

THE JOURNAL OF
PHYSICAL CHEMISTRY

Volume 69, Number 12 December 1965

Electron Capture by Solutes in the Radiolysis of Methanol and Ethanol	E. Hayon and M. Moreau	4053
Reaction Mechanism Leading to the Formation of Molecular Hydrogen in the Radiation Chemistry of Water	E. Hayon and M. Moreau	4058
The Barrier to Internal Rotation in 2-Furaldehyde	Kjell-Ivar Dahlqvist and Sture Forsén	4062
Reaction between Benzoyl Peroxide and Rhodamine 6GX Color Base	P. K. Nandi and U. S. Nandi	4071
Acid Property and Structure of a Solid Metal Sulfate Catalyst. Change in Structure of Nickel Sulfates with Heating	Tsuneichi Takeshita, Ryuichiro Ohnishi, Toshiji Matsui, and Kozo Tanabe	4077
Galvanic Cell Measurement of the Thermodynamic Interaction between Zinc and Lead in Dilute Solution in Liquid Tin	S. T. Cleveland, K. Okajima, and R. D. Pehlke	4085
A Gas Phase Electron Diffraction Study of <i>cis</i> -Dichloroethylene	M. I. Davis and H. P. Hanson	4091
Benzene and Dioxane Electric Moments of N-Alkyl-Substituted Nicotinamides from Measurements in Mixed Benzene-Dioxane Solutions	William P. Purcell and Judith A. Singer	4097
Mean Activity Coefficient of Polyelectrolytes. I. Measurements of Sodium Polyacrylates	Norio Ise and Tsuneo Okubo	4102
The Determination of the Ionization Constants of Some Sulfonic Acids by Raman Measurements	O. D. Bonner and Arnold L. Torres	4109
Structure of the Electrical Double Layer at a Mercury Electrode in the Presence of Adsorbed Nitrate Ions	Richard Payne	4113
Dissociative Equilibria in the Systems Aromatic Hydrocarbon ⁻ , Na ⁺ ⇌ Radical Anion ⁻ + Na ⁺	R. V. Slates and M. Szwarc	4124
Reactions of Alanine with the Reducing Species Formed in Water Radiolysis	Boyd M. Weeks, Sibyl A. Cole, and Warren M. Garrison	4131
Physicochemical Studies on Isotactic Polystyrene	Hiroyasu Utiyama	4138
Nuclear Magnetic Resonance Studies of Nitriles and Isocyanides: Acetonitrile and Methyl Isocyanide	A. Loewenstein and Y. Margalit	4152
Some Aspects of Gel Permeation Chromatography	William B. Smith and Anthony Kollmansberger	4157
The Dilation Contribution to the Heat Capacity of Copper and α -Brass at Elevated Temperatures	Y. Austin Chang and Ralph Hultgren	4162
Nuclear Magnetic Resonance Spectra of 2,2'-Bipyridyl	S. Castellano, H. Günther, and S. Ebersole	4166
Dielectric Dispersion of Crystalline Powders of Amino Acids, Peptides, and Proteins	S. Takashima and H. P. Schwan	4176
Complex Modulus of Concentrated Polymer Solutions in Steady Shear	Kunihiro Osaki, Mikio Tamura, Michio Kurata, and Tadao Kotaka	4183
Membrane Potential in Nonisothermal Systems	Masayasu Tasaka, Shoji Morita, and Mitsuru Nagasawa	4191
A Method for Determining Dielectric Relaxation Times	Abhai Mansingh and Pradip Kumar	4197
The Desorption and Isotopic Exchange of Oxygen at a Silver Surface	Y. L. Sandler and D. D. Durigon	4201
The Conductance of the Symmetrical Tetraalkylammonium Halides and Picrates in Methanol at 25 and 10°	Robert L. Kay, C. Zawoyski, and D. Fennell Evans	4208
The Conductance of the Tetraalkylammonium Halides in Deuterium Oxide Solutions at 25°	Robert L. Kay and D. Fennell Evans	4216

PHYSICAL CHEMISTS

Introductory Books of Merit

UNDERSTANDING PHYSICAL CHEMISTRY, Parts I and II, Arthur W. Adamson, University of Southern California

A collection of 556 problems designed to teach the fundamentals of a rigorous introductory physical chemistry course. The student must first recognize a principle and modify a standard equation to fit the situation before making his calculation. Answers are given and a time limit for the solution of problems is suggested. The book also contains complete sections on wave mechanics and group theory. 542 pages, two volume paper (121, 123) \$3.95 each, cloth (126) \$10.00.

THE CALCULUS OF CHEMISTRY, James Newton Butler, formerly University of British Columbia, and Daniel Gureasko Bobrow, Massachusetts Institute of Technology

An intuitive and pictorial approach to the mathematical ideas and techniques related to calculus are applied to chemistry for the first-year student. The concept of a function, basic to both calculus and chemistry, is given new breadth by a detailed discussion of the various forms in which a function may be expressed: graphs, tables, and algebraic rules. A function is then represented as a computer program. 160 pages, paper (1581) \$2.95, cloth (1580) \$5.00.

MATHEMATICS FOR INTRODUCTORY SCIENCE COURSES, Daniel A. Greenberg, Columbia University

Designed to meet the mathematical requirements of first year courses in physical sciences, this elementary book concentrates on calculus and vectors and reviews algebra, analytic geometry, and trigonometry. Through a clear and explicit text, supplemented by numerous exercises, examples, and illustrations, the student is rapidly brought to the point where he can understand the concepts underlying the use of graphical methods in analyzing experimental results. 228 pages, paper (3501) \$2.95, cloth (3500) \$5.00.

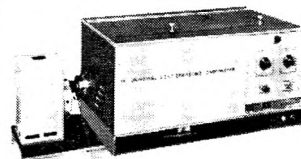
QUANTUM MECHANICS IN CHEMISTRY, Melvin W. Hanna, University of Colorado

This introduction to the application of quantum mechanics to chemistry is designed for a first-year course in undergraduate physical chemistry. It presents a detailed study of atomic and molecular electronic structure and the fundamental principles of molecular spectroscopy. The content has been selected to prepare the student to read much of the current research literature and to serve as a basis for the presentation of thermodynamics from the modern molecular viewpoint. 268 pages, paper (3701) \$3.95, cloth (3700) \$8.50.

Prepaid orders receive a 20% discount

W. A. BENJAMIN, INC.
ONE PARK AVENUE
NEW YORK

NOW YOU CAN MEASURE
MOLECULAR WEIGHTS
from 300 TO 1 BILLION*
with ONE INSTRUMENT . . .



the BRICE-PHOENIX UNIVERSAL LIGHT SCATTERING PHOTOMETER

Sounds improbable, doesn't it? But it is true. And not only does it measure molecular and micellar weights from 300 to 1 Billion, but it also measures size, shape, mass, interactions in solutions, turbidity, dissymmetry, and depolarization. With features such as absolute calibration, wavelength selection, and temperature control one would expect to pay much more than the actual price of the BRICE-PHOENIX LIGHT-SCATTERING PHOTOMETER. As a matter of fact it is far below the cost of other instruments with more limited ranges.

Certainly you will want more information. Send for Bulletin BP-2000.

*See DISSYMMETRIES, Anal. Chem. 36, 42A (1964); 36, 66A (1964); Science 143, 617 (1964) and 144, 449 (1964)



PHOENIX PRECISION INSTRUMENT COMPANY
A Subsidiary of CENCO INSTRUMENTS CORP.
3803-05 N. 5th Street, Phila., Penna. 19140, U.S.A.

14619 Germanium tetraethyl \$12.00/1g.
\$60.00/10g.
17356 Phenyl boric acid \$9.50/10g.

RARE

CHEMICALS

FINE

CATALOG NUMBER **5**

SEND FOR CATALOG #5

TELEPHONE
AREA CODE 516
GENERAL 3-6262

TELEX: 01-26464
CABLE: KALABOR PLAINVIEWNEWYORK

LABORATORIES, INC.
121 EXPRESS STREET, ENGINEERS HILL, PLAINVIEW, NEW YORK

Some Observations of Spectroscopic and Photoconductivity Effects in Permselective Membranes	Chaim Forgacs and Gabriel Stein	4221
Charge Separation in Liquid Junctions	Dennis R. Hafemann	4226
The Heats and Entropies of Dilution of the Perchlorates of Magnesium and Strontium	H. S. Jongenburger and R. H. Wood	4231
The Wetting of Gold and Platinum by Water	K. W. Bewig and W. A. Zisman	4238
The Use of Combined Schlieren and Absorption Optics in an Electrophoretic Study of the Reversibly Interacting System Dextran Sulfate-Carboxyhemoglobin	York Tsang and T. E. Thompson	4242
The Thermodynamics of Vaporization in the Beryllium Oxide-Boron Oxide System	Paul E. Blackburn and Alfred Buchler	4250
Nuclear Magnetic Resonance Absorption in Anhydrous Sodium Soaps	Kenneth D. Lawson and Thomas J. Flautt	4256
Thermodynamics of the Exchange of Tetramethylammonium with Sodium Ions in Cross-Linked Polystyrene Sulfonates at 25°	A. Schwarz and G. E. Boyd	4268
Diffusion and Frictional Coefficients for Two Concentrated Compositions of the System Water-Mannitol-Sodium Chloride at 25°; Tests of the Onsager Reciprocal Relation	Peter J. Dunlop	4276
Triplet State of Fluorobenzene	I. Unger	4284
Kinetics of the Attack of Molybdenum by Dissociated Chlorine	Daniel E. Rosner and H. Donald Allendorf	4290
Recoil Tritium Reaction: Ring Opening and Alkyl Replacement in Substituted Cyclopropanes	Yi-Noo Tang and F. S. Rowland	4297
Low-Temperature Thermodynamic Properties of <i>n</i> -Propyl- and <i>n</i> -Butylbenzene	John F. Messerly, Samuel S. Todd, and Herman L. Finke	4304
Further Critical Opalescence Measurements on the Nitrobenzene- <i>n</i> -Heptane System	H. Brumberger and R. Pancirov	4312
On the Possible Initiation of Photooxidation by Charge-Transfer Excitation	J. C. W. Chien	4317
Comparison of Nuclear Magnetic Resonance, Thermal Maximum, and Scavenging Techniques for Rate Measurement	Peter G. Evans, Gerald R. Miller, and Maurice M. Kreevoy	4325
Mechanism of the Solid-State Thermal Decomposition of Potassium Trisoxalatochromium(III) Trihydrate	R. M. Wing and G. M. Harris	4328
Infrared Reflection Spectra of Molten Fluoride Solutions. Hydrolysis of Tantalum(V) in Potassium Fluoride-Lithium Fluoride	J. Stuart Fordyce and Ruth L. Baum	4335
Mass Spectrometric Investigations of the Synthesis, Stability, and Energetics of the Low-Temperature Oxygen Fluorides. I. Dioxygen Difluoride	T. J. Malone and H. A. McGee, Jr.	4338
The Investigation of the Behavior of Some Divalent Salts of <i>p</i> -Toluenesulfonic Acid and Related Polymeric Acids in Aqueous Solutions	O. D. Bonner, W. H. Breazeale, and Carey Rushing	4345
The Chemically Activated Decomposition of <i>n</i> -Butane and of Isobutane	G. Z. Whitten and B. S. Rabinovitch	4348
Fluorine Bomb Calorimetry. XIII. The Enthalpy of Formation of Arsenic Pentafluoride	P. A. G. O'Hare and Ward N. Hubbard	4358
A Least-Squares Method for Calculating Diffusion Coefficients for Ternary Systems	R. L. Dunn and J. D. Hatfield	4361
Sedimentation Equilibrium in Reacting Systems of the Type $mA + nB \rightleftharpoons C$	L. W. Nichol and A. G. Ogston	4365
Spectral Changes in a Cationic Dye Due to Interaction with Macromolecules. III. Stoichiometry and Mechanism of the Complexing Reaction	R. C. Bean, W. C. Shepherd, R. E. Kay, and E. R. Walwick	4368
The Formation Kinetics of the Nickel Monomalonate Complex Studied by the Temperature-Jump Method	Francesco Paolo Cavalino	4380
Physical Adsorption on Low-Energy Solids. III. Adsorption of Ethane, <i>n</i> -Butane, and <i>n</i> -Octane on Poly(tetrafluoroethylene)	Donald P. Graham	4387
Internal Pressure of Simple Liquids	Umberto Bianchi, Giuseppe Agabio, and Antonio Turturro	4392

LABORATORY REPORT

Project: Separate data on the biological activity of organic compounds from the mass of published information.


By: Chemical Abstracts Service

Date: 1965

Procedure

The mass is concentrated by application of energy (selection of approximately 300 pertinent journals by CAS staff scientists). Appropriate material (articles reporting on biological activities of organic compounds) is removed, condensed (digest preparation by staff analysts), fractionated (in form of indexes) and collected into a suitable container (Chemical-Biological Activities).

Results

Structure:	Keyword-In-Context Index		Molecular Formula Index
	Author Index		Digest Section

Properties: Biweekly publication.
 25-30 access points per digest.
 Six-month cumulation of indexes.
 Registry Number for compounds for identification in CAS computer system.
 Journal references with volume and page numbers.
 Chemical structure diagrams.
 Author names for compounds used throughout.

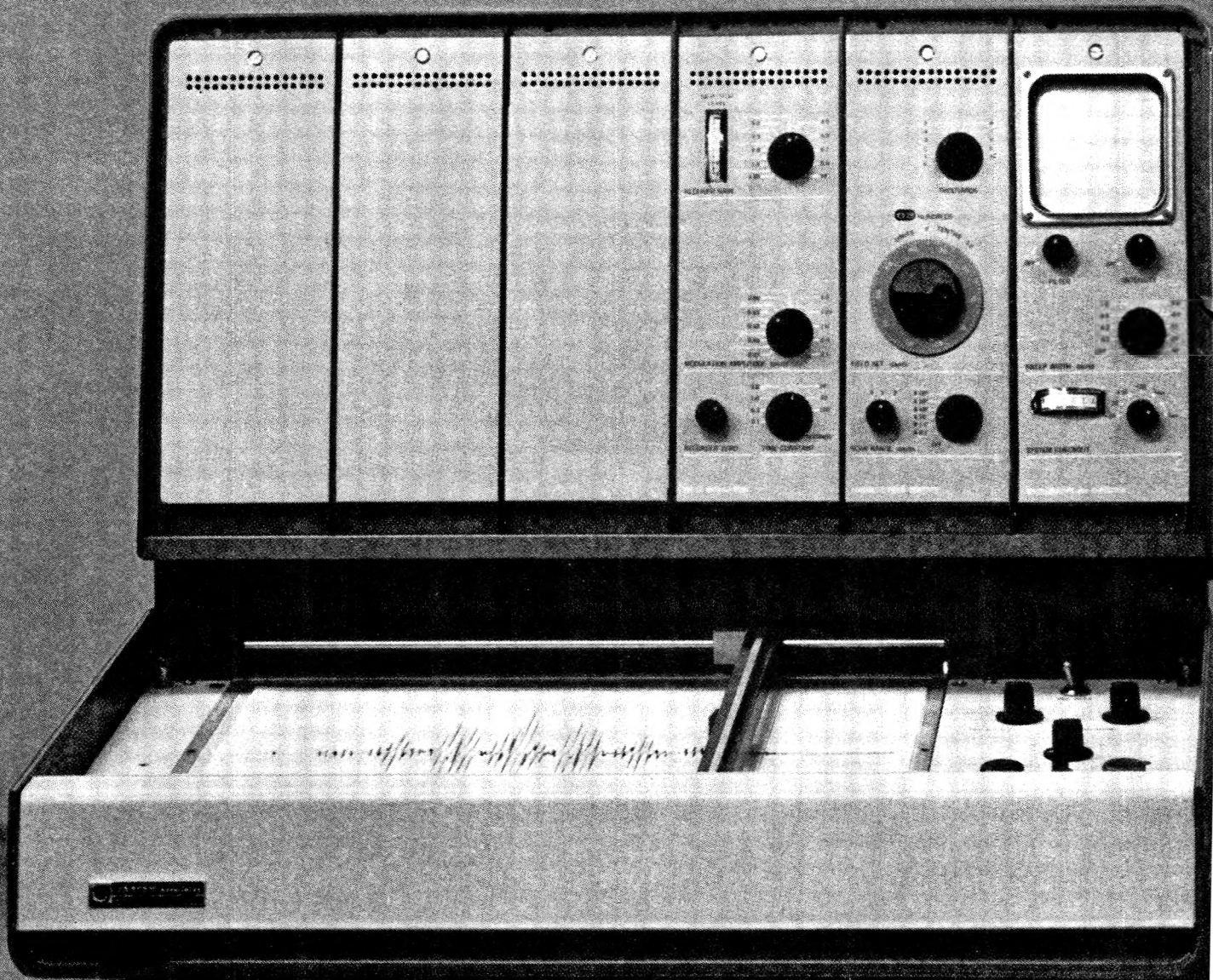
Comments

Excellent tool for removing needed facts from extraneous material. Digests reflect accurate picture of experimental results.

Low cost—\$800/year (includes up to 25 scientists at the subscriber's address). An additional charge of \$50 is made for each additional group of 25 or less scientists who will be served by CBAC. Maximum price—\$1,500.

Current coverage of life science journals.

Contact Mr. Emerson Heilman at the Chemical Abstracts Service, The Ohio State University, Columbus, Ohio 43210, for further information.



ANOTHER FIRST FROM VARIAN
NEW TABLE-TOP
LOW-PRICED EPR

Electron Capture by Solutes in the Radiolysis of Methanol and Ethanol

by E. Hayon and M. Moreau

Service de Chimie-Physique, C.E.A. Saclay (Seine et Oise), France (Received August 31, 1965)

The yields of hydrogen produced on γ -irradiation of air-free methanol and ethanol at lowest doses are $G(\text{H}_2) = 5.25$ and $G(\text{H}_2) = 5.0$, respectively. Addition of certain salts (NiCl_2 , CoSO_4) has been used to determine the "readily scavengeable" yields of solvated electrons in methanol, $G(e^-) = 1.05$, and ethanol, $G(e^-) = 0.90$. Addition of nitrate and chloroacetate ions, over a wide concentration range, gives rise to a decrease in hydrogen yields and an increase in yields of nitrite and chloride ions. Above a certain solute concentration, the sum of the yields of $G(\text{H}_2) + G(\text{NO}_2^-)$ or $G(\text{H}_2) + G(\text{Cl}^-)$ increases with further increase in $[\text{S}]$. This increase has been shown to be proportional to the rate constant of the solute with solvated electrons and is attributed to electron capture by solutes in the spurs leading to a decrease of the combination reaction $\text{RCH}_2\text{OH}^+ + \text{RCH}_2\text{OH}^- \rightarrow 2\text{RCH}_2\text{OH}$. The "total scavengeable" yield of electrons is $G(e^-) = 1.85$ in methanol and $G(e^-) = 1.65$ in ethanol.

The action of ionizing radiations on simple aliphatic alcohols is in many ways quite similar to that on water, giving rise to solvated electrons and hydrogen atoms. In the radiation chemistry of water it has recently been shown,¹ on addition of certain oxidizing agents, *e.g.*, H^+ , NO_3^- , and ClCH_2COOH , that the yield of total reducing species increase, above a certain solute concentration, with further increase in solute concentration finally reaching a maximum yield. This increase in radical yields was shown to be proportional to $k_{\text{RS}}C_{\text{S}}$, where k_{RS} is the rate constant for reaction of the solute with H_2O^- and C_{S} is the solute concentration, and was attributed to the capture by solutes of electrons produced in regions of high radical concentration, *i.e.*, spurs. Such scavenging leads to a reduction of the combination reaction $\text{H}_2\text{O}^- + \text{OH} \rightarrow \text{H}_2\text{O} + \text{OH}^-$ to form water.

It seemed of interest to demonstrate that the same phenomenon took place in the radiolysis of simple aliphatic alcohols. With this view in mind, the γ -irradiation of lithium nitrate and chloroacetate solutions was investigated.

Experimental Section

A 200-curie ^{60}Co γ source was used, and the dose rate in pure alcohols was 2.2×10^{16} e.v./g. min. based on the ferrous sulfate dosimeter, taking $G(\text{Fe}^{3+}) = 15.5$. The ethanol was a Merck "pro analysis" product and was used without further purification since it was found to give $G(\text{H}_2) = 4.85 \pm 0.05$, in good agreement with other recently published values.²⁻⁴ A

(1) E. Hayon, *J. Phys. Chem.*, **68**, 1242 (1964); *Trans. Faraday Soc.*, **61**, 723 (1965).

(2) E. Hayon and J. J. Weiss, *J. Chem. Soc.*, 3262 (1961).

later batch of Merck ethanol was found to give $G(\text{H}_2) = 5.00 \pm 0.05$ (see below). The Merck "pro analysis" methanol was found to contain aldehydes, and various ways of purifying it were tried. The best results were obtained by refluxing overnight under a nitrogen gas atmosphere about 800 ml. of methanol containing 1 ml. of H_2SO_4 and 3 g. of 2,4-dinitrophenylhydrazine sulfate. The column having been cleaned by the reflux, this methanol was discarded. On the following morning a fresh quantity (with added H_2SO_4 and hydrazine) with N_2 bubbling through the methanol was refluxed for 3 hr. The middle fraction was then collected in a receiver kept at 0° . All reagents used were analytical research grades supplied by Hopkin and Williams except LiNO_3 which was supplied by Baker and Adamson. They were all dried in a desiccator containing silica gel.

All irradiations were carried out in Pyrex ampoules of ca. 5-ml. capacity; the degassing procedure and gas analysis by chromatography have already been described.⁵ Nitrite ions were determined by the method of Shinn,⁶ using ϵ 53,200 at 5400 Å., and chloride ions determined⁷ as silver chloride.

Results

In all cases the alcohols were irradiated to low doses (7×10^{17} e.v./g.) so as to determine initial yields, and the maximum total dose given in the determination of low concentrations of chloride ions ($<50 \mu\text{M}$) was 5×10^{18} e.v./g. Linear yield-dose curves were obtained in all cases, and each G value given is the result of four or five measurements on the corresponding curve. The only products determined were hydrogen, nitrite (in LiNO_3 solutions), and chloride ions (in chloroacetate solutions).

Radiolysis of Ethanolic Solutions. The hydrogen yield obtained on γ -irradiation of air-free ethanol was $G(\text{H}_2) = 4.85 \pm 0.05$. This value was obtained in all cases, except the batch used in the determination of H_2 yields in presence of Ni^{2+} and Co^{2+} salts (see below) when $G(\text{H}_2) = 5.00 \pm 0.05$. These values are to be compared with recent $G(\text{H}_2)$ values of 4.85 obtained by Hayon and Weiss² and Adams and Sedgwick³ and 5.0 by Myron and Freeman.⁴

Most of the solutes which have been used in the radiolysis of alcohols react with both solvated electrons and H atoms, the two reducing species formed on irradiation. In order to determine accurately the yields of "readily scavengeable" electrons produced in these alcohols, it is important to use solutes where $k(e^- + \text{S}) \gg k(\text{H} + \text{S})$. This condition was not usually observed in previous studies. The radiolysis in the presence of the divalent ions Ni^{2+} and Co^{2+} was there-

fore examined since Baxendale and Dixon⁸ have indicated that these ions react very much more slowly with H atoms than with electrons in aqueous solutions, such that $k(e^- + \text{M}^{2+})/k(\text{H} + \text{M}^{2+}) \geq 10^{4,5,8}$. The H_2 yields were determined as a function of solute concentration of these divalent salts, and the results are shown in Figure 1(b) using $\text{NiCl}_2 \cdot 6\text{H}_2\text{O}$ and $\text{CoSO}_4 \cdot 7\text{H}_2\text{O}$. A plateau is obtained over almost a 40-fold change in the solute concentration to give $G(\text{H}_2) = 4.10 \pm 0.05$, as compared to $G(\text{H}_2) = 5.0 \pm 0.05$ in pure ethanol from the same batch.

Addition of lithium nitrate, which is soluble in alcohols, was found to reduce the H_2 yield in the radiolysis of 2-propanol.⁹ A similar effect was observed in the irradiation of ethanol and methanol. The decrease in H_2 yields and the formation of NO_2^- ions with increase in $[\text{LiNO}_3]$ are shown in Figure 2. There appears to be an inflection in the curves in the region of $5 \times 10^{-2} M$ LiNO_3 , and its significance is not clear. G_{total} , that is, the sum of $G(\text{H}_2) + G(\text{NO}_2^-)$, seems to reach a plateau value of 5.6 at $\sim 1.0 M$ LiNO_3 . It is interesting to note that this increase of 0.75 G units over the yield in absence of LiNO_3 is reflected in the NO_2^- yields which increase more rapidly than the corresponding decrease in the H_2 yields.

On addition of chloroacetic acid, the same effect is observed, as shown in Figure 3. At low solute concentrations, the yields of H_2 decrease more rapidly than with LiNO_3 , indicating a greater reactivity with the precursor of H_2 in this region. Similarly, the yield of Cl^- increases more rapidly with concentration than that of NO_2^- . The sum of $G(\text{H}_2) + G(\text{Cl}^-)$ is plotted in Figure 3, and one obtains a maximum G value of 5.65. Again, the increase in 0.80 G units due to scavenging by the chloroacetate is to be seen in a greater yield in $G(\text{Cl}^-)$ over and above the corresponding decrease in $G(\text{H}_2)$. Above $2 \times 10^{-1} M$ chloroacetate, the yield of H_2 continues to decrease regularly, but the yield of Cl^- increases abruptly bearing no relation to the corresponding decrease in H_2 . Such a rapid increase in Cl^- yields seems to indicate the presence of a chain reaction. The yields of H_2 in chloroacetate are somewhat different from those previously found² and are closer to those recently reported.³

(3) G. E. Adams and R. D. Sedgwick, *Trans. Faraday Soc.*, **60**, 865 (1964).

(4) J. J. Myron and G. R. Freeman, *Can. J. Chem.*, **43**, 381 (1965).

(5) E. Hayon and M. Moreau, *J. chim. phys.*, **62**, 391 (1965).

(6) M. B. Shinn, *Ind. Eng. Chem., Anal. Ed.*, **13**, 33 (1941).

(7) E. Hayon and A. O. Allen, *J. Phys. Chem.*, **65**, 2181 (1961).

(8) J. H. Baxendale and R. S. Dixon, *Proc. Chem. Soc.*, 148 (1963).

(9) L. Gilles, private communication.

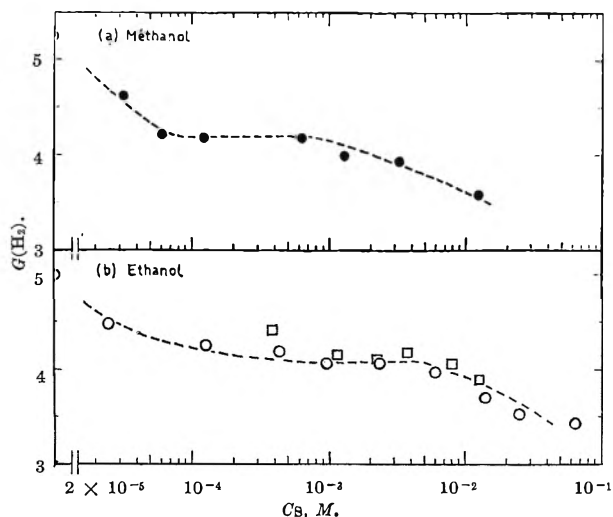


Figure 1. (a) Radiolysis of methanol in presence of NiCl_2 , ●. (b) Radiolysis of ethanol in presence of NiCl_2 , ○, and CoSO_4 , □.

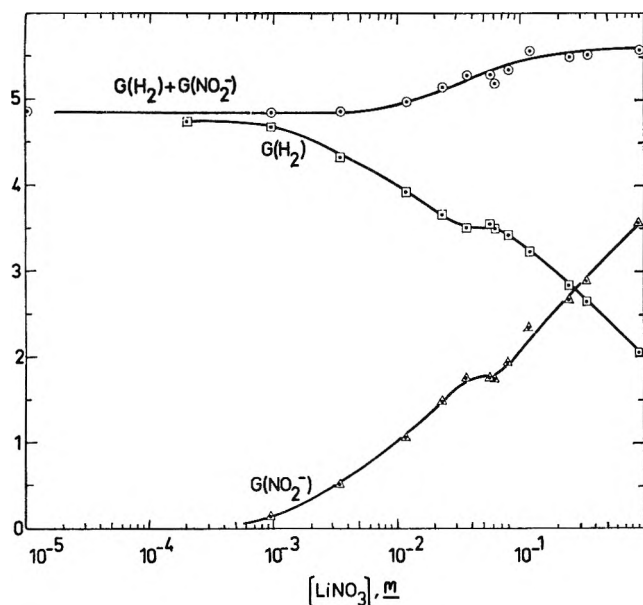


Figure 2. γ -Irradiation of air-free ethanolic solutions of LiNO_3 . Yields of $G(\text{H}_2)$, □, $G(\text{NO}_2^-)$, △, and the sum $G(\text{H}_2) + G(\text{NO}_2^-)$, ○, are shown.

Radiolysis of Methanolic Solutions. Considerable attention was given to the purification of methanol. Making the assumption that the highest yields of hydrogen obtainable are an indication of the absence of impurities capable of reacting with the solvated electrons and H atoms produced on irradiation, and hence of a higher degree of purity, we endeavored to vary our purification procedure with this end in mind. The method of purification found to give the highest $G(\text{H}_2)$ yields has been described above. A mean of 12 ir-

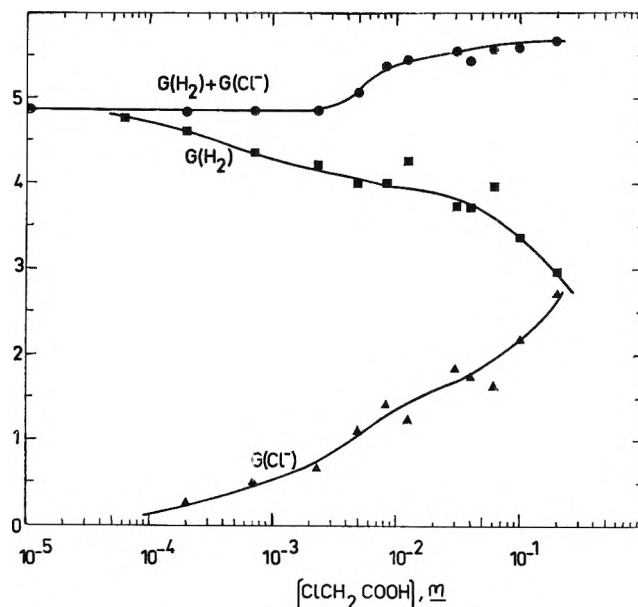


Figure 3. γ -Irradiation of air-free ethanolic solutions of chloroacetate. Yields of $G(\text{H}_2)$, ■, $G(\text{Cl}^-)$, ▲, and the sum $G(\text{H}_2) + G(\text{Cl}^-)$, ●, are shown.

radiations gave $G(\text{H}_2) = 5.26 \pm 0.1$, on γ -irradiation of deaerated methanol. This yield is to be compared with earlier values of 4.1,^{10,11} 4.8,^{12a} 4.99,^{12b} and the high values of 5.39¹³ and 5.4¹⁴ obtained after careful purification of the methanol.

As was done for ethanol, the yield of readily scavengable solvated electrons was determined by measuring the yield of hydrogen produced in the presence of NiCl_2 . A plateau value of $G(\text{H}_2) = 4.2 \pm 0.05$ was obtained, Figure 1(a), indicating $G(e^-) = 1.05 \pm 0.05$. On addition of LiNO_3 , the yields of $G(\text{H}_2)$ and $G(\text{NO}_2^-)$ were irreproducible, particularly in moderately dilute solutions. In concentrated solutions the results were better, e.g., in 1.0 M LiNO_3 , $G(\text{H}_2) = 1.82$ and $G(\text{NO}_2^-) = 4.18$, giving $G_T = 6.0$. The results in this region of concentration independence correspond to the maximum yield obtained by Baxendale and Mellows¹⁴ on addition of H^+ ions, $G(\text{H}_2) = 6.05$, and indicates that the total scavengable yield of electrons produced in methanol is $G(e^-)_T = 1.85 \pm 0.1$.

Discussion

Chemical kinetic evidence,^{2,3,10,14} as well as spectral¹⁵

- (10) E. Hayon and J. J. Weiss, *J. Chem. Soc.*, 397C (1961).
 (11) G. E. Adams and J. H. Baxendale, *J. Am. Chem. Soc.*, **80**, 4215 (1958).
 (12) (a) M. Imamura, S. U. Choi, and N. N. Lichtin, *ibid.*, **85**, 3565 (1963); (b) L. M. Theard and M. Burton, *J. Phys. Chem.*, **67**, 59 (1963).
 (13) G. Meshitsuka and M. Burton, *Radiation Res.*, **8**, 285 (1958).
 (14) J. H. Baxendale and F. W. Mellows, *J. Am. Chem. Soc.*, **83**, 4720 (1961).

and e.s.r.¹⁶ evidence, has recently established the formation of solvated electrons in the radiolysis of simple aliphatic alcohols. The curves showing the variation of $G(\text{H}_2)$ with the concentrations of various solutes (ref. 2, 3, 10, 14 and Figures 1-3) show two regions which are sometimes separated by a range of solute concentration over which $G(\text{H}_2)$ remains constant. These observations have been interpreted to indicate the presence of two precursors of hydrogen—the solvated electron and H atoms—each of which is capable of being scavenged by solutes, although with significantly different rate constants. From known reactivities of various solutes, the decrease of $G(\text{H}_2)$ down to the plateau region has been attributed to the reaction of the solute with solvated electrons, and the decrease of $G(\text{H}_2)$ at higher solute concentration to a competition between the solute and alcohol for H atoms.

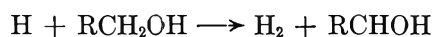
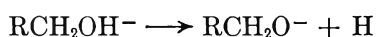
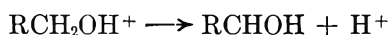
Reactions 1-3 are considered to be the main processes occurring on γ -irradiation.



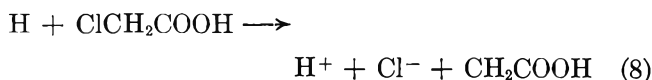
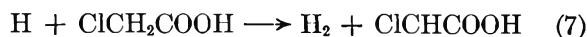
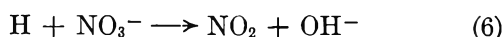
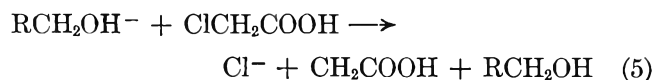
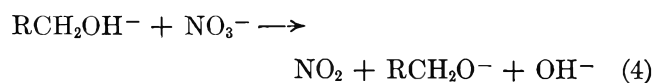
where RCH_2OH^- represents the solvated electron. Reaction 3 which could account for the formation of unscavengable (molecular) hydrogen



is followed by



On using solutes known to be good reactants for electrons, such as nitrate ions and chloroacetic acid, one can explain the results obtained up to $\sim 5 \times 10^{-3} M$ solutions when G_{total} remains constant (Figures 2 and 3) as due to reactions 4 to 8



The NO_2 formed in reactions 4 and 6 reacts, as has been

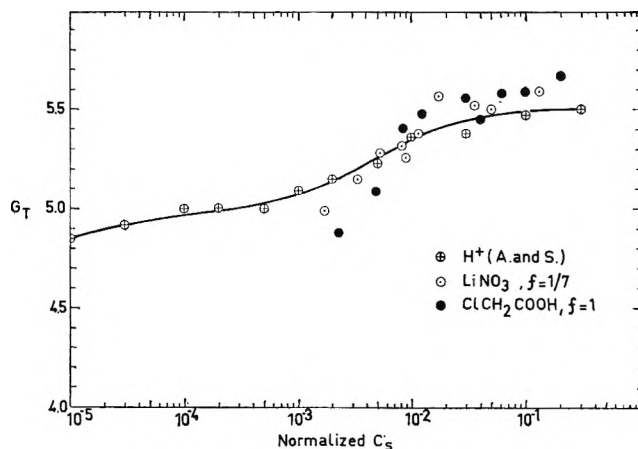


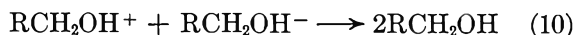
Figure 4. Plot of G_{total} as a function of solute concentration normalized with respect to $[\text{H}^+]$: $[\text{H}^+]$, \oplus , data from ref. 3; $[\text{LiNO}_3]$, \odot , $f = 1/7$; $[\text{ClCH}_2\text{COOH}]$, \bullet , $f = 1$. (f is the normalization factor.)

shown in aqueous solutions,¹⁷ with RCHOH radicals to yield NO_2^- ions and the corresponding aldehyde



In this way one reducing species leads to the formation of one NO_2^- ion.

At solute concentrations above $5 \times 10^{-3} M$ one finds, however, that the sum of the H_2 and NO_2^- (or Cl^-) yields does not remain constant but increases with further increase in $[\text{S}]$ finally reaching a plateau value. This increase is reflected in the yields of NO_2^- and Cl^- ions which are greater than the corresponding decreases in the H_2 yield. These results are interpreted to indicate a scavenging of electrons in the spurs by the solutes present in relatively high concentration, resulting in a decrease of the back reaction



As was done in the radiation chemistry of water,^{1,17} the increase in total yields with increase in solute concentration was normalized with respect to $[\text{H}^+]$ since the rate constant $k(e^- + \text{H}^+)$ is known¹⁵: in ethanol $k(e^- + \text{H}^+) = 2 \times 10^{10} M^{-1} \text{sec}^{-1}$ and in methanol $k(e^- + \text{H}^+) = 4 \times 10^{10} M^{-1} \text{sec}^{-1}$. Figure 4 shows the results normalized for LiNO_3 and ClCH_2COOH solutions against $[\text{H}^+]$, using the results of Adams and Sedgwick³ of $G(\text{H}_2)$ vs. $[\text{H}^+]$. The normalization coincidence of the curves is not so good as that ob-

(15) I. A. Taub, M. C. Sauer, and L. M. Dorfman, *Discussions Faraday Soc.*, **36**, 206 (1963).

(16) C. Chachaty and E. Hayon, *Nature*, **200**, 59 (1963); *J. chim. phys.*, **61**, 1115 (1964).

(17) E. Hayon, *Trans. Faraday Soc.*, **61**, 734 (1965).

tained in aqueous systems. However, from the normalization factors, f , obtained one can calculate rate constants to better than $\pm 40\%$. Thus, in ethanol, $k(e^- + \text{NO}_3^-) = 2.9 \pm 0.9 \times 10^9 \text{ M}^{-1} \text{ sec.}^{-1}$ and $k(e^- + \text{ClCH}_2\text{COOH}) = 2.0 \pm 0.7 \times 10^{10} \text{ M}^{-1} \text{ sec.}^{-1}$. Such rate constant values are in support of the capture by these solutes of electrons since the rate constants for reaction with H atoms are much smaller (see, *e.g.*, ref. 5).

It is seen, therefore, that in the radiolysis of ethanol the yield of readily scavengeable solvated electrons derived using Ni^{2+} or Co^{2+} salts is $G(e^-) = 0.90 \pm 0.10$, and the yield of electrons scavengeable at relatively high concentrations of LiNO_3 or ClCH_2COOH in the spurs is $G(e^-) = 0.75 \pm 0.10$. This total $G(e^-)_T = 1.65 \pm 0.20$ obtained on irradiation of liquid ethanol at room temperature is to be compared with the yield of electrons $G(e^-) = 2.3 \pm 0.7$ as determined¹⁶ by e.s.r. in the radiolysis of glassy ethanol at 77°K. On γ -irradiation of methanol, the yield of readily scavenge-

able electrons is 1.05 ± 0.05 , and the maximum yield of electrons is $G(e^-) = 1.85 \pm 0.1$. The corresponding yield obtained¹⁶ by e.s.r. on irradiation of glassy methanol at 77°K. is $G(e^-) = 2.2 \pm 0.7$. The yields of readily scavengeable electrons given above can be compared with $G(e^-) = 0.95^3$ and 0.9^4 for ethanol and $G(e^-) = 1.3^{14}$ for methanol.

In conclusion, it would appear to be a general phenomenon in the radiation chemistry of liquid systems that some of the electrons, which are produced on ionization of the medium and which normally return to the parent positive ions or react with other positive ions or radicals formed on irradiation, can be captured in the tracks or spurs by certain solutes present in relatively high concentrations provided the $k_{RS}C_S$ value is sufficiently high (where k_{RS} is the rate constant for reaction of the solute with electrons and C_S is the solute concentration). Such electron capture by solutes in the spurs leads to a higher yield of radical production and hence a higher net decomposition of the liquid.

Reaction Mechanism Leading to the Formation of Molecular Hydrogen in the Radiation Chemistry of Water

by E. Hayon and M. Moreau

Service de Chimie Physique, C.E.A. Saclay (Seine et Oise), France (Received August 31, 1965)

The yields of "molecular" hydrogen produced in the γ -radiolysis of air-free neutral solutions of potassium dichromate, potassium nitrite, and copper nitrate have been measured over a very wide range of concentrations, such that up to 99% of the hydrogen has been scavenged by these solutes. From a comparison of the scavenging efficiencies of the various solutes used, the results seem to indicate the presence of two precursors leading to the formation of "molecular" hydrogen. From a kinetic treatment of the data it is suggested that the precursors are electrons and H atoms, which react according to $\text{H}_2\text{O}^- + \text{H}_2\text{O}^- \rightarrow \text{H}_2 + 2\text{OH}^-$ and $\text{H} + \text{H}_2\text{O}^- \rightarrow \text{H}_2 + \text{OH}^-$, with a small contribution from $\text{H} + \text{H} \rightarrow \text{H}_2$. On accounting for the different rate constants for reaction of the solutes with the two reducing species, it is possible to obtain better qualitative agreement between theoretical diffusion kinetics calculations and experiment.

The "molecular" yield of hydrogen produced on γ -irradiation of aqueous solutions, $G_{\text{H}_2} = 0.45 \pm 0.01$, is known to be reduced in the presence of a number of solutes (*e.g.*, NO_2^- , NO_3^- , H_2O_2 , Cu^{2+} , acrylamide, Ce^{4+}), the variation being dependent on the scavenger used and its concentration. It was suggested by Hayon and Weiss¹ that the main precursor leading to the formation of "molecular" hydrogen is an electron, H_2O^- , which on recombination in the "spurs" produces H_2 , according to the over-all reaction



It was thus possible to explain the lowering^{2,3} of G_{H_2} in acid solutions compared to neutral solutions on the basis of a competition between $\text{H}_2\text{O}^- + \text{H}^+ \rightarrow \text{H} + \text{H}_2\text{O}$ and reaction 1, resulting in an expansion of the dimensions of the spurs. Dorfman and Taub⁴ have recently confirmed the existence of reaction 1.

Mahlman⁵ has shown that on irradiation of water with γ -rays, using nitrate ions as scavenger for the precursor of hydrogen, a plot of $G(\text{H}_2)$ vs. the cube root of $[\text{NO}_3^-] \times$ activity coefficient showed two straight lines with different slopes, indicating two different modes of formation of "molecular" H_2 . The lower slope extrapolates to $G(\text{H}_2) = 0.1$ at "infinite dilution." This value seems to correspond to the yield of H_2 ob-

tained on irradiation of frozen aqueous solutions of NaNO_3 ⁵ or H_2O_2 ⁶ at -196° . The results of Anderson and Hart,⁷ using hydrogen peroxide as solute, were also shown⁸ to give two straight lines with different slopes when plotting $G(\text{H}_2)$ vs. $[\text{H}_2\text{O}_2]^{1/3}$. Since NO_3^- ions and H_2O_2 are known to react efficiently with H_2O^- ($k = 10^{10}$ ^{9,10} and 1.3×10^{10} ^{10,11} $M^{-1} \text{ sec}^{-1}$, respectively) and relatively slowly with H atoms ($k = 2.4 \times 10^6$ $M^{-1} \text{ sec}^{-1}$ ¹² and 4×10^7 $M^{-1} \text{ sec}^{-1}$,¹³ respec-

(1) E. Hayon and J. J. Weiss, *Proc. 2nd Intern. Conf. Peaceful Uses At. Energy, Geneva*, 29, 30 (1958).

(2) E. Hayon, *J. Phys. Chem.*, 65, 1502 (1961).

(3) C. H. Cheek, V. J. Linnenbom, and J. W. Swinnerton, *Radiation Res.*, 19, 636 (1963).

(4) L. M. Dorfman and I. A. Taub, *J. Am. Chem. Soc.*, 85, 2370 (1963).

(5) H. A. Mahlman, *J. Chem. Phys.*, 32, 601 (1960).

(6) J. A. Ghormley and A. C. Stewart, *J. Am. Chem. Soc.*, 78, 2934 (1956).

(7) R. A. Anderson and E. J. Hart, *J. Phys. Chem.*, 65, 804 (1961).

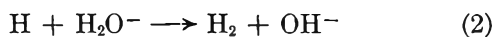
(8) E. Hayon, *Nature*, 194, 737 (1962).

(9) J. K. Thomas, S. Gordon, and E. J. Hart, *J. Phys. Chem.*, 68, 1524 (1964).

(10) J. H. Baxendale, E. M. Fielden, C. Capellos, J. M. Francis, J. V. Davies, M. Ebert, C. W. Gilbert, J. P. Keene, E. J. Land, and A. J. Swallow, *Nature*, 201, 468 (1964).

(11) S. Gordon, E. J. Hart, M. S. Matheson, J. Rabani, and J. K. Thomas, *Discussions Faraday Soc.*, 36, 193 (1963).

tively), it was proposed⁸ that the major portion of molecular hydrogen which can be readily reduced by the addition of these scavengers has as precursor H_2O^- , while the remaining portion ($G(\text{H}_2) \simeq 0.1$), less susceptible to H_2O_2 and NO_3^- ions, has H atoms as the precursor



To check this mechanism further, the variation of $G(\text{H}_2)$ with the concentration of a number of selected solutes was examined: $\text{Cu}(\text{NO}_3)_2$, KNO_2 , and $\text{Na}_2\text{Cr}_2\text{O}_7$. The solutes were chosen on the basis of increasing reactivity towards H atoms,¹² with $k(\text{H} + \text{S}) = 2.5 \times 10^8$, 6.1×10^8 , and $5.6 \times 10^9 \text{ M}^{-1} \text{ sec}^{-1}$, where S = $\text{Cu}(\text{NO}_3)_2$, KNO_2 , and $\text{Na}_2\text{Cr}_2\text{O}_7$, respectively. The corresponding rate constants for reaction with H_2O^- were 4.5×10^{10} , 4.0×10^9 ,^{9,10} and $3.3 \times 10^{10} \text{ M}^{-1} \text{ sec}^{-1}$.

Experimental Section

Copper nitrate and sodium dichromate supplied by Hopkin and Williams and potassium nitrite by Baker and Adamson were used without further purification. All other reagents were of analytical grade.

A 200-curie ^{60}Co γ -source was used with a dose rate of 6.5×10^{19} e.v./l. min. based on the Fricke dosimeter taking $G(\text{Fe}^{3+}) = 15.5$. Total doses given ranged from 4×10^{21} e.v./l. at low solute concentrations to 3×10^{22} e.v./l. for the highest solute concentrations used. The water employed was purified as described elsewhere.¹⁴ The method used for degassing, filling the 10-ml. irradiation tubes, extracting the gaseous products, and measuring them by gas chromatography has already been given.¹² The solutions containing $\text{Cu}(\text{NO}_3)_2$ and $\text{Na}_2\text{Cr}_2\text{O}_7$ were irradiated in the presence of 10^{-3} M KBr to protect the molecular hydrogen from OH radical attack. Bromide was not added to solutions of nitrite since it is a good scavenger for OH radicals.

Direct interaction of the radiation with the solutes used in this work becomes important at the high solute concentrations used. The doses absorbed in these solutions was therefore corrected^{2,15} using the equation

$$D_S = D_{\text{Fe}^{2+}} \left(\frac{\epsilon_S}{\epsilon_D} + \tau \right)$$

where D_S is the corrected dose, $D_{\text{Fe}^{2+}}$ is the dose as measured by the Fricke dosimeter, ϵ_S and ϵ_D are the electron density of the irradiated solutions and dosimeter, respectively, and τ is the correction for the photoelectric effect. The yields of H_2 and O_2 were corrected

as indicated above and are given on the basis of total energy absorbed by the solution. The correction factor used below represents the ratio $D_S/D_{\text{Fe}^{2+}}$. Each G value measured is the result of five or six irradiations carried out at different times to give linear yield-dose curves, and are good to better than $\pm 3\%$ at the low solute concentrations and $\pm 5\%$ at the high solute concentrations.

Results

The yields of hydrogen obtained on γ -irradiation of air-free aqueous solutions of sodium dichromate, copper nitrate, and potassium nitrite were determined over a wide range of concentrations such that up to 99% of the yield of H_2 was scavenged by the solutes used. In all cases the decrease in $G(\text{H}_2)$ is linear with $[\text{S}]^{1/3}$ at low solute concentrations. Extrapolation of this linear portion of the curve to infinite dilution gives $G_{\text{H}_2} = 0.44$. At higher solute concentrations the yields of H_2 are no longer linear with $[\text{S}]^{1/3}$ and a smooth curve can be drawn through the experimental points.

Figure 1 presents the results according to the method used by Schwarz.¹⁶ Here the fractional lowering of the molecular H_2 yield $G(\text{H}_2)/G_{\text{H}_2}$ is plotted against the logarithm of the solute concentration and the resulting series of curves brought into coincidence by multiplication of the concentration by a normalization factor f . This factor is chosen to give the "best" coincidence of the curves in the low concentration regions, and was obtained relative to the nitrite system. Comparison of the f values for the solutes used here shows that they are related to the reactivity of these solutes toward H_2O^- , as obtained by pulse radiolysis.

The full curve drawn in Figure 1 is theoretical and was calculated¹⁶ for the nitrite system on the basis of the one-radical diffusion model. The yields of H_2 in NaNO_3 solutions⁵ as well as those in H_2O_2 ,^{7,17} and acrylamide¹⁸ solutions have been included in Figure 1, and all have been plotted as a function of the solute concentration.

Oxygen is formed on irradiation of $\text{Na}_2\text{Cr}_2\text{O}_7$ and $\text{Cu}(\text{NO}_3)_2$ (none is observed in NaNO_2 solutions), particularly at higher solute concentrations. These

(12) E. Hayon and M. Moreau, *J. chim. phys.*, **62**, 391 (1965).

(13) J. K. Thomas, *J. Phys. Chem.*, **67**, 2593 (1963).

(14) E. Hayon, *Trans. Faraday Soc.*, **60**, 1059 (1964).

(15) H. A. Mahlman and G. K. Schweitzer, *J. Inorg. Nucl. Chem.*, **5**, 213 (1958).

(16) H. A. Schwarz, *J. Am. Chem. Soc.*, **77**, 4960 (1955).

(17) J. A. Ghormley and C. J. Hochanadel, *Radiation Res.*, **3**, 227 (1955).

(18) F. S. Dainton, *Radiation Res. Suppl.*, **1**, 25 (1959).

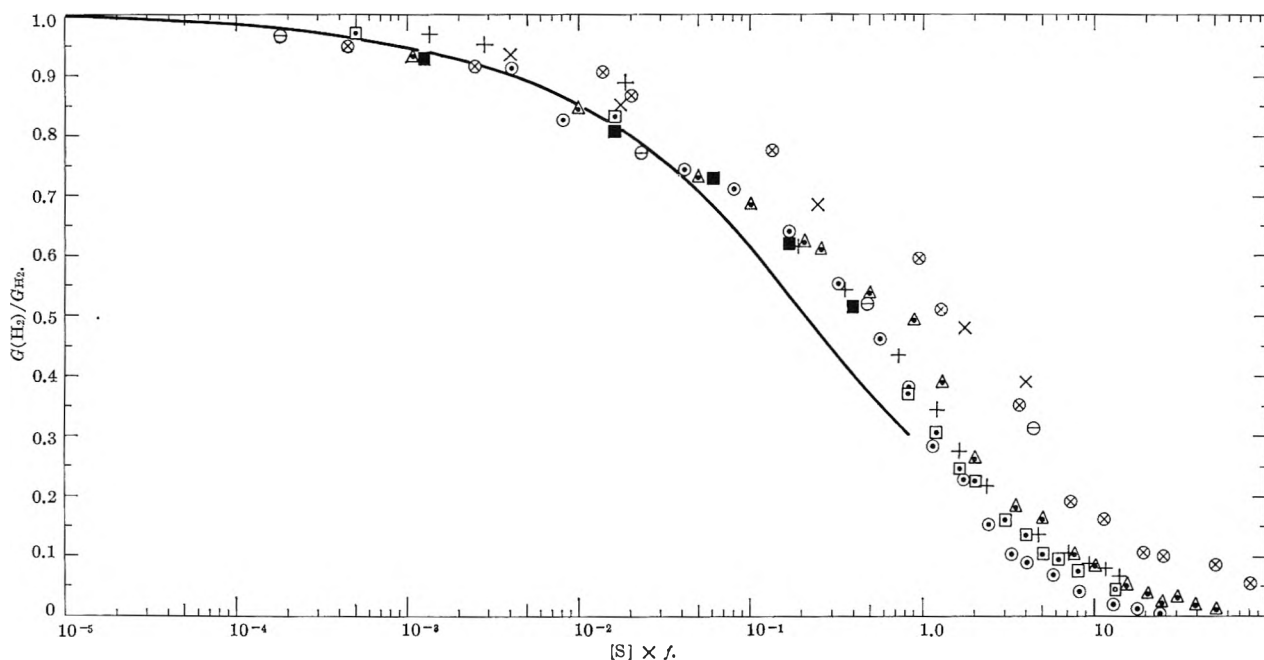


Figure 1. $G(\text{H}_2)/G_{\text{H}_2}$ as a function of the logarithm of the solute concentration multiplied by normalization factor f : KNO_2 (\square , \blacksquare) $f = 1$; NaNO_3 ($+$, ref. 5), $f = 2.4$; H_2O_2 (\otimes , ref. 7, \times , ref. 17), $f = 2.5$; acrylamide (\ominus , ref. 18), $f = 4.0$; $\text{Na}_2\text{Cr}_2\text{O}_7$ (\circ), $f = 8.2$; $\text{Cu}(\text{NO}_3)_2$ (Δ), $f = 10$.

yields were not too reproducible, and are probably a result of the "direct effect" of radiation on the solutes. The results obtained are shown in Figure 2.

In all cases these yields increase with increase in the solute concentration but with a positive $G(\text{O}_2)$ intercept. Thus the intercept for $\text{Cu}(\text{NO}_3)_2$ is approximately double that for NaNO_3 .¹⁹ No explanation is offered for these intercepts.

Molecular H_2 Yields in Alkaline Solutions. The variation of the yields of "molecular" hydrogen with $[\text{H}^+]$ having been shown,^{2,3} it seemed of interest to measure the yields of G_{H_2} in alkaline solutions. Potassium nitrite was chosen as solute since it is stable in alkaline solutions and reacts efficiently with OH radicals or O^- ions, thus protecting the hydrogen that is formed. The variation of $G(\text{H}_2)$ with $[\text{KNO}_2]^{1/3}$ is shown in Figure 3. On extrapolation to infinite dilution, one obtains G values of 0.44, 0.43, and 0.37 at pH 6, 13.7, and 14.0, respectively.

Discussion

From a plot of $G(\text{H}_2)$ vs. $[\text{S}]^{1/3}$, the slopes of the linear portions of the curves at the lower solute concentrations have been found to be greatest for those solutes which react more efficiently with H_2O^- , and the order is $\text{Cu}(\text{NO}_3)_2 \geq \text{Cr}_2\text{O}_7^{2-} > \text{NO}_2^-$ in accord with the rate constants $k(\text{H}_2\text{O}^- + \text{S})$. This is in agreement with the postulate^{1,8} that the precursors of the molecular hydrogen scavenged on this portion

of the curve are electrons, H_2O^- . At higher solute concentrations, however, the decrease of $G(\text{H}_2)$ with concentration is no longer proportional to the reactivity of the solutes toward H_2O^- . This effect can be seen in Figure 1, where the relative lowering of the molecular yield $G(\text{H}_2)/G_{\text{H}_2}$ is plotted against the logarithm of the solute concentration, after normalizing the results obtained from $\text{Cr}_2\text{O}_7^{2-}$, $\text{Cu}(\text{NO}_3)_2$, NO_3^- ,⁵ H_2O_2 ,^{7,17} and acrylamide¹⁸ systems with respect to the nitrite system on the basis of the reactivity of these solutes toward H_2O^- . Thus at high solute concentrations the decrease of $G(\text{H}_2)/G_{\text{H}_2}$ follows the order $\text{Cr}_2\text{O}_7^{2-} > \text{NO}_2^- > \text{Cu}(\text{NO}_3)_2 > \text{NO}_3^- > \text{H}_2\text{O}_2$ and acrylamide. This order is different from the one shown to exist at the lower solute concentrations: $\text{Cu}(\text{NO}_3)_2 \geq \text{Cr}_2\text{O}_7^{2-} > \text{acrylamide} > \text{H}_2\text{O}_2 > \text{NO}_3^- > \text{NO}_2^-$. With the exception of the NaNO_3 results, the order at high solute concentrations is in agreement with the reactivity of these solutes toward H atoms.^{12,13}

Diffusion kinetic computations^{16,20,21} can predict the variation of the yields of "molecular" hydrogen as a function of solute concentration, taking a certain value for the rate constant of the reaction of the solute

(19) H. A. Mahlman, *J. Phys. Chem.*, **67**, 1466 (1963).

(20) A. Kupperman and G. G. Belford, *J. Chem. Phys.*, **36**, 1427 (1962); A. Kupperman, "Action Chimique et Biologique des Radiations," Part 5, M. Haissinsky, Ed., Masson, Paris, 1961, p. 154.

(21) K. Shinohara, T. Shida, and N. Saito, *J. Chem. Phys.*, **35**, 1899 (1961).

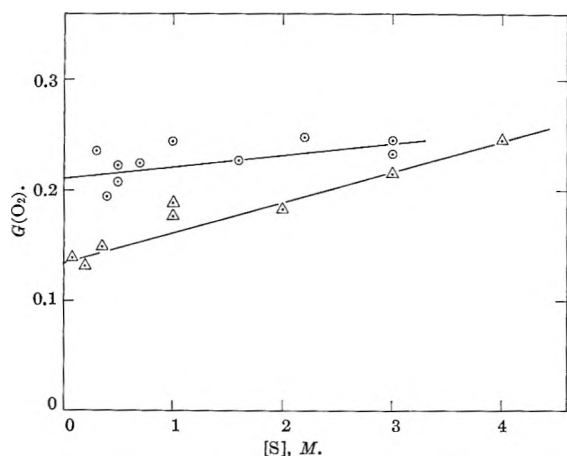


Figure 2. $G(\text{O}_2)$ yields as a junction of solute concentration: $\text{Na}_2\text{Cr}_2\text{O}_7$ (\circ); $\text{Cu}(\text{NO}_3)_2$ (Δ).

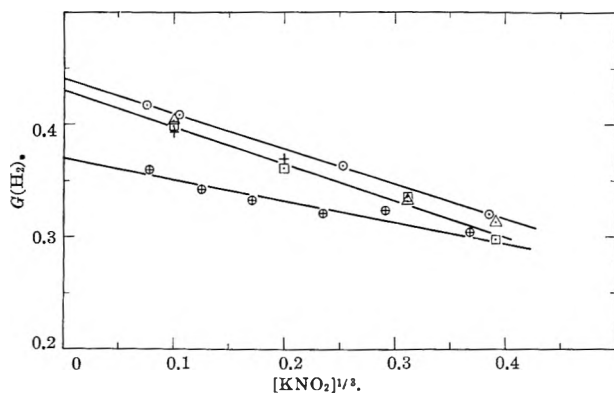


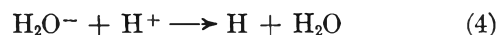
Figure 3. Yield of molecular H_2 in alkaline solutions: \circ , neutral pH; \square , pH 13; Δ , pH 13.5; $+$, pH 13.7; \otimes , pH 14.0.

with the precursor of H_2 . No agreement has, however, been observed^{7,16,20,21} between the theoretical curve and experimental data over the whole concentration range investigated. This was the case whether one dealt with cube-root or logarithmic plots, and whether one used theoretical curves derived on the basis of the one-radical¹⁶ or two-radical model.^{20,21} It was found necessary to change one or more of the parameters⁷ over some part of the curve to obtain agreement with the experimental results. This discrepancy between theory and experiment can now be explained as due to the fact that the solutes examined up to then happened to have been efficient reactants for H_2O^- but rather poor ones for H atoms. On accounting for the presence of two precursors each reacting with the solutes with significantly different rate constants, a better qualitative agreement can be obtained between theory and experiment, as can be seen in the case of potassium dichromate (Figure 1). Here the

yields are normalized relative to the nitrite system for $k(\text{H}_2\text{O}^- + \text{S}) = 4.5 \times 10^9 \text{ M}^{-1} \text{ sec}^{-1}$, and this happens to be very nearly the value for $k(\text{H} + \text{Cr}_2\text{O}_7^{2-}) = 5.6 \times 10^9 \text{ M}^{-1} \text{ sec}^{-1}$. Since the values of $k(\text{H} + \text{S})$ for all the other solutes used are lower than $4.5 \times 10^9 \text{ M}^{-1} \text{ sec}^{-1}$, one would expect to find a displacement to the right for the H_2 yields at high solute concentration. Such a displacement would be greater the lower the $k(\text{H} + \text{S})$. This is what is observed (Figure 1), and qualitatively the displacement can be seen to be proportional to the scavenging efficiencies of the solutes for H atoms.

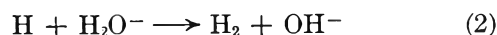
The disagreement with the NaNO_3 data is disturbing, particularly since no obvious explanation can be given at present. Nevertheless, it is our belief that the results obtained in the five other systems justifies the interpretation given to them.

Other mechanisms have recently been proposed to explain the formation of molecular H_2 . It was suggested²² that the H_3O radical is the main precursor of hydrogen. It is not apparent from this brief communication what is the evidence for introducing such a new species. Baxendale and Dixon²³ have proposed that most of the molecular H_2 is formed from H atom recombination as a result of reaction 4 occurring in the spurs



but that the decrease of G_{H_2} by solutes is due to their reaction with H_2O^- , the precursor of the H atom. If this mechanism prevailed, the decrease of G_{H_2} by solutes should be independent of $[\text{H}^+]$. In actual fact, it has been shown^{7,17,24} that the decrease of G_{H_2} is pH dependent. Schwarz²⁴ has suggested that some of the precursors of molecular H_2 are H atoms formed *via* reaction 4 in the spurs, since the local concentration of H^+ is at least equal to that of H_2O^- . For the reasons stated above, if reaction 4 occurs in the spurs, one would expect certain solutes present at high concentrations to be capable of competing with H^+ for H_2O^- . The results shown in Figure 1 indicate that such a competition does not take place.

It is concluded that H atoms as well as H_2O^- are the precursors leading to the formation of "molecular" hydrogen



(22) T. J. Sworski, *J. Am. Chem. Soc.*, **86**, 5034 (1964).

(23) J. H. Baxendale and R. S. Dixon, *Z. physik. Chem. (Frankfurt)*, **43**, 11 (1964).

(24) H. A. Schwarz, *Radiation Res. Suppl.*, **4**, 89 (1964).



The rate constants of reactions 1–3 are known: $2k_1 = 1 \times 10^{10} M^{-1} \text{ sec.}^{-1}$ (ref. 11); $k_2 = 2.5 \times 10^{10} M^{-1} \text{ sec.}^{-1}$ (ref. 25), and $2k_3 = 1.2 \times 10^{10} M^{-1} \text{ sec.}^{-1}$ (ref. 13). Since the yield of H atoms is about one-fifth that of electrons in the radiolysis of neutral solutions,²⁶ taking the above rate constants the contribution from reaction 3 compared to reaction 2 becomes rather small. Thus the main reactions forming “molecular” hydrogen are (1) and (2). The H atoms may originate from the dissociation of excited water molecules, as

has been proposed^{14,27} to explain the formation of H atoms in the bulk of the solutions.



The results obtained above would tend to favor such a mechanism, though one cannot dismiss entirely a small contribution from reaction 4.

(25) M. S. Matheson and J. Rabani, *J. Phys. Chem.*, **69**, 1324 (1965).

(26) E. Hayon, *ibid.*, **68**, 1242 (1964).

(27) J. T. Allan and G. Scholes, *Nature*, **187**, 218 (1960).

The Barrier to Internal Rotation in 2-Furaldehyde

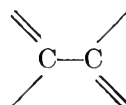
by Kjell-Ivar Dahlqvist and Sture Forsén

Research Group for NMR, Division of Physical Chemistry, The Royal Institute of Technology, Stockholm 70, Sweden (Received August 31, 1965)

The rotation barrier in 2-furaldehyde has been studied by nuclear magnetic resonance (n.m.r.) at temperatures down to -115° . The rate of interconversion of the two rotational isomers, which are present in unequal amounts, has been calculated from the line shapes of the n.m.r. signal from both the aldehyde group and the ring proton in the 3-position. A small systematic difference in interconversion rates deduced from the line shape of the signals from the aldehyde proton and the H-3 proton is noted. The results are analyzed in terms of the theory of absolute reaction rates.

1. Introduction

The factors determining the barriers restricting rotation around carbon-carbon single bonds between sp^2 -type hybridized carbon atoms



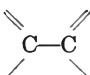
are not well known. It seems likely, however, that the study of barriers to internal rotation in systems of this type should give increased insight into the significance of π -electron delocalization in conjugated molecules. However, comparatively few rotational barriers in systems of this nature have been reported.

The technique of ultrasonic relaxation has been used by de Groot and Lamb to study the unsymmetrical rotational barriers in acrolein and a few related unsaturated aldehydes.^{1,2} Their results are summarized in Table I. Nuclear magnetic resonance spectroscopy has recently been applied by Anet and Ahmad to estimate the free energy of activation for the symmetrical rotational barriers in benzaldehyde and two *para*-substituted benzaldehyde derivatives³ (*cf.* Table I). The rotational barriers in butadiene and styrene have

(1) M. S. de Groot and J. Lamb, *Proc. Roy. Soc. (London)*, **A242**, 36 (1957).

(2) J. Lamb, *Z. Elektrochem.*, **64**, 135 (1960).

(3) F. A. L. Anet and M. Ahmad, *J. Am. Chem. Soc.*, **86**, 119 (1964).

Table I: Rotational Barriers Observed in Single Bonds of the Type 

Compound	T, °K.	ΔE_A , kcal./ mole	ΔH° , kcal./ mole	ΔH^* , kcal./ mole	ΔS° , cal. mole ⁻¹ deg. ⁻¹	ΔS^* , cal. mole ⁻¹ deg. ⁻¹	ΔF° , kcal./ mole	ΔF^* , kcal./ mole	Ref.
Butadiene		<i>cis</i> → <i>trans</i> 2.6							4
		<i>trans</i> → <i>cis</i> 4.9							
Styrene		2.2							5
Acrolein	248.6 to 298.4		2.06	<i>cis</i> → <i>trans</i> 4.96 <i>trans</i> → <i>cis</i> 7.02		<i>cis</i> → <i>trans</i> 0.44		<i>cis</i> → <i>trans</i> 4.85 ^a	1
Crotonaldehyde	273.2 to 323.3		1.93	<i>cis</i> → <i>trans</i> 5.51 <i>trans</i> → <i>cis</i> 7.44		<i>cis</i> → <i>trans</i> -2.75		<i>cis</i> → <i>trans</i> 6.10 ^a	1
Cinnamaldehyde	298.3 to 349.0		1.5	<i>cis</i> → <i>trans</i> 5.62 <i>trans</i> → <i>cis</i> 7.12		<i>cis</i> → <i>trans</i> 3.05		<i>cis</i> → <i>trans</i> 4.71 ^a	1
Methacrolein	248.4 to 298.1		3.07	<i>cis</i> → <i>trans</i> 5.31 <i>trans</i> → <i>cis</i> 8.38		<i>cis</i> → <i>trans</i> 0.475		<i>cis</i> → <i>trans</i> 5.19 ^a	1
Furacrolein	333.1 to 373.0		1.2	<i>cis</i> → <i>trans</i> 5.10 <i>trans</i> → <i>cis</i> 6.30		<i>cis</i> → <i>trans</i> -8.5		<i>cis</i> → <i>trans</i> 7.96 ^a	1
Benzaldehyde	150		0		0		0	7.9	3
<i>p</i> -Methoxybenz- aldehyde	174		0		0		0	9.2	3
<i>p</i> -Dimethylamino- benzaldehyde	202		0		0		0	10.8	3

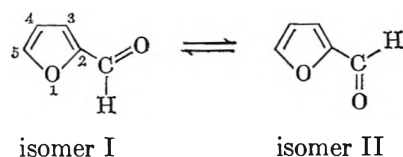
^a Calculated from the values of ΔH^* and ΔS^* at the lowest temperature in the interval given in the second column.

been calculated from infrared spectroscopic and thermodynamic data.^{4,5}

In the study of rotational barriers the techniques of ultrasonic relaxation and nuclear magnetic resonance (n.m.r.) are largely complementary. With the ultrasonic relaxation method, rotational barriers in a two-isomer system are most accurately measurable when the isomers are present in *unequal* amounts ($\Delta F^\circ/RT \sim 1-5$).² When the barrier is symmetrical and the isomers are present in equal amounts the ultrasonic relaxation method cannot be used. In such a case the n.m.r. method may be employed. On the other hand, it is difficult to extend the n.m.r. method to two-isomer systems where the ratios of the two isomers are much smaller than *ca.* $1/20$ ($\Delta F^\circ/RT \sim 3$). Detailed kinetic analysis of intramolecular interconversion processes

has, in fact, with few exceptions⁶ been devoted only to systems with the isomers present in equal amounts.

In the present work we have studied the barrier to internal rotation in 2-furaldehyde. This compound may exist in two planar or nearly planar rotational isomers



(4) J. G. Aston, G. Szasz, H. W. Woolley, and F. G. Brickwedde, *J. Chem. Phys.*, **14**, 67 (1946).

(5) K. Pitzer, L. Guttman, and E. F. Westrum, *J. Am. Chem. Soc.*, **68**, 2209 (1946).

The rotational barrier in this compound is not high enough to prevent a rapid interconversion of the two isomers at room temperature. At temperatures below *ca.* -80° , however, the interconversion is sufficiently slow to make separate n.m.r. signals from the two isomers observable. In an intermediate temperature region, the rate of interconversion has been calculated from the observed line shapes of the signals from the aldehyde proton and from the ring proton in 3-position (H-3).

Isomers I and II are present in unequal amounts, and their ratio varies with temperature; this has required a detailed analysis of the interconversion process. Despite the comparatively complex line shapes observed, it has been found possible to fit theoretical and experimental line shapes very closely.

A preliminary value for the effective free energy of activation for the hindered rotation in 2-furaldehyde (calculated from the coalescence temperature of the aldehyde signal) has previously been given by the present authors in connection with a study of the stereospecificity of the long-range aldehyde spin-coupling to the ring protons.⁷

2. Experimental Methods

The sample of 2-furaldehyde was of commercial quality (Fluka A.G.) and distilled under vacuum before use. The n.m.r. measurements were performed on a 10% solution of 2-furaldehyde in dimethyl ether with *ca.* 1% of tetramethylsilane added as internal reference. The solvent dimethyl ether was also of commercial quality (The Matheson Co., Inc.) and used without further purification.

The n.m.r. spectra were obtained at 60 Mc./sec. with a Varian A-60 spectrometer equipped with a Varian V-6031 variable-temperature probe and temperature controller. Above -70° the spectra were run on a scale of expansion of the precalibrated recorder chart of 0.5 c.p.s./cm. and below -70° on a scale of expansion of 1 c.p.s./cm. The nonstandard scale expansion of 0.5 c.p.s./cm. was accomplished by introducing an additional resistor in series with the resistor network in the sweep circuits of the spectrometer.

The n.m.r. spectra were recorded at lowest possible sweep rate (0.05 or 0.10 c.p.s./sec.) at a low amplitude of the radiofrequency field (*ca.* 0.04 mgauss) so as to minimize saturation broadening of the signals. At each temperature of measurement five to ten spectra were recorded.

The chemical shift measurements were made by linear interpolation between reference side bands from the tetramethylsilane signal. The frequencies

of the side bands were measured with a Hewlett-Packard Model 5512 A electronic counter.

In the Varian V-6031 temperature controller used to maintain a preset temperature of the gas cooling the sample the gas temperature is sensed at the inlet of the gas flow to the measuring volume. Since this temperature may differ from that inside the sample tube, the system was calibrated by the use of a copper-constantan thermocouple placed inside a dummy tube. The temperature readings inside the dummy tube were found to be affected by the flow rate of the cooling gas and by the rate of sample spinning. In the present investigation the sample temperature is estimated to be accurate to $\pm 1^{\circ}$.

A large number of theoretical n.m.r. spectra based on the equations derived in section 4 were calculated using the Swedish high-speed electronic computer BESK.

3. Measurements of Isomer Ratio and Rate of Interconversion

3.1. The N.m.r. Spectrum of 2-Furaldehyde. At room temperature (the data in the following refer to 303.7°K.) the spectrum of 2-furaldehyde consists of four groups of signals.⁸ The signal from the aldehyde group appears as a quartet at $\delta = 9.61$ p.p.m. The splitting of this signal is due to long-range coupling to the protons in the 4- and 5-positions ($J_{\text{CHO}-4} = 0.30$ c.p.s. and $J_{\text{CHO}-5} = 0.77$ c.p.s.). The signal from H-5 is found at $\delta = 7.73$ p.p.m. and is split owing to spin-coupling with the aldehyde proton and with the ring protons H-3 and H-4. The signal due to H-3 appears at $\delta = 7.23$ p.p.m. and is split into a quartet due to spin-coupling with H-4 and H-5. Finally, the signal from H-4 is found at $\delta = 6.58$ p.p.m. and shows fine structure due to spin-coupling with the aldehyde proton and with the ring protons H-3 and H-5. The experimental shifts and spin-coupling constants are summarized in the upper part of Table II.

At about -50° the n.m.r. signals due to the aldehyde proton and due to the ring proton in the 3-position become broadened. At still lower temperatures new signals appear; at -115.5° the signal from the aldehyde group consists of two doublets with the intensity ratio *ca.* 1:10, and the signal due to H-3 also consists

(6) F. A. Rovey, F. P. Hood, III, E. W. Anderson, and R. I. Kornegay, *J. Chem. Phys.*, **41**, 2041 (1964).

(7) K.-I. Dahlqvist and S. Forsén, *J. Phys. Chem.*, **69**, 1760 (1965).

(8) The room temperature spectrum of 2-furaldehyde has been reported earlier by several authors; see, for example, N. S. Bhacca, L. F. Johnson, and J. N. Shoolery, "NMR Spectra Catalog," Varian Associates, Palo Alto, Calif., 1961. In this work, however, the assignment of the signals due to the ring protons in the 3- and 4-position should be interchanged (*cf.* R. A. Hoffman, B. Gestblom, S. Gronowitz, and S. Forsén, *J. Mol. Spectry.*, **11**, 454 (1963)).

Table II: Chemical Shifts and Spin-Coupling Constants in 2-Furaldehyde. The Shifts Are Given Relative to Tetramethylsilane as Internal Reference. The Subscripts I and II Refer to the Corresponding Rotational Isomers (See Text)

Proton	Shift, p.p.m.	Spin-coupling constants, c.p.s.
303.7°K.		
CHO	9.61	$J_{35} = 0.80$; $J_{34} = 3.70$
H-3	7.23	$J_{45} = 1.75$; $J'_{\text{CHO-4}} = 0.30^a$
H-4	6.58	$J'_{\text{CHO-5}} = 0.77^a$
H-5	7.73	
157.7°K.		
(CHO) _I	9.56	$J_{35} = 0.80$; $J_{34} = 3.70$
(CHO) _{II}	9.74	$J_{45} = 1.75$
(H-3) _I	7.57	$J^{\text{I}}_{\text{CHO-5}} = 1.10$; $J^{\text{I}}_{\text{CHO-4}} < 0.2$
(H-3) _{II}	7.42	$J^{\text{II}}_{\text{CHO-5}} < 0.2$; $J^{\text{II}}_{\text{CHO-4}} = 0.85$
H-4	6.79	
H-5	8.04	

^a Weighted mean values (see text).

of two quartets with an integrated intensity ratio of *ca.* 1:10. The smaller of the aldehyde doublets is found at $\delta = 9.74$ p.p.m. and is split owing to spin-coupling with the ring proton H-4; the larger doublet is found at $\delta = 9.56$ p.p.m. and is split owing to spin-coupling with the ring proton H-5. The smaller of the two H-3 quartets occurs at $\delta = 7.42$ p.p.m. and the larger at $\delta = 7.57$ p.p.m. Shift data and spin-coupling constants obtained at -115.5° are given in the lower part of Table II.

The larger of the two signals from both the aldehyde group and from the ring proton H-3 are assigned to the rotational isomer I and the smaller signals to the isomer II. The assignment is based upon the diamagnetic anisotropy effect of the carbonyl group which is known to cause deshielding of protons near the carbonyl group in the trigonal $>\text{C}=\text{O}$ plane.⁹⁻¹² [The preceding assignment is strongly supported by a recent n.m.r. study of 3-hydroxy-2-thiophenealdehyde (private communication from Dr. R. A. Hoffman and Prof. S. Gronowitz). In this compound the aldehyde group may be assumed to be locked in a conformation corresponding to isomer I in 2-furaldehyde by an intramolecular hydrogen bond to the OH group in the 3-position. The aldehyde proton in 3-hydroxy-2-thiophenealdehyde is found to be spin-coupled only to the ring proton in the 5-position. Thus in 2-thiophenealdehydes as well as in 2-furaldehyde the rule of predominant spin-coupling *via* the straightest zig-zag path seems to be violated (*cf.* ref. 13).]

3.2. *The Ratio of the Rotational Isomers.* At low

temperatures, where separate n.m.r. signals from isomers I and II are observed, the isomer ratio was determined from the integrals of the signals of the corresponding isomer. At higher temperatures, where the signals from the two isomers have coalesced, their ratio was estimated from the "effective" spin-coupling constant between the aldehyde proton and the ring protons in the 4- and 5-positions. When the lifetimes of each rotational isomer are short, the observed aldehyde spin-coupling constants are weighted mean values of the coupling constants in the two isomers. The averaged or "effective" spin-coupling constants $J'_{\text{CHO-4}}$ and $J'_{\text{CHO-5}}$ should thus be given by

$$J'_{\text{CHO-4}} = P_I J^{\text{I}}_{\text{CHO-4}} + (1 - P_I) J^{\text{II}}_{\text{CHO-4}} \quad (1)$$

and

$$J'_{\text{CHO-5}} = P_I J^{\text{I}}_{\text{CHO-5}} + (1 - P_I) J^{\text{II}}_{\text{CHO-5}} \quad (2)$$

where P_I and $1 - P_I$ are the fractional populations of the isomers I and II, respectively. $J^{\text{I}}_{\text{CHO-4}}$, $J^{\text{II}}_{\text{CHO-4}}$, $J^{\text{I}}_{\text{CHO-5}}$, and $J^{\text{II}}_{\text{CHO-5}}$ are the spin-coupling constants between the aldehyde group and the ring protons H-4 and H-5 in isomers I and II. Now the n.m.r. spectrum of 2-furaldehyde indicates the spin-couplings of the aldehyde proton to be virtually stereospecific; *i.e.*, in isomer I the aldehyde proton is observed to be spin-coupled only to H-5 and in isomer II only to H-4.⁷ It can be estimated that the spin-couplings $J^{\text{I}}_{\text{CHO-4}}$ and $J^{\text{II}}_{\text{CHO-5}}$ are less than 0.2 c.p.s. With the assumption that the latter two spin-coupling constants are zero, eq. 1 and 2 reduce to

$$J'_{\text{CHO-4}} = (1 - P_I) J^{\text{II}}_{\text{CHO-4}} \quad (3)$$

and

$$J'_{\text{CHO-5}} = P_I J^{\text{I}}_{\text{CHO-5}} \quad (4)$$

The values of $J^{\text{II}}_{\text{CHO-4}}$ and $J^{\text{I}}_{\text{CHO-5}}$ were obtained from the spectrum of 2-furaldehyde at -115.5° (*cf.* Table II). The "effective" aldehyde coupling constants $J'_{\text{CHO-4}}$ and $J'_{\text{CHO-5}}$ were accurately determined in the temperature interval -40 to $+50^\circ$, and the fractional population of isomers I and II was calculated from eq. 3 and 4.

(9) L. M. Jackman, "Applications of Nuclear Magnetic Resonance Spectroscopy in Organic Chemistry," Pergamon Press Inc., Oxford, 1959, Chapter 7.

(10) O. L. Chapman, H. G. Smith, and R. W. King, *J. Am. Chem. Soc.*, **85**, 806 (1963).

(11) A. D. Cross and I. T. Harrison, *ibid.*, **85**, 3223 (1963).

(12) D. H. Williams, N. S. Bhacca, and C. Djerassi, *ibid.*, **85**, 2810 (1963).

(13) R. A. Hoffman, B. Gestblom, S. Gronowitz, and S. Forsén, *J. Mol. Spectry.*, **11**, 454 (1963).

Table III: Summary of Thermodynamic Data and Activation Parameters for the Interconversion of the Rotational Isomers in 2-Furaldehyde. Activation Data Obtained from Studies of the N.m.r. Signal of the CHO Proton and of the H-3 Proton Are Given Separately. The Errors Are Average Deviations (Assuming Only Random Errors). The Subscripts I and II Refer to the Corresponding Isomers (See Text)

ΔE_{AI} , kcal./mole	ΔE_{AII} , kcal./mole	ΔH° , kcal./mole	ΔH_I^* , kcal./mole	ΔH_{II}^* , kcal./mole	ΔS° , cal./mole deg.	ΔS_I^* , cal./mole deg.	ΔS_{II}^* , cal./mole deg.	ΔF° , kcal./mole	ΔF_I^* , kcal./mole	ΔF_{II}^* , kcal./mole
216°K.										
12.17 ±0.17	11.12 ±0.17	1.05 ±0.05	11.74 ±0.17	10.69 ±0.17	2.17 ±0.18	3.77 ±0.09	1.60 ±0.20	0.58 ±0.04	10.93 ±0.20	10.35 ±0.20
CHO proton, 191.7°K.										
12.17 ±0.17	11.12 ±0.17	1.05 ±0.05	11.79 ±0.17	10.74 ±0.17	2.17 ±0.18	4.00 ±0.10	1.83 ±0.18	0.63 ±0.04	11.02 ±0.21	10.39 ±0.21
216°K.										
11.68 ±0.21	10.63 ±0.21	1.05 ±0.05	11.25 ±0.21	10.20 ±0.21	2.17 ±0.18	1.21 ±0.06	0.04 ±0.19	0.58 ±0.04	10.77 ±0.23	10.19 ±0.24
H-3 proton, 191.7°K.										
11.68 ±0.21	10.63 ±0.21	1.05 ±0.05	11.30 ±0.21	10.25 ±0.21	2.17 ±0.18	2.44 ±0.07	0.27 ±0.17	0.63 ±0.04	10.83 ±0.24	10.20 ±0.24

The equilibrium constant K for the equilibrium isomer I \rightleftharpoons isomer II was calculated from $K = (1 - P_I)/P_I$. ΔH° for the isomer equilibrium was obtained from a plot of $\ln K$ against $1/T$. The experimental values of ΔH° , $\Delta F^\circ = -RT \ln K$, and ΔS° are listed in Table III.

3.3. The Rate Measurements. As mentioned in the preceding section, the two rotational isomers of 2-furaldehyde are present in unequal amounts and their ratio changes with temperature. This circumstance, in connection with the relatively complex spin-coupling pattern in the signals from the aldehyde group and the H-3 proton, necessitates a detailed consideration of the exchange process in order to derive the equations relating the signal line shapes to the rate of interconversion of the isomers.

Since the n.m.r. spectrum of 2-furaldehyde at all temperatures is of the first-order type to a good approximation, we may think of the 2-furaldehyde solution as containing a mixture of molecules with the ring protons and the aldehyde proton in different spin states (α or β). In the rate measurements we observe the energy of transitions between the two spin states for either the aldehyde proton or the H-3 proton, and in the following we thus need only consider the spin states of H-4 and H-5 since there is no observable spin-coupling between H-3 and the aldehyde proton. Now it can be assumed that a transition of the aldehyde group from one equilibrium position to the other takes place in a time so short that the spin states of all protons are preserved. (A similar assumption is always made in calculations of the effect of intercon-

version processes on n.m.r. signal shapes.¹⁴) The interconversion process can accordingly be illustrated in the way depicted in Figure 1. Interconversion is thus possible only within the pairs (a) \rightleftharpoons (e), (b) \rightleftharpoons (f), (c) \rightleftharpoons (g), and (d) \rightleftharpoons (h).

In the absence of interconversion, the n.m.r. signals of the CHO proton or the H-3 proton would consist of lines associated with the molecular species in Figure 1; the lines could be grouped into two chemically shifted multiplets, one due to isomer I and one due to isomer II. A schematic spectrum is depicted in Figure 2.

In Figure 2 ω_I and ω_{II} are the chemical shift (in angular frequency units) of the CHO proton or the H-3 proton in isomer I and II, respectively, relative to some chosen reference frequency ω_0 . (The assignment of the individual lines in Figure 2 to the molecular species in Figure 1 has been made with the assumption that the static magnetic field increases from left to right and that all spin-coupling constants are positive; cf. ref. 13.)

When the schematic spectrum in Figure 2 represents transitions of the H-3 proton, we have $J_1 = J_{3,5}^I$, $J_2 = J_{3,4}^I$, $J_3 = J_{3,5}^{II}$, and $J_4 = J_{3,4}^{II}$. Within experimental error $J_{3,5}^I = J_{3,5}^{II}$ and $J_{3,4}^I = J_{3,4}^{II}$.

When the schematic spectrum in Figure 2 represents the transitions of the CHO proton, we have $J_1 = J_{CHO-4}^I$, $J_2 = J_{CHO-5}^I$, $J_3 = J_{CHO-4}^{II}$, and $J_4 = J_{CHO-5}^{II}$. As has been shown earlier, no evidence is found for spin-couplings between the CHO proton and

(14) H. M. McConnell, *J. Chem. Phys.*, 28, 430 (1958).

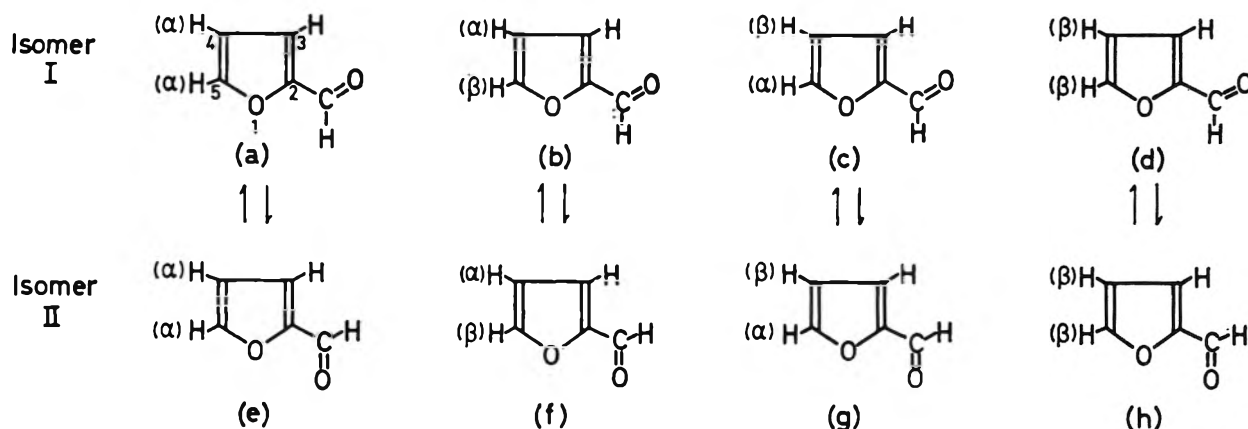


Figure 1. Schematic illustration of the interconversion of the rotational isomers in 2-furanaldehyde.

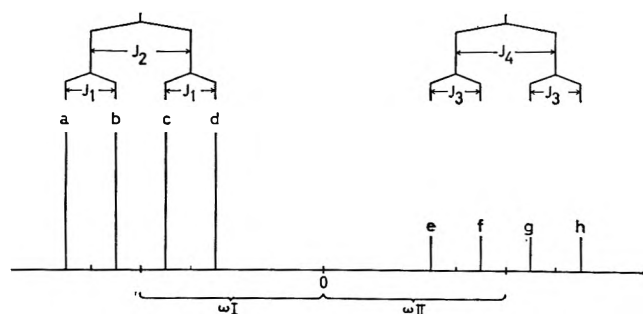


Figure 2. Schematic n.m.r. spectrum of the H-3 proton (or of the CHO proton) in 2-furanaldehyde in the limit of very slow interconversion of the rotational isomers.

the H-4 proton in isomer I or the H-5 proton in isomer II, and we have in the present work put $J^{\text{I}}_{\text{CHO-4}} = 0$ and $J^{\text{II}}_{\text{CHO-5}} = 0$. In the aldehyde spectrum at low exchange rates the signals due to isomer II are found at the low-field side of the signals from isomer I whereas the opposite is the case in the spectrum of the H-3 proton.

A quantitative description of the changes in the low-temperature n.m.r. spectrum of the H-3 or the CHO proton which appear at higher temperatures when the rate of interconversion of the isomers is increased may be derived using the modified Bloch equations including exchange phenomena first introduced by Gutowsky, McCall, and Slichter.¹⁵ In the following we will use the reformulations and notations due to McConnell.¹⁴ For the exchange between two rotational isomers in which the spin state of the H-4 and the H-5 proton remains the same, for example, the exchange (a) \rightleftharpoons (e) in Figure 1, we have for the complex magnetic moment $G (= u + iv)$

$$\frac{dG_a}{dt} + \alpha_a G_a = -i\gamma H_1 \frac{P_I}{4} M_0 + \frac{G_e}{\tau_{II}} - \frac{G_a}{\tau_I} \quad (5)$$

and

$$\frac{dG_e}{dt} + \alpha_e G_e = -i\gamma H_1 \frac{(1 - P_I)}{4} M_0 + \frac{G_a}{\tau_I} - \frac{G_e}{\tau_{II}} \quad (6)$$

where γ is the gyromagnetic ratio of the proton, H_1 is the amplitude of radiofrequency field, P_I is the population of isomer I, M_0 is the equilibrium value of the magnetization in the z direction, and τ_I and τ_{II} are the mean lifetimes of isomers I and II, respectively. α_a and α_e are complex quantities depending on the frequencies of the CHO or H-3 signals assigned to the molecular species (a) and (e) in the absence of exchange and on the frequency ω of the observing radiofrequency field

$$\alpha_a = 1/(T_2)_{\text{I}} - i[\omega_0 - (\omega_I + 0.5(J_1 + J_2)) - \omega] \quad (7)$$

$$\alpha_e = 1/(T_2)_{\text{II}} - i[\omega_0 + (\omega_{II} - 0.5(J_3 + J_4)) - \omega] \quad (8)$$

In the above equations $(T_2)_{\text{I}}$ and $(T_2)_{\text{II}}$ are the transverse relaxation times of the CHO or H-3 proton in isomers I and II in the absence of exchange. (In the following it will be assumed that $(T_2)_{\text{I}} \approx (T_2)_{\text{II}} = T_2$.)

Under conditions of slow passage, *i.e.*, $dG_a/dt = dG_e/dt = 0$, eq. 5 and 6 may be solved for the complex magnetic moments G_a and G_e .

With the short-hand notations

$$C_I = \gamma H_1 P_I M_0 / 4 \quad (9)$$

$$C_{II} = \gamma H_1 (1 - P_I) M_0 / 4 \quad (10)$$

and noting that $P_I/(1 - P_I) = \tau_{II}/\tau_I$ or $\tau_{II} = [(1 - P)/P]\tau$, where the subscripts of τ_I and P_I have been dropped, the expressions for G_a and G_e read

(15) H. S. Gutowsky, D. W. McCall, and C. P. Slichter, *J. Chem. Phys.*, 21, 279 (1953).

$$G_a = -\frac{i[C_{II}\tau - C_{I\tau}(1-P)\tau E/P]}{1 - AE\tau^2(1-P)/P} \quad (11)$$

$$G_b = -\frac{i[C_{I\tau}(1-P)/P + C_{II}\tau^2(1-P)A/P]}{1 - AE\tau^2(1-P)/P} \quad (12)$$

where $A = \alpha_a + 1/\tau$ and $E = \alpha_e + P/\tau(1-P)$.

In complete analogy with the presentation above, one may derive the complex magnetic moments G_b and G_t , G_c and G_e , G_d and G_h . The sum of all these moments gives the complex expression for the line shapes

$$G = \sum_{\nu=A}^h G_\nu \quad (13)$$

When the n.m.r. spectrum is observed in the absorption mode, the signal intensity at the radiofrequency ω is proportional to the imaginary part of G . The summation and the separation of the total complex moment G into imaginary and real parts have been accomplished by the use of a computer program which calculates the signal intensity for a range of values of ω with a given set of parameters T_2 , τ , P , J_1 , J_2 , J_3 , J_4 , ω_I , and ω_{II} .

The theoretical line shapes calculated with a relevant set of parameters accurately reproduce the observed spectra of both the CHO proton and the H-3 proton. The value of the lifetime τ at different temperatures was obtained from a comparison of experimental and theoretical spectra. In the temperature region where the experimental line shape undergoes pronounced changes (corresponding to lifetimes in the interval 0.01 to 1 sec.) the value of τ could generally be determined to within $\pm 10\%$. Examples of theoretical and experimental spectra of the CHO and H-3 protons are shown in Figures 3 and 4. Plots of $\ln(1/\tau)$ against $1/T$ are shown in Figure 5. The data obtained from the study of the CHO and the H-3 protons are considered separately. It may be seen from Figure 5 that the interconversion rate constants inferred from the measurements on the CHO proton are systematically lower (by ca. 30%) than the rates obtained from the study of the H-3 proton but that the temperature dependence of the rates are in close agreement. The reason for this disagreement is most likely not to be sought in the inadequacy of the McConnell equations to describe the present interconversion process but may have several other causes. The chemical shift of the CHO or the H-3 proton in the two isomers ($\omega_I + \omega_{II}$) may be somewhat temperature dependent and not equal to the values measurable in the limit of very slow exchange. This would lead to systematic errors in the rate measurements

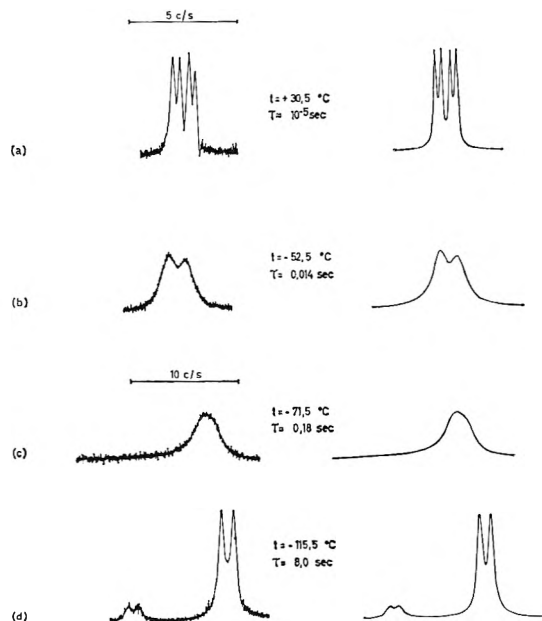


Figure 3. Examples of experimental and theoretical n.m.r. spectra of the CHO proton in 2-furanaldehyde. Note the change in linear scale between spectra a, b and c, d.

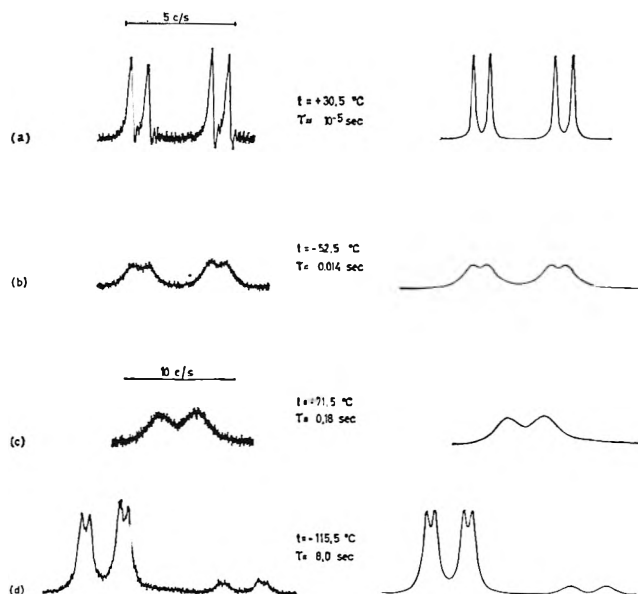


Figure 4. Examples of experimental and theoretical n.m.r. spectra of the H-3 proton in 2-furanaldehyde. Note the change in linear scale between spectra a, b and c, d.

in particular in the intermediate range where the lines begin to coalesce. Another uncertainty lies in the determination of the transverse relaxation time, T_2 , for the CHO or the H-3 proton in the absence of interconversion. The usual procedure in the analysis of rates from line shapes of single resonance spectra is to use the "effective" transverse relaxation time T_2^* for

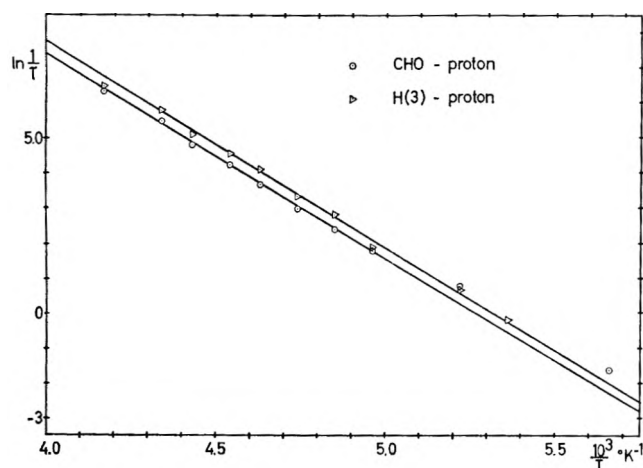


Figure 5. A plot of $\ln 1/\tau$ vs. $10^3/T$ for 2-furaldehyde.

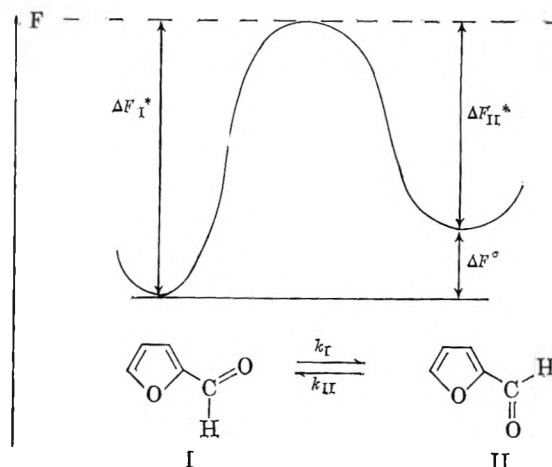
a nonexchanging nucleus. This procedure (which in the present case is the only workable one) has also been employed in this work, and at a given temperature the transverse relaxation time of the CHO and the H-3 proton was taken to be equal to the effective relaxation time calculated from the line width of the multiplet lines due to the H-4 proton. When lines are broadened due to magnetic inhomogeneities, the apparent line width, $1/T_2^*$, for a nonexchange-broadened line is given by

$$1/T_2^* = (1/T_2^0) + (1/T_2')_{\text{inhomog}} \quad (14)$$

where T_2^0 is the "true" transverse relaxation time of the nucleus, and the last term in eq. 14 is the line broadening caused by the field inhomogeneities.

Now it is known that different nuclei in the same molecule may have different values of T_2^0 . (It is even possible that the values of T_2^0 for one and the same proton in two different rotamers are different.) Furthermore, it is known, for example, from spin-echo measurements (cf. ref. 16), that transverse relaxation times vary with temperature. If T_2^0 contributes significantly to T_2^* and if T_2^0 is not the same for H-3, H-4, and the CHO proton, this would lead to systematic errors in the rate measurements—in particular, in the limits of fast and slow exchange. At present, there seems to be no objective way of deciding which of the two measured rates is the most reliable, and we will, in the following, separately give the results evaluated from both series of measurements.

The dependence of the rate of interconversion on the temperature has been interpreted in terms of the theory of absolute reactions rates.¹⁵ The free energy changes for the isomer interconversion may be illustrated by the schematic diagram



where ΔF_I^* and ΔF_{II}^* are the free energies of activation for isomers I and II, respectively.

From the theory of absolute reaction rates,¹⁷ it follows that

$$\frac{1}{\tau_I} = k_I = \frac{\kappa k T}{h} e^{-\Delta F_I^*/RT} = \frac{\kappa k T}{h} e^{\Delta S_I^*/R} e^{-\Delta H_I^*/RT} \quad (15)$$

and an analogous expression is valid for k_{II} . Furthermore, we have

$$\Delta F_I^* = \Delta F_{II}^* + \Delta F^0 \quad (16)$$

$$\Delta H_I^* = \Delta H_{II}^* + \Delta H^0 \quad (17)$$

and

$$\Delta S_I^* = \Delta S_{II}^* + \Delta S^0 \quad (18)$$

By use of eq. 15–18 and the values of ΔF^0 , ΔH^0 , and ΔS^0 obtained from the study of the temperature dependence of the isomer ratio, it is possible to calculate ΔF^* , ΔH^* , and ΔS^* for the interconversion of the two rotational isomers. The values obtained (with $\kappa = 1$) are summarized in Table III. The errors indicated in this table are average deviations (assuming only random errors).

4. Discussion

The present investigation illustrates that the ultimate accuracy to which rates of interconversion may be obtained from the line shapes in high-resolution n.m.r. spectra may be largely limited by errors of a systematic nature. A particularly deplorable example in this connection is the activation energy for restricted rotation in dimethylformamide. (Cf. ref. 16.) Today five independent determinations have been performed

(16) A. Allerhand and H. S. Gutowsky, *J. Chem. Phys.*, **41**, 2115 (1964).

(17) S. Glasstone, K. J. Laidler, and H. Eyring, "The Theory of Rate Processes," McGraw-Hill Book Co., Inc., New York, N. Y., 1941.

with results ranging from 7 to 24 kcal./mole—the probable error in each measured value being given as *ca.* ± 1 kcal./mole. This example is not very apt to arouse confidence in the n.m.r. line shape method for rate measurements. Part of the large spread in the values of the rotational barrier in dimethylformamide can probably be attributed to the use of less reliable methods for extracting the exchange rates from the observed line shapes. In the case of a collapsing doublet, exchange rates have been obtained from measurements of the distance between the two maxima or from the quotient between the signal intensities of the two maxima and the central minimum. In both of these methods, however, only a part of the available experimental information is utilized. It appears that the most reliable method for evaluating rate constants is to fit the entire experimental curve with theoretical curves calculated with different values of the characteristic lifetime. When the line shape is comparatively simple—as in the case of a collapsing doublet—the curve fitting may favorably be performed by means of an iterative computer program.

The identification of the sources of systematic errors in the n.m.r. line shape method would be greatly facilitated if the results could be checked with some independent experimental method. Recently, great interest has arisen in the use of spin-echo techniques for the study of chemical-exchange processes.¹⁶ The spin-echo method makes it possible to extend rate measurements to severalfold faster rates than are accessible with the n.m.r. line-shape method, and the spin-echo technique is not likely to be sensitive to the same type of systematic errors as is the line-shape method. However, as yet, few experimental spin-echo data are available.

A rigorous comparison of the results of the present investigation on the rotational barrier in 2-furaldehyde and the barriers listed in Table I is somewhat difficult since identical thermodynamic functions have not always been evaluated. The rotational barriers (whether taken as ΔE , ΔG^* , or ΔH^*) in the $\text{C}-\text{C}$ bonds so far studied have indicated the barriers to be higher in unsaturated and aromatic aldehydes than in the unsaturated hydrocarbons butadiene and styrene. One may inquire whether this difference is due to the different importance of conjugation across the single bond in the two types of molecules. Although the Hückel MO method admittedly is very crude and cannot be expected to reveal finer details of the conjugative interaction, a Hückel-type calculation may, however, serve as a starting point for a discussion.

We have calculated the loss in total π -electron energy which occurs when a molecule is rotated around a single bond of the type $\text{C}_{(A)}-\text{C}_{(B)}$ from a planar state to a state where the two parts of the molecule are perpendicular to each other. In the latter configuration the overlap integral between the $2p\pi$ orbitals on the sp^2 -type hybridized carbon atoms $\text{C}_{(A)}$ and $\text{C}_{(B)}$ is zero, and the resonance integral for the $\text{C}_{(A)}-\text{C}_{(B)}$ bond may also be taken as zero. The calculated loss in total π -electron energy (ΔE^π) in units of β for some compounds of interest is listed in Table IV.

Table IV: Hückel-Type Molecular Orbital Calculations of the Loss of Total π -Electron Energy (ΔE^π) upon Rotation of the Molecules around the $\text{C}-\text{C}$ Bond from a Planar State to a State Where the Two Parts of the Molecule Are Perpendicular. The Following Parameters for Heteroatoms Have Been Used: $\alpha_{=O} = \alpha + \beta$; $\alpha_{\ddot{O}} = \alpha + 2\beta$; $\alpha_{\ddot{N}} = \alpha + 1.5\beta$; $\beta_{\text{C=O}} = \beta$; $\beta_{\text{C}-\ddot{O}} = 0.8\beta$; and $\beta_{\text{C}-\ddot{N}} = 0.8\beta$

Molecule	$\Delta E^\pi(1/\beta)$
Butadiene	0.472
Styrene	0.424
Acrolein	0.523
Benzaldehyde	0.465
<i>p</i> -Methoxybenzaldehyde	0.485
<i>p</i> -Dimethylaminobenzaldehyde	0.492
2-Furaldehyde	0.562
3-Furaldehyde	0.505
2-Pyrrolealdehyde	0.561
3-Pyrrolealdehyde	0.514

It may be noted from the results in Table IV that the Hückel calculations indicate the comparatively large activation energy for the rotation of the aldehyde group in 2-furaldehyde to be related to an accompanying relatively large change in ΔE^π . Also, the loss in π -electron energy upon rotation of the aldehyde group an angle $\pi/2$ is calculated to increase in the series benzaldehyde < *p*-methoxybenzaldehyde < *p*-dimethylaminobenzaldehyde which is also the order of increasing ΔF^* found by Anet and Ahmad. However, the difference in experimental activation energies between butadiene and styrene, on the one hand, and 2-furaldehyde and the aromatic aldehydes, on the other hand, is much larger than expected on the basis of changes in π -electron energies alone. More accurate quantum chemical calculations are not likely to lead to very different relative values of ΔE^π and the

importance of other factors besides conjugation (such as intramolecular van der Waals interactions) for determining rotational barriers in $\begin{array}{c} \diagup \\ \text{C}-\text{C} \\ \diagdown \end{array}$ bonds is borne out. The Hückel calculations lead to very similar values of ΔE^\ddagger in 2-furalaldehyde and 2-pyrrolealdehyde. Preliminary rate measurements on the interconversion of the rotational isomers in the latter compound have indicated the rotational barrier to be comparable to that in 2-furalaldehyde.

Acknowledgments. The authors wish to thank Dr. E. Forslind for his kind interest in this work and Mr. Torbjörn Alm for his skillful programming of the line-shape equations. Thanks are also due to the Computing Division of the Swedish National Office for Administrative Rationalization and Economy for providing free access to the Swedish electronic computer BESK. The work has been financed by the Swedish Technical Research Council and the Swedish Natural Science Research Council.

Reaction between Benzoyl Peroxide and Rhodamine 6GX Color Base

by P. K. Nandi and U. S. Nandi

Department of Physical Chemistry, Indian Association for the Cultivation of Science, Jadavpur, Calcutta-32, India (Received February 23, 1965)

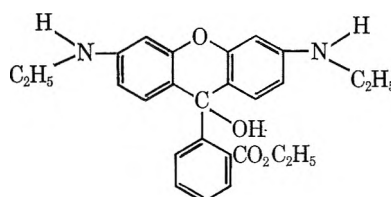
The reaction between benzoyl peroxide and Rhodamine 6GX color base in five hydrocarbon solvents has been studied in the temperature range where the thermal decomposition of benzoyl peroxide is negligible. In the very first step of the reaction an intermolecular complex is probably produced by electron transfer. The mechanism of the reaction has been discussed in the light of thermodynamic parameters.

Introduction

The reaction of benzoyl peroxide with amines is interesting and has been studied by other workers.¹ The reaction is reported to be comparatively fast at temperatures where the thermal decomposition of benzoyl peroxide is negligible. There are two mechanisms suggested for such a rapid reaction between peroxide and amines. One² is that the induced decomposition of peroxide by amine-type radicals may be an extremely rapid chain reaction, while the other^{3,4} hypothesizes a bimolecular reaction between the peroxide molecule and the amine molecule leading to the peroxide decomposition. The bimolecular reaction would most probably be a one-electron-transfer reaction. Either possibility is cogent although neither is compelling.

The disparity between the proposed mechanisms of the reaction warranted the investigation for the eluci-

ation of the involved mechanism. Here we have chosen a dye base as the amine, having chromophoric >NH groups, which has the formula



A sharp change in the color of the amine dye base as the time proceeds after the addition of benzoyl per-

- (1) A. V. Tobolsky and R. B. Mesrobian, "Organic Peroxides," Interscience Publishers, Inc., New York, N. Y., 1956.
- (2) P. D. Bartlett and K. Nozaki, *J. Am. Chem. Soc.*, **68**, 1686 (1946); **69**, 2299 (1947).
- (3) L. Horner, *Angew. Chem.*, **61**, 458 (1949).
- (4) M. Imoto and S. Choe, *J. Polymer Sci.*, **15**, 485 (1955).

oxide has been attributed to a possible charge-transfer phenomenon, thereby supporting the view that as an intermediate of the reaction an intermolecular complex is produced. This occurs by the donation of an electron from the amine to benzoyl peroxide, thereby decomposing the peroxide.

The variation of the rate constant with temperature could be utilized for the computation of thermodynamic parameters of activation which are of immense value in elucidating the mechanism. In the present paper both the amine dye and benzoyl peroxide were dissolved in hydrocarbon solvents, and the rates were measured at different temperatures.

Experimental Section

Rhodamine 6GX (C.I. No. 45160) was purified by using ether to precipitate the dye from a saturated solution in absolute alcohol.⁵ The sample supplied was the chloride salt. The color base of the dye was extracted in hydrocarbon solvents following the procedure developed in this laboratory.⁶ The Rhodamine 6GX color base extract was kept over sodium hydroxide beads. The benzoyl peroxide was reprecipitated three times, using chloroform, from a solution of benzoyl peroxide in methanol.⁷ It was kept in a desiccator containing calcium chloride in a cool, dry place.

The solvents heptane, benzene, decalin (mixed isomer), and toluene were purified by the method suggested in the references.⁸ Cyclohexane used was B.D.H. spectroscopic grade.

The characteristic yellow color of the Rhodamine 6GX color base is only obtained when it is extracted with hydrocarbon solvents. It was found that the greater the unsaturation of the solvent, the better the extraction. Any other solvent, with the exception of hydrocarbons, gives a characteristic pink color with or without fluorescence. Our experiments are limited to hydrocarbon solvents only.

The concentration of the color base in hydrocarbon solvents can be determined by shaking the nonaqueous layer with a solution containing 1 *M* HCl and 3 *M* KCl solution. The extract in the acidic layer first turns to a pink color, which, when kept for some hours, becomes completely yellow. The concentration of this solution may be obtained from the standard graph of optical density vs. concentration of Rhodamine 6GX chloride dissolved in the mixed HCl-KCl solution. Actually, the exact concentration of Rhodamine 6GX color base is not necessary as will be seen later.

The progress of the reaction of the Rhodamine 6GX color base with benzoyl peroxide was investigated by measuring the optical density at the wave lengths of maximum absorption at different intervals of time using

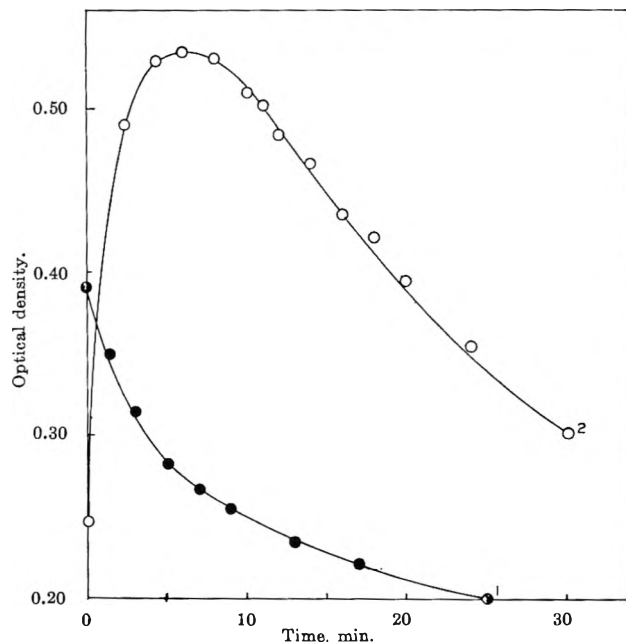


Figure 1. A typical plot of the decay of Rhodamine 6GX color base and consequent formation and decay of the intermediate with time in decalin: 1, measurements at 484 $m\mu$; 2, measurements at 515 $m\mu$. Benzoyl peroxide concentration $\approx 2.5 \times 10^{-4} M$; temperature $32 \pm 0.1^\circ$.

a Hilger Uvspeck spectrophotometer. Stopped quartz cells of 1-cm. thickness were used. The temperature in the cell compartment was maintained to within $\pm 0.1^\circ$ of the desired value by circulating water in the thermospacer set fixed in the spectrophotometer from an external thermostat controlled by a relay.

Results and Discussion

The visible spectrum of the extracted color base in heptane shows absorption peaks at 480 and 450 $m\mu$; in cyclohexane, absorption peaks are at 480 and 452 $m\mu$; and in benzene, toluene, and decalin, they are at 484 and 454 $m\mu$.

The experiments were performed at the wave lengths of maximum absorption, *viz.*, at 480 $m\mu$ in heptane and cyclohexane and at 484 $m\mu$ in benzene, decalin, and toluene. At these wave lengths the color base obeys Beer's law.

(5) R. W. Ramette and E. B. Sandell, *J. Am. Chem. Soc.*, **78**, 4872 (1956).

(6) S. R. Palit, *Chem. Ind. (London)*, 1531 (1960); *Anal. Chem.*, **33**, 1441 (1961).

(7) C. G. Swain, W. H. Stockmayer, and J. T. Clarke, *J. Am. Chem. Soc.*, **72**, 5426 (1950).

(8) A. Weissberger, Ed., "Techniques in Organic Chemistry," Vol. VII, Interscience Publishers, Inc., New York, N. Y., 1955, pp. 311, 313, 317, and 319.

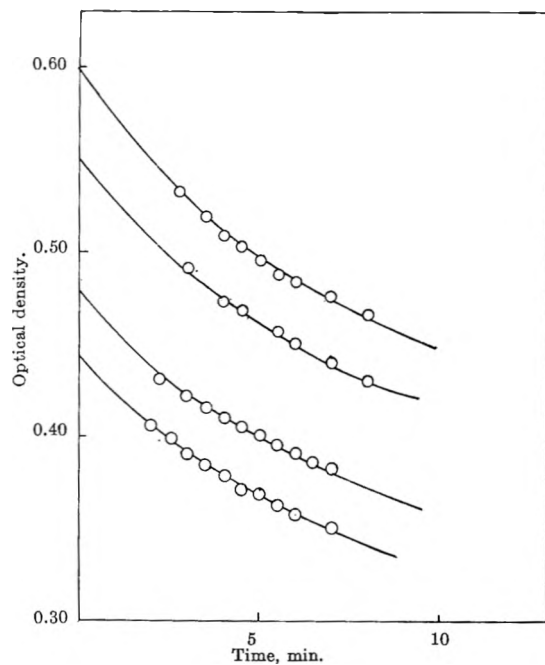


Figure 2. Variation of optical density with time using $5.205 \times 10^{-4} M$ benzoyl peroxide at $24.9 \pm 0.1^\circ$ with different concentrations of Rhodamine 6GX color base in benzene.

The experiment was performed with a dye concentration of about $2 \times 10^{-5} M$ and a benzoyl peroxide concentration ranging from 5×10^{-4} to $10^{-4} M$.

In the presence of benzoyl peroxide the characteristic yellow color of Rhodamine 6GX color base diminishes continuously, and a pink color develops. The pink color also disappears gradually, and a colorless solution is obtained in all solvents. At low benzoyl peroxide concentration ($10^{-5} M$) and at a temperature of 15° the decay of the pink color is very slow (about 1% in 20 min.). The absorption maximum of the pink color, under these conditions, was found to be $515 m\mu$. This maximum depends only slightly upon the solvents in which the experiments were performed. This absorption band corresponds with the acid color developed by the color base in acid solutions, *e.g.*, benzoic, stearic acids, etc., in the above-mentioned solvents. The component which has the absorption band at $515 m\mu$ has little effect on the absorption of the original color base as can be observed by comparing the spectra. At high temperatures the appearance of the pink color is very transitory.

The fading away of the color of the intermediate compound is most rapid in heptane and slowest in toluene at any temperature.

The comparison of the absorbance of a solution of benzoyl peroxide and Rhodamine 6GX color base kept

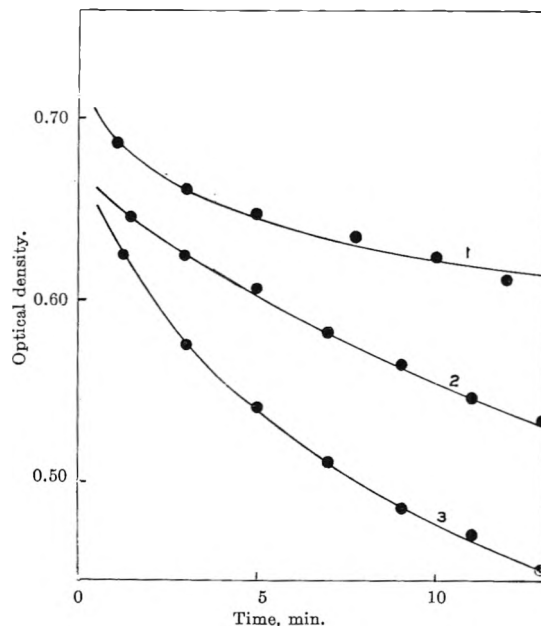


Figure 3. Variation of optical density with time using nearly the same concentration of Rhodamine 6GX color base with different concentrations of benzoyl peroxide in toluene at $26.1 \pm 0.1^\circ$: 1, $5.036 \times 10^{-4} M$; 2, $2.520 \times 10^{-4} M$; 3, $1.008 \times 10^{-4} M$ benzoyl peroxide.

in dark, with an identical solution subjected to experimentation in the spectrophotometer, for the same period, shows very little perceptible difference, thereby eliminating the possibility of a photochemical reaction.

The disappearance of the amine color, followed by the appearance of the pink color and its subsequent decay, points to the fact that the nature of the reaction is a consecutive one. However, the identification of the end product could not be made. From the comparison of spectra it seems that the intermediate compound decays giving more than one single product.

Figure 1 illustrates the behavior of the reaction in decalin. Figure 2 illustrates the variation of optical density with time at different concentration of Rhodamine 6GX color base using the same concentration of benzoyl peroxide. Figure 3 illustrates the same with a constant concentration of Rhodamine 6GX color base but different concentrations of benzoyl peroxide in benzene.

Under the conditions used, the reaction obeyed zero-order kinetics with respect to Rhodamine 6GX color base concentration and first-order kinetics with respect to benzoyl peroxide concentration.

To establish the order of the reaction and to calculate the velocity constant K from the values of concentration at different times, numerous methods have been suggested.⁹ The following equation was used for

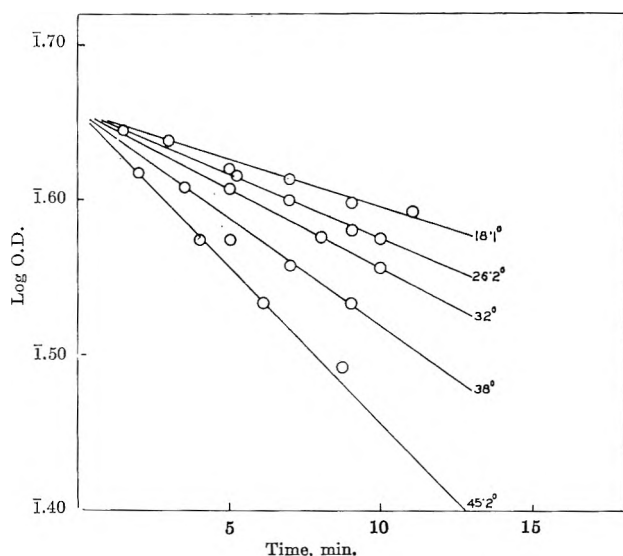


Figure 4. Variation of log (optical density) with time at different temperature in decalin.

obtaining the first-order rate constant: $\ln C = \ln C_0 - Kt$, where C_0 is the initial concentration, C is the concentration of the dye at time t , and K is the first-order velocity constant. According to this equation, the plot of $\log C$ vs. t would give a straight line for a first-order reaction, and it is actually found so, as shown in Figure 4. In Figure 4 the plots at different temperatures in decalin are given, and the first-order behavior of the reaction is confirmed. As the concentration of benzoyl peroxide is much greater than the concentration of Rhodamine 6GX carbinol base, the real velocity constant K' was obtained as

$$K' = \frac{\Delta \log [R]}{[B]\Delta t} = \frac{\Delta \log \text{O.D.}}{[B]\Delta t}$$

where $[R]$ is the concentration of Rhodamine 6GX carbinol base and $[B]$ is the concentration of benzoyl peroxide. The rate constant K' may be assumed to actually be a bimolecular rate constant for the reaction.

Dependence of K' on Temperature. The data given in Figure 4 show the variation of log O.D. at different temperatures in the range 291 to 318°K. in decalin. From the slope of the plot and known initial benzoyl peroxide concentration, the value of K' was computed and reported in Table I for the reaction in toluene. The data of Table I were analyzed using the Arrhenius equation

$$\ln K' = \ln A - \frac{E^\ddagger}{RT}$$

and the results are given in Figure 5 for the reaction

in toluene. It is found that a linear plot of $\log K'$ vs. $1/T$ is obtained in accord with the above equation. The slope of this plot yields a value of 13.2 kcal./mole for E^\ddagger , the energy of activation in toluene. The value of the frequency factor A was obtained by computing the value of E^\ddagger and K' at a fixed temperature from the above equation. This gives a value for A in toluene which is $3.84 \times 10^9 M^{-1} \text{sec}^{-1}$. The values of E^\ddagger and A in different solvents are listed in Table II. Also from the data, the different thermodynamic parameters for activation were calculated using the equations¹⁰

$$\Delta F^\ddagger = 2.303RT \left(\log \frac{RT}{Nh} - \log K' \right)$$

$$\Delta S^\ddagger = 2.303R \left(\log A - \log e \frac{RT}{Nh} \right)$$

where ΔF^\ddagger and ΔS^\ddagger are the free energy and entropy of activation, R is the gas constant, K' is the rate constant at temperature T , N is Avogadro's number, h is Planck's constant, and e is the exponential factor.

Table I: Bimolecular Rate Constant at Different Temperatures in Toluene

T , °K.	K' , M^{-1} sec^{-1}
318.4	3.57
311.4	2.32
305.2	1.46
299.1	0.91
293.1	0.58

Table II: Rate Constant, Energy of Activation, and Frequency Factor of the Reaction in Different Solvents

Solvent	K' , $M^{-1} \text{sec}^{-1}$ at 300°K.	E^\ddagger , kcal. mole ⁻¹	A , M^{-1} sec^{-1}
<i>n</i> -Heptane	4.04	6.3	1.64×10^6
Cyclohexane	4.6	6.6	2.94×10^6
Decalin	2.97	9.8	4.12×10^7
Benzene	1.42	10.4	7.76×10^7
Toluene	1.01	13.2	3.84×10^9

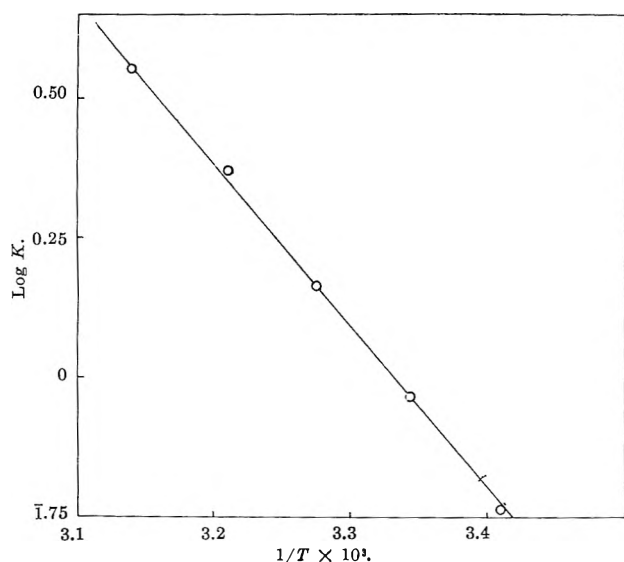
The thermodynamic quantities are entered in Table III. It is to be noted that the intermediate com-

(9) A. A. Frost and R. G. Pearson, "Kinetics and Mechanism," John Wiley and Sons, Inc., New York, N. Y., 1953, p. 40.

(10) S. Glasstone, K. J. Laidler, and H. Eyring, "The Theory of Rate Processes," McGraw-Hill Book Co., Inc., New York, N. Y., 1941.

Table III: Different Thermodynamic Parameters of Activation for the Reaction

Solvent	ΔH^\ddagger , kcal. mole ⁻¹	ΔF^\ddagger , kcal. mole ⁻¹	ΔF^* , kcal. mole ⁻¹	ΔS^\ddagger , cal. deg. ⁻¹ mole ⁻¹	ΔS^* , cal. deg. ⁻¹ mole ⁻¹	K_e
<i>n</i> -Heptane	5.7	16.7	20.8	-36.7	-24.7	9.66×10^{-9}
Cyclohexane	6.0	16.6	20.7	-35.5	-23.7	1.76×10^{-8}
Decalin	9.2	16.9	21.0	-25.7	-13.9	2.43×10^{-6}
Benzene	9.8	17.3	21.4	-25.5	-13.7	2.68×10^{-6}
Toluene	12.6	17.5	21.6	-16.3	-4.5	2.71×10^{-4}

Figure 5. Linear variation of $\log K'$ with $1/T$ in toluene.

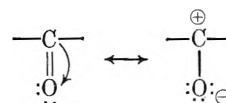
pound (maxima at $515 \text{ m}\mu$) is more stable in the solvent having double bonds, which implies the possibility of its formation by ionization.¹¹ The differences in the values of the entropy of activation¹² in different solvents may be attributed to differences in the degree of orientation of the solvent molecules under the influence of a polar transition state and to the differences in the degree of orientation of the reactants and products. The comparison of the stability of the intermediate compound with the values of the entropy of activation listed in Table III suggests that the aromatic solvent molecules are capable of further stabilizing the charge separation owing to their high capacity for polarizability of the π electron in the aromatic ring.

The activation energy in such ionogenic reactions should be antipatically related to the solvating power of the medium.¹⁰ The value of the rate constants, as well as the activation energy (Table II), leads to the fact that specific effects¹³ other than the dielectric constant may be more important.

The possibility of charge formation is favored by the presence of $>\text{NH}$ groups in the Rhodamine 6GX color

base and oxygen atoms of benzoyl peroxide. The N atom in $>\text{NH}$ donates an electron to the O atom, resulting in a charge-transfer complex having a characteristic pink color; the reaction may be termed as the acid-base¹⁴ reaction, benzoyl peroxide behaving as a Lewis acid and Rhodamine 6GX color base as a Lewis base. The reaction is catalyzed by benzoyl peroxide.

The presence of the appreciable dipole moment of $>\text{C}=\text{O}$, which probably arises as



implies that the coordination of the electron takes place between central peroxy oxygen atoms and N atoms of the NHC_2H_5 groups.

The charge-transfer interaction most probably takes place between the highest occupied orbital of the donor and the vacant antibonding orbital of the $2\rho\sigma_u$ around the O-O bond in the peroxide. The lowering of the energy level of the antibonding orbital of the O-O bond and the elevation of that of the lone pair of N atom facilitate the charge transfer.¹⁵

The product of the reaction, which has a maxima at $515 \text{ m}\mu$, is most probably of inner complex type as has been classified by Mulliken.¹⁶ It has been found that such complexes are always unstable. The formation of a charge-transfer complex lowers the activation barrier. The complex formation is the precursor of the chemical reaction, an idea which was earlier set forth by Barckmann.¹⁷ A similar case of charge-transfer complex occurs when pyromellitic dianhydride

(11) D. P. Aimes and J. E. Willard, *J. Am. Chem. Soc.*, **73**, 164 (1951).

(12) W. F. K. Wynne-Jones and H. Eyring, *J. Chem. Phys.*, **3**, 492 (1935).

(13) J. H. Beard and P. H. Plesch, *J. Chem. Soc.*, 3682 (1964).

(14) G. N. Lewis, *J. Franklin Inst.*, **226**, 293 (1938).

(15) K. Tokumaru and O. Simamura, *Bull. Chem. Soc. Japan*, **36**, 333 (1963).

(16) R. S. Mulliken, *J. Am. Chem. Soc.*, **74**, 818 (1952).

(17) W. Barckmann, *Rec. trav. chim.*, **68**, 147 (1949).

(PMDA), which acts as a π acceptor or π acid, reacts with aniline producing a red complex, but the color disappears as amine reacts with PMDA.¹⁸ Complex formation is reduced with increasing temperature. The reaction between *N,N*-dimethylaniline and chloranil produces crystal violet salt by a charge-transfer phenomenon. Diamagnetic donor-acceptor complexes and paramagnetic semiquinones are two observed intermediates.¹⁹

From the values of ΔF^\ddagger and ΔS^\ddagger the terms ΔF^* and ΔS^* can be calculated by means of the equations

$$\Delta F^\ddagger = \Delta F^* - RT \ln 1000$$

$$\Delta S^\ddagger = \Delta S^* - R + R \ln 1000$$

The terms ΔF^* and ΔS^* are the excess free energy and the excess entropy of activation, respectively. The quantity ΔF^* is the free energy of formation of the intermediate state for reacting particles in excess of what it would be if the state were simply the usual transient collision complex of two neutral nonreacting particles. ΔS^* is the corresponding entropy term.²⁰

The entropy of activation, as well as other parameters, has been calculated assuming the transmission coefficient to be equal to unity. In the case of an electron-transfer reaction, the best compromise configurations are those giving frequent electronic transitions without too high a free energy of activation. Thus, any measurable rate for an electron-transfer reaction involves a transmission coefficient of less than unity since it is arrived at using an idealized transition configuration.²¹ The electronic transmission coefficient K_e is related to the apparent entropy of activation by the formula $\Delta S^\ddagger = R \ln K_e$. The values of K_e in the solvents have been listed in Table III.

Isokinetic Temperature. Figure 6 shows a plot of the activation parameter for the reaction between benzoyl peroxide and the amine. The slope gives a temperature of 335.4°K. (62.3°C.) for the reaction which indicates that the rate of the reaction at this temperature is independent of the solvent.²²

The Validity of the ΔH^\ddagger - ΔS^\ddagger Plot. Peterson, *et al.*,²³ have pointed out that, for a reaction series involving a narrow range of ΔH^\ddagger values and considerable error in the rate constant, little validity can be assumed in any observed ΔH^\ddagger - ΔS^\ddagger relationship. The larger the range of the ΔH^\ddagger values and the smaller the experimental error, the greater is the reliability of any observed relationship.

If the range of ΔH^\ddagger values be designated by $d\Delta H^\ddagger$ and the maximum fractional error in ΔH^\ddagger by the symbol δ , Peterson, *et al.*, have shown that the ratio of $d\Delta H^\ddagger/2\delta$ must be equal to or greater than unity if

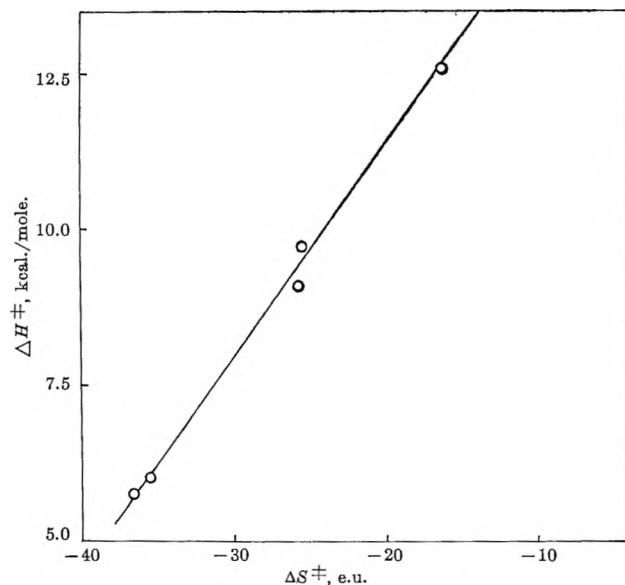


Figure 6. Least-square plot of enthalpy-entropy of activation for the reaction.

any validity can be assumed in an observed ΔH^\ddagger - ΔS^\ddagger plot. This ratio must be much greater than unity if any details of the relationship are to be inferred. The maximum fractional error in ΔH^\ddagger can be calculated using the equation $\delta = 2RT'\alpha/(T' - T)$, where α is the maximum fractional error in the rate constant, R is the gas constant, and T' and T are the upper and lower temperature limits, respectively.

The value of α may be assumed to be equal to the reproducibility of the rate constant K' . The range of the ΔH^\ddagger value is about 6.8 kcal./mole, and δ turns out to be about 0.205. The ratio of $d\Delta H^\ddagger/2\delta$ therefore turns out to be about 7. This value is much greater than 1, and the validity of the ΔH^\ddagger - ΔS^\ddagger plot may be assumed correct.

Acknowledgment. The authors are indebted to Professor Santi R. Palit for constant encouragement during the course of the work. Thanks are due to the Council of Scientific and Industrial Research for financial assistance to P. K. N.

(18) L. I. Ferstending, W. G. Toland, and C. D. Heaton, *J. Am. Chem. Soc.*, **83**, 1151 (1961).

(19) J. W. Eastman, G. Englesma, and M. Kelvin, *J. Am. Chem. Soc.*, **84**, 1939 (1962).

(20) R. A. Marcus, *J. Chem. Phys.*, **26**, 868 (1957).

(21) R. J. Marcus, B. J. Zwolinski, and H. Eyring, *J. Phys. Chem.*, **58**, 432 (1954).

(22) S. L. Fries, E. S. Lewis, and A. Weissberger, Ed., "Techniques of Organic Chemistry," Vol. VIII, Part I, 2nd Ed., Interscience Publishers, Inc., New York, N. Y., 1961, p. 207.

(23) R. C. Peterson, J. H. Markgraf, and S. D. Ross, *J. Am. Chem. Soc.*, **83**, 3819 (1961).

Acid Property and Structure of a Solid Metal Sulfate Catalyst.

Change in Structure of Nickel Sulfates with Heating¹

by Tsuneichi Takeshita, Ryuichiro Ohnishi, Toshiji Matsui, and Koza Tanabe

Research Institute for Catalysis, Hokkaido University, Sapporo, Japan (Received March 17, 1965)

The structure of nickel sulfate heat-treated at various temperatures ranging from room temperature to 550° was studied by X-rays, infrared, n.m.r., and e.s.r. to characterize the nature of the acidic sites on a metal sulfate catalyst. It was shown by X-rays that the specimen, obtained by heating $\text{NiSO}_4 \cdot 6\text{H}_2\text{O}$ at 150 to 350°, consists mainly of the monohydrate phase and that the reflection line of this phase becomes progressively diffuse as the temperature of heat treatment is raised. Since two phases exist for the specimen treated at 300–400° and since the anhydrous lines become sharper at higher temperatures, this temperature range seems to be accompanied by the greatest disorder or strain in both phases. This range also coincides with the maximum appearance of the e.s.r. signal. There was a splitting of the SO_4^{2-} infrared absorption band owing to coordination to the central metal. The extent of this splitting increased as the sample was treated at higher temperatures. There were three temperature regions characterized by the degree of this splitting for the catalyst treated at the ambient, the 150–350°, and the 400–600° temperature ranges. The pattern of the OH stretching and the bending was also significantly different in these three groups. This division of the specimen was similar to that shown by the X-ray analysis. The maximum intensity of the n.m.r. spectrum was observed at 250°, but that of the e.s.r. was at 350°. These observations indicate a strain or change in the crystal field of the sulfate heat-treated at 150–350°, at which temperatures the marked surface acidity appears. The nature of the acid sites or the catalytic activity sites is explained by postulating a metastable intermediate structure which has a vacant orbital on the nickel ion. It is formed from the loss of water before the monohydrate is thermally converted to the stable anhydrous form. Attention is given to the similarity of this structure to the SN1 intermediate with a coordination number of less than 6 during the ligand exchange.

Introduction

In 1950, Walling² discovered that the solid surface of some metal sulfates changes the color of Hammett indicators, suggesting a new series of solid acids. Several studies were followed thereafter which indicated an intrinsic solid acidity, not arising from any impurities. Metal sulfates showed this property to an unusual extent.³ The acidity usually increased remarkably on heat treatment, attained a maximum value, and then decreased at higher temperatures.^{3,4} As a typical example, the acid property of nickel sulfate, together with its catalytic activity, was studied,⁴ and the catalytic action was kinetically shown to be

similar to an enzymatic one.⁵ The reactions catalyzed by metal sulfates include the depolymerization of paraldehyde,^{4,6} the polymerization of propylene^{7,8}

(1) Presented at the 15th Discussion Meeting on Catalysis, Catalysis Society of Japan, Osaka, Japan, Nov. 9, 1964.

(2) C. Walling, *J. Am. Chem. Soc.*, **72**, 1164 (1950).

(3) K. Tanabe and M. Katayama, *J. Res. Inst. Catalysis, Hokkaido Univ.*, **7**, 106 (1959).

(4) K. Tanabe and R. Ohnishi, *ibid.*, **10**, 229 (1962).

(5) K. Tanabe and A. Arameta, *ibid.*, **8**, 43 (1960).

(6) K. Tanabe, *ibid.*, **7**, 114 (1959); K. Tanabe and Y. Watanabe, *ibid.*, **7**, 120 (1959); K. Tanabe, *Shokubai* (Tokyo), **3**, 195 (1961).

(7) K. Tarama, S. Teranishi, K. Hattori, and T. Ishibashi, *ibid.*, **4**, 69 (1962).

and of aldehydes,⁹ the hydration of propylene,¹⁰ the formation of formaldehyde from methylene chloride,¹¹ the condensation of glucose with acetone,¹² the esterification of anhydrous phthalic acid,⁷ and the synthesis of isoprene from 4,4-dimethyl-*m*-dioxane.¹³ In every case, there have been found good correlations of the acidic property of metal sulfates with their catalytic activity (see, for example, Figure 8). However, no investigation has been made on the structure of acid sites of the sulfates except X-ray studies.⁷ Since the amount of water in these metal sulfates varies with the heating temperature and seems to be a critical factor for maximum acidity, particular attention is given to the role of water in the present work. Therefore, the structural nature of nickel sulfate as an acid catalyst was studied by X-rays, infrared, n.m.r., and e.s.r. spectra.

Experimental Section

Samples. Nickel sulfate ($\text{NiSO}_4 \cdot 7\text{H}_2\text{O}$; G.R., Kanto Chemical Co.) was heated in a glass tube at various temperatures ranging from 150 to $550 \pm 5^\circ$ for 3 hr., and the ampoule was sealed off, or cooled in a vacuum desiccator. Deuterated catalysts were prepared by distilling heavy water (99.75 mole % D_2O of Showa Denko K. K., Japan) over the anhydrous salt in a vacuum line, recrystallizing, and calcining to keep out moisture from the atmosphere.

Figure 1 shows the amount of water calculated from the decrease in weight of the salt *vs.* the temperature of heat treatment and indicates that the catalyst obtained by dehydrating at 350° corresponds to a state intermediate between the monohydrate and the anhydrous salt. As previously noted, the solid acidity is maximum for specimens dehydrated at 350° .³⁻⁸

Measurement. (a) *X-Ray Diffraction.* The powder pattern of each specimen was obtained with a Norelco unit, using filtered $\text{Cu K}\alpha$ radiation. Intensities were measured with a scintillation counter with pulse-height discrimination; the ratemeter readings were recorded on a chart, and peak area above background level was taken to be an integrated intensity. The specimen was scanned between 22 and 32° (2θ). A specimen spinner was used to reduce orientation effects and to average out the intensities over a large volume of the specimen. In order to prevent moisture from entering, the sample was coated with polystyrene by immersing in a 1% benzene solution followed by evaporation of the solvent. Quantitative estimation of the phase was made by using well-crystallized silicon metal powder of high purity, amounting to as much as 10% of the sample, as an internal standard. The d value was also determined from comparison of the reflection

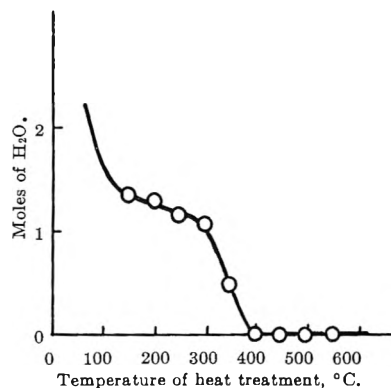


Figure 1. Variation of water (moles) in nickel sulfates treated at various temperatures.

line under investigation with that of the internal standard.

(b) *Infrared.* An Hitachi EPI-2 infrared spectrophotometer with an NaCl prism for $4000\text{--}650\text{ cm}^{-1}$ and KBr prism for $1100\text{--}360\text{ cm}^{-1}$ was used. Samples were measured either in a KBr tablet or Nujol mull. The two methods gave no significant difference. However the Nujol method is better suited for a deuterated sample since exchange with atmospheric water is slower.

(c) *N.m.r. and E.s.r.* The instruments used were both of Nippon Denshi K. K., Japan. Measurements were made at room temperature.

(d) *Change of Specific Heat with Heating.* This was measured on a Rigaku Denki DTA-SHM unit.

(e) *Lewis Acidity.* Lewis acidity was measured by the Leftin and Hall method¹⁴ for estimating the amount of the chemisorbed trityl chloride.

Results

(1) *X-Ray.* Representative patterns are given in Figure 2. Table I gives a phase composition of the nickel sulfate treated at the indicated temperatures and the amount estimated with reflections, $2\theta_{(203)} = 30.12^\circ$ for $\text{NiSO}_4 \cdot 6\text{H}_2\text{O}$, $2\theta_{(202)} = 29.47^\circ$ for $\text{NiSO}_4 \cdot \text{H}_2\text{O}$, and $2\theta_{(111)} = 24.98^\circ$ for NiSO_4 against the reference phases obtained at 50, 150, and 500° , respectively.^{15,16}

(8) Y. Watanabe and K. Tanabe, *J. Res. Inst. Catalysis, Hokkaido Univ.*, 12, 56 (1964).

(9) H. Takida and K. Noro, *Kobunshi Kagaku*, 21, 23, 109 (1964).

(10) Y. Ogino, *Shokubai* (Tokyo), 4, 73 (1962).

(11) N. Kominami and N. Sakurai, presented at 17th Annual Meeting of Chemical Society of Japan, Tokyo, April 1964.

(12) T. Sano, K. Tanabe, and T. Takeshita, to be published.

(13) Y. Hamamoto and A. Mitsutani, *Kogyo Kagaku Zasshi*, 67, 1227 (1964).

(14) H. P. Leftin and W. K. Hall, *Actes Congr. Intern. Catalyse*, 2^e, Paris, 1960, 1, 1307, 1353 (1961).

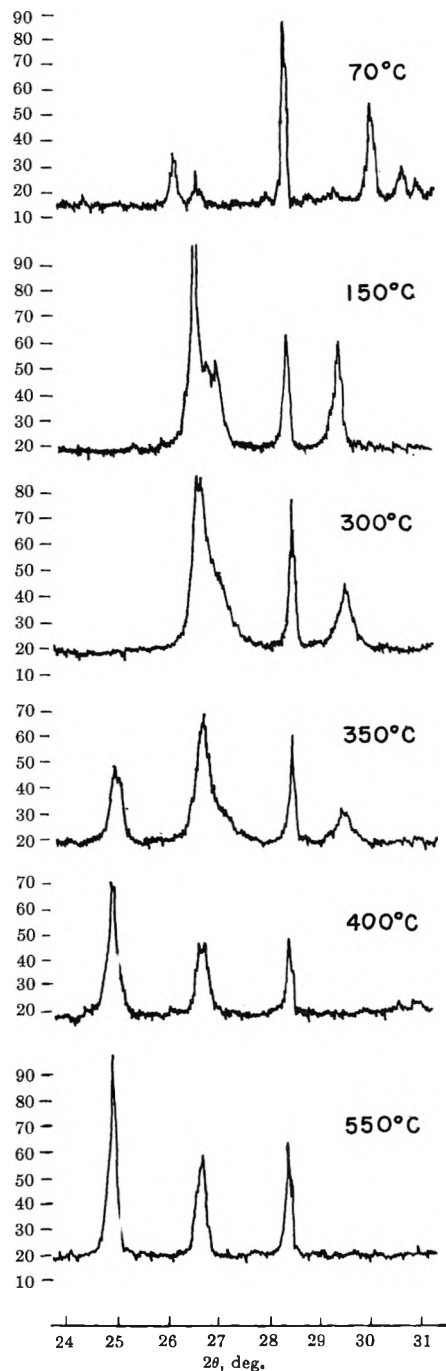


Figure 2. Diffraction pattern of nickel sulfates calcined at various temperatures.

The specimen of interest can be conveniently divided into three groups from the X-ray analysis according to the temperature range of the heat treatment, *i.e.*, (a) 150–300°, (b) 300–400°, and (c) 400–550°. (a) This specimen consists of a single phase of $\text{NiSO}_4 \cdot \text{H}_2\text{O}$ and begins to give rise to an anhydrous phase abruptly at 300–350°. It is significant that the reflection peaks

of the monohydrate become more diffuse for the specimen heated at higher temperature. This is clearly seen in an obvious change of the triplet at $2\theta = 26.6^\circ$. (b) The specimen is a mixture of two phases, $\text{NiSO}_4 \cdot \text{H}_2\text{O}$ and NiSO_4 , with an increasing amount of the anhydrous phase as the temperature is raised. (c) Only the anhydrous NiSO_4 exists in this range with a continuing trend of sharper lines as the temperature is raised above 400°, indicating gradual growth of the crystallite.

The spacing determined for each phase-characteristic reflection line is almost invariant for the hexahydrate and anhydrous phases over the temperature range in which the specimen was treated. However, that of $\text{NiSO}_4 \cdot \text{H}_2\text{O}$ apparently decreases from 3.028 Å. (150°) to 3.025 Å. (350°), which may indicate some shrinkage of the crystal owing to loss of water resulting in the creation of some strain in the intermolecular bonds.

Apparent sizes of crystallite were calculated by means of Jones' method¹⁷ from integrated breadth of each reflection under investigation, and these are shown in Figure 3 against the temperature of heat treatment with minima of both $\text{NiSO}_4 \cdot \text{H}_2\text{O}$ and NiSO_4 at temperatures of 300 to 400°. The apparent size thus obtained usually gives us a representation for a local strain within the crystal lattice, as well as an indication of the crystallite size. A previous determination⁴ indicates that the growth of crystallites is proportional to the apparent decrease in the B.E.T. area [NiSO_4 : 150° (3.7 m.²/g.), 250 (18.2), 325 (13.4), 350 (12.2), 375 (11.2), 400 (10.4), 464 (8.9), 600 (6.6)]. Therefore, the observed broadening may be attributed to increase in strain or to loss of symmetry developed in the $\text{NiSO}_4 \cdot \text{H}_2\text{O}$ phase as the specimen is heated from 150 to 300°.

(2) *Infrared.* A portion of the infrared spectra is given in Figures 4, 5, and 6, and the key bands are given in Table II with intensity values per unit weight (mg.) in a fixed amount of KBr (200 mg.). The spectra, as a whole, consist of those of H_2O and SO_4^{2-} . Most characteristic is the splitting of an SO_4^{2-} band as the dehydration proceeds. This is probably removal of degeneracy as the water is removed owing to increasing coordination of SO_4^{2-} with the Ni^{2+} ion which was free

(15) Spacings were taken from the following. $\text{NiSO}_4 \cdot 6\text{H}_2\text{O}$: National Bureau of Standards Circular 539, U. S. Government Printing Office, Washington, D. C., 1957, p. 36. $\text{NiSO}_4 \cdot \text{H}_2\text{O}$: C. W. F. T. Pistorius, *Bull. soc. chim. Belges*, 69, 570 (1960). NiSO_4 : National Bureau of Standards Monograph 25, U. S. Government Printing Office, Washington, D. C., 1962, Section 2.

(16) According to our preliminary X-ray study, the nickel sulfate heated at 150° for less than 2 hr. gives varying amounts of an amorphous phase. The constant intensity for the monohydrate phase is obtained only by heating 3 hr. or more.

(17) F. W. Jones, *Proc. Roy. Soc. (London)*, A166, 16 (1938).

Table I: X-Ray Diffraction Analysis^a of the Nickel Sulfates Treated at Various Temperatures

Temp. of heat treatment, °C., 3 hr.	Phase compn., %, probable error $\pm 5\%$ ^b			Moles of H ₂ O in NiSO ₄ · <i>x</i> H ₂ O
	NiSO ₄ ·6H ₂ O (<i>d</i> ₍₂₀₁₎ , Å.) ^c	NiSO ₄ ·H ₂ O (<i>d</i> ₍₂₀₂₎ , Å.) ^c	NiSO ₄ (<i>d</i> ₍₁₁₁₎ , Å.) ^c	
50	100 (2.965)	6.00
70	88.6 (2.964)
150	...	100 (3.028)	...	1.33
200	...	88.3 (3.028)	...	1.30
250	...	99.6 (3.029)	...	1.16
300	...	91.2 (3.025)	2.15	1.08
350	...	54.2 (3.025)	46.7	0.50
400	...	+	87.8 (3.561)	0.02
450	85.4 (3.562)	0
500	100 (3.561)	0
550	95.2 (3.562)	-0.01

^a Operating conditions: scanning speed 0.25°/min.; time constant 2 sec.; full scale 400 c.p.s.; divergent slit 1°, receiving slit 0.003 in.; P.H.A. (pulse-height analyzer), H.V. (high voltage) 860 v., B.L.V. (base-line voltage) 21 v., C.W. (channel width) 9 v. ^b This limit of error may be a somewhat overoptimistic estimate because errors due to causes other than the statistical fluctuation, such as the instability of the counter, of their associated circuits, or of the X-ray tube, and inhomogeneity of the mixture of the specimen and the internal standard, may have crept in determining the integrated intensities. ^c Spacing: (111), reflection of Si, $2\theta = 28.442^\circ$, was used as the standard.

Table II: Characteristic Bands of Nickel Sulfates Treated at Various Temperatures

Bands, ^a cm. ⁻¹	No treatment	Temp. of heat treatment, °C.						
		150	250	300	350	400	450	550
Near 3000 OH ₂ str.	3500	3300	3300	3300	3300	3400	(3400)	
	3300	3300 (0.13)	3100 (0.16)	3100 (0.22)	3100 (0.22)			
1600 OH ₂ sciss.	1630	1630	1630					
1500 OH ₂ sciss.		1530 (0.10)	1530 (0.08)	1530 (0.09)	1530 (0.10)			
900 OH ₂ rock		920 (0.57)	925 (0.53)	925 (0.60)	925 (0.63)			
750 OH ₂ rock	770							
1105 SO ₄ ²⁻ str.	1090	1120	1150	1150	1150	1230 (0.72)	1235 (0.72)	1235 (0.72)
			1090	1090	1090	1160	1160	1160
				1020 (0.35)	1020 (0.42)	1040	1040	1030
980 SO ₄ ²⁻ str.	980 sh	1020 (0.35)		980 sh (0.08)	980 sh (0.08)	980 (0.64)	980 (0.64)	980 (0.64)
610 SO ₄ ²⁻ def.	630	680	685	685	685	685	685	685
		630	630	630	630	615	615	615
		600	605	605	605	595	595	595
450 SO ₄ ²⁻ def.			420	420	485	485	485	

^a KBr disk: numerals in parentheses are intensities at 1 mg. of substance/200 mg. of KBr obtained from I_0 at 2000 cm.⁻¹ (I at 3300-3100), 1475-1625 (I at 1530), 850-1500 (I at 1235), 750 (I at 1020), and a tangent line (I at 980).

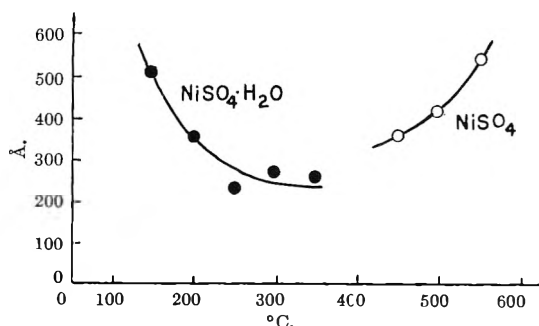


Figure 3. Apparent crystallite size vs. temperature of heat treatment.

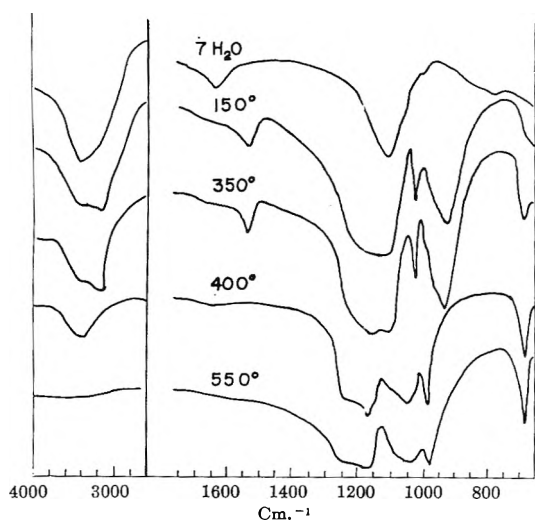


Figure 4. Infrared spectra of nickel sulfates treated at several temperatures (in KBr).

in a hexahydrate. Loss of symmetry has been reported by Nakamoto, Fujita, Tanaka, and Kobayashi¹⁸ in the observation of sulfato complexes. The removal of degeneracy increases by coordination of a bidentate SO_4^{2-} over that of monodentate. Similar reasoning has been made on nickel sulfate by Rocchiccioli.¹⁹

Accordingly, nickel sulfates treated at different temperatures are classified through sulfate absorption into three groups, those treated near room temperature, at 150–365°, and above 400°, respectively. These three groups show a parallelism in the OH absorptions; for example, the OH stretching in the sample of 150–365° is observed at 3100 cm^{-1} , shifted considerably from that of the ordinary water, such as shown in other groups. Moreover, the scissoring vibration of 1530 cm^{-1} is at an irregularly lower frequency, which probably indicates a shorter distance of metal–water bonding. The strong band of 925 cm^{-1} was assigned as an OH_2 rocking mode because this band shifted to 715 cm^{-1} in a deuterated nickel sulfate heated at 300°

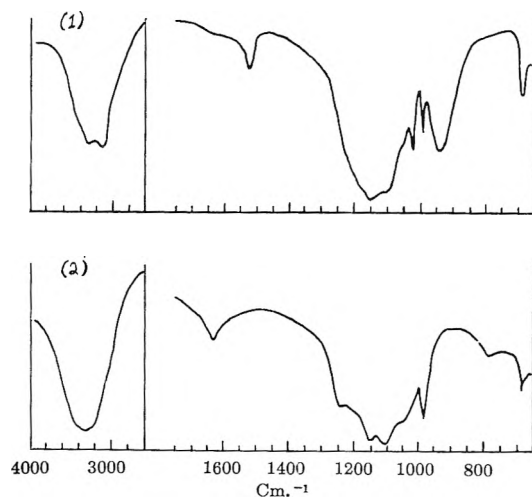


Figure 5. (1) Infrared spectra of nickel sulfates treated at 365° (in KBr). (2) Infrared spectra of nickel sulfates (550° treated) left in air overnight absorbing about 2 moles of water (in KBr).

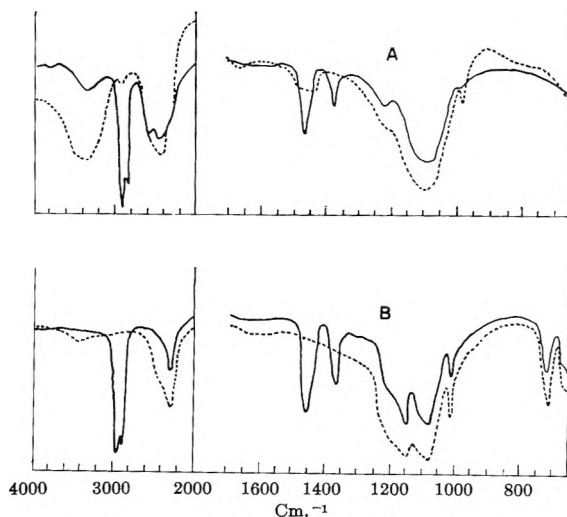


Figure 6. Infrared spectra of (A) nickel sulfate $\text{NiSO}_4 \cdot 7\text{D}_2\text{O}$; (B) A heated at 300°: — in Nujol; - - - in KBr.

(Figure 6), and the 720 cm^{-1} ²⁰ of the same mode observed in $\text{NiSO}_4 \cdot 7\text{H}_2\text{O}$ was not present. As these OH bands disappear in a sample obtained at 400°, a further splitting of SO_4^{2-} occurs. These facts—similar OH_2 and SO_4^{2-} absorption—suggest the structure of the 150° sample (approximately monohydrate) is

(18) K. Nakamoto, J. Fujita, M. Tanaka, and M. Kobayashi, *J. Am. Chem. Soc.*, **79**, 4904 (1957).

(19) C. Rocchiccioli, *Compt. rend.*, **257**, 3851 (1963).

(20) J. Fujita, K. Nakamoto, and M. Kobayashi, *J. Am. Chem. Soc.*, **78**, 3963 (1956); I. Gamo, *Bull. Chem. Soc. Japan*, **34**, 760, 765 (1961); I. Nakagawa and T. Shimanouchi, *Spectrochim. Acta*, **20**, 429 (1964).

maintained up to 350–365°. The OH absorption which is sometimes observed in the sample prepared above 450° may be due to the moisture absorbed after preparation of the specimen. These specimens do not show the absorption of the monohydrate but rather indicate a direct formation of a hexa- or heptahydrate.

(3) *E.s.r. and N.m.r.* (Figures 7, 8). Since modification of the crystal structure or some strain in a lattice was thought to be responsible for the significant acidity of the nickel sulfate heated at 150–400°, a paramagnetic resonance study was undertaken. There is no detectable e.s.r. signal for $\text{NiSO}_4 \cdot 7\text{H}_2\text{O}$ near 3000 gauss using an ordinary x band (0.3 cm.^{-1}). However, when the symmetry of the crystal is lowered or the crystal field is weakened, the extent of this splitting can be decreased to give a possibility for detecting an e.s.r. by the x band. It was only at about 150°, when the acidity of catalyst is significant, that the e.s.r. signal becomes strong enough to be recognized. This signal increases as the temperature of heat treatment is raised, gradually attaining a maximum value. It abruptly reduces its intensity above 400°, with a little signal still remaining in a 600° specimen. A relative intensity of these signals was calculated as an area by taking d^2h (half-width = d , height = h) from the differential graph. It was found to be related to the number of the acid sites previously measured,²³ as well as to the catalytic activity. If the intensity thus obtained is taken to mean some disorder within a crystal, the acidity and the activity of the catalyst appears related to the amount of the unstable phase.

A broad-line n.m.r. spectrum gives two peaks, one narrow and one broad. As the temperature of the heat treatment rises, the area of the narrow band increases, and at the same time the entire signal increases. This expansion happens in spite of the fact that the amount of water is actually decreasing, but the maximum intensity is observed for the 250° sample. Some of the narrow band remains even in 400 and 450° specimens. This indicates more freedom of water molecules in a sample treated at as high a temperature as 400°. The increase of the signal at 150–250° may be due to the influence of a paramagnetic ion (Ni^{2+}) on a spin-lattice relaxation mechanism, the coordinated water being closer to the central ion in the monohydrate.²⁴

(4) *Variation of Specific Heat.* There are three endothermic peaks at 114, 146, and 360°, respectively. They may correspond to the dehydration steps: $6\text{H}_2\text{O} \rightarrow 4\text{H}_2\text{O}$, $4\text{H}_2\text{O} \rightarrow 1\text{H}_2\text{O}$, and $1\text{H}_2\text{O} \rightarrow 0\text{H}_2\text{O}$, respectively.²⁵ The values of ΔH at these temperatures were 23.0, 12.3, and 11.9 kcal./mole, respectively.

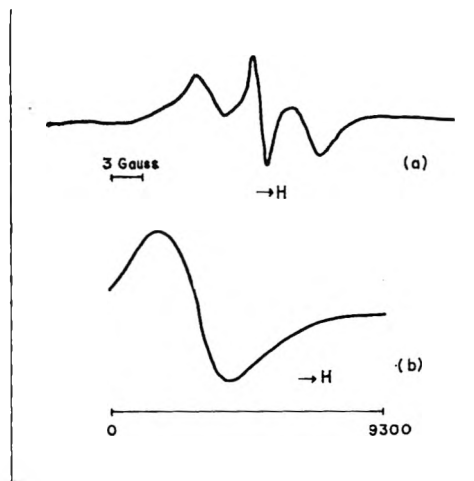


Figure 7. N.m.r. (a) and e.s.r. (b) spectra of nickel sulfates treated at 350°.

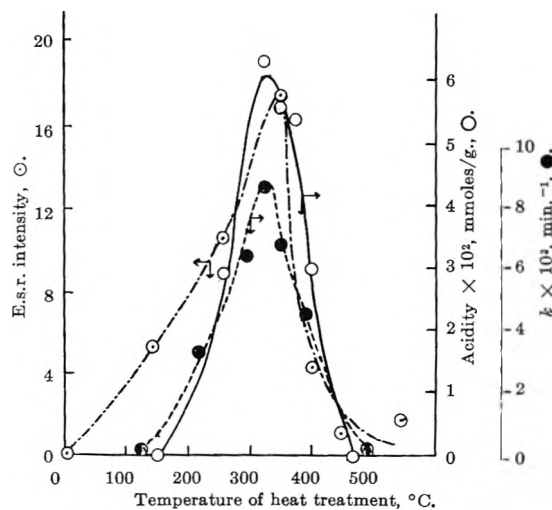


Figure 8. Correlation of e.s.r. intensity with acidities ($\text{p}K_a = -3.0$ in dicinnamalacetone) and catalytic activity (the first-order rate constant for paraldehyde depolymerization at 30°).⁴

(21) Unfortunately, the samples of infrared and X-ray analyses were not from the same batch. The X-ray analysis of the 350° specimen gives 47% of NiSO_4 , but the infrared gives no anhydrous band. This discrepancy may be due to variation in temperature of treatment and difficulty in obtaining a homogeneous specimen. The infrared sample of the 365° specimen consists of a mixture of two phases similar to the 350° specimen used for the X-ray studies. This difference is close to the temperature range ($\pm 5^\circ$) of the heat treatment for the specimen preparation.

(22) K. Ohno, *J. Phys. Soc. Japan*, 8, 802 (1953).

(23) We are comparing a strong acid site measured against dicinnamalacetone ($\text{p}K_a = -3.0$); cf. ref. 4.

(24) For line broadening in paramagnetic solids, see, for example, D. J. Kroon, *Philips Res. Rept.*, 15, 501 (1960).

(25) C. Duval, "Inorganic Thermogravimetric Analysis," translated by R. E. Oesper, 2nd Ed., Elsevier Publishing Co., Amsterdam, 1963.

(5) *Estimation of Lewis Acidity.* The catalyst prepared at 300, 350, and 400° gave Lewis acid sites¹³ of 2.9×10^{-7} , 2.7×10^{-7} , and 3.2×10^{-7} mole/g., respectively. These values are rather small in comparison to the total acidities ($\sim 10^{-4}$ mole/g.)³ obtained by the Benesi method.²⁶

Discussion

Significant acidity appears for the nickel sulfate dehydrated by heating as far as the state of the monohydrate, *i.e.*, above 150°. The acidity attains a maximum at about 0.5 mole of H₂O and decreases sharply thereafter. Tarama, *et al.*,⁷ postulated a residual water to generate a Brønsted acid. We are, however, inclined to believe that the acidity of nickel sulfate is that of both a Brønsted acid (B-acid) and a Lewis acid (L-acid) and that the acidity is associated with a metastable structure. Our reasoning is based on the foregoing experimental results summarized as follows.

(1) The monohydrate crystallinity decreases from that of a 150° specimen to a 350° specimen as revealed in the broadening of the reflection line. The contrary is the tendency of the anhydrous phase (350–550°) since line sharpening occurs at higher temperatures. Deformation of the lattice of both phases (NiSO₄·H₂O and NiSO₄) is the greatest for the 300–350° specimen, which is exactly the range observed for maximum appearance of the surface acidity.²⁷ The temperature range of lowered symmetry (150–350°) coincides with that of the appearance of the e.s.r. signal.

(2) The characteristic infrared absorption of SO₄²⁻ observed in the monohydrate persists continuously in the samples treated at 150–350°, and the pattern changes considerably above 400°. This observation suggests two forms of anhydrous NiSO₄, where the transition takes place near that temperature (365–400°). The infrared spectrum of the sample obtained at 365° consists of the peaks of these two forms.

(3) If the relative intensity of the e.s.r. signal can be related to a strain or disorder of the crystal, the maximum intensity at 350°—the same temperature as that of the highest acidity of the catalyst—may mean the greatest disorder within the crystal. This is in good agreement with the observations made from X-ray and infrared analyses in that the monohydrate structure is maintained up to 400°, supporting the change from metastable to stable NiSO₄ at 365–400°.

(4) The catalyst obtained at 550°, presumably of NiSO₄(stable), is converted to a hexa- or heptahydrate directly when moisture is admitted over the salt.^{28,29} This is also true for the sample obtained at 400–450° which contains some water. The n.m.r. spectrum of the 450° sample indicates a relatively free H₂O mole-

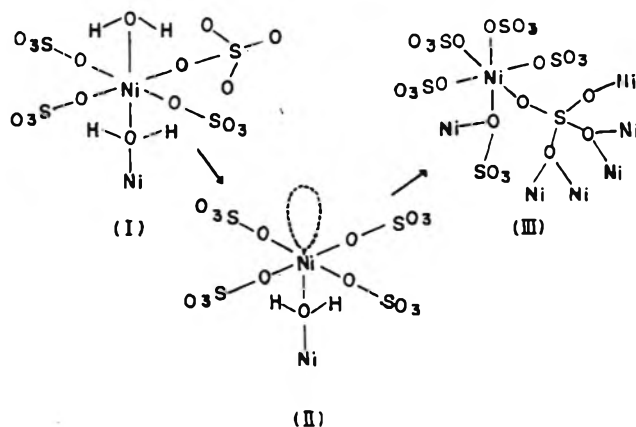
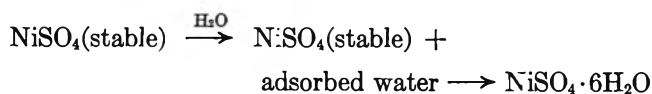
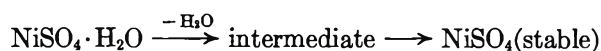


Figure 9. Structure of NiSO₄·H₂O (I), NiSO₄ (III), and metastable NiSO₄·xH₂O (II).

cule. These observations lead to the conclusion that the conversion NiSO₄(stable) → NiSO₄(metastable) → NiSO₄·H₂O is unlikely and that the following conversion probably takes place



Since the appearance of the acid sites and, therefore, activity of nickel sulfate seem to be closely related to the transition intermediate in the process



we propose that the acidity is attributed to an intermediate metastable structure as presented in Figure 9.³⁰ This has a vacant orbital (II) before the known monohydrate³¹ (I) is thermally converted to the known form (III).²⁹ Where the typical L-acid such as BF₃ and AlCl₃ owes its acidity to a vacant p orbital, the L-acidity of nickel sulfate can be ascribed to its vacant sp³d² orbital.

It is of interest at this stage to compare this model with a similar analog in a homogeneous case. The present model can be visualized as a solid-surface counterpart of the transient intermediate in an S_N1-type displacement of a ligand in a complex.³² For

(26) H. A. Benesi, *J. Phys. Chem.*, **61**, 970 (1957).

(27) We intend to study further the relationship between the strain in the crystal and the acidity of nickel sulfate.

(28) No typical monohydrate structure appears, but those of hexa- or heptahydrate do appear in both X-ray and infrared studies.

(29) P. I. Dimaras, *Acta Cryst.*, **10**, 313 (1957).

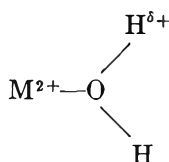
(30) We are indebted to Professor D. D. Eley for discussion of this model.

(31) J. Coing-Boyat and G. Bassi, *Compt. rend.*, **256**, 1482 (1963).

(32) F. Basolo and R. G. Pearson, "Mechanisms of Inorganic Reaction," John Wiley and Sons, Inc., New York, N. Y., 1958, p. 76.

example, a recent study of nickel(II) complexes by Hammes and Morrell³³ and others³² strongly indicates that the rate of loss of an H₂O molecule from the hydrated complex is a slow step regardless of an incoming nucleophile since the several nucleophilic reactions proceed at an identical rate. The evidence for less than six-coordination is a recently reported species as a tetrahedral Co²⁺(H₂O)₄ by the loss of the water at 94.5° in a solution.³⁴ It is thus interesting to recall that the solid surface can often accommodate an otherwise unstable cationic species as reviewed by Leftin and Hobson.³⁵

B-Acidity is postulated to arise from two sources by a second-order interaction.³⁶ One is from the water coordinated as in II.



The other type of the B-acidity may be due to the surface water acidified by a neighboring positive Lewis acid center through an inductive or field effect.³⁷ The B-acid sites will, of course, generate stronger acidity in the vicinity of a greater number of such L-acid sites. It is conceivable that some disorder in the crystal or reduction of the symmetry by forming such a vacant orbital makes this structure an unstable one. The X-ray results are compatible with the contention that the greatest strain in both phases, NiSO₄·H₂O and NiSO₄, is observed for specimens of 300–400°. A weakening in the crystal field due to loss of symmetry could decrease the zero-splitting in the case of the e.s.r. This is exactly what is found, namely, appearance of a maximum coinciding with that of the

350° specimen in the ordinary x -band region. It is also reasonable to postulate that the existence of these empty orbitals responsible for the catalytic activity will be possible only when supported with a regular monohydrate structure (I). When the amount of monohydrate (I) is reduced to a certain critical amount, the metastable anhydrous salt structure (II) apparently cannot be maintained and is converted abruptly to the stable structure (III) where H₂O is no longer necessary for stabilization of the structure. This postulate is verified by the n.m.r. and infrared spectra of the anhydrous salt which inadvertently absorbed atmospheric moisture. The n.m.r. and infrared spectra of this salt are more like those of the hexahydrate, where water is relatively weakly coordinated in comparison to that of the monohydrate.

Acknowledgment. The authors are indebted to Professor J. Sohma and Mr. T. Komatsu, of the Department of Engineering, and to Professor M. Kaneko and Dr. K. Hikichi, of the Department of Polymer Science, for the e.s.r. and n.m.r. measurements and for the discussion of the spectra. We also thank Professor K. Miyahara for his mass spectroscopic measurement of heavy water and Miss T. Sano and Messrs. T. Ido, T. Yamaguchi, and K. Arata for their earnest cooperation in part of the experimental work.

(33) G. G. Hammes and M. L. Morrell, *J. Am. Chem. Soc.*, **86**, 1497 (1964).

(34) T. J. Swift and R. E. Connick, *J. Chem. Phys.*, **37**, 307 (1962).

(35) H. P. Leftin and M. C. Hobson, Jr., *Advan. Catalysis*, **14**, 115 (1963).

(36) For Lewis and Brønsted sites in a typical solid acid, silica alumina, see, for example, N. R. Basila, T. R. Kantner, and K. H. Rhee, *J. Phys. Chem.*, **68**, 3197 (1964), and references cited therein.

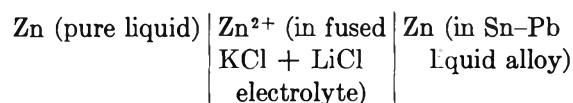
(37) L-Sites do not have to be on the surface.

Galvanic Cell Measurement of the Thermodynamic Interaction between Zinc and Lead in Dilute Solution in Liquid Tin

by S. T. Cleveland, K. Okajima, and R. D. Pehlke

Department of Chemical and Metallurgical Engineering, University of Michigan, Ann Arbor, Michigan
(Received March 31, 1965)

The interaction parameters of the ternary system tin-zinc-lead and the binary system tin-zinc were determined over the temperature range 450–650° using an electromotive force measuring technique. The concentration cell employed was



The experimental results show that the activity of zinc in the dilute binary system tin-zinc deviates only slightly from Henry's law behavior. In the ternary system tin-zinc-lead, small additions of lead tend to increase the activity of zinc in dilute solution with solvent tin. The zinc-zinc and zinc-lead interaction parameters were found to be a linear function of the reciprocal absolute temperature and can be expressed by the relations $\epsilon_{\text{Zn}}^{\text{Zn}} = -642/T + 1.02$ and $\epsilon_{\text{Zn}}^{\text{Pb}} = 2080/T - 0.30$.

Introduction

Thermodynamic interaction between solutes in metallic solutions has been of considerable interest in recent years, and much effort has been expended to develop a general model for these relationships. Several empirical approaches have been presented which attempted to predict these interactions with quantitative accuracy. Himmler¹ based his analysis on variation in electron to atom ratio, Ohtani and Gokcen² used periodicity, and Alcock and Richardson³ developed a model based on chemical binding considerations. These attempts have failed to provide an accurate predictive model that could be generally applied beyond a few selected systems.

In the development of a general model that will quantitatively predict interaction parameters for binary, ternary, and higher order systems, much needs to be accomplished in providing experimental data on atomic interactions, especially in ternary and higher order systems. It is with this purpose that the present study was undertaken.

Wagner⁴ has derived a useful relationship for expressing solute interactions in dilute solutions. He pro-

posed a Taylor series expansion of the activity coefficient around zero mole fraction for correlation purposes. The form of the expansion is

$$\ln \gamma_i = \ln \gamma_i^0 + \left[x_j \left(\frac{\partial \ln \gamma_i}{\partial x_j} \right)_{x_i=x_j=0} + x_j \left(\frac{\partial \ln \gamma_i}{\partial x_j} \right)_{x_i=x_j=0} + \dots \right] + \dots + \left[\frac{1}{2} x_i^2 \left(\frac{\partial^2 \ln \gamma_i}{\partial x_i^2} \right)_{x_i=x_j=0} + x_i x_j \left(\frac{\partial^2 \ln \gamma_i}{\partial x_i \partial x_j} \right)_{x_i=x_j=0} + \dots \right] \quad (1)$$

The second-order partial derivatives are neglected as a first approximation, and the resulting first-order partial derivatives, termed interaction parameters, are represented by the notation

- (1) W. Himmler, *Z. physik. Chem. (Leipzig)*, **195**, 244 (1950).
- (2) N. A. Gokcen and M. Ohtani, *Trans. AIME*, **218**, 533 (1960).
- (3) C. B. Alcock and F. D. Richardson, *Acta Met.*, **6**, 385 (1959).
- (4) C. Wagner, "Thermodynamics of Alloys," Addison-Wesley Press, Inc., Cambridge, Mass., 1952. p. 52.

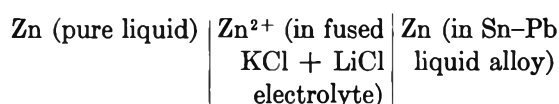
$$\epsilon_i^i = \left[\frac{\partial \ln \gamma_i}{\partial x_i} \right]_{x_i = x_j = 0} \quad \epsilon_i^j = \left[\frac{\partial \ln \gamma_i}{\partial x_j} \right]_{x_i = x_j = 0}$$

This yields the simplified relationship

$$\ln \gamma_i = \ln \gamma_i^0 + x_i \epsilon_i^i + x_j \epsilon_i^j + x_k \epsilon_i^k + \dots \quad (2)$$

Experimental Section

Method. The experimental investigation employed galvanic cells with liquid chloride electrolytes of the type



The reversible electromotive force of the cell was measured over the temperature range 450–650°. The activity coefficient of zinc was calculated using the equation

$$\gamma_{\text{Zn}} = \frac{e^{-nFE/RT}}{X_{\text{Zn}}} \quad (3)$$

where γ_{Zn} is the activity coefficient of zinc, X_{Zn} is the mole fraction of zinc, n is the number of equivalents, F is Faraday's constant, E is the cell potential, R is the gas constant, and T is the absolute temperature. Evaluation of the interaction parameters was achieved using graphical techniques.

The experimental equipment is shown schematically in Figure 1. A Vycor tube, 68.6 cm. in length and 6.4 cm. in o.d., was used to hold the galvanic cell. The tube was provided with a ground-glass removable head and inlet arms for vacuum and gas supplies. The Pyrex head had five outlets through which the electrode leads and thermocouple were passed.

A recrystallized alumina crucible was used as a container for the galvanic cell crucibles and the fused electrolyte salt. Five smaller recrystallized alumina crucibles were placed symmetrically in the large crucible.

The furnace was supplied with power from a 230-v. transformer, which was wired so that a constant voltage difference could be tapped independent of the absolute voltage setting. The furnace temperature was controlled by a recording potentiometer which allowed either the higher or the lower voltage to be imposed on the furnace windings.

The chromel–alumel control thermocouple was placed against the furnace tube at the level where the galvanic cell apparatus was positioned. This thermocouple arrangement maintained a temperature variation of less than $\pm 2^\circ$ in the galvanic cell itself.

A helium atmosphere was maintained over the cell. The helium gas was passed through a calcium sulfate drying tower, then through a small copper gauze re-

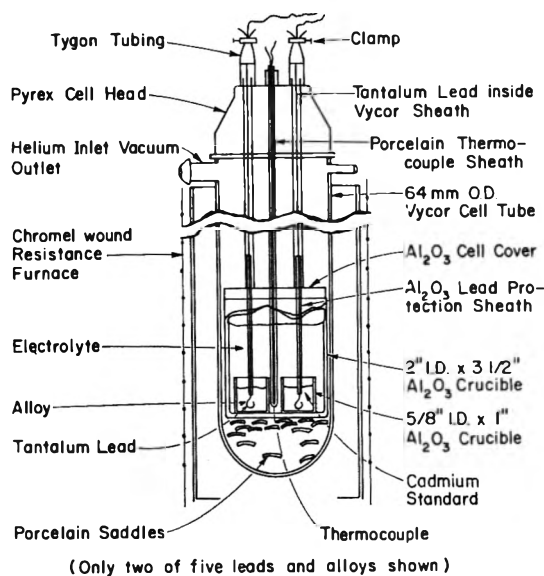


Figure 1. Experimental cell assembly.

sistance furnace at 500°, and finally through another calcium sulfate drying tower. A Leeds and Northrup No. 8687-v. potentiometer was used to measure the electromotive force of the galvanic cells and the chromel–alumel thermocouple.

The electrolytic salt was a mixture of 53% potassium chloride, 42% lithium chloride, and 5% zinc chloride by weight. All of these were reagent grade chemicals. The zinc, lead, and tin used in the experiments were of 99.999+ % purity.

Procedure. The tantalum electrode leads were carefully cleaned before each run with emery cloth to ensure better contact. Each electrode lead was next fitted with a 12.7-cm. recrystallized alumina shield. This shield was drawn to within 0.64 cm. of the end that would be in contact with the molten metal solution. The exposed tip was then bent in the shape of a circular ring of approximately the diameter of the recrystallized alumina shield.

The metals were weighed out to 0.0001 g. on an automatic analytical balance. The weighed metals were placed into the small alumina crucibles and then stored in a desiccator until the sinking operation.

In sinking the electrode leads, three of the alloy electrode crucibles, along with a crucible containing pure zinc as a standard, were placed symmetrically in a steel sinking cup. The entire assembly was placed in the Vycor cell tube, which was evacuated and flushed with helium gas prior to establishing a helium atmosphere at a slight positive pressure. The tube was lowered into a furnace maintained at 450°.

After melting, the helium supply pressure was increased, and each electrode clamp was loosened in

turn, after which each electrode was pushed down into its respective alloy until the bottom of the crucible was reached. The electrode tips were then swirled for 2 min. in a vertical direction to wet the surface. The electrode was then positioned slightly above the bottom of the crucible, not touching any of the walls, and clamped in place. Approximately 15 min. after sinking the electrodes, the tube was lifted out of the furnace and allowed to cool to room temperature under the helium atmosphere.

The mixture of potassium chloride and lithium chloride of approximately eutectic composition was prepared in advance. The salt was vacuum dried in the liquid state at a temperature of 500°. The zinc chloride was dried separately at 200°.

Five presunk electrode crucibles, including four alloy compositions and a pure zinc standard, were positioned symmetrically around the inside edge of the larger recrystallized alumina crucible. The electrode leads were then shielded with 91.4 cm. of small-diameter Vycor tubing, and the lead was run up through the outlets in the tube head. A chromel-alumel thermocouple was also placed in the cell in a Vycor protective shield. The zinc chloride was added to the crucible, and the eutectic salt mixture was immediately poured over the electrode crucibles. The salts occupied approximately three-fourths of the total height of the large crucible. The alundum cover was brought down flush with the top of the crucible, and the cell assembly was positioned in the large Vycor tube. A helium atmosphere was established in the tube which was then positioned in the furnace.

The cell was maintained at 500° for approximately 24 hr. to allow the system to reach a steady state. The e.m.f. readings were taken at 20-min. intervals over a 2-hr. period at each temperature investigated. These values were averaged in subsequent calculations.

Results

The activity of zinc in the binary liquid system tin-zinc was first reported in 1923 by Taylor.⁵ More recently, additional results^{6,7} have been reported for the tin-zinc system. The results for this binary obtained in the present investigation are summarized in Table I. Figure 2 shows the excellent agreement between the present study and the work of Taylor⁵ and Sano, Okajima, and Tatsuo.³ The experimental results on the ternary system tin-zinc-lead are summarized in Table II.

Using interpolated values for the activity coefficient, plots of $\ln \gamma_{Zn}$ vs. mole fraction of zinc were constructed for constant mole fractions of lead. The natural logarithm of the activity coefficient of zinc

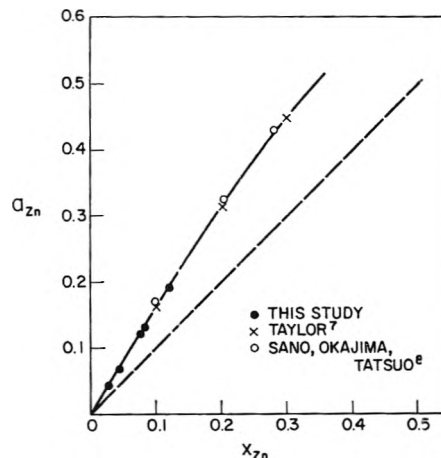


Figure 2. Activity of zinc vs. mole fraction of zinc in tin at 550°.

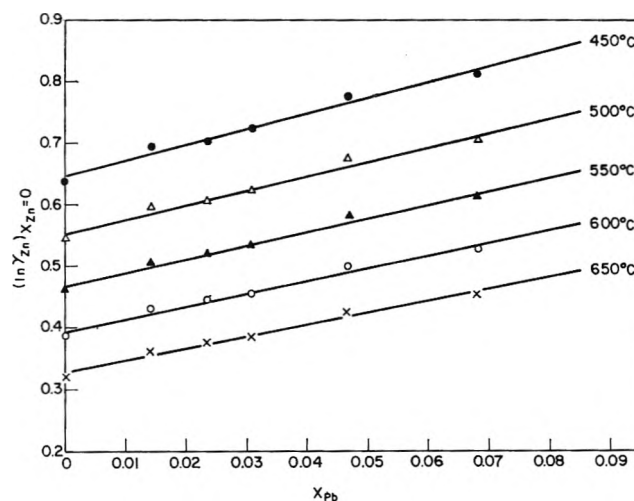


Figure 3. Determination of lead-zinc interaction in liquid tin: natural logarithm of zinc activity coefficient at infinite zinc dilution vs. mole fraction of lead.

varied linearly with the mole fraction of zinc. The intercepts for these plots are values of $\ln \gamma_{Zn}$ for various mole fractions of lead at $X_{Zn} = 0$. These results permitted the preparation of a plot of $\ln \gamma_{Zn}$ vs. X_{Pb} for zero mole fraction of zinc, as shown in Figure 3. The slope of the resulting curve at zero mole fraction of lead is the magnitude of the interaction parameter

$$\text{slope (at } X_{Pb} = 0) = \left[\frac{\partial \ln \gamma_{Zn}}{\partial X_{Pb}} \right]_{X_{Zn} = X_{Pb} = 0} = \epsilon_{Zn}^{Pb}$$

(5) N. W. Taylor, *J. Am. Chem. Soc.*, **45**, 2865 (1923).

(6) K. Sano, K. Okajima, and S. Tatsuo, *Mem. Fac. Eng. Nagoya Univ.*, **5**, 299 (1953).

(7) T. Yokokawa, A. Doi, and K. Niwa, *J. Phys. Chem.*, **65**, 202 (1961).

Table I: Experimental Results of Sn-Zn System

T, °C.	$X_{Zn} = 0.0267$			$X_{Zn} = 0.0267$			$X_{Zn} = 0.0431$			$X_{Zn} = 0.0431$		
	E, mv.	a_{Zn}	γ_{Zn}	E, mv.	a_{Zn}	γ_{Zn}	E, mv.	a_{Zn}	γ_{Zn}	E, mv.	a_{Zn}	γ_{Zn}
450	92.91	0.0506	1.89	93.06	0.0504	1.89	78.41	0.0807	1.87	78.81	0.0796	1.85
500	102.44	0.0461	1.73	102.52	0.0460	1.72	86.82	0.0737	1.71	87.20	0.0729	1.69
550	111.96	0.0425	1.59	111.98	0.0425	1.59	95.23	0.0682	1.58	95.60	0.0675	1.56
600	121.49	0.0395	1.48	121.44	0.0396	1.48	103.65	0.0636	1.47	103.99	0.0630	1.46
650	131.01	0.0371	1.39	130.90	0.0372	1.39	112.06	0.0597	1.38	112.38	0.0592	1.37
T, °C.	$X_{Zn} = 0.0750$			$X_{Zn} = 0.0825$			$X_{Zn} = 0.0825$			$X_{Zn} = 0.1188$		
	E, mv.	a_{Zn}	γ_{Zn}	E, mv.	a_{Zn}	γ_{Zn}	E, mv.	a_{Zn}	γ_{Zn}	E, mv.	a_{Zn}	γ_{Zn}
450	61.35	0.140	1.86	58.25	0.154	1.87	58.62	0.152	1.85	47.21	0.220	1.85
500	68.44	0.128	1.71	65.18	0.141	1.71	65.49	0.140	1.70	53.14	0.203	1.71
550	75.52	0.119	1.58	72.10	0.131	1.59	72.36	0.130	1.58	59.07	0.189	1.59
600	82.61	0.111	1.48	79.02	0.122	1.48	79.22	0.122	1.48	65.00	0.178	1.50
650	89.70	0.105	1.40	85.95	0.115	1.40	86.09	0.115	1.39	70.92	0.168	1.41

Table II: Experimental Results of Sn-Zn-Pb System

X_{Pb}	T, °C.	$X_{Zn} = 0.0150$			$X_{Zn} = 0.0252$			$X_{Zn} = 0.0409$			$X_{Zn} = 0.0744$		
		E, mv.	a_{Zn}	γ_{Zn}	E, mv.	a_{Zn}	γ_{Zn}	E, mv.	a_{Zn}	γ_{Zn}	E, mv.	a_{Zn}	γ_{Zn}
0.0142	450	110.90	0.0284	2.00	92.95	0.0506	2.02	71.18	0.102	2.03	58.53	0.153	2.04
	500	121.87	0.0257	1.81	102.55	0.0460	1.84	79.46	0.0920	1.84	65.74	0.139	1.85
	550	132.85	0.0236	1.66	112.14	0.0423	1.69	87.73	0.0842	1.68	72.95	0.128	1.70
	600	143.82	0.0218	1.54	121.74	0.0393	1.57	96.00	0.0779	1.55	80.17	0.119	1.58
	650	154.79	0.0204	1.43	131.33	0.0368	1.47	104.27	0.0726	1.45	87.38	0.111	1.48
0.0235	450	108.68	0.0305	2.01	92.41	0.0515	2.02	71.27	0.101	2.03	59.31	0.149	2.01
	500	119.40	0.0277	1.82	102.00	0.0468	1.83	79.44	0.0920	1.84	66.54	0.136	1.83
	550	130.12	0.0255	1.68	111.59	0.0430	1.69	87.62	0.0845	1.69	73.77	0.125	1.68
	600	140.84	0.0236	1.56	121.17	0.0399	1.56	95.79	0.0783	1.57	81.00	0.116	1.56
	650	151.56	0.0221	1.46	130.76	0.0373	1.46	103.97	0.0732	1.47	88.23	0.109	1.46
0.0307	450	108.65	0.0306	2.04	91.86	0.0524	2.07	70.76	0.103	2.08	58.87	0.151	2.04
	500	119.53	0.0276	1.84	101.46	0.0475	1.88	78.95	0.0934	1.88	66.13	0.137	1.85
	550	130.42	0.0253	1.68	111.06	0.0436	1.73	87.15	0.0856	1.72	73.40	0.126	1.70
	600	141.31	0.0233	1.56	120.66	0.0404	1.60	95.34	0.0793	1.59	80.66	0.117	1.58
	650	152.19	0.0218	1.45	130.26	0.0378	1.50	103.53	0.0740	1.49	87.93	0.110	1.48
0.0468	450	106.37	0.0329	2.14	90.73	0.0543	2.16	69.94	0.106	2.12	58.78	0.152	2.08
	500	117.25	0.0296	1.93	100.37	0.0491	1.95	77.94	0.0963	1.93	66.18	0.137	1.88
	550	128.12	0.0270	1.76	110.01	0.0449	1.78	85.94	0.0886	1.77	73.57	0.126	1.72
	600	139.00	0.0248	1.62	119.65	0.0415	1.65	93.94	0.0823	1.65	80.97	0.116	1.59
	650	149.88	0.0231	1.50	129.29	0.0387	1.54	101.94	0.0770	1.54	88.37	0.108	1.49
0.0680	450	105.51	0.0338	2.25	90.40	0.0549	2.20	69.47	0.107	2.15	56.87	0.161	2.15
	500	116.39	0.0304	2.02	100.07	0.0495	1.98	77.53	0.0975	1.95	64.15	0.146	1.94
	550	127.27	0.0276	1.84	109.75	0.0453	1.81	85.60	0.0894	1.79	71.42	0.133	1.78
	600	138.15	0.0254	1.69	119.42	0.0418	1.67	93.66	0.0829	1.66	78.70	0.123	1.65
	650	149.02	0.0236	1.57	129.09	0.0389	1.56	101.72	0.0774	1.55	85.98	0.115	1.53

A confirming graphical procedure was used to substantiate the results obtained by the procedure described above. This involved finding the slope of a plot of $\ln \gamma_{Zn}$ vs. mole fraction of lead at $X_{Pb} = 0$ for constant mole fraction of zinc. A final plot of $\partial \ln \gamma_{Zn} / \partial X_{Pb}$ vs. mole fraction of zinc was extrapolated

to zero mole fraction of zinc to give the desired interaction parameter

$$\text{intercept (at } X_{Zn} = 0) = \left[\frac{\partial \ln \gamma_{Zn}}{\partial X_{Pb}} \right]_{X_{Zn} = X_{Pb} = 0} = \frac{Pb}{\epsilon_{Zn}}$$

The procedure described for the ternary system was

also used to determine the zinc-zinc interaction parameter. A plot of $\ln \gamma_{Zn}$ vs. X_{Zn} for $X_{Pb} = 0$ is shown in Figure 4. The slope of these lines is the self-interaction parameter for zinc.

A relationship was derived by Dealy and Pehlke⁸ that indicated a linear relationship between the interaction parameter and the reciprocal of the absolute temperature. This relationship was of the form

$$\frac{d\epsilon_i^j}{d\left(\frac{1}{T}\right)} = \frac{1}{R} \left[\frac{\partial^2 H}{\partial X_i \partial X_j} \right]_{X_i=X_j=0} \quad (4)$$

This equation is valid if the right-hand derivative is not a strong function of temperature. The interaction parameters ϵ_{Zn}^{Pb} and ϵ_{Zn}^{Zn} are summarized in Table III. These interaction parameters show a strict linearity with reciprocal absolute temperature as predicted by eq. 4.

$$\epsilon_{Zn}^{Zn} = -\frac{642}{T} + 1.02$$

$$\epsilon_{Zn}^{Pb} = \frac{2080}{T} - 0.30$$

Discussion

The reversibility of the galvanic cell being measured is one of the most important considerations in the present study. One technique employed to assure cell reversibility was to observe the trend of the experimental data. It has been the experience of many researchers that side reactions or some other source of irreversibility will cause a decided drift in e.m.f. readings. Furthermore, the readings at a temperature will not be reproducible when approaching the same temperature from the opposite side. The present analysis only included those cells which showed reproducibility and no significant drift in e.m.f. at a particular temperature.

Table III: Interaction Parameters of Sn-Zn-Pb System

T, °C.	ϵ_{Zn}^{Zn}	ϵ_{Zn}^{Pb}
450	0.13	2.5
500	0.18	2.4
550	0.23	2.2
600	0.28	2.1
650	0.33	2.0

Oxygen, which would react with the cell materials, was kept out of the system by precautions in handling and in the maintenance of a helium atmosphere in the

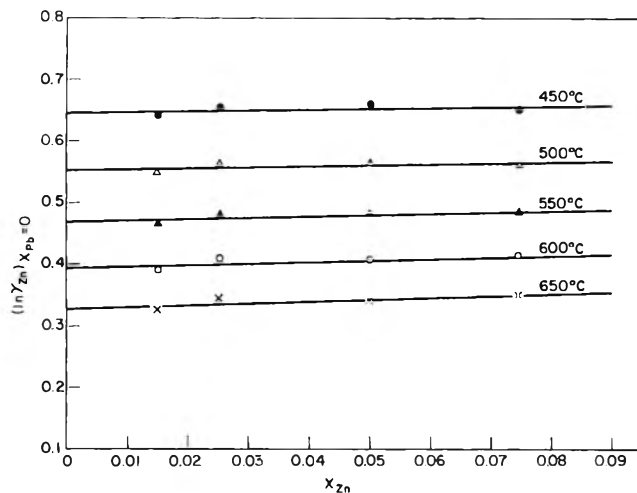
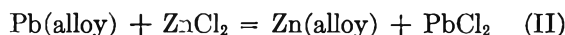
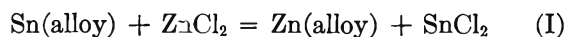


Figure 4. Determination of self-interaction parameter for zinc in liquid tin: natural logarithm of zinc activity coefficient in tin-zinc binary vs. mole fraction of zinc.

Vycor tube. Water vapor absorption leading to side reactions could occur during the salt transfer before the actual run. The cell assembly was lowered into the Vycor tube, and the helium atmosphere was introduced as quickly as possible to minimize this source of error.

Wagner and Werner⁹ have derived a relationship for estimating the error in e.m.f. measurements caused by displacement reactions. Their relationship is based on the differences in free energy of formation of the chlorides of the least noble metal and the other alloying elements present. The displacement reactions that are of interest here are



It was estimated that less than 1% error in potential should occur under conditions where 1 mole % zinc was present with 10 mole % lead and 89 mole % tin in an electrode at 550°.

Another important aspect to be considered is that the electrolyte must show only ionic conductance and the equivalence of the zinc must not fluctuate. Zinc chloride can dissolve an appreciable amount of zinc metal that might promote some nonionic behavior. However, Taylor⁵ and Seltz¹⁰ found that this undesirable effect can be virtually eliminated by dissolving only a small amount of chloride in the eutectic lithium chloride-potassium chloride mixture. The experi-

(8) J. M. Dealy and R. D. Pehlke, *Trans. AIME*, **227**, 88 (1963).

(9) C. Wagner and A. Werner, *J. Electrochem. Soc.*, **110**, 326 (1963).

(10) H. Seltz, *ibid.*, **77**, 233 (1940).

mental procedure on salt preparation was followed as outlined by Seltz.¹⁰

The valence of zinc in the electrolyte and the ionic nature of the conductance of the electrolyte were examined experimentally in a Faraday yield experiment.¹¹ This test was carried out using an external current source to transfer a given weight of zinc between a pure zinc standard and an alloy electrode (a bismuth base alloy containing a small amount of zinc and gallium). The electrolyte used was the same as that employed in all of the experiments of the present study. After transferring a given amount of zinc, the potential of the alloy electrode was measured and found to correspond to that calculated for 100% ionic current efficiency and for a zinc valence in the electrolyte of 2. The current was then reversed, and the same number of coulombs passed through the cell in the opposite direction. The alloy electrode returned to its original potential. This experiment directly verified that the electrolyte is purely an ionic conductor and that the zinc valence is 2.

The thermocouple was calibrated by comparing the recorded melting point with the known melting point of lead. The same apparatus and conditions as described for an actual run were used for the calibration. The thermocouples were found to be accurate (no correction necessary) at this point.

A statistical analysis was carried out on these data to establish the accuracy of the experimental results. The technique used a linear regression with one dependent variable. The 90% confidence level indicated was ± 0.2 for the interaction parameters ϵ_{Zn}^{Pb} and ϵ_{Zn}^{Zn} . This represents less than 10% of the values for ϵ_{Zn}^{Pb} . For ϵ_{Zn}^{Zn} , however, this represents a value which is about the same order as the parameter itself.

Conclusions

The binary data in the current work are consistent with previous work. The ternary system measurements showed that a small concentration of lead will increase the activity of zinc in the solvent tin. In the binary, Henry's law is closely followed; *i.e.*, the self-interaction parameter for zinc is very small. The binary and ternary interaction parameters showed a linear relationship with reciprocal temperature, which can be expressed by the relations

$$\epsilon_{Zn}^{Zn} = -\frac{642}{T} + 1.02$$

$$\epsilon_{Zn}^{Pb} = \frac{2080}{T} - 0.30$$

(11) J. V. Gluck, Ph.D. Thesis, University of Michigan, 1965.

A Gas Phase Electron Diffraction Study of *cis*-Dichloroethylene

by M. I. Davis

Department of Chemistry, The University of Texas, Austin, Texas

and H. P. Hanson

Department of Physics, The University of Texas, Austin, Texas (Received April 1, 1966)

The molecular structure of *cis*-dichloroethylene has been investigated by the gas phase electron diffraction method. The proposed structure is $r(\text{C}=\text{C}) = 1.354 \pm 0.005 \text{ \AA}$, $r(\text{C}-\text{Cl}) = 1.718 \pm 0.007 \text{ \AA}$, $\angle \text{CCCl} = 123.8 \pm 0.5^\circ$, $r(\text{C}-\text{H}) = 1.075 \pm 0.015 \text{ \AA}$, and $\angle \text{CCH} = 132 \pm 3^\circ$.

Introduction

The relative simplicity of the molecular structures of the halogen-substituted ethylenes has made them suitable objects for a wide variety of investigations. It has also led to the possibility of testing and formulating theories of intramolecular interactions, on the basis of comparisons of the measured molecular properties.

One member of this group that has been studied in some detail, but for which no precise molecular dimensions were available, is *cis*-dichloroethylene. Consequently, this compound was a suitable object for a gas phase electron diffraction study. Several previous studies had been made, using this technique,¹ but the level of precision was not sufficient to allow for any useful comparison with the more recent results of microwave and diffraction investigations of allied compounds.

A microwave investigation of this compound has been reported.² Although the molecular dimensions were not available from that study, values were obtained for the three moments of inertia. The existence of that information provides a basis of comparison for the results of the diffraction investigation.

Wilson³ has presented a discussion of trends which exist among the structural parameters of a number of ethylene derivatives and of various theoretical approaches that might be called upon to account for them. The dimensions of this particular compound and those of *cis*-dibromoethylene⁴ provide a further basis for evaluation of current theories.

A combination of the results of vibrational spectroscopic investigations⁵ with thermochemical data⁶ has

led to the evaluation of ΔE° for the *cis-trans* isomerization, showing the *cis* isomer to be the more stable. A tentative explanation for the stability order has been previously presented.⁴

Experimental Section

This investigation is one of the first that has been carried out with the recently constructed electron diffraction unit of The University of Texas. In this unit the high voltage and the electron optics are obtained from a 32-step Canalco electron microscope power supply. The scattering chamber is of the "big tank" variety; in this and several other details the design is similar to the unit operated at the University of Oslo.⁷ The nozzle and cold-trap assemblies are slightly modified versions of those designed by Professor Kenneth Hedberg of Oregon State University.⁸

Intensity data were collected photographically at image distances of 25, 50, and 100 cm. Two different

(1) L. E. Sutton, Ed., "Tables of Interatomic Distances," Special Publication No. 11, The Chemical Society, London, 1958.

(2) W. H. Flygare and J. A. Howe, *J. Chem. Phys.*, **36**, 440 (1961).

(3) E. B. Wilson, Jr., *Tetrahedron*, **17**, 191 (1962).

(4) M. I. Davis, H. A. Kappler, and D. J. Cowan, *J. Phys. Chem.*, **68**, 2005 (1964).

(5) H. J. Bernstein and D. A. Ramsay, *J. Chem. Phys.*, **17**, 556 (1949).

(6) R. E. Wood and D. P. Stevenson, *J. Am. Chem. Soc.*, **63**, 1650 (1941).

(7) O. Bastiansen, O. Hassel, and E. Risberg, *Acta Chem. Scand.*, **9**, 232 (1955).

(8) K. Hedberg, personal communication.

sectors were used: one for the 100-cm. distance, the other for the shorter two.

The photographic plates were developed with the aid of a thermostatically controlled photoprocessor. Values of percentage transmissions were obtained at intervals of $\Delta s = 0.25 \text{ \AA}^{-1}$ from traces of the microphotometer records.

No interference pattern, that could be measured with any expectation of reliability, was observed beyond $s = 32 \text{ \AA}^{-1}$. This is partly due to the large value of the vibrational amplitude for the dominating Cl-Cl atom pair and partly to the significant difference between the atomic phase shifts for carbon and chlorine.

The de Broglie wave lengths were obtained from the diffraction patterns of Au foil.

Preliminary Handling of Data

The transmission values were converted first to optical densities and subsequently, by means of a correction formula of the type proposed by Karle,⁹ to electron intensities.

Corrections were applied to take into account the sectoring of the electron beam and the use of flat photographic plates. The resulting intensity values were multiplied by s^4 , as required by the theoretical considerations (see eq. 1).

There exist several excellent descriptions of the way in which various groups handle their intensity data.¹⁰⁻¹² Where significant differences exist, we have tended to follow the treatment developed by the Oslo group.¹⁰ The major distinction between our procedure and those outlined in the aforementioned articles lies in the use of a numerical method of background separation.

Theory

A brief account will be given here of the various theoretical relationships that have been adopted in the analysis of the experimental data.

The classical angular intensity distribution for an electron beam, scattered by a fixed electron, is given by the well-known Rutherford equation and may be presented in the form

$$I_R(s) = k/s^4 \quad (1)$$

where s , the scattering parameter, equals $4\pi(\sin \theta)/\lambda$, 2θ being the angle of scattering and λ the de Broglie wave length; k is the product of a number of natural and experimental physical constants.

The most convenient form of the experimental intensities, for data-handling purposes, is $I_A(s)$, defined by

$$I_A(s) = I_{EX}(s)/I_R(s) \quad (2)$$

where the $I_{EX}(s)$ terms are the observed intensities

after corrections have been applied for the sector and for the use of flat plates.

The total observed scattering is considered to be made up of two distinct components

$$I_A(s) = B_A(s) + M_A(s) \quad (3)$$

$M_A(s)$ varies in an undulating fashion with the parameter s . This is the interference pattern and will be referred to as the molecular scattering. $B_A(s)$ provides a relatively smooth background for $M_A(s)$. It will be referred to as the atomic scattering, or simply as the background.

In order to avoid unnecessary confusion, it is appropriate that some comment be offered concerning the notation used to signify molecular-scattering intensities. We feel that the choice of M as a symbol is an obvious one. It is necessary, however, to include the subscripts A and B for the experimental and theoretical intensities, respectively, to distinguish them from the $M(s)$ and $M_C(s)$ used by other workers to denote slightly different entities. A comparison of this outline and ref. 11 should assist the reader in grasping the essential difference between the two approaches.

The theoretical expression for the atomic scattering is given by

$$B_B(s) = \sum_i n_i \{ (Z_i - F_i(s))^2 + S_i(s) \} \quad (4)$$

where $F_i(s)$ and $S_i(s)$ are, respectively, the atomic and the inelastic scattering factors of the element with atomic number Z_i ; n_i atoms of this element occur in the molecule.

$F_i(s)$ and $S_i(s)$ may be calculated from the best available wave functions.¹³ The scattering factor values that were employed in this investigation were calculated from Hartree-Slater self-consistent field wave functions.¹⁴

The expression that was adopted for the molecular scattering contribution is given in

$$M_B(s) = \sum_{ij} 2n_{ij} (Z_i - F_i(s))(Z_j - F_j(s)) \times \cos(\eta_i(s) - \eta_j(s)) \times \exp(-l_{ij}^2 s^2 / 2) (\sin(sr_{ij})) / (sr_{ij}) \quad (5)$$

(9) J. Karle and I. L. Karle, *J. Chem. Phys.*, **28**, 957 (1950).

(10) O. Bastiansen and P. N. Skancke, *Advan. Chem. Phys.*, **3**, 323 (1961).

(11) R. A. Bonham and L. S. Bartell, *J. Chem. Phys.*, **31**, 702 (1959).

(12) J. Karle and I. L. Karle, "Determination of Organic Structures by Physical Methods," E. A. Braude and F. C. Nachod, Ed., Academic Press Inc., New York, N. Y., 1955, Chapter X.

(13) See, e.g., N. F. Mott and H. S. W. Massey, "The Theory of Atomic Collisions," 2nd Ed., Oxford University Press, London, 1949.

(14) H. P. Hanson, F. Herman, J. D. Lea, and S. Skillman, *Acta Cryst.*, **17**, 1040 (1964); R. F. Pohler and H. P. Hanson, *J. Chem. Phys.*, in press.

n_{ij} is the number of symmetrically equivalent atom pairs with an internuclear distance r_{ij} and a mean vibrational amplitude l_{ij} . The $\eta_i(s)$ terms are the atomic phase shifts of atom i .¹⁵ In this instance the values of $\eta_i(s)$ were calculated from an empirical formula of Bonham and Ukaji.¹⁶

The derivation of eq. 5 involves the adoption of the harmonic oscillator (H.O.) model. To a first approximation r_{ij} is the H.O. equilibrium distance. A more exact interpretation of that equation, still in the context of the H.O. model, is

$$r_{ij} = r_{\text{H.O.}} - l_{ij}^2/r_{ij} \quad (6)$$

Equation 5 also serves as a reasonable representation for the anharmonic oscillator case. In that instance r_{ij} may be interpreted according to

$$r_{ij} = r_g - l_{ij}^2/r_{ij} \quad (7)$$

where r_g is the mean internuclear distance. Its relationship to the equilibrium value is given, to a reasonable approximation, by¹⁷

$$r_g = r_e + 1.5al_{ij}^2 \quad (8)$$

where a is the Morse potential constant.

Separation of the Atomic and Molecular Scattering Contributions

It is frequently found that the smooth background to an experimental intensity curve does not correspond perfectly with the predictions of eq. 4. The discrepancies are not usually large, and, whether they arise from experimental or theoretical shortcomings, it is advisable to compensate for them. Small deviations in the over-all shape of the background can be corrected for, by means of a simple two-parameter adjustment of the type

$$I_A(s) = aI_A(s)(1 + bs) \quad (9)$$

where a and b are constants which are evaluated by a suitable least-squares procedure, involving the differences between $I_A(s)$ and its theoretical counterpart. For this investigation, the values obtained for the parameter b represent maximum deviations of 1.6% for the 100-cm. curve, 3.5% for the 50-cm. curve, and 8.3% for the 25-cm. curve, from the intensity values obtained by simple normalization. Unless a great deal of error exists in the predicted values of $M_B(s)$, the values calculated for the constants a and b will depend almost exclusively upon the experimental and theoretical values for the background.

In addition to the discrepancies existing between the over-all shapes of the theoretical and experimental backgrounds, there will be differences in the more intimate details of the two total-scattering curves.

It is assumed that the difference curve $\Delta I(s)$ can be split into smooth and undulating components, as expressed in

$$I_A(s) - I_B(s) = \Delta I(s) = \Delta B(s) + \Delta M(s) \quad (10)$$

where $\Delta B(s)$ is assumed to be the best smooth curve that can be fitted to the points of $\Delta I(s)$. The curve $\Delta B(s)$ will contain some undulation, but none so sharp that it might be treated as part of the molecular interference pattern. $\Delta B(s)$ can be obtained graphically, but it may also be evaluated numerically. It is found that functions of the types given in eq. 11a and b will satisfactorily describe the form of $\Delta B(s)$.

$$\Delta B(s) = \sum_i c_i \sin(a_i s) \quad (11a)$$

$$\Delta B(s) = d + \sum_i c_i \sin(a_i s) + b_i \cos(a_i s) \quad (11b)$$

The set of constants a_i must naturally be significantly smaller than the smallest internuclear distance. With the aid of an adequate computer, values of the constant term d and the coefficients c_i and b_i may be rapidly calculated, using standard least-square procedures.

With values calculated for $\Delta B(s)$, the experimental molecular scattering intensities may be evaluated from

$$M_A(s) = M_B(s) + \Delta I(s) - \Delta B(s) \quad (12)$$

The indices of resolution were calculated and found to be 1.035, 0.99, and 1.045 for the 100-, 50-, and 25-cm. curves, respectively.

Refinement of Data

The first stage of the structure determination involved the calculation of a radial distribution curve. This was carried out in accordance with

$$\sigma(r)/r = \sum_s M_A(s) s Z_{\text{Cl}}^2 / (Z_{\text{Cl}} - F_{\text{Cl}}(s))^2 \times \exp(-ks^2) (\sin(\epsilon r)) \Delta s \quad (13)$$

where k is an artificial damping factor, introduced to compensate for the upper limit of s at which $M_A(s)$ values were obtainable. In the range $s = 0.25$ – 1.50 \AA^{-1} , where experimental intensities were either unobtainable or unreliable, theoretical values were used.

The three sharp peaks, corresponding to the Cl-Cl and the two C-Cl atom pair contributions, gave inter-

(15) V. Schomaker and R. Glauber, *Nature*, **170**, 290 (1962); *Phys. Rev.*, **89**, 667 (1953).

(16) R. A. Bonham and T. Ukaji, *J. Chem. Phys.*, **36**, 72 (1962).

(17) See, e.g., L. S. Bartell, *ibid.*, **23**, 1219 (1955).

atomic distances from which it was possible to calculate C and Cl atomic coordinates of reasonably high reliability. The length of the C=C bond, obtained from its relatively small contribution, was in good agreement with the other three distances. No really useful information could be obtained, at this stage, from the small contributions of the C-H and Cl-H atom pairs.

It was possible, using the atomic coordinates from the radial distribution treatment, to calculate a new and more reliable theoretical molecular scattering curve. The refinement procedures, represented in eq. 10 and 11, were repeated. The ensuing improved version of the experimental molecular scattering curve was used in a number of different refinement procedures.

A further radial distribution curve was calculated. It was compared with a theoretical version which had been obtained from a Fourier inversion of the theoretical molecular scattering curve. Each of the individual contributions to the theoretical molecular scattering curves was calculated in the same fashion. Adjustments were made to the individual contributions in order to improve the correlation between the theoretical and experimental curves.

Three separate methods were adopted to refine the structural parameters on the basis of optimum correlation between the theoretical and experimental molecular scattering curves. One of these was that described by Hedberg.¹⁸ This method involves the use of the first Taylor approximations of $\sin(sr_{ij})$ and $\exp(-l_{ij}^2s^2/2)$ in a least-squares procedure. The other methods entail the continuous adjustment of the independent dimensional parameters and vibrational amplitudes in the direction of improving correlation. The two methods differ in that one involves simultaneous adjustment of all parameters while, in the other, each parameter is individually changed. It was hoped that by using more than one refinement procedure it would be possible to avoid the danger of reaching false minima in the numerical values of the criteria adopted for judging the correlation.

It was first ascertained that the four methods of analysis independently led to reasonably similar values for the internuclear distances not involving the hydrogen atoms. This having been achieved, numerous attempts were made, using the various methods available, to improve the theoretical molecular scattering curve. At the same time, further efforts were made to improve the theoretical radial distribution curve. It should be borne in mind that, while the radial distribution analysis involved independent changes in all eight internuclear distances, the intensity curve was analyzed in terms of the five dimensional parameters

that describe the molecule when C_{2v} symmetry is assumed.

Results

The results of the radial distribution analysis and those corresponding to the "best" theoretical molecular scattering curve are presented in Table I.

Table I: Comparison of the Results of Three Methods^a of Structure Refinement

	Interatomic distances (Å.) and bond angles		
	R.D.	A	B
C=C	1.353	1.354	1.353
C-Cl	1.718	1.717	1.716
C-Cl'	2.713	2.714	2.713
Cl-Cl'	3.261	3.262	3.264
C-H	1.059	1.065	1.068
CCH	(131.6°) ^b	133.4°	131.6°
CCCl	123.7°	123.75°	123.8°

	Vibrational amplitudes, Å.		
	R.D.	A	B
C=C	0.039	0.033	0.043
Cl-Cl'	0.114	0.117	0.119
C-Cl	0.044	0.050	0.046
C-Cl'	0.060	0.063	0.062
C-H	0.083	0.085	0.097

^a R.D.: radial distribution curve analysis. *Intensity curve analyses*: A: Hedberg method (values corresponding to lowest calculated errors). B: continuous adjustment of independent parameters. ^b Assumed.

The proposed structure, together with limits of tolerance is given in Table II. The limits of tolerance are based upon a standard-error matrix calculation of the type described by Hedberg.¹⁸ The limits for the bond lengths have been increased by 0.2% to take

Table II: The Molecular Structure of *cis*-Dichloroethylene^a

—Vibrational amplitudes, Å.—	
$r_g(\text{C}=\text{C}) = 1.354 \pm 0.005 \text{ \AA.}$	$l(\text{C}=\text{C}) = 0.038 \pm 0.009$
$r_g(\text{C}-\text{Cl}) = 1.718 \pm 0.007 \text{ \AA.}$	$l(\text{C}-\text{Cl}) = 0.048 \pm 0.004$
$\angle \text{CCCl} = 123.8 \pm 0.5^\circ$	$l(\text{C}-\text{Cl}') = 0.062 \pm 0.005$
$r_g(\text{C}-\text{H}) = 1.075 \pm 0.015 \text{ \AA.}$	$l(\text{Cl}-\text{Cl}') = 0.117 \pm 0.004$
$\angle \text{CCH} = 132.0 \pm 3.0^\circ$	$l(\text{C}-\text{H}) = 0.088 \pm 0.016$

^a The interatomic distances (r_g) have been calculated from the r_{ij} values, using eq. 7. No corrections have been made for shrinkage.

(18) K. Hedberg and M. Iwasaki, *Acta Cryst.*, 17, 529 (1954).

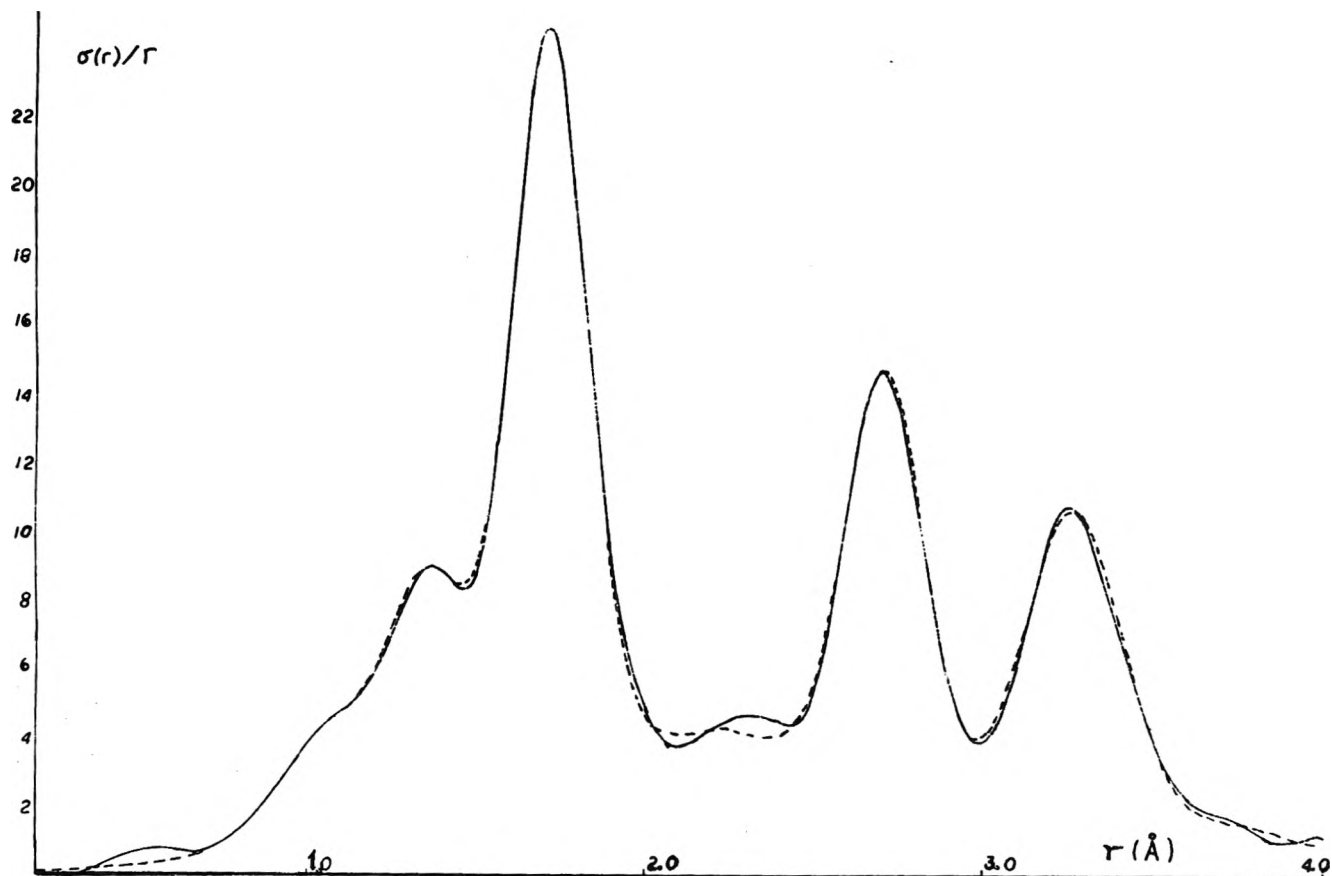


Figure 1. The radial distribution curve of *cis*-dichloroethylene. The broken line is a theoretical version. The damping factor $k = 0.0043$.

into account the errors involved in evaluating the de Broglie wave length and measuring the nozzle-to-camera distances.

The final experimental and theoretical radial distribution curves are shown in Figure 1. The theoretical curves were calculated by Fourier inversion of the molecular scattering contributions, rather than by summation of Gaussian curves.

The theoretical and experimental molecular scattering curves are shown in Figure 2. The correlation between the two is not as good as that which may be obtained for hydrocarbons. Bearing in mind the fact that for this compound the molecular scattering represents a much smaller part of the over-all, than is the case for hydrocarbons, the resemblance between the two curves is quite good.

There are two small regions of the molecular scattering curves where there exist obvious discrepancies between the shapes of the experimental and theoretical versions. These are at $s = 15$ and 22 \AA^{-1} , respectively. Despite the fact that these discrepancies are so visibly apparent, the quantitative differences are somewhat less than 0.5% of the total scattering in those

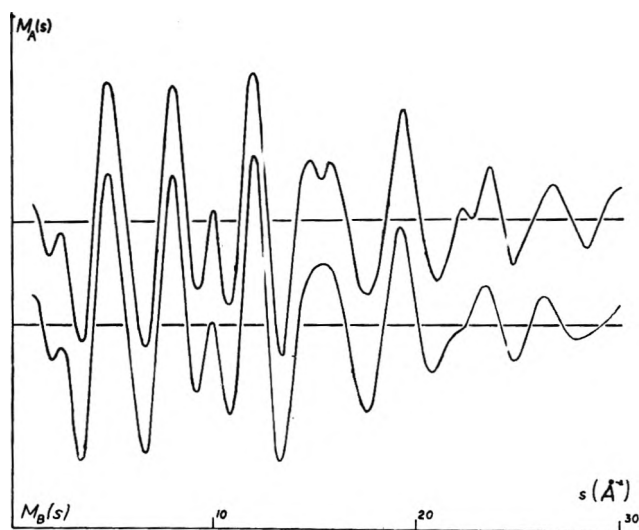


Figure 2. Theoretical and experimental versions of the molecular scattering curve of *cis*-dichloroethylene. The experimental curve M_A is the upper one.

regions. It is not improbable that suitable statistical evaluation techniques could be employed to improve the situation with respect to those regions, but it is

unlikely that such improvements would have any profound effect upon the accuracy of the experiment.

Moments of Inertia

The three moments of inertia had been obtained from a microwave study of this compound.² They have also been calculated from the results of the electron diffraction study. The two sets of values are given in Table III.

Table III: Moments of Inertia (a.m.u. Å.²)

	Microwave study	Electron diffraction study
I_A	43.890	44.0
I_B	198.628	200.4
I_C	242.747	244.4

It should be recognized that, while the microwave study observes the molecule in all of its vibrational ground states, the diffraction investigation is concerned with a Boltzmann distribution of both ground and excited states.

The discrepancy between the two sets of moments of inertia does not necessarily imply that the conduct of one or the other of the experiments has been faulty. It is more likely that the effects of vibrational-rotational coupling upon the rotational energies is such as to make the r_0 values significantly different from the r_g values of the diffraction experiment.

A value of $124^\circ 45'$ was predicted for the C-Cl bond angle,² on the basis of certain molecular orbital calculations¹⁹ and a value for the Cl³⁵ nuclear quadrupole coupling constant of *cis*-dichloroethylene in the solid state.²⁰ A value of this magnitude would require a C=C bond length considerably shorter than that obtained from the diffraction study.

Discussion of Results

The number of high-precision structure investigations, that have been carried out on the haloethylenes is surprisingly small, most of them being for fluorine derivatives. Those investigations that have been performed led to the results shown in Table IV.

The C=C bond length, like that of *cis*-dibromoethylene is of the order of 0.02 Å. larger than that found for the parent ethylene. The C=C bond in vinyl chloride, which might have been expected to have a length midway between those of ethylene and *cis*-dichloroethylene, is in fact found to be shorter. The vinyl chloride investigation was carried out by

Table IV: Reported Structures of the Haloethylenes

	$r(\text{C}=\text{C})$	$r(\text{C}-\text{X})$	Ref.	Method ^k
CH ₂ =CH ₂	1.337	1.103	<i>a</i>	E.D
CH ₂ =CHF	1.332	1.348	<i>b</i>	M.W
CHF=CHF (<i>cis</i>)	1.324	1.337	<i>b</i>	M.W
CH ₂ =CF ₂	1.320	1.321	<i>b</i>	M.W
CF ₂ =CF ₂	1.313	1.313	<i>c</i>	E.D
CH ₂ =CHCl	1.332	1.726	<i>d</i>	M.W
CHCl=CHCl (<i>cis</i>)	1.354	1.718	<i>h</i>	E.D
CH ₂ =CCl ₂	1.32 ⁱ	1.727		
	1.35 ^j	1.715	<i>e</i>	M.W
CCl ₂ =CCl ₂	1.30	1.72	<i>f</i>	E.D
CHBr=CHBr (<i>cis</i>)	1.360	1.871	<i>g</i>	E.D

^a L. S. Bartell, E. A. Roth, C. D. Hollowell, K. Kuchitsu, and J. E. Young, Jr., *J. Chem. Phys.*, **42**, 2683 (1965). ^b V. W. Laurie, *ibid.*, **34**, 291 (1961). ^c I. L. Karle and J. Karle, *ibid.*, **18**, 963 (1950). ^d D. Kivelson, E. B. Wilson, Jr., and D. R. Lide, *ibid.*, **32**, 205 (1960). ^e S. Sekino and T. Nishikawa, *J. Phys. Soc. Japan*, **12**, 43 (1957). ^f I. L. Karle and J. Karle, *J. Chem. Phys.*, **20**, 63 (1952). ^g See ref. 4. ^h This investigation. ⁱ Original authors' assumption. ^j Calculation by present author. ^k E.D, gas phase electron diffraction; M.W, microwave spectroscopy.

the microwave technique. It has already been observed that there must exist a significant difference between the r_0 and r_g values for dichloroethylene. It is therefore not improbable that a similar difference exists for vinyl chloride, and consequently a simple comparison between the results of the two techniques is not possible. To investigate this situation an electron diffraction study of vinyl chloride would be desirable.

The C-Cl bond length in *cis*-dichloroethylene is fairly close to the values obtained by microwave analysis of vinyl chloride and vinylidene chloride.

The C-H bond appears to be somewhat shorter than the value cited for ethylene. The CCH bond angle would seem to be exceptionally large. The determination of this angle cannot be accomplished with anything approaching high precision. It would appear, however, that it is significantly larger than the sp^2 value of 120° . This might be taken to indicate the presence of a fairly large attractive force between the hydrogen and chlorine atoms.

It is of interest to note that the C=C and C-H bond distances of the fluoroethylenes both appear to decrease with increasing fluorine content. The errors involved in the individual investigations, together with the possible differences between the r_0 and r_g values,

(19) J. A. Howe, J. S. Muirhead, and J. H. Goldstein, *J. Chem. Phys.*, **36**, 841 (1961).

(20) R. Livingston, *J. Phys. Chem.*, **57**, 496 (1953).

while obviously important, are probably not so large as to make this trend meaningless.

That the C=C bonds of the fluoroethylenes should be shorter than the ethylene values, while those for *cis*-dichloroethylene and its bromine analog are longer, is interesting and has prompted us to initiate structural studies of the other dichloroethylenes.

Acknowledgments. The equipment, used in this in-

vestigation, was built with financial assistance from the Graduate School of The University of Texas. A great deal of credit for its construction must go to Dr. D. M. Cowan. The research was sponsored by the Robert A. Welch Foundation of Houston, Texas. We wish to express our gratitude to Mr. Bobby Turman for his help in the collection of the experimental data and to Mr. David Loyd for his part in the construction of the equipment.

Benzene and Dioxane Electric Moments of N-Alkyl-Substituted Nicotinamides from Measurements in Mixed Benzene-Dioxane Solutions¹

by William P. Purcell and Judith A. Singer

Department of Pharmaceutical and Medicinal Chemistry, University of Tennessee College of Pharmacy, Memphis, Tennessee (Received May 10, 1966)

Dielectric constants and refractive indices of dilute mixed benzene-dioxane and pure dioxane solutions of pyridine, nicotinamide, N-methylnicotinamide, N-ethylnicotinamide, N,N-dimethylnicotinamide, N,N-diethylnicotinamide, and N,N-di-*n*-propylnicotinamide and also of dilute benzene solutions of N,N-di-*n*-propylnicotinamide were measured at 25°. The dipole moments were calculated from Smith's modification of the Guggenheim equation. The mixed-solvent moments are virtually the same as those calculated from pure-solvent measurements, and the results are consistent with the electron-releasing effect of alkyl group substitution. Differences between benzene and dioxane moments for a given compound are interpreted in terms of the expected effect of the amide substituents on the solvating dioxane molecules.

Introduction

We found the benzene solution moment of isonicotinamide² to be 0.68 D. lower when it was measured in pure benzene than when it was measured by a mixed benzene-dioxane technique.³⁻⁶ This deviation was interpreted in terms of the formation of isonicotinamide dimers with zero moment when pure benzene is the solvent.² The apparent solute-solute association problems encountered in the measurement of amides in pure benzene,⁷ coupled with our results for isonicotinamide and our interest in correlating polarities with

cholinesterase inhibitory properties,⁸ prompted us to apply the mixed benzene-dioxane solvent technique³⁻⁶

(1) This research is being supported by the National Science Foundation (B-15989). Computer facilities were provided through U. S. Public Health Service Grant HE-09495.

(2) W. P. Purcell and J. A. Singer, *J. Phys. Chem.*, **69**, 691 (1965).

(3) G. K. Estok and C. H. Stembridge, *J. Am. Chem. Soc.*, **76**, 4316 (1954).

(4) G. K. Estok and S. P. Sood, *J. Phys. Chem.*, **61**, 1445 (1957).

(5) G. K. Estok, S. P. Sood, and C. H. Stembridge, *ibid.*, **62**, 1464 (1958).

(6) G. K. Estok and S. P. Sood, *ibid.*, **66**, 1372 (1962).

Table I: Dielectric Constants Measured at 25° in Dioxane and in Mixtures of Dioxane and Benzene Solution^a and the Corresponding Slopes, α (ϵ vs. w_2)

Solvent composition, mole % dioxane	$10^3 w_2$	ϵ	Solvent composition, mole % dioxane	$10^3 w_2$	ϵ	Solvent composition, mole % dioxane	$10^3 w_2$	ϵ	Solvent composition, mole % dioxane	$10^3 w_2$	ϵ
Pyridine						$\alpha = 11.3$	2.7559	2.2435	$\alpha = 10.8$	3.1072	2.2658
100.00	0.0000	2.2075	75.27	0.0000	2.2343		5.3345	2.2721		4.3231	2.2790
		2.7850			2.8634		6.1741	2.2820		5.0042	2.2868
$\alpha = 8.82$	5.0817	2.2519	$\alpha = 7.86$	4.3446	2.2685					5.9004	2.2968
	9.2200	2.2884		5.1643	2.2743	62.74	0.0000	2.2440	46.69	0.0000	2.2561
	10.363	2.2990		5.7637	2.2792		0.9046	2.2521		1.4453	2.2684
	10.772	2.3026		10.049	2.3135	$\alpha = 10.4$	2.4405	2.2680	$\alpha = 9.95$	2.8514	2.2828
61.13	0.0000	2.2446	45.32	0.0000	2.2555		4.2791	2.2872		3.3817	2.2888
		2.0398			2.6383		5.4908	2.3004		4.0758	2.2956
$\alpha = 7.70$	3.6465	2.2722	$\alpha = 7.51$	4.8806	2.2914		7.0211	2.3169		5.3250	2.3086
	4.4439	2.2780		5.9229	2.3000	31.08	0.0000	2.2617			
	6.6386	2.2957		7.0507	2.3085		1.2602	2.2733			
	6.7425	2.2972		9.5544	2.3270	$\alpha = 9.84$	3.3177	2.2935			
Nicotinamide							4.4001	2.3042			
							5.8815	2.3196			
100.00	0.0000	2.2119	75.07	0.0000	2.2332	N,N-Dimethylnicotinamide					
		0.8136			1.1452	100.00	0.0000	2.2133	77.47	0.0000	2.2313
$\alpha = 12.6$	1.1913	2.2265	$\alpha = 11.9$	1.6010	2.2526		1.0881	2.2287		0.6859	2.2404
	2.0979	2.2380		2.2218	2.2598	$\alpha = 14.4$	1.8681	2.2395	$\alpha = 14.1$	1.9037	2.2573
	2.9995	2.2496		2.4240	2.2620		2.9544	2.2557		2.8855	2.2704
	3.8800	2.2606		2.6696	2.2651		3.7626	2.2665		3.8160	2.2850
59.64	0.0000	2.2463	53.03	0.0000	2.2499		5.6498	2.2941		5.2065	2.3039
		0.7027			0.8775		5.7944	2.2968		6.4451	2.3217
$\alpha = 11.5$	1.4447	2.2632	$\alpha = 10.9$	1.3265	2.2637	61.04	0.0000	2.2434	41.12	0.0000	2.2581
	2.0423	2.2703		1.6741	2.2678		0.9811	2.2558		0.8135	2.2686
	2.0925	2.2706		2.6138	2.2782	$\alpha = 13.6$	2.2554	2.2739	$\alpha = 13.1$	1.4632	2.2771
	2.4807	2.2746					2.8008	2.2812		1.6124	2.2786
38.93	0.0000	2.2591					4.6267	2.3056		3.0937	2.2983
		0.5122					5.2377	2.3148		3.1581	2.2997
$\alpha = 10.5$	1.3292	2.2730					5.5880	2.3187		4.5128	2.3169
	1.4350	2.2747				25.49	0.0000	2.2679			
	2.2675	2.2830					0.9537	2.2795			
	2.8105	2.2889				$\alpha = 12.6$	1.6198	2.2880			
	2.9995	2.2906					2.2159	2.2951			
N-Methylnicotinamide							2.2649	2.2961			
							2.8878	2.3047			
100.00	0.0000	2.2121	78.40	0.0000	2.2329	N,N-Diethylnicotinamide					
		0.6858			1.3097	100.00	0.0000	2.2125	56.00	0.0000	2.2466
$\alpha = 12.6$	1.5634	2.2319	$\alpha = 11.8$	3.1582	2.2692		0.7996	2.2233		1.0951	2.2596
	2.4693	2.2442		3.8412	2.2775	$\alpha = 12.9$	1.4996	2.2327	$\alpha = 12.1$	2.0963	2.2713
	2.9817	2.2502		4.8527	2.2903		1.5232	2.2320		2.1330	2.2726
	4.8949	2.2737					2.4149	2.2450		3.4954	2.2886
61.31	0.0000	2.2467	38.88	0.0000	2.2602		3.1173	2.2528		4.9151	2.3057
		0.9480			0.7804		3.9768	2.2640		5.2657	2.3105
$\alpha = 11.3$	2.3025	2.2717	$\alpha = 10.8$	1.7496	2.2782	41.91	0.0000	2.2574	29.03	0.0000	2.2658
	2.9377	2.2784		2.1535	2.2827		0.7469	2.2658		1.1170	2.2780
	3.8502	2.2898		2.8036	2.2901	$\alpha = 11.8$	1.2587	2.2721	$\alpha = 11.6$	1.6351	2.2845
	5.1723	2.3049		3.6472	2.2991		2.3789	2.2853		2.3376	2.2926
N-Ethylnicotinamide							3.1674	2.2948		2.5737	2.2951
100.00	0.0000	2.2121	76.97	0.0000	2.2332		3.7569	2.3014		3.0238	2.3009
		1.2002			1.4514		4.5058	2.3104		3.7188	2.3085

Table I (Continued)

Solvent composition, mole % dioxane			Solvent composition, mole % dioxane		
	$10^4 w_2$	ϵ		$10^4 w_2$	ϵ
N,N-Di- <i>n</i> -propylnicotinamide					
100.00	0.0000	2.2082	64.87	0.0000	2.2380
	0.7855	2.2169		1.1451	2.2499
$\alpha = 11.1$	1.8148	2.2280	$\alpha = 10.7$	1.6124	2.2544
	2.5565	2.2369		2.8321	2.2676
	3.2316	2.2440		3.5121	2.2749
	4.2018	2.2548		4.5109	2.2854
	4.4029	2.2573		6.4131	2.3063
43.84	0.0000	2.2536	21.82	0.0000	2.2667
	0.9777	2.2631		1.0911	2.2775
$\alpha = 10.2$	1.6249	2.2705	$\alpha = 9.68$	1.6244	2.2821
	2.8739	2.2831		1.9434	2.2852
	2.9905	2.2837		2.5821	2.2924
	3.2543	2.2863		2.6353	2.2921
	4.5827	2.3005		3.2742	2.2982
0.00	0.0000	2.2770			
	1.0257	2.2865			
$\alpha = 9.46$	1.1372	2.2877			
	2.4910	2.3003			
	2.7735	2.3027			
	3.7962	2.3130			
	3.8735	2.3136			

^a N,N-Di-*n*-propylnicotinamide was also measured in pure benzene.

to a series of N-alkylnicotinamides, which we had already measured in pure benzene,⁹ and to N,N-di-*n*-propylnicotinamide.

Experimental Section

Reagents. Pyridine (Spectroquality reagent, Matheson Coleman and Bell) was used without further purification; n_D^{25} 1.5074 (lit.¹⁰ n_D^{25} 1.5073). Nicotinamide (Matheson Coleman and Bell) was recrystallized four times from benzene, m.p. 126.8–127.3° (lit.¹¹ m.p. 129–130°). N-Methylnicotinamide (reagent grade, K & K Laboratories) was recrystallized four times from benzene, m.p. 104.8–105.3° (lit.¹² m.p. 104–105°). N,N-Dimethylnicotinamide (Aldrich Chemical Co.) was vacuum distilled, b.p. 97° (0.1 mm.), n_D^{25} 1.5416. N-Ethyl nicotinamide (reagent grade, K & K Laboratories) was vacuum distilled, b.p. 128° (0.12 mm.). N,N-Diethyl nicotinamide (Aldrich Chemical Co.) was vacuum distilled, b.p. 104° (0.09 mm.), n_D^{25} 1.5233. N,N-Di-*n*-propylnicotinamide was prepared by a procedure previously described¹³ and was vacuum distilled into a receiver protected from light, b.p. 116° (0.20 mm.), n_D^{25} 1.5121 (lit.¹⁴ b.p. 182–183° (16 mm.)).

Solvents. The compounds were measured in dilute solutions of SpectrAR benzene (Mallinckrodt) or Spectroquality benzene (Matheson Coleman and Bell), Spectroquality *p*-dioxane (Matheson Coleman and Bell), and in mixtures of these solvents.

Apparatus. The dielectric constants of all the solutions and the refractive indices of the pure solutes were measured at 25° as previously described.⁹ The refractive indices of the solutions were measured to ± 0.00003 at 25° with a Bausch and Lomb Precision refractometer (sodium D-line); the temperature of the solutions was controlled to $\pm 0.02^\circ$ by a NBe Haake constant-temperature circulator using a thermometer calibrated against a National Bureau of Standards certified thermometer.

Calculations. The dipole moments in pure benzene and in pure dioxane were calculated from eq. 1¹⁵ and Smith's modification¹⁶ (eq. 2) of the Guggenheim

$$\mu = 0.01281(TP_M)^{1/2} \quad (1)$$

$$P_M = 3M_2v_1[\alpha/(\epsilon_1 + 2)^2 - \gamma/(n_1^2 + 2)^2] \quad (2)$$

equation,¹⁷ where μ is the dipole moment, T is the absolute temperature, P_M is the orientation polarization, M is the molecular weight, v is the specific volume, ϵ is the dielectric constant, n is the refractive index, α is the slope of ϵ vs. the weight fraction w_2 , γ is the slope of n^2 vs. w_2 , and the subscripts 1 and 2 refer to the solvent and solute, respectively. The dipole moments from extrapolation of mixed-solvent α values to pure dioxane and to pure benzene solution were calculated from a modification of the method described by Estok, *et al.*^{3–6} The slope, α , was calculated for each mixed-solvent series by the method of least squares; these values for α were plotted against mole per cent dioxane of the mixed solvent and extrapolated to 0% dioxane to give α_{benzene} and extrapolated to 100% dioxane to give α_{dioxane} . The slopes, γ , were determined with pure benzene and pure dioxane as solvents by the method of least squares. Smith's method¹⁶ (eq. 1 and 2)

(7) P. A. Geary and J. G. Miller, *J. Electrochem. Soc.*, **97**, 54 (1950).

(8) W. P. Purcell, J. G. Beasley, and R. P. Quintana, *Biochim. Biophys. Acta*, **88**, 233 (1964).

(9) W. P. Purcell, *J. Phys. Chem.*, **68**, 2666 (1964).

(10) V. Zawidzki, *Chemiker-Ztg.*, **30**, 299 (1906).

(11) C. F. Krewson and J. F. Couch, *J. Am. Chem. Soc.*, **65**, 2256 (1943).

(12) A. Pictet and G. Sussdorff, *Chem. Zentr.*, **69**, 677 (1898).

(13) J. G. Beasley, R. P. Quintana, and G. G. Nelms, *J. Med. Chem.*, **7**, 698 (1964).

(14) K. Fricker, French Patent 791,783 (Dec. 17, 1935).

(15) C. P. Smyth, "Dielectric Behavior and Structure," McGraw-Hill Book Co., Inc., New York, N. Y., 1955, p. 221.

(16) J. W. Smith, *Trans. Faraday Soc.*, **46**, 394 (1950).

(17) E. A. Guggenheim, *ibid.*, **45**, 714 (1949).

and the values for α_{benzene} , γ_{benzene} , α_{dioxane} , and γ_{dioxane} were then used to calculate the corresponding moments. All least-squares calculations were carried out on the IBM 1620 computer, using a modification of the program TIPS, which prints slopes, intercepts, and deviations of the experimental points from the corresponding points on the least-squares line.

Results and Discussion

The dielectric constants of the solutions are given in Table I. With the exception of N,N-di-*n*-propyl-nicotinamide, the dielectric constants of solutions of these molecules in pure benzene have already been reported,⁹ and, therefore, we measured only the mixed benzene-dioxane and pure dioxane solutions. Table I also gives the slopes, α , for each series of solutions of solute at a particular solvent composition. The mixed-solvent α value (Table I) were extrapolated as described under Calculations to obtain α_{benzene} and α_{dioxane} for each compound (Table II).

Table II: Slopes, α (ϵ vs. w_2), Extrapolated to Pure-Solvent from Mixed-Solvent Data

Compound	α_{benzene}	α_{dioxane}
Pyridine	6.99	8.15
Nicotinamide	8.87	13.0
N-Methylnicotinamide	9.69	12.4
N-Ethylnicotinamide	9.08	11.2
N,N-Dimethylnicotinamide	12.0	14.7
N,N-Diethylnicotinamide	11.0	13.0
N,N-Di- <i>n</i> -propylnicotinamide	9.20	11.5

Table III gives the refractive indices for the solutions of each compound in pure benzene and pure dioxane and the corresponding slopes, γ .

The electric moments are reported in Table IV. The moments measured in pure benzene solution⁹ are repeated for comparison although the benzene moment for N,N-di-*n*-propylnicotinamide, 4.22, is new. The value is 0.07 D. larger than that for N,N-diethylnicotinamide, which is consistent with the electron releasing¹⁸ effect of alkyl groups and the trends previously reported.⁹ The N,N-di-*n*-propylamide group moment, calculated from the "75% *trans*" method,⁹ is 5.12.

Comparing the differences between the benzene and dioxane moments measured in the pure solvents, one finds an interesting trend. Nicotinamide shows the greatest difference, 0.37, and has two amide hydrogen atoms available for hydrogen bonding to the oxygen atoms in dioxane, thus inducing moments and increasing the observed moment in dioxane. N-Methyl-

Table III: Refractive Indices Measured at 25° in Dioxane and in Benzene Solution and the Corresponding Slopes, γ (n_D^2 vs. w_2)

Dioxane		Benzene	
$10^4 w_2$	n_D	$10^4 w_2$	n_D
Pyridine			
0.0000	1.41990	0.0000	1.49777
2.7850	1.42008	1.4148	1.49788
5.0817	1.42027	2.5790	1.49799
8.2146	1.42058	3.4973	1.49810
9.2200	1.42068		
10.363	1.42074		
10.772	1.42077		
$\gamma = 0.240$		$\gamma = 0.028$	
Nicotinamide			
0.0000	1.41986	0.0000	1.49782
1.5110	1.42015	0.5108	1.49782
2.6915	1.42037	1.0765	1.49788
4.0051	1.42049	1.7357	1.49791
$\gamma = 0.456$		$\gamma = 0.172$	
N-Methylnicotinamide			
0.0000	1.41990	0.0000	1.49771
1.1492	1.41999	0.8271	1.49779
3.1346	1.42030	2.1858	1.49791
4.2557	1.42046	4.5752	1.49805
$\gamma = 0.386$		$\gamma = 0.220$	
N-Ethylnicotinamide			
0.0000	1.41996	0.0000	1.49771
2.9454	1.42027	6.8431	1.49802
5.7851	1.42061	6.9379	1.49807
8.2078	1.42092	15.275	1.49849
$\gamma = 0.333$		$\gamma = 0.153$	
N,N-Dimethylnicotinamide			
0.0000	1.41990	0.0000	1.49771
5.0358	1.42049	6.6566	1.49805
6.8435	1.42071	9.7393	1.49821
15.934	1.42177	18.534	1.49861
$\gamma = 0.334$		$\gamma = 0.145$	
N,N-Diethylnicotinamide			
0.000	1.41990	0.0000	1.49777
13.575	1.42127	10.155	1.49805
18.624	1.42177	22.558	1.49841
20.995	1.42202	41.669	1.49891
$\gamma = 0.286$		$\gamma = 0.082$	
N,N-Di- <i>n</i> -propylnicotinamide			
0.0000	1.41993	0.0000	1.49779
4.0546	1.42033	4.1752	1.49788
5.5491	1.42049	9.5375	1.49799
10.368	1.42093	15.368	1.49810
$\gamma = 0.274$		$\gamma = 0.060$	

(18) C. A. Coulson, "Valence," 2nd Ed., Oxford University Press, London, 1961, pp. 356-365.

Table IV: Electric Moments, D.

Compound	μ_{benzene}	μ_{benzene}	μ_{dioxane}	μ_{dioxane}
	from pure solvent ^a	from extrapolation of mixed-solvent data to 100% benzene	from pure solvent	from extrapolation of mixed-solvent data to 100% dioxane
Pyridine	2.27	2.25	2.33	2.24
Nicotinamide	3.07	3.13	3.44	3.50
N-Methylnicotinamide	3.42	3.44	3.65	3.63
N-Ethylnicotinamide	3.44	3.51	3.63	3.62
N,N-Dimethylnicotinamide	3.99	4.04	4.11	4.16
N,N-Diethylnicotinamide	4.15	4.23	4.25	4.26
N,N-Di- <i>n</i> -propylnicotinamide	4.22	4.16	4.24	4.30

^a Electric moments in benzene at 25° of all compounds, exclusive of N,N-di-*n*-propylnicotinamide, previously reported: W. P. Purcell, *J. Phys. Chem.*, **68**, 2666 (1964).

nicotinamide, which has only one amide hydrogen available for bonding, has a smaller difference, 0.23, and the difference for N-ethylnicotinamide, 0.19, is still a little smaller, probably because the bulkier ethyl group interferes sterically with the solvating molecule(s). The disubstituted derivatives have even smaller differences which decrease with increasing size of the substituent groups—*i.e.*, N,N-dimethylnicotinamide, 0.12; N,N-diethylnicotinamide, 0.10; N,N-di-*n*-propylnicotinamide, 0.02.

Comparing the benzene moments measured in pure benzene with those calculated from mixed-solvent measurements, one sees very little difference; the greatest difference is between the two moments of diethylnicotinamide, 4.15 and 4.23, which is larger than the experimental error for this compound. Similarly,

the differences between the dioxane moments measured in pure dioxane and those calculated from mixed-solvent measurements are small, the largest difference being 0.09 D. One might conclude, therefore, that the mixed-solvent technique apparently offers little advantage (*for these homologs*) since virtually the same moments are obtained from pure-solvent measurements, and considerably less experimental work is required in the latter technique. We wish to add, however, that the dimers formed from these 3-pyridine derivatives would generally have moments not equal to zero, and, therefore, the fact that the pure-benzene moments and the benzene moments from mixed solvents are the same would not necessarily indicate that there is no solute-solute association in pure benzene. Furthermore, the benzene and dioxane mixed-solvent moments and the pure-dioxane moments increase in the same direction as the pure-benzene moments, so the application of this technique does have the advantage of corroborating our earlier discussion.⁹ There are three exceptions, however: the benzene moment of N,N-diethylnicotinamide measured by the mixed-solvent technique is larger than the corresponding N,N-di-*n*-propylnicotinamide moment by 0.07 D.; the dioxane moment of N-methylnicotinamide measured by mixed solvents is larger than the corresponding N-ethylnicotinamide moment by 0.01 D.; and the dioxane moment of N,N-diethylnicotinamide measured by mixed solvents is larger than the corresponding N,N-di-*n*-propylnicotinamide moment by 0.01 D. The first exception has a moment difference which does seem somewhat large, but the second and third are certainly within the experimental error.

Acknowledgment. The authors wish to thank Dr. R. P. Quintana for synthesizing and supplying a sample of N,N-di-*n*-propylnicotinamide and Dr. C. W. Sheppard and Mrs. A. B. McEachran of the University of Tennessee Medical Units Computer Center for their help in processing the data.

Mean Activity Coefficient of Polyelectrolytes. I. Measurements of Sodium Polyacrylates¹

by Norio Ise and Tsuneo Okubo

Department of Polymer Chemistry, Kyoto University, Kyoto, Japan (Received May 11, 1966)

Using a concentration cell with transference, the *mean* activity coefficient of a polyelectrolyte was directly measured for the first time. Control experiments were carried out with sodium chloride: The observed mean activity coefficient agreed with the literature value. Those of the polyelectrolyte were found to decrease with increasing concentration. By comparison of the observed mean activity coefficient of the polyelectrolyte with the observed single-ion activity coefficient of gegenions, it was found that these two coefficients were not generally equal. This indicates that the contribution of macroions to the thermodynamic properties of the solutions is not negligible at all but is very influential. The mean activity coefficient observed was successfully compared with that computed by a previous theory.

Introduction

In a great number of papers² concerning the solute activity of polyelectrolyte solutions, emphasis has been put on the single-ion activities of gegenions or of simple electrolytes coexisting. This situation is unsatisfactory if one admits a point of view proposed by Guggenheim³ that single-ion activities are inaccessible to exact thermodynamics, and only *mean* activities are physically significant. This situation, however, appears to be inevitable for the following reasons. The first reason comes from a consideration of the existing theories of polyelectrolyte dilute solutions. As was pointed out already,⁴ it has been assumed in most theories that macroion-macroion interactions were not as important as small ion-macroion interactions. Thus, only properties at infinite dilution are considered. It is rather difficult to derive expressions for the mean activity coefficient on the basis of this theoretical framework. The second reason is related to the experimental technique of activity measurements. Usually, in the study of polyelectrolytes, electrochemical methods, *e.g.*, e.m.f. measurements of cells, have been employed to derive the activity coefficient. According to electrochemical theory, the question as to what kind of activity has been measured is answered by finding with respect to which species of ions the electrodes were reversible. Electrodes so far known are reversible with respect to small ions such as H⁺, Cl⁻, and so on, but

not to macroions. Therefore, if one of these electrodes was used in a cell, together with a reference electrode, only the single-ion activity of the relevant small ions could be obtained, provided the liquid junction potential could be evaluated.

This unsatisfactory situation can be improved by direct or indirect measurements of the *mean* activity of polyelectrolytes.⁵ There are two well-known direct ways for electrochemical measurement of *mean* activity: e.m.f. measurement of cells with transference and of cells without transference. If the latter type of cell is employed, however, it is required to have electrodes reversible with respect to each of the ions of the polyelectrolyte, gegenions, and macroions.

(1) Presented at the 14th Annual Meeting of the Society of Polymer Science, Tokyo, Japan, May 1965.

(2) See S. A. Rice and M. Nagasawa, "Polyelectrolyte Solutions," 1st Ed., Academic Press Inc., New York, N. Y., 1961, Chapter 8.

(3) E. A. Guggenheim, *J. Phys. Chem.*, **33**, 842 (1929).

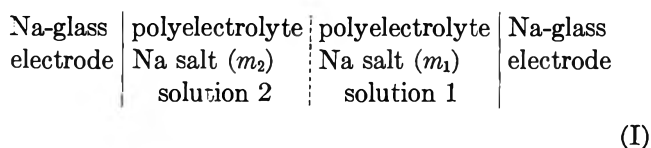
(4) (a) N. Ise and M. Hosono, *J. Polymer Sci.*, **39**, 389 (1959); (b) N. Ise, *J. Chem. Phys.*, **36**, 3248 (1962); *J. Phys. Chem.*, **67**, 382 (1963); N. Ise and P. Ander, *J. Chem. Phys.*, **39**, 592 (1963).

(5) It should be mentioned that what is described as the observed value of the mean activity coefficient of the polyelectrolyte in the present paper is the stoichiometric one, which will be denoted by γ^* . It is possible to define another mean activity coefficient for polyelectrolytes on the basis of the number of free ions, which will be denoted by γ . If confusion can be avoided, however, as in the case of low molecular weight strong electrolytes in which no ion association can be supposed to occur, the asterisk will be omitted. See Results and Discussion for the difference between γ^* and γ .

As was mentioned above, this is not possible. On the other hand, in order to set up the former type of cell, it is required to have electrodes reversible with respect to one of the ions constituting the polyelectrolyte, e.g., the gegenion. Na-glass electrodes are convenient for this purpose since they respond to some alkali metal ions which are in most cases used as gegenions of anionic macroions. The main purpose of this article is to obtain *mean* activity coefficients of sodium polyacrylate from e.m.f. data of concentration cells with transference using Na-glass electrodes.

Experimental Section

Principles. The method adopted in this paper is basically the same as the one developed earlier by Brown and MacInnes.⁶ A concentration cell with transference was set up with Na-glass electrodes as



The vertical dotted line represents a liquid junction, and m_1 and m_2 are the molalities of solutions 1 and 2, respectively. If we denote the transference number of macroions by t_p and the *mean* activity of the polyelectrolyte by \mathbf{a} and if we assume that a polyelectrolyte molecule dissociates into one (negative) macroion and α (positive) gegenions, the e.m.f. (E) of the cell shown by (I) is given by

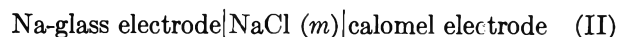
$$E = \frac{(1 + \alpha)RT}{\alpha F} \int_{a_2}^{a_1} t_p d \ln \mathbf{a} \quad (1)$$

where R is the gas constant, T temperature in °K., and F Faraday's constant. We shall use eq. 1 to obtain \mathbf{a} from E , t_p , and α .

Apparatus. (c) *Cell Design.* The cell design employed here is the one used by Stokes and Levien⁷ to obtain transference numbers from e.m.f. data of a concentration cell. In order to avoid contamination due to carbon dioxide, the air inside the half-cells was replaced with nitrogen before the cell was filled with the solution, and the volume of the gas contacting the solution was diminished as much as possible. The Na-glass electrodes were supported in silicon rubber stoppers which fit tightly into the tops of the two half-cells. Contamination was thus reduced to a minimal amount.

(b) *Electrodes.* The Na-glass electrodes,⁸ products of Horiba Manufacturing Co., Kyoto, were stored in an NaCl aqueous solution ($m = 0.100$) when not in use since it was found that dry electrodes failed to give

a stable e.m.f. Before and after e.m.f. measurement of one pair of solutions, the e.m.f. of cell II was meas-



ured at $m = 0.100$ to standardize the glass electrode.

(c) *Electric Circuits.* The e.m.f. values were measured with a precision potentiometer, Type K-2, of Shimadzu Manufacturing Co., Kyoto, in conjunction with a vibrating-reed electrometer, TR-85, manufactured by Takeda Riken Industry Co., Tokyo, as a null detector. The electrometer has an input impedance of more than 10^{14} ohms, and the maximum sensitivity was $50 \mu\text{V}$.

A standard cell was purchased from Yanagimoto Manufacturing Co., Kyoto, and had been certified by the Electrochemical Laboratory, Agency of Industrial Science and Technology, Tokyo. The concentration cell was immersed in a liquid paraffin thermostat maintained at $25 \pm 0.02^\circ$. The thermostat with its accessories was put in a metal box, which was grounded, to avoid outer disturbance, and the high-impedance side of the circuit was shielded.

Materials. Sodium chloride, reagent grade, was used for the experiments without further purification. Sodium polyacrylate was kindly furnished by Prof. M. Nagasawa, Nagoya University. It was used without fractionation for this experiment of an exploratory nature, and the weight-average degree of polymerization was 1640. Conductivity water was used in preparing all of the solutions. As collected from the delivery tip of columns of ion-exchange resins it had a specific conductance of 10^{-7} ohm $^{-1}$ cm. $^{-1}$. The solutions of sodium chloride were made up by dilution of a 0.1 *m* stock solution, which was prepared in measuring flasks. In order to obtain molalities, densities were measured. The polymer solutions were prepared from a stock solution of sodium polyacrylate; the stock solution was diluted and treated with ion-exchange resins. The polyacid thus obtained was quantitatively reconverted into sodium salt by means of potentiometric titration. Polymer concentration was determined from this titration.

Results and Discussion

Calibration of Na-Glass Electrode. Using a cell shown by (II), calibration of the Na-glass electrode was undertaken. For this type of cell, if the liquid

(6) A. S. Brown and D. A. MacInnes, *J. Am. Chem. Soc.*, **57**, 1356 (1935).

(7) R. H. Stokes and B. J. Levien, *ibid.*, **68**, 333 (1946).

(8) For a discussion of the general properties of Na-glass electrodes, see R. G. Bates, "Determination of pH, Theory and Practice," 1st Ed., John Wiley and Sons, Inc., New York, N. Y., 1964, Chapter 10.

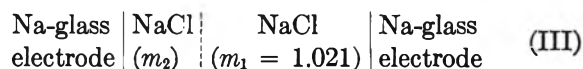
junction potential can be assumed to be negligible, the e.m.f. (E) is given by

$$E = E_0 + \frac{RT}{F} \ln a_{\text{Na}^+} \quad (2)$$

where E_0 is the standard value of the e.m.f. and a_{Na^+} is the single-ion activity of Na^+ . With the value of a_{Na^+} determined by using MacInnes' convention concerning ion activity coefficients,⁹ eq. 2 was tested. As is clear from Figure 1, a linearity between E and $\log a_{\text{Na}^+}$ was obtained over a wide range of a_{Na^+} . Between $a_{\text{Na}^+} = 1$ and 0.01, the slope was 59.0 mv., which is in good agreement with the theoretical value, 59.157 m.v., at 25°. A departure from this linearity appears at $a_{\text{Na}^+} \approx 0.001$. For comparison, a response curve of a sodium amalgam electrode used by Nagasawa and Kagawa¹⁰ is shown by a dotted curve. Although their electrode displayed better performance than is usually expected,¹¹ it is clear that the Na-glass electrodes are reversible in a much wider range of activity.

The e.m.f. reading varied appreciably at first after the electrodes were inserted into solutions. They reached a limiting value which was constant within ± 0.1 mv. over a 30-min. period. The e.m.f. value given in this paper is this limiting value.

Measurements of the E.m.f. of Concentration Cells of Sodium Chloride. It is interesting to measure the e.m.f. of the same type of cell of sodium chloride as that of polymer samples and to compare the activity coefficient thus obtained with the literature value. The cell was



The e.m.f. of the concentration cell was measured twice for each pair of solutions. In the second measurement, the positions of the two electrodes were reversed. The difference between these two measurements was always smaller than 0.5 mv. The results which were obtained by averaging these two values are given in the second column of Table I. The first column of the table gives the concentration m_2 . It should be remembered that the concentrations studied were in the range (1.0 to 0.003) where a straight line was obtained for the plot of e.m.f. vs. a_{Na^+} as was shown in Figure 1. The slope agreed with the theoretical value. Needless to say, this means that the galvanic cell was reversible, which is a basic requirement for electrochemical determination of activity coefficients.

The observed e.m.f. was constant within ± 0.5 mv. for 2 days.¹² It was also observed that the additivity of the e.m.f. holds for three pairs of three different concentrations. This additivity, together with

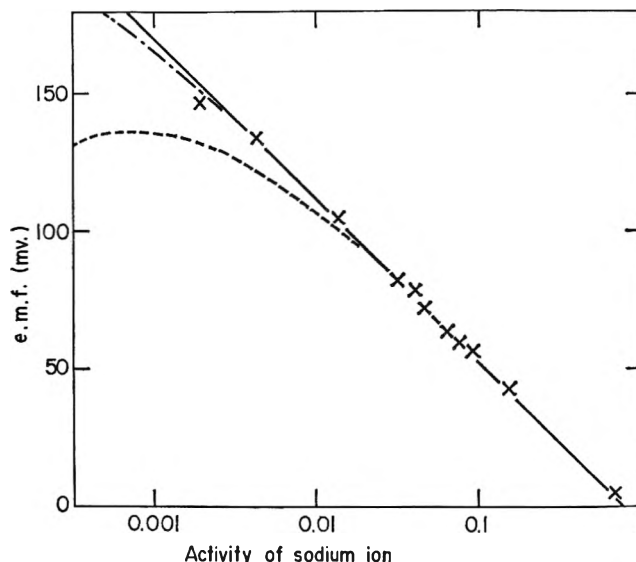


Figure 1. Calibration curve of the Na-glass electrode: —, theoretical line; -X---, observed curve; ·····, calibration curve of sodium amalgam electrode. (The original curve was vertically shifted.) See ref. 10.

Table I: Computation of Mean Activity Coefficient of Sodium Chloride

Molality	E.m.f., mv.	t_{Na}	$\log (\gamma_2/\gamma_1)$	γ_{obsd}	γ_{lit}
0.010	135.0	0.608 ^a	0.1448	0.92	0.903 ^c
0.020	115.0	0.610 ^a	0.1257	0.88	0.873 ^c
0.050	87.9	0.612 ^a	0.0947	0.82	0.822 ^c
0.100	68.2	0.615 ^a	0.0705	0.78	0.778 ^d
0.201	49.2	0.618 ^a	0.0308	0.71	0.735 ^d
0.506	21.5	0.623 ^b	0.0105	0.67	0.681 ^d
0.762	8.9	0.626 ^b	0.0050	0.66	0.665 ^d
1.021	0	0.628 ^b	0	(0.657)	0.657 ^d

^a G. L. Longworth, *J. Am. Chem. Soc.*, **54**, 2741 (1932).

^b Determined by the use of the data at 18 and 30°, "International Critical Tables," Vol. 6, 1929, p. 310. ^c G. Scatchard and S. S. Prentiss, *J. Am. Chem. Soc.*, **55**, 4355 (1933). ^d R. H. Stokes and B. J. Levien, *ibid.*, **68**, 333 (1946).

the constancy, indicates that concentration difference and diffusion at the junction do not have a serious effect upon our e.m.f. measurements.

The Na-glass electrode, as is readily seen from the present description, is not quite as accurate as the

(9) See ref. 8, Chapter 3.

(10) M. Nagasawa and I. Kagawa, *J. Polymer Sci.*, **25**, 61 (1957).

(11) It is believed that reliable measurements with amalgam electrodes cannot be carried out for solutions more dilute than about 0.1 M. See S. Glasstone, "An Introduction to Electrochemistry," D. Van Nostrand Co., Inc., Princeton, N. J., 1964, p. 198.

(12) This conclusion is right if the asymmetry potential changes slowly with time, which is believed to be the case.

silver-silver chloride electrodes used by Brown and MacInnes.⁶ For example, these authors reported a value of 0.01 mv. for the reproducibility of their measurements. In view of the performance of the commercially available glass electrode, an accuracy better than ± 0.5 mv. cannot be claimed. The reproducibility was about $\pm 2\%$. Even if it were possible to improve the electrode and set up special measuring circuits, it would be difficult to obtain transference number data of macroions accurately enough. Therefore, in the present work, efforts have not been made to aim at high precision. In the light of such accuracy, impurity problems are relatively unimportant. Brown and MacInnes⁶ have shown that the correction ΔE_i to be applied to observed e.m.f. reading (due to minute traces of salts) is given by

$$\Delta E_i = 47\kappa_i \left(\frac{1}{C_1} - \frac{1}{C_2} \right) \quad (3)$$

where κ_i is the specific conductance due to the contamination, ΔE_i is expressed in mv., and C is the electrolyte concentration in normality. For a value of $\kappa_i = 10^{-6}$ ohm⁻¹ cm.⁻¹, ΔE_i is 0.047 mv. for the cell having the concentration range 1.0 to 10^{-3} *m*. This assumed value for κ_i is certainly large compared to the actual κ value of water used. Therefore, the correction due to contamination is well within our experimental error and is neglected in this paper.

The e.m.f. of the cell shown in (III) is given by

$$E = (2RT/F) \int_{a_2}^{a_1} t_a d \ln a \quad (4)$$

Using the observed value of E and the literature value for t_a , the mean activity coefficient γ^{13} was calculated using the method described by Glasstone.¹¹ Equation 4 was rearranged to

$$\frac{FE}{4.606t_a RT} - \log \left(\frac{m_2}{m_1} \right) + \frac{F}{4.606RT} \int_0^E \delta dE \quad (5)$$

where $\delta = (1/t_a) - (1/t_{a1})$ and t_{a1} is the transference number of the anion at some reference concentration m_1 ; in this case $m_1 = 1.021$, and γ_1 is the activity coefficient at m_1 . The e.m.f. measurements allow us to evaluate the first two terms on the right-hand side of eq. 5. The third term was obtained by graphical integration of δ against E since δ can be derived from the concentration dependence of the transference number. Thus $\log (\gamma_2/\gamma_1)$ was determined and is given in the fourth column of Table I. Usually, in order to determine activity coefficients, use is made of the familiar equation of the Debye-Hückel theory. In the present paper, an expedient was adopted instead; γ_1 was as-

sumed equal to the literature value of the activity coefficient at $m_1 = 1.021$. Then it is possible to derive $\log \gamma$ for any concentration from the values of $\log (\gamma_2/\gamma_1)$ obtained previously. The activity coefficient data thus obtained (γ_{obsd}) are shown in the fifth column of Table I and can be compared with literature values of the activity coefficient (γ_{lit}) shown in the sixth column. The absolute values of the first and second term on the right-hand side of eq. 5 are close to each other, the third term making only a small contribution. Therefore $\log (\gamma_2/\gamma_1)$ is most sensitive to the e.m.f. data. Taking into consideration the reproducibility and accuracy of the measurements, we have an error which does not exceed $\pm 5\%$ for γ_{obsd} values at lower concentrations (0.020 to 0.010 *m*) and $\pm 3\%$ between 0.201 and 0.050 *m*. It can thus be said that there is good agreement between γ_{obsd} and γ_{lit} . Though the agreement is less than that reported by Brown and MacInnes, it is satisfactory for our purpose.

Measurement of the E.m.f. of Concentration Cells of Sodium Polyacrylate. Though experimental procedures and the treatment of data are basically the same as those employed in the case of sodium chloride, the study of polyelectrolytes brings forth a special problem. As was mentioned already,⁴ electrostatic interaction in polyelectrolyte solutions does not disappear at zero polymer concentration since the electric charges on the polymer chain cannot be separated from each other unless the polymer chain is broken into the corresponding monomer units. Therefore, if the adopted standard state of the free energy is the same as that chosen in the case of simple electrolytes, the activity coefficient (of ionized groups) of the polyelectrolytes converges to a value other than unity at the zero polymer concentration. This value clearly depends on the electrostatic interaction between electric charges. This interaction, by various theories, has been related to the intrinsic properties of the polyelectrolyte molecule such as the dimensions of the macroion, the number of electric charges on it, and so on. In the absence of a complete theory, however, the basis of the activity coefficient cannot be provided at zero polymer concentration.

In order to avoid this difficulty, we have used the following convention. By definition, the observed mean activity coefficient γ^* is written as

$$\gamma^{*\alpha+1} = \gamma^{*\alpha}_{2g} \gamma^{*}_{2p} \quad (6)$$

where γ^{*}_{2g} and γ^{*}_{2p} represent the single-ion activity coefficients of gegenions and macroions, respectively.

(13) In the case of sodium chloride, γ^* is equal to γ since complete dissociation can be assumed.

Since α is usually large compared to unity as far as typical polyelectrolytes are concerned, we obtain an approximate relation

$$\gamma^* = \gamma_{2g}^* \quad (7)$$

on the condition that γ_{2p}^* is not extremely small or large. While this condition cannot yet be proved to be true, we expediently determine γ_{1}^* value on the basis of eq. 7, using a γ_{2g}^* value (at a reference concentration of 0.01 *m*) determined independently by measuring the e.m.f. of a cell shown by (II).¹⁴ We then proceed to evaluate γ^* values for other concentrations using the γ_{1}^* value.

The essential data for the computation of the mean activity coefficient from e.m.f. data are gathered in Table II. In the first column, the monomolal concentration is given. The e.m.f. values of the cells shown by (I) are given in the second column. The transference numbers (third column) at each concentration were obtained from the data of Okubo, Nishizaki, and Ise,¹⁴ who carried out the transference experiment following the method developed by Huizenga, Grieger, and Wall.¹⁵ In column 4 the observed mean activity coefficients are given. Column 5 gives the single-ion activity coefficients of gegenions of the same sodium polyacrylate, which were determined independently.¹⁴

In the case of the polyelectrolyte solutions, the accuracy of the e.m.f. measurement was ± 0.5 mv., and the reproducibility was $\pm 2\%$. The accuracy of transference number data is estimated to be $\pm 2\%$. Taking these factors into consideration, the limit of error associated with the γ_{obsd}^* values was found to increase with decreasing concentration and t_{2p} value; the highest limit of error obtained was about $\pm 7\%$ for $t_{2p} = 0.48$ and $m = 0.00435$. Except for this extreme case, a value of $\pm 5\%$ was the limit of experimental error.

For convenience, the experimental data are also presented in Table III, together with theoretical values for activity coefficients. From Table II (the fifth column), it is seen that γ_{2g}^* is about 0.28, almost independent of the polymer concentration in the concentration range studied. This independence is also demonstrated in the fifth column of Table III, which shows that the ratio of γ_{2g}^* to that at the reference molality (0.01) is about unity. On the other hand, the observed value of γ^* decreases with increasing concentration, as is seen in the fourth column of Table II and the second column of Table III. Thus it is evident that γ^* is not always equal to γ_{2g}^* ; in other words, eq. 7 does not hold generally. It is then interesting to estimate the relative change of γ_{2p}^* . The eighth column of Table III gives the relative change of γ_{2p}^* obtained from the observed γ^* and γ_{2g}^* using eq. 6.

Table II: Mean Activity Coefficient of Sodium Polyacrylate

Molality	E.m.f., mv. ^a	t_{2p}^b	γ_{obsd}^*	γ_{2g}^*
0.00435	34.6	0.480	0.32	0.29
(0.01)	(0.29)	(0.29)
0.0116	27.5	0.480	0.28	0.29
0.0166	24.0	0.480	0.26	0.28
0.0331	16.0	0.481	0.25	...
0.0663	7.8	0.485	0.24	0.28
0.0995	5.7	0.494	0.19	0.28
0.167	0.0	0.522	0.18	0.28
0.227	-2.5	0.522	0.15	...

^a The e.m.f. measurements were carried out with $m_1 = 0.167$, whereas the γ_{obsd}^* values were determined using a γ_{2g}^* value at 0.01. ^b From the measurements in the work cited in ref. 14.

The enormous change of γ_{2p}^* with concentration should be noted and will be discussed later.

It would be useful to mention the single-ion activity coefficients of macroions (γ_{2p}^*) and gegenions (γ_{2g}^*). However, as explained in the Introduction to this paper, the single-ion activities are inaccessible to exact thermodynamics. It should also be noted that a meaningful discussion of γ_{2p}^* cannot be given because of experimental difficulties as well as of the basic inaccessibility alleged by Guggenheim.³ Since an electrode, reversible with respect to macroions, is not available, we are forced to estimate γ_{2p}^* indirectly by measuring γ^* and eq. 6. Usually, when polyelectrolytes are concerned, α is very large compared to unity. Therefore, it is clear from eq. 6 that γ^* must be known to a high degree of accuracy in order to obtain a reasonably accurate value of γ_{2p}^* . For example, if α is assumed to be 1000, which appears to be a reasonable estimate for ordinary polyelectrolytes, an error of γ^* of 0.1% corresponds to an error in γ_{2p}^* of 100%. Evidently, such high accuracy for γ^* cannot be expected. Thus, it is difficult to compute exact values of γ_{2p}^* from data of γ^* .¹⁶ On the other hand, eq. 6 indicates that, however large α may be, the magnification of error does not matter when the aim is to estimate γ_{2g}^* . This is one reason why γ_{2g}^* could often be used for discussion of thermodynamic properties of polyelectrolyte solutions. It should be carefully noted, however, that this usefulness relies ultimately on the well-known assumption

(14) T. Okubo, Y. Nishizaki, and N. Ise, *J. Phys. Chem.*, **69**, 3690 (1965).

(15) J. R. Huizenga, P. F. Grieger, and F. T. Wall, *J. Am. Chem. Soc.*, **72**, 2636 (1950).

(16) Note that the enormous change of γ_{2p}^* mentioned in the preceding paragraph exceeds largely the limit of error associated with γ_{2p}^* .

Table III: Relative Changes of γ^* , γ_{2g}^* , and γ_{2p}^* with Concentration and Comparison with Theory^a

Molality	$\gamma^*/\gamma_{0.01}^*$			$\gamma_{2g}^*/\gamma_{2g0.01}^*$			$\gamma_{2p}^*/\gamma_{2p0.01}^*$		
	Obsd.	Calcd.		Obsd.	Calcd.		Obsd.	Calcd.	
		$R = 100 \text{ \AA.}$	$R = 120 \text{ \AA.}$			$R = 100 \text{ \AA.}$		$R = 120 \text{ \AA.}$	
0.001	...	2.59	1.31	...	1.21	1.21	...	10^{238}	10^{26}
0.01	1.00	1.00	1.00	1.00	1.00	1.00	1.00	1.00	1.00
0.03	0.86	0.63	0.86	0.97	0.89	0.89	10^{-38}	10^{-105}	10^{-10}
0.1	0.66	0.53	0.80	0.97	0.82	0.82	10^{-120}	10^{-136}	10^{-18}

^a The reference molality is 0.01.

tion pertaining to the liquid junction potentials which has not yet been rigorously established.

In view of ambiguities associated with the single-ion activity coefficients discussed briefly in the preceding paragraph, it is desirable to discuss the solution properties of polyelectrolytes in terms of the mean activity coefficient. It is also thermodynamically significant. Furthermore, it would be interesting to show how useful the mean activity coefficient is. First of all, we have to mention a test of the Gibbs-Duhem equation in polyelectrolyte solutions.¹⁷ The test of this equation, as is well-known, had been impossible because of the lack of mean activity coefficient data. However, using the data presented in this paper and the osmometrically determined activity coefficient of solvent, the equation can now be checked. In other words, the reliability of thermodynamic solution data can be conclusively discussed. It would also be useful to recall recent observation by Nagasawa and Fujita¹⁸ that, when the mean activity coefficient in the Gibbs-Duhem equation is replaced by the single-ion activity coefficient, the modified equation gives single-ion activity coefficient values, which not only disagree numerically with values determined by other direct methods but also show a concentration dependence quite different from the experimental one. It is plausible that the origin of this contradiction is the replacement of γ^* by γ_{2g}^* in the equation, *i.e.*, the adoption of eq. 7. As a matter of fact, γ^* values calculated by the (unmodified) Gibbs-Duhem equation agreed with observed values of γ^* in a high concentration range.¹⁷ Here again, the inaccuracy of eq. 7 is clearly demonstrated.

The next step to be taken is comparison of the experimental data with theory. As may be understood from the discussion given later, in order that the experimental data of mean activity coefficient can be accounted for by any theory, the macroion-macroion interaction has to be taken into consideration in that theory. Regrettably, there are only a few theories: a theory by Harris and Rice¹⁹ and our previous theory^{4a}

appear to meet this requirement. The former theory, however, led us to a complicated expression for γ^* so that the comparison using this theory will be reported in a subsequent paper. In the present paper we confine ourselves to our theory.

As is mentioned in another paper,¹⁴ mean activity coefficient and single-ion activity coefficients of macroions and gegenions formulated in our theory are denoted by γ , γ_{2p} , and γ_{2g} , respectively, and are based on the assumption that the electrolyte is partially dissociated; that is, the macroion is not Z valent but α valent.²⁰ These quantities should not be confused with the experimentally found activity coefficients, which are "stoichiometric" ones determined on the assumption that the electrolyte is fully dissociated and which have been and will be expressed by γ^* terms in this paper. If the fraction of free gegenions is denoted by β , we obtain

$$\gamma^* = \beta\gamma, \quad \gamma_{2g}^* = \beta\gamma_{2g}, \quad \text{and} \quad \gamma_{2p}^* = \beta\gamma_{2p} \quad (8)^{21}$$

Furthermore, thermodynamics gives

$$\gamma^{\alpha+1} = \gamma_{2p}\gamma_{2g}^{\alpha} \quad (9)$$

If we assume that β is equal to the polymer charge fraction (i/s), which was determined by transference experiment,¹⁴ observed values of mean activity coefficient, γ^* , can be compared with the theoretical value by means of eq. 8. The expressions for γ_{2p}

(17) N. Ise and T. Okubo, publication in preparation.

(18) M. Nagasawa and H. Fujita, *J. Am. Chem. Soc.*, **86**, 3005 (1964).

(19) F. E. Harris and S. A. Rice, *J. Chem. Phys.*, **25**, 955 (1956).

(20) The macroion is assumed to have Z ionizable groups and λ bound gegenions, and $\alpha = Z - \lambda$.

(21) It should be recalled that the same standard state of chemical potential of polyelectrolyte as that of the 1-1 type electrolyte was adopted. To be correct, consequently, γ_{2p} must be called the "single-ion activity coefficient of α ionizable groups of the macroion," whereas γ_{2g} must be called the "single-ion activity coefficient of α ionized groups of the macroion," though the term "single-ion activity coefficient of the macroion" does not result in confusion. In the light of such a physical meaning of γ_{2p}^* , the reason for the difference between γ_{2p}^* and γ_{2p} , and between γ^* and γ would be understood.

and γ_{2g} obtained in the previous treatment^{4a} reduce to the following in salt-free polyelectrolyte solutions

$$kT \ln \gamma_{2g} = -\frac{\kappa e_0^2}{3\epsilon} \left\{ \tau(\kappa\delta_2) + \frac{[\alpha\sigma(\kappa R) + \sigma(\kappa\delta_2)](1 - 2n_2\alpha v_{2g})}{2(\alpha\mathfrak{M}_{2p} + \mathfrak{M}_{2g})} \right\} \quad (10)$$

$$kT \ln \gamma_{2p} = -\frac{\alpha^2 \kappa e_0^2}{3\epsilon} \left\{ \tau(\kappa R) + \frac{[\alpha\sigma(\kappa R) + \sigma(\kappa\delta_2)](1 - 2n_2 v_{2p})}{2(\alpha\mathfrak{M}_{2p} + \mathfrak{M}_{2g})} \right\} + \frac{e_0^2}{\epsilon} \left\{ \frac{3\alpha^2}{5R} - \frac{1}{2\delta_2}(Z + \lambda) \right\} \quad (11)$$

with

$$\kappa^2 = \frac{4\pi e_0^2}{\epsilon kT} [\alpha n_2(\alpha\mathfrak{M}_{2p} + \mathfrak{M}_{2g})]$$

where e_0 is the absolute value of the elementary charge, k the Boltzmann constant, ϵ the dielectric constant of solvent, δ_2 the mean radius of an ionized group and a gegenion, n_2 the number of macroions per unit volume of solution, r the radius of macroion sphere, \mathfrak{M}_i the exclusion volume parameter of ion i ($\mathfrak{M}_{2p} = 1 - n_2 v_{2p}$ for macroions), and v_i the exclusion volume of ion i ($v_2 = 4\pi r^3/3$ for macroions). The subscript 2 refers to polyelectrolyte. σ and τ are familiar functions which appear in the Debye-Hückel theory.²²

Using eq. 8-11, γ^* was calculated with the values of $\beta = 0.44$, $Z = 1640$, $\lambda = 920$, $\alpha = 720$,²³ $\delta_2 = 4 \text{ \AA}$., and appropriate values of r . In Table III, the theoretical values of $\gamma^*/\gamma_{0.01}^*$, $\gamma_{2g}^*/\gamma_{2g,0.01}^*$, and $\gamma_{2p}^*/\gamma_{2p,0.01}^*$ are presented. It is clear that the theoretical value of $\gamma^*/\gamma_{0.01}^*$ decreases with concentration in accordance with the observed tendency. On the other hand, the calculated value of $\gamma_{2g}^*/\gamma_{2g,0.01}^*$ is much more insensitive to the concentration than that of $\gamma^*/\gamma_{0.01}^*$. This is also a fact experimentally found (compare columns two and five). This difference can be attributed to the contribution of γ_{2p}^* , as was mentioned already. In the ninth and tenth columns of Table III, the theoretical values of $\gamma_{2p}^*/\gamma_{2p,0.01}^*$ are presented. Taking into account the fact that the calculated values are very sensitive to the assumed value of r , we note that the agreement between theoretical and observed (eighth column) values is satisfactory.

It should be further noted that γ_{2p} consists of contributions of macroion-macroion interaction and intramacroion interaction. The former is represented by the κ -containing first term²⁴ on the right-hand side of eq. 11, and the latter by the rest. According to our nu-

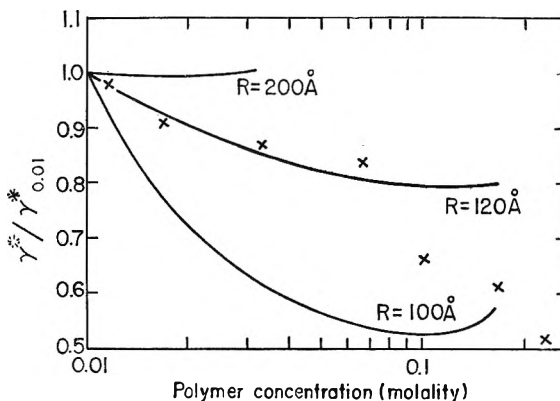


Figure 2. Concentration dependence of the mean activity coefficient: —, theory; ×, observed.

merical calculations, the intermacroion interaction is as strong as the intramacroion interaction. Therefore, the observed enormous change of γ_{2p}^* with concentration should be attributed to these two kinds of interactions and indicates that the contribution of macroion-macroion interaction in the thermodynamic properties of dilute polyelectrolyte solutions is not negligible at all, but strikingly influential. This is in contrast with what has been often assumed in many theoretical treatments of polyelectrolytes. The important role of the macroion-macroion interaction has been pointed out in a series of our previous papers⁴ and is now again demonstrated by measurements of a thermodynamically significant quantity, *e.g.*, the mean activity coefficient.

In Figure 2, the theoretical and observed values of $\gamma^*/\gamma_{0.01}^*$ are compared. Three curves represent theoretical ones obtained with r values indicated in the figure, whereas the crosses denote experimental data. Figure 2 shows that a theoretical curve obtained with $r = 120 \text{ \AA}$. is in excellent agreement with experimental data between 0.01 and 0.07 *m*, and observed values at high concentrations deviate from this curve, approaching a theoretical curve obtained with $r = 100 \text{ \AA}$. as the concentration increases. This is quite understand-

(22) R. H. Fowler and E. A. Guggenheim, "Statistical Thermodynamics," 1st Ed., Cambridge University Press, London, 1939, Chapter 9.

(23) The transference experiment in the work cited in ref. 14 shows that the polymer charge fraction i/s ($=\beta$) varies only slightly with concentration. The value adopted here, *i.e.*, 0.44, is the average one. The value of α was obtained by $\alpha = \beta Z$, where Z , the total number of ionizable groups of a macroion, happens to be equal to the degree of polymerization under our experimental condition. λ was determined by $\alpha = Z - \lambda$.

(24) This term contains also macroion-gegenion interaction. However, this interaction would be much smaller than the macroion-macroion interaction, judged from the nature of Coulombic interaction.

able since the radius of the polymer sphere would decrease with increasing polymer concentration.

Finally, mention should be made of the value of r found above. Figure 2 shows that 120 Å. for r gives a very satisfactory agreement between theory and experiment in the dilute region. Since information on this quantity at finite concentrations from other sources is not available, no convincing conclusion can be drawn. It should be noted, however, that, if this value of r is used for computation of γ_{2g} (by means of eq. 10),

an excellent agreement between theory and experiment can also be obtained as is shown in Table III.

Acknowledgments. The authors gratefully acknowledge the encouragement and useful criticisms received from Professor Ichiro Sakurada. N. I. expresses sincere thanks to Professor U. P. Strauss for having directed attention to the Na-glass electrode and to Professors F. T. Wall and J. T. Edsall for comments at the early stage of the experiments, and Professors M. Nagasawa and H. Fujita for valuable discussion.

The Determination of the Ionization Constants of Some Sulfonic Acids by Raman Measurements

by O. D. Bonner and Arnold L. Torres

*Department of Chemistry, University of South Carolina, Columbia, South Carolina
(Received May 12, 1965)*

The degrees of ionization of *p*-toluenesulfonic acid and 2,5-dimethylbenzenesulfonic acid in aqueous solutions have been determined by comparison of the ratio of intensities of the Raman lines arising from the C-H stretch in the CH₃ group and the S-O stretch for each sulfonate ion. These data have been combined with activity coefficient data to yield ionization constants of 11.6 ± 0.5 and 2.7 ± 0.5 for the two acids. A comparison of infrared spectra for samples of an ion-exchanger film indicates a degree of ionization comparable to that of the two "model" compounds.

The introduction of the sulfonic acid type of cation-exchange resins, consisting of sulfonate-exchange sites on polystyrene-divinylbenzene matrices, has resulted in the accumulation of very precise equilibrium data. The structures of these resins are reasonably well known, and resin samples from the same batch are quite uniform. There have been many attempts to interpret these data for various pairs of ions. One of the most interesting phenomena is the reversal of selectivity shown in exchanges involving an alkali metal ion, *e.g.*, sodium ion, and hydrogen ion. The resin exhibits the expected preference for sodium ion except in cases where the sodium ion loading exceeds

about 90%, in which case hydrogen ion is then preferred. This behavior has led to considerable speculation as to the strengths of sulfonic acids. Because of the insolubility of the ion-exchange resins, many studies have been made on solutions of "model" compounds similar in structure to the repeating units of the ion exchanger.

Mock and Marshall¹ have investigated a sulfonated 1:1 copolymer of styrene and vinyltoluene having a molecular weight of approximately 224,000 and report a degree of ionization, α , of 0.38 as determined from

(1) R. A. Mock and C. A. Marshall, *J. Polymer Sci.*, **13**, 263 (1954).

pH measurements on binary solutions of the polymer and HCl. The degree of polymerization was also found to be independent of concentration. In further investigations, Mock and co-workers² confirm this value by conductance measurements. The calculations assume, however, that the value of Λ^0 is chiefly a consequence of proton conductance with little contribution from the polysulfonate ion. These results may be contrasted with the work of Lapanje and Rice³ in which Raman spectra were obtained for solutions of polystyrenesulfonic acid (PSSA) and ethylbenzenesulfonic acid (EBSA). Those workers concluded that the absence of new lines in the spectrum of PSSA and the fact that the relative intensities of the lines are approximately the same as in EBSA strongly suggest that PSSA is completely ionized. This assumes, of course, the complete ionization of EBSA. This result was in qualitative agreement with the proton magnetic resonance study of Kotin and Nagasawa,⁴ who interpreted chemical shift data as indicating that PSSA is completely ionized. Dinius and Choppin⁵ have measured nuclear magnetic resonance spectra of *p*-toluenesulfonic acid as a function of concentration and find an acid ionization constant calculated from chemical shifts to be 22 ± 3 . This value lies between those found by Mock and Marshall and by Lapanje and Rice.

Bonner and co-workers have speculated on the strengths of sulfonic acids on the basis of results obtained from studies of "model" compounds and from ion-exchange equilibria involving hydrogen ion at several temperatures. Studies of soluble sulfonates indicated⁶ that sulfonic acids are only moderately strong acids; the ionization constants of the higher molecular weight acids are probably the same order of magnitude but lower than that of nitric acid. An ionization constant of the order of 5 to 10 was postulated for 16% DVB resin⁷ from equilibrium studies and calorimetric measurements indicated⁸ fewer un-ionized exchange sites on resins of lower DVB content. The investigations reported in this paper were initiated in an attempt to determine with certainty the ionization constants of representative sulfonic acids, to correlate acid strengths with structure, and to relate these results to ion-exchange equilibria.

Experimental Section

All Raman spectra were recorded by a Cary Model 81 Raman spectrophotometer. A circulating filter solution was used to isolate the 4358-Å. mercury-exciting line. This solution consisted of 125 ml. of *o*-nitrotoluene and 1.75 g. of ethyl violet in 3 l. of isopropyl alcohol. The frequencies of all sharp lines are expected to be accurate to ± 5 cm.⁻¹. A standard

Cary 7-mm. cell with a volume of 5 ml. was employed. A spectral slit width of 10 cm. and slit height of 10 cm. were used to record all spectra. Varying amplifications and scanning times were used for the solutions of different concentrations.

Osmotic and activity coefficients of the acids were determined by isopiestic comparison of solutions of these electrolytes with solutions of lithium chloride which were used as standards. Osmotic coefficients were calculated from the equation

$$\nu\phi = \nu_{\text{ref}} \frac{m_{\text{ref}}}{m} \phi_{\text{ref}}$$

Activity coefficients were calculated from the equation

$$\log \gamma = \log \gamma_{\text{ref}} + \log \frac{m_{\text{ref}}}{m} +$$

$$\frac{2}{2.303} \int_0^{m_{\text{ref}}^{1/2}} \frac{\frac{m_{\text{ref}}}{m} - 1}{(m\gamma)_{\text{ref}}^{1/2}} d(m\gamma)_{\text{ref}}^{1/2}$$

Aqueous solutions of *p*-toluenesulfonic acid and 2,5-dimethylbenzenesulfonic acid were prepared from reagent grade material. The sodium salts were prepared by neutralization of the acid solutions with reagent grade hydroxides.

Results and Discussion

Raman band frequencies and relative intensities are reported for sodium *p*-toluenesulfonate and sodium 2,5-dimethylbenzenesulfonate in Table I. The same band frequencies are observed for the corresponding acids. In each instance the band occurring at 2925 cm.⁻¹ is assigned to the C-H stretch of the methyl group. The bands which occur at 1125 cm.⁻¹ in the case of the *p*-toluenesulfonates and 1025 cm.⁻¹ in the case of the 2,5-dimethylbenzenesulfonates are due to the sulfonate ion.^{3,9,10} Preliminary ultraviolet absorption spectra revealed that at the wave length of the exciting line (4358 Å.) these substances absorb light. Further, acids and salts of the same concentration absorb differently, indicating different extinction co-

(2) R. A. Mock, C. A. Marshall, and T. E. Slykhouse, *J. Phys. Chem.*, **58**, 498 (1954).

(3) S. Lapanje and S. A. Rice, *J. Am. Chem. Soc.*, **83**, 496 (1961).

(4) L. Kotin and M. Nagasawa, *ibid.*, **83**, 1026 (1961).

(5) R. H. Dinius and G. R. Choppin, *J. Phys. Chem.*, **66**, 268 (1962).

(6) O. D. Bonner and O. C. Rogers, *ibid.*, **64**, 1499 (1960).

(7) O. D. Bonner and R. R. Pruett, *ibid.*, **63**, 1417 (1959).

(8) O. D. Bonner and J. R. Overton, *ibid.*, **65**, 1599 (1961).

(9) G. Zundel, H. Noller, and G. M. Schwab, *Z. Elektrochem.*, **66**, 129 (1962).

(10) G. Zundel, H. Noller, and G. M. Schwab, *ibid.*, **66**, 122 (1962).

efficient for the un-ionized acid and the sulfonate ions. This prevented direct comparisons of the intensities of the sulfonate bands occurring in the salt solutions and the various acid solutions. The ratio of the intensities of the sulfonate ion and C-H bands in the same solution was found, however, to be proportional

Table I: Raman Intensities

Sodium toluenesulfonate		Sodium 2,5-dimethylbenzenesulfonate	
Frequency, ^a cm. ⁻¹	Intensity	Frequency, ^a cm. ⁻¹	Intensity
225	12	285 b	20
295	31	345	30
395 b	6	465	65
495 b	3	705	32
560 b	6	745	22
630	24	880	37
680 b	6	1025	92
805	50	1100	17
1005	10	1150 sh	10
1030	22	1215	67
1125	100	1280	8
1180 sh	10	1380	48
1210	23	1440 b	12
1375	15	1565 sh	15
1600	65	1510	70
2875 sh	12	2375 sh	22
2925	48	2325	100
2975 sh	12	2375 sh	37
3060	58	3360	54

^a b, broad; sh, shoulder.

to the fraction of sulfonate ion (sulfonate ion concentration divided by the stoichiometric sulfonate concentration). The band at 2925 cm.⁻¹ was chosen as the reference band rather than the C-H stretch of the hydrogen atoms on the aromatic ring because it is not affected by other ring substituents and, therefore, is independent of the degree of ionization of the sulfonic acids. Plots of these intensity ratios are shown in Figure 1. The degree of ionization of the acid in the various solutions was calculated from these data, and the stoichiometric ionization quotient $Q_m = \alpha^2 m / (1 - \alpha)$ was determined. This quotient must be corrected by the term $f_+ f_- / \beta$ in order to obtain the ionization constant. Activity coefficients have been reported for *p*-toluenesulfonic acid up to 5.0 *m*¹¹ and osmotic coefficients up to 10.0 *m*.¹² Osmotic and activity coefficients are available for solutions of 2,5-dimethylbenzenesulfonic acid solutions up to 5.0 *m*.¹³ In order to make activity coefficient corrections, further isopiestic equilibrations have been carried out which permit the data for both acids to be extended to more concentrated

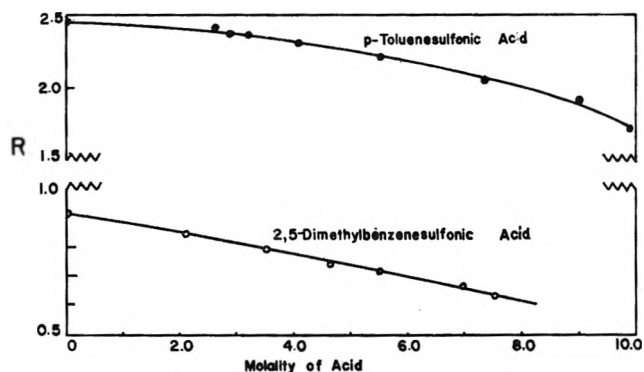


Figure 1. Ratio of intensities of the bands arising from the sulfonate groups and the methyl groups in *p*-toluenesulfonic and 2,5-dimethylbenzenesulfonic acids. Intensity ratios at zero concentration are for solutions of the sodium salts. These ratios are independent of the concentrations of the salt solution. Degree of ionization = R_{acid}/R_{salt} .

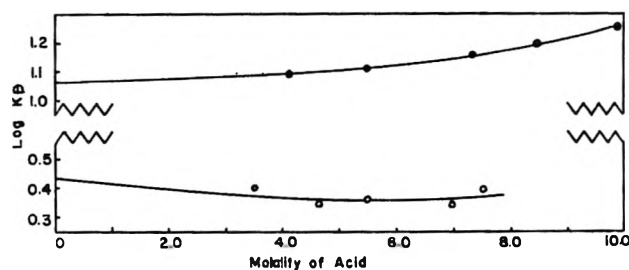


Figure 2. Ionization constants of *p*-toluenesulfonic and 2,5-dimethylbenzenesulfonic acids.

Table II: Osmotic and Activity Coefficients

<i>p</i> -Toluenesulfonic acid		2,5-Dimethylbenzenesulfonic acid	
<i>m</i>	γ	ϕ	γ
5.0	0.453	0.773	0.298
5.5	0.471	0.796	0.299
6.0	0.492	0.821	0.301
6.5	0.516	0.848	0.305
7.0	0.542	0.874	0.310
7.5	0.572	0.899	0.316
8.0	0.606	0.923	0.322
8.5	0.639	0.946	0.328
9.0	0.675	0.966	0.334
9.5	0.715	0.984	0.339
10.0	0.754	1.000	0.344

solutions (Table II). These data, however, represent mean *stoichiometric* activity coefficients, γ_{\pm} , and the

(11) O. D. Bonner, G. D. Basterling, D. L. West, and V. F. Holland, *J. Am. Chem. Soc.*, **77**, 242 (1955).

(12) O. D. Bonner and O. C. Rogers, *J. Phys. Chem.*, **65**, 981 (1961).

(13) O. D. Bonner, V. F. Holland, and L. L. Smith, *ibid.*, **60**, 1102 (1956).

ionic activity coefficients necessary for the corrections were calculated from the relationship $\gamma_{\pm} = \alpha f_{\pm}$, where f_{\pm} is now the mean *ionic* activity coefficient. The extrapolation of a plot of $\log K\beta$ vs. molality to infinite dilution (Figure 2) yields ionization constants of 11.6 ± 0.5 and 2.7 ± 0.5 for *p*-toluenesulfonic and 2,5-dimethylbenzenesulfonic acids, respectively.

These two sulfonic acids may be considered as "models" of the repeating units in a sulfonated styrene-divinylbenzene ion-exchange resin. The values obtained for the ionization constants indicate that all exchange sites on the resin are not identical, and the incomplete ionization of the sulfonic acids explains some of the phenomena occurring in exchanges involving hydrogen ion. The relatively large difference

in the strengths of these acids leads one to the conclusion that the difference in the behavior of resins of different DVB content is due to the properties of the sulfonated DVB bridges to at least as great an extent as to the differences in concentration. The direct calculation of the ionization constant of a resin sample is difficult since the resins will not swell sufficiently for one to obtain very dilute solutions. The results reported by Zundel and co-workers^{9,10} of infrared spectra of ion-exchange films indicate, however, that the degree of ionization of the ion exchanger is similar to that of these "model" sulfonates at comparable concentrations.

Acknowledgment. The support of this research by the Atomic Energy Commission under Contract At-(40-1)-1437 is gratefully acknowledged.

Structure of the Electrical Double Layer at a Mercury Electrode in the Presence of Adsorbed Nitrate Ions

by Richard Payne

*Air Force Cambridge Research Laboratories, L. G. Hanscom Field, Bedford, Massachusetts
(Received June 4, 1966)*

The adsorption of the nitrate ion on a mercury electrode from mixed solutions of ammonium nitrate and ammonium fluoride has been studied by measuring the double-layer capacity as a function of solution composition at 25°. The adsorption can be described by Frumkin's modification of the Langmuir isotherm with a small repulsive lateral interaction coefficient, a nonlinear charge dependence of the standard free energy of adsorption, and a low saturation coverage. The large apparent area occupied by the adsorbed ion is tentatively interpreted in terms of two-dimensional hydration. The amounts adsorbed are calculated and the capacity is resolved into its component parts with the aid of the isotherm and diffuse-layer theory. The (integral) capacity measured at constant amount adsorbed decreases linearly with the amount adsorbed, and the capacity measured at constant charge is a function of the charge. These observations are critically discussed in terms of the Grahame-Stern model of the double layer, and an alternative interpretation based on a model of mixed adsorption of the anion and the solvent is suggested.

Introduction

The specific adsorption of the nitrate ion at the mercury-solution interface is more complex than the adsorption of the structurally simpler halide ions which have been studied in some detail.¹⁻³ Grahame and Soderberg⁴ first recognized this anomalous behavior which they attributed to the operation of weaker adsorption forces of the van der Waals type in the case of the nitrate ion. However, the nitrate ion appears to be at least as extensively adsorbed as the chloride ion although the adsorption increases more rapidly with the potential in the former case. For this reason, the characteristic capacity "hump" which is largely obscured by the adsorption in chloride solutions is well developed in nitrate solutions. The interpretation of the hump is of considerable theoretical interest in view of its close connection with the structure of the solvent dielectric in the inner region of the double layer.⁵ Considerable insight into the structure of the inner region is possible from a study of specific adsorption of the anion.^{1,2}

Because the adsorption of the nitrate ion is not so strongly potential dependent as that of previously

studied anions, it is difficult to obtain accurate measurements of the amount adsorbed especially at the lower concentrations because of uncertainties in the diffuse layer concentration of anions.⁶ For this reason, measurements have been made in mixed solutions of ammonium nitrate and ammonium fluoride of constant ionic strength. This method possesses the double advantage of eliminating the diffuse-layer correction to the amount adsorbed and of minimizing the effect of the diffuse-layer capacity in the subsequent analysis.

Experimental Section

The double-layer capacity at a dropping mercury electrode was measured for eight solutions of $x M \text{NH}_4\text{NO}_3 + (1 - x) M \text{NH}_4\text{F}$ in water for the range $0 \leq x \leq 1$ at 25° using the a.c. bridge method de-

- (1) D. C. Grahame, *J. Am. Chem. Soc.*, **80**, 4201 (1958).
- (2) D. C. Grahame and R. Parsons, *ibid.*, **83**, 1291 (1961).
- (3) R. Payne, *J. Chem. Phys.*, **42**, 3371 (1965).
- (4) D. C. Grahame and B. Soderberg, *ibid.*, **22**, 449 (1954).
- (5) R. Parsons, "Advances in Electrochemistry and Electrochemical Engineering," Vol. I, Interscience Publishers, Inc., New York, N. Y., 1961, p. 1.
- (6) K. M. Joshi and R. Parsons, *Electrochim. Acta*, **4**, 129 (1961).

scribed previously.⁷ A calomel reference electrode in 1 *M* KCl was used for all the measurements. The reference electrode solution was isolated from the test solution by a closed stopcock to reduce instability of the liquid junction potential. The reproducibility of the liquid junction potential was checked repeatedly by measurements of the potential of the electrocapillary maximum (e.c.m.) for the base solution (*i.e.*, 1 *M* NH₄F). The e.c.m. potential was measured for each solution by the method of the streaming mercury electrode.⁸

Solutions were prepared volumetrically from permanganate-distilled water and A.R. grade salts. NH₄NO₃ was recrystallized before use but NH₄F was used without further purification after attempts to purify this salt by vacuum sublimation resulted in decomposition. However, no evidence of organic or inorganic impurity was detected in the impedance measurements. Mercury was prepared by agitating with dilute nitric acid followed by multiple distillation *in vacuo*. Details of the preparation of capillaries and other details are given elsewhere.⁹ The measurements were made in a water thermostat controlled to $\pm 0.05^\circ$.

Results

The capacity of the double layer is shown as a function of the potential for seven solutions of x *M* NH₄NO₃ + (1 - x) *M* NH₄F in Figure 1. The characteristic hump in the anodic branch of the curve for the base solution is further developed by addition of NH₄NO₃ to the solution owing to specific adsorption of the NO₃⁻ ion. Coincidence of the curves for all solutions at potentials more negative than -1.2 v. shows that the NO₃⁻ ion is completely desorbed in this region. The potentials and capacities at the e.c.m. are summarized in Table I.

The capacity data were integrated on an Elliot 803 computer to give values of the capacity (C), potential measured with respect to a hypothetical reference electrode reversible to the cation (E^+), the interfacial tension (γ') relative to that of the base solution at the same value of the surface charge density on the metal (q), and the function $\xi^+ = \gamma' + qE^+$ all interpolated to integral values of q . The constants of integration were evaluated by assuming equality of the charge and interfacial tension for all solutions at sufficiently negative values of q ($-20 \mu\text{coulombs/cm}^2$). A check of the accuracy of this procedure was made by comparing the values of the e.c.m. potential obtained by the back-integration method with independent values measured by the streaming mercury electrode method. The agreement found was usually better

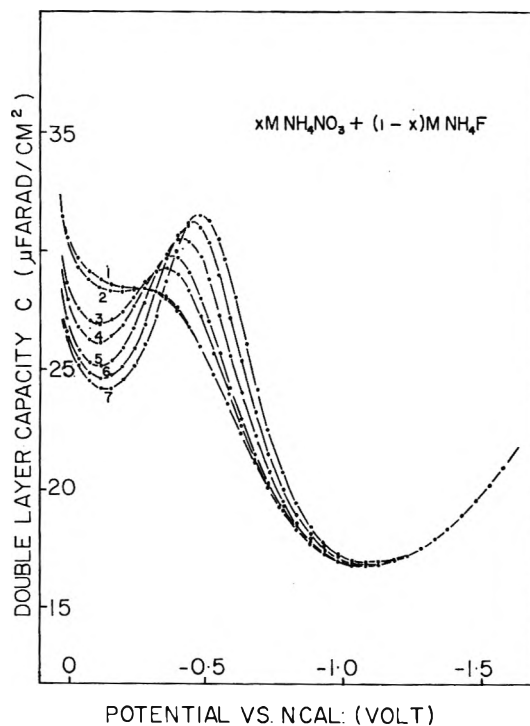


Figure 1. Differential capacity of the electrical double layer in contact with solutions of x *M* NH₄NO₃ + (1 - x) *M* NH₄F in water at 25°: x = (1) 0; (2) 0.01; (3) 0.01; (4) 0.02; (5) 0.05; (6) 0.1; (7) 0.2.

Table I: Potential and Capacity at the Electrocapillary Maximum for Solutions of x *M* NH₄NO₃ + (1 - x) *M* NH₄F in Water at 25°

x , mole l. ⁻¹	$-E_{\text{meas}}^a$, mv.	$-E_{\text{calcd}}^b$, mv.	C , $\mu\text{f. cm}^{-2}$
0.0	474.0	...	26.13
0.001	474.7	473.6	26.27
0.005	476.6	477.0	26.74
0.01	480.4	480.1	27.27
0.02	484.4	484.3	27.96
0.05	495.9	495.5	29.33
0.1	509.1	508.7	30.39
0.2	523.2	523.6	31.06
1.0	563.6	565.1	31.18

^a E_{meas} was measured directly by the streaming mercury electrode method.⁸ ^b E_{calcd} was calculated by back-integration of the capacity-potential curve from the far cathodic end using a value of $q = -20 \mu\text{coulombs cm}^{-2}$ at $E = 1.5215$ v. obtained from the data for 1 *M* NH₄F.

than 1 mv. (Table I). Since the cation concentration was kept constant throughout, the experimental E

(7) G. J. Hills and R. Payne, *Trans. Faraday Soc.*, **61**, 316 (1965).

(8) D. C. Grahame, E. M. Coffin, J. T. Cummings, and M. A. Poth, *J. Am. Chem. Soc.*, **74**, 1207 (1952).

(9) R. Payne, *J. Electroanal. Chem.*, **7**, 33 (1964).

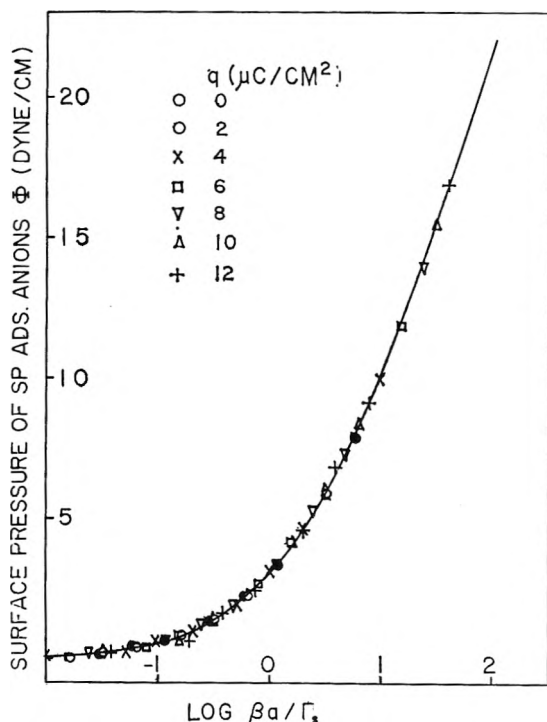


Figure 2. Composite curve of the surface pressure (Φ) of specifically adsorbed nitrate ions measured at constant charge as a function of the chemical potential of anions in the solution.

values could be equated to E^+ . No correction for the variation of the cation activity with solution composition was considered necessary.

The Gibbs adsorption equation for the present system takes the form¹⁰

$$-d\xi^+ = kT\Gamma_{\text{NO}_3^-} d \ln x - E^+dq \quad (1)$$

where $\Gamma_{\text{NO}_3^-}$ is the surface concentration of specifically adsorbed NO_3^- ions; *i.e.*, no correction for the diffuse-layer concentration of NO_3^- is necessary.¹¹ The surface pressure (Φ) of the specifically adsorbed ions was therefore simply evaluated as $\xi^+ - \xi_0^+$ where ξ_0^+ refers to the base solution. Φ was then plotted against $\log x$ for constant integral values of q . As before,^{3,12,13} it was found possible to construct a single composite surface pressure curve by superimposing the individual curves for different values of q by sliding them along the $\log x$ axis. The results of this fit are shown in Figure 2. The majority of the points are indistinguishable from the common curve, and the maximum deviation is no more than 0.4 dyne/cm.

The results were fitted to a Frumkin isotherm which has the form¹⁴

$$\ln \frac{\theta}{1-\theta} + A\theta = \ln \frac{\beta a}{\Gamma_s} \quad (2)$$

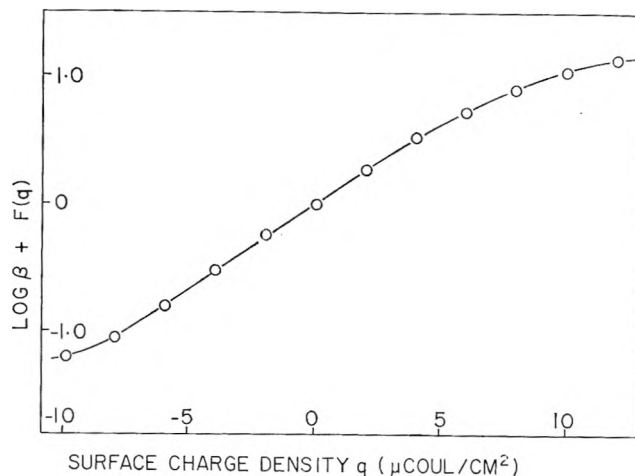


Figure 3. Dependence of the standard free energy of adsorption ($\log \beta$) of nitrate ions on the surface charge density (q) for a constant-charge isotherm.

where θ is the fractional surface coverage, A the dimensionless lateral interaction coefficient, a the activity of the adsorbate, and Γ_s the saturation coverage. β is a constant related to the standard free energy of adsorption by

$$\ln \beta = -\Delta G^\circ/RT \quad (3)$$

The method of fitting the data was, as before, by comparing the experimental surface pressure data with theoretical values calculated by integrating the isotherm. The curves were compared in the form of universal plots of $\log \Phi$ vs. $\log a$ (see ref. 12). In this way the value of the interaction coefficient A and a rough fit were obtained. The fit was then improved by comparing the curves in the form of Φ vs. $\log a$. The solid line in Figure 2 was calculated from a Frumkin isotherm having the constants

$$\begin{aligned} A/2.303 &= 1 \\ \left\{ \begin{aligned} \Gamma_s &= 1.54 \times 10^{14} \text{ molecules/cm}^2 \\ q_s^1 &= 24.7 \text{ } \mu\text{coulombs/cm}^2 \end{aligned} \right. & (4) \\ \log \beta &= 14.95 + f(q) \end{aligned}$$

The dependence of $\log \beta$ on q found from the amount by which the individual surface pressure curves in

(10) E. Dutkiewicz and R. Parsons, *J. Electroanal. Chem.*, in press.

(11) It is assumed in (1) that the activity coefficient of the nitrate ion is independent of the composition of the solution and in the calculation of the standard free energy of adsorption it will be arbitrarily set to unity.

(12) R. Parsons, *Proc. Roy. Soc. (London)*, **A261**, 79 (1961).

(13) J. M. Parry and R. Parsons, *Trans. Faraday Soc.*, **59**, 241 (1963).

(14) A. N. Frumkin, *Z. physik. Chem.*, **116**, 466 (1925).

Figure 2 had to be shifted along the $\log a$ axis in making the fit is shown in Figure 3. Unlike previously reported systems of anion adsorption,¹⁻³ the variation in this case is nonlinear so that $f(q)$ in (4) is not specified.

The choice of the charge rather than the potential as the independent electrical variable has recently been strongly criticized by Frumkin and his co-workers,^{15,16} especially in connection with the adsorption of neutral organic molecules. Damaskin,¹⁶ in particular, has attempted to show that the application of a constant-charge isotherm to the adsorption of *t*-amyl alcohol results in apparent reversal of the lateral interaction of the adsorbed molecules from a predominantly attractive force to a repulsive force as the electrode charge is made more negative. However, as Parsons¹⁷ has pointed out, this argument presupposes the correctness of the constant-potential isotherm, which is implicit in Frumkin's original model of the double layer in the presence of the adsorbed species as a pair of parallel connected condensers, so that the argument is essentially a circular one. The amounts adsorbed calculated from an equation based on a specific model of the double layer will obviously be consistent with that model, but this provides no evidence whatsoever for the correctness of the initial assumptions. In a recent paper, Frumkin and co-workers¹⁵ have recognized this point and have shown that whereas the Frumkin isotherm leads to the well-known parallel condenser equation

$$C = C_0(1 - \theta) + C' \quad (5)$$

for constant-potential adsorption, the corresponding constant charge equation represents a *series* combination

$$1/C = (1 - \theta)/C_0 + 1/C' \quad (6)$$

where C_0 and C' are the capacities of the double layer corresponding to values of the fractional coverage θ equal to 0 and 1, respectively. It can easily be shown from (5) and (6) that

$$\varphi_{q=0} = \varphi_N \theta \left/ \left[\frac{C_0}{C'}(1 - \theta) + \theta \right] \right. \quad (7)$$

for the constant-potential isotherm and

$$\varphi_{q=0} = \varphi_N \theta \quad (8)$$

for the constant-charge isotherm where φ is the potential measured with respect to the point of zero charge in the absence of the adsorbate and φ_N is the value of φ corresponding to $\theta = 1$. Equations 7 and 8, therefore, provide a simple method of distinguishing between the two types of isotherm and for testing the more ap-

propriate electrical variable to describe a specific system.

In order to test the validity of the constant-charge approach to ionic adsorption originally proposed by Parsons,¹⁸ the present data were subjected to two tests. First, the surface pressure (π) of the adsorbed layer measured at constant potential, given by

$$\pi = \gamma' - \gamma'_0 \quad (9)$$

where γ'_0 is the interfacial tension of the base solution relative to the electrocapillary maximum, was computed and a composite surface pressure curve constructed as before by superimposing the individual curves for different values of E , sliding the curves along the $\log x$ axis by an amount proportional to E to achieve the fit. The results of this fit are shown in Figures 4 and 5. The solid line is again calculated from a Frumkin isotherm having exactly the same constants as that fitted to the constant-charge data. In the present system, therefore, not only the *form* but also the *constants* of the isotherm are indistinguishable for the constant-potential and constant-charge cases when compared by this method. This may seem at first sight a surprising result but can be readily understood when it is recalled that the charge is almost linearly dependent on the potential in this system because of the small dependence of the capacity on the potential in the anodic region of polarization. It is evident, therefore, that the results in Figure 4 really represent a constant-charge isotherm since the potential drop across the diffuse-layer, which varies by amounts of up to 40 mv. at constant total potential over the concentration range used here, has been neglected. This is a serious criticism of the choice of constant-potential conditions since the diffuse-layer potential can vary appreciably even for a neutral adsorbate and a solution of 1 *M* electrolyte concentration, and should be taken into account.

The data were next tested by plotting $\varphi_{q=0}$ against the fractional coverage θ . The result is shown in Figure 6. It is evident that $\varphi_{q=0}$ is linearly dependent on θ within the experimental error suggesting that (8) is applicable and therefore that the charge is the correct electrical variable. The slope of the plot in Figure 6, which according to (8) is equal to φ_N is -0.22 v. which leads to the reasonable value for the extrapolated zero charge potential when $\theta = 1$ of -0.69 v. It was con-

(15) A. N. Frumkin, B. B. Damaskin, V. M. Gerovich, and R. I. Kaganovich, *Dokl. Akad. Nauk SSSR*, **158**, 706 (1964).

(16) B. B. Damaskin, *J. Electroanal. Chem.*, **7**, 155 (1964).

(17) R. Parsons, *ibid.*, **8**, 93 (1964).

(18) R. Parsons, *Trans. Faraday Soc.*, **51**, 1518 (1955).

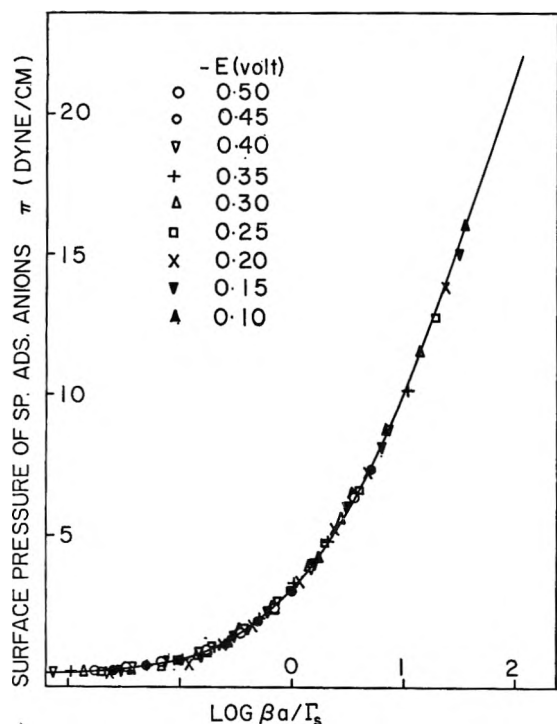


Figure 4. Composite curve of the surface pressure (π) of specifically adsorbed nitrate ions measured at constant potential as a function of the chemical potential of anions in the solution.

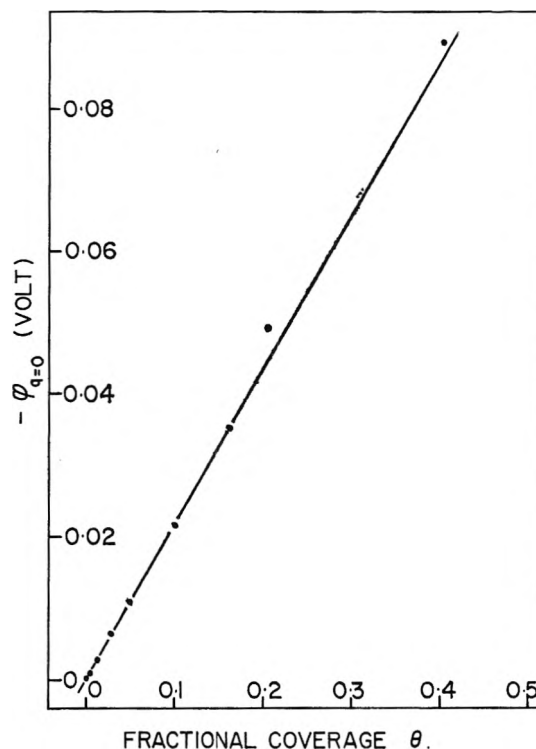


Figure 6. Dependence of the potential of zero charge ($\phi_{q=0}$) relative to the value for a nonadsorbed electrolyte (-0.474 v.) on the fractional coverage of the electrode with specifically adsorbed nitrate ions.

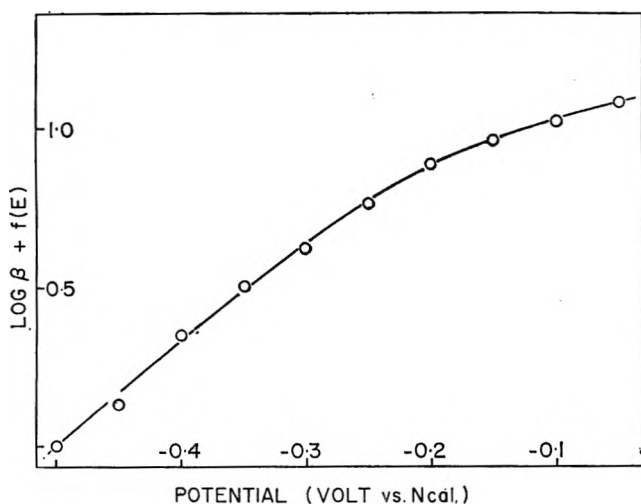


Figure 5. Dependence of the standard free energy of adsorption ($\log \beta$) of nitrate ions on the electrode potential for a constant-potential isotherm.

cluded, therefore, that the constant-charge isotherm is the more appropriate form to describe the present data.

Values of q^1 , the charge due to specifically adsorbed NO_3^- ions were calculated from the isotherm (2) and

checked by comparison with values found by graphical differentiation of the experimental data according to (1). Agreement was generally good except at the higher concentrations and low values of q where deviations of up to $2 \mu\text{coulombs/cm}^2$ occurred. This was considered within the probable error of the graphical differentiation which is greatest at the ends of the curve. q^1 is shown as a function of charge and concentration of NH_4NO_3 in Figure 7. The curves differ radically from the corresponding curves for the KI^1 and KCl^2 systems in two respects, namely the clear approach to saturation at the higher concentrations and charges and the wide divergence of the curves.

The potential difference across the inner region of the double layer (ϕ^{m-2}) was calculated from the measured potential by subtracting the potential of the e.c.m. in the absence of specific adsorption (-0.474 v. vs. N cal.) and the potential of the outer Helmholtz plane (ϕ_2) calculated from diffuse-layer theory¹⁹ assuming cations and F^- ions to be nonspecifically adsorbed. ϕ^{m-2} is shown as a function of q^1 for integral values of q in Figure 8. As before, ϕ^{m-2} is a linear function of

(19) D. C. Grahame, *Chem. Rev.*, **41**, 441 (1947).

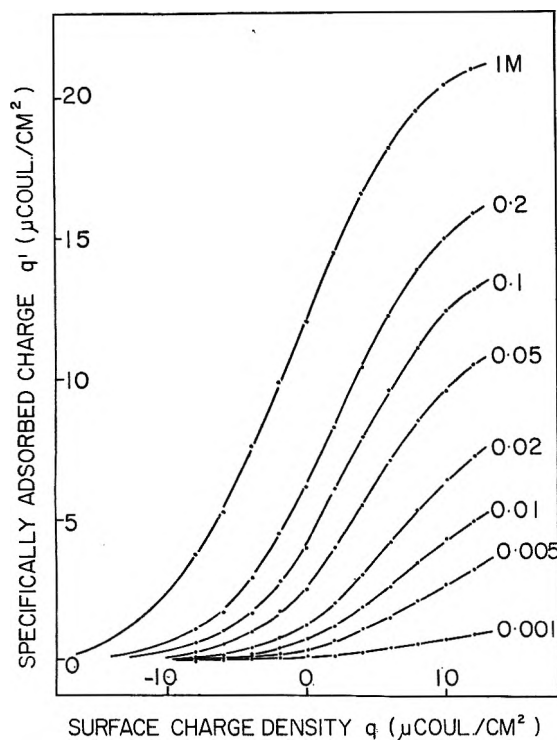


Figure 7. Charge due to specifically adsorbed nitrate ions (q^1) as a function of the surface charge density (q) and the bulk concentration of nitrate ions.

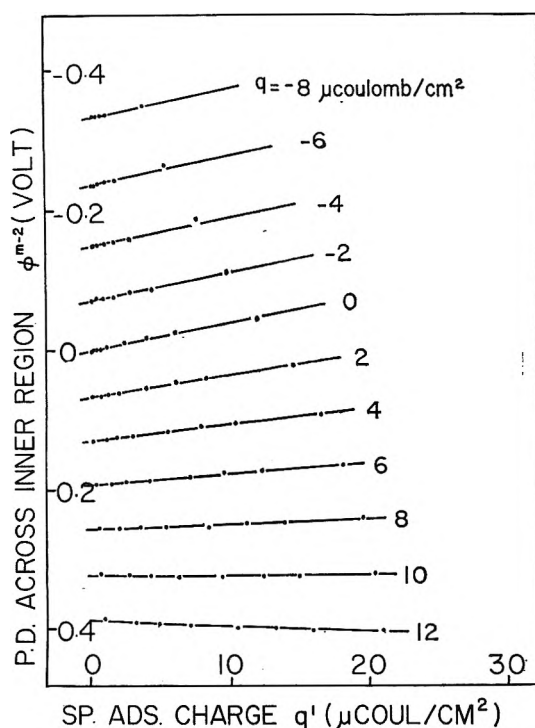


Figure 8. Potential difference across the inner region of the double layer (ϕ^{m-2}) as a function of the charge due to specifically adsorbed nitrate ions (q^1) and the charge on the metal (q).

q^1 , but in contrast with previously studied systems the lines are not parallel. This is to be expected from the nonlinear dependence of $\log \beta$ on q in view of the approximate relationship²⁰

$$\left(\frac{\partial \phi^{m-2}}{\partial q^1}\right)_q = \frac{RT}{F} \frac{d \ln \beta}{dq} \quad (10)$$

The term of the left-hand side of (10) is equal to the reciprocal of the component of the inner-layer capacity previously denoted¹³ by ${}_q C^i$, which in view of its constancy (at constant q) can be replaced by the corresponding integral capacity ${}_q K^i$.

The total inner-layer capacity C^i was calculated from diffuse-layer theory according to the equation¹³

$$\frac{1}{C} = \frac{1}{C^i} + \frac{1}{C^d} \left(1 + \frac{\partial q^1}{\partial q}\right) \quad (11)$$

where C^d is the capacity of the diffuse double layer. Values of $\partial q^1 / \partial q$ were obtained from the isotherm by differentiation

$$\frac{\partial q^1}{\partial q} = \frac{\partial \ln \beta}{\partial q} \left[\frac{1}{q^1} + \frac{1}{q_s^1 - q^1} + A \right] \quad (12)$$

The components of the inner-layer capacity were then calculated from the identity²⁰

$$\frac{1}{C^i} = \frac{1}{{}_q C^i} + \frac{1}{{}_q K^i} \frac{\partial q^1}{\partial q} \quad (13)$$

where ${}_q C^i$ is the capacity measured at constant amount adsorbed, *i.e.*, $(\partial q / \partial \phi^{m-2})_{q^1}$. ${}_q C^i$ has been referred to as the "base-solution" capacity²⁰ by analogy with the adsorption of neutral molecules from a base solution of constant salt concentration. The second term in (13) will be referred to as the "adsorption" term in the following discussion.

Discussion

1. *Origin of the Capacity Hump.* The total differential capacity (C), the inner-layer capacity (C^i), and the inner-layer capacity measured at constant amount adsorbed (${}_q C^i$) are compared for four concentrations of NH_4NO_3 in Figure 9. The effect of the diffuse layer and the adsorption on the total capacity is readily apparent. The hump in the total capacity (Figure 9(a)) is developed by progressive decrease in the capacity on the positive side and increase at the negative side as the concentration of NO_3^- increases. At the same time, the position of the hump is shifted in the negative direction. Removal of the contribution of the diffuse-layer capacity leaves the hump intact (Figure 9(b)) although the height of the peak now

(20) R. Parsons, *Trans. Faraday Soc.*, 55, 999 (1959).

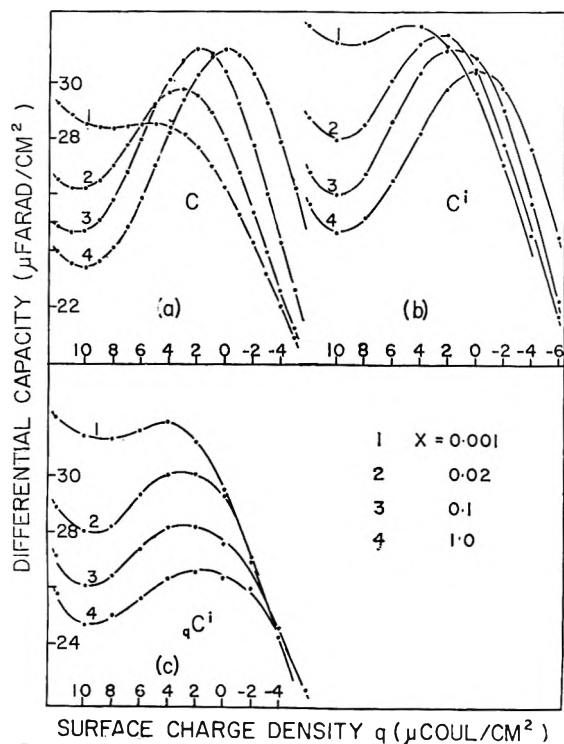


Figure 9. Components of the capacity: (a) total capacity (C); (b) capacity of the inner region (C^i); (c) capacity of the inner region measured at constant amount adsorbed (${}_qC^i$).

decreases systematically with increasing concentration of NO_3^- . The capacity is, however, still increased by the adsorption process on the negative side of the e.c.m. (This is brought out more clearly in Figure 10.) The curves of ${}_qC^i$ (Figure 9(c)) show that the major contribution to the development of the hump in concentrated nitrate solutions is the decrease in ${}_qC^i$ at the anodic end. The effect of the adsorption term on C^i diminishes as q becomes more positive due to the approach of $1/{}_qK^i$ to zero in (13). This behavior is quite different from that of iodide adsorption, for example, in which the capacity is dominated by the adsorption term, and the base-solution term (${}_qC^i$) is apparently independent of concentration within the experimental error.¹

The effect of the adsorption on the capacity is best illustrated by the plot of the change in reciprocal capacity of the inner layer against charge shown in Figure 10. These curves are characteristic of an adsorption isotherm in which the standard free energy of adsorption is a quadratic function of the charge,²¹ and are remarkably similar to typical capacity curves found in the adsorption of neutral organic molecules.^{22,23} Because of the negative charge on the ion, the adsorption is shifted in the positive direction so that the posi-

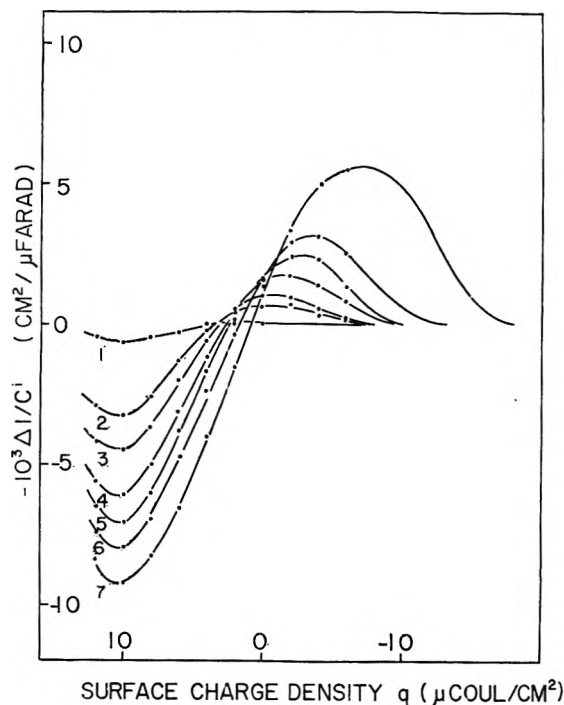


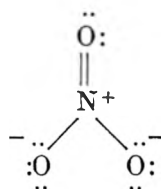
Figure 10. Change of the inner-layer capacity resulting from specific adsorption of nitrate ions: $x =$ (1) 0.001; (2) 0.01; (3) 0.02; (4) 0.05; (5) 0.1; (6) 0.2; (7) 1.0.

tive end of the curves is outside the experimental range. However, the minimum on the curve is apparently developed close to $q = 12 \mu\text{coulombs/cm}^2$ in the most concentrated solution. The minimum in $-\Delta 1/C^i$ corresponds to a maximum in the amount adsorbed²⁴ (assuming that $\ln \beta$ is a quadratic function of q) which is also suggested by the plots of q^1 vs. q in Figure 7. It is clear, therefore, that unless the form of the isotherm changed radically, the nitrate ion would be desorbed at more positive values of q if these were attainable. In view of the negative charge on the ion, this is a remarkable result which can only mean that what is being observed is a mixed adsorption of the nitrate ion and some other unidentified species. The fluoride ion appears to be nonspecifically adsorbed over a wide range of concentration and temperature^{25,26} and in any case is certainly less specifically adsorbed than the nitrate ion.⁴ It is, therefore, difficult to resist the conclusion that the solvent is the competing species. If this is the case, it must

- (21) R. Parsons, *J. Electroanal. Chem.*, **5**, 397 (1963).
- (22) M. Breiter and P. Delahay, *J. Am. Chem. Soc.*, **81**, 2938 (1959).
- (23) B. B. Damaskin, *Electrochim. Acta*, **9**, 231 (1964).
- (24) R. Parsons, *J. Electroanal. Chem.*, **7**, 136 (1964).
- (25) D. C. Grahame, *J. Am. Chem. Soc.*, **76**, 4819 (1954).
- (26) D. C. Grahame, *ibid.*, **79**, 2093 (1957).

also be concluded that the water molecule undergoes a specific (*i.e.*, nonelectrostatic) interaction with the metal, unless for geometrical reasons the electrostatic interaction of the water dipole with the field is more favorable than that of the ion with the field. Any specific interaction of the water with the metal constitutes additional support for the view²⁷ that the preferred orientation of the dipole is that with the negative (oxygen) end facing the metal since this must be the orientation at extreme positive polarizations. In any case, chemical interaction with the metal seems certain to be between the mercury and oxygen rather than hydrogen in view of the well-known low adsorbability of hydrogen on mercury, characterized by the large hydrogen over-voltage and low catalytic activity of the mercury electrode.²³

2. *The Saturation Area.* The nitrate ion is planar with the electronic structure²⁹



The double bond resonates between the three oxygen atoms so that the ion is symmetrical. The most probable orientation of the adsorbed ion would seem to be flat on the metal surface. Figure 11 shows a model of the ion constructed from the measured value of the N–O bond length (1.21 Å.) and an estimated value for the van der Waals radius of the oxygen atom of 1.4 Å.²⁹ The area generated by rotating the ion about its axis of symmetry is 21.2 Å.². The saturation area given by the isotherm fit (4), however, is 65 Å.² or roughly three times the geometric area of the ion.

Although it is possible that the data could be fitted equally well to an isotherm having slightly different constants, it is unlikely that the saturation area could be in error by a factor of three. When the lateral interaction term is large, a considerable range of combinations of A and Γ_s will give similar isotherms. This is because of the arbitrariness involved in separating the interactions into long-range and short-range contributions. However, in the present case the long-range interaction is weak ($A/2303 = 1$) compared with, for example, iodide ion adsorption from formamide ($A/2303 = 6$) where the interaction is sufficient to make not only the constants but also the form of the isotherm uncertain.³ It is therefore necessary to look elsewhere for the explanation of the large apparent area occupied by the nitrate ion.

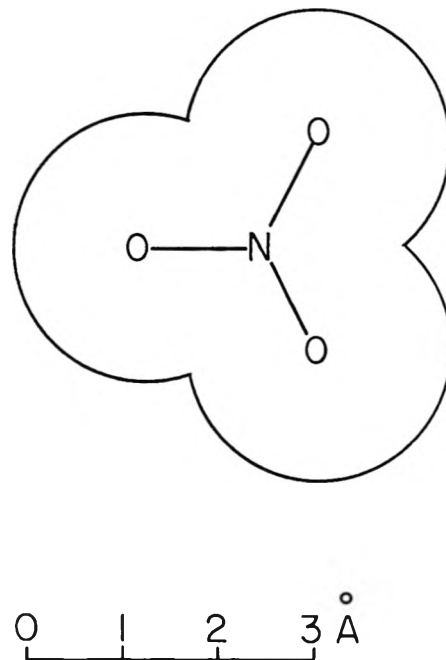


Figure 11. Model of the nitrate ion.

A possible explanation is that the ion is adsorbed with strongly bound primary water of solvation. Figure 12 shows a model of such a hydrated ion assuming three water molecules each "bonded" to the oxygen atoms of the ion by way of a hydrogen atom and separated by a distance equal to the hydrogen bond length. The area of this model calculated by summing the areas of the circles circumscribing each water molecule (12.6 Å.²) and the ion (21.2 Å.²) is 59 Å.². (It seems reasonable to assume that the space between the water molecules would be available for occupation by adjacent solvated ions.) The evidence for hydration of the nitrate ion in solution is scanty. Recent measurements³⁰ based on ionic transport processes through membranes indicate a primary hydration number of 6, whereas previously reported data³¹ based on compressibility measurements suggest a value of 1. A value of 3 seems reasonable in view of the structure of the nitrate ion. However, as was pointed out previously²⁷ the nature of the ion–solvent complex in the bulk solution is not strictly relevant. If the unsolvated

(27) G. J. Hills and R. Payne, *Trans. Faraday Soc.*, **61**, 326 (1965).

(28) A. N. Frumkin, "Advances in Electrochemistry and Electrochemical Engineering," Vol. I, Interscience Publishers, Inc., New York, N. Y., 1961, p. 65.

(29) L. Pauling, "The Nature of the Chemical Bond," Cornell University Press, Ithaca, N. Y., 1948.

(30) A. J. Rutgers, W. Rigole, and V. Hendrickx, *Chem. Weekblad*, **59**, 33 (1963).

(31) J. Padova, *Bull. Res. Council Israel*, **A10**, 63 (1961).

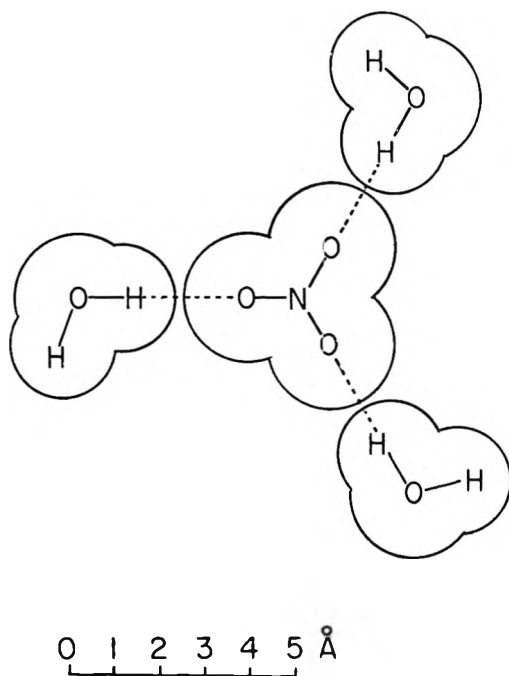


Figure 12. Model of a hypothetical hydrated nitrate ion.

ion were adsorbed into the water-populated inner layer, with consequent strong polarization of three nearest-neighbor water molecules, the result would be the same. This amounts to postulating that the ion-solvent interaction in the double layer is different from that in the bulk solution due to the different electrical conditions. Some previously reported measurements of entropy and volume changes accompanying the adsorption of nitrate and other ions²⁷ were, however, interpreted in terms of displacement of bound water (adsorbed or solvation) which requires that the ion be solvated in the bulk.

3. *Potential Difference Generated by Specifically Adsorbed Anions.* The potential difference (ϕ^{m-2}) generated across the inner region of the double layer by the specifically adsorbed nitrate ions is shown as a function of the amount adsorbed (q^1) for various constant values of q in Figure 8. As in all previously reported studies of anion adsorption, ϕ^{m-2} is a linear function of q^1 but whereas the plots were parallel or nearly so in all cases, in the present system the slope decreases as q becomes more positive, passing through zero at $q \approx 8 \mu\text{coulombs/cm}^2$ and actually reversing sign at more positive values. This surprising result is difficult to interpret in terms of the Grahame-Stern model^{1,19} of the inner layer.

The reciprocal slope ($\partial q^1 / \partial \phi^{m-2}$) _{q} of the lines in Figure 8 has the dimensions of capacity which as already noted can be regarded as an integral capacity

(${}_q K^i$) since it is independent of q^1 . ${}_q K^i$ was previously interpreted^{2,3,13} as the capacity of the parallel plate condenser with the plates located at the inner Helmholtz plane (I.H.P.) and the outer Helmholtz plane (O.H.P.) so that

$${}_q K^i = \frac{\epsilon^i}{4\pi(x_2 - x_1)} \quad (14)$$

where ϵ^i is the dielectric constant of the inner layer and x_1 and x_2 are the distances of the I.H.P. and O.H.P., respectively, from the metal surface. The increasing value of ${}_q K^i$ with increasing q can therefore be interpreted in terms of this simple model as an increase in ϵ^i or decrease in the thickness $x_2 - x_1$. Although the dielectric constant would be expected to depend on the amount of adsorbed material because of the change in composition, it seems unreasonable to suppose that this could account for the large variation of ${}_q K^i$ observed. In view of the discontinuous variation of ${}_q K^i$ with q and especially the occurrence of negative values, it must be assumed that variation of $x_2 - x_1$ is responsible.

The notion that the location of the specifically adsorbed anions moves away from the metal (*i.e.*, x_1 increases) as the positive charge on the metal increases is difficult to accept on electrostatic grounds. However, according to the arguments outlined earlier, it seems probable that anions are "out-squeezed" by solvent molecules when q is large so that x_1 may tend to increase.

The alternative possibility that x_2 , the thickness of the inner layer, decreases with increasing positive charge must also be considered although this also appears unlikely since the capacity at constant amount adsorbed is only slightly dependent on q (see Figure 13). A further difficulty arises irrespective of whether the variation of $x_2 - x_1$ is regarded as a variation of x_1 or of x_2 , since negative values of $x_2 - x_1$ imply that diffuse-layer ions penetrate closer to the metal than specifically adsorbed ions. This raises the whole question of the nature of the specific adsorptive forces and the location of the adsorbed ions. It is assumed in the Grahame-Stern model that specifically adsorbed ions are in direct contact with the metal and that the adsorption forces fall off sharply with distance so that ions at or beyond the O.H.P. can only experience coulombic forces. There is a possibility that diffuse-layer ions could be specifically adsorbed, by way of a bridging solvent molecule in much the same way as ion-pair association can occur in solution. Ions adsorbed in this way would contribute little to ϕ^{m-2} because their centers of charge would be in the diffuse layer and subject to the screening effect of ions in

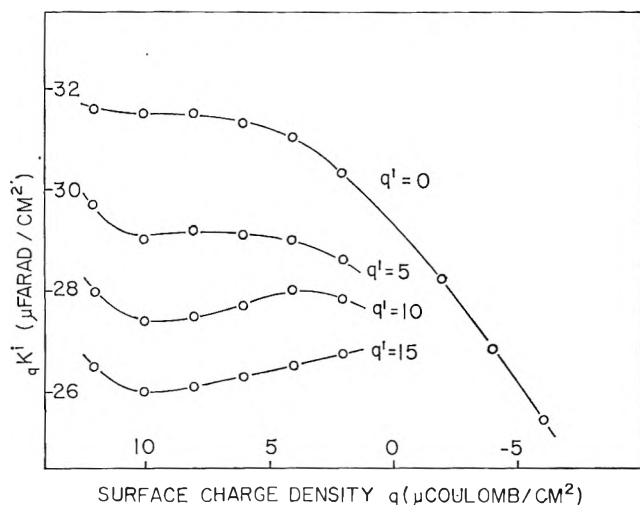


Figure 13. Integral capacity of the inner region of the double layer measured at constant amount adsorbed (q^1) as a function of the charge on the metal (q) at constant values of the amount of specifically adsorbed nitrate ion (q^1). Units of q^1 are microcoulombs per square centimeter.

the bulk solution. This is similar to an argument recently put forward by Mott, Parsons, and Watts-Tobin³² to explain the absence of the predicted correlation between the cathodic capacity and the cation radius. In this case, however, the cation is not specifically adsorbed to any appreciable extent (which is to be expected since the water molecules in the hydration shell would be oriented with the oxygen end of the dipole toward the cation and the hydrogen toward the metal).

A clue to a possible source of the increase of the adsorption energy of the solvent relative to that of the anion which results in the out-squeezing effect is found in the large apparent saturation area of the anion which suggests that approximately five water molecules occupy the space vacated by a single anion. It is clear, therefore, that the replacement of the ion is considerably more favorable energetically than it would be if the anion occupied a single site. The delicate balance between the adsorption of the solvent and the anion set up in this way appears to be responsible for many of the unusual properties of this system.

So far, we have neglected the contribution to ϕ^{m-2} of the permanent dipole moment of the adsorbed water molecules, a contribution which is increasingly negative as q becomes more positive and the dipoles are aligned by the field. The potential difference ϕ_d generated by a layer of N dipoles of moment μ at an angle θ with the field and immersed in a medium of dielectric constant ϵ is given by

$$\phi_d = \frac{4\pi N\mu \cos \theta}{\epsilon} \quad (15)$$

With the values given by Watts-Tobin³³ of $\epsilon = 3.1$, $\theta = \cos^{-1}(1/\sqrt{3})$, $N = 10^{15}$ molecules/cm², and $\mu = 1.84 \times 10^{-18}$ e.s.u., the value of ϕ_d in (15) is equal to 1.29 v. It appears, therefore, that ϕ_d can be an important contributing factor to ϕ^{m-2} . If n dipoles are replaced by the adsorption of one anion located at the I.H.P., ϕ^{m-2} will shift in the positive direction if

$$n\bar{\mu} > (x_2 - x_1)e \quad (16)$$

where $\bar{\mu}$ is the average component of the adsorbed dipoles perpendicular to the interface and e is the electronic charge³⁴; it is therefore apparently possible to explain the zero or positive shift of ϕ^{m-2} with q^1 in Figure 8 in this simple way without recourse to a detailed model of the inner layer. It is evident that ϕ^{m-2} is a complex parameter and that both of the simple interpretations discussed above are unlikely to be better than crude approximations even under favorable conditions. This is mainly because the double layer is of molecular dimensions so that a classical electrostatic approach cannot be applied unambiguously. It seems reasonable to conclude that any interpretation must recognize the finite size of the ion and the molecular structural properties of the dielectric, *i.e.*, that the problem is one of mixed adsorption of similar chemical entities. This view is consistent with the evidence in Figures 3 and 10 of the nonlinear dependence of the standard free energy of adsorption on the charge. However, the experimental evidence is not completely self-consistent. For example, if the removal of a solvent dipole is supposed to affect ϕ^{m-2} , then the plots of ϕ^{m-2} vs. q^1 would be expected to be nonlinear. More serious is the apparently ideal behavior of the benzenedisulfonate ion which should replace large numbers of water molecules but which is actually found to give both *linear* and *parallel* plots of ϕ^{m-2} vs. q^1 .¹³ It should also be mentioned that the adsorption of nitrate ions from KNO₃ solutions in the absence of an inert base electrolyte behaves in a similar manner.³⁵ This suggests strongly that the ionic strength of the bulk solution influences the properties of the double layer in a way that is not wholly accounted for by diffuse-layer theory. A satisfactory answer to these and other problems requires more extensive measurements both in water and in other solvent systems.

(32) N. F. Mott, R. Parsons, and R. J. Watts-Tobin, *Phil. Mag.*, **7**, 483 (1962).

(33) R. J. Watts-Tobin, *ibid.*, **6**, 133 (1961).

(34) It is assumed that both the dipole and the ion are immersed in the same dielectric medium.

(35) R. Payne, to be published.

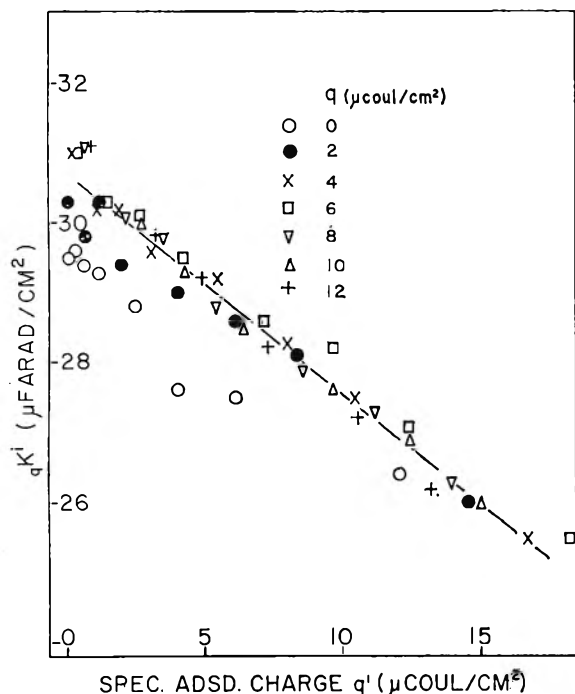


Figure 14. Integral capacity of the inner region of the double layer measured at constant amount adsorbed (${}_qK^i$) as a function of the specifically adsorbed charge (q^1) at constant values of the surface charge density (q).

4. *Capacity of the Inner Region at Constant Amount Adsorbed.* According to the curves in Figure 9(c), the capacity of the inner region measured at constant amount adsorbed (${}_qC^i$) is strongly dependent on the composition of the solution, and therefore the amount of specifically adsorbed nitrate ion, in the anodic region of polarization. The decrease of the capacity with amount adsorbed is clearly illustrated in Figure 14 in which the corresponding integral capacity ${}_qK^i$ is plotted against q^1 for integral values of q . ${}_qK^i$ is evidently linearly dependent on q^1 , and the slope of the variation is the same within the experimental error for all values of q .³⁶

The strong dependence of ${}_qC^i$ (or ${}_qK^i$) on the amount adsorbed is not found for other systems in which the plots of ϕ^{m-2} vs. q^1 are parallel or nearly so.^{1-3,13} The integral capacity can be regarded as the capacity of a parallel plate condenser given by

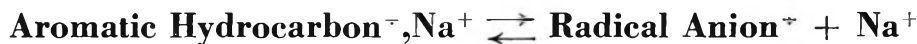
$${}_qK^i = \frac{\epsilon^i}{4\pi x_2} \quad (17)$$

where ϵ^i and x_2 are the dielectric constant and thickness, respectively, of the inner layer. Both ϵ^i and x_2 would be expected to depend on the composition of the layer, so that it is somewhat surprising to find for the adsorption of iodide ions from water,¹ for example, that ${}_qK^i$ is essentially independent of the coverage. It is even more surprising in the case of the benzenedisulfonate anion in which ${}_qK^i$ remains independent of q even under conditions approaching saturation coverage.¹³ Because of the large geometric size of the benzenedisulfonate ion (97 Å.² assuming a flat orientation) there can be little or no water remaining in the inner layer at saturation coverage (125 Å.²/ion). It must be concluded, therefore, that in this and other systems the constancy of ${}_qK^i$ is due to a remarkable accidental compensation in the variations of ϵ^i and x_2 and that the behavior of the present system may be more typical. The replacement of water in the inner layer is consistent with decreasing ϵ^i resulting in a decreasing capacity. This may seem inconsistent with the dependence of ${}_qK^i$ on q discussed in the previous section since ${}_qK^i$ apparently approaches infinity and eventually reverses sign as q becomes more positive. However, as already pointed out, this behavior could hardly be due to variation of the dielectric constant and must therefore be due either to a thickness effect or breakdown of the simple model.

The close similarity of the forms of C^i for the pure NH_4F solution and ${}_qC^i$ for the nitrate solutions strongly suggests that the origin of the capacity hump is the same in both cases, namely mixed adsorption of the anion and the solvent. Although the adsorption of the fluoride ion can be shown to conform to diffuse-layer behavior *within the experimental error*, there is no reason to believe that fluoride differs essentially from other ions but merely represents extreme behavior. Where the metal-ion interaction is purely coulombic, the solvent is able to compete more favorably and a higher capacity results as found experimentally.

(36) The overlap of the data for different values of q in Figure 9 should not be taken to imply that the points lie on a common line. It is due to the small dependence of ${}_qK^i$ on q in this region of polarization.

Dissociative Equilibria in the Systems



by R. V. Slates and M. Szwarc

Department of Chemistry, State University College of Forestry at Syracuse University, Syracuse, New York 13210 (Received June 9, 1965)

The conductance of the sodium salts of aromatic radical ions has been investigated in THF. The dissociation constants of the respective ion pairs were determined and found to increase with the size of the anion, being $1.5 \times 10^{-6} M$ for biphenyl $^{\cdot-}, \text{Na}^+$ and $23 \times 10^{-6} M$ for perylene $^{\cdot-}, \text{Na}^+$. An exceptionally low value was found for naphthalene $^{\cdot-}, \text{Na}^+$, viz., $\sim 0.2 \times 10^{-6} M$. The Λ_0 and Λ_0^- values were determined, and their significance is discussed. The Λ_0^- values derived from the conductance studies are slightly smaller than those calculated from the diffusion constants of the respective aromatic hydrocarbons, and thus the diffusion of an aromatic radical ion appears to be only slightly slower than that of the parent aromatic hydrocarbon. Knowledge of K_{diss} allows us to correct the values of the electron affinities of aromatic hydrocarbons which were previously determined potentiometrically and spectrophotometrically. The relation between the equilibrium constants derived by these two methods is discussed in terms of the equilibria established between ion pairs and those involving free ions, viz., $\text{A}^{\cdot-} + \text{B} \rightleftharpoons \text{B}^{\cdot-} + \text{A}$ (K_{pt}) as compared with $\text{A}^{\cdot-}, \text{M}^+ + \text{B} \rightleftharpoons \text{B}^{\cdot-}, \text{M}^+ + \text{A}$ (K_{sp}). The two constants are related, namely, $K_{\text{sp}}/K_{\text{pt}} = K_{\text{diss}, \text{A}^{\cdot-}, \text{M}^+}/K_{\text{diss}, \text{B}^{\cdot-}, \text{M}^+}$. A similar problem arises when one considers the disproportionations of radical anions into dianions since the following equilibria have to be considered: $2\text{A}^{\cdot-} \rightleftharpoons \text{A} + \text{A}^{2-}$; $\text{A}^{\cdot-} + \text{A}^{\cdot-}, \text{Na}^+ \rightleftharpoons \text{A}^{2-}, \text{Na}^+ + \text{A}$; and $2\text{A}^{\cdot-}, \text{Na}^+ \rightleftharpoons \text{A}^{2-}, 2\text{Na}^+ + \text{A}$.

The chemistry of radical anions derived from aromatic hydrocarbons and related compounds is now rapidly developing. In solution these species exist in at least two distinct forms¹ as ion pairs and as free ions. Other associates such as contact ion pairs and solvent-separated pairs,^{1b} triple ions, dimeric ion pairs,² etc., may also be encountered. Since each of these species has its own characteristics and usually differs from the others in its reactivity, it is necessary to learn more about the equilibria established between them in order to interpret correctly their behavior in various processes. In this work we shall deal with the dissociative equilibria, $\text{Ar}^{\cdot-}, \text{Na}^+ \rightleftharpoons \text{Ar}^{\cdot-} + \text{Na}^+$, established at 25° in tetrahydrofuran. The following aromatic hydrocarbons were investigated: biphenyl, naphthalene, triphenylene, pyrene, anthracene, tetracene, and perylene. The results reported here were obtained from conductance studies of their sodium

salts. However, before considering the experimental details of this work, the significance of such studies will be discussed in relation to other experiments involving radical ions. Two examples have been chosen: (1) electron-transfer equilibria involving aromatic hydrocarbons and (2) disproportionation equilibria of radical anions.

Electron-Transfer Equilibria

Following the pioneering work of Paul, Lipkin, and

(1) (a) H. V. Carter, B. J. McClelland, and E. Warhurst, *Trans. Faraday Soc.*, **56**, 455 (1960); (b) A. C. Aten, J. Dieleman, and G. J. Hoijsink, *Discussions Faraday Soc.*, **29**, 182 (1960); (c) B. J. McClelland, *Trans. Faraday Soc.*, **57**, 1458 (1961); (d) N. M. Atherson and S. I. Weissman, *J. Am. Chem. Soc.*, **83**, 1330 (1961); (e) E. de Boer and E. L. Mackor, *ibid.*, **86**, 1513 (1964); (f) J. Bolton and G. K. Fraenkel, *J. Chem. Phys.*, **40**, 3307 (1964).

(2) (a) K. H. J. Buschlow, J. Dieleman, and G. J. Hoijsink, *ibid.*, **42**, 1993 (1965); (b) K. H. J. Buschlow, Ph.D. Thesis, Amsterdam, 1963.

Table I

Pair	$K_{diss},$ $M \times 10^6$	$K_{sp},$ obsd.	$\Delta\epsilon_{1,2,sp} =$ $0.06 \log$ K_{sp}	$\Delta\epsilon_{1,2},$ measd.	$\Delta\epsilon^{\circ}_{1,2},$ v.	$\Delta\epsilon_{1,2,sp},$ calcd. from $\Delta\epsilon_{1,2}$ measd.	$K_{diss,1}/$ $K_{diss,2},$ obsd.	$K_{diss,1}/$ $K_{diss,2},$ calcd. ^a
(1) Naphthalene (2) Terphenylene	0.2 } 4.85 }	3	0.029	0.047 ^b	0.095	0.000	0.041	0.25 ^b
(1) Pyrene (2) Anthracene	6.8 } 4.55 }	111	0.125	0.119	0.114	0.124	1.5	1.6
(1) Tetracene (2) Perylene	15 } 23 }	52	0.102	0.108	0.113	0.103	0.65	0.62
(1) Pyrene (2) 9,10-Dimethyl- anthracene	6.8 } (2.2) ^c }	91	0.117	0.102	(0.087) ^c	3.2

^a The values given in the last column are calculated from $\log(K_{diss,1}/K_{diss,2}) = (\Delta\epsilon_{1,2,sp} - \Delta\epsilon_{1,2,measd})/0.03$. ^b This value is the least reliable. It involves a substantial correction (see ref. 4). ^c These values are calculated from the $K_{diss,1}/K_{diss,2}$ given in the last column.

Weissman,³ the electron-transfer equilibria between aromatic hydrocarbons and their radical anions were investigated spectrophotometrically in tetrahydrofuran⁴ (THF). The investigated processes involved essentially ion pairs, *viz.*

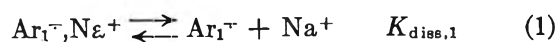


because in the 10^{-4} to 10^{-3} M THF solutions used in those studies the concentrations of free ions were negligible. The pairs naphthalene-triphenylene, pyrene-anthracene, pyrene-dimethylantracene, and tetracene-perylene were chosen since their spectra do not overlap, and the respective equilibrium constants are not too large. The results are listed in Table I, and the respective spectrophotometric equilibrium constants are denoted by K_{sp} .

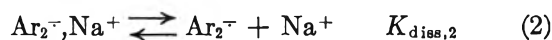
In the same paper,⁴ the results of potentiometric titrations of aromatic hydrocarbons were reported, the technique developed by Hoijtink, *et al.*,⁵ being used. Thus, the differences in the reduction potentials, $\Delta\epsilon^{\circ}_{1,2}$, were determined. These are related to the respective equilibrium constants K_{pt}



by the conventional equation $\Delta\epsilon^{\circ}_{1,2} = (RT/23,000) \ln K_{pt}$. It should be noticed that K_{sp} and K_{pt} differ from each other since one refers to a process involving ion pairs and the other to free ions. They are, however, related through the equation $K_{sp}/K_{pt} = K_{diss,1}/K_{diss,2}$, where $K_{diss,1}$ and $K_{diss,2}$ are the respective dissociation constants of



and



Moreover, the directly *measured* potentials, *i.e.*, those established between the electrodes when half of the titrated hydrocarbon is reduced, differ from the standard potentials $\Delta\epsilon^{\circ}$. As was shown previously,⁴ the latter are related to the former through the equation

$$\Delta\epsilon^{\circ}_{1,2} = \Delta\epsilon_{1,2,measd} - (1/2RT/23,000) \ln (K_{diss,1}/K_{diss,2})$$

Hence, the following relations apply at 25°

$$\Delta\epsilon_{1,2,sp} = 0.06 \log K_{sp} = \Delta\epsilon_{1,2,measd} + 0.03 \log (K_{diss,1}/K_{diss,2})$$

$$\Delta\epsilon^{\circ}_{1,2} = \Delta\epsilon_{1,2,measd} - 0.03 \log (K_{diss,1}/K_{diss,2})$$

These potentials, as well as the respective K_{diss} , are also given in Table I. The agreement between the experimental data obtained by the two different techniques becomes better when the dissociation processes are accounted for. This is clearly seen from Table I when the observed and the calculated ratios of the dissociation constants (the last two columns) are compared or when $\Delta\epsilon_{1,2,sp} = 0.06 \log K_{sp}$ (the fourth column) is compared with $\Delta\epsilon_{1,2,sp}$ (the seventh column), the latter being derived from the $\Delta\epsilon_{1,2,measd}$ by means of the above given equation.

(3) D. E. Paul, D. Lipkin, and S. I. Weissman, *J. Am. Chem. Soc.*, **78**, 116 (1956).

(4) J. Jagur-Grodzinski, M. Feld, S. L. Yang, and M. Szwarc, *J. Phys. Chem.*, **69**, 628 (1965).

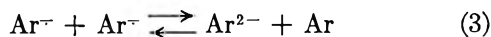
(5) G. J. Hoijtink, E. de Boer, P. H. van der Meij, and W. P. Weijland, *Rec. trav. chim.*, **75**, 487 (1956).

It should be stressed that the values of $\Delta\epsilon^{\circ}_{1,2}$, given in the sixth column of Table I, represent the potentials which should be considered when theoretical electron affinities of aromatic hydrocarbons in THF are discussed. For example, the difference of $\Delta\epsilon^{\circ}_{1,2}$ values of anthracene and dimethylantracene, *viz.*, 0.027 v., is more plausible than the small difference derived from the spectrophotometric data (0.008 v.) or even from a direct titration. The interaction of the anion with its counterion is not given by a constant term, and therefore it distorts the results obtained by either spectrophotometric or potentiometric methods. It is also interesting to notice that the dissociation constant of dimethylantracene⁻,Na⁺ (calculated from the difference between $\Delta\epsilon_{1,2,sp}$ and $\Delta\epsilon_{1,2,pt}$) is lower than that of anthracene⁻,Na⁺. This is to be expected since the electron-donating power of the methyl group should increase the attraction between the anion and its counterion, and apparently the steric effect of the CH₃ groups is not large.

Finally, the exceptionally low value of K_{diss} for naphthalene⁻,Na⁺, which is deduced from the conductance studies, is, at least partially, justified by the large difference between $\Delta\epsilon_{1,2,sp}$ and $\Delta\epsilon^{\circ}_{1,2}$.

Disproportionation of Radical Anions

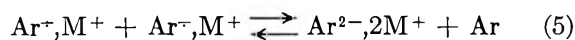
The disproportionation processes



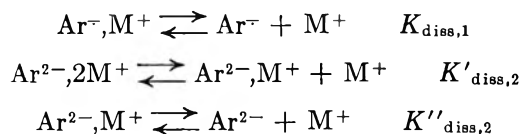
have been discussed by many workers, initially by Hush,⁶ and later by Hoijtink^{2,5} and others. At higher dilution, the process



may become significant, whereas reaction 3—which is the most interesting theoretically—may hardly be observed. Under normal experimental conditions the reaction involves ion pairs, and hence the observed spectrophotometric equilibria refer to



The equilibrium constants K_3 , K_4 , and K_5 are correlated with the dissociation constants



namely

$$K_4/K_5 = K'_{diss,2}/K_{diss,1}$$

and

$$K_3/K_5 = K'_{diss,2}K''_{diss,2}/(K_{diss,1})^2$$

Spectrophotometric studies are usually concerned with the sums $\text{Ar}^{\cdot-},\text{Na}^+ + \text{Ar}^{\cdot-} = \text{Ar}^{\cdot-}_{total}$, and $\text{Ar}^{2-},2\text{M}^+ + \text{Ar}^{2-},\text{M}^+ + \text{Ar}^{2-} = \text{Ar}^{2-}_{total}$. Hence, the apparent spectrophotometric equilibrium constant for disproportionation, K_{sp} , is given by

$$K_{sp} = K_5(1 + K'_{diss,2}/\text{M}^+)/ (1 + K_{diss,1}/\text{M}^+)^2$$

where M^+ denotes the concentration of the counterions in the investigated solution. For a very low degree of dissociation $K_{sp} = K_5$.

The potentiometric titration gives the difference between the first and second reduction potential, $(\epsilon' - \epsilon'')_{pt}$, which is related to the potential of reaction 4, $(\epsilon' - \epsilon'')_4 = -0.06 \log K_4$, *viz.*

$$\begin{aligned} (\epsilon' - \epsilon'')_4 &= (\epsilon' - \epsilon'')_{pt} + \\ &0.06 \log (K_{diss,1}/K'_{diss,2})([\text{M}^+]_2/[\text{M}^+]_1) \end{aligned}$$

Similarly

$$\begin{aligned} (\epsilon' - \epsilon'')_3 &= (\epsilon' - \epsilon'')_{pt} + \\ &0.06 \log (K^2_{diss,1}/K'_{diss,2}K''_{diss,2})([\text{M}^+]_2/[\text{M}^+]_1) \end{aligned}$$

$[\text{M}^+]_1$ and $[\text{M}^+]_2$ denote the concentrations of the counterion in the titrated solutions. It is obvious, therefore, that the theoretically interesting difference, $(\epsilon' - \epsilon'')_3$, may substantially differ from that obtained in a potentiometric titration. $[(\epsilon' - \epsilon'')_{pt}$ is the potential established between two electrodes, one immersed in a solution containing an equimolar amount of Ar and Ar⁻,M⁺, the other maintained in a solution of equimolar amounts of Ar⁻,M⁺ and Ar²⁻,2M⁺.]

Results of the Conductance Studies

The conductances of the monosodium salts of the following hydrocarbons were investigated: biphenyl, naphthalene, triphenylene, pyrene, anthracene, tetracene, and perylene. In addition, the conductance of the disodium salt of anthracene was also studied. All of the investigations were carried out in THF, at 25°, using an apparatus described in a previous communication.⁷ The concentrations of the radical ions were determined spectrophotometrically, the optical cells being part of the apparatus. The technique of dilution is also described in ref. 7, and it suffices to say that this was accomplished by removal of the solute and not by addition of the solvent. Thus, salt solutions as dilute as 10⁻⁶ M could be prepared without introducing any impurities or foreign materials.

All of the investigated hydrocarbons were twice

(6) N. J. Hush and J. Blackledge, *J. Chem. Phys.*, **23**, 514 (1955).

(7) D. N. Bhattacharyya, C. L. Lee, J. Smid, and M. Szwarc, *J. Phys. Chem.*, **69**, 612 (1965).

crystallized and then sublimed under high vacuum by gentle heating. To prevent any contamination the sublimed material was never exposed to air. The solvent (THF) was purified by a standard procedure. The purified material was kept on a high vacuum line over sodium-potassium alloy to which some anthracene or benzophenone was added, and eventually it was distilled directly, whenever required, to an appropriate ampoule.

The solutions of the radical anions were prepared by leaving overnight a THF solution of the investigated hydrocarbon in contact with a sodium mirror. In this way biphenyl, naphthalene, and triphenylene were converted into Ar⁻, Na⁺ (the first one being only partially converted). The remaining hydrocarbons, however, yield under these conditions the disodium salts, Ar²⁻, 2Na⁺. The following procedure was therefore adopted when dealing with the latter compounds. Their solution was divided into two nearly equal portions; the smaller one reacted with sodium and then mixed with the other. The Ar²⁻, 2Na⁺ was converted then into Ar⁻, Na⁺, leaving in the solution a small residue of the unreacted hydrocarbon.

The reliability of the dilution technique was checked for sodium tetracene. The solution contained some excess of tetracene, and its concentration was determined by the optical density at λ_{\max} 444 and 474 m μ , whereas the concentration of tetracene⁻ was determined by the optical density at the λ_{\max} 711 m μ . The results in Table II were obtained. These data clearly

Table II

Concn., M	Diln. on basis of tetracene ⁻	Diln. on basis of tetracene
1.6 × 10 ⁻³ } 4.5 × 10 ⁻⁴ }	3.54	3.50
4.5 × 10 ⁻⁴ } 5.7 × 10 ⁻⁵ }	7.90	7.97
Solution left overnight after being diluted		
5.7 × 10 ⁻⁵ } (Previous day)	4.27 (Killed during the night)	2.67
1.34 × 10 ⁻⁵ } (Following day)		
1.34 × 10 ⁻⁵ } 0.66 × 10 ⁻⁵ }	2.04	2.03

indicate the correctness of the spectrophotometric determination of the tetracene⁻ concentration and show that a negligible killing takes place within a few hours. However, the extremely dilute solutions were partially

destroyed by the solvent if left for 12 hr. or more. Therefore, only a concentrated solution was kept overnight, and it was stored in a refrigerator.

Killing produces a new type of ion pair, e.g., X-(CH₂)₄O⁻, Na⁺, which may contribute to the conductivity of the solution; however, usually its contribution is negligible.

The equivalent conductances and the concentrations of the investigated solutions are given in Table III, and the calculated Fuoss lines are shown in Figures 1 and 2. Their slopes, which give $1/\Lambda_0^2 K_{diss}$, are well determined and reliable within 3-5%. However, the intercepts are less reliable, particularly for the less dissociated radical ions. Since the latter give the values of $1/\Lambda_0$, the accuracy of K_{diss} is affected by the reliability of the intercept. The final results are collected in Table IV.

Table III^a

C × 10 ⁶ , M	Λ	C × 10 ⁶ , M	Λ
Biphenyl ⁻ , Na ⁺		Triphenyl ⁻ , Na ⁺	
1120	4.85	1850	7.200
398	7.69	467	12.696
128	12.38	187	18.286
41.3	20.48	30.9	38.556
15.5	30.99	16.8	49.871
6.28	44.33	11.14	58.870
0.541	104.25	3.87	60.238
Pyrene ⁻ , Na ⁺		Perylene ⁻ , Na ⁺	
1540	14.05	865	20.22
290	26.0	263	29.00
68.3	44.3	84.8	42.26
20.5	65.8	23.1	61.40
12.4	78.5	8.46	76.01
2.51	120.6	3.90	85.28
		0.95	89.95
Anthracene ⁻ , Na ⁺		Tetracene ⁻ , Na ⁺	
8150	6.01	1600	13.631
1630	9.24	451	20.99
336	16.18	194	29.21
317	17.40	57.2	42.98
75.6	29.36	13.4	64.75
15.8	54.55	6.57	75.73
13.2	56.38	3.00	85.73
Naphthalene ⁻ , Na ⁺		Anthracene ²⁻ , 2Na ⁺	
554	2.27	206	2.5
225	3.32	51.5	5.4
85	5.17	25.2	7.6
35	8.10	15.4	11.6
15.6	11.38	6.55	15.74
7.7	15.60	6.11	17.00
4.7	17.84	4.11	14.58

^a Solvent, THF; temperature, 25°.

Table IV

Radical anion	Concn. range, <i>M</i>	Λ_0 , cm. ² /ohm equiv.	Slope	$10^6 K_{\text{diss}}$, <i>M</i>
Biphenyl ⁻	0.5×10^{-6} – 1×10^{-3}	125	55.0	1.15
Naphthalene ⁻	4×10^{-6} – 5×10^{-4}	(120)	460.0	0.15
Triphenylene ⁻	4×10^{-6} – 2×10^{-3}	110	17.0	4.85
Pyrene ⁻	2.5×10^{-6} – 1.5×10^{-3}	148 (128) ^a	7.0	6.75 (9.0) ^a
Anthracene ⁻	1.3×10^{-5} – 8×10^{-3}	125	14.0	4.55
Tetracene ⁻	3×10^{-6} – 1.6×10^{-3}	100	6.75	15.0
Perylene ⁻	1×10^{-6} – 9×10^{-4}	95	4.90	23.0
Anthracene ²⁻	10^{-6} – 10^{-4}	(?)	~600.	~0.1

^a The results given in parentheses are based on the assumed value of 128 for Λ_0 of pyrene⁻, Na⁺. The value 148 seems to be unduly high.

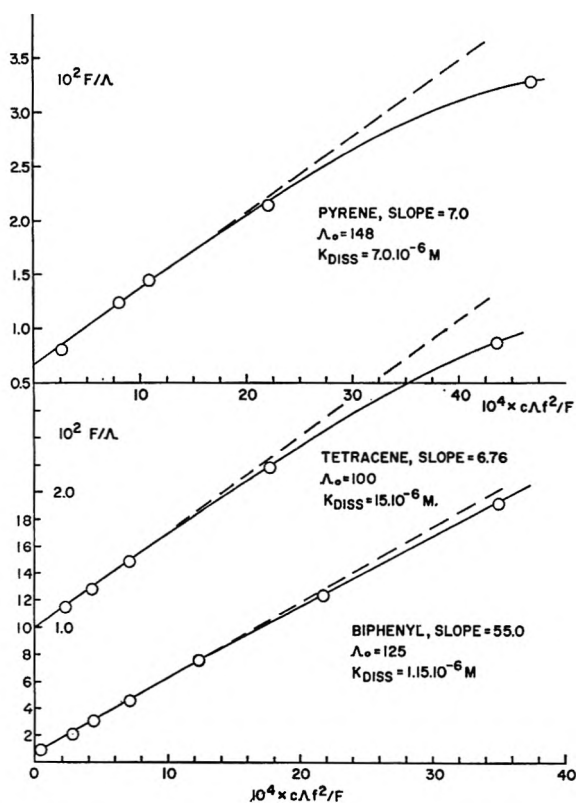


Figure 1.

The Significance of Λ_0 Values

A brief discussion of Λ_0 is not out of place. Inspection of Figures 1 and 2 indicates that Λ_0 is reliable at least within 10% for perylene⁻, anthracene⁻, and tetracene⁻ and is good within 15% for pyrene⁻. The observed gradation is plausible. Λ_0 should increase with decreasing size of the ions, and indeed Λ_0 values are 95 and 100 cm.²/ohm equiv., respectively, for the largest anions, perylene⁻ and tetracene⁻, and still larger for anthracene⁻ (125) and for pyrene⁻ (148). Hence, the

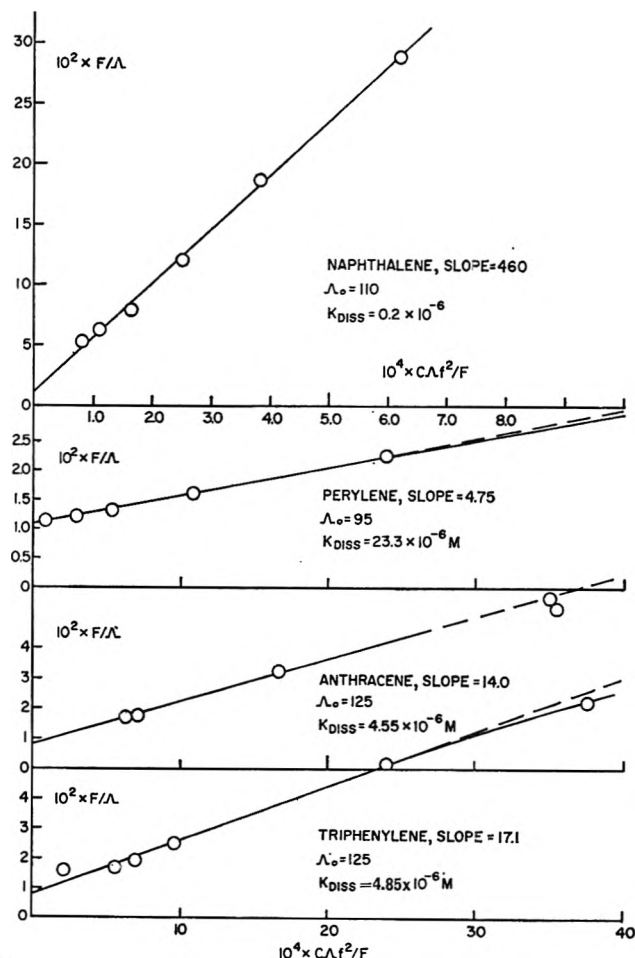


Figure 2.

values of $\Lambda_0 = 110$ for triphenylene⁻ and $\Lambda_0 = 125$ for biphenyl⁻ appear to be reasonable although they might be slightly too low. For naphthalene⁻ we assume, rather arbitrarily, $\Lambda_0 = 120$. Nevertheless, it will be seen that the true Λ_0 value for naphthalene⁻, Na⁺ cannot be much different from the chosen one.

There is an alternative method to check the reliability of the proposed Λ_0 values. The mobility of a salt is given by the sum of Λ_0^+ and Λ_0^- , *viz.*, the mobilities of the cations and anions. For the Na⁺ ion in THF at 25°, Λ_0^+ was determined⁸ to be 48 cm.²/ohm equiv., and hence the data given in Table IV lead to the values for Λ_0^- listed in Table V.

Table V: Λ_0^- of Aromatic Radical Ions in THF at 25°^a

Aromatic radical ion	10 ⁶ <i>D</i> , cm. ² /sec.	Λ_0^- calcd. from <i>D</i> , cm. ² /ohm equiv.	Λ_0^- calcd. from Λ_0^+ , cm. ² /ohm equiv.
Biphenyl ⁻	2.3	85	77
Naphthalene ⁻	2.3	85	(70)
Triphenylene ⁻	62
Pyrene ⁻	100(80)
Anthracene ⁻	2.2	81	77
Tetracene ⁻	52
Perylene ⁻	47

^a Diffusion constant *D* is calculated from the data of ref. 9 using their average values for the product *D* η and taking 4.6 mp. for the viscosity of THF at 25°.

On the other hand, the phenomenological relation between Λ_0^- of an ion and its diffusion coefficient, $6.47 \times 10^6 \Lambda_0^- = D/kT$, permits the calculation of one from the other. It is probable that the diffusion coefficient of the Ar⁻ radical ion is only slightly smaller than that of the corresponding hydrocarbon, and therefore the latter may be used to calculate the relevant Λ_0^- . The diffusion coefficients of some aromatic hydrocarbons have recently⁹ been determined, and from the published data, which show the constancy of *D* η , the diffusion constants in THF at 25° were calculated. These are listed in the second column of Table V, the following column giving the Λ_0^- computed from these *D* values. Comparison of the last two columns of Table V is most gratifying; it shows that our Λ_0^- values are indeed only slightly smaller than those derived from the diffusion constants of the respective hydrocarbons. This agreement indicates that Λ_0^- for naphthalene⁻ is ~70. The low conductance of its solution made it difficult to determine directly the Λ_0 of this salt from the conductance data, and therefore we estimated its value from the diffusion constant of naphthalene.

Having established the degree of reliability of the Λ_0^- values of aromatic radical ions, we may compare them with the Λ_0^+ of Li⁺, Na⁺, Cs⁺, and Bu₄N⁺, *viz.*, 36.6, 48, 63, and 44.5, respectively.⁸ In spite of their large areas, the radical anions are more mobile

than the Li⁺ or Na⁺ cations, strongly indicating a lack of any specific coordination of the negative ions with the solvent (THF). The aromatic radical anions have apparently the shape of a relatively thin platelet which moves easily, whereas the Li⁺ or Na⁺ ions, which are probably coordinated with at least four molecules of THF, form large, slowly moving spheres.

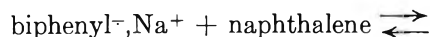
Discussion

The values of the electron affinities of aromatic hydrocarbons in THF, which were reported in the previous paper,⁴ need some corrections to account for the variable degree of association of the respective radical anions with Na⁺ counterions. These corrections can now be calculated, and the adjusted electron affinities, together with the original ones, are listed in Table VI.

Table VI: Electron Affinities of Aromatic Hydrocarbons in THF at 25°, Corrected for the Variable Degree of Association with Na⁺ Ions

Hydrocarbon	Original ϵ° , v., ref. 4	Corrected ϵ° , v.
Biphenyl	(0.0)	(0.0)
Naphthalene	0.066 ± 0.02	0.043
Triphenylene	0.113 ± 0.01	0.128
Phenanthrene	0.124 ± 0.005	...
Pyrene	0.505 ± 0.005	0.529
9,10-Dimethylanthracene	0.607 ± 0.005	0.616
Anthracene	0.624 ± 0.005	0.642
Perylene	0.917 ± 0.005	0.956
Tetracene	1.025 ± 0.01	1.058

On the whole, the corrected ϵ° values are only slightly larger than those reported in ref. 4, the largest increase of about 0.04 v. being found for perylene (0.917 to 0.956). Naphthalene is an exception, its electron affinity being by about 0.02 v. lower than that reported previously. The extremely strong association of naphthalene⁻ with Na⁺ increases, however, the spectrophotometric equilibrium constant



The large degree of association between naphthalene⁻ and Na⁺ calls for some comments. Because of its exceptional behavior, the conductance studies of its

(8) D. N. Bhattacharyya, C. L. Lee, J. Smid, and M. Szwarc, *J. Phys. Chem.*, **69**, 608 (1965).

(9) T. A. Miller, B. Prater, J. K. Lee, and R. N. Adams, *J. Am. Chem. Soc.*, **87**, 121 (1965).

solutions were repeated several times. There is, therefore, little doubt about its low dissociation constant.

The dissociation of naphthalene⁻,Na⁺ was investigated also by Atherson and Weissman^{1d} who used an e.s.r. technique. This interesting method distinguishes ion pairs, in which an additional splitting of the e.s.r. signal occurs due to the presence of Na²³, from the free ions which do not show further splitting. Experimentally, the method is not too reliable, as far as absolute values are concerned (see the text of ref. 1d), and moreover it determines probably only the contact ion pairs, counting the solvent separated pairs as free ions. Hence, the dissociation constant, $1.5 \times 10^{-6} M$, determined by this technique may be too high.

The relative smallness and symmetry of the anion probably leads to a central location of the Na⁺ cation in the ion pair, and the proximity of *all* of the negative charge to Na⁺ accounts therefore for the large binding energy. The greater delocalization of the negative charge in the larger radical ions reduces the attraction and probably causes an unsymmetrical placement of the counterion. Perylene⁻,Na⁺ represents one of the extreme cases since the counterion can only be associated with one of the two naphthalene rings that form this hydrocarbon. Thus, Na⁺ is in the proximity of only 0.5 of the negative charge residing on this anion, and hence the high degree of dissociation of the perylene⁻,Na⁺ pair is understandable.

It should not be concluded that the counterion is rigidly located with respect to the anion. On the contrary, there is evidence^{1d,10} that the counterion vibrates rapidly between the positions of the highest negative density if two or more of such positions exist in the anion.

Remarks Concerning the Paper by Buschlow, Dieleman, and Hoijtink^{2a}

In a most interesting paper, Hoijtink, *et al.*,^{2a} discussed the dissociation of ion pairs—aromatic⁻, alkali ion⁺—in tetrahydrofuran (THF) and methyltetrahydrofuran (MTHF). The conductance of each of the investigated ion pairs was determined over a wide temperature range (25 to -75°) but at one concentration ($10^{-4} M$) only. The degree of dissociation was estimated from the temperature dependence of the conductance. Although this method may give some qualitative information about the extent of the dissociation, often it could be misleading. For example, Hoijtink considers a salt to be completely dissociated if no maximum is shown in the conductance-temperature curve. This is not a valid conclusion, and indeed it led Hoijtink to believe that in THF at 25° anthracene⁻,Na⁺

is completely dissociated at the concentration of $10^{-4} M$, while its dissociation under these conditions amounts to 8% only.

At a constant salt concentration, the temperature dependence of the conductance curve is governed by several factors: (1) the temperature dependence of the solvent viscosity, (2) the heat of dissociation of the investigated ion pair, (3) the temperature dependence of $\Lambda_0\eta$, and (4) the degree of dissociation of the salt.

The viscosities of THF and MTHF have been shown¹¹ to be given by a linear, Arrhenius-type relation which is valid over the whole temperature range of 25 to -75°. Thus,

$$\log \eta_{\text{THF}} = -3.655 + 393/T$$

and

$$\log \eta_{\text{MTHF}} = -3.625 + 384/T$$

and the respective "activation energies" are ~ 1.76 and 1.72 kcal./mole. The heat of dissociation of the Na⁺, Cs⁺, and NBU₃(*i*-Am)⁺ salts of BPh₄⁻ have also been investigated in this temperature range,¹¹ and in THF the heat of dissociation of Na⁺BPh₄⁻ was found to increase from the -1.3 kcal./mole at 25° to about 0 kcal./mole at -70°. The concentration of the ions is proportional to $K_{\text{diss}}^{1/2}$ if the degree of dissociation is low, and therefore the temperature coefficient of conductance is given by " $E\eta$ " + $1/2\Delta H_{\text{diss}}$. The conductance of Na⁺BPh₄⁻ decreases, therefore, steadily on lowering the temperature, clearly indicating the unreliability of Hoijtink's criterion.

There are good reasons to believe that in THF solutions Li⁺X⁻ ion pairs may form solvent-separated pairs, and, since the exothermicity of their dissociation is quite low,¹² their conductance may not show a maximum. Hence, the criterion discussed above might again be misleading.

The contribution of triple ions to the conductance must not be neglected, and, since their concentration decreases at lower temperatures, this effect may lead to the disappearance of the maximum in the conductance-temperature curve.

Finally, if the investigated ion pairs are completely dissociated, the observed Λ should be close to Λ_0 . It was shown⁸ that Λ_0^+ of Li⁺ and Na⁺ in THF at 25° are 36.6 and 48, respectively, whereas the Λ values of the Li⁺ and Na⁺ salts of anthracene⁻ reported in ref. 2a are ~ 18 and 28 only. This proves again

(10) E. de Boer and E. L. Mackor, *J. Am. Chem. Soc.*, **86**, 1513 (1964).

(11) C. Carvajal, J. K. Tölle, J. Smid, and M. Szwarc, *ibid.*, in press.

(12) T. E. Hogen-Esch and J. Smid, *ibid.*, **87**, 666 (1965).

that under those conditions the dissociation is less than 50%.

Conductance of Anthracene²⁻, 2Na⁺

Several samples of anthracene²⁻, 2Na⁺ were prepared, and their conductances were investigated. Unfortunately, the scatter is too great to allow a reliable determination of Λ_0 or $1/\Lambda_0^2 K_{\text{diss}}$; however, the very low conductance of these solutions proves the low degree of dissociation which we estimate at about $10^{-7} M$. Our findings agree again with the qualitative observations of Hoijtink, *et al.*^{2a} Apparently, A²⁻, 2Na⁺ are contact agglomerates whereas A⁻, Na⁺ may be, to a large extent, a solvent-separated ion pair. See in this

connection ref. 13. Discussion of the disproportionation of 2A⁻ into A²⁻ + A which resembles ours was published by Shatenstein¹⁴ in 1964. See also ref. 13.

Acknowledgment. The financial support of this study by the U. S. Army Research Office (Durham), Grant DA-ARO(D)-31-124-G521, Texaco, Inc., and the National Science Foundation is gratefully acknowledged.

(13) R. C. Roberts and M. Szwarc, *J. Am. Chem. Soc.*, in press.

(14) A. I. Shatenstein, E. S. Petrov, and M. I. Belusova, "Organic Reactivity," Vol. 1, Tartu State University, Estonia, U.S.S.R., 1964, p. 191.

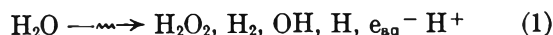
Reactions of Alanine with the Reducing Species Formed in Water Radiolysis¹

by Boyd M. Weeks, Sibyl A. Cole, and Warren M. Garrison

Lawrence Radiation Laboratory, University of California, Berkeley, California (Received June 10, 1965)

A detailed study has been made of the effects of pH and of added scavengers on the reactions of alanine with the reducing species formed in water radiolysis. A principal reaction of the hydrated electron (e_{aq}^-) leads to degradation of the N-C linkage, *e.g.*, $e_{\text{aq}}^- + \text{RNH}_3^+ \rightarrow \text{R} + \text{NH}_3$. The rate of removal of e_{aq}^- by such reaction is strongly dependent on the ionic form of the α -amino acid; β -alanine is relatively less reactive toward e_{aq}^- under all conditions of pH. A suggested reaction scheme accounts both qualitatively and quantitatively for the observed effects of pH on product yields from oxygen-free solutions of alanine under γ rays.

The principal actions of ionizing radiations on solutes in dilute aqueous solution are initiated by the radiation-induced step²



Subsequent reactions of these oxidizing and reducing species with the simpler amino acids such as glycine and alanine in oxygen-free solutions lead to both oxidative and reductive deamination with formation of the corresponding keto acid and fatty acid as major degradation products.³ The relative and absolute yields of both major and minor products from glycine and alanine are strongly dependent on the pH of the

irradiated solution. One pH-dependent reaction that must be considered is of course the conversion of e_{aq}^- to H by the hydronium ion²



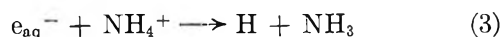
However, conversion of e_{aq}^- to H is not specific to the

(1) This work was done under the auspices of the U. S. Atomic Energy Commission.

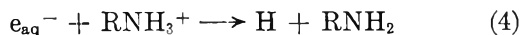
(2) E. J. Hart, *Science*, **146**, 19 (1964).

(3) (a) G. Stein and J. Weiss, *J. Chem. Soc.*, 3256 (1949); (b) N. E. Sharpless, A. E. Blair, and C. R. Maxwell, *Radiation Res.*, **2**, 135 (1955); (c) B. M. Weeks and W. M. Garrison, *ibid.*, **9**, 291 (1958).

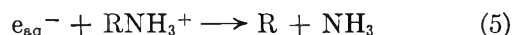
H_3O^+ ion. Other proton donors are also effective; ammonium ion, for example, converts e_{aq}^- to H *via*⁴



and the analogous reaction



might be expected to be of importance in the radiolysis of aqueous solutions of organic compounds containing the NH_2 function. With the amines, a dissociative cleavage of the N-C bond may also be envisaged



Some preliminary evidence on the role of reaction 5 in the radiolysis of the α -amino acids in aqueous solution has been described.⁵ We report here a detailed study of the several processes involved in the deamination of alanine in oxygen-free solution under γ rays. Data on the glycine-water system have also been included for purposes of comparison.

Experimental Section

Materials. Alanine and glycine (Nutritional Biochemicals) were recrystallized several times from water. The labeled alanine and glycine (C^{14}OOH) were purified chromatographically on Dowex 50 (hydrogen form). Hydrochloric acid in progressively increasing concentration (0 to 4 *N*) was used as the eluting agent. The separated amino acid hydrochlorides were passed through Dowex 1 (acetate form) to remove chloride ion; the acetic acid was removed under vacuum, and the amino acids were then recrystallized from water. The detailed procedures have been described.^{3c} Water from a Barnstead still redistilled first from alkaline permanganate and then from sulfuric acid was used in the preparation of the solutions. The chloroacetic acid (Eastman) was redistilled *in vacuo*. All other chemicals were reagent grade and were used without further purification. The pH adjustments were made with sulfuric acid or sodium hydroxide.

Irradiations. The Pyrex irradiation cells were cleaned in nitric acid-hydrogen peroxide solution and rinsed with triply distilled water. The samples (10-ml.) were irradiated in cylindrical Pyrex cells with a total volume of ~ 40 ml. The samples containing C^{14} -labeled amino acid were irradiated at a volume of 1 ml. in a proportionately smaller cell. Samples were degassed by evacuation. The irradiations were made with CO^{60} γ rays from a 200-curie source. The dose rate, $\sim 5 \times 10^{16}$ e.v. $\text{g}^{-1} \text{min}^{-1}$ over the period of this study, was determined by the Fricke dosimeter ($G(\text{Fe}^{3+}) = 15.5$, $\epsilon_{305} 2180$ at 24°). Energy deposition in

solutions was taken to be proportional to the electron density.

Analytical Procedures. Gaseous products volatile at -80° were transferred to a gas buret by means of a Toepler pump. After the total volume was measured, a sample was withdrawn for mass spectrometric analysis. The system was designed so that the neutral and alkaline samples could be acidified to $\text{pH} < 1$ to ensure quantitative recovery of carbon dioxide.

The Conway diffusion method⁶ was used to separate ammonia from the irradiated solutions. The difusates were assayed by means of the Nessler reagent. Pyruvic acid and acetaldehyde from alanine and glyoxylic acid and formaldehyde from glycine were identified by paper chromatography of the 2,4-dinitrophenylhydrazones^{3c}; their separate amounts were quantitatively determined by the method of Johnson and Scholes.⁷ The appropriate "blank" and control runs were made. Ammonia and carbonyl measurements were reproducible to within 5%.

The fatty acid yields were determined radiometrically. Solutions containing the C^{14} -labeled amino acids at a known specific activity were irradiated and then "spiked" with measured amounts of appropriate carrier (propionic and acrylic acids in the case of alanine and acetic acid in the case of glycine). The entire sample was then placed on a silicic acid column and chromatographed with the butanol-chloroform solvent system after the method of Marvel and Rands^{3c,8} to separate the fatty acids from the amino acid and from other products. Propionic and acrylic acids are eluted together in a single peak, and to separately determine them it was convenient to brominate the mixture and rechromatograph. The mono- and dibromopropionic acids are well separated from propionic acid. Yields were calculated from the specific activities of the initial amino acid solution and the isolated fatty acid.

Results

We find, in agreement with Maxwell and co-workers,^{3b} that the major degradation products from unbuffered alanine solutions ($\text{pH} 6.4$) include ammonia, propionic acid, pyruvic acid, and acetaldehyde. In addition,

(4) J. Jortner, M. Ottolenghi, J. Rabani, and G. Stein, *J. Chem. Phys.*, **37**, 2488 (1962).

(5) (a) W. M. Garrison, *Radiation Res. Suppl.*, **4**, 158 (1964); (b) B. M. Weeks, S. A. Cole, and W. M. Garrison, Chemistry Division Annual Report UCRL-11213, 1963, p. 112.

(6) E. J. Conway and A. Berne, *Biochem. J.*, **27**, 419 (1933).

(7) G. R. A. Johnson and G. Scholes, *Ind. Eng. Chem. Anal. Ed.*, **79**, 217 (1954).

(8) C. S. Marvel and R. Rands, Jr., *J. Am. Chem. Soc.*, **72**, 2642 (1950).

we find acrylic acid; the observed yield of this product varies considerably from one run to the next but in neutral solution averages about 10% of the propionic yield. Product yields from alanine and also from glycine increase rapidly with increasing solute concentration up to $\sim 0.3 M$ and then tend toward the limiting values in the concentration range ~ 0.5 to $\sim 1 M$. Typical yield-concentration plots are given in Figure 1 for alanine at pH 6.4, 2.8, and 0.3. Yields of all major products from 1 M alanine at pH 6.4 are summarized in Table I.

Table I: Observed and Calculated Yields of Products from 1 M Alanine at pH 6.4

Product	G	
	Obsd.	Calcd. ^a
Ammonia	4.3	4.8
Propionic acid	1.0	1.0 ^b
Pyruvic acid	1.6	1.4
Acetaldehyde	0.5	0.60
Carbon dioxide	0.60	0.60 ^b
Hydrogen	1.25	1.0

^a Based on the accepted yields for water decomposition (ref. 11) and the reaction scheme formulated in the present work. ^b The observed yields of propionic acid and carbon dioxide give directly the yields of reactions 8b and 14a, respectively. Other yields may then be calculated on the basis of eq. 1, 6, 7, 8a, 8b, 9, 10b, 11, 13, 14, and 14a.

The effects of an added radical scavenger, formate ion, on $G(\text{NH}_3)$ from neutral 1 M solutions of alanine and glycine are shown in Figure 2. The ammonia yields from both the alanine and glycine systems drop sharply with increasing concentrations of formate and then approach steady values at formate concentrations in the range 0.1 to 0.25 M. The limiting ammonia yields extrapolated to zero formate concentration correspond to $G(\text{NH}_3) = 2.5$ for alanine and $G(\text{NH}_3) = 1.6$ for glycine. The effects of 0.25 M sodium formate on the yields of fatty acids and carbonyl products from alanine and glycine, 1 M, pH 6.4, are summarized in Table II. If there is any effect at all of added formate on $G(\text{propionic})$ and $G(\text{acetic})$, it is to increase the yields by a small amount. At the same time we find that the production of carbonyl products is almost completely quenched by formate ion at 0.25 M. Table II also shows that addition of increasing amounts of chloroacetic acid to the 1 M alanine-0.25 M formate system leads to a sharp decrease in the yield of propionic acid; at 0.15 M chloroacetic acid, $G(\text{propionic})$ is essentially zero.

The effect of pH on $G(\text{NH}_3)$ for 1 M alanine in the

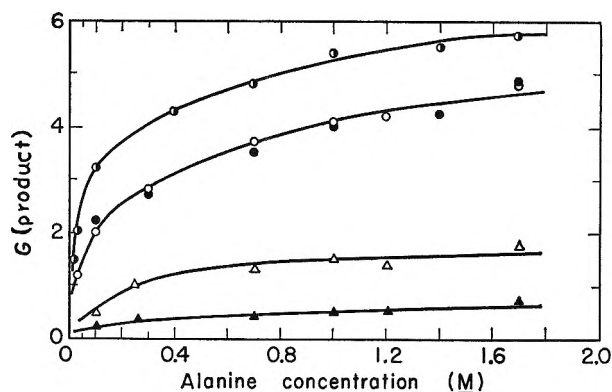


Figure 1. Product yields as a function of alanine concentration: ammonia at pH 0.3 (●), pH 2.8 (○), pH 6.4 (○); pyruvic acid (▲) and acetaldehyde (△) at pH 6.4.

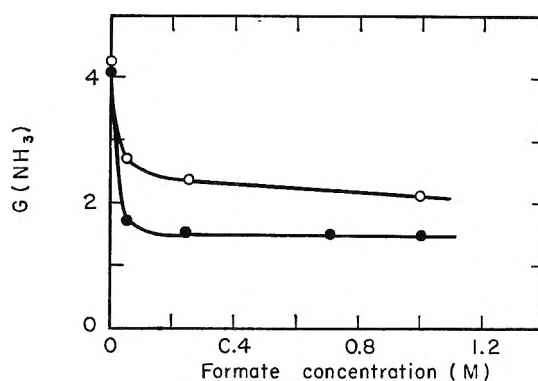


Figure 2. Yield of ammonia from 1.0 M alanine (○) and 1.0 M glycine (●) as a function of sodium formate concentration at pH 6.4.

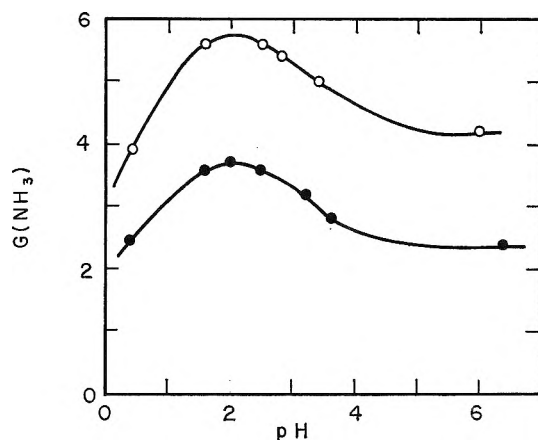


Figure 3. Yield of ammonia from 1 M alanine (○) and 1.0 M alanine-0.25 M formate (●) as a function of pH.

presence and in the absence of 0.25 M formate scavenger are given in Figure 3 for the range pH 6.4 down to 0.3. That the effect of 0.25 M formate is maximal over the entire pH range studied is shown by the data of Figure

Table II: Effect of Scavengers on the Yields of Organic Products from Solutions of Alanine and Glycine at pH 6.4

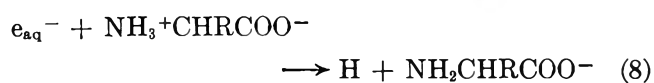
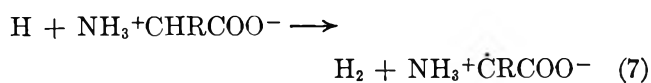
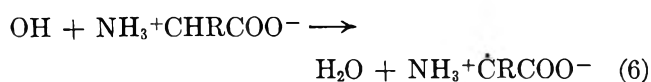
	[Formate]	Fatty acid	Keto acid	Aldehyde
1.0 M alanine	None	1.0	1.5	0.5
1.0 M alanine	0.25	1.1	<0.1	<0.1
1.0 M glycine	None	1.7	2.3	0.6
1.0 M glycine	0.25	1.8	<0.1	<0.1
	[Chloroacetate]			
1.0 M alanine	None	1.1	<0.1	<0.1
+	0.02	0.25
0.25 M formate	0.15	<0.1	<0.1	...

4, $G(\text{NH}_3)$ decreases sharply with increasing formate at pH 0.3 and pH 2.8 as well as at pH 6.4 and in all cases approaches a steady value at formate concentration above 0.25 M. The yield of pyruvic acid plus acetaldehyde is decreased to $G < 0.1$ by 0.25 M formate over the whole pH range studied.

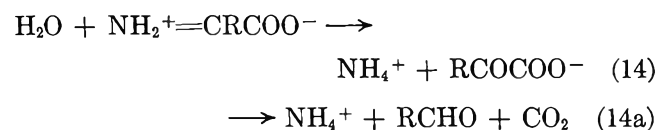
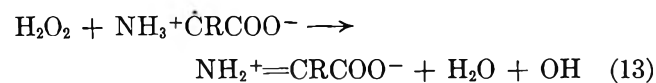
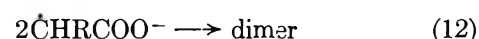
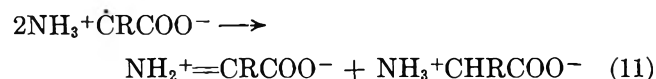
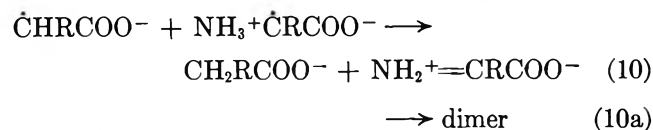
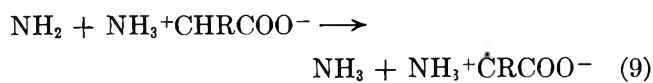
Propionic acid production over the pH range 6.4 to 0.3 in 1 M alanine and in 0.1 M alanine solutions is plotted in Figure 5. Note that the form of the G -(propionic)-pH plot for 1 M alanine has essentially the same form as the $G(\text{NH}_3)$ -pH plot for 1 M alanine-0.25 M formate (Figure 3). Hydrogen and carbon dioxide yields for 1 M alanine over the corresponding pH range are given in Figure 6. The hydrogen yield shows little dependence on hydrogen ion concentration at pH values > 2 . The increase in $G(\text{H}_2)$ with decreasing pH below ~ 2 is accompanied by a decrease in both $G(\text{NH}_3)$ and $G(\text{propionic})$.

Discussion

We consider first the radiation chemistry of alanine and glycine in neutral solution under which condition the amino acids are almost exclusively in the zwitterion form.⁹ The proposed reaction scheme for formation of the principal products is summarized by eq. 1^{10,11} and 6 through 14a

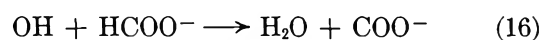
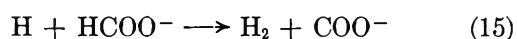


followed by

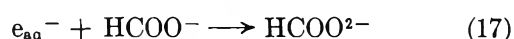


The removal of OH and H *via* steps 6 and 7 and the further oxidation of $\text{NH}_3^+\dot{\text{C}}\text{RCOO}^-$ to yield ammonia and carbonyl products is in accord with earlier work.^{3c} Our primary concern here is in regard to the validity of reactions 8, 8a, and 8b as paths for removal of e_{aq}^- .

Now, the formate ion reacts rapidly with H and OH



($k_{15} = 2 \times 10^8 \text{ M}^{-1} \text{ sec}^{-1}$, $k_{16} = 10^9 \text{ M}^{-1} \text{ sec}^{-1}$) but is relatively unreactive towards e_{aq}^-



($k_{17} < 10^6 \text{ M}^{-1} \text{ sec}^{-1}$).^{11,12} We find that the ammonia yields from both alanine and glycine in 1 M solution drop rapidly with increasing formate concentrations but then level off at formate concentrations above $\sim 0.1 \text{ M}$ to the limiting $G(\text{NH}_3)$ value shown in Figure 2. And, this drop in $G(\text{NH}_3)$ is accompanied by a complete quenching of carbonyl production whereas the fatty acid yield remains essentially unchanged (Table II). At sufficiently high concentrations of formate ion we may assume that both H and OH are

(9) J. P. Greenstein and M. Winitz, "Chemistry of the Amino Acids," John Wiley and Sons, Inc., New York, N. Y., 1961.

(10) We assume for reaction 1 the 100-e.v. yields: $G_{\text{H}_2} = 0.45$, $G_{\text{H}_2\text{O}_2} = 0.7$, $G_{\text{OH}} = 2.9$, $G_{\text{H}} = 0.55$, $G_{e_{\text{aq}}^-} = 2.3$ (ref. 11).

(11) (a) A. O. Allen, *Radiation Res. Suppl.*, **4**, 54 (1964); (b) J. T. Allan, *J. Phys. Chem.*, **68**, 2697 (1964).

(12) E. J. Hart, J. K. Thomas, and S. Gordon, *Radiation Res. Suppl.*, **4**, 74 (1964).

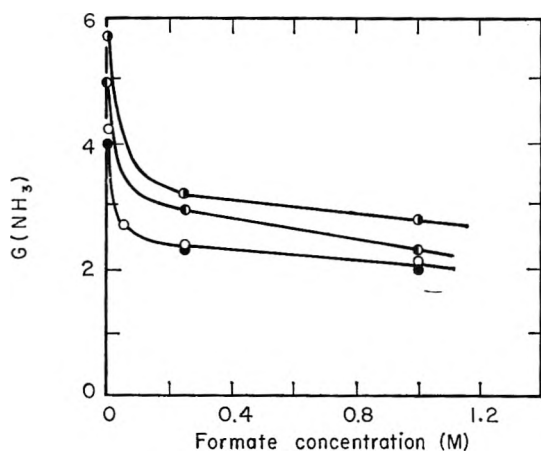


Figure 4. Yield of ammonia from 1 *M* alanine as a function of sodium formate concentration: pH 0.3 (●), pH 2 (●), pH 3.4 (○), pH 6.4 (○).

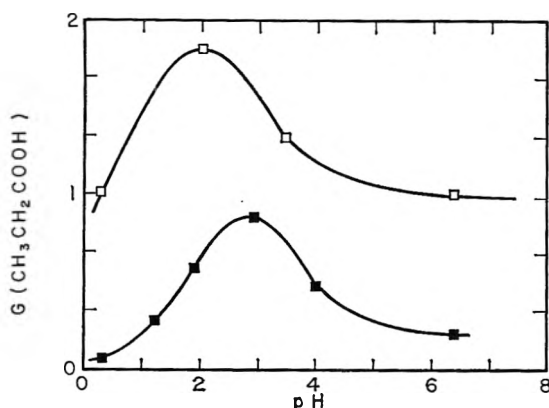


Figure 5. Yield of propionic acid as a function of pH in 1.0 *M* alanine (□) and 0.1 *M* alanine (■).

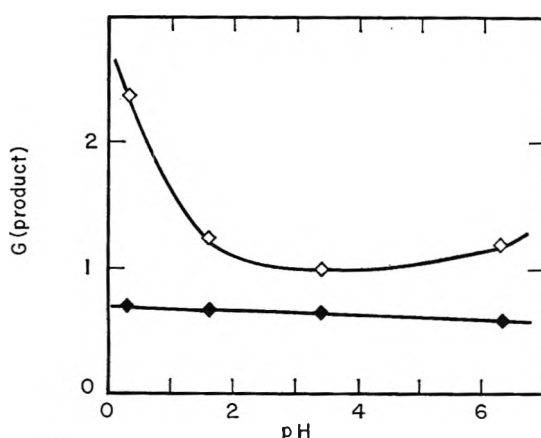
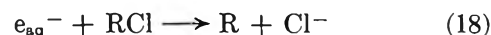


Figure 6. Yields of hydrogen (◇) and carbon dioxide (◆) from 1 *M* alanine as a function of pH.

preferentially removed through reactions 15 and 16, respectively, and that the COO^- radicals so formed are ineffective in initiating deamination. The produc-

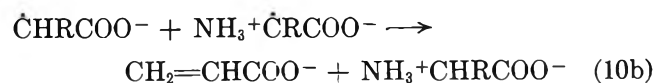
tion of fatty acid and ammonia in the presence of excess formate (Table II, Figure 2) is then assigned to reactions of e_{aq}^- with the amino acid zwitterion as given eq. 8a and 8b. This assignment is also substantiated by the observation that chloroacetic acid at a concentration of 0.1 *M* effectively blocks the production of the fatty acid (Table II); the chloroacetate ion is extremely reactive towards e_{aq}^-



($k_{18} \approx 10^{10} \text{ M}^{-1} \text{ sec}^{-1}$).^{12,13}

In 1 *M* solutions of the glycine zwitterion, the yield for removal of e_{aq}^- through reactions 8a and 8b is given by $G(\text{NH}_3) \approx G(\text{CH}_3\text{COOH}) \approx 1.6$ as indicated by the data of Figure 2 and Table II. We suggest in the case of the glycine zwitterion that reactions 8a and 8b occur in parallel with the conversion reaction (8) and that the yield of reaction 8 in neutral 1 *M* glycine is given by $G_{e_{\text{aq}}^-} - 1.6 \approx 1.2$. Reaction 8 does not lead to glycine deamination in the presence of formate by virtue of reaction 15, but, in the absence of formate, the combined yield of H atoms available for reaction 7 becomes $G_{\text{H}} + 1.2 \approx 1.7$ to give $G(\text{H}_2) \approx G_{\text{H}} + 1.7 \approx 2.2$ which is close to the experimentally observed hydrogen yield from neutral 1 *M* glycine under γ rays.¹⁴

In the radiolysis of 1 *M* alanine, pH 6.4, the ammonia yield levels off at $G(\text{NH}_3) \approx 2.5$ with increasing formate concentration (Figure 2), and as with glycine the carbonyl yield goes to zero while the fatty acid yield remains constant (Table II). We conclude that the alanine zwitterion scavenges e_{aq}^- almost quantitatively *via* steps 8a and 8b. The fact that the propionic yield from alanine is considerably less than the limiting $G(\text{NH}_3)$ value in the presence of formate indicates that the radical product of reaction 8a, $\dot{\text{C}}\text{HRCOOH}$, reacts preferentially as a reducing species in both the presence and absence of added formate. In the alanine case then reaction 10 is of the form



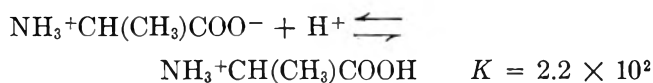
which also accounts for the formation of acrylic acid. The acrylic acid yield on this basis should approximate $G_{e_{\text{aq}}^-} - G(\text{CH}_3\text{CH}_2\text{COOH}) \approx 1.8$ since the yield of higher molecular weight products (reactions 10a and 12) is negligible. That the observed yield is only a fraction of this is not surprising in view of the efficiency of the radical-induced chain polymerization of vinyl

(13) E. Hayon and A. O. Allen, *J. Phys. Chem.*, **65**, 2181 (1961).

(14) C. R. Maxwell, D. C. Peterson, and N. E. Sharpless, *Radiation Res.*, **6**, 530 (1954).

compounds in dilute aqueous solution.¹⁵ Product yields calculated on the basis of the above reaction scheme for neutral 1 *M* alanine are compared in Table I with the experimentally observed values.

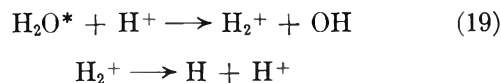
The removal of e_{aq}^- by the zwitterion forms of glycine and alanine, which, as we have shown here, gives rise to the chemistry of eq. 8a and 8b, is a relatively slow process. Hart¹² has followed spectrophotometrically the disappearance of e_{aq}^- in neutral solutions of glycine and alanine and finds that both of these solutes react with e_{aq}^- with a bimolecular rate constant of $\sim 7 \times 10^7 M^{-1} \text{ sec.}^{-1}$; and, Maxwell¹⁶ finds from competition studies with the NO_3^- ion a rate constant of $\sim 2 \times 10^7 M^{-1} \text{ sec.}^{-1}$ for the reaction of e_{aq}^- with glycine in neutral solution. Since these rates are only 10^{-3} that for the reaction of e_{aq}^- with H_3O^+ ($k = 2 \times 10^{10} M^{-1} \text{ sec.}^{-1}$) and since, for example, in the case of alanine⁹



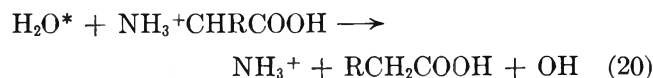
it follows that the probability of capture of e_{aq}^- by the alanine zwitterion decreases rapidly with decreasing pH. Since formate effectively quenches the oxidative deamination of alanine over the entire pH range ~ 7 to ~ 0.3 , it is apparent from the data of Figures 3 and 5 that e_{aq}^- also reacts with the alanine cation and more rapidly than with the zwitterion to give the product analogs of reactions 8a and 8b. The magnitude of $G(\text{NH}_3)$ from 1 *M* alanine–0.25 *M* formate at the lower pH values (Figure 3) shows that the velocity constants for the reaction of $\text{NH}_3^+\text{CH}(\text{CH}_3)\text{COOH}$ and of H_3O^+ with e_{aq}^- are within the same order of magnitude.¹⁷

We note, in regard to the pronounced maximum in the pH–yield plot shown in Figure 3, the addition of increasing amounts of formate scavenger to 1 *M* alanine at pH ~ 2 decreases the ammonia yield from ~ 5.4 to ~ 3.5 (Figures 3 and 4) which is significantly greater than the value anticipated from reactions 8a and 8b on the basis of $G_{e_{aq}^-} = 2.8$. And, in the absence of formate the yields of all products from 1 *M* alanine at pH 2 to 3 are greater^{3c} than we can account for in terms of the accepted yields^{10–12} for the decomposition of neutral water *via* reaction 1. Now, Platzman¹⁸ has pointed out that subexcitation electrons, *i.e.*, secondary electrons with kinetic energies below that corresponding to the lowest excitation potential of water, can be effective in the direct excitation of solute species in the decimolar concentration range. And, it is not unreasonable to suggest that the chemical effectiveness of such excitation of the α -amino acids

might depend on their ionic form. However, we know from other studies that the direct excitation of alanine and other amino acids by ionizing radiation^{3b,19} and by ultraviolet light²⁰ leads to modes of decomposition that yield carbon dioxide as a major decomposition product. Since we find that $G(\text{CO}_2)$ for 1 *M* alanine is essentially constant from pH 6.4 down to 0.3 (Figure 6), our conclusion is that the enhanced yield for alanine decomposition in acid solution is not the result of subexcitation electron effects. We note, however, that there is accumulating evidence²¹ that, as the pH of a solution is reduced below 3 to 4, the yield for water decomposition actually increases presumably as a result of the stoichiometry^{21b}



where H_2O^* represents either an excited water molecule or an isolated radical pair (H, OH), species which revert to water at pH > 4 by first-order kinetics. It is clear, however, that scavenging of H_2O^* by H^+ to yield additional H and OH cannot be responsible for the enhancement with decreasing pH of product yields from 1 *M* alanine containing excess formate scavenger. On the other hand, the present experimental requirements appear to be wholly satisfied by a reductive deamination of the amino acid by H_2O^* *via* the stoichiometry



where $G_{\text{H}_2\text{O}^*} \simeq 0.8$ and where the radical products of reaction 20 are subsequently removed through steps 6 and 9.

As the pH is decreased below ~ 2 , the hydrogen yield begins to increase as a consequence of the competition of H_3O^+ for reducing species according to reactions 2 and 19. The present data do not provide a basis for estimating the relative importance of reac-

(15) E. Collinson, F. S. Dainton, and G. S. McNaughton, *Trans. Faraday Soc.*, **53**, 357 (1957).

(16) C. R. Maxwell, unpublished results.

(17) Although HCOOH is considerably more reactive towards e_{aq}^- than is HCOO^- (ref. 12), this solute still acts preferentially as a scavenger of H and OH in acidic 1 *M* alanine because of the increased reactivity of the cation form towards e_{aq}^- .

(18) R. L. Platzman, *Radiation Res.*, **2**, 1 (1955).

(19) B. Rajewsky and K. Dose, *Z. Naturforsch.*, **12b**, 384 (1947).

(20) K. Pfordte and G. Leuschner, *Strahlentherapie*, **119**, 278 (1962).

(21) (a) A. O. Allen, "The Radiation Chemistry of Aqueous Solutions," D. Van Nostrand Co., Inc., New York, N. Y., 1961; (b) F. S. Dainton and D. B. Peterson, *Proc. Roy. Soc. (London)*, **A267**, 443 (1962).

tions 2 and 19 in the production of the additional hydrogen.

From the radiation chemistry reported here thus far, one might assume that reductive cleavage of the N-C bond represents a characteristic radiation chemical property of amines generally. However, Riesz²² finds no evidence for such reaction in the radiolysis of oxygen-free solutions of the methylammonium ion, nor do we find any important contribution of reductive deamination in our preliminary studies of the effects of H and OH scavengers on the radiation chemistry of β -alanine. The α -amino acids appear to represent a special case, and we can only speculate at the present time on the role of α substitution in the reductive

cleavage of the N-C bond by e_{aq}^- . One possibility, of course, is that e_{aq}^- interacts with the π electrons of the C=O group and that dissociation of the N-C bond at the α position occurs on rearrangement of the intermediate complex. It would appear that further consideration of these reactions must await additional information on the radiation chemistry of the variously substituted amines.

Acknowledgment. We are indebted to Dr. M. E. Jayko for the mass spectrometric analysis and to Mrs. Harriet L. Atkins for technical assistance in certain phases of the experimental work.

(22) P. Riesz, *Radiation Res.*, **26**, 1 (1965).

Physicochemical Studies on Isotactic Polystyrene

by Hiroyasu Utiyama¹

Institute for Chemical Research, Kyoto University, Takatsuki, Osaka-fu, Japan (Received June 10, 1965)

An isotactic polystyrene sample prepared by using a Ziegler-type catalyst has been fractionated by a stepwise separation of crystalline solid precipitate from isotactic polystyrene-monochlorobenzene-cyclohexanol at 8°. Measurement of crystallinity of the films of the fractionated samples by an infrared spectroscopic method has shown that the fractions differ in their speed and degree of crystallization. Light-scattering and viscosity measurements have been carried out at 25.3° on the fractionated samples using monochlorobenzene as solvent and 2,4,6-trimethylphenol as antioxidant. One of the fractions (F-4), the films of which readily crystallize at relatively low temperature, has shown a negative initial slope and a minimum in the plot of the conventional reciprocal scattered intensity function *vs.* $\sin^2(\theta/2)$. From theoretical considerations, it has been concluded that this anomaly is due to a large optical anisotropy, 40 times as large as that for atactic polystyrene. This conclusion has been confirmed by the separate measurement of vertical and horizontal components of scattered light using vertically or horizontally polarized light. It has also been found that optical anisotropy of highly crystallizable samples of isotactic polystyrene fractions decreases with increase in temperature, while that of the conventional atactic polystyrene is very small and increases slightly with temperature. The second virial coefficient corrected for the effect of the optical anisotropy of sample F-4 is exceptionally small. While definitive estimations of the unperturbed chain dimension *A* and of the interaction parameter *B* were not possible, consideration of the data suggests that, as the degree of isotactic stereoregularity increases, the short-range parameter *A* increases and the long-range interaction parameter *B* decreases. A consideration of the estimated value of the optical anisotropy of the styrene monomer as a function of the mode of rotation of the benzene ring has led to the conclusion that the optical anisotropy is a good measure of the degree of the isotactic stereoregularity of polystyrene. The optical anisotropy increases as the degree of isotactic stereoregularity increases. This increase is due to the hindered rotation around the C-C bond connecting the benzene ring to the main chain. The hindrance is due to the larger interaction between neighboring benzene rings, which simultaneously decreases the flexibility of the chain.

Introduction

Since the first success of Natta and his co-workers in the production of crystalline high polymers of α olefins and the identification of their local stereochemical configurations,^{2,3} the physical chemical properties of these polymers in solution have been the subject of extensive investigation. The hindrance, due to internal rotation around each C-C bond along the main chain, may be affected by stereochemical configuration of the asymmetric carbon atoms. Thus, dimensions and the electric dipole moments of isotactic polymers in dilute solutions will differ to some

extent from those of atactic polymers. Furthermore, particular attention has been paid to establishing reliable techniques for estimation of the stereoregularity. Such techniques should, if possible, be based on measurements of quantities reflecting directly the structure of

(1) On leave of absence at the Department of Chemistry, Harvard University, Cambridge, Mass.

(2) (a) G. Natta, P. Pino, P. Corradini, F. Danusso, E. Mantica, G. Mazzanti, and F. Moraglio, *J. Am. Chem. Soc.*, **77**, 1708 (1955); (b) G. Natta, *J. Polymer Sci.*, **16**, 143 (1955).

(3) G. Natta, *Makromol. Chem.*, **16**, 77, 213 (1955).

individual molecules and being free from any influence of secondary effects.^{4,5}

Numerous studies have been carried out on the solution properties of stereoregular polymers, particularly of isotactic polystyrene.

Among these studies is that of Natta, Danusso, and Moraglio,⁶ who concluded, on the basis of the results of viscosity and osmotic pressure data, that the relation between molecular weight and limiting viscosity number was the same for both isotactic and atactic polystyrene. This conclusion was confirmed repeatedly by subsequent investigators.⁷⁻¹⁰ Danusso and Moraglio⁷ fractionated isotactic and atactic polystyrene simultaneously by fractionating precipitates from a solution which contained an equal amount of both polymers. They made osmotic pressure measurements on the fractionated samples and found that the second virial coefficient and its molecular weight dependence for isotactic polystyrene were both smaller than those of atactic polystyrene. On the basis of light-scattering data for fractionated samples with the use of a semioctagonal cell, Trossarelli, Campi, and Saini¹⁰ found that no differences exist between the molecular dimension of isotactic and atactic polystyrene in toluene. However they also found that the ratios $A_2M_w/[\eta]$ of isotactic polymer fractions were smaller than those of atactic polystyrene and essentially independent of molecular weight. Krigbaum, Carpenter, and Newman¹¹ made viscosity, osmotic pressure, and light-scattering measurements on two fractionated samples of isotactic polystyrene in *p*-chlorotoluene and in *o*-dichlorobenzene. They concluded that the unperturbed dimension of isotactic polystyrene was 25-30% larger than that of its atactic counterpart.

All of these authors state that, of the second virial coefficient and the molecular dimension, only the former was affected by stereoregularity. If so, the properties of dilute solutions of isotactic polystyrene may not be explained within the frame of the two-parameter theory without making any additional assumptions. It should be remarked, in this connection that the analysis of the experimental data by Krigbaum, *et al.*,¹¹ is somewhat ambiguous in that their treatment inevitably results in assuming the dependence of interaction parameter *B* on molecular weight. The present study has been performed in an attempt to resolve this ambiguity and to clarify the characteristic properties of isotactic polystyrene in solution by examining them with a different experimental approach.

Now, in order to answer whether the physical properties of an isotactic polymer are affected by the stereoregularity, it is necessary before making any physicochemical measurement (i) to employ a solvent that will

dissolve the highly crystalline portion of the polymer, (ii) to develop a method to separate out a highly stereoregular fraction, and (iii) to estimate its stereoregularity. Since an isotactic polystyrene sample is a mixture of molecules with various degrees of stereoregularity and of polymerization, the use of a solvent which does not dissolve the highly crystalline fraction of the polymer will usually result in extracting a part of the original sample with less than the maximum obtainable isotacticity. Moreover, under such conditions, the fractions of different molecular weight may not necessarily be samples of the same degree of stereoregularity, so that it is not always safe to use such fractions to study the dependence of various solution properties on molecular weight. Except in the work of Krigbaum, *et al.*,¹¹ the isotactic polystyrene samples investigated heretofore were either the toluene-soluble fractions^{6,8-10} or the fraction extracted with benzene.⁷ Although it was not always mentioned specifically, the amount of the polymer extracted from the original material by the use of boiling toluene seems not to have exceeded 50%, and the amount seems to have varied from case to case from 6%¹⁰ up.

We have found that isotactic polystyrene could be completely dissolved in monochlorobenzene by a specific heat treatment. The use of a process of separation of crystalline solid particles from a system consisting of isotactic polystyrene-monochlorobenzene-cyclohexanol has been shown to be effective in separating out highly isotactic material. The increase in stereoregularity of a sample has been observed to be accompanied by the increase in optical anisotropy, which can be estimated by light-scattering measurement with polarized incident light and by analyzing the data according to a theory developed previously by the author.¹² The increase in the optical anisotropy has been explained in terms of the larger interaction between the benzene rings of polystyrene in the isotactic configuration. Finally, we have found that

(4) V. N. Tsvetkov, S. Y. Magarik, N. N. Boitsova, and M. G. Okuneva, *J. Polymer Sci.*, **54**, 635 (1961).

(5) F. A. Bovey and G. V. D. Tiers, *Fortschr. Hochpolymer. Forsch.*, **3**, 139 (1963).

(6) G. Natta, F. Danusso, and G. Moraglio, *Makromol. Chem.*, **20**, 37 (1956).

(7) F. Danusso and G. Moraglio, *J. Polymer Sci.*, **24**, 161 (1957).

(8) F. Ang, *ibid.*, **25**, 126 (1957).

(9) F. Ang and H. Mark, *Monatsh. Chem.*, **88**, 427 (1957).

(10) L. Trossarelli, E. Campi, and G. Saini, *J. Polymer Sci.*, **35**, 205 (1959).

(11) W. R. Krigbaum, D. K. Carpenter, and S. Newman, *J. Phys. Chem.*, **62**, 1586 (1958).

(12) H. Utiyama and M. Kurata, *Bull. Inst. Chem. Res. Kyoto Univ.*, **42**, 128 (1964); H. Utiyama, to be published.

the experimental results of light-scattering and viscosity measurements on the fractionated samples can be put into the frame of the two-parameter theory if we assume that, as the degree of isotacticity increases the unperturbed dimension of polystyrene increases, and the interaction parameter B decreases. Therefore, the polymer dimension or the limiting viscosity number of isotactic polystyrene may be either larger or smaller than those of its atactic counterpart, depending upon its molecular weight and the degree of stereoregularity.

Experimental Procedures

Synthesis of Isotactic Polystyrene. A Ziegler-type catalyst used for polymerization of styrene was prepared by reacting titanium tetrachloride in heptane solution with triethylaluminum in a 1:4 molar ratio in the same solvent. The reaction mixture for the polymerization contained 2 moles of styrene, 0.4 mole of triethylaluminum (20% monomer), 0.16 mole of titanium tetrachloride (40% triethylaluminum), and 170 ml. of hexane. It was kept at 80° for 11.5 hr. and then at room temperature for 16 hr. The reaction was stopped by the addition of a large excess of methanol. The precipitate from the mixture was recovered and was washed repeatedly with methanol and dried under vacuum at room temperature. Sixty-seven per cent of the monomer was converted to polymer.

Choice of Solvent and Purification of the Sample and Solvent. The solubility of the crude polymer product was tested in benzene and toluene, but the polymer was found to be practically insoluble in either of the solvents. In the course of testing the solvent power of other solvents, monochlorobenzene was found to be satisfactory although a small quantity of polymer was undissolved and remained in the swollen state until the mixture was heated. In order to obtain a clear and stable solution, it was necessary first to keep it at room temperature for 48 hr. and then to heat it to the boiling temperature of monochlorobenzene at 130° for about 2 hr. The monochlorobenzene solution of isotactic polystyrene prepared in this way was very stable, and it did not bring about any detectable change in the limiting viscosity number at 20° even after the solution was kept at temperatures as low as 8°. Therefore we employed monochlorobenzene as solvent.

Reagent grade monochlorobenzene was washed five times with equal volumes of concentrated sulfuric acid. To remove the acid, it was then washed with water and with an aqueous solution of potassium bicarbonate several times each and dried over phosphorus pentoxide overnight. Finally, it was distilled

before use. The refractive index of the purified monochlorobenzene was n_D^{25} 1.52154 (lit. 1.52212). The crude polymer product was then dissolved in the purified monochlorobenzene, by the procedure mentioned above, to make a solution of about 2%. The solution was centrifuged to produce a force 20,000 times that of gravity for 1 hr. The supernatant was poured into an excess of methanol, and solid pieces of decomposed catalyst and a very small amount of remaining undissolved polymer gel were discarded. The polymer precipitate was washed carefully with methanol and then dried under vacuum at room temperature. The amount obtained was 138 g. The purified product was then annealed in boiling *n*-heptane for 12 hr. to increase the degree of crystallization. Finally, it was washed with methyl ethyl ketone to extract the soluble fraction which was presumably nonisotactic material.

Fractionation. The next step was the separation of highly stereoregular fraction and the comparison of its solution properties with those of conventional atactic polystyrene of the same molecular weight. Here, we briefly explain the principle of fractionation employed in this work. As is well known, it is frequently observed that, on standing, crystalline solid particles separate out from a metastable solution of crystalline polymer, such as polyvinyl chloride and polyvinyl alcohol. This process is a kind of cooperative phenomenon, and processes of both nucleation and growth of nuclei are probably regulated not only by the stereoregularity but also by the molecular size as well. For example, the nucleation rate will be largest for the molecules of moderate size and of highest stereoregularity. The larger molecules will need a longer time to orient into an ordered conformation, and the smaller molecules may not form a stable nucleus which will grow at an appreciable rate. Therefore, if we successively separate the liquid phase from the crystalline solid precipitate, which is brought about by the addition of an appropriate nonsolvent to a dilute solution and by standing long enough at an appropriate temperature, the fractions may have different molecular weight. However, the possibility of obtaining a fraction with large stereoregularity is substantial.

Among the nonsolvents tested, cyclohexanol was most suitable for the present purpose because a sufficiently large amount can be added to the monochlorobenzene solution of isotactic polystyrene without instantaneous formation of threadlike solid particles. On the contrary, when we used *n*-heptane, methanol, butanol, and diisopropyl ether as nonsolvents, the addition of even a very small amount of any one of them into the solution resulted in an appearance of threadlike crystalline particles. The solid threads could not be redis-

solved even after complete mixing of the solution and heating to a temperature as high as 70°.

Purified isotactic polystyrene (25 g.) was dissolved in 2.5 l. of monochlorobenzene by the procedure stated previously. An equal volume of cyclohexanol was added to the clear monochlorobenzene solution at room temperature, and the mixture was kept overnight at 8°. Although the mixture remained transparent in the beginning, the formation of a white, gellike precipitate proceeded within the next 24 hr. to about 3 days. The mixture was then centrifuged at 20,000 times the force of gravity for 30 min., and the precipitate was separated out by decantation from the supernatant, which did not become turbid on further standing. The supernatant portion was concentrated by vacuum distillation, and a proper amount of monochlorobenzene was added. The solution was centrifuged to eliminate dust and precipitated by addition to a large excess of methanol. If the amount of the precipitate was appropriate, say between 1.5 and 3 g., it was recovered as a fraction. When the amount was less than this, it was added to the subsequent supernatant portion; if greater, it was subjected to further fractionation under milder conditions. The precipitate portion, the white, gellike material, was easily dissolved in monochlorobenzene by heating the mixture to about 80° for 30 min. This solution was subjected to the same procedure: the addition of cyclohexanol, standing for up to 3 days, and the centrifugal separation of precipitates from the solution. This procedure was repeated until finally the amount of the precipitate became too small for further fractionation. In this way, the original isotactic polystyrene sample was divided into ten fractions and one extraneous fraction (assigned as F-0) which was no longer soluble in monochlorobenzene by our procedure. Recovery of 85.6% of the polymer was made. A schematic diagram of the fractionation process is shown in Figure 1. The thick lines in the figure represent the precipitated fractions, and the number in the brackets shows the weight of each fraction. It may be seen that the fractions from F-3 through F-9 were fractionated essentially by the extraction of nonprecipitating material.

Preparation of Solutions. Before the measurements of light scattering and viscosity were made, it was necessary to check whether the polymeric material was dissolved in a molecularly dispersed state. In the case of usual amorphous polymers, the presence of aggregated particles may be easily checked if one measures the molecular weight of the polymeric solute in two solvents which differ appreciably in their solvent power. On the other hand, crystalline polymers cannot, in general, be dissolved in poor solvents, and this

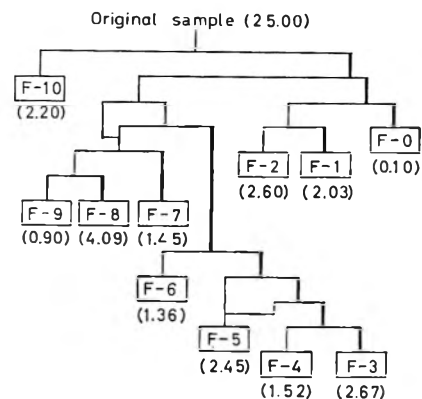


Figure 1. Schematic representation of the fractionation procedure.

type of test is not applicable. The dispersed state of crystalline polymer molecules in solution, however, depends largely on the temperature at which the polymer is dissolved and also on the subsequent heat treatment. The heat treatment at higher temperature will of course give more dispersed solutions, but the thermal and oxidative degradation of the polymer molecule will take place to a greater extent.¹¹ In order to find an optimal condition of heat treatment (temperature and duration) for dissolving the polymer in a molecularly dispersed state with minimal degradation, a simple test was made by measuring viscosity on solutions of the unfractionated sample pretreated with heat under various conditions. The test solutions were made as follows. The original solution of about 1 g./dl. concentration was divided into several assay tubes, and each of them was sealed after replacing the air by nitrogen. Unless otherwise stated, 10 mg. of 2,4,6-trimethylphenol was added to 100 ml. of solution as an antioxidant. Figure 2 represents the variation of the limiting viscosity number with the time of heating. It is seen that the decrease in the limiting viscosity number is greatest for the sample which was heated at 130° in the absence of the antioxidant and that all three samples give practically the same limiting viscosity number unless the heating time exceeds 2 hr. If only the melting of aggregated particles takes place, the limiting viscosity number will decrease rapidly at short heating times and then level off. The final equilibrium value will depend on temperature of heat treatment. The present results indicate that the state of molecular dispersion is not affected by heat treatment longer than 2 hr. at temperatures higher than 120°, at which the thermal and oxidative degradation of molecules becomes noticeable. Hence, we employ as the standard condition of heat treatment: 120°, 2 hr.

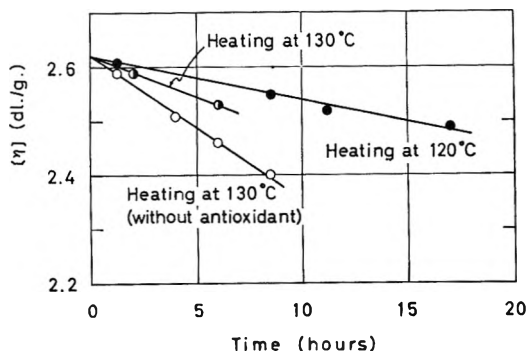


Figure 2. The variation of the limiting viscosity number of the unfractionated isotactic polystyrene sample in monochlorobenzene at 25° with time of heat treatment at 120° and at 130° in the presence and absence of antioxidant, 2,4,6-trimethylphenol.

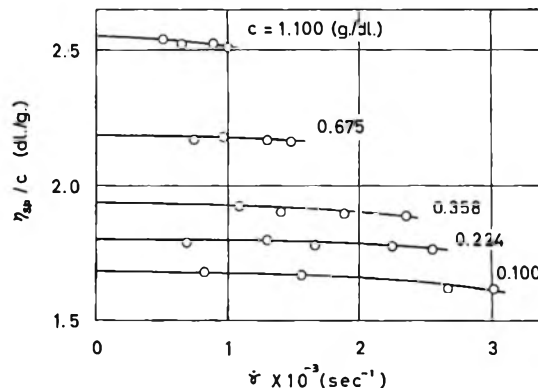


Figure 3. Dependence of reduced viscosity of a fractionated sample F-3 in monochlorobenzene at 25° on the rate of shear at different solute concentrations. Measurement was made by using a tilting-type Ostwald viscometer.

Viscosity Measurements. In order to study the shear rate dependence of the reduced viscosity of monochlorobenzene solution of isotactic polystyrene, viscosity measurements were made using a tilting-type Ostwald viscometer.¹³ Figure 3 represents an example of the experimental results on fractionated sample F-3. It may be seen that isotactic polystyrene solutions do not exhibit an exceptionally large dependence of viscosity on the rate of shear. Therefore further measurements of specific viscosity were made by using Ostwald-Fenske viscometers. The constants of the apparatus were as follows: the radius of capillary, 0.0296 cm.; the capillary length, 14.3 cm.; volume of the bulb, 1.98 ml.; average head, 2.13 cm.; the maximum rate of shear, $3.12 \times 10^2 \text{ sec.}^{-1}$. The correction for the kinetic energy was negligible.

Refractive Index Increment. Specific refractive index increments were determined by using a differential refractometer of the Debye type¹⁴ (Shimadzu Seisakusho Co., Kyoto, Japan). Temperature was maintained to within $\pm 0.05^\circ$. The distance of the vertical displacement of the image of the horizontal narrow slit on the focal plane of the telescope was determined photoelectrically. For the calibration of the refractometer, reference was made to the data reported by Kruis¹⁵ for KCl aqueous solutions at 25°.

Light Scattering. Light-scattering measurements were carried out in a modified Brice-type light-scattering photometer¹⁶ (Shimadzu Seisakusho Co., Kyoto, Japan) over the angular range from 30 to 140°. The wave length of incident light *in vacuo* was 436 m μ . Polaroid disks which serve as polarizer and analyzer could be set at the appropriate positions. The Brewster law was used in the final alignment of the analyzer. That is, a glass plate was set vertically at the cell position, and unpolarized parallel light was incident

at the polarizing angle on the glass plate. The intensity of the reflected ray will be maximum (minimum) when the plane of the analyzer is vertical (horizontal). Once the plane of the analyzer was set correctly, the alignment of the polarizer could be readily performed. The sensitivity of the photomultiplier tube (Type 1P21) to horizontally polarized light was 1.0% greater than its sensitivity to vertically polarized light. The degree of extinction of the crossed polaroids was determined by ratios of deflections in the photomultiplier at 0° with the aid of neutral filters. The results for the incident light of 436 m μ were $H_v/V_v = 0.00181$ and $V_h/H_h = 0.00181$. Therefore the measurements of small depolarization were possible. A cylindrical cell with specifically ground flats of the 0 and 180° faces was used, and the circular uniformity of the cell was demonstrated by the fact that the reduced intensity of fluorescence emitted by a dilute aqueous solution of fluorescein was constant within $\pm 2\%$ in the angular range studied in the present investigation. In order to calibrate the cell, the intensity of the light scattered from purified benzene was measured at 30° at a right angle to the incident beam. The Rayleigh ratio of benzene was taken to be 4.95×10^{-6} at 30° for the incident light of 436 m μ . The appropriate corrections for the Fresnel reflection of the incident light were applied to the experimental data. In order to obtain the calibration constant for the measurements with monochlorobenzene, the n^2 correction of Hermans¹⁷

(13) E. Wada, *J. Polymer Sci.*, **16**, 305 (1954).

(14) P. Debye, *J. Appl. Phys.*, **17**, 392 (1946).

(15) A. Kruis, *Z. physik. Chem.*, **34B**, 13 (1936).

(16) B. A. Brice, M. Halwer, and R. Speiser, *J. Opt. Soc. Am.*, **40**, 768 (1950).

(17) J. J. Hermans and S. Levinson, *ibid.*, **41**, 406 (1951).

was applied to correct for the difference in refractive index. The temperature of the test solution was kept at $25.3 \pm 0.2^\circ$ by circulating water through the thermostating mantle. The test solution in the cell was stirred with a magnetic stirrer. Five test solutions of different concentrations were made from a 1% stock solution which was prepared and heat treated in a sealed tube as mentioned previously. For the optical purification, each test solution was filtered first through a No. 5 sintered glass filter and then through two sheets of Grade M Cellafilter directly into the light-scattering cell. The concentration of each test solution was determined by measuring dry weight after evaporation of the solvent when the light-scattering measurements were completed.

Degree of Crystallinity. The degrees of crystallization of the fractionated samples in the solid state were determined in the following way.¹⁸ A monochlorobenzene solution of each fractionated sample at about 2% concentration was made in a sealed tube by the same procedure stated previously. Each solution was poured into a square-shaped mold with a bottom consisting of a horizontal flat, glass surface, and the solvent was evaporated by keeping the solution at 60° for 4 hr. Thus, transparent films of about 50μ in thickness were made. These were soaked in methanol for 1 week and dried *in vacuo* in order to remove the remaining solvent. Each film was then cut into eight equal pieces. Pairs of them were annealed at 160° ¹⁹ for 0, 1, 2, and 5 hr. in Wood's metal.

The degree of crystallization of films prepared in this way was determined by the method of infrared absorption. The per cent of absorption (D) at the crystalline-sensitive band (wave number: 984 cm.^{-1}) and at the CH-bending band (wave number: 1945 cm.^{-1}) were measured by a recording infrared spectrophotometer, Type IR-S (Nihonbunkokogyo Co., Hachioji, Japan). The ratio D_{980}/D_{1945} was used for evaluation of the degree of crystallization according to the equation²⁰

$$X_{\text{IR}} = 0.5(D_{980}/D_{1945}) - 0.170 \quad (1)$$

where X_{IR} , defined by eq. 1, is known to be in good agreement with the degree of crystallization determined by the X-ray diffraction method.

Experimental Results

Solubilities of the Fractionated Samples. In order to examine the solubilities of the fractionated samples qualitatively, each sample was put into a sealed tube, a proper amount of monochlorobenzene was added to it to make a 1% solution, and each was kept overnight at room temperature. There were marked and sig-

nificant differences in the state of dissolution of the samples. The fractions F-10, F-9, and F-8 were readily soluble in monochlorobenzene even at room temperature without the heat treatment. However, the fractions F-7, F-6, and F-5 were partially insoluble although they were brought to an appreciably swollen state. The fractions F-4, F-3, F-2, and F-1 were much less soluble in monochlorobenzene at room temperature. Notably, fraction F-1 did not swell. Moreover, the solutions of the samples from F-10 to F-2 were very stable after they had been heated at 120° for 2 hr., while the solution of F-1 was unstable and the solid-liquid separation occurred readily below 10° . Hence, this sample was again divided into two portions by keeping the solution at 10° , and only the soluble fraction which was designated as F-1' was used for further experiments.

Light-Scattering Behavior of Fractionated Samples. The specific refractive index increment of isotactic polystyrene fractions (F-2, F-4, F-8, and F-10) in monochlorobenzene at 25.3° was 0.085 ml./g. , which is in good agreement with that of atactic polystyrene.²¹

Light-scattering measurements on fractionated samples were made first without the use of polarizer and analyzer. The reduced scattered intensity under this experimental condition of polarization of incident and scattered light is written as $R_{V_u}(\theta)$. As typical examples of the results of light-scattering measurements, the reciprocal scattered intensity functions, $Kc(1 + \cos^2 \theta)/2R_{V_u}(\theta)$, where K is given by $4\pi^2 n_0^2 (dn/dc)^2/\lambda_0^4 N_A$ of F-4, F-5, and F-8 are plotted as functions of concentration and of $\sin^2(\theta/2)$ in Figures 4, 5, and 6, respectively. The open circles represent the angular dependence of the reciprocal intensity function at constant concentration, and the filled circles represent the concentration dependence of the extrapolated values of the reciprocal intensity function to zero angle of observation. The same plots for the samples F-1', F-6, F-7, F-9, and F-10 are all similar to that of F-8 (Figure 6) and similar to patterns usually obtained in amorphous polystyrene solutions. From the data, the weight-average molecular weight, second virial coefficient, and z -average mean-square radius of gyration were estimated by the usual method, and the values obtained are listed in Table I.

(18) The degrees of crystallization of the three fractions F-1' (the difference between F-1' and F-1, will be stated later), F-5, and F-6 could not be determined because of the lack of sufficient amounts of these samples.

(19) This is the optimum temperature for the crystallization of isotactic polystyrene. See A. S. Kenyon, R. C. Growth, and A. L. Wurster, *J. Polymer Sci.*, **40**, 159 (1959).

(20) F. Sakaguchi and W. Tsuji, private communication.

(21) H. Utiyama, M. Kurata, and M. Tamura, to be published.

Table I: Light-Scattering and Viscosity Results for Fractionated Samples of Isotactic Polystyrene in Monochlorobenzene at 25.3°

Sample	$[\eta]$, dl./g.	M_w $\times 10^{-6}$	$M_{w,app}$ $\times 10^{-6}$	A_2 $\times 10^4$	$A_{2,app}$ $\times 10^4$	$\langle S^2 \rangle_z$ $\times 10^{10}$	$\langle S^2 \rangle_{z,app}$ $\times 10^{10}$	δ $\times 10^3$
F-1'	1.77	7.47	0.250
F-2	1.25	4.03	4.63	3.64	4.70	0.158	0.124	1.78
F-3	1.62	5.75	5.99	3.83	4.00	0.172	0.090	3.13
F-4	1.15	3.41	4.13	0.76	0.25	0.120	Negative	53.30
F-5	0.78	2.18	2.29	3.04	2.80	0.082	0.021	8.34
F-6	1.40	5.81	...	4.52	...	0.266
F-7	1.14	3.85	...	3.92	...	0.141
F-8	1.17	5.00	...	4.28	...	0.155
F-9	0.87	2.93	...	3.64	...	0.103
F-10	1.23	4.31	...	4.13	...	0.168

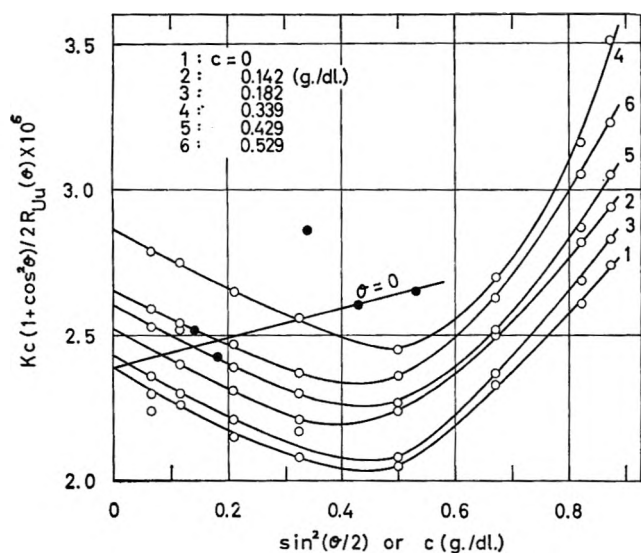


Figure 4. Light-scattering results of the fractionated sample F-4 in monochlorobenzene at 25.3°. The open circles represent the angular dependence of the reciprocal intensity function at finite concentrations, and the filled circles represent the concentration dependence of the extrapolated values of the reciprocal intensity function to the zero angle of observation.

On the other hand, the results of samples F-4 and F-5 (Figures 4 and 5) are apparently quite anomalous. The angular dependencies of reciprocal scattered intensity curves for different solute concentrations are all concave upward, and the initial tangent of the plot at infinite dilution, which is proportional to the z -average mean-square radius of gyration in the conventional analysis, appears to be too small. Samples F-2 and F-3 also showed similar behavior. In the case of sample F-4, the initial tangent of the same plot becomes negative. These anomalies in the reciprocal angular envelopes distinctly imply the presence of a sufficiently large optical anisotropy of the optical segment.²² Thus, none of the above three quantities

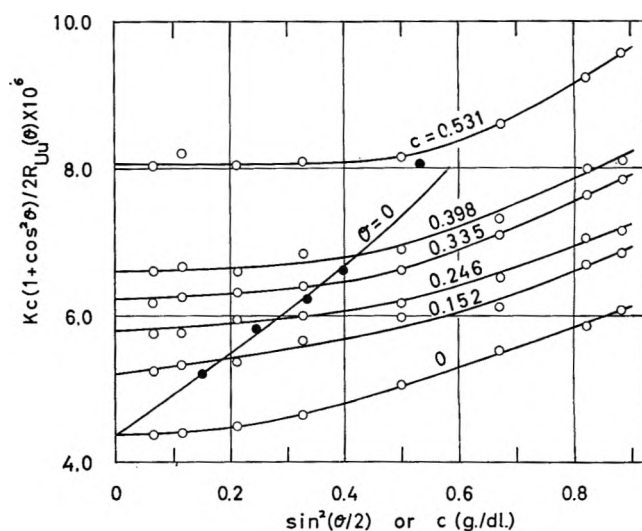


Figure 5. Light-scattering results of the fractionated sample F-5 in monochlorobenzene at 25.3°. The open and closed circles have the same meaning as in Figure 4.

derivable from light-scattering measurements can be estimated correctly without making a correction for the effect of segmental anisotropy. A correction for this effect will be discussed in the subsequent section. Table I also lists the values of M_w , A_2 , and $\langle S^2 \rangle_z$ for these fractions estimated before and after making the correction for the anisotropy effect.

Analysis of Anomalous Light-Scattering Data. According to a theory recently developed by the author,¹² the reciprocal scattered intensity function $Z(\theta)$ ($\equiv Kc \times (1 + \cos^2 \theta)/2R_{UU}(\theta)$) for flexible-chain polymers consisting of optically anisotropic segments is given by

$$1/Z(\theta) = M(1 - 2A_2Mc) -$$

$$MK(1 - 4A_2Mc) \sin^2(\theta/2) +$$

$$M\delta(13 + \cos^2 \theta)/(1 + \cos^2 \theta) \quad (2)$$

(22) H. Utiyama, Doctoral Thesis, Kyoto University, 1963.

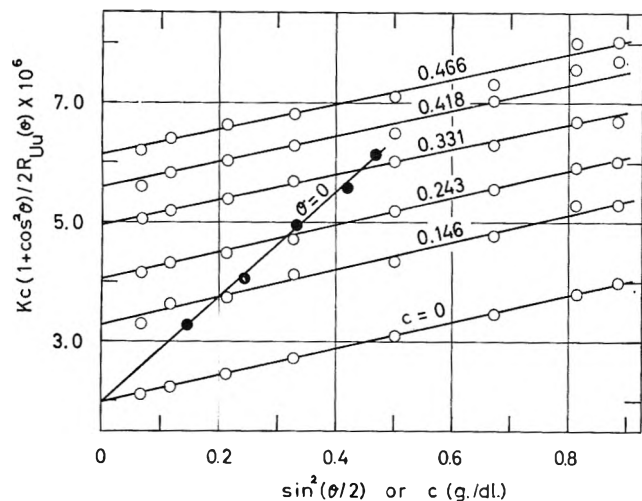


Figure 6. Light scattering results of the fractionated sample F-8 in monochlorobenzene at 25.3°. The open circles and closed circles have the same meaning as in Figure 4.

where M is the molecular weight of polymeric solute, A_2 the second virial coefficient, c the solute concentration expressed in weight per unit volume, $K = (4/3) \times (2\pi/\lambda)^2 \langle S^2 \rangle$, and λ is the wave length of incident light in solution. δ is a parameter representing the anisotropy of the optical segment and is expressed in terms of three principal polarizabilities α_1 , α_2 , and α_3 ; the number of segments in a chain is expressed as

$$\delta = \frac{\{(\alpha_1 - \alpha_2)^2 + (\alpha_2 - \alpha_3)^2 + (\alpha_3 - \alpha_1)^2\}}{10n(\alpha_1 + \alpha_2 + \alpha_3)^2} \quad (3)$$

Equation 2 readily leads to the relation

$$\frac{1}{Z(\theta)} - \frac{1}{Z(\pi - \theta)} = MK(1 - 4A_2Mc)\{1 - \sin^2(\theta/2)\} \quad (4)$$

Therefore, we can estimate the quantity $MK(1 - 4A_2Mc)$ from the slope of the plot $1/Z(\theta) - 1/Z(\pi - \theta)$ vs. $1 - 2\sin^2(\theta/2)$. Once the quantity $MK(1 - 4A_2Mc)$ is determined by use of eq. 4, then a plot of $1/Z(\theta) + MK(1 - 4A_2Mc)\sin^2(\theta/2)$ against $(13 + \cos^2\theta)/(1 + \cos^2\theta)$ enables one to estimate both $M(1 - 2A_2Mc)$ and M from the intercept and the slope of the plot, respectively. The latter plot will be a flat straight line for the solution of a polymer consisting of isotropic segments since $\delta \equiv 0$ for such a polymer. The analysis of experimental data of $Z(\theta)$ at various solute concentrations by the method illustrated above enables us to make a separate estimation of the quantities M , A_2 , δ , and $\langle S^2 \rangle$.

By way of illustration, light-scattering data for F-5 were analyzed following the above procedure and plotted in Figures 7 and 8. It appears that the anomalous light-scattering data can be explained quan-

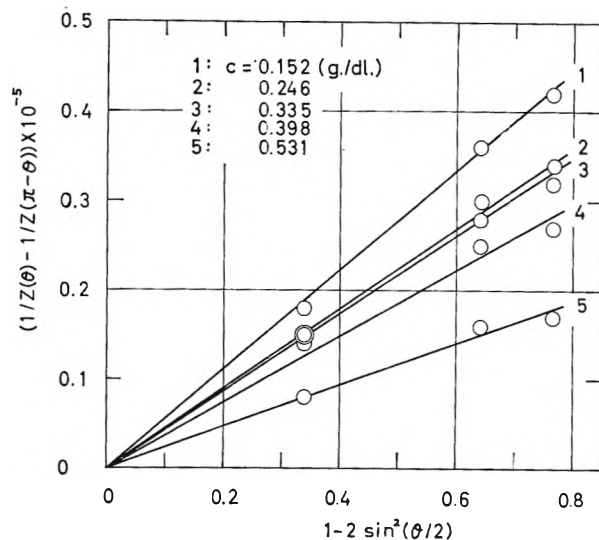


Figure 7. Plots of $1/Z(\theta) - 1/Z(\pi - \theta)$ at various concentrations as a function of $1 - 2\sin^2(\theta/2)$ from the data shown in Figure 6 for the fraction F-8.

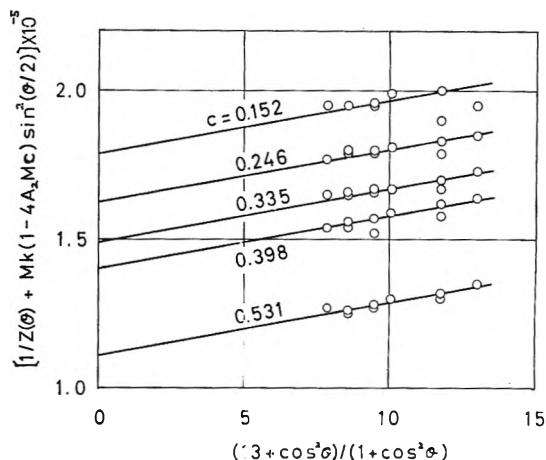


Figure 8. Plots of $1/Z(\theta) + MK(1 - 4A_2Mc)\sin^2(\theta/2)$ at various solute concentrations as a function of $(13 + \cos^2\theta)/(1 + \cos^2\theta)$ for the fractionated sample F-8. The original data are taken from Figure 6.

titatively in the present theory. The experimental data of F-2, F-3, F-4, and F-5 were re-examined and corrected for the effect of anisotropy. The light-scattering data of other samples are normal and analyzed by the usual method. The results are listed in Table I. The optical anisotropies of the above four samples are, in fact, all larger than that of atactic polystyrene (see the next section) as shown in the last column of Table I. Furthermore, it should be mentioned that the optical anisotropy of F-4 is extraordinarily large, while the second virial coefficient is very small compared with those of other samples of comparable molecular weights. The molecular weight

of F-4 is rather small in spite of the fact that the fraction was obtained in the final stage of extraction.

Results of Light-Scattering Measurements with Polarized Incident Light. When a polymer molecule consists of optically anisotropic segments, the theoretical expressions of the reduced intensity of light scattered from the solution for the V_v and H_v components (vertical and horizontal components of the scattered light when incident light is vertically polarized) and for the V_h and H_h components are given by¹²

$$R_{V_v}(\theta) = KcMP(\theta) - 2A_2MQ(\theta)c + 4\delta \quad (5)$$

$$R_{V_h}(\theta) = R_{H_v}(\theta) = 3\delta KcM \quad (6)$$

$$R_{H_h}(\theta) = KcM[P(\theta) - 2A_2MQ(\theta)c + \delta] \cos^2 \theta + 3\delta \quad (7)$$

where $P(\theta)$ is the well-known particle scattering factor and $Q(\theta)$ is the intermolecular correlation function.²³

These equations show (1) that the H_h component at $\theta = \pi/2$ coincides with the V_h ($=H_v$) component, (2) that the V_h component is independent of the angle of observation and proportional to the optical anisotropy, and (3) that the anisotropy effect in the V_v component can be eliminated by using another component at $\theta = \pi/2$. In order to compare these formal properties with experimental results and to estimate δ directly, four components of the scattered light were measured separately.

First, the accuracy of the measurement was tested by using a pure liquid such as benzene or carbon tetrachloride, in which the V_v , H_v , and V_h components of the scattered light are constant irrespective of the angle, and the H_h component, which agrees with the H_v and V_h components at $\theta = \pi/2$, is symmetrical about $\theta = \pi/2$. Typical experimental results for four components of the reduced scattered intensity of benzene are shown in Figure 9. The reduced scattered intensity of the U_v component and the depolarization ratio ρ_u are estimated from the data and listed in Table II. It is shown that the above requirements are fulfilled with sufficient accuracy and that the agreement of ρ_u values estimated in the present experiment with those reported in the literature are satisfactory.

The experimental results of similar measurements on an isotactic polystyrene sample (a sample recovered from the fraction F-4 after the first light-scattering and viscosity measurements were completed and designated as F-4') are shown in Figure 10. The H_v and V_h components of the reduced scattered intensity agree well with each other, but they show a tendency to increase slightly with the angle of observation. An explanation of this discrepancy has not been obtained

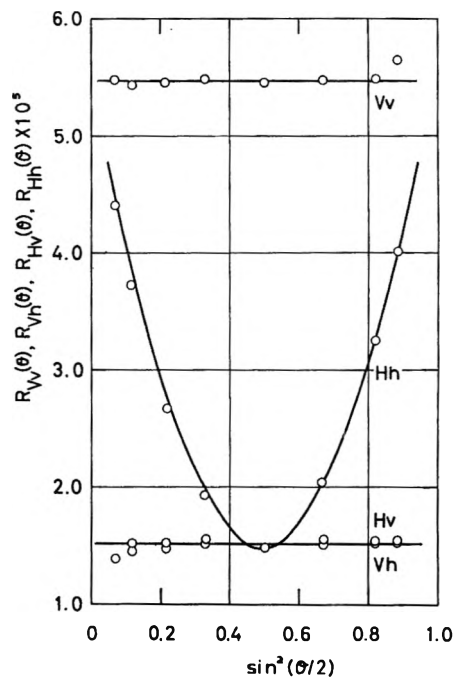


Figure 9. The angular variation of four components of the reduced scattered intensity of benzene at 30.0°. The wavelength of incident light *in vacuo*, λ_0 , was 436 m μ . V_v and H_v represent the vertical and horizontal components of the scattered light when the incident light is vertically polarized. V_h and H_h have a corresponding significance for horizontally polarized light.

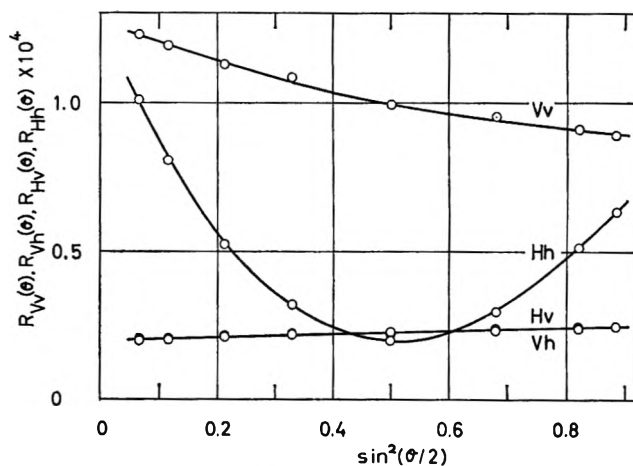


Figure 10. Angular variations of four components of the reduced scattered intensity of F-4' in monochlorobenzene at 25.3°; $c = 0.107$ g./dl.

as yet. However, the value of the H_v or V_h component extrapolated to the zero angle of observation appears to be in good agreement with that of the H_h component at $\theta = \pi/2$ and was therefore used for estimating the

(23) B. H. Zimm, *J. Chem. Phys.*, **16**, 1093 (1948).

Table II: Experimental Results of Depolarization Ratio and Reduced Scattered Intensity for Pure Liquids

Solvent	Temp., °C.	Refractive index (436 mμ)	δ, g./ml.	$R_{Uu} \times 10^6$		ρ_u	
				Exptl.	Lit.	Exptl.	Lit.
Benzene	25	1.5225	0.8735	48.5	48.0 ^a	0.43	0.43 ^a
Carbon tetrachloride	30	1.4709	1.575	16.2	15.8 ^a	0.05	0.05 ^a
Toluene	35	1.5107	0.8509	58.1	56.3 ^{a,b}	0.52	0.49 ^{a,b}
Monochlorobenzene	25.3	1.5334	1.102	76.3	...	0.64	...
	40.8	1.5250	1.084	78.2	...	0.61	0.60
	61.1	1.5142	1.062	79.4	...	0.58	...
	82.2	1.5031	1.038	83.2	...	0.55	...
n-Butyl chloride	36	1.4019	0.8689	17.4	...	0.23	...
Cyclohexane	35	1.4233	0.7648	18.2	...	0.06	...
Methyl ethyl ketone	40	1.3769	0.7839	15.4	...	0.23	...

^a J. P. Kratozil, G. J. Dezelic, M. Kerker, and E. Matijevic, *J. Polymer Sci.*, 57, 59 (1962). ^b Values at 25°.

optical anisotropy parameter δ . Then the V_v component was corrected for the anisotropy effect with the use of this δ value. The reciprocal scattered intensity function of the corrected V_v component is plotted in Figure 11 as a function of $\sin^2(\theta/2)$ together with a conventional plot of the function $Kc(1 + \cos^2 \theta)/2R_{Uu}(\theta)$ vs. $\sin^2(\theta/2)$. The latter gives an anomalous curve similar to that shown in Figure 4, while the plotted points of the former function fall strictly on a straight line, as the theory predicts, with a positive slope which is proportional to the mean-square radius of gyration $\langle S^2 \rangle$.

The temperature dependence of the optical anisotropy parameter δ was estimated in the same way from the light-scattering measurement on F-4' over the temperature range from 25.3 to 82.2°. The result is shown in Figure 12, which also includes, for comparison, a result on a polystyrene sample obtained by the thermal bulk polymerization and fractionating procedure ($M_w = 51.2 \times 10^4$). The optical anisotropy parameter was multiplied by the molecular weight in order to compensate for the difference in molecular weight.²⁴ It can be seen in this figure that there is a remarkable and significant difference in the values of the optical anisotropy parameter $M\delta$ of isotactic and atactic polystyrene. The value of $M\delta$ of isotactic polystyrene is almost 40 times as large as that of the atactic sample and markedly decreases with temperature, while that of atactic polystyrene slightly increases. A reason for this difference between the two will be discussed in a later section.

Crystallinity of Fractionated Samples. The degrees of crystallization X_{IR} of fractionated samples, estimated from infrared spectroscopic measurement, are shown in Figure 13 as a function of the time of annealing at 160°. Before proceeding further, however, several

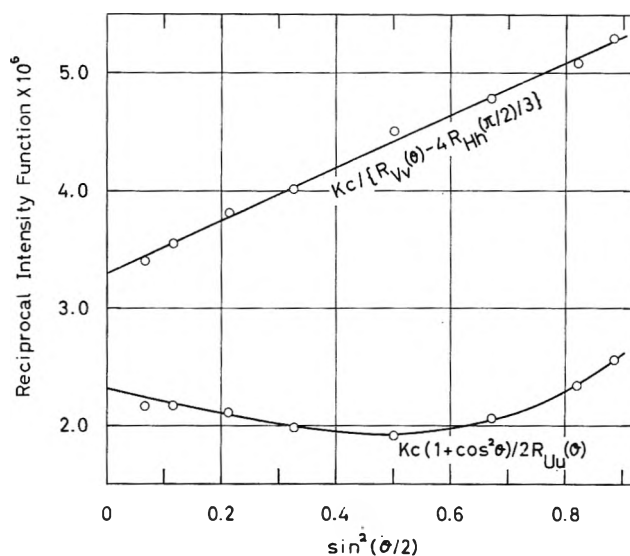


Figure 11. Reciprocal reduced intensity plots for F-4' in monochlorobenzene at 25.3°; $c = 0.107$ g./dl. The lower plotted points are the conventional reciprocal light-scattering intensity function and the upper points show the function corrected for the effect of optical anisotropy.

remarks must be made. For the quantitative discussion of the crystalline state of a polymer film, such procedures as melting and quenching of the film may be necessary before the process of annealing can be carried out, and the annealing itself should be done at several different temperatures. Such experiments were impossible because of the lack of material. Our aim here, therefore, is not to investigate the solid properties by themselves but to look for some qualitative cor-

(24) H. Benoit and G. Weill, "Proceedings of the International Symposium on Macromolecular Chemistry," Prague, Czechoslovakia, Sept. 1957, p. 35.

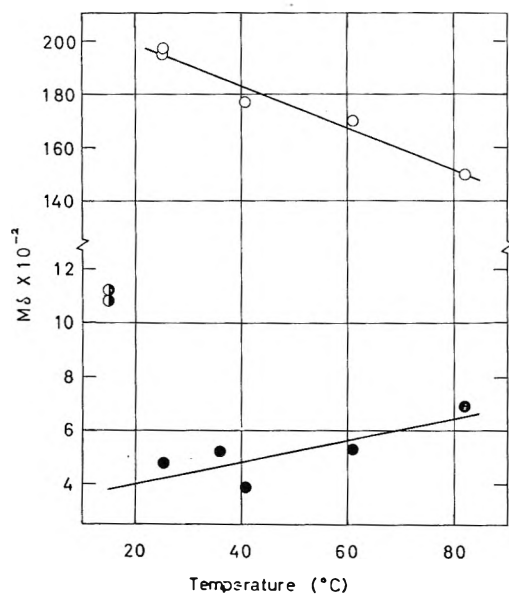


Figure 12. Optical anisotropy vs. temperature relationships for the isotactic polystyrene fraction F-4' (open circles) and an atactic polystyrene sample ($M_w = 51.2 \times 10^4$, closed circles) in monochlorobenzene. The half-filled circles are for the atactic polystyrene in benzene.

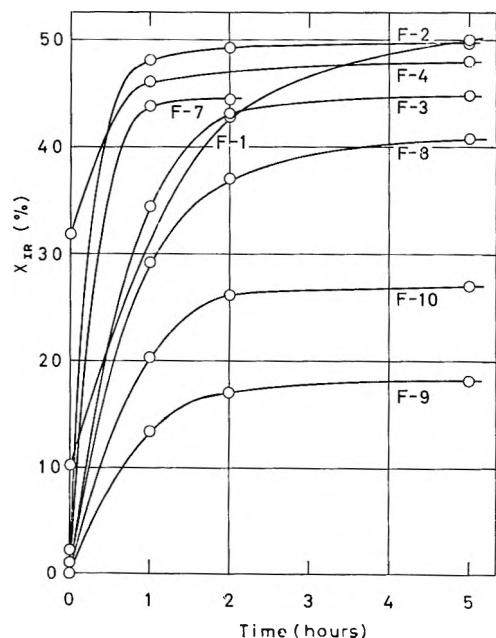


Figure 13. Crystallinity of films of isotactic polystyrene fractions estimated on the basis of infrared absorption measurements as a function of duration of annealing at 160° .

relations between the properties of isotactic polystyrene in the solid and dissolved states.

The most interesting point in this figure is that the fraction F-4 exhibits an extraordinarily high degree of crystallinity at $t = 0$. In other words, fraction F-4

can crystallize during the film formation, during which the temperature was not greater than 60° . Fraction F-1 also shows a high X_{IR} value at $t = 0$, but the initial rate of crystallization is rather small, and the value of X_{IR} after 2-hr. annealing is still lower than the equilibrium value. The reason for this may perhaps be the high molecular weight of F-1, which can also be the origin of the separation of crystalline solid particles from the solution. By the same token, because of the small molecular weight, the solution of F-4 is stable at room temperature, and the measurement of solution properties was possible.

Now, the large tendency of sample F-4 to crystallize at a low temperature is probably due to its high degree of stereoregularity. If we consider the previous result, that this sample showed exceptionally large optical anisotropy, the present results on measurements of crystallinity may confirm our view that the optical anisotropy is an intrinsic property which is closely connected with the isotactic configuration of the asymmetric carbon atoms along the main chain of the isotactic polymer.

The equilibrium values of X_{IR} of the fractionated samples, which are listed in Table III, are not of the order of the fraction number as was expected. However, it is interesting to note that samples F-9 and F-10, which are readily soluble in monochlorobenzene at room temperature, have a lower degree of crystallinity than the other samples.

Table III: Derived Results of Unperturbed Dimension K , Optical Anisotropy $M\delta$, and Crystallinity X_{IR} for Fractionated Samples of Isotactic Polystyrene

Sample	$K \times 10^3$	$A_2 M_w / [\eta]$	$M\delta \times 10^{-2}$	$X_{IR}, \%$ ($t = 5$)	$X_{IR}, \%$ ($t = 0$)
F-1'	0.68	...	6.4 ^a	(49.7) ^b	(10.2) ^b
F-2	0.96	117	7.2	49.7	2.5
F-3	0.93	136	18.0	44.9	0
F-4	1.04	22.5	182.0	47.9	31.9
F-5	0.93	85	18.2
F-6	0.63	188	5.0 ^a
F-7	0.85	132	3.3 ^a	45.0	1.0
F-8	0.67	183	4.3 ^a	40.7	0
F-9	0.76	123	2.5 ^a	18.6	0
F-10	0.82	145	3.7 ^a	26.9	0

^a Estimated values based on the result for atactic polystyrene.

^b Experimental data on F-1.

Discussion

Unperturbed Dimension A of Isotactic Polystyrene. Our problem here is to estimate the effect of stereoregularity on the unperturbed dimension A and the

interaction parameter B of polystyrene in dilute solution. A and B are defined by

$$A = a/M_0^{1/2} \quad B = \beta/M_0^2 \quad (8)$$

where a is the effective bond length, M_0 the molecular weight of a segment, and β the binary cluster integral for a pair of segments. The short-range parameter A is determined directly and unambiguously only by the measurement of the molecular weight and the dimension of the polymer in a θ -solvent in which β vanishes. However, this cannot be done for an isotactic polymer because of the absence of an appropriate θ -solvent. At the moment, the most promising method of estimating the unperturbed dimension from a system with positive β may be by means of the relation between the limiting viscosity number and molecular weight of polymer.

The excluded volume effect on the polymer dimension is a problem yet to be solved, but several useful approximate theories have been developed by Ptitsyn,²⁵ by Kurata, Stockmayer, and Roig,²⁶ and by Fixman.²⁷ Of the three theories, Ptitsyn's equation appears to best agree with experimental results, but the functional form is not convenient for estimating the parameters A and B from intrinsic viscosity results.^{21,22} Kurata and Stockmayer²⁸ analyzed the dependence of intrinsic viscosity on molecular weight for a large number of pairs of solvent and polymer, showing that their relation is quite useful in obtaining the two parameters separately from viscosity and molecular weight measurements. Later, Stockmayer and Fixman showed that Fixman's equation, when applied to viscosity, is different in functional form from that of Kurata, *et al.*, but the two equations are essentially equivalent.²⁹

Because of the simpler functional form, we employ the latter, which reads

$$[\eta]/M_w^{1/2} = qK + 0.5\Phi_0 B M_w^{-1/2} \quad (9)$$

where Φ_0 is the Flory constant under the θ -condition, $K = \Phi_0 A^3$, and q is the correction factor for heterogeneity in molecular weight. From the intercept of the plot of $[\eta]/M_w^{1/2}$ vs. $M_w^{1/2}$, parameter A may be estimated by assuming Φ_0 as constant $\Phi_0 = 2.5 \times 10^{23}$.³⁰ The results obtained are shown in Figure 14. The solid line in the figure expresses the correlation line for atactic polystyrene corresponding to $q = 0.93$.^{21,31} Since the points are widely scattered, they cannot be extrapolated properly. The fractionated samples, however, should not be taken as samples of the same nature differing only in the molecular weight. Since the samples show different optical anisotropy, different solubilities, and different degrees of crystallinity in the solid state, they probably represent different

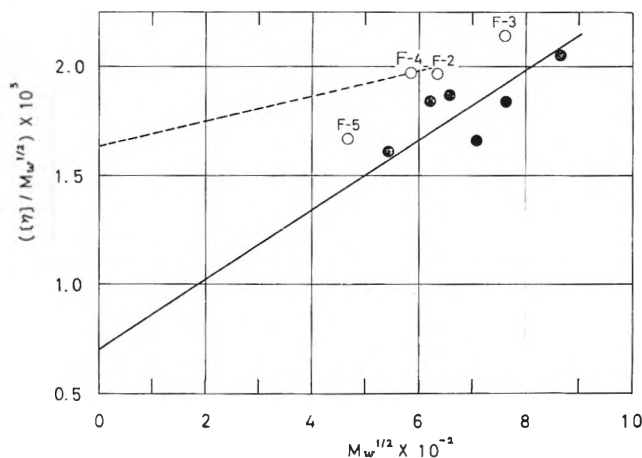


Figure 14. $[\eta]/M_w^{1/2}$ vs. $M_w^{1/2}$ for isotactic polystyrene fractions in monochlorobenzene at 25.3°. The straight line is for atactic polystyrene with $q = 0.93$, and the dashed line is drawn through the experimental point of the sample F-4 with $\Phi_0 B = 0.11 \times 10^{-5}$. The closed circles represent the fractions with negligible optical anisotropy, and the open circles are for the samples of large optical anisotropy.

molecular species. Hence, it may not be appropriate to draw a line best fitting the experimental points in order to estimate the K value. It is interesting to note, however, that the plotted points for the samples of small optical anisotropy fall close to the correlation line (closed circles), but those of large anisotropy are located well above the line (open circles).

For the estimation of the unperturbed dimension of each fraction, we need an alternative means which provides information about the expansion factor α_η ($\equiv [\eta]/[\eta]_0$), but no possible method is left except the use of the relation $A_2 M_w / [\eta]$ vs. $\alpha_\eta^2 - 1$.³² Experi-

(25) O. B. Ptitsyn, *Vysokomolekul. Soedin.*, **1**, 715 (1959).

(26) M. Kurata, W. H. Stockmayer, and A. Roig, *J. Chem. Phys.*, **33**, 151 (1960).

(27) M. Fixman, *ibid.*, **36**, 3123 (1962).

(28) M. Kurata and W. H. Stockmayer, *Fortschr. Hochpolymer. Forsch.*, **3**, 196 (1963).

(29) (a) W. H. Stockmayer and M. Fixman, *J. Polymer Sci.*, **C1**, 137 (1963); (b) Various theoretical relations between the expansion factor and molecular weight were examined recently by G. C. Berry and T. G. Fox, *J. Am. Chem. Soc.*, **86**, 3540 (1964).

(30) Burchard had made use of the same relation before it was worked out in an experimental study of solvent effects on the unperturbed dimension. It should be mentioned that the second term in the right-hand side of eq. 9 is simply the first term of series expansion of $[\eta]$ about $[\eta]_0$. See: W. Burchard, *Makromol. Chem.*, **50**, 20 (1961).

(31) The polydispersity of the isotactic polystyrene fraction is not known, but it must be large considering the broad molecular weight distribution of the crude sample. (See, for example, K. Kawahara and R. Okada, *J. Polymer Sci.*, **56**, S7 (1962).) We assume for the present samples $M_w/M_n = 3$, but the assignment is not important for the subsequent discussion.

mental values of $A_2M_w/[\eta]$ of atactic polystyrene samples²¹ are plotted in Figure 15 against $[\eta]/[\eta]_0 - 1$ (filled circles), together with those of isotactic polystyrene (half-filled circles). The numerical values of $[\eta]/[\eta]_0 - 1$ for the latter were estimated by assuming that K is the same as for atactic polystyrene. The solid line was drawn so as to best fit the experimental points of atactic polystyrene. The plotted points of the fractions F-2 through F-5 (shown by the arrows in the figure) deviate again appreciably from the correlation line, while the other experimental points appear to be in rough agreement. This result may suggest that the second virial coefficient of isotactic polystyrene is smaller and/or the unperturbed dimension is larger than that of the conventional atactic polymer. The results shown in Figures 14 and 15 indicate that, as long as we assume the same unperturbed dimension for both isotactic and atactic polymers, it may be concluded that the isotactic polystyrene is characterized by the larger intramolecular interaction (the larger value of B or the steeper correlation line in Figure 14) and abnormally smaller intermolecular interaction (smaller value of A_2) than the atactic counterparts. However, it may be unrealistic to assume different interaction parameters for intra- and intermolecular interaction since there is no theoretical or experimental evidence indicating that the crystalline polymer solutions do not obey the two-parameter theory. Alternatively, we may tentatively assume the same B values for both polymers. Each experimental point in Figure 14 is extrapolated with the same slope as that of atactic polystyrene to obtain a qK value from the intercept on the ordinate axis. Table III lists the K values obtained by this procedure making use of the assumed q value. The experimental points of $A_2M_w/[\eta]$ replotted using these K values fall near the universal correlation line as shown by open circles in Figure 15. This agreement seems too good to be taken as fortuitous. It may be said that the samples of larger optical anisotropy are characterized by larger unperturbed dimensions. Furthermore, in view of the smaller second virial coefficient, B values of isotactic polymer should be smaller, and the K value must therefore be larger to some extent than the figures listed in Table III. In fact, the plotted point of F-4 Figure 15 falls on the universal correlation line if we employ 0.11×10^{-5} for $\Phi_0 B$, which is about one-third that of atactic polystyrene, and estimate the K value as 1.76×10^{-3} (the dashed line in Figure 14).

Molecular Conformation of Isotactic Polystyrene in Dilute Solution. In summarizing the experimental results obtained in the present investigation and some

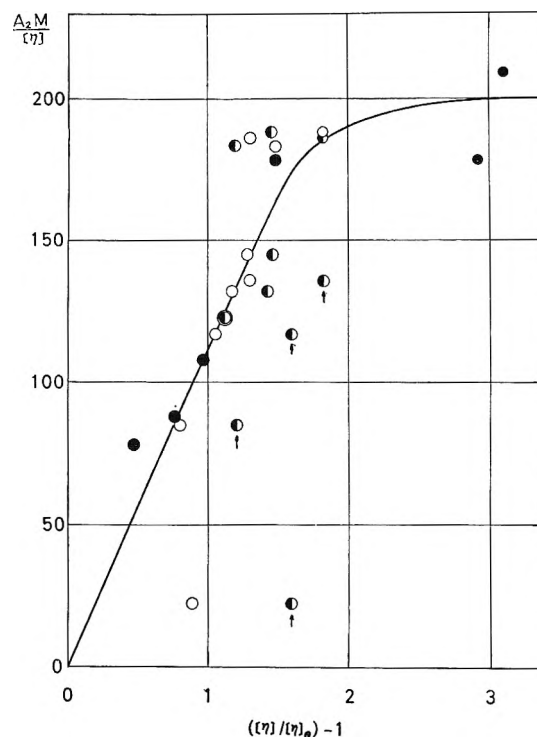


Figure 15. $A_2M_w/[\eta]$ as a function of $[\eta]/[\eta]_0 - 1$ for isotactic (half-filled circles and open circles) and atactic polystyrene fractions (filled circles). See text.

conclusions from the previous discussion, it has been shown (1) that we can separate by the present method of fractionation a fraction which has a large optical anisotropy, high crystallizability, and rapid rate of crystallization at low temperature, (2) that the solubility and crystallizability do not always parallel each other, (3) that consideration of the data suggests that, with increasing optical anisotropy, the unperturbed dimension of isotactic polystyrene increases and the interaction parameter decreases, and (4) that the optical anisotropy of isotactic polystyrene decreases rapidly with increase of temperature, while atactic polystyrene exhibits only a negligibly small optical anisotropy which slightly increases with temperature.

Here we may briefly discuss the relation between optical anisotropy and the stereoregularity of polystyrene. According to the calculation by Stein and Tobolsky,³³ the optical anisotropy of styrene monomer depends significantly upon the mode of the orientation of the benzene ring. The difference between the principal polarizabilities along and perpendicular to the contour of the C-C bond is (1) -4.9×10^{-22}

(32) W. H. Stockmayer, *Makromol. Chem.*, **35**, 54 (1960).

(33) R. S. Stein and A. V. Tobolsky, *J. Polymer Sci.*, **11**, 285 (1953).

cm.³ if all single bonds within the monomer are freely rotating, (2) -6.2×10^{-22} cm.³ if the benzene ring may rotate freely about the bond which connects the benzene ring to the chain, and (3) -62.8×10^{-22} cm.³ if the benzene ring is oriented within the plane perpendicular to the axis of the chain. In addition, the similar value corresponding to the optical segment³⁴ may be generally greater than that of a monomer unit owing to the restricted internal bond rotation. When the asymmetric carbon atoms in a polystyrene chain assume the isotactic configuration, the rotating motion of each benzene ring around the bond which connects the benzene ring to the chain may be more restricted by the larger steric hindrance between the neighboring benzene rings than in the atactic configuration. Therefore, if we extend the above discussion, the large optical anisotropy exhibited by the highly crystallizable fraction might be due to hindrance of benzene ring rotation, which in turn might reflect the degree of stereoregularity. Therefore, the optical anisotropy could be a measure for determining stereoregularity at least in the case of polystyrene. In addition, the increase in the stiffness of the isotactic polystyrene chain, as shown by the larger unperturbed dimension, supports the view that the larger interaction between the benzene rings is the main cause of the increase in optical anisotropy. If this statement is true, then optical anisotropy is very important in characterizing stereoregularity because it is an in-

trinsic property which is not influenced by secondary effects.

It is interesting to note that Tsvetkov and his co-workers³⁵ observed in the study of flow birefringence that isotactic polymethyl methacrylate was characterized by a large optical anisotropy. The 40-fold increase in the optical anisotropy of the fraction F-4' may be due to the restriction of benzene ring rotation caused by the stereoregular structure, which is preserved even in solution. As the temperature is raised, the freedom of rotation of the benzene ring and the freedom of internal bond rotation will increase owing to the violent thermal motion, which would cause optical anisotropy to decrease.

Acknowledgments. The author is indebted to Professor Michio Kurata for discussion and criticism of this work. The technical assistance of Mr. J. Komiya, Mr. H. Itani, and Mr. M. Tsuji is gratefully acknowledged. This work was supported in part by a grant-in-aid of research from the Ministry of Education of Japan.

(34) The size of the optical segment is not necessarily equal to the size of the statistical segment. See, for example, M. V. Volkenstein, "Configurational Statistics of Polymer Chains," translated by S. N. Timasheff and M. J. Timasheff from the Russian edition, Interscience Publishers, Inc., New York, N. Y., 1963.

(35) V. N. Tsvetkov, S. Y. Magarik, N. N. Boitsova, and M. G. Okuneva, *J. Polymer Sci.*, **54**, 635 (1961).

Nuclear Magnetic Resonance Studies of Nitriles and Isocyanides:

Acetonitrile and Methyl Isocyanide

by A. Loewenstein and Y. Margalit

Department of Chemistry, Technion, Israel Institute of Technology, Haifa, Israel (Received June 10, 1965)

The positions and line widths of H^1 , C^{13} , and N^{14} resonances in CH_3NC and CH_3CN are reported and discussed. The positions of the H^1 resonances of the OH group in methanol in mixtures with CH_3CN , CH_3NC , and CCl_4 were measured. From these measurements the enthalpies of hydrogen-bonded complex formation with CH_3CN and CH_3NC are estimated. The values obtained are $\Delta H = 0.9$ and 2.0 kcal./mole for CH_3CN and CH_3NC , respectively.

Introduction

Acetonitrile and methyl isocyanide are isoelectronic symmetric top molecules which show close similarities in their molecular parameters such as the bond lengths¹⁻³ and electric dipole moments.⁴ The significant difference between CH_3CN and CH_3NC is that whereas the former can be presented in terms of classical bond structures, the latter structures such as $CH_3-N^+ \equiv C^-$ or $CH_3-\ddot{N}=C:$ must be postulated.⁵ This report presents a study of CH_3CN and CH_3NC using the H^1 , N^{14} , and C^{13} nuclear magnetic resonance spectra. The major emphasis is on the study of the hydrogen bond formation of both molecules to CH_3OH . Additional information on the electric field gradient at the N^{14} nucleus is obtained through the study of the N^{14} n.m.r. line widths.

Infrared investigations⁶⁻⁹ have indicated that in acetonitrile, hydrogen bonds are formed to the nitrogen atom whereas in methylisocyanide, the carbon acts as a proton acceptor. The change in the OH stretching frequency due to H bond formation was found to be smaller in CH_3CN as compared to CH_3NC ,⁶ indicating a stronger H-bond formation in the latter. Mitra⁷ estimates a value of $\Delta H = 2.25$ kcal./mole (at 30–50°) for the complexation constant between CH_3CN and CH_3OH ; no data for the corresponding CH_3NC system are available.

Nuclear magnetic resonance has been applied extensively to the study of hydrogen bonding and complex formation¹⁰ in solutions. Similar procedures are used in the present work to evaluate the complexa-

tion constants and enthalpies between CH_3CN or CH_3NC and methanol.

The N^{14} n.m.r. line width is proportional to the electric field gradient at the N^{14} nucleus and to a correlation time. The latter quantity is approximately equal in liquids of similar viscosity and molecular diameter. A variety of nitrogen-containing compounds has recently been studied in this manner.¹¹ In a previous study of the N^{14} n.m.r. of methyl isocyanide,¹² under low resolution conditions, the resonance was found to be relatively sharp. This indicates a very

(1) M. Kessler, H. Ring, R. Trambarulo, and W. Gordy, *Phys. Rev.*, **79**, 54 (1950).

(2) J. B. Moffat, *Can. J. Chem.*, **42**, 1323 (1964).

(3) C. C. Costain, *J. Chem. Phys.*, **29**, 864 (1958).

(4) S. N. Ghosh, R. Trambarulo, and W. Gordy, *ibid.*, **21**, 308 (1953).

(5) L. Pauling, "The Nature of the Chemical Bond," 3rd Ed., Cornell University Press, Ithaca, N. Y., 1960, p. 270.

(6) A. Allerhand and P. von R. Schleyer, *J. Am. Chem. Soc.*, **85**, 866 (1963).

(7) S. S. Mitra, *J. Chem. Phys.*, **36**, 3286 (1962).

(8) W. H. Fletcher, C. S. Shoup, Jr., and W. T. Thompson, *Spectrochim. Acta*, **20**, 1065 (1964).

(9) L. L. Ferstrandig, *J. Am. Chem. Soc.*, **84**, 1323, 3553 (1962).

(10) Cf. (a) C. M. Huggins, G. C. Pimentel, and J. N. Shoolery, *J. Chem. Phys.*, **23**, 1244 (1955); (b) H. A. Christ and P. Diehl, *Helv. Phys. Acta*, **36**, 170 (1963); (c) E. Gore and S. S. Danyluk, *J. Phys. Chem.*, **69**, 89 (1965).

(11) (a) W. B. Monitz and H. S. Gutowsky, *J. Chem. Phys.*, **38**, 1155 (1963); (b) D. Herbison-Evans and R. E. Richards, *Mol. Phys.*, **7**, 515 (1964).

(12) J. D. Ray, L. H. Piette, and D. P. Hollis, *J. Chem. Phys.*, **29**, 1022 (1958).

Table I: N.m.r. Parameters of CH_3NC and CH_3CN^a

Solvent	H^1 (ref. TMS)		N^{14} (ref. HNO_3 70%)		C^{13} (ref. CE_3 in CH_3CN)	
	Position	Width ^b	Position	Width	Position	
	CH_3NC				CH_3	NC
Neat	-3.17	0.5	196	0.5 ^b	-24	-157.5
CHCl_3 (1:1 vol.)	-3.12	0.5	$\delta_{\text{CH}_3\text{NC}}^d = 133.5$	
CCl_4 (1:1 vol.)	-3.17	0.5	196	0.5 ^b	$\delta_{\text{CH}_3\text{NC}}^d = 131.5$	
CH_3OH^c	-3.17 to -3.01	0.5	197	0.5 ^b	$\delta_{\text{CH}_3\text{NC}}^d = 133.5$ to 108.5^e	
	CH_3CN				CH_3	CN
Neat	-2.03	0.5	104	81	0	-123
CCl_4 (1:1 vol.)	-2.03	0.5	104 to 101 ^c	100	0	-121
H_2O (1:1 vol.)	-2.05	0.5	104 to 114 ^c	113	0	-123
CH_3OH (1:1 vol.)	-2.03 to -1.98	0.5	104 to 107.5 ^c	81	0	-123

^a Positions are given in p.p.m. and width in c.p.s. ^b Resolution determined by field inhomogeneity. ^c Concentration dependence was studied; see Figures 1 and 2. ^d Chemical shift between C^{13} resonances of CH_3 - and $-\text{NC}$ groups.

low electric field gradient at the N^{14} nucleus in CH_3NC which has been further proven by the observation¹³ of a sharp H^1 n.m.r. triplet in CH_3NC with $J_{\text{NH}} = 2.7$ c.p.s. These measurements show that with respect to the electric field gradient at the N^{14} nucleus, CH_3NC displays a similar behavior to symmetrical species such as the ammonium or tetramethylammonium ions. We have extended these observations by high-resolution N^{14} n.m.r. measurements and attempted to measure the N^{14} resonance in solid CH_3NC . We are at present unable to offer any quantitative explanation of this rather surprising phenomenon. Proton n.m.r. work on other isocyanides¹³ seems to indicate that a low electric field gradient is not a unique characteristic of CH_3NC but may apply to other isocyanides as well. Further investigation of this problem is planned.

Experimental Section

Materials. Commercially available C.P. acetonitrile and carbon tetrachloride were used without further purification. Methanol was distilled over CaH_2 to remove traces of water. Methyl isocyanide was prepared by a procedure similar to that given by Lifshitz, Carroll, and Bauer.¹⁴ The product contained about 4% acetonitrile which was not removed. Other solvents were all C.P. products.

Spectrometer. Hydrogen-1 spectra were taken with a Varian A-60 spectrometer equipped with a variable-temperature accessory. Tetramethylsilane was used as an internal reference. Carbon-13 spectra, at natural abundance, were taken with a Varian DP-60 spectrometer equipped with a V4210A variable-frequency unit operating at 15 Mc. Nitrogen-14 spectra were taken with a Varian DP-60s spectrometer equipped with a V4311 fixed-frequency unit operating at 4.33 Mc.

The samples for both N^{14} and C^{13} spectra were contained in 15-mm. o.d. Pyrex tubes. The C^{13} resonances were measured from an internal reference (the CH_3 resonance of CH_3NC or CH_3CN), while the N^{14} resonance were measured relative to an external reference (70% HNO_3 , or saturated NH_4Cl solution) contained in an inner 8-mm. o.d. tube. No susceptibility corrections were applied. The attempts to detect the N^{14} resonance in solid CH_3NC were performed with the V-4210A variable-frequency unit operating at 4.3 Mc. and a specially constructed dewar insert.

Results and Discussion

A. Measurements on CH_3CN and CH_3NC . The positions and widths of the H^1 , C^{13} , and N^{14} resonance in CH_3NC and CH_3CN are given in Table I.

1. H^1 Resonances. The methyl resonance in CH_3NC is shifted about 1 p.p.m. lower than the corresponding resonance in CH_3CN . This shift is probably due to different bond anisotropy and to the partial positive charge on the nitrogen atom in CH_3NC . The methyl resonance in CH_3NC displays a triplet of equal intensities with $J_{\text{NH}} = 2.35$ c.p.s. This value is slightly lower than the value of 2.7 c.p.s. reported previously.¹³ The C^{13} -H spin-spin interaction in the methyl group of CH_3CN has been measured previously¹⁵ and found to be 136 c.p.s. We have measured the same quantity for CH_3NC and found it to be equal in magnitude to that in CH_3CN .

(13) I. D. Kuntz, P. von R. Schleyer, and A. Allerhand, *J. Chem. Phys.*, **35**, 1533 (1961).

(14) A. Lifshitz, H. F. Carroll, and S. H. Bauer, *J. Am. Chem. Soc.*, **86**, 1488 (1964).

(15) N. Muller and D. E. Pritchard, *J. Chem. Phys.*, **31**, 1471 (1959); H. Dreeskamp, E. Sackmann, and G. Stegmeier, *Ber. Bunsenges. Physik. Chem.*, **67**, 860 (1963).

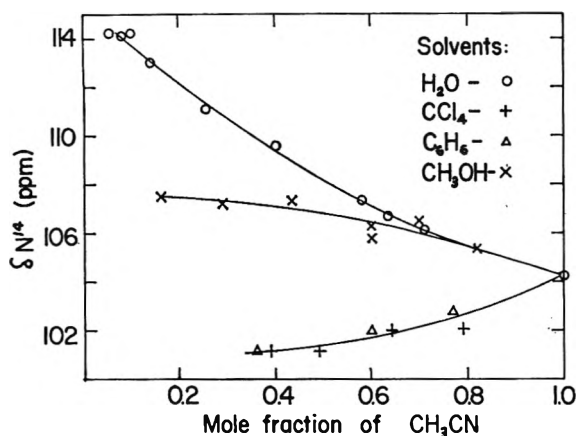


Figure 1. Chemical shift of the N^{14} resonance in CH_3CN as a function of its mole fraction in various solvents. Shifts are measured relative to the N^{14} resonance in 70% aqueous HNO_3 at $30 \pm 2^\circ$.

2. N^{14} Resonance. The N^{14} resonance in CH_3NC is shifted to higher field than in CH_3CN by about 90 p.p.m. It displays a 1:3:3:1 spin-spin quadruplet with $J_{NH} = 2.3$ c.p.s. which agrees well with the value obtained from the H^1 spectra.

The position of N^{14} resonance in CH_3NC does not change on dilution with polar or nonpolar solvents. In CH_3CN however, such a dependence is observed and is particularly large in aqueous solutions. The results are presented in Figure 1. The shift in hydrogen bond forming solvents is to higher fields, opposite to H^1 shifts which are to lower fields. This suggests that the hydrogen bonds are formed to the nitrogen atom in CH_3CN . A larger shift, to higher field, of the N^{14} resonance in pyridine-methanol solutions was observed¹⁶ and attributed to hydrogen-bond formation. The shifts to lower fields in CCl_4 or C_6H_6 are solvent effects not related to intermolecular hydrogen bonding.

The line width in CH_3NC is only about $1/100$ to $1/300$ as large as it is in CH_3CN . We may use the relationship¹¹

$$\frac{1}{T_1} = \frac{3}{8} \left(\frac{e^2 Qq}{\hbar} \right)^2 \tau_q \quad (1)$$

where T_1 is the longitudinal relaxation time, $e^2 Qq/\hbar$ the quadrupole coupling constant (in Mc.), and τ_q is the correlation time (assuming the asymmetry factor $\eta = 0$), to estimate the upper limit of $e^2 Qq/\hbar$ in CH_3NC . Taking $T_2 = T_1$, where T_2 is the transverse relaxation time, and assuming equal τ_q values for both CH_3NC and CH_3CN and $e^2 Qq/\hbar = 4.35$ Mc. for CH_3CN ,¹¹ we obtain $e^2 Qq/\hbar < 0.3$ Mc. for CH_3NC . From microwave spectra,¹ an upper limit of 0.5 Mc. was estimated for this quantity. If the solid, state line width is com-

pletely determined by the quadrupolar interaction, we should be able to observe this resonance, provided the interaction is smaller than about 6×10^{-3} Mc. (corresponding to about 20-gauss line width). Attempts to observe the N^{14} resonance in solid CH_3NC (at -70°) failed. In solid NH_4Cl , where the electric field gradient is zero, N^{14} resonances were observed, which suggests that dipolar broadening is not the cause for not observing the resonance in solid CH_3NC .

The N^{14} line width in CH_3CN is slightly solvent-dependent and probably related to small changes in τ_q . Similar observations have been noticed before.^{11b}

3. C^{13} Spectra. Line widths could not be measured with our experimental setup. The chemical shift between the CH_3- and the $-CN$ or $-NC$ is larger in methylisocyanide than in acetonitrile by about 10 p.p.m. Also, all resonances are shifted to higher fields in the latter. The most significant, result however, is that in a hydrogen bond forming solvent (methanol) the C^{13} resonance of the $-NC$ group is concentration-dependent (shifts to higher fields) whereas the resonance position of the $-CN$ group in CH_3CN remains unchanged. This strongly indicates (*cf.* N^{14} shifts) H-bond formation to the C atom in CH_3NC . The detailed shifts and the calculated curve (which shall be discussed later) are given in Figure 2.

B. Measurements on CH_3OH . The equilibrium constants of hydrogen-bonded complexes of CH_3CN and CH_3NC with CH_3OH were estimated from the H^1 resonance shifts of the OH group in the methanol. The results are shown in Figures 3 and 4. In order to take into account the shifts due to changes in the self-association of the methanol we have measured the OH shift of methanol in CCl_4 (Figure 5). The curves given in Figures 3-5 were analyzed by a procedure analogous to that given by Huggins, Pimentel, and Shoolery.^{10a}

The observed chemical shift, δ_{obsd} , is the sum of two terms

$$\delta_{obsd} = \frac{x}{c} \delta_x + \frac{c-x}{c} \delta_c \quad (2)$$

where x is the concentration of the complex, c is the concentration of the methanol, and δ_x and δ_c are the shifts of pure complex and pure methanol, respectively.

Assuming that by subtracting from δ_{obsd} the shift of CH_3OH in CCl_4 a correction for the self-association effects is applied, we obtain

$$\delta'_{obsd} = \frac{x}{c} \delta_x \quad (3)$$

(16) H. Saitô and K. Nukada, *Tetrahedron Letters*, 2, 111 (1965).

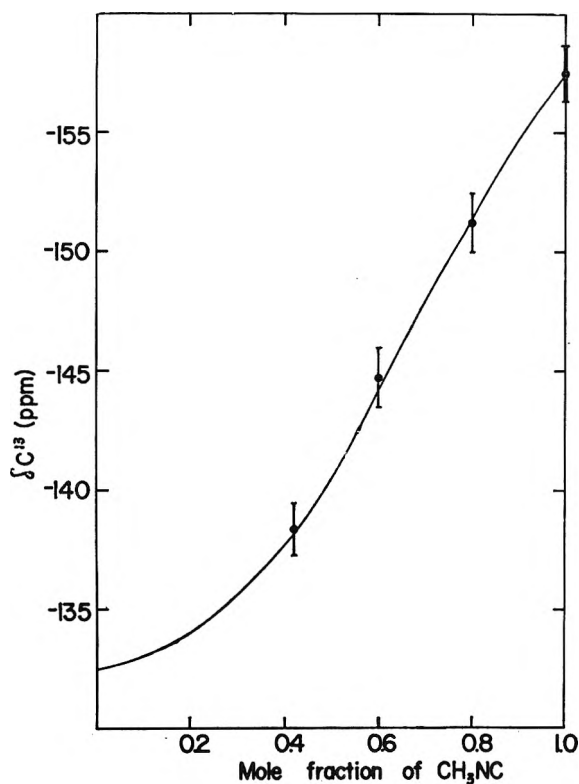


Figure 2. The C^{13} chemical shift of the NC group in CH_3NC as a function of its mole fraction in methanol. Shifts are measured relative to the C^{13} resonance of the CH_3 group in CH_3CN . The line is the calculated curve (see text); temperature, $30 \pm 2^\circ$.

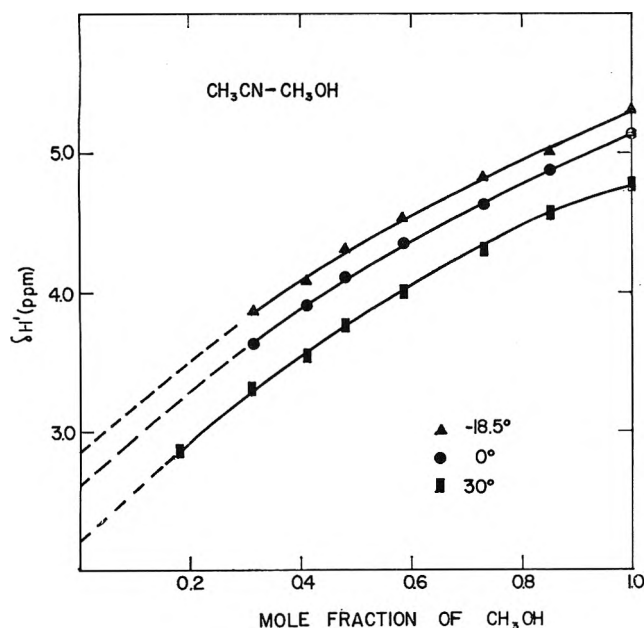


Figure 3. The H^1 chemical shift of the OH group in methanol in mixtures with CH_3CN at various temperatures. Shifts are to lower magnetic fields relative to the internal reference tetramethylsilane.

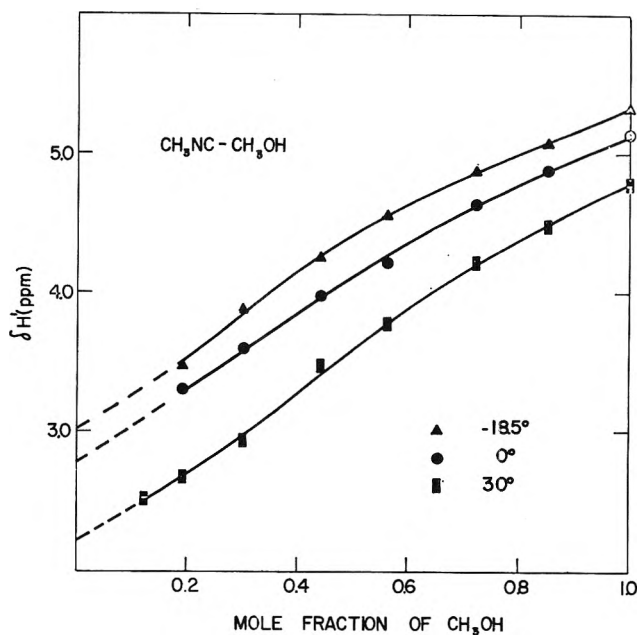


Figure 4. The H^1 chemical shift of the OH group in methanol in mixtures with CH_3NC at various temperatures. Reference is the same as in Figure 3.

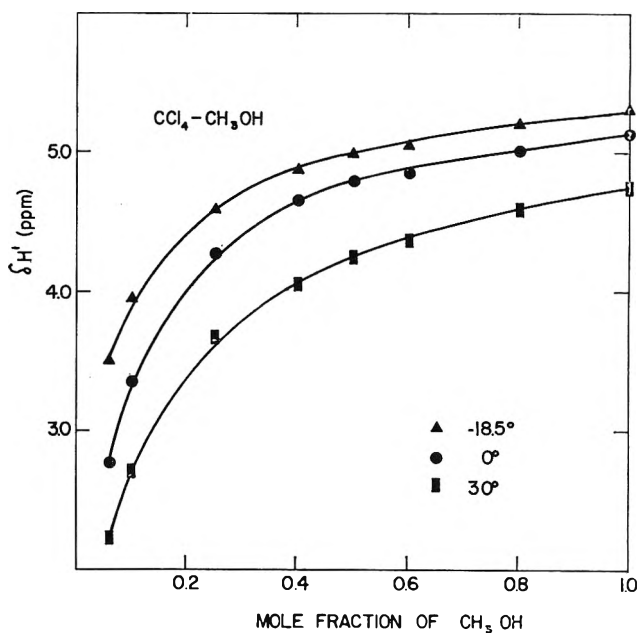


Figure 5. The H^1 chemical shift of the OH group in methanol in mixtures with CCl_4 at various temperatures. Reference is the same as in Figure 3.

where δ'_{obsd} is the difference between the OH shift in CH_3CN (or CH_3NC) and CCl_4 at the same concentration of methanol. Assuming further that as $c \rightarrow 0$, also $x \rightarrow 0$, one obtains^{10a}

$$\delta_x = (\delta_{\text{obsd}})_{c \rightarrow 0} + \frac{1}{K} [(\delta_{\text{obsd}})_{c \rightarrow 0} - \delta_c] \quad (4)$$

where $(\delta_{\text{obsd}})_{c \rightarrow 0}$ is the extrapolated value of the OH shift in infinite dilutions in CH_3CN (or CH_3NC) and is taken from Figure 3 or 4. The equilibrium constant K is defined as

$$K = \frac{x(b + c - x)}{(c - x)(b - x)} \quad (5)$$

where b is the concentration of the CH_3CN (or CH_3NC).

Combining eq. 3, 4, and 5, one may write δ'_{obsd} in terms of K and the concentrations of methanol and CH_3CN (or CH_3NC) in the solution. The values of K were then computed by a trial and error procedure. The best values of K thus obtained are given in Table II. The temperature dependence of K can be represented by $\Delta H = 0.9$ and 2.0 kcal./mole for CH_3CN and CH_3NC , respectively.

Table II: Equilibrium Constants for Hydrogen-Bonded Complexes in CH_3CN and CH_3NC

Temp., °C.	K	
	CH_3CN	CH_3NC
30	2.6	3.0
8	2.4	2.1
-18.5	2.0	1.6

Obviously, the model on which this calculation is based involves some rather over-simplifying approximations. The worst assumptions probably are the correction applied for self-association and the neglect of specific solvent effects. Another uncertainty lies in the extrapolation to obtain $(\delta_{\text{obsd}})_{c \rightarrow 0}$ shown in Figure 3 or 4. At relatively high methanol concentrations its spectrum already turns into an AB_3 type which makes the determination of the OH position rather difficult. Furthermore, δ_x might be temperature-dependent¹⁷ and this may account, in part, for the variation of the calculated equilibrium constant with the

temperature. Therefore, no estimate for the limits of errors was calculated. The orders of magnitude of the data are, however, very plausible and roughly agree with infrared data.^{6,7} The stronger H bonds to CH_3NC as compared to CH_3CN are evident from the larger value of ΔH for the former. Also, this result is consistent with the data obtained from infrared spectra.

A correction for self-association was applied in a study of hydrogen bonding of alcohols in various solvents.¹⁸ This method, which involves computer curve fitting, should, in principle, give more reliable results. However, the low precision of our measurements and the other approximations still uncorrected for put in doubt the justification for the use of this method in our case.

An independent check on the consistency of the results was performed in the following manner: The C^{13} shifts of the NC group in CH_3NC solutions in methanol (Figure 2) can be written as

$$\delta_{\text{C}^{13}(\text{obsd})} = x_{(\text{complex})} \delta_{\text{C}^{13}(\text{complex})} + x_{(\text{CH}_3\text{NC})} \delta_{\text{O}^{13}(\text{CH}_3\text{NC})} \quad (6)$$

where the x 's denote mole fractions. The x values at 30° were calculated from the equilibrium constant (Table II) and the value of $\delta_{\text{C}^{13}(\text{complex})}$ was chosen so as to give best fit with the measured points. We thus obtained $\delta_{\text{C}^{13}(\text{complex})} = -124$ p.p.m. and calculated the curve which is shown in Figure 2. Measurement of the C^{13} resonance in the range of $x_{\text{CH}_3\text{NC}} < 0.4$ would serve as a critical test to this calculation. Unfortunately, however, C^{13} resonances at these low concentrations could not be measured with sufficient accuracy due to experimental difficulties. Similar calculations on the N^{14} resonance in the $\text{CH}_3\text{CN}-\text{CH}_3\text{OH}$ system were not performed due to the small over-all shift of the N^{14} .

(17) Cf. N. Muller and R. C. Reiter, *J. Chem. Phys.*, **42**, 3265 (1965); we are indebted to a referee for pointing out this reference.

(18) C. Lussan, *J. chim. phys.*, **60**, 1100 (1963); we are indebted to a referee for pointing out this reference.

Some Aspects of Gel Permeation Chromatography

by William B. Smith and Anthony Kollmansberger

Department of Chemistry, Texas Christian University, Fort Worth, Texas (Received June 14, 1965)

The separation of a number of alkanes and aromatic compounds by chromatography through cross-linked polystyrenes has been carried out using tetrahydrofuran as the eluting solvent. It was established that molecular volume is fundamental in determining the degree of separation. The variation of the height equivalent to a theoretical plate with flow rate was studied, and a comparison of the elution volumes with diffusion coefficients for a series of compounds was also made. These data are compared to the expectations from recent chromatographic theory.

It has been known for some time that molecular separation can be effected by the passage of solutions through solvent-swollen, cross-linked gels.¹ While much of this work has been done with water solutions and hydrophilic gels, recently the use of organic solvents and hydrophobic gels has been reported. Using a vulcanized rubber latex with heptane as the solvent, Brewer separated polymers from low molecular weight compounds.² Vaughan³ has reported the separation of low molecular weight polystyrenes upon passage through a cross-linked polystyrene swollen with benzene.

Recently, Moore^{4a} and Moore and Hendrickson^{4b} have described an elegant procedure for obtaining polymer molecular weight distributions by chromatography of the polymer sample through cross-linked polystyrenes of graded permeabilities. By calibrating these columns with carefully characterized polymers, it was possible to prepare a curve relating the elution volume to the logarithm of the average molecular chain length. It was observed that these calibration curves were often linear over a large range of chain lengths. From the calibration curve, the molecular weight distribution of unknown samples could then be calculated.

Moore has termed this process as "gel permeation chromatography" which seems more accurately descriptive of the process involved than the previously used term "gel filtration." The simplest model consistent with this method of separation envisions the permeation of the solute into the gel from the flowing solution. In both aqueous and nonaqueous solvents

and with both hydrophilic and hydrophobic gels, it is observed that larger, higher molecular weight materials are eluted from the columns first since, presumably, these substances diffuse less rapidly (or not at all) into the gel structure when compared to smaller molecules.

In view of the importance which gel permeation chromatography is likely to assume in polymer chemistry, it seems highly desirable that the details of the mode of separation be ascertained.⁵ In order to eliminate the difficulties in working with poorly defined high molecular weight mixtures, it was decided that separations with smaller molecules should be used in this study.

Experimental Section

Benzene and the halobenzenes used in this study were all commercial products with properties in agreement with the literature values. The iodobenzene and *p*-diiodobenzene were distilled and recrystallized, respectively, before use. The normal hydrocarbons

(1) For a review of these techniques see P. Flodin and J. Porath, "Chromatography," E. Heftmann, Ed., Reinhold Publishing Corp., New York, N. Y., 1961, Chapter 13.

(2) P. S. Brewer, *Nature*, **188**, 935 (1960).

(3) M. F. Vaughan, *ibid.*, **188**, 55 (1960).

(4) (a) J. C. Moore, *J. Polymer Sci.*, **A2**, 835 (1964); (b) J. C. Moore and J. G. Hendrickson, *ibid.*, **C8**, 233 (1965); see also (c) D. J. Harmon, *ibid.*, **C8**, 243 (1965); and (d) L. E. Maley, *ibid.*, **C8**, 253 (1965).

(5) For recent attempts to define the separations with aqueous systems see: P. Flodin, *J. Chromatog.*, **5**, 103 (1961); J. Porath, *Pure Appl. Chem.*, **6**, 232 (1963); G. K. Ackers, *Biochemistry*, **3**, 723 (1964); and M. Kubin, *Collection Czech. Chem. Commun.*, **30**, 1104 (1965).

were high purity materials obtained from the Aldrich Chemical Co. as was the 2-methylpentane. Each checked as one compound upon vapor phase chromatography, and each gave the correct index of refraction.⁶

The preparations of 2-methyloctane, 3-methyloctane, 3-ethyloctane, 3-methylnonane, 4-ethylnonane, and 4-methyldecane each proceeded in the same fashion. The appropriate Grignard reagent was reacted with either 2-octanone or 3-octanone, and the resultant alcohol was dehydrated by distillation from a trace of iodine. The crude distillate, consisting of a mixture of olefins and some of the starting ketone, was hydrogenated with Adams' platinum in acetic acid, and the hydrogenated material was washed with cold, concentrated sulfuric acid. Each substance was then washed with water, dried over magnesium sulfate, distilled, checked for purity by v.p.c., index of refraction, and infrared spectroscopy.

Tetrahydrofuran was refluxed for at least 1 day over solid potassium hydroxide and was then distilled before use.

Gel Permeation Chromatography. A commercial instrument manufactured by Waters Associates, Framingham, Mass., was used in this study. The instrument was equipped with two 4-ft. columns of 40-Å. gel and one 4-ft. section of 20-Å. gel in series (permeabilities assigned by the manufacturer).⁷ Tetrahydrofuran was used as the solvent throughout. All determinations were carried out at the ambient temperature (23–25°). Since the instrument uses a differential refractometer as the detector, the concentrations of solutes used in this study were determined, in part, by the refractive index differences between the solutes and the solvent (THF).

In one study a mixture containing 0.020 g., respectively, of benzene and *p*-dibromobenzene/ml. of tetrahydrofuran was used to determine the variations caused by differing flow rates. The same sample size was injected in each case. The peaks were symmetrical and cleanly separated to the base line. The total number of plates in the column for each substance was calculated from the usual chromatographic formula: plates = $(4V_e/w)^2$, where V_e is the elution volume to the peak from the time of injection, and w is the width in volume at the base of the peak and is determined by drawing the tangents to the inflection points on each side of the peak. The height equivalent to a theoretical plate (HETP) was determined by dividing the total number of plates into 12 ft., the length of the columns. The results of this study are given in Table I.

Elution volumes at a constant flow rate were then de-

Table I: HETP vs. Flow Rate

Solute	Flow rate, ml./min.	V_e , ml.	w , ml.	HETP $\times 10^3$, ft.
Benzene	0.074	99.51	2.70	0.55
DBB ^a		92.54	3.12	0.85
Benzene	0.286	104.89	3.60	0.88
DBB		97.55	4.13	1.34
Benzene	0.390	105.34	4.17	1.18
DBB		97.55	4.39	1.51
Benzene	0.744	107.94	5.08	1.66
DBB		100.12	5.17	2.00
Benzene	1.612	109.64	6.63	2.75
DBB		102.01	6.63	3.17

^a *p*-Dibromobenzene.

Table II: Elution Volumes (at 0.736 ml./min.) in THF

Compound	Concn., g./ml.	V_e , ml.	HETP $\times 10^3$, ft.
<i>n</i> -Pentane	0.02	98.48	1.36
<i>n</i> -Hexane	0.03	95.19	1.28
<i>n</i> -Heptane	0.05	91.98	1.49
<i>n</i> -Octane	0.09	89.17	1.39
<i>n</i> -Nonane	0.20	86.67	1.30
<i>n</i> -Decane	0.20	83.41	1.42
<i>n</i> -Undecane	0.15	81.86	1.69
<i>n</i> -Dodecane	0.13	79.97	1.70
2-Methylpentane	0.04	94.01	1.66
3-Methyloctane	0.11	86.29	1.34
2-Methyloctane	0.10	85.76	1.45
3-Methylnonane	0.20	84.39	2.01
3-Ethyloctane	0.11	84.78	2.30
4-Methyldecane	0.14	81.91	1.52
4-Ethylnonane	0.11	82.32	2.30
Benzene	0.02	107.39	1.57
Chlorobenzene	0.02	101.96	1.61
Bromobenzene	0.02	102.83	1.77
Iodobenzene	0.02	102.21	1.81
<i>p</i> -Dichlorobenzene	0.02	97.30	2.06
<i>p</i> -Dibromobenzene	0.02	99.70	1.88
<i>p</i> -Diiodobenzene	0.02	97.30	2.06

termined for a series of normal alkanes, branched alkanes, and aromatic compounds. The results of these determinations are presented in Table II. Both here

(6) All boiling points, indices of refraction, and densities were taken from R. R. Dreisbach, "Physical Properties of Chemical Compounds," Vol. I, American Chemical Society, Washington, D. C., 1955.

(7) The instrument has been described in ref. 4d, and the preparation of the gels in ref. 4a.

and in the flow rate study described above, at least three determinations of V_e and w per compound were carried out, and the values reported are the average values. Values of V_e were reproducible with an average deviation of ± 0.05 – 0.07% , while values of w agreed with average deviations of ± 1 – 2% .

Diffusion Coefficients. The apparatus and techniques used in the determination of the diffusion coefficients were similar to those described by Stokes.⁸ The diffusion cell consisted of a glass tube bisected by a medium-porosity glass frit (2-cm. diameter). The ends of the glass tube were pulled down and joined to stopcocks (one at each end) which were mounted axially. Ten small glass beads were sealed in each compartment for stirring purposes. The two cell compartments so formed contained 13.31 and 10.15 ml., respectively. The cell was mounted horizontally in the constant-temperature bath. The glass tubing leading away from each stopcock was used as an axle and mounted in small ball bearings. Stirring was accomplished by turning the cell axially about its mounting using a motor-driven rubber pulley. The temperature bath was maintained at $25.0 \pm 0.02^\circ$.

The compartments were filled and emptied with the cell mounted vertically using a long hypodermic needle and syringe. The larger side was first filled with pure solvent, and solvent was allowed to fill the frit. The cell was then inverted, and the solvent which passed through the frit was withdrawn. This compartment was then filled with the desired solution. The cell was placed in its mounting and stirred for the appropriate length of time.

Upon completion of a run, the cell was again vertically clamped with the smaller compartment, containing the more concentrated solution, uppermost. The end tubes were washed with acetone and dried with an air jet. This compartment was quickly emptied with the syringe. Then the lower compartment was emptied.

The concentrations of the solutions in each compartment were determined from the refractive indices at 25° . Calibration curves for each solute at various concentrations in THF were prepared in advance. Once the diffusion time and the two concentrations were determined, the diffusion coefficient was obtained by the relation: $D = (1/KT) \log [C_1/(C_2 - C_3)]$, where D is the diffusion coefficient, T is the temperature, C_1 is the initial concentration (g./ml.) of the solution, C_2 and C_3 are the final concentrations of the initial solution and solvent side, respectively, and K is the cell constant. In order to determine the cell constant, three runs were made using biphenyl in benzene.⁹ An average value of 0.112 was found with a precision of fractional standard deviation of 5.27% .

In order to check the accuracy of the method, the diffusion coefficient for toluene in hexane was determined as 4.10×10^{-5} with a fractional deviation of 4.54% for three runs. The reported value is 4.21×10^{-5} .¹⁰ The results for the seven compounds used in this study are given in Table III.

Table III: Diffusion Coefficients in THF at 25°

Solute	Initial concn., g./ml.	$D \times 10^{-5}$	Fractional std. dev., %
Benzene	0.0704	3.84	4.07
Chlorobenzene	0.1026	3.28	1.38
Bromobenzene	0.1392	2.69	1.06
Iodobenzene	0.1844	2.06	3.62
<i>p</i> -Dichlorobenzene	0.1354	2.21	2.87
<i>p</i> -Dibromobenzene	0.2080	1.94	9.61
<i>p</i> -Diiodobenzene	0.2961	1.69	3.52

Apparent Molar Volumes. The apparent molar volumes of the aromatic compounds used in this study were determined in THF solution by a standard technique.¹¹ The results were as follows where the value in parentheses are the molar concentrations: benzene, 89.15 ml. (0.9004); chlorobenzene, 100.07 ml. (0.9000); bromobenzene, 103.36 ml. (0.9002); iodobenzene, 109.78 ml. (0.9003); *p*-dichlorobenzene, 113.49 ml. (0.8999); *p*-dibromobenzene, 119.79 ml. (0.9000); and *p*-diiodobenzene, 128.67 ml. (0.8999).

Results and Discussion

The separation of various mixtures into discrete molecular species by means of gel permeation chromatography presumably depends on the relative rates of diffusion of the various species into the gel. In the polymer systems studied previously,⁴ calibration of the columns was carried out on the basis of an average molecular chain length calculated from the number-average molecular weight and assuming a planar zig-zag backbone structure. While this procedure has been found empirically to give useful results, intuitively it would seem that molecular volumes would be a more fundamental parameter with which to calibrate the columns.

The elution volumes for a series of normal and

(8) R. H. Stokes, *J. Am. Chem. Soc.*, **72**, 763 (1950).

(9) R. Mills, *J. Phys. Chem.*, **67**, 600 (1963).

(10) P. Chang and R. C. Wilke, *ibid.*, **59**, 592 (1955).

(11) N. Bauer and S. Z. Lewin, "Technique of Organic Chemistry," Vol. I, A. Weissberger, Ed., Interscience Publishers, Inc., New York, N. Y., 1959, pp. 141, 142.

Table IV: Chain Length vs. Molar Volume Comparisons

Compound	Length, Å. ^a	Effective length, Å.	% error	Molar vol., ^b ml.	Effective molar vol., ml.	% error
<i>n</i> -Pentane	9.0			116.1		
<i>n</i> -Hexane	10.3			131.6		
<i>n</i> -Heptane	11.7			147.5		
<i>n</i> -Octane	13.1			163.5		
<i>n</i> -Nonane	14.4			179.7		
<i>n</i> -Decane	15.8			195.9		
<i>n</i> -Undecane	17.2			212.2		
<i>n</i> -Dodecane	18.6			228.6		
2-Methylpentane	9.0	10.1	12.2	132.9	136	2.3
3-Methyloctane	13.1	14.6	11.5	178.9	179	0.0
2-Methyloctane	13.1	15.0	15.3	180.8	182	0.5
3-Methylnonane	14.4	15.8	9.7	195.0	191	2.1
3-Ethyloctane	13.1	15.5	18.4	193.3	188	2.6
4-Methyldecane	15.8	17.3	9.5	...	210	...
4-Ethylnonane	14.4	17.0	11.8	...	206	...
Benzene	7.1	6.4	9.9	89.2	85	4.5
Chlorobenzene	8.4	7.9	6.0	100.1	104	4.0
Bromobenzene	8.8	7.6	13.6	103.4	100	2.9
Iodobenzene	9.1	7.8	14.3	109.8	103	6.4
<i>p</i> -Dichlorobenzene	9.7	9.5	2.0	113.5	122	8.0
<i>p</i> -Dibromobenzene	10.5	8.6	20.0	119.8	113	5.8
<i>p</i> -Diiodobenzene	11.1	9.5	16.8	128.7	122	5.4

^a Measured from LaPine-Leybold models prepared according to Stuart and Briegleb, LaPine Scientific Co., Chicago, Ill. ^b Molar volumes determined from the densities at 25° for the alkanes. For the aromatic compounds, the values are apparent molar volumes in THF at 25°.

branched alkanes, as well as a series of aromatic compounds, are given in Table II. Plots of log (chain length) and log (molar volume), respectively, vs. V_e for the normal hydrocarbons gave very good straight lines. Using these lines as calibrations then allows one to determine an "effective chain length" and an "effective molar volume" for the other compounds in the series. The comparison of the chain lengths and molar volumes determined by the g.p.c. is given in Table IV. For 14 compounds, the "effective chain lengths" were found to show a 12.1% average deviation; while for 12 cases, the molar volumes gave only a 3.7% average deviation. As expected, the molecular volume is the more fundamental yardstick relating elution volume to molecular structure.

Regarding the model to be used in considering the g.p.c. process, we first rather naively assumed that the general chromatography equation would apply.¹² According to this equation (known as the van Deemter equation when applied to gas chromatography) the height equivalent to a theoretical plate is given by: $HETP = A + B/u + Cu$, where A is a constant describing the "multipath" or eddy diffusion effect which is a function of the packing and particle size of the

column packing; the term B/u describes the longitudinal diffusion of the solute into the bulk of the solvent and varies inversely as the flow rate, u ; and Cu is a term describing the state of the partition equilibrium between solute in the bulk solution and the packing. According to this equation, the variation in HETP with flow rate follows a hyperbola with HETP decreasing with flow rate until a minimum is reached. At slower flow rates, the HETP then increases rapidly owing to the longitudinal diffusion term.

A plot of the data in Table I is given in Figure 1, and it is clear that the behavior expected, based upon the above reasoning, is not observed. At the lowest flow rate used in this study, benzene was eluted after over 24 hr. on the column. The deleterious effect of longitudinal diffusion, even over this long period, has not yet started to evidence itself.

Others have noted chromatographic behavior at odds with that expected from the above equation, and at least two theories have been proposed to account for the departure. Giddings¹³ has proposed a modifica-

(12) See ref. 1, pp. 27, 97, and 170.

(13) J. C. Giddings, *Anal. Chem.*, **35**, 1338 (1963); see also ref. 1, p. 98.

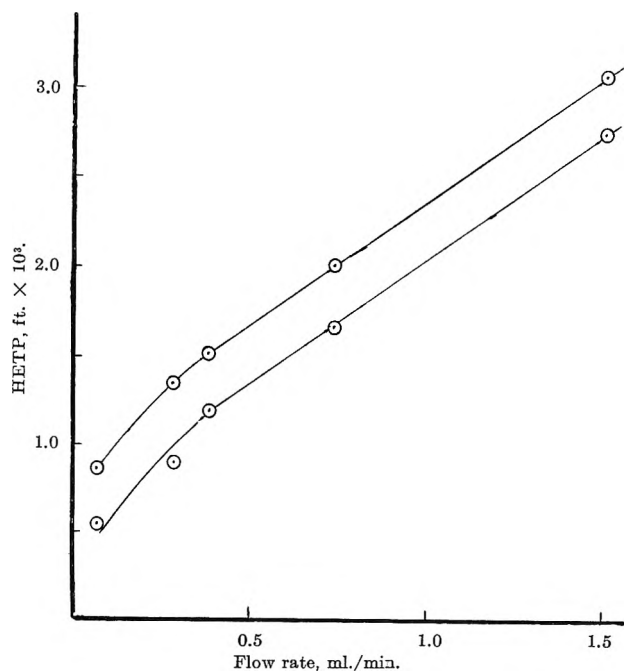


Figure 1. A plot of flow rate vs. HETP for the g.p.c. data with benzene (lower) and *p*-dibromobenzene (upper).

tion of the eddy diffusion term to take into account mass-transfer processes in the mobile phase. His theory, known as the coupling theory, may be summarized by the equation

$$\text{HETP} = \frac{AEu}{A + AEu} + Cu$$

where the first term replaces the former term for eddy diffusion, and E is a constant (or better a series of constants) proportional to the square of the channel diameter and the reciprocal of the diffusion coefficient of the solute in the mobile phase. The longitudinal diffusion term has been omitted here as it seems to make no important contribution under the conditions of this study.

Walton¹⁴ has proposed a modified equation to account for behavior in ion-exchange chromatography. Walton's equation, as defined by his film diffusion theory, is

$$\text{HETP} = A + \frac{Bu}{D_s} + \frac{Cu}{(1 + Fu)D_1}$$

where A again describes the eddy diffusion effect; B , C , and F are composites of several constants; and D_s and D_1 are diffusion coefficients for the solute in the gel and the diffusion of solute through a static liquid film surrounding the gel particles.

No obvious choice between the two above equations is suggested by the data in Figure 1. Both should lead to linear behavior at the extremes of flow rate with

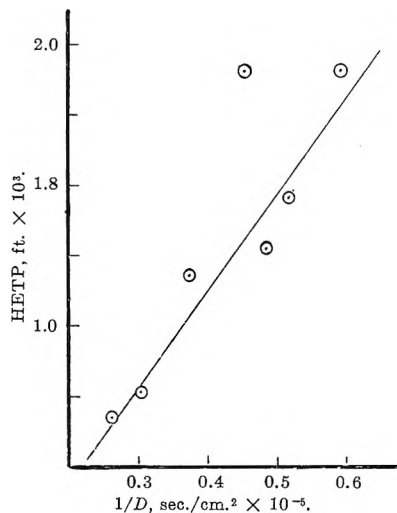


Figure 2. A plot of HETP vs. the reciprocal of the diffusion coefficients for a series of aromatic compounds. The point off the line is *p*-dichlorobenzene.

a nonlinear intermediate region. The curves in Figure 1 exhibit just such behavior. Furthermore, both models suggest a higher slope for the curve at lower flow rates in agreement with Figure 1. Giddings¹³ has offered considerable data to support his theory and has criticized the film diffusion theory.¹⁵

Examination of the details of either theory suggests a reciprocal relation between HETP and the diffusion coefficients for the different solute species. It is evident from the data in Table II that HETP increases with molecular size, and, of course, diffusion coefficients vary in the opposite fashion. Unfortunately, there is no exact theory relating molecular size or shape to diffusion coefficients for small molecules at this time. A plot of $1/D$ vs. HETP for the aromatic compounds is shown in Figure 2, and, with the unexplained exception of dichlorobenzene, a linear relation is observed.

In summary, it is evident from this study that useful separations of small molecules may be effected by this technique and that molecular volume is the important parameter influencing the degree of separation. The variation of HETP with flow rate follows either of the two most current chromatographic equations and shows a linear inverse variation with the diffusion coefficients for various solutes.

Acknowledgment. The authors wish to acknowledge the financial support of the Dow Chemical Co. in the conduct of this research. Grateful thanks is also expressed to J. C. Moore for helpful discussions.

(14) H. F. Walton, ref. 1, p. 299.

(15) J. C. Giddings, *Anal. Chem.*, **34**, 1186 (1962).

The Dilation Contribution to the Heat Capacity of Copper and α -Brass at Elevated Temperatures¹

by Y. Austin Chang and Ralph Hultgren

Department of Mineral Technology, College of Engineering, University of California, Berkeley, California (Received June 14, 1965)

For pure copper and an α -brass containing 9.7 atom % Zn, the compressibilities were measured from 77 to 800°K. and the heat contents of the brass, from 298 to 800°K. From these and other data found in the literature, the dilation term $C_p - C_v$ of the heat capacity was calculated. The Nernst-Lindemann approximate formula was found to express accurately the dependence of the dilation term on temperature for these two substances. However, data found in the literature for eight other substances indicate the Nernst-Lindemann approximation more usually gives too rapid an increase of the dilation term with temperature.

Introduction

Heat capacities of solids and liquids are always measured at constant pressure, C_p , while theoretical treatments apply to C_v , the heat capacity at constant volume. The difference, $C_p - C_v$, is called the dilation contribution. At the molal volume, V , and temperature, T , the dilation can be shown to equal

$$C_p - C_v = \alpha^2 VT / \kappa_T \quad (1)$$

where α is the volume coefficient of thermal expansion and κ_T is the isothermal compressibility.

While the other terms are relatively well known, data on compressibilities are few except for the elements at room temperature and below. In the present work the compressibilities of copper and of an α -brass with 9.7 atom % zinc were measured from 77 to 800°K. with an ultrasonic pulse-echo technique. The method failed at higher zinc concentrations because of increased attenuation of the echoes.

Experimental Section

The copper specimen was machined to a cylinder 1.6 cm. in diameter and 1.27 cm. long from a cold-rolled OFHC grade ingot. Spectroscopic analysis showed impurities as Ag, 0.003, and Ni, 0.003 wt. %. The brass specimen in the form of a 1.9-cm. rod was kindly supplied by the Bridgeport Brass Co., from which a specimen 1.27 cm. long was machined. Their analysis showed Cu, 90.05, Zn, 9.93, Bi, 0.001, Fe, 0.005, Ni, 0.01, Pb, 0.003, and Sn, 0.00 wt. %.

The faces of the specimens were ground and polished parallel within 0.0005 cm. After annealing, the average grain sizes for the copper and brass were 0.015 and 0.025 mm., respectively. X-Ray diffraction showed sharp back-reflection lines and respective lattice constants of 3.6152 and 3.6355 Å., in good agreement with Pearson² for copper and 9.7 atom % zinc.

Ultrasonic Velocity Measurement. A Sperry ultrasonic attenuation comparator, Style 56A001, was used. Waves and their echoes were displayed on an oscilloscope from which the time of travel and the velocity could be measured. Longitudinal and transverse velocities were separately measured, using 10Mc X-cut and Y-cut quartz crystals. The adiabatic compressibility is

$$\kappa_S = \frac{1}{\rho(V_1^2 - \frac{4}{3}V_t^2)} \quad (2)$$

(where ρ is the density, V_1 is the longitudinal velocity, and V_t is the transverse velocity) from which the isothermal compressibility can be calculated.

$$\kappa_T = \kappa_S + \alpha^2 TV / C_p \quad (3)$$

The principal experimental difficulty was firmly

(1) Much of this material in this publication has been abstracted from the Ph.D. Thesis of Y. A. Chang, University of California, 1963.

(2) W. B. Pearson, "A Handbook of Lattice Spacings and Structures of Metals and Alloys," Pergamon Press, Inc., New York, N. Y., 1958.

binding the quartz transducer to the specimen at elevated temperatures. At low temperatures Fisher nonaqueous stopcock grease served very well, but a number of bonding materials failed at elevated temperatures, including Sauereisen cement P-31, Biggs epoxy resin R-335, and a mixture of $\text{Na}_2\text{SiF}_6 + \text{BaSO}_4 + \text{Na}_2\text{SiO}_4$. Dr. Harold Chen of the Shell Development Co. kindly supplied the formula which proved to be the best of those tested. The bonding material was an epoxy resin formed by mixing Epon 1031 and nadic methyl anhydride, catalyzed by benzene-dimethylamine added at about 50° . This bond was excellent to 500°K ., above which the echo intensity dropped sharply. However, it was usable to 800°K . The bond broke during cooling of the specimens leaving some black powder, probably carbon from decomposition of the resin.

The experimental arrangement is shown in Figure 1. Elevated temperatures were attained by means of a glass heating tape wrapped around the Pyrex tube; low temperatures, by immersing it in liquid nitrogen.

Results and Discussion

Ultrasonic Velocity and Compressibility. The measured longitudinal and transverse velocities are shown in Figure 2. The scatter of data is less than the stated accuracy ($\pm 1\%$) of the Sperry instrument. This corresponds to a somewhat larger ($\pm 3\%$) scatter in the compressibilities calculated from them. Calculations were made using thermal expansion data from the literature.³⁻⁵

It can be seen in Table I that compressibilities increase with temperature and with zinc content. Measurements with higher zinc alloys also showed qualitatively that compressibility increased with zinc content.

Heat Content. Because the high-temperature heat capacities of brass measured by Kussmann and Wollen-

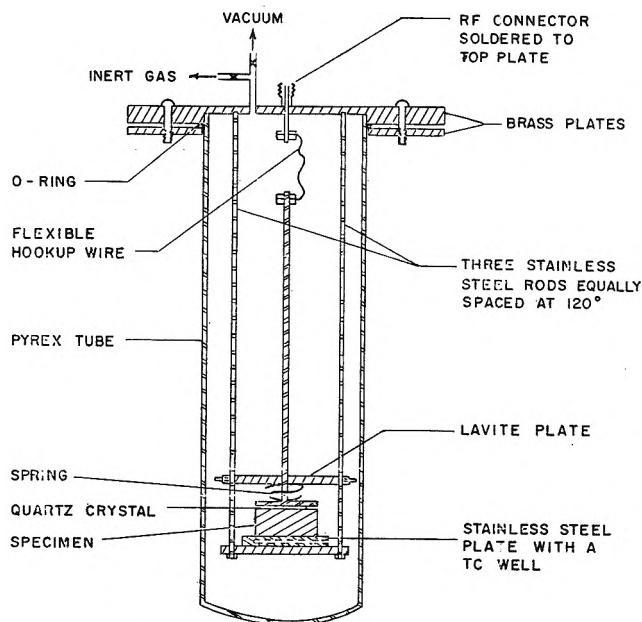


Figure 1. Apparatus.

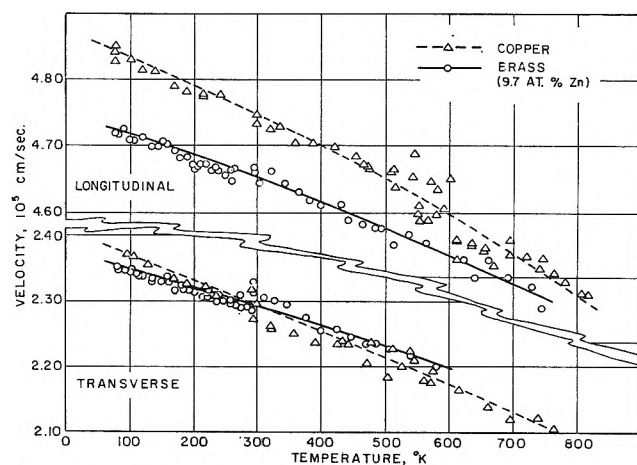


Figure 2. Sonic velocities.

Table I: Measured Compressibilities

T, °K.	Compressibility, $\text{cm}^2/\text{dyne} \times 10^{12}$			
	χ_S		χ_T	
	Copper	Brass, $z_{\text{Zn}} = 0.097$	Copper	Brass, $z_{\text{Zn}} = 0.097$
77	6.96	7.53	7.00	7.56
100	6.99	7.55	7.03	7.59
200	7.09	7.65	7.21	7.79
298.15	7.20	7.77	7.42	8.00
400	7.32	7.89	7.63	8.23
500	7.48	8.04	7.88	8.48
600	7.67	8.20	8.18	8.76
700	7.87	8.37	8.50	9.07
800	8.10	8.86		

berger⁶ disagreed with low-temperature values of Huffstutler⁷ by about 0.45 cal./g.-atom deg. at room temperature, it was decided to repeat the work and extend it to higher temperatures by heat content measurements in a diphenyl ether drop calorimeter described

(3) (a) F. C. Nix and D. MacNair, *Phys. Rev.*, **60**, 597 (1941); **61**, 74 (1942); (b) P. Hidnert, National Bureau of Standards Scientific Paper 410, Vol. 17, U. S. Government Printing Office, Washington, D. C., 1922, p. 91.

(4) P. D. Merica and L. W. Schad, *Bull. Bur. Std.*, **14**, 571 (1919).

(5) H. W. Altman, T. Rubin, and H. L. Johnston, Report TR-264-28, Cryogenic Laboratory, Ohio State University, ASTIA Document AD-31268, 1954.

(6) A. Kussmann and H. Wollenberger, *Z. Metallk.*, **50**, 94 (1959).

(7) M. C. Huffstutler, Ph.D. Thesis, University of California, Berkeley, Calif., 1961.

elsewhere.^{8,9} Results are shown in Table II. Derived C_p values are shown in Table III. They extrapolate to $C_p = 5.84$ at 298.15°K., agreeing with Huffstutler's determination. For copper, C_p values were taken from the literature.¹⁰

Table II: Experimental Heat Contents of α -Brass (cal./g.-atom deg.)

T , °K.	$H_T - H_{298}$	T , °K.	$H_T - H_{298}$	T , °K.	$H_T - H_{298}$
373.8	441	637.9	2079	656.5	2237
404.0	636	699.5	2481	606.5	1872
451.9	915	752.1	2704	551.9	1551
497.0	1203	806.3	3189	488.8	1156
564.9	1626	808.0	3130	447.2	897
611.2	1900	756.2	2847	405.8	636
611.6	1922	697.1	2441	345.2	282

Table III: Heat Capacities (cal./g.-atom deg.) and Dilation Term

T , °K.	Copper			α -Brass		
	C_p	$C_p - C_v$	$10^5 A$	C_p	$C_p - C_v$	$10^5 A$
77	2.98	0.02	2.21	3.05	0.01	1.58
100	3.84	0.02	1.68	3.95	0.03	1.68
200	5.41	0.10	1.68	5.42	0.10	1.68
298.15	5.84	0.17	1.68	5.84	0.17	1.68
400	6.04	0.24	1.68	6.06	0.25	1.68
500	6.19	0.32	1.68	6.21	0.32	1.68
600	6.34	0.40	1.64	6.33	0.40	1.68
700	6.48	0.48	1.64	6.42	0.49	1.72
800	6.62	0.57	1.63			

Dilation Contribution. Values of the dilation contribution (Table III) were calculated from eq. 1, using measured values of the compressibility (Table I) and other quantities from the literature.²⁻⁵

The resulting dilation terms were used to test the validity of the Nernst-Lindemann semiempirical equation. This equation, derived with the aid of certain considerations of Gruneisen, has been frequently used to estimate the dependence on T of $C_p - C_v$ at elevated temperatures, though it has been inadequately tested above room temperature. According to the Nernst-Lindemann equation

$$C_p - C_v = AC_p^2 T \quad (4)$$

where A ($=\alpha^2 V/C_p^2 \kappa_T$) is assumed constant with temperature. As can be seen in Table III, A is satisfactorily constant except at 77°K. for both copper and α -brass.

The applicability of the Nernst-Lindemann equation

was tested for five additional metals and three non-metallic substances for which sufficient data were found in the literature (see Table IV). For each of these a constant, A , was chosen which fitted the data exactly at 300°K. For a rather high temperature in each case, the experimental $C_p - C_v$ was compared with the calculated value as shown in Table IV. Evidently, the equation tends to overestimate the dilational con-

Table IV: Dilatation Heat Capacities

Substance	Temp., °K.	Data source	$C_p - C_v$, cal./g.-atom deg.		Dev., %
			Exptl.	Calcd.	
Cu	800		0.57	0.59	+ 3.5
Brass, 9.7 atom % Zn	750		0.53	0.52	- 1.9
Zn	650	<i>a-d</i>	0.72	0.86	+19.4
In	400	<i>a, e, f</i>	0.75	0.79	+ 5.3
Al	800	<i>a, b, g, h</i>	0.90	1.15	+27.8
Pb	600	<i>a, e, g</i>	0.87	1.22	+40.2
Sn	500	<i>a, e, i</i>	0.53	0.62	+17.0
KCl	1000	<i>j-o</i>	1.34	1.44	+ 7.5
NaCl	700	<i>l, o-r</i>	0.92	1.03	+12.0
MgO	1400	<i>l, o, s, t</i>	0.49	0.59	+20.4

^a See ref. 2. ^b See ref. 10. ^c G. A. Alers and J. R. Neighbours, *J. Phys. Chem. Solids*, **7**, 58 (1958). ^d E. Gruneisen and E. Goens, *Z. Physik*, **29**, 141 (1924); E. A. Owen and E. L. Yates, *Phil. Mag.*, **17**, 113 (1934). ^e A. I. Kaznoff, Ph.D. Thesis, University of California, Berkeley, Calif., 1961. ^f J. Graham, A. Moore, and G. V. Raynor, *J. Inst. Metals*, **84**, 86 (1955). ^g See ref. 4. ^h P. M. Sutton, *Phys. Rev.*, **91**, 816 (1953). ⁱ H. D. Erling, *Ann. Physik*, **34**, 136 (1939); B. G. Childs and S. Weintraub, *Proc. Phys. Soc. (London)*, **B63**, 267 (1950). ^j M. H. Norwood and C. V. Briscoe, *Phys. Rev.*, **112**, 45 (1958). ^k F. D. Enck, *ibid.*, **119**, 1873 (1960). ^l K. K. Kelley and E. G. King, U. S. Bureau of Mines Bulletin No. 592, U. S. Government Printing Office, Washington, D. C., 1961. ^m F. D. Enck, D. G. Engle, and K. I. Marks, *J. Appl. Phys.*, **33**, 2070 (1962). ⁿ K. E. Salimaki, *Ann. Acad. Sci. Fennicae, Ser. A VII*, **56**, 40 (1960). ^o C. O. Hodgman, "Handbook of Chemistry and Physics," 36th Ed., Chemical Rubber Publishing Co., Cleveland, Ohio, 1956. ^p W. C. Overton, Jr., and R. T. Swin, *Phys. Rev.*, **84**, 758 (1951). ^q A. Eucken and W. Dannohl, *Z. Elektrochem.*, **40**, 814 (1934). ^r L. Hunter and S. Siegel, *Phys. Rev.*, **61**, 84 (1942). ^s C. Susse, *J. Rech. Centre Natl. Rech. Sci. Lab. Bellevue (Paris)*, **54**, 23 (1961). ^t M. Durand, *Physics*, **7**, 297 (1936).

(8) R. Hultgren, P. Newcombe, R. L. Orr, and L. Warner, National Physical Laboratory Symposium No. 9, Paper 1H, HMSO, London, 1959.

(9) W. Kendall, R. L. Orr, and R. Hultgren, *J. Chem. Eng. Data*, **7**, 516 (1962).

(10) R. Hultgren, R. L. Orr, P. D. Anderson, and K. K. Kelley, "Selected Values of Thermodynamic Properties of Metals and Alloys," John Wiley and Sons, Inc., New York, N. Y., 1963.

tribution; copper and brass are the most favorable of all the substances. However, in spite of the considerable overestimate, the magnitude of the error seldom exceeds 0.2 cal./deg. g.-atom and is usually of the order of 0.1.

The experimental values of the heat capacity of copper and brass were satisfactorily accounted for at all temperatures as the sum of a lattice vibrational (Debye) term, C_D , the dilation term, and an electronic contribution term, C_{e1} .

$$C_p = C_D + (C_p - C_v) + C_{e1} \quad (5)$$

In these calculations C_D was taken from an assumed Debye temperature for copper and brass of 315 and

308°K., respectively. Electronic heat capacities were assumed to be $1.64 \times 10^{-4} T$ for copper¹⁰ and $1.78 \times 10^{-4} T$ for brass.¹¹

Acknowledgment. The authors are indebted to the Office of Scientific Research, U. S. Air Force, and to the U. S. Atomic Energy Commission for its support of this work. They are also grateful to Dr. Harold Chen of the Shell Development Co., who supplied the high-temperature epoxy resin; Bridgeport Brass Co., who supplied the brass specimen; and Donald Hawkins, who carried out the heat content measurements.

(11) J. Rayne, *Phys. Rev.*, **108**, 22 (1957).

Nuclear Magnetic Resonance Spectra of 2,2'-Bipyridyl

by S. Castellano, H. Günther, and S. Ebersole

Mellon Institute, Pittsburgh, Pennsylvania (Received June 14, 1965)

The n.m.r. spectra of 2,2'-bipyridyl (I) in solution in 11 different solvents (CCl_4 , CCl_3H , CH_3OH , $\text{C}_2\text{H}_5\text{OH}$, $(\text{CH}_3)_3\text{CC}\equiv\text{CH}$, $\text{CH}_2\text{ClCH}_2\text{OH}$, CH_3COOH , $\text{C}_2\text{H}_5\text{COOH}$, $\text{CH}_3\text{CHBrCOOH}$, $\text{C}_3\text{H}_7\text{COOH}$, CF_3COOH) and in binary mixtures of solvents (CCl_4 - CCl_3H , CCl_4 - CH_3OH , CCl_3H - CF_3COOH) have been recorded and completely analyzed in terms of the fundamental n.m.r. parameters. The n.m.r. spectrum of the iron complex $[\text{Fe}^{\text{II}}(\text{C}_{10}\text{N}_2\text{H}_8)_3]\text{Cl}_2$ (II) in CH_3OH solution has also been recorded and exactly analyzed. The n.m.r. parameters of I show remarkable changes with the nature of solvent used; in particular, the behavior of the chemical shift of the proton 3 (and 3') indicates the existence of a strong deshielding effect exerted by the nitrogen atom of the adjacent ring. The several effects which determine the low-field occurrence of the resonance of protons 3 (and 3') are discussed and their contribution to the shift calculated. It is shown that the van der Waals dispersion forces may cause, at the 3 position, downfield shifts of 0.20–0.30 p.p.m. in the *trans*-planar conformation of I. As a result of the calculations, different conformations are assigned to 2,2'-bipyridyl in inert and proton donor solvents. The conformations of the mono- and diprotonated cations are also discussed and orders of magnitude of the dihedral angle between the two pyridine rings estimated. The chemical shifts of the protons of II are interpreted and calculated in terms of the anisotropy and dispersion force effects which arise because of the relative orientations of the bipyridyl groups in the molecule.

Introduction

The n.m.r. spectrum of 2,2'-bipyridyl has been already described in general terms^{1,2} and analyzed by a first-order approximation by Kramer and West³ and by Gil.⁴

Our interest in the study of the n.m.r. spectrum of this molecule has been motivated by the previous observations of the large deshielding effects exerted by the nitrogen atom of aromatic heterocyclic systems at the *ortho* protons of a phenyl ring attached at the α position. Data obtained in this laboratory from the n.m.r. spectra of 2,4-diphenyl-6-methyl-*s*-triazine, 3,6-diphenyltetrazine, and 2-phenylpyridine⁵ clearly suggested the existence of a strong interaction between the nitrogen and the opposed aromatic protons. A comparison of the chemical shifts of the *ortho* protons of the phenyl groups in 2-benzoylpyridine⁶ and benzophenone⁷ suggests that the interaction occurs through space and is still present even if a carbonyl group is inserted between the two rings.

A preliminary investigation showed that a similar interaction is also present in 2,2'-bipyridyl whose n.m.r. spectrum shows an unusual downfield shift for the resonance of protons 3 and 3'. The spectrum of I appeared to be much simpler than the spectra of any one of the previously mentioned compounds and was therefore considered better suited for a study of the observed phenomenon. Since the latter appeared to be strongly dependent on the nature of the solvent used, it was felt that a systematic investigation of the

(1) M. Freymann and R. Freymann, *Arch. Sci. (Geneva)*, **13**, 506 (1960).

(2) M. Freymann, R. Freymann, and D. Libermann, *Compt. rend.*, **250**, 2185 (1960).

(3) F. A. Kramer, Jr., and R. West, *J. Phys. Chem.*, **69**, 673 (1965).

(4) V. M. S. Gil, *Mol. Phys.*, **9**, 97 (1965).

(5) H. Günther and S. Castellano, unpublished results.

(6) S. Castellano and A. A. Bothner-By, *J. Chem. Phys.*, **41**, 3863 (1964).

(7) S. Castellano and J. Lorenc, *Chim. Ind. (Milan)*, **47**, 643 (1965).

behavior of the spectral parameters of 2,2'-bipyridyl in different solvents could be highly rewarding in terms of a better understanding of the nature of the studied interaction. Accordingly, we have performed the analysis of the n.m.r. spectra of 2,2'-bipyridyl in different media and in mixtures of different solvents; the experimental results found in this study and their interpretation form the body of this paper.

Experimental Section

Materials. Samples of 2,2'-bipyridyl were of commercial origin (Calbiochem Co. and Eastman Organic Chemicals). Solvents used were Merck, Fisher Certified, Baker Analyzed, and Matheson Coleman Spectro-quality chemicals. All compounds were used without further purification. In no case were extraneous peaks detected in the n.m.r. spectra, and this was considered as a sufficient criterion of purity for all materials. Repeated experiments with samples from different manufacturers gave identical results. No attempt was made to determine traces of water possibly present in the acids.

The iron complex $[\text{Fe}^{\text{II}}(\text{C}_{10}\text{N}_2\text{E}_8)_3]\text{Cl}_2$ was prepared according to standard procedures.⁸ The n.m.r. spectrum of this compound showed barely detectable signals from proton-containing impurities.⁹

Sample Preparation and N.m.r. Spectra. Solutions of I were prepared by weighing the compound directly in standard 5-mm. n.m.r. tubes and by adding the solvent with a calibrated syringe. All tubes were degassed on a vacuum line and sealed after addition of about 1% of tetramethylsilane (TMS), which was used as an internal reference. For the solution of II in methanol, the concentration (less than 0.03 mole fraction) is not exactly known. No TMS was added to the solution; the shifts were measured in this case from the methyl peak of the solvent and referred thence to TMS.

Proton spectra were obtained on a Varian A-60 spectrometer. Calibration of the spectra was by means of the audio side band technique. Peak positions were the average of at least four measurements, two made with increasing and two with decreasing field using a 50-c.p.s. full-sweep width.

Spectral Analysis. The n.m.r. spectra of I and II are of the type ABCD since no long-range coupling between the two aromatic rings is detectable experimentally. The spectra often show the characteristic first-order pattern of a 2-substituted pyridine ring,^{6,10,11} and the assignment of the resonances of the different protons is straightforward. However, in the course of this study, several cases were met in which the resonances of two protons overlap and the spectrum con-

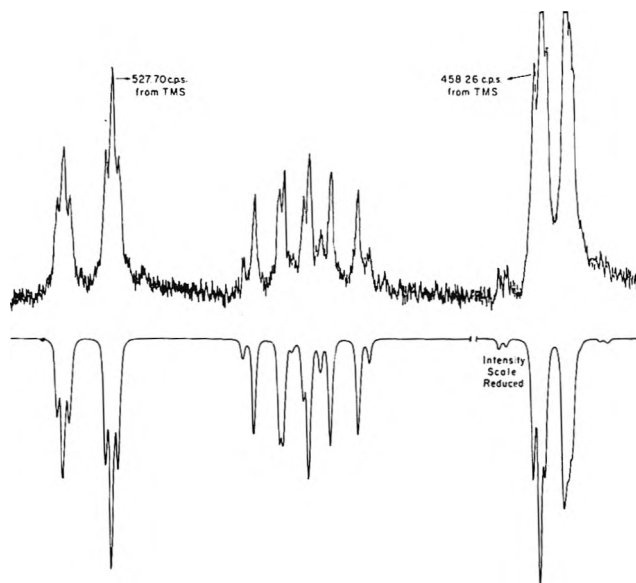


Figure 1. Experimental and calculated n.m.r. spectrum of $[\text{Fe}^{\text{II}}(\text{C}_{10}\text{N}_2\text{E}_8)_3]\text{Cl}_2$ in CH_3OH solution.

volutes remarkably. For all the cases here reported, the analyses of the spectra were performed with the aid of the LAOCOON II program using a 7090 IBM computer. As a typical example of the fitting of the experimental spectra achieved in this way, we have reported in Figure 1 the experimental and calculated n.m.r. spectrum of II. For the majority of the spectra the probable error of any parameter came out to be about ± 0.05 c.p.s. In some cases, however (solution of I in α -bromopropionic and trifluoroacetic acids, solution of II in methanol), severe broadening of the spectra was observed, and the resulting parameters are thought to be accurate only to within ± 0.2 c.p.s. For one of the solutions in $\text{CCl}_3\text{H}-\text{CF}_3\text{COOH}$ mixtures, the fit of the experimental spectrum was achieved by varying only the chemical shifts⁶ and using for the coupling constants (not reported in Table II) the averages of the values obtained in solutions at lower and higher acid concentrations.

Results

The parameters resulting from the analyses of the experimental spectra are reported in Tables I and II. In Figures 2 and 3, the chemical shifts of the protons of I are plotted *vs.* the compositions of the binary mixtures used as solvents. Other tables and figures

(8) F. Blau, *Monatsh. Chem.*, **19**, 647 (1898).

(9) Traces of paramagnetic solid material had, however, to be removed from the solution by centrifugation.

(10) W. Brügel, *Z. Elektrochem.*, **66**, 159 (1962).

(11) V. J. Kowalewski and D. G. de Kowalewski, *J. Chem. Phys.*, **37**, 2603 (1962).

Table I: N.m.r. Parameters of 2,2'-Bipyridyl in Different Solvents^a

Solvent	Mole fraction of C ₁₀ N ₂ H ₈	Chemical shifts				Coupling constants					
		ν_2	ν_4	ν_6	ν_8	J_{24}	J_{26}	J_{28}	J_{46}	J_{48}	J_{68}
CCl ₄	0.203	509.77	459.47	427.43	515.19	8.01	1.16	1.00	7.53	1.80	4.75
CCl ₄	0.089	507.65	461.32	429.30	514.24	8.02	1.19	1.00	7.49	1.84	4.84
(CH ₃) ₃ CC≡CH	0.091	509.33	461.72	430.50	515.54	8.06	1.17	0.96	7.49	1.81	4.78
CCl ₃ H	0.161	505.08	463.62	432.51	519.19	8.04	1.21	0.95	7.51	1.81	4.80
CCl ₃ H	0.075	504.16	467.71	436.91	520.37	8.02	1.22	0.95	7.54	1.83	4.81
C ₃ H ₇ COOH	0.092	499.58	470.87	441.16	525.24	8.00	1.15	0.91	7.62	1.77	4.97
CH ₃ OH	0.084	498.77	471.07	441.17	518.13	8.03	1.17	0.95	7.50	1.78	4.85
CH ₃ OH	0.074	498.33	471.06	441.20	517.63	7.98	1.17	0.93	7.57	1.76	4.88
C ₂ H ₅ OH	0.100	502.24	471.74	441.67	517.66	8.03	1.16	0.92	7.57	1.76	4.84
CH ₃ OH	0.040	497.72	473.01	443.05	518.03	8.00	1.17	0.95	7.56	1.78	4.87
C ₂ H ₅ COOH	0.089	498.70	473.20	443.57	526.69	7.99	1.15	0.93	7.59	1.80	4.97
CH ₂ ClCH ₂ OH	0.091	495.73	476.63	446.60	520.61	8.02	1.16	0.95	7.62	1.76	4.92
CH ₂ ClCH ₂ OH	≪0.091	498.30	483.93	453.64	523.68	8.04	1.16	0.92	7.62	1.74	5.02
CH ₃ COOH	0.100	501.50	491.02	460.83	531.21	8.13	1.16	0.86	7.71	1.73	5.17
CH ₃ CHBrCOOH ^b	0.090	512.85	509.69	477.43	538.78	7.95	1.44	0.66	7.62	1.43	5.31
CF ₃ COOH ^b	0.089	520.66	532.95	501.38	549.39	8.12	1.03	0.37	8.09	1.30	5.79
CF ₃ COOH ^b	0.050	521.07	533.76	502.30	549.81	8.12	1.18	0.57	8.02	1.54	5.75
CH ₃ OH ^{b,c}	Fe(C ₁₀ N ₂ H ₈) ₃ Cl ₂	531.24	495.76	455.35	454.84	8.14	1.19	0.77	7.53	1.58	5.67

^a All data in c.p.s.; ν_0 60 Mc.p.s. Chemical shifts referred to TMS as internal standard. ^b Data accurate to within ± 0.2 c.p.s. ^c Concentration less than 0.03 mole fraction. Chemical shift measured from the methyl peak of CH₃OH and then referred to TMS.

Table II: N.m.r. Parameters of 2,2'-Bipyridyl in Mixtures of Different Solvents^a

Mole fraction			Chemical shifts				Coupling constants					
CCl ₄	CCl ₃ H	C ₁₀ N ₂ H ₈	ν_2	ν_4	ν_6	ν_8	J_{24}	J_{26}	J_{28}	J_{46}	J_{48}	J_{68}
0.911	0.000	0.089	507.65	461.32	429.30	514.24	8.02	1.19	1.00	7.49	1.84	4.84
0.654	0.261	0.085	506.22	463.08	431.58	516.32	8.02	1.20	0.98	7.50	1.86	4.84
0.417	0.501	0.082	506.00	464.44	433.27	518.12	8.03	1.20	0.97	7.53	1.82	4.84
0.200	0.722	0.078	505.09	465.41	434.28	518.96	7.98	1.19	0.94	7.50	1.81	4.79
0.000	0.925	0.075	504.16	467.71	436.91	520.37	8.02	1.22	0.95	7.54	1.83	4.81
CCl ₄	CH ₃ OH	C ₁₀ N ₂ H ₈										
0.911	0.000	0.089	507.65	461.32	429.30	514.24	8.02	1.19	1.00	7.49	1.84	4.84
0.650	0.265	0.085	503.00	465.99	434.54	515.34	8.08	1.19	0.95	7.52	1.82	4.84
0.413	0.506	0.081	501.35	467.82	436.87	515.85	8.00	1.21	0.96	7.50	1.81	4.84
0.197	0.725	0.078	500.08	469.77	439.41	516.94	8.02	1.19	0.96	7.57	1.81	4.85
0.000	0.926	0.074	498.33	471.06	441.20	517.63	7.98	1.17	0.92	7.57	1.76	4.88
CCl ₃ H	CF ₃ COOH	C ₁₀ N ₂ H ₈										
0.925	0.000	0.075	504.16	467.71	436.91	520.37	8.02	1.22	0.95	7.54	1.83	4.81
0.818	0.091	0.091	506.60	492.47	460.81	532.14	8.13	1.14	0.87	7.71	1.69	5.26
0.667	0.237	0.096	506.31	501.70	468.83	533.16	8.11	0.95	0.87	7.89	1.62	5.36
0.419	0.490	0.091 ^{b,c}	507.68	509.06	476.00	535.30						
0.000	0.911	0.089 ^b	520.66	532.95	501.38	549.39	8.12	1.03	0.37	8.09	1.30	5.79

^a All data in c.p.s.; ν_0 60 Mc.p.s. Chemical shifts referred to TMS as internal standard. ^b Data accurate to within ± 0.2 c.p.s. ^c Coupling constants not determined. See text.

will be described during the discussion of the data. The chemical shifts are usually given in c.p.s. from TMS at 60 Mc.p.s.; however, shifts resulting from calculations are reported in p.p.m.

Discussion

The experimental data (Tables I and II) show that the n.m.r. parameters of all the protons of 2,2'-bipyridyl change remarkably in passing from solution in inert

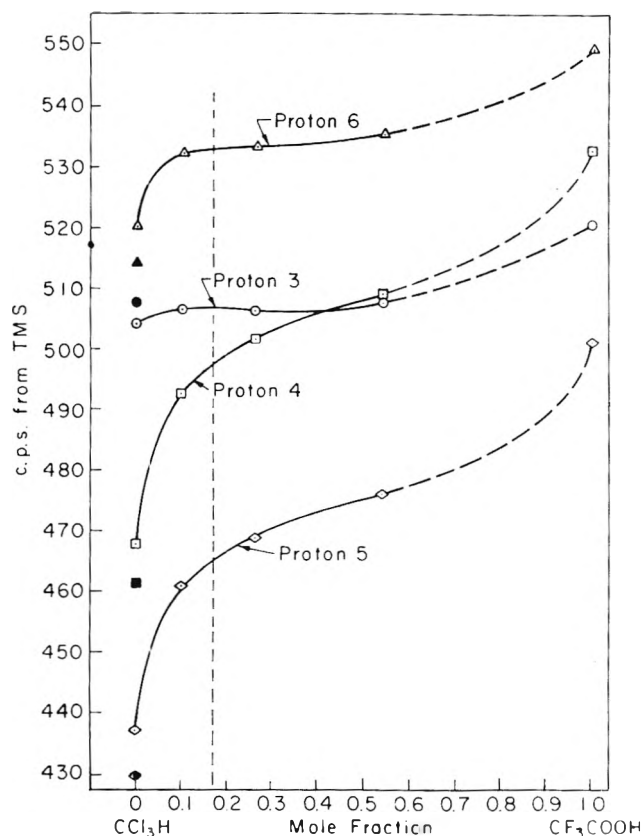


Figure 2. Chemical shifts of the protons of 2,2'-bipyridyl in solution in mixtures of CCl_3H and CF_3COOH .

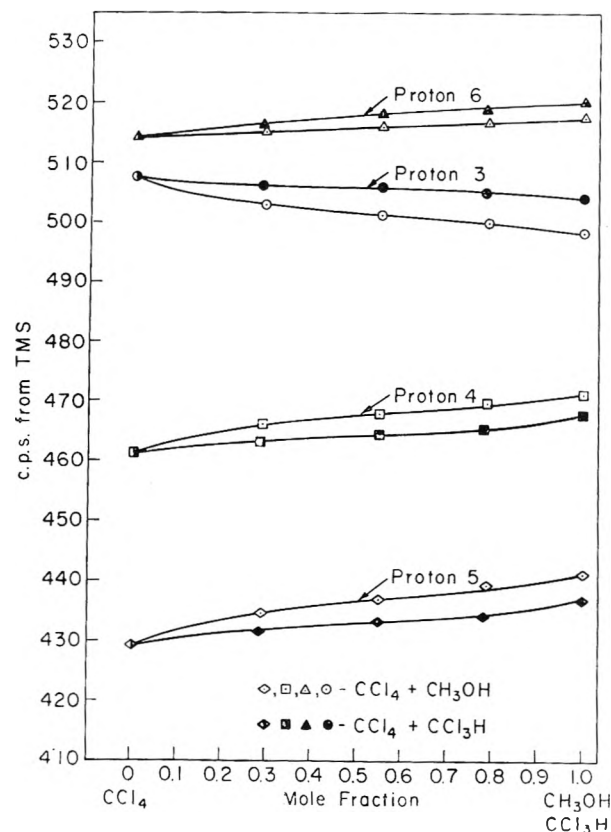


Figure 3. Chemical shifts of the protons of 2,2'-bipyridyl in solution in mixtures of CCl_4 and CH_3OH and of CCl_4 and CCl_3H .

solvents to solutions in more acidic media, the largest variations being associated, as expected, with the chemical shifts. Several papers¹²⁻¹⁴ in the recent literature have dealt with the interpretation of the same variations observed in the n.m.r. spectra of pyridine. Since the data available for this compound are limited to solutions in inert solvents (CCl_4 , C_6H_{12}) or in strong acids (CF_3COOH), in order to establish a comparison between these data and our experimental results, we will discuss the n.m.r. parameters of 2,2'-bipyridyl in the same media first. A discussion of the n.m.r. data of I in proton donor solvents and weak acids will then follow. The n.m.r. spectrum of II will be discussed last.

N.m.r. Spectra of 2,2'-Bipyridyl in Inert Solvents (CCl_4). The parameters of the proton spectrum of I at two different concentrations in CCl_4 are reported in Table I. The small differences observed between corresponding values of the chemical shifts are indicative of the order of magnitude of the dilution shifts in that range of concentrations. For pyridine at infinite dilution in the same solvent, the chemical shifts, in c.p.s., for the α , β , γ protons, in this order, are^{15,16} 513.96, 435.96, and 458.16. A comparison between

these values and our experimental data shows that the presence of the second pyridine ring affects only slightly the chemical shifts of protons 4, 5, and 6. For proton 3 a large downfield shift is observed; if referred to the chemical shift of proton 5 (both protons are *meta* to the nitrogen), it amounts to -1.34 p.p.m.

2,2'-Bipyridyl is known to be in the *trans*-planar conformation (I), in the solid.^{17,18} Measurements¹⁹ of the electric dipole moment (0.6 D.), as well as ultraviolet

(12) V. M. S. Gil and J. N. Murrell, *Trans. Faraday Soc.*, **60**, 248 (1964).

(13) I. C. Smith and W. G. Schneider, *Can. J. Chem.*, **39**, 1158 (1961).

(14) G. Kotowycz, T. Schaefer, and E. Bock, *ibid.*, **42**, 2541 (1964).

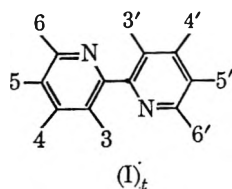
(15) G. Fraenkel, R. E. Carter, A. McLachlan, and J. H. Richards, *J. Am. Chem. Soc.*, **82**, 5846 (1960).

(16) Other data, given in ref. 13, for the chemical shifts of pyridine in C_6H_{12} are 520.4, 432.4, and 457.4.

(17) F. Bertinotti, A. M. Liquori, and R. Parisi, *Gazz. chim. ital.*, **86**, 893 (1956).

(18) L. L. Merritt, Jr., and E. D. Schroeder, *Acta Cryst.*, **9**, 801 (1956).

(19) P. H. Cureton, C. G. Le Fevre, and R. J. W. Le Fevre, *J. Chem. Soc.*, 1736 (1963). These authors, however, propose a *trans* conformation with an angle of twist of $10-17^\circ$ between the two pyridine rings.



spectroscopic data,²⁰ are also consistent with a *trans*-planar conformation in solution (CCl₄, C₆H₆). Proton 3 is, therefore, the closest to the adjacent pyridine ring and to its nitrogen atom. The magnetic anisotropies of the aromatic ring²¹ and of the nitrogen atom,¹² as well as the electric field²² produced at the 3 position by the electric dipole of the second pyridine group, will cause a deshielding of that proton. The existence of a van der Waals interaction between the lone-pair electron of the nitrogen and proton 3 may also be very effective in reducing the shielding of that proton.²³

The contributions of all these effects to the chemical shift of proton 3 have been calculated and are presented in Table III. The molecular dimensions used in the calculations are those given in ref. 18. The deshielding caused by the ring current effect ($\Delta\sigma_R$) has been determined by the use of the tables of Johnson and Bovey²⁴ under the assumption²⁵ that the ring currents in pyridine and benzene are essentially the same. The value $\Delta\chi = -7.21 \times 10^{-30}$ cm.³/molecule has been used for the magnetic anisotropy of the nitrogen¹² in order to estimate the deshielding ($\Delta\sigma_N$) due to this effect. The field, produced by the electric dipole (2.15 D.) of pyridine²⁶ at the 3 position has been calculated by localizing the dipole at the nitrogen atom. The calculations of the shifts ($\Delta\sigma_E$) due to the electric field effect have been performed by the use of both Buckingham's²² ($A = 2 \times 10^{-12}$, $B = 10^{-18}$) and

along the C-H bond and to the E^2 term. The downfield shift due to the van der Waals forces has been determined by the use of Bothner-By's²³ scheme of calculation, later revised by Buckingham.²⁸ The mean-square electric field, caused by the dispersion forces, has been estimated through the equation: $E^2 = 3h\nu\alpha/r^6$, where ν is the mean frequency of electronic excitation, α the electric polarizability, and r the distance between the centers of the charges.^{29,30} The deshielding ($\Delta\sigma_W$) was then calculated by both Buckingham's and Musher's coefficients.

The results presented in Table III show that the use of both equations leads to the same values of the total shift ($\Delta\sigma_T$) although the partial contributions of the electric field effects—dipole field and van der Waals forces field—are different as expected in the two cases. The value found for $\Delta\sigma_T$ appears to be quite reasonable and in good agreement with other experimental results. If the chemical shift of proton 3 is corrected by the calculated amount, the difference between the shifts of protons 3 and 5, which may be considered as a measure of the "chemical effect" due to the substitution at the 2 position, becomes equal to -0.15 p.p.m. This value correlates reasonably well with the corresponding differences measured⁹ in 2-methyl- and 2-ethylpyridine (-0.08), in 2-vinylpyridine (-0.11), and in 2-phenylpyridine^{6,31,32} (-0.15). Particularly interesting is the fact that the van der Waals forces effect comes out, in both cases, of the same order of magnitude as the dipolar field effect and contributes substantially to the

Table III: Calculated Values of the Deshielding of Proton 3 in 2,2'-Bipyridyl^a

Effect		Deshielding	
		B	M
Anisotropy of the aromatic ring	$\Delta\sigma_R$	-0.49	-0.49
Anisotropy of the nitrogen	$\Delta\sigma_N$	-0.16	-0.16
Dipolar electric field	$\Delta\sigma_E$	-0.25	-0.33
van der Waals forces	$\Delta\sigma_W$	-0.29	-0.21
Total deshielding	$\Delta\sigma_T$	-1.19	-1.19

^a All data in p.p.m. B and M refer to the use of Buckingham's and Musher's equations for the calculations of the electric field effects.

Musher's²⁷ ($A = 2.9 \times 10^{-12}$, $B = 7.38 \times 10^{-19}$) coefficients in the equation ($\Delta\sigma_E = -A \times E_{C-H} - B \times E^2$) relating the shift to the component of the field

(20) K. Nakamoto, *J. Phys. Chem.*, **64**, 1420 (1960).

(21) J. A. Pople, W. G. Schneider, and H. J. Bernstein, "High Resolution Nuclear Magnetic Resonance," McGraw-Hill Book Co., Inc., New York, N. Y., 1959.

(22) A. D. Buckingham, *Can. J. Chem.*, **38**, 300 (1960).

(23) A. A. Bothner-By, *J. Mol. Spectry.*, **5**, 52 (1960).

(24) C. E. Johnson, Jr., and F. A. Bovey, *J. Chem. Phys.*, **29**, 1012 (1958).

(25) G. G. Hall, A. Hardisson, and L. M. Jackmann, *Discussions Faraday Soc.*, **34**, 15 (1962).

(26) B. B. De More, W. S. Wilcox, and J. H. Goldstein, *J. Chem. Phys.*, **22**, 876 (1954).

(27) J. I. Musher, *ibid.*, **37**, 34 (1962).

(28) W. T. Raynes, A. D. Buckingham, and H. J. Bernstein, *ibid.*, **36**, 3481 (1962).

(29) The actual values used in the calculations were as follows. $\alpha = 1.12 \text{ \AA}^3$; this value was determined from the geometrical mean of the refractions of the groups³⁰ C-H (1.70) and $\overset{\text{C}}{\text{C}}\text{>N}$: (4.65).

$r = 2.21 \text{ \AA}$; this value represents the distance between proton 3 and the center of charge of the nitrogen lone pair.¹² $\nu = 50,000 \text{ cm}^{-1}$ was taken from ref. 23.

(30) C. P. Smyth, "Dielectric Behavior and Structure," McGraw-Hill Book Co., Inc., New York, N. Y., 1955.

(31) After correction for the ring current effect of the benzene group. Angle of twist assumed³² 25°.

(32) G. Favini, *Gazz. chim. ital.*, **94**, 1287 (1965).

shielding of proton 3. A still more dramatic demonstration of the shifts produced by these forces will be presented in the discussion of the n.m.r. spectrum of II.

The same calculations, performed in order to evaluate $\Delta\sigma_R$, $\Delta\sigma_N$, and $\Delta\sigma_E$ for the other protons, furnished the result that in each case $\Delta\sigma_N$ and $\Delta\sigma_E$ are very small and of opposite sign and practically cancel each other. The shifts of these protons are therefore dominated by the value of $\Delta\sigma_R$, which has to be calculated by the use of the dipole approximation. With the value of the anisotropy of benzene, recommended by Dailey³³ for use in this kind of calculation, the following values, in p.p.m., of $\Delta\sigma'_T = \Delta\sigma_R + \Delta\sigma_N + \Delta\sigma_E$ have been obtained³⁴ for protons 4, 5, and 6 in that order: -0.07 , -0.05 , -0.06 . The experimental chemical shifts of protons 4 and 6, by comparison with pyridine, are moved slightly downfield (by less than the calculated amount, however); the resonance of proton 5 occurs at higher fields. It must be inferred, therefore, that in 2,2'-bipyridyl a compensation of these small downfield shifts does occur, possibly through the polarization induced in the π system of one ring by the electric dipole field of the adjacent pyridine group.

The values for the coupling constants for I in CCl_4 solutions are to be considered normal in the sense that they follow the general pattern already observed in many other 2-substituted pyridines.^{9,10,11}

N.m.r. Spectra of 2,2'-Bipyridyl in Strong Acids (CF_3COOH). Both rings of I are protonated in solution in trifluoroacetic acid; this conclusion follows from the direct comparison of the chemical shifts measured for the protons of I (Table I) and the corresponding shifts of the pyridinium ion. The latter, for the α , β , and γ protons are¹² 535.4, 496.4, and 530.4 c.p.s., respectively. For any of the protons of I, shifts larger than the previous values have always been found experimentally. Further evidence of the complete protonation has been obtained from the constancy of these shifts to variations in the concentration of I (Table I).

By protonation, electronic charge is withdrawn toward the nitrogen from all positions in the ring; consequently, a downfield shift of the resonance of all the protons is observed. Since the magnitude of the latter is in some way¹⁵ a measure of the decrease of charge density at the carbon to which the proton is bonded, it is interesting to compare the downfield shifts, occurring by protonation, in pyridine and in each one of the rings of 2,2'-bipyridyl. For pyridine itself, these shifts, in p.p.m., for the α , β , and γ protons are²⁵ $0.357 + [0.720]$, $1.073 + [0.200]$, and $1.206 + [0.134]$, respectively. The total downfield shift³⁶ for the whole molecule is therefore equal to 6.040 p.p.m. In the protonation of I the downfield shifts of protons 6, 5, and 4 are 0.710

+ $[0.720]$, $1.217 + [0.200]$, and $1.207 + [0.134]$, respectively. For proton 3 only limiting estimates of this shift are possible. If one supposes that the whole shift,³⁷ $0.224 + [0.200] + (1.190)$, be attributed to the decrease of electronic density at the 3 position, the total downfield shift, for each of the pyridine rings, becomes 5.802 p.p.m. If, instead, the withdrawal of charge is supposed to be equal to the one occurring at the 5 position, the total shift obtained is 5.597 p.p.m. In both cases, values smaller than for pyridine are obtained, in good qualitative agreement with the highly acidic character of the dication.³⁸

There are good reasons to believe that the difference between the chemical shifts of protons 3 and 5 due to the "chemical effect" of the substitution at the 2 position lies between the values, previously calculated for 2,2'-bipyridyl, -0.15 and -0.25 p.p.m. (See next section.) If these values are subtracted from the difference of the chemical shifts of these protons determined experimentally (-0.31 p.p.m.) and the residuals attributed to the anisotropy effect of the adjacent aromatic ring, by the use of Johnson and Bovey's tables,²⁴ angles of twist³⁹ of 55° (125°) and 72° (108°) between the two rings are obtained for the dication.

In CF_3COOH solutions broadening of all the lines of the spectrum takes place.⁴⁰ Consequently, the errors of all the n.m.r. parameters, particularly of the coupling constants, increase considerably. The large changes, however, observed for some of these parameters, are safely outside the experimental error and are consistently interpretable under the assumption that by protonation the two pyridine rings become more benzene-like. In particular, J_{56} increases by about 1 c.p.s.

(33) B. P. Dailey, *J. Chem. Phys.*, **41**, 2304 (1964).

(34) Values about twice as large are obtained by the use of the experimentally measured anisotropy of benzene.

(35) The numbers in brackets represent the total "hidden" contributions to the shifts, due to the disappearance in the ion, of the anisotropy effect of the nitrogen and of the electric dipolar field effect as illustrated by Gil and Murrell.¹² In this paper, however, there is a numerical error in the calculations of the shift due to the electric field effect for the α proton. The correct value is 0.42 p.p.m.

(36) Because of the direct relationship between proton chemical shift and charge density,¹⁶ we have used this locution in order to avoid the introduction of a more or less arbitrary constant of proportionality.

(37) It must be pointed out that this represents a maximum. The anisotropic effects of the ring current at the 3 position always produce a downfield shift which may become zero for a perpendicular orientation of the two rings. The number in parentheses is $\Delta\sigma_T$ previously calculated.

(38) P. Krumholz, *J. Am. Chem. Soc.*, **73**, 3487 (1951). In the above calculations, however, no changes in the electronic densities at the carbons joining the two rings have been considered.

(39) In our notation angles of twist of 0 and 180° correspond to the *trans*- or *cis*-planar conformations.

(40) The same phenomenon has been observed¹³ in the n.m.r. spectrum of pyridine in the same medium and explained in terms of the low rate of exchange between the acid and the cation.

and becomes larger than in pyridine.⁴¹ J_{45} becomes about equal to the other *ortho* coupling constant, J_{34} , whose value is only slightly affected by protonation. J_{46} decreases by about 0.4 c.p.s., whereas J_{35} remains practically unchanged. The *para* coupling constant, J_{36} , drops from the typical value of pyridine (0.9 c.p.s.) to the more benzene-like value of 0.5–0.6 c.p.s. As a general and expected trend, the larger changes are observed for the coupling constants between protons closer to the nitrogen atom.

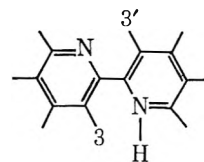
The protonation of 2,2'-bipyridyl has also been studied in solutions of mixtures of chloroform and trifluoroacetic acid (Table II). Particularly interesting is the behavior of the chemical shifts on varying the concentration of the acid (Figure 2). The chemical shifts of protons 4 and 5 decrease initially very rapidly until the monoprotonated 2,2'-bipyridyl cation is formed. Thereafter, they decrease slowly and reach their minimum values for the solution in the neat acid. The concentrations of I, used in the experiments (Table II), were such that the stoichiometric amount of acid, required for the formation of the monocation, corresponded to a mole fraction of about 0.1. The pK_a values of the mono- and diprotonated 2,2'-bipyridyl are 4.43 and -0.52 , respectively.^{38,42} Therefore, in presence of a strong acid, the first protonation occurs with about stoichiometric quantities of reagents, whereas the formation of the dication requires a large excess of acid.

The chemical shifts of protons 4 and 5 reach the values of the arithmetic means of the corresponding shifts for solutions⁴³ in CCl_4 and CF_3COOH (492.14 and 465.19 c.p.s., respectively) for a concentration of acid (~ 0.17 mole fraction) close to the stoichiometric value. These mean values have been therefore considered as the chemical shifts of these protons in the monoprotonated cation. Furthermore, hereafter the chemical shifts of protons 4 and 5 have been chosen as parameters measuring the degree of protonation in other media.⁴⁴

The behavior of the chemical shifts of protons 6 and 3 is of particular interest. The shielding of these protons is largely determined by the anisotropic and electric field effects associated with the nitrogen atom and the pyridine ring. By protonation these effects, in turn, may vary either through a change of the intensive parameter associated with each one of them—magnetic anisotropy, electric dipole, etc.—or through a variation of the geometrical parameter which determines the spatial dependence of the effect. By protonation, only the changes due to the variations of the first kind of parameters are sensed by proton 6 since its position is fixed with regard to the nitrogen in the same ring, and

the anisotropic effects due to the twisting of the two rings are very small at its position.⁴⁵ In the monocation, proton 6 resides on either the protonated ring or the other,⁴⁶ and its chemical shift is given, as for protons 4 and 5, by the mean of the shifts observed in 2,2'-bipyridyl and in the dication.

A completely different behavior is observed for the chemical shift of proton 3. In this case the downfield shift expected from the withdrawal of charge occurring during protonation is compensated by the contributions of the "hidden" shifts released by the decrease of the magnitude of the intensive parameters, as well as by the variations of the geometrical factors caused by the twisting of the two aromatic rings. Assuming a reasonable angle of twist, $\varphi = 30^\circ$, and that the downfield shift caused by the withdrawal of charge at the 3' position is equal to that occurring at position 5', the varia-



tion of the chemical shift of proton 3 (and 3') has been calculated as follows: by protonation of the adjacent pyridine ring, the resonance of proton 3 is shifted upfield by⁴⁷ $\delta\Delta\sigma_{T^3} = 0.80$ p.p.m. and the resonance of proton 3' downfield by⁴⁸ $\delta\Delta\sigma_{T^{3'}} = 1.02$ p.p.m. The net shift, resulting from the average of the calculated data, is therefore $\delta\Delta\sigma_{T^{3,3'}} = -0.11$ p.p.m. Experimentally, an extremely small upfield shift is obtained from the comparison of the chemical shifts of proton 3 in the monoprotonated species and in CCl_4 solution.⁴⁹ The

(41) W. G. Schneider, H. J. Bernstein, and J. H. Pople, *Can. J. Chem.*, **35**, 1487 (1957).

(42) F. H. Westheimer and O. T. Benfey, *J. Am. Chem. Soc.*, **78**, 5309 (1956).

(43) The average has been made with the values of the shifts in CCl_4 solutions (black symbols in Figure 2) since chloroform, like any proton-donor solvent, influences the shifts of the protons of I through the formation of hydrogen bonds with the nitrogen.

(44) The chemical shift of proton 5 should be insensitive to any variation of the anisotropic effect—ring current effect—related to twist of the two pyridine rings. Theoretically that is not true for the shift of proton 4; however, the practically complete parallelism of the two curves in Figure 2 clearly suggests that at position 4 these variations are also very poorly sensed. By symmetry the same should be true at position 6.

(45) See footnote 44 and the discussion of the previous section.

(46) Experimentally both rings give a unique n.m.r. spectrum because of the rapid rate of exchange of the H^+ ion.

(47) δ refers to the variations of the several $\Delta\sigma$ previously defined. $\delta\Delta\sigma_{T^3} = \delta\Delta\sigma_{R^3} + \delta\Delta\sigma_{N^3} + \delta\Delta\sigma_{E^3} + \delta\Delta\sigma_{W^3} = 0.10 + 0.16 + 0.25 + 0.29$.

(48) $\delta\Delta\sigma_{T^{3'}} = \Delta\sigma^{5'} + \delta\Delta\sigma_{R^{3'}} + \delta\Delta\sigma_{N^{3'}} + \delta\Delta\sigma_{E^{3'}} + \delta\Delta\sigma_{W^{3'}} = -1.42 + 0.10 + 0.08 + 0.10 + 0.12$.

calculations, however, show very well the compensating effects previously discussed and the reasons for the flat behavior of the chemical shift of proton 3 vs. the acid concentration in Figure 2.

In Table II are also reported the coupling constants found in this series of measurements. It is worthwhile to point out that the variations of these parameters more or less follow the same trend observed for the chemical shift, in the sense that about half of the change is obtained at concentration of acid corresponding to the formation of the monocation.

N.m.r. Spectra of 2,2'-Bipyridyl in Proton-Donor Solvents and in Weak Acids. In the study (Table II) of the n.m.r. spectra of 2,2'-bipyridyl in mixtures of inert (CCl_4) and proton-donor solvents (CCl_3H , CH_3OH), it was noticed that, on increasing the concentration of the latter (Figure 3), the resonance signals of protons 4, 5, and 6 moved toward lower fields, whereas that of proton 3 moved upfield.⁵⁰ In order to investigate further this anomalous behavior, we have analyzed the spectra of I in other proton-donor solvents, as well as in weak acids. The data obtained in this study are summarized in Table I and graphically displayed in Figure 4, where the chemical shifts of all the protons have been plotted vs. the chemical shift of proton 5 for all the solutions investigated in the same order as they appear in Table I. The parallelism of behavior between the chemical shifts of protons 4 and 5, already observed in mixtures of $\text{CCl}_3\text{H}-\text{CF}_3\text{COOH}$, was also found in all of the other solutions studied. Clearly noticeable, however, is the slightly sigmoid shape of the curve representing the chemical shifts of proton 4. The corresponding curve for proton 6 passes through a small minimum and a small maximum before assuming the monotonic trend toward lower fields. For this proton, however, the chemical shift (black symbols in Figure 4) always lies at lower fields in solutions of acids than in other solvents. The chemical shift of proton 3 increases initially about linearly, passes through a pronounced maximum, and then decreases with an increase of the acidity of the medium.

Focusing attention on the behavior of the chemical shift of the latter proton, we interpret the data of Figure 4 as follows: in proton-donor solvents or weak acids, 2,2'-bipyridyl forms a 1:1 complex by hydrogen bonding between the nitrogen and the acidic proton of the medium. The formation of the hydrogen bond would involve pronounced twisting of the two pyridine rings about the central single bond which in turn determines, through a decrease of $\Delta\sigma_N$, $\Delta\sigma_E$, $\Delta\sigma_W$, and mainly of $\Delta\sigma_R$, the upfield shift observed for proton 3. In more strongly acidic media, one or two protons are transferred completely from the acid to the pyridine

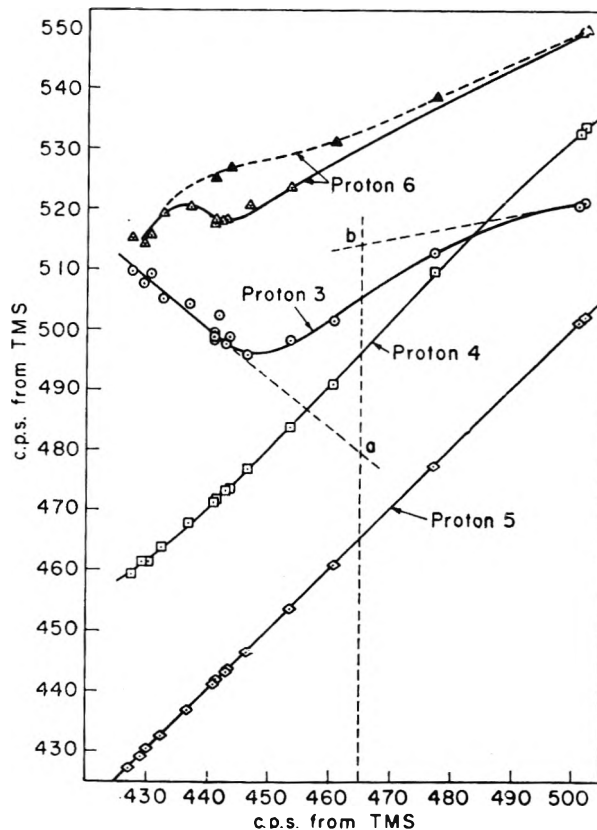


Figure 4. Plot of the chemical shifts of the protons of 2,2'-bipyridyl vs. the chemical shift of proton 5.

nitrogens, and, because of the smaller steric requirement of the proton, the angle of twisting is less, and the downfield trend of the chemical shift of proton 3 is established.

In order to formulate quantitative estimates of the phenomena observed, we have assumed that in proton-donor solvents or in weak acids only 1:1 complexes are involved⁵¹ in the equilibrium between 2,2'-bipyridyl and the medium. We have also assumed that the chemical shifts of the protons in the complex, no matter which the partner in the association,⁵² differ from the

(49) If the same calculations are repeated by assuming a nonplanar *cis* conformation ($\varphi = 150^\circ$), an upfield shift $\delta\Delta\sigma_{T^{2,3,7}} = 0.11$ p.p.m. is obtained. No conclusion, however, may be drawn from these calculations since other types of interactions occur at high concentrations of CCl_3H . See next section.

(50) This trend in solutions in CH_3OH has also been reported by Gil.⁴

(51) This assumption has been made according to the weak basicity already established for the 2,2'-bipyridyl monocation. It may not be true for solutions in stronger acidic media corresponding to the central part of Figure 4; this, however, does not invalidate the rationalization scheme given below.

(52) In the spectrum of $[\text{Fe}^{II}(\text{C}_{10}\text{N}_2\text{H}_8)_3]\text{Cl}_2$ the chemical shift of proton 4 is identical with the value found for the monocation. The chemical shift of proton 5 is only slightly different than the corresponding shift in the monocation; this difference, as well as those observed for protons 6 and 3, is, however, clearly attributable to the particular geometry of the molecule. See next section.

ones in the monocation only by virtue of the electric and magnetic shielding effects brought about by the different dihedral angles between the pyridine rings.

With these assumptions, the data on the left-hand portion of the curve of the chemical shifts of proton 3 have been interpreted as representing the weighted average of the shifts of this proton, over the species present at equilibrium (2,2'-bipyridyl and complex); the position of the equilibrium being determined by the different nature of the solvents used in the experiments. We draw a tangent to the curve, from the extreme left; the point a, where this tangent intersects the vertical line drawn from the chemical shift of proton 5 in the monocation, is taken as the chemical shift of proton 3 in the complex. The value so found (480 c.p.s.) differs by 0.46 p.p.m. from the corresponding shift obtained experimentally for proton 3 in 2,2'-bipyridyl (CCl₄ solution).

According to the scheme of calculation described in the preceding section, the values of $\delta\Delta\sigma_T^{3,3'}$ (upfield shifts) calculated for dihedral angles of 60, 70, 80, 90, 100, 110, and 120° are, respectively, 0.30, 0.38, 0.45, 0.47, 0.46, 0.42, and 0.35 p.p.m. From the direct comparison between the experimentally derived and calculated values, we argue that in the hydrogen-bonded complex the dihedral angle between the two pyridine rings lies between 80 and 100°. It is interesting to note that a dihedral angle within these limits is probably best suited for an intramolecular exchange of the hydrogen bond between the nitrogens of the two rings. It is also worthwhile to mention that the calculated chemical shift of proton 3 lies 0.25 p.p.m. downfield from the chemical shift of proton 5; in view of all the simplifications involved in all this kind of calculations, this is in excellent agreement with the corresponding difference calculated for 2,2'-bipyridyl in the *trans*-planar conformation (-0.15 p.p.m.).

In the central and right-hand portions of Figure 4 much more complex equilibria are probably involved. We consider that toward the extreme right side of Figure 4—between the points corresponding to solutions in α -bromopropionic and trifluoroacetic acids—the main species present at equilibrium are the mono- and dications. Using the same arguments previously given,⁵³ we have drawn the tangent from the extreme right side of the curve and considered point b, in which it intersects the vertical line at 465 c.p.s., as the chemical shift of proton 3 in the monocation. This point lies 0.11 p.p.m. to lower field from the corresponding shift found in 2,2'-bipyridyl (CCl₄ solution) in excellent agreement with the value calculated, in the preceding section, from an estimated angle of twist of 30°. ⁵⁴

The behavior of the chemical shifts of proton 4 has

also been found to be in good agreement with the assumptions made. The small anisotropic effect felt at this position and due to the twisting out of plane of the two rings should move the resonance of this proton slightly upfield producing the observed upward convexity of the curve on the left side of Figure 4. On the right side of Figure 4, the anisotropic effect should produce shifts in the opposite direction, causing the observed upward concavity.

For proton 6, the assumption that the nature of the complexing solvent molecule does not influence directly the chemical shift is not correct. The clearly different behavior of the shifts of this proton in solvents containing the carbonyl group, as compared to the behavior in other solvents, strongly suggests that the electric field and magnetic anisotropic effects produced by the proximity of the incoming proton-donor group are noticeably sensed at this position. These differences of behavior should, however, be lessened by the occurrence of true protonation, and under this assumption the full and dashed lines of Figure 4 have been merged at the points corresponding to solutions in CF₃COOH. Any attempt to rationalize the minimum and the maximum presented by the shifts in nonacidic media, in terms of the twisting of the two pyridyl rings, must also be regarded with skepticism because of the different electric and magnetic properties of CCl₃H (points near the minimum) and of the solvents containing the alcoholic group (points near the maximum).

The changes in the coupling constants observed in these media are similar to the ones already discussed for solutions in CCl₃H-CF₃COOH mixtures and do not require further comment.

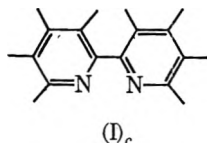
N.m.r. Spectrum of [Fe^{II}(C₁₀N₂H₈)₃]Cl₂. The parameters resulting from the analysis of the n.m.r. spectrum of II in CH₃OH solution are given in the last line of Table I. Particularly interesting is the switch of the resonances of protons 3 and 6, which causes the loss of any resemblance of the spectrum (Figure 1) with the pattern characteristic of the n.m.r. spectra of α -substituted pyridines. With references to the shifts assigned to the protons of the complex formed by hydrogen bonding in proton-donor solvents (point a, for proton 3 and, similarly, the other points in which the vertical line intersects the curves in Figure 4), only the chemical shift of proton 4 remains unchanged. The resonance of proton 3 is shifted downfield by 0.85 p.p.m.

(53) As in the case of the complex, it has been here assumed, *mutata mutandis*, that the presence of different counterions does not change sensibly the chemical shifts of the protons in the cations.

(54) This agreement strongly supports a *transoid* skew conformation of the monocation. By induction it is very likely that the dication is also in the same conformation, the dihedral angles being, of course, different for the two species.

and that of proton 5 and 6 upfield by 0.16 and 1.28 p.p.m., respectively.

The ion $[\text{Fe}^{\text{II}}(\text{C}_{10}\text{N}_2\text{H}_8)_3]^{2+}$ is an octahedral complex⁵⁵ in which the bipyridyl groups are fixed in the *cis*-planar conformation (I)_c with the nitrogens of the three group



arranged⁶⁶ approximately at the corners of a regular octahedron.

Protons 3 and 3' lie, therefore, very close to each other, and the van der Waals forces are expected to contribute substantially, together with the anisotropic effect of the ring current, to the observed deshielding. By the use of the equations already described, total downfield shifts⁵⁷ ($-\Delta\sigma_{\text{T}}^3$) of 0.86 and of 0.77 p.p.m. have been, respectively, calculated with Buckingham's and Musher's coefficients. The agreement between calculated and experimental values is surprisingly good and gives further support to the results obtained by the extrapolation in the previous section and to the conclusions there drawn. It is also worthwhile to underline, once again, the large contribution ($\sim 40\%$) of the dispersive forces to the total shielding.

By the use of a model it may be noticed, at once, that in II, proton 6 lies very close to and above the plane of the pyridine ring of a second ligand group. The reason for the large upfield shift of this proton is thereby clear. The magnetic anisotropy of the same pyridine ring in the second ligand group is also responsible for the shift toward higher fields of the resonance of proton 5.

We have reported in Table IV, the shieldings of protons 5 and 6 as calculated from the geometry of the molecule and the use of the tables of Johnson and Bovey²⁴ by varying the distance D between the center of the carbon-carbon bond joining the two rings and the Fe atom. Also reported in Table IV for each value of D is the corresponding distance ($D_{\text{Fe-N}}$) between the iron and nitrogen. For proton 6 the shielding of 1.28 p.p.m., previously estimated, corresponds to an Fe-N distance of about 2 Å, which is in excellent agreement with the expectation.⁵⁸ For the same distance, the calculated value $\Delta\sigma_{\text{R}}^5 = 0.28$ p.p.m. is a little larger than the one estimated from Figure 4, but still in reasonable agreement, in view of the approximations involved in the assumptions made about the geometry of the molecule.

Finally, it is interesting to note in Table I the large values—of the same order of magnitude of the ones observed for 2,2-dipyridyl in CF_3COOH solutions—of

Table IV: Calculated Values of the Shielding of Protons 5 and 6 in $[\text{Fe}^{\text{II}}(\text{C}_{10}\text{N}_2\text{H}_8)_3]\text{Cl}_2$

D^a	$D_{\text{Fe-N}}^b$	$\Delta\sigma_{\text{R}}^{5c}$	$\Delta\sigma_{\text{R}}^{6c}$
2.00	1.56	0.53	3.97
2.50	1.86	0.34	1.81
2.65	1.97	0.30	1.37
2.75	2.04	0.27	1.12
3.00	2.23	0.22	0.69

^a Distance (in Å.) between the carbon-carbon bond joining the two rings and Fe. ^b Distance (in Å.) between iron and nitrogen. ^c Shieldings in p.p.m.

J_{35} , J_{46} , and J_{56} against the stationary values of the other coupling constants.

Conclusions

It has been shown that in 2,2'-bipyridyl several effects contribute in producing the large downfield shift observed in the resonance of proton 3. The van der Waals forces are among these, and their contribution to the deshielding is large any time the geometry of the molecule allows for close contact between protons or between protons and nitrogen lone-pair electrons. The results of this study support the proposal of Schaefer, Reynolds, and Yonemoto⁵⁹ that intramolecular dispersion forces may play an important role in determining proton chemical shifts.

The n.m.r. parameters found in this study are consistent with a *trans*-planar conformation ($\varphi = 0^\circ$) of 2,2-bipyridyl in inert solvents, and with *trcnsoïd* skew conformations of the monocation ($\varphi = 25\text{--}30^\circ$) and of the dication ($\varphi = 55\text{--}72^\circ$) in solutions in strong acids.⁶⁰

(55) A. F. Wells, "Structural Inorganic Chemistry," Oxford University Press, London, 1962.

(56) Since no crystallographic data are available, we have maintained the same molecular parameters given for the *trans*-planar conformation¹⁸ and have merely rotated the two rings by 180° . We have also assumed that the bonds Fe-N are directed as the lines passing through the nitrogen and the γ proton of each ring, which intersect at an angle smaller than 90° .

(57) $\Delta\sigma_{\text{T}}^3 = \Delta\sigma_{\text{R}}^3 + \Delta\sigma_{\text{W}}^3 = -0.49 - 0.37 = -0.86$ p.p.m. (Buckingham's equation) and $\Delta\sigma_{\text{T}}^3 = \Delta\sigma_{\text{R}}^3 + \Delta\sigma_{\text{W}}^3 = -0.49 - 0.28 = -0.77$ p.p.m. (Musher's equation). The symbol δ has been dropped since the shieldings are calculated with reference to the chemical shifts in a conformation ($\varphi = 90^\circ$) in which $\Delta\sigma_{\text{R}} = \Delta\sigma_{\text{W}} = \Delta\sigma_{\text{N}} = \Delta\sigma_{\text{E}} = 0$. The parameters used in the calculations were $\tau = 1.94$ Å., $\alpha = 0.67$ Å.³, and $\nu = 50,000$ cm.⁻¹.

(58) The sum of the covalent radii⁶⁶ of Fe^{II} (1.23 Å.) and of N (0.74 Å.) is 1.97 Å.

(59) T. Schaefer, W. F. Reynolds, and T. Yonemoto, *Can. J. Chem.*, **41**, 2969 (1963).

(60) For the monocation the conclusions drawn in this paper do not agree with the structure proposed by Nakamoto²⁰ from the analysis of ultraviolet spectroscopic data obtained in aqueous acidic solutions. It must be pointed out, however, that our experimental data in proton-donor solvents do not exclude the possibility of more complex equilibria in the central region of Figure 4. Solvation processes may be very effective in producing variations of the dihedral angles proposed for the monocation.

In proton-donor solvents, the formation of hydrogen-bonded complexes is consistently interpreted in terms of a perpendicular orientation ($\varphi = 80\text{--}100^\circ$) of the two pyridine rings. For the iron complex $[\text{Fe}^{\text{II}}(\text{C}_{10}\text{N}_2\text{H}_8)_3]\text{Cl}_2$ the *cis*-planar conformation of the pyridyl groups has been found perfectly in line with the measured values of the chemical shifts. From the latter data a metal-nitrogen distance of 2 Å. has been derived.

Finally, we want to point out that, although only static molecular models have been used in the calculations, the dihedral angles proposed must be interpreted as averaged positions of equilibrium over all the possible vibrational and torsional states present in the molecule. Several secondary effects (reaction field

effect,²² electric field effect due to the presence of positive charges on the nitrogens in the cations, etc.) have not been taken into account; it is very likely, however, that their contributions to the chemical shifts are small and do not invalidate the internally consistent interpretation of the results presented in this paper.

Acknowledgments. We are profoundly indebted to Dr. A. A. Bothner-By for many helpful and constructive suggestions given to us during the course of the present work as well as for reading this manuscript. Computations were performed at the University of Pittsburgh Computer Center with the partial support of the National Science Foundation.

Dielectric Dispersion of Crystalline Powders of Amino Acids, Peptides, and Proteins¹

by S. Takashima and H. P. Schwan

Electromedical Division, Moore School of Electrical Engineering, University of Pennsylvania, Philadelphia, Pennsylvania (Received June 17, 1965)

The dielectric constants of crystalline powders of glycine, tyrosine, glycyglycine, and ovalbumin were measured in the frequency range of 20 c.p.s. to 200 kc.p.s. It was found that dry crystals did not have an appreciable dielectric constant but that adsorbed water increased the dielectric constant markedly. The static dielectric constants, their dispersions, and the dielectric losses were measured with varied amounts of adsorbed water. The increase of the dielectric constant is proportional to the increase of water of adsorption until the first water layer is completed. The second and third layers are formed if the vapor pressure is increased. The dielectric constant, however, does not increase any more and practically levels off. The formation of multilayers does not seem to affect the dielectric constant of crystals. Apparently, only the first layer of water of adsorption makes the major contribution to the dielectric constant of wet crystals.

Introduction

The dielectric constants of crystalline powders of amino acids, peptides, and proteins were measured by Bailey² in the dry and wet state. His results indicate that these materials have very small dielectric constants when they are carefully dried. He observed,

however, that the adsorption of water was accompanied by considerable increases in the dielectric constant and the dielectric loss. Unfortunately, Bailey

(1) This study was supported by National Institutes of Health Grant No. 1253.

(2) S. T. Bailey, *Trans. Faraday Soc.*, **47**, 509 (1951).

did not establish complete dispersion curves, probably because of the frequency limitation of his instrument.

The dielectric constant of sodium bicarbonate crystalline powder was studied by O'Konski.³ He observed that bicarbonate crystals did not have an appreciable dielectric constant when they were thoroughly dried but that a small amount of adsorbed water increased the dielectric constant markedly. The crystals of ferroelectric potassium dihydrogen phosphate, however, showed a considerably larger dielectric constant than those of sodium bicarbonate, even in the dry state.

On the other hand, the dielectric constants of microscopic particles of synthetic polymers, clay, and living cells have been extensively investigated by Fricke, Cole, and Schwan.⁴ The enormously large dielectric polarization in the low-frequency region is evidently not due to particle orientation but is considered to be due to the time-dependent surface conductance of these particles. The frequency-dependent character of this surface conductance is explained by Schwarz⁵ to be the result of counterion movement.

The purpose of this experiment is to establish the static dielectric constant and dispersion of crystalline materials and to analyze the mechanism of the dielectric polarization in terms of the electrical double layer formed between the crystal surface and the water of adsorption.

Technique and Materials

Impedance Bridge. The bridge has been designed and constructed to meet a wide range of requirements of conductivity and capacity within a frequency range from 20 c.p.s. to 200 kc.p.s. The details of this bridge are given in review articles by Schwan.^{6,7}

Electrode Polarization and Sample Cell. Since the dielectric constant of these materials exhibits an anomalous dispersion in the audiofrequency range, correction for electrode polarization errors is crucial in order to obtain significant dispersion curves. Noting that the electrode admittance is in series with the admittance of the sample, the following derived equation is pertinent^{7,8}

$$C = C_s + 1/\omega^2 R^2 C_p \quad (1)$$

where C is the total observed capacity, C_s is the capacity of the sample, ω is the angular frequency, R is the resistance, and C_p is the electrode capacity. The following technique was chosen to facilitate the use of eq. 1.⁸ It is known that the electrode polarization capacity varies as a power function of frequency, and the power factor is usually between 0.3 and 0.5. Hence, in a plot of $\log C$ against $\log f$, a straight line results with a slope of about -1.6 if C_s is small compared

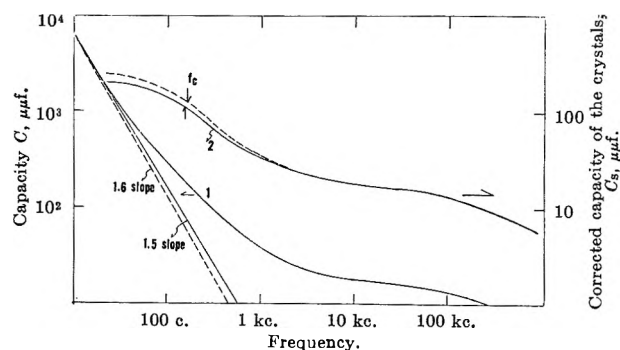


Figure 1. Logarithmic plot of the electric sample capacity C of glycine crystals against frequency: curve 1, the total capacity before correction; curve 2, the capacity after correction. Curve 2 is obtained by taking the difference between curve 1 and the limit slope of 1.5. The dashed curves pertain to a slope value of 1.6. They are shown to demonstrate the effect of the chosen slope value on the dispersion curve and the insensitivity of the characteristic frequency f_c (arrow) from the limiting slope.

to the second term of the equation, *i.e.*, at sufficiently low frequencies. If C_s is appreciable, a curve will result which will deviate from this straight line. Thus, by taking the difference between the experimental curve and the limiting slope, approached at very low frequencies, we can obtain the true capacity of the sample. The validity of this procedure is illustrated by the example in Figure 1, using a dilute KCl solution.

This correction procedure also permits evaluation of the electrode polarization capacitance C_p . C_p data, presented in Table I, increase rapidly with increasing water content according to an approximate relationship, $C_p = aw^m$, where w is water content. The data in Table I indicate m to be between 3 and 4. Extrapolation to 100% water content gives quite reasonable C_p values near 100,000 μf . Note that the strong dependence of C_p on the water content w readily can be rationalized. The polarization capacitance is determined by the amount of electrode area in contact with the water of adsorption. If C_p were in direct proportion to this contact area, C_p would change in proportion to w . However, each particle near the electrodes exerts a restriction on the current

(3) C. T. O'Konski, *J. Am. Chem. Soc.*, **73**, 5093 (1951).

(4) (a) See the review article by H. P. Schwan, *Advan. Biol. Med. Phys.*, **5**, 148 (1957); (b) H. P. Schwan, G. Schwarz, J. Maczuk, and H. Pauly, *J. Phys. Chem.*, **66**, 2626 (1962).

(5) G. Schwarz, *ibid.*, **66**, 2636 (1962).

(6) H. P. Schwan and K. Sittel, *Trans. AIEE*, **114** (1953).

(7) H. P. Schwan, "Physical Techniques in Biological Research," Vol. 6, Academic Press Inc., New York, N. Y., 1963, p. 323.

(8) H. P. Schwan, *Z. Naturforsch.*, **6b**, 121 (1951).

strength at the electrode surface. This restriction effectively causes C_p to decrease as w decreases.⁸ Thus, C_p should change more rapidly than linearly with w .

In the case of pronounced electrode polarization, the accuracy with which the low-frequency limit of the dielectric constant ϵ_0 can be stated is poorest and is about 20% as indicated in Figure 1. This figure demonstrates a case in which electrode polarization is particularly prominent. Even here it is possible readily to establish the limiting slope of about 1.6. This slope of about 1.6 is, of course, characteristic of the second term of eq. 1 even in cases where polarization at the electrodes does not contribute strongly. In such cases, the ordinate level at which the limiting slope curve must be placed in order reasonably to explain the observed data is usually rather well defined. Usually ϵ_0 and the characteristic frequency can be estimated with an accuracy of about 10%. In cases of still lesser contribution of the electrodes to the total polarization, correction techniques can be omitted altogether. More detailed discussions of the limitations of this technique are in ref. 8.

Table I: Increase of Electrode Polarization with Increasing Water of Adsorption^a

Water content, %	Resistance, ohms	C_p
0.15	10^9	33.3 $\mu\mu\text{f.}$
0.20	5×10^8	60.6 $\mu\mu\text{f.}$
0.67	10^7	44,000 $\mu\mu\text{f.}$ (0.044 $\mu\text{f.}$)
1.50	5×10^6	0.13 $\mu\text{f.}$
2.50	3×10^6	0.58 $\mu\text{f.}$

^a Frequency 20 c.p.s., electrode area 4.4 cm.².

A dielectric cell, the details of which are described in a previous publication,⁷ was used. It consists of two parallel platinum electrodes whose diameter is 2.54 cm. Stray field errors cancel out since the sample thickness is small compared with its diameter, and the results obtained with the filled and the empty sample cell are subtracted from each other. Capacitance and conductance values as measured by the bridge are converted into dielectric constants and conductivities by using cell constants which are calculated from the geometry of the sample.

Materials and Procedure. Dried crystalline powders of amino acids, peptides, and proteins, spread in petri dishes as thin layers, were placed in a desiccator over a small amount of water. After some time, an

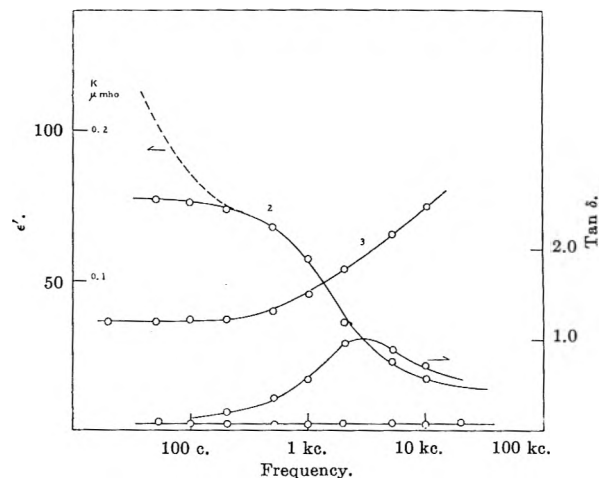


Figure 2. Dielectric dispersion and loss tangent of glycine crystals: curve 1, dry crystal; curve 2, dielectric constant with 0.67% water; curves 3 and 4, the specific conductivity and the loss tangent of the same sample. The dashed branch of curve 2 holds before electrode polarization is corrected for.

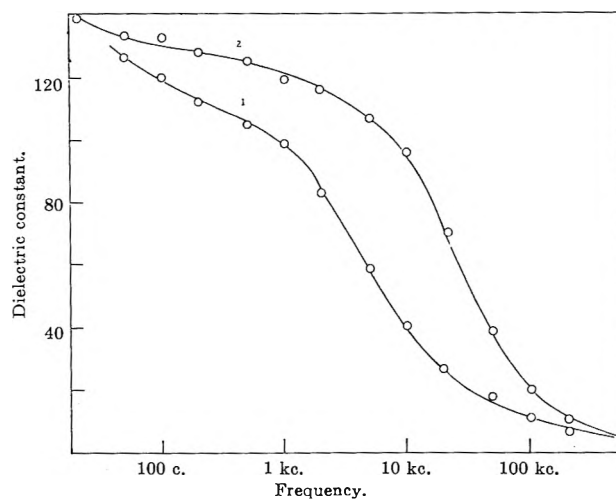


Figure 3. Dependence of the dielectric dispersion of solid glycine on the crystal size: curve 1, average diameter 0.3–0.5 mm.; curve 2, 0.02–0.08 mm. Curves are not corrected for a small electrode polarization contribution at low frequencies. Water content is 2.5%.

aliquot of the powder was examined for its water content. The rest of the powder was placed in the cylindrical test cell and pressed moderately between the electrodes, which were usually heavily platinized with platinum black. The polarization capacity as determined with a 0.1 N NaCl solution was about 200,000 $\mu\text{f.}$ at 20 c.p.s. for the total area of the electrode.

Results

Glycine. The dielectric constant of a dry crystalline powder of glycine is shown by curve 1 in Figure 2.

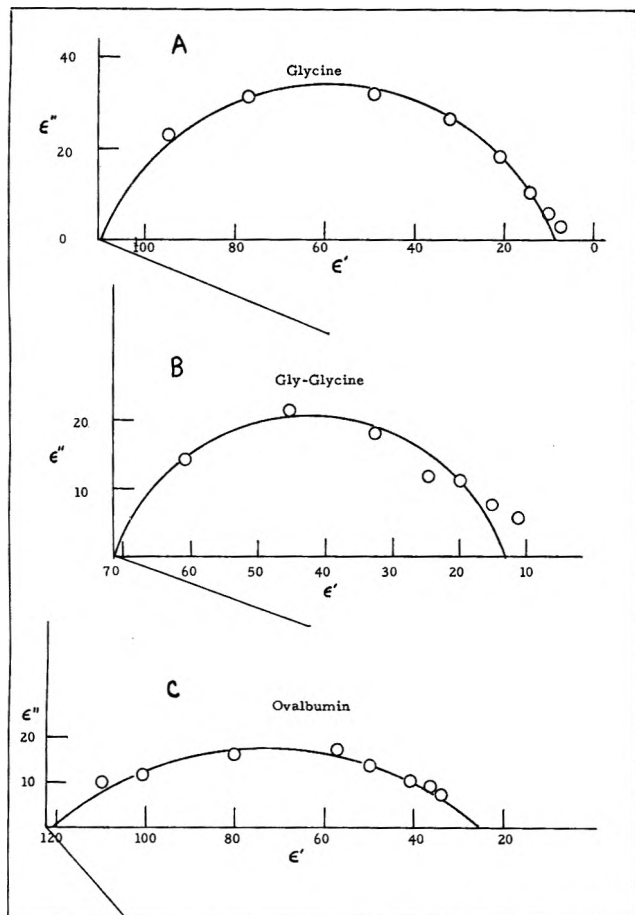


Figure 4. Cole-Cole plot of (A) glycine with 1.5% water, (B) glycyglycine with 1.0% water, and (C) albumin with 11% water.

The dielectric constant is very small even at 20 c.p.s., and the dielectric loss of the sample is negligible over the whole frequency range. However, as the water content is increased, the dielectric constant and the dielectric loss increase rapidly, as shown by curves 2 and 3 in the same figure.

The effect of crystal size was studied with coarse crystals whose average diameter was about 0.3–0.5 mm. and a fine powder of particles whose average diameter was 0.02–0.08 mm. As illustrated in Figure 3, the size of the crystals does not have a marked effect on the magnitude of the dielectric constant, but it greatly influences the relaxation times. The dispersion curve shifts considerably towards higher frequencies with smaller particle size, indicating that the relaxation time decreases as the particle size decreases.

The dielectric loss of the glycine crystals was calculated according to the equation $\epsilon'' = [(\kappa - \kappa_0)/\omega]\epsilon_r$, where ϵ'' is the dielectric loss, κ_0 is the conductivity approached at low frequency, ω is the angular frequency,

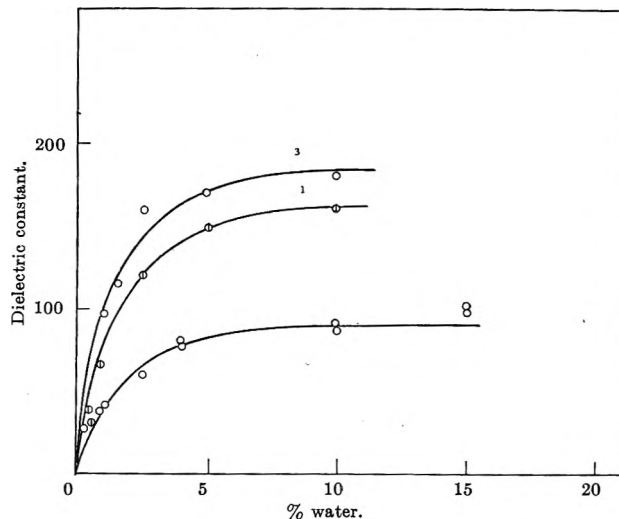


Figure 5. Plot of the static dielectric constant ϵ against the amount of water of adsorption: curve 1, glycine; curve 2, glycyglycine; curve 3, tyrosine.

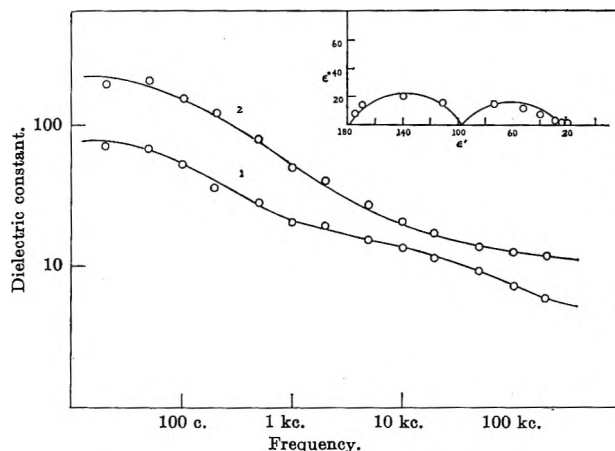


Figure 6. The dielectric dispersion of (1) glycyglycine with 2.5% water and (2) tyrosine with 2.5% water. The figure in the upper corner shows a Cole-Cole plot for tyrosine crystals.

and $\epsilon_r = 8.85 \times 10^{-14}$. The real and imaginary parts of the dielectric constant were plotted on a complex plane. The resultant Cole-Cole plot is shown in Figure 4. The Cole-Cole parameter which indicates the distribution of relaxation times is found to be 0.25. The loss tangent was calculated by $\tan \delta = \epsilon''/\epsilon'$.

The low-frequency dielectric constant ϵ_0 for the crystalline powder of glycine changes with its water content as shown in Figure 5 (curve 1). The curve consists of two parts: (1) below 5%, the dielectric constant increases very rapidly; (2) above 5%, the dielectric constant tends to level off and reaches a constant value.

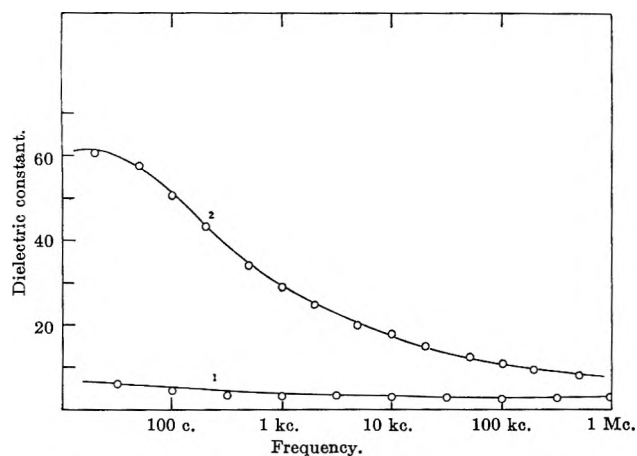


Figure 7. The dielectric dispersion of ovalbumin at low (curve 1) and 11% water content (curve 2).

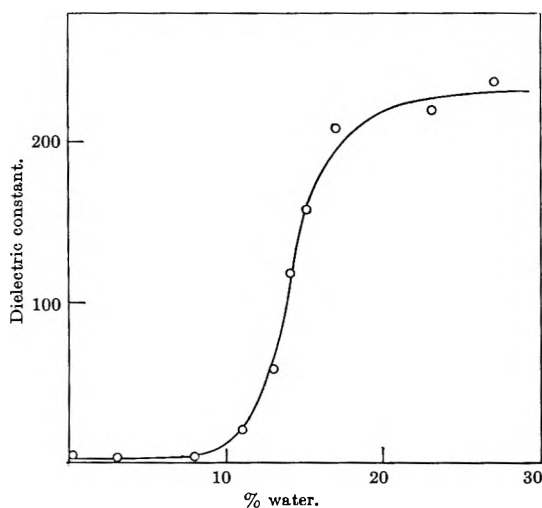


Figure 8. The static dielectric constant of albumin crystals as function of water content. The data in Figures 7 and 8 were obtained by Takashima at the Institute for Protein Research, Osaka University.

Tyrosine. In spite of the much smaller solubility of tyrosine in water, the dielectric behavior of the tyrosine crystals is qualitatively the same as that of glycine (Figure 6, curve 2). However, the shape of the dispersion curves is very flat, indicating a wide distribution of relaxation times. The Cole-Cole plot, also shown in Figure 6, indicates perhaps two circular portions, suggesting that the dielectric behavior of tyrosine crystals involves two separate relaxation processes. The relationship between the dielectric increment and the water content is shown in Figure 5 (curve 3).

Glycylglycine. The dielectric dispersion of crystalline glycylglycine is shown in Figure 6. Apparently, it exhibits two dispersion curves, but the magnitude of

the one at the higher frequency region is not clearly established. The Cole-Cole plot, which is shown in Figure 4 (B) does not strongly indicate a dual circle, and the distribution parameter obtained from this plot corresponds to a fairly well-defined spectrum of relaxation times. The dielectric increment of glycylglycine crystals is plotted against the water content in Figure 5 (curve 2). Obviously, the saturation level of ϵ_0 is considerably smaller than for glycine and tyrosine.

Ovalbumin. The dielectric dispersion of freeze-dried powder is shown in Figure 7 (curve 2). This specimen, however, was found to contain approximately 10 to 11% water. Although we were not able to remove with certainty all of the water molecules from the proteins, we assumed that another specimen which was dried over phosphorus pentoxide under vacuum was a dry protein. The dielectric constant of this dry powder is shown in Figure 7 (curve 1). As shown, the dielectric constant of the dry ovalbumin powder is as small as 2-3 in the frequency range between 60 c.p.s. and 200 kc. p.s. It, therefore, is obvious that the electric polarization of the freeze-dried powder is due to water of hydration or adsorption.

The dispersion curves are very flat which indicates a wide distribution of the relaxation times. The Cole-Cole plot is shown in Figure 4. In contrast to those of glycine and glycylglycine, the distribution parameter is much larger, and a value 0.41 was obtained. The relationship between the dielectric constant ϵ_0 and the water content is shown in Figure 8. It is worth noting that the curve consists of three portions. Up to a water content of 10%, the dielectric constant is independent of the water content, and the value is close to 3 or 4. The dielectric constant increases rapidly between 10 and 20% and then slows down above 20%.

Fuoss-Kirkwood Plot. Since the Cole-Cole distribution parameters of some crystals such as ovalbumin were observed to be large, the Cole-Cole plot was not suitable for an accurate determination of α . A different method was introduced by Fuoss and Kirkwood⁹ which often gives better results. Their equation states

$$\epsilon''/\epsilon_m'' = \operatorname{sech} \left(\beta \ln \frac{f}{f_m} \right) \quad (2)$$

where ϵ_m'' is the imaginary dielectric constant at the maximum of the dielectric loss, f_m is the frequency at maximum loss, and β is a distribution parameter which is numerically different from the Cole-Cole parameter.

(9) R. M. Fuoss and J. G. Kirkwood, *J. Am. Chem. Soc.*, 63, 385 (1941).

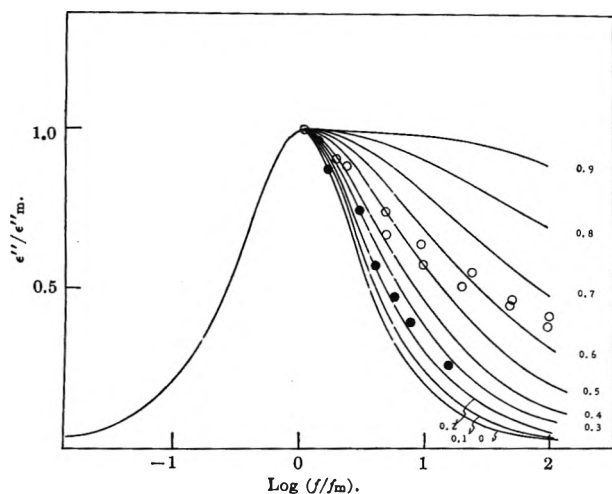


Figure 9. Fuoss-Kirkwood plot. Solid lines are theoretical curves for various values of β . The low-frequency side of the plot is omitted because of symmetry: open circles, ovalbumin; closed circles, glycine.

The relationship between this parameter and the Cole-Cole parameter is given by the following good approximation

$$\beta\sqrt{2} = \frac{\alpha}{\cos \frac{\pi}{4}} \quad (3)$$

Plots of the Fuoss-Kirkwood equation are given in Figure 9. The curves are fairly close to each other when β is small. They separate more as β becomes larger. The dielectric losses of glycine fit the curve $\beta = 0.2$. This value converts to the Cole-Cole parameter ($=0.27$) which is in excellent agreement with the value obtained from the Cole-Cole plot.

The Fuoss-Kirkwood plots of two samples of albumin also are shown in Figure 9. Obviously these data do not fit the Fuoss-Kirkwood plot. Hence, the dielectric dispersion of albumin involves a different distribution function of relaxation times than that in the underlying equation (2).

Discussion

Carefully dried crystalline powders of glycine, glycyglycine, and protein have low and nearly frequency-independent dielectric constants even at very low frequencies. This fact suggests that the individual molecule in the crystals has no freedom of rotation and that the contribution of ion transfer to the polarization in a dry crystal is negligible for the frequencies employed.

It was already found by Bailey that the dielectric constant of crystalline powders of dipolar ions increased with an increasing amount of water of adsorption.

He did not, however, establish the static, low-frequency dielectric constant of these crystals, probably owing to a limitation of his instrumentation. By using high-resolution, low-frequency techniques, we succeeded in determining the low-frequency, static dielectric constants of various crystals with various amounts of water of adsorption. The wet crystals exhibit an anomalous dispersion even below 1 kc., and static dielectric constant values are first approached below 100 c.p.s.

The increased dielectric constant of wet crystals may be caused by a conductivity on the surface between the adsorbed water and the crystal surface.^{4,5} The rapid increase of the dielectric constant at the early stage of adsorption is proportional to the increase of the surface area which is covered by the adsorbed water. Thus, the linear increase of the dielectric constant with the initial increase in adsorbed water could be easily understood.

The dielectric constant levels off sharply near a 2.5% water content. This may indicate some change in the properties of the crystal surfaces. It is interesting to note that the actual adsorption isotherms of dipolar ion crystals show an obvious break at a water content level near 2-5%,¹⁰⁻¹² and additional adsorption, if any, proceeds with a smaller slope. According to the theory of Brunauer, Emmet, and Teller,¹³ the change of the slope is due to the completion of the first layer of adsorbed water, and the further rise of the adsorption curve is due to the formation of additional layers. The fact that both dielectric constant and adsorption curve change slope at nearly the same water content value may indicate that the leveling off of the dielectric constant is due to the completion of the first layer of adsorbed water. It is not understood why the water in excess of 2-3% which probably forms additional layers does not contribute to the polarizability of the wet crystals.

The mean thickness of the water layer at 2.5% water content can be calculated to check the above hypothesis. If we assume that all water molecules are adsorbed on the surface of the crystals and do not penetrate into the crystals, we can estimate the thickness of the water layer by the formula

$$\Delta R = R \left(\frac{1}{\sqrt[3]{1-w}} - 1 \right) \sim \frac{R}{3} w \quad (4)$$

(10) H. Bull, *J. Am. Chem. Soc.*, **66**, 1499 (1944).

(11) W. S. Hnojewyj and L. H. Reyerson, *J. Phys. Chem.*, **65**, 1694 (1961).

(12) R. L. Altman and S. W. Benson, *ibid.*, **64**, 851 (1960).

(13) S. Brunauer, P. H. Emmet, and E. Teller, *J. Am. Chem. Soc.*, **60**, 309 (1938).

where ΔR is the thickness of the water layer, R is the mean radius of the crystals assuming spherical shape, and w is the weight fraction of water.¹⁴ For example, assuming 2.5% adsorbed water, the water layer thickness ΔR on a crystal for which $R = 0.002$ cm. is about 1600 Å., which is far more than the thickness of a single water layer. Clearly, either the assumption that the water of adsorption does not penetrate into crystals is wrong or the concept that leveling off of the curves occurs upon completion of a monolayer of water is erroneous.

An alternative explanation is to assume that leveling off of the curves of the dielectric constant takes place when the water layer is sufficiently thick so that the electrical double layer can be completed. The thickness of electrical double layers ranges from 3 to 30 Å. for moderate ionic strength values. These values are still much smaller than 1600 Å. In any case, the assumption that the water of adsorption does not penetrate into the crystals is an oversimplification, and it is

reasonable to assume that water molecules go into the crystals and occupy interstitial spaces.

As shown in Figure 8, the relationship between the water of adsorption and the static dielectric constant of protein crystals is much more complicated than in the case of amino acid crystals. The dielectric constant of protein crystals is not affected by the adsorption of water until the water content is about 10–12%. A similar phenomenon was observed also by Rosen,¹⁵ with various proteins, and it seems to be a general characteristic of the water of adsorption on protein crystals. No detailed explanation may be given of this observation at present.

(14) This equation was derived on the assumption that crystals are spherical with a radius of R and that the thickness of the water layer is ΔR . Then, the volume fraction of adsorbed water will be

$$V = \frac{4/3\pi(R + \Delta R)^3 - 4/3\pi R^3}{4/3\pi(R + \Delta R)^3}$$

from which eq. 4 is obtained.

(15) D. Rosen, *Trans. Faraday Soc.*, **59**, 489, 2178 (1963).

Complex Modulus of Concentrated Polymer Solutions in Steady Shear¹

by Kunihiro Osaki, Mikio Tamura, Michio Kurata, and Tadao Kotaka

*Department of Industrial Chemistry and Institute for Chemical Research,
Kyoto University, Kyoto, Japan (Received June 18, 1965)*

Complex moduli of concentrated polymer solutions in steady shear were measured with a rheometer of the coaxial cylinder geometry. The outer cylinder was given a synthetic motion of pure rotation and sinusoidal oscillation, and the inner cylinder was suspended concentrically in the outer cylinder by a torsion wire. The oscillatory part of the inner cylinder motion was detected separately from the stationary part of the motion to determine the complex modulus $G_{\kappa}^*(\omega)$ as a function of angular frequency ω for various fixed values of the rate of the superimposed shear κ . Measurements of the complex modulus with superimposed steady shear, $G_{\kappa}^*(\omega)$, were performed at 30° on four polymer-solvent systems, *i.e.*, 15% solutions of polystyrenes with molecular weight $M = 1.95 \times 10^6$ and 2.51×10^6 in toluene; a 10% solution of poly(methyl methacrylate) with $M = 1.60 \times 10^6$ in diethyl phthalate, and a 5% solution of poly(*n*-butyl methacrylate) with an extremely high molecular weight, 1.2×10^7 , in diethyl phthalate. From these measurements, the following results were found. (1) In the low-frequency range, both the real and imaginary parts of the complex modulus in steady shear, $G_{\kappa}'(\omega)$ and $G_{\kappa}''(\omega)$, decreased with increasing rate of shear κ . The effect was more remarkable in the real part than in the imaginary part, and at very low frequencies, $\log [G_{\kappa=0}'(\omega)/G_{\kappa}'(\omega)]$ was appreciably larger than $\log [G_{\kappa=0}''(\omega)/G_{\kappa}''(\omega)]^2$. (2) In the range of high frequency which corresponds to the rubbery plateau region of the relaxation spectrum, $G_{\kappa}'(\omega)$ still decreased with increasing rate of shear, whereas $G_{\kappa}''(\omega)$ increased. (3) The effect of superimposed shear on G_{κ}^* was practically negligible for Newtonian fluids. The molecular weight dependence of the steady-shear viscosity was also studied on a series of polystyrene-toluene systems under various fixed values of κ . Based on the results obtained, a discussion is given of the entanglement couplings in concentrated polymer systems.

Introduction

Polymer molecules in bulk or in concentrated solution exhibit a marked non-Newtonian effect in steady-shearing flow as well as the normal stress effect. Both effects are observed also in dilute solution, but usually to a far lesser degree in magnitude. Another feature of bulk polymers or concentrated polymer solutions is the so-called box-type distribution of relaxation times which characterizes the linear viscoelastic behavior in the range of a relatively long time scale. In all of these features the presence of the entanglement couplings between polymer chains seems to be playing an important role. The characteristic modes of chain motion participating in the box-type distribution of relaxation times may be ascribed to cooperative motions of many molecules joined by the entangle-

ments.² The non-Newtonian effect in the steady-shear viscosity may also be explained as a result of a decrease in degree of entanglement with increasing rate of shear,³ and the normal stress effect as a result of a large elastic deformation of the quasi-network structure formed by the entanglements.^{3,4} The role of the entanglement coupling in viscoelasticity is qualitatively well recognized, but molecular theoretical understand-

(1) A brief preliminary note has been published in *J. Soc. Mater. Sci. Japan*, 12, 339 (1963).

(2) See, for example, J. D. Ferry, "Viscoelastic Properties of Polymers," John Wiley and Sons, Inc., New York, N. Y., 1961.

(3) M. Yamamoto, *J. Phys. Soc. Japan*, 11, 413 (1956); 12, 1148 (1957); 13, 1200 (1958).

(4) A. S. Lodge, *Trans. Faraday Soc.*, 52, 120 (1956).

ing of the coupling still remains at an early stage of development in spite of several pioneering works.³⁻⁶

In terms of linear viscoelasticity, the simultaneous motion of polymer segments can be expressed as a sum of a series of characteristic modes of cooperative segmental motions in a phase space, each being specified by its own relaxation time. The distribution of the (characteristic) relaxation times depends on the nature of the system, especially on the nature of coupling between segments, and is most conveniently determined by analyzing the complex modulus as a function of the angular frequency of excitation. Thus measurements of the complex modulus provide important information on the nature of segmental coupling. In this way, Ferry and co-workers⁷ have recently been able to estimate the magnitude of the hydrodynamic coupling between polymer segments in dilute solutions with the aid of the molecular theories developed by Rouse⁸ and Zimm.⁹ In concentrated solutions, on the other hand, quantitative interpretation of the box-type distribution of relaxation times is seriously hampered by the lack of molecular theoretical knowledge of the entanglement coupling. Undoubtedly, other types of experimental information are needed for obtaining a more clear understanding of the entanglement.

The normal stress effect and the non-Newtonian effect are related to an over-all contribution of all the modes of segmental motion, and no information on the separate contribution of each individual mode is obtained by this type of experiment. However, as was mentioned, the existing data on these effects indicate that an entanglement network is probably formed in concentrated polymer systems and is degraded to some extent as the rate of shear is increased.¹⁰ This suggests that the steady-shearing rate can be adopted as a state variable affecting the degree of the entanglement coupling.¹¹ Consequently, measurement of the complex modulus with superimposed shear can be used as a tool for analyzing the distribution of characteristic modes associated with the entanglement coupling in polymer solutions subjected to steady shear. This paper describes the results of such measurements performed on some typical polymer-solvent systems, *i.e.*, polystyrene in toluene, poly(methyl methacrylate) in diethyl phthalate, and poly(*n*-butyl methacrylate) in diethyl phthalate.

Apparatus and Preliminary Measurements

a. Apparatus.^{12,13} The apparatus used is of the coaxial cylinder type with rotating outer cylinder. Two sets of driving devices are used, one being for pure rotation and the other for rotational oscillation.

Each set consists of a 0.5-h.p. induction motor, a gear box of the ring-cone type with a gear ratio of 1:4, and an eight-step gear box of a planetary gear system with gear ratio of 1:3 per step. These two devices are connected through a superimposer with the drive shaft of the main assembly, on which the outer cylinder is mounted. The superimposer consists of a central cogwheel, two planetary gears, and a circular rack. The cogwheel is mounted on the shaft of the drive unit for pure rotation. Two planetary gears are fitted into an annular space between the cogwheel and the circular rack. The axes of the gears are attached to a disk, on the center of which the drive shaft of the main assembly is attached. On the rim of the circular rack a lever arm of the drive unit for oscillatory motion is attached. The whole cog engagement must be very precise so as not to leave any slight gap between them; otherwise smooth motions of the main drive shaft cannot be attained. The axes of the planetary gears and accordingly the disk on which the main shaft is attached can be either rotated unidirectionally by rotation of the central wheel or oscillated sinusoidally by oscillatory motion of the circular rack. The unidirectional rotation and the oscillation can be superposed to give an oscillatory rotation by simultaneous application of both motions to the superimposer.¹⁴

By this means, three types of motion can be given to the outer cylinder, depending upon the purpose of measurement. These are: (1) pure rotation within the range of speed between 1.24×10^{-3} and 10 revolutions per sec. (r.p.s.) for measurement of the steady-shear viscosity η as a function of the rate of shear κ ; (2) sinusoidal oscillation within the range of frequency

(5) (a) M. S. Green and A. V. Tobolsky, *J. Chem. Phys.*, **14**, 80 (1946); (b) F. Bueche, *ibid.*, **20**, 1959 (1952).

(6) S. Hayashi, *J. Phys. Soc. Japan*, **18**, 249 (1963).

(7) N. W. Tschoegl and J. D. Ferry, *Kolloid-Z.*, **189**, 37 (1964); N. W. Tschoegl and J. D. Ferry, *J. Phys. Chem.*, **68**, 867 (1964); J. E. Frederick, N. W. Tschoegl, and J. D. Ferry, *ibid.*, **68**, 1974 (1964).

(8) P. E. Rouse, Jr., *J. Chem. Phys.*, **21**, 1272 (1953).

(9) B. H. Zimm, *ibid.*, **24**, 269 (1956).

(10) (a) T. Kotaka, M. Kurata, and M. Tamura, *J. Appl. Phys.*, **30**, 1705 (1959); (b) T. Kotaka, M. Kurata, and M. Tamura, *Rheol. Acta*, **2**, 179 (1962).

(11) The temperature as a state variable affects the hydrodynamic coupling between segments, but does not affect the entanglement coupling. See ref. 10.

(12) The apparatus was designed and completed with the cooperation of Iwamoto Seisakusho Co. Ltd., Kyoto. A brief description of the apparatus was first published by M. Tamura, M. Kurata, and T. Kotaka, *J. Soc. Mater. Sci. Japan*, **8**, 335 (1959).

(13) A description of the apparatus, particularly when it was used for dynamic moduli measurements, also appeared in T. Kotaka and K. Osaki, *Bull. Inst. Chem. Res., Kyoto Univ.*, **39**, 331 (1961).

(14) M. Tamura, M. Kurata, T. Kotaka, and G. Iwamoto, unpublished.

between 4.5×10^{-3} and 30 c.p.s. for measurement of the complex modulus G^* as a function of the angular frequency ω ; and (3) superimposed motion of rotation and oscillation for measurements of the complex modulus with superimposed steady-shear G_e^* as a function of ω and κ .

The outer cylinder is enclosed with a jacket in which oil is circulated from a thermostated bath to keep the temperature of test fluids constant in the range between room temperature and 100° to within an accuracy of $\pm 0.2^\circ$. An inner cylinder is concentrically suspended in the outer cylinder by a wire of known torsional stiffness. The dimensions of two cylinders are

$$R_1 \text{ (radius of inner cylinder)} = 19.0 \text{ mm.}$$

$$R_2 \text{ (radius of outer cylinder)} = 20.0 \text{ mm.}$$

$$L \text{ (immersed length of inner cylinder)} = 150 \text{ mm.} \quad (1)$$

A differential transformer unit is attached to the lever which transmits oscillatory motion from one of the drive units to the superimposer. This allows us to detect only the oscillatory part of the outer cylinder motion regardless of whether or not a steady rotation is being superimposed. A pair of differential transformers is also used for detecting the inner cylinder motion. Here two cores are attached to the ends of a beam whose center is in turn attached to the top of the inner cylinder. Two solenoids are mounted on adjustable saddles so that each core is located at the center of the hollow of each solenoid when the inner cylinder is at rest. The output voltage of the transformers is directly proportional to the torque acting on the cylinder. In steady-shear experiments the torque is measured as a function of the velocity of rotation. In dynamic measurements, the alternating voltages generated in the transformer units at the oscillator lever and at the inner cylinder are simultaneously fed to the horizontal and the vertical plates of a cathode ray tube, respectively. The Lissajous pattern thus obtained on the screen is recorded. Then the real, G' , and imaginary, G'' , components of the complex modulus can be determined as shown later. In dynamic experiments superimposed on steady shear, the torsion wire is twisted up to a certain angle in response to the superimposed steady shear and oscillates around this angle in response to the oscillatory part of the outer cylinder motion. First, on imposing only a steady rotation, the position of the solenoids on the adjustable saddle is adjusted to cancel the output voltage due to the steady shear. Then the oscillatory motion is superimposed, and oscillatory components of the output voltages are treated in the same way as above.

b. Principle of Measurements and Determination of Apparatus Constants. (i) Steady-Shear Viscosity. Determination of the steady-shear viscosity by this type of apparatus is now a routine procedure, and the detailed description is not reproduced here. The so-called "single-bob" method of Krieger and Maron was used throughout this work.¹⁵ The range of shear rate covered in this study was from 1.7×10^{-1} to $3.3 \times 10^2 \text{ sec.}^{-1}$.

*(ii) Ordinary Complex Modulus.*¹³ The oscillatory motion of a viscoelastic fluid in an annular space between walls of two coaxial cylinders has been investigated in detail by Markovitz.¹⁶ Giving the amplitude and frequency of the outer cylinder, and assuming the end effect of both cylinders to be negligible, he has shown that

$$1 - p^{-1}(\cos \varphi + i \sin \varphi) + \sum_{n=1}^{\infty} (-1)^n (\rho \omega^2 / G^*)^n [(I - k \omega^{-2}) \rho^{-1} A_n + B_n] = 0 \quad (2)$$

$$G^* = G' + iG''$$

where p is the complex ratio of amplitudes of two cylinders, φ is the phase difference between two cylinders, i is the imaginary unit $\sqrt{-1}$, ρ is the density of the test fluid, ω is the angular frequency, I is the moment of inertia of the inner cylinder assembly, and k is the torsional constant of the suspending wire. G^* is the complex modulus, and G' and G'' are its real and imaginary components, respectively. A_n and B_n are geometric constants of the apparatus. Their first two terms are

$$A_1 = (R_2^2 - R_1^2) / 4\pi L R_1^2 R_2^2;$$

$$B_1 = (R_2^2 - R_1^2)^2 / 8R_2^2;$$

$$A_2 = [4 \ln (R_1/R_2) + (R_2^2/R_1^2) - (R_1^2/R_2^2)] / 32\pi L;$$

$$B_2 = (1/192R_2^2) [(R_2^2 - R_1^2)(R_2^4 - 5R_2^2R_1^2 - 2R_1^4) + 12R_2^2R_1^4 \ln (R_2/R_1)] \quad (3)$$

where R_1 , R_2 , and L represent the dimensions of two cylinders as defined in eq. 1. In our case,¹³ using the values given in eq. 1, we found

$$\begin{aligned} A_1 &= 1.432 \times 10^{-4}; & A_2 &= 2.39 \times 10^{-7} \\ B_1 &= 4.75 \times 10^{-4}; & B_2 &= 2.80 \times 10^{-6} \end{aligned} \quad (4)$$

The terms with indexes higher than $n = 3$ were all negligible.

The moment of inertia I of the inner cylinder assembly including the core of the differential trans-

(15) I. M. Krieger and S. H. Maron, *J. Appl. Phys.*, **25**, 72 (1954).

(16) H. Markovitz, *ibid.*, **23**, 1070 (1952).

formers was determined from the frequency ν of free oscillation by using the well-known relation that $\nu = (1/2\pi)(k/I)^{1/2}$ where k is the torsion constant of the wire employed. For the wire with $k = 1.615 \times 10^6$ dyne-cm./rad, the observed value of ν was 1.111 sec.⁻¹, which led to $I = 3.314 \times 10^3$ g. cm.². The above test was performed without applying an exciting current to the solenoidal coils of differential transformers. In the presence of the exciting current, it was recognized that the frequency of free oscillation was increased up to $\nu' = 1.124$ sec.⁻¹ for the same torsion wire. This increase in ν may be attributed to the influence of restoring force acting on the cores due to their interaction with the magnetic field of the solenoids. In order to take this effect into account, we used an effective wire constant k' defined as $k' = k + \Delta k$ instead of k where $\Delta k = (2\pi)^2 I (\nu'^2 - \nu^2) = 3.6 \times 10^3$ dyne-cm./rad. It was found that the correction Δk did not depend on the wire constant k , nor on the frequency so long as the displacement of the cores was not very large. The real wire constants k of the torsion wires used were 1.578×10^6 for the most rigid one and 1.015×10^6 dyne-cm./rad for the least rigid one.

The amplitude ratio p and the phase difference φ of two cylinders can be determined at each angular frequency of oscillation ω from the Lissajous ellipse and its circumscribed rectangle which is determined by lines parallel to the horizontal axis and to the vertical axis of the oscilloscope: that is, p can be given as the ratio of two sides of the rectangle, and φ can be estimated by the use of the relation¹⁷ $|\sin \varphi| = (4/\pi) \{(A)/[A]\}$. Here (A) and $[A]$ are the area of the ellipse and of the rectangle, respectively. In this way, by the analysis of the Lissajous pattern at various frequencies, two components, real and imaginary, of the complex modulus can be determined as function of angular frequency ω .

(iii) *Complex Modulus with Superimposed Steady Shear.* The principle for measurement of the dynamic complex modulus with superimposed steady shear is essentially the same as above. When the outer cylinder is given a constant angular velocity, the inner cylinder is rotated up to an equilibrium angle where the torque exerted by the torsion wire is counterbalanced by the viscous force. A sinusoidal oscillation superimposed on the rotation of the outer cylinder then gives rise to an oscillation of the inner cylinder around this equilibrium angle. The oscillation of the inner cylinder is also sinusoidal if the amplitude of oscillation of the outer cylinder is kept sufficiently small. A complex quantity corresponding to the ordinary complex modulus can then be determined by analyzing the oscillatory parts of motions of two cylinders, again

with the use of eq. 2. This quantity is denoted by G_s^* , and is temporarily termed the complex modulus with superimposed steady shear. The complex modulus with superimposed steady shear varies not only with the angular frequency ω , but also with the rate of shear κ , the latter being determined by the steady motion of the outer cylinder.

c. *Preliminary Test of Dynamic Measurement with Superimposed Steady Shear.* Castor oil, as an example of purely viscous fluids, was used for a preliminary test of the dynamic measurements with superimposed steady shear. The steady-shear viscosity of the castor oil was 5.8 poises. A series of tests was performed at 25° by using a series of torsion wires with different torsion constants. A typical result is given in Figure 1. In this particular example, a wire with $k = 9.253 \times 10^6$ dynes cm. rad⁻¹ was employed. In Figure 1, the open circles represent the experimental points obtained for pure oscillation and three types of shaded circles represent those obtained for oscillation super-

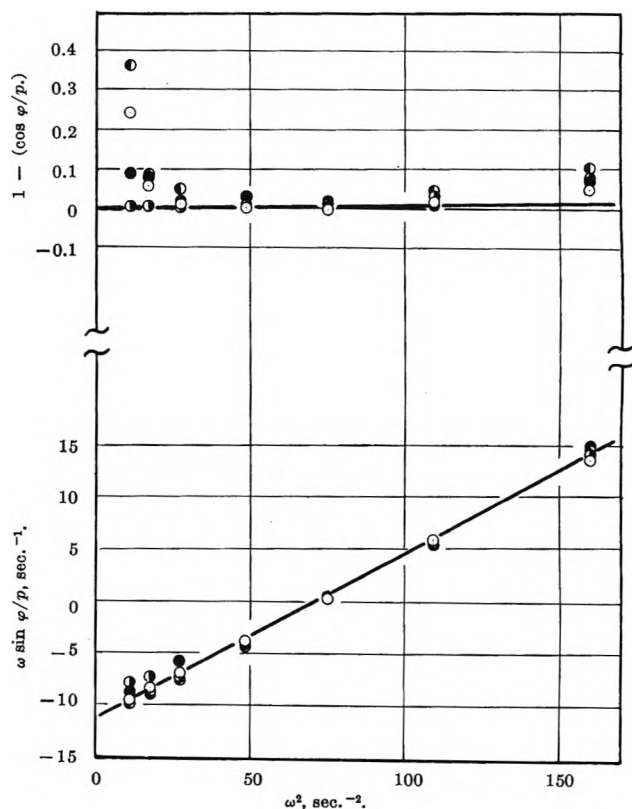


Figure 1. $\omega \sin \varphi/p$ and $1 - (\cos \varphi/p)$ plotted against ω^2 for castor oil at 25° ($\eta = 5.7$ poises). Superimposed rate of shear, κ , in sec.⁻¹: O, 0; ◐, 0.162; ◑, 0.482; ●, 1.46. Solid lines: calculated values by eq. 5 and 6.

(17) L. A. Wood, *Rev. Sci. Instr.*, 2, 644 (1931).

imposed on rotation. Different marks correspond to different values of rate of shear. In the case of a purely viscous fluid with a constant viscosity η , the real part of the complex modulus, G'_κ , should be identically zero irrespective of the rate of shear κ , and the imaginary part G''_κ should be given by $\eta\omega$. Equation 2 then becomes

$$[(A_1I + B_1\rho)\omega^2 - kA_1]/\eta = \omega \sin \varphi/p \quad (5)$$

$$[(A_2I + B_2\rho)\rho\omega^2 - kA_2\rho]/\eta^2 = 1 - (\cos \varphi/p) \quad (6)$$

Accordingly, the plots of $\omega \sin \varphi/p$ and $1 - (\cos \varphi/p)$ against ω^2 both should give straight lines whose slopes and intercepts are determined by eq. 5 and 6. These lines are shown in Figure 1 by the solid lines. Agreement between the calculated and experimental values was satisfactory in the plot of $\omega \sin \varphi/p$ vs. ω^2 over a wide range of frequency. On the other hand, in the plot of $1 - (\cos \varphi/p)$ vs. ω^2 , the agreement was limited to within a narrow range of frequency, for ω^2 about 30 to 100. The frequency range of application of eq. 6, of course, depended on the torsion constant of the wire employed. A series of torsion wires with a wide variety of torsional constant was needed for covering a wide range of frequency. Generally, the thinner wire was suitable for lower frequencies. When steady shear was superimposed, however, a thin wire was often twisted too much by the torque due to the steady motion of the fluid. This introduced a difficulty in the measurements for the combination of a low frequency and a high rate of shear. However, for a suitable combination of ω and κ , we were able to determine G_κ^* as a function of ω and κ . The results will be shown below.

Experimental Section

a. Materials. Polymers used in this investigation were polystyrene, poly(methyl methacrylate), and poly(*n*-butyl methacrylate). Nine samples of polystyrene were used, of which five samples with relatively high molecular weights were whole polymers specially prepared for this study by thermal bulk polymerization at various temperatures. Conversions were kept below 10% in order to avoid the possibility of chain branching. The viscosity-average molecular weight M_v was evaluated from the intrinsic viscosity in cyclohexane at 35° with the use of¹⁸

$$[\eta] = 8.2 \times 10^{-4} M_v^{0.50} \quad (7)$$

Polymerization temperatures, conversion, and M_v of these samples are given in Table I.

Four other samples with relatively low molecular weights were the fractions of a low conversion product of thermally polymerized styrene (polymerization

Table I: Molecular Weights of Polystyrene Samples

Polymerization temp., °C.	Conversion, %	M_v
115	5.1	0.56×10^6
95	10.7	0.72×10^6
80	8.5	1.04×10^6
60	8.6	1.95×10^6
40	7.3	2.51×10^6

^a Designated as PS(A). ^b Designated as PS(B).

temperature, 230°; these samples were kindly given us by Dr. H. Utiyama, Kyoto University). Their viscosity-average molecular weights were 1.18×10^6 , 8.62×10^4 , 2.43×10^4 , and 1.05×10^4 , respectively, as evaluated by eq. 7.

Poly(methyl methacrylate) was prepared by thermal polymerization at 47° without solvent or catalyst. The conversion was 8.5%. The viscosity-average molecular weight was 1.60×10^6 as was evaluated by¹⁹

$$[\eta] = 5.7 \times 10^{-5} M_v^{0.76} \quad (\text{benzene, } 25^\circ) \quad (8)$$

Poly(*n*-butyl methacrylate) was prepared by emulsion polymerization with the use of potassium persulfate as initiator and sodium lauryl sulfate as emulsifier. This sample has an extremely high intrinsic viscosity, 8.17 dl./g., in methyl ethyl ketone at 23°, which corresponds to a viscosity-average molecular weight of 1.18×10^7 as evaluated by the equation of Chinai, *et al.*²⁰

$$[\eta] = 1.56 \times 10^{-5} M_v^{0.81} \quad (9)$$

Toluene and diethyl phthalate, G.R. grades, were used as solvents without further purification. Each solution was prepared in a sealed ampoule at an elevated temperature (about 50°). Several weeks was necessary before obtaining homogeneous solutions.

b. Superimposed Oscillation Measurement in Polymer Solutions. Measurements of the dynamic modulus with superimposed steady shear were performed at 30° for four types of polymer solutions, a 15% solution in toluene of polystyrene A (PS(A)-Tol), a 15% solution in toluene of polystyrene B (PS(B)-Tol), a 5% solution in diethyl phthalate of poly(*n*-butyl methacrylate)

(18) W. R. Krigbaum and P. J. Flory, *J. Polymer Sci.*, **11**, 37 (1953).

(19) P. J. Flory, "Principles of Polymer Chemistry," Cornell University Press, Ithaca, N. Y., 1953, p. 312.

(20) S. N. Chinai and R. N. Guzzi, *J. Polymer Sci.*, **21**, 417 (1956). The use of eq. 9 in such a high molecular weight range as this is somewhat questionable. This value of M_v is therefore only a tentative estimate.

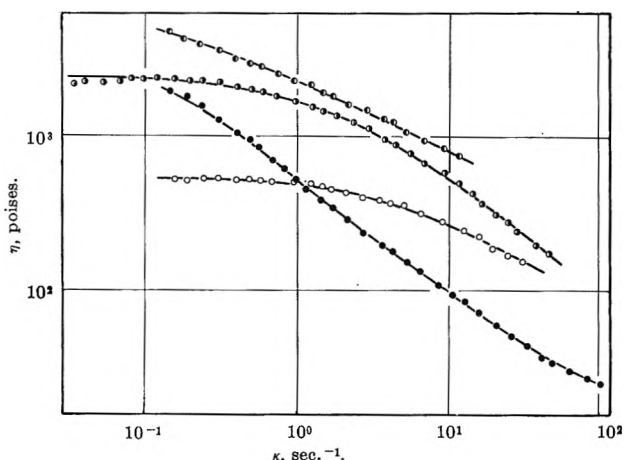


Figure 2. Steady-shear viscosity, η , plotted against rate of shear κ at 30° for four polymer-solvent systems: O, PS(A)-toluene; \odot , PS(B)-toluene; \circ , PMMA-diethyl phthalate; \bullet , PBMA-diethyl phthalate.

(PBMA-DEP), and a 10% solution in diethyl phthalate of poly(methyl methacrylate) (PMMA-DEP). The viscosity data in steady shear of these solutions are shown in Figure 2, where the viscosity η_κ is plotted against the rate of shear κ in double logarithmic scale. As is seen from the figure, these four solutions are examples of polymer solutions which show the non-Newtonian effect to a different degree; *i.e.* the effect increases in the order PS(A)-Tol < PS(B)-Tol < PMMA-DEP < PBMA-DEP.

Figure 3 shows the result of superimposed oscillation measurements obtained for the 15% toluene solution of polystyrene A, where the open circles represent the real and the imaginary parts of the complex modulus, G' and G'' , as function of ω , and the four types of shaded circles represent those of the complex modulus with superimposed steady shear, G'_κ and G''_κ , obtained at various rates of shear κ . Apparently, the superimposed steady shear produces a rather minor effect on the complex modulus so far as the rate of shear is sufficiently small to keep the non-Newtonian effect in the viscosity less significant. The effect of the rate of shear becomes significant in the real part of the complex modulus only at the highest shear rate investigated. The imaginary part seems insensitive to the steady shear.

Figure 4 shows the result of the superimposed oscillation measurements for the 15% solution of high molecular weight polystyrene B in toluene. This polymer exhibits a stronger non-Newtonian effect than does polystyrene A. A remarkable effect of the rate of shear on the complex modulus is observed in this figure. As the rate of the applied shear is increased, the real part of the complex modulus is significantly

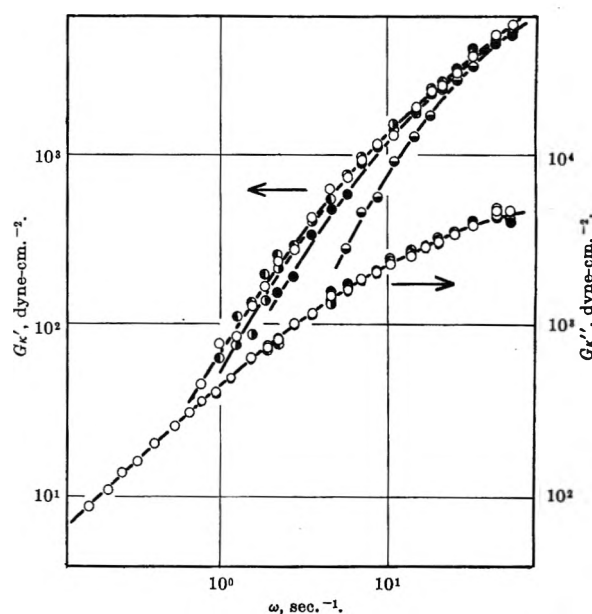


Figure 3. Real and imaginary parts of complex modulus in shear, G'_κ and G''_κ , plotted against angular frequency, ω , for 15% solution of polystyrene A in toluene at 30° . Superimposed rate of shear in sec.^{-1} : O, 0; \odot , 0.162; \bullet , 0.482; \circ , 1.46; \ominus , 4.60.

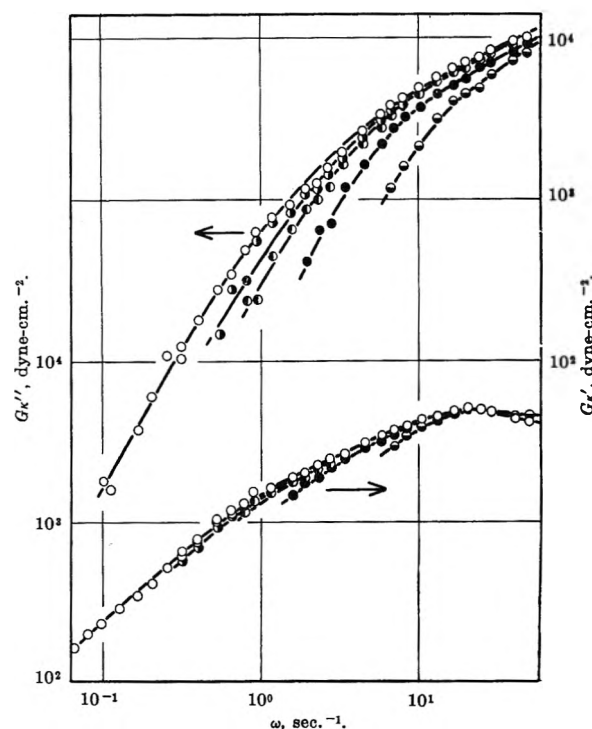


Figure 4. Real and imaginary parts of complex modulus in shear, G'_κ and G''_κ , plotted against angular frequency, ω , for 15% solution of polystyrene B in toluene at 30° . Superimposed rate of shear in sec.^{-1} : O, 0; \odot , 0.162; \bullet , 0.505; \circ , 1.62; \ominus , 5.13.

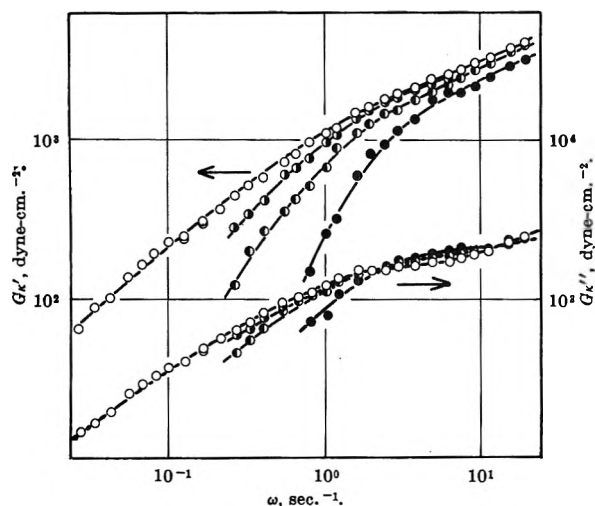


Figure 5. Real and imaginary parts of complex modulus in shear, G' and G'' , plotted against angular frequency, ω , for 10% solution of poly(methyl methacrylate) in diethyl phthalate at 30°. Superimposed rate of shear in sec.^{-1} : \circ , 0; \odot , 0.188; \ominus , 0.560; \bullet , 1.71.

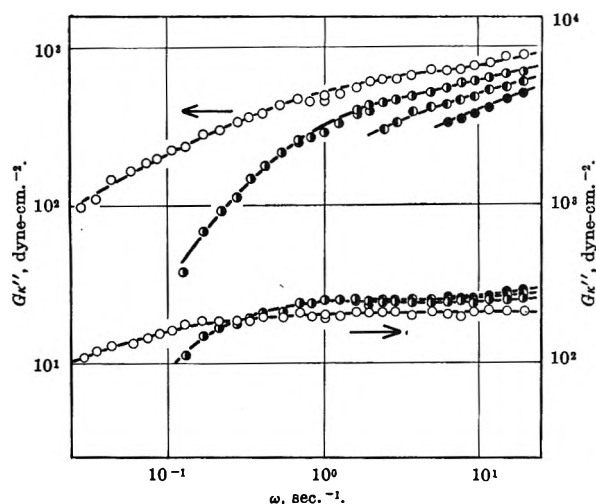


Figure 6. Real and imaginary parts of complex modulus in shear, G' and G'' , plotted against angular frequency, ω , for 5% solution of poly(*n*-butyl methacrylate) in diethyl phthalate at 30°. Superimposed rate of shear in sec.^{-1} : \circ , 0; \odot , 0.190; \ominus , 0.580; \bullet , 1.76.

diminished over almost the whole range of frequency observed. However, the imaginary part is again less sensitive to the rate of shear, particularly at high frequencies. The lower the frequency becomes, the larger is the relative decrease in G'_κ or G''_κ observed. In addition, the curves for the complex modulus with superimposed steady shear are different in shape from those for the complex modulus without superimposed steady shear, especially at a high rate of shear. Simple sliding of the curves for different shear rates

along the coordinate axis does not provide a composite curve as the WLF shift does for data of different temperatures.²¹ This fact implies that the effect of the steady shear on the complex modulus is more complicated than is the effect of temperature.

Figures 5 and 6 show the superimposed oscillation data obtained for the 10% solution of poly(methyl methacrylate) in diethyl phthalate and for the 5% solution of poly(*n*-butyl methacrylate) in diethyl phthalate, respectively. These solutions show stronger non-Newtonian behavior than do the polystyrene solutions. As is seen in Figures 5 and 6, the effect of the steady shear on G'_κ is very significant in these solutions. The qualitative feature of the effect is the same as in the polystyrene solutions described above. A closer inspection indicates, however, that the imaginary part of the complex modulus increases with increasing shear in the high-frequency range. Now returning to Figure 4, we may observe the same effect at the highest frequency, though to a slight degree. Thus we may conclude that this effect is not a characteristic of a special type of polymers, *e.g.*, poly(methyl methacrylate) and poly(*n*-butyl methacrylate), but is common to all concentrated polymer solutions.

c. Steady-Shear Viscosity. The effect of molecular weight on the steady-shear viscosity was also investigated at various rates of shear for 15% solutions of polystyrene in toluene at 30°. The results are shown in Figure 7.

The molecular weight dependence of the zero-shear viscosity shows the well-known feature²; that is, the log-log plot of η_0 vs. M_v displays a sharp turn at about $M_v = 3 \times 10^5$, and beyond it, increases with 3.4 power of M_v . This turning point is often referred to as the critical molecular weight M_c for the onset of the entanglement network.

At a given rate of shear, say $\kappa = 0.482 \text{ sec.}^{-1}$, the polymers with a relatively low molecular weight, say less than about 10^6 , are practically Newtonian. The non-Newtonian deviation becomes significant at and above a certain molecular weight. It is of course unlikely that, in the log-log plot of η_κ vs. M_v with a given rate of shear κ , a sharp turning point is defined between the Newtonian and non-Newtonian regions. The transition from one region to the other is gradual as η_κ decreases gradually with increasing κ for a fixed M_v (see Figure 2). It is nevertheless worthwhile to note that the log η_κ vs. log M_v plot most closely resembles type A in Figure 8, but neither type B nor C, and that the boundary between Newtonian and non-Newtonian regions shifts to lower M_v as κ increases.

(21) M. L. Williams, R. F. Landel, and J. D. Ferry, *J. Am. Chem. Soc.*, **77**, 3701 (1955).

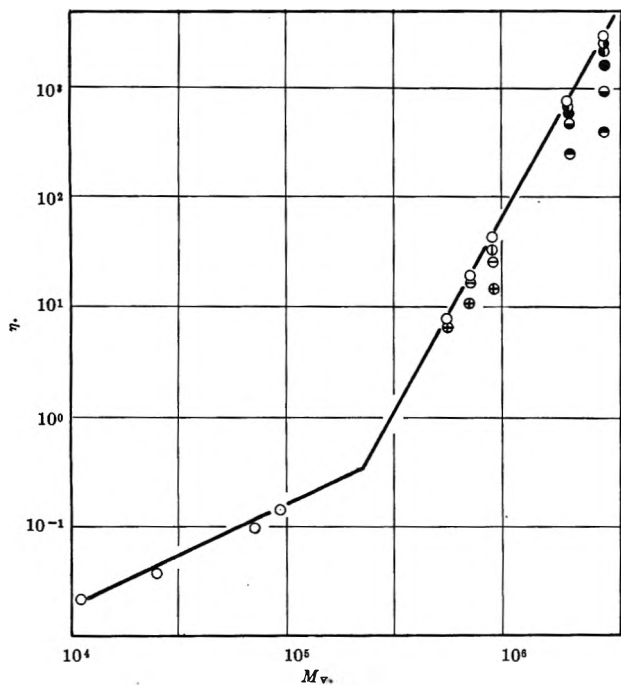


Figure 7. Steady-shear viscosity, η , as functions of viscosity-average molecular weight, M_v , for polystyrene at 30°. Rate of shear in sec.⁻¹: ○, 0; ●, 0.162; ○, 0.482; ●, 1.46; ○, 4.40; ●, 13.2; ○, 39.6; ●, 119; ○, 357.

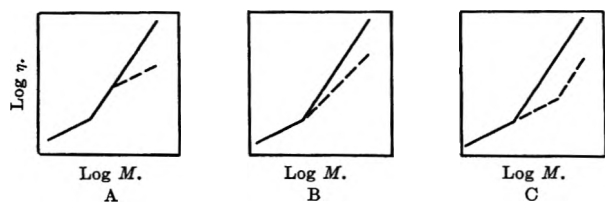


Figure 8. Schematic representation of three possible types of $\log \eta$ vs. $\log M$ relationship. Solid line: zero shear viscosity; dashed line: viscosity under a constant value of the rate of shear.

Discussion

The present measurements were performed only within a rather restricted range of frequency for each given system. It is, however, clear from the shape of the double logarithmic plots for G' and G'' vs. ω that the frequency range covered in Figure 4 roughly corresponds to the so-called flow region of the relaxation spectrum, while the frequency range covered in Figure 6 corresponds to the rubbery plateau region. Figure 5 may then be regarded as an example for showing the shear rate effect in the intermediate region between the above two. Thus, we are able to deduce a general picture of the shear rate effect on the relaxation spectrum from comparison or synthesis

of the two following features obtained in the three regions of different time scales.

(i) In the flow region, the decrease in the real part of the complex modulus due to the superimposed shear is larger than the square of the decrease in the imaginary part. In fact, the value of n_κ defined by

$$n_\kappa = \lim_{\omega \rightarrow 0} \frac{\ln [G'_\kappa(\omega)/G'_{\kappa=0}(\omega)]}{\ln [G''_\kappa(\omega)/G''_{\kappa=0}(\omega)]} \quad (10)$$

was about 3–4 in Figure 4.

(ii) In the plateau region, the imaginary part of the complex modulus increases with increasing rate of shear (see Figures 5 and 6).

Rough estimates of the relaxation spectrum can be based on either component of the complex modulus, $G'_\kappa(\omega)$ and $G''_\kappa(\omega)$. The results are such that the relaxation spectrum $H(\ln \tau)$ as a function of logarithmic relaxation time is markedly cut off at the long time end and is heightened in the plateau region of shorter time scales. Figure 9 gives a schematic representation of the result.

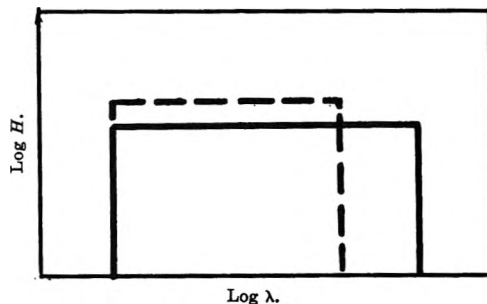


Figure 9. Schematic representation of shear effect on the relaxation spectrum H . Solid line corresponds to zero rate of shear, and dashed line to a finite rate of shear.

The type of behavior observed has a unique feature different from that observed for the effect of temperature. In the latter case, a single shift factor a_T can be assigned for all relaxation times (the WLF shift²¹), and the relative effect of the variable on G' and G'' can be given as

$$n_T = \lim_{\omega \rightarrow 0} \frac{\ln [G'_T(\omega)/G'_{T_0}(\omega)]}{\ln [G''_T(\omega)/G''_{T_0}(\omega)]} = 2 \quad (11)$$

Here T_0 is a reference temperature. The observed value of n_κ was found to be much larger than 2 as mentioned above. In a sense, the effect of the rate of shear resembles the effect of molecular weight depression as exemplified by the sharp cut of the long time end of the relaxation spectrum. Quantitative analysis of the

experimental results in terms of the existing theories such as Marvin's²² will be published elsewhere.

Acknowledgment. Talking with Dr. R. S. Marvin, who was a visiting professor of this university in the period 1961–1962, was indispensable at an early stage of this study. We are indebted to him for many

valuable discussions. Thanks are also tendered to Prof. S. Onogi of this university for stimulating discussions and to the Ministry of Education of Japan for a grant-in-aid.

(22) R. S. Marvin and H. Oser, *J. Res. Natl. Bur. Std.*, **66B**, 171 (1962); **67B**, 87 (1963).

Membrane Potential in Nonisothermal Systems

by Masayasu Tasaka, Shoji Morita, and Mitsuru Nagasawa

Departments of Applied and Synthetic Chemistry, Faculty of Engineering, Nagoya University, Furo-cho, Chikusa-ku, Nagoya, Japan (Received June 21, 1965)

Applying nonequilibrium thermodynamics, a theory of membrane potential in nonisothermal systems was obtained. Measurements of membrane potential across an ion-exchange membrane separating two solutions which are at different temperatures were carried out to be compared with the theory. Agreement between the theory and the observed results is satisfactory. The present experimental results are in agreement with the results reported by Tyrrell, *et al.*, who used strips of ion-exchange resin, but are different from those reported by Ikeda, *et al.*, using collodion membranes.

Introduction

It is well known that an electrostatic potential difference appears across a membrane separating two electrolyte solutions of different concentrations. However, since not only a concentration gradient but also a temperature gradient across the membrane is a driving force for the permeation of ions, a potential difference must also appear when there is a temperature difference on both sides of the membrane. The study of such "thermal membrane potentials" is important because they are often observed in physiology, in electrodialysis, or in desalination operations, though little attention has thus far been devoted to this phenomenon.

Some experimental results were reported by Ikeda, *et al.*,¹ who found that the thermal membrane potential across oxidized collodion membranes separating two solutions of 0.1 *M* KCl at different temperatures is quite low, lower than 0.05 mv./deg. On the other

hand, Tyrrell, *et al.*,² measured thermal diffusion potentials in strips of ion-exchange resin and reported a value about 10 times higher than that reported by Ikeda, *et al.*, at 0.1 *M* KCl. Since the fundamental principles in these two experiments are the same except for the shapes of the ion exchangers used, the difference observed between both results is quite a dilemma.

Hills, *et al.*,³ derived an equation of nonisothermal membrane potential by using nonequilibrium thermodynamics, but the effect of temperature difference on membrane potential could not be clearly predicted from their theory, since their theory includes the heat

(1) T. Ikeda, *J. Chem. Phys.*, **28**, 166 (1958); T. Ikeda, M. Tsuchiya and M. Nakano, *Bull. Chem. Soc. Japan*, **37**, 1482 (1964).

(2) H. J. Tyrrell, D. A. Taylor, and C. M. Williams, *Nature*, **177**, 668 (1956).

(3) G. J. Hills, P. W. M. Jacobs, and N. Lakshminarayanaiah, *Proc. Roy. Soc. (London)*, **A262**, 246 (1961).

of transfer of each component, *i.e.*, the Soret coefficient of a single component.

In the present work, an equation for the membrane potential in nonisothermal systems is derived by using nonequilibrium thermodynamics, and measurements of membrane potential across a few ion-exchange membranes separating two KCl solutions at different temperatures are compared with the theory.

Theory

Applying nonequilibrium thermodynamics to ion-transport processes in 1-1 electrolyte solution, in the absence of viscous force, the entropy production σ is given by the equation^{4,5}

$$-T\sigma = J_s \cdot \text{grad } T + \sum_{i=+,-,0} J_{mi} \cdot \text{grad } \bar{\mu}_i \quad (1)$$

where

$$\bar{\mu}_i = \mu_i + z_i \mathcal{F} \psi \quad (2)$$

T is the temperature, J_s is the total entropy flux, J_{mi} is the absolute mass flux, $\bar{\mu}_i$ is the electrochemical potential, μ_i is the chemical potential, z_i is the valence of component i , \mathcal{F} is the Faraday constant, and ψ is the electrical potential. Subscripts $+$, $-$, and 0 refer to cation, anion, and water molecule, respectively. The force $\text{grad } \bar{\mu}_i$ is a function of temperature and, hence, eq. 1 differs from the starting equation of Hills, *et al.*, who used $(\text{grad } \bar{\mu}_i)_T$, *i.e.*, the gradient of $\bar{\mu}_i$ at constant temperature, as a force.

The fluxes and forces in eq. 1 are not all independent. A mass flux J_{m0} vanishes from the condition that the sum of weighed mass fluxes must be zero,⁵ that is

$$\sum_{i=+,-,0} w_i J_{mi} = 0$$

where w_i is a weight factor. Another mass flux, for instance, J_{m-} , may also be replaced by the total electric current I , as I is the sum of $z_i \mathcal{F} J_{mi}$. Thus we obtain

$$T\sigma = -J_s \cdot \text{grad } T - J_{m+} \cdot \text{grad} \left(\mu_+' - \frac{z_+}{z_-} \mu_-' \right) - I \cdot \text{grad} \left(\frac{\mu_-'}{z_- \mathcal{F}} + \psi \right) \quad (3)$$

where the abbreviation

$$\mu_i' = \mu_i - \frac{w_i}{w_0} \mu_0 \quad (4)$$

has been used.

Then, the phenomenological equations for the fluxes and thermodynamic forces of eq. 3 are given by

$$\begin{aligned} -J_s &= \Omega_{ss} \text{grad } T + \Omega_{sm} \text{grad} \left(\mu_+' - \frac{z_+}{z_-} \mu_-' \right) + \Omega_{se} \text{grad} \left(\frac{\mu_-'}{z_- \mathcal{F}} + \psi \right) \\ -J_{m+} &= \Omega_{ms} \text{grad } T + \Omega_{mm} \text{grad} \left(\mu_+' - \frac{z_+}{z_-} \mu_-' \right) + \Omega_{me} \text{grad} \left(\frac{\mu_-'}{z_- \mathcal{F}} + \psi \right) \\ -I &= \Omega_{es} \text{grad } T + \Omega_{em} \text{grad} \left(\mu_+' - \frac{z_+}{z_-} \mu_-' \right) + \Omega_{ee} \text{grad} \left(\frac{\mu_-'}{z_- \mathcal{F}} + \psi \right) \end{aligned} \quad (5)$$

To take into account the fact that the membrane is not an infinitely thin film but has a finite thickness, we now adopt the method which was used by Kirkwood⁶ in isothermal systems. By solving eq. 5 for the forces and integrating them from one side of the membrane to the other keeping the fluxes constant, we obtain

$$\begin{aligned} -J_s &= \omega_{ss} \Delta T + \omega_{sm} \Delta \left(\mu_+' - \frac{z_+}{z_-} \mu_-' \right) + \omega_{se} \Delta \left(\frac{\mu_-'}{z_- \mathcal{F}} + \psi \right) \\ -J_{m+} &= \omega_{ms} \Delta T + \omega_{mm} \Delta \left(\mu_+' - \frac{z_+}{z_-} \mu_-' \right) + \omega_{me} \Delta \left(\frac{\mu_-'}{z_- \mathcal{F}} + \psi \right) \\ -I &= \omega_{es} \Delta T + \omega_{em} \Delta \left(\mu_+' - \frac{z_+}{z_-} \mu_-' \right) + \omega_{ee} \Delta \left(\frac{\mu_-'}{z_- \mathcal{F}} + \psi \right) \end{aligned} \quad (6)$$

where Δ shows the differences between two fluid phases on both sides of the membrane and $\omega_{\alpha\beta}$ is the permeability coefficient of the membrane of finite thickness. $\omega_{\alpha\beta}$ is a matrix which is related to the matrix $\Omega_{\alpha\beta}$ as

(4) S. R. de Groot, "Thermodynamics of Irreversible Processes," North-Holland Publishing Co., Amsterdam, 1951.

(5) S. R. de Groot and P. Mazur, "Nonequilibrium Thermodynamics," North-Holland Publishing Co., Amsterdam, 1962.

(6) J. G. Kirkwood, "Ion Transport across Membranes," H. T. Clarke, Ed., Academic Press Inc., New York, N. Y., 1954, p. 119.

$$\begin{aligned} \frac{|\Omega|_{\alpha\beta}}{|\Omega|} &= R_{\beta\alpha} \\ \gamma_{\beta\alpha} &= \int_0^\delta R_{\beta\alpha}(x) dx \\ \omega_{\alpha\beta} &= \frac{|\gamma|_{\beta\alpha}}{|\gamma|} \end{aligned} \quad (7)$$

where $|\Omega|$ or $|\gamma|$ is the determinant of the matrix $\Omega_{\alpha\beta}$ or $\gamma_{\alpha\beta}$, $|\Omega|_{\alpha\beta}$ or $|\gamma|_{\alpha\beta}$ is the appropriate cofactor, and δ is the thickness of the membrane. $\Omega_{\alpha\beta}$ or $\omega_{\alpha\beta}$ is not an absolute constant for membrane-electrolyte systems but can practically be treated as constant.

Let us now employ eq. 6 for the determination of the electrical potential difference $\Delta\psi$ appearing across the membrane at zero electric current. That is, from the condition of $I = 0$, we have

$$\begin{aligned} -\Delta\psi &= \eta\Delta T + \sum_{i=+,-} \frac{t_i}{z_i\mathcal{F}} \Delta\mu_i' \\ &= \eta\Delta T + \sum_{i=+,-,0} \tau_i \Delta\mu_i \end{aligned} \quad (8)$$

where

$$\begin{aligned} \eta &= \frac{\omega_{ee}}{\omega_{ee}} \\ t_i &= \left(\frac{z_i\mathcal{F}J_{mi}}{I} \right)_{\Delta T=0, \Delta\mu_i=0} \\ \tau_i &= \left(\frac{J_{mi}}{I} \right)_{\Delta T=0, \Delta\mu_i=0} \end{aligned} \quad (9)$$

η is the differential thermoelectric potential, t_i is the transport number, and τ_i is the reduced transport number of i th species. Employing the mean activities of electrolytes instead of the single activities of ions in eq. 8 to calculate the chemical potentials, we have

$$\begin{aligned} -\Delta\psi &= (2t_+ - 1) \frac{RT}{\mathcal{F}} \ln \frac{a_{\pm}(2)}{a_{\pm}(1)} + \\ & (2t_+ - 1) \frac{R\Delta T}{\mathcal{F}} \ln a_{\pm}(2) + \tau_0 RT \ln \frac{a_0(2)}{a_0(1)} + \\ & \tau_0 R\Delta T \ln a_0(2) + \left[t_+ \left\{ \eta - \left(\frac{s_+^0}{\mathcal{F}} + \tau_0 s_0^0 \right) \right\} + \right. \\ & \left. t_- \left\{ \eta + \left(\frac{s_-^0}{\mathcal{F}} - \tau_0 s_0^0 \right) \right\} \right] \Delta T \end{aligned} \quad (10)$$

where

$$s_i^0 = \frac{\partial \mu_i^0}{\partial T} \quad (11)$$

s_i^0 is the partial molal entropy which is the partial

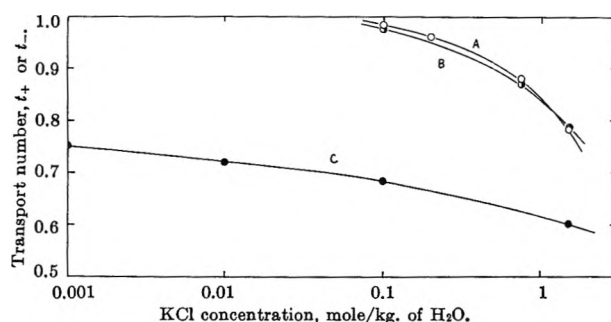


Figure 1. The dependence of the transport number on electrolyte concentration. Membrane: A, C-1; B, A-1; C, C-2.

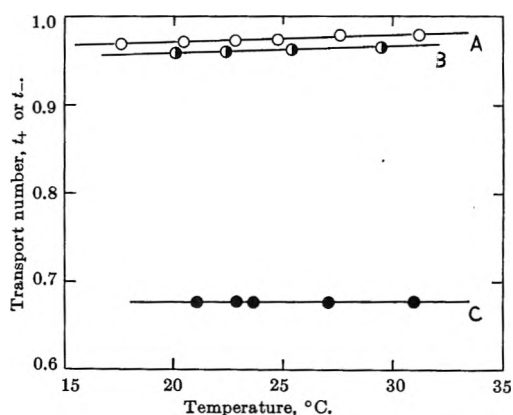


Figure 2. The temperature dependence of the transport number between 0.1 and 0.2 *m* KCl solutions. Membrane: A, C-1; B, A-1; C, C-2.

derivative of standard chemical potential μ_i^0 with respect to temperature. At $\Delta T = 0$, eq. 10 becomes the equation for isothermal systems.^{6,7} In dilute solutions the activity of water is nearly unity and, hence, $\ln(a_0(2)/a_0(1))$ and $\ln a_0$ terms are negligible compared with the other terms. Therefore eq. 10 may be written as

$$\begin{aligned} -\Delta\psi &= (2t_+ - 1) \frac{RT}{\mathcal{F}} \ln \frac{a_{\pm}(2)}{a_{\pm}(1)} + \\ & (2t_+ - 1) \frac{R\Delta T}{\mathcal{F}} \ln a_{\pm}(2) + (t_+\alpha_+ + t_-\alpha_-) \Delta T \end{aligned} \quad (12)$$

where the abbreviations

$$\begin{aligned} \alpha_+ &= \eta - \left(\frac{s_+^0}{\mathcal{F}} + \tau_0 s_0^0 \right) \\ \alpha_- &= \eta + \left(\frac{s_-^0}{\mathcal{F}} - \tau_0 s_0^0 \right) \end{aligned} \quad (13)$$

are used.

(7) A. J. Staverman, *Trans. Faraday Soc.*, **48**, 176 (1952).

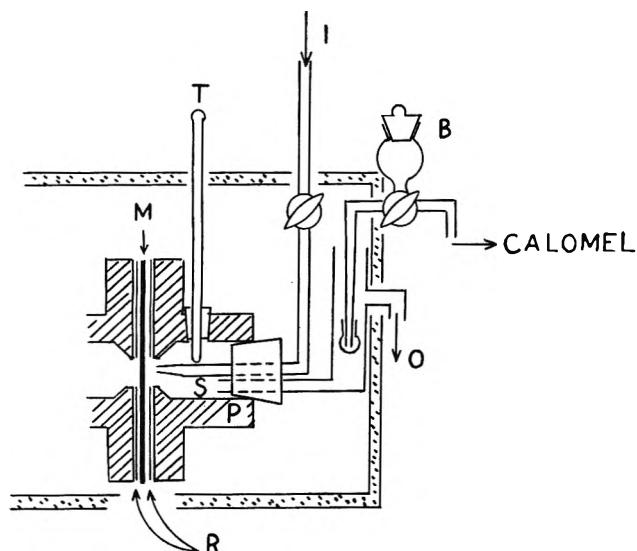


Figure 3. Membrane potential cell: P, poly(methyl methacrylate) resin cell; M, membrane; R, rubber gaskets; T, thermometer; S, solution; B, salt bridge (satd. KCl); I, solution inlet; O, solution outlet.

If there is no activity difference across the membrane, moreover, $\Delta\psi/\Delta T$ may be written as

$$-\frac{\Delta\psi}{\Delta T} = 2.303(2t_+ - 1)\frac{R}{\mathcal{F}} \log a_{\pm}(2) + (t_+\alpha_+ + t_-\alpha_-) \quad (14)$$

If the selectivity of membrane is ideal, *i.e.*, $t_+ \text{ or } t_- = 1$, therefore the slope of the $\Delta\psi/\Delta T$ vs. $\log a_{\pm}(2)$ plot must be $\pm 2.303R/\mathcal{F}$ and its intercept at the $\log a_{\pm}(2)$ axis gives α_+ or α_- . Since the concentration of electrolyte absorbed in the membrane varies slightly with the electrolyte concentration in the outer solutions, the phenomenological coefficients $\Omega_{\alpha\beta}$ or $\omega_{\alpha\beta}$ in eq. 5 or 6 and, consequently, α_+ and α_- of eq. 13 may vary slightly with the electrolyte concentration in membrane systems but can be practically treated as constant, as is seen in the experimental results.

Experimental Section

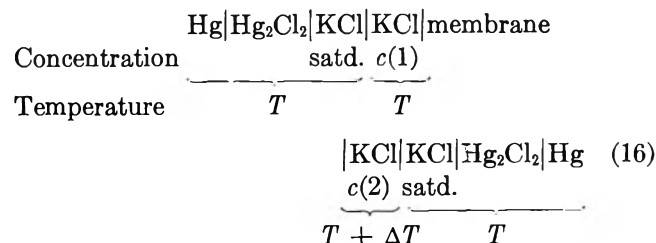
Preparation and Properties of Membranes. Heterogeneous cation- and anion-exchange membranes were prepared from Amberlite XE-69 and XE-119 of about 300 mesh and polyvinyl chloride (a copolymer containing 5% vinyl acetate) as a binder. The membranes used are the following three: (C-1), XE-69 60%, $t_+^{0.1} = 0.98$; (A-1), XE-119 60%, $t_-^{0.1} = 0.97$; (C-2), XE-69 33%, XE-119 27%, $t_+^{0.1} = 0.68$, where $t_{\pm}^{0.1}$ is the transport number of cation or anion at $c_{\text{KCl}} = 0.1$ m (mole/kg. of H_2O) and at 25° . The changes in t_+ and t_- of these membranes with KCl

concentration are shown in Figure 1. The temperature dependence of t_+ and t_- was negligible in the present experimental region as shown in Figure 2. These transport numbers of cation and anion in the membranes were calculated from membrane potentials at $\Delta T = 0$ using the equation

$$-\Delta\psi = \pm(2t_{\pm} - 1)\frac{RT}{\mathcal{F}} \ln \frac{a_{\pm}(2)}{a_{\pm}(1)} \quad (15)$$

Actually, the transport number at an electrolyte concentration was determined by interpolating the values obtained at various values of $a_{\pm}(2)/a_{\pm}(1)$ ($a_{\pm}(2)$ being kept constant) to $a_{\pm}(2)/a_{\pm}(1) = 1$.⁸

Membrane Potential Cell and Measurements. The membrane potential cell was constructed from two sections made of poly(methyl methacrylate) resin and a calomel electrode was connected to each section as shown in Figure 3 or eq. 16.



A membrane, whose effective area was 0.78 cm^2 , was mounted between the half-cells. The solution inlet and outlet as well as a mercury thermometer were inserted in each half-cell to disturb a diffusion layer on the membrane surface.⁹ The nozzle of the inlet tube, whose internal diameter was about 3 mm., was fixed at a position 2–3 mm. apart from the membrane surface. In order to prevent the temperature rise of the calomel electrodes two saturated KCl bridges were used to connect the half-cell and the calomel electrode and, moreover, the membrane potential cell was carefully insulated from the calomel electrode compartment which was kept at 20° . That the two calomel electrodes do not show any potential difference was checked before and after every measurement of membrane potential by dipping the two electrodes into a saturated KCl solution. Sometimes, however, a small potential difference such as 0.1 mv. was observed. If so, the value was subtracted from the observed membrane potential.

Strictly speaking, the observed potential differences include not only the electrical potential difference

(8) Y. Oda and T. Yawataya, *Bull. Chem. Soc. Japan*, **29**, 673 (1956).

(9) M. Nagasawa and I. Kagawa, *Discussions Faraday Soc.*, **21**, 52 (1956).

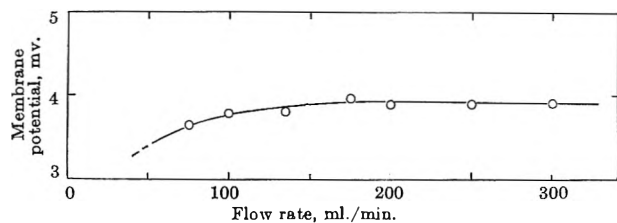


Figure 4. The influence of flow rate on membrane potential for membrane C-1 at 0.1 *m* KCl solution. Membrane thickness, 1.13; temperature difference, ΔT , 10°.

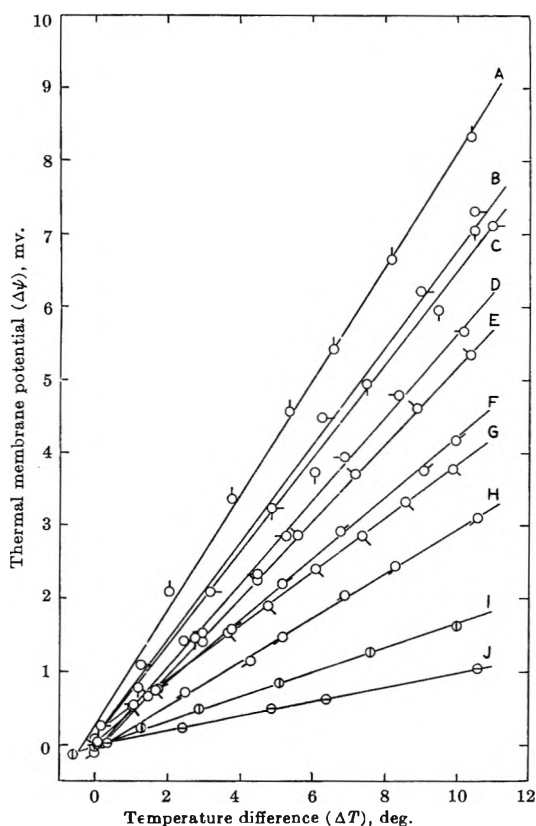


Figure 5. Thermal membrane potentials of membrane C-1. KCl concentrations: A, 0.001 *m*; B, 0.002 *m*; C, 0.005 *m*; D, 0.01 *m*; E, 0.02 *m*; F, 0.05 *m*; G, 0.1 *m*; H, 0.2 *m*; I, 0.75 *m*; J, 1.5 *m*.

across the membranes but also certain small thermal junction potentials in solution. In this paper, it is assumed that such thermal junction potentials in solution are negligible. This assumption is justified in this context because the potassium chloride solutions never differed in temperature by more than 10° and the transference numbers of potassium and chloride ions, which are almost equal at room temperature, do not change significantly with temperature.¹⁰

While in isothermal systems a reproducible stationary membrane potential was observed at relatively low

flow rates of KCl solutions (60–150 ml./min.) and even with thin membranes, in nonisothermal systems high flow rates (250–300 ml./min.) and thicker membranes (of about 1-mm. thickness) were required to obtain reproducible membrane potentials independent of the flow rate. If a thin membrane of 0.3 mm. is used, reproducible membrane potentials independent of the flow rate cannot be obtained even at very high flow rates. An example of the dependence of membrane potential on flow rate is shown in Figure 4. The measurements of membrane potentials were carried out by using a potentiometer of Type K2 and a galvanometer of Shimadzu Inst. Co. The sensitivity in measurement was 0.01 mv.

Two series of measurements of membrane potentials were carried out: (i) between KCl solutions which have the same concentration but are at different temperatures; and (ii) between KCl solutions which are at different temperatures and also have different concentrations. The lower temperature $T(1)$ was about 20° and was controlled to the same temperature as the outside thermostat. The temperature difference $T(2) - T(1) = \Delta T$ between two solutions was varied between 0 and 10°, with an accuracy of 0.1°.

Results

Figure 5 shows that the membrane potential $\Delta\psi$ for the cation-exchange membrane (C-1) in the absence of a concentration difference varies linearly with the temperature difference ΔT , as predicted by eq. 14. Each straight line was calculated by the method of least squares. Quite similar results were also obtained for both the anion-exchange membrane (A-1) and another cation-exchange membrane (C-2) as shown in Figure 6. For the cation- and anion-exchange membranes the slopes, $\Delta\psi/\Delta T$ (mv./deg.), obtained are plotted as a function of the activity of KCl in the outer solutions in Figure 7. The straight lines were calculated by using the method of least squares assuming the slope of $2.303R/\bar{t}$ in the range of 0.001 to 0.1 *m* concentrations. All observed values are seen to be near the straight line and, therefore, the second term of eq. 14, α_+ or α_- , may be considered to be practically constant. At higher concentrations $\Delta\psi/\Delta T$ values are deviated from linearity. This deviation is due to the fact that the transport number decreases with increase of the concentration. The half-black circles in Figure 7 are the values corrected for the concentration dependence of the transport number. The thermal change of the activity coefficient was also

(10) H. S. Harned and B. B. Owen, "The Physical Chemistry of Electrolytic Solutions," Reinhold Publishing Corp., New York, N. Y., 1950, pp. 224–234.

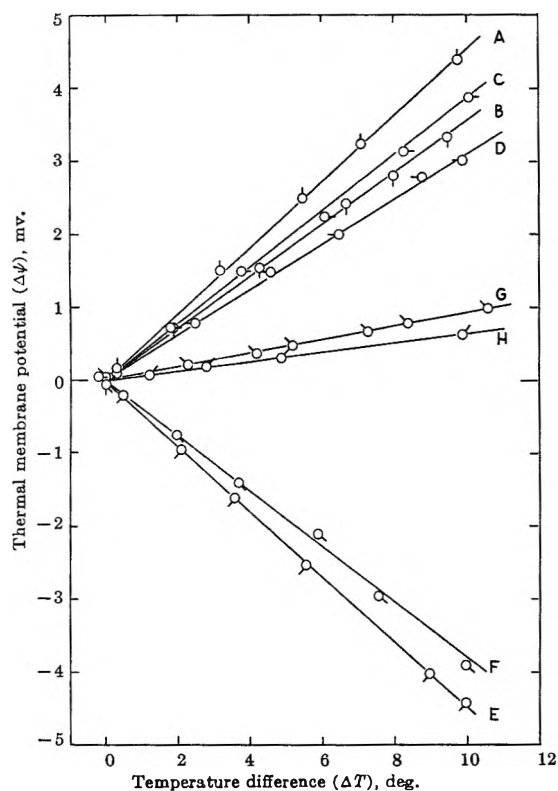


Figure 6. Thermal membrane potentials of membranes C-1, A-1, and C-2. The contribution of the concentration difference was eliminated by using eq. 12. The temperature in phase 2 is always higher than that in phase 1. C-1: A, $t_+ = 1.0$, $c(1) = 0.1$ m, $c(2) = 0.05$ m; B, $t_+ = 1.0$, $c(1) = 0.05$ m, $c(2) = 0.1$ m; C, $t_+ = 0.97$, $c(1) = 0.2$ m, $c(2) = 0.1$ m; D, $t_+ = 0.97$, $c(1) = 0.1$ m, $c(2) = 0.2$ m; A-1: E, $t_- = 0.97$, $c(1) = 0.2$ m, $c(2) = 0.1$ m; F, $t_- = 0.97$, $c(1) = 0.1$ m, $c(2) = 0.2$ m; C-2: G, $t_+ = 0.68$, $c(1) = 0.2$ m, $c(2) = 0.1$ m; H, $t_+ = 0.68$, $c(1) = 0.1$ m, $c(2) = 0.2$ m.

taken into account when the concentration was high.¹¹ The values thus corrected are all close to the straight lines.

For the membrane C-2, the graph of $\Delta\psi/\Delta T$ against $\log a_{\pm}(2)$ was calculated from eq. 14 with the values of t_+ as shown in Figure 1, assuming the same α_+ and α_- as obtained for C-1 and A-1. The agreement between the calculated curve and the observed values is satisfactory.

The membrane potentials obtained in the present work are much different from the values reported by Ikeda, *et al.*,¹ who used oxidized collodion membranes, but are in almost complete agreement with the values by Tyrrell, *et al.*,² who used quite a different shape of ion-exchange resin.

The membrane potentials across the membranes separating two solutions which are at different temperatures and also have different concentrations include

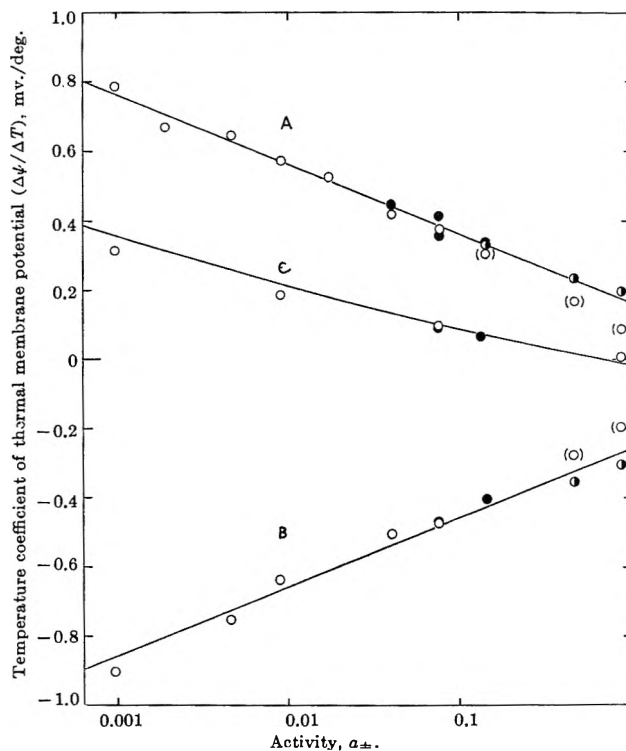


Figure 7. The dependence of temperature coefficient, $\Delta\psi/\Delta T$, on KCl concentration: O, observed values (no corrections were given); \odot , corrected for the low transport number; \bullet , corrected for the concentration difference and the low transport number.

terms due to the concentration difference in addition to the terms due to the temperature difference, as seen in eq. 12. Therefore, if the term due to the concentration difference (*i.e.*, the first term in eq. 12) is subtracted from the observed values, the remaining values must be the values for the presence of temperature difference only, and, therefore must be in agreement with the potential differences which were obtained with no concentration difference. The relationship between the thermal potential (*i.e.*, the potential due to temperature difference only) and the temperature difference is shown in Figure 6. The slopes of the graphs in Figure 6 are compared with the values obtained without concentration difference in Figure 7. All values are seen to be on the same theoretical lines, as shown in Figure 7.

In conclusion, the present theory for nonisothermal membrane systems agrees with the experimental results both in the absence and in the presence of concentration difference. The membrane potential $|\Delta\psi|$ increases linearly with increase of the temperature difference and the slope of $\Delta\psi/\Delta T$ vs. $\log a_{\pm}(2)$ plot is $2.303R/\bar{v}$ if the transport number of anion is unity.

(11) See ref. 10, p. 558.

Acknowledgment. The authors wish to thank Professor I. Kagawa of Nagoya University for his continuing interest and encouragement, and also Pro-

fessor L. Kotin of University of Illinois (Chicago) and Professor Y. Kobatake of Osaka University for critically reading our manuscript.

A Method for Determining Dielectric Relaxation Times

by Abhai Mansingh and Pradip Kumar

Physics Department, Allahabad University, Allahabad, India (Received June 21, 1965)

A graphical method has been proposed to solve Fröhlich's expression for complex dielectric constant at microwave frequencies in order to evaluate the minimum and maximum dielectric relaxation times τ_1 and τ_2 . Calculations have been made at three frequencies for ethyl bromide and butyl bromide at 25° and dibenzyl ether at 20, 40, and 60°. It has been found that the results are affected considerably by the inaccuracy of measurements and by the nonapplicability of Fröhlich's distribution function.

Introduction

Dielectric relaxation is the lag in dipole orientation behind an alternating electric field.¹ Bergmann, Roberti, and Smyth² have given a method for analyzing the dielectric relaxation of some substances in terms of two relaxation times, one for the molecular orientation and the other for the intramolecular orientation process. Recent experimental observations³ have been made showing very clearly the existence of the two processes. When the dielectric relaxation occurs by two or more mechanisms giving more or less overlapping dispersion regions, the analysis of the corresponding dielectric constant and loss values and the calculation of the relaxation times are often difficult and approximate. Fong and Smyth⁴ have described a method for such cases in terms of the Debye theory.

Fröhlich⁵ considered that a distribution in relaxation time might arise from a distribution of activation energies in a given system. This is consistent with the model that each rotating segment is surrounded by a different field of force, but the lengths of the relaxing segments are equal throughout the system. Fröhlich⁵ assumed that each process obeyed the Arrhenius relation $\tau = \tau_0 \exp(v/kT)$, H to $H + v$ being the range of

activation energy, H being the minimum potential barrier.

To explain the circular arc plot for a large number of molecules Cole and Cole⁶ empirically introduced a parameter α in Debye's expression for complex dielectric constant ϵ^* , and called α the distribution parameter for the relaxation time. Instead of using α , Fröhlich⁵ assumed minimum and maximum relaxation times, τ_1 and τ_2 , and used a distribution function of the form

$$\begin{aligned} f(\tau) &= 1/A\tau & (\tau_1 < \tau < \tau_2) \\ f(\tau) &= 0 & (\tau > \tau_1, \tau_2 < \tau) \end{aligned} \quad (1)$$

where $A = v/kT$.

(1) P. Debye, "Polar Molecules," Chemical Catalog, New York, N. Y., 1929.

(2) K. Bergmann, D. M. Roberti, and C. P. Smyth, *J. Phys. Chem.*, **64**, 665 (1960).

(3) W. P. Purcell, K. Fish, and C. P. Smyth, *J. Am. Chem. Soc.*, **82**, 6299 (1960).

(4) F. K. Fong and C. P. Smyth, *J. Phys. Chem.*, **67**, 226 (1963).

(5) H. Fröhlich, "Theory of Dielectrics," Oxford University Press, London, 1949, pp. 93-95.

(6) K. S. Cole and R. H. Cole, *J. Chem. Phys.*, **9**, 341 (1941).

With such a distribution function, he derived expressions for ϵ' and ϵ'' , the dielectric constant and the dielectric loss, respectively. Assuming Fröhlich's distribution function, Higasi^{7,8} gave a method for determining τ_1 and τ_2 .

It is observed that different relaxation mechanisms are not equally probable. Smaller values of τ indicate more probable mechanisms. Matsumoto and Higasi,⁹ therefore, modified the eq. 1 as

$$f(\tau) = 1/A\tau^n \quad (0 < n < \infty, \tau_1 < \tau < \tau_2)$$

$$f(\tau) = 0 \quad (\tau_1 > \tau, \tau_2 < \tau)$$

In some substances, Davidson and Cole¹⁰ showed that as the temperature of measurement is lowered, skewed arcs are obtained. These were beautifully explained by Matsumoto and Higasi⁹ by putting $n = 3/2, 1, 2/3, 1/2,$ and $1/3$. When the experimental values of Davidson-Cole parameter β are very near to the theoretical values obtained by putting $n = 3/2, 1, 2/3, 1/2,$ and $1/3$, the method described here may also be applied. For intermediate values of β it may be difficult to choose a proper value of n and evaluate the integral.

The purpose of the present paper is to determine τ_1 and τ_2 using Fröhlich's equation and making no approximation. Since an algebraic solution was impossible, a graphical approach has been followed. The results are considerably affected by the inaccuracy of measurements.

Theory

Taking into consideration the distribution of relaxation time, Fröhlich's⁵ expression for the complex dielectric constant is

$$\epsilon^* = \epsilon_\infty + \int_0^\infty \frac{(\epsilon_0 - \epsilon_\infty)f(\tau)d\tau}{(1 - j\omega\tau)} \quad (2)$$

where ϵ_0 and ϵ_∞ are the static and optical dielectric constants, respectively, τ is the relaxation time, ω is the angular frequency, $f(\tau)$ is the distribution function for the relaxation time given by eq. 1, and $j = \sqrt{-1}$. Only the case where $n = 1$ will be considered. Using eq. 1, eq. 2 can be written as

$$\frac{\epsilon^* - \epsilon_\infty}{\epsilon_0 - \epsilon_\infty} = \frac{1}{A} \int_{\tau_1}^{\tau_2} \frac{d\tau}{\tau(1 - j\omega\tau)} \quad (3)$$

where τ_1 and τ_2 are the minimum and maximum relaxation times. Multiplying the numerator and denominator of the right-hand side of this equation by $(1 + j\omega\tau)$ and equating the real and imaginary parts of both sides and using $\epsilon^* = \epsilon' + j\epsilon''$, the following equations are obtained

$$\frac{\epsilon' - \epsilon_\infty}{\epsilon_0 - \epsilon_\infty} = \frac{1}{A} \int_{\tau_1}^{\tau_2} \frac{d\tau}{\tau(1 + \omega^2\tau^2)} \quad (4a)$$

and

$$\frac{\epsilon''}{\epsilon_0 - \epsilon_\infty} = \frac{1}{A} \int_{\tau_1}^{\tau_2} \frac{\omega d\tau}{(1 + \omega^2\tau^2)} \quad (4b)$$

Dividing eq. 4b by eq. 4a and evaluating the integrals

$$\frac{\epsilon''}{\epsilon' - \epsilon_\infty} = \frac{2\left\{\tan^{-1} \omega\tau_2 - \tan^{-1} \omega\tau_1\right\} \left/ \ln \frac{\tau_2^2 (1 + \omega^2\tau_1^2)}{\tau_1^2 (1 + \omega^2\tau_2^2)} \right.}{}$$

Introducing two variables, $\omega_1 = 1/\tau_1$ and $\omega_2 = 1/\tau_2$, and rearranging the terms one gets

$$\left(\frac{\epsilon''}{\epsilon' - \epsilon_\infty}\right) \ln (\omega_1^2 + \omega^2) + 2 \tan^{-1} \frac{\omega}{\omega_1} = \left(\frac{\epsilon''}{\epsilon' - \epsilon_\infty}\right) \ln (\omega_2^2 + \omega^2) + 2 \tan^{-1} \frac{\omega}{\omega_2}$$

or

$$f(\omega_1) = f(\omega_2) = f(\omega_k)$$

where

$$f(\omega_k) = \left\{ \left(\frac{\epsilon''}{\epsilon' - \epsilon_\infty}\right) \ln (\omega_k^2 + \omega^2) + 2 \tan^{-1} \frac{\omega}{\omega_k} \right\} \quad (5)$$

The factor $\epsilon''/\epsilon' - \epsilon_\infty$, for any substance at a constant temperature and a given angular frequency ω , is a constant. Now a graphical solution to eq. 5 is sought. Experimentally observed values of ϵ' , ϵ'' , and ϵ_∞ at a given temperature, and the angular frequency (ω) are substituted into eq. 5. A curve of $\log \omega_k$ vs. $f(\omega_k)$ is traced by varying ω_k independently. A typical curve (dibenzyl ether) is shown in Figure 1a. An infinite number of lines parallel to the abscissa can be drawn to cut the curve at two points which correspond to equal values of $f(\omega_k)$. For every such line the condition $f(\omega_1) = f(\omega_2)$ is satisfied. The infinite number of solutions clearly show that observation at one single frequency is not sufficient to determine the correct values of τ_1 and τ_2 . Therefore, another curve must be traced (Figure 1b) with the help of observed data for a different value of ω . To find the relaxation times τ_1 and τ_2 , two curves between $\log \omega_1$ and $\log \omega_2$, as ob-

(7) K. Higasi, "Dielectric Relaxation and Molecular Structure," Hokkaido University, Sapporo, Japan, 1961, Chapters VI and VII.

(8) K. Higasi, K. Bergmann, and C. P. Smyth, *J. Phys. Chem.*, **64**, 880 (1960).

(9) A. Matsumoto and K. Higasi, *J. Chem. Phys.*, **36**, 1776 (1962).

(10) D. W. Davidson and R. H. Cole, *ibid.*, **12**, 1484 (1951).

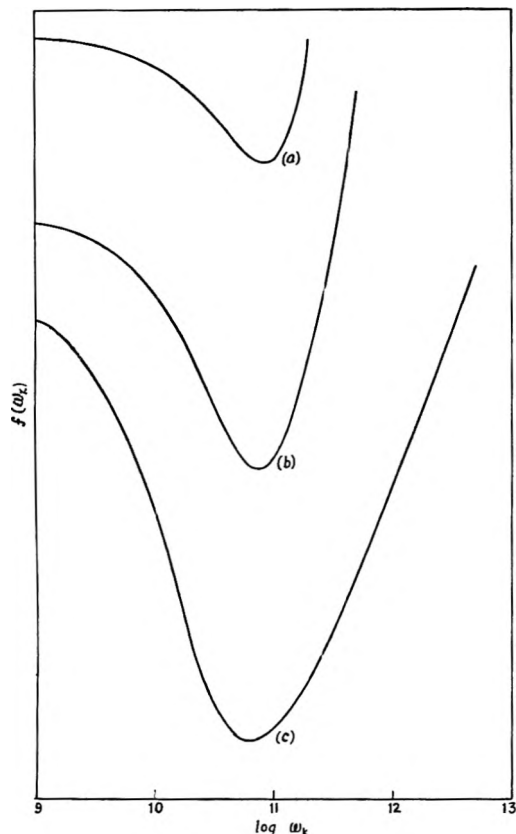


Figure 1. Plots of $f(\omega_k)$ vs. $\log \omega_k$ for dibenzyl ether at 60° for three wave lengths: (a) 1.25 cm.; (b) 3.22 cm.; and (c) 10.0 cm.

tained from different lines parallel to the abscissa for the two curves a and b in Figure 1, are traced. The point of intersection of the two curves thus drawn, Figure 2, gives the relaxation times.

If the accuracy of measurement is very good, observations at two frequencies only will suffice and give good values of τ_1 and τ_2 . With anything less than very good accuracy observations at more frequencies will be needed. Curves corresponding to different observation frequencies ω may not intersect at a common point; thus several values of τ_1 and τ_2 may be obtained. If the spread of the calculated values is not large, an average may be taken and better values of relaxation times τ_1 and τ_2 may be obtained. If the inaccuracies are large, the lines may not intersect or the spread in the values may be large.

The relaxation times for a few substances have been determined by the above method and the results are compared with other methods. The data were easily available from the Princeton group.^{11,12} The results of the calculations are given in Tables I and II. The points of intersection of the lines for observations at wave lengths 10 and 3.22 cm., 10 and 1.27 cm., and

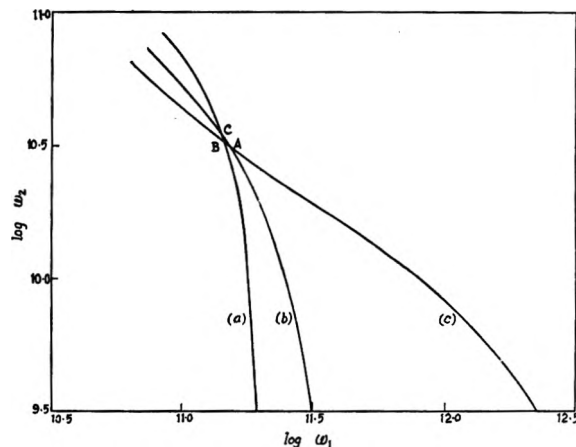


Figure 2. Plots of $\log \omega_1$ and $\log \omega_2$. Curves a, b, and c here correspond to curves a, b, and c, respectively, of Figure 1.

Table I: Values of the Relaxation Times τ_1 and τ_2 for Ethyl Bromide and Butyl Bromide

Substances		Authors' values		Higasi's values ^a	
		$\tau_1 \times 10^{12}$ sec.	$\tau_2 \times 10^{12}$ sec.	$\tau_1 \times 10^{12}$ sec.	$\tau_2 \times 10^{12}$ sec.
Ethyl bromide at 25°	A	0.5	16.6		
	B	1.2	11.0	1.8	8.0
	C	1.8	7.3		
<i>n</i> -Butyl bromide at 25°	A	8.5	10.1		
	B	3.4	20.2	3.1	24.6
	C	3.0	28.2		

^a See ref. 7.

3.22 and 1.27 cm. are given in Table IA, B, and C, respectively. Table IIA, B, and C lists the points of intersection of the lines for observations at wave lengths 10 and 3.22 cm., 10 and 1.25 cm., and 3.22 and 1.25 cm., respectively.

Discussion

In the case of ethyl bromide and butyl bromide, the spread in the calculated values is very large and hence these values cannot be averaged to given correct values for τ_1 and τ_2 . The large discrepancies in the values of τ_1 and τ_2 are apparently due to experimental inaccuracy. This may also be due to the nonapplicability of the Fröhlich distribution function. If observations at a larger number of frequencies are available, the average

(11) W. M. Heston, Jr., E. J. Hennelly, and C. P. Smyth, *J. Am. Chem. Soc.*, **70**, 4093 (1948); H. L. Laquer and C. P. Smyth, *ibid.*, **70**, 4097 (1948); E. J. Hennelly, W. M. Heston, Jr., and C. P. Smyth, *ibid.*, **70**, 4102 (1948); F. H. Branin, Jr., and C. P. Smyth, *J. Chem. Phys.*, **20**, 1121 (1952).

(12) D. M. Roberti, O. F. Kalman, and C. P. Smyth, *J. Am. Chem. Soc.*, **82**, 3523 (1960).

Table II: Values of the Relaxation Times τ_1 and τ_2 for Dibenzyl Ether

Substance		Authors' values		Bergmann's values by Higasi's method ^a		Bergmann's values by his method ^a	
		$\tau_1 \times 10^{13}$ sec.	$\tau_2 \times 10^{13}$ sec.	$\tau_1 \times 10^{13}$ sec.	$\tau_2 \times 10^{12}$ sec.	$\tau_1 \times 10^{12}$ sec.	$\tau_2 \times 10^{12}$ sec.
Dibenzyl ether at 20°	A	12.6	64.5				
	B	11.2	72.5	11.0	79.0	3.9	33.0
	C	10.2	127.4				
Dibenzyl ether at 40°	A	8.1	51.5				
	B	8.4	50.4	8.0	42.0	4.2	25.0
	C	8.8	43.1				
Dibenzyl ether at 60°	A	6.5	31.8				
	B	6.7	30.9	8.0	19.0	4.2	17.0
	C	6.8	29.8				

^a See ref. 2.

of the calculated τ_1 and τ_2 would give a better estimation of the relaxation times.

The accuracy of measurements for dibenzyl ether is definitely greater than that for the alkyl bromides. In the case of dibenzyl ether, it is seen that as the temperature increases, the spread in the values of τ_1 and τ_2 decreases. Assuming the accuracy of measurements to remain the same, it seems possible that Fröhlich's distribution function becomes more probable as the temperature increases.

The methods of Bergmann, Roberti, and Smyth² and Fong and Smyth⁴ are approximate. The former method is good for the cases where two widely separated relaxation times occur, while the latter one is

applicable to the cases where the distribution function is completely unknown. Higasi's^{7,8} method may be called a semiempirical method. It is based on a comparison of the Cole-Cole arc plot and the pseudo-elliptic plot. The results, therefore, depend on the empirical parameter α .

Since the method suggested here depends on the solution of Fröhlich's equation without any approximations, it is expected to give better results, provided Fröhlich's distribution function is applicable.

Acknowledgments. Thanks are due to Professor Krishnaji for supervision and to the C.S.I.R. (India) for financial assistance.

The Desorption and Isotopic Exchange of Oxygen at a Silver Surface¹

by Y. L. Sandler and D. D. Durigon

Westinghouse Research Laboratories, Pittsburgh, Pennsylvania 15236 (Received June 21, 1965)

Pressure-temperature scans with oxygen on porous silver, as well as the onset of the homonuclear exchange $O^{16}_2 + O^{18}_2 \rightarrow 2O^{16}O^{18}$, show that the chemisorption becomes partly reversible at about 160°. Measurements of the exchange rate were carried out at 160–180°, followed by fast removal of the gas phase and determination of the desorption rate and of the isotopic composition of the desorbing gas. It is thus shown in two independent ways that the desorption rate is equal to the rate of exchange. The chemisorbed oxygen exists in two binding states, but no evidence is found that one of these is in undissociated form. Increase in the proportion of the firmly bound form reduces the desorption rate but causes no change in the activation energy of desorption which is 32.5 kcal./mole of O_2 . The results show that while rapid diffusion and exchange takes place over the entire outer surface, desorption occurs only from those regions which are free of the firmly bound oxygen.

Introduction

The understanding of the chemisorption of oxygen on silver is of great interest in view of the importance of silver as an oxidation catalyst, as an oxygen electrode in fuel cells, and as a base material in electron emissive devices and photocathodes. Previous adsorption work on silver indicates the existence of different types of oxygen chemisorptions. This was concluded from the discontinuity in the rate of adsorption with increasing coverage.^{2a,b} Furthermore, studies of the catalytic oxidation of ethylene to ethylene oxide and carbon dioxide indicate that the reactions occur by two distinct mechanisms which involve two different types of chemisorption.^{3,4}

Isotopic exchange experiments^{5,6} were interpreted as showing that one of the modes of adsorption is non-dissociative. This was concluded from results which seemed to show that the desorption rate of oxygen in the region of 200° is faster than the rate of the homonuclear exchange reaction, $O^{16}_2 + O^{18}_2 \rightarrow 2O^{16}O^{18}$. The present work did not confirm these results.

The poor reproducibility and conflicting results in kinetics and adsorption behavior^{7,8} and in surface potential measurements⁹ have been noted. To a large extent, this has been due to the presence of impurities. Much of the work was done on catalyst powders of low purity and evacuated only slightly above the operating temperature (200–300°).

In the present work, attention was thus paid to the cleanliness of bulk and surface of the silver. A study was made of the properties of the different modes of adsorption of oxygen and their mutual interaction. Experiments will be described and discussed in which the adsorption and desorption of oxygen and isotopic exchange reactions were studied. The present paper only deals with the silver-oxygen system proper; the effect of added impurities, including hydrogen, will be the subject of another communication.¹⁰

(1) Work supported by the Advanced Research Projects Agency through the U. S. Army Electronics Laboratories and the Office of Naval Research.

(2) (a) A. F. Benton and L. C. Drake, *J. Am. Chem. Soc.*, **56**, 255 (1934); (b) W. W. Smeltzer, E. L. Tollefson, and A. Cambron, *Can. J. Chem.*, **34**, 1046 (1956).

(3) G. H. Twigg, *Proc. Roy. Soc. (London)*, **A118**, 92, 105, 123 (1946).

(4) Cf. L. Y. Margolis, *Advan. Catalysis*, **14**, 451 (1963).

(5) R. G. Meisenheimer, A. W. Ritchie, D. O. Schlissler, D. P. Stevenson, H. H. Voge, and J. N. Wilson, *Proceedings of the Second International Congress on Surface Activity*, Vol. II, Butterworth and Co., Ltd., London, 1957, p. 337.

(6) L. Y. Margolis, *Izv. Akad. Nauk SSSR*, 225 (1959).

(7) M. I. Temkin and N. V. Kulkova, *Proc. Acad. Sci. USSR*, **105**, 1021 (1955).

(8) J. N. Wilson, H. H. Voge, D. P. Stevenson, A. E. Smith, and L. T. Atkins, *J. Phys. Chem.*, **63**, 463 (1959).

(9) J. T. Kummer, *ibid.*, **63**, 460 (1959).

(10) Y. L. Sandler, S. Z. Beer, and D. D. Durigon, forthcoming publication.

Experimental Section

Experimental Setup. The reaction system of about 30 cc. volume consisted of 2–4 g. of silver powder in a quartz vessel, a thermistor gauge, and a Hoke metal valve (No. 411). The latter separated the system through liquid nitrogen traps from the gas handling system, in which lubricated stopcocks were used, and from the mercury diffusion pumps. Further details are described elsewhere.¹¹

The system was coupled to a small mass spectrometer (Consolidated Electrodynamics Model 21-620A) from which the standard 3-l. volume was isolated in order to facilitate the use of smaller gas samples for analysis. The instrument was used for monitoring impurities desorbing from the samples and for analyzing isotopic oxygen mixtures. One control experiment, described in Table I, run 5, was carried out on a larger sample and was analyzed on a larger analytical mass spectrometer (Consolidated Electrodynamics Model 21-103C).

Surface Areas. These were determined by the B.E.T. method by means of thermistor gauges. Krypton was used as an adsorbent at liquid nitrogen temperature and helium for dead space determinations. The surface area amounted to about 600 cm.²/g. after cleaning and degassing the powder. The monolayer of chemisorbed oxygen will be defined as 1.2×10^{15} atoms/cm.², in accordance with previous literature.^{2,5}

Material. The silver was procured from Engelhard Industries. It was prepared from carbonate by reaction with formic acid. It contained only 4 p.p.m. of copper as determined by spark source mass spectrometric analysis; this is equivalent to only $1/30$ of a monolayer. The carbon content,¹¹ however, was considerably larger and was removed *in situ*.

Degassing Procedure. Except in the preliminary experiments described, the empty reaction vessel was first pumped at 600–700°. The metal valve and thermistor were degassed at 180° for several days with frequent contact of low pressure oxygen. During the later stages only traces of hydrogen desorbed from the valve. The powder was then placed in the vessel and pumped. On raising the temperature to 150°, hydrocarbons and water were observed to desorb. After their removal, the temperature was gradually raised to about 520°. Oxygen below 1 torr pressure was repeatedly added to remove residual carbon¹¹ as CO₂. After several days of treatment the pressure build-up in the reaction vessel was measured when closed at 500° overnight; it amounted to an equivalent of less than 10^{-3} monolayer. No hydrogen was used for cleaning in the present experiments because it was found¹¹ that some hydrogen is retained by the metal and modifies its surface properties.

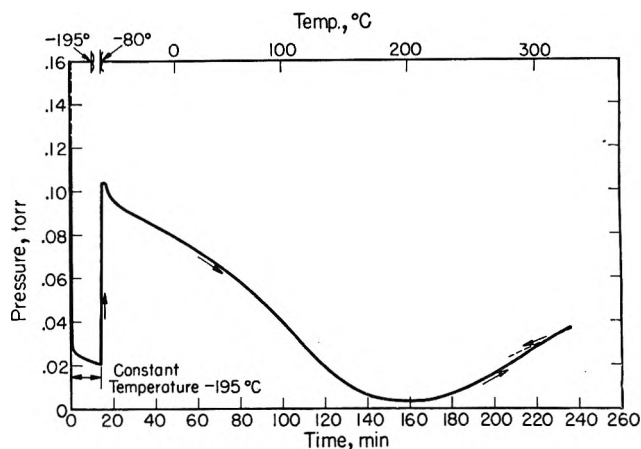


Figure 1. Pressure-temperature scan for oxygen on silver with fixed amount of oxygen in reaction vessel.

Results

Pressure-Temperature Scans. These provide rapid qualitative information on different types of adsorption active in different temperature ranges. In Figure 1, a pressure-temperature scan is shown taken at an early stage (on a powder of lesser purity). The oxygen pressure, for a constant amount of oxygen in the reaction vessel, is plotted *vs.* time and temperature. Oxygen (8×10^{-3} cc. (STP)) was first adsorbed on 2 g. of silver at -195° in a vessel of 30-cc. volume. The temperature was then raised in a single step to -80° . The sharp pressure rise is due to release of physically adsorbed gas. The temperature from there on was raised at a uniform rate to 240° within 4 hr. It may be seen that already at -80° a slow readsorption takes place due to chemisorption. At about 160° the pressure begins to increase as expected when the chemisorption becomes partly reversible. When the temperature was reversed, the curve in the last region essentially retraced itself, apart from a small hysteresis which can be attributed to lack of temperature equilibrium.

The Homonuclear Exchange Reaction $O^{16}_2 + O^{18}_2 \rightarrow 2O^{16}O^{18}$. An early exchange experiment is presented in Table I. Two grams of high-purity silver powder, in a vessel of 30-cc. volume, was first degassed for 24 hr. at temperatures up to 360° . Twenty torr of a nonequilibrium isotopic oxygen mixture was then admitted at room temperature. Table I gives the analyses of the oxygen mixture used and of samples withdrawn after 30 min. contact at various temperatures up to 250° .

The following conclusions can be drawn from this. (1) Below 150° no measurable amount of $O^{16}O^{18}$ is

(11) Y. L. Sandler and D. D. Durigon, *Trans. Faraday Soc.*, in press.

Table I: Reaction of 20-Torr O¹⁶₂ + O¹⁸₂ Mixture with Silver Powder

	Mole %							
	O ¹⁶ O ¹⁶	O ¹⁶ O ¹⁷	O ¹⁶ O ¹⁸	O ¹⁷ O ¹⁸	O ¹⁸ O ¹⁸	CO ¹⁶ O ¹⁶	CO ¹⁶ O ¹⁸	CO ¹⁸ O ¹⁸
O ¹⁶ ₂ + O ¹⁸ ₂ mixture	47.5	0.04	7.7	0.40	44.3	0.04
(1) 25°, 30 min.	47.2	0.04	7.7	0.39	44.6	0.03
(2) 150°, 30 min.	47.0	0.04	7.5	0.37	44.4	0.53	0.15	...
(3) 200°, 30 min.	47.2	0.06	8.0	0.36	42.5	1.3	0.44	0.05
(4) 200°, 60 min.	48.0	0.08	8.7	0.35	40.9	1.3	0.55	0.06
(5) 250°, 30 min.	50.2	0.11	12.3	0.32	34.8	1.2	0.84	0.17

formed. This is in agreement with the conclusions drawn from the pressure-temperature scan which showed lack of reversibility of the gas uptake below that temperature. (2) Residual O¹⁶, which is retained by the silver during the evacuation, participates in the exchange. This follows from the increase in the O¹⁶/O¹⁸ ratio and is most evident from the increase in the concentration of O¹⁶₂ with increasing temperature while the concentration of O¹⁸₂ decreases. (3) Carbon dioxide was evolved in fairly large quantities in this early experiment. Temperature and time of degassing and cleaning with oxygen were therefore considerably raised in the subsequent experiments. Conclusions 1 and 2 were, nevertheless, confirmed in the experiments described later.

From the temperature dependence of the exchange reaction, measured on nine different samples, an apparent activation energy of 30-37 kcal./mole was found between 200 and 280°. The reaction order was found to be 0.5 at 250° at 2-20 torr pressure and about 0.1 at 180°.

Desorption of Isotopic Oxygen Mixtures. Previously published experiments,^{5,6} involving a preadsorbed oxygen isotope, were interpreted as showing that the desorbing gas is equilibrated only in part and the conclusion was drawn that a substantial part of the chemisorbed oxygen must exist in undissociated form. To test this conclusion, desorption experiments were carried out in which the degree of equilibrium in the desorbing gas was directly determined after rapid removal of the gas phase. The experiments were carried out in the temperature region of 160 to 200° in which the homonuclear exchange is slow but still measurable and the rate of desorption is slow enough so that removal of the gas phase can be accomplished with negligible loss in coverage.

In Table II, results of desorption experiments are presented. A nonequilibrium equimolar mixture of O¹⁶₂ and O¹⁸₂, containing 6.5% O¹⁶O¹⁸, was first adsorbed at about 2 torr pressure for 15 to 45 min. When possible, the apparent rate constant was measured for

the small change in O¹⁶O¹⁸ which took place in the relatively short time. The reaction vessel was then pumped 40 to 60 sec. and small samples of desorbing gas were collected in the reaction vessel for analysis.

Argon was admixed to the isotopic mixture because it is not adsorbed on the metal and is pumped at a rate similar to oxygen. The completeness of the gas removal before taking desorbed samples can thus be checked. This is important because removal of the gas phase had to be rapid and complete in order to keep the loss in surface coverage low (to about 10⁻³ of the adsorbed gas) and to avoid mixing of the small amounts of desorbed gas with residual gas phase oxygen.

The first four examples given in Table II were measured in a vessel of 33-cc. volume on a 4-g. sample of silver having a surface area of 2000 cm.². In the first example, the sintered powder was pretreated at 500° with O¹⁶₂ at a few torr pressure and was pumped for 2.5 hr. at the same temperature. Then 2.2 torr of an oxygen mixture of the given composition was adsorbed for 15 min. at 180°. In all experiments the amount of adsorbed oxygen was about equal to the amount in the gas phase to within a factor of 3. The O¹⁶O¹⁸ may be seen to have changed little during this period. (The figures given in brackets in Table II represent the oxygen concentration given in the preceding line, normalized to 100% for oxygen only.) After pumping the gas phase for 40 sec., successive gas samples were collected in the reaction vessel for 3 min. each. It may be seen that already the first gas sample from the adsorbed phase had a high O¹⁶O¹⁸ concentration. For strictly equimolar mixtures of O¹⁶₂ + O¹⁸₂ the equilibrium concentration of O¹⁶O¹⁸ would be 50% corresponding to an equilibrium constant $K = (O^{16}O^{18})^2 / (O^{16}_2)(O^{18}_2) = 4.0$. At the O¹⁶/O¹⁸ ratios in the present experiments, the equilibrium concentration is 45-47% O¹⁶O¹⁸.

An increased O¹⁶ concentration was found in the desorbing gas after removal of the gas phase. This is due to residual oxygen which was not removed even

Table II: Desorption Experiments on Silver

No.	System	Pretreatment at 500°	Approximate temp., °C.	Pressure, torr	Pump, sec.	Gas collected
1	Small mass spectrometer, 4 g. of Ag, 33-cc. volume	O ¹⁶ ₂ Evacuated 2.5 hr.	180	2.2	~40	
					45	
					45	
2		O ¹⁶ ₂	180	1.7		
3		Evacuated 4 hr.	180	2.2	40	
					45	
					45	
4		O ¹⁶ ₂ + O ¹⁸ ₂	180	2.2	60	2.8 μ
					45	3.3 μ
					45	3.1 μ
5	Large mass spectrometer, 20 g. of Ag, 135-cc. volume	O ¹⁶ ₂ + O ¹⁸ ₂	160	2.3	50	2.0 μ
					45	2.3 μ
			160	1.20 at 45 min.		0.135 cc. (=99% of gas phase) 0.0031 cc.

Time		Analysis, mole %			A	k_{app} , min. ⁻¹
From	To	O ₂	O ₁₈ O ₂	O ₂		
0	15 min.	37.6 (45.5)	5.4 6.5	39.8 48.0)	17.2	
		37.4	5.5	38	19.0	
		(46.2)	6.8	47.0)		
15 min. 40 sec.	18 min. 40 sec.	46	31 ± 5	23	0.0	
19 min. 25 sec.	22 min. 25 sec.	45	40	15	0.0	
23 min. 10 sec.	26 min. 10 sec.	46	40	14	0.0	
		37.8	5.3	39.5	17.4	
		(45.9)	6.4	47.8)		
0	15 min. 20 sec.	37.0	5.4	37.7	19.9	
		(46.2)	6.8	47.1)		
16 min. 0 sec.	19 min. 0 sec.	22	39 ± 3	39	0.0	
19 min. 45 sec.	22 min. 45 sec.	17	46	37	0.0	
23 min. 30 sec.	28 min. 15 sec.	11	44	45	0.0	
		46.1	6.1	45.3	2.5	
0	16 min.	46	6.1	44.3	2.9	5.4×10^{-4}
17 min. 0 sec.	20 min. 0 sec.	29	46 ± 5	25	0.0	
20 min. 45 sec.	24 min. 15 sec.	28	50	22	0.0	
25 min. 0 sec.	28 min. 30 sec.	25	51	24	0.0	
		38.4	5.4	39.4	16.8	
0	15 min.	37.5	5.1	38.1	19.3	
15 min. 50 sec.	30 min. 10 sec.	26	48 ± 5	26	0.0	
30 min. 55 sec.	48 min. 0 sec.	27	46	27	0.0	
		11.79	1.39	10.29	76.53	
		(50.24)	5.94	43.82)		
0	45 min.	7.40	0.99	6.54	85.07	3.5×10^{-4}
		(49.56)	6.63	43.81)		
49 min.	50 min.	7.51	1.01	6.72	84.67	
		(49.28)	6.63	44.09)		
90 min.	150 min.	30.97	49.5 ± 0.5	19.55	0.00	

after pumping at 500°. Samples pumped for 16 hr. at the high temperature showed the same behavior. In spite of its firm binding, this oxygen rapidly equilibrates on the surface with the adsorbing oxygen mixture.

In the second example given in Table II, an experiment similar to the first is presented in which, however, the residual oxygen was first replaced by O¹⁸. This was done by contacting the metal several times with O¹⁸₂ at 500°. At this temperature all residual oxygen is exchanged at a very high rate. It may be seen from Table II that the oxygen desorbed at 180° is now richer in O¹⁸ than is the gas adsorbed during the experiment.

The O¹⁶O¹⁸ concentration of the gas after 40 sec. of pumping and 3 min. of collecting was again relatively close to equilibrium as compared to the negligible change in concentration from 6.4 to 6.8% in 15 min. before removal of the gas phase.

The small deviation from complete equilibrium found in examples 1 and 2, and in four more experiments in which a single isotope was also used for pretreatment, is at least in part due to a poor temperature distribution found to exist over the sample. This may cause an uneven distribution of residual oxygen over the different regions of the porous metal when pumping at 500° and thus a varying O¹⁶/O¹⁸ ratio in the adsorbed phase after the oxygen mixture has been adsorbed. Then, even if the gas desorbing from each region is in isotopic equilibrium, the entire gas phase may not be in complete equilibrium. This holds to a larger extent for nonequimolar mixtures and could have been one reason for the apparent lack of isotopic equilibrium in the desorbing gas found in previously published work.^{5,6}

In examples 3 and 4 of the same table, the results are given for two runs in which the silver was pretreated with an equimolar mixture of O¹⁶₂ + O¹⁸₂ instead of a single isotope. In both experiments the desorbed samples were in isotopic equilibrium (50% O¹⁶O¹⁸) within the error of measurement.

The pressure of the desorbing gas was measured by the thermistor attached to the reaction vessel. In example 3, the apparent exchange constant at 180° was determined in a separate experiment. Since the desorbing gas was in equilibrium, the rate of exchange should be equal to the rate of desorption. Then the exchange rate constant must be equal to $(1/p)dp/dt$, *i.e.*, the rate of pressure increase per unit time divided by the pressure of the system. This latter quantity was $(1/2000 \mu) \times 1 \mu/\text{min.} = 5 \times 10^{-4} \text{ min.}^{-1}$, in agreement with the apparent exchange rate constant.

An independent experiment was also carried out on a larger reaction system which was attached to a

spectrometer of higher accuracy. The amounts of the various gases present in the gas phase and adsorbed at any time were now accurately determined from the measured oxygen/argon ratios and the gas amounts withdrawn. The latter were determined in a standard volume by means of a capacitance micromanometer. The gas phase in these experiments was removed by condensing it in a liquid helium trap. Measurement of the quantity of this gas as well as comparison of its composition with the composition of the gas phase before its condensation makes it possible to see if the adsorbed phase contains any weakly chemisorbed gas. The latter would have been lost during the pumping period in the previous experiments.

The results of one run are presented in Table II, experiment no. 5. The exchange rate was determined by a series of measurements in the first 45 min., the last of which is given in the table. The reaction vessel was then connected to a liquid helium trap, and 99% of the amount present in the gas phase was recovered from the trap. The composition of the trapped gas can be seen to be the same as in the gas phase before condensation. The adsorbed phase thus does not contain any measurable amount of weakly adsorbed oxygen. After a few expansions, the gas was collected in the trap for 1 hr. This gas was now in complete equilibrium as may be seen from the data in the last row of the table. The O¹⁶O¹⁸ concentration found was 49.5 ± 0.5 while the calculated equilibrium value is 49.4. The measured desorption rate again was equal to the exchange rate, determined in the first 45 min. before condensation of the gas. In no case was it found that the desorption is faster than the exchange as previously claimed.⁶ Exchange experiments thus provide no evidence that a part of the chemisorbed oxygen is undissociated.

Influence of Oxygen in the Stronger Binding State on the Desorption Rate. The presence of residual oxygen in the exchanged gas, as found in the described experiments, indicates the existence of chemisorbed oxygen in two different binding states.

In the following experiments the mutual interaction between the two types was studied by investigating the effect of varying the amounts of firmly bound oxygen on the rate and activation energy of desorption. The temperature distribution in these experiments was improved by surrounding the reaction vessel with a metal shield.

In Figure 2 the results of measurements of the rate of desorption as a function of oxygen pretreatment and temperature are given. The logarithm of the desorption rate per square centimeter is plotted *vs.* $1/T$. The silver was first pretreated in oxygen at

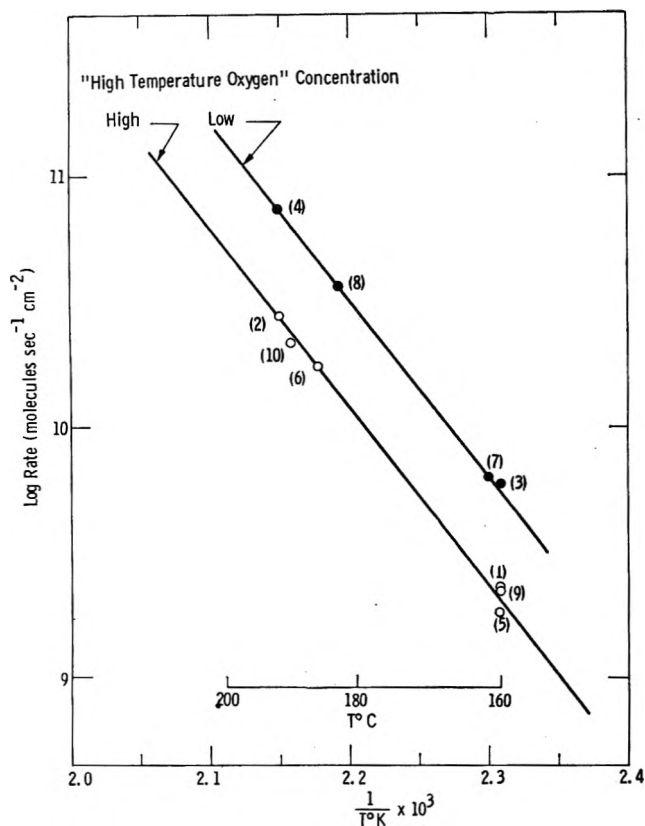


Figure 2. Effect of gas pretreatment at 500° on the oxygen desorption between 160 and 190°.

500° in all runs, and was then either pumped overnight to remove some of the firmly bound oxygen (upper line) or, alternately, was cooled in 5 torr of oxygen to 250° and then pumped for 1 hr. (lower line). In all cases, oxygen was then adsorbed at 5-torr pressure at 160° for 1 hr., the system was pumped, and the rate of desorption was followed by the recorded output of a thermistor gauge, first at about 160°, then after rapidly raising the temperature by 20–30°. The numbers on the two curves in Figure 2 give the sequence of the measurements. It may be seen that there is a well-reproducible effect of the high-temperature pretreatment. The higher concentration of the strongly bound "high-temperature oxygen" caused a rate of desorption which was roughly one-third as high. The activation energy corresponding to the two lines was the same within the error of the measurements, being 32.2 kcal./mole \pm 2.3 (maximum deviation) for the case of high "high-temperature oxygen" concentration, and 32.7 kcal./mole \pm 1.1 for the lower concentration.

Figure 3 shows a retraced pressure recording obtained for one of the runs represented in Figure 2. The pressure increase was linear before as well as after the temperature rise in all runs. The small loss of

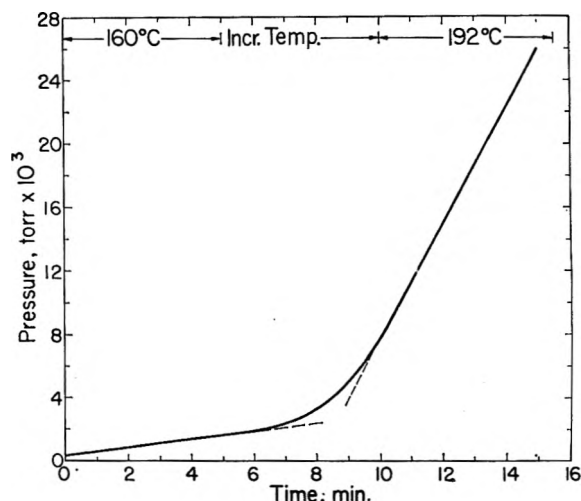


Figure 3. Pressure increase with time at two temperatures after rapid removal of the gas phase.

coverage during desorption thus had no effect on the desorption rate.

The desorption rate r is

$$r = 5 \times 10^{26} \exp(-32,500/RT) \text{ molecules sec.}^{-1} \text{ cm.}^{-2}$$

for the lower content in strongly bound oxygen, and about one-third as high for the higher content. It should be noted that the activation energy of desorption found by the desorption method is a "true" activation energy since it is measured at constant coverage. The activation energy of the exchange reaction is an apparent one since it is measured at constant pressure, but was found to be roughly the same. Assuming that the number and character of the adsorption sites do not appreciably change in the narrow temperature range between 160 and 200°, the following relationship¹² holds

$$E_{app} = E_{true} - nq$$

where n is the reaction order and q the differential heat of adsorption. With $n \approx 0.1$ and $q \approx 16$ kcal./mole,¹ the correction term nq is relatively small in the chosen temperature range, approximately 1.6 kcal./mole of O₂.

Discussion

It can be seen from the linearity of the pressure rise of the desorption and the good agreement of the desorption rates with exchange rates that meaningful desorption rates were obtained. Objections were previously raised^{12a,b} concerning the significance of desorp-

(12) Y. L. Sandler, *J. Chem. Phys.*, **21**, 2243 (1953).

(13) (a) B. M. W. Trapnell, "Chemisorption," Butterworth and Co., Ltd., London, 1955, p. 44; (b) A. W. Czanderna, *J. Phys. Chem.*, **68**, 2765 (1964).

tion data because of the possibility of readsorption during diffusion through the porous mass. Under the chosen condition, however, the depletion in coverage was small, below 1%, and the rate of chemisorption was very low.

The reproducible change in the desorption rate with oxygen pretreatment at high temperatures shows in a particularly clear way the existence of two types of chemisorbed oxygen, a low-temperature form which is reversible above 160° and a high-temperature form of much higher binding energy. The heat of adsorption in the weaker binding state is about 16 kcal./mole.^{2a} The adsorption heat for the stronger binding state is not known. A very high heat of adsorption, 108 kcal./mole of O₂, was found by Gonzales and Parravano¹⁴ at very low coverages. This was determined by the use of the hydrogen-water equilibrium. However, since the coverage amounted to only 10⁻² to 10⁻³ monolayer and no special precautions were apparently taken, the heat of adsorption may have been determined by surface impurities. Also, the chosen method is unsuitable for the oxygen-silver system proper because the presence of hydrogen modifies the oxygen adsorption on silver, as will be shown in a subsequent paper.

The present exchange and desorption experiments show that at least a portion of the residual firmly bound oxygen rapidly equilibrates with the adsorbing oxygen. Similar conclusions follow from experiments at 200° with an oxygen isotope preadsorbed on silver at the same temperature which are described elsewhere.¹⁵ The amount involved in the exchange is shown to be approximately one monolayer and includes firmly bound oxygen. Only at higher temperatures a larger amount of oxygen, in surface solution or occluded in the solid, is involved.

Boreskov and Kassin¹⁶ reported on exchange experiments with evaporated silver films which can be interpreted in the same manner. The rate constant of exchange between O¹⁶₂ gas with preadsorbed O¹⁸ was found to be constant to the extent of about one monolayer and the conclusion was drawn that the adsorbed

layer is "energetically uniform." According to our interpretation, the results mean that the desorption is rate-determining and the equilibration in the surface between different types of adsorbed oxygen is fast. This indicates a state of high mobility, but energetic uniformity of a complete monolayer cannot be reconciled with our results.

On a uniformly mobile surface, the changed mode of adsorption after high-temperature treatment would be expected to cause a change in the interaction energy between oxygen and surface. However, the desorption experiments show that the high-temperature oxygen treatment causes a decrease in the desorption rate without a change in the activation energy. The treatment causes an increase in the stronger oxygen adsorption on the expense of the weaker one and presumably involves a surface rearrangement¹⁷ or a growth of the low index crystal facets. Thermal etching in oxygen at high temperatures is known¹⁸ to bring out the low index planes.

The silver surface then consists of two distinct regions which differ in the arrangement of the silver atoms and the way in which the oxygen atoms are embedded between them. The more weakly chemisorbed oxygen atoms can diffuse over the outer surface and exchange with the more strongly bound oxygen. On the other hand, desorption of chemisorbed oxygen is restricted to those parts of the metal surface which are free of tightly bound oxygen. High-temperature oxygen pretreatment will decrease the size of the latter regions, but will not affect the desorption energy.

Acknowledgment. The authors are indebted to W. M. Hickam and his group for performing the control experiments on the analytical mass spectrometer.

(14) O. D. Gonzales and G. Parravano, *J. Am. Chem. Soc.*, **78**, 4533 (1956).

(15) Y. L. Sandler and W. M. Hickam, *Proc. Third Intern. Congr. Catalysis, Amsterdam, 1964*, 227 (1965).

(16) Discussion to ref. 15.

(17) Cf. A. V. MacRae, *Science*, **139**, 379 (1963).

(18) G. E. Read and H. Mykura, *Acta Met.*, **10**, 843 (1962).

The Conductance of the Symmetrical Tetraalkylammonium Halides and Picrates in Methanol at 25 and 10°

by Robert L. Kay, C. Zawoyski, and D. Fennell Evans

Mellon Institute, Pittsburgh, Pennsylvania (Received June 22, 1965)

Conductance measurements are reported for Me_4NCl , Bu_4NCl , Me_4NBr , Et_4NBr , Pr_4NBr , Bu_4NBr , $n\text{-Am}_4\text{NBr}$, Me_4NI , Pr_4NI , Bu_4NI , $n\text{-Am}_4\text{NI}$, Me_4NPi , and Bu_4NPi in methanol solutions at 25° and the bromides and iodides at 10°. The ion-size parameter \bar{d} had a constant value of 3.6 ± 0.2 at 25° and 3.5 ± 0.2 at 10° for all the salts. Only the tetramethyl- and tetraethylammonium halides are significantly associated among the bromides and chlorides, but all of the picrates and iodides and even the large tetraphenylborides are definitely associated in methanol solutions. A decrease in temperature has little effect on the association of the iodides but decreases the association of the bromides in proportion to the ϵT product. Dielectric constants of 38.01, 35.70, and 32.62 are reported for methanol at 0, 10, and 25°, respectively.

Introduction

The conductance of the tetraalkylammonium halides in aqueous solution has been found to be abnormal² in that the conductance decrease with concentration becomes greater as the anion size increases, in contrast to the predictions of the Fuoss-Onsager theory.³ It is possible to explain this abnormal conductance decrease by an appeal to ion association that increases as the anion size increases. The same type of abnormal behavior was found by Lindenbaum and Boyd⁴ for the activity coefficients of these salts in aqueous solution, which they explained by ion association. However, they postulated that ionic association was enhanced to a considerable extent by water-structural effects rather than by simple coulombic interaction.

In this paper, we report the association behavior of these salts in methanol solutions as obtained from conductance measurements at two temperatures. Methanol is a structured solvent with a dielectric constant in the intermediate range (32.6) that is not too different from that of acetonitrile (36.0). We have determined the association behavior of these salts in acetonitrile⁵ and found the association to depend primarily on ion size, increasing as the crystallographic size of both anion and cation decreases. The reverse behavior is reported here for the same salts in methanol solutions; that is, the association behavior is in agreement

with that required to explain the results for aqueous solutions. A considerable amount of data from the literature for methanol and other alcohol solutions has been recalculated to bring it into conformity with the Fuoss-Onsager theory and is reported here for comparison purposes.

Experimental Section

The resistance measurements and weighings were carried out with a precision of better than 0.02%. The details of the conductance bridge and cells have been described elsewhere,^{5,6} as has the procedure followed in making the measurements, with the exceptions as noted below. The cells were of the Erlenmeyer type and contained 500 ml. of solution, to which the weighed salt was added in Pyrex cups from the dispensing device in a closed system.⁶ All resistance measurements were corrected for the usual small frequency dependence.

(1) Presented in part at the 147th National Meeting of the American Chemical Society, Chicago, Ill., Sept. 1964.

(2) D. F. Evans and R. L. Kay, *J. Phys. Chem.*, in press.

(3) R. M. Fuoss and F. Accascina, "Electrolytic Conductance," Interscience Publishers, Inc., New York, N. Y., 1959.

(4) S. Lindenbaum and G. E. Boyd, *J. Phys. Chem.*, **68**, 911 (1964).

(5) D. F. Evans, C. Zawoyski, and R. L. Kay, *ibid.*, **69**, 3878 (1965).

(6) J. L. Hawes and R. L. Kay, *ibid.*, **69**, 2420 (1965).

All salts used for the measurements at 25°, with the exception of the chlorides, were the same samples as were used for the acetonitrile⁵ and aqueous² solutions. The measurements at 10° were carried out with freshly prepared salts purified as previously described.⁵ The chlorides were prepared by metathesis of the corresponding purified iodides by AgCl in methanol, the absence of iodide being determined by the starch test. The resulting AgI was removed by a fine, fritted-glass filter. Me₄NCl was recrystallized twice from methanol by the addition of peroxide-free ether and dried at 140° in a vacuum oven, while Bu₄NCl was recrystallized twice from acetone by the addition of ether and dried at 56° in a vacuum oven. Owing to the extreme hygroscopic nature of these chlorides, extreme care was taken to avoid contact of these salts with water vapor. All manipulations involving the chlorides were carried out in a drybox with appropriate precautions to avoid explosive concentrations of ether and acetone in the drybox atmosphere. We are indebted to Dr. J. Gordon for samples of his highly purified *n*-Am₄NBr and *n*-Am₄NI.

All solutions were prepared by weight and vacuum corrected. Owing to the hygroscopic nature of the chlorides, the usual 11-mm. Pyrex cups containing these salts were weighed in capped, soft-glass, 7-ml. standard weighing bottles that had been reduced in size by a factor of 3. All salt transfers involving the chlorides were carried out in a drybox. The salt cup dispensing device was of considerable help during the measurements on these hygroscopic salts.

Extremely high solvent conductances were encountered initially during measurements at 10°. This was found to be due to the contraction of the solvent on cooling which pulled air into the cells. The problem was overcome by maintaining positive pressure of N₂ in the cells during the cooling process.

Reagent grade methanol was purified by passage through reagent grade, mixed-bed, ion-exchange resin, followed by a fractional distillation in a 1.2-m. Stedman column. The ion-exchange resin had been previously treated with methanol until all water had been removed. Titration with Karl Fischer reagent indicated no more than 0.01 wt. % water in the final product, which had a specific conductance of $5-12 \times 10^{-8}$ at 25°. The measured density was 0.78658 at 25° and 0.80073 g. ml.⁻¹ at 10°. The viscosity at 10° was found to be 0.672 cp. as measured with a Ubbelohde-type viscometer, using as standard the methanol viscosity at 25° of 0.5445 cp.⁷ More recent measurements, carried out in this laboratory using a different viscometer of the same type, indicate this value to be low and 0.676 cp. to be more nearly correct at 10°. All calculations

reported here were carried out using the lower value since it was found that this small change in the solvent viscosity had a negligible effect on the conductance parameters.

The absolute dielectric constant of methanol was measured in the completely guarded three-terminal dielectric cells of Vidulich and Kay,⁸ using the General Radio Type 1615A transformer bridge. The cell constant of approximately 2.2 pf. was determined by direct measurement and corrected to vacuum. All measurements were carried out at 10 kHz. since there was a negligible frequency effect. The values of ϵ obtained at 0, 10, and 25° were 38.01, 35.70, and 32.62, respectively. Our result at 25° is in excellent agreement with that of Gosting and Albright⁹ and of Jones and Davies,¹⁰ but at every temperature our values are about 1% higher than those reported by Koizumi and Hanai.¹¹

The absolute temperature at 10° was determined within $\pm 0.002^\circ$ by means of a calibrated platinum resistance thermometer and a Mueller bridge, as was the case at 25°.

The cell constant at 10° was determined by measuring the conductance of aqueous KCl solutions and comparing the Λ_0 with that predicted by the conductance equation for the temperature dependence of the conductance of KCl between 5 and 55°, as given by Harned and Owen.¹² The resulting change in the cell constant between 25 and 10° was less than 0.01% and in good agreement with the change calculated from cell geometry and coefficients of expansion as given by Stokes and Robinson.¹³

Results

The equivalent conductances and concentrations (M) are given in Table I for 25° and in Table II for 10°. Included with each run is the solvent specific conductance, κ_0 , in ohm⁻¹ cm.⁻¹. The values of the density increments A are given for each salt. These were obtained at 25° from density measurements on the most concentrated solution studied in the conductance with the assumption that solution densities follow

(7) G. Jones and H. J. Fornwalt, *J. Am. Chem. Soc.*, **60**, 1683 (1938).

(8) G. A. Vidulich and R. L. Kay, *J. Phys. Chem.*, **66**, 383 (1962).

(9) P. S. Albright and L. J. Gosting, *J. Am. Chem. Soc.*, **68**, 1061 (1946).

(10) T. T. Jones and R. M. Davies, *Phil. Mag.*, **28**, 307 (1939).

(11) N. Koizumi and T. Hanai, *Bull. Inst. Chem. Res., Kyoto Univ.*, **33**, 14 (1955).

(12) H. S. Harned and B. B. Owen, "The Physical Chemistry of Electrolytic Solutions," 3rd Ed., Reinhold Publishing Corp., New York, N. Y., 1958, p. 233.

(13) R. A. Robinson and R. H. Stokes, "Electrolyte Solutions," 2nd Ed., Butterworth and Co. Ltd., London, 1959, p. 97.

Table I: Equivalent Conductances in Methanol at 25°

10°C	A	10°C	A	10°C	A	10°C	A	10°C	A	10°C	A
—Me ₄ NCl—		69.611	99.354	15.659	85.528	—Me ₄ NI—		33.319	91.769	—Me ₄ NPi—	
10 ⁸ κ ₀ =	A =	79.155	97.911	21.157	83.984	10 ⁸ κ ₀ =	A =	39.190	90.411	10 ⁸ κ ₀ =	A =
7.6	0.031			26.883	82.630	8.6	0.076	47.330	88.745	9.6	0.107
10.316	111.395	—Et ₄ NBr—		32.638	81.441	5.992	123.367			3.272	110.867
20.240	107.463	10 ⁸ κ ₀ =	A =	38.487	80.360	12.902	119.178	—Bu ₄ NI—		7.621	107.892
30.756	104.419	7.3	0.078	43.995	79.432	20.601	115.765	10 ⁸ κ ₀ =	A =	12.934	105.414
46.883	100.865	2.980	112.094			28.750	112.903	5.4	0.100	18.394	103.270
54.731	99.442	10.329	107.619			37.408	110.358	3.830	96.347	24.598	101.346
65.237	97.758	17.025	104.908	10 ⁸ κ ₀ =	A =	47.709	107.822	8.292	93.622	30.699	99.726
75.502	96.289	25.154	102.400	7.3	0.088	59.591	105.307	14.557	90.854	39.336	97.741
86.136	94.915	31.763	100.700	3.307	90.882	72.009	103.043	20.478	88.802	46.763	96.167
		39.165	99.056	8.084	88.285			27.594	86.757	10 ⁸ κ ₀ =	A =
—Bu ₄ NCl—		46.246	97.661	12.526	86.552	—Pr ₄ NI—		33.297	85.343	7.0	0.107
10 ⁸ κ ₀ =	A =	56.429	95.909	17.185	85.052	10 ⁸ κ ₀ =	A =	40.665	83.732	4.255	109.880
4.6	0.050			23.041	83.504	5.1	0.091	47.272	82.457	9.522	106.797
9.249	84.127	—Pr ₄ NBr—		28.310	82.306	2.949	104.108			14.640	104.553
18.099	81.538	10 ⁸ κ ₀ =	A =	33.398	81.269	8.956	100.041	— <i>n</i> -Am ₄ NI—		20.254	102.571
26.945	79.582	5.7	0.083	40.387	80.017	14.576	97.467	10 ⁸ κ ₀ =	A =	26.319	100.785
36.267	77.981	2.848	98.171	46.689	79.004	20.591	95.285	8.0	0.108	33.076	99.064
47.003	76.441	7.987	95.101			25.988	93.632	4.620	91.602	41.405	97.224
56.495	75.264	15.165	92.268	— <i>n</i> -Am ₄ NBr—		33.069	91.773	10.142	88.593	49.332	95.704
65.192	74.311	21.093	90.469	10 ⁸ κ ₀ =	A =	38.882	90.426	15.663	86.346	—Bu ₄ NPi—	
		27.080	88.962	9.1	0.104	48.875	88.414	22.633	84.106	10 ⁸ κ ₀ =	A =
—Me ₄ NBr—		33.060	87.645	3.485	86.851	10 ⁸ κ ₀ =	A =	30.654	81.978	11.2	0.117
10 ⁸ κ ₀ =	A =	40.228	86.254	8.719	84.179	6.0	0.091	37.199	80.497	2.848	82.021
5.2	0.062	49.851	84.638	14.996	81.973			44.033	79.119	8.135	79.120
4.905	118.394	—Bu ₄ NBr—		21.704	80.111	3.887	103.226	52.144	77.661	14.507	76.768
14.737	112.903	10 ⁸ κ ₀ =	A =	28.395	78.598	8.307	100.419	63.656	75.942	20.985	74.831
23.854	109.495	7.2	0.088	35.277	77.264	13.849	97.834	75.496	74.303	27.245	73.331
34.779	106.320	3.962	90.416	41.581	76.190	19.862	95.578	85.661	73.067	34.023	71.929
45.787	103.730	9.633	87.641	50.592	74.821	25.424	93.856	97.002	71.765	42.093	70.473
56.648	101.555							107.414	70.683	50.460	69.167

the linear relationship $d = d_0 + A\bar{m}$ where \bar{m} is the concentration in moles per kilogram of solution. The values of A at 10° were assumed to be the same as those at 25°, and measurement on a few salts indicated that the difference in A at the two temperatures was no greater than 0.005.

The conductance parameters for both 25 and 10°, obtained from least-squares analyses⁸ of the conductance data using a computer and the Fuoss-Osager³ equations in the form

$$\Lambda = \Lambda_0 - SC^{1/2} + EC \log C + (J - F\Lambda_0)C \quad (1)$$

or, if the electrolytes were associated, in the form

$$\Lambda = \Lambda_0 - S(C\gamma)^{1/2} + EC\gamma \log C\gamma + (J - F\Lambda_0)C\gamma - K_A C\gamma\Lambda\gamma^2 \quad (2)$$

are given in Table III. Included in Table III is σ_Λ , the standard deviation of the individual points. With two exceptions, it was found that treating the salts as

unassociated electrolytes resulted in σ_Λ that were from 2 to 14 times larger than those resulting from assuming association and using eq. 2. We have considered this a reliable criterion for association and have not included the results for the analyses with eq. 1 except for Bu₄NCl and Bu₄NBr at 10°.

The constants α , β , E_1 , and E_2 had the values 0.8545, 153.59, 7.350, and 193.5 at 25° and 0.8206, 122.76, 6.778, and 148.5 at 10°, respectively, where, in eq. 1 and 2, $S = \alpha\Lambda_0 + \beta$ and $E = E_1\Lambda_0 - E_2$.

The quantity F in eq. 1 and 2 corrects for the increase in the solution viscosity due to the addition of salt. For the large salts involved here, the increase in viscosity is not negligible, although not nearly so large as in aqueous solutions. We have followed Fuoss^{3,14} in setting F equal to the viscosity B coefficient. It should be remembered that only J and,

(14) R. M. Fuoss, *J. Am. Chem. Soc.*, **79**, 3301 (1957).

Table II: Equivalent Conductances in Methanol at 10°

10°C	Λ	10°C	Λ	10°C	Λ
—Me ₄ NBr—		—Bu ₄ NBr—		—Pr ₄ NI—	
10 ^s κ_0 = 10.5		10 ^s κ_0 = 5.5		10 ^s κ_0 = 11.3	
7.529	95.165	3.371	73.348	3.963	83.574
16.632	91.627	9.017	71.066	8.885	81.160
26.810	88.803	15.065	69.421	15.578	78.901
41.456	85.732	21.761	67.902	23.224	76.679
55.743	83.364	31.049	66.218	30.623	75.012
70.024	81.254	40.763	64.778	38.866	73.434
80.714	79.978	47.778	63.865	47.583	71.972
96.549	78.305	55.722	62.955	55.635	70.781
10 ^s κ_0 = 6.0		10 ^s κ_0 = 5.7		10 ^s κ_0 = 5.2	
8.705	94.594	4.341	72.892	4.020	83.617
19.461	90.758	8.995	71.107	10.670	80.519
30.507	87.939	14.853	69.409	19.000	77.839
39.969	86.008	21.146	67.976	26.058	76.064
50.342	84.189	29.087	66.590	44.175	72.595
60.620	82.637	36.743	65.324	55.400	70.914
74.463	80.819	46.135	64.064	62.337	69.995
91.411	78.925	57.330	62.767		
—Et ₄ NBr—		10 ^s κ_0 = 4.6		—Bu ₄ NI—	
10 ^s κ_0 = 5.7				10 ^s κ_0 = 10.2	
5.319	89.727	3.525	73.321	3.923	78.044
13.953	86.426	13.198	69.887	9.019	75.632
22.662	84.062	18.846	68.526	15.201	73.539
37.351	81.155	24.658	67.339	22.972	71.439
44.942	79.955	32.001	66.088	30.285	69.838
53.767	78.674	38.540	65.114	38.889	68.239
62.351	77.606	44.508	64.314	48.272	66.818
72.437	76.422	51.991	63.390	58.348	65.409
—Pr ₄ NBr—		—Me ₄ NI—		10 ^s κ_0 = 5.0	
10 ^s κ_0 = 12.1		10 ^s κ_0 = 9.6			
4.948	78.484	6.820	100.165	4.049	77.658
10.982	76.237	14.074	96.850	9.270	75.204
19.684	73.844	20.297	94.683	15.256	73.214
27.340	72.278	28.390	92.381	22.209	71.329
36.689	70.693	38.507	90.006	29.516	69.722
48.239	68.971	48.278	88.061	37.538	68.216
57.756	67.831	57.462	86.474	44.437	67.063
69.405	66.603	71.812	84.363	50.891	66.115

consequently, the ion-size parameter \bar{a} are affected by the particular choice for F . The viscosity B coefficients used are given in Table IV. They are based on the Tuan and Fuoss¹⁶ values for Me₄NBr and Bu₄NBr at 25°, on our own measurements for Bu₄NI, Bu₄NBr, Me₄NI, and Me₄NBr at 25 and 10°, on Jones and Fornwalt's¹⁶ difference in B for KCl and KBr of 0.024, and on the assumptions that interpolated values for the tetraethyl- and tetrapropylammonium salts are valid and that B for the picrate ion in methanol is close to the value obtained for acetonitrile solutions.¹⁶ In any case, the total change in \bar{a} due to inclusion of the

F term is small, amounting to only 0.15 Å. for Me₄NBr and 0.25 Å. for Bu₄NBr at both temperatures. The B coefficients are based on a molar concentration scale.

The results listed in Table III are reduced to a more concise form in Table V, where the conductance parameters resulting from multiple runs have been averaged after weighting each value of the parameter by its standard deviation.

Discussion

Ion Conductances. The limiting ionic conductances for the quaternary ammonium ions in methanol solutions at 25° can be calculated from our results since transference data for KCl,¹⁷ NaCl,¹⁷ and LiCl¹⁸ and precise conductance data for most of the alkali halides^{19,20} are available. From these data, the average values of 52.36, 56.45, and 62.78 were obtained for λ_0 for the chloride, bromide, and iodide ions, respectively, after recomputation by the Fuoss-Onsager theory.²¹ When these values are subtracted from the corresponding Λ_0 for the quaternary ammonium halides given in Table V, the limiting cation conductances in Table VI result. The agreement is as good as can be expected for the bromides and iodides, with the exception of the n -Am₄N⁺ ion. The values obtained from the chlorides are not in so good agreement as we would hope, but we attribute this to the experimental difficulties resulting from their extremely hygroscopic nature. The agreement with the halides reported by Hartley²² and co-workers is within the precision of their data after recomputation to bring them into agreement with eq. 1. Knox and Evers²³ measured the quaternary ammonium picrates in methanol at 25°, and their value of $\Lambda_0(\text{KPi}) = 99.71$ (after recomputation with eq. 1) results in $\lambda_0(\text{Pi}^-) = 47.27$. Their resulting λ_0^+ values for the quaternary ammonium ions are given in Table VI and are somewhat lower than our values. We get $\lambda_0(\text{Pi}^-) = 47.07$ from the Me₄N⁺ salt and 47.20 from the Bu₄N⁺ salt (average value $\lambda_0(\text{Pi}^-) = 47.14 \pm 0.07$). If our value of $\lambda_0(\text{Pi}^-)$ is

(15) D. F.-T. Tuan and R. M. Fuoss, *J. Phys. Chem.*, **67**, 1343 (1963).

(16) G. Jones and H. J. Fornwalt, *J. Am. Chem. Soc.*, **57**, 2041 (1935).

(17) J. A. Davies, R. L. Kay, and A. R. Gordon, *J. Chem. Phys.*, **19**, 749 (1951).

(18) G. A. Vidulich and R. L. Kay, to be published.

(19) J. P. Butler, H. I. Schiff, and A. R. Gordon, *J. Chem. Phys.*, **19**, 752 (1951).

(20) R. E. Jervis, D. R. Muir, J. P. Butler, and A. R. Gordon, *J. Am. Chem. Soc.*, **75**, 2855 (1953).

(21) R. L. Kay, *ibid.*, **82**, 2099 (1960).

(22) See footnote a of Table VI.

(23) See footnote b of Table VI.

Table III: Conductance Parameters for Methanol Solutions at 25 and 10°

Salt	Λ_0	\bar{a}	K_A	J	$\sigma\Delta$
Me ₄ NCl	120.82 ± 0.06	3.28 ± 0.09	7.3 ± 0.8	1557	0.04
Bu ₄ NCl	91.38 ± 0.04 ^a	3.94 ± 0.04 ^a		1385	0.05
Me ₄ NBr	125.16 ± 0.04	3.50 ± 0.09	14.0 ± 0.7	1689	0.03
Et ₄ NBr	116.95 ± 0.03	3.81 ± 0.11	9.8 ± 0.7	1697	0.02
Pr ₄ NBr	102.55 ± 0.01	3.72 ± 0.07	6.3 ± 0.4	1470	0.01
Bu ₄ NBr	95.37 ± 0.02	3.49 ± 0.09	2.6 ± 0.6	1307	0.01
	95.42 ± 0.01	3.68 ± 0.05	4.1 ± 0.3	1365	0.007
<i>n</i> -Am ₄ NBr	91.41 ± 0.01	3.51 ± 0.06	2.5 ± 0.4	1267	0.009
Me ₄ NI	131.35 ± 0.05	3.51 ± 0.10	18.0 ± 0.8	1769	0.03
Pr ₄ NI	108.99 ± 0.04	4.52 ± 0.20	21.4 ± 1	1807	0.03
	108.84 ± 0.01	3.83 ± 0.08	16.3 ± 0.5	1591	0.01
Bu ₄ NI	101.72 ± 0.006	3.76 ± 0.03	15.6 ± 0.2	1473	0.004
<i>n</i> -Am ₄ NI	97.42 ± 0.02	3.70 ± 0.08	15.7 ± 0.6	1399	0.01
Me ₄ NPi	115.99 ± 0.07	3.81 ± 0.32	11 ± 2	1678	0.05
	115.76 ± 0.02	3.78 ± 0.09	10.5 ± 0.6	1664	0.01
Bu ₄ NPi	86.14 ± 0.03	3.4 ± 0.2	7 ± 1	1172	0.02
10°					
Me ₄ NBr	101.78 ± 0.07	3.1 ± 0.1	11 ± 1	1125	0.05
	101.77 ± 0.03	3.28 ± 0.06	12.1 ± 0.5	1174	0.02
Et ₄ NBr	94.82 ± 0.04	3.4 ± 0.1	6.7 ± 0.9	1121	0.03
Pr ₄ NBr	83.07 ± 0.05	3.3 ± 0.2	5 ± 1	992	0.03
Bu ₄ NBr	76.90 ± 0.01 ^a	2.97 ± 0.02 ^a		840	0.02
	76.90 ± 0.02 ^a	2.95 ± 0.03 ^a		837	0.03
	76.92 ± 0.01 ^a	2.96 ± 0.02 ^a		837	0.02
Me ₄ NI	106.95 ± 0.02	3.61 ± 0.06	19.2 ± 0.4	1328	0.01
Pr ₄ NI	88.02 ± 0.07	3.4 ± 0.4	15 ± 2	1059	0.05
	88.11 ± 0.01	3.88 ± 0.06	17.5 ± 0.4	1177	0.008
Bu ₄ NI	82.36 ± 0.03	3.9 ± 0.2	18 ± 1	1124	0.02
	82.00 ± 0.02	3.7 ± 0.1	16.5 ± 0.9	1069	0.01

^a Evaluated from eq. 1.**Table IV:** Viscosity B Coefficients for Methanol Solutions at 10 and 25°

Salt	10°	25°	Salt	25°
Me ₄ NBr	0.42	0.43	Me ₄ NCl	0.45
Et ₄ NBr	0.58	0.56	Bu ₄ NCl	0.86
Pr ₄ NBr	0.73	0.70	<i>n</i> -Am ₄ NBr	0.98
Bu ₄ NBr	0.89	0.84	<i>n</i> -Am ₄ NI	0.94
Me ₄ NI	0.38	0.38	Me ₄ NPi	0.78
Pr ₄ NI	0.70	0.66	Bu ₄ NPi	1.13
Bu ₄ NI	0.85	0.80		

used with the Knox and Evers data for the tetraalkylammonium picrates, their resulting λ_0^+ values for the tetraalkylammonium ions agree well with ours, except for the Et₄N⁺ ion. On the other hand, Fuoss and Copland²⁴ report an average value $\lambda_0(\text{Pi}^-) = 46.86 \pm 0.02$ from very precise and multiple measurements

on NaPi and KPi. Since their $\Lambda_0(\text{Bu}_4\text{NPi}) = 86.12$ is in excellent agreement with our value of 86.14, the discrepancy in $\lambda_0(\text{Pi}^-)$ could be explained by our Λ_0 for the halides being about 0.34 too high or Fuoss and Copland's value of Λ_0 for NaPi and KPi being low by the same amount. We prefer the latter conclusion since Fuoss and Copland have measured *i*-Am₃BuNI, which gives $\lambda_0(i\text{-Am}_3\text{BuN}^+) = 36.61$. If this is subtracted from their value of $\Lambda_0(i\text{-Am}_3\text{BuNPi}) = 83.69$, a $\lambda_0(\text{Pi}^-) = 47.08$ results, which is in better agreement with our value of 47.14 than with their value of 46.86 obtained from the alkali picrates. Furthermore, if we combine our value for the picrate ion with their $\Lambda_0(i\text{-Am}_3\text{BuNPi})$, we obtain $\lambda_0(i\text{-Am}_3\text{BuN}^+) = 36.55$, in excellent agreement with the value 36.61 obtained from the iodide (see above) and in fair agreement with the value 36.78, which results from the measurements

(24) See footnote *c* of Table VI.

Table V: Summary of Averaged Conductance Parameters for Methanol Solutions at 25 and 10°

Salt	Λ_0	d	K_A
25°			
Me ₄ NCl	120.82	3.3	7
Bu ₄ NCl	91.38	3.9	0
Me ₄ NBr	125.16	3.5	14
Et ₄ NBr	116.95	3.8	10
Pr ₄ NBr	102.55	3.7	6
Bu ₄ NBr	95.39	3.6	3
<i>n</i> -Am ₄ NBr	91.41	3.5	2
Me ₄ NI	131.35	3.5	18
Pr ₄ NI	108.85	3.8	17
Bu ₄ NI	101.72	3.8	16
<i>n</i> -Am ₄ NI	97.42	3.7	16
Me ₄ NPi	115.80	3.8	11
Bu ₄ NPi	86.14	3.4	7
10°			
Me ₄ NBr	101.77	3.2	12
Et ₄ NBr	94.82	3.4	7
Pr ₄ NBr	83.07	3.3	5
Bu ₄ NBr	76.90	3.0	0
Me ₄ NI	106.95	3.6	19
Pr ₄ NI	88.11	3.8	17
Bu ₄ NI	82.12	3.7	17

unity than that quoted by Copland and Fuoss. This confirms their contention that *i*-Am₃BuNBPh₄ should be an excellent reference electrolyte for the determination of single-ion conductances in methanol solutions since, by assuming an equal split in Λ_0 for both ions in other solvents, it could be invaluable in extending our knowledge of single-ion conductances without the arduous chore of measuring transference numbers.

Unfortunately, the lack of transference data for methanol solutions at 10° prevents a calculation of limiting ion conductances. As a matter of fact, conductance measurements at any temperature other than 25° appear not to exist for methanol solutions, except for the data reported here for 10°. The consistency of the Λ_0 obtained can be checked by comparing the differences in Λ_0 for the bromides and iodides with a common cation. These differences amount to 5.18, 5.04, and 5.22 from the Me₄N⁺, Pr₄N⁺, and Bu₄N⁺ salts, respectively. The Walden product can be used to calculate limiting ion conductances at 10° from the corresponding values at 25°, and the results can be compared to the measured Λ_0 . Such calculations result in Λ_0 values that are 0.4 unit too low for the Me₄N⁺ salts, about correct for the Pr₄N⁺ salts, and 0.3 unit too high for the Bu₄N⁺ salts.

Ion-Size Parameters. An inspection of the d values

Table VI: Cation-Limiting Conductances for Methanol Solutions at 25°

	Cl ⁻	Br ⁻	I ⁻	Pi ⁻	Best values	$\lambda_0 + \eta_0$
Me ₄ N ⁺	68.46	68.71	68.75		68.73	0.3742
	68.7 ^a	68.9 ^a	69.1 ^a	68.6 ^b		
Et ₄ N ⁺		60.50			60.5	0.329 ₄
	61.1 ^a	60.7 ^a	60.9 ^a	60.1 ^b		
Pr ₄ N ⁺		46.08	46.07		46.08	0.2509
				45.9 ^b		
Bu ₄ N ⁺	39.02	38.94	38.94		38.94	0.2120
				38.8 ^b		
<i>i</i> -Am ₃ BuN ⁺			36.61 ^c		36.6	0.199 ₃
<i>i</i> -Am ₄ N ⁺				35.4 ^b	35.4	0.192 ₈
<i>n</i> -Am ₄ N ⁺		34.96	34.64		34.8	0.189 ₅

^a T. H. Mead, O. L. Hughes, and H. Hartley, *J. Chem. Soc.*, 1207 (1933); A. Unmack, E. Bullock, D. M. Murray-Rust, and H. Hartley, *Proc. Roy. Soc. (London)*, **A132**, 427 (1931). ^b E. C. Evers and A. G. Knox, *J. Am. Chem. Soc.*, **73**, 1739 (1951). ^c M. A. Copland and R. M. Fuoss, *J. Phys. Chem.*, **68**, 1177 (1964).

of Kunze and Fuoss on the alkali tetraphenylborides,²⁵ that give $\lambda_0(\text{BPh}_4^-) = 36.50$, and from the Copland and Fuoss²⁴ value of $\Lambda_0(i\text{-Am}_3\text{BuNBPh}_4) = 73.28$. We have given this latter value little weight in the "best values" quoted in the last column of Table VI. It is interesting to note that the ratio $\lambda_0(i\text{-Am}_3\text{BuN}^+)/\lambda_0(\text{BPh}_4^-) = 36.6/36.50 = 1.003$ is even closer to

in Table V shows that they are surprisingly constant, as was the case for the tetraalkylammonium salts in nitromethane and acetonitrile solutions. An average value of 3.6 ± 0.2 at 25° and 3.5 ± 0.2 at 10° for d is obtained for all the salts in methanol solutions.

(25) R. W. Kunze and R. M. Fuoss, *J. Phys. Chem.*, **67**, 385 (1963).

Table VII: Conductance Parameters of Other Workers for Methanol Solutions at 25°

Salt	Λ_0	\bar{a}	K_A	σ_A	Ref.
<i>i</i> -Am ₃ BuNI	99.38 ± 0.04	4.5 ± 0.5	18 ± 3	0.01	<i>a</i>
Me ₄ NPi	115.89 ± 0.02	4.2 ± 0.4	13 ± 2	0.01	<i>b</i>
	116.0 ± 0.1	4.0 ± 0.8	13 ± 5	0.03	<i>c</i>
Et ₄ NPi	107.31 ± 0.02	4.2 ± 0.6	18 ± 3	0.02	<i>b</i>
	107.63 ± 0.06	4 ± 1	13 ± 5	0.02	<i>c</i>
Pr ₄ NPi	93.12 ± 0.01	6.4 ± 0.3	21 ± 3	0.006	<i>b</i>
Bu ₄ NPi	86.12 ± 0.01	3.7 ± 0.1	10 ± 1	0.002	<i>a</i>
	86.04 ± 0.02	4.5 ± 0.2	13 ± 1	0.01	<i>b</i>
<i>i</i> -Am ₃ BuNPh ₄	83.68 ± 0.01	4.2 ± 0.1	12 ± 1	0.002	<i>a</i>
<i>i</i> -Am ₄ NPi	82.54 ± 0.02	4.3 ± 0.8	15 ± 3	0.007	<i>b</i>
Bu ₄ NBPh ₄	75.99 ± 0.01	5.1 ± 0.4	37 ± 4	0.006	<i>a</i>
<i>i</i> -Am ₃ BuNBPh ₄	73.3 ± 0.1	5.3 ± 0.6	32 ± 3	0.004	<i>a</i>

^a See footnote c of Table VI. ^b See footnote b of Table VI. ^c F. Accascina and S. Petrucci, *Ric. Sci. Suppl.*, **29**, 1383 (1959); F. Accascina and L. Antonucci, *ibid.*, **29**, 1391 (1959).

This is identical with the \bar{a} values found for the alkali halides in methanol,²¹ in excellent agreement with the 3.6 ± 0.2 obtained for these salts in acetonitrile,⁵ and in good agreement with the value 3.9 ± 0.3 obtained for some of these salts in nitromethane solutions.^{26,27} It would appear that the tetraalkylammonium halides and picrates, salts that involve a considerable variation in crystallographic radii, produce the same electrophoretic and relaxation effects in these three solvents once differences in Λ_0 , η , and ϵ have been taken into account. Thus, the continuum theory seems totally adequate to describe the concentration dependence of the conductance of the free ions in these three solvents; however, the size dependence in the Fuoss–Onsager theory appears to need revision.

On the other hand, it should be noted that \bar{a} for the larger tetraphenylborides listed in Table VII are greater than those reported for the halides and picrates in agreement with what was found in acetonitrile solution,⁵ where an \bar{a} of 5.3 was also reported for Bu₄NBPh₄.²⁸

The significance of the trends in \bar{a} in these solvents will be clearer when the electrophoretic effect has been obtained independently from the concentration dependence of transference numbers. Transference data^{17,18} have already indicated that the electrophoretic effect as calculated²⁹ from the Fuoss–Onsager theory³ is essentially correct for the alkali halides in methanol solutions. A project to obtain this information for the tetraalkylammonium halides is under way.

Association Constants. The results of an analysis of all of the data in the literature for the symmetrical tetraalkylammonium salts in methanol solutions with the required precision for an application of eq. 2 are given in Table VII. The viscosity *B* coefficient for

the two tetraphenylborides was estimated to be 1.2.¹⁵ It can be seen that Knox and Evers data for Me₄NPi are in good agreement with our own (Table V), whereas the data of Copland and Fuoss agree better with our data for Bu₄NPi. It would appear, from the results in Table VII, that all of the tetraalkylammonium picrates are associated to the same degree.³⁰

The most outstanding feature of the association constants given in Tables V and VII is the fact that salts containing large ions show a considerable amount of association. This can perhaps be seen better in Figure 1, where $\log K_A$ is plotted *vs.* the reciprocal of the sum of the estimated ion radii.³¹ The data of Fuoss and Copland²⁴ for Bu₄NBPh₄, *i*-Am₃BuNBPh₄, and *i*-Am₃BuNI have been included; and, for ease of representation, the picrates and tetraphenylborides were assumed to have the same size as the corresponding iodides. The dotted line in this plot represents the slope which was computed from the coulombic term $e^2/ekT = 7.44$. It can be seen in Figure 1 that,

(26) R. L. Kay, S. C. Blum, and H. I. Schiff, *J. Phys. Chem.*, **67**, 1223 (1963).

(27) A small correction due to the solution viscosity has been added to the average value of 3.7 obtained from the \bar{a} reported by Kay, Blum, and Schiff²⁶ after correction of the misprint for Bu₄NBr from 3.19 to 3.91. Since viscosity data are not available for nitromethane solutions, the *F* in eq. 1 was assumed to be the same as found for acetonitrile solutions which in turn are almost identical with those used here for methanol solutions.¹⁵

(28) D. S. Berns and R. M. Fuoss, *J. Am. Chem. Soc.*, **82**, 5585 (1960).

(29) R. L. Kay and J. L. Dye, *Proc. Natl. Acad. Sci. U. S.*, **49**, 5 (1963).

(30) The somewhat high K_A of 21 and the high \bar{a} of 6.4 for Pr₄NPi can be attributed to a poor split in the last two terms of eq. 2. If \bar{a} is changed to agree with our average value of 3.6 Å., a K_A of about 12 results since $\partial J/\partial \bar{a} = 250$. This is in much better accord with the data for the other picrates.

(31) See ref. 13, p. 125.

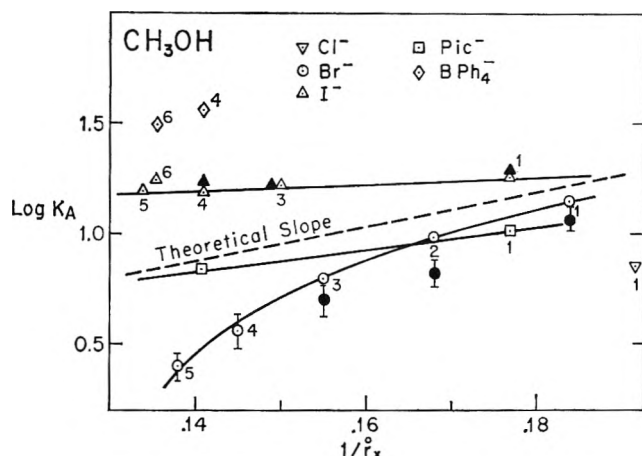


Figure 1. Association constants for the tetraalkylammonium halides, picrates, and tetraphenylborides as a function of crystallographic ion size at 25° (open symbols) and 10° (filled symbols). The picrates and tetraphenylborides are assumed to have the same size as the iodides for comparison purposes. All data are from this research except for the tetraphenylborides and *i*-Am₃BuNI which are from ref. 24. The numbers next to the points on the plot identify the cations: (1) Me₄N⁺, (2) Et₄N⁺, (3) Pr₄N⁺, (4) Bu₄N⁺, (5) *n*-Am₄N⁺, (6) *i*-Am₃BuN⁺.

as the anion size increases, the association increases, and the increase appears to be greater in the case of the large cations than of the small cations. Of particular importance is the fact that the iodides are more associated than the corresponding bromides since the conductance data for aqueous solutions of these salts can be explained best by assuming that the iodides are associated to a much greater extent than the bromides. The results shown in Table VIII for ethanol (ϵ 24.3) and 1-propanol (ϵ 20.4) show the same variation of K_A with size in that association increases as the halide ion increases in size and, owing to the lower dielectric constant, the effect is much more pronounced.

The large association constants shown here for salts of such large ions as tetrabutylammonium iodide and tetrabutylammonium tetraphenylboride are completely unexpected since these salts show very little, if any, association in acetonitrile.⁵ In acetonitrile, the K_A for these salts was less than 5. The same behavior is found for the tetraalkylammonium picrates. Generally, association of large ions is attributed to the lack of solvation of the ions. The known association behavior for methanol solutions could be explained on this basis alone since the highly solvated alkali halides^{18,19,21} have been found to be completely dissociated except for the larger cesium chloride, which has an association constant of about 9.³² However, although the lack of solvation would explain the high degree

Table VIII: Conductance Parameters for Ethanol and 1-Propanol Solutions at 25°

Salt	Δ_0	d	K_A	Ref.
C ₂ H ₅ OH				
Me ₄ NCl	51.87 ± 0.04	4.2 ± 0.4	141 ± 8	<i>a</i>
Me ₄ NBr	54.03 ± 0.02	5 ± 1	164 ± 3	<i>a</i>
Et ₄ NBr	53.54 ± 0.03	3.9 ± 0.5	96 ± 8	<i>b</i>
Et ₄ NI	56.5 ± 0.6	4 ± 1	130 ± 13	<i>b</i>
Me ₄ NPi	55.03 ± 0.05	6 ± 4	110 ± 40	<i>a</i>
Et ₄ NPi	54.2 ± 0.1	3.7 ± 0.2	69 ± 6	<i>c</i>
<i>n</i> -C ₃ H ₇ OH				
Et ₄ NBr	27.07 ± 0.02	5.2 ± 0.4	393 ± 9	<i>d</i>
Et ₄ NI	28.52 ± 0.02	6.4 ± 0.5	503 ± 10	<i>d</i>
Pr ₄ NBr	24.43 ± 0.06	5.0 ± 1.6	311 ± 35	<i>d</i>
Pr ₄ NI	25.80 ± 0.03	4.6 ± 0.7	418 ± 17	<i>d</i>

^a See footnote *a* of Table VI. ^b M. Barak and H. Hartley, *Z. physik. Chem. (Leipzig)*, **A165**, 273 (1933). ^c R. Whorton and E. S. Amis, *Z. physik. Chem. (Frankfurt)*, **17**, 300 (1958). ^d T. A. Grover and P. G. Sears, *J. Phys. Chem.*, **60**, 330 (1956).

of association of salts containing large ions in methanol solution, the lack of association of these salts in acetonitrile solutions would have to be attributed to a considerable increase in solvation energy in that solvent over that found in methanol solutions. We believe that this is unlikely and that a more plausible explanation rests in assuming that some factor is stabilizing the formation of ion pairs of large ions in methanol solutions. It is possible that structural features brought on by the hydrogen-bonding character of the alcohols plays a part in the association process.

In an attempt to study the possible effect of solvent structure on the association behavior of these large electrolytes, we extended our measurements to 10°. The association constants are represented in Figure 1 by the filled-in symbols, as compared to the open symbols for the measurements at 25°. The small decrease in K_A for the bromides is of about the correct magnitude to be attributed to the change in the ϵT product due to the decrease in temperature. The slight increase in K_A for the iodides, after taking into account the change in the ϵT product, could be an indication that the increased amount of methanol chains present at the lower temperature stabilizes the ion pairs. Data for much lower temperatures will be required before this hypothesis can be tested.

Acknowledgment. This work was supported by Contract 14-01-0001-359 with the Office of Saline Water, U. S. Department of the Interior.

(32) R. L. Kay and J. L. Hawes, *J. Phys. Chem.*, **69**, 2787 (1965).

The Conductance of the Tetraalkylammonium Halides in Deuterium Oxide Solutions at 25°

by Robert L. Kay and D. Fennell Evans

Mellon Institute, Pittsburgh, Pennsylvania 15213 (Received June 28, 1965)

Precise conductance measurements were carried out on dilute solutions of Me_4NBr , Et_4NBr , Pr_4NBr , Bu_4NBr , Me_4NI , and Bu_4NI in essentially pure D_2O at 25°. The change in the ratio of the Walden product for D_2O solutions relative to H_2O solutions is explained by the increased structure in D_2O solutions. The concentration dependence of conductance for these salts in dilute solution is almost identical with that found for H_2O solutions in that unrealistically low ion size parameters are obtained which decrease with the increasing anion size. As was the case with H_2O solutions, the data for Bu_4NI analyzed for a small amount of association.

Introduction

The increases in such properties as the heat capacity, the melting point, and the viscosity of D_2O over that of H_2O in the liquid state have been attributed to more structural order in liquid D_2O .¹ This subject has been reviewed in detail recently.² The increase in structural order has been attributed to an increase in the strength of the hydrogen bonding in D_2O solutions as compared to H_2O solutions. In concentrated H_2O solutions, the properties of the tetraalkylammonium ions are known to be affected by structural order in the solvent,³ and even at infinite dilution⁴ it has been shown that, as the hydrocarbon portion of these electrolytes increases in length, water structure enforcement about these chains affects the ionic mobility. In this paper, we wish to investigate the same effect for these ions in D_2O solutions. At the same time, we wish to determine if the greater structure present in liquid D_2O has any effect on the concentration dependence of the conductance for these ions by comparison with known results for H_2O solutions.⁴

Very few investigations of the transport properties of electrolytes in D_2O have been reported. Most of the early work was carried out at a time when D_2O was both scarce and extremely expensive. Only very small quantities of solution could be prepared and, for that reason, many of the data were restricted in scope and not too precise. Recently, precise conductance measurements for the alkali halides in pure D_2O have been

reported.⁵ These data indicate that both the alkali and the halide ions behave in a similar manner in D_2O as in H_2O , and the main effect is the decrease in mobility due to the 23% increase in viscosity. The quaternary ammonium salts have never been systematically investigated in D_2O .

Experimental Section

The conductance bridge, conductance cells, method of procedure, and purification of salts have been amply described elsewhere and will not be repeated in detail here, except where the procedure was changed owing to the particular properties of D_2O . A precision of 0.01% was sought in all the quantities measured. The resistance measurements were carried out on a calibrated Dike-Jones bridge. The 500 ml. Erlenmeyer-type conductance cell was fitted with the cup dropping device,^{6,7} which enabled the salt samples to be added to the solvent without exposing the cell and its contents to the atmosphere. The salt samples themselves were weighed in small Pyrex cups on a microbalance, and all

- (1) G. Némethy and H. A. Scheraga, *J. Chem. Phys.*, **41**, 680 (1964).
- (2) J. L. Kavanau, "Water and Solute-Water Interaction," Holden-Day, Inc., San Francisco, Calif., 1964.
- (3) W. Y. Wen and S. Saito, *J. Phys. Chem.*, **68**, 2639 (1964).
- (4) D. F. Evans and R. L. Kay, *ibid.*, in press.
- (5) C. G. Swain and D. F. Evans, to be published.
- (6) J. L. Hawes and R. L. Kay, *J. Phys. Chem.*, **69**, 2420 (1965).
- (7) D. F. Evans, C. Zawoyski, and R. L. Kay, *ibid.*, **69**, 3878 (1965).

solutions were made up by weight and vacuum corrected. The solutions were stirred continuously while the resistance measurements were being made. The constant-temperature oil bath was maintained at $25 \pm 0.002^\circ$ by means of a mercury in glass thermoregulator, and the absolute temperature was determined by a calibrated platinum resistance thermometer and a Mueller bridge.

The preparation of the salts has been described in detail elsewhere.⁷

The unpurified D₂O (Atomic Energy Commission, normal O¹⁸) content was found to have a conductance of about 10^{-6} mho cm.⁻¹ after distillation. This small conductance was due not to CO₂ but rather to some solid dissolved impurity. The conductance of the D₂O was reduced further to $0.7\text{--}1.4 \times 10^{-7}$ mho cm.⁻¹ by passage through a 33-cm. column containing 100 ml. of mixed-bed, ion-exchange resin⁵ that had been equilibrated with D₂O for more than 6 months and was the same sample as was used previously⁸ to prepare at least 10 l. of conductance grade D₂O. The density of the final product was found to be 1.1044 g. ml.⁻¹. The pure product is considered to have a density of 1.10451.⁹ The isotopic content is difficult to obtain from density measurements alone, owing to an unknown but small O¹⁸ content.

All manipulations involving the D₂O were carried out in a drybox or in a closed system. Before each run, 60 ml. of the D₂O was passed through the resin and used to rinse the conductivity cell. The cells were thoroughly flushed with dry nitrogen and filled with 500 ml. of D₂O by connecting the cells directly to the ion-exchange column with catalyst-free polyethylene tubing while dry nitrogen flowed through the cell. The prolonged contact of the D₂O with the glass walls of the cell and all of the manipulations of the D₂O appeared to have no measurable effect on the isotopic content as verified by the fact that redistillation of a used solution in a Vigreux column gave a product with no change in density when compared to the value quoted above.

The density of D₂O was measured in a single-capillary pycnometer which contained 25 ml. of liquid. The viscosity measurements were carried out in a Ubbelohde suspended level type of viscometer with a flow time of 540 sec. for water at 25° (0.008903 poise). The viscosity of D₂O measured at 25° was 0.01094 poise, which agrees favorably with the 0.010963 poise obtained by Hardy and Cottington.¹⁰ A dielectric constant of 78.06 was measured¹¹ for D₂O at 25° using the Cole-Gross transformer bridge and the completely guarded and shielded dielectric cells of Vidulich and Kay.¹² These cells were developed for absolute meas-

urements and have been shown to introduce less than 0.1% error in the determination of dielectric constants as high as 80. The value obtained here for D₂O at 25° is somewhat larger than 77.94, which has been reported by Malmberg and Mayott.¹³

The same salt samples were used here as have been shown to give excellent checks with transference data for aqueous⁴ and methanol solutions.¹⁴

Results

The measured equivalent conductances, molar con-

Table I: Equivalent Conductances in D₂O at 25°

10°C	Λ	ΔΛ	10°C	Λ	ΔΛ
—Me ₄ NBr, 10 ⁷ κ ₀ = 0.83—			—Bu ₄ NBr, 10 ⁷ κ ₀ = 0.91—		
8.613	99.111	0.022	3.344	78.396	-0.010
21.582	97.802	-0.004	10.284	78.318	0.017
36.502	96.756	-0.007	20.504	77.014	0.002
51.094	95.924	-0.017	30.350	76.257	-0.006
65.636	95.235	-0.003	40.578	75.593	-0.003
87.052	94.333	-0.007	52.792	74.889	-0.004
103.260	93.740	0.004	64.869	74.269	0.000
120.777	93.153	0.012	75.857	73.747	0.004
—Et ₄ NBr, 10 ⁷ κ ₀ = 1.1—			—Me ₄ NI, 10 ⁷ κ ₀ = 0.70—		
4.479	89.569	-0.009	6.348	98.545	0.012
13.735	88.440	0.030	16.957	97.319	0.008
26.643	87.319	-0.015	28.126	96.393	-0.003
38.162	86.577	-0.005	41.038	95.528	-0.015
50.767	85.869	-0.009	55.321	94.731	-0.011
65.855	85.146	0.001	71.206	93.963	-0.004
81.006	84.492	0.003	82.820	93.452	-0.002
91.912	84.059	0.004	106.423	92.528	0.015
—Pr ₄ NBr, 10 ⁷ κ ₀ = 1.4—			—Bu ₄ NI, 10 ⁷ κ ₀ = 1.0—		
4.001	82.087	-0.003	5.325	77.701	0.050
12.655	80.973	0.017	13.432	76.550	-0.003
22.359	80.081	-0.008	23.365	75.550	-0.001
33.321	79.296	-0.012	33.644	74.663	-0.019
45.982	78.545	-0.001	44.371	73.831	-0.049
62.725	77.682	0.004	58.329	72.910	-0.028
73.632	77.174	0.002	72.674	72.056	0.003
91.250	76.425	0.000	85.406	71.365	0.048

(8) We are indebted to Dr. C. G. Swain of the Massachusetts Institute of Technology for donation of this equilibrated resin which had been used in the preparation of conductance grade D₂O for the alkali halides. (See ref. 5.) The removal of all exchangeable protons was followed by density measurements.

(9) I. Kirshenbaum, "Physical Properties and Analysis of Heavy Water," McGraw-Hill Book Co., Inc., New York, N. Y., 1951, p. 14.

(10) H. C. Hardy and R. L. Cottington, *J. Res. Natl. Bur. Std.*, **42**, 573 (1949).

(11) G. A. Vidulich, D. F. Evans, and R. L. Kay, to be published.

(12) G. A. Vidulich and R. L. Kay, *J. Phys. Chem.*, **66**, 383 (1962).

(13) C. G. Malmberg and A. A. Mayott, *J. Res. Natl. Bur. Std.*, **56**, 1 (1956).

(14) R. L. Kay, C. Zawoyski, and D. F. Evans, *J. Phys. Chem.*, **69**, 4208 (1965).

centrations, and solvent conductances, κ_0 , in mho cm.⁻¹ are given in Table I along with $\Delta\Lambda$, the difference between the measured conductances and those calculated from eq. 1 below. Solution concentrations were calculated with the aid of densities obtained from the expression $d = d_0 + A\bar{m}$, where \bar{m} is the concentration in moles per kilogram of solution. The values of A given in Table II were the result of density measurements on 0.05 \bar{m} solutions of the salts in D₂O.

Table II: Density Increments A and Viscosity B Coefficients for D₂O Solutions at 25°

Salt	A	B
Me ₄ NBr	0.032	0.08
Et ₄ NBr	0.019	0.33
Pr ₄ NBr	0.005	0.79
Bu ₄ NBr	0.000	1.26
Me ₄ NI	0.069	0.04
Bu ₄ NI	0.028	1.21

The conductance parameters given in Table III were obtained by applying the Fuoss–Onsager conductance equation¹⁵ in the form

$$\Lambda = \Lambda_0 - SC^{1/2} + EC \log C + (J - B\Lambda_0)C \quad (1)$$

In the case of Bu₄NI, some association was suspected owing to the exceedingly low \bar{d} obtained from J .

Table III: Conductance Parameters for D₂O Solutions at 25°

Salt	Λ_0	\bar{d}	K_A	σ_A	J
Me ₄ NBr	101.27 ± 0.009	1.64 ± 0.02		0.01	69.6
Et ₄ NBr	91.10 ± 0.01	1.60 ± 0.04		0.01	63.5
Pr ₄ NBr	83.50 ± 0.006	1.71 ± 0.03		0.009	66.0
Bu ₄ NBr	80.29 ± 0.006	1.94 ± 0.03		0.009	74.5
Me ₄ NI	100.42 ± 0.008	1.10 ± 0.02		0.01	39.3
Bu ₄ NI	79.34 ± 0.02	0.08 ± 0.02		0.04	-48.1
	79.42 ± 0.02 ^a	3.8 ± 0.7 ^a	4 ± 1 ^a	0.01	149.0

^a From eq. 2.

Consequently, the conductance parameters for Bu₄NI were obtained as well by means of the equation for associated electrolytes

$$\Lambda = \Lambda_0 - S(C\gamma)^{1/2} + EC\gamma \log C\gamma + (J - B\Lambda_0)C\gamma - K_A C\gamma\Delta f^2 \quad (2)$$

In eq. 1 and 2, B is the Jones–Dole¹⁶ viscosity B coefficient given by

$$(\eta - \eta_0)/\eta_0 = \phi C^{1/2} + BC \quad (3)$$

and takes into account the rather large change of viscosity with concentration encountered with solutions of these large cations. The values of B given in Table II were obtained from direct measurement of the viscosities of concentrated solutions.¹⁷ The least-squares computer programs for eq. 1 and 2 are described in detail elsewhere.^{6,18} The conductance parameters reported here in Table III were computed using unweighted values of Λ since the measurements were carried out at approximately equal intervals in C . Included in Table III are the standard deviations for each parameter along with the standard deviations of the individual points, σ_A .

The values of α , β , E_1 , and E_2 for D₂O solutions at 25° are 0.2310, 49.38, 0.5374, and 16.82, respectively, where S and E in eq. 1 and 2 are given by $S = \alpha\Lambda_0 + \beta$ and $E = E_1\Lambda_0 - E_2$.

Limiting cation conductances and Walden products of the tetraalkylammonium ions are given in Table IV, along with R , the ratio of the Walden product in D₂O to its value in H₂O, both at 25°; that is

$$R = (\lambda_0\eta_0)_{D_2O}/(\lambda_0\eta_0)_{H_2O} \quad (4)$$

The limiting conductances were computed from Longworth's transference data¹⁹ for KCl and NaCl and $\Lambda_0(\text{KBr}) = 126.07$ and $\Lambda_0(\text{KCl}) = 124.23$, as reported by Evans⁵ for D₂O at 25°. Since the transference data were measured at rather high concentrations,

they were re-extrapolated⁵ using the Fuoss–Onsager evaluation of the electrophoretic effect which has been shown to give the correct concentration dependence

(15) R. M. Fuoss and F. Accascina, "Electrolytic Conductance," Interscience Publishers, Inc., New York, N. Y., 1959.

(16) G. Jones and M. Dole, *J. Am. Chem. Soc.*, **51**, 2950 (1929).

(17) R. L. Kay, D. F. Evans, and T. Vituccio, to be published.

(18) R. L. Kay, *J. Am. Chem. Soc.*, **82**, 2099 (1960).

(19) L. G. Longworth and D. A. MacInnes, *ibid.*, **59**, 1666 (1937).

Table IV: Limiting Cation Conductances and Walden Products in D₂O at 25°

	Br ⁻	I ⁻	$\lambda_0^* \eta_0$	<i>R</i>
Me ₄ N ⁺	36.61	36.62	0.4009	1.0124
Et ₄ N ⁺	26.44		0.2895	1.008
Pr ₄ N ⁺	18.84		0.2063	0.9981
Bu ₄ N ⁺	15.62	(15.63)	0.1711	0.9948

for aqueous solutions.²⁰ The final values obtained for T_0^+ were 0.4943 and 0.3985 for KCl and NaCl, respectively, and resulted in $\lambda_0(\text{Br}^-) = 64.67$ for D₂O at 25°. A value of $\lambda_0(\text{I}^-) = 63.79$ was obtained from our data for Bu₄NI, which leads to an excellent check since $\lambda_0(\text{Me}_4\text{N}^+) = 36.62$ from the iodide and 36.61 from the bromide.

Discussion

Limiting Conductances. Since this is the first determination of limiting conductances for the tetraalkylammonium ions in D₂O with one possible exception,⁵ no independent check for our data is available. However, the excellent agreement in $\lambda_0(\text{Me}_4\text{N}^+)$ obtained from the bromide and iodide and the fact that the same salts were used here as gave excellent agreement with the data of other workers for H₂O solutions at 25° adds considerably to the confidence to be placed on the reliability of our data.

The lower limiting conductances in D₂O as compared to H₂O, of course, reflect the 23% increase in the viscosity. However, the ratio of the conductance-viscosity product for D₂O relative to H₂O, as given by *R* in Table IV, shows systematic and significant deviations from unity. Although the deviations of *R* from unity are small, the differences between H₂O and D₂O in the properties which classical electrolyte theory takes into account are also very small. The dielectric constant and molar volume of H₂O at 25° are 78.38 and 18.05 ml./mole while for D₂O at the same temperature the values are 78.06 and 18.11 ml./mole. In Figure 1, the *R* values reported are compared, on a size basis, to those reported by Swain and Evans⁵ for a number of alkali and halide ions. Considerable data from thermodynamic, transport, and dielectric relaxation measurements involving these smaller ions have been interpreted satisfactorily^{21,22} by assuming that these ions are structure breakers in that they tend to break down the three-dimensional water structure in their vicinity. The resulting decrease in the local viscosity would be greater in the case of D₂O than H₂O owing to the greater structural order known to be present in liquid D₂O at the same temperature.¹ It is

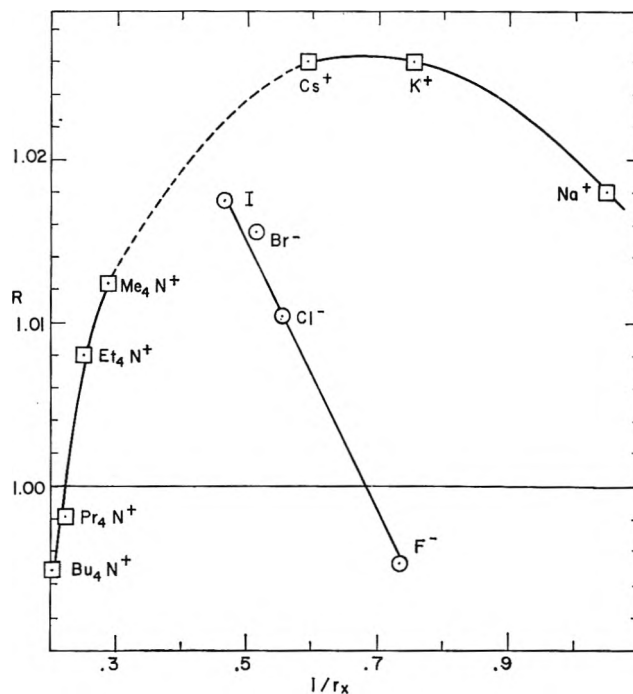


Figure 1. The limiting conductance-viscosity product in D₂O divided by that in H₂O at the same temperature as a function of ion size.

this greater decrease in the local viscosity around the alkali and halide ions in D₂O over that of H₂O that produces the increase in the conductance-solvent viscosity product for these ions in D₂O over that in H₂O. The value of *R* less than unity for the fluoride ion indicates that ion to be more highly hydrated in D₂O than in H₂O so that the increased viscous drag of the larger moving particle in D₂O outweighs any structure-breaking properties of the ion. For Pr₄N⁺ and Bu₄N⁺, *R* is significantly less than unity owing to greater enforcement of water structure about the hydrogen chains of these ions in D₂O as compared to the effect in H₂O. This hydration of the second kind has been detected by other independent measurements^{3,21} on the quaternary ammonium ions and is verified here by their transport properties. The values of *R* slightly above unity for the Et₄N⁺ and Me₄N⁺ ions indicate that the structure-breaking tendencies of these large ions more than match the structure-making tendencies due to hydration of the second kind.

The conclusions reached here concerning the relative effect of solvent structure in D₂O and H₂O on the

(20) R. L. Kay and J. L. Dye, *Proc. Natl. Acad. Sci.*, **49**, 5 (1963).

(21) H. S. Frank and W. Y. Wen, *Discussions Faraday Soc.*, **24**, 133 (1957).

(22) R. W. Gurney, "Ionic Processes in Solution," McGraw-Hill Book Co., Inc., New York, N. Y., 1953.

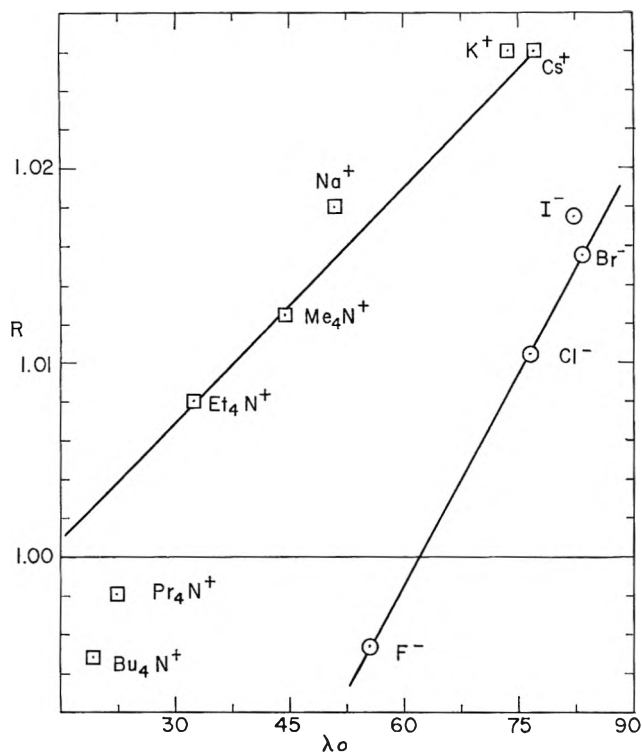


Figure 2. The conductance-viscosity product ratio R as a function of the limiting ion conductance in H_2O .

mobilities of ions are in agreement with the explanation used by Greyson²³ to account for the negative excess entropies and heats of transfer of ions from D_2O to H_2O at infinite dilution.

The results in Figure 1 demonstrate also that the interaction of a cation with water is different from that of an anion. This is brought out more clearly in Figure 2 where the R values are plotted against the limiting equivalent conductance of the ions in H_2O .

In conclusion, it should be said that the explanation for the solvent isotope effect given here is in complete agreement with the model of Frank and Wen²¹ for ionic solutions. In this model, they postulate three regions around an ion in aqueous solution. The first contains water molecules immobilized owing to hydration of the first kind (electrostriction) or hydration of the second kind (clathratelike cages). A second region separates the third region containing the bulk or normal water from the water of hydration around the ion. In this second region, the amount of hydrogen bonding or structure is less than in bulk water, owing to competition between the orienting influence of the central ion and that of the neighboring water molecules. The relative size or effect of these three regions depends on the charge, size, composition, and shape of the central ion. In general, high charge and small size or low

charge and large hydrophobic surface area increase the size of the first region, whereas low charge and large size increase the effect of the second area on ionic properties. From the data represented in Figure 1, it would be possible to order the ions according to their structure-breaking ability. Strictly speaking, this order would apply only to the effect of solvent structure on ionic mobilities, and a somewhat different order could be obtained from thermodynamic data or other measurements. However, the order found here for the cations and the anions is in good agreement with that obtained from other measurements although the structure-breaking effect of cations relative to anions seems to depend more on the particular property investigated.

Concentration Dependence. The δ values shown in Table III for the tetraalkylammonium bromides and iodides are relatively low and of about the same magnitude as those found for the same salts in H_2O solution.⁴ An analysis of the data for Bu_4NI showed much better precision when eq. 2 was used, indicating a significant amount of association was present for that salt relative to the other salts studied. The magnitude of the association constant is the same as that found for this salt in H_2O at two temperatures⁴ within experimental error. Thus, the concentration dependence for these salts in D_2O appears to be identical with that obtained in H_2O solutions.

This apparent association of Bu_4NI and the lack of association for Bu_4NBr is the most notable feature of the concentration dependence of conductance. Lindenbaum and Boyd²⁴ required the same assumption of greater association of the quaternary ammonium iodides, as compared to the bromides, to explain their activity coefficient data in aqueous solution. It is difficult to explain association constants that increase with increasing anion size. Errors in the theory used for the evaluation of the conductance of the free ions should be present for both salts, and the excellent agreement obtained in the limiting conductance for our salts in H_2O and D_2O rules out salt impurities. Likewise, Diamond's suggestion²⁵ that large ions will tend to form ion pairs more readily in aqueous solution owing to the fact that ion pairs will cause the least interference with the solvent structure is ruled out since a much larger K_A would be expected for D_2O solutions owing to the more extensive structure in D_2O as compared to H_2O . It is possible that the fact that large ions come into contact more often may not be properly

(23) J. Greyson, *J. Phys. Chem.*, **66**, 2218 (1962).

(24) S. Lindenbaum and G. E. Boyd, *ibid.*, **68**, 911 (1964).

(25) R. N. Diamond, *ibid.*, **67**, 2513 (1963).

taken care of in the theory. This will explain the higher association of the iodides in aqueous and alcoholic solutions but leaves the lack of association of Bu_4NI in acetonitrile⁷ to be explained. It would appear that the effect is characteristic of alcoholic¹⁴ and aqueous solutions⁴ but not solvents like acetonitrile,⁷ nitromethane,²⁶ and nitrobenzene.⁷ It would appear to be insensitive to the degree of hydrogen bonding in the solvent, as seen here for D_2O solutions and previously for aqueous solutions where a decrease in temperature had

little effect. It would appear that some as yet unidentified specific solvent effect must be present in alcoholic and aqueous solutions to account for the abnormally high association of the tetraalkylammonium iodides.

Acknowledgment. This work was supported by Contract 14-01-0001-359 with the Office of Saline Water, U. S. Department of the Interior.

(26) R. L. Kay, S. C. Blum, and S. I. Schiff, *J. Phys. Chem.*, **67**, 1223 (1963).

Some Observations of Spectroscopic and Photoconductivity

Effects in Permselective Membranes

by Chaim Forgacs and Gabriel Stein

Negev Institute for Arid Zone Research, Beersheba, and Department of Physical Chemistry, Hebrew University, Jerusalem, Israel (Received June 22, 1965)

Some permselective membranes colored through the existence of conjugated double bonds in the polymer backbone were investigated. Changes in the absorption spectrum due to different gegenions were found. The current through the membranes increases on illumination. The additional current depends on the magnitude of the dark current, light intensity, existence of double-bond structure, and the spectrum employed. Saturation of the double bond occurs during prolonged current transfer in the dark or light. The characteristics of such membranes as mixed ionic and electronic conductors and the role of internal polarization within the body of the membrane are discussed.

We have reported briefly¹ observations which showed that the absorption spectrum of some charged permselective membranes immersed in different electrolyte solutions is affected by the nature of the gegenion, opposite in sign to the charge of the membrane. It was also shown there that the conductivity of such membranes is increased by illumination. Both observations appeared to be related to the electric field existing *within* the membrane. They offered a method of obtaining further information on this component of membrane processes, which hitherto could not be investigated. In the present paper, we report more

detailed results and attempt to give a largely qualitative interpretation of the phenomena.

Experimental Section

Permselective Membranes. Most experiments were carried out using positively charged membranes synthesized at the Negev Institute for Arid Zone Research according to the process described by Körösy and Shorr.²

(1) G. Stein and Ch. Forgacs, *Science*, **142**, 953 (1963).

(2) F. de Körösy and J. Shorr, *Dechema Monograph.*, **47**, 477 (1963).

These membranes are made of poly(vinyl chloride), the active positive amine groups being formed on the membrane through treatment with poly(ethyleneamines), alkylized with alkyl bromides. After synthesis, the membranes are brought into the chloride form by soaking in dilute aqueous HCl, then washed with distilled water, and stored in 0.1 *N* KCl solution. These membranes are colored deeply reddish brown. Other experiments were made using positively charged membranes obtained from American Machine and Foundry Co. (AMF60A). These are colorless and are polyethylene-polystyrene based, containing quaternary ammonium groups.

Negatively charged permselective membranes were obtained from American Machine and Foundry Co. (AMF60C) and were polyethylene-polystyrene based with active sulfonate negative groups. These membranes have a reddish brown color. For comparison, experiments were also carried out using membranes which were colored and permselective through the chemical attachment of commercially available ionic dye molecules to a membrane, which itself was neither colored nor permselective. The membrane matrix itself does not contain double bonds either before or after the incorporation of the ionic groups. These membranes were prepared by Mr. A. Susser and will be described separately.

Materials. The water used was demineralized by double-bed ion exchange followed by mixed-bed treatment. It had more than 10^6 ohms cm. specific resistance. All chemicals used were analytical grade.

Spectra. These were measured and recorded with a Beckman DB instrument and potentiometric recorder.

Illumination. The light sources used were: for steady illumination, a 750-w. incandescent lamp and, for flash illumination, an Eltronic Cornet SK xenon photographic flash. With this, two intensity settings were available, giving about 10 and 5 joules, respectively, per flash. Optical-glass filters (Chance Bros. Co., Birmingham, Great Britain) were used to isolate spectral regions from the flash light. One face only of the membrane was illuminated.

Electrical Measurements. The results obtained in four types of experimental arrangements will be referred to.

(A) Strips of the permselective membrane, 10×60 mm., were introduced into a 1-cm. optical path length quartz or Pyrex spectrophotometric cell, provided (parallel to and outside the light path) with insulating frames to hold the membrane strip and to minimize the current leakages. Of course, in this arrangement the same electrolyte solution is present of necessity on both sides of the membrane. Electrical

contact was made to either side through 0.1 *N* KCl agar bridges, kept outside the light path, and leading to cups containing Ag-AgCl electrodes in 0.1 *N* KCl solution. The bridges, cups, and electrodes were shielded from the light. The electrodes were connected to a Metrohm Polarecord E261R instrument, which both provided the polarizing potential and recorded the current flowing through the cell and membrane, with a maximum sensitivity of 10^{-10} amp./mm. The compensating current available permits in the limit a change of 1/2000 in the total current flowing to be recorded and determined.

(B) Here the cell used allows the use of different electrolytes in the two compartments fully separated by the membrane. Two electrodes only were used, as in (A), but the Ag-AgCl electrodes were now introduced directly into the cell, well shielded from the light, and led to the Polarecord instrument as under (A).

(C) The same cell as in (B) was used. Into each compartment were placed two electrodes, one Ag-AgCl electrode and one of bright Pt. A potentiostat, manufactured for us by Messrs. Elron Ltd., Haifa, Israel, permitted a constant potential drop (0 to ± 3 v.) to be maintained across the membrane between the Ag-AgCl electrodes. Through the Pt electrodes the current needed to maintain this constant potential was passed. The voltage drop caused by this current flowing through an external resistance, in series with the cell, was then measured and recorded on the mv. measuring scale of the Metrohm Polarecord instrument. Once again, a change of 1/2000 in the total current could be determined and recorded.

(D) The cell used was as in (B) and (C), but only the Pt electrodes were used. The electrodes were connected through an external resistance. When the two compartments of the cell are filled with solutions of different salt concentrations, a potential difference arises across the membrane. This generates a current flowing *via* the Pt electrodes and the external resistance, which increasingly polarizes the electrodes. When the electrodes become sufficiently polarized to counterbalance the membrane potential, the current decreases to zero. On illumination of the membrane, we expected this balance between the opposing potentials to break down and looked for a momentary current flow through the circuit. We attempted to measure this as a voltage across the external resistance and to integrate it using a Dymec Model 2210 voltage-to-frequency converter and Elron El-54-C. electronic scaler.

The use of the first three methods enabled us to cover six orders of magnitude of dark current in the same experiments. The fourth method was used to

investigate whether there is a photocurrent when a potential difference exists across the membrane without dark current flowing.

In all experiments, two kinds of blank controls were measured. (1) With the membrane in position, the lamp (steady or flash) was actuated; however, the light was masked to prevent illumination of the cell. In this way, electric transients due to the operation of the light source itself could be ascertained. (2) The entire setup was operated in the absence of the membrane only. In this way, one could show that the photoeffects are due to light falling on the membrane and not other parts of the system. Experiments using heat filters were carried out to show that transients observed are not due to heat effects.

Results

Effect of the Gegenion on the Absorption Spectrum of Membranes. Körösy-type membranes, 0.1 mm. thick, were brought into equilibrium through prolonged soaking with saturated solutions of various salts, then rinsed thoroughly with distilled water, and their absorption spectra were measured with the membranes immersed in distilled water in the spectrophotometer cell. Under these conditions, only the negative gegenions attached to the positive membrane are retained. Absorption is total in the ultraviolet and the visible range to 550 m μ ; it decreases and reaches a minimum around 700 m μ , rising again toward the infrared and far-infrared range. Table I shows the results for λ_{\min} and $\lambda_{1/2}$ (at $\lambda_{1/2}$, the transmittance of the membrane reaches 50% of its maximum) for the halide gegenions. Table II shows, for Cl⁻ as the gegenion, that the position of $\lambda_{1/2}$ remained reasonably constant when five different membrane samples of varying transmittance were used.

Table I: Absorption Spectrum as a Function of Gegenion

Ion	λ_{\min} , m μ	$\lambda_{1/2}$, m μ
F ⁻	705 \pm 5	622
Cl ⁻	710 \pm 5	632
Br ⁻	717 \pm 5	648
I ⁻	722 \pm 2	655

The absorption spectrum of the membrane is due to a system of conjugated double bonds formed in the poly(vinyl chloride) polymer during the process of introduction of the positively charged groups. The positively charged poly(ethyleneamine) groups themselves do not absorb in the visible nor can they form

Table II: Position of $\lambda_{1/2}$ with Cl⁻ as Gegenion for Various Membrane Samples

Sample	λ_{\min} , m μ	% transmittance at λ_{\min}	$\lambda_{1/2}$, m μ
1	708 \pm 4	47	631
2	710 \pm 2	27	638
3	712 \pm 5	24	638
4	713 \pm 5	24	630
5	715 \pm 6	19	639

colored ion-pair charge-transfer complexes with halide ions. On the other hand, similar coloring may be formed in uncharged poly(vinyl chloride) sheets by dehydrochlorination through treatment with hot KOH solution. In this case, conjugated double-bond systems are known to be formed. Accordingly, the effects now observed are attributed to the influence of the halide negative gegenions in the body of the membrane on the conjugated double-bond system of the polymer. The correlation with the electron affinity and ionic radius of the halide ion would be consistent with the assumption that donor-acceptor interactions are involved; however, since absorption maxima could not be determined, this point is left open. The ion-exchange capacity of the membranes used was 2 mequiv./g. of chloride form (dry weight). Thus, the concentration of halide ions is high enough to ensure spatial proximity to any conjugated double-bond system.

Changes in the Current through the Membrane on Illumination. Effect of Double Bonds in the Membrane Structure. In all of the experiments reported in the present work, it must be emphasized that with membranes from all sources there was considerable variation in their optical properties and in their response to illumination. Indeed, even cuttings from the same sheet responded somewhat differently under otherwise identical experimental conditions. However, it became apparent that there is a correlation between the absorbance of the sample in the visible region and the effect of light on the current flowing. Therefore, we investigated whether the conjugated double bonds, responsible for the color and thus absorbing the light in the visible region, are those responsible for the conductivity effect as well. Samples of Körösy-type membranes were chosen, as optically homogeneous as possible, and divided into two, one sample being brominated under mild conditions to saturate the double bonds. Excess bromine was washed off. The resulting membrane showed an electrical performance (conductivity and permselectivity) nearly identical

with that of the untreated sample. The color, however, changed from translucent deeply red-brown to only slightly yellow, but rather opaque. On illumination under arrangement C in 0.1 *N* KCl with 1.5-ma. dark current applied, the additional current was +3.0 $\mu\text{a.}$ for the untreated colored membrane and only +0.8 $\mu\text{a.}$ for the treated decolorized membrane.

Using uncolored positive membranes, no change in current occurred on illumination. Using colored negative membranes (AMF60C), effects similar to those with colored positive membranes were obtained. Thus, it appeared that it is the conjugated double-bond systems in the membranes that are responsible for the additional current under illumination.

Effect of Wave Length of Illuminations. Using experimental arrangement C, 0.1 *N* KCl solution, and 10-ma. dark current, a Kőrös-type membrane was illuminated with the full light of the xenon flash, which contained all wave lengths down to 300 $m\mu$. We measured the maximum value of additional current recorded.

$\Delta I = 32 \mu\text{a.}$ was obtained. Using a Chance filter No. OY4, which does not transmit below 500 $m\mu$ and which has an integrated visible transmission of 84%, $\Delta I = 13 \mu\text{a.}$ was obtained; *i.e.*, $\Delta I_{\text{equiv}} = 15.5 \mu\text{a.}$, for light above 500 $m\mu$. Here, ΔI_{equiv} is the calculated value of the current if allowance is made for the decrease in per cent transmission. Using Chance filter No. ORD2, which does not transmit below 600 $m\mu$ and which transmits 90% of all light above 650 $m\mu$, $\Delta I = 5 \mu\text{a.}$ was obtained; *i.e.*, $\Delta I_{\text{equiv}} = 5.5 \mu\text{a.}$

It is thus seen that a major part of the added current on illumination is due to absorption above 500 $m\mu$ where only the conjugated double-bond system absorbs.

Thus, the experiments on the spectra and current changes on illumination both support the assumption that these effects are connected with the existence of conjugated double bonds in the body of the membrane.

The Effect of Light Intensity. Using the same experimental setup as in the preceding sections, 1-ma. steady dark current was applied. On illumination of a membrane sample with the full light of the flash, $\Delta I = 2.0 \pm 1.0 \mu\text{a.}$ was obtained in a series of illuminations, while, using the half-energy setting on the flash, $\Delta I = 1.0 \pm 0.5 \mu\text{a.}$ was obtained with the same sample.

Dependence of Additional Photocurrent on the Steady-State Dark Current. The experiments in 0.1 and 1 *N* KCl solutions in experimental arrangements A, B, and C are shown in Figure 1, where ΔI is plotted as a function of I using the full intensity of the flash.

It will be seen that $\Delta I \rightarrow 0$ as $I \rightarrow 0$. The photocurrent is therefore not a property of the membrane

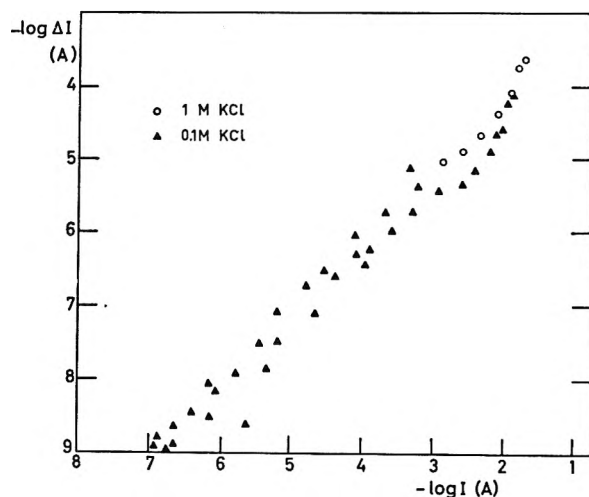


Figure 1. Relation between the dark current and the peak value of the additional current obtained on illumination.

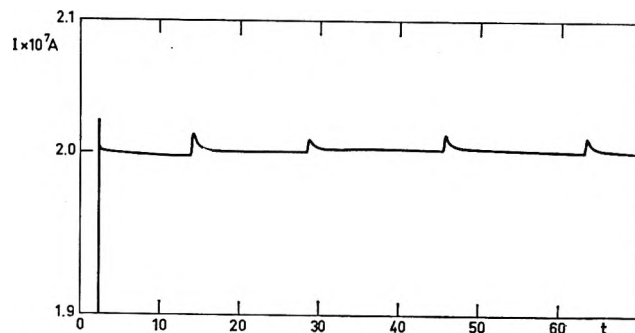


Figure 2. Rise and decay of additional current after flash illumination. Time scale: 10 units = 12 sec.

alone but depends on the electrical state inside the membrane, produced by the current flowing. Figure 2 shows one example of the recording of current changes on illumination. The time scale is a function of the particular circuitry employed, and it is not determined how the specific properties of the membrane influence it. Reversal of the direction of the dark current did not affect the photocurrent, which always added to the dark current.

Experiments Using Susser-Type Membranes. Using these membranes, where the absorbing color was not due to conjugated double bonds in the membrane matrix itself but to chemically attached colored, charged dye molecules, additional photocurrents were not obtained on illumination. Moreover, no change in the absorption spectrum was observed on changing the gegenions as in Tables I and II.

Results in the Absence of Dark Current. A potential difference was produced across a membrane by introducing different concentrations of KCl solution (0.001 and 1 *N*) in the two compartments. Then,

according to arrangement D, no current flows through the membrane when full polarization is established. The illumination of the membrane under these conditions did not produce a detectable current.

Influence of Current Transfer on the Conjugated Double Bonds of the Membrane Matrix. It was known of the Körösy-type membranes that they are gradually discolored by transferring current through them. However, it was thought that this effect is caused by chemical reagents present in the solutions. In order to find the reasons for the effect, arrangement C was used with large-surface Ag-AgCl electrodes instead of the Pt, to avoid electrode reactions which may produce reactive substances. With a potential drop of 2 v. between the two reference electrodes, a current of 30 ma./cm.² passed through the membrane immersed in 0.1 N KCl solution. The current was passed for 10 hr., in the first experiment without and in the second with illumination by a 100-w. incandescent lamp. In this second experiment, two samples of the same membrane were placed in the same solution, one illuminated and the other in the dark. In the course of the experiment, the solution was tested for free chlorine production and for changes in pH. No chlorine was found, and the pH did not change significantly. Gas formation on the electrodes was not observed.

After 10 hr. of experiment, the part of the membranes which was exposed to current transfer was lighter in color, with and without illumination. No color changes occurred in membranes immersed into such solutions without current flowing.

Discussion

An additional current, some tenths of 1% of the dark current, flows through the membranes under illumination with the light intensities here employed. This additional current may be attributed to the existence of two factors: a potential difference between two points inside the membrane and a system of conjugated double bonds linking these two points, enabling the electron excited by the light to flow along the potential difference.

The decoloration of the membranes during prolonged current flow is connected with the saturation of the double-bond systems. The order of magnitude of the yield of this process may be calculated from the known ionic capacity of the membranes (1 mequiv./g. or 10 μ equiv./cm.² of the membranes used) and by assuming that 1-10 double bonds are associated with every

ionic group. (There are 10 PVC units per ionic group in our membranes.) For the number of faradays used in our experiments, the yield is of the order of 0.1%.

Both effects are thus small, but significant. We may account for them by assuming that, between points inside the membrane, there arises a potential difference during current flow by ion transport. If the two points are connected by a system of conjugated double bonds, electrochemical reactions resulting in the saturation of the double bonds may occur across the two ends of the system as a result of the potential difference, the circuit being completed by electron flow along the conjugated double-bond system.

On illumination, electrons are raised into the conduction band of the conjugated double-bond system, resulting in additional current flow between the points of potential difference.

The effects observed cannot be derived from the existing models of permselective membrane processes. It is known³ that some aspects of the experimental behavior of permselective membranes, particularly during ion transport, cannot be quantitatively fully described by the existing theoretical models. Such, for example, are the magnitude of membrane potentials^{3a} under equilibrium conditions during current transfer,^{3b} and the relaxation of residual potentials on switch off (electret effect).^{3c}

The effects now observed are relatively small. However, they offer an experimental way for obtaining further information concerning processes inside the membrane and may shed light on the cause of the more general observations.

It is to be remarked that the special membranes now used behave as mixed ionic-electronic conductors. The influence of current density, light intensity, saturation of double bonds by halogenation, and wave length of light employed on the additional light-induced current support this qualitative picture, in which only the electronic mode of conduction is affected by illumination.

We should like to draw attention to some phenomena observed in biological membranes⁴ which appear to be similar to our observations.

(3) (a) G. F. Hills, P. W. M. Jacobs, and N. Lakshminarayanaiah, *Proc. Roy. Soc. (London)*, **A262**, 246, 257 (1961); (b) B. A. Cooke, *Electrochem. Acta*, **3**, 307 (1961); **4**, 179 (1961); P. A. Cooke and S. F. van der Walt, *ibid.*, 216 (1961); (c) D. Cowan, *Dechema Monograph.*, **47**, 565 (1963).

(4) N. Chalazonitis, *Photochem. Photobiol.*, **3**, 539 (1964).

Charge Separation in Liquid Junctions

by Dennis R. Hafemann

Department of Chemistry, University of California, San Diego, La Jolla, California 92038
(Received June 23, 1965)

Liquid junction potentials are calculated by a computer simulation method. The charge distribution generated by the interdiffusion of two electrolyte solutions is computed explicitly and used to evaluate the liquid junction potential as a function of time. A rise time of about 10^{-9} sec. is calculated for the potentials of junctions between ordinary salt solutions. The steady-state results agree with previous calculations which were made by assuming electroneutrality throughout the junction and performing a thermodynamic integration of transport numbers. The application of the simulation method to more complex systems, including biological membrane systems, is discussed.

Introduction

Steady-state values for the electrostatic potential difference across variously constrained liquid junctions are calculable by several methods.¹⁻¹⁰ In some methods reversible thermodynamics is applied to an irreversible process. Such treatments can be expected to be valid only for the analysis of diffuse junctions on a long-time scale. Other methods treat the irreversible phenomena more or less correctly, but they depend on the assumption of electroneutrality throughout the junction. This assumption is self-contradictory because there can be no potential difference if there is no charge separation. To rationalize the electroneutrality condition, it has been assumed that the deviations from electroneutrality are so small that they have no effect on the result. No electrostatic charge distributions have previously been calculated to support this rationalization.

The generation of an electrostatic potential between two initially electrically neutral solutions is the subject of the present work. The electroneutrality condition is eliminated, and transient charge distributions are calculated using a digital computer. The results show that the electroneutrality assumption is approximately valid for the time scales on which experiments are usually performed. A liquid junction which is formed from a sharp initial boundary and not subsequently constrained with respect to width is shown to give rise to a charge distribution that changes with time in such a way that a steady liquid junction potential results.

Method

Consider an experiment in which two uncharged solutions are initially brought together to form a planar junction of large area. In the limiting case of infinite area, neglecting gravity and assuming no bulk flow or convection, the one-dimensional nature of the initial condition will persist throughout the experiment. The x direction is defined to be perpendicular to the plane of the junction.

To construct a digital model, one subdivides the region around the junction into $m + 1$ "cells," separated by planes parallel to the junction at fixed intervals along the x axis. The cells are numbered in spatial sequence from 0 to m . The model is represented by an $n(m + 1)$ concentration matrix C

$$C = \begin{pmatrix} c_{10} & \cdots & c_{1m} \\ \vdots & & \vdots \\ c_{n0} & \cdots & c_{nm} \end{pmatrix} \quad (1)$$

- (1) H. von Helmholtz, "Wissenschaftliche Abhandlungen," J. A. Barth, Leipzig, Vol. 1, 1882, p. 840; Vol. 2, 1895, p. 979.
- (2) W. Nernst, *Z. physik. Chem.* (Leipzig), **2**, 613 (1888).
- (3) M. Planck, *Ann. Phys. Chem.*, **39**, 161 (1890); **40**, 561 (1890).
- (4) P. Henderson, *Z. physik. Chem.* (Leipzig), **59**, 118 (1907); **63**, 325 (1908).
- (5) H. Pleijel, *ibid.*, **72**, 1 (1910).
- (6) P. B. Taylor, *J. Phys. Chem.*, **31**, 1478 (1927).
- (7) R. Schlögl, *Z. physik. Chem.* (Frankfurt), **1**, 305 (1954).
- (8) H. Cohen and J. W. Cooley, *Biophys. J.*, **5**, 145 (1965).
- (9) S. R. de Groot, "Thermodynamics of Irreversible Processes," North-Holland Publishing Co., Amsterdam, 1952, pp. 133-140.
- (10) D. T. J. Hurtle, J. B. Mullin, and E. R. Pike, *J. Chem. Phys.*, **42**, 1651 (1965).

where n is the number of distinct species (ions and neutral molecules) considered. It is assumed that each of the cells is homogeneous, the entire difference between c_{ij} and $c_{i,j+1}$ being displayed as a discontinuity in $c_i(x)$ at the boundary between cell j and cell $j + 1$. The charge density ρ_j in cell j is

$$\rho_j = \sum_{i=1}^n z_i c_{ij} \quad (2)$$

where z_i is the charge of species i .

Let us consider all of the charge in cell j to lie on a plane at the midpoint of the cell. The surface charge density σ_j on this plane is

$$\sigma_j = \rho_j d_j \quad (3)$$

where d_j is the thickness of cell j . The planes of charge are located x_0, x_1, \dots, x_m , respectively. The surface charge densities are subject to the condition

$$\sum_{j=0}^m \sigma_j = 0 \quad (4)$$

because the system as a whole has no net charge.

Consider a point with coordinate x lying between x_k and x_{k+1} . By application of Gauss' theorem¹¹ one can show that the electric field intensity E at x is

$$E(x) = \frac{1}{\epsilon(x)} \sum_{j=0}^{k(x)} \sigma_j \quad (5)$$

where $\epsilon(x)$ is the permittivity of the medium, which is in general a function of x . The upper limit on the summation of (5) is chosen so that the sum includes only the charges lying to the left of point x . Formally k is determined by the inequality

$$x_k < x < x_{k+1} \quad (6)$$

The potential difference V across the system is given by (see Appendix)

$$V = \frac{d}{\epsilon} \sum_{j=0}^m j \sigma_j \quad (7)$$

where d is the constant cell thickness and ϵ is assumed to be independent of x . For detailed computations, (A3) is a more general equation.

To simulate the effect of elapsed time, the numbers in the C matrix must be changed according to an algorithm using the methods of irreversible thermodynamics. In the present work, it is assumed that the flux of species i depends on the electric field intensity and the gradient of the activity of i at the point in question but that it does not depend on the gradient of the activity of any other species. This oversimplification is made to provide a simple test for the method.

Nonlinear force-flux relationships and coupling of fluxes can be treated by the method described here. Assuming constant temperature and pressure, the equation¹² for the flux J_i of species i is

$$J_i = -c_i g_i \frac{d}{dx} \mu_i^* \quad (8)$$

where c_i is the concentration, g_i the mobility ($g_i \equiv L_{ii}/c_i$), and μ_i^* the electrochemical potential of species i . A more detailed expression, neglecting the polarizability¹³ of the component species, is

$$J_i = -g_i \left\{ RT \frac{\partial c_i}{\partial x} + RT c_i \frac{\partial \ln \gamma_i}{\partial x} + z_i c_i \mathcal{F} \frac{\partial \psi}{\partial x} \right\} \quad (9)$$

where γ_i is the activity coefficient of species i , ψ is the electrostatic potential, and \mathcal{F} is the Faraday. For uncharged species

$$g_i = \frac{D_i}{RT} \quad (10)$$

where D_i is the solvent-fixed diffusion coefficient. For ionic species

$$g_i = \frac{t_i \Lambda}{z_i^2 \mathcal{F}^2} \quad (11)$$

where t_i is the solvent-fixed transference number of species i in a solution of conductance Λ . In the present calculation, solvent flow is neglected. Both g_i and γ_i are assumed for simplicity to be functions of total ionic strength only.

Single-ion activity coefficients are estimated by use of the MacInnes assumption¹⁴

$$\gamma_{\text{Cl}^-}^{\text{MCl}} = \gamma_{\text{Cl}^-}^{\text{KCl}} = \gamma_{\pm}^{\text{KCl}} \quad (12)$$

Since these activity coefficients are not thermodynamically measurable,¹⁵⁻¹⁸ their use introduces an error of unknown magnitude. However, it is better to include an estimate in the calculation than to ignore

(11) L. Page and N. I. Adams, "Principles of Electricity," D. Van Nostrand Co., Inc., New York, N. Y., 1931, p. 25.

(12) H. S. Harned and B. B. Owen, "The Physical Chemistry of Electrolytic Solutions," Reinhold Publishing Corp., New York, N. Y., 1958, p. 119.

(13) I. Pregogine, P. Mazur, and R. Defay, *J. chim. phys.*, **50**, 146 (1953).

(14) D. A. MacInnes, "The Principles of Electrochemistry," Reinhold Publishing Corp., New York, N. Y., 1939, p. 242.

(15) E. A. Guggenheim, *J. Phys. Chem.*, **33**, 842 (1929); **34**, 1540 (1930).

(16) J. G. Kirkwood and I. Oppenheim, "Chemical Thermodynamics," McGraw-Hill Book Co., Inc., New York, N. Y., 1961, p. 211.

(17) I. Oppenheim, *J. Phys. Chem.*, **68**, 2959 (1964).

(18) H. S. Frank, *ibid.*, **67**, 1554 (1963).

activity coefficients altogether. It is possible that calculations of the kind described here may eventually make possible more accurate estimates of single-ion activity coefficients.

At time 0 matrix C is set to the initial conditions of the experiment being simulated, and values of $\partial c_i/\partial x$ and $\partial \ln \gamma_i/\partial x$ for every species i and $\partial \psi/\partial x$ are determined at the intersections of adjacent cells. Then the fluxes J_i are calculated from (9). These fluxes are assumed to remain constant over an appropriately short time interval Δt , and a new set of values for C is determined. From these values $\partial c_i/\partial x$, $\partial \ln \gamma_i/\partial x$, and $\partial \psi/\partial x$ are again calculated, and the process is repeated as often as desired. A typical calculation, for which $n = 2$, $m + 1 = 100$, and the Δt iteration is repeated 500 times, requires about 1 min. of computation on a CDC 3600.

Results

The junction NaCl (0.099570 M)–NaCl (0.049833 M) has been studied, using the data^{19–21} in Table I. The values in this table have been adjusted to provide the most accurate interpolation possible in the concentration range of interest. Figure 1 shows the calculated variation of V with time. The three curves are results obtained with three sets of values for Δt and d . The shortest value of Δt probably gives the most reliable curve. Because V reaches its final value very rapidly (10^{-9} sec.), no comparison of the rise time with published experiments can be made. It is possible, however, that methods could be devised to measure the radiofrequency energy which is generated by a flowing junction. After the initial fast rise, the liquid junction potential remains constant (except for some overshoot in cases where Δt is too long), in agreement with experiment.

Table I: Data Used in the Computations^a

Concn., M	$\ln \gamma_{K^+} =$ $\ln \gamma_{Cl^-}$	$\ln \gamma_{Na^+}$	$\theta_{K^+}^b$	θ_{Cl^-}	θ_{Na^+}
0	-0.079	-0.077	7.54	7.83	5.08
0.05	-0.202	-0.188	7.02	7.31	4.62
0.10	-0.264	-0.240	6.78	7.07	4.41
0.15	-0.302	-0.264	6.57	6.85	4.20

^a See ref. 19–21. ^b The units of g are 10^{-16} mole sec. g^{-1} .

Figure 2 shows the broadening of the junction that is continually taking place. Although a junction of specified width will reach a steady-state charge distribution, the charge distribution in a junction unconstrained with respect to width is a strong function of

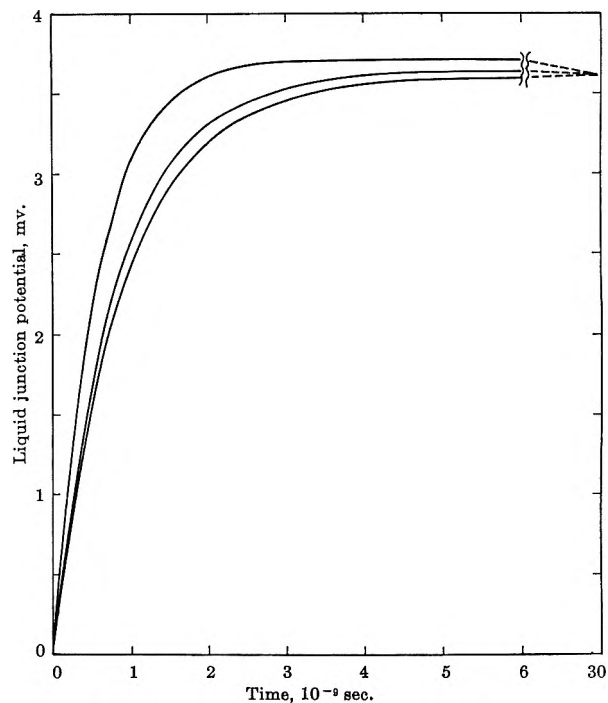


Figure 1. Liquid junction potential vs. time after formation of a sharp junction between NaCl (0.099570 M) and NaCl (0.049833 M): top curve, $\Delta t = 5 \times 10^{-10}$ sec.; middle curve, $\Delta t = 10^{-10}$ sec.; bottom curve, $\Delta t = 10^{-11}$ sec.; $\Delta t/d^2 = 10^4$ sec. cm^{-2} ; $T = 25^\circ$ for all curves.

time after formation from an initially sharp boundary. At 1.2×10^{-8} sec. after formation of the junction, there is a 0.36% excess of Cl^- ions at the trough of the charge distribution. After 6.2×10^{-8} sec., the excess is reduced to 0.075%. It is only for a very sharp junction that the electroneutrality assumption is incorrect.

The junction NaCl (0.1 M)–KCl (0.1 M) has also been studied because this is a case in which the Planck and Henderson methods fail to predict the correct result.²² In Figure 3 the concentrations of Na^+ , K^+ , and Cl^- are shown 6.2×10^{-8} sec. after the formation of a NaCl–KCl junction. Note that the chloride concentration profile is distorted by the inequality of the mobilities of the two counterions, in qualitative agreement with the calculation of Taylor⁶ on the junction HCl–KCl.

Figure 4 shows the dependence of liquid junction potential rise time on the assumed dielectric constant

(19) See ref. 12, Appendix A.

(20) R. A. Robinson and R. H. Stokes, "Electrolyte Solutions," Butterworth and Co. Ltd., London, 1959.

(21) A. S. Brown and D. A. MacInnes, *J. Am. Chem. Soc.*, **57**, 1356 (1935).

(22) See ref. 14, p. 236.

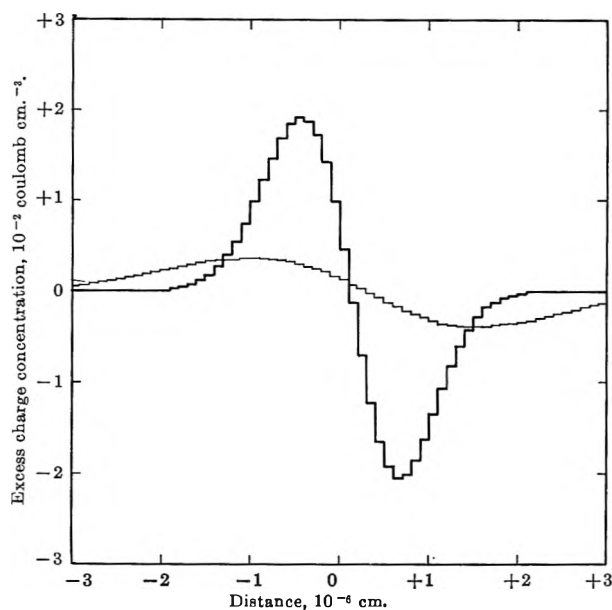


Figure 2. Concentration of excess charge vs. distance in the junction NaCl (0.099570 M)-NaCl (0.049833 M) at 10^{-8} sec. (heavy curve) and at 6.2×10^{-8} sec. (light curve) after formation. For both curves $\Delta t = 10^{-10}$ sec., $\Delta t/d^2 = 10^4$ sec. cm.^{-2} .

of the solution. A low dielectric constant decreases the time for attainment of a steady potential difference.

Discussion

The following two conditions have been found to be important to the model's stability and to the fidelity with which it simulates a physical process.

The ratio $\Delta t/d^2$ must be such that d is approximately equal to the root-mean-square distance a molecule travels in time Δt . For diffusion of uncharged species $\Delta t/d^2 = O(D^{-1})$. For charged species the ratio is also affected by the strengths of the electric fields present and by the dielectric constant of the medium. If $\Delta t/d^2$ is too small, the result will be only slightly in error, but, if $\Delta t/d^2$ is too large, the calculation will be unstable and lead to meaningless results.

The interval Δt must be short compared with the natural rise time of the liquid junction potential. The method may give an accurate long-time value of the liquid junction potential if this condition is not met, but it cannot yield the correct time dependence. As $\Delta t \rightarrow 0$, keeping $\Delta t/d^2$ constant, the fidelity of the model increases monotonically, but less rapidly than the computation time increases. The value of Δt used in a calculation must be determined by a compromise between high fidelity and short computation time.

The potential calculated for the NaCl (0.1 M)-KCl (0.1 M) junction, 4.83 mv., differs significantly

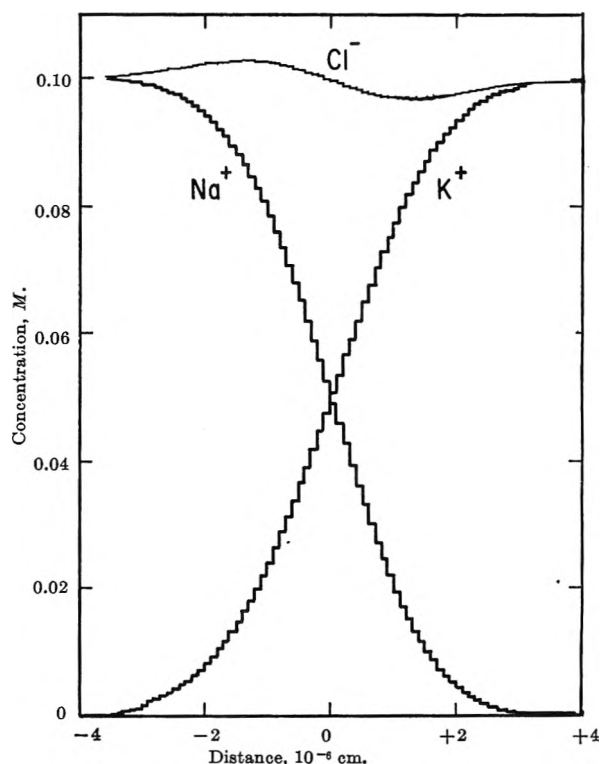


Figure 3. Concentration of Na^+ , K^+ , and Cl^- vs. distance in the junction NaCl (0.1 M)-KCl (0.1 M) at 6.2×10^{-8} sec. after formation. $\Delta t = 10^{-10}$ sec., $\Delta t/d^2 = 10^4$ sec. cm.^{-2} .

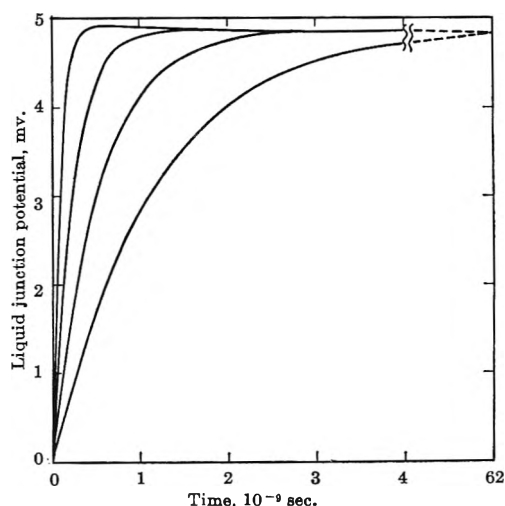


Figure 4. Liquid junction potential vs. time for the junction NaCl (0.1 M)-KCl (0.1 M), $\Delta t = 10^{-10}$ sec., $\Delta t/d^2 = 10^4$ sec. cm.^{-2} ; top curve, dielectric constant $K = 19.63$; second curve, $K = 39.27$; third curve, $K = 78.54$; bottom curve, $K = 157.08$. Top curve overshoots because the value of $\Delta t/d^2$ is too high.

from the measured²² Cl^- ion potential difference of 6.42 mv. Essentially the same result, 4.86 mv., is ob-

tained by the Planck and Henderson methods of calculation.²² Therefore, one of the following assumptions is probably incorrect.

(1) The activity coefficient of Cl^- is the same in a given concentration of NaCl as it is in the same concentration of KCl .

(2) The flux of a given component is independent of the flux of any other component, except that the fluxes of charged species will influence each other electrostatically.

(3) The mobility of a given component depends only on the total ionic strength of the solution.

(4) The dielectric constant of the solution is constant and equal to that of water. This includes the assumption that the effect of the force tending to pull the most polarizable species to the point of highest field strength is negligible for the solutions treated here. The use of the bulk dielectric constant, or of any dielectric constant, on the distance scale encountered here (10 Å.) is questionable, but, since the value of the dielectric constant affects only the rate of change of the potential and not its steady-state value, this is probably not the cause of the discrepancy.

(5) The junction is isothermal. If the heat of mixing of the two solutions were large, this simplifying assumption could not be made.

(6) Solvent flow is negligible.

The error probably results from the first and second assumptions.

The NaCl (0.099570 M)– NaCl (0.049833 M) results agree within 1% with experiment.²¹ Table II shows that the result obtained using the Guggenheim assumption ($\gamma_{\text{M}^+} = \gamma_{\text{Cl}^-} = \gamma_{\pm}^{\text{MCl}}$) is not significantly different from that obtained using the MacInnes assumption. However, complete neglect of activity coefficients leads to an 8% error in the calculated cell potential.

Table II: Effect of Activity Coefficient Assumption on the Calculated Potential of the Concentration Cell

	Ideal soln. assump- tion	Mac- Innes assump- tion	Guggen- heim assump- tion
A. Concentration potential ^a	17.783	16.191	16.345
B. Liquid junction potential	-4.062	-3.611	-3.745
C. Calculated cell potential (A + B)	13.721	12.580	12.600
D. Observed cell potential ^b	12.692	12.692	12.692
E. Deviation (C - D)	+1.029	-0.112	-0.092

^a All potentials are in millivolts. ^b See ref. 21.

Calculation of this cell potential by means of the thermodynamically exact Helmholtz method, with experimentally determined transport numbers and activity coefficients, leads to a much more accurate result than any quoted in Table II but gives no information about time dependence or activity coefficient asymmetry.

Although the present investigation has been limited to the study of one-dimensional isothermal liquid junctions between simple salt solutions, the method developed also is applicable to: (1) more complex geometries, providing the electrostatic part of the problem can be solved; (2) nonisothermal systems, if the irreversible thermodynamic treatment is extended to include the effect of temperature gradients; (3) solutions which are reacting chemically, provided the rates of reaction, equilibrium constants, and heats of reaction are known; (4) diffusion in ionic solids, in which experimentally observable rise times may be predicted; (5) membrane phenomena, including analysis of the generation and time variations of electrostatic potentials across biological membranes. The temporal and spatial variations of the ionic mobilities which are important in the description of biological membrane phenomena could easily be included in the treatment described above.

Acknowledgments. The author wishes to thank Dr. Stanley L. Miller, Dr. Donald G. Miller, and Dr. Alexander Mauro for their helpful criticisms and suggestions. The work was supported by U. S. Public Health Service Grant No. 11906.

Appendix

Potential Difference across a System of Infinite Planes of Uniform Surface Charge. From elementary electrostatics

$$V \equiv V_m - V_0 = - \int_{x_0}^{x_m} E(x) dx \quad (\text{A1})$$

If eq. 5 is substituted for $E(x)$, (A1) becomes

$$V = - \int_{x_0}^{x_m} \frac{1}{\epsilon(x)} \sum_{j=0}^{k(x)} \sigma_j dx \quad (\text{A2})$$

Making explicit the discrete nature of the charge distribution, we write

$$V = - \sum_{k=0}^{m-1} \frac{x_{k+1} - x_k}{\epsilon_k} \sum_{j=0}^k \sigma_j \quad (\text{A3})$$

if ϵ has the value ϵ_k at all points between x_k and x_{k+1} . The upper limit on the first summation in (A3) can be changed to m since by (4) the added term will equal

zero. For the special case where ϵ is independent of x and the planes are equally spaced

$$d_j = d \quad (\text{A4})$$

for all j , (A3) can be reduced to

$$V = -\frac{d}{\epsilon} \sum_{j=0}^m \sigma_j \sum_{k=j}^m 1 \quad (\text{A5})$$

Evaluating the final sum in (A5) and using (4) to simplify the expression, we arrive at the result

$$V = \frac{d}{\epsilon} \sum_{j=0}^m j \sigma_j \quad (\text{A6})$$

which has been used in all the calculations reported above.

The Heats and Entropies of Dilution of the Perchlorates of Magnesium and Strontium¹

by H. S. Jongenburger and R. H. Wood

Department of Chemistry, University of Delaware, Newark, Delaware (Received June 28, 1965)

The heats of dilution of magnesium perchlorate and strontium perchlorate have been measured at 25° from 0.002 up to 4.4 *m*. The results were extrapolated to infinite dilution using an extended Debye-Hückel equation. The values of the relative apparent molal heat content are intermediate between the corresponding chlorides and nitrates. The corresponding entropies of dilution have been calculated. The results indicate that the perchlorates are not strongly ion paired.

This paper is one of a series² on the heats and entropies of dilution of electrolyte solutions. The regularities found in the entropies of dilution offer some hope of achieving a deeper understanding of the structural effects in concentrated electrolytes. The perchlorates of the alkali metals show an increasing degree of ion pairing as the alkali metal gets heavier. The same sequence holds for the nitrates of the alkali metals and the alkaline earths. This study was undertaken to see if the alkaline earth perchlorates showed a similar behavior.

Experimental Section

Materials. All chemicals used were reagent grade. The magnesium perchlorate was prepared from MgO and HClO₄. The oxide was digested several times with large amounts of water to reduce further the alkali salts content. After three recrystallizations the stock

solution was prepared by dissolving the wet salt in the required amount of water and adjusting the pH to about 4.

Strontium perchlorate stock solution I was prepared from SrCO₃ and HClO₄. The procedure was similar to the above. For stock solution II the SrCO₃ was prepared from Sr(NO₃)₂ and (NH₄)₂CO₃. The SrCO₃ was dried at 600° to remove all ammonium salts.

Stock solutions were analyzed for Na, K, and Ca by flame photometry using a Beckman DU spectrophotometer, Model 2400, with an oxygen-acetylene flame attachment. The procedure was to compare a solution of the salt with one to which known amounts of

(1) The authors thank the National Science Foundation for financial aid under Grant NSF-G14304.

(2) (a) R. H. Wood, *J. Phys. Chem.*, **63**, 1347 (1959); (b) F. R. Jones and R. H. Wood, *ibid.*, **67**, 1576 (1963).

impurities (about 0.1 mole %) had been added. Proportionality between readings and concentrations was assumed after correcting for background emission. The results were: sodium 0.06, 0.2, and 0.1 mole %; potassium 0.00, 0.0, and 0.0 mole %; calcium 0.002, 0.15, and 0.06 mole % for magnesium perchlorate and strontium perchlorate stock solutions I and II, respectively.

The concentration of the $\text{Mg}(\text{ClO}_4)_2$ stock solution was determined by titration with 0.01 *M* disodium dihydrogen ethylenediaminetetraacetate (EDTA) solution. The EDTA solution was obtained by dissolving the exact amount of the dried salt (12 hr. at 80°). The titer was checked against a standard solution of zinc prepared from zinc metal.³ The maximum deviation of six titrations of the stock solution was 0.08%. The concentrations of the $\text{Sr}(\text{ClO}_4)_2$ stock solutions were determined by precipitating the strontium as the sulfate.⁴ The results showed maximum deviations of 0.1 and 0.2% for stock solutions I and II, respectively.

All other solutions were prepared from the stock solutions by diluting with water by weight. Stock solution II ($\text{Sr}(\text{ClO}_4)_2$) was used in runs 68 and 69 only.

*Description of Calorimeter.*⁵ The isothermal differential calorimeter was constructed entirely of aluminum⁶ coated inside with Penton.⁷ The design differs from that by Gucker, *et al.*,⁸ mainly with respect to the construction and arrangement of heaters, pipets, and the differential thermopile.

The vessels have a net capacity of 700 ml. The lids and stirring assembly are permanently attached to the top of the submarine which was immersed in a constant-temperature bath ($\pm 0.001^\circ$).

Four rectangular wells extended from each lid into the vessels. The wells were placed symmetrically and were welded to the lids. The heater was placed in two opposite wells and the thermopiles in the two remaining wells of each lid. The stirrer was placed in the center of the vessel and the pipets in the spaces between each pair of wells and the wall of the vessel. This arrangement is advantageous in that it provides a technique for obtaining conveniently and quickly heats of dilution data over short concentration intervals in the very low concentration ranges required for the extrapolation of the data to zero concentration. The air spaces in the vessel (10 ml.) and pipets (1 ml.) were small enough so that changes in the amount of water vapor caused negligible heat effects.

The pipets were made of 22-mm. glass tubing and contained about 22 ml. Teflon sleeves and stoppers were used to close and open the pipets. The stoppers were screwed on a tantalum rod. The glass tubes were blown out in a triangular shape between the sleeves.

This provided enough open area around the top stopper in the opened position for flushing of the pipets. The heat of opening was determined for each of the eight available pipets and found to be 0.0085 cal. with a standard deviation of 0.004 cal. The heat of opening was the same for all eight pipets, within the experimental error. The data as reported have been corrected for this effect.

The thermopile consisted of 76 junctions of No. 30 B and S gauge constantan and chromel-P. The junctions were soldered into $5 \times 5 \times 2$ mm. copper blocks and held in a slotted Teflon plate which pressed the junction against the aluminum wall. A sheet of mica (0.02 mm.)⁹ was used for insulation. A four-junction thermopile was constructed in a similar manner between each vessel and the submarine. The thermopile voltage was measured by means of a galvanometer amplifier with negative feedback, which has been described elsewhere.¹⁰

The 500-ohm heaters were constructed of No. 33 B and S gauge Evanohm¹¹ wound around a 0.16-cm. aluminum plate and immersed in a well which was filled with silicone oil. The current-carrying leads were of No. 24 B and S copper which caused negligible heat loss and lead resistance errors.

The electrical heat inputs were measured ($\pm 0.04\%$) with a standard circuit (1 cal. = 4.1840 absolute joules). The experiments were performed at $25.00 \pm 0.02^\circ$. The pipets were filled by weight, and the vessels were filled with 580 ± 0.2 g. of water.

The results were corrected for heat losses during the experimental period using the formula

$$\Delta Q = C_p \int K \Delta \theta dt \quad (1)$$

where ΔQ is the heat exchanged, C_p is the heat capacity of the vessel, K is the over-all heat leak constant between vessels, $\Delta \theta$ is the difference in temperature between the two vessels, and t is the time. The integral

(3) F. J. Welcher, "The Analytical Uses of Ethylenediamine Tetraacetic Acid," D. Van Nostrand Co., Inc., New York, N. Y., 1958, p. 117.

(4) A. I. Vogel, "Quantitative Inorganic Analysis," 3rd Ed., Longmans, Green and Co., London, 1961, p. 552.

(5) For further details see H. S. Jongenburger, Ph.D. Thesis, University of Delaware, 1963.

(6) Obtained through the courtesy of the Aluminum Co. of America, Pittsburgh, Pa.

(7) Penton resin and technical information supplied through the courtesy of the Hercules Powder Co., Wilmington, Del.

(8) F. T. Gucker, H. B. Pickard, and R. W. Planck, *J. Am. Chem. Soc.*, **61**, 459 (1939).

(9) Obtained through the courtesy of the Tar Heel Mica Co., Plumtree, N. C.

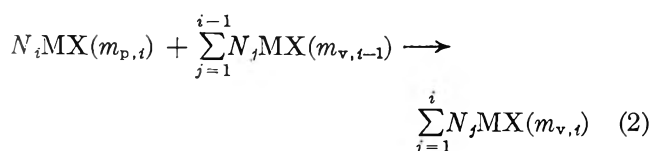
(10) R. H. Wood and H. S. Jongenburger, *Rev. Sci. Instr.*, **35**, 407 (1964).

(11) Courtesy of Wilber B. Driver Co., Newark, N. J.

is evaluated during the experimental period. The constant K was evaluated by experiments in which known amounts of heat were put into both vessels at different times, and ΔQ was measured. The value of K was 0.34%/min., and the corrections varied from 0 to 1% of the total heat.

The over-all performance of the calorimeter was checked by means of some dilution experiments with 0.816 M sodium chloride. Except for the experiments using the first pipet, the results checked the values of the heat liberated calculated from the experiments of Gulbransen and Robinson¹² to within 0.01 cal. The later experiments with the calorimeter did not show any inconsistency in the results using the first pipet.

Program of Dilutions. The equation for the reaction upon opening the i th pipet is



where N_i moles of the salt MX (molality $m_{p,i}$) in the i th pipet to be opened are mixed with the sum of the number of moles in the preceding pipets at a molality in the vessel $m_{v,i-1}$ to give a final solution of molality $m_{v,i}$. The heat of mixing for this process is

$$q_i = N_i[\phi_L(m_{p,i}) - \phi_L(m_{v,i})] + \sum_{j=1}^{i-1} N_j[\phi_L(m_{v,i-1}) - \phi_L(m_{v,i})] \quad (3)$$

If the pipets all contain solutions of the same molality (m_p), the results can be combined to give

$$\sum_{i=1}^i q_i = \sum_{j=1}^i N_j[\phi_L(m_p) - \phi_L(m_{v,i})] \quad (4)$$

and also

$$\left(\frac{\sum_{j=1}^i q_j}{\sum_{j=1}^i N_j} \right) - \left(\frac{\sum_{l=1}^k q_l}{\sum_{l=1}^k N_l} \right) = \phi_L(m_{v,k}) - \phi_L(m_{v,i}) \quad (5)$$

All of the direct data (eq. 4) and all of the indirect data (eq. 5) which were in an appropriate concentration range were used in the extrapolation. The extrapolation of the weighted experimental data to zero concentration was carried out on an IBM 1620 computer¹³ using the extended Debye-Hückel equation.¹⁴

$$\phi_L = Sm^{1/2}[1/(1 + Am^{1/2}) - \sigma(Am^{1/2})/3] + Bm + Cm^{3/2} \quad (6)$$

where

$$\sigma(Y) = 3Y^{-3}[1 + Y - 2 \ln(1 + Y) - 1/(1 + Y)] \quad (7)$$

and S is the Debye-Hückel slope ($S = 3580$). Appropriate values for A were calculated from activity data. Values for B and C were found by applying the least-squares technique, using $\Delta\phi_L$ data derived from Table I. Relative weights were calculated from estimated probable errors. In treating the data, an F test¹⁵ was used to determine whether the C coefficient was significant.

The accuracy of the extrapolation method was checked using salts for which very low concentration measurements were available. Extrapolations of the same data, using only the higher concentration data, indicated that, for 1-1 electrolytes with ϕ_L greater than -36 cal./mole at 0.1 M and for 2-1 electrolytes with ϕ_L greater than 360 cal./mole at 0.1 M , the extrapolation using the concentration range 0.1 to 0.01 M yields ϕ_L values accurate to ± 1.5 cal./mole at 0.01 M . For 1-2 electrolytes with ϕ_L greater than 140 cal./mole at 0.1 M more dilute data (0.05 to 0.005 M range) must be used to obtain ϕ_L values accurate to ± 2 cal./mole at 0.01 M .

The exact value of the limiting slope S is in some doubt.^{16,17} The value derived from the dielectric constant measurements of Malmberg and Maryott¹⁶ has been used. The uncertainty in slope represents a difference in extrapolation of about 4 cal./mole.

Results and Discussion

The calorimetric data are given in Table I. The data are given in order of opening of the pipets in each run with results from the left vessel alternating with values for the right vessel. To minimize the calculations for assigning weights to the data, duplicate runs were not averaged but were treated individually. Originally, all possible $\Delta\phi_L$ values up to 0.1 M were used in the extrapolation. In a second trial the data were limited to about 0.06 M . No significant change was found in the case of $\text{Mg}(\text{ClO}_4)_2$. However, the standard deviation of the fit for $\text{Sr}(\text{ClO}_4)_2$ decreased from 2.1 to 1.0 cal. mole⁻¹, and at 0.068 M the ϕ_L

(12) E. A. Gulbransen and A. L. Robinson, *J. Am. Chem. Soc.*, **56**, 2637 (1934).

(13) The authors thank the Computing Center of the University of Delaware for the use of its facilities.

(14) A copy of the Fortran program is available from R. H. Wood.

(15) W. J. Dixon and F. J. Massey, "Introduction to Statistical Analysis," 2nd Ed., McGraw-Hill Book Co., Inc., New York, N. Y., 1957.

(16) G. C. Malmberg and A. A. Maryott, *J. Res. Natl. Bur. Std.*, **56**, 1 (1956).

(17) B. B. Owen, R. C. Miller, C. E. Milner, and H. L. Cogan, *J. Phys. Chem.*, **65**, 2065 (1961).

Table I

Run no.	$10^4 n_i$	$10^4 m_{p,i}$	$10^4 m_{v,i}$	% cal.	$\phi_L(m_{p,i}) - \phi_L(m_{v,i})$, cal./mole	$\phi_L(m_{v,i})$, cal./mole	$\phi_L(m_{p,i})$, cal./mole	Av. $\phi_L(m_{p,i})$, cal./mole		
Calorimetric dilution data of $Mg(ClO_4)_2$ at 25°										
51	1.103	50.03	1.833	0.252	228.4	91.2	319.6	316.9		
	1.103		1.833	0.248	224.8		316.0			
	1.102		3.534	0.182	196.8		121.2		318.0	
	1.101		3.533	0.185	196.4		317.6			
	1.103		5.120	0.140	173.5		145.2		318.7	
	1.102		5.118	0.130	170.3		315.5			
	1.105		6.606	0.127	158.6		157.4		316.0	
	1.104		6.602	0.127	156.5		313.9			
58	2.188	99.86	3.635	0.567	259.1	122.4	381.5	385.5		
	2.188		3.635	0.582	266.0		388.4			
	2.191		7.020	0.979	223.5		160.9		384.4	
	2.191		7.020	1.007	229.9		390.8			
	2.192		10.18	1.311	199.5		186.0		385.5	
	2.188		10.17	1.338	203.7		389.7			
	2.192		13.12	1.591	181.6		205.1		386.7	
	2.189		13.11	1.591	181.7		386.8			
45	4.965	192.1	8.211	1.355	272.9	171.6	444.5	448.3		
	4.963		8.207	1.374	277.4		449.0			
	4.969		15.78	0.904	227.4		219.5		446.9	
	4.973		15.78	0.902	229.4		448.9			
	4.967		22.78	0.714	199.5		249.4		448.9	
	4.976		22.79	0.705	200.1		449.5			
	4.972		29.27	0.568	178.2		271.0		449.2	
	4.978		29.29	0.562	178.3		449.3			
46	19.30	812.7	31.97	6.179	320.2	278.7	598.9	599.6		
	19.30		31.97	6.177	320.1		598.8			
	19.31		61.54	3.936	261.9		338.0		599.9	
	19.33		61.56	3.940	261.9		599.9			
	19.24		88.85	3.060	227.7		372.0		599.7	
	19.24		88.86	3.056	227.7		599.7			
	19.29		114.3	2.571	204.1		395.6		599.7	
	19.30		114.3	2.589	204.3		599.9			
47	19.29	812.7	31.96	6.212	322.0	278.7	600.7	600.8		
	19.30		31.96	6.233	323.0		601.7			
	19.31		61.52	3.916	262.4		338.0		600.4	
	19.31		61.53	3.879	261.9		599.9			
55	45.94	2467	76.75	44.25	963.1	358	1321	1321		
	45.95		76.77	44.16	960.9		1319			
	45.97		148.7	38.45	899.7		422		1322	
	45.94		149.0	38.41	898.0		1320			
	45.89		216.7	36.43	864.5		459		1324	
	45.88		216.8	36.48	863.7		1323			
	45.81		280.6	35.17	840.3		480		1320	
	45.90		280.8	35.36	840.4		1320			
54	12.71	599.9	21.14	3.957	311.3	242.6	553.9	553.4		
	12.70		21.13	3.943	310.3		542.9			
	14.75		700.2	44.14	3.156		269.4		307.3	576.7
	14.73		700.2	44.09	3.149		269.2		576.5	
	18.74		899.0	71.84	3.773		266.8		351.8	618.6
	18.58		899.0	71.58	3.774		268.7		620.5	
	20.64		1001	100.7	3.916		260.0		383.6	643.6
	20.63		1001	100.4	3.954		261.8		645.4	

Table I (Continued)

Run no.	$10^4 m_i$	$10^4 m_{p,i}$	$10^4 m_{v,i}$	q_i , cal.	$\phi_L(m_{p,i}) - \phi_L(m_{v,i})$, cal./mole	$\phi_L(m_{v,i})$, cal./mole	$\phi_L(m_{p,i})$, cal./mole	Av. $\phi_L(m_{p,i})$, cal./mole
57	26.29	1303	43.81	11.31	430.1	307.0	737.1	738.5
	26.26	1303	43.75	11.37	433.0		740.0	
	31.64	1600	93.44	13.27	477.3	376.5	853.8	852.7
	31.57	1600	93.29	13.17	475.1		851.6	
	38.66	2018	151.1	21.84	634.5	422.5	1057.0	1056
	38.71	2018	151.1	21.84	633.4		1055.9	
	56.82	3195	235.5	77.92	1444	467	1911	1911
	56.80	3195	235.5	77.93	1444		1911	
Calorimetric dilution data of $\text{Sr}(\text{ClO}_4)_2$ at 25°								
67	1.373	62.36	2.281	0.259	188.6	97.5	286.1	285.7
	1.373		2.281	0.248	180.6		278.1	
	1.370		4.396	0.177	158.9	128.8	287.7	
	1.370		4.397	0.174	153.8		282.6	
	1.369		6.368	0.141	140.3	147.6	287.6	
	1.369		6.368	0.137	135.9		283.5	
	1.373		8.214	0.106	124.5	162.3	286.8	
	1.371		8.214	0.103	120.7		283.0	
60	2.799	128.1	4.652	0.524	187.1	130.7	317.8	311.4
	2.798		4.651	0.498	177.9		308.6	
	2.799		8.977	0.296	146.5	167.4	313.9	
	2.798		8.973	0.289	140.6		308.0	
	2.802		13.01	0.223	124.1	190.5	314.6	
	2.800		13.01	0.196	117.1		307.6	
	2.798		16.78	0.155	107.0	206.8	313.8	
	2.813		16.79	0.142	100.3		307.1	
61	2.806	128.1	4.662	0.508	181.0	130.9	311.9	312.2
	2.801		4.655	0.504	179.9	130.7	310.6	
	2.801		8.990	0.313	146.4	167.7	314.1	
62	2.805	128.1	4.662	0.503	179.3	130.9	310.2	309.8
	2.807		4.664	0.508	181.0		311.9	
	2.803		8.992	0.282	139.9	167.7	307.6	
	2.802		8.993	0.295	143.1		310.8	
	2.800		13.03	0.200	117.1	190.5	307.6	
	2.802		13.03	0.214	120.9		311.4	
	2.802		16.80	0.160	102.1	206.8	308.9	
	2.801		16.80	0.156	103.1		309.9	
64	6.488	300.0	10.77	0.730	112.7	178.5	291.2	291.9
	6.472		10.76	0.740	114.3		292.8	
	6.472		20.78	0.191	71.7	220.5	292.2	
	6.476		20.78	0.180	71.0		291.5	
	6.478		30.15	0.008	47.4	244.4	291.8	
	6.473		30.12	0.002	47.3		291.7	
63	8.368	390.3	13.91	0.644	77.0	194.6	271.6	271.4
	8.354		13.89	0.643	77.0		271.6	
	8.377		26.88	0.066	34.5	237.1	271.6	
	8.374		26.86	0.071	34.2		271.3	
	8.381		38.99	0.306	10.8	260.4	271.2	
	8.381		38.97	0.308	10.5		270.9	
	8.372		50.31	0.401	-3.9	275.2	271.3	
	8.354		50.27	0.387	-3.7		271.5	
65	20.51	1001	35.33	-3.348	-163.3	254.4	91.1	90.5
	20.52		35.35	-3.374	-164.4		90.0	
	20.51		68.25	-4.898	-201.0	292.0	91.0	
	20.49		68.24	-4.895	-201.6		90.4	

Table I (Continued)

Run no.	$10^2 m_i$	$10^2 m_{p,i}$	$10^2 m_{v,i}$	q_i , cal.	$\phi_L(m_{p,i}) - \phi_L(m_{v,i})$, cal./mole	$\phi_L(m_{v,i})$, cal./mole	$\phi_L(m_{p,i})$, cal./mole	Av. $\phi_L(m_{p,i})$, cal./mole
	20.51		99.00	-5.066	-216.4	307	90.6	
	20.49		98.96	-5.054	-216.6		90.4	
	20.54		127.8	-4.959	-222.6	313	90.4	
	20.51		127.7	-4.921	-222.5		90.5	
66	48.32	2666	80.79	-12.12	-250.8	300	49.2	
	48.32		80.79	-12.11	-250.6		49.4	
	48.26		156.7	-13.57	-266.0	313	47.0	
	48.22		156.7	-13.60	-266.3		46.7	48.3
	48.27		228.4	-11.90	-259.5	307	47.5	
	48.37		228.3	-11.87	-259.5		47.5	
	48.25		296.0	-9.83	-245.5	295	49.5	
	48.33		296.0	-9.82	-245.4		49.6	
68	17.89	864.3	29.78	-2.114	-118.1	243.7	125.6	125.8
	17.89	864.3	29.78	-2.106	-117.7		126.0	
	14.94	715.2	52.82	-2.263	-110.1	278.2	168.1	169.5
	14.94	715.2	52.80	-2.220	-107.3		170.9	
	13.39	636.8	71.94	-1.894	-101.1	294.7	193.6	193.7
	13.40	636.8	71.93	-1.892	-100.9		193.8	
	10.43	490.7	85.34	-0.979	-60.5	302.2	241.7	240.5
	10.43	490.7	85.33	-1.005	-63.0		239.2	
69	29.36	1488	48.95	-7.85	-267.4	273.9	6.5	7.0
	29.36	1488	48.95	-7.82	-266.4		7.5	
	42.47	2283	116.2	-14.33	-311.3	311.2	-0.1	-0.6
	42.46	2283	116.2	-14.36	-312.3		-1.1	
	52.54	2970	195.5	-11.45	-214.1	314.0	99.9	99.8
	52.69	2970	195.7	-11.49	-214.3		99.7	
	70.92	4429	299.5	16.29	195.0	294	489	490
	70.77	4429	299.5	16.37	196.6		491	

value changed from 294.5 to 292.0 cal. mole⁻¹. A further reduction in the concentration range did not result in significant changes of the fit. Table II summarizes the relevant data.

Table II: Least-Squares Fit of Eq. 6

	A	B	C	Concn. range, M	σ_{fit} , cal./mole
Mg(ClO ₄) ₂	3.25	-833.7	1074	0.002-0.114	1.36
Sr(ClO ₄) ₂	3.44	-185.5	2332	0.002-0.068	1.03

The values of $\phi_L(m_{p,i}) - \phi_L(m_{v,i})$ given in column 6 of Table I were calculated from eq. 3. Values of $\phi_L(m_{v,i-1}) - \phi_L(m_{v,i})$ for use in this equation and the values of $\phi_L(m_{v,i})$ in column 7 were derived from the extrapolation or, for data outside the range of the extrapolation, from large-scale plots of ϕ_L vs. m . The values of $\phi_L(m_{p,i})$ in columns 8 and 9 are calculated from the data in columns 6 and 7.

Relative apparent molal enthalpies ϕ_L and relative partial molal enthalpies \bar{L}_2 were calculated at even concentrations using a method similar to that suggested by Scatchard and Epstein.^{2b,18} Excess partial molal entropies were also calculated using the relation

$$T\Delta S^E = \bar{L}_2 - RT\nu \ln \gamma_{\pm}$$

The mean molal activity coefficients were taken from Robinson and Stokes.¹⁹ These results are given in Tables III and IV.

The ϕ_L for Mg(ClO₄)₂ near 0.1 M is close to those for all of the alkaline earth halides. In the case of Sr(ClO₄)₂ the ϕ_L curve is a little below that of the halides. The results of Swanson²⁰ for Ba(ClO₄)₂ show that ϕ_L for this salt is over 100 cal./mole below those for the halides and close to that for Sr(NO₃)₂

(18) G. Scatchard and L. F. Epstein, *Chem. Rev.*, **30**, 211 (1942).

(19) R. A. Robinson and R. H. Stokes, "Electrolyte Solutions," 2nd Ed., Academic Press Inc., New York, N. Y., 1955.

(20) J. A. Swanson, Ph.D. Thesis, University of Nebraska, Lincoln, Neb.

Table III: ϕ_L , \bar{L}_2 , and $T\bar{S}^E$ for $Mg(ClO_4)_2$

Concn., m , moles/ kg.	B	$dB/dm^{1/2}$	ϕ_L , cal./ mole	\bar{L}_2 , cal./ mole	γ_{\pm}	$T\bar{S}^E$
0.05	-522	854.8	319	410		
0.1	-439	937.5	383	477	0.577	1455
0.2	-324	666.6	449	541	0.565	1556
0.3	-267	517.8	485	574	0.576	1555
0.4	-224	467.4	512	606	0.599	1517
0.5	-190	430.2	534	637	0.633	1450
0.6	-162	364.7	554	662	0.673	1366
0.8	-111	423.8	596	775	0.780	1217
1.0	-66	435.2	645	909	0.925	1048
1.5	37	470.6	810	1402	1.498	684
2.0	130	490	1044	2095	2.59	404
3.0	303	640	1731	4392	8.99	489

Table IV: ϕ_L , \bar{L}_2 , and $T\bar{S}^E$ for $Sr(ClO_4)_2$

Concn., m , moles/ kg.	B	$dB/dm^{1/2}$	ϕ_L	\bar{L}_2	γ_{\pm}	$T\bar{S}^E$
0.05	-1398	2591	275	332		
0.1	-1193	2125	308	345	0.528	1480
0.2	-1005	1151	313	290	0.494	1543
0.3	-900	928.5	295	228	0.488	1503
0.4	-830	738.5	269	155	0.494	1408
0.5	-780	600.0	239	77	0.507	1284
0.6	-742	562.5	206	12	0.525	1157
0.8	-676	548.7	144	-84	0.573	906
1.0	-620	540.5	91	-147	0.638	652
1.5	-498	529.8	8	-148	0.868	103
2.0	-398	511.1	-12	13	1.220	-340
3.0	-240	461.5	102	671	2.57	-1006

at 0.1 M . Thus, ϕ_L values for the perchlorates seem to be lower than those for the halides in general but not nearly so low as those for the corresponding nitrates. For the alkaline earth nitrates the low values of ϕ_L are associated with ion pairing.²¹ Thus, strontium and barium perchlorates appear to be slightly ion paired, but the effect is not so marked as with the nitrates.

The experimental values of the excess partial molal entropies and those predicted by the correlation of Wood^{2a} at 0.1 m are compared in Table V. The correlation of Wood is of the form

$$T\bar{S}^E = A + B(P_+ + P_- - C)$$

where A and B depend on the concentration. The P_+ values were taken from Wood, and the P_- value for the perchlorate ion was taken from Jones and Wood.^{2b} The value for barium perchlorate is based

on the ϕ_L data given by Swanson.²⁰ The correlation and the data for the chlorides, bromides, nitrates, and perchlorates of the alkaline earth metals are given in Figure 1. The line represents the correlation of

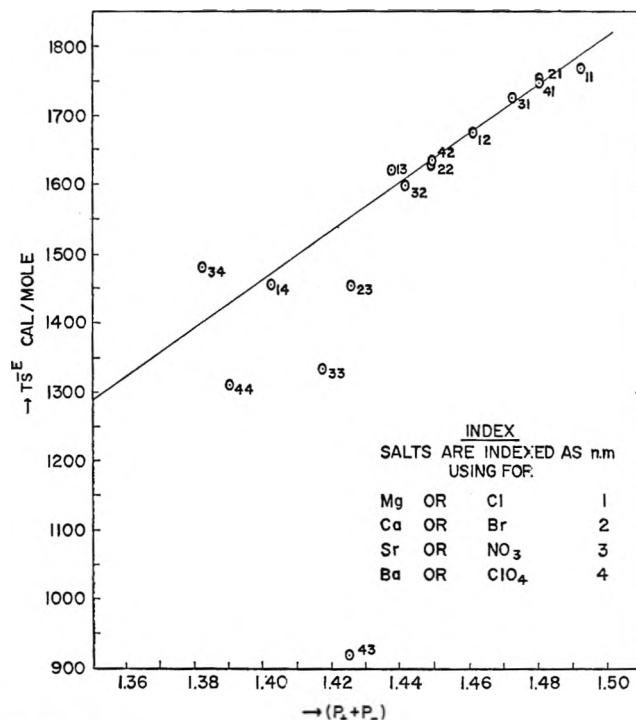


Figure 1.

Table V: Test of $T\bar{S}^E$ Correlation

	$P_+ + P_-$	$T\bar{S}^E_{\text{exptl}}$	$T\bar{S}^E_{\text{calcd}}$	$T\bar{S}^E_{\text{calcd}} - T\bar{S}^E_{\text{exptl}}$
$Mg(ClO_4)_2$	1.402	1455	1465	+10
$Sr(ClO_4)_2$	1.382	1480	1395	-85
$Ba(ClO_4)_2$	1.390	1548	1430	+118

Wood. Of the perchlorates, only the magnesium salt fits the correlation well. The value for strontium perchlorate is above the line while the value for barium perchlorate is below the line in the same direction as barium nitrate. The fact that the perchlorates are much closer to the line than the corresponding nitrates indicates that, although there may be some ion pairing in the heavier alkaline earth perchlorates, it is much less than with the nitrates. The deviations of perchlorates of strontium and barium are small enough

(21) E. C. Righellato and C. W. Davies, *Trans. Faraday Soc.*, 26, 592 (1930).

that they may be due to effects other than ion pairing. Small differences in the water structure around the ions could easily explain the deviations.

Acknowledgments. The authors thank Dr. Ronald W. Smith for his help in establishing the accuracy of the extrapolation procedure.

The Wetting of Gold and Platinum by Water

by K. W. Bewig and W. A. Zisman

U. S. Naval Research Laboratory; Washington, D. C. (Received July 6, 1965)

When a sessile drop of pure water is placed on a clean surface of pure, polished gold or platinum, it will spread spontaneously over the metal and exhibit a zero contact angle. However, in order to rid these metal surfaces of adsorbed hydrophobic contaminants, it is necessary to heat them to white-hot temperatures in flowing streams of high purity gases. After such a heat treatment, a prolonged exposure of the metals to these gases rendered them nonwetting because of the gradual adsorption of trace hydrophobic contaminants present in the gas streams. However, if the gases were freed from such trace contaminants by an adsorbent cold trap and the gold and platinum specimens were initially clean, they were completely wetted by pure water and exhibited zero contact angles.

Introduction

There has been a 50-year history of difficulties in determining the surface properties of inorganic solids in the absence of organic contaminating films. The contaminant problem has been especially important in fundamental studies of the wetting, adhesive, and frictional properties of such solids because of the well-demonstrated fact that an adsorbed monolayer of an organic compound can cause major changes. Much of the early research in these properties was vitiated by inadequate attention to this problem. Adam¹ briefly summarized in 1941 the state of knowledge of the spreading of ordinary liquids on inorganic solids with the statement: "Most organic liquids and water form zero (contact) angles with *clean* glass and silica, also with clean metallic surfaces." Authoritative reviews by Wark and Sutherland² and Gaudin³ covering the field of ore flotation reveal that really clean surfaces of nearly all minerals, including oxides and sulfides, have zero or small contact angles. The later extensive investigation of the wetting of high-energy sur-

faces by Fox, Hare, and Zisman⁴ led to the conclusion that *all pure liquids* spread spontaneously on high-energy surfaces unless they belong to the special class of *organic* liquids which were either "autophobic" or were hydrolyzed on contact with the solid surface. From their work as an important special case, it can be concluded that pure water will spread on any high-energy surface if it is free from adsorbed organic films.

Prolonged exposure of a clean (*i.e.*, organic-free) hydrophilic solid surface to any atmosphere, other than a most carefully purified gas, will result in the surface exhibiting water contact angles from a few degrees up to 90°, depending on the nature of the organic contaminant present and its surface concentration. As we

(1) N. K. Adam, "The Physics and Chemistry of Surfaces," 3rd Ed., Oxford University Press, London, 1941.

(2) K. L. Sutherland and I. W. Wark, "Principles of Flotation," Australasian Institute of Mining and Metallurgy, Melbourne, 1955.

(3) A. M. Gaudin, "Flotation," 2nd Ed., McGraw-Hill Book Co., Inc., New York, N. Y., 1957.

(4) H. W. Fox, E. F. Hare, and W. A. Zisman. *J. Phys. Chem.*, **59**, 1097 (1955).

have recently demonstrated,⁵ even nonpolar organic vapors, such as those of pure hexane or benzene, can adsorb on clean metal surfaces, including gold and platinum, and the last monolayer of the resulting film will not evaporate from the surface unless the temperature of the metal is raised by 100°. The apparent irreversibility encountered arises from polarization of the adsorbed vapor by the electrostatic field emanating from the metal surface. Such monolayers are usually adsorbed with the molecules lying as flat as possible in the surface; the condensed monolayer causes the water contact angle to be from 55 to 75°, depending on the metal surface.

However, in the past 12 years a few investigators have reported results to the contrary. Especial emphasis was given in their experiments to such readily cleaned metals as gold and platinum. Bartell and Smith⁶ obtained advancing water contact angles in water vapor or air of $7 \pm 1^\circ$ on gold. More recently, White's⁷ experiments on the contact angle of condensed water vapor on gold in a Pyrex and metal system led him to conclude that an unoxidized surface of pure gold is hydrophobic, and only when there is a surface oxide present, is there a zero water contact angle. Erb⁸ also measured the contact angle of water on pure gold under continuous condensing conditions in pure steam and observed contact angles of 55–85°. He concluded that physically adsorbed organic contamination could be removed in his apparatus within a few hours and chemisorbed contamination within a few days. After several thousand hours of continuous operation in his apparatus, the metals should have been clean, and yet gold continued to exhibit an advancing contact angle from 50 to 90°. He also concluded that gold needed surface oxidation to exhibit a zero contact angle with water.

Because of these recent published observations and opinions, we have re-examined the wetting of pure gold and platinum surfaces in a much simpler system by first reducing the metals in extremely pure flowing hydrogen gas streams at high temperatures and then measuring the water contact angle of the cooled surface at different times after each heat treatment. We have also conducted similar experiments in gaseous atmospheres of other pure gases. The results are summarized here.

Experimental Techniques

The same procedures used in our previous study⁵ of the changes caused in the contact potentials of metals by adsorbed nonpolar compounds were also followed here in the first stage of preparing the gold and platinum specimens. Three gold specimens were employed

from the following sources: (1) Englehard Industries, 99.99% purity; (2) Handy and Hartman, 99.9999% purity; and (3) National Bureau of Standards electrolytic gold, kindly supplied by Dr. E. Wichers and later molded into an ingot in an inert argon atmosphere using special molybdenum crucibles by Mr. E. J. Chapin of the Metallurgy Division of N.R.L. No distinction was observed in the experimental behavior of the three gold samples. The platinum used was supplied by Englehard Industries and was 99.99% pure. Each metal specimen was abraded, polished, and dried as in the previous work.⁵ Metal specimens were 0.95 cm. in diameter and 0.16 cm. thick; each had been fabricated with an integral pin of the same material, 0.25 cm. in diameter and 0.64 cm. long on its back surface, in order to facilitate the mechanical handling of the specimen and to be sure that the free surface would not be touched during manipulations.

Each metal specimen to be studied was next introduced into the glass system shown in Figure 1. In this system the only nonglass materials present between the gas adsorbent system and the specimen chamber were two small, clean Teflon connecting collars in the gas stream. The simple, compact, specimen chamber (volume only 50 ml.) was devised because it was necessary that each piece of glassware in it had to be capable of being disassembled and cleaned by acid washing and

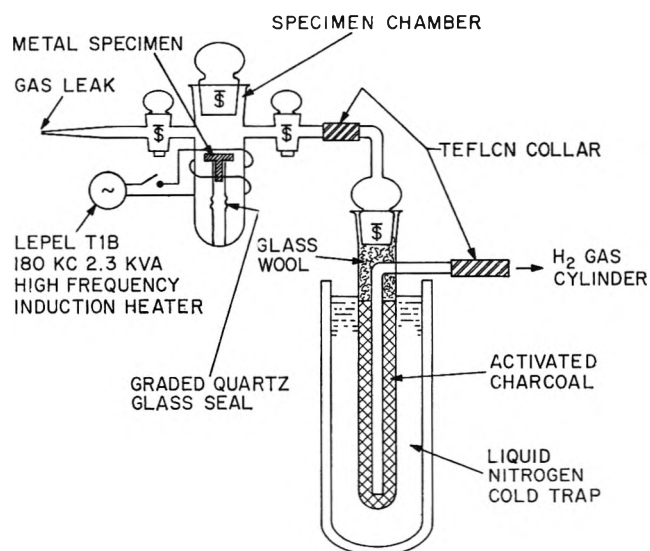


Figure 1. Gas purification apparatus and metal specimen heat cell.

- (5) K. W. Bewig and W. A. Zisman, *J. Phys. Chem.*, **68**, 1804 (1964).
- (6) F. E. Bartell and J. T. Smith, *ibid.*, **57**, 165 (1953).
- (7) M. L. White, *ibid.*, **68**, 3083 (1964).
- (8) R. A. Erb, *ibid.*, **69**, 1306 (1965).

baking just before each experiment in order to avoid the evolution of organic contaminants by the interior wall to contaminate the gas stream. The stopcocks and ground joints of the system were not lubricated. The cold trap and adsorbent system cooled by liquid nitrogen is of the same design used successfully by the National Bureau of Standards⁹ in the purification of helium gas; it contained Fisher activated coconut charcoal adsorbent, 6–14 mesh, which was outgassed frequently at 320° and 10⁻⁴ mm. Without this cold trap to remove the last traces of organic contaminants in the gas stream, appreciable contact angles were encountered on the metal specimens even when the purest obtainable commercial hydrogen gas was used. Hydrogen cylinder gas used was Linde Co. research grade having the following analysis of impurities: oxygen <1 p.p.m., nitrogen <5 p.p.m., carbon monoxide <1 p.p.m., carbon dioxide <1 p.p.m., argon <1 p.p.m., hydrocarbons <1 p.p.m., methane <1 p.p.m., and moisture <1 p.p.m.

After each metal specimen was polished and cleaned as previously described, it was placed in the specimen chamber on the quartz tube holder. A gas flow rate of 150 ml./min at 15° was allowed to purge the specimen chamber for 30 min. Then, the metal specimen was heated with a high-frequency induction heater for 3 min. while remaining in the flowing gas stream. The specimen was next allowed to cool to the temperature of the flowing gas stream, and this usually required 10 min. After that, the ground-glass cap of the specimen chamber was removed, a small sessile drop of clean pure water was touched to the polished metal surface by means of a previously flame-cleaned platinum wire, and the chamber was closed again by replacing the cap. This operation required about 1 sec. The test water was obtained by passing the effluent of a Stokes wall still through an Amersil Bi-Distillation unit of fused quartz. If the water drop did not spread completely over all of the plane surface of the metal disk, its contact angle was measured by means of a telescope fitted with a goniometer eyepiece.¹⁰ No attempt was made to distinguish between an advancing and a receding contact angle.

Experimental Results

A. Results of Heating and Cooling Metal Specimens in a Hydrogen Stream. The output power of the induction heater was adjusted to heat the metal specimen to an initial observable dull red color. Results on the wettability were erratic with both gold and platinum. Occasionally, each metal was completely wet by the water drop and showed zero contact angles. In repeat experiments the water drop sometimes did not com-

pletely wet either metal, and contact angles between 4 and 8° were observed. Increasing the time of heating to a dull red from 3 min. to as long as 30 min. did not improve reliability. Increasing the hydrogen flow rate from 150 to 500 ml./min. also produced no observable change in the results of repeated experiments. Reducing the hydrogen flow rate to zero by closing the stopcocks on either side of the specimen chamber increased the contact angles to about 6 to 13°, and no zero contact angles were observed.

The metals were next heated until white hot, and great care had to be exercised with the gold in order to prevent it from melting. In fact, the output coupling of the induction heater was increased until the surface of the gold was observed to begin melting; then the output coupling was reduced just below the setting where melting of the gold would not occur under continuous prolonged heating. After the 3-min. heat treatment, followed by quick cooling in a 150-ml./min. hydrogen stream, the platinum and the three gold specimens always exhibited zero water contact angles. When the hydrogen flow rate was cut off, water contact angles of about 6 to 13° were again observed; however, in three of these experimental runs zero contact angles were still obtained. Longer metal heating times did not change the results.

From 10 to 15 repeated experiments were made on each one of the platinum and gold specimens. If a completely wetting water film was allowed to evaporate in the 150-ml./min. dry hydrogen stream, after 6 min. the film began to recede as a flat lens from the edges of the metal surfaces. These water lenses showed immeasurably small contact angles (<1°), and optical interference colors could be observed beyond the edges of the evaporating flat water lens by reflecting light from a white paper card placed behind the specimen chamber. The light source was either a focused microscope lamp with a blue filter over its object lens or a Gates sodium vapor lamp.

In other experiments, after the white-hot heat treatment of the metal specimen, it was allowed to remain in the flowing hydrogen stream for extended times beyond the 10 min. required for cooling off. After 30 min. in the hydrogen stream, small water contact angles began to be observed, and after 60 min. contact angles of 5 to 11° were observed on gold and on platinum specimens. Experiments lasting longer were not conducted in order to conserve the supply of research grade hydrogen.

(9) R. B. Scott, "Cryogenic Engineering," D. Van Nostrand Co., Inc., New York, N. Y., 1959, Chapter 3.

(10) W. C. Bigelow, D. L. Pickett, and W. A. Zisman, *J. Colloid Sci.*, 1, 513 (1946).

B. *Results of Heating Specimens in Room Air and in Navy Grade, Water-Pumped Breathing Air.* For comparison with the preceding results observed in a pure hydrogen atmosphere, the ground-glass cap on the specimen chamber was removed, and the metal specimen was heated to a white heat while being exposed to the air of an unusually "clean" laboratory. In no case was complete wetting by water obtained after this treatment; contact angles varying from 6 to 21° were measured on successive days of the experiment. There were no significant differences in experiments with gold and platinum.

In another experiment, a cylinder of Navy stores, water-pumped breathing air was substituted for the Linde research grade hydrogen gas cylinder. This air was also run through the cold gas adsorption trap and the closed specimen chamber at a flow rate of 150 ml./min.; an acetone-Dry Ice mixture was used as a refrigerant instead of the liquid nitrogen. After heating the metal specimen to a white heat and then cooling it, the results of placing drops of water on both the gold and the platinum metals were practically identical with those observed in the hydrogen gas reduction treatment. These experiments were run for as long as 120 min. after heating the specimens, and zero contact angles were still obtained. Since sufficient quantities of breathing air were available, elapsed time runs of 24 hr. were also made; after such long exposures to the air, the gold and platinum specimens gradually evidenced increasing water contact angles which attained values from 24 to 30° owing to the accumulated adsorption on the clean metal of hydrophobic contamination from the air stream. Thus, even after passage through the gas adsorption trap, cooled by acetone and Dry Ice, the air still contained a trace of organic contamination.

C. *Results of Heating Specimens in High Purity Inert Gases.* Further experiments were performed using cylinders of the following Linde Co. research grade gases: krypton, neon, argon, and nitrogen. The procedures were identical with those employed using hydrogen, except that a mixture of acetone and Dry Ice was used as a refrigerant in order to prevent these gases from liquefying in the cold trap. The output coupling of the induction heater also had to be decreased since the inert gases have lower thermal conductivities than hydrogen, and consequently the efficiency of the induction heater was increased. Complete wetting and zero contact angles could always be obtained with white-hot heating of the gold and platinum metals. At dull red heating, just as with the hydrogen stream, finite contact angles were observed with each of these gases. The exposure times for which spon-

taneous wetting could be maintained after the heat treatment of the metals varied between 30 and 120 min. The concentrations of impurities in these inert gases (as specified by the supplier) were close to those present in the cylinder of research grade hydrogen.

Discussion

According to Kubaschewski and Hopkins,¹¹ although platinum is considered to be a noble metal and in bulk is not easily converted into oxides, nevertheless a strongly adsorbed layer of oxygen is formed during exposure to air. At temperatures even above 1200° repeated hydrogen reduction and vacuum outgassing is required in order to remove this adsorbed oxygen film. On the other hand, recent papers by Mair, *et al.*,¹²⁻¹⁴ describe low-energy electron diffraction, electron microscopy, and X-ray emission experiments which indicate that heating gold in oxygen does not produce stable oxides on the surface at room temperature, and heating it to about 900° in oxygen can remove contamination more readily than heating in other gases.

Thus, the high-temperature reduction of our very pure gold specimens in cleaned-up research grade hydrogen was done to assure that a minimum oxidation of the surface would occur. Certainly no gross anodic oxide as mentioned by White⁷ and referred to by Erb⁸ could have been present on these gold surfaces. Even in the case of the platinum specimen, the high-temperature hydrogen reduction treatment used makes very improbable the presence of any significant oxide or adsorbed oxygen.

The inconsistent wetting results obtained with lower dull red temperatures was somewhat surprising. However, Wheeler¹⁵ and Kaminsky¹⁶ state that the temperature required to guarantee an adequate thermal cleaning of a metal surface can be estimated roughly as 20 times the binding energy in kcal./mole of the layer of impurity atoms on the surface. Thus, according to Kaminsky,¹⁶ a temperature of 1770° would be required to desorb ethene from tungsten.

(11) O. Kubaschewski and B. E. Hopkins, "Oxidation of Metals and Alloys," 2nd Ed., Butterworths and Co. Ltd., London, 1962.

(12) D. Clark, T. Dickinson, and W. N. Mair, *J. Phys. Chem.*, **65**, 1470 (1961).

(13) D. Clark, T. Dickinson, and W. N. Mair, *Trans. Faraday Soc.*, **55**, 1937 (1959).

(14) L. G. Carpenter and W. N. Mair, *ibid.*, **55**, 1929 (1959).

(15) A. Wheeler, "Structure and Properties of Solid Surfaces," R. Gomer and C. S. Smith, Ed., University of Chicago Press, Chicago, Ill., 1953, p. 455.

(16) M. Kaminsky, "Atomic and Ionic Impact Phenomena on Metal Surfaces," Academic Press Inc., New York, N. Y., 1965, pp. 28, 29.

It is well known that polished metal surfaces are not nascently clean, crystalline lattice planes. However, such a surface (and for that matter an oxidized metal) otherwise free from *organic* contamination should have a critical surface tension of wetting¹⁷ which would cause a sessile drop of water to spread spontaneously on the metal. A metal surface entirely free from oxides would have a higher surface energy than an oxidized metal; consequently, water should spread more readily on the former surface rather than the latter. If a sessile water drop does not spontaneously wet a "clean" metal surface, it is probably an

indication of measurable contamination by a hydrophobic organic impurity. An exception to this would be contamination by an organic wetting agent¹⁸ having a polar group in the outermost surface of the adsorbed molecule; such an impurity on a metal surface would promote the spontaneous spreading of a sessile drop of water.

(17) W. A. Zisman, *Advances in Chemistry Series*, No. 43, American Chemical Society, Washington, D. C., 1964, p. 12.

(18) S. J. Gregg, "The Surface Chemistry of Solids," 2nd Ed., Reinhold Publishing Corp., New York, N. Y., 1961, p. 220.

The Use of Combined Schlieren and Absorption Optics in an Electrophoretic

Study of the Reversibly Interacting System Dextran Sulfate-Carboxyhemoglobin^{1,2}

by York Tsang and T. E. Thompson

Department of Physiological Chemistry, Johns Hopkins University, School of Medicine, Baltimore, Maryland (Received July 6, 1965)

The behavior during moving-boundary electrophoresis of interacting dextran sulfates-carboxyhemoglobin in aqueous solution has been studied utilizing combined schlieren and absorption optics. Interaction was studied over a pH range of 7.4 to 8.5 and ionic strength range of 0.05 to 0.20 *M* and at various concentration ratios of interactants. The variation of the interaction, decreasing with increasing pH and ionic strength, can be explained as due to attraction between the anionic sulfate groups of the dextran sulfates and cationic groups on the hemoglobin. Interaction constants have been calculated by two different methods. The information provided by the combined schlieren and absorption optical systems enables a more accurate estimate of the effects of nonideal electrophoresis and reduces uncertainties involved in the interpretation of the moving-boundary patterns of interacting macromolecules to a level comparable with that involved for non-interacting systems of macromolecules.

Numerous studies have been reported on the behavior in free-boundary electrophoresis of systems of interacting macromolecules.³ For many of these systems, the behavior as reflected in the refractometrically determined moving-boundary patterns is such as to suggest that continuous readjustment of the con-

centrations of each species is occurring in the boundary region. The patterns can no longer be related in any

(1) Presented in part at the 145th National Meeting of the American Chemical Society, New York, N. Y., Sept. 1963.

(2) Portions of this paper are derived from the Ph.D. dissertation of Y. T., Johns Hopkins University, 1964.

simple manner to conditions in the homogeneous solution.

Several methods have been developed to evaluate the patterns of rapidly equilibrating systems. Calculations have usually utilized the relationships derived from the moving-boundary equations.⁴ Alternately, the differential equations describing the transport behavior of the interacting systems can be used. Analytical solutions have been obtained for the equations describing the reaction $A + B \rightleftharpoons C$, assuming instantaneous equilibration and neglecting the effects of diffusion.⁵ Computer solutions⁶ have been obtained for the equations describing the isomerization reaction $A \rightleftharpoons B$ for different reaction rates and diffusion constants and, more recently, for equations⁷ describing the reaction $A + nB \rightleftharpoons C$, assuming instantaneous equilibration.

The problem of interpreting the moving-boundary pattern obtained with interacting systems is complicated by the fact that the usual refractometric methods for recording concentration distributions sum the contributions of all species present in the boundary. What, in fact, is desired is the concentration distribution of each individual interactant in the boundary region. This information can be obtained in a two-interactant system by employing light absorption measurements in conjunction with a refractometric method, provided that one interactant has suitable absorption characteristics.

In this investigation the electrophoretic boundaries of the interacting system carboxyhemoglobin-dextran sulfate have been investigated using a Tiselius apparatus equipped with both schlieren and absorption optics. This interactant system was selected for study because of the convenient light absorption characteristics of the carboxyhemoglobin and because of the general interest in interaction between proteins and charged polysaccharides.⁸⁻¹⁴

Experimental Section

Human carboxyhemoglobin (COHb) was twice crystallized by the method of Drabkin.¹⁵ Stock solutions ranging from 8 to 12% (g./100 ml. of solution) were kept under CO at 4°. In the buffer systems used, the electrophoretic mobility was linear with pH over the range 6.0 to 9.0 with the isoelectric point at pH 6.8. No variation in mobility with ionic strength was observed in the experimental range 0.05 to 0.20 *M*. Single symmetrical boundaries were obtained in both cell limbs under all conditions of pH and ionic strength employed.

Sodium dextran sulfates (DS) were synthesized from dextran samples prepared by acetone fractionation of acid hydrolysates of native dextrans. The composi-

tion and electrophoretic properties are given in Tables I and II. D-8 and E-4 were gifts of Dr. Colin Ricketts of the University of Birmingham, England. Ph-150 was synthesized according to the procedure of Ricketts.¹⁶ The ascending electrophoretic peak was

Table I: Properties of Dextran Sulfates

Prepn.	Mol. wt. (number-average)	% sulfur	No. of sulfate groups per glucose
D-8	1.0×10^6	18.9	2.3
E-4	6.0×10^4	11.1	1.4
Ph-150	3.0×10^6	16.7	2.0

Table II: Electrophoretic Mobilities of Dextran Sulfates

Prepn.	pH	$\Gamma/2, M$	$u \times 10^5, \text{cm.}^2 \text{sec.}^{-1} \text{v.}^{-1}$
D-8	7.4	0.05	17.8
		0.10	14.4
		0.20	11.9
	8.0	0.05	15.5
		0.10	14.2
		0.20	11.9
	8.5	0.05	15.6
		0.10	14.2
		0.20	11.8
E-4	7.4	0.10	14.4
		0.20	12.0
Ph-150	7.4	0.10	14.4
		0.20	12.0

(3) R. A. Brown and S. N. Timasheff in "Electrophoresis," M. Bier, Ed., Academic Press Inc., New York, N. Y., 1959.

(4) L. G. Longworth in "Electrophoresis," M. Bier, Ed., Academic Press Inc., New York, N. Y., 1959.

(5) G. A. Gilbert and R. C. Ll. Jenkins, *Proc. Roy. Soc. (London)*, **A253**, 420 (1959).

(6) J. R. Cann and H. R. Bailey, *Arch. Biochem. Biophys.*, **93**, 576 (1961).

(7) J. R. Cann and W. M. Goad, *J. Biol. Chem.*, **240**, 148 (1965).

(8) P. Bernfeld, V. M. Donahue, and M. E. Berkowitz, *ibid.*, **226**, 51 (1957).

(9) S. E. Kornguth and M. A. Stahmann, *Arch. Biochem. Biophys.*, **91**, 32 (1960).

(10) M. Schubert and E. C. Franklin, *J. Am. Chem. Soc.*, **83**, 2920 (1961).

(11) P. Bernfeld and T. Kelley, *J. Biol. Chem.*, **238**, 1236 (1963).

(12) H. Noguchi, *Biochim. Biophys. Acta*, **22**, 459 (1959).

(13) H. Noguchi, *J. Phys. Chem.*, **64**, 185 (1960).

(14) T. E. Thompson and W. M. McKernan, *Biochem. J.*, **81**, 12 (1961).

(15) D. A. Drabkin, *Arch. Biochem. Biophys.*, **21**, 224 (1949).

(16) C. R. Ricketts, *Biochem. J.*, **51**, 129 (1952).

always hypersharp, and the descending peak, broad and asymmetrical.

The moving-boundary apparatus was of the Klett-Longworth type equipped with phase plate and cylindrical lens.⁴ A single set of optical components proved adequate for both schlieren and absorption measurements. The modifications necessary for absorption measurements included the installation of a precisely adjustable mount for the light source, the use of a pencil-type tungsten filament lamp (GE T3Q/Cl Quartzline), interference filters to isolate the desired wave length, and a mechanical scanner located at the image plane of the camera lens.

The search-head unit carrying a photomultiplier (IP 21) was mounted on a 0.5-in. no. 16 brass screw driven by a Bodine synchronous motor (KYC-23RB). The unit was positioned to scan a 2.5 cm. wide strip at the image plane located on the opposite side from the schlieren base line. Thus, except when the gradient was very steep, the scan was not cut by the schlieren peak. Scanning slit width was 0.6 mm. Micro-switches served to limit the scan to 7.5 cm. Scanning time was fixed at 20 sec. corresponding to a recorder strip of 17.2 cm.

The recording circuit consisted of the IP21 tube, a d.c. amplifier, a logarithmic conversion circuit, and a 10-mv. Brown recorder. The photomultiplier signal was d.c. amplified, converted to its logarithm, and read out into the recorder. The logarithmic conversion circuit was of the biased diode type and used four 6A15's to approximate the log of the amplified signal over a two-decade range. The linearity was $\pm 1\%$, full scale. Photomultiplier power was supplied by 67.5-v. batteries. Current drain was below 100 ma. with maximum anode current 0.3 ma. Drift of the over-all circuit when in continuous operation over several days was 0.2% of the full-scale input.¹⁷

Typical linearity and reproducibility are shown in Figure 1. Points for different preparations of COHb all fell within the circles. Linearity was preserved up to 0.4% COHb concentration (one decade) with the 596-m μ interference filter and up to 0.8% with the 610-m μ filter. Point reproducibility was better than $\pm 2\%$, full scale. Tubes were aged, as were the batteries, and matched if necessary, before use. For comparison, the linearity of the integrated schlieren pattern *vs.* concentration of COHb is shown in Figure 2. The agreement of these two types of measurement is shown in Figure 3. The nonlinearity at higher COHb concentrations observed with the absorption record was probably due to the finite band width of the light isolated by the interference filter. Both the extinction coefficient of COHb and the sensitivity of the photo-

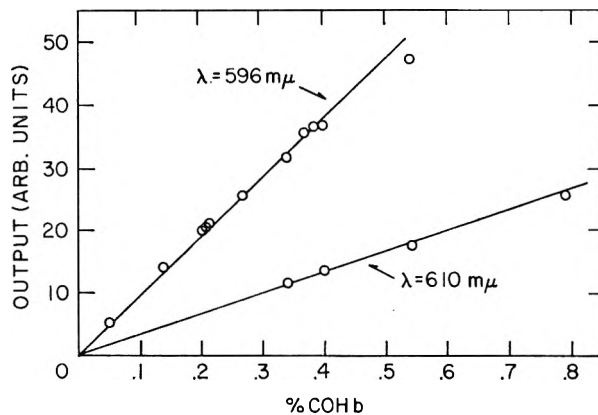


Figure 1. Linearity and reproducibility of absorption scanning system. Plot of pen deflection *vs.* COHb concentration.

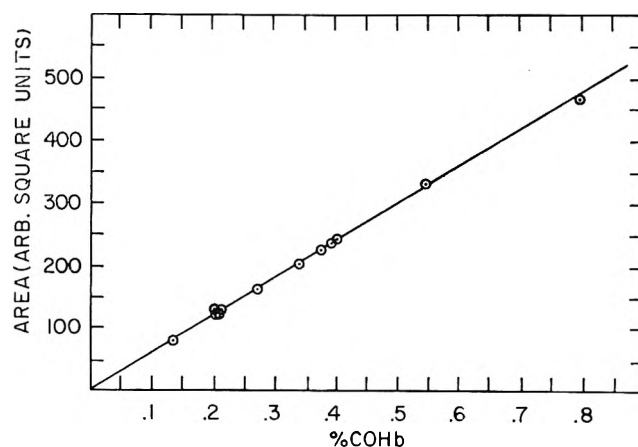


Figure 2. Linearity and reproducibility of schlieren system. Plot of integrated schlieren area (arbitrary square units) *vs.* COHb concentration.

multiplier in the wave length region of the filters used decreased appreciably with increasing wave length. Calibrated neutral density filters gave linear response up to 1.8 decades.

The concentration of COHb was determined with a Beckman DU spectrophotometer at 538 and 568 m μ using $E_{1\text{cm}}^{1\%} = 8.55$. Dextran sulfate concentrations were determined by dry weight.

Sodium phosphate buffers were used at pH 7.5 and 7.0. Cacodylate buffer was used at pH 6.0. Tris-(hydroxymethyl)aminomethane (Tris) buffers were used at all other pH values. All solutions were 0.05 ionic strength in the buffer with sodium chloride making up the rest of the ionic strength. Solution conductivities were determined in a dipping-type cell with either an Industrial Instrument bridge (Model RC16B2) or an LKB Type 3216 B instrument. All pH and con-

(17) Y. Tsang, Thesis, Johns Hopkins University, 1964.

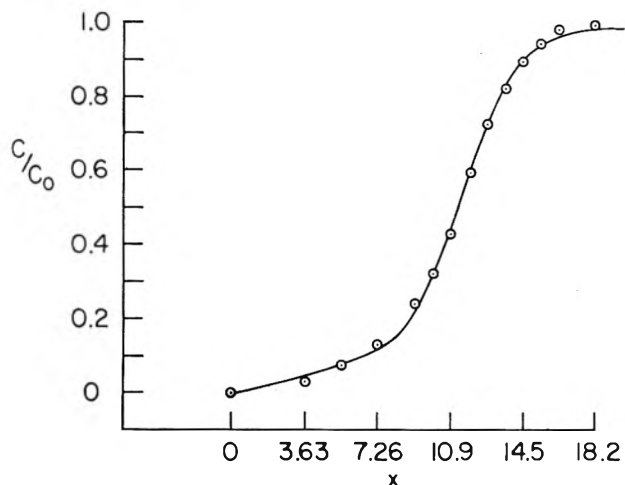


Figure 3. Superposition of absorption and integrated schlieren patterns. COHb alone; phosphate buffer; pH 7.4; $r/2 = 0.20$.

ductance determinations were corrected to 1° , the temperature at which the electrophoretic measurements were made.

A minimum of three sets of schlieren and absorption patterns was taken during each run. The schlieren photograph was first taken, then the search-head unit swung into place, and the absorption scan made. A maximum of 4 min. was required for these operations. Before comparing the absorption scan with the integrated schlieren pattern, correction was made for the absorption base line, the resulting pattern reduced by dividing the density at each point by the maximum density, and the reduced pattern then multiplied by the refractive index increment in arbitrary square units.

Results

The interaction studies were carried out over a pH range of 7.4 to 8.5, at an ionic strength range of 0.05 to 0.20 M , and at different interactant concentration ratios. The criteria for ascertaining whether interaction occurs have been discussed in other studies.^{4,14} By these criteria the systems studied here were of the reversible, rapidly equilibrating type. Both schlieren and absorption patterns indicated that the concentration distributions in all runs showing interaction could be classified as of the "two-moving-boundary" type. In the descending limb, the slow boundary, which was symmetric or only very slightly skewed, moved with the mobility of free hemoglobin. A comparison of schlieren and absorption patterns showed that this boundary consisted of hemoglobin only. The fast, descending boundary was an asymmetric reaction boundary.⁴ In the ascending limb, the sharp, sym-

metric, fast boundary consisted entirely of dextran sulfate and moved with the mobility of free dextran sulfate. The slow, ascending boundary was an asymmetric reaction boundary.

The electrophoretic results are summarized in Table III. In the table, α is the fraction of total COHb moving with the mobility of free COHb in the descending cell unit. The free COHb concentration was obtained directly from the absorption pattern. The empirical measure of interaction used was $1 - \alpha$ which may vary from 0 for no interaction to 1 for maximum interaction without equilibration.¹⁴ It can be seen that, at constant ionic strength, the interaction as measured by $1 - \alpha$ decreased sharply with increasing pH. At pH 8.5, the patterns were those of a simple, noninteracting system of two macromolecular components. At constant pH, the interaction decreased rapidly with increasing ionic strength. The interaction increased somewhat with increasing molecular weight of the dextran sulfate. It should be mentioned that preliminary experiments with dextran sulfates of the same molecular weight as the E-4 preparation but with sulfur contents of 15.2 and 18.2% gave nearly identical patterns, with the degree of interaction increasing only slightly with increasing sulfur content. Variation of the concentration ratios or the total concentrations did not appreciably change the value of $1 - \alpha$.

Additional information can be obtained by considering the relative mobilities, r , of the reaction boundaries. A relative mobility r_{DS} can be defined for the fast, descending boundary as

$$r_{DS} = (u'_{DS} - u_{COHb}) / (u_{DS} - u_{COHb})$$

and in a similar manner r_{COHb} can be defined for the slow, ascending boundary

$$r_{COHb} = 1 - (u_{DS} - u'_{COHb}) / (u_{DS} - u_{COHb})$$

Here u_{DS} and u_{COHb} are the mobilities of uncomplexed dextran sulfate and carboxyhemoglobin, respectively, u'_{DS} and u'_{COHb} are the weight-average mobilities of the fast, descending boundary and the slow, ascending boundary, respectively, calculated from the centroidal ordinate of the gradient curve.⁴ If the weight-average mobilities of the reaction boundaries are taken as measures of the constituent mobilities,¹⁸ then it is evident that the relative mobility is a convenient measure of the difference between the constituent mobility and the mobility of the corresponding free interactant. It can be seen by examination of Table III that r_{DS}

(18) R. A. Alberty and E. H. Marvin, *J. Phys. Colloid Chem.*, **54**, 47 (1950).

Table III: Summary of Electrophoretic Data

pH	$\Gamma/2$	COHb, g./100 ml.	DS, g./100 ml.	DS, mol. wt.	$1-\alpha$	r_{DS}	r_{COHb}	n	n'	$\Delta\Gamma/2$
7.42	0.10	0.205	0.470	1.0×10^6	0.85	0.88	0.70	5.5	10	0.0085
8.00	0.10	0.208	0.455	1.0×10^6	0.32	0.92	0.50	2.0	6	0.004
8.52	0.10	0.305	0.455	1.0×10^6	0.02	1.0	0.10	0.004
7.40	0.20	0.207	0.450	1.0×10^6	0.45	0.92	0.45	3.0	9	0.008
7.96	0.20	0.209	0.460	1.0×10^6	0.07	0.91	0.10	0.5	...	0.005
8.45	0.20	0.202	0.415	1.0×10^6	0	1.0	0	0.004
7.44	0.05	0.208	0.302	1.0×10^6	1.00	0.85	0.85	10.2	15	0.004
7.42	0.10	0.205	0.470	1.0×10^6	0.85	0.88	0.70	5.5	10	0.0085
7.40	0.20	0.207	0.450	1.0×10^6	0.45	0.92	0.45	3.0	9	0.008
7.98	0.05	0.205	0.460	1.0×10^6	0.92	0.86	0.95	6.0	18	0.003
8.00	0.10	0.208	0.455	1.0×10^6	0.32	0.92	0.50	2.0	6	0.004
7.96	0.20	0.209	0.460	1.0×10^6	0.07	0.91	0.10	0.5	...	0.005
7.43	0.10	0.170	0.420	6.0×10^4	0.25	0.98	0.30	0.1	3	0.007
7.40	0.20	0.156	0.245	6.0×10^4	0	1.0	0	0.005
7.43	0.10	0.170	0.420	6.0×10^4	0.25	0.98	0.30	0.10	3	0.007
7.43	0.10	0.271	0.435	3.0×10^6	0.22	0.84	0.10	0.7	2	0.0095
7.43	0.10	0.205	0.470	1.0×10^6	0.85	0.88	0.70	5.5	10	0.0085
7.43	0.10	0.298	0.63	6.0×10^4	0.29	0.95	0.30	0.12	2	0.011
7.43	0.10	0.360	0.265	6.0×10^4	0.15	0.92	0.20	0.18	4	0.004
7.42	0.10	0.170	0.420	6.0×10^4	0.25	0.98	0.30	0.10	3	0.007
8.00	0.10	0.208	0.455	1.0×10^6	0.32	0.92	0.50	2.0	6	0.004
8.00	0.10	0.77	0.390	1.0×10^6	0.37	0.77	0.40	10.8	26	0.004
7.96	0.20	0.209	0.460	1.0×10^6	0.07	0.91	0.10	0.5	...	0.005
7.96	0.20	0.395	0.440	1.0×10^6	0.08	0.93	0.05	1.5	...	0.005

is equal to 1 or very nearly so in all cases. This can obtain only if the mobilities of all the complexes are essentially equal to u_{DS} . If this is the case, then r_{COHb} should decrease as the degree of interaction decreases. Examination of Table III shows that this is indeed the case. Hence, it is apparent that all DS-COHb complexes present in the system, regardless of their stoichiometry, have mobilities essentially equal to u_{DS} .

The minimum number of moles, n , of COHb complexed per mole of dextran sulfate can be directly estimated from the known concentrations of total COHb and total dextran sulfate and from the concentration of uncomplexed COHb as determined from the slow, descending boundary assuming that all the dextran sulfate is available for association. The maximum quantity, n' , of moles of COHb complexed per mole of dextran sulfate can be obtained from the uncomplexed dextran sulfate concentration in the fast, ascending boundary. As the mobilities of the complexes are not very different from that of the dextran sulfate, the quantity n cannot be very much less than the actual value in the homogeneous interaction solution.

It can be seen in Table III that these quantities run parallel to the degree of interaction. With the mole ratios used, it can be concluded that, except at low degrees of interaction, the average composition of the complex changed with both pH and ionic strength.

Interaction (dissociation) constants were calculated from the moving-boundary equations^{4,18} or from the partial differential equations of Gilbert and Jenkins.⁶ For the moving-boundary calculations, the interaction was considered to be of the type $A + nB \rightleftharpoons AB_n$, where A is the dextran sulfate, B is the carboxyhemoglobin, and n is the number of moles of COHb associated per mole of dextran sulfate. In the Gilbert calculations, $n = 1$.

In utilizing the Gilbert and Jenkins equations, a procedure employing information derived from both absorption and schlieren patterns was developed. The asymptotic equations were rearranged to give

$$\frac{da_T}{db_T} = \frac{v_A - v_C}{v_B - v_C} \frac{v - v_B}{v - v_A}$$

where $a_T = a + c$ and $b_T = b + c$. The symbols are those of Gilbert and Jenkins.⁶ Here a represents the

Table IV: Summary of Interaction Constant Calculations

	Mol. wt. of DS							
	6.0×10^4	6.0×10^4	6.0×10^4	1.0×10^5	1.0×10^5	1.0×10^5	1.0×10^5	3.0×10^5
pH	7.43	7.43	7.43	8.00	8.00	7.95	7.95	7.43
$\Gamma/2$	0.10	0.10	0.10	0.10	0.10	0.20	0.20	0.10
[COHb], $M \times 10^{-5}$	4.40	5.30	2.50	3.06	11.3	3.07	5.80	4.00
[DS], $M \times 10^{-5}$	10.5	4.4	7.0	0.46	0.39	0.46	0.44	1.40
[COHb], free, $M \times 10^{-5}$	3.10	4.50	1.85	2.10	7.1	2.85	5.20	3.10
$u'_{DS} \times 10^{-6}$, cm. ² sec. ⁻¹ v. ⁻¹	13.8	13.3	14.1	13.2	11.3	11.2	11.1	12.2
Moving boundary								
n	1	1	1	12	12	2	2	1
K , $M \times 10^5$	12.5	12.5	13.0	25×10^{-53}	86×10^{-49}	18×10^{-5}	12×10^{-5}	1.3
Gilbert-Jenkins								
$v_A = v_{DS} \times 10^4$, cm./sec.	6.6	6.6	6.6	5.4	5.4	2.31	2.31	6.7
$v_B = v_{COHb} \times 10^4$, cm./sec.	0.33	0.33	0.33					
$v_C = v_{AB} \times 10^4$, cm./sec.	5.5	4.1	5.5	5.3	5.3	2.10	2.10	6.2
K , $M \times 10^5$, eq. 16, ref. 5	0.0085	0.0110	0.011	0.96	0.96	0.80	0.80	0.85
K , $M \times 10^5$, eq. 19, ref. 5	0.185	0.30	0.65					
K , $M \times 10^5$ ($v_A = v_C$)	22	20	18					1.7

concentration of uncomplexed DS, b represents the concentration of uncomplexed COHb, and c represents the concentration of the 1-1 complex. The value of the derivative, da_T/db_T , was obtained by differentiation of a plot of the values of a_T vs. b_T in the boundary regions. The value of v_C could thus be unequivocally determined. With v_C known, the dissociation constants were calculated using either eq. 16 or 19 of ref. 5.

In addition, dissociation constants were calculated assuming v_C is equal to v_A . It is of interest to note that with the combined schlieren and absorption data, such a procedure, using only the derivatives of the partial differential system, could, in principle, be extended to higher order complexes to include the effect of changes in conductances through the reaction boundary. However, the precision of the data obtained in this study did not warrant such a procedure.

The results of calculations using both the moving-boundary equations and the Gilbert-Jenkins differential equations for selected runs are summarized in Table IV. In the case of the interaction of E-4 and Ph-150 with COHb at pH 7.3, ($\Gamma/2$) = 0.10, the best fit with the moving-boundary equations was obtained for $n = 1$. In these systems dissociation constants calculated

by the two methods agree well, provided $v_A = v_C$. The agreement is poor when eq. 16 or 19 of ref. 5 are used with values of v_C calculated from dx_T/db_T . At higher values of pH and ionic strength, the moving-boundary equations required values of $n > 1$. Under these circumstances, application of the Gilbert-Jenkins equations leads to negative values for the dissociation constants.

Discussion

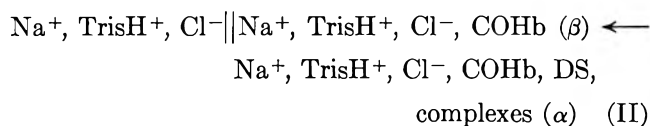
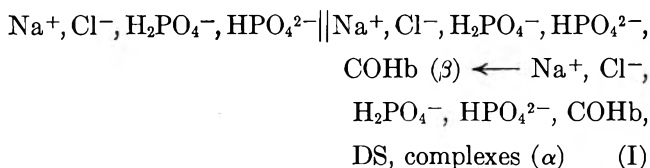
In addition to the assumptions of homogeneous solutes and of simple stoichiometry, both the treatment utilizing the moving-boundary equations and the Gilbert-Jenkins equations assume that experimentally attainable constant weight-average velocities can be reached and that electrophoresis is in all other respects ideal.

In fact, electrophoresis was nonideal as evidenced by the large area due to the stationary boundaries. At the ionic strength and pH range for which interaction was observed, nonideality can be attributed to the large equivalent concentration of the dextran sulfate. Thus, in runs with dextran sulfate alone, the descending, stationary boundary accounted for 15-

30% of the total area under the schlieren curves. The area was usually linear with respect to the per cent concentration of dextran sulfate but varied with the buffer system used. For a given concentration it was nearly independent of ionic strength. The areas of the stationary boundaries in runs with COHb alone were near the experimental error for area measurements.

An estimate of the ionic strength change through the reaction boundaries can be obtained by use of the moving-boundary equations.^{4,19} The results are shown in the last column of Table III. Sodium or Tris dextran sulfate was assumed to behave as a univalent electrolyte in its contribution to the ionic strength.²⁰ Equivalent concentrations were estimated from the area of the descending, stationary boundary in runs with dextran sulfate alone. Comparison of the absorption and schlieren patterns indicated that the stationary areas in the interaction experiments were the same as those estimated for the interacting systems. These results are in agreement with counterion binding studies on other polyelectrolytes.²¹

The two types of boundary systems assumed for the calculations were



Since the interaction as measured by the parameter $1 - \alpha$ decreased with increasing ionic strength at a given pH, it may be expected that, owing to this effect alone, the observed degree of interaction would be 0.02–0.05 lower than in the homogeneous interaction solution. In addition, the conductivity of the β solution would be higher than that of the α solution. The increase in the degree of interaction would be small since the mobility of the reaction boundary is close to that of free dextran sulfate.

The effects of nonideal electrophoresis would be more serious in calculations involving the Gilbert-Jenkins equations than with the moving boundary equations. For the latter, the increase of the $u_{\text{DS}}^- - u_{\text{COHb}}^+$ would be offset by a decrease in $[\text{COHb}] - [\text{COHb}]_{\text{T}}$. In the former calculations, $[\text{DS}]_{\text{T}}$, the total concentration of dextran sulfate, was obtained by subtracting the absorption pattern from the schlieren pattern and assuming that the change in refractive index caused by changes in the concentration of buffer and salt ions

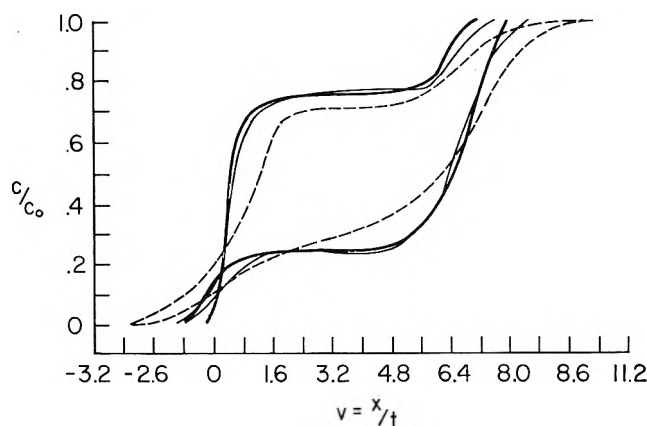


Figure 4. Variation of concentration distribution with time: —, 20 min.; - - -, 50 min.; ····, 95 min. pH 7.43; $\Gamma/2 = 0.10$; COHb and DS concentrations 0.170 and 0.420 g./100 ml., respectively; DS molecular weight 6.0×10^4 .

through the reaction boundary was linear in the change in refractive index due to changes in the sodium (or Tris) dextran sulfate concentration. For the concentration range used, a given per cent deviation in the assumed linear relation would cause an error in the experimental value ranging from 0.25 to 0.50 of the per cent deviation.

The point at which the original homogeneous solution begins and the point at which the solution containing uncomplexed components begins were difficult to determine with precision. Plots of $v(x/t)$ vs. c/c_0 (Figure 4) indicate that, for all systems studied, a "quasi-steady-state" was reached within the experimental time limits.

There have been numerous studies on the interaction between different macromolecules carrying net charges of the same sign.^{3,8-14} Usually, there are other attractive forces which compensate for the long-range repulsion. Thus, for antibody-antigen interaction, the large surface area available for short-range attraction contributing to steric fit is sufficient to balance out the coulombic repulsion. For interactions involving polyelectrolytes, the flexible-coil properties are probably as important as the charge densities. Dipole and non-polar effects are probably not sufficient.¹²

The marked variation of interaction with ionic strength and pH observed in this study indicates that the interaction probably involves the sulfate anion of the dextran sulfate and cationic groups on the COHb.¹⁴

(19) J. de Wael and E. Wegelin, *Rec. trav. chim.*, **71**, 1035 (1952).

(20) C. Tanford, "Physical Chemistry of Macromolecules," John Wiley and Sons, Inc., New York, N. Y., 1961, p. 468.

(21) G. Sitaramaiah and D. A. I. Goring, *J. Polymer Sci.*, **58**, 1107 (1962).

While the total charge per polyelectrolyte molecule is high (even with extensive counterion binding), it is distributed through a large volume. Thus, for example, E-4, which has approximately the same average molecular weight as COHb, can be calculated to have an equivalent hydrodynamic radius of 280 Å. as compared to 32 Å. for COHb.^{22,23} The near neutrality of this large permeable sphere,²⁴ in addition to the nearly random motions of the fixed charges within the volume, is favorable for a close approach by the COHb molecule and multiple interactions of the local field of unlike charges. With increasing pH, the decrease in the available cationic groups on the COHb would be a cause for decreased interactions. The titration charges of COHb are -2, -7, and -14 at pH 7.4, 8.0, and 8.5, respectively,²⁵ and the calculated electrophoretic charges are -2, -4, and -6.²⁶ The disappearance of interaction occurs at a much lower charge than that observed for dextran sulfate-bovine serum albumin interaction.¹⁴ This correlates with the extensive anion-binding properties of BSA which is in contrast with the behavior of human hemoglobin which exhibits little or no binding of monovalent and divalent cations and monovalent anions.²⁷ The decrease in interaction may also be partly attributed to counterion binding of TrisH⁺ ion resulting in a greater excluded volume within the equivalent sphere.

It has been observed that values of interaction constants obtained from transport experiments usually

do not agree with values obtained from equilibrium experiments.^{4,28} It has been suggested that transport and equilibrium experiments constitute two general classes of experiments from which two different quantities can be obtained.²⁹ An applied field will modify the charge density in the ionic atmosphere, quite apart from any effect due to the finite mobilities of the ion.³⁰ In the studies reported here, as has been mentioned, the field strength was varied over a sixfold range with currents from 2.5 to 15 ma. with only slight changes occurring in the patterns.

Acknowledgments. We wish to thank the Johns Hopkins School of Medicine for Post-Sophomore fellowships for Y. T. Some of the calculations were done at the Rockefeller Institute, and we wish to thank Dr. G. E. Perlmann for providing facilities. This research was supported by U. S. Public Health Service Research Grant GM-08411.

(22) P. J. Napijus and J. J. Hermans, *J. Colloid Sci.*, **14**, 252 (1959).

(23) J. J. Hermans, *J. Polymer Sci.*, **18**, 529 (1955).

(24) P. Debye and A. M. Beuche, *J. Chem. Phys.*, **16**, 573 (1948).

(25) K. F. Guthe, *J. Biol. Chem.*, **234**, 3167 (1959).

(26) D. C. Henry, *Proc. Roy. Soc. (London)*, **A135**, 106 (1931).

(27) C. Van Os and W. Moeller, *Rec. trav. chim.*, **77**, 297 (1958).

(28) O. Kedem and A. Katchalsky, *J. Polymer Sci.*, **15**, 32 (1955).

(29) Z. Alexandrowicz and E. Daniels, *Biopolymers*, **1**, 447 (1963).

(30) F. Booth, *Proc. Roy. Soc. (London)*, **A203**, 514 (1950).

The Thermodynamics of Vaporization in the Beryllium Oxide-Boron Oxide System¹

by Paul E. Blackburn and Alfred Büchler

Arthur D. Little, Inc., Cambridge, Massachusetts 02140 (Received July 8, 1966)

Vaporization and the phase relationships in the beryllium oxide-boron oxide system were studied by Knudsen effusion using a vacuum balance and a mass spectrometer and by differential thermal analysis. Gaseous beryllium metaborate, $\text{Be}(\text{BO}_2)_2$, was identified mass spectrometrically in the vapor above the system. Solid $\text{Be}_3\text{B}_2\text{O}_6$ (m.p. $1495 \pm 5^\circ$) was found to be the only condensed mixed oxide. The following thermodynamic values were obtained for the formation of gaseous beryllium metaborate from beryllium oxide and gaseous boron oxide: $\text{BeO}(\text{c}) + \text{B}_2\text{O}_3(\text{g}) = \text{Be}(\text{BO}_2)_2(\text{g})$ ($\Delta H_{1500} = 22 \pm 5$ kcal./mole; $\Delta S_{1500} = 6 \pm 2$ e.u./mole). For the formation of solid $\text{Be}_3\text{B}_2\text{O}_6$ from the condensed oxides, $3\text{BeO}(\text{c}) + \text{B}_2\text{O}_3(\text{l}) = \text{Be}_3\text{B}_2\text{O}_6(\text{c})$ ($\Delta H_{1500} = -23 \pm 5$ kcal./mole; $\Delta S_{1500} = -13 \pm 3$ e.u./mole). The metal-anion bond strengths in the gaseous lithium and beryllium metaborates show the same relation to each other as the bond strengths in the corresponding chlorides, thus further confirming the pseudohalide character of the gaseous metaborates.

Introduction

A mass spectrometric study^{2a} of gaseous sodium and lithium metaborate showed considerable similarity between these compounds and the gaseous alkali halides.^{2b} We were therefore led to investigate the existence of group II metaborates in the vapor phase. Gaseous beryllium metaborate, $\text{Be}(\text{BO}_2)_2$, was in fact identified mass spectrometrically in the vapor above a mixture of beryllium oxide and boron oxide.³ To derive reliable thermodynamic data for the gas phase compound, condensed phase data for the $\text{BeO-B}_2\text{O}_3$ system are required. While one condensed beryllium borate has been identified,^{4,5} no phase diagram for the entire system has been reported, nor are thermodynamic data available. A study of the phase relations in the $\text{BeO-B}_2\text{O}_3$ system by means of weight-loss effusion experiments and melting point measurements was therefore undertaken. The results of both these and the mass spectrometric studies are reported here.

Experimental Section

The experiments to be discussed below include (1) weight change measurements by means of an automatically recording microbalance, (2) melting

point measurements by differential thermal analysis, and (3) mass spectrometric measurements of heats of vaporization of individual vapor species.

Microbalance Measurements. Vapor pressure as a function of composition in the $\text{BeO-B}_2\text{O}_3$ system was obtained by determining the rate of effusion from a Knudsen cell whose weight change was continuously

(1) This work was supported by the U. S. Air Force Office of Scientific Research, Contract No. AF 49(638)-1171, ARPA Order No. 315-62 and by the U. S. Army Research Office, Contract No. DA-19-020-ORD-5584, ARPA Order No. 40-62, with funds provided by the Advanced Research Projects Agency.

(2) (a) A. Büchler and J. B. Berkowitz-Mattuck, *J. Chem. Phys.*, **39**, 286 (1963); (b) for a review of alkali halide vaporization, cf. S. H. Bauer and R. F. Porter in "Molten Salt Chemistry," M. Blander, Ed., Interscience Publishers, Inc., New York, N. Y., 1964, pp. 607-680.

(3) A. Büchler, J. B. Berkowitz-Mattuck, and J. L. Stauffer, paper presented at Tenth Annual Meeting, ASTM Committee E-14 on Mass Spectrometry, New Orleans, La., June 1962. On the basis of these experiments a preliminary value of 35 kcal./mole was reported for the heat of reaction $\text{BeO}(\text{c}) + \text{B}_2\text{O}_3(\text{g}) \rightarrow \text{Be}(\text{BO}_2)_2(\text{g})$ with the assumption that $\text{BeO}(\text{c})$ was present at unit activity. The present work shows that the phases present were in fact $\text{Be}_3\text{B}_2\text{O}_6(\text{c}) + \text{B}_2\text{O}_3(\text{l})$.

(4) H. Menzel and S. Slivinski, *Z. anorg. allgem. Chem.*, **249**, 357 (1942); H. Menzel and J. Adams, *Glastech. Ber.*, **22**, 237 (1949).

(5) L. Y. Mazelev, *Izv. Akad. Nauk Belorussk. SSR*, **4**, 105 (1953).

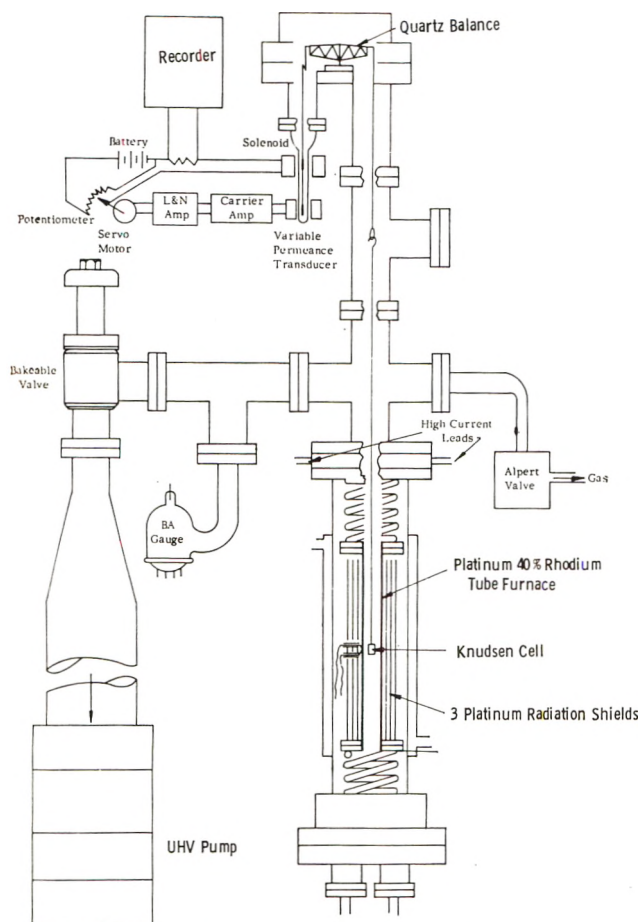


Figure 1. Automatic recording vacuum microbalance.

measured by means of an automatic recording microbalance.

The microbalance (Figure 1) consists of a quartz truss beam supported at the fulcrum by steel pivots resting in sapphire cups. The pan-support knife edges at the end of each arm are replaced by quartz fibers sealed directly to the beam and to quartz hooks.

The balance is held at its null position automatically by an electromagnet acting on a magnet rod suspended from one arm of the balance. The null position is detected with a variable permeance transducer which surrounds a steel rod hanging below the magnet rod. When the balance is displaced from its null point, a signal is generated by the transducer-controller which drives a potentiometer through a servo mechanism. The potentiometer changes the current flowing in the electromagnet restoring the balance to its null position. The current, which is proportional to the weight change, is recorded continuously. Cochran's control design⁶ was used for governing the balance.

The vacuum system, designed to achieve pressures in the high-vacuum range, is pumped with a Consoli-

dated PMCU 721 diffusion pump, a foreline trap, and a 5-ft.³/min. mechanical pump. The system is surrounded by a large degassing oven, and hence can be baked out at a temperature of about 500°. The vacuum system is made of stainless steel, Pyrex glass, and Kovar. All joints are sealed with metal gaskets of gold or copper. Both the electromagnet and the transducer mentioned above are mounted outside the system so that they may be removed during bakeout.

After bakeout, pressures as low as 2×10^{-9} torr have been achieved. With the vacuum furnace at 1300°, the pressure generally rises to the 10^{-7} to 10^{-8} torr range.

The furnace consists of a water-cooled stainless shell containing a 25-cm. long resistance-heated platinum-40% rhodium tube with three platinum radiation shields. The furnace ends are platinum rims clamped between water-cooled nickel flanges. The electrical leads are water-cooled tubing brought through the furnace wall with Varian high current feedthroughs. A platinum-10% rhodium-platinum control thermocouple is welded to the center of the furnace tube. The leads are insulated from the radiation shields by sapphire tubes. The furnace is calibrated with a thermocouple inside the vacuum system. This calibration is checked against the melting point of gold. The furnace has been used at temperatures up to 1600° with temperatures controlled to $\pm 1^\circ$.

The furnace is fed by a stepdown transformer, governed by a Leeds and Northrup CAT controller through a magnetic amplifier and saturable reactor. Voltage from the control thermocouple is recorded together with the weight change.

The experiments were carried out both in platinum Knudsen cells of conventional design, and in platinum cells which were 0.63 cm. in diameter and 0.94 cm. high with a conical base projecting into the cylinder. The sample was contained in the groove between the cylindrical wall and the conical base. The orifice was at the vertex of the cone. These cells, designed after Freeman,⁷ were used to direct the effusing gas toward the bottom of the apparatus, thus reducing condensation on the support wire. Since temperature is noted and controlled automatically, continuous measurements may be made for weeks at a time.

Differential Thermal Analysis. The experimental procedure used is described below together with the measurements.

High-Temperature Mass Spectrometry. The experiments were carried out with a Nuclide Corporation

(6) C. N. Cochran, *Rev. Sci. Instr.*, 29, 1135 (1958).

(7) R. D. Freeman, private communication, March 1963.

12-in. radius, 60° sector, magnetic deflection mass spectrometer. Two types of crucibles were used. The first was a two-piece nickel crucible of the design described earlier.^{2a} The second, illustrated in Figure 2, was a platinum-lined two-piece molybdenum crucible into which a small platinum cell was placed.

Materials. Crystalline B_2O_3 was furnished by the U. S. Borax and Chemical Corp. No significant impurities were indicated by spectrographic analysis. A water content of 4.5 wt. % in material as received was found by titrating samples acidimetrically for their B_2O_3 content, then calculating for water by difference. Samples were therefore carefully dried by heating at 950° for several hours under vacuum before using. Absence of H_2O was indicated by lack of weight loss during heating at lower temperatures during effusion measurements. High purity BeO was supplied by Nuclear Metals, Inc.

$BeO-B_2O_3$ samples were prepared from the pure oxides and loaded into Knudsen cells at Nuclear Metals. Weighed powders were thoroughly mixed, fused at 950° *in vacuo* for 2 hr., ground, and mixed again. Samples from a single batch were analyzed photometrically for BeO and B_2O_3 to test for uniform mixing.

Mass spectrometric samples were prepared in our laboratories. To obtain the mixed oxide $Be_3B_2O_6$, a mixture of BeO and B_2O_3 powders was allowed to react in sealed platinum capsules at 1300° for 100 hr.

Results

Weight Change Measurements. The first weight change measurements were made in the temperature range between 1080 and 1250°, with orifice areas between 2.3×10^{-3} and 1.8×10^{-2} cm.². These data indicated the existence of a two-phase region extending from $B_2O_3(l)$ to at least 50 mole % BeO, as manifested by a constant pressure equal to that of $B_2O_3(l)$. The existence of at least one compound was revealed, for the pressure decreased in the range from 50 to 75 mole % BeO. In none of these measurements, however, was equilibrium established after the pressure dropped. This is evidenced by the lack of constant pressure regions corresponding to other two-phase domains. To obtain consistent results, as shown by well-defined two-phase areas, it was necessary to use very small orifices. Two separate measurements were made, one at 1562°K. with an orifice area of 5.5×10^{-4} cm.², and a second at 1398°K. with an orifice area of 1.4×10^{-3} cm.². The larger orifice was necessary at the lower temperature because of time limitations. Even with an orifice of this size, the measurement required 3 weeks. Duplicate measurements

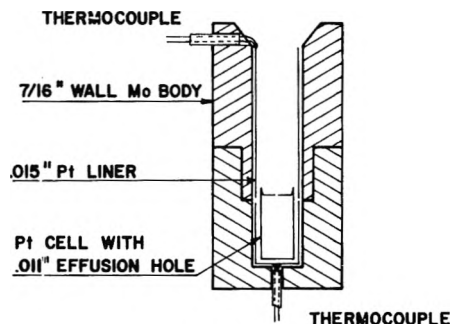


Figure 2. Molybdenum-platinum crucible.

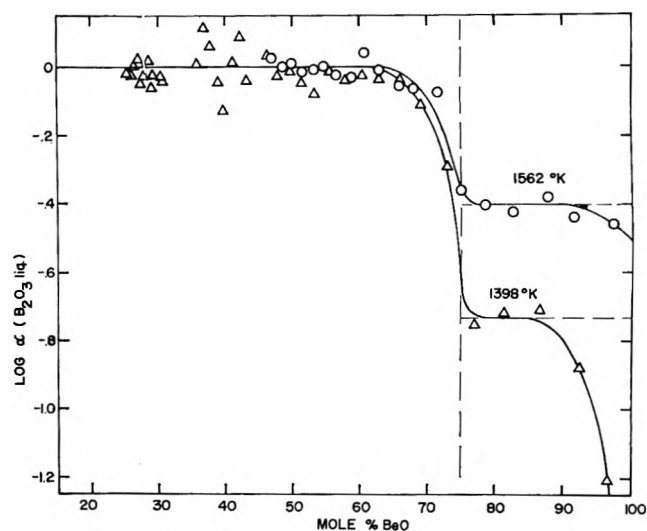


Figure 3. Boric oxide activity as a function of composition.

on B_2O_3 pressures were reproducible to between 3 and 7%.

The results of the two experiments are shown in Figure 3, in which the logarithm of the B_2O_3 activity with $B_2O_3(l)$ as standard state is plotted against composition. The data of Figure 3 indicate that the compound $Be_3B_2O_6$ identified earlier by low-temperature X-ray studies^{4,5} is in fact the only stable intermediate phase in this system. The drop-off in B_2O_3 activity as the 75% composition is approached is typical of a phase change in binary systems.^{8,9} A drop-off in activity as pure BeO is approached may be due to a decrease in effective evaporating surface through formation of BeO and to a low evaporation coefficient for the vaporization of B_2O_3 from $Be_3B_2O_6$.

Differential Thermal Analysis Measurements. To construct a phase diagram for the $BeO-B_2O_3$ system consistent with the vaporization data, it was neces-

(8) P. E. Blackburn, *J. Phys. Chem.*, **62**, 897 (1958).

(9) O. Kubaschewski and E. L. Evans, "Metal Physics and Physical Metallurgy," Pergamon Press, New York, N. Y., 1958, p. 66.

sary to establish the melting point of the compound Be₃B₂O₆. The liquidus in the neighborhood of this compound was found by differential thermal analysis. In this procedure, the difference in temperature between a sealed capsule containing a mixture of BeO and B₂O₃ in the ratio 3BeO:1.15B₂O₃ and a second capsule containing aluminum oxide was measured during cooling. The two capsules, placed side by side, were heated in a globar tube furnace. Platinum-platinum-10% rhodium thermocouples inserted in wells inside each capsule were used to measure temperature. One recorder was used to indicate the temperature of the capsule containing the experimental mixture, while a second recorder was used for the temperature difference between the two capsules. Three inflections were observed: (1) the point at which freezing started, 1488°; (2) the temperature where freezing ceased, *i.e.*, the eutectic temperature, 1441°; (3) the point where the cooling differential between the two capsules was re-established. No other inflections were observed in the differential curve, indicating the absence of other phases stable at lower temperatures. Our data yield a melting point for the stoichiometric compound Be₃B₂O₆ of 1495 ± 5°. Thus, all vapor pressure measurements were made over solid Be₃B₂O₆ and either BeO(c) or B₂O₃(l). On the basis of the data a phase diagram of the B₂O₃-BeO system can be drawn as shown in Figure 4.

Mass Spectrometric Studies. Four series of mass spectrometric measurements were made, three over the two-phase region B₂O₃(l) + Be₃B₂O₆(c) and one over the two-phase region Be₃B₂O₆(c) + BeO(c). In each case, the principal ionic species observed was B₂O₃⁺, corresponding to the neutral boron oxide B₂O₃(g). The principal beryllium-containing ionic species was Be(BO₂)₂⁺, corresponding to neutral beryllium metaborate Be(BO₂)₂(g).

The three measurements on the sample containing excess B₂O₃ yielded results apparently unaffected by the quantity of sample material or the cell orifice areas. Two of these measurements were made with nickel cells of the design described earlier,^{2a} one containing about 5 mg. each of BeO and B₂O₃, and one containing 26 mg. of B₂O₃ and 10 mg. of Be₃B₂O₆. Both cells had orifices of 7.8 × 10⁻³ cm.². In the third experiment the crucible design of Figure 2 was used with the platinum cell having an orifice area of 4.8 × 10⁻⁴ cm.². The results of the three experiments were combined to give the data shown in Figure 5 which gives the temperature dependence of the B₂O₃⁺ and Be(BO₂)₂⁺ ion intensities. The second-law heat of vaporization for B₂O₃ found from these experiments is 91 kcal./mole with a standard deviation of ±0.5

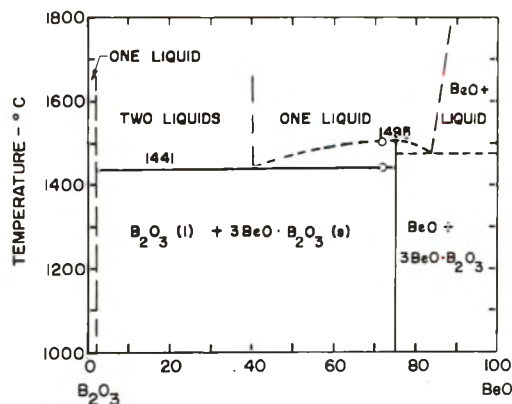


Figure 4. B₂O₃-BeO phase diagram.

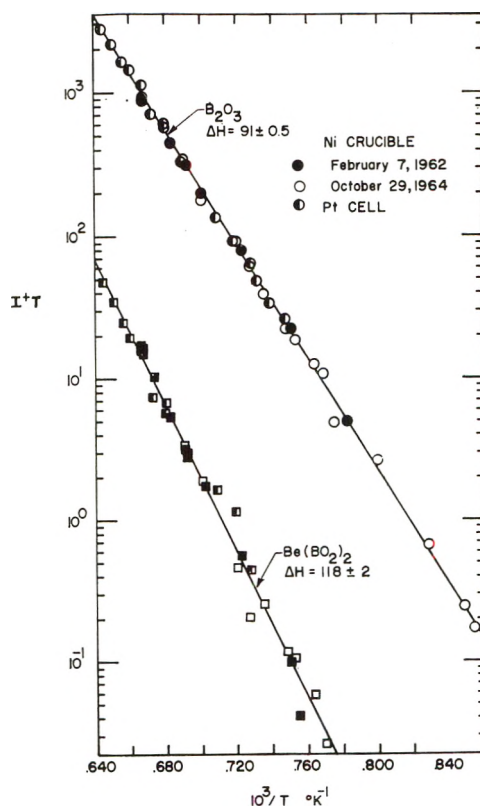


Figure 5. Plot of $I+T$ vs. $1/T$ for vaporization of B₂O₃(g) and Be(BO₂)₂(g) from the system Be₃B₂O₆(c)-B₂O₃(l).

kcal./mole, in good agreement with 93 ± 3 kcal./mole obtained in earlier experiments.^{2a} To obtain data for the BeO-rich side of the diagram a molybdenum crucible was used with a platinum cell liner containing 68 mg. of Be₃B₂O₆ and 12 mg. of BeO and having an orifice area of 4.8 × 10⁻⁴ cm.². The data obtained for both B₂O₃ and beryllium metaborate gas are shown in Figure 6.

The second-law heats indicated in Figures 5 and 6 correspond to the following reactions.

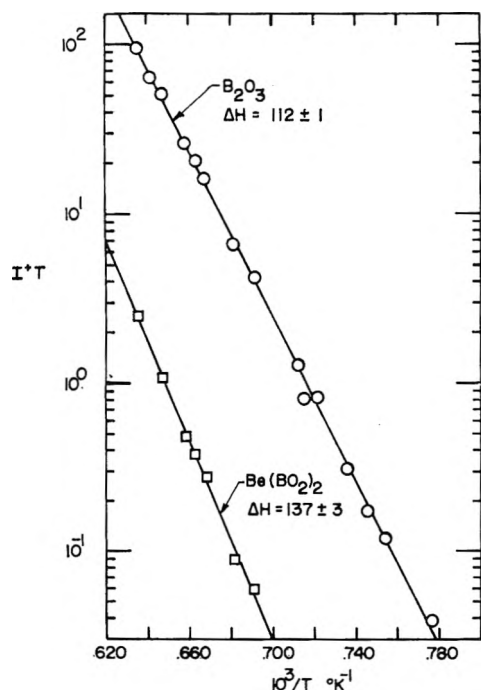
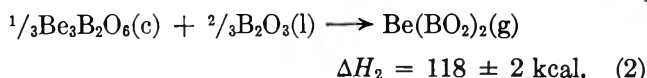
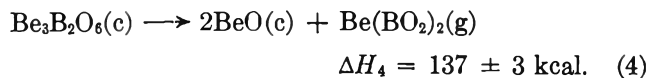
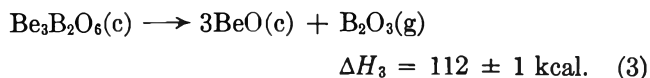


Figure 6. Plots of $I+T$ vs. $1/T$ for vaporization of $B_2O_3(g)$ and $Be(BO_2)_2(g)$ from the system $Be_3B_2O_6(c)$ - $BeO(c)$.

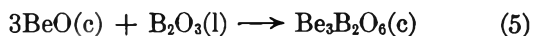
(a) $B_2O_3(l)$ - $Be_3B_2O_6(c)$ (Figure 5)



(b) $Be_3B_2O_6(c)$ - $BeO(c)$ (Figure 6)

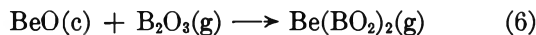


From these least-squares data the heats of formation of the condensed phase mixed oxide, $Be_3B_2O_6(c)$, and the gaseous mixed oxide, $Be(BO_2)_2(g)$, can be obtained. The heat of reaction for



can be obtained from the pairs of reactions 1 and 3 and 2 and 4, which give -21 ± 2 and -28.5 ± 5 kcal./mole, respectively. A third value for the heat of this reaction can be derived from the B_2O_3 activity data obtained in the weight loss experiments (at $1398^\circ K.$, $a_{B_2O_3} = 0.18$ and at $1562^\circ K.$, $a_{B_2O_3} = 0.39$), which give -20 ± 2 kcal./mole (estimated uncertainty). The best estimate for reaction 5 is therefore $\Delta H_5 = 23 \pm 5$ kcal./mole. The uncertainty in

ΔH_5 is within the standard deviations of the slopes from which it was computed. For the heat of formation of the gaseous beryllium metaborate from the oxides



a value of 25 ± 3 kcal./mole is obtained directly from the gaseous equilibrium on the BeO-rich side. The $Be(BO_2)_2(g)$ data on the B_2O_3 -rich side in combination with ΔH_5 give a value of 19 ± 3 kcal./mole. From these two values we therefore obtain as the best estimate for reaction 6, $\Delta H_6 = 22 \pm 5$ kcal./mole. The uncertainty in ΔH_6 is statistically consistent with the values for reactions 1 through 4.

In order to obtain entropy values consistent with the measured pressures and second-law heats, entropy changes for reactions 1 through 4 were calculated from

$$\Delta S_{1500} = \frac{\Delta H_{1500}}{1500} + R \ln p \quad (7)$$

where p is the vapor pressure of the gaseous species and ΔH_{1500} is the heat of reaction computed from the values in Table I.¹⁰ The B_2O_3 pressure at $1500^\circ K.$ given by our vacuum balance data is 2.70×10^{-5} atm. Using this pressure, the ion intensities of $B_2O_3^+$ and $Be(BO_2)_2^+$ from the mass spectrometric data, and Otvos and Stevenson's¹¹ ionization cross sections, the pressures were computed at $1500^\circ K.$ for reactions 2 through 4. The data taken from platinum cells over the BeO- $Be_3B_2O_6$ system were normalized to the orifice area and sample-to-ion source distance of the nickel cells.

Table I: Thermodynamic Values for the Be-B-O System

	$\Delta H_f^{\circ 1500}$, kcal./mole	$S^{\circ 1500}$, e.u./mole
$BeO(c)^a$	-142.3	19.8
$B_2O_3(l)^a$	-294.7	61.3
$B_2O_3(g)^b$	-204	101
$Be_3B_2O_6(c)^b$	-745	108
$Be(BO_2)_2(g)^b$	-324	127

^a See ref. 10. ^b This work.

Using the above procedure, the following pressures (in atmospheres) and entropy changes were calculated for reactions 1 through 4: (1) $P_{B_2O_3} = 2.7 \times 10^{-5}$,

(10) "JANAF Thermochemical Tables," The Dow Chemical Co., Midland, Mich.; BeO, Sept. 1963; B_2O_3 , Dec. 1964.

(11) J. W. Otvos and D. P. Stevenson, *J. Am. Chem. Soc.*, **78**, 546 (1956).

$\Delta S_1 = 39.6 \pm 0.3$ e.u.; (2) $P_{\text{Be}(\text{BO}_2)_2} = 2.5 \times 10^{-7}$, $\Delta S_2 = 50.3 \pm 1.4$ e.u.; (3) $P_{\text{B}_2\text{O}_3} = 9.3 \times 10^{-6}$, $\Delta S_3 = 53.0 \pm 0.7$ e.u.; (4) $P_{\text{Be}(\text{BO}_2)_2} = 1.1 \times 10^{-7}$, $\Delta S_4 = 59.1 \pm 2$ e.u. The deviations in the entropy changes were calculated from those in the heats assuming the pressures to be exact.

The entropies for reactions 5 and 6 were calculated from the entropy changes for reactions 1 through 4 by the same methods as the heats. In this manner one obtains $\Delta S_5 = -13 \pm 3$ e.u./mole and $\Delta S_6 = 6 \pm 2$ e.u./mole at 1500°K. ΔS_1 , ΔS_5 , and ΔS_6 are combined with JANAF¹⁰ entropies at 1500°K. for B₂O₃(l) and BeO(c) to give the remaining entropies in Table I.

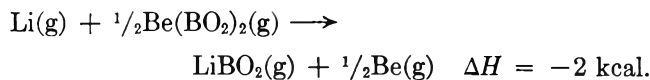
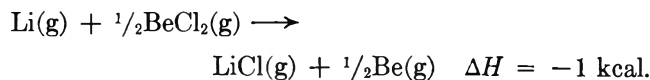
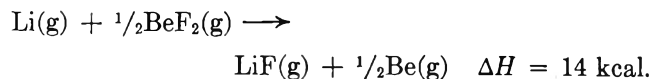
It should be noted that our value of $S_{1500} = 101$ e.u. for B₂O₃(g) compares well with Sommer, White, Linevsky, and Mann's¹² value $S_{1500} = 100.2$ e.u. The model assumed by these authors is that of a V-shaped molecule.

Discussion

Phase Diagram. The BeO-B₂O₃ phase diagram of Figure 4 has been drawn in analogy with the diagram for the MgO-B₂O₃ system.¹³ The alkaline earth oxide-boron oxide systems all show regions of liquid miscibility. However, from magnesium onward boron oxide rich solid oxides with low melting points are also stable. BeO-B₂O₃ appears to be the highest melting system. The thermodynamic data for the various compounds in this system are summarized in Table I.

The properties of the gaseous alkali metaborates suggested that these compounds could be regarded as pseudo-halides and the existence of gaseous beryllium metaborate was originally postulated on this basis.

It is therefore of interest to compare the heats of formation of beryllium and lithium metaborate with those of the corresponding fluorides and chlorides. Using heats of formation of the atoms and halides given by the "JANAF Tables,"¹⁰ we obtain the following heats of reaction at 1500°



The first of these reactions shows that the beryllium fluoride single bond is actually stronger than the lithium fluoride bond, whereas in the corresponding chlorides the two bond strengths are essentially equal. The relation of the lithium metaborate and beryllium metaborate single bond strength is very close to that of the chlorides and supports the description of the gaseous metaborates as pseudo-halides.

Acknowledgment. We are grateful to Mr. James L. Stauffer, Mr. John T. Larson, and Miss Barbara D. Peatie in assisting with the measurements, and to Dr. Joan B. Berkowitz-Mattuck for many valuable discussions.

(12) A. Sommer, D. White, M. J. Linevsky, and D. E. Mann, *J. Chem. Phys.*, **38**, 87 (1963).

(13) H. M. Davis and M. A. Knight, *J. Am. Ceram. Soc.*, **28**, 100 (1945).

Nuclear Magnetic Resonance Absorption in Anhydrous Sodium Soaps

by Kenneth D. Lawson and Thomas J. Flautt

The Procter & Gamble Company, Miami Valley Laboratories, Cincinnati, Ohio 45239 (Received July 9, 1965)

Nuclear magnetic resonance absorption in anhydrous sodium stearate, sodium palmitate, sodium myristate, and sodium laurate has been investigated in the temperature range from 90 to 473°K. Abrupt changes in the line widths have been observed which correspond to previously reported crystalline-crystalline, crystalline-mesomorphic, and mesomorphic-mesomorphic phase transitions. The widths of the lines resulting from the mesomorphic phases have been measured using two conditions of modulation: $H_m \ll \Delta H$ and $\nu_m \gg \gamma \Delta H$. The latter method of measurement is found to be more sensitive to line width changes in these systems. A possible explanation of the crystalline-crystalline transitions is given in terms of rotatory and oscillatory molecular motions in the solid state. The mesomorphic phases in the four soaps produce lines which have a "super-Lorentzian" shape. This shape is believed to result from a distribution of correlation times. The results for sodium stearate, palmitate, and myristate are closely similar. The sodium laurate data suggest that this soap may be significantly different in its crystal structure and possibly in the structure of the mesophases. A phase transition not previously reported has been detected in sodium myristate. In general, the results for the four soaps are consistent with the structural picture suggested for these systems by X-ray studies.

Introduction

It has long been known that the alkali metal salts of long-chain fatty acids are capable of existing in several phases in addition to the crystalline phases—of which there are at least four—and the isotropic liquid phase. These additional phases which exist in the temperature range from roughly 100 to 300° are of the mesomorphic or liquid-crystalline type frequently observed in surfactants, polymers, lipids, and other biological systems.^{1,2}

Mesomorphic phases in anhydrous soaps and soap-water systems have been studied by several physical methods. Phase transitions between mesomorphic phases have been detected by X-rays,³⁻⁵ dilatometry and microscopy,⁶⁻¹⁰ light transmission,¹¹ nuclear magnetic resonance spectroscopy,¹²⁻¹⁶ and calorimetry,¹⁷⁻¹⁹ as well as other methods.

Nuclear magnetic resonance spectroscopy (n.m.r.) can detect phase transitions^{20,21} as well as give some indication of the kinds and the extent of molecular motions present in the solid state.²²⁻²⁴ Some n.m.r. studies of the alkali metal salts of long-chain fatty acids

have been made previously.¹²⁻¹⁶ In all of these studies the transitions between the crystalline phase and the first mesomorphic phase have been easily detected.

- (1) G. W. Gray, "Molecular Structure and the Properties of Liquid Crystals," Academic Press Inc., New York, N. Y., 1962.
- (2) G. H. Brown and W. G. Shaw, *Chem. Rev.*, **57**, 1049 (1957).
- (3) A. E. Skoulios and V. Luzzati, *Acta Cryst.*, **14**, 278 (1961).
- (4) H. Nordsieck, F. B. Rosevear, and R. H. Ferguson, *J. Chem. Phys.*, **16**, 175 (1948).
- (5) F. G. Chesley, *ibid.*, **8**, 643 (1940).
- (6) M. J. Vold, M. Macomber, and R. D. Vold, *J. Am. Chem. Soc.*, **63**, 168 (1941).
- (7) M. J. Vold, *ibid.*, **63**, 160 (1941).
- (8) R. D. Vold, F. B. Rosevear, and R. H. Ferguson, *Oil & Soap*, **16**, 48 (1939).
- (9) M. J. Vold and R. J. Vold, *J. Am. Chem. Soc.*, **61**, 808 (1939).
- (10) R. D. Vold, R. Reivere, and J. W. McPain, *ibid.*, **63**, 1293 (1941).
- (11) D. P. Benton, P. G. Howe, and I. E. Puddington, *Can. J. Chem.*, **33**, 1384 (1955).
- (12) R. F. Grant and B. A. Dunell, *ibid.*, **38**, 1951, 2395 (1960).
- (13) M. B. Barr and B. A. Dunell, *ibid.*, **42**, 1098 (1964).
- (14) D. J. Shaw and B. A. Dunell, *Trans. Faraday Soc.*, **58**, 132 (1962).
- (15) R. F. Grant and B. A. Dunell, *Can. J. Chem.*, **39**, 359 (1961).

However, the mesomorphic-mesomorphic transitions have generally not been observed. The inability to detect transitions between mesomorphic phases in past n.m.r. experiments is understandable when the widths of the lines resulting from these phases are considered. The line widths from mesomorphic phases are almost always less than 500 mgauss. In many previous studies the inhomogeneities of the static magnetic field used in the n.m.r. experiment have been large enough to mask partially any changes in spectra occurring as a result of phase transitions. In addition, the conventional derivative method of obtaining n.m.r. resonances in the wide-line experiment results in lines which are often artificially broadened by modulation²⁵; this tends also to mask small line-width changes. This paper reports the results of an n.m.r. study of anhydrous sodium stearate ($C_{17}H_{35}CO_2Na$), sodium palmitate ($C_{15}H_{31}CO_2Na$), sodium myristate ($C_{13}H_{27}CO_2Na$), and sodium laurate ($C_{11}H_{23}CO_2Na$) in the temperature range from 90 to about 473°K. In this study both of the handicaps mentioned above have been overcome.

Experimental Section

a. Samples. The sodium stearate used in this study was prepared from an Eastman Kodak White Label grade acid which was found to be about 99% pure by gas chromatographic analysis of the methyl ester. The palmitic, myristic, and lauric acids were prepared by saponification of methyl esters, which by chromatographic analysis were 99+ % pure, with alcoholic KOH followed by acidification with an excess of aqueous HCl. Special care was taken to remove any traces of methyl or ethyl esters from the resulting acids. Gas chromatographic analysis indicated that these acids were 99+ % pure.

To prepare the sodium salts the acids were dissolved in an 80:20 ethanol-water (V_1/V_2) mixture and titrated to an alkaline end point. The indicator, thymol blue, was used externally. During the titration and all other operations, a stream of dry nitrogen was continually bubbled through the solutions to prevent dissolution of carbon dioxide. The excess solvent was evaporated using a steam bath and the resulting precipitate dried on a freeze drier. The fused soaps were then crushed and dried in an oven, under a nitrogen stream, at 150° for about 1 hr. This treatment produces completely anhydrous soaps.

The n.m.r. samples were prepared by sealing portions of the soaps into either 10- or 5-mm. o.d. tubes under a nitrogen atmosphere. The samples were maintained under these conditions throughout the studies.

b. Instrumentation. The n.m.r. experiments were

conducted on a spectrometer assembled mainly from Varian Associates components. The magnet system consists of a 9-in. Model V-3400 magnet equipped with tapered pole caps and homogeneity control coils and powered by a Model VFR-2501 power supply equipped with a Fieldial sweep unit. A Varian 40-Mc. radiofrequency unit is used in conjunction with a Princeton Applied Research Model JB-5 lock-in amplifier. The output of the internal oscillator of the lock-in amplifier is fed through an Eico Model ST-70 stereo amplifier to the modulation coils. The resonances were recorded on a strip chart recorder and the widths measured from the recordings. The intrinsic inhomogeneity of the magnetic field is about 7 mgauss as determined from the half-maximum intensity line width of a spinning 5-mm. sample of distilled water.

The heating and cooling of the samples were accomplished by using a Varian Model V-4340 variable temperature probe unit. Temperatures below room temperature were obtained by passing a stream of dry nitrogen through a copper coil immersed in either a liquid nitrogen or a Dry Ice-acetone bath. The sample temperature was measured with a Brown recording potentiometer using a copper-constantan thermocouple placed about 1.5 cm. above the surface of the sample. The reading from this thermocouple was calibrated against a second thermocouple placed directly into a sample.

Normally in the wide-line n.m.r. experiment the modulation frequency, ν_m , and the modulation amplitude, H_m , are chosen so that $H_m \ll \Delta H$ and $\nu_m \ll \bar{\gamma}\Delta H$, where ΔH is the width of the line to be measured. However, it is not always possible to obtain a small enough H_m consistent with good signal-to-noise ratio. When $H_m \gtrsim 0.25\Delta H$, the measured line width will be greater than the true line width, and corrections for the effect of both the modulation frequency and amplitude must be applied.^{25,26} If, however, the modulation

(16) W. R. Janzen and B. A. Dunell, *Trans. Faraday Soc.*, **59**, 1260 (1963).

(17) F. H. Stross and S. T. Abrams, *J. Am. Chem. Soc.*, **73**, 2825 (1951).

(18) R. D. Vold, *ibid.*, **63**, 2915 (1941).

(19) R. D. Vold, *J. Phys. Chem.*, **49**, 315 (1945).

(20) C. K. Coogan, G. G. Belford, and H. S. Gutowsky, *J. Chem. Phys.*, **39**, 3061 (1963).

(21) C. K. Coogan and H. S. Gutowsky, *ibid.*, **40**, 3419 (1964).

(22) E. R. Andrew, *ibid.*, **18**, 607 (1950).

(23) E. R. Andrew and R. G. Eades, *Proc. Roy. Soc. (London)*, **A218** 537 (1953).

(24) H. S. Gutowsky and G. E. Pake, *J. Chem. Phys.*, **18**, 162 (1950).

(25) E. R. Andrew, *Phys. Rev.*, **91**, 425 (1953).

(26) K. Halbach, *ibid.*, **119**, 1230 (1960).

frequency is chosen so that it is large compared to the line width, separate side band resonances will be obtained.²⁷ The width of the side band resonances is then the true line width. Under normal operating conditions the center band resonance is removed by suitable phasing. This type of detection is normally called the "first side band" method.

The upper limit of line width which can be measured by this method depends upon the highest modulation frequency which can be obtained. In addition to the high modulation frequency, the amplitude of the modulation field must also be high. The upper frequency limit depends, for the most part, upon the amount of eddy current losses occurring in the probe. With the instrument used in this study, it is possible to produce modulation fields which range in frequency from 20 c.p.s. to 10 kc.p.s. With this range of frequencies, proton resonances which are about 1 gauss or less in width can be detected by the first side band method.

c. Methods. The line width at any given temperature represents the average of from two to six recordings. Both increasing and decreasing magnetic field sweeps were used in recording the spectra. The variations in the measured line widths are about ± 0.15 gauss for the wide lines and about ± 5.0 mgauss for the narrow lines. The accuracy of the line widths measured at 90°K., however, is probably not better than ± 0.5 gauss because of the relatively poor signal-to-noise ratio at this temperature.

The accuracy of the stated temperatures is within $\pm 0.2^\circ$ at and near room temperature but only within $\pm 2.0^\circ$ around 200°. The 90°K. value is probably not better than $\pm 5.0^\circ$ K.

The lines which have widths greater than approximately 1 gauss were recorded as the derivative, and the widths were determined between points of maximum slope. When obtaining these lines, a modulation frequency of either 80 or 20 c.p.s. was used, and the radiofrequency power level was maintained well below that required for saturation. In most cases the modulation amplitude was chosen so that $H_m/\Delta H < 0.2$, where ΔH is the line width. Amplitudes of this magnitude should produce errors of less than 2% between the measured and true line widths.²⁸ No attempt was made to correct the line widths themselves for the effect of either the modulation frequency or the modulation amplitude.

Lines which are less than about 1 gauss in width were obtained by two different methods. In addition to obtaining the line widths by using very small modulation amplitudes, which become increasingly difficult when the lines become very sharp, the lines were re-

corded under modulation conditions such that $\nu_m \gg \bar{\gamma}\Delta H$; usually $\nu_m/\bar{\gamma}\Delta H > 5$. These conditions produce the absorption curve. The width, which now is not affected by the modulation amplitude, is measured at the point of half-maximum intensity. In addition to the advantage of obtaining the true line width by this method, there is additional information to be gained by measuring the widths by two different methods. A comparison of the line widths, as measured at the half-maximum intensity and at the point at which the slope changes, provides information about the shape of the line. Likewise, the difference between the widths obtained by the two methods, observed as a function of temperature, provides information about the effect of temperature on the line shape. These points will be discussed in more detail in following sections.

Results and Discussion

a. Temperature Dependence of the Line Widths. The line widths of anhydrous sodium stearate (hereafter NaS), sodium palmitate (NaP), sodium myristate (NaM), and sodium laurate (NaL) are shown in Figures 1 through 4, respectively, for temperatures between 0 and 200°. In these figures the line widths have been placed on a log scale to afford more meaningful comparisons of the line width changes. In addition to the measurements shown in the figures, the line widths of all four of the materials were determined at liquid nitrogen temperature ($\sim 90^\circ$ K.). Some measurements were also made between 0 and -25° for NaP. The liquid nitrogen temperature line widths are 13.9 ± 0.5 , 14.6 ± 0.5 , 14.1 ± 0.5 , and 13.7 ± 0.5 gauss, respectively, for NaS, NaP, NaM, and NaL.

Before each line width determination was made, sufficient time was allowed for the system to reach thermal equilibrium. The length of time varied, depending upon the point on the line width vs. temperature curve where the measurement was being made. In some cases only about 1 hr. was found to be sufficient to establish equilibrium, but in the regions where the line width changes rapidly, several hours was allowed. If there was any doubt about whether or not the system had attained equilibrium at any temperature, the temperature was held constant overnight and the line width remeasured. In all of the cases in which this happened the line width did not change significantly from the value which had been obtained after the system had equilibrated for 2 or 3 hr. Sodium laurate appears to require more time to equilibrate than do the other

(27) W. A. Anderson, "NMR and EPR Spectroscopy," Pergamon Press Inc., New York, N. Y., 1960, Chapter 14.

(28) G. W. Smith, *J. Appl. Phys.*, **35**, 1217 (1964).

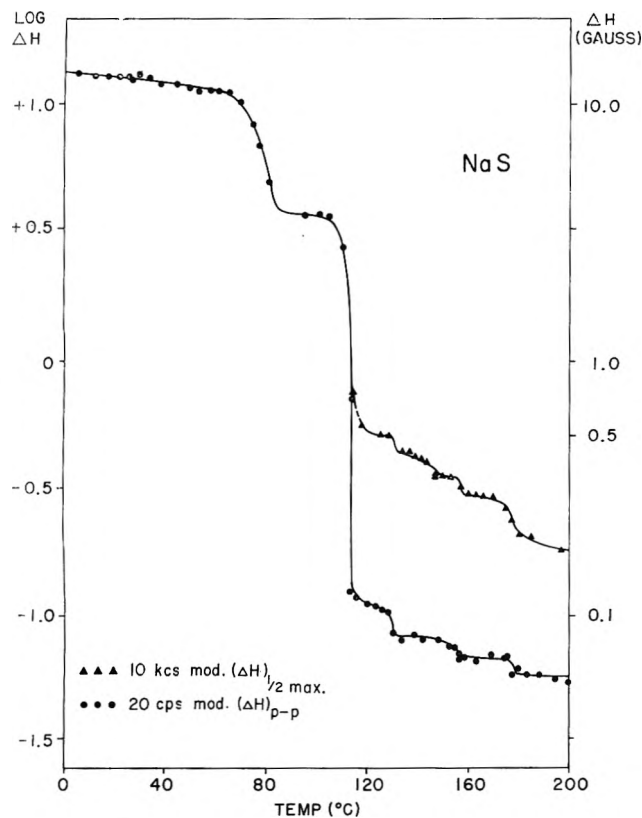


Figure 1. The line width of sodium stearate as a function of temperature.

samples, particularly in the 150 to 200° temperature range.

Several discontinuities are present in the line width vs. temperature curves of the four soaps. These transitions correspond reasonably well with phase transitions which have been found to occur in these materials by other means.^{3-13,17-19} The temperatures at which the line width changes occur are tabulated in Table I along with the range of transition temperatures previously reported by other methods.

There is some question of whether the names given in Table I to the various phases should be applied to all four of these soaps. The name "subwaxy," for example, was originally associated with those particular phases found in NaP and NaS,⁶ but more recent X-ray studies by Skoulios and Luzzati³ indicate that all of the phases mentioned in Table I are distinct phases and are similar in structure in all four soaps.

The first two transitions listed in Table I require some comment. The existence of a transition in anhydrous soaps at or near the melting point of the corresponding fatty acid was first reported by Thiessen and Ehrlich²⁹ and given the name "genotypical." This transition has been observed by other workers

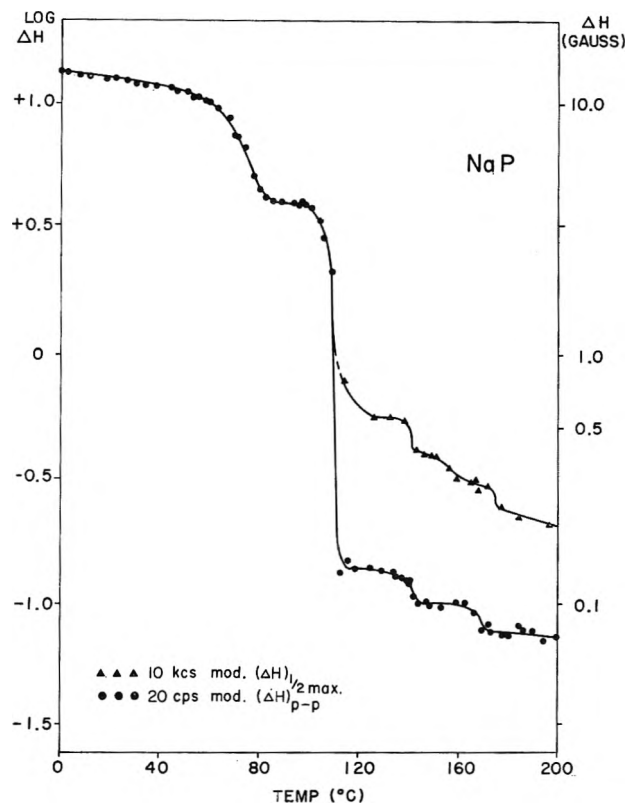


Figure 2. The line width of sodium palmitate as a function of temperature.

in NaP and NaS^{6,19} and is believed to be a second-order transition. Of the four soaps studied here, only NaL shows any line width change at or near the melting point of the corresponding fatty acid. (The melting points are: NaS, 69°; NaP, 63°; NaM, 54°; and NaL, 44°.) In NaL the line width changes by about 1 gauss at 42°. The nature of the structural change producing this line width change is not understood. The sample of NaL used in this study does not contain free acid which has been suggested as being the cause of this transition.

Several workers^{6,18,19} have observed a transition in anhydrous soaps which occurs below the crystalline-mesomorphic transition. This transition has been designated as a curd-curd or a curd-supercurd transition by Vold.^{18,19} X-Ray data collected in these laboratories indicate that no major structural changes occur in this temperature range, but there do appear to be some structure modifications. Pronounced changes occur around 80° in the n.m.r. line widths of NaS, NaP, and NaM. These transitions are listed in Table I as crystalline-crystalline transitions. The absence

(29) P. A. Thiessen and E. Ehrlich, *Z. physik. Chem. (Leipzig)*, **A165**, 453, 464 (1933).

Table I: Phase Transitions in Anhydrous Sodium Soaps

Phase transitions	Transition temperatures, °C.							
	Sodium stearate		Sodium palmitate		Sodium myristate		Sodium laurate	
	This work	Lit. values ^a	This work	Lit. values ^b	This work	Lit. values ^c	This work	Lit. values ^d
Genotypical	...	65-70	...	67	42	M.p. of lauric acid = 44
Crystalline-crystalline ^{e,f}	85	86-96	82	...	80	79-80
Crystalline-subwaxy	114	108-118	113	114-125	108	98-113	104	98-100
Subwaxy-waxy	131	129-134	142-144	134-140	141	133-142	147-149	130-142
					(162)			
Waxy-superwaxy	157-159	165-180	172-175	172-176	182	175-182	190-192	182-187
Superwaxy-subneat	178-181	188-210	>200	195-211	202-204	204-218	>200	200-220

^a Taken from ref. 3, 6, 7, 11-13, and 17-19. ^b Taken from ref. 3-9 and 18. ^c Taken from ref. 3, 6, 10, and 18. ^d Taken from ref. 3, 6, 7, and 18. ^e The crystalline phase present in these soaps at 25° is the ω -phase as described by R. H. Ferguson, *Oil & Soap*, 21, 6 (1944). ^f This transition is probably the curd-curd transition reported by Vold.¹⁸

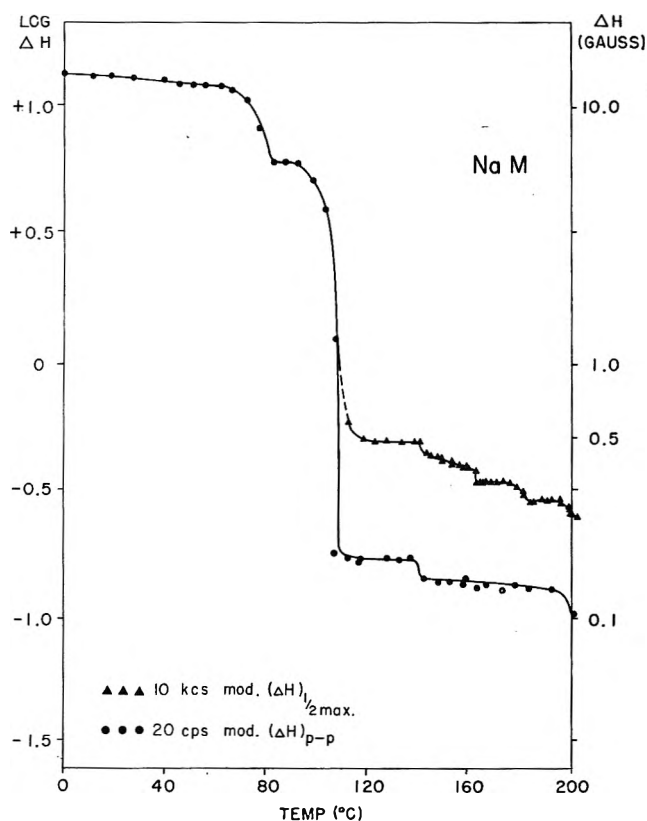


Figure 3. The line width of sodium myristate as a function of temperature.

of this transition in NaL is puzzling; however, it may be attributed to the relatively larger effect of the polar groups in this material due to the shorter length of the hydrocarbon chains. It could be argued that the small change in line width which occurs at 42° in NaL should be grouped with the transitions designated as crystalline-crystalline, but the large temperature difference

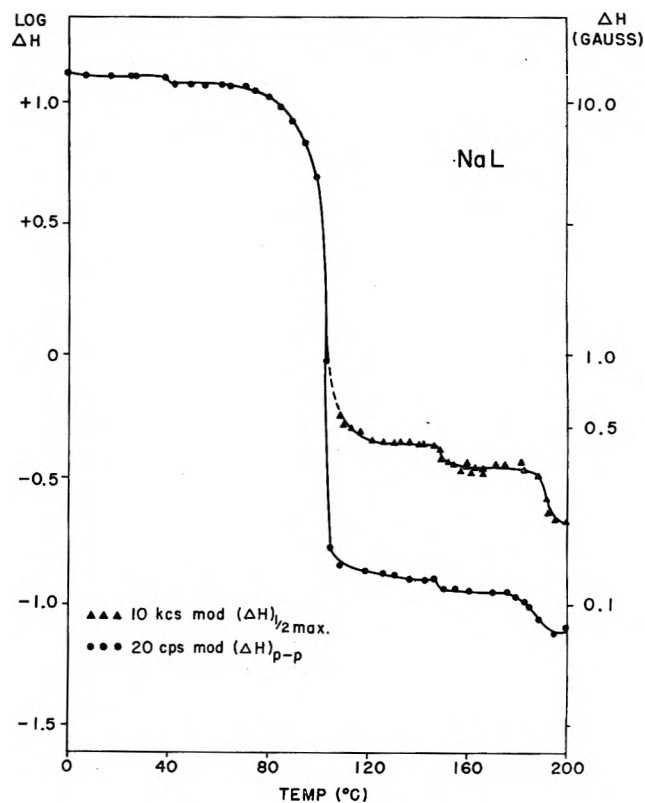


Figure 4. The line width of sodium laurate as a function of temperature.

between this and the transitions in NaS, NaP, and NaM, plus the large difference in the magnitude of change in the line width, seems to preclude this grouping. It appears more reasonable to place the crystalline-crystalline transition in NaL, if it is present at all, at about 100°, where it merges with the crystalline-subwaxy transition.

The line width transitions occurring near 80° for NaS, NaP, and NaM are interpreted as arising from increased molecular motion in the hydrocarbon chains of the soaps. It was with this origin of the line width decrease in mind that the suggestion was made that the same transition may occur in NaL at a higher temperature. The larger effect of the polar end of the molecule in this material should reduce the amount of motion present in the paraffinic chains.

The type of molecular motion assumed to be present here could give rise to a second-order phase transition,³⁰ and preliminary calorimetric studies made in our laboratories do indeed indicate that these transitions are of the second kind.

A comparison of the transition temperatures determined by other methods with those found in this study (see Table I) indicates that for the most part the agreement is relatively good. The largest discrepancies occur in the waxy-superwaxy and the superwaxy-subneat transitions in sodium stearate. Both of these transition temperatures are about 8° below any previously reported values. This difference is too large to be attributed to errors in measuring the temperature, and other explanations must be sought.

It is not completely unexpected that n.m.r. transition temperatures would differ somewhat from those found by other methods. One reason that one would expect to find differences is that, in addition to structural changes, molecular motions play a large part in determining where n.m.r. line width transitions occur, and, in fact, these motions can be relatively small in both frequency and amplitude. To narrow an n.m.r. line, the motion must have a frequency of only the order of the line width in frequency units. This means, for the most part, frequencies no greater than 10⁴ to 10⁵ c.p.s. In a system such as sodium stearate, where the motions of the hydrocarbon chains are the dominant ones, it is not unreasonable to expect that the rate of reorientation of those chains becomes comparable to the line width before actual structural changes occur since changes in structure involve the polar groups of the molecules. Premelting-narrowing of n.m.r. lines has been observed previously in several systems.^{22,23} As a further indication of the sensitivity of n.m.r. line widths and second moments to low-frequency motions, recent n.m.r. and X-ray studies of the benzene-silver perchlorate complex should be mentioned.³¹ The n.m.r. results indicate that the benzene molecule rotates about the hexad axis more or less freely at room temperature while X-ray diffraction measurements indicate that the carbon atoms spend a significant amount of their time at specific positions.

Aside from the fact that n.m.r. lines are affected by

relatively low frequency motions, which in itself may cause n.m.r. transition temperatures to differ from those found by other means, X-ray studies of mesomorphic phases in anhydrous soaps³ indicate that transitions between two phases may take place through a mixture zone made up of the two surrounding phases. This perhaps is a result of the high viscosity of the systems which slows up the establishment of equilibrium. The coexistence of two phases would probably lead to narrowing of the n.m.r. line since the recorded line is an average line for the system.

In addition to the discrepancies in transition temperatures already discussed, the n.m.r. line width of NaM decreases quite sharply at about 152°. This change is reproducible with both increasing and decreasing temperature and has all the indications of a phase change; however, a phase transition has not been reported at this temperature by other methods.

The line widths of the various soaps show some consistency with chain length changes. For example, in the crystalline phase at room temperature (28°), the lines increase slightly with decreasing chain length. The values are 12.4, 12.6, 12.9, and 13.0 gauss, respectively, for NaS, NaP, NaM, and NaL. This small change results undoubtedly from a slight difference in the amount of motion present in these systems at a given temperature. The longer chains would be expected to possess more freedom of motion.

In the mesomorphic phases, however, the same order is not observed. The widths of the lines from NaS, NaP, and NaM appear to be in order, but the lines of NaL have widths which in general are intermediate between those of NaP and NaM. This may indicate that the structures of the mesomorphic phases in NaL are not the same as that in the higher homologs although X-ray studies have not indicated that this is true.³

b. Line Shapes in the Mesomorphic Phases. It is obvious from the data shown in Figures 1 through 4 that the sensitivity of the line width to changes in the system depends to some extent upon the manner in which the widths are measured. In these systems the line widths measured at half the maximum intensity are more sensitive to changes in the system than those measured at the inflection points. This difference in sensitivity is produced by the peculiar line shapes which are found in the mesomorphic phases of these soaps. In all of the mesomorphic phases in the

(30) J. R. Partington, "An Advanced Treatise on Physical Chemistry," Vol. 3, Longmans, Green and Co., London, 1952, pp. 399-406.

(31) (a) D. F. R. Gilson and C. A. McDowell, *J. Chem. Phys.*, **39**, 1825 (1963); (b) H. G. Smith, *ibid.*, **40**, 2412 (1964); (c) D. F. R. Gilson and C. A. McDowell, *ibid.*, **40**, 2413 (1964).

anhydrous soaps, the n.m.r. lines are very narrow in the center portion but have more intensity in the wings than does a lorentzian line. A typical example of the line shape is shown in Figure 5. A calculated lorentzian line shape is also shown to illustrate the difference. The points at which the slope changes—where the width is measured from the derivative curve—are very near the top of the line, and thus any changes occurring in the wings would not produce a change in the line width measured between these points.

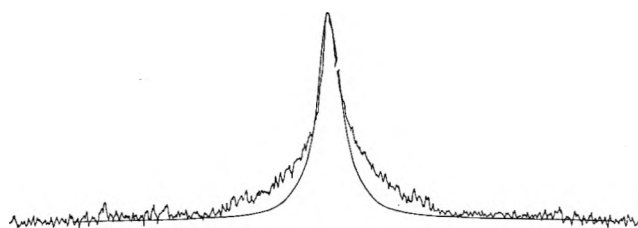


Figure 5. The n.m.r. spectrum of sodium stearate at 126°. The smooth curve is a calculated lorentzian line.

The ratio between the widths measured at the two points, half-maximum intensity ($\Delta H_{1/2\max}$) and inflection points (ΔH_{p-p}), further illustrates the difference between the lines found in the mesomorphic phases and a lorentzian or gaussian line. This ratio for a lorentzian line is 1.73 and for a gaussian line is 1.18. For the lines found in these soap phases, the ratio is temperature dependent but varies from about 5 to about 3 in NaS, decreasing with increasing temperature. The directional variation with temperature is the same in all of the soaps, and the ratio decreases from about 4 to 3, 3.5 to 2.6, and 3.2 to 2.6 for NaP, NaM, and NaL, respectively. The lines from the mesomorphic phases can possibly be best described by the term "super-lorentzian" since the ratio of the two widths ($\Delta H_{1/2\max}/\Delta H_{p-p}$) is greater than that found in a lorentzian curve. In none of the mesomorphic phases do the lines become pure lorentzian in shape, but they do tend to become more nearly so at the higher temperatures. This leads one to expect that the isotropic phases of these soaps, which generally occur above 300°, would have lines very nearly lorentzian in shape.

Some insight into how such a line shape could arise in systems of this type can perhaps be gained by considering the proposed structures of the mesomorphic phases in anhydrous soaps.

Skoulios and Luzzati³ have grouped the mesomorphic phases of anhydrous soaps into two structural families. The first family is made up of the subwaxy, waxy, superwaxy, and subneat phases; the second family

contains only the neat phase. In the first group of phases, which includes all of the phases occurring in the temperature range covered in this study, the polar ends of the soap molecules are believed to be arranged in double layers. These layers are "ribbonlike" in structure with finite widths and indefinite lengths. The layering of the polar groups results in the formation of "ribbons" of molecules having a thickness of approximately two molecular lengths. The hydrocarbon chains fill in the space between the polar "ribbons" and exist more or less as they would in a liquid with the exception of a partial loss in translational freedom. Differences in the width of the ribbons are believed to be the predominant difference among the various members of this family of phases in a given soap. The structure of the neat phase, although not encountered in this study, is considered to be a lamellar-type structure. The polar groups are again located in double layers which are parallel and equidistant from each other, the distance between layers being substantially less than twice the length of the hydrocarbon chains. These layers do not have finite widths.

In all of the mesomorphic phases, the structures are such that the hydrocarbon chains of the soap molecules are rather strongly fixed in place on the one end with the opposite end more or less enjoying the kinds of freedom found in the liquid phase, with the exception of translational freedom. If one then considers the effect of molecular motion upon an n.m.r. line, it is apparent that the line one obtains should be made up of a distribution of lines resulting from the individual methylene groups in the hydrocarbon chains. The positions of these lines would be almost the same, with the exception of the methylene group adjacent to the polar group, but the widths of the lines should change depending upon the amount of motion available to the group giving rise to the line. The line shapes found in these systems—very sharp in the center but having very wide wings—appear to be a reflection of the distribution of motion in the paraffin chains.

Whenever a transition between two of these mesomorphic phases occurs, the width of the polar layer decreases, according to Luzzati's proposed structure, thus affecting that portion of the line arising from methylene groups nearer the polar groups to a much greater extent than those near the end of the hydrocarbon chains. This then explains why more change is seen in the line width when measured at half-maximum intensity than if measured at the inflection points, the former points being farther from the center of the line. As the temperature is increased, of course, the amount of motion enjoyed by the fixed ends increases, the relative difference between the two ends of the

chains becomes less, and the line shape thus approaches a lorentzian shape.

A comparison of the ratios stated above indicates that, as the length of the hydrocarbon chains decreases, the lines also become more lorentzian in shape. This change results, no doubt, from the smaller motional gradient in the shorter chains, perhaps not from a decrease in the rigidity of the polar "ribbons" but by a decrease in the amount of motion present in the free ends of the chains. This decrease in the amount of motion in the chain as the length decreases also would predict the order of the line widths mentioned in the previous section. However, it must be mentioned again that NaL is an exception.

c. Molecular Motion in the Solid State—Crystalline—Crystalline Transition. The narrowing of n.m.r. lines by molecular motion, so-called "motional narrowing," has been observed in many solid systems.²²⁻²⁴ Discussions of motional narrowing are facilitated by employing a correlation time or correlation frequency. The correlation frequency (ν_c) can be considered as the rate at which the molecular or atomic environment about a given nucleus changes significantly.³² In terms of the line widths the correlation time (τ_c) can be expressed as²⁴

$$\tau_c = 1/(2\gamma\Delta H) \tan \left[(\pi/2) \frac{(\Delta H^2 - \Delta H''^2)}{(\Delta H'^2 - \Delta H''^2)} \right] \quad (\text{I})$$

where ΔH is the line width in the line-narrowing region, $\Delta H'$ is the line width before motional narrowing (rigid lattice), and $\Delta H''$ is the line width after motional narrowing has taken place.

By assuming that the molecular motions can be described by a single correlation time (this has been found in other systems^{22,23}) which varies with temperature according to an Arrhenius-type equation

$$\tau_c = \tau_0 \exp(E_{\text{act}}/RT) \quad (\text{II})$$

values of E_{act} can be obtained from plots of the $\ln \tau_c$ against $1/T$. E_{act} is an energy related to the height of the potential barrier which must be overcome in order for the nucleus or molecule to reorient. Its magnitude produces information about the nature of the reorientation process. However, because of the uncertainties in eq. I^{23,24} and because the line shape undoubtedly changes with temperature, the numbers obtained by this method have little significance beyond orders of magnitude.

Plots of the type described above have been made for the soaps studied here (Figures 6 and 7). The values of $\Delta H'$ are the rigid lattice line widths determined at liquid nitrogen temperatures. They are listed above. The values of $\Delta H''$ used are the line widths

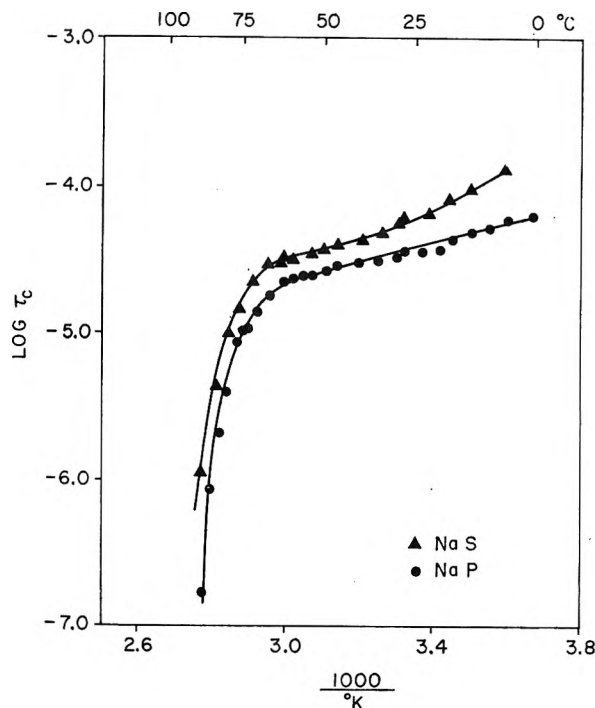


Figure 6. The correlation times of sodium stearate and sodium palmitate as a function of the inverse temperature.

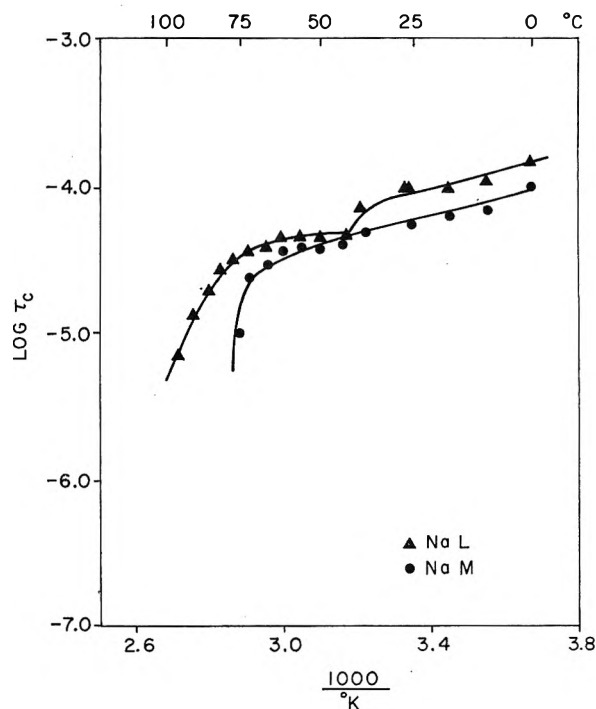


Figure 7. The correlation times of sodium myristate and sodium laurate as a function of the inverse temperature.

(32) K. Bloembergen, E. M. Purcell, and R. V. Pound, *Phys. Rev.*, 73, 679 (1948).

just prior to the crystalline-subwaxy transitions. These widths are 3.67, 4.00, 6.00, and 5.12 gauss, respectively, for NaS, NaP, NaM, and NaL.

The data for the four soaps, Figures 6 and 7, do not fall on particularly straight lines, and, in addition, the data for NaL are complicated by the presence of the genotypical transition; however, from the slopes of the best straight lines drawn through the points, values of E_{act} of about 3 kcal./mole are obtained from the low-temperature segments for all four soaps. This value is about the order of magnitude usually associated with the rotation and/or small-amplitude torsional oscillations of the ends of hydrocarbon chains,³³ a reasonable motion in this temperature range.

In view of the limitations in eq. I and of the large size of these molecules, it is not surprising that the plots are not completely linear. Even if the treatment were exact, the presence of a single correlation time in such systems would be surprising. In a long chain of methylene groups, fixed rather firmly in place on one end, each individual group would be in a potential well whose depth and shape would depend upon the distance of the methylene group from the fixed end of the chain. In these systems the fixed end of the chain might be bound by the ionic layers. Molecular motions in such a system could be governed by a distribution of correlation times and activation energies. Multiple dielectric relaxation times have been observed in long-chain halides³⁴ and in methyl palmitate.³⁵

d. Second-Moment Data—Crystalline Phases. The second moments of the four soaps are shown in Figures 8 and 9 as a function of temperature. At the crystalline-subwaxy transition the second moments drop

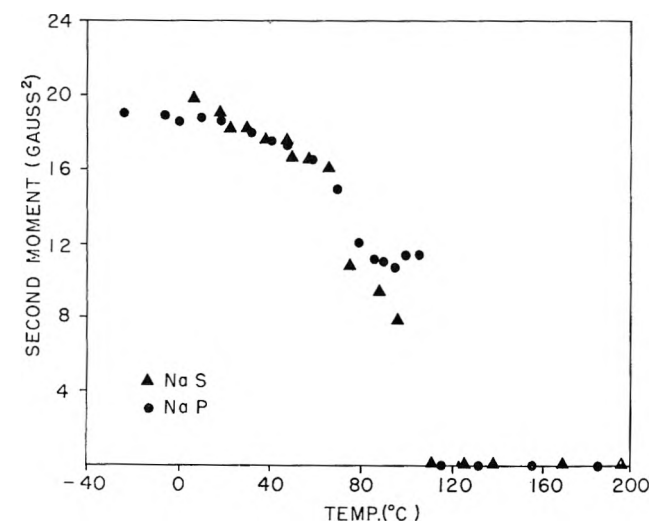


Figure 8. The second moments of sodium stearate and sodium palmitate as a function of temperature.

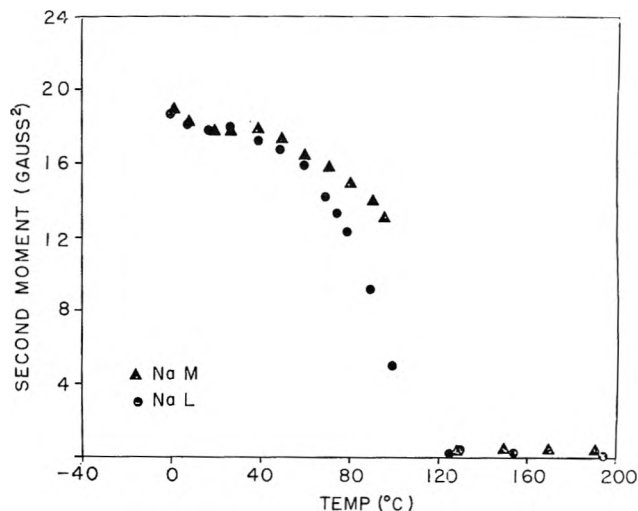


Figure 9. The second moments of sodium myristate and sodium laurate as a function of temperature.

abruptly from values of several gauss² to values which are less than 1 gauss². The values shown in Figures 8 and 9 and elsewhere have been corrected for the effect of modulation amplitude²⁵ but not for modulation frequency.²⁶ This latter correction is considered to be negligible under the conditions used here. The moments were not measured at every temperature at which a line-width measurement was made but were measured about every 8 to 10°.

In Table II are listed the theoretical moments expected for certain molecular motions and also the values expected for rigid-lattice conditions. Also shown in Table II are the experimental moments measured at various significant temperatures.

The theoretical rigid-lattice moments were obtained by using the equation of Van Vleck³⁶ for a powdered sample. For a system of this type, containing two kinds of magnetic nuclei, this equation is

$$\overline{\Delta H^2} = (6/5)I(I+1)g^2\mu_0^2N^{-1}\sum_{i>j}r_{ij}^{-6} + (4/15)I_I(I_I+1)g_I^2\mu_0^2N^{-1}\sum_{j,j'}r_{jj'}^{-6} \quad (\text{III})$$

Here $g\mu_0I$ and $g_I\mu_0I_I$ are the magnetic moments of the hydrogen and sodium atoms, respectively, and N is the number of magnetic nuclei over which the sums are taken. In these salts the contribution to the second moment from the sodium atoms (the last part of eq. III) is very small and has been disregarded.¹²

(33) D. W. McCall and W. P. Slichter, *J. Polymer Sci.*, **26**, 171 (1957).

(34) J. D. Hoffman, *J. Chem. Phys.*, **20**, 541 (1952).

(35) W. Jackson, *Nature*, **164**, 486 (1949).

(36) J. H. Van Vleck, *Phys. Rev.*, **74**, 1168 (1948).

Table II: Experimental and Theoretical Second Moments for Anhydrous Sodium Soaps

Condition	Moments, gauss ²			
	NaS	NaP	NaM	NaL
	Experimental			
90°K.	25.8 ± 1.5	27.9 ± 1.5	27.6 ± 1.6	19.7 ± 3.0
After the crystalline-crystalline transition	9.6 ± 0.2 (88.0°)	11.2 ± 0.2 (86.7°)	13.8 ± 0.2 (89.7°)	... ^a
Prior to the crystalline-subwaxy transition	7.8 ± 0.2 (95.4°)	11.6 ± 0.2 (105.5°)	12.7 ± 0.2 (95.2°)	... ^b
	Theoretical			
Rigid lattice	28.2 ± 1.0	27.9 ± 1.0	27.6 ± 1.0	27.4 ± 1.0
Rotation of the methyl groups	24.3	23.9	23.1	22.2
Rotation of the hydrocarbon chains as a unit about the long axes	9.6	9.4	9.3	9.1

^a This transition is not present in NaL. ^b The line-width change is not sufficiently sharp to allow an exact point to be chosen.

The details of the molecular arrangements in the unit cells have not yet been determined for these sodium soaps. However, it has been assumed that the structures are similar to those of the silver salts for which the structures are known.³⁷ The intramolecular contribution to the rigid-lattice moments were calculated by assuming that the hydrocarbon chains are arranged in a zigzag configuration with tetrahedral angles throughout. The carbon-hydrogen bond length was taken as 1.094 Å. and the carbon-carbon distance as 1.54 Å. Because of the uncertainty about the crystal structures of the sodium salts, the intermolecular contributions were not calculated in detail but were estimated from the values which have been calculated for other sodium and potassium soaps.^{12,16} The values of the intermolecular contributions which have been used for the rigid-lattice calculations are 9.4, 9.1, 8.8, and 8.5 gauss² for NaS, NaP, NaM, and NaL, respectively. These values are estimated to be within ±0.5 gauss² of the actual values unless the structures of sodium and silver salts differ considerably.

A comparison of the calculated rigid-lattice moments and the experimental moments determined at liquid nitrogen temperature indicates that some rotation of the end methyl groups is probably occurring in NaS even at liquid nitrogen temperature. However, the NaP and NaM lattice appear to be rigid at this temperature. Unfortunately, the experimental data for NaL are not sufficiently accurate to allow definite conclusions about the degree of rigidity to be made. It appears that there is more motion present in this material, however, than would be expected if NaL has the same crystal structure as the longer chain soaps. This idea will be discussed in more detail later.

Of interest also are the values of the experimental moments just prior to the crystalline-subwaxy transitions and just after the crystalline-crystalline transitions. The values of the moments at these points allow conclusions to be drawn about the kinds and magnitude of motions present in the crystalline phases.

Gutowsky and Pake²⁴ have shown that the reduction in the second moment resulting from molecular motions can be calculated if the nature of the motion is known. For rotational motions, this calculation involves multiplying each term in the summation in eq. III by the factor

$$F(\phi) = 1/4(3 \cos^2 \phi_{ij} - 1)^2 \quad (\text{IV})$$

where ϕ is the angle between the radius vector r_{ij} and the axis of motion. When the two axes are parallel, there is no reduction, and, when the two axes are perpendicular, the second moment is one-fourth of the rigid-lattice value. Andrew²² has treated the effect of torsional oscillations upon the second moments and found that the reduction is given by

$$\rho = 1 - 3/4[(1 - J_0^2(\alpha)) \sin^2 2\gamma + (1 - J_0^2(2\alpha)) \sin^4 \gamma] \quad (\text{V})$$

In this equation ρ is the ratio of the moments for the oscillating and rigid cases, γ is the angular amplitude of the motion, α is the angle between the axis of reorientation and the internuclear vector r_{ij} , and J_0 is a Bessel function.

From the data shown in Table II it appears that in NaS the hydrocarbon chains are effectively rotating

(37) V. Vand, A. Aitken, and R. K. Campbell, *Acta Cryst.*, 2, 398 (1949).

freely about their long axes just after the crystalline-crystalline transition. However, as pointed out by Andrew,²² it is impossible to decide which kind of motion is responsible for the reduction in the second moment without a detailed knowledge of the depth and shape of the potential wells, but it is quite likely that both rotations and oscillations are present. The rotational states, no doubt, become more populated as the temperature is increased. Using the calculations of Grant and Dunell¹² for the effect of torsional oscillations upon the second moment of NaS, one would require torsional oscillations with amplitudes of about 150° alone to account for the observed second moment. The observed values of 7.8 gauss² for the second moment of NaS prior to the crystalline-subwaxy transition indicates that some longitudinal flexing of the hydrocarbon chain may also be present at this temperature.

The data for NaP and NaM suggest that as the chain length decreases, the amount of motion decreases. The values of the moments for these two soaps could be accounted for either by torsional oscillations or by rotations about the long axes of the hydrocarbon chains.

It appears quite reasonable, on the basis of the second moment values, just after the crystalline-crystalline transition in NaS, NaP, and NaM, that this transition is a second-order transition resulting from molecular rotations and/or oscillations. It is interesting that preliminary calorimetric data collected in our laboratories indicate the presence of a transition of the second kind in the temperature ranges in which the crystalline-crystalline transitions occur.

The behavior of NaL in the crystalline phase appears to be significantly different from the other soaps. A comparison of Figure 4 with Figures 1 through 3 will disclose the difference in the behavior of the line width. The crystalline-crystalline transition observed in the other three homologs is not present in NaL. A comparison of the second-moment data of NaL with those of the other soaps (see Figures 8 and 9) also illustrates the peculiar behavior of NaL as compared to NaS, NaP, and NaM. In the temperature range between about 80 and 100° the second moment of NaL is less than that of NaM. However, Figures 3 and 4 show that in this same temperature region the line width of NaL is the larger. This results from a difference in the line shape. In this region the NaM lines evidently have a larger proportion of the total intensity in the wings although this is not too obvious from comparison of the spectra.

The value of the second moment of NaL around 80°, about the point where the line width begins to decrease

significantly, is about 12 gauss². Table II indicates that this value would be indicative of violent oscillations, or almost free rotation, about the long axes of the hydrocarbon chains based on a structure of the crystalline phase similar to that of the other homologs. In addition, the second-moment value at 100°, the point at which the last of the crystalline phase is present, is 5.0 gauss². On the basis of the calculations illustrated in Table II, this value would indicate that translational motions are present at this temperature. Very little translational motion is expected in the crystalline state; however, self-diffusion of molecules in the crystalline state has been observed.³⁸ Self-diffusion results from the formation of lattice vacancies as a crystalline material is brought to its melting point.

e. Second-Moment Data—Mesomorphic Phases. The measurable second moment expected from an isotropic liquid is of the order of 10⁻⁴ to 10⁻⁵ gauss². As mentioned previously, the second moments of NaS, NaP, NaM, and NaL decrease from values of several gauss² to values of less than 1 gauss² at the crystalline-subwaxy transitions. The moments did not drop to the values one would expect for isotropic liquids. In Table III the second moments of the various phases in the four soaps are tabulated. The values for the subwaxy phase are the least reliable of the mesomorphic phase moments because of the extreme wings on the spectra at these temperatures. The moments were not measured at all points within a given phase at which line width measurements were made. The moments listed in Table II are, for the most part, near the center of the temperature ranges in which the various phases exist. The moments probably show

Table III: Experimental Moments of the Mesomorphic Phases in Anhydrous Soaps

Phase	M_2 , gauss ²	M_4 / M_2^2	Temp., °C.	M_2 , gauss ²	M_4 / M_2^2	Temp., °C.
	NaS			NaP		
Subwaxy	0.84	8.5	126.4	0.29	5.5	133.6
Waxy	0.36	5.8	139.7	0.25	6.0	157.0
Superwaxy	0.24	7.1	169.7	0.13	9.5	185.0
Subneat	0.11	8.5	196.5
	NaM			NaL		
Subwaxy	0.92	4.3	132.6	0.37	6.0	130.3
Waxy	0.60	4.9	149.8	0.21	6.3	155.0
		6.2	169.6			
Superwaxy	0.24	6.5	190.2	0.18	4.8	195.0
Subneat	0.16	8.9	200.0

(38) L. Petrakis and A. Rao, *J. Chem. Phys.*, **39**, 1633 (1963).

approximately the same temperature dependence within a given phase as do the line widths. Two moment values are listed for the waxy phase of NaM. It should be recalled that the line width indicates a phase transition in the temperature range which has previously been considered to cover only the waxy phase. The moments in Table III were measured above and below that transition temperature and offer further proof of the transition.

The values of the moments in the mesomorphic phases indicate that isotropic molecular motion is certainly not present; however, the motion is more extensive than just rotational and/or oscillatory. The moment values are quite reasonable for the kind of structure believed to exist in these phases—that of the hydrocarbon chains existing in a “liquidlike” state with diffusion restrained. Completely free translational motion is restrained by the ionic layers. The width of the polar “ribbons” decreases at the phase transitions, allowing more motion and thus reducing the moment. The moments approach the value expected for an isotropic liquid as the temperature increases.

A comparison of the moments for each of the soaps in a given phase indicates that of the two factors mainly responsible for the values of the moments, temperature and structure, the temperature determines the moment value for the most part. Although the moments were not determined at the same temperatures for each of the samples, it appears that the moments follow about the same order with respect to chain length as do the line widths.

Of interest also are the ratios of the fourth moment to the square of the second moment (M_4/M_2^2) for the mesomorphic phases. This ratio is an indication to some extent of how the line shape changes with temperature. For a lorentzian line, of course, the ratio depends upon the points at which the wings are truncated, but, for a gaussian line, the ratio is 3.³⁹ This ratio is greater than 3 in all cases and in general increases with temperature. This fact, coupled with the knowledge that the ratio of the line width measured at half-maximum intensity to the line width measured at the inflection points decreases with increasing temperature, illustrates, to some extent, how the line shapes in the mesomorphic phases change with temperature. It appears that the lines become sharper near the center with relatively more change occurring in the vicinity of half-maximum intensity than toward the top of the line where the width is determined at the inflection points. While this is happening, however, the intensity far out in the wings remains relatively large. This latter fact accounts for the increase

in the ratios of fourth to second moment squared. Actually, the wings tend to shrink in toward the center but not as rapidly as the center sharpens. This behavior is consistent with the motion of the hydrocarbon chains increasing with temperature while one end remains fixed rather firmly in place by the action of the ionic layer.

Summary

From the line widths, second moments, and line shapes some conclusions can be made about the behavior of the four soaps in the temperature range covered in this study.

There are only small differences among the data for sodium stearate, sodium palmitate, and sodium myristate, and these can be accounted for reasonably well by the differences in the length of the hydrocarbon chains. The data from sodium laurate suggest that there may be significant differences between the crystal structure of this material and those of the other soaps, and possibly some differences also between the structures of the mesomorphic phases.

The prominent forms of motion in the crystalline state are probably oscillations and rotations of the paraffin chains. This motion appears to be completely frozen out in sodium palmitate and sodium myristate at liquid nitrogen temperature, but in sodium stearate there appears to be some rotation of the methyl groups at this temperature. Again, it appears that the value of the second moment of sodium laurate at this temperature cannot be reconciled with the expected motions if the crystalline structure is assumed to be the same as the other homologs.

Crystalline-crystalline phase transitions, which appear to be of the second kind, are present in sodium stearate, sodium palmitate, and sodium myristate. If an identical transition is present in sodium laurate, it evidently merges with the crystalline-subwaxy transition. The widths and moments of the lines from the mesomorphic phases are consistent with the structural picture suggested by X-ray studies for these phases.³ The shape of the lines—“super-lorentzian”—observed in the mesomorphic phases appears to result from the hydrocarbon chains existing in a “liquidlike” environment on the one end and a “solidlike” environment on the other. This situation produces a distribution of correlation times which, in turn, produces a resonance band which is made up of a distribution of lines having varying widths.

(39) A. Abragam, “The Principles of Nuclear Magnetism,” Oxford University Press, London, 1961.

Measurement of the lines arising from the mesomorphic phases under the condition $\nu_m \gg \bar{\gamma}\Delta H$ produces a line width which is very sensitive to changes in the systems and, in addition, removes the artificial line broadening produced by the modulation field H_m .

All known phase transitions in the temperature range covered in this investigation have been detected. In addition, in sodium myristate an apparent transition

at 162° has been detected. This transition has not previously been reported.

Acknowledgments. The authors wish to express their appreciation to their associates who aided in this investigation. Special thanks are due to M. C. Beisner for recording the spectra, to R. G. Folzenlogen for preparing the acids, and finally to A. J. Mabis and F. B. Rosevear for instructive advice and criticism.

Thermodynamics of the Exchange of Tetramethylammonium with Sodium Ions in Cross-Linked Polystyrene Sulfonates at 25°¹

by A. Schwarz and G. E. Boyd

Oak Ridge National Laboratory, Oak Ridge, Tennessee 37831 (Received July 12, 1965)

A thermodynamic computation of the selectivity coefficient for the ion-exchange equilibrium between tetramethylammonium (TMA) and sodium ion in dilute aqueous mixtures and cross-linked polystyrene sulfonates was carried out by applying the Gibbs-Donnan equation to measurements of equivalent water contents and volumes on lightly cross-linked preparations. A comparison of the experimentally determined selectivity coefficients with those computed showed satisfactory agreement within the errors involved. The configurational free energy increase in the molecular network of the ion exchanger when the relatively large TMA cation was taken up was shown to be an important factor in determining the observed strong inversion in the selectivity coefficient as the cross linking was increased. Indirect indication of "site binding" of Na⁺ ion in the more highly cross-linked preparations was obtained from the calculated behavior of the activity coefficient ratio for sodium and TMA ions in the exchanger.

Ion-exchange reactions involving the quaternary ammonium ions in aqueous solutions are of interest because studies with them serve to shed light on the role of size and hydration in determining the selective uptake of cations by cross-linked organic ion exchangers. In previous work,^{2a,b} a quantitative description of the dependence of the mass law concentration product ratio for ion-exchange equilibria on exchanger cross linking and ionic composition was achieved with the Gibbs-Donnan equation.³ This equation, which may be written as

$$\log K_a = P\Delta\bar{v}/2.3RT \quad (1)$$

relates the thermodynamic equilibrium constant, K_a , for an exchange reaction to the configurational

(1) Presented before the Division of Physical Chemistry, 150th National Meeting of the American Chemical Society, Atlantic City, N. J., Sept. 1965. Research sponsored by the U. S. Atomic Energy Commission under contract with the Union Carbide Corp.

(2) (a) G. E. Myers and G. E. Boyd, *J. Phys. Chem.*, **60**, 521 (1956); (b) G. E. Boyd, S. Lindenbaum, and G. E. Myers, *ibid.*, **65**, 577 (1961).

(3) F. G. Donnan and E. A. Guggenheim, *Z. physik Chem.*, **162A**, 346 (1932).

free energy change in the molecular network of the ion exchanger, which may be expressed as a product of a pressure and a partial molal volume change. A method for estimating the mass law concentration product ratio, or selectivity coefficient, D , can be based on eq. 1. Thus, the selectivity coefficient for the exchange of singly charged cations, 1 and 2, with 2, the preferred ion, is^{2a}

$$\log D_1^2 = P(\bar{v}_1 - \bar{v}_2)/2.3RT + \log (\gamma_1/\gamma_2)_r - 2 \log (\gamma_1/\gamma_2)_w \quad (2)$$

When the quantity P in eq. 2 is large, as with highly cross-linked exchangers, and/or when $(\bar{v}_1 - \bar{v}_2)$ is large, as in exchange reactions with large cations, neglect of the first term on the right-hand side of eq. 2 may lead to large errors. For example, in the exchange of tetraalkylammonium ion with Na^+ ion, the quantity $P\Delta\bar{v}/2.3RT$ may be more important in setting the value of $\log D_1^2$ than the term $\log (\gamma_1/\gamma_2)_r$. In our earlier investigations^{2a} on the exchange of H^+ , Li^+ , K^+ , and Cs^+ ions with Na^+ ion, the term $\log (\gamma_1/\gamma_2)_r$ was dominant. This paper reports a study of the exchange of tetramethylammonium ion (TMA) with Na^+ ion in several cross-linked polystyrene sulfonates. Each of the terms on the right-hand side of eq. 2 will be computed, and their sum will be compared with values of $\log D_1^2$ measured in equilibrium distribution experiments at 25°.

Experimental Section

Materials. Four polystyrene sulfonate exchangers nominally cross linked with 0.5, 2, 4, and 8% divinylbenzene (DVB) were used. These preparations were obtained from the Dow Chemical Co. and were designated as Dowex 50W. Their exchange capacities, measured by electrometric pH titrations in 2 *N* aqueous salt solutions, were 5.46, 5.20, 5.32, and 5.19 mequiv./g. of dry H-form, respectively.⁴ The exchange capacity for tetramethylammonium ion (TMA), which was determined by self-exchange with ¹⁴C-labeled TMA and by elution of an aliquot of exchanger in the ¹⁴C-labeled TMA form with HCl, was the same as for sodium ion within experimental error for all but the 8% DVB preparations where a value of 5.01 (96.6% of full capacity) was found.

After pretreatment to remove metallic impurities and linear polyelectrolyte, a bed of exchanger in the Na-form was placed in a jacketed column maintained at 25°, and an excess of solution of the desired composition was passed until equilibrium was reached. After removing the solution from the bed, the exchanger was washed and stored in a closed vessel over saturated MgCl_2 solution at room temperature. The water content of an aliquot was determined by drying to a con-

stant weight under vacuum trapped with liquid nitrogen. These preparations of varying ionic composition⁵ and cross linking were employed in the measurements of selectivity coefficients and in the equivalent water and equivalent volume determinations described below.

Reagent grade chemicals were used as received except for the tetramethylammonium chloride, which was purified additionally by recrystallization from methanol-water.

Selectivity Coefficient Measurements. Determinations of the equilibrium selectivity coefficients, $D_{\text{Na}}^{\text{TMA}}$ were performed with mixed aqueous electrolyte solutions at an ionic strength, $\mu = 0.1$, except with the 0.5% DVB exchanger where $\mu = 0.01$. Carbon-14-labeled TMA⁶ and 14.8-hr. ²⁴Na were employed as tracers. Further purification of the TMA ¹⁴C was achieved by heating the compound under reduced pressure (2–3 mm.) at 50° and collecting the volatile impurities in a liquid nitrogen-chilled trap. This operation was repeated until negligibly small amounts of ¹⁴C activity (4–5 times background) were condensed. Proof of the purity of the TMA ¹⁴C employed was obtained by eluting a small sample from the top of a columnar ion-exchange bed (Dowex 50W-8, Na form) with 0.1 *M* NaCl. The elution curve showed but a single peak whose area was equal to the initial activity placed on the bed. Additionally, the weight distribution coefficient computed from the column parameters was in agreement with that estimated from other experiments.

Assays of the γ -ray emitting ²⁴Na were performed with a well-type thalliated NaI crystal scintillation counter. Carbon-14 was measured by liquid scintillation methods; however, it was necessary to count aqueous electrolyte solutions so that the more highly efficient toluene-base counting mixture could not be used. The following mixture gave a 47% counting yield (including instrument losses) without phase separation when 1 ml. of 0.1 *M* neutral aqueous electrolyte was dissolved in 15 ml.: (a) 3000 ml. of *p*-dioxane (Matheson Coleman and Bell); (b) 300 g. of naphthalene recrystallized from alcohol (Eastman Organic Chemical Co.); 28.0 g. of 2,5-diphenyloxazole, PPO (Packard Instrument Co.); (d) 1.0 g. of 1,4-bis-2-(5-phenyloxazolyl)benzene, POPOP (Packard Instrument Co.); (e) 200.0 g. of deionized water. A Model

(4) Analyses for the sulfur content of the exchangers were in agreement with these exchange capacity values.

(5) Ionic composition was expressed as equivalent fraction of TMA, x_{TMA} .

(6) Nuclear Chicago Co., Des Plaines, Ill. Specific activity = 1.5 meuries/mmole; radiochemical purity 99% by dilution analysis.

314 EX Tri-Carb liquid scintillation counting system was employed.

A rate study was conducted to determine the time necessary for the attainment of ion-exchange equilibrium. The homoionic ^{14}C -labeled TMA salt of the 8% DVB cross-linked exchanger was caused to exchange with TMA in aqueous solution in a "finite bath" experiment. Eighty per cent of equilibrium was reached in 2.0 min.; a 24-hr. period, accordingly, was considered sufficient for the establishment of an isotopic redistribution.

The possibilities that ^{14}C in the TMA might exchange with the ion-exchange copolymer or that not all of the labeled TMA is removed from the exchanger when it was eluted with 1 *M* HCl⁷ were investigated. A ^{14}C -labeled TMA salt of the 8% DVB exchanger was prepared and allowed to stand. The exchanger was then converted to the H form by treatment with an excess of 1.0 *M* HCl. Approximately 1.6 g. was dissolved in 100 ml. of 6% H_2O_2 containing 150 mg. of $\text{FeSO}_4 \cdot 7\text{H}_2\text{O}$ and the gases evolved were collected in 0.1 *M* NaOH. Virtually no ^{14}C activity was found in either the aqueous solution or in the base, indicating that the amount of ^{14}C that might have entered the structure of the exchanger or remained attached to exchange sites was negligible.

Self-exchange reactions with ^{14}C -labeled TMA and ^{24}Na were employed in the selectivity coefficient determinations. Aliquots of pre-equilibrated exchanger whose preparation was described above were placed in contact with solution identical in composition with that with which it had been brought to equilibrium but containing ^{24}Na and TMA- ^{14}C tracers. After mixing in a thermostated bath at 25.0° for 24 hr., the phases were separated and the exchanger was regenerated with 1.0 *M* HCl. The ^{24}Na γ -ray activity in an aliquot of the eluate was counted with a well-type crystal scintillation counter setting the discriminator level high enough to exclude pulses from ^{14}C bremsstrahlen. The ^{24}Na half-life and γ -ray spectrum were compared with standards to establish the purity of the tracer. The ratio of γ -activity in the exchanger to that in the aqueous phase was observed not to change with time, indicating that an isotope of constant half-life was measured in both phases. On several occasions in self-exchange experiments where $x_{\text{TMA}} = 1.00$ the aqueous phase was analyzed for sodium by flame photometry. The amount of Na found was close to the limit of detection of the method and, hence, was vanishingly small. The absence of sodium confirmed the assumption that a valid self-exchange experiment had been performed.

The ^{14}C -labeled TMA in the 1 *M* HCl eluate⁸ was

measured after a lapse of at least 12 half-lives of the ^{24}Na . The activity of the latter was found to have decreased to background after this time when measured either with a multichannel analyzer or by an integral count rate determination. As an additional check, the β activities of two samples, one of which had ^{24}Na added, were compared with a liquid scintillation counter. There was no interference by the ^{24}Na with the ^{14}C activity measurement after a decay of 7 days.

Numerical values for the selectivity coefficient for the uptake of the preferred TMA ion⁹ were derived from measurements of the radioactivities of the TMA and Na^+ ions in the exchanger and in the aqueous phase, respectively

$$D_{\text{Na}}^{\text{TMA}} = \frac{[(\text{TMA})_r/(\text{TMA})_w]}{[(\text{Na}^+)_r/(\text{Na}^+)_w]} \quad (3)$$

The equivalent fraction of TMA in the exchanger, x_{TMA} , was obtained from

$$x_{\text{TMA}} = \frac{D_{\text{Na}}^{\text{TMA}}(x_{\text{TMA}})_w}{1 + (D_{\text{Na}}^{\text{TMA}} - 1)(x_{\text{TMA}})_w} \quad (4)$$

where $(x_{\text{TMA}})_w$ is the aqueous phase equivalent fraction. An activity balance was made in each experiment to reduce the possibility of systematic errors caused by adsorption losses, etc.

The fact that only 96.6% of the exchange capacity of the 8% DVB preparation was available for the TMA ion (see above) made it necessary to correct $D_{\text{Na}}^{\text{TMA}}$ for the unavailable exchange sites. The selectivity coefficients reported for this preparation, therefore, must be considered less accurate than with the other preparations because they have been based on capacity rather than on counting ratio determinations.

Equivalent Water Content Measurements. The isopiestic vapor pressure comparison procedure for the measurement of the equivalent water contents, x_w , of the various ion exchanger preparations as a function of water activity, a_w , has been described.¹⁰ Saturated salt solutions of accurately known a_w were used as references¹¹ when available; otherwise, NaCl solutions

(7) Micro amounts of tetraethylammonium ion were found by D. K. Hale, D. I. Packham, and K. W. Pepper, *J. Chem. Soc.*, 844 (1953), to be taken up strongly by the H-form of a 15% DVB cross-linked polystyrene sulfonate.

(8) The presence of acid or salts at concentrations above 0.1 *m* caused an appreciable lowering in the efficiency for counting TMA- ^{14}C . Unsuccessful attempts were made to overcome this "chemical quenching." The procedure finally used was to adjust the counting mixtures prepared from the aqueous and eluent phases, respectively, to the same composition.

(9) The "preferred ion" was defined as that ion which is selectively extracted by the most weakly cross-linked exchanger (*i.e.*, the 0.5% DVB preparation).

(10) S. Lindenbaum and G. E. Boyd, *J. Phys. Chem.*, 68, 911 (1964).

(11) R. H. Stokes and R. A. Robinson, *Ind. Eng. Chem.*, 41, 2013 (1949).

were employed. These latter solutions were analyzed for Cl^- ion by potentiometric titration when vapor pressure equilibrium had been attained. Isopiestic equilibrium with the exchangers was approached from both directions (*i.e.*, by the uptake or loss of water), and measurements were conducted in duplicate on the 0.5, 2, and 8% DVB exchangers. Water contents of the 4% DVB preparation in equilibrium with 0.1 *m* electrolyte solutions were found by measuring the increase in concentration of a ^{32}P -tagged high molecular weight polyphosphate solution when partially dried exchanger was immersed in it and osmotic equilibrium was established.

Equivalent Volume Measurements. Varying compositions (*i.e.*, x_{TMA}) of the 2% DVB exchanger in equilibrium with various known water activities were employed in the equivalent volume measurements. Dry *n*-octane (synthetic, Matheson Coleman and Bell) was used as a displacement liquid in a pycnometric technique described elsewhere.^{2b} The *n*-octane was dried by passing it through a deep bed of Linde 4A molecular sieve. The density of the dried liquid was found in good agreement with the literature value.

Experimental Results and Treatment of Data

The variation of the selectivity coefficient, $D_{\text{Na}^{\text{TMA}}}$ for the uptake of TMA with exchanger cross linking and composition is shown in Figure 1. The curves drawn through the experimental points shown represent a least-squares fit to a quadratic equation in x_{TMA} . An unusual feature is the strong selectivity reversal as the cross linking of the polystyrene sulfonate increased. With the 0.5% DVB exchanger, tetramethylammonium ion was preferred for all compositions; with the 8% DVB exchanger, Na^+ ion was preferred for all compositions.¹² This behavior contrasts with the selective uptake of Cs^+ ion by the sodium form of polystyrene sulfonates where $D_{\text{Na}^{\text{Cs}^+}}$ was observed to increase with cross linking.^{2a}

The measurements of the equivalent water contents, x_w , are given in Table I as a function of water activity (*i.e.*, $-\log a_w$) and ionic composition for the 0.5 and 2% DVB preparations. These data, and those for the 8% DVB exchanger which are not listed, were converted to weight normalities by the relation $N_m = 1000/x_w$ and fitted by least squares to a polynomial in $-\log a_w$.¹³

$$N_m = \alpha + \beta(-\log a_w) + \gamma(-\log a_w)^2 \quad (x_{\text{TMA}} \text{ constant}) \quad (5)$$

Equation 5 was applied in several ways in the computation of the first and second terms on the right-hand

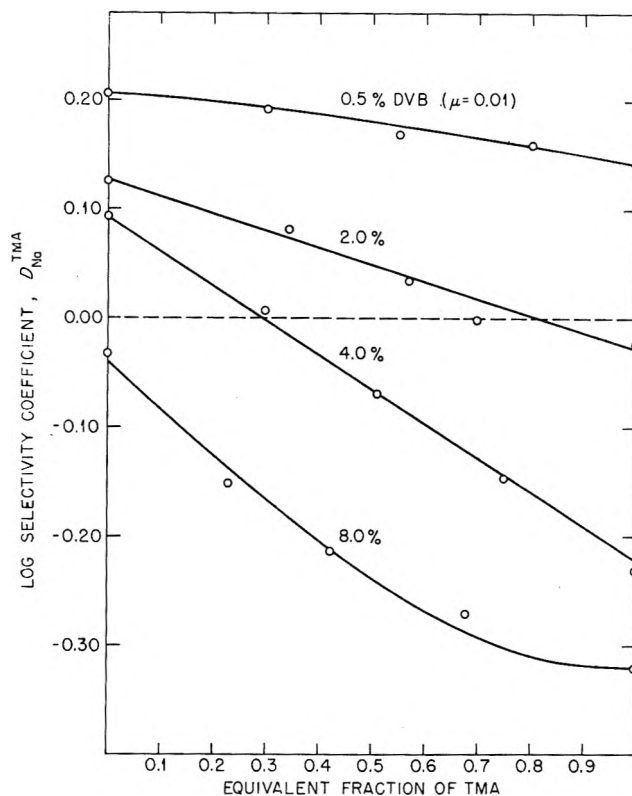


Figure 1. Equilibrium selectivity coefficients at 25° for the exchange of tetramethylammonium with sodium ions on variously cross-linked polystyrene sulfonate; ($\mu = \text{C.10}$).

side of eq. 2. In the estimation of the configurational free energy, the quantity P is computed from¹⁴

$$P = (RT/\bar{v}_w) \ln (a_w'/a_w) \quad (N_m \text{ constant}) \quad (6)$$

where \bar{v}_w is the partial molal volume of water in the exchanger and a_w' and a_w are the water activities in a cross-linked preparation and in a chemically identical exchanger so lightly cross linked that $P = 0$, respectively.

The data of Table I also were employed in the evaluation of the activity coefficient ratio, $\log (\gamma_{\text{Na}^+}/\gamma_{\text{TMA}^+})_r$, by means of the equation^{2a}

$$\log (\gamma_{\text{Na}^+}/\gamma_{\text{TMA}^+})_r = \log (\gamma_{\text{Na}^+}^*/\gamma_{\text{TMA}^+}^*)_r - 0.05551I_R \quad (7a)$$

where the integral, I_R , is defined by

(12) A pronounced reversal in the selectivity coefficient with cross linking in polystyrene sulfonate exchangers also has been observed in the exchange of tetramethylammonium ion with potassium ion by H. P. Gregor and J. I. Bregman, *J. Colloid Sci.*, **6**, 323 (1951).

(13) The constants α , β , and γ in eq. 5 will be supplied on request.

(14) G. E. Boyd and B. A. Soldano, *Z. Elektrochem.*, **57**, 162 (1953).

$$I_R = \int_0^{-\log a_w} (\partial x_w / \partial x_{TMA})_{a_w} d(-\log a_w) \quad (x_{TMA} \text{ constant}) \quad (7b)$$

The quantity, $\log (\gamma_{Na^*} / \gamma_{TMA^*})_r$, was obtained from measurements of the selectivity coefficient, D^* , on the 0.5% DVB preparation in equilibrium with highly dilute aqueous electrolyte mixtures. In this case the first and third terms on the right-hand side of eq. 2 become negligibly small, and

$$\log D^* = \log (\gamma_{Na^*} / \gamma_{TMA^*})_r \quad (8)$$

The required values of the coefficient, $(\partial x_w / \partial x_{TMA})_{a_w}$, which is a function of $-\log a_w$ and x_{TMA} , were found by computing x_w for chosen values of x_{TMA} and $-\log a_w$ from eq. 5. These interpolated x_w values were fitted by least-squares methods to an empirical equation of the form

$$x_w = a + bx_{TMA} + cx_{TMA}^2 \quad (-\log a_w \text{ constant}) \quad (9)$$

A plot of the derived $(\partial x_w / \partial x_{TMA})_{a_w}$ values as a function of $-\log a_w \equiv y$ for the 0.5% DVB and 2% DVB exchangers with $x_{TMA} = 0.0, 0.5$, and 1.0 is given in Figure 2. The curves shown were computed from the "least-squares" equation

$$(\partial x_w / \partial x_{TMA})_{a_w} = A_1 e^{-A_2 y} + A_3 e^{-A_4 y} \quad (10)$$

This equation was employed because of the unsymmetric maxima observed in Figure 2. The appropriate values of $-\log a_w$ for the upper limit of the integral in eq. 7b were obtained by substituting the x_w values for the more highly cross-linked exchangers in eq. 5 for the 0.5% DVB preparation and solving the quadratic. It is evident from Figure 2 that the quantity I_R is positive over a wide range in $-\log a_w$.

The measured equivalent volumes, V_e , were employed to compute the quantity $(\bar{v}_{Na} - \bar{v}_{TMA})$, also required to estimate the configurational free energy of the copolymer molecular network. The experimental V_e (ml. equiv.⁻¹) for $x_{TMA} = 0.00, 0.342, 0.569, 0.800$, and 1.00 taken on the 2% DVB exchanger with varying x_w (g. of H₂O equiv.⁻¹) were fitted to the empirical equation^{2b}

$$V_e = V_a + 1.00298x_w^2 / (b + x_w) \quad (11)$$

where V_a is the equivalent volume of the anhydrous exchanger and b is the fractional molar volume defect (Table II). Values of 142.0 and 221.0 ml. equiv.⁻¹ were observed experimentally for V_a for the sodium and tetramethylammonium forms, respectively. The computation of the difference in the partial molal volumes of these forms was based on the equation^{2a}

Table I: Equivalent Water Contents (g. of H₂O/equiv.) of the Sodium and Tetramethylammonium (TMA) Salts of Nominal 0.5% and 2.0% DVB Cross-Linked Polystyrene Sulfonate as a Function of Water Activity and TMA Equivalent Fraction

Equivalent fraction, x_{TMA}	$-\log a_w$																
	0.00131	0.00160	0.00168	0.00189	0.00877	0.01176	0.01495	0.03395	0.04484	0.07438	0.09807	0.12332	0.14978	0.20901	0.27687	0.4815	
	0.5% DVB																
0.000	2052	1290	474.8	...	314.0	179.8	148.8	114.9	98.2	83.5	76.2	63.1	51.2	38.6	
0.401	2045	1291	505.0	...	344.1	206.0	171.3	125.2	106.1	90.3	80.1	65.0	50.9	36.2	
0.643	2071	1289	516.4	...	350.8	219.5	183.4	130.9	111.1	94.7	81.3	(62.5)	52.5	35.4	
0.853	2056	521.8	428.8	...	228.2	192.2	138.9	119.6	99.1	84.7	67.3	54.8	39.5	
1.000	2087	525.1	433.1	...	233.2	197.1	(137.3)	124.0	99.7	89.1	69.4	57.3	40.1	
	2.0% DVB																
0.000	...	508.6	511.8	...	342.5	298.7	...	174.2	152.9	117.3	104.8	89.3	82.3	68.3	54.5	40.7	
0.342	495.1	481.7	351.0	...	276.3	187.6	160.6	120.0	105.6	89.2	80.3	65.1	51.9	35.8	
0.569	489.7	475.5	356.8	...	285.6	198.1	169.7	125.8	109.3	92.2	82.7	66.3	53.3	36.7	
0.800	...	479.8	482.2	...	359.1	324.0	...	206.8	178.2	133.0	116.1	97.1	85.6	68.9	56.4	38.4	
1.000	...	474.0	475.9	...	359.5	326.5	...	212.1	183.9	136.8	121.2	100.0	89.3	72.2	59.6	41.8	

$$(\bar{v}_{\text{Na}} - \bar{v}_{\text{TMA}}) = \Delta V_a - \int_0^{x_w} (\partial \bar{v}_w / \partial x_{\text{TMA}})_{x_w} dx_w \quad (x_{\text{TMA}} \text{ constant}) \quad (12)$$

The required values of the partial molal volume of water, $\bar{v}_w = (\partial V_a / \partial x_w)_{x_{\text{TMA}}}$, were computed from eq. 11 and fitted to the empirical equation

$$\bar{v}_w = a + bx_{\text{TMA}} + cx_{\text{TMA}}^2 \quad (x_w \text{ constant}) \quad (13)$$

from which $(\partial \bar{v}_w / \partial x_{\text{TMA}})_{x_w}$ values were computed. These differential coefficients were fitted to empirical equations which were used to evaluate the integral

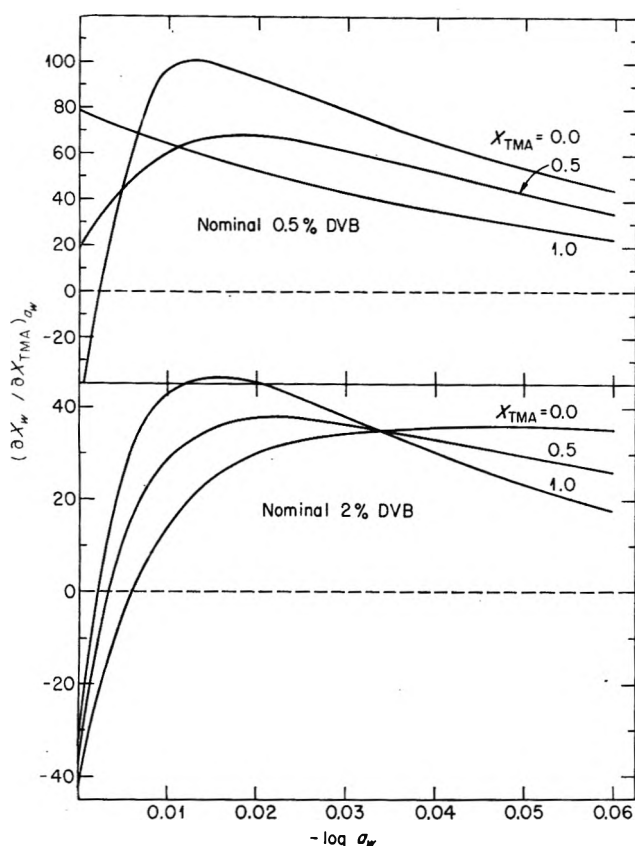


Figure 2. Variation of $(\partial x_w / \partial x_{\text{TMA}})_{a_w}$ with $-\log a_w$ for cross-linked polystyrene sulfonate.

Table II: Least-Squares Parameters for the Variation of Equivalent Volumes (ml.) of Tetramethylammonium-Sodium Salt Forms with Equivalent Water Content (g. equiv.⁻¹) According to Eq. 11

x_{TMA}	V_a	b	Range of x_w
0.000	144.8	25.1	0.1-385.9
0.342	168.4	21.4	0.1-395.3
0.569	187.7	17.3	0.1-420.1
0.800	203.9	13.7	0.1-373.7
1.000	219.2	12.6	0.1-408.3

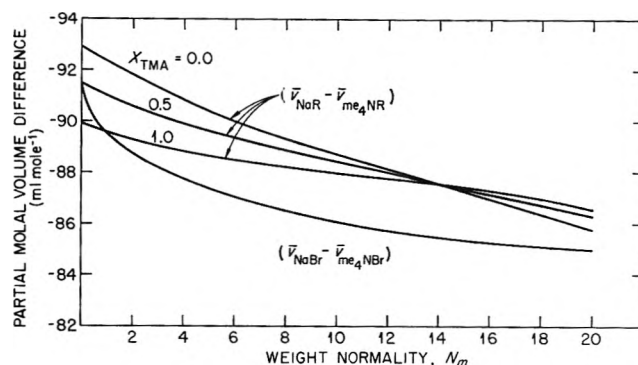


Figure 3. Variation of partial molal volume difference of tetramethylammonium and sodium resinate with weight normality.

in eq. 12. The results of the calculations based on eq. 12 are shown in Figure 3 where it may be seen that the difference, $(\bar{v}_{\text{Na}} - \bar{v}_{\text{TMA}})$, is relatively quite large. For example, the difference, $(\bar{v}_{\text{Na}} - \bar{v}_{\text{Ca}})$ was but -18 ml. equiv.⁻¹, approximately.^{2a} Recent measurements¹⁵ of the partial molal volumes of tetramethylammonium bromide in aqueous solutions allow a calculation of the difference, $(\bar{v}_{\text{NaBr}} - \bar{v}_{\text{TMABr}})$, which is shown in Figure 3 for purposes of comparison.¹⁶ It is seen that a fair concordance between the two sets of measurements exists as would be expected; this fact suggests that V_a values measured on the 2% DVB exchanger are reliable.

The third term on the right-hand side of eq. 2, $-2 \log (\gamma_{\text{NaCl}} / \gamma_{\text{TMACl}})_w$, is a measure of the ionic interactions in the dilute aqueous electrolyte mixture in equilibrium with the ion exchanger. The contribution of this term for a 0.1 *m* solution is expected to be small. Its evaluation was accomplished by applying Harned's rule and estimating α with a procedure¹⁷ suggested by Guggenheim. The equation was

$$\log (\gamma_{\text{NaCl}} / \gamma_{\text{TMACl}})_w = \log (\gamma_{\text{NaCl}(0)} / \gamma_{\text{TMACl}(0)}) - (b'_{\text{NaCl}} - b'_{\text{TMACl}})m \quad (14)$$

where $\gamma_{\text{NaCl}(0)}$ and $\gamma_{\text{TMACl}(0)}$ are the activity coefficients of pure NaCl and TMACl solutions at molality, *m*, and the quantities b' are obtained from the relation $b' = 0.4342 (10\phi - 9.19)$, where ϕ is the molal osmotic coefficient at *m*. The derived value of $2 \log (\gamma_{\text{NaCl}} / \gamma_{\text{TMACl}})_w$ was 0.0210 when *m* = 0.1, independent of the equivalent fraction of TMACl in the mixed

(15) W. Y. Wen and S. Saito, *J. Phys. Chem.*, **68**, 2639 (1964).

(16) Values for \bar{v}_{NaBr} as a function of concentration were computed with the equations and values of ϕ^0 and S_v given by H. S. Harned and B. B. Owen, "Physical Chemistry of Electrolyte Solutions," Reinhold Publishing Corp., New York, N. Y., 1959, p. 361.

(17) R. A. Robinson and R. H. Stokes, "Electrolyte Solutions," Butterworth and Co. Ltd., London, 1955, p. 440.

Table III: Computation of the Equilibrium Selectivity Coefficient, D_{Na}^{TMA} , for the Exchange of Tetramethylammonium with Sodium Ion for Various Ionic Compositions of Nominal 2, 4, and 8% DVB Cross-Linked Polystyrene Sulfonate^a

$$\log D_{Na}^{TMA} = P\Delta\bar{v}/2.3RT + \log (\gamma_{Na}/\gamma_{TMA})_r - 0.0210$$

% DVB	x_{TMA}	x_w	$-\log a_w$	$\log (\gamma_{Na}^*/\gamma_{TMA}^*)_r$	$0.05551I_R$	$\log (\gamma_{Na}/\gamma_{TMA})_r$	P	$-\Delta\bar{v}$	$-P\Delta\bar{v}/2.3RT$	D_{calcd}	D_{obsd}/D_{calcd}
2	0.00	503	0.0077	0.2058	0.0136	0.1922	20	91.9	0.0317	1.38	0.97
	0.50	497	0.0084	0.1830	0.0192	0.1638	22	90.6	0.0350	1.28	0.88
	1.00	486	0.0099	0.1408	0.0410	0.0998	26	89.3	0.0417	1.09	0.86
4	0.00	310	0.0157	0.2058	0.0557	0.1501	45	91.2	0.0721	1.14	1.08
	0.50	249	0.0266	0.1830	0.0854	0.0976	79	89.8	0.1251	0.89	0.97
	1.00	190	0.0467	0.1408	0.1330	0.0078	141	88.4	0.2215	0.58	1.03
8	0.00	192	0.0306	0.2058	0.1300	0.0758	91	90.1	0.1451	0.81	1.13
	0.50	180	0.0431	0.1830	0.1390	0.0440	130	89.2	0.2058	0.66	0.88
	1.00	174	0.0529	0.1408	0.1430	-0.0022	161	88.3	0.2517	0.53	0.91

^a Based on the 0.5% DVB exchanger.

Table IV: Computation of the Equilibrium Selectivity Coefficient, D_{Na}^{TMA} , for the Exchange of Tetramethylammonium with Sodium Ion for Various Ionic Compositions of Nominal 4 and 8% DVB Cross-Linked Polystyrene Sulfonate^a

$$\log D_{Na}^{TMA} = P\Delta\bar{v}/2.3RT + \log (\gamma_{Na}/\gamma_{TMA})_r - 0.0210$$

% DVB	x_{TMA}	x_w	$-\log a_w$	$\log (\gamma_{Na}^*/\gamma_{TMA}^*)_r$	$0.05551I_R$	$\log (\gamma_{Na}/\gamma_{TMA})_r$	P	$-\Delta\bar{v}$	$-P\Delta\bar{v}/2.3RT$	D_{calcd}	D_{obsd}/D_{calcd}
4	0.00	310	0.0114	0.1801	0.0145	0.1656	45	91.2	0.0721	1.18	1.04
	0.50	249	0.0214	0.1047	0.0263	0.0784	79	89.8	0.1251	0.86	1.01
	1.00	190	0.0416	0.0349	0.0505	-0.0156	141	88.4	0.2215	0.55	1.08
8	0.00	193	0.0295	0.1801	0.0593	0.1208	91	90.1	0.1451	0.90	1.01
	0.50	180	0.0390	0.1047	0.0614	0.0433	130	89.2	0.2058	0.66	0.88
	1.00	174	0.0486	0.0349	0.0645	-0.0296	161	88.3	0.2517	0.50	0.97

^a Based on the 2.0% DVB exchanger corrected to $P = 0$ and $\mu = 0.01$.

electrolyte. The values for $\gamma_{TMACl(0)}$ and ϕ_{TMACl} at 0.1 *m* were taken from a recent publication.¹⁰

Discussion and Conclusions

A summary of the calculations of the selectivity coefficient, D_{Na}^{TMA} , as a function of the cross linking and ionic composition of the exchanger is afforded by Table III. These calculations were based on the measured properties of the most lightly cross-linked preparation (*e.g.*, 0.5% DVB) which was taken as the reference exchanger. In principle, the thermodynamic procedure described above allows the calculation of the selectivity coefficient for any cross-linked exchanger relative to the properties of a more lightly cross-linked one. This point is illustrated by Table IV, where the 2% DVB exchanger was taken as the reference.

The calculated D_{Na}^{TMA} values in Tables III and IV are believed to show a satisfactory agreement with the experimentally measured values. The agreement is

better with the 2% DVB cross-linked exchanger as the reference principally because of the greater accuracy with which its equivalent water content was measured for small values of $-\log a_w$. However, an additional cause was the fact that the equivalent weight of the 2% DVB exchanger (192.1) was much closer to that for the 4% (188.1) and for the 8% (192.6) preparations than was the equivalent weight of the 0.5% DVB exchanger (183.0). The thermodynamic calculations were based on the assumptions that: (a) the ion exchangers may be regarded as homogeneous, ternary mixtures of tetramethyl resinate, sodium resinate, and water, and (b) the lightly cross-linked reference exchangers are chemically identical with the more highly cross-linked exchangers. Assumption b especially breaks down for preparations with 8% DVB and greater because of the increased organic content of these exchangers, and because of the increasing number of sulfonate groups on the cross links. The importance

of such changes in composition and structure have been elucidated in the extensive research of Bonner¹⁸ with aqueous solutions of "model" compounds. It may be concluded from these investigations that an increase in selectivity coefficient should accompany an increase in the equivalent weight of an exchanger, and it is of interest to note that the differences between the experimental and calculated selectivity coefficients given in Table III are in this direction.

The relative contributions of the various terms in eq. 2 to $\log D_{\text{Na}^+/\text{TMA}^+}$ for varying water content (and, hence, cross linking) when $x_{\text{TMA}} = 0.0$ are shown in Figure 4. It is evident that an important cause of the large decrease in the selective uptake of tetramethylammonium ion with increasing cross linking is the large increase in the configurational free energy (*i.e.*, the $P\Delta\bar{v}/2.3RT$ term) of the polymer molecular network when the large quaternary ammonium ion enters the exchanger. The magnitude of the selectivity coefficient reversal is accounted for quantitatively by the right-hand side of eq. 2, and this fact greatly increases our confidence in the essential correctness of the model on which the thermodynamic derivation of eq. 1 was based. The observed selectivity coefficient decrease, as the fraction of TMA in all the exchangers was increased (Figure 1), and the reversal found with the 4% DVB exchanger also were reflected in the thermodynamic calculations (*cf.* Tables III and IV).

It is of further interest to note that the ionic interactions in the exchanger, which are reflected by the term $\log(\gamma_{\text{Na}^+}/\gamma_{\text{TMA}^+})_r$, were such as to decrease the selectivity for tetramethylammonium ion with increased cross linking. This behavior, of course, indicates that the activity coefficient for Na^+ ion in the exchanger decreases more rapidly with increased N_m than does γ_{TMA^+} , and it suggests that possibly "site binding" of Na^+ ion becomes increasingly important as the water content of the exchanger decreases. The TMA ion is believed to be only slightly hydrated,¹⁹ and the mechanism of its interaction with the sulfonate groups probably does not change significantly as x_w is decreased. This difference in the interaction of TMA and sodium ions with the sulfonate group also manifests itself in aqueous solutions. Recent measurements²⁰ of thermodynamic activity coefficients of the sodium and tetramethylammonium salts of ethanesulfonic acid have shown that γ_{\pm} for the latter salt at small concentrations is less than that for the Na salt, but that when $m > 1.5$ the reverse is true.

The selective uptake of the tetramethylammonium cation by the most lightly cross-linked exchanger may be regarded as a consequence of water-water interac-

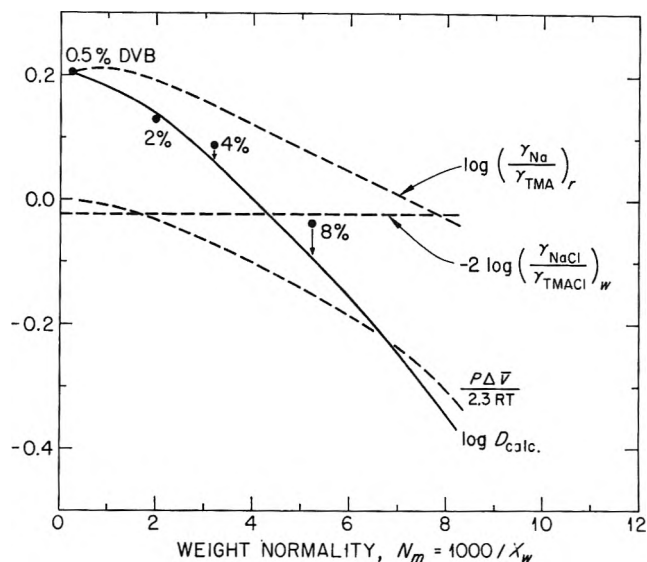


Figure 4. Comparison of terms contributing to calculated $\log D$ for the tetramethylammonium-sodium exchange on variously cross-linked Dowex 50 at 25°; $x_{\text{TMA}} = 0.0$.

tions which act to force large unhydrated ions from their aqueous solutions. This type of an effect has been proposed²¹ to explain the large selectivity coefficients shown by strong-base anion exchangers for large, unhydrated anions such as ClO_4^- , ReO_4^- , I^- , ions, etc., and for the uptake of quaternary ammonium ions by cation exchangers in which "structure-enforced ion pairs"²² in the exchanger presumably are formed. It seems unlikely, however, that such ion pairs even if they are formed with polystyrene sulfonates can be very stable because of the strong hydration of the sulfonate group. When the cross linking is increased, these pairs become progressively more unstable and strong selectivity reversals occur. The conclusion from this research is that both ionic size and hydration are important in determining the uptake of tetramethylammonium ion by cross-linked polysulfonate cation exchangers.

Acknowledgment. It is a pleasure to acknowledge the interest and help given during the course of this research by our colleague, Dr. S. Lindenbaum.

(18) O. D. Bonner and O. C. Rogers, *J. Phys. Chem.*, **64**, 1499 (1960); **65**, 981 (1961); O. D. Bonner and J. R. Overton, *ibid.*, **67**, 1035 (1963).

(19) E. R. Nightingale, Jr., *ibid.*, **66**, 894 (1962), on the basis of viscosity measurements has described the $(\text{CH}_3)_4\text{N}^+$ ion as weakly perisurface hydrated.

(20) H. P. Gregor, M. Rothenberg, and N. Fine, *ibid.*, **67**, 1110 (1963).

(21) B. Chu, D. C. Whitney, and R. M. Diamond, *J. Inorg. Nucl. Chem.*, **24**, 1405 (1962).

(22) R. M. Diamond, *J. Phys. Chem.*, **67**, 2513 (1963).

Diffusion and Frictional Coefficients for Two Concentrated Compositions of the System Water-Mannitol-Sodium Chloride at 25°; Tests of the Onsager Reciprocal Relation¹

by Peter J. Dunlop²

Chemistry Department and Institute for Enzyme Research, University of Wisconsin, Madison, Wisconsin 53706 (Received July 12, 1965)

Using a Gouy diffusimeter, diffusion and refractive index data have been measured for two concentrated compositions of the system H₂O-mannitol-NaCl at 25° and compared with other diffusion data which were obtained by Kelly with a diaphragm cell for the same system. Frictional coefficients for four compositions of this system have been computed from the diffusion data reported here, the diffusion data of Kelly, and the activity data of Kelly, Robinson, and Stokes. The frictional coefficients indicate that the Onsager reciprocal relation for isothermal diffusion is valid for this system. Diffusion, density, and refractive index data are also reported for the systems H₂O-mannitol and H₂O-NaCl at 25°.

In the last decade, a number of papers in the literature have reported diffusion data for isothermal ternary systems. For some of these systems,³⁻⁸ thermodynamic data have also been available and this has permitted the Onsager reciprocal relation (ORR) for isothermal diffusion in these systems to be rigorously tested.³⁻⁹ For other systems,¹⁰ it was necessary to make certain simplifying assumptions for the thermodynamic data before approximate tests of the ORR could be made. However, in all cases the ORR was found to be valid within the estimated error of measurement.

This paper reports diffusion data which were obtained with the Gouy diffusimeter for two concentrated compositions of the system H₂O-mannitol-NaCl. The experiments were undertaken to complement data obtained by Kelly⁸ with the diaphragm cell for two other compositions of this system. Diffusion and refractive index data, obtained with the Gouy diffusimeter, are also reported for the binary systems H₂O-mannitol and H₂O-NaCl. The former are compared with the data of Kelly.⁸ The ternary diffusion data are combined with the thermodynamic data of Kelly, Robinson, and Stokes¹¹ to test the ORR

by computing frictional coefficients for this system both from the data reported here and also from the data of Kelly.⁸

(1) This investigation was supported in part by National Science Foundation research grant GP-179 and by National Institute of Arthritis and Metabolic Diseases (U. S. Public Health Service) Research Grant AM-05177.

(2) Department of Physical and Inorganic Chemistry, Adelaide University, South Australia.

(3) I. J. O'Donnell and L. J. Gosting, "The Structure of Electrolytic Solutions," W. J. Hamer, Ed., John Wiley and Sons, Inc., New York, N. Y., and Chapman and Hall, London, 1959. See also, H. Fujita and L. J. Gosting, *J. Phys. Chem.*, **64**, 1256 (1960), where these data were analyzed by an improved procedure for calculating the diffusion coefficients.

(4) P. J. Dunlop, *ibid.*, **63**, 612 (1959).

(5) D. G. Miller, *ibid.*, **63**, 570 (1959).

(6) L. A. Woolf, D. G. Miller, and L. J. Gosting, *J. Am. Chem. Soc.*, **84**, 317 (1962).

(7) R. P. Wendt, *J. Phys. Chem.*, **66**, 1279 (1962).

(8) F. J. Kelly, Ph.D. Thesis, University of New England, Armidale, New South Wales, Australia, 1961.

(9) P. J. Dunlop and L. J. Gosting, *J. Phys. Chem.*, **63**, 86 (1959).

(10) F. O. Shuck and H. L. Toor, *ibid.*, **67**, 540 (1963).

(11) F. J. Kelly, R. A. Robinson, and R. H. Stokes, *ibid.*, **65**, 1958 (1961).

Theory

It is possible to describe ternary isothermal diffusion by two equivalent formulations.¹² The first involves flow equations for the two (arbitrarily chosen) solutes, 1 and 2, diffusing in a solvent denoted by 0. The flows $(J_1)_V$ and $(J_2)_V$ of these components are written as linear functions of the independent solute concentration gradients at constant temperature, T , and pressure, P . The equations which have been suggested¹³ and tested experimentally¹⁴ are

$$(J_1)_V = -(D_{11})_V(\partial C_1/\partial x)_{T,P,t} - (D_{12})_V(\partial C_2/\partial x)_{T,P,t} \quad (1)$$

$$(J_2)_V = -(D_{21})_V(\partial C_1/\partial x)_{T,P,t} - (D_{22})_V(\partial C_2/\partial x)_{T,P,t} \quad (2)$$

$$(D_{12})_V \longrightarrow 0 \text{ as } C_1 \longrightarrow 0$$

$$(D_{21})_V \longrightarrow 0 \text{ as } C_2 \longrightarrow 0$$

where C_1 and C_2 are the solute concentrations in moles cc.⁻¹, $(D_{11})_V$ and $(D_{22})_V$ are the *main* diffusion coefficients, and $(D_{12})_V$ and $(D_{21})_V$ are the *cross-term* diffusion coefficients. The subscript V is used to indicate the volume frame of reference defined by

$$\sum_{i=0}^2 \bar{V}_i(J_i)_V = 0 \quad (3)$$

where the \bar{V}_i are the partial molar volumes of the components. In spite of the fact that four diffusion coefficients appear in these flow equations, only three are independent^{5,15,16} if the principle of *microscopic reversibility*^{17,18} is invoked. However, experimentally it is almost always necessary to measure all four coefficients in order to completely describe ternary diffusion. It should be noted that no "activity data" appear explicitly in eq. 1 and 2.

The second method for describing ternary diffusion has been suggested by both Onsager¹⁹ and Lamm,²⁰ though in slightly different forms. Their formulations are equivalent to the suggestion that it is possible to describe relative motion between components in terms of a set of frictional coefficients R_{ik} defined by the equations²¹⁻²⁵

$$X_i = \sum_{k=0}^2 R_{ik}C_k[(v_i)_V - (v_k)_V] \quad (4)$$

$$R_{ik} = R_{ki} \quad (4a)$$

where the X_i are the gradients of the chemical potentials, μ_i , and are assumed to be the forces causing relative motion of the components

$$X_i = -(\partial\mu_i/\partial x)_{T,P,t} \quad (5)$$

$$\sum_{i=0}^2 C_i X_i = 0 \quad (5a)$$

and the $(v_i)_V$ are diffusion velocities, for the volume frame of reference, defined by

$$(J_i)_V = C_i(v_i)_V \quad (6)$$

Thus for ternary systems the diffusion process may be described in terms of only *three independent* frictional coefficients.

For ternary diffusion the equalities expressed by eq. 4a are equivalent to the linear relationship^{5,15,16} which reduces the four dependent diffusion coefficients to three which are independent. It should be noted that, because velocity differences appear in eq. 4, the R_{ik} are *independent* of the frame of reference used to define the diffusion coefficients.

The above two formulations are entirely equivalent and it has been shown²⁵ for ternary systems that the R_{ik} may be expressed in terms of the $(D_{ij})_V$ by the relations²⁶

$$R_{10} = \frac{C_1(C_1P_{11} + C_2P_{12})}{C_0(C_1a_{11} + C_2a_{12})} \quad (7)$$

$$R_{12} = \frac{C_1(a_{12}P_{11} - a_{11}P_{12})}{(C_1a_{11} + C_2a_{12})} \quad (8)$$

$$R_{21} = \frac{C_2(a_{21}P_{22} - a_{22}P_{21})}{(C_1a_{21} + C_2a_{22})} \quad (9)$$

$$R_{20} = \frac{C_2(C_1P_{21} + C_2P_{22})}{C_0(C_1a_{21} + C_2a_{22})} \quad (10)$$

where

- (12) S. Ljunggren, "Ultracentrifugal Analysis in Theory and Experiment," J. W. Williams, Ed., Academic Press, Inc., New York, N. Y., and London, 1963, p. 29.
- (13) R. L. Baldwin, P. J. Dunlop, and L. J. Gosting, *J. Am. Chem. Soc.*, **77**, 5235 (1955).
- (14) P. J. Dunlop and L. J. Gosting, *ibid.*, **77**, 5238 (1955).
- (15) G. Hooyman, *Physica*, **22**, 751 (1956).
- (16) J. G. Kirkwood, R. L. Baldwin, P. J. Dunlop, L. J. Gosting, and G. Kegeles, *J. Chem. Phys.*, **33**, 1505 (1960).
- (17) L. Onsager, *Phys. Rev.*, **37**, 405 (1931).
- (18) L. Onsager, *ibid.*, **38**, 2265 (1931).
- (19) L. Onsager, *Ann. N. Y. Acad. Sci.*, **46**, 241 (1945).
- (20) O. Lamm, *Acta Chem. Scand.*, **11**, 362 (1957).
- (21) A. Klemm, *Z. Naturforsch.*, **8a**, 397 (1953).
- (22) R. W. Laity, *J. Phys. Chem.*, **63**, 80 (1959).
- (23) R. J. Bearman, *ibid.*, **65**, 1961 (1961).
- (24) S. Ljunggren, *Trans. Roy. Inst. Tech., Stockholm*, **172**, 1 (1961).
- (25) P. J. Dunlop, *J. Phys. Chem.*, **68**, 26 (1964).
- (26) It should be noted that the frictional coefficients used by Bearman, Klemm, and Dunlop are the negative of those suggested by Onsager. Laity adopted those of Onsager.

$$a_{ik} = \delta_{ik} + (C_i \bar{V}_k / C_0 \bar{V}_0) \quad (i, k = 1, 2) \quad (11)$$

$$P_{11} = -(N_{22}/K); P_{12} = (N_{12}/K) \quad (12)$$

$$P_{21} = (N_{21}/K); P_{22} = -(N_{11}/K)$$

$$K = |N_{ij}| = (N_{11}N_{22} - N_{12}N_{21}) \quad (12a)$$

$$N_{11} = -[(D_{11})_{V\mu_{22}} - (D_{12})_{V\mu_{21}}]/\theta$$

$$N_{12} = [(D_{11})_{V\mu_{12}} - (D_{12})_{V\mu_{11}}]/\theta \quad (13)$$

$$N_{21} = [(D_{22})_{V\mu_{21}} - (D_{21})_{V\mu_{22}}]/\theta$$

$$N_{22} = -[(D_{22})_{V\mu_{11}} - (D_{21})_{V\mu_{12}}]/\theta$$

$$\theta = |\mu_{ij}| = (\mu_{11}\mu_{22} - \mu_{12}\mu_{21}) \quad (13a)$$

and

$$\mu_{ij} = (\partial\mu_i/\partial C_j)_{T,P,C_{k \neq 0,j}} \quad (13b)$$

The validity of the ORR for a given system at a certain composition would result in the equality²⁵ of the frictional coefficients R_{12} and R_{21} , the numerical values of which are independent of the frame of reference. The difference between these two quantities is a measure of the accuracy of the test of the ORR. Thus it is convenient to define

$$\Delta\% \text{ (exptl.)} \equiv 100(R_{12} - R_{21})/\bar{R} \quad (14)$$

where

$$\bar{R} = [(|R_{12}| + |R_{21}|)/2] \quad (14a)$$

In this paper eq. 7-13 are used to compute frictional coefficients for four compositions of the ternary system H₂O-mannitol-NaCl from the diffusion data reported here and from the data of Kelly,⁸ by using the thermodynamic data of Kelly, Robinson, and Stokes.¹¹ A detailed description of the method used to compute the R_{ik} is given in a later section.

Experimental Section

Materials. The mannitol used in all experiments was a British Drug Houses microanalytical reagent and the sodium chloride was a B.D.H. Analar product. Both of these chemicals were used without further purification and were dried *in vacuo* over phosphorus pentoxide. The diffusion coefficients and refractive index derivatives obtained for the two-component experiments with mannitol agreed, within the experimental error, with the results of an experiment performed in this laboratory with another sample of mannitol that had been recrystallized three times by Kelly⁸ and used for his work. Diffusion experiments performed by Ellerton²⁷ with another sample of B.D.H. microanalytical grade mannitol also agreed, within the error of measurement, with the results reported here.

All solutions were prepared with distilled water that had been treated in a Barnstead water purification system.²⁸ The molecular weights²⁹ of water, mannitol, and sodium chloride were taken to be 18.015, 182.175, and 58.443, respectively, while the corresponding component densities which were used to reduce all weighings to vacuum were 0.997048, 1.489, and 2.165 g. cc.⁻¹, respectively. The density of brass was taken to be 8.40 g. cc.⁻¹ and the density of the stainless steel Mettler weights to be 7.76 g. cc.⁻¹. The correct procedure for reducing weights to vacuum is described in a Mettler publication.³⁰

Solutions. All solutions were prepared by weight and the solute concentrations³¹ in moles/1000 cc., C_i , calculated by means of the solution densities, ρ , in g. cc.⁻¹, and the solute molecular weights. All solution densities were determined in quadruplicate with Pyrex matched 30-cc. single-neck pycnometers.

Apparatus, Experimental Quantities, and Computations. The Gouy diffusimeter used for all of the experiments reported here has been adequately described elsewhere.^{14,32,33} All of the experimental quantities used in this paper have been defined in another publication.⁶ This paper should be read in conjunction with that article which also gives a description of the method of performing the experiments and the calculation procedures for obtaining the final results. Occasionally equation numbers in that article will be referred to here and identified by the letter W (*e.g.*, 31W). The same fused quartz cell, SH-1 (cell 2 of ref. 7), was used for all experiments: its thickness, a , along the light path was 2.5075 cm. and the optical lever arm, b , was 306.64 cm. All experiments were performed within $\pm 0.003^\circ$ of 25° .

Results

Two-Component Systems. Seven diffusion experiments were performed with the system H₂O-mannitol. The data obtained are reported in Table I. The value of \bar{c} corresponds to the average of the concentrations of the two solutions which were used in each experiment while the value of Δc is the corresponding difference between these two concentrations. The total

(27) H. D. Ellerton, private communication.

(28) G. Reinfelds and L. J. Gosting, *J. Phys. Chem.*, **68**, 2464 (1964).

(29) Using atomic weights compiled in International Union of Pure and Applied Chemistry, Information Bulletin No. 14b (1961).

(30) Mettler News, (1-22)E, 81 (1961). This publication is available from local Mettler agents.

(31) $C_i = 1000C_i$; and $(\partial C_i/\partial C_j)_{T,P,C_{k \neq 0,i}} = 1000$.

(32) L. J. Gosting, E. M. Hanson, G. Kegeles, and M. S. Morris, *Rev. Sci. Instr.*, **20**, 209 (1949).

(33) P. J. Dunlop and L. J. Gosting, *J. Am. Chem. Soc.*, **75**, 5073 (1953).

Table I: Diffusion Data for the Binary Systems at 25°

System	c	Δc	J	$(\Delta n/\Delta c) \times 10^3$	$D \times 10^6$	$Q \times 10^4$
H ₂ O-mannitol	0.026183	0.052366	62.42	25.958	0.6608	0.1
H ₂ O-mannitol ^b	0.032690	0.065380	77.92	25.954	0.6597	0.2
H ₂ O-mannitol	0.040918	0.081836	97.51	25.948	0.6576	0.0
H ₂ O-mannitol	0.195452	0.064971	77.26	25.896	0.6274	1.5
H ₂ O-mannitol	0.399622	0.064359	76.34	25.831	0.5867	-1.3
H ₂ O-mannitol	0.688826	0.057741	68.17	25.710	0.5360	0.5
H ₂ O-mannitol	0.799871	0.060561	71.49	25.707	0.5170	0.4
H ₂ O-NaCl	1.50046	0.19988	84.04	9.156	1.4948	-1.6
H ₂ O-NaCl	3.00010	0.20013	78.26	8.516	1.5555	-1.5

^a Units: concentrations c , moles 1000 cc.⁻¹; diffusion coefficients D , cm.² sec.⁻¹; refractive index derivatives $(\Delta n/\Delta c)$, 1000 cc. mole⁻¹, referred to the velocity of light in air at standard temperature and pressure and for wave length 5460.7×10^{-8} cm. in air.

^b This sample was obtained from R. H. Stokes and had been recrystallized three times by F. J. Kelly.

number of fringes, J , obtained in each Gouy experiment together with the corresponding refractive index derivatives, $(\Delta n/\Delta c)$, and diffusion coefficients, D , are also included in the table. The Q values⁵ are the areas of the graphs of the relative fringe deviations, Ω , vs. the reduced fringe numbers $f(\xi)$.⁶ If the Gouy apparatus is optically perfect, the magnitude of Q is a measure of the deviation of the refractive index gradient curve from gaussian shape.

Several density measurements were made with the mannitol solutions to complement results which had been obtained elsewhere.³⁴ The results of a total of twelve experiments are best represented by the equation

$$\rho = 0.99704g + 0.063110c - 0.000754c^2 \quad (c \leq 0.9) \quad (15)$$

with an average deviation of $\pm 0.0002\%$. These density results are approximately 0.005% lower than those of Kelly,⁸ who obtained 118.96 cc. mole⁻¹ for the limiting partial molar volume of mannitol. The results summarized by eq. 15 give 119.42 cc. mole⁻¹ for the same limiting partial molar volume. Equation 15 was used to compute the solute concentrations for all the mannitol diffusion experiments in Table I.

The densities for the sodium chloride solutions were computed using the following equation³⁵ for the apparent molar volume of NaCl, Φ

$$\Phi_{\text{NaCl}} = 16.50 + 2.034c^{1/2} + 0.0121c^{3/2} \quad (c \leq 5.3) \quad (16)$$

Using the diffusion and refractive index data for the system H₂O-mannitol in Table I, the method of least squares was used to obtain the equations

$$D \times 10^6 = 0.6664 - 0.2088c + 0.0278c^2 \quad (c \leq 0.8) \quad (17)$$

with an average deviation of $\pm 0.05\%$, and

$$(\Delta n/\Delta c) \times 10^3 = 25.964 - 0.340c \quad (c \leq 0.8) \quad (18)$$

with an average deviation of 0.02%. The limiting diffusion coefficient obtained for this system is 2.2% lower than that obtained by Kelly,⁸ while both sets of data agree when $c = 0.2$. The refractive index data obtained in this work are an average of 1% lower than that of Kelly. A somewhat similar situation was found by Woolf³⁶ when comparing his diffusion results for the system pentaerythritol-H₂O with the corresponding data of Kelly. Woolf³⁶ has discussed several possibilities which might explain the discrepancies between the data reported here and the results of Kelly.

Table II: Comparison of Diffusion and Refractive Index Data at 25° for Two Compositions of the System NaCl-H₂O

	Stokes ³⁷ (diaphragm cell)	Lyons ³⁸ (Gouy)	Woolf ³⁶ (Gouy)	Dunlop (Gouy)
($c = 1.5$)				
$D \times 10^6$	1.495	1.498	1.4966	1.4948
$(\Delta n/\Delta c) \times 10^3$...	9.170	9.182	9.156
($c = 3.0$)				
$D \times 10^6$	1.544	1.565	...	1.5555
$(\Delta n/\Delta c) \times 10^3$...	8.564	...	8.516

(34) P. J. Dunlop, unpublished data.

(35) H. S. Harned and B. B. Owen, "The Physical Chemistry of Electrolyte Solutions," Reinhold Publishing Corp., New York, N. Y., 1958, p. 397.

(36) L. A. Woolf, *J. Phys. Chem.*, **67**, 273 (1963).

Table III^a: Experimental Data for the System H₂O–Mannitol–NaCl at 25° (0 = H₂O; 1 = Mannitol; 2 = NaCl)

	$\bar{c}_1 = 0.75; \bar{c}_2 = 1.50$ $\bar{c}_0 = 48.675$				$\bar{c}_1 = 0.75; \bar{c}_2 = 3.00$ $\bar{c}_0 = 46.819$			
	SH-1	SH-1	SH-1	SH-1	SH-1	SH-1	SH-1	SH-1
1 Cell								
2 $(\bar{c}_1)_A$	0.750051	0.743058	0.722058	0.716633	0.749897	0.748429	0.716889	0.714131
3 $(\bar{c}_2)_A$	1.40404	1.40718	1.48129	1.50176	2.89322	2.90652	2.99662	3.00394
4 $(\rho)_A$	1.097609	1.097334	1.098819	1.099239	1.151621	1.152025	1.153374	1.153470
5 $(\bar{c}_1)_B$	0.749988	0.757238	0.778304	0.783165	0.750375	0.751815	0.783104	0.785982
6 $(\bar{c}_2)_B$	1.60284	1.59700	1.52047	1.50285	3.10339	3.09649	2.99685	2.99595
7 $(\rho)_B$	1.104991	1.105181	1.103613	1.103243	1.159112	1.158928	1.157204	1.157326
8 \bar{c}_1	0.750020	0.750148	0.750181	0.749899	0.750136	0.750122	0.749996	0.750056
9 \bar{c}_2	1.50344	1.50209	1.50088	1.50230	2.99830	3.00150	2.99674	2.99994
10 J_{exptl}	80.20	92.82	80.17	76.49	79.95	75.44	73.71	76.84
11 J_{calcd}	80.20	92.86	80.13	76.51	79.89	75.50	73.70	76.85
12 α_1	-0.0009	0.1746	0.8026	0.9942	0.0066	0.0498	0.9988	1.0393
13 $(\mathcal{D}_A)_{\text{exptl}} \times 10^5$	1.3801	1.1026	0.57565	0.48925	1.4629	1.3609	0.43129	0.41507
14 $(\mathcal{D}_A)_{\text{calcd}} \times 10^5$	1.3815	1.1014	0.57561	0.48934	1.4628	1.3611	0.43099	0.41534
15 $Q_{\text{exptl}} \times 10^4$	-154.86	3.47	106.51	45.85	-198.30	-129.50	106.34	85.82
16 $Q_{\text{calcd}} \times 10^4$	-156.04	5.25	104.94	46.81	-198.74	-129.01	105.78	86.33
17 I_A		269.21				259.99		
18 S_A		183.91				221.97		
19 E_0^b		-4.1743				-5.4679		
20 E_1^b		28.7542				41.0490		
21 E_2^b		22.5569				30.5117		
22	$\bar{V}_0 = 17.997$	$\bar{V}_1 = 122.58$	$\bar{V}_2 = 21.39$		$\bar{V}_0 = 17.909$	$\bar{V}_1 = 123.79$	$\bar{V}_2 = 22.89$	
23	$\mathcal{R}_1 \times 10^3 = 24.898$	$\mathcal{R}_2 \times 10^3 = 8.793$			$\mathcal{R}_1 \times 10^3 = 24.208$	$\mathcal{R}_2 \times 10^3 = 8.224$		
24	$\mathcal{I}_1 \times 10^2 = 5.947$	$\mathcal{I}_2 \times 10^2 = 3.703$			$\mathcal{I}_1 \times 10^2 = 5.765$	$\mathcal{I}_2 \times 10^2 = 3.542$		
25	$\rho(\bar{c}_1, \bar{c}_2) = 1.101170$				$\rho(\bar{c}_1, \bar{c}_2) = 1.155409$			

^a Units: concentrations \bar{c}_i , moles 1000 cc.⁻¹; densities ρ , g. cc.⁻¹; reduced height-area ratios \mathcal{D}_A , cm.² sec.⁻¹. ^b More than the minimum number of significant digits were retained in these values to minimize the accumulation of errors in the calculations.

Experiment 5 in Table I was performed with the same sample as was used by Kelly.

Two binary diffusion experiments were also performed with the B.D.H. Analar sodium chloride sample. The results are listed in Table I. Table II gives a comparison of the results obtained with those of three other workers.^{37,38}

It is seen that all the results at $\bar{c} = 1.5$ show quite good agreement, but that at $\bar{c} = 3.0$ the deviations between the various results in Table II are much larger than one would expect with an estimated accuracy in D for the Gouy and diaphragm cell methods of 0.1 and 0.2%, respectively. However, because most diffusion coefficients are functions of concentration, it is possible that these deviations may be due to the fact that the Gouy data reported in Table II are, strictly speaking, integral values. Inspection of all the Q values in Table I indicates that the refractive index gradient curves obtained with the samples used in this work were of gaussian shape within the error of measurement.

Three-Component Systems. All of the pertinent experimental data for the two compositions of the system H₂O–mannitol–NaCl studied in this work are

reported in Table III. Throughout this paper 0 is used to designate the solvent (an arbitrary choice) while 1 and 2 are used to designate the solutes mannitol and NaCl, respectively.

Lines 2 to 7 give the concentrations and the corresponding densities of the two solutions A (upper) and B (lower) used in each diffusion experiment, while lines 8 and 9 give the arithmetic averages, \bar{c}_i , of these solution concentrations. The total number of fringes, J_{exptl} , used for each experiment are listed in the table together with the corresponding values of J_{calcd} which were computed from the concentration differences, $\Delta\bar{c}_i$, and the two refractive index derivatives,³⁹ \mathcal{R}_i , calculated by the method of O'Donnell and Gosting.³ The values of α_1 (see eq. 39W) are given in line 12. The experimental and computed height-area ratios, \mathcal{D}_A , are listed in lines 13 and 14 while lines 15 and 16 give the corresponding experimental and computed areas of the fringe deviation graphs for each experiment. It is

(37) R. H. Stokes, *J. Am. Chem. Soc.*, **72**, 2243 (1950).

(38) V. Vitagliano and P. A. Lyons, *ibid.*, **78**, 1549 (1956).

(39) A script letter has been used here to represent the refractive index increments to avoid confusion with the frictional coefficients, R_{ik} .

believed that, in this work, each Q_{exptl} value is known to approximately $\pm 2.0 \times 10^{-4}$. Lines 17 to 21 report certain intermediate quantities which are obtained in the calculations⁶ for the $(D_{ij})_V$ values.

Stability criteria^{20,40} were applied to the ternary diffusion experiments and indicated in each case that the diffusion boundaries were gravitationally stable.

The method of least squares was used to express the solution densities for each composition of the system by means of the equation

$$\rho = \rho(\bar{c}_1, \bar{c}_2) + \mathcal{K}_1(c_1 - \bar{c}_1) + \mathcal{K}_2(c_2 - \bar{c}_2) \quad (19)$$

where \bar{c}_1 and \bar{c}_2 define the composition of the system and the \mathcal{K}_i are defined by the equation

$$\mathcal{K}_i = (\partial\rho/\partial c_j)_{T,P,c_l \neq 0,j} \quad (19a)$$

Values of \mathcal{K}_1 , \mathcal{K}_2 , and $\rho(c_1, c_2)$ are reported in lines 24 and 25 of Table III. The \mathcal{K}_i values were employed to compute⁴¹ the partial molar volumes, \bar{V}_i , listed in line 22 of the same table. In both cases the density data are represented by eq. 19 with an average deviation of $\pm 0.0007\%$.

The pertinent data in Table III were then used to compute the $(D_{ij})_V$ values which appear in columns C and D of Table IV. The diffusion data of Kelly which were obtained with the diaphragm cell method are listed in the same table for comparison. The methods used for computing the $(D_{ij})_V$ have been given in great detail elsewhere.⁶ All computations in this article were performed with programs previously written by R. P. Wendt (Intercom 1000) and H. D. Ellerton (IBM 1620). The errors in each $(D_{ij})_V$ in Table IV were computed by assuming errors of $\pm 2.0 \times 10^{-4}$ in each Q value. As has been previously indicated,^{7,42} the errors in the values of Q cause much greater errors in the $(D_{ij})_V$ than the corresponding errors in the values of the \mathcal{D}_A .

It is interesting to note that the $(D_{12})_V$ and $(D_{21})_V$ values in Table IV can be represented within the error of measurement by the two equations

$$(D_{12})_V = c_1(0.06332 - 0.00033c_2) \quad (20)$$

$$(D_{21})_V = c_2(0.16290 - 0.05218c_1) \quad (21)$$

which also satisfy the restrictions $(D_{12})_V \rightarrow 0$ as $c_1 \rightarrow 0$ and $(D_{21})_V \rightarrow 0$ as $c_2 \rightarrow 0$ (see eq. 1 and 2).

Tests of the Onsager Reciprocal Relation

Derivatives of the Solute Chemical Potentials. In order to evaluate the derivatives μ_{ij} in eq. 13, these derivatives are first related to the corresponding derivatives on the molality concentration scale by the relation

Table IV^{a,b}: Diffusion and Frictional Coefficients

	A	B	C	D
c_1	0.20	0.20	0.75	0.75
c_2	1.50	3.00	1.50	3.00
$(D_{11})_V \times 10^6$	0.559 ±0.004	0.446 ±0.006	0.4598 ±0.0012	0.3848 ±0.0010
$(D_{12})_V \times 10^6$	0.016 ±0.010	0.013 ±0.008	0.0462 ±0.0006	0.0466 ±0.0004
$(D_{21})_V \times 10^6$	0.2315 ±0.0010	0.456 ±0.003	0.1794 ±0.0084	0.3744 ±0.0075
$(D_{22})_V \times 10^6$	1.390 ±0.002	1.469 ±0.003	1.0989 ±0.0034	1.1403 ±0.0030
$R_{10} \times 10^{-17}$	0.7563	0.8877	1.0192	1.1194
$(\delta R_{10})_1 \times 10^{-17}$	±0.0477	±0.0922	±0.0046	±0.0061
$(\delta R_{10})_2 \times 10^{-17}$	±0.0016	±0.0027	±0.0040	±0.0062
$R_{12} \times 10^{-17}$	3.4309	3.8627	4.5022	5.8726
$(\delta R_{12})_1 \times 10^{-17}$	±1.5858	±1.4441	±0.0387	±0.0264
$(\delta R_{12})_2 \times 10^{-17}$	±0.0358	±0.0348	±0.0410	±0.0381
$R_{21} \times 10^{-17}$	4.1825	4.2472	4.1201	5.5604
$(\delta R_{21})_1 \times 10^{-17}$	±0.0219	±0.0507	±0.0971	±0.3085
$(\delta R_{21})_2 \times 10^{-17}$	±0.0790	±0.1057	±0.1106	±0.1381
$R_{20} \times 10^{-17}$	0.6922	0.8412	0.9123	1.1312
$(\delta R_{20})_1 \times 10^{-17}$	±0.0010	±0.0014	±0.0097	±0.0068
$(\delta R_{20})_2 \times 10^{-17}$	±0.0035	±0.0069	±0.0062	±0.0115
$\Delta\%$ (exptl.)	-19.7	-9.6	8.8	5.6
$\Delta\%$ (calcd.)	±45.2	±40.3	±15.9	±8.9

^a Units: concentrations c_i , moles 1000 cc.⁻¹; diffusion coefficients $(D_{ij})_V$, cm.² sec.⁻¹; frictional coefficients R_{ik} , erg cm. sec. mole⁻². ^b The $(D_{ij})_V$ in columns A and B were obtained by Kelly with the diaphragm cell.

$$\mu_{ij} = \sum_{k=1}^2 A_{ik} B_{kj} \quad (i, j = 1, 2) \quad (22)$$

where

$$A_{ik} = (\partial\mu_i/\partial m_k)_{T,P,m_l \neq k} \quad (22a)$$

and

$$B_{kj} \times 10^{-3} = (\partial m_k/\partial c_j)_{T,P,c_l \neq 0,j} \quad (22b)$$

The molalities m_k are related to the corresponding c_k and the solution density ρ by

$$m_k = (c_k/\beta) \quad (k = 1, 2) \quad (23)$$

where

$$\beta = \left[\rho - \sum_{i=1}^2 M_i c_i / 1000 \right] \quad (23a)$$

and M_i is the molecular weight of component i . Ex-

(40) R. P. Wendt, *J. Phys. Chem.*, **66**, 1740 (1962).

(41) See the Appendix of ref. 9.

(42) P. J. Dunlop and L. J. Gosting, *J. Phys. Chem.*, **68**, 3874 (1964).

pressions for the B_{kj} may be readily obtained by differentiating eq. 23 with respect to c_j

$$B_{kj} \times 10^{-3} = [\beta\delta_{kj} - c_k(3c_j - M_j/1000)]/\beta^2 \quad (24)$$

The derivatives A_{ik} are functions of the solute concentrations, m_i , and the corresponding activity coefficients, γ_i ,⁴³ which appear in the expressions for the chemical potentials, μ_i , of the two-solute components

$$\mu_1 = \mu_1^0 + \nu_1 RT \ln \gamma_1 m_1 \quad (25)$$

$$(\nu_1 = 1; \nu_2 = 2)$$

$$\mu_2 = \mu_2^0 + \nu_2 RT \ln \gamma_2 m_2 \quad (26)$$

In these expressions μ_1^0 and μ_2^0 are the standard chemical potentials and R is the gas constant. Differentiation of these equations with respect to the appropriate molalities gives

$$A_{ik} = RT\nu_i[(\delta_{ik}/m_i) + \Gamma_{ik}] \quad (i, k = 1, 2) \quad (27)$$

where

$$\Gamma_{ik} = (\partial \ln \gamma_i / \partial m_k)_{T,P,m_l \neq k} \quad (27a)$$

$$\nu_i \Gamma_{ik} = \nu_k \Gamma_k \quad (i \neq k) \quad (27b)$$

The derivatives Γ_{ik} may be obtained directly from the series expressions for the $\ln \gamma_i$ reported by Kelly, Robinson, and Stokes¹¹ for the system H₂O-mannitol-NaCl, the data of Robinson and Stokes⁴⁴ for the system H₂O-mannitol, and the vapor pressure data⁴⁵ for the system H₂O-NaCl which is used as a reference standard for the isopiestic vapor pressure method. The data for these two-component systems are reported as osmotic coefficients, φ_i , as functions of the solution molality, m_i

$$\varphi_i \equiv -(1000/\nu_i m_i M_0) \ln a_0 \quad (28)$$

$$= 1 + \frac{1}{m_i} \int_0^{m_i} m_d \ln \gamma_i^0 \quad (i = 1, 2)$$

where γ_i^0 is the activity coefficient of the solute and a_0 and M_0 are the activity and molecular weight, respectively, of the solvent. An intermediate quantity Γ_{ii}^0 , which is used in obtaining the Γ_{ik} , may be obtained by differentiating the expression for the φ_i with respect to m_i and using the Gibbs-Duhem relation. Thus we obtain

$$\begin{aligned} \Gamma_{ii}^0 &\equiv (\partial \ln \gamma_i^0 / \partial m_i)_{T,P} \quad (i = 1, 2) \\ &= (\partial \varphi_i / \partial m_i)_{T,P} + [(\varphi_i - 1)/m_i] \end{aligned} \quad (29)$$

If the experimental osmotic coefficients are expressed as series expansions in the molality, the Γ_{ii}^0 may be found by differentiation of these series expressions and using eq. 29.

As a first step in obtaining the μ_{ij} for testing the ORR

for several compositions of the system H₂O-mannitol-NaCl, it is necessary to compute values for the Γ_{ik} . These values were obtained by differentiation of the four equations^{11,44,46}

$$\ln \gamma_1 = \ln \gamma_1^0 + am_2 + (b/2)m_2^2 + (c/3)m_2^3 + em_1 m_2 \quad (30)$$

$$\ln \gamma_2 = \ln \gamma_2^0 + (a/2)m_1 + (b/2)m_1 m_2 + (c/2)m_1 m_2^2 + (e/4)m_1^2 \quad (31)$$

$$\begin{aligned} [a = -0.0145, b = 0.00184, \\ c = -0.0022, e = 0.0032] \\ \varphi_1 = 1 + 0.0034m_1 + 0.0042m_1^2 \end{aligned} \quad (32)$$

$$\begin{aligned} \varphi_2 = 0.9353 + 0.034997(m_2 - 1) + \\ 0.017450(m_2 - 1)^2 - \\ 0.005765(m_2 - 1)^3 + 0.001241(m_2 - 1)^4 - \\ 0.0001091(m_2 - 1)^5 \quad [1.0 < m_2 < 5.0] \end{aligned} \quad (33)$$

together with eq. 27a-29 and are listed in Table V.

Table V^{a,b}: Computation of the Chemical Potential Derivatives μ_{ij}

	I	II	III	IV
c_1	0.20	0.20	0.75	0.75
c_2	1.50	3.00	1.50	3.00
m_1	0.21178	0.21926	0.85531	0.88921
m_2	1.5884	3.2889	1.71062	3.55682
Γ_{11}^0	0.00947	0.00956	0.01758	0.01800
Γ_{22}^0	0.02589	0.08856	0.03358	0.09434
Γ_{11}	0.01455	0.02008	0.02305	0.02938
$\Gamma_{12} = 2\Gamma_{21}$	-0.01645	-0.03155	-0.01505	-0.03295
Γ_{22}	0.02534	0.08717	0.03115	0.08820
$A_{11} \times 10^{-10}$	11.74172	11.35609	2.95553	2.86072
$(A_{12} = A_{21}) \times 10^{-10}$	-0.04078	-0.07821	-0.03731	-0.08168
$A_{22} \times 10^{-10}$	3.24704	1.93970	3.05283	1.83125
$B_{11} \times 10^{-3}$	1.08608	1.12516	1.26010	1.31689
$B_{12} \times 10^{-3}$	0.00461	0.00534	0.02088	0.02428
$B_{21} \times 10^{-3}$	0.20389	0.44502	0.23937	0.52511
$B_{22} \times 10^{-3}$	1.09348	1.17633	1.18218	1.28271
$\mu_{11} \times 10^{-13}$	12.7442	12.7518	3.7153	3.7244
$\mu_{12} \times 10^{-13}$	0.0095	-0.0314	0.0176	-0.0353
$\mu_{21} \times 10^{-13}$	0.6178	0.7751	0.6837	0.8540
$\mu_{22} \times 10^{-13}$	3.5505	2.2813	3.6082	2.3470

^a More than the minimum number of significant digits have been retained on the A_{ij} , B_{ij} , and μ_{ij} values to minimize the accumulation of errors in calculating the R_{ik} . ^b The μ_{ij} have units cc. erg mole⁻¹.

(43) γ_1 and γ_2 are functions of both m_1 and m_2 .

(44) R. A. Robinson and R. H. Stokes, *J. Phys. Chem.*, **65**, 1954 (1961).

(45) R. A. Robinson and R. H. Stokes, "Electrolyte Solutions," Butterworth and Co., Ltd., London, 1959, p. 476.

(46) Equation 33 was obtained from the data cited in ref. 45 by the method of least squares.

The A_{ik} were then obtained from the Γ_{ik} and the m_i by means of eq. 27 and are also listed in the same table. The B_{kj} , the other quantities which appear in the expressions for the μ_{ij} , were computed from the \mathcal{F}_j in Table III and eq. 24. Equation 20 was then used to calculate the μ_{ij} in Table V.

Calculation of the R_{ik} . Frictional coefficients R_{ik} were computed from the pertinent data in Tables III to V by means of eq. 7 to 13. The values so obtained are listed in Table IV. In these calculations the value of the gas constant, R , and the value of the absolute zero of temperature were taken to be 8.3144×10^7 ergs deg.⁻¹ mole⁻¹ and -273.16° , respectively.

At the bottom of Table IV the $\Delta\%$ (exptl.) values, which were calculated by means of eq. 14, provide a measure of the validity of the ORR (microscopic reversibility) for a given composition of the system. The $\Delta\%$ (calcd.) values in the next line were calculated as follows. The main errors in the R_{ik} were assumed to be due to the errors in the $(D_{ij})_V$ listed in Table IV and to the errors in the Γ_{ik} .⁴⁷ On this basis it was possible to compute both the errors $(\delta R_{ik})_1$ caused by the errors in the $(D_{ij})_V$ and the errors $(\delta R_{ik})_2$ caused by the estimated errors⁴⁸ of ± 0.002 in Γ_{12} and Γ_{21} and ± 0.003 in Γ_{11} and Γ_{22} . Values for $(\delta R_{ik})_1$ and $(\delta R_{ik})_2$ are listed in Table IV. In computing the $\Delta\%$ (calcd.) values the absolute values of the estimated errors in R_{12} and R_{21} were substituted in the relation

$$\Delta\% \text{ (calcd.)} = \pm (100/\bar{R}) \sum_{\substack{i,k,l=1 \\ (i \neq k)}}^2 |(\delta R_{ik})_l| \quad (34)$$

where \bar{R} is defined by eq. 14a. The errors in R_{12} and R_{21} in Table IV indicate that, as far as the data obtained with the Gouy diffusimeter are concerned (columns C and D), the errors in the R_{ik} are somewhat larger for the estimated errors in the $(D_{ij})_V$ than for the estimated errors in the Γ_{ik} .

The $(D_{ij})_V$ values in Table IV indicate that the diffusion coefficients obtained for this system by the diaphragm cell⁸ and the results obtained in this work with the Gouy diffusimeter are known, when all the $(D_{ij})_V$ are considered, with essentially the same accuracy. However, for ternary diffusion, a complete check of the accuracies of the two methods has yet to be made. This would require measuring the $(D_{ij})_V$ by the Gouy and diaphragm cell methods in the same laboratory and with the same samples of the solutes and solvent.

Acknowledgment. The author wishes to thank Professor L. J. Gosting for many stimulating discussions and suggestions and Professor R. H. Stokes for his criticism of this article.

(47) Thus it is assumed that errors in the C_i , the m_i , the \bar{V}_i , and the φ_i are negligible compared to the errors in the Γ_{ik} .

(48) It is extremely difficult to estimate the errors in the Γ_{ik} . The error of ± 0.002 in Γ_{12} and Γ_{21} was adopted on the basis of similar isopiestic results obtained in this laboratory by Mr. H. D. Ellerton for the system H₂O-sucrose-urea. He was able to represent his 150 experimental points by a series of expansion in both m_1 and m_2 with an average deviation of ± 0.0017 . Since integration followed by differentiation is involved in obtaining Γ_{11} and Γ_{22} , the larger error of ± 0.003 was adopted for these quantities.

Triplet State of Fluorobenzene

by I. Unger¹

Department of Chemistry, University of Texas, Austin, Texas (Received July 12, 1965)

The sensitized emission of biacetyl and the *cis-trans* isomerization of butene-2 have been applied to fluorobenzene. Approximately 90% of the fluorobenzene molecules excited by 2537-Å. radiation cross over to the triplet state. The effect of wave length has also been studied.

Introduction

Although the triplet state of benzene was detected by Lewis and Kasha in 1944,² by its strong phosphorescence in a rigid medium at low temperatures, it was not found either in solution or in the gas phase until much later. Ishikawa and Noyes³ developed a technique based on the sensitized emission of biacetyl which clearly demonstrated the existence of triplet benzene. These authors also showed that, within experimental error, all of the benzene molecules which had absorbed 2537-Å. radiation and did not fluoresce crossed over to the triplet state. Cundall and co-workers⁴⁻⁷ used the sensitized *cis-trans* isomerization of butene-2 to detect the triplet state of benzene. Their estimate of the amount of triplet produced is in agreement, within experimental error, with that given by Ishikawa and Noyes.

It was thought of interest to apply the above-outlined techniques to some halogenated derivatives of benzene to detect indirectly their triplet states and to try to observe a McClure effect.⁸ Fluorobenzene is the only monohalogenated benzene which does not decompose when irradiated at 2537 Å.⁹ (Loeff, Ravetti, and Stein¹⁰ have noted a very small quantum yield of decomposition of fluorobenzene in solution when irradiated at 2537 Å.)

Fluorobenzene shows strong absorption over the same region as benzene. Its triplet state (detected by oxygen perturbation) lies very close to that of benzene.¹¹ It has a weak fluorescent emission in all phases but does not show any triplet state emission even in a glassy matrix.¹² It seemed therefore that this molecule would be very well suited for the type of study outlined above.

Experimental Section

Materials. The fluorobenzene used was Eastman White Label, purified by bulb-to-bulb distillation *in vacuo*. The cyclohexane was Matheson Coleman and Bell Chromatoquality reagent used without further purification; benzene was Matheson Coleman and Bell Spectroquality reagent purified in the same way as the fluorobenzene; biacetyl was also obtained from Matheson Coleman and Bell and purified by bulb to bulb distillation *in vacuo*. Research grade *cis*- and *trans*-butene-2 were obtained from the Phillips Petroleum Co., and vapor phase chromatography showed them to be essentially pure.

A conventional high-vacuum, grease-free line was employed. All experiments were carried out in a 60 mm. long T-shaped cell. The horizontal windows of

- (1) The University of New Brunswick, Saint John, New Brunswick, Canada.
- (2) G. N. Lewis and M. Kasha, *J. Am. Chem. Soc.*, **66**, 2100 (1944).
- (3) (a) H. Ishikawa and W. A. Noyes, Jr., *ibid.*, **84**, 1502 (1962); (b) H. Ishikawa and W. A. Noyes, Jr., *J. Chem. Phys.*, **37**, 583 (1962).
- (4) R. B. Cundall and T. F. Palmer, *Trans. Faraday Soc.*, **56**, 1211 (1960).
- (5) R. B. Cundall and D. G. Milne, *J. Am. Chem. Soc.*, **83**, 3902 (1961).
- (6) R. B. Cundall, F. J. Fletcher, and D. G. Milne, *J. Chem. Phys.*, **39**, 3536 (1963).
- (7) R. B. Cundall, F. J. Fletcher, and D. G. Milne, *Trans. Faraday Soc.*, **60**, 1146 (1964).
- (8) D. S. McClure, *J. Chem. Phys.*, **17**, 905 (1949).
- (9) O. P. Semenova and G. S. Tsiknov, *Zh. Fiz. Khim.*, **18**, 311 (1944).
- (10) I. Loeff, L. M. Ravetti, and G. Stein, *Nature*, **204**, 1300 (1964).
- (11) D. F. Evans, *J. Chem. Soc.*, 2753 (1959).
- (12) E. H. Gilmore, G. E. Gibson, and D. S. McClure, *J. Chem. Phys.*, **20**, 829 (1952), and correction to this publication: *ibid.*, **23**, 399 (1955).

the cell were 30 mm. in diameter while the vertical or emission window was 20 mm. in diameter. The cell was encased in an aluminum block which served a dual purpose in that it reduced stray light and could be used as a furnace. High-vacuum Teflon stopcocks (Delmar Corp.) were installed close to the cell in order to diminish the "dead space."

The light source was a Hanovia S-100 medium-pressure mercury arc (Alpine Burner) whose emission was focused by two quartz lenses on the entrance slit of a Bausch and Lomb grating monochromator, Model 33-86-45. The reciprocal linear dispersion of this monochromator is given as 6.6 Å./mm., and the slit widths used in this study were entrance slit 4 mm. and exit slit 1 mm. The light from the monochromator was focused by a quartz lens onto the window of the cell. The light transmitted through the cell was measured with an RCA 935 phototube connected to a Keithley Micro-Microammeter, Model 410. The emission intensity was measured by an RCA 1P28 photomultiplier. The associated electronics have been previously described.¹³ Fluorobenzene and benzene emission was viewed through a Corning No. 9863 filter which transmits from 2400 to 4000 Å., while biacetyl emission was viewed through a Corning C.S. 373 filter which transmits wavelength longer than about 4400 Å.

All materials were thoroughly degassed before admission to the cell. Mixing was accomplished by flash vaporization, and in the cases where the components had widely separated boiling points the flash vaporization procedure was repeated several times. Pressures below 3 mm. were measured by allowing a relatively large pressure into the cell and then expanding into large calibrated flasks.

In order to measure fluorobenzene fluorescence and the sensitized emission of biacetyl, the following technique was used. Benzene or benzene biacetyl mixtures were introduced into the cell and photolyzed at 2537 Å. The absorbed and emitted intensities were noted at several pressures for which quantum yields of emission and sensitized emission have been given by Ishikawa and Noyes.^{3b} These quantum yields were then set equal to

$$Q = \frac{I_e}{I_a} Z \quad (1)$$

where Q is the absolute quantum yield of either fluorescence or sensitized emission, I_e is the photocurrent due to emitted light, I_a is the difference in photocurrent due to transmitted light when the cell is empty and when it is full, and Z is a dimensionless constant of the system which allows the conversion of these arbitrary photocurrents into quantum yields. Z values

obtained in this way could then be used to obtain quantum yields of fluorescence either of fluorobenzene or of biacetyl emission sensitized by fluorobenzene. These Z values were reproducible and were checked prior to and at the end of each set of experiments. When measuring emission of biacetyl sensitized by fluorobenzene the pressure of fluorobenzene was kept at about 3 mm. This pressure of fluorobenzene has an absorption equal to about 20 mm. of benzene. To keep these experiments consistent with those of Ishikawa and Noyes, cyclohexane was introduced to make up the difference in pressure. The added cyclohexane has no effect on the fluorobenzene but does inhibit biacetyl decomposition. The potassium ferrioxalate actinometer described by Parker¹⁴ and by Hatchard and Parker¹⁵ was used in conjunction with the Cundall technique.

cis- and *trans*-butene-2 were analyzed on a Wilkens HyFi Aerograph Chromatograph, Model 600-C equipped with a 7.6-m. benzyl ether (20%) on firebrick (60–80 mesh) column followed by a 3.05-m. silicone gum rubber column which acted as a scrubber. Both columns were at room temperature. The retention time for *trans*-butene-2 under these conditions was 12 min. 19 sec. and for *cis*-butene-2 was 14 min. 2 sec.

Although Beer's law is not obeyed for fluorobenzene (see Table I) absorption by fluorobenzene, particularly at the pressures used in this study, is so much higher than that of biacetyl that, for most of the mixtures used, effectively all of the light was absorbed by fluorobenzene.

Table I: Variation of Apparent Extinction Coefficient ϵ with Fluorobenzene Pressure at 2537 Å. and 27°^a

Fluorobenzene press., mm.	C , $10^4 M$	ϵ^b
43.5	23.272	128
33.5	17.922	129
24.5	13.107	156
9.0	4.815	202

^a Length of cell: 6 cm. ^b $\epsilon = 1/Cl \log I_0/I_t$ where I_0 is the incident intensity and I_t is the transmitted intensity at C moles/liter of fluorobenzene in the cell.

Results

A. Fluorobenzene Fluorescence. Fluorobenzene when excited at 2537 Å. shows a relatively strong

(13) J. Hecklen, Ph.D. Thesis, University of Rochester, 1958.

(14) C. A. Parker, *Proc. Roy. Soc. (London)*, **A220**, 104 (1953).

(15) C. G. Hatchard and C. A. Parker, *ibid.*, **A235**, 518 (1956).

fluorescence, and the fluorescence yield is almost as great as that of benzene. The absolute fluorescence yield based on benzene extrapolates to 0.235 at zero pressure. It should be emphasized that this extrapolation to zero pressure cannot be used to predict behavior at very low pressures. Plots of $1/Q_f$ vs. P are probably not linear at low pressures.¹⁶ Self-quenching for fluorobenzene is small but larger than that of benzene. Since fluorobenzene absorbs very strongly at 2537 Å., it is possible that the observed self-quenching is mainly due to a geometrical effect and that actual self-quenching is much smaller. Fluorescence quenching by biacetyl is stronger than self-quenching while cyclohexane has little or no effect on the fluorescence of fluorobenzene.

A plot of $1/Q_f$ vs. (fluorobenzene) at room temperature follows the equation

$$1/Q_f = 4.22 + 2.05 \times 10^3(\text{FPh}) \quad (2)$$

where (FPh) is the fluorobenzene concentration in moles per liter.

A plot of $1/Q_f$ vs. (biacetyl) follows the equation

$$1/Q_f = 4.44 + 6.1 \times 10^3(\text{B}) \quad (3)$$

where (B) is the biacetyl concentration in moles per liter. (All concentrations in this paper are expressed in moles per liter.) The data mentioned above are summarized in Figure 1.

The addition of *cis*-butene-2 has no effect on the fluorescence of fluorobenzene (see Table II and Figure 1). There is a considerable amount of scatter in the data. This is probably due to the inefficient mixing of the two gases.

B. Sensitized Emission of Biacetyl. A sensitized emission of biacetyl is observed when fluorobenzene is excited in the presence of biacetyl. The sensitized

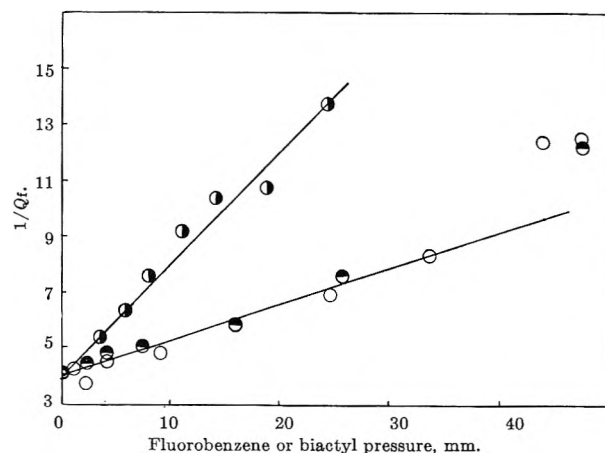


Figure 1. Variation of $1/(\text{fluorescence yield of fluorobenzene})$ with increasing fluorobenzene pressure, O; at 3.5 mm. of fluorobenzene and increasing pressure of biacetyl, ●; and the effect of 40 mm. of cyclohexane on $1/(\text{fluorescence yield of fluorobenzene})$ at various fluorobenzene pressures, ●. Temperature 27°.

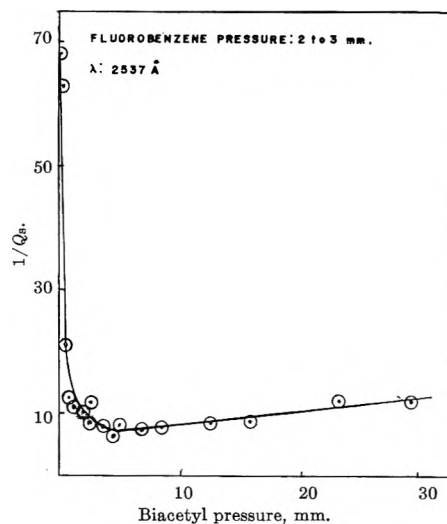


Figure 2. Variation of $1/(\text{sensitized emission yield of biacetyl})$ with biacetyl pressure at constant fluorobenzene pressure. Temperature 27°.

Table II: Effect of *cis*-Butene-2 on the Fluorescence Yield of Fluorobenzene at 2537 Å. and 27°^a

<i>cis</i> -Butene-2 press., mm.	Fluorescence yield of fluoro- benzene
54	0.23
48	0.24
42	0.21
36	0.20
30	0.23
24	0.23
17.5	0.25
12	0.24
6	0.24
0	0.24

^a Fluorobenzene pressure: 3 mm.

emission yield of biacetyl passes through a maximum at approximately 4.5 mm. of biacetyl. The sensitized emission yield at 3 mm. of fluorobenzene and room temperature follows the equation (see Figure 2)

$$1/Q_s = 5.5 + 4.4 \times 10^3(\text{B}) \quad (4)$$

Equation 4 is not obeyed at very high and very low values of (B). Increasing the pressure of fluorobenzene decreases the sensitized emission yield. The

(16) P. Sigal, *J. Chem. Phys.*, **42**, 1953 (1965).

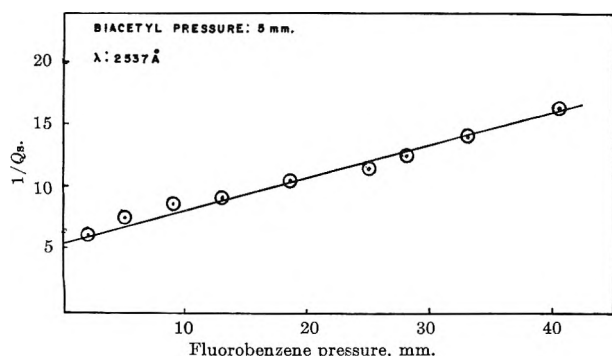


Figure 3. Variation of $1/($ sensitized emission yield of biacetyl) with increasing fluorobenzene pressure, biacetyl pressure remaining constant at 5 mm. Temperature 27° .

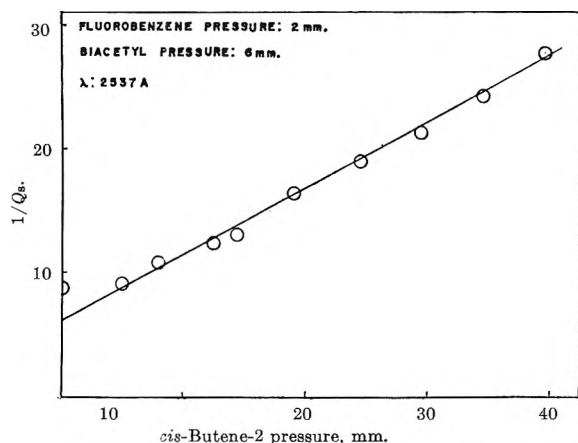


Figure 4. Variation of $1/($ sensitized emission yield of biacetyl) with *cis*-butene-2 pressure. Fluorobenzene pressure 2 mm.; biacetyl pressure 6 mm. Temperature 27° .

equation for $1/Q_s$ for a constant biacetyl pressure of 5 mm. and room temperature is given by (see Figure 3)

$$1/Q_s = 5.5 + 4.67 \times 10^3(\text{FPh}) \quad (5)$$

The sensitized emission yield is strongly quenched by *cis*-butene-2, and the data may be represented by (see Figure 4)

$$1/Q_s = 6 + 1.02 \times 10^4(\text{cis-butene-2}) \quad (6)$$

In this connection it should be noted that *cis*-butene-2 was found to have no effect on the emission of biacetyl when biacetyl was excited at 4050 and 4358 Å. This would be expected because of the low energy values for the singlet and triplet states of biacetyl and is in agreement with data in the literature.¹⁷

C. Variation of Sensitized Emission with Incident Wave Length. The sensitized emission yield of biacetyl is essentially constant from 2640 to 2420 Å. but appears to drop off sharply at 2350 Å.; the data are summarized in Table III. The value at 2350 Å. must be regarded

with caution because the low-incident intensity at this wave length will magnify any error. It is interesting to contrast these data with those obtained for the benzene-sensitized emission of biacetyl. Benzene-sensitized emission of biacetyl drops off rapidly with wave length and is zero, within experimental error, at 2420 Å. even in the presence of large pressures of a quenching gas such as cyclohexane.

Table III: Variation of Sensitized Emission Yield of Biacetyl with Wave Length^a

Wave length, Å.	Sensitized emission yield
2350	0.036
2420	0.139
2480	0.121
2537	0.148
2537	0.123
2537	0.137
2640	0.125

^a Pressure: biacetyl, 5 mm.; fluorobenzene, 2-3 mm.; cyclohexane, 20 mm. Temperature 27° .

D. cis-trans Isomerization of cis-Butene-2. Fluorobenzene excited at 2537 Å. sensitizes the *cis-trans* isomerization of *cis*-butene-2. This was found to be true even at 2420 Å. where there is no longer any observable fluorescence from fluorobenzene. In marked contrast, no *cis-trans* isomerization was observed when benzene was used as sensitizer at 2420 Å. even under prolonged irradiation. The experimental technique used in this study, in conjunction with the Cundall type of experiments, was not precise enough to allow accurate estimates of the amount of triplet state molecules of fluorobenzene produced, mainly because of difficulty with the chromatography. It was, however, sufficient to show unequivocally that isomerization of *cis*-butene-2 had occurred and that it did not occur in blank runs. One of the better results indicated that 90% of the fluorobenzene molecules which adsorbed radiation ended up in the triplet state.

Discussion

There are several ways of determining whether or not one is dealing with a triplet state. These methods must be used with caution since triplet states of different molecules will not respond to any given test in the same manner.¹⁸ The experimental observation of a strong,

(17) N. A. Coward and W. A. Noyes, Jr., *J. Phys. Chem.*, **22**, 1207 (1954).

(18) D. W. Sester, D. W. Placzek, R. J. Cvetanovic, and B. S. Rabinovitch, *Can. J. Chem.*, **40**, 2179 (1962).

sensitized emission of biacetyl when fluorobenzene is excited at 2537 Å. is not in itself sufficient evidence for postulating the existence of a triplet state of fluorobenzene. Only if the ratio of the integrated green to the integrated blue is much larger than 60:1^{19,20} can biacetyl emission be used as conclusive evidence of triplet sensitization. To obtain good values of the blue-to-green ratio requires exposures of up to 12 days at the intensities available. In the present study, rather than go to such long exposures, the *cis-trans* isomerization of butene-2 was used as confirming evidence for triplet fluorobenzene. The evidence for the formation of triplet fluorobenzene may now be summarized as follows.

(1) The sensitized emission yield of biacetyl reaches a maximum value of 0.136 ± 0.013 at 2537 Å. The value for the phosphorescence efficiency when biacetyl is excited directly at 4358 Å. has been given by Almy and Gillette²¹ as 0.15 ± 0.03 . The data on sensitized emission therefore indicate that 80 to 97% of all the initially excited fluorobenzene molecules transfer their energy to biacetyl. The fluorescence yield of fluorobenzene with the presence of biacetyl at the maximum is about 0.16. The total lies between 0.96 and 1.13. With the rather large errors in the data, all of the initially excited fluorobenzene molecules either fluoresce or cross over to the triplet state.

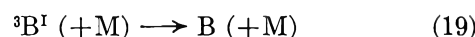
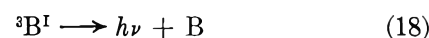
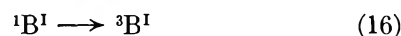
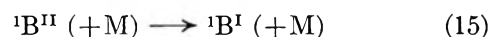
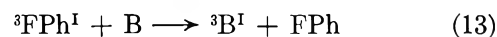
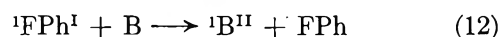
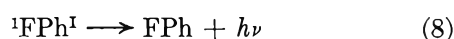
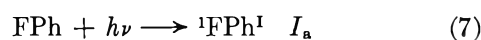
(2) One plate of the sensitized emission was taken, and it showed the integrated green-to-blue ratio to be much larger than the 60:1 value obtained when biacetyl is excited directly.

(3) Michael and Noyes²² have given a derivation which shows that, if one takes slope over intercept from a plot of biacetyl concentration, over sensitized emission *vs.* biacetyl concentration, $(B)/Q_s$ *vs.* (B), it will be equal to slope over intercept of a plot of $1/Q$ (where Q is the quantum yield of any measurable quantity for some process such as fluorescence or decomposition) *vs.* biacetyl concentration if both processes occur from the same spin state. In our case, slope over intercept for sensitized emission is 0.72 whereas slope over intercept for fluorescence quenching of fluorobenzene by biacetyl is 0.13, or that state of fluorobenzene which undergoes fluorescence cannot be the same one which passes on its energy to biacetyl. The kinetics shown below elucidate this point.

(4) The observations in the presence of *cis*-butene-2 are in themselves quite strong evidence that a large fraction of the excited fluorobenzene molecules reaches the triplet state. The singlet state of fluorobenzene cannot transfer energy to the olefin since the singlet state of the former is lower in energy than the singlet state of the latter.²³ The olefin has no effect on the

emission of biacetyl, but it does strongly quench the sensitized emission. It is, therefore, removing triplet fluorobenzene molecules before they can sensitize the emission of biacetyl. Moreover *cis-trans* isomerization of the olefin is observed when fluorobenzene is excited in its presence. This is typical of triplet state behavior.²⁴

The following mechanism is consistent with the experimental results and the photochemical behavior of biacetyl²⁵



In the above scheme FPh represents a ground-state fluorobenzene molecule, B is a ground-state biacetyl molecule, M is any molecule capable of removing vibrational energy, the superscripts refer to singlet and triplet states, and the Roman numerals refer to the first and second excited states.

All radiationless processes are shown as possibly being bimolecular. It is difficult to conceive of any of the occurring without the removal of vibrational energy although this may not be the rate-determining

(19) H. Okabe and W. A. Noyes, Jr., *J. Am. Chem. Soc.*, **79**, 801 (1958).

(20) H. L. J. Bäckstrom and K. Sandros, *Acta Chem. Scand.*, **14**, 48 (1960).

(21) G. M. Almy and P. R. Gillette, *J. Chem. Phys.*, **11**, 188 (1943).

(22) J. L. Michael and W. A. Noyes, Jr., *J. Am. Chem. Soc.*, **85**, 1027 (1963).

(23) P. G. Wilkinson and R. S. Mulliken, *J. Chem. Phys.*, **23**, 1895 (1955).

(24) H. M. Frey, *J. Am. Chem. Soc.*, **82**, 5947 (1960).

(25) W. A. Noyes, Jr., G. B. Porter, and J. E. Jolley, *Chem. Rev.*, **56**, 49 (1956).

step.²⁶ Reaction 14 is much more rapid than (15).²⁷ We may therefore neglect steps 15, 16, and 17.

For the scheme shown above the expression for fluorescence efficiency of fluorobenzene can be shown to be

$$1/Q_f = 1 + \frac{k_9}{k_8} + \frac{k_{10}}{k_8}(\text{FPh}) + \frac{k_{12}}{k_8}(\text{B}) \quad (20)$$

For the case of no biacetyl present, the last term on the right-hand side of (20) vanishes, and one should have a straight line with slope equal to k_{10}/k_8 . When the fluorobenzene is kept constant, we should again have a straight line, and this time the slope will be k_{12}/k_8 . The experimental results show that this is indeed the case and that $k_{10}/k_8 = 2.05 \times 10^3$ whereas $k_{12}/k_8 = 6.1 \times 10^3$; these data indicate that k_{12} is about three times as large as k_{10} . Slope over intercept for constant fluorobenzene in eq. 20 will be given by

$$\frac{\text{slope}}{\text{intercept}} = \frac{k_{12}}{k_8 + k_9 + k_{10}(\text{FPh})} \quad (21)$$

If reaction 13 does not occur and sensitized emission is due to (12) followed by (15)–(19), then one obtains for $(\text{B})/Q_s$

$$\frac{(\text{B})}{Q_s} = \frac{(k_{18} + k_{19})(k_{16} + k_{17})(k_{14} + k_{15}) \times (k_8 + k_9 + k_{10}(\text{FPh}) + k_{12}(\text{B}))}{k_{18}k_{16}k_{15}k_{12}} \quad (22)$$

At constant (FPh) the slope of (22) will be

$$\text{slope} = \frac{k_{12}(k_{18} + k_{19})(k_{16} + k_{17})(k_{15} + k_{14})}{k_{18}k_{16}k_{15}k_{12}} \quad (23)$$

and the intercept of (22) will be

$$\text{intercept} = \frac{(k_8 + k_9 + k_{10}(\text{FPh}))(k_{18} + k_{19}) \times (k_{16} + k_{17})(k_{15} + k_{14})}{k_{18}k_{16}k_{15}k_{12}} \quad (24)$$

and the slope over the intercept is the same as (21). On the other hand, if (13) does occur, then $(\text{B})/Q_s$ will be given by

$$\frac{(\text{B})}{Q_s} = \frac{(k_{18} + k_{19})(k_{13}(\text{B}) + k_{11}) \times (k_8 + k_9 + k_{10}(\text{FPh}) + k_{12}(\text{B}))}{k_{18}k_{13}k_9} \quad (25)$$

From the above we can conclude that the singlet

state of fluorobenzene is not the one which causes the sensitized emission of biacetyl since slope over intercept can in no way equal (21). An examination of eq. 25 shows that k_{11} is not negligible with respect to k_{13} (B). If this were the case, the slope over intercept of $1/Q_s$ vs. (B) should equal the slope over intercept for $1/Q_f$ vs. (B) at constant fluorobenzene pressure.

The integrated molar absorptivity of fluorobenzene has been given as 2.03×10^6 ²⁸; this leads to a fluorescence lifetime (τ) of 1.14×10^{-7} sec.

$$\tau = \frac{1}{k_8} \quad (26)$$

The above yields 8.77×10^6 sec.⁻¹ as the limiting value of k_8 . From eq. 2 and 20 and k_8, k_9 is found to be 2.82×10^7 sec.⁻¹. From the slope of eq. 20 at zero biacetyl pressure, k_{10} can be calculated and is found to be 2.98×10^{-11} molecule⁻¹ cm.³ sec.⁻¹. This leads to a self-quenching cross section of 2.07×10^{-16} cm.² for fluorobenzene. The ratio of k_{12} to k_{10} is 3. This leads to a value of 8.8×10^{-11} molecule⁻¹ cm.³ sec.⁻¹ for k_{12} . We may now use k_{12} to estimate an effective cross section for quenching of singlet fluorobenzene by biacetyl which turns out to be about 6.0×10^{-16} cm.². Should this be the correct value, then one would be forced to conclude that biacetyl quenches the singlet state of fluorobenzene very effectively.

Earlier in this discussion it was noted that k_{11} is not negligible with respect to k_{13} (B). If, however, this assumption is made and the appropriate values are inserted into eq. 25, we can obtain $k_{18}/(k_{18} + k_{19})$, i.e., the fraction of triplet state biacetyl molecules which emits. On going through the above procedure, $k_{18}/(k_{18} + k_{19})$ is found to be about 0.24 which is rather high but not too far out of agreement with the value obtained by Almy and Gillette.²¹

Acknowledgments. The author is deeply indebted to Dr. W. A. Noyes, Jr., for many helpful discussions and suggestions during the course of this work. Financial support from the Robert A. Welch Foundation is also gratefully acknowledged.

(26) W. A. Noyes, Jr., *Proc. Acad. Sci. Lisbon*, 3 (1962).

(27) A. G. Harrison and F. P. Lossing, *Can. J. Chem.*, 37, 1478 (1959).

(28) M. Ballester, J. Palau, and J. Riera, *J. Quant. Spectry. Radiative Transfer*, 4, 819 (1964).

Kinetics of the Attack of Molybdenum by Dissociated Chlorine¹

by Daniel E. Rosner and H. Donald Allendorf

*AeroChem Research Laboratories, Inc., Subsidiary of Pfudler Permutit Inc.,
Princeton, New Jersey 08540 (Received July 13, 1965)*

The true kinetics of the attack of molybdenum surfaces by both atomic and diatomic chlorine have been studied using microwave discharge-fast flow system techniques coupled with electrical resistance heating and monitoring of the reacting specimens. Experimental results are reported herein over the surface temperature range from 400 to 1530°K., at reactant partial pressures of the order of 10^{-3} to 10^{-1} torr. In contrast to the behavior of nickel, dissociation markedly increases the chlorination probability of molybdenum over the entire temperature range investigated, the enhancement being of the order of 100-fold at about 1000°K. The high reaction probability for $\text{Cl}_2(\text{g})$ attack of high-temperature nickel, previously reported by McKinley and Shuler, has been verified. When exposed to dissociated chlorine, the ratio of the nickel chlorination rate to the Cl atom recombination rate decreases with decreasing surface temperature—on 420°K. nickel filaments the recombination coefficient γ has been found to be $1/2$. The implications of these results with regard to dissociative adsorption on and evaporation from nickel and molybdenum surfaces are discussed in the light of available kinetic and thermochemical data for these and related heterogeneous reactions.

Introduction

Dissociative adsorption on either metal surface sites or chemisorbed halogen atom monolayers plays a major role in determining the observed kinetics of the high-temperature heterogeneous reactions between metals and the gaseous diatomic halogens X_2 ($=\text{Cl}_2$, Br_2 , ...).²⁻⁴ While many such reactions (*e.g.*, the chlorination of copper⁵ and nickel^{2,6}) have been reported to occur with very high reaction probabilities ($\epsilon > 10^{-1}$) over a wide temperature range, several (*e.g.*, the reaction between platinum and iodine⁷ and the molybdenum-chlorine reaction discussed below) exhibit much lower reaction probabilities and correspondingly high activation energies. In view of these differences, a series of studies of the kinetics of high-temperature metal halogenation reactions in partially dissociated gas mixtures has been initiated at this laboratory with the expectation that a comparison of the results with those obtained in undissociated gases will shed light on the relative importance of dissociative adsorption as a rate-limiting step in this class of heterogeneous reactions. These data should also provide valuable information on the response of refractory metals in partially dissociated halogen-con-

taining gas mixtures, such as occur in lamps and thermionic devices utilizing chemical-transport reactions^{7,8} and in the combustion products of current and future generation solid propellants.

The experiments reported herein were designed to provide the first high-temperature data on the attack of polycrystalline molybdenum by atomic chlorine under conditions such that the observed reaction rates (a) would not be falsified by reactant or product diffusional limitations^{9,10} and thermal accommodation

(1) Supported by the Propulsion Division of the Air Force Office of Scientific Research under Contract AF 49(638)1195.

(2) J. D. McKinley, *J. Chem. Phys.*, **40**, 120 (1964).

(3) J. N. Smith, Jr., and W. L. Fite, "Rarefied Gas Dynamics," Vol. 1, J. A. Laurmann, Ed., Academic Press, Inc., New York, N. Y., 1963, p. 430.

(4) (a) J. D. McKinley, *J. Chem. Phys.*, **40**, 576 (1964); (b) *ibid.*, **41**, 2814 (1964).

(5) L. Frommer and M. Polanyi, *Z. physik. Chem.* **137A**, 201 (1928).

(6) J. D. McKinley and K. E. Shuler, *J. Chem. Phys.*, **28**, 1207 (1958).

(7) L. K. Tower, *Advan. Energy Conversion*, **3**, 185 (1963).

(8) H. Schäfer, "Chemical Transport Reactions," translated by H. Frankfort, Academic Press Inc., New York, N. Y., 1964.

effects and (b) could be directly compared with chlorination rates for diatomic chlorine on the same molybdenum surface using the same experimental techniques. Despite the rapidity of the Cl atom attack, this has been accomplished at surface temperatures up to 1530°K. by combining the conditions of low pressure, high pumping speed, and small specimen size, as described below. In addition, we have determined the recombination coefficient for Cl atoms on nickel and confirmed the high reaction probability for Cl₂ on nickel filaments above 1000°K., first reported by McKinley and Shuler.⁶

Experimental Section

The techniques used here are similar to those developed in our previous kinetic studies of the oxygen atom attack of molybdenum¹¹ and graphite,^{12,13} the principal differences being those necessitated in the area of chlorine atom detection.

Atom Production. As indicated schematically in Figure 1, the apparatus consists of a part Vycor, part Pyrex vacuum flow system coupled to a 25-l./sec. mechanical pump (not shown). Metered Ar-Cl₂ gas mixtures (dilute in Cl₂) are passed through a 2450-Mc./sec., 125-w. microwave discharge cavity,¹⁴ 28 cm. downstream of which the gas encounters the electrically heated filament being studied. Flow metering was accomplished using sonic flow orifices fabricated from jeweled watch bearings.¹⁵ The Cl₂ flow rate was calibrated using absorption by Indicarb¹⁶ as the primary standard. Unless otherwise specified, the static pressure level at the specimen location was maintained at 1 torr, and the flow rate was maintained at 21.7 cc. (STP)/sec. This corresponded to a linear velocity of approximately 2×10^4 cm./sec. in the discharge tube or a residence time of 45 μsec./cm.

H₃PO₄ was used to poison the Vycor walls of the discharge tube to the heterogeneous recombination of Cl atoms.¹⁷ At comparable pressure and gas compositions (and at much lower flow rates) Ogryzlo¹⁷ verified the production of Cl atoms using a Wrede gauge, the discoloration of silver mirrors, and the removal of Cl atoms by homogeneous reaction with NOCl (using a calorimetric probe as the titration end point detector). Indeed, comparison of the chemical titration method with the output of a calorimetric detector led to the conclusion that below 4 torr Cl atom recombination was solely responsible for the surface-catalyzed heating of nickel detectors at $T \approx 400^\circ\text{K}$. In the present experiments a nickel wire detector revealed that a tenfold variation in Cl atom concentration (at detectable levels) was obtained through variations of the Cl₂ mole fraction in the feed gas and changes in

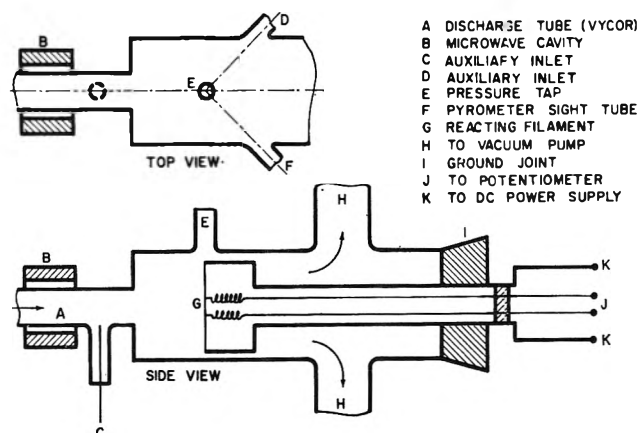


Figure 1. Filament chlorination apparatus.

microwave cavity tuning. In most of the experiments reported below, the Cl atom mole fraction was maintained at 4.3×10^{-3} and the initial Cl₂ mole fraction in the feed was 10^{-2} . This condition corresponds to the dissociation of roughly 22% of the Cl₂ molecules passing through the microwave discharge.

Reaction Rate. The technique used for following the rate of the heterogeneous chlorination reaction was to monitor continuously the resistance-time curve of an electrically heated filament and to relate this to the diameter reduction caused by the reaction of molybdenum to form volatile products.¹¹ The molybdenum filaments, of initial diameter 0.0281 cm. (15 mils) and total length 3 cm., were electrically heated using a regulated d.c. power supply. Together with current measurements, the voltage drop across the central 0.55 cm. of the filament was continuously monitored using spring-loaded contacts (cf. Figure 1) leading to a recording potentiometer. During a run the filament was maintained at constant surface temperature by manually altering the current in accord with an optical pyrometer output (for $T > 900^\circ\text{K}$.) or a thermocouple output¹⁸ ($T < 900^\circ\text{K}$.),

- (9) D. E. Rosner, *AIAA J.*, **2**, 593 (1964).
 (10) D. E. Rosner, AeroChem TP-111, April 1965; *Intern. J. Heat Mass Transfer*, submitted.
 (11) D. E. Rosner and H. D. Allendorf, *J. Chem. Phys.*, **40**, 3441 (1964).
 (12) D. E. Rosner and H. D. Allendorf, *Carbon*, in press.
 (13) D. E. Rosner and H. D. Allendorf, *AIAA J.*, **3**, 1522 (1965).
 (14) Raytheon Microtherm generator and cavity supplied by Ophos Instrument Co., Rockville, Md.
 (15) D. E. Rosner, *J. Basic Eng.*, **84**, 458 (1962).
 (16) Fisher Scientific Co. acid absorbent.
 (17) E. A. Ogryzlo, *Can. J. Chem.*, **39**, 2556 (1961).
 (18) A 0.0127-cm. chromel-alumel thermocouple junction diagonally lashed (with spring loading) across the center of the reacting molybdenum filament was used for this purpose. As will be seen below, data at the upper end of this temperature range satisfactorily matched data obtained using optical pyrometer temperature control.

thereby allowing the decrease in filament diameter caused by the reaction (typically less than a total of 0.005 cm.) to be related to the observed increase in electrical resistance. It should be stressed that, while the optical pyrometer or thermocouple was used to maintain constant filament temperature during an experiment, the *absolute value* of the surface temperature, which in the present experiments was in the range 400–1530° K., was determined from the initial filament resistance in accord with its resistivity–temperature relation.¹⁹ A typical plot of inferred filament diameter *vs.* time is shown in Figure 2, in which data for both undissociated and dissociated chlorine are included for comparison. In each case the reaction rate (proportional to the absolute value of the slope) is seen to be constant in time, as is to be expected for heterogeneous reactions forming volatile (nonprotective) products. Owing to the large increase in reaction rate upon activation of the electrical discharge and the small concentrations of Cl₂(g) present, the observed reaction rate for the dissociated gas condition is fortunately dominated by the Cl atom contribution, thereby necessitating only small corrections (typically less than 3%) for the Cl₂ contribution.

Atom Detection. Owing to the high flow rates used, it was not possible to utilize the NOCl titration to determine absolute Cl atom concentrations. Instead, calorimetric techniques based on the heat release upon surface-catalyzed Cl atom recombination were invoked.^{17,20} Two types of nickel catalytic detectors were used, one for relative atom concentration determinations and the other for absolute determination at one flow condition. The first consisted of an electrically heated 0.0381-cm. diameter nickel wire spanning the flow (at the molybdenum specimen location when the specimen was removed). In this case the atom concentration is taken to be proportional to the change in power required to maintain constant filament temperature (~420° K.) in the presence and absence of Cl atoms.²¹ Absolute atom concentrations were determined in a similar way, but using instead a 163-cm. length of nickel wire wrapped in the shape of a cone (base diameter 1.2 cm, altitude 6.4 cm., apex downstream) mounted at the end of the discharge tube in such a way as to recombine all of the atoms passing through the tube into the test section. The observed power difference²¹ was converted to Cl atom concentration by assuming that each atom releases its thermodynamic heat of recombination at the nickel calorimeter surface. This measurement was repeated seven times, with the result displaying a 7% average deviation from the mean. Confirmation that all atoms were removed from the stream was obtained based on com-

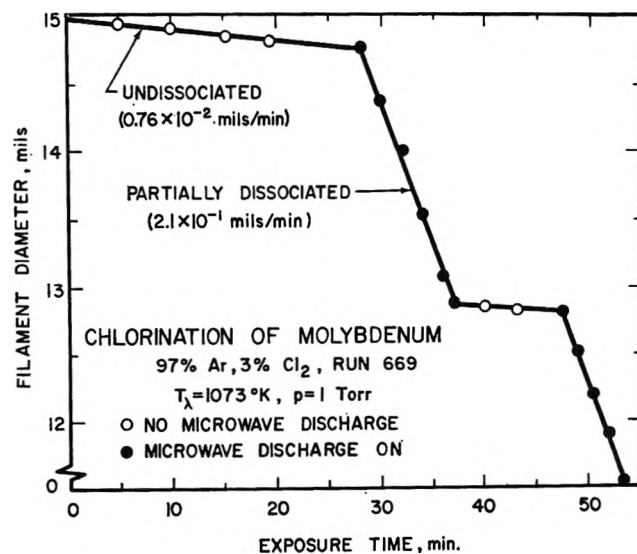


Figure 2. Effect of dissociation on the chlorination rate of molybdenum.

parisons with similar results using longer filaments (length 237 cm.) coiled in the same fashion.

Materials. All the data included herein were obtained using commercially available polycrystalline molybdenum (Westinghouse Lamp Division, Bloomfield, N. J., Type A, Process C3H) and nickel (International Wire Products Co., New York, N. Y., Grade A) filaments. High Purity grade (Matheson) chlorine and Welding grade (Air Reduction Corp.) argon cylinder gases were used without pretreatment. Static pressure at the filament location was measured using a U-tube manometer (equipped with a micrometer depth gauge) containing dibutyl phthalate.

Results

It will prove instructive to cast the experimental results for both the Cl(g)–Mo(s) and Cl₂(g)–Mo(s) reactions in terms of dimensionless reaction probabilities. In the present case this can be done without a knowledge of the product gas species distribution by introducing the *chlorination probability* ϵ , defined here

(19) J. L. Everhart, W. E. Lindlie, J. Kanegis, P. G. Weissler, and F. Siegel, National Bureau of Standards Circular No. C447, U. S. Government Printing Office, Washington, D. C., 1943.

(20) D. E. Rosner, *J. Am. Rocket Soc.*, **32**, 1065 (1962); see also L. Elias, E. A. Ogryzlo, and H. I. Schiff, *Can. J. Chem.*, **37**, 1680 (1959).

(21) Since the gas temperature (as measured by a poisoned, glass-covered thermocouple) is appreciably altered by the presence of the electrical discharge, as well as by the presence or absence of Cl₂ when the discharge is on, the following modified procedure was adopted. The power required in the presence of a discharge through the Cl₂–Ar mixture was compared to the power required to maintain the same detector surface temperature in a pure argon discharge at the same flow rate but with the tuning adjusted to maintain the same gas temperature.

as the ratio of the flux of molybdenum atoms (regardless of their chemical state of aggregation) away from the surface to the collision flux of Cl(g) or Cl₂(g) with the surface. The molybdenum atom flux, Z''_{Mo} , is obtained from the observed rate of filament diameter change, the density of the filament (10.0 g./cc.), and the molecular weight of molybdenum (95.95 g./mole). The incident Cl(g) or Cl₂(g) flux (Z''_{Cl} , Z''_{Cl_2}) is directly proportional to their known partial pressures and is obtained from the Hertz-Knudsen equation evaluated at the filament surface temperature T

$$Z''_i = \left(\frac{p_i}{kT}\right) \left(\frac{kT}{2\pi m_i}\right)^{1/2} \quad (1)$$

where $i = \text{Cl}$ or Cl_2 , p_i and m_i are, respectively, the partial pressure and molecular mass of species i , and k is the Boltzmann constant. Thus, if Z''_{Mo} is experimentally found to be proportional to the n th power of the chlorine partial pressure, where n is the reaction order, the probability ϵ will be proportional to the $n - 1$ power of chlorine partial pressure (and, hence, independent of the latter when the reaction is first order, *i.e.*, when $n = 1$). It is also seen from eq. 1 that the apparent activation energy locally inferred from an Arrhenius plot of $\ln \epsilon$ vs. $1/T$ will exceed that obtained from a plot of $\ln Z''_{Mo}$ vs. $1/T$ by the amount $RT/2$, where R is the universal gas constant.

The Chlorination Probability and Its Temperature Dependence. Figure 3 summarizes the results of 27 experiments on the chlorination probability as a function of molybdenum surface temperature, for both chlorine atom and chlorine molecule attack. It is clear that over the entire temperature range studied Cl atom strikes are significantly more effective than Cl₂ strikes in removing molybdenum atoms from the filament. Even at 400°K. roughly 1 out of every 35 Cl atom strikes is successful, and at temperatures near 1000°K. the reaction probability attains values of the order of 2 out of every 3 collisions. In contrast, the Cl₂ reaction probability (at $p_{Cl_2} = 3 \times 10^{-2}$ torr) never exceeded $\sim 1/100$ and, at temperatures less than 1000°K., differed from the corresponding Cl atom reaction probability by more than two orders of magnitude. Neither reaction probability displays simple Arrhenius (constant activation energy) behavior, and each, in fact, exhibits a true maximum. However, this maximum is very shallow in the case of the Cl atom attack, for which a temperature change of some 400°K. produces no appreciable change in the reaction probability. At surface temperatures below about 1100°K. the Cl₂ data can be represented by a straight line, corresponding to an observed activation energy of 13.7 kcal./mole. For the Cl data the observed

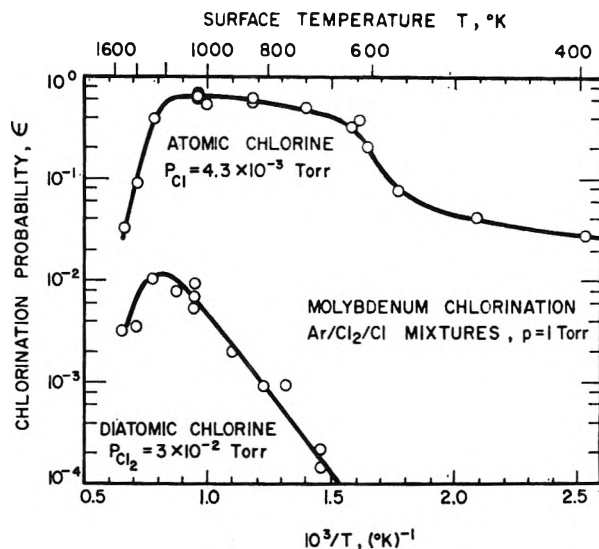


Figure 3. Chlorination probabilities for the attack of molybdenum by atomic and diatomic chlorine.

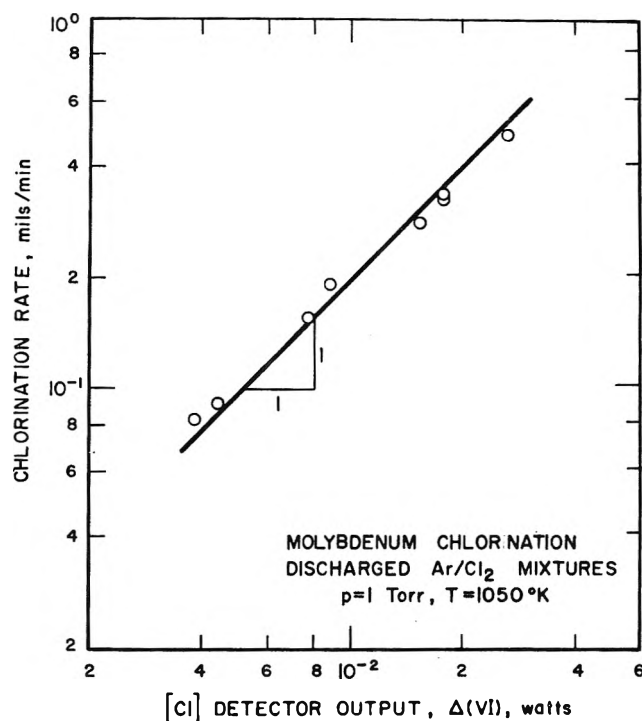


Figure 4. Kinetic order plot for the attack of molybdenum by atomic chlorine.

activation energy varies continuously with temperature and appears to pass through a maximum near 600°K.

Kinetic Order of the Cl Atom Attack. A series of experiments was performed on 1050°K. molybdenum filaments to determine the kinetic order of the Cl atom attack mechanism in the range of maximum reaction

probability. The Cl atom concentration was varied over about a sevenfold range, as determined from the output of a 420°K. nickel filament catalytic detector.²¹ This produced the variations in chlorination rate ($\propto Z''_{Mo}$) shown in Figure 4. Since these data are well represented by a straight line of unit slope (on log-log coordinates), one may conclude that the reaction order is unity under these conditions, and hence the maximum Cl atom reaction probabilities, shown in Figure 3 for the case $p_{Cl} = 4.3 \times 10^{-3}$ torr, would remain invariant with (at least comparable) changes in Cl atom pressure.

Chlorination of High-Temperature Nickel. McKinley and Shuler have reported⁶ values for the reaction probability for the attack of nickel by diatomic chlorine of the order of²² $1/2$ at filament temperatures between 1200 and 1700°K. and at chlorine partial pressures of 0.8×10^{-1} to 4×10^{-1} torr. If the $Cl_2(g)$ reaction probability on a nickel surface is indeed this high, then one should not expect a drastic increase in reaction efficiency upon prior dissociation of chlorine. To test this prediction and to confirm the results of ref. 6, several experiments were performed on the chlorination of nickel filaments of the type previously used for atom detection. In this case the filaments were electrically heated to an estimated temperature of 1080°K. in an argon-chlorine stream containing 1% $Cl_2(g)$ at a total pressure of 1 torr. In the absence of a discharge, the observed rate of diameter decrease ($\sim 1.3 \times 10^{-4}$ cm./sec.) indeed corresponded to a reaction probability of approximately $1/2$. Moreover, in contrast to the corresponding result for molybdenum (*cf.* Figure 2), activation of the discharge produced virtually no change in the observed rate of diameter decrease. These results, which are consistent with those of ref. 6, reveal significant differences between the nickel and molybdenum chlorination reactions.

Cl Atom Recombination Probability on a Nickel Surface. The output of the relative atom concentration detector described earlier is proportional to the product of the recombination coefficient γ and the Cl atom concentration. Consequently, an independent determination of the absolute Cl atom concentration using the coiled nickel filament detector made possible the quantitative estimate $\gamma \approx 1/2$ for Cl atom recombination on a 420°K. nickel surface. This result, when taken together with the observation that the nickel chlorination rate at this low temperature was not measurable, reveals that, as the filament temperature is decreased, recombination (rather than chlorination) becomes the favored fate for the Cl atom. Similar trends apparently characterize the interaction

of O atoms with graphite^{12,13}; *i.e.*, the ratio of ϵ to γ is an increasing function of surface temperature.

Discussion

Identity of the Active Species. Based on the work of Ogryzlo¹⁷ using similar atom production and detection techniques, as well as the data presented in Figure 4, it is concluded that the observed reactivity of the chlorine passed through the microwave discharge is due to the presence of ground state $Cl(^2P_{3/2})$ atoms.

At comparable microwave power levels and pressures Ogryzlo¹⁷ reported agreement between the Cl atom concentration as determined from the quantitative gas phase titration reaction



and the output of a calorimetric nickel detector. While $Cl_2(A^3\Pi_{ou+})$ has been identified in the products of chlorine discharges,²³ its presence here due to production in the discharge or by subsequent preassociation of $Cl(^2P_{3/2})$ atoms can be ruled out on the basis of residence time considerations.²⁴

Finally, the fact that the observed chlorination rate increased linearly with the Cl atom concentration inferred from the output of a nickel calorimeter detector (see Figure 4) constitutes further indirect evidence that excited Cl_2 molecules (written Cl_2^*) play a negligible role in the present work. These experiments cover a twofold range of initial Cl_2 mole fractions and were carried out at microwave power levels from 60 to 90% of full power. If excited chlorine molecules played a significant role both in the observed kinetics and in the nickel detector response, it is unlikely that a linear correlation would be observed over the resulting range of $[Cl_2^*]/[Cl]$ ratios.

Absence of Transport Limitations. While reductions in the apparent activation energy of high-temperature heterogeneous reactions are frequently associated with a local depletion of reactant due to physical limitations on its rate of supply (by convective diffusion),^{9,10,25,26} previous studies of the oxidation of molybdenum, tungsten, and graphite at comparable reaction rates,

(22) Based on the filament temperature. The corresponding value based on the use of the upstream gas temperature in eq. 1 was $1/6$.

(23) L. W. Bader and E. A. Ogryzlo, *J. Chem. Phys.*, **41**, 2926 (1964).

(24) The radiative lifetime of $Cl_2(^3\Pi_{ou+})$ is shorter²³ than 10^{-8} sec. Moreover, using the termolecular rate constant $k_{Ar} = 4 \times 10^{16}$ cm.⁶ mole⁻² sec.⁻¹ for the homogeneous recombination of Cl atoms with argon as a third body (L. W. Bader and E. A. Ogryzlo, *Nature*, **201**, 491 (1964)), the residence time required for the initial Cl atom concentration to fall to half of its original value would exceed 10 sec. in the present experiments.

(25) D. E. Rosner and H. D. Allendorf, *J. Electrochem. Soc.*, **111**, 759 (1964).

(26) D. E. Rosner and H. D. Allendorf, *ibid.*, **112**, 653 (1965).

reactant flow rates, surface temperatures, and reactant partial pressures have demonstrated the absence of this class of physical phenomena in the present reactor.¹¹⁻¹³ Thus, reported reaction rates¹¹⁻¹³ are found to be independent of both reactant flow rate and identity of the carrier gas.²⁶ Consequently, the observed departures of the molybdenum chlorination probabilities from simple Arrhenius behavior are believed to be true kinetic phenomena, characteristic of the temperature and chlorine partial pressure levels encountered herein and not peculiar to this particular reactor configuration.

Mechanistic Considerations. If every incident Cl₂ molecule produced one MoCl₂(g) product molecule, ϵ would be unity. Similarly, if every incident Cl atom is used to produce one MoCl₂(g) molecule, ϵ would be 1/2. When ϵ is considerably below these values,²⁷ it is clear that some chlorine is being reflected from the surface and/or is adsorbed but later evaporated as either Cl₂(g) or Cl(g) before chemical reaction can occur.

Considering first the reaction of Cl₂(g) with Mo(s) and Ni(s), we note that the molybdenum chlorination probability passes through a maximum and then falls off sharply at higher temperatures (cf. Figure 3) whereas, under similar conditions, the nickel chlorination probability does not exhibit this feature.⁶ This suggests that the chlorine adsorbed on molybdenum is more weakly bound and thus more likely to evaporate²⁸ as Cl(g) and Cl₂(g). This reduces the high-temperature reaction probability of molybdenum.²⁹ The large value of ϵ for high-temperature nickel also implies a high sticking probability when Cl₂(g) is incident upon this surface; i.e., a significant fraction of incident molecules dissociatively adsorb on the Cl atom covered nickel surface.³⁰ With this combination of high sticking probability and low evaporation rate of unreacted chlorine, it is not surprising to find that prior dissociation of the incident chlorine causes no significant increase in the high-temperature reaction probability of nickel. In the case of molybdenum, however, the sticking probability is apparently low, and the evaporation rate of unreacted chlorine is larger. Prior dissociation can therefore greatly increase the over-all reaction probability ϵ in two distinct ways: (i) by increasing the sticking probability, leaving the remainder of the reaction mechanism essentially unaltered, and (ii) by introducing a Rideal-type mechanism in which a Cl atom from the gas phase can react directly with adsorbed chlorine atoms to form a complex leading to the desorption either of reaction product or of diatomic chlorine.³¹ Both of these mech-

anisms are readily reconciled with the observed first-order kinetic behavior of this reaction (cf. Figure 4).³²

Homogeneous Thermal Dissociation. At 1500°K. the extent of Cl₂ dissociation predicted *thermo-dynamically* is appreciable. Indeed, based on the 1500°K. equilibrium constant, $p_{Cl}/p_{Cl_2}^{-1/2} = 10^{-1.226}$ atm.^{1/2},

(27) The corresponding values for the reaction product MoCl₂(g) are 2/3 and 1/3, respectively. For MoCl(g) they are 2 and 1, respectively.

(28) In the absence of adsorption heat data some insight into the relevant binding energies can be obtained from an examination of the relative bond strengths of the gaseous metal chlorides. At 298.16°K. the dissociation energy of NiCl(g) is given as 115 kcal./mole: A. G. Gaydon, "Bond Dissociation Energies," Chapman and Hall, 1953. From the heats of formation of the tungsten chlorides WCl_n(g) ($n = 2, 4, 5, 6$) given in the "JANAF Thermochemical Tables," Dow Chemical Co., Midland, Mich., we estimate the WCl bond strength to be about 113 kcal./mole. While a reliable value for the MoCl bond does not appear to be available, the tungsten value given here and ratios taken from L. L. Quill, "The Chemistry and Metallurgy of Miscellaneous Materials, Thermodynamics," McGraw-Hill Book Co., Inc., New York, N. Y., 1950, indicate an MoCl bond strength of about 99 kcal./mole. For comparison, note that the Cl-Cl bond in Cl₂(g) has a strength of only 57.1 kcal./mole (cf. Gaydon, cited previously in this footnote) and the heat of sublimation of molybdenum is 155.5 kcal./mole: T. L. Cottrell, "The Strengths of Chemical Bonds," Butterworth and Co. Ltd., London, 1958.

(29) While reliable data on the thermodynamics of the Mo-Cl system do not appear to be available, calculations of the partial pressures of WCl_n(g) ($n = 2, 4, 5, 6$), Cl(g), and Cl₂(g) in equilibrium with a tungsten surface can be made based on the JANAF thermochemical data. When this is done we find that the equilibrium Cl(g) and Cl₂(g) pressures become comparable to the imposed Cl(g) and Cl₂(g) pressures (in the present experiments) at surface temperatures in the range 1050-1250°K. At these and higher surface temperatures, the reaction to form the stable metal chlorides is thus thermodynamically not favored. Further verification of this tendency is provided by similar thermodynamic calculations and experiments on the molybdenum-oxygen and tungsten-oxygen systems. In contrast to the chlorination reactions studied here, we expect and find that, at comparable reactant partial pressures, the oxidation probability of tungsten and molybdenum monotonically increases in precisely the temperature range in which the chlorination probability drops off. For the attack of molybdenum and tungsten by O₂(g) these kinetic measurements extend to a surface temperature of 2600°K.: D. E. Rosner and H. D. Allendorf, AeroChem TN-61, May 1964; DDC AD 438 927. However, at lower O₂ pressures, maxima in ϵ have been experimentally observed below this surface temperature (cf., e.g., J. B. Berkowitz-Mattuck, *et al.*, *J. Chem. Phys.*, 39, 2722 (1963), Figure 8, and P. O. Schissel and O. C. Trulson, *ibid.*, 43, 737 (1965)).

(30) It is interesting to note here that, quite apart from bond strength considerations, the (2.49-Å.) minimum internuclear distance in the nickel crystal is closer to the (1.99-Å.) internuclear distance in chlorine than is the (2.72-Å.) minimum internuclear distance in the molybdenum lattice. Moreover, since the metal specimens studied are polycrystalline, the nickel structure, being f.c.c., presents more closely packed crystal faces to the chlorine than the b.c.c. molybdenum structure.

(31) It is anticipated that the relative importance of these routes can be assessed by independent measurements of the atom recombination probability on high-temperature reacting surfaces, or transient measurements of the average residence time of a Cl atom on the surface (when the specimen is subjected to a modulated atomic beam, in the spirit of ref. 2).

(32) Interestingly enough, at these reactant partial pressure levels, all high-temperature kinetic studies carried out thus far of O atom reactions on the refractory metals (Mo, W),¹¹ graphite,^{12,13} and platinum (cf. G. C. Fryberg, *J. Chem. Phys.*, 24, 175 (1956)) have revealed large enhancements in the reaction rate and first-order kinetic behavior.

the gas wetting the filament would contain a Cl atom partial pressure of 5.60×10^{-2} torr, even in the absence of a microwave discharge. At first sight, this casts doubt on the significance of the data in "undissociated chlorine" at these filament temperatures. However, while it is likely that the gas temperature is raised locally to the filament surface temperature,³³ it is unlikely that adequate time is available for homogeneous dissociation in the vicinity of the filament. This can be verified by comparing the residence time for a gas molecule within the thermal layer of the filament (at most of the order of $d^2/D_{\text{Cl}_2-\text{Ar}}$, where d is the filament diameter and $D_{\text{Cl}_2-\text{Ar}}$ is the Fick Cl_2 -Ar interdiffusion coefficient) to the characteristic time $(k_{d,\text{Ar}}n_{\text{Ar}})^{-1}$ for homogeneous Cl_2 dissociation (where $k_{d,\text{Ar}}$ is the appropriate dissociation rate constant³⁴ and n_{Ar} is the argon molecule number density). Since the residence time is found to be too small by more than five orders of magnitude, we are led to the conclusion that even at the highest filament temperatures investigated Cl atoms were effectively absent as a potential reactant in all chlorination experiments carried out with the electrical discharge off.

Conclusions

Based upon the experimental data and the discussion above, the following conclusions may be drawn.

(1) A convenient experimental technique, making use of a microwave discharge, a fast-flow subatmospheric pressure system, and resistance heating-monitoring of the specimen, has been developed to study the true kinetics of rapid metal chlorination by both $\text{Cl}(\text{g})$ and $\text{Cl}_2(\text{g})$ at partial pressures of the order of 10^{-3} torr and greater. The molybdenum and nickel chlorination reactions occur at constant (time-independent) rates, as expected for reactions forming volatile (non-protective) products.

(2) The high reaction probability ($\epsilon \sim 1/2$) of $\text{Cl}_2(\text{g})$ on nickel at surface temperatures above 1000°K ., first reported by McKinley and Shuler,⁶ has been verified. Consistent with this result, partial dissociation of chlorine in the microwave discharge has no appreciable effect on the chlorination rate of nickel.

(3) In contrast, with molybdenum, Cl atoms are considerably more reactive than diatomic chlorine

over the entire temperature range investigated (400 – 1530°K .). Even at 400°K ., only 35 Cl atom strikes are necessary to remove one molybdenum atom from the filament, and at temperatures near 1000°K . the reaction probability (which is independent of Cl atom concentration) attains values of the order of 2 out of every 3 collisions. Corresponding reaction probabilities for $\text{Cl}_2(\text{g})$ attack of molybdenum never exceeded $\sim 1/100$ (at $p_{\text{Cl}_2} = 3 \times 10^{-2}$ torr).

(4) These results suggest that the sticking probability for $\text{Cl}_2(\text{g})$ dissociative adsorption on (chlorine atom covered) nickel is much larger than on (chlorine atom covered) molybdenum. In the presence of $\text{Cl}(\text{g})$, this kinetic difficulty on molybdenum is circumvented, and a new (Rideal-type) mechanism, involving reaction as a result of direct gas phase atom strikes, also becomes available.

(5) Above about 1200°K . the molybdenum chlorination probability (for both attack by $\text{Cl}(\text{g})$ and $\text{Cl}_2(\text{g})$) decreases with increasing surface temperature, indicating appreciable evaporation of Cl_2 and/or Cl from the filament at these temperatures. The corresponding behavior for the oxidation of molybdenum and tungsten by $\text{O}_2(\text{g})$ at these partial pressure levels has not been observed at temperatures up to 2600°K .

(6) The recombination probability for Cl atoms on 420°K . nickel filaments is about $1/2$. As the surface temperature increases, the ratio of the chlorination rate to the recombination rate increases sharply.

Acknowledgment. The authors gratefully acknowledge the advice and assistance of Dr. A. Fontijn in the areas of the generation and detection of atomic species. We are especially indebted to the Propulsion Division of the United States Air Force Office of Scientific Research for its interest in and financial support of this research. In addition, we wish to thank Drs. J. D. McKinley and O. C. Trulson for helpful comments on this work.

(33) Since the filament diameter is of the order of 10 times the mean free path of the gas, molecules approaching the filament make an appreciable number of collisions with molecules which have either already interacted with the filament or collided with those that have.

(34) $k_{d,\text{Ar}} \sim 10^8 \text{ cm}^3 \text{ mole}^{-1} \text{ sec}^{-1}$ at 1500°K .: H. Hiraoka and R. Hardwick, *J. Chem. Phys.*, **36**, 1715 (1962).

Recoil Tritium Reaction: Ring Opening and Alkyl Replacement in Substituted Cyclopropanes¹

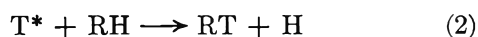
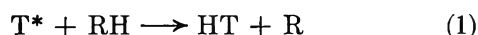
by Yi-Noo Tang and F. S. Rowland²

Departments of Chemistry, University of Kansas, Lawrence, Kansas, and University of California, Irvine, California (Received July 14, 1965)

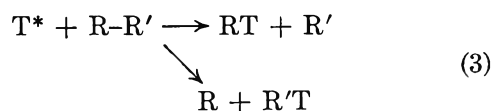
In addition to the two common reactions of abstraction of and substitution for hydrogen atoms, energetic recoil tritium atoms react with substituted cyclopropanes by attack on the C-C bond with ring opening and the formation of an excited, tritium-labeled radical. These free radicals subsequently decompose both by C-C bond break to a smaller radical and an olefin and also by the higher activation energy process of loss of a hydrogen atom, in about equal yields. The replacement of alkyl groups substituted on the cyclopropane ring by energetic tritium atoms also occurs, and the excited methylcyclopropane-*t* and cyclopropane-*t* molecules so formed are sufficiently excited to undergo unimolecular isomerization. The higher yields of olefinic products from the ring-opening reaction obscure these isomerization reactions and prevent quantitative estimates of the energies of excitation involved in the substitution of an energetic tritium atom for an alkyl group.

Introduction

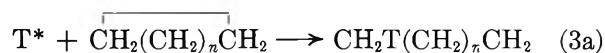
Energetic tritium atoms formed by nuclear recoil react with cyclanes, as with alkanes, primarily by the two hot reactions of abstraction of hydrogen atoms and substitution for them, as in reactions 1 and 2.³⁻¹⁶



In the hydrocarbon and halocarbon systems, smaller yields are regularly found for the products corresponding to the substitution of hot tritium for alkyl groups, as in reaction 3. Investigations of these reactions in



alkane systems are comparatively straightforward since both RT and R'T are stable molecules, each simple, smaller relatives of the parent molecule R-R'. In experiments carried out with cyclanes, however, these reactions are not so directly investigated since the equivalent replacement by the hot tritium atom of a carbon atom bonded to another should lead to the formation of a labeled free radical, as in (3a), whose subsequent reaction must also be understood.



Several years ago, the substitution of tritium for hydrogen in cyclopropane was postulated to leave the

(1) This research was supported by A.E.C. Contract No. AT-(11-1)-407.

(2) Department of Chemistry, University of California, Irvine, Calif.

(3) J. K. Lee, B. Musgrave, and F. S. Rowland, *J. Am. Chem. Soc.*, **81**, 3803 (1959).

(4) J. K. Lee, B. Musgrave, and F. S. Rowland, *Can. J. Chem.*, **38**, 1756 (1960).

(5) E. K. C. Lee and F. S. Rowland, *J. Am. Chem. Soc.*, **85**, 897 (1963).

(6) M. Henchman, D. Urch, and R. Wolfgang, "Chemical Effects of Nuclear Transformations," Vol. 2, International Atomic Energy Agency, Vienna, 1961, p. 83.

(7) F. S. Rowland, J. K. Lee, B. Musgrave, and R. M. White, ref. 6, p. 67.

(8) J. K. Lee, B. Musgrave, and F. S. Rowland, *J. Am. Chem. Soc.*, **82**, 3545 (1960).

(9) R. Odum and R. Wolfgang, *ibid.*, **85**, 1050 (1963).

(10) J. W. Root and F. S. Rowland, *ibid.*, **84**, 3027 (1962).

(11) E. K. C. Lee and F. S. Rowland, *ibid.*, **85**, 2907 (1962).

(12) J. W. Root and F. S. Rowland, *J. Chem. Phys.*, **38**, 2030 (1963).

(13) H. C. Jurgeleit and R. Wolfgang, *J. Am. Chem. Soc.*, **85**, 1057 (1963).

(14) W. Breckenridge, J. W. Root, and F. S. Rowland, *J. Chem. Phys.*, **39**, 2374 (1963).

labeled cyclopropane molecule in such an excited state that the molecule was able to undergo subsequent isomerization to propylene, and both labeled cyclopropane and labeled propylene are found in the system in agreement with this postulate.^{3,4} Furthermore, the measured yield of cyclopropane-*t* increases with the gas pressure during irradiation, as expected for a competition between isomerization and collisional stabilization for an energetic excited molecule.⁴ Subsequently, a careful investigation of the cyclobutane system disclosed complementary pressure-dependent yields of cyclobutane-*t* and the expected product of its decomposition, C₂H₃T, and led to an estimate of 5 e.v. as the average excitation energy of *c*-C₄H₇T molecules formed by reaction 2 with cyclobutane.⁵ Excitation energies in this range are already sufficient to produce various decomposition and isomerization processes with activation energies in the 3–4-e.v. range.^{17–19}

Small yields of butene-1 from recoil tritium reactions with cyclobutane support the hypothesis of the ring-opening reaction (3a) in cyclane systems.⁵ However, corresponding detailed studies of the cyclopropane system are complicated by the fact that the expected product of reaction 3a, following loss of an H atom from the excited radical, will be CH₂TCH=CH₂, while the isomerization of excited cyclopropane-*t* formed by reaction 2 would also lead to tritium-labeled propylene.^{20,21} Our present study of similar reactions with substituted cyclopropanes has been undertaken to furnish more definitive information about the occurrence of the ring-opening reaction in cyclane systems. Simultaneously, the possibility also exists for investigation of the secondary reactions following replacement by tritium atoms of alkyl groups bonded to cyclopropane rings, thereby providing a rough estimate of the average excitation energy remaining in the molecule after that hot reaction. These recoil tritium experiments have been carried out with ethylcyclopropane (EC), *cis*-1,2-dimethylcyclopropane (*cis*-DMC), and *trans*-1,2-dimethylcyclopropane (*trans*-DMC).

Experimental Section

The experimental methods are quite similar to those described in recent recoil tritium publications from this research group. The gas phase samples utilized the nuclear reaction He³(n,p)H³ as tritium source; the liquid samples were condensed onto LiF in capillaries, in which tritium was formed by the Li⁶(n,α)H³ reaction.^{19,22} Neutron irradiations were carried out primarily in a nominal neutron flux of 10¹¹ neutrons/cm.² sec. for periods as long as 3 hr. The actual

neutron flux within the irradiation bulbs was about 5 × 10¹⁰ neutrons/cm.² sec. because of neutron attenuation in the boron-rich 1720 Pyrex glass used in the bulbs.

The distribution of tritium activity among various molecules was determined by radio gas chromatography.²³ The chief difficulties in the analyses of these recoil tritium systems arose from the large number of labeled molecules observed, even in scavenged systems, and the necessity for measuring certain particular components in rather low yields. The radio gas chromatogram of Figure 1 is illustrative of the complexity of the analysis for the labeled molecules formed in a system thoroughly scavenged to eliminate all thermal reactions.

The total hydrocarbon analyses were made primarily on one or two of the following three columns (all packed in 0.64-cm. o.d. Cu tubing): (1) 15.25-m. DMS: 35% dimethylsulfolane on 30–60-mesh firebrick, operated at 24.5°, 20 p.s.i. of He, and 25 ml./min. (2) 15.25-m. SAF: 35% safrole on 30–60-mesh acid-washed firebrick operated at 0°, 20 p.s.i. of He, and 44 ml./min. (3) 24.4-m. AA: 16% acetylacetone on 30–40-mesh acid-washed firebrick, operated at 0°, 12 p.s.i. of He, and 30 ml./min. The lightest molecules were separated on the following column: 15.25-m. PCA: 9.6% propylene carbonate on 30–50-mesh activated alumina (F-1), operated at 0°, 10 p.s.i. of He, and 29 ml./min.

The parent molecules, EC, *cis*-DMC, and *trans*-DMC, were all A.P.I. prepared samples with a stated purity of >99.7%, confirmed by gas chromatography. The experiments involving gas phase irradiations were limited on the upper end of the pressure range by the vapor pressure at the 20° temperature of the irradiation facility: *cis*-DMC, 38 cm.; *trans*-DMC, 52 cm.; EC, 39 cm.

(15) A. Odell, A. Rosenberg, R. D. Fink, and R. Wolfgang, *J. Chem. Phys.*, **40**, 3730 (1964).

(16) Y. N. Tang, E. K. C. Lee, and F. S. Rowland, *J. Am. Chem. Soc.*, **86**, 1280 (1964).

(17) E. K. C. Lee, Y. N. Tang, and F. S. Rowland, *ibid.*, **86**, 5038 (1964).

(18) Y. N. Tang and F. S. Rowland, *ibid.*, **87**, 1265 (1965).

(19) Y. N. Tang and F. S. Rowland, *ibid.*, **87**, 3304 (1965).

(20) The recent development of isotopic separation techniques for radio gas chromatography permits some estimate of the relative contributions of these two processes, for the former produces propylene with tritium only in the alkyl position, while the latter forms propylene with both alkyl and olefinic tritium.²¹ Both contributions have been shown to be present in unpublished experiments by E. K. C. Lee.

(21) E. K. C. Lee and F. S. Rowland, *Anal. Chem.*, **36**, 2181 (1964).

(22) Y.-N. Tang, Ph.D. Thesis, University of Kansas, 1964.

(23) J. K. Lee, E. K. C. Lee, B. Musgrave, Y.-N. Tang, J. W. Root, and F. S. Rowland, *Anal. Chem.*, **34**, 741 (1962).

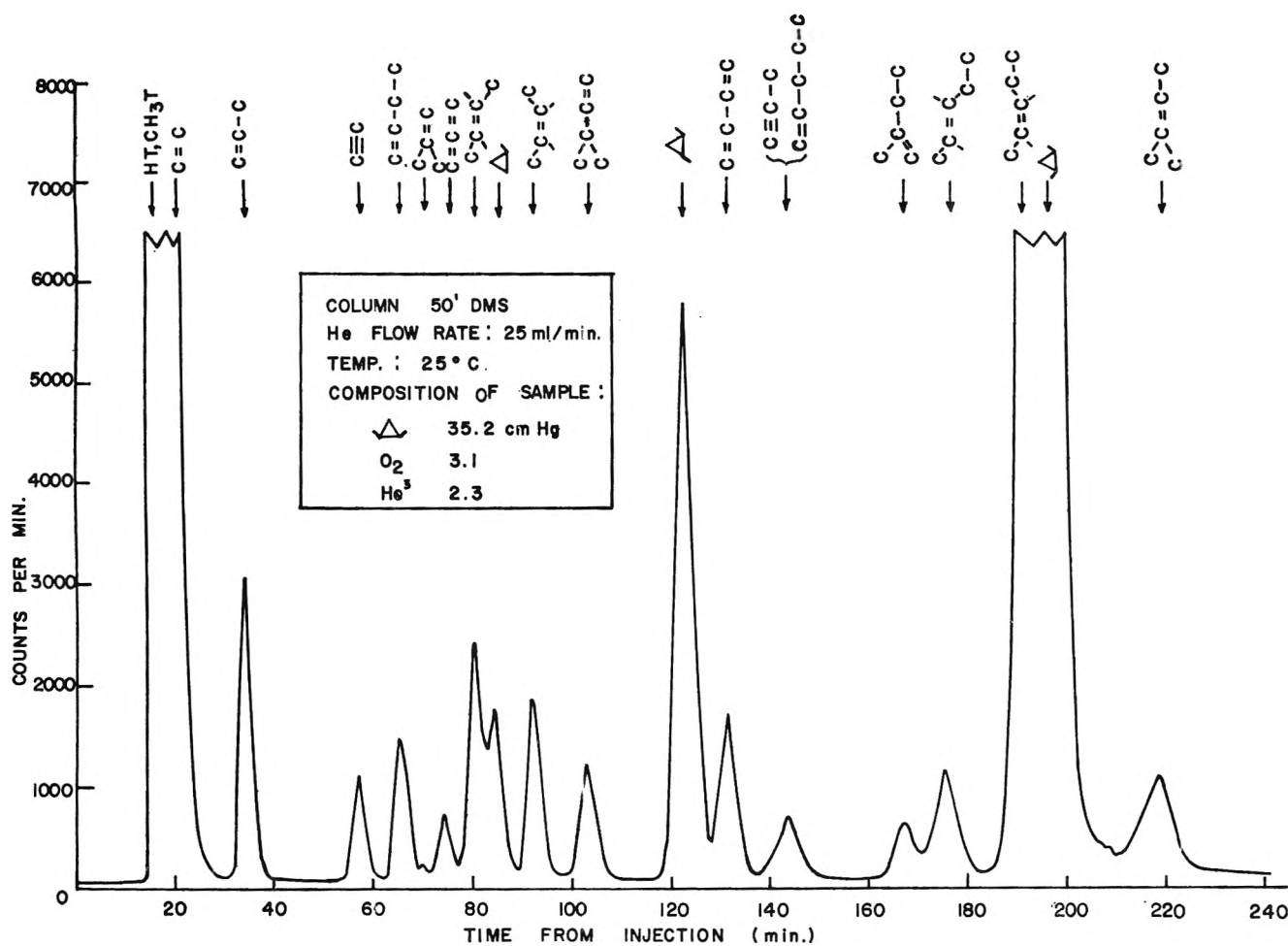


Figure 1. Radio gas chromatographic analysis of radioactive products from recoil tritium reactions with *cis*-1,2-dimethylcyclopropane.

Results and Discussion

Grouping of Hot Products. The radioactivity analyses of these samples show at least 20 significant tritiated species in well-scavenged runs and many additional saturated hydrocarbons in experiments carried out in the absence of scavengers. We believe that these results can be more meaningfully presented if they are listed in small correlated groups rather than in a large table of all products formed under a variety of experimental conditions. Further, we shall present the results intermixed with a discussion of the reactions involved since the appropriate small groups may best be chosen with the mechanisms in mind. The data are all presented as relative yields, with the measured yield of the parent hydrocarbon serving as the base ($=100$). Any comparison of samples irradiated at different pressures therefore requires proper correction for any variations in the parent yield with the pressure of irradiation.

Energetic Addition of Tritium Accompanied by Ring Opening. The reaction of an energetic tritium atom





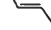


with one of the ring carbon atoms to form a stable C-T bond, while simultaneously opening the ring as in reaction 3a, would produce the labeled free radicals shown in the center column of Table I. The labeled olefins and free radicals expected from the decomposition of these radicals through breakage of the weakest C-C bonds are summarized in the right-hand columns. In addition, since these reactions are exothermic even without the kinetic energy of the reacting tritium atom, these radicals will probably be found in very excited states, and decomposition by other paths, *e.g.*, loss of H atoms, could also be expected.

Energetic Substitution of Tritium for Alkyl Groups. The replacement of an alkyl group by an energetic tritium atom, as in reaction 3, has been observed with every alkane larger than CH_4 and has further been noted for all possible R groups in each of these molecules. The corresponding reactions in EC will produce CH_3T , $\text{C}_2\text{H}_5\text{T}$, $\text{CH}_2\text{T}-c\text{-C}_3\text{H}_5$, and $c\text{-C}_3\text{H}_5\text{T}$, while those with either DMC will form CH_3T and $\text{CH}_3-c\text{-C}_3\text{H}_4\text{T}$. If the methylcyclopropane-*t* and cyclopropane-*t* mole-

Table I: Ring-Opening Reactions with Substituted Cyclopropane Molecules by Energetic Tritium Atoms

Reactants	Excited radical	Labeled products	
		Radicals	Olefins
$\begin{array}{c} \text{T}^* \\ + \\ \text{CH}_2 \\ \\ \text{CH}_3\text{CH}_2\text{CH} \\ / \quad \backslash \\ \text{CH}_2 \end{array}$	$\begin{array}{c} \text{CH}_2 \\ \\ \text{CH}_3\text{CH}_2\text{CHT} \quad \text{CH}_2 \cdot \\ \\ \text{CH}_2\text{T} \\ \\ \text{CH}_3\text{CH}_2\text{CH} \quad \text{CH}_2 \cdot \\ \\ \text{CH}_2\text{T} \\ \\ \text{CH}_3\text{CH}_2\text{CH} \quad \text{CH}_2\text{T} \\ \\ \text{CH}_2 \end{array}$	$\text{CH}_3\text{CH}_2\text{CHT} \cdot$ $\text{CH}_2\text{T} \cdot$ $\text{CH}_2\text{T} \cdot$	\dots $\text{CH}_2\text{TCH}=\text{CH}_2$ $\text{CH}_2\text{TCH}_2\text{CH}=\text{CH}_2$
$\begin{array}{c} \text{T}^* \\ + \\ \text{CH}_2 \\ \\ \text{CH}_3\text{CHCHCH}_3 \end{array}$	$\begin{array}{c} \text{CH}_2 \\ \\ \text{CH}_3\text{CHT} \quad \text{CHCH}_2 \\ \\ \cdot\text{CH}_2 \\ \\ \text{CH}_3\text{CHTCHCH}_3 \\ \\ \text{CH}_2\text{T} \\ \\ \text{CH}_3\text{CH}-\text{CHCHCH}_3 \end{array}$	$\text{CH}_3\text{CHT} \cdot$ $\text{CH}_3\text{CHT} \cdot$ $\text{CH}_2\text{T} \cdot$	\dots $\text{CH}_3\text{CHTCH}=\text{CH}_2$ $\text{CH}_2\text{TCH}=\text{CHCH}_3$ <i>(cis + trans)</i>

Table II: Relative Yields of Butenes, Propylene, Cyclopropane, and Methylcyclopropane from Recoil Tritium Reactions with Substituted Cyclopropanes^a (Parent Molecule = 100)^b

Product	Parent molecule			Relative rates of formation	
	EC	<i>cis</i> -DMC	<i>trans</i> -DMC	Ref. 25, 468°K., pyrolysis	Ref. 26, 2600 Å., ketene + cyclopropane
	<u>4.0 ± 0.2</u>	<u>1.6 ± 0.1</u>	<u>1.5 ± 0.1</u>	1.00	1.00
	0.14 ± 0.05	<i>c</i>	0.15 ± 0.05	0.16	0.27
	0.11 ± 0.05	<u>2.3 ± 0.2</u>	<u>2.0 ± 0.1</u>	0.63	0.66
	0.13 ± 0.05	<u>2.6 ± 0.1</u>	<u>2.5 ± 0.2</u>	0.28	0.63
	<u>8.2 ± 0.2</u>	2.8 ± 0.2	2.5 ± 0.2		
	1.3 ± 0.1	1.9 ± 0.1	1.6 ± 0.2		
	0.9 ± 0.1	0.0 ± 0.1	0.0 ± 0.1		

^a Those underlined are products expected from ring-opening mechanism. ^b Experiments carried out at approximately 0.5 atm.; O₂-scavenged. ^c Concealed in butene-1 peak.

cules thus formed are created with excess vibrational energy in the gas phase, unimolecular isomerizations in measurable yields would be expected. Thermally excited cyclopropane isomerizes to propylene,²⁴ while methylcyclopropane isomerizes to each of the four possible butenes in varying yields.^{25,26} A qualitative distinction can then be drawn between the ring-opening mechanism and the sequence of isomerization following






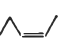



alkyl replacement: all butenes are expected from the latter, while only butene-1 is anticipated from EC and isobutene is not expected from DMC from the former.

(24) See S. Benson, "The Foundations of Chemical Kinetics," McGraw-Hill Book Co., Inc., New York, N. Y., 1962, p. 252.

(25) J. P. Chesick, *J. Am. Chem. Soc.*, **82**, 3277 (1960).

(26) J. N. Butler and G. B. Kistiakowsky, *ibid.*, **82**, 759 (1960).

Table III: Relative Yields of Geometrical and Structural Isomers from Recoil Tritium Reactions with Substituted Cyclopropanes

Products	<i>cis</i> -DMC			<i>trans</i> -DMC			EC		
	Thermal isomerization, ref. 27	Ring-opening reaction	Obsd. yields	Thermal isomerization, ref. 27	Ring-opening reaction	Obsd. yields	Thermal isomerization, ref. 29	Ring-opening reaction	Obsd. yields
	Parent	No	(100) ^a	(28) ^c	No	~5.2 ^f	...	No	0
	(66) ^c	No	8.2 ^e	Parent	No	(100) ^a	...	No	0
	...	No	0	...	No	0	Parent	No	(100) ^a
	0	Yes	1.0	0	Yes	0.8	(1.0) ^d	Yes	2.5
	0.93	Yes	2.2	0.54	Yes	2.2	0.4	Yes	1.5
	0.81	Yes	<i>b</i>	0.35	Yes	<i>b</i>	0.6	Yes	<i>b</i>
	0.58	Yes	1.0	0.58	Yes	1.2	0.2	Yes	0.9
	0	Yes	1.6	0	Yes	1.7	0	No	0
	0.55	Yes	2.2	0.54	Yes	1.9	0	No	0

^a Arbitrary yield standard for comparison purposes. Samples were O₂-scavenged at ~0.5 atm. ^b Concealed in *cis*-DMC or EC peak. ^c Rate constants for isomerization²⁷ at 430.9° in units of 10⁵k₁, sec.⁻¹. ^d Relative rates of formation at 467.8°. ^e 2.6 in liquid phase; 10.6 in gas sample at 10 cm. ^f Ca. 1 in liquid; ~6 in gas sample at 10 cm.

Yields of C₃H₅T and C₄H₇T Molecules. The radioactivity yields of propylene, the butenes, cyclopropane, and methylcyclopropane observed for comparable samples of each of three C₃ cyclopropanes are collected in Table II. For convenience in comparison of the data, those yields are underlined in the table for which the ring-opening reaction is a suitable mechanism. The data show immediately that the two high yield olefins from EC are propylene and butene-1, as expected from the ring-opening mechanism, while the remaining three butenes have yields an order of magnitude less than that of butene-1. The butenes observed from DMC include the anticipated ring-opening products in high yields, while that of isobutene, which should not be formed by the ring-opening reactions, is an order of magnitude less. The methylcyclopropane-*t* and cyclopropane-*t* yields are measurable when a simple T-for-R reaction will form them, but cyclopropane-*t* is not formed from the DMC molecules, for which a more complex mechanism would be required.

On the other hand, none of the butene yields is ever zero, and repeated experiments show these yields to be quite reproducible. We interpret the data of Table II to indicate that the addition reaction with ring opening, followed by C-C bond break in the excited radical, accounts for the major fraction of butene production in each case but that isomerization of methylcyclopropane-*t* is also contributing to the formation of the butene-*t* molecules in lesser yields.

The yields of propylene-*t* from each of the DMC molecules are not accounted for by either of the mechanisms above and will be considered again later. The high yield of propylene-*t* from EC suggests a contribution to it from the same mechanism operative in the DMC cases. The isomerization of cyclopropane-*t* may also contribute to the formation of propylene-*t* from EC, but the yield is completely obscured by the much larger yield observed from ring opening.

Geometrical and Structural Isomerizations. The cyclopropane hydrocarbons are susceptible toward the

same isomerization reaction to propylenic compounds observed with cyclopropane itself if the excitation energy is sufficiently high. However, the isomerization rates of DMC and EC are much slower than those for cyclopropane molecules with equal excitation energies.²⁵⁻²⁹ The fastest observed isomerization reactions of both *cis*- and *trans*-DMC are the geometric isomerizations to the opposite isomer; structural isomerizations to pentenes occur with rate constants one-tenth to one-twentieth times as fast,²⁷ as shown in the "thermal isomerization" columns of Table III.

The radioactive yields of the various C₆H₉T molecules from each of the parent cyclopropanes are summarized in Table III. The *cis*-DMC is found as a radioactive product from T* reactions with *trans*-DMC, and *vice versa*; no isomerization in either direction is observed between EC and either of the DMC molecules; the yields of *cis*- and *trans*-DMC from each other are both small (<10%) relative to the activity found in the same form as the irradiated parent molecule. Although the *cis-trans* isomerization is a reversible process,²⁷ equilibrium is not observed in either system. Some of the labeled parent molecules (*i.e.*, *cis*-DMC-*t* from T* + *cis*-DMC, etc.) are formed with excitation energies insufficient for the isomerization; others are formed with sufficient energy but lose it by collision before the isomerization can actually occur. Since the environmental system is at room temperature during the irradiation and only the freshly substituted molecules themselves have high excitation energy, collisional de-excitation quickly reduces the internal energy of excited molecules down to levels for which the isomerization process is negligibly slow. The results given in Table III, showing that the *cis-to-trans* isomerization proceeds more readily than the reverse, are in agreement with previous observations of the relative rates of isomerization.²⁷

The total gas pressures for the systems shown in Table III are all approximately 35 cm. At this pressure, only 8 and 5% of the labeled opposite geometrical isomers were observed relative to the activity observed in the chemical form of the parent substance. If the relative rate constants obtained in thermal pyrolysis experiments are used to predict relative yields of structural isomerization processes in recoil tritium systems, the yields of the appropriate pentenes would be estimated to be of the order 0.1 or less. For each parent molecule, only four (one group of four for EC and another one for the DMC substances) of the pentenes are expected from structural isomerization reactions. The presence of appreciable yields of the two unexpected pentene-*t* products in each system would be strong evidence for another source of the pentene-*t* molecules.

Pentene-t. Another potential source of pentene-*t* molecules in these cyclopropane systems arises through the loss of an H atom from the excited radicals formed in the initial addition process. Examination of the radicals shown in Table I discloses that the pentenes expected from EC by H-atom loss from an excited radical are the same four pentenes expected from the structural isomerization mechanism. The absence of radioactivity as 3-methylbutene-1 and 2-methylbutene-2 is good evidence for the specific nature of the pentene-forming reaction processes. However, in the two DMC cases, all of the pentene-*t* molecules are formed in roughly comparable yields although neither 3-methylbutene-1 nor pentene-1 is expected through the thermal isomerization process. These observations clearly indicate that the primary source of pentene-*t* in these systems is through the loss of H atoms from the excited radicals formed by hot tritium addition, with opening of the cyclopropane ring. The total yields of pentene-*t* molecules are comparable to the yields of the labeled smaller olefins shown in Table II, indicating that many of the radicals are decomposing while very excited, inasmuch as decomposition by the much higher activation energy path accounts for about half of the reactions.

Substitution with Inversion. If the energetic substitution of T for H at an asymmetric carbon position followed a course involving inversion of the configuration, the opposite geometric isomer would be the direct result. Previous experiments with glucose-galactose,³⁰ L(+)-alanine,³¹ and *sec*-butyl alcohol (only the latter in the gas phase)³² have all shown that such hot substitutions take place predominantly ($\geq 90\%$) with retention of configuration in those molecules and would indicate that little inversion should be expected here. In these experiments, it is not feasible to set any limits on the amount of substitution with inversion because of the larger amounts formed by geometric isomerization. In principle, the two mechanisms are distinguishable since the inversion mechanism would form molecules labeled only at the asymmetric carbon positions. However, in this system at least, the experimental difficulties in determining the chemical location of the

(27) M. C. Flowers and H. M. Frey, *Proc. Roy. Soc. (London)*, **A257**, 122 (1960).

(28) M. C. Flowers and H. M. Frey, *ibid.*, **A260**, 424 (1961).

(29) M. L. Halberstadt and J. P. Chesick, *J. Phys. Chem.*, **69**, 429 (1965).

(30) F. S. Rowland, C. N. Turton, and R. Wolfgang, *J. Am. Chem. Soc.*, **78**, 2354 (1956); H. Keller and F. S. Rowland, *J. Phys. Chem.*, **62**, 1373 (1958).

(31) J. G. Kay, R. P. Malsan, and F. S. Rowland, *J. Am. Chem. Soc.*, **81**, 5050 (1959).

(32) M. Henchman and R. Wolfgang, *ibid.*, **83**, 2991 (1961).

tritium in *cis*-DMS from *trans*-, or *vice versa*, have precluded determination of the intramolecular tritium distribution. Even the formation of the labeled opposite geometric isomer in liquid phase irradiations is not proof of the inversion mechanism, for previous work with hexene-2 has demonstrated the decomposition of excited radicals in the liquid phase.³³

Highly Unsaturated Products. Several highly unsaturated tritium-labeled products, including acetylene, allene, propyne, and 1,3-butadiene, are all observed in low, but definite, yields from these substituted cyclopropane systems, as summarized in Table IV. Products of this type are regularly found in alkane systems and are postulated as arising from the decomposition of the most highly excited molecules formed in the initial hot substitution reactions. Inasmuch as these molecules are thus considered as the end products of a sequence of two or more reactions, it is relatively difficult to isolate the various steps in the chain leading to their formation.

A similar set of reactions has been written for the formation of propylene-*t* in reactions of T with neopentane, in which the T atom replaces one CH₃ group, and the excited isobutane-*t* then decomposes to propylene-*t* plus methane. In the neopentane system, confirmation of this mechanism has been obtained through analysis of the intramolecular location of the tritium atom in the propylene molecule. The only propylene-*t* molecule expected from this set of reactions is CH₃CT=CH₂, and radio gas chromatographic analysis has demonstrated that the tritium activity is found only in olefinic positions.^{17,34} Reactions of this kind, occurring in low yields, should be found in the cyclane systems, as well as in the alkane and alkene systems, and can readily account for the highly unsaturated products of Table IV.

The formation of appreciable yields of C₂H₃T in each system, the observation of propylene-*t* in the DMC systems, and the relatively high yield of propylene-*t* from EC all indicate the existence of mechanisms for the formation of small olefins. These mechanisms are probably similar to that suggested above for the formation of butadiene—the breakup of a very excited parent molecule after the substitution of T for H or for an alkyl group. One possible form for such breakup can be suggested from the observed split, after absorption of ultraviolet light, of cyclopropane into methylene plus ethylene.³⁵ The analogous reaction with DMC could produce directly propylene and the ethylidene radical, with the latter isomerizing to ethylene. Similarly, such a reaction with EC could form directly ethylene and propylidene, with isomerization to propylene for the latter. These mechanisms are only speculative suggestions from the present data, and are not readily investigated further in the complexity of these systems.

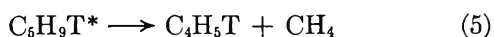
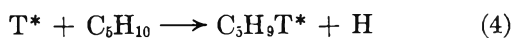
Hot Abstraction Reaction. The product of highest yield in each of these systems is HT, formed by hot abstraction from the parent molecule. Experiments with simpler molecules have amply demonstrated that the yield of HT depends strongly on the bond dissociation energy of the C–H bond attacked and will therefore vary substantially from position to position within the DMC and EC molecules. The high yield relative to those of the labeled parent molecules indi-

Table IV: Relative Yields of Light and Highly Unsaturated Products from Recoil Tritium Reactions with Substituted Cyclopropanes^a

Products	<i>cis</i> - DMC	<i>trans</i> - DMC	EC
C ₂ H ₃ T	10.0	9.6	9.9 ^c
C ₂ HT	1.1	N.M. ^b	0.2
Allene	0.7	0.7	0.9
Propyne	0.3	N.M.	N.M.
1,3-Butadiene	2.3	N.M.	2.1

^a Product yields are all relative to tritium-labeled parent as 100. ^b N.M.: not measured. ^c Including C₂H₆T yield.

1,3-Butadiene has been observed as a thermal decomposition product in the EC system at 454°, with a yield in the same order of magnitude as that of the pentenes formed by structural isomerization.²⁹ The mechanism suggested for its formation in pyrolysis involves an intermediate in which the ethyl group bends back over the cyclopropane ring and would not be expected to form butadiene in the DMC compounds. The actual measured yields of 1,3-butadiene are comparable from both EC and DMC and are yields an order of magnitude higher than observed for the pentenes from structural isomerization. Accordingly, we assume the bulk of 1,3-butadiene formed from reaction with EC and DMC arises from a different mechanism corresponding to the same equations



(33) E. K. C. Lee and F. S. Rowland, *J. Chem. Phys.*, **36**, 554 (1962).

(34) E. K. C. Lee, J. W. Root, and F. S. Rowland, "Chemical Effects of Nuclear Reactions and Radioactive Transformations," International Atomic Energy Agency, Vienna, 1965, in press.

(35) C. L. Currie, S. J. H. Okabe, and J. R. McNesby, *J. Phys. Chem.*, **67**, 1494 (1963).

cates that some of the C-H bond positions in both EC and DMC have bond dissociation energies substantially lower than those of cyclopropane or cyclobutane, but no significant measurements can be made

without experiments on selectively deuterated compounds.

Acknowledgment. The cooperation of Dr. J. K. Lee and Dr. E. K. C. Lee is deeply appreciated.

Low-Temperature Thermodynamic Properties of *n*-Propyl- and *n*-Butylbenzene

by John F. Messerly, Samuel S. Todd, and Herman L. Finke

Contribution No. 142 from the Thermodynamics Laboratory of the Bartlesville Petroleum Research Center, Bureau of Mines, U. S. Department of the Interior, Bartlesville, Oklahoma (Received July 16, 1965)

The heat capacities from 12 to 370°K., heats of fusion, triple points, and purities of *n*-propylbenzene and *n*-butylbenzene were measured in an adiabatic calorimeter. Both compounds exhibited monotropism with the metastable crystals melting 2.02° below the stable crystals in the case of *n*-propylbenzene and 0.16° below the stable crystals in the case of *n*-butylbenzene. From the calorimetrically measured data the thermodynamic functions ($G_s - H^\circ_0$)/ T , ($H_s - H^\circ_0$)/ T , $H_s - H^\circ_0$, S_s , and C_s were calculated at selected temperatures for each compound for both the metastable and stable crystals and the liquid phase. For each compound, the entropies at 298.15°K. in the liquid state calculated by metastable and by stable paths agreed within experimental error, providing another check of the third law of thermodynamics. The entropy increment obtained between *n*-propyl- and *n*-butylbenzene is about 0.25 e.u. greater than the constant entropy increment for the normal paraffins from C₆ to C₁₈ in both the liquid and ideal gas states. This slightly larger increment from *n*-propyl to *n*-butyl substitution has been noticed earlier in monoalkyl-substituted cyclopentanes and cyclohexanes. From incomplete measurements on *n*-decylbenzene, values of the heat of melting and triple point temperature were obtained. Estimates of the entropies of *n*-decylbenzene at 298.15°K. in the liquid and ideal gas states were made.

Introduction

As part of the continuing program of research conducted in this laboratory on the thermodynamic properties of hydrocarbons and related substances, low-temperature calorimetric studies have been made on corresponding members of several homologous series of compounds. From the study of selected members of each series, it has been possible to calculate the effect on the entropy of the liquid for each methylene group added. For the *n*-paraffins this entropy increment has been found^{1,2} to be essentially constant for C₅ through C₁₈. For the *n*-1-olefins this increment was found by McCullough, *et al.*,³ to be constant from

C₅ to C₁₀ but became irregular from C₁₀ to C₁₆ owing to orientation disorder in the crystals. The data of Messerly, *et al.*,⁴ on *n*-alkylcyclopentanes and of Finke, *et al.*,⁵ on *n*-alkylcyclohexanes have shown that the entropy increment from *n*-propyl to *n*-butyl is slightly

(1) H. L. Finke, M. E. Gross, G. Waddington, and H. M. Huffman, *J. Am. Chem. Soc.*, **76**, 333 (1954).

(2) Unpublished data, this laboratory.

(3) J. P. McCullough, H. L. Finke, M. E. Gross, J. F. Messerly, and G. Waddington, *J. Phys. Chem.*, **61**, 289 (1957).

(4) J. F. Messerly, S. S. Todd, and H. L. Finke, *ibid.*, **69**, 353 (1965).

(5) H. L. Finke, S. S. Todd, and J. F. Messerly, *ibid.*, **69**, 2094 (1965).

Table I: Heat Capacity (cal. deg.⁻¹ mole⁻¹)

<i>T</i> , °K. ^a	<i>C_s</i> ^b	<i>T</i> , °K. ^a	<i>C_s</i> ^b	<i>T</i> , °K. ^a	<i>C_s</i> ^b	<i>T</i> , °K. ^a	<i>C_s</i> ^b	<i>T</i> , °K. ^a	<i>C_s</i> ^b	<i>T</i> , °K. ^c	<i>C_s</i> ^b
<i>n</i> -Propylbenzene						<i>n</i> -Butylbenzene					
Stable crystals						Stable crystals					
11.36	0.7929	30.09	6.283	108.04	20.143	11.40	0.943	32.84	7.967	114.16	23.569
11.99	0.9598	33.40	7.273	113.49	20.812	12.04	1.106	36.34	9.069	118.65	24.209
12.45	1.0515	37.04	8.273	117.10	21.258	12.52	1.243	40.05	10.149	124.61	25.052
13.12	1.208	40.88	9.267	119.23	21.543	13.04	1.380	43.93	11.206	130.37	25.891
13.65	1.348	44.90	10.225	122.27	21.924	13.72	1.589	48.54	12.373	135.96	26.706
14.37	1.525	49.67	11.275	127.76	22.602	14.16	1.718	54.19	13.647	140.23	27.284
14.98	1.689	55.10	12.350	133.08	23.258	14.93	1.940	54.60	13.737	141.40	27.483
15.78	1.913	55.21	12.366	138.60	23.938 ^c	15.46	2.103	59.64	14.816	146.07	28.147
16.47	2.090	59.82	13.230	142.22	24.372 ^c	16.25	2.356	65.35	15.963	147.21	28.327 ^e
17.52	2.397	64.77	14.100	144.31	24.647 ^c	17.06	2.600	71.11	16.988	152.26	29.058 ^e
18.16	2.606	70.37	14.980	146.43	24.906 ^c	17.83	2.845	76.88	17.979	153.37	29.256 ^e
19.59	3.024	76.07	15.836	147.82	25.079 ^c	18.72	3.148	82.71	18.991	155.21	29.513 ^e
20.09	3.179	81.83	16.724	147.88	25.068 ^c	19.74	3.496	85.52	19.457	158.28	29.929 ^e
21.87	3.742	87.67	17.567	149.87	25.359 ^c	20.48	3.756	88.26	19.898	159.37	30.146 ^e
22.12	3.811	93.60	18.335	152.13	25.645 ^c	21.93	4.256	90.52	20.211	161.23	30.473 ^e
24.33	4.515	97.63	18.828	154.43	25.935 ^c	22.54	4.476	94.13	20.737	163.12	30.702 ^e
24.44	4.552	99.63	19.092	158.22	26.479 ^c	24.29	5.086	95.76	20.959	164.14	30.900 ^e
26.91	5.312	102.89	19.495	160.79	26.829 ^c	24.79	5.263	101.34	21.755	167.07	31.505 ^e
27.15	5.392	105.41	19.825	164.40	27.394 ^c	26.82	5.956	102.75	21.943	169.33	31.904 ^e
29.90	6.216					27.23	6.106	107.21	22.592	169.82	32.079 ^e
						29.45	6.838	108.56	22.773	176.91	34.640 ^e
						29.82	6.969	112.85	23.393		
Metastable crystals						Metastable crystals					
11.45	0.964	30.44	6.824	101.81	19.452						
12.37	1.204	33.56	7.763	107.40	20.148						
13.43	1.493	37.03	8.721	107.90	20.199	55.25	13.937	117.08	24.064	159.64	30.111 ^f
13.59	1.553	40.81	9.683	113.32	20.876	60.19	14.982	123.13	24.916	160.35	30.118 ^f
14.66	1.837	45.25	10.723	119.03	21.578	65.81	16.089	128.97	25.729	161.85	30.498 ^f
14.99	1.939	50.35	11.806	124.57	22.263	71.47	17.093	135.19	26.586	163.12	30.710 ^f
16.07	2.238	54.57	12.601	130.29	22.951	77.25	18.083	141.76	27.501	165.18	30.937 ^f
16.58	2.394	55.35	12.750	136.20	23.658	83.16	19.107	148.14	28.392	165.40	31.050 ^f
17.69	2.736	59.55	13.508	141.93	24.356 ^d	88.45	20.027	149.99	28.637	165.44	31.152 ^f
18.49	2.998	65.25	14.470	143.96	24.556 ^d	89.26	20.078	153.73	29.221	169.89	31.799 ^f
19.56	3.334	71.29	15.372	147.52	25.044 ^d	93.80	20.788	154.33	29.284	171.19	32.346 ^f
20.63	3.691	76.90	16.185	151.25	25.458 ^d	99.49	21.598	156.01	29.560	174.49	32.763 ^f
21.72	4.040	82.59	17.023	152.83	25.727 ^d	105.46	22.447	157.63	29.797 ^f	180.15	35.826 ^f
22.92	4.446	85.87	17.492	153.76	25.869 ^d	111.19	23.254	159.51	30.158 ^f		
24.03	4.800	88.39	17.831	155.73	25.869 ^d						
25.31	5.222	91.10	18.161	158.31	26.357 ^d						
26.51	5.619	96.50	18.820	159.75	26.639 ^d	193.81	49.760	260.84	54.472	319.52	60.486
27.73	5.987	101.75	19.465	160.92	26.631 ^d	197.29	49.919	270.91	55.416	329.67	61.593
29.25	6.448					205.85	50.356	280.81	56.389	340.00	62.728
						211.83	50.698	290.55	57.366	350.16	63.842
180.87	43.689	246.19	46.990	310.45	52.465	221.83	51.356	300.15	58.375	360.17	64.947
186.47	43.838	256.30	47.726	320.98	53.489	231.69	52.051	309.92	59.432	370.02	66.011
194.80	44.121	266.24	48.524	331.34	54.495	241.42	52.807				
204.78	44.531	276.02	49.345	341.52	55.476						
204.89	44.542	285.65	50.188	351.54	56.479						
214.57	45.025	295.13	51.014	361.50	57.433						
225.11	45.614	300.12	51.460	370.54	58.362						
235.95	46.291	304.48	51.902								

^a *T* is the mean temperature of each heat capacity measurement. ^b *C_s* is the heat capacity of the condensed phase under saturation pressure. Values of *C_s* for the crystals are *not* corrected for effects of premelting caused by impurities. ^{c,d,e,f} The temperature increments of these measurements are, in order of increasing temperature, in °K.: (c) 5.794, 5.665, 5.633, 5.515, 5.525, 6.654, 5.486, 5.905, 6.455, 6.276, 6.269, 6.086; (d) 5.663, 7.413, 5.515, 7.175, 7.031, 5.302, 5.284, 6.951, 6.818, 5.144; (e) 6.255, 6.102, 6.077, 6.105, 5.939, 5.918, 5.929, 6.132, 5.778, 5.765, 6.110, 5.596, 8.595; (f) 5.062, 6.019, 5.834, 4.895, 5.769, 5.914, 4.779, 5.676, 5.844, 4.666, 5.661, 4.548, 6.786.

Table II: Equations for Heat Capacity of Liquid

$$C_s = A + BT + CT^2 + DT^3, \text{ cal. deg.}^{-1} \text{ mole}^{-1}$$

Compd.	A	B	10 ⁴ C	10 ⁷ D	Range, °K.	Average dev., cal.	Max. dev., cal.
<i>n</i> -Propylbenzene	58.710	-0.22063	9.2097	-8.8580	180-370	0.01	0.02
<i>n</i> -Butylbenzene	65.158	-0.24196	10.343	-10.108	195-380	0.01	0.02

larger than that found for *n*-alkanes, but the average values obtained on the *n*-butyl- to *n*-decyl-substituted compounds agree well with those obtained for the *n*-alkanes and *n*-1-olefins. The data of Person and Pimentel⁶ on the entropies of the *n*-alkanes from C₈ to C₁₆ in the ideal gas state at 298.15°K. have shown the entropy increment per methylene group to be essentially constant. This constant entropy increment has been shown to be the same as the average entropy increment found for the *n*-alkylcyclopentanes⁴ and *n*-alkylcyclohexanes⁶ from *n*-butyl to *n*-decyl.

This work was projected as a study of *n*-propyl-, *n*-butyl-, and *n*-decylbenzenes to verify these relationships found for the entropy increment. Although data on *n*-butylbenzene were available,⁷ the limited range of the data and the unknown purity of the sample made a restudy of this compound desirable. The measurements were completed on *n*-propyl- and *n*-butylbenzene, but work had to be abandoned on *n*-decylbenzene owing to experimental difficulties. (Two sample containers were found to be ruptured after repeated cycling of the vessels through the solid-solid phase transition at approximately 235°K.)

Efforts were made to procure a pure sample of a heavier *n*-alkylbenzene in order to determine if the average entropy increment beyond *n*-butyl was the same as in the *n*-alkylcyclopentanes and -cyclohexanes. A sample of *n*-dodecylbenzene was obtained, but the purity, as determined, was too low to obtain a reliable value of $S_{298.15}$ for this compound.

Experimental Section

Apparatus and Physical Constants. The low-temperature calorimetric measurements were made with apparatus described by Huffman and co-workers.⁸ The 1951 International Atomic Weights⁹ and values of the fundamental physical constants¹⁰ were used. Measurements of temperature were made with platinum resistance thermometers calibrated in terms of the International Temperature Scale of 1948¹¹ from 90 to 400°K., and the provisional scale of the National Bureau of Standards¹² from 11 to 90°K. Celsius temperatures were converted to Kelvin temperatures

by the addition of 273.15°.¹³ Energy was measured in joules and converted to calories by the relation, 1 cal. = 4.184 (exactly) joules. Measurements of mass, electrical potential, and resistance were made in terms of standard devices calibrated at the National Bureau of Standards.

Some of the results in this paper were originally calculated with physical constants and temperatures related to the definition 0° = 273.16°K. Temperatures reported here are in terms of the newer definition,¹³ but only part of the experimental results were recalculated. Numerical inconsistencies less than the precision of the experimental data may have been introduced by this procedure.

Materials. All of the samples used in this study were API Research hydrocarbons.¹⁴ The samples were frozen in the ampoules as received, and the liquid just above the melting point was examined for traces of ice. In only one sample, *n*-butylbenzene, was there enough ice present to warrant drying. In this case the sample was dried with calcium hydride in the liquid phase. Each sample was transferred to the calorimeter without exposure to oxygen or water.

Results

Heat Capacities. Both *n*-propylbenzene and *n*-

- (6) W. B. Person and G. C. Pimentel, *J. Am. Chem. Soc.*, **75**, 532 (1953).
- (7) H. M. Huffman, G. S. Parks, and M. Barmore, *ibid.*, **53**, 3876 (1931).
- (8) (a) H. M. Huffman, *Chem. Rev.*, **40**, 1 (1947); (b) H. M. Huffman, S. S. Todd, and G. D. Oliver, *J. Am. Chem. Soc.*, **71**, 584 (1949); (c) D. W. Scott, D. R. Douslin, M. E. Gross, G. D. Oliver, and H. M. Huffman, *ibid.*, **74**, 883 (1952); (d) R. A. Ruehrwein and H. M. Huffman, *ibid.*, **65**, 1620 (1943).
- (9) E. Wichers, *ibid.*, **74**, 2447 (1952).
- (10) F. D. Rossini, F. T. Gucker, Jr., H. L. Johnston, L. Pauling, and G. W. Vinal, *ibid.*, **74**, 2699 (1952).
- (11) H. F. Stimson, *J. Res. Natl. Bur. Std.*, **42**, 209 (1949).
- (12) H. J. Hoger and F. G. Brickwedde, *ibid.*, **22**, 351 (1939).
- (13) H. F. Stimson, *Am. J. Phys.*, **23**, 614 (1955).
- (14) These samples of API Research hydrocarbons were made available through the American Petroleum Institute Research Project 44 on the collection, analysis, and calculation of data on properties of hydrocarbons and were purified by the American Petroleum Institute Research Project 6 on the analysis, purification, and properties of hydrocarbons.

Table III: Triple Point Temperatures, Heats of Fusion, and Cryoscopic Constants

Compd.	T_{tp} , °K.	ΔH_m , cal. mole ⁻¹	A , deg. ⁻¹	B , deg. ⁻¹
<i>n</i> -Propylbenzene				
Stable crystals	173.59	2215 ± 2 ^a	0.03699	0.00235
Metastable crystals	171.6	2031 ± 50 ^a	0.03470	0.00204
<i>n</i> -Butylbenzene				
Stable crystals	185.30	2682 ± 2 ^a	0.03931	0.00289
Metastable crystals	185.14	2691 ± 4 ^a	0.03951	0.00264

^a The uncertainty shown here is the maximum deviation from the mean of two or more determinations.

butylbenzene exhibit monotropism, and in each case the metastable form could be readily obtained and supercooled. Complete measurements of the heat capacities on both metastable and stable crystals from 12°K. to the melting points were obtained for these compounds. The heat capacities of the liquids were measured from just above the melting point to approximately 370°K. Only one of the two crystalline forms of *n*-butylbenzene, which melt 0.16°K. apart, was reported by Huffman, *et al.*,⁷ and by Rossini.¹⁵ The incomplete study on *n*-decylbenzene showed at least two crystalline polymorphs.

The observed values of heat capacity at saturation pressure, C_s , are recorded for each compound in Table I. The temperature increments used in the measurements were small enough to obviate corrections for nonlinear variation of C_s with T . Corrections for the effect of premelting have not been made to these data, but pertinent ΔT values are included to permit their calculation.

The precision uncertainty of the results was, in general, less than 0.1%, and above 30°K. the accuracy uncertainty should not exceed 0.2%, except in regions near phase transformations. Near phase changes the data for the solid state is less precise and accurate because of rapid changes of C_s with T , slow equilibration, or uncertainties caused by the presence of impurities.

Cubic equations in T were fitted to the heat capacity of each compound in the liquid state. The constants for these equations are listed in Table II, together with values of the deviations from observed data as an estimate of reliability.

Heats of Fusion, Triple Point Temperatures, and Purity of Samples. The heats of fusion, ΔH_m , were determined from the heat capacity data and enthalpy measurements made over appropriate temperature

Table IV: Melting Point Summaries

F	1/F	T_F , °K.	T_{calcd} , °K.
<i>n</i> -Propylbenzene (impurity = 0.03 mole %) ^c			
Stable crystals			
0.0988	10.12	173.5123	173.5076
0.2603	3.842	173.5575 ^a	173.5575
0.5150	1.942	173.5719	173.5727
0.7466	1.339	173.5775 ^a	173.5775
0.9318	1.073	173.5820	173.5796
1.0000	1.000		173.5802
Pure	0		173.5882
Metastable crystals			
0.1300	7.69	171.5100 ^a	171.51
0.2542	3.93	171.5321	171.54
0.4025	2.48	171.5566 ^a	171.55
0.8474	1.18	171.6224 ^b	171.56
1.0000	1.00		171.57
Pure	0		171.58
<i>n</i> -Butylbenzene (impurity = 0.08 mole %) ^c			
Stable crystals			
0.0971	10.299	185.0961	185.0786
0.2459	4.067	185.2093 ^a	185.2093
0.4872	2.053	185.2511	185.2516
0.6878	1.454	185.2648	185.2641
0.8912	1.122	185.2711 ^a	185.2711
1.0000	1.000		185.2737
Pure	0		185.2947
Metastable crystals			
0.3892	2.569	185.0746	185.0726
0.5928	1.687	185.0940 ^a	185.0940
0.8578	1.166	185.1066 ^a	185.1066
1.0000	1.000		185.1106
Pure	0		185.1348
<i>n</i> -Decylbenzene (impurity = 0.05 mole %)			
0.0880	11.36	258.6699	258.6494
0.2374	4.21	258.7185	258.7147
0.4870	2.05	258.7345 ^a	258.7345
0.6867	1.46	258.7405	258.7399
0.8865	1.13	258.7429 ^a	258.7429
1.0000	1.000		258.7441
Pure	0		258.7532

^a Straight lines through these points were extrapolated to $1/F = 0$ to calculate triple point temperature. ^b This point was thought to be high owing to the partial transposition to the higher melting (*i.e.*, stable) form. ^c The impurities listed are those calculated from the melting point studies on the stable crystals. From the melting point study of the metastable crystals of *n*-propylbenzene an impurity of 0.03 mole % was also found; for *n*-butylbenzene the impurity was estimated at between 0.05 and 0.09 mole %, from a study of the metastable form.

(15) A. F. Forziati, W. R. Norris, and F. D. Rossini, *J. Res. Natl. Bur. Std.*, 43, 555 (1949).

Table V: Thermodynamic Functions for Condensed Phases^a

T, °K.	$-(G_s - H^{\circ}_s)/T,$	$(H_s - H^{\circ}_s)/T,$	$H_s - H^{\circ}_s,$	$S_s,$	$C_s,$	T, °K.	$-(G_s - H^{\circ}_s)/T,$	$(H_s - H^{\circ}_s)/T,$	$H_s - H^{\circ}_s,$	$S_s,$	$C_s,$
	cal. deg. ⁻¹ mole ⁻¹	cal. deg. ⁻¹ mole ⁻¹					cal. deg. ⁻¹ mole ⁻¹	cal. deg. ⁻¹ mole ⁻¹			
n-Propylbenzene						16	0.219	0.624	9.98	0.843	2.224
Stable crystals						18	0.305	0.835	15.03	1.140	2.830
10	0.047	0.140	1.40	0.187	0.557	20	0.404	1.067	21.33	1.471	3.471
12	0.080	0.242	2.90	0.322	0.954	25	0.711	1.712	42.80	2.423	5.138
14	0.128	0.376	5.27	0.504	1.428	30	1.086	2.427	72.82	3.513	6.715
16	0.188	0.541	8.65	0.729	1.963	35	1.513	3.143	110.00	4.656	8.156
18	0.262	0.731	13.15	0.993	2.542	40	1.979	3.855	154.19	5.834	9.490
20	0.350	0.942	18.83	1.292	3.147	45	2.474	4.547	204.62	7.021	10.667
25	0.623	1.540	38.49	2.163	4.718	50	2.987	5.214	260.68	8.201	11.734
30	0.961	2.198	65.93	3.159	6.254	60	4.050	6.458	387.5	10.508	13.585
35	1.352	2.884	100.93	4.236	7.719	70	5.132	7.594	531.6	12.726	15.195
40	1.782	3.572	142.88	5.354	9.044	80	6.215	8.635	690.8	14.850	16.641
45	2.242	4.248	191.15	6.490	10.243	90	7.289	9.603	864.3	16.892	18.029
50	2.724	4.903	245.16	7.627	11.343	100	8.348	10.507	1,050.7	18.855	19.247
60	3.728	6.140	368.4	9.868	13.262	110	9.389	11.357	1,249.3	20.746	20.474
70	4.761	7.280	509.6	12.041	14.922	120	10.412	12.168	1,460.1	22.580	21.695
80	5.803	8.329	666.3	14.132	16.439	130	11.417	12.948	1,683.2	24.365	22.911
90	6.842	9.312	838.1	16.154	17.877	140	12.405	13.702	1,918.3	26.107	24.108
100	7.871	10.232	1,023.2	18.103	19.139	150	13.375	14.437	2,165.5	27.812	25.334
110	8.887	11.098	1,220.8	19.985	20.385	160	14.330	15.157	2,425.1	29.487	26.606
120	9.889	11.924	1,430.9	21.813	21.649	170	15.27	15.87	2,697.6	31.14	27.882
130	10.874	12.724	1,654.1	23.598	22.885	171.67	15.42	15.99	2,744.3	31.41	28.098
140	11.846	13.492	1,888.9	25.338	24.100	Metastable liquid					
150	12.802	14.241	2,136.1	27.043	25.354	171.67	15.42	27.82	4,775	43.24	43.50
160	13.745	14.976	2,396.2	28.721	26.659	173.60	15.74	27.99	4,859	43.73	43.55
170	14.68	15.70	2,669.4	30.38	27.976	n-Butylbenzene					
173.60	15.01	15.96	2,770.9	30.97	28.458	Stable crystals					
Liquid						10	0.057	0.169	1.69	0.226	0.669
173.60	15.01	28.72	4,986	43.73	43.55	12	0.098	0.288	3.46	0.386	1.115
180	16.06	29.25	5,265	45.31	43.67	14	0.153	0.444	6.22	0.597	1.662
190	17.65	30.02	5,703	47.67	43.95	16	0.225	0.634	10.15	0.859	2.275
200	19.22	30.72	6,144	49.94	44.33	18	0.312	0.851	15.32	1.163	2.903
210	20.73	31.38	6,590	52.11	44.79	20	0.413	1.090	21.80	1.503	3.583
220	22.21	32.00	7,040	54.21	45.32	25	0.728	1.763	44.08	2.491	5.331
230	23.64	32.60	7,497	56.24	45.91	30	1.113	2.501	75.02	3.614	7.035
240	25.04	33.16	7,959	58.20	46.56	35	1.557	3.265	114.29	4.822	8.655
250	26.41	33.71	8,428	60.12	47.26	40	2.043	4.033	161.33	6.076	10.135
260	27.74	34.25	8,904	61.99	48.02	45	2.561	4.787	215.43	7.348	11.486
270	29.04	34.77	9,389	63.81	48.84	50	3.103	5.520	275.98	8.623	12.713
273.15	29.44	34.94	9,543	64.38	49.11	60	4.234	6.903	414.2	11.137	14.893
280	30.31	35.29	9,881	65.60	49.69	70	5.396	8.184	572.9	13.580	16.797
290	31.56	35.80	10,382	67.36	50.58	80	6.567	9.369	749.5	15.936	18.524
298.15	32.56	36.22	10,798	68.78	51.32	90	7.735	10.480	943.2	18.215	20.153
300	32.78	36.31	10,893	69.09	51.49	100	8.894	11.517	1,151.7	20.411	21.553
310	33.99	36.81	11,412	70.80	52.43	110	10.037	12.495	1,374.4	22.532	22.990
320	35.16	37.32	11,941	72.48	53.38	120	11.165	13.428	1,611.4	24.593	24.399
330	36.31	37.82	12,480	74.13	54.34	130	12.275	14.327	1,862.5	26.602	25.821
340	37.45	38.32	13,028	75.77	55.32	140	13.369	15.199	2,127.9	28.568	27.258
350	38.57	38.82	13,587	77.39	56.31	150	14.45	16.05	2,407.6	30.50	28.683
360	39.67	39.32	14,155	78.99	57.31	160	15.51	16.89	2,701.8	32.40	30.17
370	40.75	39.82	14,733	80.57	58.31	170	16.56	17.72	3,012	34.28	31.89
Metastable crystals						180	17.60	18.57	3,343	36.17	34.46
10	0.055	0.164	1.64	0.219	0.651	185.30	18.14	19.05	3,530	37.19	35.96
12	0.094	0.282	3.38	0.376	1.105						
14	0.149	0.437	6.12	0.586	1.644						

$T, ^\circ\text{K.}$	$-(G_s - H^\circ_0)/T,$	$(H_s - H^\circ_0)/T,$	$H_s - H^\circ_0,$	$S_s,$	$C_s,$
	cal. deg. ⁻¹ mole ⁻¹	cal. deg. ⁻¹ mole ⁻¹			
Liquid					
185.30	18.14	33.52	6,212	51.66	49.41
190	18.98	33.92	6,444	52.90	49.60
200	20.75	34.71	6,942	55.46	50.05
210	22.45	35.46	7,446	57.91	50.59
220	24.12	36.16	7,955	60.28	51.23
230	25.74	36.83	8,470	62.57	51.93
240	27.33	37.47	8,993	64.80	52.69
250	28.87	38.10	9,524	66.97	53.52
260	30.37	38.71	10,064	69.08	54.40
270	31.85	39.30	10,612	71.15	55.33
273.15	32.31	39.49	10,787	71.80	55.63
280	33.28	39.90	11,171	73.18	56.31
290	34.69	40.48	11,739	75.17	57.31
298.15	35.82	40.95	12,209	76.77	58.16
300	36.08	41.06	12,317	77.14	58.36
310	37.44	41.63	12,906	79.07	59.44
320	38.76	42.21	13,506	80.97	60.54
330	40.07	42.78	14,117	82.85	61.63
340	41.36	43.35	14,739	84.71	62.73
350	42.62	43.92	15,371	86.54	63.83
360	43.86	44.49	16,015	88.35	64.93
370	45.10	45.05	16,670	90.15	66.01
380	46.30	45.62	17,335	91.92	67.12
Metastable crystals					
10	0.056	0.170	1.70	0.226	0.675
12	0.097	0.289	3.47	0.386	1.117
14	0.153	0.446	6.24	0.599	1.666
16	0.225	0.636	10.17	0.861	2.277
18	0.312	0.853	15.36	1.165	2.912
20	0.414	1.093	21.85	1.507	3.590
25	0.729	1.767	44.18	2.496	5.340
30	1.115	2.506	75.17	3.621	7.043
35	1.560	3.271	114.50	4.831	8.674
40	2.046	4.041	161.65	6.087	10.161
45	2.566	4.798	215.90	7.364	11.520
50	3.110	5.533	276.64	8.643	12.757
60	4.243	6.923	415.4	11.166	14.944
70	5.407	8.209	574.6	13.616	16.838
80	6.582	9.395	751.6	15.977	18.563
90	7.754	10.506	945.5	18.260	20.196
100	8.916	11.550	1,155.0	20.466	21.671
110	10.063	12.535	1,378.8	22.598	23.087
120	11.194	13.472	1,616.6	24.666	24.476
130	12.308	14.372	1,868.4	26.680	25.860
140	13.406	15.241	2,133.8	28.647	27.240
150	14.48	16.09	2,413.2	30.57	28.641
160	15.55	16.92	2,707.1	32.47	30.18
170	16.60	17.74	3,016	34.34	31.69
180	17.64	18.57	3,342	36.21	33.49
185.14	18.17	18.99	3,517	37.16	34.47
Metastable liquid					
185.14	18.17	33.53	6,208	51.70	49.40
185.30	18.19	33.55	6,216	51.74	49.41

^a The values tabulated are the Gibbs energy function, enthalpy function, enthalpy, entropy, and heat capacity of the condensed phase at saturation pressure.

intervals that included the triple point temperature. Corrections to ΔH_m for the effect of premelting caused by impurities were applied to each measurement. For *n*-propylbenzene and *n*-butylbenzene, measurements were also made for the heat of fusion of the metastable phase. The large uncertainty in the heat of fusion of the metastable crystalline form of *n*-propylbenzene is probably caused by difficulties in securing pure metastable crystals owing to partial transposition to the stable phase if crystallization is too slow and to incomplete crystallization if it is too rapidly cooled. The values of ΔH_m listed in Table III represent the average of two or more measurements for each form of each compound. (An approximate value of 7790 cal. mole⁻¹ was found for the heat of fusion of *n*-decylbenzene.)

The triple point temperature and sample purity for each compound were determined from studies of the equilibrium melting temperature as a function of the fraction of sample melted.¹⁶ The melting point data for both stable and metastable crystals are summarized in Table IV. Also listed in Table IV is a melting point study of *n*-decylbenzene. In all cases the equilibrium temperatures, T_F , were plotted as functions of $1/F$, the reciprocal of the fraction of the total sample in the liquid state. The triple point temperatures, T_{tp} , were determined by linear extrapolations to the zero value of $1/F$. If the impurities form ideal solutions in the liquid phase and are insoluble in the solid phase, the relation between mole fraction of total impurity, N_2^* , and melting point depression, $\Delta T = T_{tp} - T_F$, is¹⁷

$$-\ln(1 - N_2) = \Lambda \Delta T(1 + B \Delta T + \dots) \quad (1)$$

where $N_2 = N_2^*/F$. The cryoscopic constants, $\Lambda = \Delta H_m/RT_{tp}^2$ and $B = 1/T_{tp} - \Delta C_m/2\Delta H_m$, were calculated from the values of ΔH_m and T_{tp} in Table V, and values of ΔC_m , the difference between the heat capacities of the compound in the solid and liquid states at the triple point, were obtained from data in Table V (discussed in the following section). Values of Λ and B are included in Table III. Impurity values given in Table IV were calculated using eq. 1 in its simplified form (for $N_2^* \ll 1$), $N_2^* = \Lambda F \Delta T$. The melting point data for the alkyl-substituted benzenes showed a greater departure from linearity than usual, but it was felt a solid solution treatment of the data was not applicable.¹⁶

(16) J. P. McCullough and G. Waddington, *Anal. Chim. Acta*, **17**, 80 (1957).

(17) A. R. Glasgow, Jr., A. J. Streiff, and F. D. Rossini, *J. Res. Natl. Bur. Std.*, **35**, 355 (1945).

Table VI: Vapor Pressure Expressed by the Cox Equation^a

Compd.	B, °K.	a	10 ^b	10 ^c	Dev. from obsd. data, mm.		Range, mm.
					Av.	Max.	
<i>n</i> -Propylbenzene	432.368	0.865134	-0.666546	0.559068	0.02	0.06	48-780
<i>n</i> -Butylbenzene	456.420	0.895932	-0.743599	0.627427	0.05	0.32	48-780

^a $\log p(\text{mm.}) = A(1 - B/T)$, where B is n.b.p. in °K. and A is defined by $\log A = a + bT + cT^2$; T in °K.

Chemical Thermodynamic Properties in the Solid and Liquid States. The low-temperature data for both the stable and metastable forms of *n*-propylbenzene and *n*-butylbenzene were used in calculating values of the Gibbs energy function, enthalpy function, enthalpy, entropy, and heat capacity for the compounds in the solid and liquid states at selected temperatures from 10 to 370°K. The values at 10°K. were computed from a Debye function, the parameters¹⁸ of which were evaluated from the heat capacity data between 11 and 20°K. Thermodynamic properties above 10°K. were calculated from values of heat and temperature of phase changes and from appropriate numerical integration of smoothed values of C_p at regular intervals. The results in Table V show that the entropies of both polymorphs of each compound agree within experimental error at the melting point of the stable form; corrections for the effects of premelting were applied as necessary in computing the "smoothed" data in Table V.

Vapor Pressures and Calculation of Heats and Entropies of Vaporization. In order to calculate the entropy and enthalpy of the compounds in the ideal gas state at 298.15°K., values of the heat of vaporization and vapor pressure were required for each compound. For *n*-propylbenzene the heat of vaporization measured by Osborne and Ginnings¹⁹ was used. For *n*-butylbenzene an experimentally determined heat of vaporization was not available. To obtain a reliable heat of vaporization,⁴ a Cox equation was fitted to the experimentally determined vapor pressures from the literature.¹⁵ From the Clapeyron equation and the value of dp/dT determined from the Cox equation, the heats and entropies of vaporization were calculated. Corrections for effects of gas imperfection were negligible and were omitted. The constants for the Cox equation and maximum and average deviations from the experimentally observed data are given for both compounds in Table VI. The heats of vaporization at 298.15°K. calculated for both compounds are given in Table VII, together with experimentally determined value of Osborne and Ginnings¹⁹ for *n*-propylbenzene.

Table VII: Heats and Entropies of Vaporization at 298.15°K.

Compd.	Calcd.		Lit. ΔH_{vap} , cal. mole ⁻¹
	ΔH_{vap} , cal. mole ⁻¹	ΔS_{vap} , cal. deg. ⁻¹ mole ⁻¹	
<i>n</i> -Propylbenzene	11,020 ± 50	36.96	11,037 ¹⁹
<i>n</i> -Butylbenzene	12,202 ± 70	40.93	

Table VIII: Molal Entropies at 298.15°K. (cal. deg.⁻¹ mole⁻¹)

Ring	Substituents				
	<i>n</i> -Propyl S°	$\Delta S/$ CH ₂	<i>n</i> -Butyl S°	$\Delta S/$ CH ₂	<i>n</i> -Decyl S°
	Liquid				
Cyclopentane	74.29	7.89	82.18	7.76	128.71
Cyclohexane	74.54	7.91	82.45	7.78	129.10
Benzene	68.78	7.99	76.77	...	123.4 ^a
	Ideal gas				
Cyclopentane	99.06	9.40	108.46	9.33	164.45
Cyclohexane	100.35	9.54	109.89	9.35	165.97
Benzene	95.09	9.56	104.65	...	161.1 ± 0.5 ^a

^a Estimated.

Discussion

The entropies at 298.15°K., determined by this research for *n*-propyl- and *n*-butylbenzene in the liquid and ideal gas state, are given in Table VIII together with previously determined values for the *n*-alkylcyclopentanes⁴ and *n*-alkylcyclohexanes.⁵ In every case the entropy increment observed between an *n*-propyl- and *n*-butyl-substituted ring is somewhat greater than the average increment found between *n*-butyl-

(18) The number of degrees of freedom and the characteristic Debye temperature, respectively, were as follows: *n*-propylbenzene: stable crystals, 5.5 and 114.8°; metastable crystals, 5.5 and 108.8°; *n*-butylbenzene: stable crystals, 5.5 and 107.8°; metastable crystals, 5.5 and 107.8°.

(19) N. W. Osborne and D. C. Ginnings, *J. Res. Natl. Bur. Std.*, **39**, 468 (1947).

and *n*-decyl-substituted rings. As satisfactory data could not be obtained on *n*-decylbenzene or *n*-dodecylbenzene, this deviation was not confirmed for the *n*-alkylbenzenes. The entropy increment, 7.99 cal. deg.⁻¹ mole⁻¹, found from *n*-propyl- to *n*-butylbenzene is a little larger than the analogous increments found for the substituted cyclopentanes and cyclohexanes and is, like them, substantially larger than the average methylene entropy increment (7.74 cal. deg.⁻¹ mole⁻¹) for the *n*-alkanes. The average values of methylene entropy increment from *n*-butyl- to *n*-decylcyclopentanes and -cyclohexanes are nearly those observed for *n*-alkanes.^{1,2} By the use of an average value of 7.77 cal. deg.⁻¹ mole⁻¹, the entropy of *n*-decylbenzene at 298.15°K. is estimated to be 123.39 cal. deg.⁻¹ mole⁻¹ for the liquid.

The agreement between the average entropy increment for the substituted *n*-alkylcyclopentanes and -cyclohexanes in the ideal gas state and the average ideal gas increment of 9.31 cal. deg.⁻¹ mole⁻¹ calculated for the *n*-alkanes by Person and Pimentel⁶ is quite good. Again, the *n*-propyl to *n*-butyl increment is higher than the average and indicates that irregularity is obtained for substituents lower than butyl. For this reason, the large value of the entropy increment for the ideal gas state found in going from *n*-propyl- to *n*-butylbenzene is not unexpected, and a somewhat lower methylene increment would be expected in estimating the entropy of *n*-decylbenzene in the ideal gas state. This may be done by two paths: one, by estimating the entropy of vaporization of *n*-decylbenzene at 298.15°K. and the entropy of compression and adding these to the estimated entropy in

the liquid state at 298.15°K.; or, two, by adding an estimated entropy increment to the calculated entropy of *n*-butylbenzene in the ideal gas state. For the first path, the entropy of vaporization is estimated by adding 7×1180 to the observed heat of vaporization of *n*-propylbenzene of Osborne and Ginnings¹⁹ according to the method outlined by Loeffler and Rossini.²⁰ This calculation gives a heat of vaporization of 19,297 cal. mole⁻¹ and an entropy of vaporization at 298.15°K. of 64.72 cal. deg.⁻¹ mole⁻¹. The entropy of compression was calculated from a Cox equation fitted to the vapor pressure data of Camin, *et al.*,²¹ and found to be -26.62 cal. deg.⁻¹ mole⁻¹. The entropy of *n*-decylbenzene in the ideal gas state calculated by this method is 161.49 cal. deg.⁻¹ mole⁻¹.

The second path used yielded a value of 160.69 cal. deg.⁻¹ mole⁻¹ for the entropy of *n*-decylbenzene in the ideal gas state when a reasonable value of 9.34 cal. deg.⁻¹ mole⁻¹ was used for the methylene entropy increment for the gas. The discrepancy, 0.8 cal. deg.⁻¹ mole⁻¹, observed between these two paths, is not unexpected in view of the long extrapolation involved. The mean value of 161.1 ± 0.5 cal. deg.⁻¹ mole⁻¹ is found in Table VIII.

Acknowledgments. The assistance of Mrs. M. E. Gross, Mrs. T. C. Kincheloe, and Dr. J. P. McCullough with some of the measurements is gratefully acknowledged.

(20) M. C. Loeffler and F. D. Rossini, *J. Phys. Chem.*, **64**, 1530 (1960).

(21) D. Camin, A. Forziati, and F. D. Rossini, *ibid.*, **58**, 440 (1954).

Further Critical Opalescence Measurements on the Nitrobenzene-*n*-Heptane System¹

by H. Brumberger and R. Pancirov

Department of Chemistry, Syracuse University, Syracuse, New York 13210 (Received July 19, 1965)

Light scattering measurements on the nitrobenzene-*n*-heptane system near the critical demixing temperature can be represented to a good approximation by the Ornstein-Zernike-Debye formalism and yield a Debye l value of ~ 9 Å. Small-angle X-ray results yield parameters inconsistent with light scattering; there is a strong suggestion that plots of I^{-1} vs. $\sin^2(\theta/2)/\lambda^2$ are curved over a sufficiently large range of the latter variable, and that an extension of the present theories is required to account for these observations.

Introduction

The theory of critical phenomena has received considerable attention in recent years.^{2,3} In order to test some of the predictions and to furnish an increasingly reliable body of experimental data, we have undertaken a series of experiments measuring the scattering of electromagnetic radiation from critically opalescent systems.^{4,5} This paper reports light scattering measurements on the nitrobenzene-*n*-heptane system, and compares them to small-angle X-ray measurements.⁴

Experimental Techniques

Purification of Materials. Nitrobenzene was purified by triple vacuum fractionation and checked by v.p.c. Only one peak was observed. *n*-Heptane, used without further purification, was obtained at a purity of 99.96 mole % from Phillips Petroleum Co.

Sample Preparation. All samples were prepared by direct weighing into the light scattering cells inside a drybox under an inert atmosphere. Compositions were known to ± 0.03 wt. %. No observable difference in the scattering was noticed for filtered and unfiltered samples.

Phase Diagram. The phase diagram of the system in the critical region was determined by the method of Rice and Atack.⁶ The separation temperature at the critical composition, 49.60 ± 0.03 wt. % *n*-heptane, was found to be $19.03 \pm 0.005^\circ$ for the samples used in this investigation.

Temperature Measurements. All temperature differences were measured with a Beckmann thermometer which had been calibrated and checked for linearity in the appropriate range against a certified platinum resistance thermometer, using a G-2 Leeds and Northrup Muller bridge.⁷ The same thermometer was used to determine the critical temperatures at various compositions and the temperature of the samples in the light scattering cell.

Temperature Control. Figure 1 shows the temperature-controlled light scattering cell. Water from a constant-temperature bath was circulated rapidly to the heat exchanger coil, F, through heavily insulated copper tubing; intake and outflow pipes in the bath were located to encourage maximum mixing. The cylindrical cell jacket was constructed of brass, with a

(1) This paper represents part of a Ph.D. dissertation submitted to the Department of Chemistry, Syracuse University, by R. Pancirov. Portions of this work were reported at the IUPAP Conference on Thermodynamics and Statistical Mechanics, Aachen, June 1964.

(2) (a) M. Fixman, *Advan. Chem. Phys.*, **6**, 175 (1964); (b) M. E. Fisher, *J. Math. Phys.*, **5**, 944 (1964).

(3) A. Münster in "Fluctuation Phenomena in Solids," R. E. Burgess, Ed., Academic Press, New York, N. Y., 1965, p. 180.

(4) H. Brumberger and W. C. Farrar, "Proceedings of the Interdisciplinary Conference on Electromagnetic Scattering," Pergamon Press, London, 1963, p. 403.

(5) R. Pancirov and H. Brumberger, *J. Am. Chem. Soc.*, **86**, 3562 (1964).

(6) O. K. Rice and D. Atack, *J. Chem. Phys.*, **22**, 382 (1954).

(7) The authors are grateful to the Carrier Corporation Laboratory, Syracuse, N. Y., for its assistance.

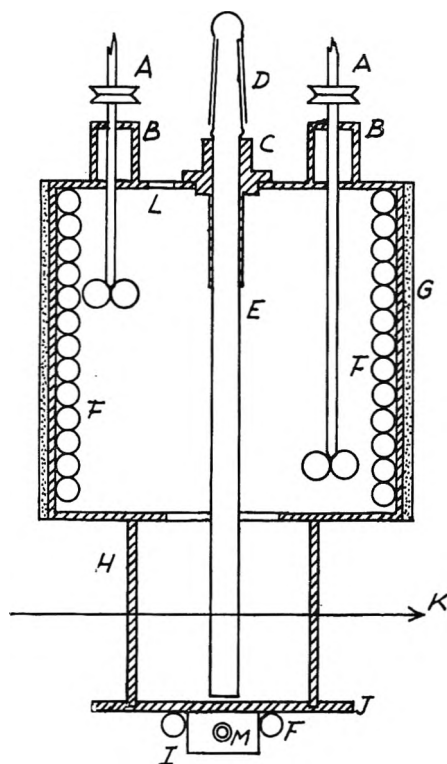


Figure 1. Temperature-controlled light scattering cell: A, stirrers; B, stirrer bearings; C, centering collar for E; D, cap for E; E, light scattering sample cell; F, heat exchanger coil of copper tubing, soldered to brass wall; G, insulation; H, glass portion of constant-temperature bath; I, centering sleeve for insertion of cell into photometer; J, brass base plate; K, direction of primary light beam; L, well for Beckmann thermometer; M, set screw.

transparent portion, H, cemented to it and to a brass base plate, J. H was a length of precision-bore 5-cm. Pyrex tubing; J and I permitted centering the entire apparatus relative to the optical system of the light scattering photometer by means of a sleeve and set screw. The jacket was filled with stirred carbon tetrachloride to minimize interfacial reflections. Turbidity due to the stirring action was found to be negligible.

Measured cell temperatures were constant to $\pm 0.005^\circ$ for several hours, and to $\pm 0.002^\circ$ during a single run. Temperature gradients were found to be unimportant in determining ΔT values, within these limits.

Light Scattering Photometer. A Brice-Phoenix photometer, modified substantially by introducing two 1×10 -mm. two-slit collimators (between source and sample, and between sample and photomultiplier), was used. The light source was monitored and adjusted to maintain constant intensity for all experiments.

Light Scattering Measurements. All of the measurements of angular distribution of scattered intensity

were made with vertically polarized incident radiation. Two wave lengths, 4360 and 5460 Å. (*in vacuo*), were used and observations were made at six to eight temperatures near the critical temperature T_c , for each of three compositions—42.97, 49.60, and 50.99 wt. % *n*-heptane. Several cell diameters were used, of which 8 and 6 mm. were found to give the most reproducible data. No qualitative differences in scattering behavior were observed for the 6- and 8-mm. cells. All of the data reported here were obtained with the latter cell diameter at 5460 Å., and have been corrected for changes in scattering volume by multiplication with $\sin \theta$. The measurements made at the shorter wave length displayed definite intensity maxima between 60 and $70^\circ \theta$, probably due to multiple scattering.

All cells were tested for symmetry with fluorescein solution. Corrections for internal reflections were found negligible. It was assumed that attenuation corrections are temperature dependent only,⁸ and would thus have no effect on the slope-intercept ratios of the Ornstein-Zernike (OZ) plots, which are used to calculate the Debye parameters.

No effect of continued irradiation on the light scattering behavior of the nitrobenzene-heptane samples was noted; changes in composition due to evaporation in the course of a run were found to be negligible. Runs made at widely different times were reproducible within the experimental error.

Experimental Results

Figure 2 shows typical curves of intensity *vs.* scattering angle at various temperature distances ΔT from the critical temperature T_c , at three compositions. Table I indicates the compositions and critical temperatures of these mixtures. The maximum observed intensity drops substantially even 1 wt. % away from the critical composition, and the dissymmetry noticeably decreases as well.

According to the Debye theory^{8,9} in the approximation including the effect of the average square of the

Table I

Composition, wt. % <i>n</i> -heptane	Demixing temp., °C.	I_{rel} at $\Delta T = 0.02^\circ$, $\theta = 30^\circ$
42.97 \pm 0.03	18.92 \pm 0.005	69
49.60 (critical comp.)	19.03	179
50.99	18.99	123

(8) P. Debye, B. Chu, and H. Kaufmann, *J. Chem. Phys.*, **36**, 3378 (1962).

(9) P. Debye, *ibid.*, **31**, 680 (1959).

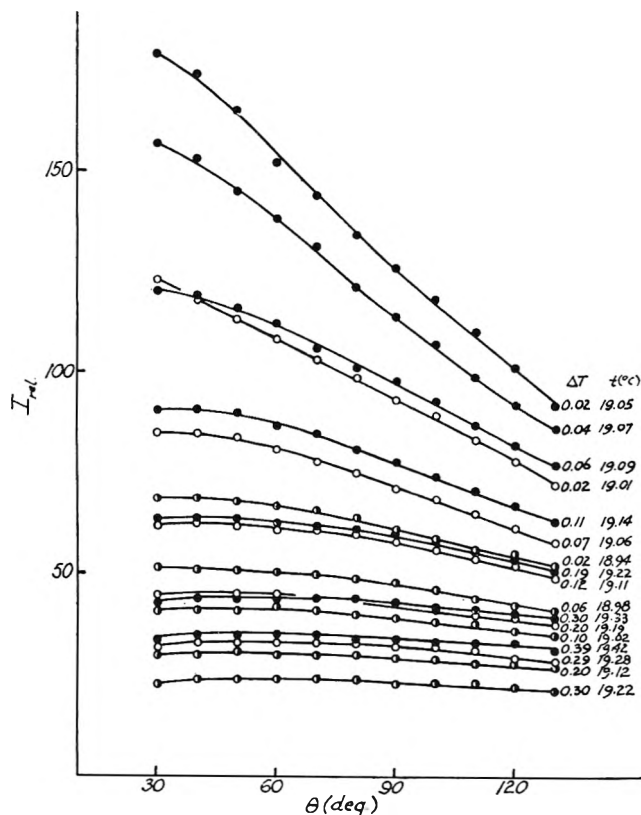


Figure 2. Angular distribution of relative intensities as a function of $\Delta T = T - T_c$ for three compositions: \circ , 50.99 wt. % heptane; \bullet , 49.60 wt. % heptane; \odot , 42.97 wt. % heptane.

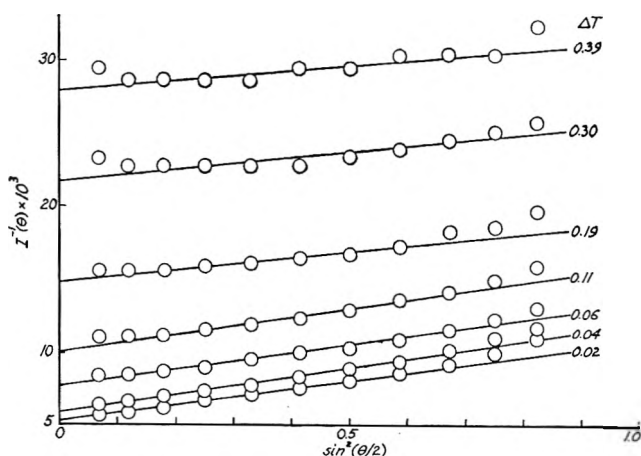


Figure 3. Typical Ornstein-Zernike plot at the critical composition.

concentration fluctuation amplitude and the average square of the fluctuation gradient, the intensity of light scattered at an angle θ from a system near T_c can be represented by

$$I^{-1} = CF(T) \frac{T_c}{T} \left[\frac{T - T_c}{T_c} + \frac{8\pi^2 l^2}{3\lambda^2} \sin^2(\theta/2) \right] \quad (1)$$

where C is a proportionality constant, $F(T)$ is a temperature-dependent attenuation factor, l is the Debye "range of intermolecular forces," and λ is the wave length in the medium. For a given composition and wave length

$$I^{-1} = A(T) + B(T) \sin^2(\theta/2) \quad (2)$$

A plot of inverse intensity vs. $\sin^2(\theta/2)$ should therefore be linear at each temperature. A similar result is obtained if the Ornstein-Zernike pair correlation function $G(r)$, where

$$G(r) = Ar^{-1} \exp(-\kappa r) \quad (3)$$

in the asymptotic approximation for $r \rightarrow \infty$,¹⁰ is inserted into the general scattering equation for a fluid medium

$$I(s) \propto \int_0^\infty 4\pi r^2 G(r) \frac{\sin sr}{sr} dr \quad (4)$$

where $s = 4\pi\lambda^{-1} \sin(\theta/2)$.

An OZ plot of the data obtained at the critical composition is shown in Figure 3; one does indeed find

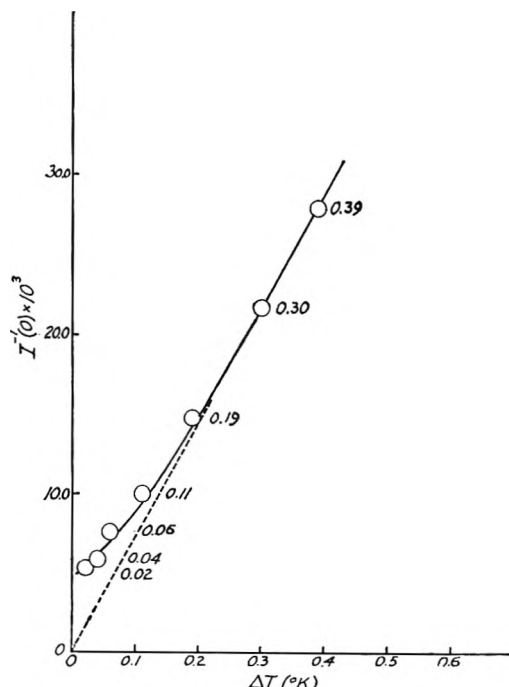


Figure 4. Plot of extrapolated zero-angle intercepts from Figure 3 vs. ΔT .

(10) L. S. Ornstein and F. Zernike, *Proc. Roy. Acad. Sci. Amsterdam*, 17, 793 (1914).

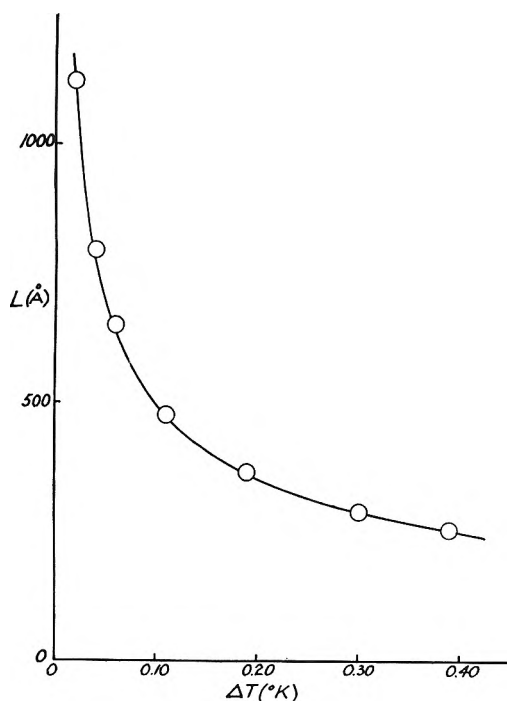


Figure 5. Plot of Debye L parameter vs. ΔT at the critical composition.

reasonably linear behavior except at the smallest and largest scattering angles. A systematic upward deviation at high angles and an upward deviation at small angles which decreases with ΔT are obtained; such observations seem fairly general, and have also been found for the 2,6-dimethylpyridine-water system⁵ and for the polystyrene-cyclohexane system.¹¹ Possibly multiple scattering effects are responsible, but this hypothesis has not so far been tested in a clearcut fashion.

The temperature dependence of the extrapolated zero-angle intercepts of the OZ plot is predicted to be linear for a model such as Debye's. Figure 4 indicates that an upward deviation from linearity is found, again in agreement with other such observations. There is, of course, a measure of doubt concerning the reliability of the extrapolation, particularly in view of the results of McIntyre, *et al.*,¹¹ and of our own low-angle X-ray data for the nitrobenzene-*n*-heptane system, discussed below.

From the OZ plots, the Debye l parameter can be calculated using eq. 1; a value of 9.3 ± 0.94 Å. is found and the correlation range, L , determined with this l value from

$$L^2 = \frac{\langle l \rangle^2}{\tau - 1} \quad (5)$$

(where $\tau = T/T_c$), is plotted vs. ΔT in Figure 5. As is

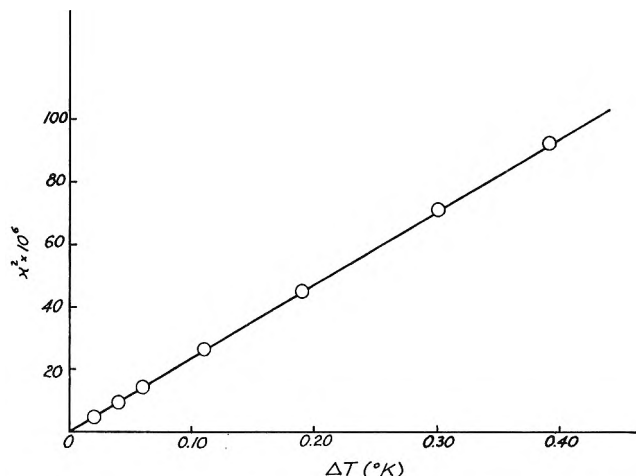


Figure 6. Plot of κ^2 vs. ΔT .

expected, the correlation range increases very rapidly as the critical temperature is approached. From the definition of L

$$L^2 = \frac{\int G(r)r^2 dv}{\int G(r) dv} \quad (6)$$

values for the OZ constant κ may be obtained by substitution of (3) yielding

$$\kappa = (\sqrt{6})/L \quad (7)$$

κ values vs. ΔT are shown in Table II. Figure 6 shows a plot of κ^2 vs. ΔT , and indicates a smooth extrapolation through the origin.

Table II

ΔT , °K.	κ , Å. ⁻¹ × 10 ⁴
0.39	9.62
0.30	8.45
0.19	6.72
0.11	5.13
0.06	3.77
0.04	3.07
0.02	2.18

Comparison to X-Ray Observations

The X-ray data so far available for this system have not as yet been extended to small enough angles to overlap the light scattering curves, and to this extent are still unsatisfactory. There is, however, sufficient evidence to indicate that the OZ plot is inadequate

(11) D. McIntyre, A. Wims, and M. S. Green, *J. Chem. Phys.*, **37**, 3019 (1962).

over a large range of $\sin(\theta/2)/\lambda$. The most striking facts are these: the OZ plot for the light scattering data shows a series of curves for the different temperatures which are nearly parallel over the temperature interval of about 0.4° from T_c which we examined. The corresponding X-ray curves (in the same temperature interval from T_c for the original X-ray sample) show a change in slope by a factor of nearly five. Further, the l value calculated from the X-ray data is $3.5 \pm 0.4 \text{ \AA.}$, about one-third of the light scattering value. The zero-angle extrapolation from the X-ray data is thus almost certainly unreliable. There is, in fact, no assurance that the same may not be true of the light scattering extrapolation; there is some experimental evidence that OZ curves may show a downward trend at smallest angles.^{5,11}

The most reasonable conclusion one may draw from these facts is that the OZ plot is likely to be curved over a sufficiently large range of $[\sin(\theta/2)/\lambda]^2$. Such observations were also made by Chu¹² and Debye.^{13,14}

Debye^{13,14} has suggested that curvature may be introduced by including higher-order terms in the series expansion for the inverse scattered intensity. In a recent publication,¹⁴ the system perfluorotributylamine-isopentane is indicated to show a curved OZ plot over a large range of s . While the inversion of the intensity curve to obtain information about the interaction potentials remains an unsolved problem for the two-component system, Debye argues by analogy to

the one-component system, for which relatively simple models are available, that only the initial slopes of the OZ curves yield a measure of the range of intermolecular interaction l , and that the slopes at large values of s have a different (though unknown) physical interpretation. Presumably deviations from linearity will be more easily observed in two-component systems.

It appears, from our measurements and those of others, that deviations from the OZD theory are in fact real and not experimental artifacts. The exact nature of these deviations is by no means well known, however, and much more precise experiments very close to T_c and over a large range of s will need to be done to ascertain it. Such measurements will require a closer look at the problem of multiple scattering, and are likely to be complicated by new phenomena which will become increasingly important near T_c .¹⁵

Acknowledgment. The authors are grateful to the National Science Foundation for supporting this research under N.S.F. Grant G-19282.

(12) (a) B. Chu, *J. Chem. Phys.*, **42**, 2293 (1965); (b) B. Chu and W. P. Kao, *ibid.*, **42**, 2608 (1965).

(13) P. Debye, ref. 4, p. 393.

(14) P. Debye, D. Caulfield, and J. Bashaw, *J. Chem. Phys.*, **41**, 3051 (1964).

(15) D. McIntyre, private communication. Dr. McIntyre observes a change in T_c when cell thicknesses are made very small (~ 0.1 mm.).

On the Possible Initiation of Photooxidation by Charge-Transfer Excitation

by J. C. W. Chien

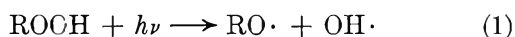
Hercules Research Center, Wilmington, Delaware 19899 (Received July 19, 1965)

The photooxidations of methylcyclohexane, cyclooctene, octene-1, benzene, toluene, cumene, and chlorobenzene have been investigated under conditions which minimized initiation by the photolysis of "impurities." The dependences of the initial rate of oxidation upon the oxygen pressure, the substrate concentration, and the incident light intensity were obtained for some of the systems. The results are interpreted assuming two primary processes, the charge-transfer excitation and the oxygen-perturbed $S \rightarrow T$ excitation. The relative significance of these two processes in photooxidation is discussed. The over-all quantum yields of initiation are given.

Introduction

The primary processes initiated by allowed transitions in the photooxidation of aromatic hydrocarbons have been reviewed^{1,2}; the photooxidation of aliphatic hydrocarbons has not received much attention. The primary concern of this communication is the mechanism of initiation of photooxidation in the wave length regions where there are no allowed transitions: $>2000 \text{ \AA}$. for aliphatic hydrocarbons and $>3100 \text{ \AA}$. for aromatic and olefinic hydrocarbons.

There are several possible primary processes. The first possibility (I) is the photolysis of "impurities" such as hydroperoxides



According to this mechanism, the induction period should increase and the rate of oxidation³ should decrease with increasing purity of the substrate. At the limit of high oxygen pressure,⁴ the rate is independent of oxygen pressure.

The second possible process (II) is the excitation of oxygen *via* the Herzberg forbidden transition to the $^3\Sigma_u^+$ state. This state could react with the substrate by either a direct reaction or an energy-transfer process.⁵ Furthermore, it could cross over to the reactive $^1\Sigma_g^+$ or $^1\Delta_g$ state. The rate of oxidation should increase with oxygen pressure. The reactions of O_2 ($^1\Delta_g$) are strongly dependent upon the nature of the substrate.⁶ From consideration of the occupational number of the antibonding orbitals, O_2 ($^1\Sigma_g^+$) could be a more electrophilic and selective species than O_2 ($^1\Delta_g$).

A third possible process (III) is the oxygen-perturbed $S \rightarrow T$ transition which is known in olefinic and aromatic hydrocarbons.⁷ For aromatic hydrocarbons, the triplet state is presumed to interact with oxygen to give directly the product peroxide²; it is not very reactive in hydrogen abstraction reactions.⁸⁻¹¹ There is no simple relationship between the $S \rightarrow T$ absorption intensity and the oxygen concentration. Little or nothing is known about the triplet state energy and the $S \rightarrow T$ transition for aliphatic hydrocarbons.

Ultraviolet absorptions have been reported¹² for

- (1) R. M. Hochstrasser and G. B. Porter, *Quart. Rev. (London)*, **14**, 146 (1960).
- (2) W. A. Noyes, Jr., G. S. Hammond, and J. N. Pitts, Jr., "Advances in Photochemistry," Vol. 1, Interscience Publishers, Inc., New York, N. Y., 1963, p. 23.
- (3) Unless otherwise stated, the rate of oxidation refers to the initial rate (*vide infra*).
- (4) L. Bateman, *Quart. Rev. (London)*, **8**, 147 (1954); L. Bateman and A. L. Morris, *Trans. Faraday Soc.*, **49**, 1026 (1953).
- (5) Analogous to the mercury photosensitization. See ref. 2, p. 209.
- (6) E. J. Corey and W. C. Taylor, *J. Am. Chem. Soc.*, **86**, 3881 (1964); C. S. Foote, private communication.
- (7) D. F. Evans, *J. Chem. Soc.*, 1735 (1960).
- (8) The ground triplet state of naphthalene does not react with alcohol or ether solvent but the excited triplet state does.⁹ The $\pi\pi^*$ triplet state of 1-naphthaldehyde is found to be unreactive in photo-reductions.¹⁰ The lower $\pi\pi^*$ triplet state of acridine is also said to be unreactive.¹¹
- (9) S. Siegel and K. Eisenthal, *J. Chem. Phys.*, **42**, 2494 (1965).
- (10) G. S. Hammond and P. A. Leermakers, *J. Am. Chem. Soc.*, **84**, 207 (1962).
- (11) A. Kellmann and J. T. Dubois, *J. Chem. Phys.*, **42**, 2518 (1965).
- (12) A. V. Munck and J. R. Scott, *Nature*, **177**, 587 (1956).

cyclohexane and for ethanol (both saturated with oxygen). Similar absorptions were also reported for aromatic compounds¹³ and for nitrogen-containing compounds.¹⁴ These absorptions have been identified¹⁴ as contact charge-transfer absorptions. These excited ³CT states (process IV) could initiate photooxidation by several possible reactions (*vide infra*). The rate of oxidation may be expected to increase with both the concentrations of oxygen and of the substrate.

The purpose of this communication is to examine the possible roles of these processes in the initiation of photooxidations of hydrocarbons.

Experimental Section

The alkanes used in this work are Phillips research grade chemicals. These are cyclohexane, methylcyclohexane, *n*-heptane, 2,3-dimethylpentane, 2,2-dimethylbutane, 2-methylpentane, 2,4-dimethylpentane, and 2,2,4-trimethylpentane (isooctane). In various experiments, these alkanes were purified by any one of the following methods. In method A, the compound was passed through a 0.6-m. column of freshly activated alumina^{15,16} immediately before use. In method B, the compound was fractionally distilled in a 100-plate Todd column. The middle third (b.p. range +0.05°) was used. Treatment with concentrated sulfuric acid was involved in method C, followed by drying, fractionation, and treatment with alumina. In method D, the compound was refluxed over copper powder under a nitrogen atmosphere and then flash-distilled at reduced pressure.

The following compounds were fractionated at reduced pressure and stored in darkness at 5°: diethyl ketone, di-*t*-butyl peroxide, cumene, octene-1, cyclooctene, and chlorobenzene.

The procedure used to measure the ultraviolet absorption intensities of compounds saturated with oxygen was essentially identical with that described by Tsubomura and Mulliken.¹⁴ The dependence of absorption intensity upon oxygen concentration was determined at 1 atm. of oxygen and at 1 atm. of air; the applicability of Henry's law was assumed. The dependence upon donor concentration was measured using suitable solvents which in the presence of oxygen do not absorb in the wave length region of interest (*i.e.*, CH₂Cl₂ at ≥2150 Å.; heptane and isooctane at ≥2600 Å.). To avoid concentration changes in these experiments, the oxygen was bubbled in at reduced temperature.

Two light sources were used: a Hanovia S-100 lamp for the monochromatic 2537-Å. radiation¹⁷ and a GE AH-6 lamp with a NiSO₄-CoSO₄-Corning 0160 filter

system for the 3130-Å. radiation (the band width at half-intensity is about 70 Å.). The output of the S-100 lamp was unchanged after 300 hr. of operation. The output of the AH-6 lamp decreased by as much as a factor of 2 in some experiments; the arithmetic mean of intensity measurements¹⁸ made before and after an experiment was taken to be the average intensity.

Photooxidation was carried out in a cylindrical cell, 10 cm. in length and 3 cm. in diameter, which was thermostated (±0.25°) in a water bath constructed of optical grade quartz. All irradiations of saturated hydrocarbons, octene-1, benzene, toluene, cumene, and chlorobenzene, were on neat compounds. For cyclooctene, both the neat compound (7.62 *M*) and solutions in isooctane were irradiated. Photooxidation of the solvent in this system is negligible.^{19,20}

In some experiments, the rate of oxidation was measured volumetrically by a gas buret operated automatically at constant pressure. The position of the mercury-leveling bulb was continuously recorded. The oxidation curve is characterized by: (1) an initial period of relatively slow and constant oxygen consumption, referred to as the initial rate; (2) an increase in the rate beginning about one-third to one-half way through the induction period; and (3) a period of "maximum rate."²¹ Unless otherwise specified, the oxygen pressure was 1 atm.

In other experiments, the substrate was distilled on a greaseless vacuum line through a column of alumina into the reaction cell. One atmosphere of an oxygen mixture (81% O₂³², 4.6% O₂³⁶, and 6.5% Ar) was introduced with stirring. Aliquots of gaseous samples (0.67 ml.) were taken during the photochemical oxidation for mass spectrometric analysis. No isotopic

(13) D. F. Evans, *J. Chem. Soc.*, 345 (1953).

(14) H. Tsubomura and R. S. Mulliken, *J. Am. Chem. Soc.*, 82, 5966 (1960).

(15) It was reported¹⁶ and substantiated in our laboratory that alumina quantitatively removes hydroperoxides.

(16) K. U. Ingold and J. R. Morton, *J. Am. Chem. Soc.*, 86, 3400 (1964).

(17) The S-100 lamp also emits about 10% of 1850-Å. radiation which was completely absorbed by the quartz cell and the quartz bath.

(18) The intensity of the incident light was measured by uranyl oxalate actinometry: W. A. Noyes, Jr., and P. A. Leighton, "The Photochemistry of Gases," Reinhold Publishing Corp., New York, N. Y., 1941, p. 78.

(19) The charge-transfer absorption of cyclooctene-O₂ at 3130 Å. is about 500 times more intense than the corresponding absorption of isooctane and the allylic hydrogens of cyclooctene are much more active than the tertiary hydrogen of isooctane.²²

(20) A. L. Williams, E. A. Oberright, and J. W. Brooks, *J. Am. Chem. Soc.*, 78, 1190 (1954).

(21) A. V. Tobolsky, D. J. Metz, and R. B. Mesrobian, *ibid.*, 72, 1942 (1950).

mixing was detected when the gaseous oxygen mixture was irradiated by 3130-Å. light for 15 hr. in the absence of a substrate. Only the compositions of the oxygen isotopes in an irradiated solution are reported here. A description of other products of oxidation will be given elsewhere.

The ratios of rate constants, $k_2/k_3^{1/2}$, where k_2 and k_3 are the rate constants of propagation and termination, respectively, are needed in calculations of quantum yields. Values of this ratio in the autoxidation of methylcyclohexane at 62.5 and 72.5° were determined by the method of Hammond, *et al.*²² The rate constant of decomposition (k_1) of azobis(isobutyronitrile)(AIBN) in methylcyclohexane was found to be 1.4×10^{-5} and 5.2×10^{-5} sec.⁻¹ at 62.5 and 72.5°, respectively. The efficiency of radical production (α), was found to be 0.61 at 62.5° and 0.73 at 72.5°. For comparison,²² values of 1.4×10^{-5} sec.⁻¹ and 0.65 for k_1 and α , respectively, have been reported at 62.5° in chlorobenzene. The values of $k_2/k_3^{1/2}$, calculated from the observed rates of oxidation by

$$-\frac{d[\text{O}_2]}{dt} = \frac{k_2}{k_3^{1/2}} [\text{RH}](2\alpha[\text{AIBN}]k_1)^{1/2} - (1 - \alpha)[\text{AIBN}]k_1$$

are 3.95×10^{-4} and 8.3×10^{-4} l.^{1/2} mole^{-1/2} sec.^{-1/2} at 62.5 and 72.5°, respectively. The rate is independent of oxygen pressure from 15 to 76 cm.

The values of $k_2/k_3^{1/2}$ for cumene oxidation, interpolated from the work of Melville and Richards,²³ are 1.48×10^{-3} , 2.1×10^{-3} , and 2.94×10^{-3} l.^{1/2} mole^{-1/2} sec.^{-1/2} at 30, 45, and 62.5°, respectively. For octene-1, this ratio was given²⁴ to be 5.47×10^{-4} l.^{1/2} mole^{-1/2} sec.^{1/2} at 25°.

Results and Discussion

Minimum Effective Concentration of "Impurity" in Photooxidation. In the preliminary experiments reported in this section, the measured induction period is used to estimate the effect of "impurity" and of purification. Unpurified alkane undergoes photooxidation after a relatively short induction period. Purified alkane photooxidizes after a longer induction period which does not increase with further purification. This limiting induction period appears to depend upon light intensity, wave length, and temperature. Table I summarizes some of the results, each entry representing the average of duplicate experiments.

Results similar to those given in Table I were also obtained in the photooxidations of ethanol, 1-butanol, isopentyl alcohol, and tetrahydrofuran. When suffi-

Table I: Effect of Purification on Photooxidation of Alkanes

Compound	Method ^a of purification	$I_0 \times 10^3$, einsteins cm. ⁻² sec. ⁻¹	λ , Å.	Temp., °C.	$t_{ind} \times 10^{-4}$, sec.
Methylcyclohexane	A	0.46	2537	62.5	1.62
Methylcyclohexane	A	0.46	2537	62.5	1.55
Methylcyclohexane	A	2.52	3130	62.5	5.90
Methylcyclohexane	B	2.33	3130	62.5	5.50
Methylcyclohexane	C	3.07	3130	62.5	6.70
Methylcyclohexane	D	2.33	3130	72.5	4.90
Isooctane	A	0.46	2537	62.5	6.95
Isooctane	A	0.46	2537	62.5	5.36
Isooctane	B	0.46	2537	62.5	6.36
Isooctane	D	1.05	2537	62.5	4.60
Isooctane	A	2.32	3130	72.5	15.7
Isooctane	C	2.32	3130	72.5	16.7
2,4-Dimethylpentane	B	2.60	3130	72.5	5.58
2,4-Dimethylpentane	A	2.53	3130	72.5	5.30

^a See Experimental Section.

ciently pure compounds are used, it appears to be meaningful to speak of a limiting induction period for specified experimental conditions.

The minimum concentration of "impurities" necessary to show an effect in photooxidations was determined. Because in most photooxidations the oxidation products (peroxides and carbonyl compounds) can be photolyzed to initiate further oxidations²⁵ (secondary initiations), the initial rates of oxidation were measured before the concentrations of oxidation products exceeded their respective minimum effective concentrations.

The "impurities" chosen in this study are di-*t*-butyl peroxide (DTBP) and diethyl ketone (DEK). The photochemistry of both of these compounds has been studied extensively.²⁵ When either of these compounds is introduced, the induction period is greatly reduced, depending upon the concentration of the added "impurity" (Table II). Under these experimental conditions, the minimum effective concentration of DTBP in the photooxidation of cyclooctene is about 10^{-3} mole l.⁻¹; it is about 10^{-4} mole l.⁻¹ in the photooxida-

(22) G. S. Hammond, J. N. Sen, and C. E. Boozer. *J. Am. Chem. Soc.*, **77**, 3244 (1955).

(23) H. W. Melville and S. Richards, *J. Chem. Soc.*, 944 (1954).

(24) L. Bateman and G. Gee, *Proc. Roy. Soc. (London)*, **A195**, 391 (1948).

(25) For example, G. R. McMillan, *J. Am. Chem. Soc.*, **84**, 2514 (1962); R. D. Doepker and G. J. Mains, *J. Phys. Chem.*, **66**, 690 (1962).

Table II: Minimum Effective "Impurity" Concentration in Photooxidations

Compound	Concn., mole l. ⁻¹	$t_{ind} \times 10^{-4}$, sec. in photooxidation of	
		Iso- octane ^a	Cyclo- octene ^b
DTBP ^c	10 ⁻¹	0.13	0.26
DTBP	10 ⁻²	2.52	0.46
DTBP	10 ⁻³	5.54	0.76
DTBP	10 ⁻⁴	7.55	1.25
DTBP	10 ⁻⁵	11.9	1.33
DTBP	10 ⁻⁶	10.85	1.28
DEK ^d	10 ⁻¹	0.42	
DEK	10 ⁻²	5.70	
DEK	10 ⁻³	6.50	
DEK	10 ⁻⁴	12.0	
DEK	10 ⁻⁵	11.2	

^a Temperature 72.5°; λ 3130 Å.; $I_0 \sim 3 \times 10^{-8}$ einstein cm.⁻² sec.⁻¹. ^b Temperature 25°; λ 3130 Å.; $I_0 \sim 1.6 \times 10^{-9}$ einstein cm.⁻² sec.⁻¹. ^c Di-*t*-butyl peroxide. ^d Diethyl ketone.

tion of isooctane. The minimum effective concentration of DEK in the photooxidation of isooctane is about 10⁻³ mole l.⁻¹. Since ϵ_{3130} for DTBP is 0.93 and ϵ_{3130} for DEK is 2.07, DTBP is about 20 times as active as DEK. This is consistent with the observed²⁵ low quantum yield of dissociation of DEK ($\sim 10^{-2}$) in perfluorodimethylcyclobutane solution.

If the same amount of "impurity" is needed to have an effect on both the rate of oxidation and the induction period, the measurement of initial photooxidation rate is meaningful if the quantity of oxygen consumed is less than the minimum effective peroxide concentration. In 50 ml. of cyclooctene, absorption of 1 ml. of oxygen (STP) corresponds to about 10⁻³ mole l.⁻¹ of oxygen reacted. Experimentally, the rate of oxidation remained relatively constant up to about 0.5 ml. of oxygen reacted (Figure 1). This rate is reported in the following sections as the initial rate in 3130-Å. photooxidations of cyclooctene, octene-1, and cumene, and 2537-Å. photooxidation of methylcyclohexane. For the 3130-Å. photooxidation of methylcyclohexane, the initial rate is calculated from the time required to consume 0.05 ml. of oxygen. These measurements were made with precision microburets.

(b) *Ultraviolet Absorption Spectra of RH-O₂ Systems.* All of the alkanes studied in this work, when saturated with oxygen, possess ultraviolet absorptions (Figures 2 and 3). The absorption intensities are directly proportional to the optical path length, to the oxygen concentration, and to the substrate concentration. The relationship with substrate concentration is illustrated for the methylcyclohexane-O₂ system in

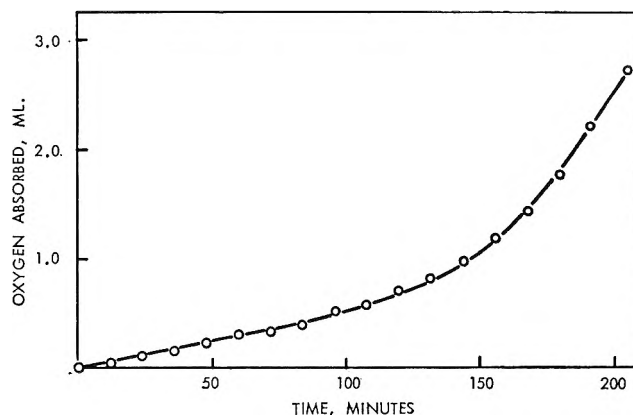


Figure 1. Photooxidation of cyclooctene: $I_a = 1.61 \times 10^{-6}$ einstein l.⁻¹ sec.⁻¹, temperature 25°, $p_{O_2} = 1$ atm., path length, 10 cm.

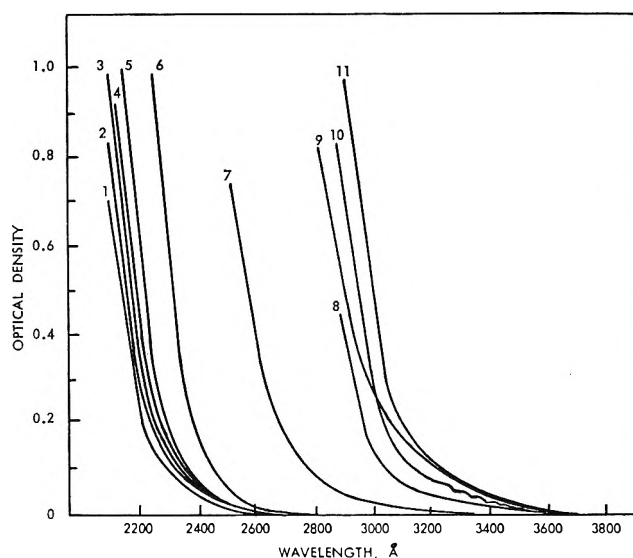


Figure 2. Ultraviolet absorption spectra (1-cm. path length, 1 atm. of oxygen) of: (1) 2,2-dimethylbutane; (2) 2-methylpentane; (3) 2,3-dimethylbutane; (4) *n*-heptane, 2,2,4-trimethylpentane (isooctane) and 2,4-dimethylpentane; (5) 2,3-dimethylpentane; (6) cyclohexane and methylcyclohexane; (7) octene-1; (8) chlorobenzene; (9) cyclohexene and cyclooctene; (10) benzene; (11) cumene and toluene.

Figure 4. In this system, the absorption intensity increases by a factor of 2.7 as the temperature is lowered from 25 to -60°.

These absorptions are not believed to be perturbed $S \rightarrow T$ transitions because there is no indication of unperturbed $S \rightarrow T$ absorptions in the same wave length region. Our experimental conditions excluded the assignment of these absorptions to the "high pressure" bands of O₂ discovered by Wulf.²⁶ The Herzberg

(26) O. R. Wulf, *Proc. Natl. Acad. Sci., U. S. A.*, **14**, 609 (1928).

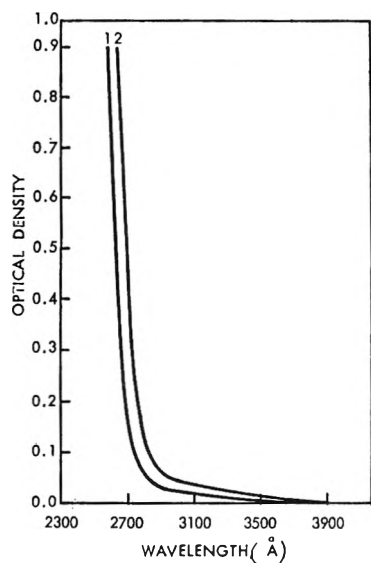


Figure 3. Ultraviolet absorption spectra (at 1 atm. of oxygen; path length = 10 cm.) of: (1) isooctane, and (2) methylcyclohexane.

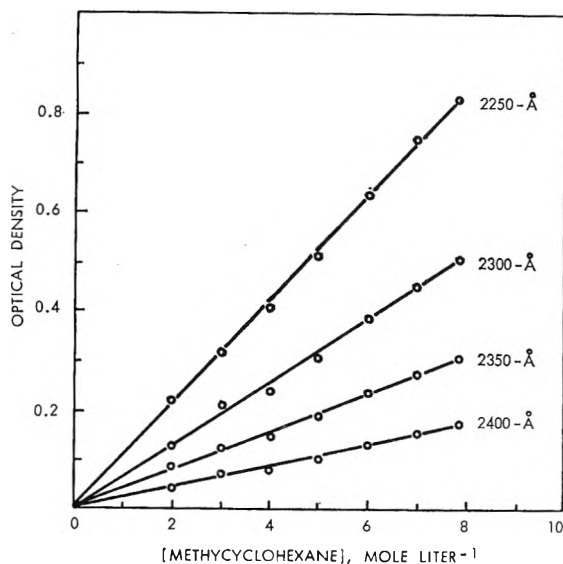


Figure 4. Variation of ultraviolet absorption intensity of methylcyclohexane- O_2 with methylcyclohexane concentration (solvent, CH_2Cl_2 ; path length, 1 cm.; $p_{O_2} = 1$ atm.).

forbidden continuum has a very low absorption coefficient.²⁷ For example, the observed 2150-Å. ultraviolet absorption of isooctane at 1 atm. pressure of oxygen has an optical density of 0.65 at 1 cm. of path length, whereas the corresponding absorption intensity of Herzberg bands for 1 atm. of gaseous oxygen is only 1.6×10^{-6} optical density unit. The same absorption in solution is expected to have much lower intensity because of the solubility of oxygen.²⁸ To some extent, this reduction of absorption intensity may be counter-

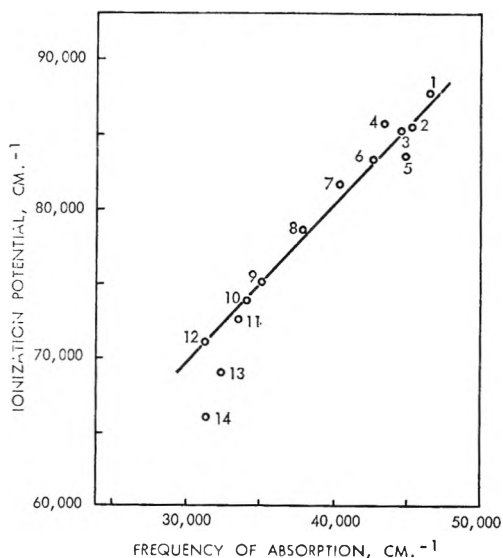


Figure 5. Frequency of ultraviolet absorption vs. ionization potentials: (1) 2,2-dimethylbutane; (2) isooctane; (3) 2,4-dimethylpentane; (4) ethanol; (5) *n*-heptane; (6) cyclohexane; (7) tetrahydrofuran; (8) diethyl ether; (9) benzene; (10) cumene; (11) toluene; (12) dialkyl sulfides; (13) xylene; (14) mesitylene.

acted by the perturbation of the forbidden transition by the interaction between oxygen and the solvent.

A plot of the wave length for equal absorption intensity, corrected for the solubility of oxygen in these compounds,^{29,30} vs. their respective ionization potentials³¹ gives a reasonably straight line (Figure 5). On the basis of these considerations, the observed ultraviolet absorptions for the alkane- O_2 systems are attributed primarily to the charge-transfer transitions.

Comparison of the spectra of olefins and aromatic compounds saturated with oxygen with those of alkanes in Figure 2 showed that the former have more intense long wave length tail absorptions. In particular, vibrational fine structures are clearly discernable in the spectrum of benzene. Both the unperturbed³²

(27) R. M. Langer, *Phys. Rev.*, **85**, 740 (1952).

(28) In fact, compounds with high ionization potentials, such as CH_3CN and H_2O , have no absorptions down to the short wave length limit of the Cary-14 spectrometer.

(29) This treatment, similar to that employed by Tsubomura and Mulliken,¹⁴ is necessitated by the lack of absorption maxima in these spectra. The solubilities were obtained from the literature.³⁰

(30) A. B. McKeown and R. R. Hibbard, *Anal. Chem.*, **28**, 1490 (1956); C. B. Kretschmer, J. Nowakowka, and R. Wiebe, *Ind. Eng. Chem.*, **38**, 506 (1946); "International Critical Tables," Vol. III, McGraw-Hill Book Co., Inc., New York, N. Y., 1928, pp. 262, 263.

(31) F. H. Field and J. L. Franklin, "Electron Impact Phenomena," Academic Press Inc., New York, N. Y., 1957, pp. 243-309; G. Briegleb, "Elektronen-Donator-Acceptor-Komplexe," Springer-Verlag, Berlin, 1961; W. C. Price, *Chem. Rev.*, **41**, 257 (1947); J. N. Murrell, *Quart. Rev. (London)*, **15**, 191 (1961).

(32) C. Reid, *J. Chem. Phys.*, **18**, 1299 (1950).

Table III: Ultraviolet Absorption Intensities^a

Compound	Optical density $\times 10^2$	
	3130 Å.	2537 Å.
Methylcyclohexane	0.045	2.5
Cyclooctene	1.5	
Octene-1	0.5	
Benzene	7.0	
Toluene	16.0	
Cumene	10.0	
Chlorobenzene	5.7	

^a At 3130 Å., the oxygen-free absorption intensities for aromatic compounds are less than 0.005 optical density unit; none is measurable for olefins and methylcyclohexane.

and the perturbed⁷ S \rightarrow T absorptions have been reported at these wave lengths for olefins and aromatic compounds. However, the continuous increase of absorption intensity with decreasing wave length cannot be accounted for by S \rightarrow T transition. It is reasonable to consider that these ultraviolet absorptions represent the sum of charge-transfer and S \rightarrow T absorptions. Without more quantitative measurement, the relative contributions of each transition to the over-all absorption intensities cannot be estimated. Tsubomura and Mulliken¹⁴ considered that charge-transfer interaction is largely responsible for the perturbation of S \rightarrow T absorption by oxygen.

In Figure 5, the points representing xylene and mesitylene, and possibly toluene as well, appear to deviate from the line shown. This deviation is possibly due to the enhanced S \rightarrow T absorptions in these compounds.

The total absorption intensities of several compounds

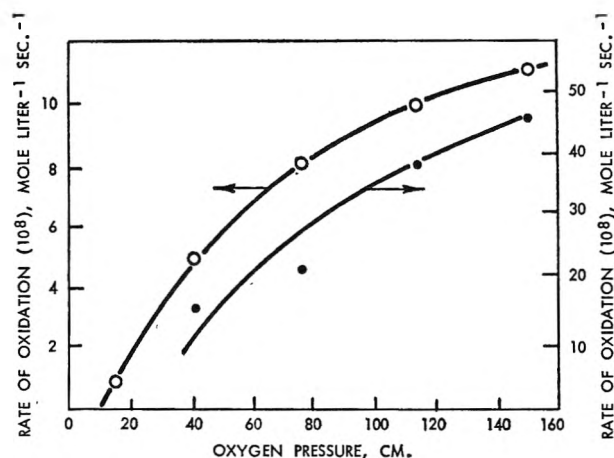


Figure 6. Variation of rate of photooxidation of methylcyclohexane with oxygen pressure at 62.5°C: ○, λ 3130 Å., $I_0 = 2.52 \times 10^{-8}$ einstein $\text{cm.}^{-2} \text{sec.}^{-1}$; ●, λ 2537 Å., $I_0 = 4.6 \times 10^{-3}$ einstein $\text{cm.}^{-2} \text{sec.}^{-1}$

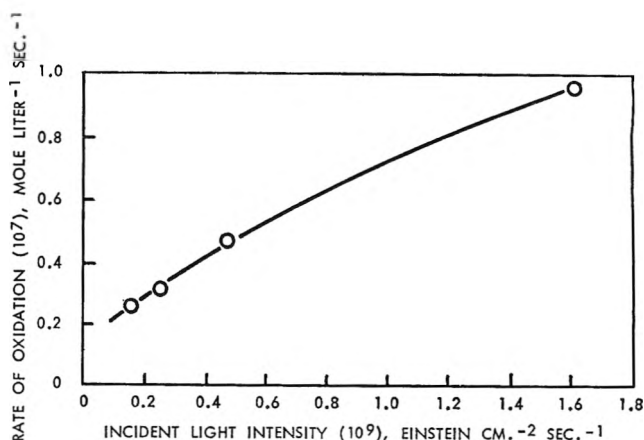


Figure 7. Initial rate of photooxidation of cyclooctene as a function of incident light intensity (temperature 25°C; $p_{\text{O}_2} = 1$ atm.; path length = 10 cm.; λ 3130 Å.; [cyclooctene] = 7.62 mole l.^{-1}).

to be used in the calculation of absorbed light intensities are summarized in Table III.

(c) *Photooxidation of Methylcyclohexane.* Figure 6 shows the dependence of the rate of photooxidation of methylcyclohexane upon oxygen pressure at 3130 and 2537 Å. Since the rate of thermal oxidation of methylcyclohexane under otherwise similar conditions is independent of oxygen pressure, the observed dependence is assumed to arise from the changes in the absorbed light intensity with oxygen pressure.

(d) *Photooxidation of Olefins.* The intense ultraviolet absorption intensity of the cyclooctene- O_2 system enables us to examine the dependence of initial oxidation rate upon oxygen pressure, cyclooctene concentration, and incident light intensity. The last relationship is shown in Figure 7. The other results are given in Table IV. A linear plot of $-d[\text{O}_2]/dt \cdot (I_a)^{-1}$ vs. $I_a^{-1/2}$, where I_a is the absorbed light intensity, for the first four experiments in Table IV, is shown in Figure 8.

Table IV: Photooxidation of Cyclooctene at 25 and 3130 Å.

Oxygen pressure, cm.	[Cyclooctene], mole l.^{-1}	$I_a \times 10^9$, einsteins $\text{cm.}^{-2} \text{sec.}^{-1}$	$d[\text{O}_2]/dt \times 10^7$, mole $\text{l.}^{-1} \text{sec.}^{-1}$
76	7.62	16.1	3.9
50	7.62	4.4	1.1
31	7.62	1.7	0.58
15.2	7.62	5.6	0.75
76	5.72	8.0	1.65
76	3.81	12.0	1.39
76	1.90	24.0	0.99
76	0.76	32.0	0.45

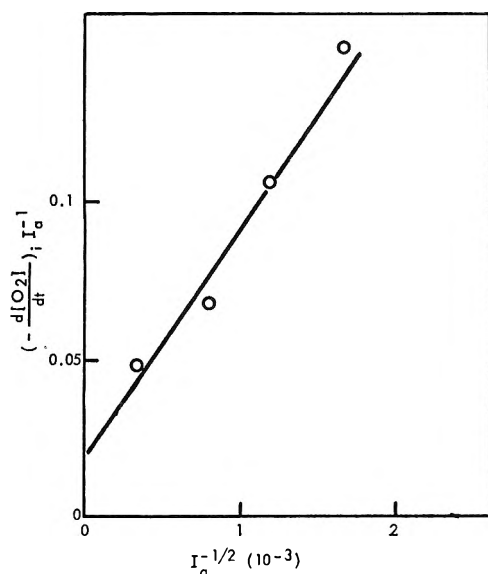


Figure 8. Photooxidation of cyclooctene at 25° and 3130 Å. (both the oxygen pressure and incident light intensity were varied, [cyclooctene] = 7.62 mole l.⁻¹).

The results of the photooxidation of octene-1 and of cumene are summarized in Table V.

(e) *Photooxidation of Aromatic Compounds.* The results in Table V allow a comparison between the photooxidations of octene-1 and cumene. The maximum rate of oxidation,²³ given in the last column, is a function of the "steady-state" hydroperoxide concentration, of the quantum yield of its decomposition, and of $k_2/k_3^{1/2}$. On the basis of consideration of the last and the most significant factor, cumene is expected to oxidize more rapidly than octene-1. Cumene's more rapid oxidation is substantiated by the observed maximum rates. In contrast, the initial rates of oxidation, as well as the induction periods, are nearly the same for both systems within the temperature range studied. Furthermore, the ultraviolet absorption intensity of cumene-O₂ is about seven times that

Table V: Photooxidation of Octene-1 and of Cumene at 3130 Å. and 1 Atm. of O₂

Compound	$I_0 \times 10^8$, einstein cm. ⁻² sec. ⁻¹	Temp., °C.	$d[O_2]/dt$ $\times 10^7$, mole l. ⁻¹ sec. ⁻¹	$t_{ind} \times$ 10^{-4} , sec.	$\left(-\frac{d[O_2]}{dt}\right)_M$ $\times 10^7$, mole l. ⁻¹ sec. ⁻¹
Octene-1	1.43	30	2.2	3.32	4.1
Octene-1	1.50	45	5.9	1.85	9.1
Octene-1	2.04	62.5	14.0	0.65	22
Cumene	1.43	30	2.3	2.43	17
Cumene	1.50	45	5.7	1.2	28
Cumene	2.04	62.5	14.0	0.73	94

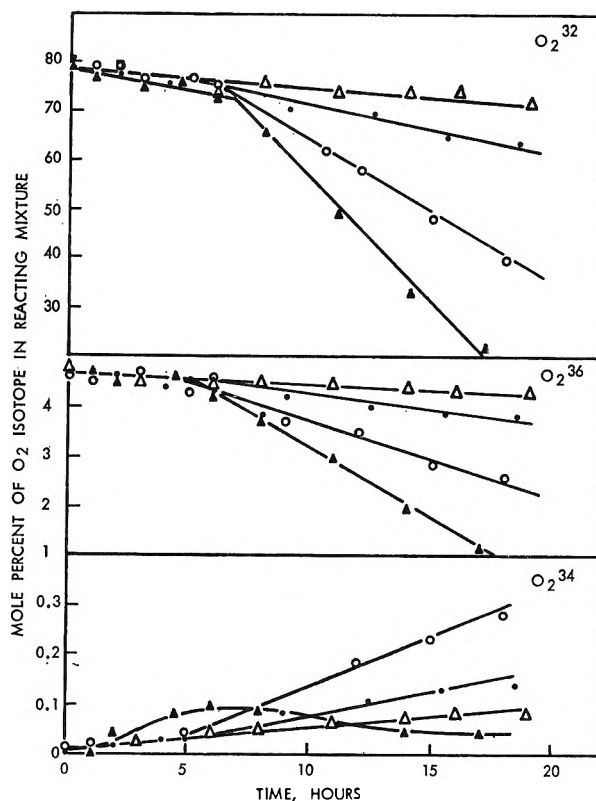


Figure 9. Rates of oxidation of neat compounds at 25° and 1 atm. pressure of isotopic O₂: Δ , benzene; \bullet , chlorobenzene; \circ , toluene; \blacktriangle , cumene.

of the octene-1-O₂ system at 3130 Å. (Table III); the primary quantum processes in cumene appear to initiate photooxidation less efficiently than those in octene-1. The photooxidations of other aromatic compounds were also examined. The results of oxygen consumption and isotopic mixing³³ caused by photooxidations are summarized in Figure 9.

In benzene, chlorobenzene, and toluene, whose hydrogens are much less reactive than the benzylic hydrogen in cumene,²⁰ the initial rates of oxygen consumption and isotopic mixing are not significantly different. Possibly the photochemical reaction is primarily that of formation of peroxides. Only cyclic peroxides and not hydroperoxides are detected by potentiometric titration in these oxidizing mixtures sampled during the induction period.

The initial rate of isotopic mixing in cumene is noticeably faster and it appears to reach a maximum near the end of the induction period. This isotopic mixing could result from the interaction of two peroxy radicals,³³ suggesting the occurrence of free-radical reactions as well as reaction 7. Semiquantitative potentiometric

(33) T. G. Traylor and P. D. Bartlett, *J. Am. Chem. Soc.*, **85**, 2407 (1963).

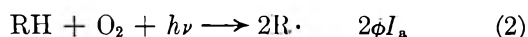
Table VI: Quantum Yields for Photooxidations

Compound	λ , Å.	ϕ
Methylcyclohexane	2537	0.023
Methylcyclohexane	3130	0.02
Cyclooctene	3130	0.018
Octene-1	3130	0.01
Cumene	3130	0.002

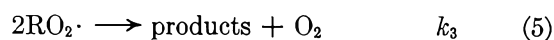
metric determinations showed the presence of both cyclic peroxides and hydroperoxides in this system; the former are present in larger amounts during the induction period.

The results with chlorobenzene are particularly noteworthy. Chlorine is known³⁴ to exert a significant heavy atom effect on intersystem transitions. The lifetime of the benzene triplet is more than a thousandfold longer than that of the chlorobenzene triplet state. Since the ultraviolet absorption intensity of chlorobenzene- O_2 is no more intense than those of the other aromatic systems, it is suggestive that the primary processes in photooxidation are fast compared to the decay of the triplet state.

(f) *Quantum Yields of Photooxidations.* If we exclude either the photolysis of "impurities" or the direct absorption by oxygen molecules as important primary processes (*vide infra*), then the most likely process is



where the nature of $R\cdot$ is not specified and the reaction includes both charge-transfer and perturbed $S \rightarrow T$ excitations. Together with the other reactions commonly accepted in autoxidation³⁵

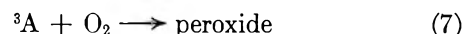


We obtained, for the initial rate of oxidation

$$-\frac{d[O_2]}{dt} = \frac{k_2}{k_3^{1/2}}[RH](\phi I_a)^{1/2} + \phi I_a \quad (6)$$

Equation 6 takes into account the evolution of oxygen³³ in the termination reaction (5). This equation predicts a linear plot of $(-d[O_2]/dt)(I_a)^{-1}$ vs. $I_a^{-1/2}$, such as that shown in Figure 8. The quantum yield can be obtained directly from the intercept. Alternatively, it can be calculated from the observed rate of oxidation using measured or literature values of $k_2/k_3^{1/2}$ (*vide supra*). Average values of ϕ are summarized in Table VI.

The values of ϕ for methylcyclohexane and olefins are not greatly difficult. On the other hand, ϕ in cumene is significantly smaller. Because the $S \rightarrow T$ transition is more easily perturbed in aromatic compounds than in olefins,⁷ it is possible that the low value of ϕ may be associated with the chemistry of the 3A state. Thus, in addition to reactions 2 to 5, one may add²



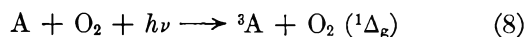
That this reaction does not entirely exclude the other reactions, at least in the case of cumene, is evident from the temperature dependence of the photooxidation rate (Table V). Possibly also the 3A state has low intrinsic reactivity because of electron delocalization.

From the slope of the plot in Figure 8, a value of $7.0 \times 10^{-5} \text{ l.}^{1/2} \text{ mole}^{-1/2} \text{ sec.}^{-1/2}$ for $k_2/k_3^{1/2}$ in cyclooctene oxidation at 25° can be calculated. This value agrees well with that reported²⁶ for cyclohexene oxidation at 25° , which is $8.5 \times 10^{-5} \text{ l.}^{1/2} \text{ mole}^{-1/2} \text{ sec.}^{-1/2}$.

Conclusions

The results presented above rather convincingly eliminated the photolysis of "impurities" (I) as an important primary process. Process II, which involves the direct excitation of oxygen, is also unlikely. Using the upper limit for the Herzberg band absorption intensity, we estimate that the quantum yield of radical formation must exceed 4, even at 2537 Å., to account for the observed oxidation rate.

Initiation by the triplet state, process III, is probably important in the photooxidations of olefins and aromatic compounds. We assume that this process is unimportant in the photooxidations of alkanes for reasons given above. In process III, reaction 7 probably predominates. Even though singlet oxygen may be produced in the $S \rightarrow T$ transition, *i.e.*



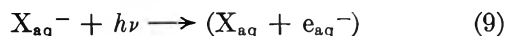
reaction of $O_2 (^1\Delta_g)$ is probably of minor importance in these systems. The reactivity of $O_2 (^1\Delta_g)$ is highly selective,^{6,7} whereas the observed initial rates of oxidation of benzene, toluene, and chlorobenzene are not significantly different. However, if the singlet oxygen is vibrationally excited, the statement above may not be valid.

The dependence of the oxidation rate upon O_2 and substrate concentrations parallels the dependence of ultraviolet absorption intensity upon these same variables. Since these absorptions are either entirely

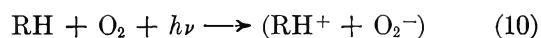
(34) D. S. McClure, *J. Chem. Phys.*, **17**, 905 (1949).

(35) C. Walling, "Free Radicals in Solution," John Wiley and Sons, Inc., New York, N. Y., 1957, pp. 397-466.

or partly attributed to charge-transfer transitions, the latter are assumed to contribute toward the initiation of oxidation of all the systems studied, particularly in the photooxidation of methylcyclohexane. The photochemistry following charge-transfer excitation of halide ions in aqueous solution has been studied.³⁶ The primary quantum process was postulated to be

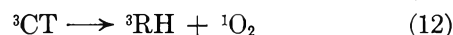
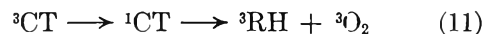


Those solvated electrons which had escaped cage recombination were observed by reaction with N_2O . Photochemistry of charge-transfer excitation in organic systems has not been studied, to the author's knowledge, but an analogous reaction can be written



Separation of ionic species in nonsolvating media has low probability.³⁷ However, since these photooxidations are low quantum efficiency processes, reaction

of those ionic species which have escaped cage recombination cannot be entirely discounted as an initiating species. There are several other alternative possibilities. The cage recombination of RH^+ and O_2^- could produce radicals or the charge-transfer absorption could be partly dissociative; these two possibilities cannot be readily differentiated. Two other possible reactions are



The results obtained so far are insufficient to justify speculation about the relative importance of these reactions in photooxidation.

(36) J. Jortner, M. Ottolenghi, and G. Stein, *J. Phys. Chem.*, **68**, 247 (1964).

(37) In the absence of an electric field, irradiation of hexane by 1.5-Mev. γ -rays gave less than 0.09 separated ion pairs per 100 e.v. of energy absorbed; A. O. Allen and A. Hummel, *Discussions Faraday Soc.*, **36**, 95 (1963).

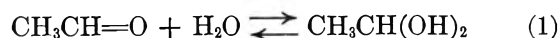
Comparison of Nuclear Magnetic Resonance, Thermal Maximum, and Scavenging Techniques for Rate Measurement

by Peter G. Evans,^{1a} Gerald R. Miller,^{1b} and Maurice M. Kreevoy^{1c}

Physical Chemistry Laboratory, Oxford, England (Received July 19, 1966)

Rates of dehydration of acetaldehyde hydrate have been studied by a scavenging method and an n.m.r. line-broadening technique. The latter has also been used to determine the hydration rate for the aldehyde. The agreement between the two methods and with the older, thermal maximum results is satisfactory and suggests that all of the methods involved are reasonably reliable.

The rate of the hydronium ion catalyzed approach to equilibrium for the reaction shown in eq. 1 has been measured by a method based on its evolution of heat.² The quantity obtained directly in such a measurement



is $k_2 + k_{-2}$, where k_2 is the second-order rate constant for the acid-catalyzed hydration (first order in sub-

strate, first order in H^+) and k_{-2} is the second-order rate constant for dehydration. The individual rate

(1) (a) U. K. Gas Council Research Scholar, 1962-1964; (b) U. S. National Science Foundation Postdoctoral Fellow 1961-1963; (c) U. S. National Science Foundation Senior Postdoctoral Fellow 1962-1963; Department of Chemistry, University of Minnesota, Minneapolis, Minnesota.

(2) (a) R. P. Bell, M. N. Rand, and K. M. A. Wynne-Jones, *Trans. Faraday Soc.*, **52**, 1093 (1956); (b) L. C. Gruen and P. T. McTigue, *J. Chem. Soc.*, 5224 (1963).

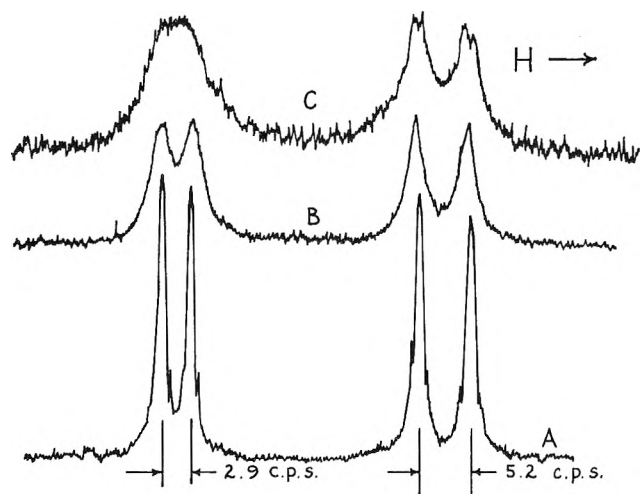


Figure 1. The methyl group doublets for acetaldehyde and its hydrate in (A) $4.4 \times 10^{-3} M$ $HClO_4$, (B) $1.2 \times 10^{-2} M$ $HClO_4$, and (C) $2.3 \times 10^{-2} M$ $HClO_4$.

constants can be obtained from this sum by combining it with the equilibrium constant, K . The best available value for the sum would seem to be about $950 M^{-1} \text{sec.}^{-1}$,² and for K , about 1.5³ (using the convention of unit activity for the solvent, water) giving a value of $570 M^{-1} \text{sec.}^{-1}$ for k_2 and $380 M^{-1} \text{sec.}^{-1}$ for k_{-2} .

We have now remeasured both k_2 and k_{-2} by an n.m.r. line-broadening technique⁴ and k_{-2} by scavenging acetaldehyde with semicarbazide.⁵ The values are all in reasonable agreement, contributing to confidence in all the methods involved.

Experimental Section

Scavenging. Reaction mixtures were made containing about $5 \times 10^{-5} M$ acetaldehyde, $2\text{--}7 \times 10^{-3} M$ semicarbazide, an acetic acid-sodium acetate buffer, and enough sodium chloride to bring the ionic strength to 0.2. Reactions were initiated by adding an aqueous solution of acetaldehyde to a mixture already containing all the other ingredients. The progress of the reaction was observed by following the buildup of the semicarbazone band at $236 m\mu$ with a Unicam SP500 spectrophotometer, the cell compartment of which was maintained at $25.0 \pm 0.1^\circ$. The unhydrated acetaldehyde all reacted with the semicarbazide before measurements were begun, and the observed optical densities obeyed a pseudo-first-order rate law with good precision.⁶ The pseudo-first-order rate constants, k_1 , were shown to be invariant under changes in the initial semicarbazide concentration between 2 and $7 \times 10^{-3} M$. Repetition indicated that they had a precision of $\pm 2\%$.

From the ratio of semicarbazone intensity produced immediately, on mixing, to that ultimately produced, K could be estimated. The value obtained was 1.5.

Line Broadening. In a $2.5 M$ neutral, aqueous solution of acetaldehyde, n.m.r. spectra show the doublet and quartet characteristic of the hydrate (J , 5.2 ± 0.1 c.p.s.) as well as those for the aldehyde (J , 2.9 ± 0.1 c.p.s.). No attempt was made to assign values of the chemical shifts in the present work, but qualitatively they seemed reasonable. As acid was added to such solutions, the multiplets first broadened and merged into singlets, and then, as still more acid was added, the two methyl peaks merged to a single line and the two methine peaks did likewise. Line widths were determined for both doublets in perchloric acid ranging from 4 to $12 \times 10^{-3} M$, a region of acidity in which the multiplet structure is still discernible. Nuclear magnetic resonance spectra were obtained using the Richards⁷ high resolution n.m.r. spectrometer operating at 29.9 Mc. The temperature could not be controlled but was measured and found to be within 1° of 25.8° for all measurements. Each spectrum on which quantitative measurements were made was reproduced six times, and the results were averaged. Spectra were sufficiently expanded so that measurements could be made with a ruler. Figure 1 shows typical spectra at the high and the low ends of the acid range used for quantitative measurements.

Results

The k_1 values obtained in the scavenging experiments were found to fit eq. 2,² with an average deviation of $\sim 3\%$. The value of k_{-2} was $565 M^{-1} \text{sec.}^{-1}$.

$$k_1 = k_{H_2O} + k_{-2}(H^+) +$$

$$k_{HA}(CH_3COOH) + k_A(CH_3COO^-) \quad (2)$$

The others will be discussed elsewhere. In eight of the scavenging experiments, the term $k_{-2}(H^+)$ in eq. 2 made up half or more of k_1 , so the reliability of k_2 would seem to be about $\pm 5\%$. Hydronium ion concentrations were obtained from the buffer ratio, the dissociation

(3) (a) E. Lombardi and P. B. Sogo, *J. Phys. Chem.*, **32**, 635 (1960); (b) R. P. Bell and J. C. Clunie, *Trans. Faraday Soc.*, **48**, 439 (1952); (c) L. C. Gruen and P. T. McTigue, *J. Chem. Soc.*, 5217 (1963).

(4) (a) A. Lowenstein and T. M. Connor, *Ber. Bunsenges. physik. Chem.*, **67**, 280 (1963); (b) J. Hine and J. G. Houston, *J. Org. Chem.*, **30**, 1328 (1965).

(5) P. L. Hénaff, *Compt. rend.*, **256**, 1752 (1963).

(6) A. A. Frost and R. G. Pearson, "Kinetics and Mechanism," John Wiley and Sons, Inc., New York, N. Y., 1962, pp. 27-31.

(7) J. B. Leane, R. E. Richards, and T. Schaefer, *J. Sci. Instr.*, **36**, 230 (1959).

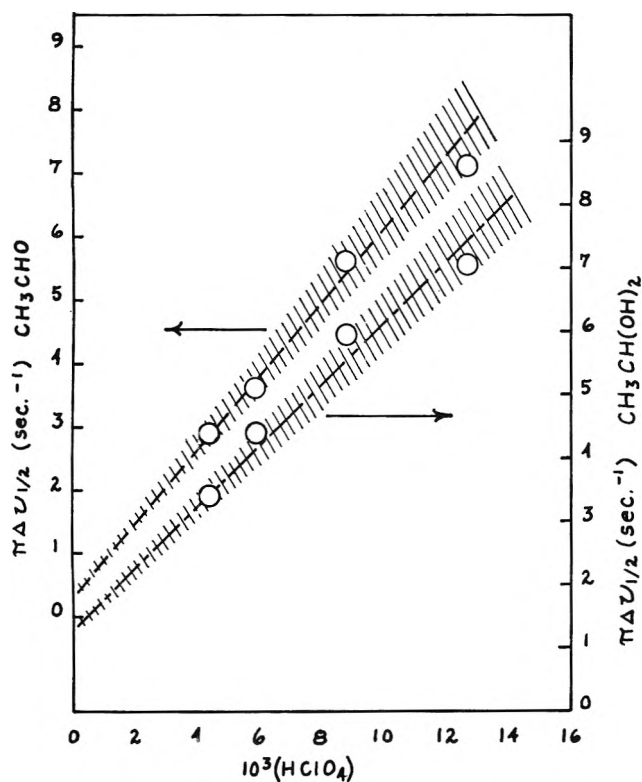


Figure 2. Plots of $\pi\Delta\nu_{1/2}$ against perchloric acid concentration for acetaldehyde, ---, and its hydrate, — · —. The former slope is k_2 , and the latter is k_{-2} . The shaded areas show a 10% uncertainty in the slopes.

tion constant of acetic acid, and the ionic strength by conventional equations previously discussed.²

To evaluate the n.m.r. results graphs were constructed of R , the ratio of intensity at the higher peak to that in the valley, vs. $\Delta\nu_{1/2}/J$, for Lorentzian doublets, for ratios of intensity in the two lines composing the doublet of 1.03 and 1.09. The latter are the intensity ratios appropriate to the doublet parts of the two A_2B spectra with the indicated spectroscopic parameters and experimental conditions. The full width at half-height is $\Delta\nu_{1/2}$. By these graphs the values of $\Delta\nu_{1/2}$ were obtained from experimental R and J .

At fairly low exchange rates k_1 is given by eq. 3,⁴ in which $\Delta\nu_{1/2}^0$ is the width at half-height for a line unbroadened by chemical exchange. Combining this

$$\Delta\nu_{1/2}^0 + k_1/\pi = \Delta\nu_{1/2} \quad (3)$$

with eq. 2 gives eq. 4 for strong acid solutions. An entirely equivalent equation can be obtained for hy-

$$\pi\Delta\nu_{1/2} = \pi\Delta\nu_{1/2}^0 + k_{H_2O} + k_{-2}(H^+) \quad (4)$$

dration, except that k_2 replaces k_{-2} . From this it is plain that plots of $\pi\Delta\nu_{1/2}$ against perchloric acid concentration should be linear with slope, k_2 or k_{-2} . Figure 2 shows that such plots, both for the aldehyde and the hydrate, are acceptably linear. They give slopes k_2 of $605 M^{-1} \text{ sec.}^{-1}$ for the aldehyde and k_{-2} of $490 M^{-1} \text{ sec.}^{-1}$ for the hydrate (determined by inspection). The scatter shown in Figure 2 suggests an uncertainty of $\pm 10\%$ for these values, which is consistent with the previous experience with the n.m.r. method.^{4,8,9} Imprecision in the intercept and in any estimated value of $\Delta\nu_{1/2}^0$, made it impossible to evaluate k_{H_2O} .

Discussion

Considering the precision of the two methods and the differences in conditions, the agreement between the scavenging k_{-2} and that from the n.m.r. measurements is entirely satisfactory. The sum of k_2 and k_{-2} from the n.m.r. measurements, $1095 M^{-1} \text{ sec.}^{-1}$, is in fair agreement with the thermal maximum value of $k_2 + k_{-2}$ ($950 M^{-1} \text{ sec.}^{-1}$),² and their ratio, 1.22, is in fair agreement with the accepted value of K , 1.5.^{3,10} Both values of k_{-2} and the n.m.r. value of k_2 are in fair agreement with recently reported n.m.r. values, $480 M^{-1} \text{ sec.}^{-1}$ for k_2 and $400 M^{-1} \text{ sec.}^{-1}$ for k_{-2} , obtained at a single-acid concentration.¹¹ (The method used was somewhat different from ours and the acid concentration somewhat higher.) The agreement between the scavenging k_{-2} and that from the thermal maximum method is a little disappointing, but taken all together the general pattern of agreement among values determined by diverse, indirect techniques contributes considerable confidence in the efficacy of all of them.

Acknowledgment. The authors want to thank Mr. R. P. Bell and Dr. R. E. Richards of the Physical Chemistry Laboratory, Oxford, England, for their hospitality and encouragement.

(8) M. M. Kreevoy, D. S. Sappenfield, and W. Schwabacher, *J. Phys. Chem.*, **69**, 2287 (1965).

(9) H. B. Charman, D. R. Vinard, and M. M. Kreevoy, *J. Am. Chem. Soc.*, **84**, 347 (1962).

(10) NOTE ADDED IN PROOF. This agreement would be even better if the nonideality of 2.5 *M* aqueous acetaldehyde solutions was taken into account.

(11) M. L. Ahrens and H. Strehlow, *Discussions Faraday Soc.*, in press.

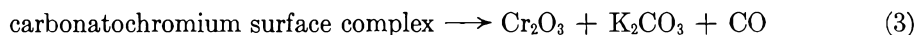
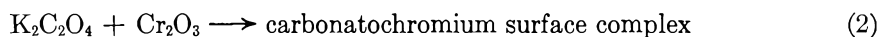
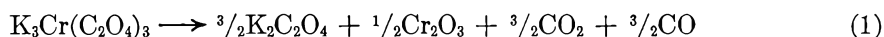
Mechanism of the Solid-State Thermal Decomposition of Potassium

Trisoxalatochromium(III) Trihydrate

by R. M. Wing¹ and G. M. Harris

*Department of Chemistry, State University of New York at Buffalo, Buffalo 14, New York
(Received July 20, 1965)*

The stoichiometry of the decomposition was studied by use of a simple nitrogen-swept tube furnace, with an absorption train for gas analysis; solid residues were examined by a combination of "wet" chemical analysis, X-ray powder diffraction, and infrared spectrophotometry. The dehydration of the complex is complete at 150°, far below the temperature required for a measurable rate of decomposition of the anhydrous material (350°). This latter process takes place, in the absence of oxygen, according to the scheme



The rates of the above reactions were determined manometrically on a vacuum furnace assembly, supplemented by periodic solid residue analysis. All obey first-order kinetics. Some carbon-13-carbon-12 discrimination studies provide strong evidence that the rate-controlling step in reaction 1 is C-O bond cleavage, following a short initial inhibition period. Reactions 2 and 3 occur on the subcrystalline Cr₂O₃ surface, as proven by spectroscopic identification of the surface intermediate, CO₂ gas pressure-dependence studies of the rate constant of (2), and separate measurements of their action rates of pure K₂C₂O₄ and hand-made Cr₂O₃-K₂C₂O₄ mixtures. Possible structures of the surface species and its mode of formation and disintegration are discussed.

No previous kinetic studies have been made of the thermolysis of solid oxalatochromium(III) complexes, although some significant information has been obtained by t.g.a. and d.t.a. techniques.² Data of this latter type, however, do not in themselves offer clear-cut chemical evidence concerning the nature of the reactions involved. Some recent papers by Yankwich, *et al.*,³ have reported complete studies of the decomposition kinetics and carbon isotope effects in the pyrolysis of simple oxalates of the type MC₂O₄ (M = Mg, Mn, and Zn), where the over-all reaction is invariably equimolar production of MO, CO, and CO₂. In the present work, detailed stoichiometric and kinetic experiments were performed on racemic crystalline K₃Cr(C₂O₄)₃·3H₂O. The techniques used included gaseous product determination and a combination of

"wet" chemical analysis, X-ray powder diffraction, and spectral examination of the solid residues. The results of these experiments, supplemented by some carbon-12-carbon-13 discrimination studies, lead to a reasonably definitive conception of the process. In contrast with the "simple" oxalates mentioned above, both metal oxide and metal carbonate products are obtained, and the process occurs in several well-defined steps. One of these sub-reactions involves chromic

(1) Work done by R. M. Wing as part of the Ph.D. requirement of State University of New York at Buffalo, June 1964. Complete dissertation available from University Microfilms, Ann Arbor, Mich.

(2) (a) W. W. Wendlandt, T. D. George, and K. V. Krishnamurty, *J. Inorg. Nucl. Chem.*, **21**, 69 (1961); (b) N. Dollimore and D. Nicholson, *ibid.*, **25**, 739 (1963).

(3) P. E. Yankwich and P. D. Zavitsanos, *J. Phys. Chem.*, **69**, 442 (1965), and other papers referred to therein.

oxide promoted surface catalysis of oxalate ion decomposition.

Experimental Section

Crystalline $K_3Cr(C_2O_4)_3 \cdot 3H_2O$ was obtained by standard procedure⁴ and purified by repeated recrystallization from water. Analyses for water and oxalate confirmed its purity, which was also checked by spectrophotometric measurements.⁵ When required, carbon dioxide gas was obtained by sublimation of Dry Ice. All other gases were taken directly from high-purity commercial cylinders. The metal oxides and graphite used were of reagent grade.

The *stoichiometric data* were obtained by use of a simple tube furnace coupled with a conventional absorption train. A Pyr-O-Vane controller maintained the furnace within $\pm 0.5^\circ$ of the desired temperature. The weighed samples were first introduced into an unheated zone of the furnace assembly, while the system was flushed with pure dry nitrogen, which served as the driver gas. To commence a run, the sample was pushed into the heated zone and its temperature was continuously recorded by means of a thermocouple attached to the Pyrex glass sample holder. The normal "heat-up" time was only a few minutes.

Water determinations were made by both weight loss of the sample and collection of the escaping water vapor on anhydrous magnesium perchlorate. Carbon dioxide was determined by absorption on Ascarite and carbon monoxide similarly, after its oxidation to carbon dioxide on copper oxide wire at 300° . The solid residues were analyzed for oxalate by permanganate titration, for chromium by iodimetry following peroxide oxidation, and for carbonate by treatment with dilute acid, collection of the evolved carbon dioxide in alkali, and back-titration. Uncomplexed oxalate was distinguished from complexed by precipitation of the former as the calcium salt, and uncomplexed chromium from complexed by use of a Dowex-50X cation-exchange column.

Infrared spectra of the solid residues were run in Nujol mulls on a Perkin-Elmer Model 21 spectrophotometer, and visible and ultraviolet spectra on a Beckmann Model DU instrument. X-Ray powder patterns of capillary-mounted samples were obtained on a Norelco X-ray diffraction setup, using either photographic or ionization-chamber recording techniques. Surface area measurements were made on a Brunauer-Emmett-Teller apparatus, using nitrogen as a reference gas.⁶ Carbon-12-carbon-13 isotopic discrimination data were obtained by conventional isotope ratio mass spectrometry of carbon dioxide samples.⁷

Most of the *kinetic runs* were made in a vacuum

furnace apparatus by following the rate of gas evolution manometrically. A magnetically controlled sample introduction device was employed, and samples of about 200-mg. size were introduced which were estimated to reach temperature equilibrium in the furnace almost immediately. A liquid nitrogen cooled trap effected the separation of CO_2 from CO , gas handling being facilitated by a Toepler pump assembly. The mercury manometer readings were made with a cathetometer and were accurate to about 0.001 cm. in a total displacement of 1 or 2 cm. per run. The gas pressure data were converted to molar units by use of the ideal gas law, with corrections for the heated volume of the gas-handling system. This volume constituted about 10% of the total.

Results and Discussion

(A). *Dehydration* of the sample goes to completion in a short time near 100° . If done slowly on a thin sample below 100° , a noncrystalline product is obtained. However, if the process is carried out more rapidly by raising the temperature to 110° and a thick sample is used (or a thin sample in a sealed ampoule), a fully crystalline anhydrous salt is obtained. It thus appears that the crystallinity of the anhydrous complex is dependent upon the existence of hydrothermal conditions during dehydration. X-Ray examination showed that the anhydrous material has a completely different crystal habit from that of the hydrate (triclinic rather than monoclinic, two formula weights per unit cell rather than four). No kinetic studies were made of the dehydration process, but it clearly comprises a nucleation-crystal growth phenomenon, at least in the presence of residual water vapor. Decomposition of the anhydrous complex does not take place until the temperature exceeds 300° .

(B). *The stoichiometry of the decomposition* in an oxygen-free atmosphere was determined on the basis of the following observations.

(a) CO and CO_2 are evolved in a 1:1 ratio until 1.5 moles of each per mole of complex is released. Then CO_2 evolution ceases, but another 1.5 moles of CO is evolved for a final total of 4.5 moles of carbon oxides released per mole of trisoxalatochromium(III) salt.

(4) J. C. Bailar, Jr., and E. M. Jones, *Inorg. Syn.*, **1**, 37 (1939).

(5) Peaks were observed at 5720 and 4200 \AA ., with molar extinction coefficients of 74.9 and 97.5, respectively. A. W. Anderson and H. Sporer, *J. Am. Chem. Soc.*, **80**, 3867 (1958), report corresponding values of 5720 (75) and 4200 (97).

(6) Courtesy of Dr. D. A. Cadenhead and Mr. Russe. McCallum of this laboratory. Details reported by R. McCallum, Senior Thesis, Chemistry Department, State University of New York at Buffalo, June 1963.

(7) Through the kind cooperation of the mass spectrometry group, McMaster University, Hamilton, Ont., Canada.

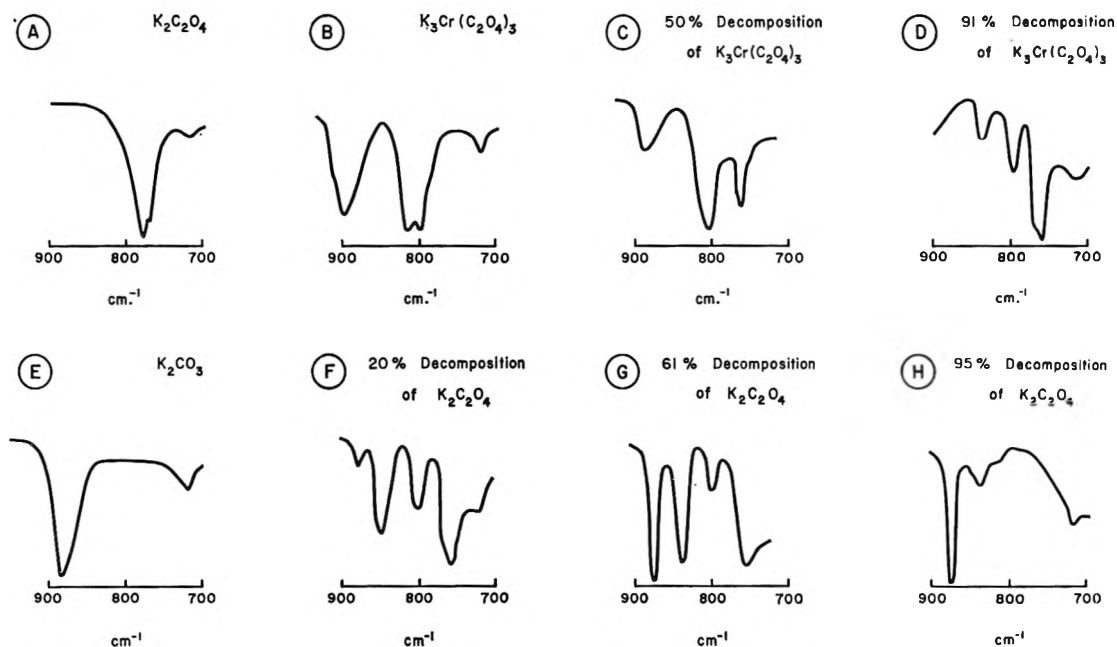


Figure 1. Infrared spectra of various samples.

(b) X-Ray powder patterns of the residues show clear evidence for the existence of $K_2C_2O_4$ crystals at the point where CO_2 evolution ceases. However, only K_2CO_3 crystals are present after gas evolution is complete. Cr_2O_3 , which must necessarily be a final product of the decomposition, does not show in the X-ray patterns, as it is apparently too finely divided.

(c) Infrared spectra of residues taken at various fractions of total reaction clearly indicate the disappearance of the coordinated C_2O_4 , which is complete by the time CO_2 evolution ceases, and the concomitant buildup of "free" $C_2O_4^{2-}$ ion (see Figure 1, curves A, B, C, and D). One then notes a decay of the $C_2O_4^{2-}$ peak, without equivalent buildup of the CO_3^{2-} peak, though a new peak develops near 850 cm^{-1} as the $C_2O_4^{2-}$ ion is used up. The 850-cm^{-1} peak later decays as CO_3^{2-} ion appears in quantity (Figure 1, curves E,

F, G, and H). Carbonato complexes of other transition metals are known to exhibit characteristic infrared absorption peaks⁸ near 850 cm^{-1} , so we interpret our observations to indicate the appearance of a carbonatochromium surface complex as a reaction intermediate in the conversion of $C_2O_4^{2-}$ ion to CO_3^{2-} ion.

(d) A comparison was made of quantities of carbon-containing products in four partially reacted samples, as calculated from the gas evolution data⁹ and similar results based on the results of "wet" analysis for carbonate (by acid decomposition) and total oxalate (by permanganate titration). The data are recorded in terms of moles of the various carbon-containing compounds present in the product mixture per mole of carbon in the original sample of trisoxalatochromium(III) complex, as shown in Table I.

These data confirm the conclusion drawn earlier that some of the carbonate does appear as a carbonato complex which later decomposes. The discrepancies

Table I: Analytical Data for Partial Trisoxalatochromium(III) Decomposition

Gas analysis data ^a			Wet analysis data ^a			Differences ^b	
A'	B'	C'	A''	B''	C''	ΔA	ΔB
0.00	0.33	0.67	0.05	0.31	0.64	0.05	0.02
0.03	0.73	0.24	0.30	0.47	0.23	0.27	0.26
0.00	0.84	0.16	0.17	0.66	0.17	0.17	0.18
0.00	0.87	0.13	0.23	0.64	0.13	0.23	0.23

^a Fractions A, B, and C refer to the mole fraction of carbon appearing as CO_3^{2-} ion, $C_2O_4^{2-}$ ion, and C_2O_4 complex, respectively. ^b $\Delta A = (A'' - A')$; $\Delta B = (B'' - B')$.

(8) J. Figata, A. E. Martell, and K. Nakamoto, *J. Chem. Phys.*, **36**, 339 (1962), and other references given therein.

(9) This calculation is based on the assumption that the total stoichiometry for complete decomposition is given by eq. 1, plus the reaction $K_2C_2O_4 \rightarrow K_2CO_3 + CO$. Then, if $[K_3Cr(C_2O_4)_3]_0$ is the initial number of moles of complex compound taken, after partial decomposition the following relations hold

$$[K_3Cr(C_2O_4)_3] = [K_3Cr(C_2O_4)_3]_0 - \frac{2}{3}[CO_2]$$

$$[K_2C_2O_4] = 2[CO_2] - [CO]$$

$$[Cr_2O_3] = \frac{1}{3}[CO_2]$$

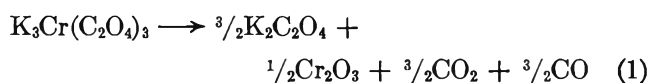
$$[K_2CO_3] = [CO] - [CO_2]$$

in the carbonate determinations (ΔA) balance out, within experimental error, those in the oxalate ion determinations (ΔB), showing that the carbonate complex "lost" in the gas evolution data computation appears, as it must, as ionic oxalate. It is also obvious that no intermediate is formed in the conversion of complexed oxalate to "free" oxalate ion since ΔC is zero within experimental error.

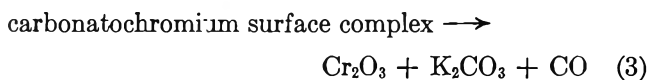
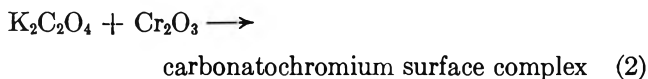
(e) Finally, it was confirmed by "wet" analysis that completely reacted residues contain 1.5 moles of CO_3^{2-} per mole of chromium(III). This, when added to the total of gaseous carbon oxides evolved, completes the carbon balance for the system.

A suitable reaction scheme to interpret the material balance data for decomposition in a nitrogen atmosphere follows.

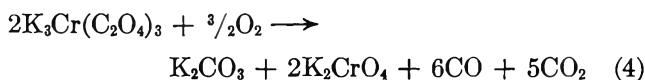
Decomposition of Anhydrous Trisoxalatochromium(III) Complex



Catalyzed Potassium Oxalate Decomposition



A few decomposition experiments were carried out in air instead of nitrogen. Invariably, only 0.5 mole of CO_3^{2-} remains at complete reaction per mole of chromium, and the latter all appears as chromate. Clearly, "carbonate fusion oxidation" occurs under these conditions, according to the over-all stoichiometry



No study has been made of the kinetics of this process in the present work.

(C). *The kinetics of the trisoxalatochromium(III) complex decomposition* (reaction 1) is clearly first order after a brief induction period. As indicated by the infrared spectra and analytical data discussed above, there is no evidence for intermediate products of any kind. A plot of the data for a typical run is presented in Figure 2. The first-order rate constant was found to be only slightly dependent on the addition of inert gases to the system, and equally so for argon, CO , and CO_2 . For example, a pressure of 48 cm. of initially added CO_2 reduced the rate constant from the *in vacuo* value of $5.0 \times 10^{-2} \text{ min.}^{-1}$ at 400° to $3.5 \times 10^{-2} \text{ min.}^{-1}$.

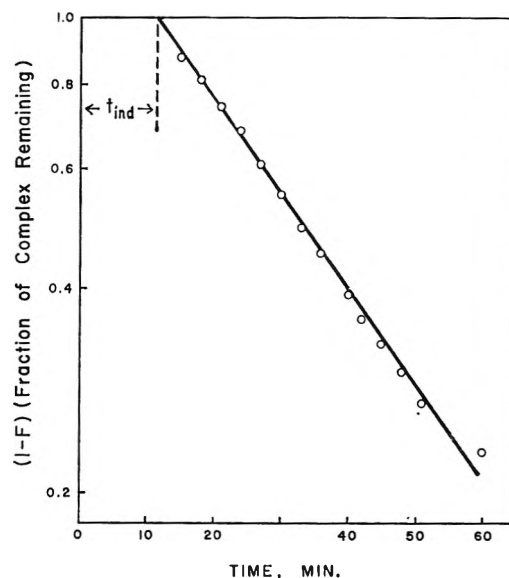


Figure 2. Typical first-order kinetic plot for the complex decomposition.

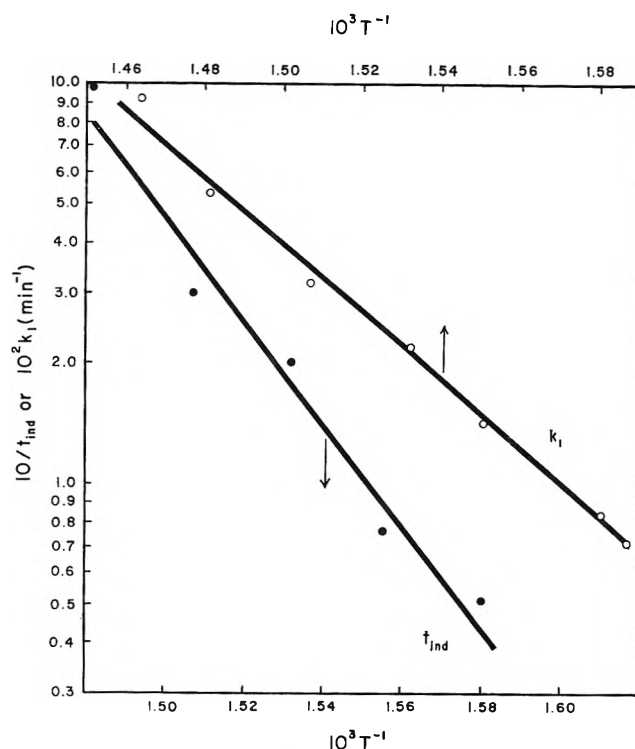


Figure 3. Temperature dependence of the induction period, t_{ind} , and the rate constant, k_1 , for the decomposition of anhydrous $\text{K}_3\text{Cr}(\text{C}_2\text{O}_4)_3$.

Both the induction period and the decomposition rate constant are strongly temperature dependent (see Figure 3). The induction period has an Arrhenius activation energy of 59 kcal./mole. The Eyring-Polanyi activation parameters for the decomposition

Table II

Species	CO	CO ₂	K ₂ C ₂ O ₄
C ¹³ atom % excess ^a (×10 ⁵)	-15 ± 1	8 ± 1	5 ± 1

^a As compared to a standard CO₂ sample with a carbon-13 atom percentage of 1.113.

reaction are $\Delta H_1^* = 34$ kcal./mole and $\Delta S_1^* = -21$ e.u.

The *isotope effect study* consisted of determining the carbon-12-carbon-13 ratios in each of the carbon-containing products of reaction 1. The averages of three independent sets of data, taken from experiments in which the complex oxalate was 50% decomposed, are shown in Table II. It must in logic be assumed that each pair of CO and CO₂ molecules produced in reaction 1 originates from a single C₂O₄ unit. These units must therefore, on the average, have an isotopic composition of about -4×10^{-5} atom % excess of carbon-13, which comes close to balancing out¹⁰ the observed 5×10^{-5} value for the undissociated C₂O₄ units appearing in the K₂C₂O₄. It seems likely that the initial step of the reaction which produces the oxides of carbon is oxygen-carbon bond cleavage, with the O-C¹² bond favored over the O-C¹³ in the conventional manner.¹¹ Succeeding steps then produce CO and CO₂, with the CO always originating from the end of the oxalate group which was the site of the initial O-C bond cleavage.

The total mechanism of the trisoxalato complex ion decomposition is more difficult to visualize. There are two distinct possibilities which lead to the observed product distribution. One comprises chromium-oxygen bond breakage¹² at one end of a chelated oxalate group, followed by release of the carbon oxides and rearrangement of the amorphous oxalate ion-chromic oxide-potassium ion residue into crystalline K₂C₂O₄ and subcrystalline Cr₂O₃. Such a mechanism is supported by data on the aquation of Cr(C₂O₄)₃³⁻ ion in acidic solution.¹³ Since the reaction takes place in aqueous medium, the coordination positions reversibly vacated by one-ended dissociation of oxalate groups are immediately re-occupied by water molecules. This preserves octahedral symmetry in the activated state for complete release of oxalate ion, thus causing little change in the crystal field stabilization energy, since water and oxalate have very nearly identical crystal field strengths. In the solid-state decomposition reaction, however, a square-pyramidal activated state is almost a necessity, resulting in a loss of crystal

field stabilization energy of about 10 kcal./mole.¹⁴ It is interesting that the activation enthalpy of the thermal decomposition does exceed that of aquation by about this amount (34 kcal./mole as compared to 23 kcal./mole).

Since it appears possible that oxalate ions are released intact from the decomposing trisoxalato-chromium(III) complex, a mechanism can be suggested for the thermolysis in purely ionic terms. It can be visualized that half of the oxalate ions, on release from the complex, break up by an ion-radical mechanism to yield CO, CO₂, and O²⁻ ions, while the remainder pair up with K⁺ ions to yield crystalline K₂C₂O₄. "Free" oxalate ions with the two electronic charges divided equally between the four oxygens would have a carbon-carbon bond energy of less than 10 kcal./mole.¹⁵ This is much smaller than the minimum decomposition enthalpy defined by the observed enthalpy of activation (34 kcal./mole), so it is obvious that the positive ions must play a critical role in stabilizing the oxalate ions which survive as K₂C₂O₄.

(D). *The catalyzed potassium oxalate decomposition*, symbolized by reactions 2 and 3, was studied by using samples of trisoxalato complex which had been heated until all complexed oxalate was decomposed according to reaction 1 (*i.e.*, no more CO₂ was being evolved). Then reaction 2 was followed by observing K₂C₂O₄ decomposition (determined by permanganate titration) and reaction 3 by manometry of carbon monoxide evolved. The data were treated on the basis of successive first-order reactions. The Eyring-Polanyi activation parameters for the two processes, obtained from

(10) The carbon-13 balance should be reckoned as follows, assuming no isotopic discrimination in the residual complex

$$2\Delta C^{13}_{K_2C_2O_4} + \Delta C^{13}_{CO} + \Delta C^{13}_{CO_2} = 0$$

The actual summation gives $3 (\pm 2) \times 10^{-5}$ atom % excess, which is not quite zero. The discrepancy may result from the assumption made concerning the residual complex isotopic composition.

(11) The expected isotope effect would be of the order of magnitude of 2% (see L. C. Melander, "Isotope Effects on Reaction Rates," Ronald Press Co., New York, N. Y., 1960). The apparent value in the present study is $(\Delta C^{13}_{CO_2} - \Delta C^{13}_{CO})/C^{13}_{standard} = 2.1\%$.

(12) There is no direct evidence for this type of mechanism in the case of chromium(III)-carboxylic chelates. However, studies of the acid hydrolysis of chelated carbonate in Co(NH₃)₄CO₃⁺ ion clearly support the concept of metal-oxygen bond opening in the dechelation step prior to CO₂ liberation (see F. A. Posey and H. Taube, *J. Am. Chem. Soc.*, **75**, 4099 (1953)).

(13) K. V. Krishnamurty and G. M. Harris, *J. Phys. Chem.*, **64**, 346 (1960); H. Kelm and G. M. Harris, to be published.

(14) F. Basolo and R. G. Pearson, "Mechanisms of Inorganic Reactions," John Wiley and Sons, Inc., New York, N. Y., 1958, p. 108 ff.

(15) This estimate is based on a simple electrostatic repulsion calculation, assuming a charge separation of 5 Å. (a reasonable maximum, since the diagonal O-O distance in oxalate ions is less than 4 Å.) and a "normal" carbon-carbon bond energy of 80 kcal./mole.

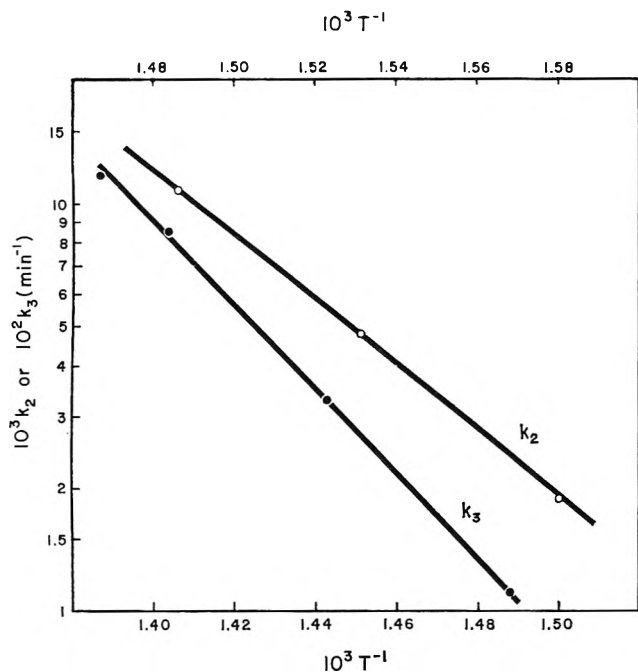


Figure 4. Temperature dependence of the rate constant for $K_2C_2O_4$ disappearance, k_2 , and for CO_2 evolution, k_3 , during Cr_2O_3 -catalyzed $K_2C_2O_4$ decomposition.

temperature dependence data (see Figure 4), are $\Delta H_2^* = 35$ kcal./mole, $\Delta S_2^* = -25$ e.u., $\Delta H_3^* = 46$ kcal./mole, and $\Delta S_3^* = -9$ e.u.

The effect of CO_2 pressure on reaction 2 at 420° was studied, yielding the results

P_{CO_2} , cm.	0.0	2.6	6.0	20.0
$10^2 k_2$, min. ⁻¹	4.3	3.0	1.7	1.2

An inhibition is seen to occur which is interpreted in terms of successively greater contamination of the active Cr_2O_3 surface by adsorbed CO_2 as the pressure of the latter is increased. This interpretation is supported by treatment of the data on the basis of the Langmuir isotherm, which leads to a rate expression of the form¹⁶

$$p/(k_0 - k) = a/k_0 + p/k_0 \quad (5)$$

In this equation, p is the pressure of CO_2 , $k_0 = k_2 =$ rate constant of reaction *in vacuo* (as regularly determined above), and k is the rate constant of the inhibited reaction. Figure 5 shows the application of this relation to the data given. It is seen to be a very satisfactory confirmation of the concept, since the observed slope of the curve (26 min.) is very close to the expected value of $1/k_2 = 23$ min.

The nature of the catalysis in this process was examined by another procedure. Hand-mixed samples of finely divided Cr_2O_3 and $K_2C_2O_4$ were prepared by

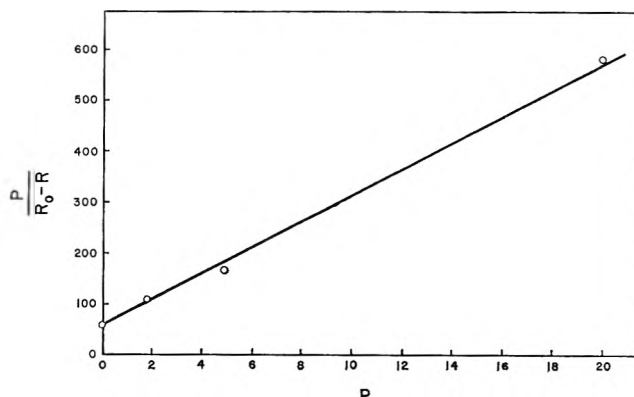


Figure 5. Dependence of $K_2C_2O_4$ decomposition rate (catalyzed by Cr_2O_3) on external gas pressure.

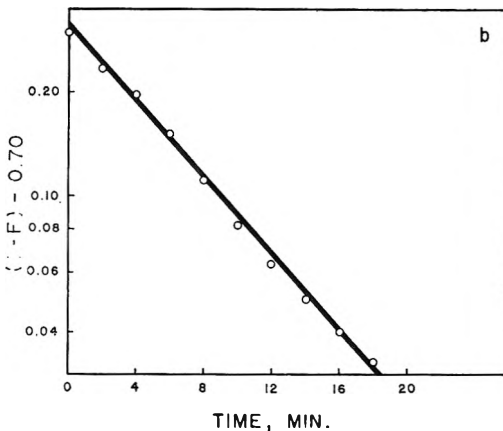
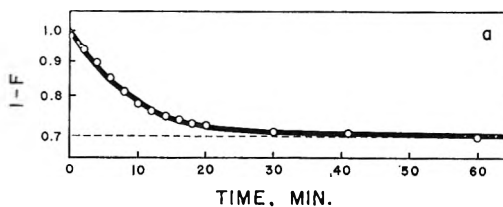


Figure 6. Kinetic plots for decomposition of a hand mixture of $K_2C_2O_4$ and Cr_2O_3 .

thorough grinding with mortar and pestle. The progress of the reaction of this material, determined at 450° by the usual oxalate decomposition procedure, is illustrated in Figure 6. It is noted that the catalyzed reaction is incomplete (curve A), but that the initial rapid process is first order (curve B), with a half-time of 5.7 min. The corresponding rate constant is

(16) The Langmuir isotherm is usually written $(1 - \theta) = a/(a + p)$, where θ is the fraction of surface covered, a is a constant determined by the relative rates of adsorption and desorption, and p is the pressure of the gas being adsorbed. If it is assumed that the rate constant of reaction on the surface, k , is proportional to the fraction of surface available, then $k = k_0(1 - \theta)$, where k_0 is the maximum rate constant, achieved *in vacuo*. Substituting for $(1 - \theta)$ and rearranging, one derives eq. 5.

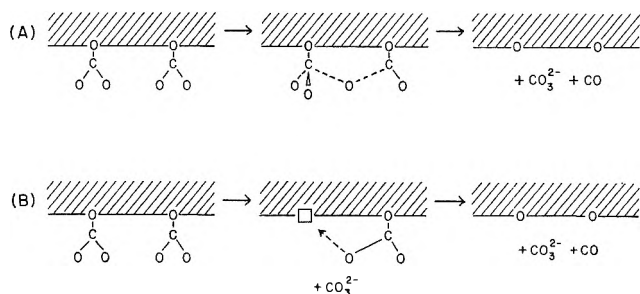


Figure 7. Mechanisms of reaction.

0.12 min.⁻¹, identical with the k_2 value at this temperature for Cr₂O₃-K₂C₂O₄ mixtures prepared *in situ* by K₃Cr(C₂O₄)₃ decomposition. The only difference is the lack of completeness of the reaction of the hand-made mixture, undoubtedly because of the impossibility of achieving totally intimate contact between Cr₂O₃ surfaces and C₂O₄²⁻ ions by this procedure. The *in situ* material, however, decomposes completely by the catalyzed mechanism, since here total mixing has been achieved by the preparation procedure, as shown by the extremely high state of subdivision of the material.¹⁷ Good first-order kinetics are thus observed over several half-times of reaction of the *in situ* preparations.

The effectiveness of some other substances as catalysts for K₂C₂O₄ thermal decomposition was also studied by use of the hand-made mixture technique. The results of the experiments, all performed at 450°, were

Catalyst	Cr ₂ O ₃	ZnO	Al ₂ O ₃	Graphite	None ¹⁸
Rate constant, min. ⁻¹	0.12	2.1 × 10 ⁻²	8.7 × 10 ⁻⁴	6.9 × 10 ⁻⁴	1.7 × 10 ⁻⁴

The metal oxides are all notably better catalysts than graphite. This supports our concept of a metal-carbonato surface complex intermediate, formed by addition of CO₂⁻ radicals to the electron-accepting metal oxide surfaces at exposed oxygen sites. Also, the catalytic activity of the three oxides falls into an order similar to their n-type character order of ZnO > Cr₂O₃ > Al₂O₃. Graphite can act as an electron acceptor, but can hold the CO₂ only as adsorbed gas, not as a carbonato complex species, and so is less effective by one order of magnitude.

One can visualize the completion of the catalysis process in either of two ways, both of which assume initial splitting of C₂O₄²⁻ ion into CO₂⁻ radical ions, with simultaneous attachment of the latter as carbonato

groups on adjacent surface oxygen sites. In one mechanism, CO₃²⁻ and CO are liberated by simple exchange of oxygen between the radicals (Figure 7a). In the other, an oxide vacancy must be temporarily formed in the metal oxide surface (Figure 7b). A choice between these mechanisms might be possible by means of experiments with oxygen-18-labeled oxalate, though other paths of oxygen exchange might obscure the result.

Carbonato surface complexes have been proposed before, in connection with the oxidation of CO to CO₂ on metal oxide surfaces,¹⁹ including some supporting infrared data.²⁰ However, Courtois and Teichner²¹ do not concur in the carbonato complex concept for the CO + O₂ reaction on nickel oxide catalyst. They may well be correct in reference to carbon dioxide adsorption, since it has linear geometry. However, the CO₂⁻ radical ion of our concept satisfies the geometrical requirements much better, since it has the same C_{2v} point symmetry as a carbonate group.²² Also, the excess electron should promote strong bond formation with surface oxygen.

Finally, some comment should be made concerning the significance of the first-order kinetics observed in all three reactions studied. Usually, this type of solid-state kinetics is associated with random nucleation by single-molecule decomposition as the rate-controlling process.²³ This is fully consistent with our identification of the rate-controlling steps in all three reactions as intramolecular processes involving only one ionic species at a time, following an equilibration period of buildup of decomposition nuclei. The latter process accounts for the short inhibition time observed in the study of reaction 1.

Acknowledgment. Financial support of this work through Contract No. AT(30-1)-1578 with the U. S. Atomic Energy Commission is gratefully acknowledged. This paper constitutes Report No. NYO-1578-32 to the Commission.

(17) The surface area of these preparations was between 10 and 16 m.²/g., as determined by B.E.T. procedure.⁶

(18) An extrapolation of the data of S. Akalan, *Rev. Fac. Sci. Univ. Istanbul*, **21C**, 184 (1956), leads to a value of $k = 1.4 \times 10^{-4}$ min.⁻¹, in good agreement with our determination at 450°.

(19) See F. S. Stone in "Chemistry of the Solid State," W. E. Garner, Ed., Butterworth and Co. Ltd., London, 1955, Chapter 15, p. 397 ff.

(20) R. P. Eischens and W. A. Plisken, *Advan. Catalysis*, **9**, 662 (1957).

(21) M. Courtois and S. J. Teichner, *J. Catalysis*, **1**, 121 (1962).

(22) D. W. Ovenall and D. H. Whiffen, *Mol. Phys.*, **4**, 135 (1961).

(23) See ref. 19, Chapter 7.

Infrared Reflection Spectra of Molten Fluoride Solutions. Hydrolysis of Tantalum(V) in Potassium Fluoride-Lithium Fluoride

by J. Stuart Fordyce and Ruth L. Baum

Union Carbide Corporation, Development Department, Parma Research Laboratory, Parma, Ohio (Received July 20, 1965)

Infrared absorption spectra, derived from reflectivity measurements, over the range 4000 to 200 cm.^{-1} for hydrolyzed melts of Ta (V) in KF-LiF have been studied. A band characteristic of a tantalum-oxygen multiple bond is found at 900 cm.^{-1} , the intensity of which is stoichiometrically related to the amount of water reacted with the melt. On the basis of these results and spectroscopic and X-ray diffraction studies of the solidified melts, the TaOF_6^{3-} anion is presumed to be the stable species in these molten solutions.

Introduction

A previous paper¹ discussed the complex anionic species present in alkali fluoride melts containing tantalum fluoride. In the KF-LiF solvent, the TaF_7^{2-} species was found by infrared reflection spectroscopic techniques to be the predominant one over a range of concentrations and temperatures.

The present investigation is an extension of this work to systems in which water is added to study the hydrolysis reactions which take place in molten fluorides and to determine what species are the stable products in such melts.

Experimental Section

The infrared reflectance measurements, reduction of data, and the preparation of anhydrous melts were carried out as previously described.¹

Qualitative hydrolysis experiments were conducted by adding 1 or 2 drops of water to the cooled solid at room temperature. The wet sample was transferred to an enclosed furnace assembly, provided with an argon flow, and was heated to just above the melting point ($\sim 720^\circ$). After holding it at this temperature for 1 hr., or so, it was cooled and transferred to the spectroscopic assembly where the infrared reflectance spectrum of the melt at 720° was determined.

Quantitative experiments were performed by maintaining the anhydrous melt in the closed-furnace assembly provided with an argon flow. Through a nickel tube placed about 0.64 cm. above the melt

surface, argon, saturated with water vapor at 25° , was passed in at a rate of 61.2 l./hr. (~ 0.078 mole of $\text{H}_2\text{O/hr.}$) for various time periods. At the end of each period the wet stream was closed off and the temperature maintained for 1 hr., or so, to drive off the hydrogen fluoride. It was then cooled, and the reflectance spectrum of the melt at 720° was obtained. Further hydrolysis was carried out the same way.

Chemical analyses were carried out on the samples following grinding in a drybox and drying overnight at 110° . The pyrohydrolysis method was used for fluorine, the gravimetric cupferron method for tantalum, and flame photometry for lithium, potassium, and nickel. The inert gas fusion method (using Laboratory Equipment Corp. apparatus) was used for oxygen which always gives high results for these samples and is not too reliable.

Results and Discussion

Figure 1 shows the infrared absorption spectrum from 1000 to 200 cm.^{-1} of a hydrolyzed melt with an initial composition of 9 mole % TaF_6 in KF-LiF. Nothing of interest was observed in the 4000- to 1000- cm.^{-1} region. In particular, the hydroxyl OH stretching band in the 3500- to 3700- cm.^{-1} region was not observed. This spectrum closely resembles that of the

(1) J. S. Fordyce and R. L. Baum, submitted to *J. Chem. Phys.*; see *J. Electrochem. Soc.*, 112, 82C (1965), and Extended Abstracts of Electrothermics and Metallurgy Division, Vol. 3, Electrochemical Society, New York, N. Y., 1965, p. 135.

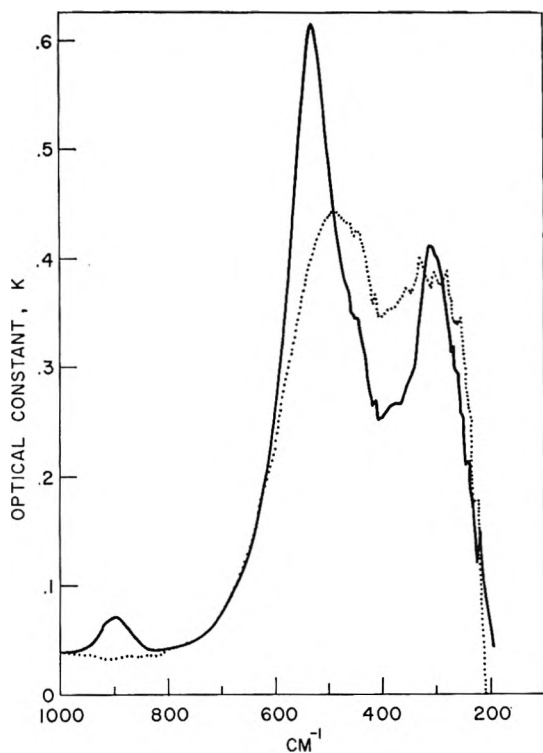


Figure 1. Infrared spectra of melts: hydrolyzed Ta(V) in KF-LiF, —; KF-LiF,

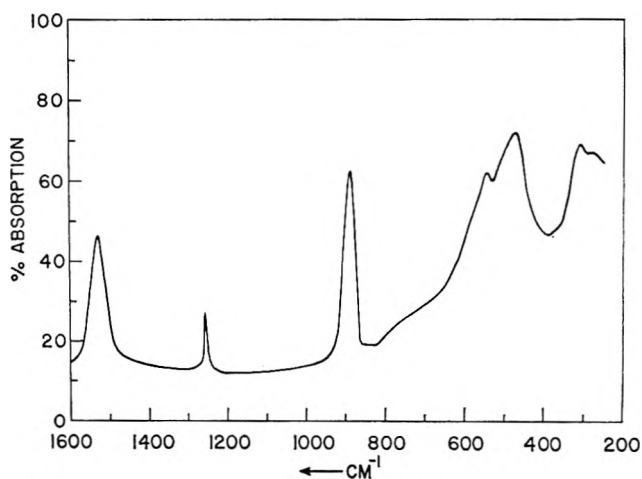


Figure 2. Infrared spectrum (KBr disk) of solidified, hydrolyzed Ta(V) in KF-LiF.

anhydrous melt with the exception of the band at 900 cm^{-1} . Chemical analysis of this system gave a composition: Ta, 22.1; K, 29.2; Li, 6.1; Ni, 0.93; F, 40.1; and O, 4.8%. The nickel analysis was performed because in these hydrolysis experiments slight attack on the nickel crucible was experienced. The X-ray diffraction powder pattern of the solid showed the presence of a face-centered-cubic material with a cell edge of 8.87 Å. This cell dimension and the line in-

tensities are in good agreement with the pattern for K_3TaOF_6 given in the literature² ($a_0 = 8.90$ Å). The remaining lines could be assigned to KF and LiF, and the few other weak ones, to K_2TaF_7 . The analytical results can be explained on the basis of a mixture: K_2TaF_7 , 18.62; K_3TaOF_6 , 31.95; LiF, 22.80; KF, 24.95; and NiF_2 , 1.53. Therefore, the melt spectrum is for a mixture of hydrolyzed and unhydrolyzed material.

The infrared absorption spectrum of the solid in a KBr disk is shown in Figure 2. The strong band at 888 cm^{-1} is apparent. The low-frequency region is characteristic of K_2TaF_7 ,¹ except that the 535- cm^{-1} band of that compound is superimposed on a band peaked at 475 cm^{-1} . In mulls, all of the bands above 1000 cm^{-1} were very weak and appeared at different frequencies. In view of these difficulties, this spectrum will not be interpreted in detail.

The appearance of a band in the 900- to 1100- cm^{-1} region is a clear indication of a metal-oxygen bond of multiple character as several authors have pointed out, particularly Kharitonov and Buslaev,³ who studied a series of oxyfluorides of metals in groups IV and V of the periodic table. Field and Hardy⁴ give 922 cm^{-1} for the $\text{Nb}=\text{O}$ stretch in K_3NbOF_6 and 927 cm^{-1} in $\text{K}_2\text{NbOF}_5 \cdot \text{H}_2\text{O}$. Unfortunately, no data for the $\text{Ta}=\text{O}$ stretch in similar compounds have been reported; it should lie very close to but slightly lower than the frequency for the niobium case. This is consistent with the present findings, *i.e.*, 900 cm^{-1} in the melt (888 cm^{-1} in the solid). On the basis of these results, it can be concluded that an oxyfluoro anion of tantalum is the stable hydrolysis product in these melts. In view of the excess fluoride present and the identity of the compound in the solid, it is most likely that the TaOF_6^{3-} species is predominant, showing that seven-coordination of the tantalum is preserved. This ion has an octahedral arrangement of fluorines around the tantalum with the oxygen off one triangular face (point group C_{3v})⁵ and would be easy to form from the TaF_7^{2-} ion (trigonal prism with one fluorine above a square face) if the two fluorines on the apex of the trigonal prism were most labile to substitution by oxygen. If only one reacts with water, the TaOF_6^{3-} ion is formed. If both react, the octahedral TaOF_5^{2-} ion would be formed, but in the presence of excess fluoride this may not be stable. The TaOF_5^{2-} ion would also possess

(2) A. E. Baker and H. M. Haendler, *Inorg. Chem.*, **1**, 127 (1962).

(3) Y. Y. Kharitonov and Y. A. Buslaev, *Izv. Akad. Nauk SSSR Otd. Khim. Nauk*, 393 (1962).

(4) B. O. Field and C. J. Hardy, *Proc. Chem. Soc.*, 11 (1963).

(5) M. B. Williams and J. L. Hoard, *J. Am. Chem. Soc.*, **64**, 1139 (1942).

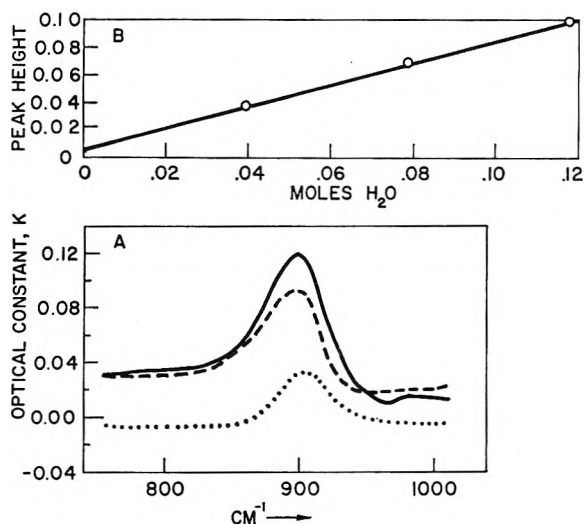


Figure 3. A. 900-cm.⁻¹ band of hydrolyzed Ta(V) in KF-LiF melts for various times of exposure to water-saturated argon stream:, 30 min.; —, 60 min.; — — —, 90 min. B. 900-cm.⁻¹ band intensity plotted against the number of moles of water vapor passed into the melt.

an absorption band at about 900 cm^{-1} and therefore cannot definitely be ruled out as a possibility.

The quantitative hydrolysis study was undertaken to relate the intensity of the 900-cm.⁻¹ band to the amount of water reacted. The reflection data were obtained only over the range of interest for the study of the 900-cm.⁻¹ band. The integration was carried out from 766 to 1010 cm^{-1} .⁶ The raw reflection data gave negative values for k because a sloping background was encountered. To overcome this, the background was approximated by a curve: $R = -14.6/\nu + 1.905 \times 10^{-2}$, which was subtracted from the observed reflectance curve. The optical constants were determined and are shown in Figure 3A. Even though in one case the k values are negative in the band tails, it is felt that this procedure allows a better determination of the intensity. The band intensity (peak height) is plotted *vs.* the number of moles of water passed over the melt in Figure 3B. The linear rela-

tionship indicates that the 900-cm.⁻¹ band intensity and the concentration of the TaOF_6^{3-} species to which it belongs is stoichiometrically related to the number of moles of water added, and presumably all or at least a constant fraction of the water reacts with the melt under these conditions to form this species. On the basis of the reaction $\text{K}_2\text{TaF}_7 + \text{KF} + \text{H}_2\text{O} \rightarrow \text{K}_3\text{TaOF}_6 + 2\text{HF}\uparrow$ and the assumption that all the water reacted in this manner, ~80% conversion to the oxyfluoride is expected with the addition of 0.118 mole of water. This is consistent with the diffraction pattern of the solid which showed only K_3TaOF_6 , KF, and LiF with a trace of K_2TaF_7 .

In one experiment a large stoichiometric excess of water vapor was added to the melt. X-Ray diffraction examination of the solid after reaction showed a precipitation of Ta_2O_5 . K_3TaOF_6 was homogeneously distributed throughout with the KF and LiF. This is consistent with the inability of KF-LiF to dissolve Ta_2O_5 at temperatures up to 800°. This was demonstrated by the infrared reflection spectrum of molten KF-LiF with Ta_2O_5 present as a solid phase which remained unchanged from the pure solvent. On prolonged heating at 850° in KF-LiF, the solid Ta_2O_5 is converted to solid KTaO_3 in agreement with the work of Ping-hsin, *et al.*⁷

Summary

The stable species in hydrolyzed molten solutions of Ta(V) in KF-LiF has been shown to be the TaOF_6^{3-} anion. This species is formed in a quantitative reaction of water with the TaF_7^{2-} anion. Extensive hydrolysis leads to the precipitation of Ta_2O_5 from the melt.

Acknowledgment. The authors wish to thank the analytical group of these laboratories for their contribution and Drs. G. W. Mellors and S. Senderoff for stimulating discussions.

(6) H. J. Bowlden and J. K. Wilmshurst, *J. Opt. Soc. Am.*, **53**, 1073 (1963).

(7) T. Ping-hsin, V. I. Konstantinov, and N. P. Luzhnaya, *Russ. J. Inorg. Chem.*, **8**, 204 (1963).

Mass Spectrometric Investigations of the Synthesis, Stability, and Energetics of the Low-Temperature Oxygen Fluorides. I. Dioxygen Difluoride

by T. J. Malone and H. A. McGee, Jr.

School of Chemical Engineering, Georgia Institute of Technology, Atlanta, Georgia 30332 (Received July 20, 1965)

A mass spectrometric arrangement is described which permits the study of compounds that are stable only at cryogenic temperatures. The low-temperature oxygen fluorides were synthesized and their mass spectra were studied between 77 and 200°K., but neither the parent ion of O₂F₂, O₃F₂, or O₄F₂ nor the unambiguously assignable fragment ions of O₃F₂ or O₄F₂ were observed. However, $A(\text{O}_2\text{F}^+)$ and $A(\text{OF}^+)$ were measured to be 14.0 ± 0.1 e.v. and 17.5 ± 0.2 e.v., respectively, at 130°K. These values are consistent with other related data and indicate that these ions are being produced by electron impact fragmentation of O₂F₂. The data permit the development of the energetics of the O₂F₂ molecule.

With the exception of OF₂, the other known and pseudo-known oxygen fluorides (O₂F₂, OF, O₂F, O₃F₂ and O₄F₂) constitute a family of compounds that exist as stable entities only so long as they are maintained at some very low temperature. This particular family, as well as other instances of species exhibiting this unusual cryogenic stability, have been discussed in a recent review.¹

The microwave spectra of O₂F₂ have indicated that the species is a nonplanar symmetric chain molecule, but no unequivocal direct observations of the other low-temperature oxygen fluorides have been reported. For example, O₃F₂ is reported by numerous investigators to be a blood-red liquid at 90°K. and to be evidently the most powerful oxidizer known, but whether or not this red liquid is actually pure molecular O₃F₂ is quite unknown. Direct observations of these species are needed first to clarify their existence, and second, because of their significance in an exploration of that little known, but very interesting, realm of chemistry below about 150°K., which may reasonably be called *cryochemistry*. Mass spectrometry offers a means for the unambiguous observation of these molecules as well as a means to study their synthesis, their stability, their chemistry, and their energetics. Because of the unusual thermal instability at cryogenic temperatures, absolute temperature control is imperative at all times, and hence

new equipment and procedures had to be developed. A thermal gradient cryogenic inlet system has been developed in which a mixture of these highly reactive species can be synthesized, separated, and vaporized directly into the ionizing electron beam of a time-of-flight mass spectrometer.

Experimental Section

Apparatus. A Bendix time-of-flight mass spectrometer, Model 12-107 with a Model S-14-107 source, was used in these experiments. Although the rather unusual auxiliary equipment that was used is described elsewhere,² a brief description of the cryogenic reactor and inlet system seems appropriate. Essentially, the system is designed such that a cold, gaseous sample can be injected directly into the ionizing electron beam of the spectrometer. Since the species are stable only at very low temperatures and since the ion source is at room temperature, the necessary fast pumping to remove thermally cracked background gas from the source rapidly was provided by a 750 l./sec. diffusion pump system (National Research Corporation, Model HS4-750).

(1) H. A. McGee, Jr., and W. J. Martin, *Cryogenics*, 2, 257 (1962).

(2) H. A. McGee, Jr., T. J. Malone, and W. J. Martin, to be published.

Referring to the schematic shown in Figure 1, the outer sleeve, A, slides through a double O-ring seal into a vacuum lock arrangement and then into the spectrometer. This permits the removal of the cryogenic assembly for adjustments or repairs without the necessity of breaking vacuum in the main spectrometer system. In essence, the unit consists of a straight tubular reactor and condensation space with a thermostated chamber (B and C) at each end. The temperatures of the two chambers are controlled independently by accurately balancing the heat required to vaporize a finely controlled liquid nitrogen input stream against the heat added by means of a resistance heater wound on the center posts, D and E. By varying the liquid nitrogen rate and the heater power, each chamber could be readily maintained at any temperature above the normal boiling point of nitrogen (77°K). The temperatures were automatically controlled within $\pm 1.0^\circ\text{K}$ of the desired values by two Leeds and Northrup Speedomax H, AZAR recorder-controllers which operated the heaters in the simple on-off mode.

A mixture of very reactive species can be either injected into or synthesized in the reactor space, F, while both B and C are at some low temperature. Then by raising the temperature of B, a thermal gradient is imposed along the connecting tube, G, between B and C causing the species to be successively vaporized and recondensed at distances along G which depend upon the volatility of the individual species. Then by manipulating the temperatures of B and C the species may be successively transported through the channel, H, and into the spectrometer. The blade-shaped nose, I, which is at the same temperature as C, is inserted directly into the ion source so that the electron beam is actually in grazing, tangential incidence with the sample inlet hole, J. Hence, mass spectrometric analysis of the vapors is achieved without warmup above the temperature of C.

Procedure. The syntheses were conducted in the assembly shown in Figure 1 by using a 1100-v., 60-cycle annular discharge between the single electrode,

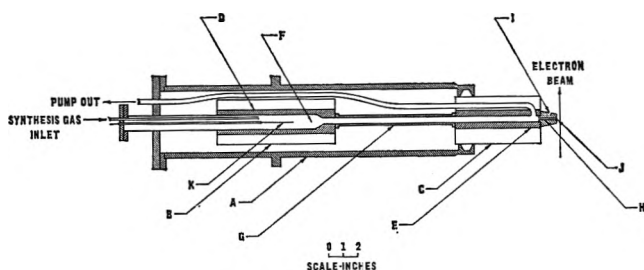


Figure 1. Schematic diagram of thermal gradient, cryogenic reactor, and inlet assembly.

K, and the grounded monel walls of the reactor space. The synthesis gas was an O_2 and F_2 mixture in the stoichiometric ratio corresponding to either O_2F_2 or to O_3F_2 , which yields O_2F_2 or O_3F_2 as the predominant product, respectively.³

The reactor pressure and temperature were 25–35 torr and 77°K ., respectively. The mixture of fluorides was partially separated and vaporized directly into the spectrometer as described above. The appearance potentials of the ions of interest were determined using the Fox retarding potential difference (RPD) method,⁴ with the energy scale calibrated immediately before and after each energy measurement using both argon and nitrogen. In making the energy measurements on the highly reactive fluorine compounds, it was necessary for the ion source to become partially passivated before the spectrometer would stabilize enough to make accurate and reproducible measurements. With continuous injection of the fluoride samples, the trap current decreased to an inoperable level after 12–15 hr.

Results

Mass Spectrum as a Function of Temperature. Several hundred traces of the mass spectrum were made over the temperature range of 77 – 200°K . in four O_3F_2 syntheses and four O_2F_2 syntheses. In addition, mass spectra as a function of temperature were obtained for the unreacted feed gas mixture of O_2 and F_2 , as well as for SiF_4 , which turned out to be a particularly troublesome impurity in the product mixtures. Relative intensities of all ion currents were tabulated at each temperature.

The limitations of the spectrometer and complicated features of the spectra combined to necessitate care in making mass assignments for the observed ions. Mass scales were prepared for each scan rate using m/e 16 (O atom) and m/e 32 (O_2 molecule) as reference masses. Using only the measured distance between the reference masses as verified from several traces, the distance from m/e 16 to all other masses out to m/e 130 was calculated and plotted to yield completely unbiased scales. The use of these scales resulted in consistent and unambiguous mass assignments for $12 \leq m/e \leq 130$ for more than 98% of all traces. The source of each ion was then determined from the observed relative intensities and reported cracking patterns of species known to be present as impurities in commercial fluorine and oxygen (*i.e.*, OF_2 , CF_4 , C_2F_6 , N_2 , HF , NF_3 , CO_2 , SF_6 , and SiF_4). In

(3) A. D. Kirshenbaum and A. V. Grosse, *J. Am. Chem. Soc.*, **81**, 1277 (1959).

(4) E C.. Melton and W. H. Hamill, *J. Chem. Phys.*, **41**, 546 (1964).

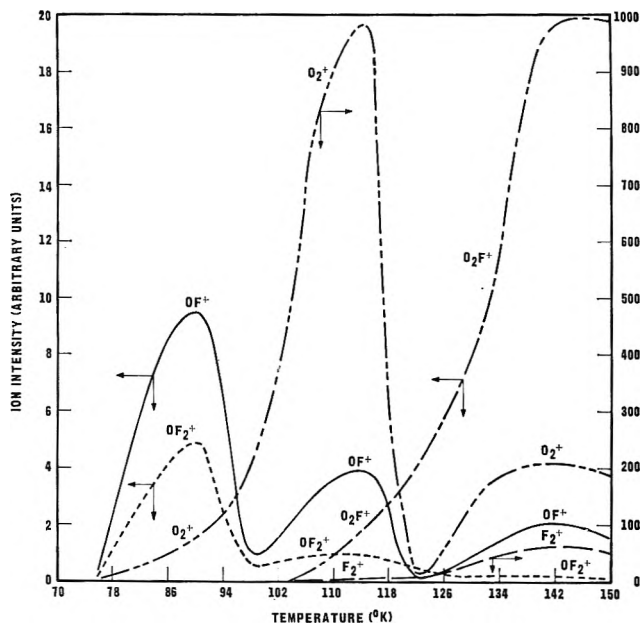


Figure 2. Representative variation of ion current intensities with temperature of the most interesting ions observed in the O_3F_2 synthesis experiments.

order to identify each impurity present in the O_2 and F_2 feed gas and to determine the volatility, and hence the temperature dependence of the mass spectra, the unreacted feed gas was pumped through the system with both B and C at $77^\circ K.$, whereupon all significant impurities were condensed. Spectra were then recorded at $2\text{--}3^\circ K.$ intervals over the temperature range of $77\text{--}200^\circ K.$ From the temperature required for the observation of the various condensed impurities of known vapor pressure, it was determined that a species exerted a vapor pressure of $0.01\text{--}0.1$ torr in E (see Figure 1) when it was first detected in the spectrometer.

Ozone Difluoride. Figure 2 illustrates the general variation of the more interesting ion currents as a function of temperature for the experiments in which O_3F_2 was the principal reaction product. The curves give a composite representation of the ion current intensities observed in three of the O_3F_2 synthesis runs. The intensity *vs.* temperature curves from the fourth O_3F_2 run exhibited a somewhat different character that was similar to that of the O_2F_2 synthesis experiments. Hence, it was concluded that O_2F_2 was likely the principal reaction product in that experiment. In Figure 2, three temperature ranges are apparent ($80\text{--}95$, $102\text{--}118$, and $126\text{--}150^\circ K.$) within which significant changes in the mass spectra occur. These temperature ranges coincide with the melting point of O_3F_2 ($83\text{--}84^\circ K.$), the decomposition temperature of O_3F_2 ($110\text{--}116^\circ K.$), and the temperature region (126--

$150^\circ K.$) in which O_2F_2 , as a stable entity, exerts a smoothly rising vapor pressure. The vapor pressure of O_2F_2 is 1 torr at approximately $130^\circ K.$

The parent ion of O_2F_2 (m/e 70) was not observed even when the inlet system was raised above $150^\circ K.$ A very small signal at m/e 70 was observed only when a very large ion current was present at m/e 69 due to CF_3^+ from CF_4 or C_2F_6 , and was evidently due to the isotope $C^{13}F_3^+$ which is reported to be approximately 1% of the $C^{12}F_3^+$ current.

Oxygen Difluoride. In the experiments in which the principal synthesis product was O_2F_2 , the mass spectra as a function of temperature from 77 to $150^\circ K.$ were essentially the same as for the O_3F_2 experiments except that at $110\text{--}115^\circ K.$ the O_2^+ current was much less intense and no excess OF^+ was observed.

No ion current was observed at m/e 67 (O_3F^+), 70 ($O_2F_2^+$), 86 ($O_3F_2^+$), or 102 ($O_4F_2^+$) in either the O_2F_2 or O_3F_2 experiments. However, there were rather intense currents at m/e 66, 69, 85, and 104 due to SiF_2^+ , COF_2 , and $N_2F_2^+$; CF_3^+ ; SiF_3^+ and $N_2F_3^+$; and SiF_4^+ and $N_2F_4^+$, respectively. The nitrogen fluorides were formed during the oxygen fluoride syntheses due to small amounts of N_2 and NF_3 in the feed gas. The presence of these masses adjacent to the expected ions from the oxygen fluorides made the unprejudiced procedure described above for making mass assignments definitely necessary. In all of these experiments the only impurities observed were those present in the O_2 and F_2 feed gas as given above and small amounts of nitrogen fluorides formed during the syntheses.

Energy Measurements. The appearance potentials were measured at several temperatures for the most interesting fragments in the mass spectrum from the O_3F_2 experiments. The appearance potential of O_2^+ was measured at 77 , 90 , 112 (O_3F_2 decomposition temperature), and $130^\circ K.$ It was found that $A(O_2^+)$ at each of these temperatures was equal to $I(O_2)$. The large amount of molecular O_2 present as background interfered with the measurement of the appearance potential of O_2^+ from the fragmented oxygen fluorides, but under the usual assumptions it is clear that $A(O_2^+)$ from these species is greater than $I(O_2)$.

The appearance potential of OF^+ at $90^\circ K.$ was measured to be 15.8 ± 0.2 e.v. which is the value reported by Dibeler, Reese, and Franklin⁵ for $A(OF^+)$ from OF_2 . Attempts to measure the appearance potential of the OF^+ ion at the decomposition temperature of O_3F_2 ($110\text{--}115^\circ K.$) have been unsuccessful due to the rapidity of the loss process which causes the

(5) V. H. Dibeler, R. M. Reese, and J. L. Franklin, *J. Chem. Phys.*, **27**, 1296 (1957).

ion current to diminish to an immeasurable level within 5–10 min.

At 130°K., $A(\text{O}_2\text{F}^+)$ and $A(\text{OF}^+)$, were measured to be 14.0 ± 0.1 and 17.5 ± 0.2 e.v., respectively, and they were found to be the same for both the O_2F_2 and O_3F_2 experiments. The larger possible error in $A(\text{OF}^+)$ is due to the fact that the OF^+ current was small, and it was much more difficult to make accurate measurements. $A(\text{O}_2\text{F}^+)$ was measured ten times in a total of four synthesis experiments with an average deviation of ± 0.05 e.v. from 14.0 e.v., and with a maximum deviation of 0.15 e.v.

Discussion

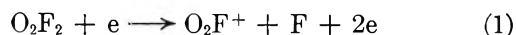
For the O_3F_2 synthesis experiments, the intense OF^+ and OF_2^+ ion currents observed at 85–90°K. were evidently arising from OF_2 since the measured $A(\text{OF}^+)$ of 15.8 e.v. was the same as reported from an earlier electron impact study of OF_2 . The OF^+ current observed at the decomposition temperature of O_3F_2 (110–115°K.) was nearly twice as intense as could reasonably be arising from both OF_2 and O_2F_2 , as estimated from the observed fragmentation pattern of these species. Attempts to measure the appearance potential of this excess OF^+ have so far been unsuccessful, but modifications in the inlet assembly have indicated that it should now be possible to make this measurement. The OF_2^+ current was apparently due to free OF_2 which had not been pumped out of the system. The O_2F^+ current appeared to be due to O_2F_2 which has a vapor pressure of about 0.05 torr at 110–115°K. The fact that the O_2^+ current is of the order of 1000 times as intense as the oxygen fluoride ion currents is further evidence that the O_3F_2 substance decomposes at this temperature to form O_2 and O_2F_2 . At 110°K., O_3F_2 has a vapor pressure of about 1 torr and reportedly⁶ can be distilled at this low pressure with only slight decomposition. If this is true, this molecule or certainly some of its possible cracking species should have been observed between 105 and 115°K. Also, at least a small amount of O_4F_2 should have been formed during the syntheses, but neither of these species was observed in these experiments. Since neither O_3F_2 nor O_4F_2 was observed, the obvious question is raised as to whether or not these species really exist as such in the vapor phase. This is a particularly interesting question in view of the fact that several investigators feel that these substances might well be an equilibrium mixture of lower molecular weight species (such as possibly O_2F and OF , or $2\text{O}_2\text{F}$ and O_2F_2) in a ratio to give a 3:2 oxygen to fluorine ratio. Another possibility is that the fragment ions are not sufficiently stable at the temperatures at which

they are being studied (100–115°K.) to exist for the 50 $\mu\text{sec.}$ required by the Bendix machine. The cryogenic inlet assembly used in this work has been modified to permit detection of species exerting a vapor pressure of only 10^{-4} to 10^{-5} torr, which will make it possible to observe the equilibrium vapors of the oxygen fluorides at much lower temperatures than were necessary for these experiments.

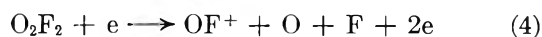
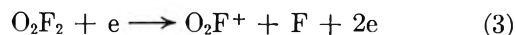
Nielson⁷ investigated the reaction products resulting from the irradiation of OF_2 at 77°K. using a mass spectrometer similar to that used in these experiments. He supposedly observed and identified O_2F_2 as well as O_3F_2 and O_4F_2 as reaction products. The ions attributed to O_3F_2 and O_4F_2 were never observed below 130°K., and in some experiments these species were not observed until the temperature was greater than 200°K. Since both O_3F_2 and O_4F_2 have vapor pressures greater than 1.0 torr at 112°K., they should have been observed at this much lower temperature. Regardless of this fact, it is well known that these compounds decompose very rapidly at temperatures (105–115°K.) much lower than those at which he reported them (130–211°K.). In view of the above as well as the fact that no cooled delivery system was used, but rather the gaseous samples were transported from their reservoir at cryogenic temperatures into the spectrometer through a tube at room temperature, it seems impossible for his reported identification of O_3F_2 and O_4F_2 to be reliable.

Energetics of O_2F_2 . In determining the source of the O_2F^+ and OF^+ ions for which the appearance potentials were measured, several possibilities were considered, including ion-pair production. However, all possibilities except the following three were easily eliminated on the basis of energetic arguments.

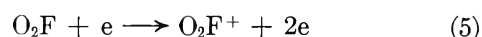
Case I



Case II



Case III (Free O_2F as the Source)



(6) A. D. Kirshenbaum, J. G. Aston, and A. V. Grosse, U. S. Department of Commerce, Office Technical Services, PB Report 149,443 (1961).

(7) R. P. Nielsen, paper presented at the Symposium on Advanced Propellant Chemistry, 149th National Meeting of the American Chemical Society, Detroit, Mich., April 1965.

Dibeler, Reese, and Franklin⁵ (DRF) made electron impact studies on the OF_2 molecule and reported $A(\text{OF}^+)_{\text{DRF}} = 15.8$ e.v., $I(\text{OF}) = 13.0$, and $D(\text{OF}) = 1.1$ e.v.⁸ From these values and the appearance potentials of the O_2F^+ and OF^+ ions measured in our experiments at 130°K ., it can be shown rather conclusively that these ions are fragments of the O_2F_2 molecule formed by the processes represented by eq. 1 and 2 in case I. Therefore, this case will be discussed first, and justification for elimination of cases II and III will be discussed last.

Case I. Neglecting any excess kinetic energy or internal excitation, the appearance potentials are given by

$$A(\text{O}_2\text{F}^+)_{\text{I}} = D(\text{F-O}_2\text{F}) + I(\text{O}_2\text{F}) \quad (7)$$

$$A(\text{OF}^+)_{\text{I}} = D(\text{FO-OF}) + I(\text{OF}) \quad (8)$$

From our measured $A(\text{OF}^+)_{\text{I}}$ of 17.5 e.v. and eq. 8, the O-O bond energy in O_2F_2 can be calculated directly. $D(\text{FO-OF}) = 17.5 - 13.0 = 4.5 \pm 0.2$ e.v. or 103.5 ± 5 kcal. This results in an experimental energy of atomization for O_2F_2 , $E_a(\text{O}_2\text{F}_2)_{\text{E}}$, of $103.5 + 2(25.4) = 154.3$ kcal. = 6.7 e.v., for the process $\text{O}_2\text{F}_2 \rightarrow 2(\text{OF}) \rightarrow 2(\text{O}) + 2(\text{F})$. Since the heat of formation of O_2F_2 has been measured calorimetrically,⁹ the energy of atomization can also be calculated thermodynamically using $\Delta H_f^\circ(\text{O}_2\text{F}_2) = 4.7$ kcal./mole, $\Delta H_f^\circ(\text{O}) = 59.2$ kcal./mole, and $\Delta H_f^\circ(\text{F}) = 18.9$ kcal./mole to give a heat of atomization at 298°K . of 6.55 e.v. Calculations have shown that this value is equal to the thermochemical energy of atomization, $E_a(\text{O}_2\text{F}_2)_{\text{T}}$, at 130°K . within the experimental error, and it is seen to agree very well with the value obtained from our low-temperature electron impact data.

The consistency of the $A(\text{OF}^+)$ from O_2F_2 obtained in our experiments and the data reported by DRF in their investigation of OF_2 can be better illustrated by the equation

$$E_a(\text{O}_2\text{F}_2)_{\text{E}} = A(\text{OF}^+)_{\text{I}} - A(\text{OF}^+)_{\text{DRF}} - A(\text{F}^-) - EA(\text{F}) + \text{K.E.} + 2E_a(\text{OF}_2)_{\text{T}} \quad (9)$$

where $A(\text{F}^-) = 1.2$ e.v. and $\text{K.E.} = 2.0$ e.v. are the appearance potential of the negative fluorine atom and the excess kinetic energy, respectively, measured by DRF for the process $\text{OF}_2 + e \rightarrow \text{OF} + \text{F}^- + \text{K.E.}$ $EA(\text{F}) = 3.6$ e.v. is the electron affinity of the fluorine atom and $E_a(\text{OF}_2)_{\text{T}} = 3.9$ e.v. is the thermochemical energy of atomization of OF_2 calculated from its heat of formation of 7.6 kcal. Substituting these values into eq. 9 gives $E_a(\text{O}_2\text{F}_2)_{\text{E}} = 17.5 - 15.8 - 1.2 - 3.6 + 2.0 + 2(3.9) = 6.7$ e.v., which is in very good agreement with $E_a(\text{O}_2\text{F}_2)_{\text{T}} = 6.55$ e.v.

This excellent agreement between $E_a(\text{O}_2\text{F}_2)_{\text{T}}$ and $E_a(\text{O}_2\text{F}_2)_{\text{E}}$ indicates that the experimental values obtained by DRF and our measured $A(\text{OF}^+)_{\text{I}}$ are reasonably accurate and the process given by eq. 2 really does occur without any significant excess kinetic energy. This in turn would indicate that the resulting $D(\text{FO-OF}) = 4.5$ e.v. is a good value. The fact that this bond energy is nearly as large as that of O_2 , $D(\text{O}_2) = 5.08$ e.v., also agrees qualitatively with the microwave data of Jackson,¹⁰ who reported a very short O-O bond length in O_2F_2 of 1.217 Å., which is nearly equal to the bond length in O_2 of 1.21 Å.

Since the energy of atomization of a molecule is independent of the path followed, we can write

$$E_a(\text{O}_2\text{F}_2)_{\text{E}} = 6.7 \text{ e.v.} = D(\text{F-O}_2\text{F}) + D(\text{O}_2\text{-F}) + D(\text{O}_2) \quad (10)$$

$$= D(\text{F-O}_2\text{F}) + D(\text{O-OF}) + D(\text{OF}) \quad (11)$$

From the known bond energy of oxygen, $D(\text{O}_2) = 5.1$ e.v., and eq. 10

$$D(\text{F-O}_2\text{F}) + D(\text{O}_2\text{-F}) = 6.7 - 5.1 = 1.6 \text{ e.v.} \quad (12)$$

and from eq. 11

$$D(\text{F-O}_2\text{F}) + D(\text{O-OF}) = 6.7 - 1.1 = 5.6 \text{ e.v.} \quad (13)$$

Equation 12 shows that the O-F bonds in O_2F_2 are unusually weak. This also agrees qualitatively with the microwave results which indicated an unusually long O-F bond length of 1.575 Å. for this molecule.

In order to calculate $D(\text{O-OF})$ from eq. 13, it is necessary to estimate the relative values of $D(\text{F-O}_2\text{F})$ and $D(\text{O}_2\text{-F})$. A reasonable assumption would be that these two bond energies are equal. This would give $D(\text{F-O}_2\text{F}) = D(\text{O}_2\text{-F}) = 0.8$ e.v. Actually, we might expect $D(\text{F-O}_2\text{F})$ to be 10-15% greater than $D(\text{O}_2\text{-F})$, but this would result in an error of only ~ 0.1 e.v. in the estimated value of 0.8 e.v. Levy and Wesley¹¹ have estimated that $D(\text{O}_2\text{-F}) = 15$ kcal. = 0.7 e.v. from kinetic data on the thermal decomposition of O_2F_2 .

Using the estimated value of $D(\text{F-O}_2\text{F}) = 0.8$ e.v., eq. 13 gives $D(\text{O-OF}) = 5.6 - 0.8 = 4.8$ e.v. = 110 kcal. This appears qualitatively in the right range since we would expect $D(\text{O-OF})$ to be greater than

(8) $D(\text{OF})$ of 2.4 e.v. has been estimated from data of A. Arkell, R. R. Reihard, and L. P. Larson, *J. Am. Chem. Soc.*, **87**, 1016 (1965).

(9) A. D. Kirshenbaum, A. V. Grosse, and J. G. Aston, *ibid.*, **81**, 6398 (1959).

(10) R. H. Jackson, *J. Chem. Soc.*, 4585 (1962).

(11) J. B. Levy and B. K. Wesley, *J. Phys. Chem.*, **69**, 408 (1965).

$D(\text{FO}-\text{OF})$ which was found to be 4.5 e.v., and it would certainly be less than $D(\text{O}_2)$ of 5.08 e.v. In view of this last statement, we would also have predicted from eq. 13 that $D(\text{F}-\text{O}_2\text{F})$ would be less than $5.6 - 4.5 = 1.1$ e.v. and certainly greater than $5.6 - 5.1 = 0.5$ e.v. Using these extreme limits we would say that $D(\text{F}-\text{O}_2\text{F}) = 0.8 \pm 0.3$ e.v., which is the value obtained above by simply assuming that $D(\text{F}-\text{O}_2\text{F}) = D(\text{O}_2-\text{F})$.

We have not needed our measured appearance potential of the O_2F^+ ion, $A(\text{O}_2\text{F}^+) = 14.0 \pm 0.1$ e.v., to obtain any of the above results, but it is needed to estimate the ionization potential of the O_2F free radical. In order to check qualitatively the consistency of the measured $A(\text{O}_2\text{F}^+)$ and the assumption that no excess kinetic energy is formed in the process given by eq. 1, the energy of atomization can be written as

$$E_a(\text{O}_2\text{F}_2)_E = A(\text{O}_2\text{F}^+)_I + D(\text{O}_2^+-\text{F}) + D(\text{O}_2^+) - I(\text{O}) \quad (14)$$

Using the known values of $D(\text{O}_2^+) = 6.48$ e.v. and $I(\text{O}) = 13.6$ e.v., eq. 14 gives $D(\text{O}_2^+-\text{F}) = 6.7 - 14.0 - 6.48 + 13.6 = -0.18$ e.v. This would indicate that the O_2F^+ ion is unstable, but we know that it is stable for at least 50 μsec . since it is observed in the mass spectrometer. The most reasonable explanation of this observation is that the formation of the O_2F^+ ion is actually accompanied by at least a small amount of excess kinetic energy. Without actually measuring the excess kinetic energy, an accurate value for $I(\text{O}_2\text{F})$ cannot be calculated. However, using the observed $A(\text{O}_2\text{F}^+)_I = 14.0$ gives an upper limit from eq. 7 of $I(\text{O}_2\text{F}) \leq 14.0 - 0.8 = 13.2$ e.v. A reasonable estimate of the excess kinetic energy can be made from an analogy with the hydrogen peroxide molecule. The dissociation energies of the analogous species from H_2O_2 have been measured by electron impact methods to be $D(\text{H}-\text{O}_2) = 2.0$ e.v. and $D(\text{H}-\text{O}_2^+) = 1.9$ e.v.,¹² or the dissociation energies of the free radical and the ion are essentially equal. If we assume that this is the case for the O_2F_2 molecule, then $D(\text{O}_2^+-\text{F}) = D(\text{O}_2-\text{F}) = 0.8$ e.v. Then we can calculate a probable upper limit of the excess kinetic energy from the equation

$$E_a(\text{O}_2\text{F}_2)_E = 6.7 = A(\text{O}_2\text{F}^+)_I - \text{K.E.} + D(\text{O}_2^+-\text{F}) + D(\text{O}_2^+) - I(\text{O}) \quad (15)$$

This gives $\text{K.E.} = 14.0 + 0.8 + 6.48 - 13.6 - 6.7 = 1.0$ e.v. Making a correction for this excess energy of 1.0 e.v. in eq. 7 gives an approximate value of $I(\text{O}_2\text{F}) = 14.0 - 1.0 - 0.8 = 12.2$ e.v. This seems like a reasonable value in view of the fact that $I(\text{O}_2) = 12.2$ e.v. and $I(\text{HO}_2) = 11.5$ e.v.¹³ The fact that this esti-

mated value of $I(\text{O}_2\text{F})$ is equal to $I(\text{O}_2)$ is coincidental but we would expect that it would probably be between $I(\text{O}_2)$ and $I(\text{HO}_2)$ since the fluorine atom is only loosely bonded to O_2 in O_2F .

Since the parent peak of O_2F_2 was not observed, it is impossible to measure the $I(\text{O}_2\text{F}_2)$ directly, but we can say that $I(\text{O}_2\text{F}_2) \leq A(\text{O}_2\text{F}^+) = 14.0$ e.v. This gives a maximum for $I(\text{O}_2\text{F}_2)$, but a more reasonable value would be nearer 13.0 e.v. which takes into account the estimated excess kinetic energy of 1.0 e.v.

Case II. The appearance potential of the O_2F^+ ion is the same as in case I and is given by eq. 7. The appearance potential of the OF^+ ion is given by

$$A(\text{OF}^+)_{II} = D(\text{F}-\text{O}_2\text{F}) + D(\text{O}-\text{OF}) + I(\text{OF}) \quad (16)$$

The $A(\text{OF}^+)_{II}$ required for this process can be readily calculated from eq. 16 using $D(\text{F}-\text{O}_2\text{F}) + D(\text{O}-\text{OF}) = E_a(\text{O}_2\text{F}_2)_T - D(\text{OF}) = 6.6 - 1.1 = 5.5$ e.v. This gives $A(\text{OF}^+)_{II} = 5.5 + 13.0 = 18.5$ e.v., which is 1.0 e.v. greater than the measured value of 17.5 e.v. which means that the process of eq. 4 is not correct.

Case III. In this case it is assumed that the O_2F^+ and OF^+ ions are arising from the O_2F free radical. Therefore, $A(\text{O}_2\text{F}^+)_{III} = I(\text{O}_2\text{F}) = 14.0$ e.v. and the appearance potential of the OF^+ ion is given by

$$A(\text{OF}^+)_{III} = I(\text{O}_2\text{F}) + D(\text{O}-\text{OF}^-) \quad (17)$$

Equation 17 gives $D(\text{O}-\text{OF}^+) = 17.5 - 14.0 = 3.5$ e.v. From the relation

$$D(\text{O}-\text{OF}^+) + D(\text{O}^+-\text{F}) = D(\text{O}_2^+-\text{F}) + D(\text{O}_2^+) \quad (18)$$

and the dissociation energy of the OF^+ ion, $D(\text{OF}^+) = 1.7$ e.v., reported by DRF, a value of $D(\text{O}_2^+-\text{F}) = 3.5 + 1.7 - 6.48 = -1.3$ e.v. is obtained. This is an unlikely value and indicates that the observed appearance potentials are not consistent for the assumption of a free O_2F radical.

Since there are no other processes that are energetically reasonable and the results obtained for case I are consistent with both the available thermochemical and microwave data, it is evident that the O_2F^+ and OF^+ ions are formed by the processes given by eq. 1 and 2. The results that were obtained are summarized in Table I.

Several laboratories, including our own, are presently investigating the possible free existence of the OF free radical. In the mass spectrum given in Table I it can be seen that the ratio of O_2F^+ to OF^+ from O_2F_2 is about 10. In view of this and the very strong O-O bond (104 kcal.) and very weak O-F bonds (approx-

(12) A. J. B. Robertson, *Trans. Faraday Soc.*, **48**, 229 (1952).

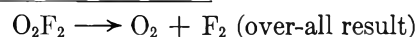
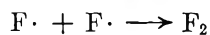
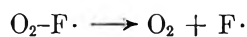
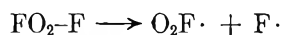
(13) S. N. Foner and R. L. Hudson, *J. Chem. Phys.*, **36**, 2681 (1962).

Table I: Relative Abundance and Appearance Potentials of Positive Ions in the Mass Spectrum of Dioxygen Difluoride

Ion	Relative abundance, %	Appearance potential, e.v.	Remarks
$O_2F_2^+$	$I(O_2F_2) \leq 14.0$ e.v. (~ 13.0 e.v. ^b)
O_2F^+	100	14.0 ± 0.1	$I(O_2F) \leq 13.2$ e.v. (~ 12.2 e.v. ^b)
OF^+	10.1	17.5 ± 0.2	$I(OF) = 13.0$ e.v. ^c
O_2^+	(1020) ^a	...	$D(FO-OF) = 4.5 \pm 0.2$ e.v.
O^+	(305) ^a	...	$D(F-O_2F) = 0.8$ e.v. $D(O_2-F) = 0.8$ e.v.
F_2^+	(300) ^a	...	$D(OF) = 1.1$ e.v. ^c
F^+	(120) ^a	...	$D(O-OF) = 4.8$ e.v.

^a Includes very large background due to decomposition of O_2F_2 in the spectrometer. ^b Accounts for excess kinetic energy in ($O_2F^+ + F$). ^c From ref. 5.

mately 18.5 kcal.), it is almost certain that the thermal decomposition does not involve the formation of OF as an intermediate. A reasonable mechanism would be that proposed by Grosse and Kirshenbaum¹⁴



This would indicate that if OF is to be formed in any appreciable amount from O_2F_2 , physical techniques for fragmentation other than pyrolysis (such as irradiation, electrical discharge, etc.) will likely be required. With any of these techniques it would be expected that considerably more O_2F free radical would be formed than OF. We are presently attempting to prepare O_2F and OF as free species using the cryogenic temperature procedures that have been outlined here.

Acknowledgments. The authors gratefully acknowledge support of this research by NASA Grants NsG-337 and NsG-657. T. J. M. also expresses thanks to NSF and to the Procter and Gamble Company for providing fellowships during two years of graduate study.

(14) A. V. Grosse and A. D. Kirshenbaum, "Production, Isolation, and Identification of the OF, O_2F , and O_3F Radicals," Second Quarterly Progress Report, Air Force Contract No. AF 04(611)-9555, The Research Institute of Temple University, March 31, 1964.

The Investigation of the Behavior of Some Divalent Salts of *p*-Toluenesulfonic Acid and Related Polymeric Acids in Aqueous Solutions

by O. D. Bonner, W. H. Breazeale, and Carey Rushing

Department of Chemistry, University of South Carolina, Columbia, South Carolina (Received August 23, 1965)

Osmotic and activity coefficients are reported for certain divalent salts of *p*-toluenesulfonic, bibenzylidisulfonic, and 1,2,3-triphenylpropanetrisulfonic acids. Correspondence with the behavior of sulfonated polystyrene-divinylbenzene ion exchangers is noted in the sequence of activity and osmotic coefficients and in the effect of temperature on these coefficients. Ion pairing appears to be greatly reduced in the polysulfonates in comparison with that observed in "normal" electrolytes of similar valence types. Limiting Debye-Hückel behavior is approached by these electrolytes only in extremely dilute solutions, if at all.

The osmotic and activity coefficients of several aromatic sulfonic acids and their salts have been reported, and these data have been related to the interpretation of ion-exchange equilibrium data on sulfonated styrene-divinylbenzene copolymers. These reported investigations have been limited so far to acids and monovalent cationic salts although polysulfonate anions containing varying numbers of sulfonate groups per molecule have been used. It has been observed in concentrated solutions where the distances of separation of ionic groups are virtually independent of the degree of polymerization that the lowering of the water activity is primarily a function of the concentration of ionic groups and not of the number of ions present.¹ The disulfonates have been found to differ markedly from sulfates in dilute solutions because of the separation of the two negative charges.² Osmotic and activity coefficients of trisulfonates and higher polymers or of divalent salts of "model" sulfonates in dilute solutions have not been reported. Atkinson³ and co-workers have, however, made an extensive investigation of the conductance of divalent salts of *m*-benzenedisulfonic acid and other bolaform electrolytes. They report that the ion pairing exhibited by "normal" 2-2 electrolytes is absent in these solutions. Brubaker⁴ confirms these observations with his measurements of the osmotic and activity coefficients of certain *m*-benzenedisulfonates. It seemed desirable, therefore, to extend the measurements of the colligative properties to solutions of divalent salts and simultaneously

to relate the results to the ion-exchange equilibrium data which are available.

Experimental Section

The osmotic properties of certain divalent salts of three sulfonic acids have been investigated. In each instance, the salts were prepared by reaction of the acid with the metal carbonates which could be obtained in very high purity. The salts were then recrystallized at least three times from water or water-methanol solutions. Equivalent weights were checked by compleximetric titration of samples which had been dried over P₂O₅.

The toluenesulfonates were prepared from reagent grade *p*-toluenesulfonic acid. Bibenzylidisulfonic acid was prepared by the dropwise addition of liquid SO₃, dissolved in CCl₄, to a solution of bibenzyl in CCl₄.⁵ The parent hydrocarbon, 1,2,3-triphenylpropane, was synthesized in the previously described manner,¹ and the trisulfonic acid was prepared by the same procedure used for bibenzylidisulfonic acid.

The osmotic coefficients were measured in dilute solutions at several temperatures by the adiabatic

- (1) O. D. Bonner and J. R. Overton, *J. Phys. Chem.*, **67**, 1035 (1963).
- (2) O. D. Bonner and O. C. Rogers, *ibid.*, **65**, 981 (1961).
- (3) *E.g.* (a) G. Atkinson, M. Yokoi, and C. J. Hallada *J. Am. Chem. Soc.*, **83**, 1570 (1961); (b) G. Atkinson and S. Petrucci, *J. Phys. Chem.*, **67**, 1880 (1963).
- (4) C. Brubaker and P. G. Rasmussen, *ibid.*, **67**, 330 (1963).
- (5) H. H. Roth, *Ind. Eng. Chem.*, **46**, 2435 (1954).

isopiestic method using the Mechrolab vapor pressure osmometer. The usual isopiestic technique⁶ was used to obtain data on the more concentrated solutions. Individual measurements of dilute solutions are accurate to about 0.5%. The reported values are, however, the average of three of five measurements of each solution and should have an accuracy of 0.2 to 0.4%. The tabular values were obtained from interpolations of plots of the original data.

Discussion and Results

The data obtained for these "model" sulfonates are of interest for correlation with ion-exchange equilibrium measurements in that the order of decreasing osmotic or activity coefficients (Tables I-III) of both the mono-sulfonates and disulfonates is the same as the order of increasing selectivity of a cross-linked ion exchanger for these same ions.⁷ This is in agreement with the interpretation of Myers and Boyd⁸ that the activity coefficients of the resin sulfonates make the greatest contribution to the ion-exchange selectivity coefficient.

Table I: Osmotic Coefficients of Some Divalent *p*-Toluenesulfonates

Concn., <i>M</i>	CuTol ₂			ZnTol ₂ 37°	CdTol ₂ 37°	CaTol ₂ 37°
	25°	37°	50°			
0.01	0.900	0.898		0.898	0.898	0.897
0.02	0.881	0.878		0.878	0.878	0.877
0.05	0.854	0.850		0.850	0.849	0.848
0.10	0.833	0.827		0.828	0.825	0.823
0.20	0.812	0.803		0.806	0.798	0.795
0.30	0.795	0.785	0.775	0.789	0.778	0.771
0.40	0.783	0.772	0.754		0.762	0.750
0.50	0.773	0.761	0.746		0.749	0.733
0.60	0.764	0.752	0.734		0.738	0.719
0.70	0.756	0.745	0.724			
0.80	0.749	0.739	0.716			
0.90		0.734	0.709			

A second substantiation of the validity of using these models in the interpretation of the ion-exchange equilibria is noted when one compares the effect of temperature on both the selectivity coefficient of the exchanger and the activity coefficients of the "model" sulfonates. The behavior of the activity coefficients of certain monovalent *p*-toluenesulfonates⁹ was found to parallel the decrease in the selectivity of the exchanger for pairs of monovalent ions as the temperature is increased. The selectivity trend is reversed, however, in exchanges involving a divalent and a monovalent ion; *i.e.*, the selectivity increases at higher temperatures. This requires a relatively larger change

Table II: Activity Coefficients of Some Divalent *p*-Toluenesulfonates

Concn., <i>M</i>	CuTol ₂		ZnTol ₂ 37°	CdTol ₂ 37°	CaTol ₂ 37°
	25°	37°			
0.01	0.712	0.711	0.705	0.710	0.693
0.02	0.649	0.646	0.641	0.645	0.630
0.05	0.557	0.531	0.547	0.550	0.537
0.10	0.490	0.480	0.480	0.481	0.469
0.20	0.423	0.411	0.414	0.409	0.398
0.30	0.384	0.371	0.373	0.368	0.356
0.40	0.357	0.344		0.339	0.325
0.50	0.337	0.324		0.314	0.303
0.60	0.320	0.306		0.297	0.284
0.70	0.305	0.292			
0.80	0.302	0.281			
0.90		0.271			

Table III: Osmotic Coefficients of Some Divalent Bibenzylidissulfonates

Concn., <i>M</i>	NiBB		ZnBB		CuBB 25°	CaBB 37°
	25°	37°	25°	37°		
0.05	0.761	0.743	0.785	0.768	0.748	0.757
0.10	0.714	0.694	0.740	0.725	0.700	0.702
0.20	0.660	0.638	0.690	0.668	0.642	0.644
0.30			0.659	0.638		0.613
0.40				0.630		

in the activity coefficient of the divalent ion resinate than is the case for the monovalent ion resinate. The data for both the model monosulfonates and disulfonates confirm this effect.

Although all of the data which have been accumulated to this time indicate that the order of increasing activity coefficients of monovalent or divalent cationic sulfonates is independent of the degree of polymerization over the range from monomers to cross-linked polymers, it is interesting to observe the differences in behavior between these electrolytes and "normal" electrolytes of the same valence types. The limiting-law type of equation for the slope of the osmotic coefficient *vs.* the square root of the molality curve may be written as

(6) R. A. Robinson and O. A. Sinclair, *J. Am. Chem. Soc.*, **56**, 1830 (1934).

(7) O. D. Bonner and L. L. Smith, *J. Phys. Chem.*, **61**, 326 (1957).

(8) G. E. Myers and G. E. Boyd, *ibid.*, **60**, 521 (1956). The selectivity coefficient for the exchange of ions of like charge is $D \equiv (m_2/m_1)_{\text{resin}} / (m_2/m_1)_{\text{aqueous}}$. Upon applying Gibbs-Donnan equilibrium conditions it is found that $\log D = P(\bar{v}_1 - \bar{v}_2)/RT + \log (\gamma_1/\gamma_2)_{\text{resin}} - 2 \log (\gamma_1/\gamma_2)_{\text{aqueous}}$.

(9) O. D. Bonner and W. C. Rampey, *ibid.*, **65**, 1602 (1961).

$$d\phi/d\sqrt{m} = -\frac{2.303}{3}AZ_+Z_-K$$

where $K = (\mu/m)^{1/2}$, μ is the ionic strength, and A is 0.509 for water at 25°. Monovalent bolaform electrolytes have been shown² to exhibit significant deviations from this "ideal" behavior because of the incomplete overlap of the ionic atmospheres. It would be expected that the deviations would be even greater for divalent cations³ or for trisulfonate salts. The data for copper bibenzylidisulfonate (Figure 1) and salts of 1,2,3-triphenylpropanetrisulfonic acid (Table IV, Figure 2) indicate that this is true. The osmotic coefficients of copper bibenzylidisulfonate are significantly higher than that of the normal 2-2 electrolyte, copper sulfate. The same observation may be made for copper triphenylpropanetrisulfonate and potassium ferricyanide although the difference is not as pronounced since the negative charges on the ferricyanide ion are also somewhat diffuse. In the case of the

Table IV: Osmotic and Activity Coefficients of Some 1,2,3-Triphenylpropanetrisulfonates (Z)

Concn., <i>m</i>	Na ₃ Z		Cu ₃ Z ₂ ^a ϕ
	ϕ	γ	
0.01	0.877	0.691	
0.04	0.816	0.523	0.664
0.09	0.773	0.425	0.616
0.16	0.740	0.357	0.636
0.2	0.725	0.332	0.654
0.3	0.707	0.289	0.740
0.4	0.701	0.265	0.891
0.5	0.700	0.248	1.046
0.6	0.704 ^b	0.235	
0.7	0.711 ^b	0.227	
0.8	0.720 ^b	0.220	
0.9	0.732 ^b	0.216	
1.0	0.746 ^b	0.213	
1.2	0.777 ^b	0.210	
1.4	0.813 ^b	0.211	
1.6	0.851 ^b	0.214	
1.8	0.890	0.220	

^a Activity coefficients were not calculated for Cu₃Z₂ because of the uncertainty in the extrapolation of the osmotic coefficient data to infinite dilution. ^b Also reported previously in ref. 1.

copper salt of the trisulfonate, the osmotic coefficient behavior bears no resemblance to that of the normal 3-2 electrolyte Cr₂(SO₄)₃. This behavior illustrates further the minimal importance of ion pairing in these electrolytes and explains the similarity of the properties

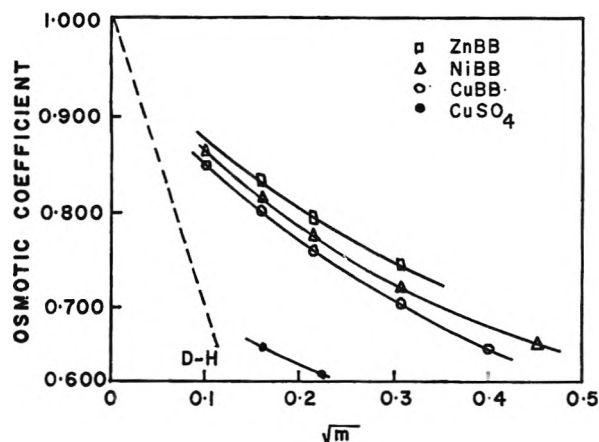


Figure 1. Osmotic coefficients of bibenzylidisulfonate salts at 25° (BB = bibenzylidisulfonate). Coefficients of CuSO₄ in two dilute solutions were also measured for comparisons.

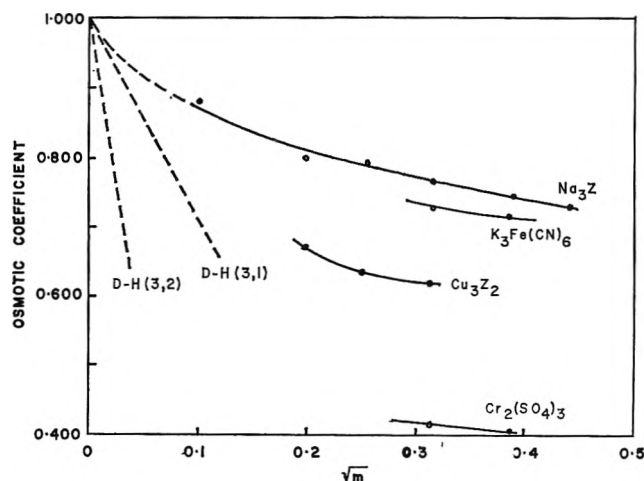


Figure 2. Osmotic coefficients of triphenylpropanetrisulfonate salts at 25° (Z = 1,2,3-triphenylpropanetrisulfonate). Data for K₃Fe(CN)₆ and Cr₂(SO₄)₃ from R. A. Robinson and R. H. Stokes, "Electrolyte Solutions," 2nd Ed., Academic Press Inc., London, 1959, p. 490.

of salts having different degrees of polymerization. A comparison of the water activity data for solutions of the copper monosulfonate and trisulfonate suggests that in concentrated solutions the vapor pressure lowering of solutions of the same weight normality would become virtually independent of the degree of polymerization of the sulfonate anion. This same behavior was noted for the monovalent cationic salts.

Acknowledgment. The support of this research by the Atomic Energy Commission under Contract At-(40-1)-1437 is gratefully acknowledged.

The Chemically Activated Decomposition of *n*-Butane and of Isobutane

by G. Z. Whitten¹ and B. S. Rabinovitch

Department of Chemistry, University of Washington, Seattle, Washington 98105 (Received July 23, 1965)

The unimolecular decomposition of *n*-butane and isobutane ($n\text{-C}_4\text{H}_{10}^* \xrightarrow{k_1} 2\text{C}_2\text{H}_5\cdot$; $n\text{-C}_4\text{H}_{10}^* \xrightarrow{k_2} \text{CH}_3\cdot + n\text{-C}_3\text{H}_7\cdot$; $i\text{-C}_4\text{H}_{10}^* \xrightarrow{k_3} \text{CH}_3\cdot + s\text{-C}_3\text{H}_7\cdot$), chemically activated by addition of methylene radicals to propane, has been studied at 25° from 0.03 to 500 mm. in the presence and absence of oxygen. The pressure course of the principal products has been determined. The data have been solved by an iteration procedure for k_1 , k_2 , and k_3 , which are equal to the collision rate at 0.25, 0.50, and 1.50 mm., respectively. Explanation of the products supports earlier findings (ref. 7 and 12) that triplet methylene can arise in diazomethane-substrate systems in relative amounts which increase with pressure up to 25–30% at high pressures, and that, as the proportion of triplet decreases, the methylene insertion rates into various C–H bonds approaches the statistical ratio. It is proposed that triplet methylene complicates the apparent insertion ratio by acting as the principal H-atom abstraction agent. RRKM calculations have been made which fit the observed decomposition rates and the model for which agrees with a value for ethyl recombination of $\sim 0.08Z$. The data require minimum butane vibrational energy of 102.3 kcal. mole⁻¹. Together with data on chemically activated cyclopropanes, ethane, and methane decompositions, this suggests that methylene radicals transport progressively less of their excess energy, acquired during genesis by diazomethane photolysis, into their combination products with olefins, with propane, with methane, and with hydrogen; the transported excesses are estimated as 20–25, 12, 9, and 0–2 kcal. mole⁻¹, respectively. This is explicable in terms of increasing inefficiency of methylene reaction along the series, with progressively increasing probability of collisional transfer of the excess energy.

Introduction

The simple alkanes are notorious for their reluctance toward yielding simple, accurate data for the rates of primary decomposition in thermal collisional activation systems.² The high temperatures which prevail in such systems encourage abstraction and other secondary reactions which lead to complex chain mechanisms and which obscure the primary rates. These systems have ill repaid the effort lavished on them and few reliable primary rate measurements of this kind exist. With the aid of improvements in experimental and analytical technique, some progress has been made very recently, particularly for the decomposition of methane,³ ethane,^{4a} and *n*-butane.^{4b,c} Even for these examples, controversy has not been lacking with regard to fact as well as interpretation.^{2–5}

Very few measurements of the decomposition rates of vibrationally excited alkanes have been made in

other than thermal systems. Recently, Bell and Kistiakowsky⁶ have described the decomposition of chemically activated methane and ethane as produced

(1) Weyerhaeuser Predoctoral Fellow.

(2) (a) E. W. R. Steacie, "Atomic and Free Radical Reactions," 2nd Ed., Reinhold Publishing Corp., New York, N. Y., 1954; (b) D. W. Setser and B. S. Rabinovitch, *J. Chem. Phys.*, **40**, 2427 (1964); B. S. Rabinovitch and D. W. Setser, *Advan. Photochem.*, **3**, 1 (1964) [in Table XIV, under k_{∞} , change 5.57 and 5.45 to 7.6 and 7.5; in Table XIII, multiply k_{∞} by 2].

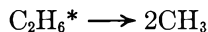
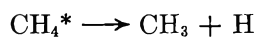
(3) (a) G. B. Skinner and R. A. Ruchrwein, *J. Phys. Chem.*, **63**, 1736 (1959); (b) H. B. Palmer and T. J. Hirt, *ibid.*, **67**, 709 (1963).

(4) (a) C. P. Quinn, *Proc. Roy. Soc. (London)*, **A275**, 190 (1963); (b) J. H. Purnell and C. P. Quinn, *ibid.*, **A270**, 267 (1962); *Can. J. Chem.*, **43**, 721 (1965), where the possible existence of a molecular decomposition mechanism for butane is opposed; (c) A. Kupperman and J. G. Larson, *J. Chem. Phys.*, **33**, 1264 (1960).

(5) R. W. Dexter and A. B. Trenwith, *Proc. Chem. Soc.*, 392 (1964); Y. I. Kudryavtseva, V. I. Vedenev, and B. V. Pavlov, *Russ. J. Phys. Chem.*, **38**, 530 (1964).

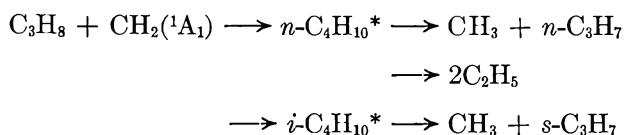
(6) J. Bell and G. B. Kistiakowsky, *J. Am. Chem. Soc.*, **84**, 3417 (1962).

by the addition of methylene radicals to hydrogen and methane, respectively



A comparison of these data with the predictions of RRKM theory has been made and reasonable agreement has been obtained^{2b}; extension of the theoretical tests to higher members was not possible and the desirability of accumulating further experimental information was noted. It was the purpose of the present research to make an experimental determination of the rates of decomposition of the two higher alkanes, *n*-butane and isobutane. Comparison with the lower members seemed of even greater interest since it has been found very recently for the analogous alkenes⁷ that the decomposition of butene, or pentene, to give alkyl radical plus allyl radical proceeds through a much tighter activated complex than does the decomposition of the smaller member, propylene, to give H atom plus allyl.⁸

Chemically activated decomposition possesses some advantages over thermal activation systems. By the addition of methylene to propane, *n*-butane and isobutane were produced with enough excess vibrational energy to decompose by carbon-carbon rupture



The reactions were carried out at room temperature so that abstraction and other unwanted secondary processes of the radical products were reduced. Oxygen and nitric oxide were also used, ostensibly as simple scavengers of free radicals at this temperature (but see later), in order to test the mechanism further. The species formed by the various recombination and disproportionation reactions of the initial radical decomposition products have been investigated over a wide range of pressure. This system has been previously studied briefly,⁹ but at pressures above those at which decomposition occurs.

Experimental Section

Materials. Diazomethane (DM) was prepared by treating *N,N'*-nitrosomethylurea with KOH solution and was stored in a di-*n*-butyl phthalate matrix at -196° .

Propane was Matheson instrument grade and was used without further treatment. Gas chromatographic analysis indicated some butane (about 0.01%) and some ethane (about 0.002%), which were not sufficient to

warrant any corrections. Propane-1,1,1,3,3,3-*d*₆ was obtained from Merck Sharpe and Dohme, Montreal. It had 6% *d*₅ impurity. It contained 0.4% ethane and 0.003% butane as the principal impurities, and no methane.

Oxygen was Air Reduction Co. tank grade and was used without purification. Nitric oxide was Matheson 98% purity. It was passed through silica gel at -78° several times and was then subjected to a number of freeze-pump-melt cycles at -196° . The purified solid was light blue in color.

Apparatus and Procedure. A conventional vacuum system was used for gas handling. Small samples of DM were distilled into a volume of 0.96 cc. The average pressure of DM was 2 cm. so that the total amount of butanes formed was less than 1 μmole. The DM was admixed with propane and/or other gases. Runs were made in seasoned Pyrex bulbs. A G.E. AH-6 high-pressure, water-cooled mercury arc lamp (Pyrex jacket) was used as the light source for the photolysis. A combination of Dow Corning No. 5543 and 3389 filters centered the radiation proximate to the 4358-Å. peak. A summary of the various experimental combinations employed is given in Table I.

Results and Interpretation of the Data

Reaction products were normalized with respect to *n*-butane product and are plotted in Figure 1 to 4.

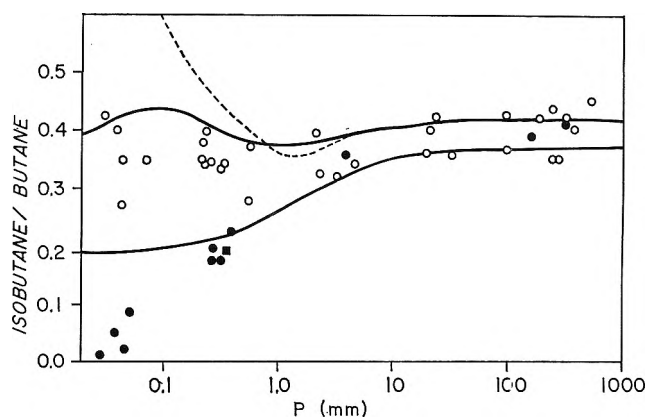


Figure 1. Plot of isobutane:butane ratio vs. pressure; pure system, O; oxygen added, ●; NO added, ■. Solid curves represent calculated fit, as in text; dashed curve assumes no decrease in abstraction at lower pressures and rises to 0.9 at 10^{-2} mm.

(7) F. H. Dorer and B. S. Rabinovitch, *J. Phys. Chem.*, **69**, 1952, 1964 (1965).

(8) J. W. Simons, B. S. Rabinovitch, and F. H. Dorer, to be published.

(9) H. M. Frey, *Proc. Chem. Soc.*, 318 (1959); *J. Am. Chem. Soc.*, **80**, 5005 (1958).

Table I: Summary of Experimental Run Conditions

Run no.	Pressure, mm.	Photolysis time, hr.	Propane/DM	Reactor size, cc.
22	540	1	16.6	0.562
20	394	0.75	16.7	0.562
49	320	2	10.5	0.95
45	280	2	12.6	0.95
50	250	2	9.1	0.95
32	250	2	10.4	0.562
16	194	1	16.0	1.32
8	100	0.5	10.4	1.32
9	100	0.67	9.6	1.32
19	32.6	1	21.6	9.95
17	24.5	1	16.0	9.95
21	21.6	1	15.1	9.95
31	20.0	3	10.3	9.95
12	4.7	1	20.7	57.9
34	3.4	3	8.3	57.9
38	2.4	3	7.1	57.9
11	2.2	1	10.2	57.9
23	0.59	2	19.0	547
26	0.57	2	22.0	547
13	0.35	2	15.9	547
35	0.33	3	8.3	547
59	0.24	4	11.0	1000
63	0.26	3	11.6	1000
48	0.24	3	13.4	1000
61	0.23	3	10.0	1000
44	0.23	3	12.6	1000
54	0.073	3	19.7	5000
30	0.045	3	11.0	5000
60	0.043	3	10.3	5000
62	0.040	4	10.5	5000
7	0.032	2	9.5	5000
O ₂ added: O ₂ /CH ₂ N ₂ = 2				
42	450	3	10.4	0.95
51	340	2	9.2	0.95
15	168	1	15.0	1.32
36	4.0	3	7.7	57.9
37	0.4	3	7.6	547
14	0.35	2	15	547
65	0.28	3	11.2	1000
67	0.28	3	10.0	1000
66	0.053	4	10.2	5000
64	0.052	4	11.3	5000
39	0.047	5	8.8	5000
40	0.038	5	6.9	5000
41	0.028	5	8.9	5000
NO added: NO/CH ₂ N ₂ = 2				
81	0.31	3	12.5	1000
82	0.30	4	9.7	1000
Runs with 1,1,1,3,3,3-propane-d ₆				
76	0.30	3	13.0	1000
75	0.24	5	8.9	1000
74	0.22	4	8.3	1000
Runs with propane-d ₆ ; O ₂ as above				
78	0.28	5.5	10.6	1000
79	0.25	3	11.2	1000

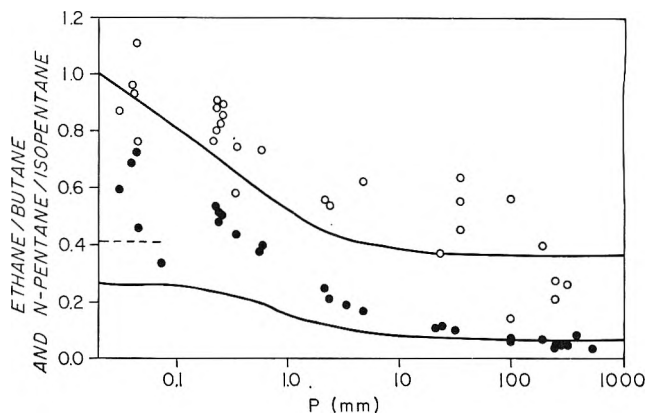


Figure 2. Plots of ethane:butane and *n*-pentane:isopentane ratios vs. pressure: ●, for ethane; ○, for pentanes. Solid lines represent calculated fit; dashed line is ethane fit corrected as in text.

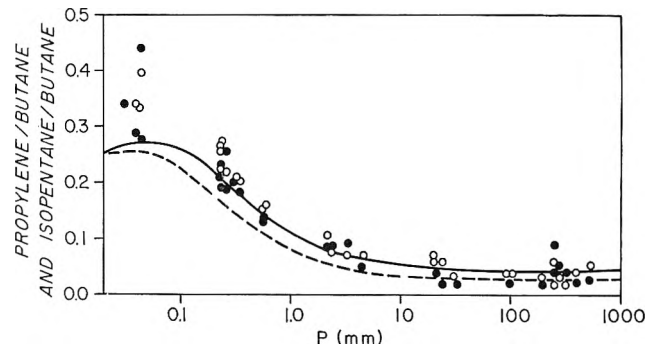


Figure 3. Plots of propylene:butane and isopentane:butane ratios vs. pressure: propylene, ○; isopentane, ●. Solid curve represents calculated fit for propylene, dashed curve is for isopentane.

In the presence of oxygen, isobutane and butane were the principal products at high pressure; their total yields were drastically reduced at lower pressures, as expected, since decomposition led to radical capture by oxygen with no return by recombination. Thus isobutane was wiped out (Figure 1) at 0.03 mm. as were other radical combination products—pentanes and hexanes. This appears surprising, since *n*-butane should also approach zero, until it is recalled that butane is an important product in the photolysis of pure DM in the presence of O₂. Thus under our conditions, the proportions of the products C₂H₆:C₂H₄:C₃H₆:*n*-C₄H₁₀:*i*-C₄H₁₀ were found in blank experiments with DM and D₂ to be on the average 1:575:2.5:130:4, respectively (the quantitative precision in check experiments was poor, but was qualitatively consistent).¹⁰ Thus the main source of butane in the low-

(10) By contrast, the pure DM photolysis products were (average), 1:0.67:0.06:0.008:~0; the radical origin of the ethane is thus evident.

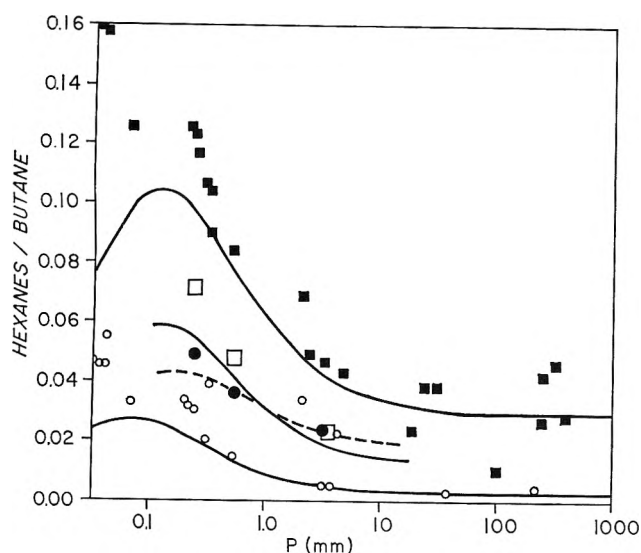
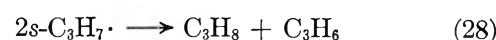
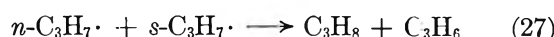
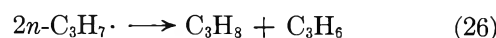
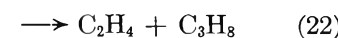
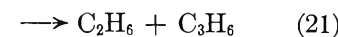
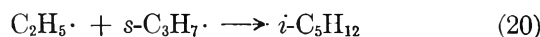
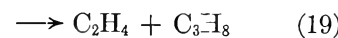
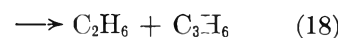
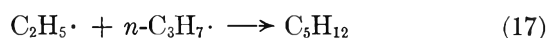
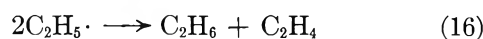
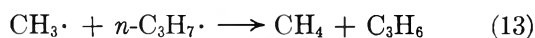
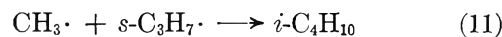
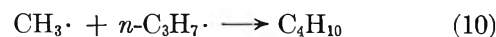
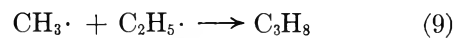
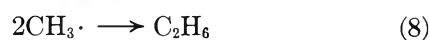
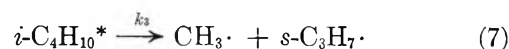
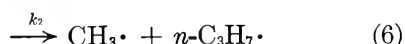
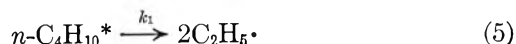
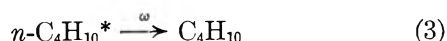
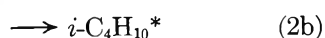
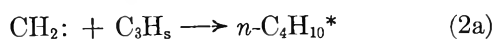
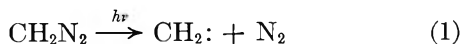


Figure 4. Plots of various hexane:butane ratios vs. pressure: *n*-hexane, O; isohexane, □; 2,3-dimethylbutane, ●; sum of isohexane and 2,3-dimethylbutane, ■. Solid curves represent computer fit for *n*-hexane, isohexane, and the sum of isohexane and 2,3-dimethylbutane; the dashed curve is for 2,3-dimethylbutane.

pressure oxygen work below 0.1 mm. was the DM substrate itself, and the relative decline of isobutane to zero is only apparent. By contrast, the amounts of isobutane and butane above 0.1 mm. rise to values which are sufficiently large even in the presence of oxygen to be independent of the DM-related contributions and thus are significant.

Ethylene and propylene were also formed in large relative amounts at low pressure in the oxygen system. The proportions to butane were $\sim 7:1$ and $\sim 3:1$, respectively, dropping to 0.4:1 for ethylene and to trace for propylene, at high pressure. Evidently, the low-pressure ethylene:butane ratio represents DM reaction products in large part; the high propylene value is discussed later.

Reaction Scheme. The present system can be largely accounted for by the reaction scheme



Some C_2H_4 and C_2H_6 are also formed on diazomethane photolysis, and this will be considered again later.

Some abstraction by CH_2 was evidenced by the occurrence of the various hexanes and propylene even at the highest pressure; these arise by recombination and disproportionation of *n*-propyl and isopropyl radicals (eq. 23–28). Also, ethyl radicals were evidently present at high pressure since *n*-pentane and isopentane were also formed (eq. 17–22).

Analysis of the Data. Due to the complex nature of the above scheme and the scatter of some of the data, it was not practical analytically to derive values for k_1 , k_2 , and k_3 directly from the experimental data. Instead an IBM 7094 computer was programmed to solve the steady-state equations with an assumed set of k values for reactions 3 through 28 and to plot the calculated products as a function of pressure. The assumed set of k values was optimized to give the best fit to the experimental results by trial combinations.

The oxygen data helped to provide very strong constraints on the allowed values of $(k_1 + k_2)/k_3$. In practice, as will be discussed later, this procedure turned out to be neither difficult nor arduous since the computational results were only a weak function of the rate constants for reactions 8 to 28, provided certain reasonable restrictions were observed; in fact, this calculational procedure provided clearer insights than would an analytical solution into the effect of various parameter changes on the amounts and pressure dependence of the various products. The program was written so as to include both H atom abstraction, with propyl radical formation, and also ethyl radical "input," so that the higher pressure data could be reproduced; the proportion of the abstraction reaction was also reduced at lower pressures for reasons discussed later. It will also be assumed, in anticipation of later discussion, that reactions 2a and 2b produced activated *n*-butane and isobutane in a slightly less than statistical 3:1 ratio. Then, at any pressure the relative amounts of ethyl, *n*-propyl, *s*-propyl, and methyl radicals which arose in the system were

$$\begin{aligned} [\text{C}_2\text{H}_5\cdot]_{\text{in}} &= 2.7k_1/(k_1 + k_2 + \omega) + 0.68 \\ [n\text{-C}_3\text{H}_7\cdot]_{\text{in}} &= 2.7k_1/(k_1 + k_2 + \omega) + 0.31 \\ [s\text{-C}_3\text{H}_7\cdot]_{\text{in}} &= k_3/(k_3 + \omega) + 0.93 \\ [\text{CH}_3\cdot]_{\text{in}} &= [n\text{-C}_3\text{H}_7\cdot]_{\text{in}} + [s\text{-C}_3\text{H}_7\cdot]_{\text{in}} \end{aligned}$$

The numbers 0.31 and 0.93 represent total H atom abstraction equal to 25% of the total product formation; abstraction was determined here from the pentane products to favor *s*-propyl formation by a net ratio of 3.0:1. The number 0.68 represents an amount of ethyl radical formation (15%) necessary to fit the high-pressure pentane products. The origin of all of this ethyl is not clear; it could arise by attack of methyl on diazomethane. Stabilized *n*-butane and isobutane (reactions 3 and 4) are then represented by

$$\begin{aligned} [n\text{-C}_4\text{H}_{10}]_{\text{s}} &= 2.7\omega/(k_1 + k_2 + \omega) \\ [i\text{-C}_4\text{H}_{10}]_{\text{s}} &= 1.0\omega/(k_3 + \omega) \end{aligned}$$

To obtain the steady-state values of the radical concentrations the following simultaneous quadratic equations were solved at each pressure

$$\begin{aligned} [\text{C}_2\text{H}_5\cdot]_{\text{in}} &= [\text{C}_2\text{H}_5\cdot]_{\text{ss}} \{ [\text{CH}_3\cdot]_{\text{ss}} [k(9) + k(12)] + \\ &[\text{C}_2\text{H}_5\cdot]_{\text{ss}} [k(15) + k(16)] + \\ &[n\text{-C}_3\text{H}_7\cdot]_{\text{ss}} [k(17) + k(18) + k(19)] + \\ &[s\text{-C}_3\text{H}_7\cdot]_{\text{ss}} [k(20) + k(21) + k(22)] \} \quad (\text{a}) \end{aligned}$$

$$\begin{aligned} [n\text{-C}_3\text{H}_7\cdot]_{\text{in}} &= [n\text{-C}_3\text{H}_7\cdot]_{\text{ss}} \{ [\text{CH}_3\cdot]_{\text{ss}} [k(10) + k(13)] + \\ &[\text{C}_2\text{H}_5\cdot]_{\text{ss}} [k(17) + k(18) + k(19)] + \\ &[n\text{-C}_3\text{H}_7\cdot]_{\text{ss}} [k(23) + k(26)] + \\ &[s\text{-C}_3\text{H}_7\cdot]_{\text{ss}} [k(24) + k(27)] \} \quad (\text{b}) \end{aligned}$$

$$\begin{aligned} [s\text{-C}_3\text{H}_7\cdot]_{\text{in}} &= \\ &[s\text{-C}_3\text{H}_7\cdot]_{\text{ss}} \{ [\text{CH}_3\cdot]_{\text{ss}} [k(11) + k(14)] + \\ &[\text{C}_2\text{H}_5\cdot]_{\text{ss}} [k(20) + k(21) + k(22)] + \\ &[n\text{-C}_3\text{H}_7\cdot]_{\text{ss}} [k(24) + k(27)] + \\ &[s\text{-C}_3\text{H}_7\cdot]_{\text{ss}} [k(25) + k(28)] \} \quad (\text{c}) \end{aligned}$$

$$\begin{aligned} [\text{CH}_3\cdot]_{\text{in}} &= [\text{CH}_3\cdot]_{\text{ss}} \{ [\text{CH}_3]_{\text{ss}} [k(8)] + \\ &[\text{C}_2\text{H}_5\cdot]_{\text{ss}} [k(19) + k(12)] + \\ &[n\text{-C}_3\text{H}_7\cdot]_{\text{ss}} [k(10) + k(13)] + \\ &[s\text{-C}_3\text{H}_7\cdot]_{\text{ss}} [k(11) + k(14)] \} \quad (\text{d}) \end{aligned}$$

where $k(n)$ represents the bimolecular rate constant for reaction n . The solutions were found by iteration. The first set was

$$\begin{aligned} [\text{C}_2\text{H}_5\cdot]_{\text{ss}(1)} &= \{ [\text{C}_2\text{H}_5\cdot]_{\text{in}} / [k(15) + k(16)] \}^{1/2} \\ [n\text{-C}_3\text{H}_7\cdot]_{\text{ss}(1)} &= \{ [n\text{-C}_3\text{H}_7\cdot]_{\text{in}} / [k(23) + k(26)] \}^{1/2} \\ [s\text{-C}_3\text{H}_7\cdot]_{\text{ss}(1)} &= \{ [s\text{-C}_3\text{H}_7\cdot]_{\text{in}} / [k(25) + k(28)] \}^{1/2} \\ [\text{CH}_3\cdot]_{\text{ss}(1)} &= \{ [\text{CH}_3\cdot]_{\text{in}} / k(8) \}^{1/2} \end{aligned}$$

The second set was calculated from the first; e.g., for ethyl one solves eq. a for the i th $[\text{C}_2\text{H}_5\cdot]_{\text{ss}}$ from the $(i - 1)$ values of $[\text{C}_2\text{H}_5\cdot]_{\text{ss}}$, $[n\text{-C}_3\text{H}_7\cdot]_{\text{ss}}$, $[s\text{-C}_3\text{H}_7\cdot]_{\text{ss}}$ and $[\text{CH}_3\cdot]_{\text{ss}}$

$$[\text{C}_2\text{H}_5\cdot]_{\text{ss}(i)} = -B + (B^2 + C)^{1/2}$$

where

$$\begin{aligned} B &= \{ [\text{CH}_3\cdot]_{\text{ss}(i-1)} [k(9) + k(12)] + \\ &[n\text{-C}_3\text{H}_7\cdot]_{\text{ss}(i-1)} [k(17) + k(18) + k(19)] + \\ &[s\text{-C}_3\text{H}_7\cdot]_{\text{ss}(i-1)} [k(20) + k(21) + \\ &k(22)] \} / 2[k(15) + k(16)] \\ C &= [\text{C}_2\text{H}_5\cdot]_{\text{in}} / [k(15) + k(16)] \end{aligned}$$

Note that B and C are positive; only the positive root is possible. After 50 cycles the solutions had converged to closer than 1%. The steady-state values were then used to produce calculated results, such as the curves in Figures 1 through 4. Table II gives the values of k_1 , k_2 , and k_3 and $k(8)$ through $k(28)$ which were used to obtain these particular calculated curves; the amount of abstraction was allowed to decline with pressure as $p/(0.1 + p)$. The fit of these curves to the data is best for *n*-hexane, for *n*- and isopentanes, for propylene, and for isobutane. The fit is correct

Table II: Rate Constants Used in Data Analysis Program^a

$k_1 = 0.50^b$	$k(17) = 9.5$
$k_2 = 0.25^b$	$k(18) = 0.75$
$k_3 = 1.50^b$	$k(19) = 0.55$
$k(8) = 8.8^c$	$k(20) = 7.5$
$k(9) = 14.0^c$	$k(21) = 3.23$
$k(10) = 12.0$	$k(22) = 1.5$
$k(11) = 9.0$	$k(23) = 4.0$
$k(12) = 0.63$	$k(24) = 6.0$
$k(13) = 0.60$	$k(25) = 2.5$
$k(14) = 1.8$	$k(26) = 0.56$
$k(15) = 5.1^c$	$k(27) = 2.4$
$k(16) = 0.66$	$k(28) = 1.6$

^a The rates of disproportionation are relative to the recombination rates and values have been taken primarily from ref. 11 and from S. W. Benson, *Ann. Rev. Phys. Chem.*, **16**, 397 (1965).

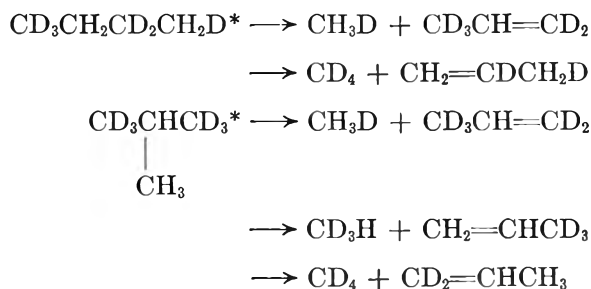
^b k_1 , k_2 , and k_3 are expressed here in terms of pressure (mm.); i.e., the rate of decomposition (k_i) equals the rate of stabilization by collision (ω) at the pressure specified. All other rates simply appear as relative values since the calculated data are normalized to *n*-butane. ^c Specific rates $k(8)$, $k(9)$, and $k(15)$ were adjusted by the following expressions to allow for onset of fall-off in recombination at lower pressures as governed by the constant in the denominator: $k(8) = 8.8p/(0.5 + p)$, $k(9) = 14.0p/(0.06 + p)$, $k(15) = 5.1p/(0.01 + p)$, where p is the pressure in millimeters.

with regard to pressure dependence, but somewhat off in magnitude, for ethane. This will be considered in the Discussion.

Test for Molecular Decomposition. Some low-pressure work was also done with 1,1,1,3,3,3-propane-*d*₆ in order to test for molecular elimination, since it was found that a considerable amount of propylene product (one-tenth in absolute amount of that produced in the pure system) still arose in the runs with added oxygen. If propylene and methane can arise from molecular elimination



then use of labeled propane in oxygen runs should allow a molecular decomposition methane product to be distinguished from any methane formed as a product from DM photolysis. It is assumed that the deuteriobutanes would decompose by a molecular mechanism to give products such as



It is evident that CD₄ and CD₃H products could not arise in methane formed by some molecular process from DM; dideuteration would be the maximum extent of such deuteration of methane.

In actual fact, *no* methane could be detected in the oxygen system (the limit of sensitivity was ~10% of the pure system amount) at a pressure (Table I) at which decomposition is virtually complete, so that on this basis no molecular decomposition to give propylene occurred. In the pure system, rupture of C-C bonds produces CD₃, CH₂D, and CH₃ radicals, with the first preponderating. CD₃ should give rise to a proportion of CD₄ and CD₃H products governed by the relative abstraction probabilities of secondary-H and primary-D from propane. For light propane, the *secondary:primary* abstraction ratio¹¹ is $7/3 = 2.33$; from primary-D, this ratio would be much higher. Methane was trapped in silica gel at -208° and analyzed on a mass spectrometer. The following relative amounts of methane were found

CH ₄	CH ₃ D	CH ₂ D ₂	CHD ₃	CD ₄
5.0	3.0	0.40	2.4	1.0

The observed ratio 2.4:1.0 suggests some small amount of molecular reaction. Although most of the methane product obviously has a free-radical origin, we conclude that the present data allow the possibility of a very minor or trace amount of a molecular process of this type.^{4b,c}

Propylene product was reduced by still another factor of 5 when NO was used instead of O₂. What propylene was left in the NO system was small enough to be explicable as DM photolysis product, as secondary reaction of methylene with ethylene, and as some other undetermined minor mechanism. Hence, there was no evidence of molecular elimination, and most of the propylene found in the presence of oxygen is conjectured as arising in the course of an oxidation chain sequence; in this sense, oxygen did not function entirely as an idealized radical getter.

Discussion

Decomposition Rates; Fit of Data. The various alkyl radical rates of recombination, $k(8)$ - $k(28)$, are not known precisely, particularly for the higher alkyls; if they were, the corresponding average thermal unimolecular rate constants for decomposition of alkanes could, of course, be easily deduced. In the light of this, several sets of product data were calculated to test their dependence on these rates; for fixed values of k_1 , k_2 , and k_3 , the values of $k(8)$ - $k(28)$ were varied

(11) J. A. Kerr and A. F. Trotman-Dickenson, *Progr. Reaction Kinetics*, **1**, 114 (1961).

widely. An interesting result was found: when rough obedience to the "rule of 2" (*i.e.*, $k_{ab}/(k_{aa}k_{bb})^{1/2} \simeq 2$) was required for alkyl radical combinations, the calculated data were virtually independent of the assumptions regarding $k(8)$ – $k(28)$. This requirement is well founded, particularly for alkyl radicals.¹¹ Various combinations of the ratios of recombination rates for the series methyl–methyl:ethyl–ethyl:*n*-propyl–*n*-propyl: and *s*-propyl–*s*-propyl, *i.e.*, of $k(8):k(15):k(23):k(25)$, were used. The following extreme variation of rate ratios all gave similar calculated results, 8.8:5.1:4.0:2.5, 1:1:1:1, 4:1:1:4, 1:4:4:1, and 2.5:4.0:5.1:8.8. Of these, the first set was used in Table II since it is considered to be the most reasonable. It is unnecessary to illustrate all of these calculated results with detailed figures. If the calculated solid line curves in Figures 1–4 were replaced by heavy brush strokes (and not all curves would have to be so broadened, nor at all pressures) it would encompass virtually all of the variation. By contrast, a change in any single $k(i)$ by only a factor of 2 made a significant change in at least some of the calculated values. In the same way, a change in any one of k_1 , k_2 , or k_3 by a factor of 2 changed the calculated relative product amounts substantially; also a uniform change of total rates at constant ratios, *e.g.*, of the values of k_1 , k_2 , and k_3 while maintaining $(k_1 + k_2)/k_3 = \text{constant}$, caused a marked and observable variation in the pressure at which characteristic changes in product amounts occurred. Various systematic combinations of the k_i were explored over a range of a factor of 10 to 100 in each. This method of data analysis led to the evaluation of the absolute and relative magnitudes of the unimolecular constants k_1 , k_2 , and k_3 to within a factor of 2; more consistent data could have produced better precision.

Some error in the determination of the k_i arises from the fact that the calculated fit of all of the product variations was not of uniform merit for all products. The ratio of $(k_1 + k_2)/k_3$ was weighted considerably by the oxygen data (the low isobutane/*n*-butane ratio found below 0.1 mm. was ignored as false for the reasons given above, and any attempt to fit that region caused the remainder of the fit to blow up completely). The ethane data could not be fitted much more closely without doing violence to the better agreement found for other products. The propylene, isobutane, pentanes, and hexanes were considered as the most crucial for optimization of fit in evaluation k_1 , k_2 , and k_3 . The total isohexane fit (Figure 4) is acceptable at pressures above 0.1 mm. but very poor below. The source of this discrepancy is not clear other than that the accuracy of determination of isohexane was less than

that for isobutane, isopentane, or propylene, which are closely related products; a more efficient recombination reaction than assumed for methyl radicals at low pressures would remove part of the discrepancy.

Actually, the ethane fit is better in two respects than first appears: first, the relative variation of ethane with pressure—which is important for the magnitude of k_1 —is correct (Figure 2); second, much of the discrepancy between the low-pressure experimental and calculated ratio to butane is explicable as follows. The low-pressure proportion of DM in the reaction mixture was $\sim 10\%$ (Table I). Thus if 10% of the ethane product which is normally yielded by pure DM photolysis¹⁰ arose, this would be an amount equal roughly to 5% of the DM used. But at low pressures *n*-butane is only two-fifths to one-third of the total products, *i.e.*, as little possibly as 33% of the DM. Thus the ethane formation directly from DM photolysis may reach 0.15 relative to the *n*-butane which, when added to the ethane calculated from the formal mechanism, puts the calculated ethane ratio up to 0.41 which is in better agreement with the data of Figure 2.

Methylene Insertion Ratios. The measured relative amount of *n*-butane to isobutane at the high-pressure end was ~ 2.5 , which agrees with the work of Frey.⁹ It should be kept in mind that some pentanes and hexanes arise at high pressures from radicals formed from propane by abstraction, say by methylene. The *sec*-propyl predominates in these products, so that combination with methyl gave additional butanes (especially iso-) such that the final calculated true insertion ratio becomes 2.7. This effect is probably present in many or most other gas phase systems; presumably, addition of O₂ (which scavenges alkyl radicals) would alter the observed apparent insertion ratio. In the present oxygen systems, the absolute amounts of butanes formed were reduced at high pressures. However, the ratio of *n*-butane to isobutane was substantially unchanged (Figure 1). The oxygen data were too few to verify the expected increase.⁹

Effects Due to Triplet Methylene. It has recently been shown that 20 to 30% of triplet methylene can be formed in ketene and DM systems at higher pressures, the percentage decreasing with lowering of system pressure.^{7,12} Nominally, little effect on the formation of the butanes in this system would be expected if, as is commonly believed, triplet radicals do not insert into carbon–hydrogen bonds. In any case,

(12) J. W. Simons and B. S. Rabinovitch, *J. Phys. Chem.*, **68**, 1322 (1964).

any effects due to the presence of triplet methylene in this system would be most pronounced at the higher pressures. Actually, it was found that the calculated low-pressure isobutane ratio in the pure system was much too high and would not fit the experimental values unless the amount of abstraction (which gives rise predominantly to isopropyl radical and eventually to isobutane) was drastically reduced as low pressure (Figure 1). The sets of data in the figures were calculated on the assumption that the abstraction reaction decreased at lower pressures as $p/(0.1 + p)$. The constant, 0.1 mm., was subjected to variation. The optimum value used is lower than that found (>1 mm.) in our previous work,^{7,12} although all studies are in qualitative agreement regarding the effect of pressure. Since the reactions of such methylene species as are produced is independent of the mean time between collisions with substrate molecules, in a system of constant composition, it is plausible that reduction of abstraction at low pressures by methylene is associated with the reduced proportions of triplet CH_2 at lower pressures and that virtually all H atom abstraction by methylene is due to the triplet species.¹³ As mentioned in a prior section, when account is taken of abstraction, the apparent insertion values are corrected in the direction of the statistical ratio. The effect of triplet methylene in altering insertion ratios away from the statistical value has already been noted.⁷ Virtually all old gas phase data in DM and ketene systems will bear correction of the apparent insertion ratios of C-H bonds of various types.

Recently, Placzek and Rabinovitch^{14a} offered an amplification of the "pressure-independent" formation of product alkenes which arise from triplet cyclopropanes upon reaction of triplet methylene with substrate alkenes^{15a}; specifically considered was triplet state dimethylcyclopropane which, as pointed out earlier,^{14b} may be regarded as a triplet trimethylene diradical, I. Placzek and Rabinovitch proposed that the triplet



cyclopropane led by H migration steps on a triplet surface to relatively long-lived α,β diradicals; these correspond to triplet state olefins that are known from $\text{Hg}(^3\text{P}_1)$ photosensitization studies to be readily interceptible by collision.¹⁶ This mechanism does still not explain the "pressure-independent" pentene-2 formation, unless CH_3 migration^{15a} or alternative diradical state, II^{15b,c} is invoked. We consider it likely that some of the pressure-independent alkene products

of triplet methylene with *cis*- or *trans*-butene-2 arise *via* H abstraction: allylic H abstraction, the most favored, leads to both *cis*- and *trans*-pentene-2 on CH_3 combination if the methallyl radical does not completely retain configuration, as is possible¹⁷; it should also lead to lesser amounts of 3-methylbutene-1, corresponding to a canonical methallyl radical structure, which is less favored.¹⁷ Abstraction of vinylic H leads to 2-methylbutene-2. Insofar as 2-methylbutene-1 product is not explicable on this basis, support is still lent to the original interpretation of Cvetanović and Duncan, and possibly that of Bell,^{16b} as having relevance for some of the products.

We are currently extending our investigations to higher pressures and liquid phase in an effort to discover the nature of the intersystem crossing mechanism leading to triplet methylene *via* the triplet precursor. Comparative absence of triplet methylene in liquid media studies of this type¹⁸ could occur either because of specific ternary interactions which alter the effective rates of various processes or, quite possibly, because other collisional processes must be invoked. If so, the enhancement of triplet production in the gas phase with increase in pressure should eventually pass through a maximum at very high pressures.^{18a}

Theoretical Calculations. The recombination of methyl radicals is known to occur at a rate very close to their singlet-state collision rate.¹⁹ This is usually accepted as signifying a very low activation energy for recombination. The critical energies for dissociation of alkanes into alkyl radicals may be taken as given by the heat of reaction at 0°K. If an Arrhenius-type dissociation rate equation is evaluated from the equilibrium constant and the radical recombination

(13) H. M. Frey and G. B. Kistiakowsky have independently come to the same conclusion (H. M. Frey, private communication).

(14) (a) D. W. Placzek and B. S. Rabinovitch, *Can. J. Chem.*, **43**, 820 (1965); (b) D. W. Setser, B. S. Rabinovitch, and E. G. Spittler, *J. Chem. Phys.*, **35**, 1840 (1961).

(15) (a) F. J. Duncan and R. J. Cvetanović, *J. Am. Chem. Soc.*, **84**, 3593 (1962); (b) J. Bell, *Progr. Phys. Org. Chem.*, **2**, 45 (1964). (c) Although this same intermediate is believed to arise in the pentene-1 $\text{Hg}(^3\text{P}_1)$ -photosensitized isomerization to 1,2-dimethylcyclopropane,^{14a} virtually no pentene-2 was formed in that process; this suggests the desirability of confirmatory evidence that this intermediate diradical is the precursor of the pentene-2 in the triplet methylene system, as proposed by Bell.

(16) R. J. Cvetanović and L. C. Doyle, *J. Chem. Phys.*, **37**, 543 (1962).

(17) R. F. Kubin, B. S. Rabinovitch, and D. W. Setser, *ibid.*, **37**, 937 (1962).

(18) D. B. Richardson, M. C. Simmons, and I. Dvoretzky, *J. Am. Chem. Soc.*, **83**, 1934 (1961).

(18a) NOTE ADDED IN PROOF. H abstraction by triplet methylene and the maximum suggested have now both been verified with *cis*-butene-2.

(19) G. B. Kistiakowsky and E. K. Roberts, *J. Chem. Phys.*, **21**, 1637 (1953).

rate, very large pre-exponential or 'A' factors are obtained. The well-known Gorin treatment by absolute rate theory deals with these reactions as proceeding through a loose activated complex having free internal rotations. Such a model is fairly successful for the lower alkanes, methane, and ethane, but seems inappropriate in general.²⁰ When applied to *n*-butane decomposition^{2b} it yields a frequency factor, 7.6×10^{18} sec.⁻¹, which is too high by a factor of ~ 8 at 873°K., relative to a classical recombination rate of the radicals. For the present calculations, a loosened vibrational model rather than the loose model was used.

For *n*-butane, a decomposition complex having lowered bending and torsional modes was constructed by fitting a calculated thermal pre-exponential factor, *A*, which was obtained by elimination between the ethyl radical-*n*-butane equilibrium constant at room temperature and the recombination rate for ethyl radicals. Shepp and Kutschke²¹ have measured the recombination at 50°; their value of 0.09*Z* was adjusted to 0.08*Z* for 25°. The moments, frequencies, and cross sections used previously^{2b} for ethyl radicals, plus the butane frequencies in Table III and the E_0 value in Table IV gave rise to a calculated *A* factor of 1.4×10^{17} sec.⁻¹. To fit this, the adiabatic moment of inertia ratio was taken as 1.6 (as described for decomposition of butene⁷), and in the activated complex four bending and rocking frequencies were lowered to one-tenth of their value and three torsions to one-sixth. This rather simplified description of frequency changes (Table III, complex 1) can nevertheless provide realistic calculated values under the constraint that these changes have given the desired *A* value.^{2b} This prescription for degree of loosening was applied to the construction of the other two complexes in Table III.

RRKM rate theory gives the well-known specific reaction rate expression for k_E as

$$k_E = \frac{I_r}{h} \frac{\sum_{E_{vr}}^{E^+} P(E_{vr})}{N^*(E)}$$

where *I* is an adiabatic partition function ratio and may include reaction path degeneracy considerations. $\sum P(E_{vr})$ represents the total sum of vibration-rotation states at an energy E^+ for the complex. E_0 is the critical energy for reaction. $N^*(E)$ is the density of states for the molecule.²²

The average observed rates for a competitive decomposition system such as butane are given by

$$k_{a1} = \omega \int_{E_{min}}^{\infty} \frac{k_{E1} f(E) dE}{(k_{E1} + k_{E2} + \omega)} \bigg/ \int_{E_{min}}^{\infty} \frac{\omega f(E) dE}{(k_{E1} + k_{E2} + \omega)}$$

$$k_{a2} = \omega \int_{E_{min}}^{\infty} \frac{k_{E2} f(E) dE}{(k_{E1} + k_{E2} + \omega)} \bigg/ \int_{E_{min}}^{\infty} \frac{\omega f(E) dE}{(k_{E1} + k_{E2} + \omega)}$$

$$k_{a3} = \omega \int_{E'_{min}}^{\infty} \frac{k_{E3} f(E) dE}{k_{E3} + \omega} \bigg/ \int_{E'_{min}}^{\infty} \frac{\omega f(E) dE}{k_{E3} + \omega}$$

Table III: Frequency Assignments (cm.⁻¹) for Molecules and Activated Complexes^a

	Butane ^b			Isobutane ^c	
	Molecule	Complex 1	Complex 2	Molecule	Complex
CH ₂ , CH ₃ bending	1180		118	1168	117
	1152	115	115	981	98
	972	97	97		
C-C-C bending	431	43	43	381	38
	271	27		418	42
Torsion	225	38	38	203 (2)	34 (2)
	194	32	32	198	33
	102	16	16		
C-C stretch	1008		...	791	...
	835	...			

^a Only molecule frequencies which change in the complex are given; all other frequencies are assigned in footnotes *b* and *c*.

^b J. H. Schachtschneider and R. G. Snyder, *Spectrochim. Acta*, **19**, 117 (1963). ^c R. G. Snyder and J. H. Schachtschneider, *ibid.*, **21**, 169 (1965).

Table IV: Rate Constants and Energy Parameters

Reaction	Pressure, mm.	$k_{exptl.}$, sec. ⁻¹	$k_{calcd.}$, sec. ⁻¹	E_0^a , kcal. mole ⁻¹	$E_{min.}$, kcal. mole ⁻¹
<i>n</i> -C ₄ → 2C ₂	10 ²		1.58 × 10 ⁸	81.5	102.3
		1.4 × 10 ⁸			
<i>n</i> -C ₄ → C + <i>n</i> -C ₃	10 ⁻²		1.21 × 10 ⁸		
	10 ²		4.96 × 10 ⁷	84.0	102.3
<i>i</i> -C ₄ → C + <i>s</i> -C ₃	10 ⁻²	7.0 × 10 ⁷	3.62 × 10 ⁷		
	10 ²		5.18 × 10 ⁸	81.6	103.9 ^b
	10 ⁻²	4.2 × 10 ⁸	3.95 × 10 ⁸		

^a An error of 1 kcal. in this quantity alters the calculated rate by a factor of ~ 2 . ^b Based on $\Delta H_f^\circ(n\text{-butane}) - \Delta H_f^\circ(s\text{-butane}) = 1.6$ kcal. mole⁻¹.

(20) H. S. Johnston and P. Goldfinger, *J. Chem. Phys.*, **37**, 700 (1962).

(21) A. Shepp and K. O. Kutschke, *ibid.*, **26**, 1020 (1957).

(22) The accuracy of the Haarhoff approximation as described by M. J. Pearson, B. S. Rabinovitch, and G. Z. Whitten [*ibid.*, **42**, 2470 (1965) (footnote 13)], has been overestimated somewhat: 3% should be changed to 8% and 10,000 cm.⁻¹ to 20,000 cm.⁻¹ in that reference.

where integration is over the range of the distribution function $f(E)$. The appropriate representation of energy distribution functions for methylene systems has been discussed earlier.²³ $f(E)$ may simply be chosen to be a room temperature thermal spread, appropriate for the butane and isobutane molecules. k_E was evaluated over a wide energy range. The required level of minimum energy, E_{\min} , upon which $f(E)$ is to be imposed was then found by trial to be 102.3 kcal. for *n*-butane in order to match k_{a1} (calcd.) to k_1 (exptl.). The level of E_{\min} for isobutane is then 103.9 kcal., as governed by heats of formation.

Excess Methylene Energy. Heats of formation at 0°K. from the A.P.I.-W Tables (1952) were used, together with election of the values 102, 97, 97, and 93 kcal. mole⁻¹ for $D_0(\text{C-H})$ for methane, ethane, primary, and secondary propane, respectively. These gave the values shown in Table IV. Table IV summarizes the results of these calculations.

The average internal energy of the formed *n*-butane, calculated from $f(E)$ is $102.3 + 2.6 = 104.9$ kcal. mole⁻¹. Taking $\Delta H_{f_0}^\circ(\text{CH}_2) = 87$ kcal. mole⁻¹ for methylene,⁶ this gives a heat of reaction, ΔH° , of 91.2 kcal. at 0°K. and an excess energy of 13.7 kcal. mole⁻¹. Similar calculations yield $\Delta H^\circ = 83.5$ and 27 kcal. excess for methylene in the dimethylcyclopropane isomerization system (using 7.0 kcal.²³ for $\Delta H_{f_0}^\circ$, dimethylcyclopropane). In the cyclopropane system, $\Delta H^\circ = 86$ and 22 kcal. excess is found.²⁴ Likewise, for ethane decomposition, ΔH° is 87.5 kcal. It has been found for ethane^{2b} that at 90 kcal. the calculated rate is too low by a factor of 20 relative to the observed value⁶ to fit which an average of 98

kcal. is required for a bending vibration model. Thus 10.5 kcal. excess energy applies. Finally, $\Delta H^\circ = 103$ kcal. and 1-3 kcal. excess for methane can be obtained.^{2b} Any neglected energy distribution of the methylene formed in these photolysis systems, or error in $\Delta H_{f_0}^\circ(\text{CH}_2)$, cancels for relative comparisons. The average heat capacity of reactants at 25° are only a few kcal. mole⁻¹ and do not differ by more than 1-2 kcal. mole⁻¹. Hence the above excess energy quantities, if lower by 1-3 kcal. are the amounts transmitted by methylene into combination reactions.

In conclusion, the high-frequency factors predicted for alkane decomposition seem to be justified. The rates given here, although accurate to only a factor of 2, can be fitted only by very loose-vibration complexes. The excess energy thereby predicted for the methylene seems quite reasonable when compared to related systems: the efficiency of C-H insertion is enhanced by the number of sites available per molecule, yet is not as efficient as addition to double bonds as in the cyclopropane systems; the amount of energy transmitted increases with reaction cross section; collisional transfer probability and loss of excess energy from the methylene increases inversely with reaction efficiency.

Acknowledgment. This work was supported in part by the Petroleum Research Fund of the American Chemical Society and in part by the National Science Foundation.

(23) D. W. Setser and B. S. Rabinovitch, *Can. J. Chem.*, **40**, 1425 (1962).

(24) D. W. Setser, B. S. Rabinovitch, and J. W. Simons, *J. Chem. Phys.*, **40**, 1751 (1964); **41**, 800 (1964).

Fluorine Bomb Calorimetry. XIII. The Enthalpy of Formation

of Arsenic Pentafluoride¹

by P. A. G. O'Hare and Ward N. Hubbard

Chemical Engineering Division, Argonne National Laboratory, Argonne, Illinois (Received August 2, 1965)

The energy of formation of arsenic pentafluoride was measured by direct combination of the elements in a bomb calorimeter. From these measurements the standard enthalpy of formation, $\Delta H_f^\circ_{298.15}(\text{AsF}_5, \text{g})$, was calculated to be -295.59 ± 0.19 kcal. mole⁻¹. The average bond strength in AsF_5 (92.4 kcal. mole⁻¹) is about 20 kcal. mole⁻¹ less than it is in AsF_3 .

This investigation is part of a continuing program to determine the enthalpies of formation of various compounds by fluorine bomb calorimetry. An accurate value for the enthalpy of formation of arsenic pentafluoride is a necessary prerequisite to the study of arsenic compounds by this method. This paper reports a value for $\Delta H_f^\circ(\text{AsF}_5, \text{g})$ calculated from measurement of the energy of combustion of crystalline black arsenic in fluorine, a spontaneous and complete reaction.

Experimental Section

Calorimetric System. The calorimeter, laboratory designation ANL-R2, has been described in detail.² The reaction vessel, laboratory designation NI6-T2, was the bomb-and-tank device previously described,³ except that a direct screw drive of the valve stem was substituted for the toggle arrangement. The energy equivalent of the calorimetric system was measured by combustion of benzoic acid (National Bureau of Standards Sample 39i) in oxygen. A series of eight calibration experiments yielded a value for $\epsilon(\text{Calor.})$ of 3363.94 cal. deg.⁻¹ with a standard deviation of the mean of 0.21 cal. deg.⁻¹ (1 cal. \equiv 4.1840 abs. joules).

Materials. High-purity, zone-refined, crystalline black arsenic (Grade 1, Batch R77) was purchased from Johnson, Matthey and Co., London. No metallic impurities were detected by spectrochemical analysis (detection limit 5 p.p.m.). Chemical analyses by Ledoux and Co., Teaneck, N. J., showed 39 p.p.m. of carbon and 10 p.p.m. of nitrogen. Neutron activation analysis, performed by Drs. E. H. Strain and W.

Ross, Oak Ridge National Laboratory, showed an oxygen content less than 10 p.p.m. Fluorine of 99.99% purity was prepared by distillation of a commercial sample in a low-temperature still.⁴

Procedure. Arsenic samples could be weighed in air as a 24-hr. exposure showed a weight change of less than 1×10^{-5} g. Before the calorimetric series, the bomb was preconditioned by several combustions of arsenic in fluorine. All subsequent operations in which the bomb was opened were performed in a helium atmosphere glove box ($\text{H}_2\text{O} \sim 0.1$ p.p.m.). The sample on a 33-g. nickel dish was introduced into the bomb which was then connected to the tank charged with fluorine at 190 p.s.i.a. pressure. After overnight evacuation, the reaction vessel was transferred into the calorimeter and measurements were made in the usual manner.⁵

After selected experiments, the product gases were condensed in a liquid nitrogen-cooled trap. Excess fluorine was removed by repeatedly freezing, pumping, and melting the condensate. The liquid nitrogen

(1) (a) This work was performed under the auspices of the U. S. Atomic Energy Commission; (b) for the previous paper in this series, see H. A. Porte, E. Greenberg, and W. N. Hubbard, *J. Phys. Chem.*, **69**, 2308 (1965).

(2) E. Greenberg, J. L. Settle, H. M. Feder, and W. N. Hubbard, *ibid.*, **65**, 1168 (1961).

(3) R. L. Nuttall, S. S. Wise, and W. N. Hubbard, *Rev. Sci. Instr.*, **32**, 1402 (1961).

(4) L. Stein, E. Rudzitis, and J. L. Settle, "Purification of Fluorine by Distillation," Argonne National Laboratory, ANL-6364, 1961. (Available from Office of Technical Services, U. S. Department of Commerce, Washington, D. C.)

(5) W. N. Hubbard, C. Katz, and G. Waddington, *J. Phys. Chem.*, **58**, 142 (1954).

Table I: Results of Combustion Experiments

1. m' , g.	1.21521	1.37874	1.34229	0.97003	0.87221	0.70216	1.53364
2. Δt_c , deg.	1.42474	1.61563	1.56795	1.13928	1.01903	0.81992	1.79960
3. $\varepsilon(\text{Calor.})(-\Delta t_c)$, cal.	-4792.68 ^d	-5434.88	-5274.49	-3832.47	-3427.96	-2758.16	-6053.75
4. $\Delta E_{\text{contents}}$, cal. ^{a,c}	-6.14	-6.99	-7.47	-4.80	-4.30	-3.45	-8.23
5. ΔE_{gas} , cal. ^b	-0.16	-0.18	-0.21	-0.13	-0.11	-0.09	-0.24
6. ΔE_{blank} , cal.	1.48	1.48	1.48	1.48	1.48	1.48	1.48
7. ΔE_{NiF_2} , cal.	12.44	10.22	2.04	22.07	0.13	0.00	29.52
8. $\Delta Ec^\circ/M(\text{sample})$, cal. g. ⁻¹	-3937.64	-3938.63	-3932.57	-3931.68	-3933.41	-3931.04	-3932.62

Average $\Delta Ec^\circ/M(\text{sample}) = -3933.94$ cal. g.⁻¹
 Std. dev. of mean = 1.1 cal. g.⁻¹
 Impurity correction = 0.5 cal. g.⁻¹
 $\Delta Ec^\circ/M(\text{As, c, black}) = -3933.4$ cal. g.⁻¹

^a $\Delta E_{\text{contents}} = \varepsilon(\text{Cont.})(t_i - 25) + \varepsilon'(\text{Cont.})(25 - t_f + \Delta t_{\text{cor}})$. ^b $\Delta E_{\text{gas}} = \Delta E^\circ(\text{gas})_0^{P_i(\text{gas})} + \Delta E^\circ(\text{gas})_0^{P_f(\text{gas})}$. ^c The internal volume of the empty bomb was 0.307 l. and of the tank, 0.232 l. ^d For this experiment $\varepsilon(\text{Calor.})$ was 3363.90 cal. deg.⁻¹.

was then replaced by a -70° slush bath and a similar procedure was used to remove AsF_5 . At -70° the vapor pressure of AsF_3 is minute, whereas that of AsF_5 is 290 torr.⁶ Thus, any AsF_3 that might have been produced as a by-product of the combustion reaction should have been retained in the trap. A subsequent infrared analysis of its contents failed to reveal any evidence for the presence of AsF_3 . In synthetic mixtures as little as 0.02% AsF_3 in AsF_5 could be detected by this method.

The nickel dish increased in weight by varying amounts in each experiment. No arsenic was detected spectrochemically in scrapings from the surface of the dish after the calorimetric series was completed. The weight gain was ascribed to the formation of NiF_2 .

Results

Combustion Experiments. The data for seven acceptable calorimetric experiments are summarized in Table I. The symbols in Table I are those used in ref. 7. Standard state corrections were made in the usual manner.⁷ For the conversion of the weight of arsenic to true mass its density was taken as 5.778 g. cc.⁻¹.⁸ For the calculation of item 4 the following heat capacity data were used: $c_p = 0.106$ and 0.080 cal. deg.⁻¹ g.⁻¹ for Ni^9 and As^{10} ; $C_v = 5.50$ and 21.27 cal. deg.⁻¹ mole⁻¹ for F_2^{11} and AsF_5 ,¹² respectively. For the calculation of item 5, values of μ (atm.⁻¹) and $(\partial E/\partial P)_T$ (cal. atm.⁻¹ mole⁻¹) were derived from the force constants of F_2^{13} and the estimated force constants for AsF_5 .¹⁴ These quantities, as functions of composition at 25° , are given by

$$\mu = 0.000801(1 + 3.33x[1 + 0.83x]) \quad (1)$$

and

$$(\partial E/\partial P)_T = 1.780(1 + 1.98x[1 + 0.49x]) \quad (2)$$

where x is the mole fraction of AsF_5 in the final combustion gas mixture.

In spite of the preconditioning of the bomb and its prolonged evacuation, an exothermic effect ("blank") was observed when fluorine was expanded into the empty bomb. Determinations of the magnitude of this blank were alternated with combustion experiments. Item 6, ΔE_{blank} , 1.48 ± 0.51 cal., is the uniform correction applied. Item 7 is the correction applied for the formation of NiF_2 , based on a value of -2.76 cal. mg.⁻¹ for the energy of combustion of nickel in fluorine.¹⁵ No correction was applied for the possible formation of less than 0.02% AsF_3 .

The sum of items 3 through 7 was divided by m' to obtain $\Delta Ec^\circ/M$, the energy of combustion of the sample in fluorine. No obvious trends are apparent in the results although the mass of sample reacted was varied by a factor of two. The carbon, nitrogen, and

(6) O. Ruff, *Z. anorg. allgem. Chem.*, **206**, 59 (1932).

(7) W. N. Hubbard in "Experimental Thermochemistry," Vol. II, H. A. Skinner, Ed., Interscience Publishers Ltd., London, 1962, Chapter 6.

(8) H. E. Swanson, R. K. Fuyat, and G. M. Ugrinic, "Standard X-ray Diffraction Patterns," Vol. III, National Bureau of Standards Circular 539, U. S. Government Printing Office, Washington, D. C., 1954.

(9) R. H. Busey and W. F. Giaque, *J. Am. Chem. Soc.*, **74**, 3157 (1952).

(10) K. K. Kelley, U. S. Bureau of Mines Bulletin 476, U. S. Government Printing Office, Washington, D. C., 1963.

(11) W. H. Evans, T. R. Munson, and D. D. Wagman, *J. Res. Natl. Bur. Std.*, **55**, 147 (1955).

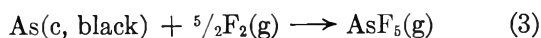
(12) L. K. Akers, Ph.D. Thesis, Vanderbilt University, 1955.

(13) D. White, J. H. Hu, and H. L. Johnston, *J. Chem. Phys.*, **21**, 1149 (1953).

(14) J. O. Hirschfelder, C. F. Curtiss, and R. B. Bird, "Molecular Theory of Gases and Liquids," John Wiley and Sons, Inc., New York, N. Y., 1954.

(15) E. Rudzitis, this laboratory, unpublished measurements.

oxygen in the sample were assumed to be present as uncombined carbon and nitrogen, and as As_2O_3 , respectively; the products of combustion were assumed to be CF_4 , N_2 , AsF_5 , and O_2 . Auxiliary enthalpies of formation (in kcal. mole⁻¹) were taken as -221 for CF_4 ¹⁶ and -155 for As_2O_3 .¹⁷ The net impurity correction, 0.46 ± 0.1 cal. g.⁻¹, was applied to give the standard energy of combustion of arsenic in fluorine, $\Delta E_c^\circ/M$, according to



Derived Data. Thermodynamic data for arsenic pentafluoride are presented in Table II. The atomic weight of arsenic¹⁸ was taken as 74.9216. Standard entropies, S° , at 25° of crystalline arsenic,¹⁰ fluorine,¹¹ and arsenic pentafluoride¹² were taken as 8.40, 48.45, and 78.00 cal. deg.⁻¹ mole⁻¹, respectively. The uncertainties given are uncertainty intervals¹⁹ equal to twice the combined standard deviation contributed by all known sources.

Table II: Derived Data at 25°

$\text{As(c, black)} + \frac{5}{2}\text{F}_2(\text{g}) \rightarrow \text{AsF}_5(\text{g})$	
Energy of formation	
$\Delta E_f^\circ = \Delta E_c^\circ$, kcal. mole ⁻¹	-294.70 ± 0.19
Enthalpy of formation	
ΔH_f° , kcal. mole ⁻¹	-295.59 ± 0.19
Entropy of formation	
ΔS_f° , cal. deg. ⁻¹ mole ⁻¹	- 51.53
Gibbs energy of formation	
ΔG_f° , kcal. mole ⁻¹	-280.23 ± 0.19

The only previously reported value for $\Delta H_f^\circ(\text{AsF}_5)$ was an estimate (-265 kcal. mole⁻¹) by Glassner.²⁰

Bond Dissociation Energies in Arsenic Fluorides

The average As-F bond dissociation energy in AsF_5 , $\bar{D}(\text{As-F})_{\text{AsF}_5}$, is given by

$$\bar{D}(\text{As-F})_{\text{AsF}_5} = \frac{1}{6}[\Delta H_f^\circ(\text{As}, {}^4\text{S}_{3/2}) + 5\Delta H_f^\circ(\text{F}, {}^2\text{P}_{3/2}) - \Delta H_f^\circ(\text{AsF}_5)] \quad (4)$$

The enthalpy of formation of gaseous atomic arsenic may be calculated from

$$\Delta H_f^\circ(\text{As}, {}^4\text{S}_{3/2}) = \frac{1}{2}[D(\text{As}_2) + \Delta H_f^\circ(\text{As}_2, \text{g})] \quad (5)$$

Inserting values of $D(\text{As}_2) = 90.8$ kcal. mole⁻¹²¹ and $\Delta H_f^\circ(\text{As}_2) = 53.1$ kcal. mole⁻¹,²² we obtain $\Delta H_f^\circ_{298}(\text{As}, {}^4\text{S}_{3/2}) = 72.0$ kcal. mole⁻¹. The latter value was combined with $\Delta H_f^\circ(\text{F}, {}^2\text{P}_{3/2}) = 18.9$ kcal. mole⁻¹,¹¹ and $\Delta H_f^\circ_{298}(\text{AsF}_5) = -295.6$ kcal. mole⁻¹ to give $\bar{D}(\text{As-F})_{\text{AsF}_5} = 92.4$ kcal. mole⁻¹ at 25°. An equation analogous to eq. 4 can be set up for $\bar{D}(\text{As-F})_{\text{AsF}_3}$. Taking $\Delta H_f^\circ(\text{AsF}_3, \text{g}) = -218.3$ kcal. mole⁻¹,²³ we obtain $\bar{D}(\text{As-F})_{\text{AsF}_3} = 115.7$ kcal. mole⁻¹. Thus the average bond strength in AsF_3 is about 20 kcal. mole⁻¹ greater than that in AsF_5 . A similar situation exists for the corresponding fluorides of phosphorus²⁴ and antimony.²⁵

Acknowledgments. The authors are grateful to Drs. H. M. Feder and Henry Mackle for helpful discussions. They are also indebted to Drs. E. H. Strain and W. Ross for the neutron activation analyses, and to Dr. R. P. Larsen for help in analytical matters. Thanks are due to Mr. G. K. Johnson for preparation and analysis of high-purity fluorine, and to Mr. J. L. Settle for checking the calculations.

(16) W. H. Evans, National Bureau of Standards, private communication.

(17) A. de Passillé, *Ann. chim. (Paris)*, [11]5, 83 (1936).

(18) A. E. Cameron and E. Wichers, *J. Am. Chem. Soc.*, **84**, 4175 (1962).

(19) F. D. Rossini, *Chem. Rev.*, **18**, 233 (1936).

(20) A. Glassner, "The Thermochemical Properties of the Oxides, Fluorides, and Chlorides to 2500°K.," Argonne National Laboratory, ANL-5750, 1957.

(21) H. J. Spangenberg, *Z. Chem.*, **3**, 315 (1963).

(22) J. Drowart and P. Goldfinger, *J. chim. phys.*, **55**, 721 (1958).

(23) F. D. Rossini, D. D. Wagman, W. H. Evans, S. Levine, and I. Jaffe, "Selected Values of Chemical Thermodynamic Properties," National Bureau of Standards Circular 500, U. S. Government Printing Office, Washington, D. C., 1952.

(24) P. A. G. O'Hare and W. N. Hubbard, to be published.

(25) N. Bartlett, "Chemistry in Canada," Chemical Institute of Canada, Ottawa, Can., Aug. 1963, p. 33.

A Least-Squares Method for Calculating Diffusion Coefficients for Ternary Systems

by R. L. Dunn and J. D. Hatfield

*Division of Chemical Development, Tennessee Valley Authority, Wilson Dam, Alabama
(Received August 2, 1965)*

A least-squares iterative method for determining Γ_n for n measurements of diffusion in a ternary system with the Gouy interferometer is described. The method minimizes the sums of squares of the differences between experimental and calculated relative fringe deviations. When $n > 2$, σ_+ , σ_- , θ_1 , and θ_2 are also determined by least squares which minimize the variances of calculated and experimental values of $1/\sqrt{D_A}$ and the quantity $(1/\sigma_-) - (1 - \Gamma_n)[(1/\sigma_-) - (1/\sigma_+)]$.

Several procedures¹⁻⁶ for calculating the four relevant diffusion coefficients that apply to isothermal diffusion in a ternary system were reviewed recently,⁶ and a general analytical method for their computation was described. Many of the earlier reported results have been recalculated⁷ by the analytical method.⁶ The earlier methods included simplifications that made the calculations practicable without high-speed computers. In one method,³ the calculation was simplified by restricting experiments to concentrations in which diffusion is gaussian—a serious limitation for ternary systems. Wendt⁸ has programmed the analytical method⁶ for the Bendix G-15 computer.

The analytical method of Fujita and Gosting⁶ requires a plot of the relative fringe deviations, Ω_j , against the reduced fringe number, $f(\zeta)$, from which the area, Q , is obtained. In this paper, a method is described that evaluates the Ω_j - $f(\zeta)$ curve from the most precise relationship available by the method of least squares. This obviates the somewhat subjective construction of the curve and permits a complete analytical treatment for the calculation of the diffusion coefficients by an IBM 704 computer.

Throughout this paper, the symbols have the meanings used in related publications.¹⁻⁶ Published equations are referred to by their numbers in the original reference; for example, eq. 23-1 refers to eq. 23 in ref. 1.

Method

The theory relating Gouy diffusiometer data to the

diffusion coefficients of ternary systems has been published by Gosting and his collaborators.¹⁻⁶

Here a method is described which yields the values of the quantities Γ_- , σ_+ , and σ_- , which minimizes $\Sigma(\Delta\Omega_j)^2$, and which, when more than two experiments are made at the same average concentration, minimizes $\Sigma[\Delta(1/\sqrt{D_A})]^2$ and $\Sigma(\Delta\sigma)^2$, where Δ denotes the difference between calculated and experimental values. In the method, the best fit of the experimental and calculated relative fringe deviations and reduced-height/area ratios are obtained simultaneously with determination of the best values for Γ_- , σ_+ , and σ_- . Values of the functions θ_1 and θ_2 and of the four diffusion coefficients are calculated by substituting values of the experimental quantities α_i (refractive fraction) and R_i (refractive index derivative) along with the best-fit values of Γ_- , σ_+ , and σ_- into eq. 25-2 and 26-2, and 30a-5, 31a-5, 51-5, and 64-5.

The least-squares treatments for calculating the dif-

(1) D. F. Akeley and L. J. Gosting, *J. Am. Chem. Soc.*, **75**, 5085 (1953).

(2) R. L. Baldwin, P. J. Dunlop, and L. J. Gosting, *ibid.*, **77**, 5235 (1955).

(3) P. J. Dunlop, *J. Phys. Chem.*, **61**, 994 (1957).

(4) P. J. Dunlop and L. J. Gosting, *J. Am. Chem. Soc.*, **77**, 5238 (1955).

(5) H. Fujita and L. J. Gosting, *ibid.*, **78**, 1099 (1956).

(6) H. Fujita and L. J. Gosting, *J. Phys. Chem.*, **64**, 1256 (1960).

(7) P. J. Dunlop, *ibid.*, **68**, 3062 (1964).

(8) R. D. Wendt, *ibid.*, **66**, 1279 (1962).

fusion coefficients for ternary systems are developed below.

Equations for Two Experiments. When the calculation is based on data from only two experiments at the same average composition, the expressions used to minimize the sum of the squares of the differences between the experimental and the calculated relative fringe deviations are obtained from the following equations. Here, and in all subsequent equations, all Γ 's are Γ_- , but the subscript minus sign is dropped for convenience.

$$\frac{1}{\sqrt{\mathcal{D}_A}} = (1 - \Gamma)\sqrt{\sigma_+} + \Gamma\sqrt{\sigma_-} \quad (55-5)$$

$$\Omega = e^{-t^2} - \frac{(1 - \Gamma)\sqrt{\sigma_+}e^{-\sigma_+y^2} + \Gamma\sqrt{\sigma_-}e^{-\sigma_-y^2}}{(1 - \Gamma)\sqrt{\sigma_+} + \Gamma\sqrt{\sigma_-}} \quad (A8-6)$$

where the value for Y_j/C_i of eq. A6-6 has been substituted in eq. A8-6.

Differences between calculated and experimental values of the relative fringe deviations are minimized by the least-squares method according to the equations

$$S_I = \sum_{i=1}^n [\Omega_{Ei} - \Omega_i]^2 \quad (1)$$

$$S_{II} = \sum_{k=1}^n [\Omega_{Ek} - \Omega_k]^2 \quad (2)$$

where Ω_i and Ω_k are calculated by eq. A8-6, i and k refer to experiments I and II, respectively, and the subscript E represents the experimental values of the relative fringe deviations.

Approximate values of Γ_i and Γ_k for experiments I and II can be obtained by any one of several published methods, such as the area method of Fujita and Gosting.⁶ These approximate values, Γ_{iA} and Γ_{kA} , are substituted in eq. 55-5 to obtain values of σ_+ and σ_- by solution of the two equations obtained from experiments I and II for which \mathcal{D}_A and Γ are different (eq. 55-5) and for which the σ values are constant.

The difference between the observed and calculated fringe deviations is now expressed approximately by⁹

$$\Delta_i = \Omega_{Ei} - \Omega_i = \Delta\Gamma_I\Omega'_{Ii} + \Delta\Gamma_{II}\Omega'_{IIi} \quad (3A)$$

$$\Delta_k = \Omega_{Ek} - \Omega_k = \Delta\Gamma_I\Omega'_{Ik} + \Delta\Gamma_{II}\Omega'_{IIk} \quad (3B)$$

where the primes are used to express the partial derivative, the first subscript of the Ω terms indicating with respect to which Γ (Γ_{IA} or Γ_{IIA}), and the second subscript of which Ω . For example

$$\Omega'_{Ii} = \partial\Omega_i/\partial\Gamma_{IA}$$

$$\Omega'_{IIi} = \partial\Omega_i/\partial\Gamma_{IIA}, \text{ etc.}$$

The terms $\Delta\Gamma_I$ and $\Delta\Gamma_{II}$ are corrections to the original estimates, Γ_{IA} and Γ_{IIA}

$$\Gamma_I = \Gamma_{IA} + \Delta\Gamma_I \quad (4A)$$

$$\Gamma_{II} = \Gamma_{IIA} + \Delta\Gamma_{II} \quad (4B)$$

The corrections are evaluated such that $\Sigma(\Delta_i^2 + \Delta_k^2)$ is minimized by

$$\begin{bmatrix} \Sigma(\Omega'_{Ii})^2 & \Sigma\Omega'_{Ii}\Omega'_{IIi} \\ \Sigma\Omega'_{Ik}\Omega'_{IIk} & \Sigma(\Omega'_{IIk})^2 \end{bmatrix} \begin{bmatrix} \Delta\Gamma_I \\ \Delta\Gamma_{II} \end{bmatrix} = \begin{bmatrix} \Sigma\Omega'_{Ii}\Delta_i \\ \Sigma\Omega'_{IIk}\Delta_k \end{bmatrix} \quad (5A)$$

$$\begin{bmatrix} \Sigma(\Omega'_{Ii})^2 & \Sigma\Omega'_{Ii}\Omega'_{IIi} \\ \Sigma\Omega'_{Ik}\Omega'_{IIk} & \Sigma(\Omega'_{IIk})^2 \end{bmatrix} \begin{bmatrix} \Delta\Gamma_I \\ \Delta\Gamma_{II} \end{bmatrix} = \begin{bmatrix} \Sigma\Omega'_{Ii}\Delta_i \\ \Sigma\Omega'_{IIk}\Delta_k \end{bmatrix} \quad (5B)$$

Equations 5A and 5B contain Γ , σ , and y terms and cannot be solved in the forms shown. It can be seen from eq. 55-5, however, that σ_+ , σ_- , $\partial\sqrt{\sigma_+}/\partial\Gamma$, $\partial\sqrt{\sigma_-}/\partial\Gamma$, and $\partial\Omega/\partial\Gamma$ can be expressed in terms of Γ_{IA} and Γ_{IIA} for experiments I and II, respectively. Values for y and $\partial y/\partial\Gamma$ for use in eq. 5A and 5B can be obtained from eq. A5-6 written in the form

$$f(y) = (1 - \Gamma_A)f(\sqrt{\sigma_+}y_A) + \Gamma_A f(\sqrt{\sigma_-}y_A) \quad (6)$$

where f is defined by

$$f(\xi) = \frac{2}{\sqrt{\pi}} \left[\int_0^\xi e^{-B^2} dB - \xi e^{-\xi^2} \right]$$

For example

$$\begin{aligned} \frac{\partial\Omega_i}{\partial\Gamma_{IA}} = & -\sqrt{\mathcal{D}_{AI}} \left\{ -\sqrt{\sigma_+} + (1 - \Gamma_{IA}) \frac{\partial\sqrt{\sigma_+}}{\partial\Gamma_{IA}} - \right. \\ & 2(1 - \Gamma_{IA})\sigma_+ \left(\frac{\partial\sqrt{\sigma_+}}{\partial\Gamma_{IA}} \right) y_i^2 - \\ & 2(1 - \Gamma_{IA})\sigma_+^{3/2} y_i \left. \frac{\partial y_i}{\partial\Gamma_{IA}} \right] e^{-\sigma_+ y_i^2} + \\ & \left[\sqrt{\sigma_-} + \Gamma_{IA} \frac{\partial\sqrt{\sigma_-}}{\partial\Gamma_{IA}} - 2\Gamma_{IA}\sigma_- \left(\frac{\partial\sqrt{\sigma_-}}{\partial\Gamma_{IA}} \right) y_i^2 - \right. \\ & \left. 2\Gamma_{IA}\sigma_-^{3/2} y_i \frac{\partial y_i}{\partial\Gamma_{IA}} \right] e^{-\sigma_- y_i^2} \left. \right\} \quad (7) \end{aligned}$$

$$\frac{\partial\sqrt{\sigma_+}}{\partial\Gamma_{IA}} = \frac{\Gamma_{IIA} \left[\frac{1}{\sqrt{\mathcal{D}_{AI}}} - \frac{1}{\sqrt{\mathcal{D}_{AII}}} \right]}{(\Gamma_{IIA} - \Gamma_{IA})^2} \quad (8)$$

$$\frac{\partial y_i}{\partial\Gamma_{IA}} =$$

$$\begin{aligned} & \left\{ [f(\sqrt{\sigma_+}y_i) - f(\sqrt{\sigma_-}y_i)] - (1 - \Gamma_{IA}) \times \right. \\ & \left. \frac{\left[\frac{\partial f(\sqrt{\sigma_+}y_i)}{\partial\sqrt{\sigma_+}} \right] \left[\frac{\partial\sqrt{\sigma_+}}{\partial\Gamma_{IA}} \right] - \Gamma_{IA} \left[\frac{\partial f(\sqrt{\sigma_-}y_i)}{\partial\sqrt{\sigma_-}} \right] \left[\frac{\partial\sqrt{\sigma_-}}{\partial\Gamma_{IA}} \right]}{(1 - \Gamma_{IA}) \frac{\partial f(\sqrt{\sigma_+}y_i)}{\partial y_i} + \Gamma_{IA} \frac{\partial f(\sqrt{\sigma_-}y_i)}{\partial y_i}} \right\} \quad (9) \end{aligned}$$

Equation 6 can be solved for y by Newton's method. Good starting values for y can be obtained from the exact equation

$$y = \frac{\sqrt{\mathcal{D}_A}}{\frac{1}{\zeta} + \frac{2}{\sqrt{\pi}} \frac{d\Omega}{df(\zeta)}} = \frac{\zeta \sqrt{\mathcal{D}_A}}{1 + \frac{2\zeta}{\sqrt{\pi}} \frac{d\Omega}{df(\zeta)}} \tag{10}$$

which is derived from eq. 9-5 and 34-1.

Equations 5A and 5B are solved simultaneously for $\Delta\Gamma_I$ and $\Delta\Gamma_{II}$. These incremental quantities are added to the values of Γ_A to yield improved values for Γ_I and Γ_{II} . The process is repeated with the improved values, and the iteration is continued until $\Delta\Gamma$ is less than 0.0001; three iterations usually are sufficient.

From the derived values for Γ , σ_+ , and σ_- , values for θ_1 and θ_2 for experiments I and II, respectively, are obtained by use of eq. 23 below. From eq. 25-2 and 26-2 and 30a-5, 31a-5, and 64-5

$$D_{11} = \frac{\frac{1}{\theta_2\sigma_+\sigma_-} + \theta_1 - \left[\frac{1}{\sigma_+} + \frac{1}{\sigma_-} \right] \theta_1}{1 - \frac{\theta_1}{\theta_2}} \tag{11}$$

$$D_{22} = \frac{1}{\sigma_+} + \frac{1}{\sigma_-} - D_{11} \tag{12}$$

$$\frac{R_2}{R_1} D_{21} = \theta_1 - D_{11} \tag{13}$$

$$\frac{R_1}{R_2} D_{12} = \theta_2 - D_{22} \tag{14}$$

If $(\alpha_1)_I = 1$ and $(\alpha_1)_{II} = 0$, the equation for D_{11} becomes

$$D_{11} = \frac{\frac{\Gamma_I}{\sigma_-} - \Gamma_{II}\theta_1}{\Gamma_I - \Gamma_{II}} \tag{15}$$

from which the values for D_{ij} can be calculated.

Equations for More Than Two Experiments. With data from more than two experiments, σ_+ and σ_- are best determined by least squares. If there are m such experiments, the quantity

$$S_{\mathcal{D}_A} = \sum_{l=1}^m \left[\frac{1}{\sqrt{\mathcal{D}_{AEI}}} - \frac{1}{\sqrt{\mathcal{D}_{AI}}} \right]^2 \tag{16}$$

is minimized where $1/\sqrt{\mathcal{D}_{AEI}}$ is experimental and $1/\sqrt{\mathcal{D}_{AI}}$ is calculated by eq. 55-5. The equations are

$$\begin{bmatrix} \sum_{l=1}^m (1 - \Gamma_l)^2 & \sum_{l=1}^m \Gamma_l(1 - \Gamma_l) \\ \sum_{l=1}^m \Gamma_l(1 - \Gamma_l) & \sum_{l=1}^m \Gamma_l^2 \end{bmatrix} \times \begin{bmatrix} \sqrt{\sigma_+} \\ \sqrt{\sigma_-} \end{bmatrix} = \begin{bmatrix} \frac{1 - \Gamma_l}{\sqrt{\mathcal{D}_{AI}}} \\ \frac{\Gamma_l}{\sqrt{\mathcal{D}_{AI}}} \end{bmatrix} \tag{17}$$

where Γ_l (that is, $\Gamma_I, \Gamma_{II}, \dots, \Gamma_m$) for each experiment is determined initially by the area method.⁶

Solution of eq. 17 and 18 gives the best values of σ_+ and σ_- for use in refining the values of Γ_l . As in eq. 5A and 5B, the equations for two, three, or four experiments are written in matrix form.

$$\begin{bmatrix} \Sigma(\Omega'_{Ii})^2 & \Sigma\Omega'_{Ii}\Omega'_{IIi} & \Sigma\Omega'_{Ii}\Omega'_{IIIi} & \Sigma\Omega'_{Ii}\Omega'_{IVi} \\ \Sigma\Omega'_{IIj}\Omega'_{IIj} & \Sigma(\Omega'_{IIj})^2 & \Sigma\Omega'_{IIj}\Omega'_{IIIj} & \Sigma\Omega'_{IIj}\Omega'_{IVj} \\ \Sigma\Omega'_{IIIk}\Omega'_{IIIk} & \Sigma\Omega'_{IIIk}\Omega'_{IIIk} & \Sigma(\Omega'_{IIIk})^2 & \Sigma\Omega'_{IIIk}\Omega'_{IVk} \\ \Sigma\Omega'_{IVl}\Omega'_{IVl} & \Sigma\Omega'_{IVl}\Omega'_{IVl} & \Sigma\Omega'_{IVl}\Omega'_{IVl} & \Sigma(\Omega'_{IVl})^2 \end{bmatrix} \times \begin{bmatrix} \Delta\Gamma_I \\ \Delta\Gamma_{II} \\ \Delta\Gamma_{III} \\ \Delta\Gamma_{IV} \end{bmatrix} = \begin{bmatrix} \Sigma\Omega'_{Ii}\Delta_i \\ \Sigma\Omega'_{IIj}\Delta_j \\ \Sigma\Omega'_{IIIk}\Delta_k \\ \Sigma\Omega'_{IVl}\Delta_l \end{bmatrix} \tag{19}$$

where

$$\Omega'_{Ii} = \partial\Omega_i/\partial\Gamma_{IA}$$

$$\Omega'_{IIj} = \partial\Omega_j/\partial\Gamma_{IIA}$$

$\Omega_i \dots i$ are functions of the corresponding $\Gamma_{IA} \dots IVA$; I ... IV and $i \dots l$ denote experiments 1 ... 4; and $\Delta_i \dots i = \Omega_{\text{obsd}} - \Omega_{i \dots i \text{ calcd}}$.

The matrix equations may be represented by $[X][Y] = [A]$, where $[X]$ is the square matrix and $[Y]$ and $[A]$ are the respective column matrices. For two or three experiments, the matrix equations are indicated by dotted and dashed lines, respectively. The total matrix equations are required for four experiments, and equations for more experiments can be written by expansion of those given.

Values of $\Delta\Gamma$ obtained from eq. 19 to 22 are added to the initial estimates of Γ (as in eq. 4A and 4B), and the improved values of Γ are used to obtain better values

(9) R. H. Moore and R. K. Zeigler, "The Solution of the General Least Squares Problem with Special Reference to High-Speed Computers," Los Alamos Scientific Laboratory (LA-2367), March 4, 1960; available from Office of Technical Services, U. S. Department of Commerce, Washington 25, D. C.

of σ_+ and σ_- by eq. 17 and 18. The process is repeated until the corrections to Γ are insignificant.

θ_1 and θ_2 are derived from the definition for Γ , eq. 51-5, where $\theta_1 = D_{11} + (R_2/R_1)D_{21}$ and $\theta_2 = D_{22} + (R_1/R_2)D_{12}$. Rearrangement of eq. 51-5 gives

$$\Gamma = \frac{\theta_1\alpha_1 + \theta_2(1 - \alpha_1) - (1/\sigma_+)}{(1/\sigma_-) - (1/\sigma_+)} \quad (23)$$

or

$$\theta_1(\alpha_1)_I + \theta_2[1 - (\alpha_1)_I] = \left[\frac{1}{\sigma_-} - (1 - \Gamma_I) \left(\frac{1}{\sigma_-} - \frac{1}{\sigma_+} \right) \right] \quad (24)$$

where $(\alpha_1)_I$ is α_1 of experiment I. Since there are m such experiments, and m equations like eq. 24, θ_1 and θ_2 are calculated by least squares from the normal equations

$$\begin{bmatrix} \sum_{i=1}^m (\alpha_{1i})^2 & \sum_{i=1}^m \alpha_{1i}(1 - \alpha_{1i}) \\ \sum_{i=1}^m \alpha_{1i}(1 - \alpha_{1i}) & \sum_{i=1}^m (1 - \alpha_{1i})^2 \end{bmatrix} \times \begin{bmatrix} \theta_1 \\ \theta_2 \end{bmatrix} = \begin{bmatrix} \sum_{i=1}^m W_i(\alpha_{1i}) \\ \sum_{i=1}^m W_i(1 - \alpha_{1i}) \end{bmatrix} \quad (25)$$

where W_i is the value of the right-hand side of eq. 24 for the i th experiment.

To calculate D_{ij} for a given composition of a ternary system, the refined values of Γ , σ , and θ are used in eq. 11 to 15, as was outlined for two experiments. The experimental and derived quantities required are the reduced-height/area ratio \mathfrak{D}_A , the experimental Gouy fringe deviations Ω_j , the differential refractivities R_1 and R_2 , the refractive fraction α_1 which is derived from the primary experimental data ΔC_1 , ΔC_2 , and J ,

and $f(\zeta)$, ζ , and $e^{-\zeta^2}$ which are calculated from J and Z_j .

As with other methods for calculating D_{ij} , it is desirable, and sometimes necessary, that the values of \mathfrak{D}_A at α_1 near 0 and at α_1 near 1 differ by several per cent, preferably by more than 10%. The importance of this requirement and its relationship to the accuracy required of the value of J are discussed in a companion paper.¹⁰

Previous methods¹⁻⁶ for calculating the diffusion coefficients depended upon graphs of relative fringe deviations that were drawn by hand through the average experimental Ω points. Despite the fact that the location of a curve is of utmost importance in the determination of the best values of the diffusion coefficients, probably no two men would draw the curve in exactly the same position. With the least-squares method the data are smoothed mathematically with the theoretical equation for the relative fringe deviation curve. This treatment gives the best possible agreement between the calculated and experimental relative fringe deviations and thus the best values for D_{ij} that can be derived from the experimental data. The performance of the method is illustrated in the treatment of experimental data in the companion paper.¹⁰

The Fortran program for processing experimental Gouy diffusimeter data with an IBM 704 computer to yield diffusion coefficients by the least-squares method is available at the TVA Computing Center, Chattanooga, Tenn. The program automatically tests the data for constancy of $y_j\sqrt{t}$, calculates $f(\zeta)$, ζ , Γ , Δt , C_i , \mathfrak{D}_A , and Ω_j and compares the values of Ω_j with the experimental values and determines the values of D_{11} , D_{22} , D_{12} , and D_{21} . The IBM 704 computer requires about 6 min. for these calculations with data from four experiments at a single average composition.

(10) O. W. Edwards, R. L. Dunn, J. D. Hatfield, E. O. Huffman, and K. L. Elmore, *J. Phys. Chem.*, in press.

Sedimentation Equilibrium in Reacting Systems of the Type $mA + nB \rightleftharpoons C$

by L. W. Nichol and A. G. Ogston

Department of Physical Biochemistry, John Curtin School of Medical Research, Australian National University, Canberra, A.C.T., Australia (Received August 4, 1965)

Equations are derived which permit the interpretation of sedimentation equilibrium results obtained with reacting systems involving two dissimilar reactants and a single complex. The use of the equations is outlined in evaluating the apparent equilibrium constant and the composition of the complex. The theoretical treatment applies to thermodynamically ideal situations, but its possible application to biologically important systems is discussed.

Data obtained in mass transport experiments may be used to determine the single equilibrium constant for the reaction $mA + nB \rightleftharpoons C$, provided (1) the system is thermodynamically ideal, (2) the complex ($C = A_mB_n$) is of known composition,¹⁻³ and (3) frictional effects do not complicate the experimental pattern.^{4,5} In view of the latter restriction, sedimentation equilibrium data are better suited for the determination of the equilibrium constant, and in this communication the necessary relations are derived to permit the evaluation when m and n are known. In addition, methods will be presented to determine the stoichiometry when m and n are unknown.

In previous treatments^{6,7} of sedimentation equilibrium of chemically reacting systems involving monomer and higher polymers, it has been shown that the distribution of each solute is unaffected by the chemical equilibrium between the species. The argument can be extended to show that this is true for any number of components in chemical equilibrium. This interesting property will be demonstrated for the present case in an alternative way. It will be assumed that the system is ideal in that the activity coefficient of each solute species equals unity, the system is incompressible, and that all density increments are equal. The latter assumption implies that there is no volume change on chemical reaction. For each solute, i ($i = A, B, \text{ or } C$), the condition for sedimentation equilibrium may be expressed by the differential equation⁸

$$\frac{d \ln c_i}{dr^2} = \frac{\omega^2(\partial\rho/\partial c_i)M_i}{2RT} = \phi M_i \quad (1)$$

where c_i is the concentration in grams per unit volume,⁸ r is the radial distance from the center of rotation, ω is the angular velocity of the rotor, M_i is the molecular weight, R is the gas constant, and T is the temperature. The partial differential, $\partial\rho/\partial c_i$ (at constant concentration of all other species) replaces the conventional $(1 - \bar{v}_i\rho)$ term⁹ and it is assumed to be identical for each solute. Accordingly, the single symbol, ϕ , suffices to describe the constant term in eq. 1. It is possible to integrate this equation between any two limits, *i.e.*, between r_1 , $c_i = c_i(r_1)$ and r_2 , $c_i = c_i(r_2)$, provided $r_m \leq r_1$ and $r_2 \leq r_b$, where r_m and r_b refer to meniscus and base of cell, respectively. It follows that

$$m \ln c_A(r_1) - m \ln c_A(r_2) = m\phi M_A(r_1^2 - r_2^2) \quad (2a)$$

$$n \ln c_B(r_1) - n \ln c_B(r_2) = n\phi M_B(r_1^2 - r_2^2) \quad (2b)$$

(1) L. G. Longworth in "Electrophoresis, Theory, Methods and Applications," M. Bier, Ed., Academic Press, New York, N. Y., 1959, p. 91.

(2) L. W. Nichol and D. J. Winzor, *J. Phys. Chem.*, **68**, 2455 (1964).

(3) L. W. Nichol and D. J. Winzor, *Biochim. Biophys. Acta*, **94**, 591 (1965).

(4) M. Davies, L. W. Nichol, and A. G. Ogston, *ibid.*, **75**, 436 (1963).

(5) L. W. Nichol and A. G. Ogston, *Proc. Roy. Soc. (London)*, submitted.

(6) E. T. Adams, Jr., and H. Fujita in "Ultracentrifugal Analysis in Theory and Experiment," J. W. Williams, Ed., Academic Press, New York, N. Y., 1963, p. 119.

(7) E. T. Adams, Jr., and J. W. Williams, *J. Am. Chem. Soc.*, **86**, 3454 (1964).

(8) T. Svedberg and K. O. Pedersen, "The Ultracentrifuge," Oxford University Press, London and New York, N. Y. (Johnson Reprint Corp., New York, N. Y.), 1940.

(9) E. F. Casassa and H. Eisenberg, *Advan. Protein Chem.*, **19**, 287 (1964).

$$\ln c_C(r_1) - \ln c_C(r_2) = \phi(mM_A + nM_B)(r_1^2 - r_2^2) \quad (2c)$$

By adding eq. 2a and 2b and subtracting eq. 2c we obtain

$$\frac{c_A(r_1)^m c_B(r_1)^n}{c_C(r_1)} = \frac{c_A(r_2)^m c_B(r_2)^n}{c_C(r_2)} = K \quad (3)$$

As the integration leading to eq. 3 may be performed between any limits, where the solute concentration is finite, the equation shows that, provided chemical equilibrium is attained at one point in the cell, it is attained at all others. The case under discussion reverts to a polymerizing system involving monomer and a single higher polymer (*cf.* Adams and Fujita⁶) by placing either m or $n = 0$.

As the distribution of each solute at equilibrium is independent of all others, eq. 1 may be rewritten and summed over all species.

$$c_i \frac{d \ln c_i}{dr^2} = \frac{dc_i}{dr^2} = \phi M_w c_i \quad (4)$$

$$\sum_i \frac{dc_i}{dr^2} = \phi \sum_i M_w c_i = \frac{\phi \sum_i M_w c_i \sum_i c_i}{\sum_i c_i} \quad (5)$$

$$\frac{d \ln \sum_i c_i}{dr^2} = \phi M_w \quad (6)$$

Thus, provided c_i is expressed in grams per unit volume, the weight-average molecular weight, M_w , at any point r may be found from the slope of the curve obtained by plotting $\ln \sum c_i$ against r^2 . In order to determine this by optical methods it must be assumed that the specific refractive increment is identical for each species. It might be advantageous to adopt the experimental technique devised by Yphantis,¹⁰ where conditions are chosen such that the total concentration near the meniscus is zero. Either Rayleigh interference or schlieren optics may be used: while the latter requires integration of the pattern to determine $\sum c_i$ at any r , it may permit higher concentrations to be examined by employing the available single sector centerpieces of small optical path.

The data collected from the above determinations apply to two equations

$$\sum_i c_i(r) = c(r) = c_A(r) + c_B(r) + c_C(r) \quad (7)$$

and

$$M_A c_A(r) + M_B c_B(r) + (mM_A + nM_B) c_C(r) = M_w(r) c(r) \quad (8)$$

Eliminating $c_C(r)$ between eq. 7 and 8 yields

$$c_A(r) [M_A - mM_A - nM_B] + c_B(r) [M_B - mM_A - nM_B] = c(r) [M_w(r) - mM_A - nM_B] \quad (9)$$

It will be assumed in what follows that M_A and M_B may be determined in separate experiments. In the simplest case, where m and n are known, eq. 9 contains two unknown quantities, $c_A(r)$ and $c_B(r)$, and cannot therefore be solved, despite the fact that it may be rewritten for r_1, r_2 , etc. However, eq. 2 may be rearranged in general form to give

$$c_i(r_1) = c_i(r_2) e^{\phi M_w (r_1^2 - r_2^2)} \quad (10)$$

Combination of eq. 9 and 10, which are valid for all r , gives

$$c_A(r_2) e^{\phi M_w (r_1^2 - r_2^2)} [M_A - mM_A - nM_B] + c_B(r_2) e^{\phi M_w (r_1^2 - r_2^2)} [M_B - mM_A - nM_B] = c(r_1) [M_w(r_1) - mM_A - nM_B] \quad (11a)$$

Also

$$c_A(r_2) [M_A - mM_A - nM_B] + c_B(r_2) [M_B - mM_A - nM_B] = c(r_2) [M_w(r_2) - mM_A - nM_B] \quad (11b)$$

Equations 11a and 11b provide two simultaneous equations in two unknown quantities and may be solved to obtain $c_A(r_2)$ and $c_B(r_2)$. In turn, from eq. 7, $c_C(r_2)$ may be evaluated. As m and n are known (which has been assumed for the present case), K may be found at r_2 from eq. 3. In a similar way it may be found at any r . It is clear, however, from numerical example that measurements made near the bottom of the cell in a Yphantis experiment¹⁰ are most useful because, with suitable choice of conditions, in this region all three species coexist in appreciable amounts.

In the general case, where m and n are unknown, two additional and independent relations (besides eq. 11a and 11b are required to solve for the four unknown quantities. One equation follows from a knowledge of the initial amounts of A and B (in grams) added to form the reaction mixture contained in the cell: these amounts are termed Q_A and Q_B , respectively.

$$Q_A = \theta b \int_{r_m}^{r_b} r c_A(r) dr + \theta b \int_{r_m}^{r_b} r \alpha c_C(r) dr \quad (12a)$$

$$Q_B = \theta b \int_{r_m}^{r_b} r c_B(r) dr + \theta b \int_{r_m}^{r_b} r \alpha' c_C(r) dr \quad (12b)$$

(10) D. A. Yphantis, *Biochemistry*, **3**, 297 (1964).

where θ is the sector angle in radians, b is the cell thickness, $\alpha = mM_A/mM_A + nM_B$, and $\alpha' = nM_B/mM_A + nM_B$. The terms involving $c_C(r)$ may be eliminated by multiplying eq. 12a by nM_B , eq. 12b by mM_A , and subtracting the resulting expressions. This provides a single equation which may be integrated by using eq. 10 to give

$$\frac{nM_B Q_A - mM_A Q_B}{\theta b} = \frac{nM_B c_A(r_b) e^{-\phi M_A r_b^2}}{2\phi M_A} (e^{\phi M_A r_b^2} - e^{\phi M_A r_m^2}) - \frac{mM_A c_B(r_b) e^{-\phi M_B r_b^2}}{2\phi M_B} (e^{\phi M_B r_b^2} - e^{\phi M_B r_m^2}) \quad (13)$$

Equation 13 may be rewritten using eq. 10 in terms of $c_A(r_2)$ and $c_B(r_2)$, and this together with eq. 11a and 11b gives three simultaneous equations in the unknown quantities, $c_A(r_2)$, $c_B(r_2)$, m , and n .

One procedure, permitting an approximate solution, is to assume a value for (say) m and thereby compute K at r_2 : reiterating the process at other values of r would permit a test of the assumed m value on the basis of constancy of K at various r values (and hence at different total concentrations). It is important to note that, although eq. 13 requires the determination of r_b by using an inert base fluid, it is not necessary to determine M_w at r_b . Alternatively, the problem may be approached by applying the fourth simultaneous equation.

$$\lim_{\sum c_i \rightarrow \infty} M_w = mM_A + nM_B = M_C \quad (14)$$

As the above equations assume thermodynamic ideality, it is hazardous to apply them in their simple form to results obtained at relatively high concentration. Accordingly, it would be necessary to extrapolate values of M_w found at relatively low concentrations to determine the molecular weight of the complex, M_C ; no theory is available at the present time to guide this extrapolation.

In summary, it is possible to use sedimentation equilibrium data to determine K for the reaction specified if one or both values of m and n are known. Two methods have been suggested to determine K , m , and n in the general case. The above theory could be elaborated to include effects due to nonideality or to a difference in $\partial\rho/\partial c_i$ for the different solute species. This would introduce several more quantities, which in general are extremely difficult to evaluate for biological systems. In addition, it is clear that a system involving several complexes of different composition cannot be treated by the present method. Additional information, such as the determination of the concentration distribution of a single species using absorption optics or a statistical approach may prove fruitful in these more complicated cases. Nevertheless, in several reacting systems of biological interest a single complex has been postulated^{2,3,11} and it is with these systems that the present treatment may find application.

(11) L. W. Nichol, J. L. Bethune, G. Kegeles, and E. L. Hess in "The Proteins," 2nd Ed., H. Neurath, Ed., Academic Press, New York, N. Y., 1964, p. 305.

Spectral Changes in a Cationic Dye Due to Interaction with Macromolecules.

III. Stoichiometry and Mechanism of the Complexing Reaction¹

by R. C. Bean, W. C. Shepherd, R. E. Kay, and E. R. Walwick

*Applied Research Laboratories, Aeronutronic Division, Philco Corporation, Newport Beach, California
(Received July 1, 1965)*

The stoichiometry of the reaction of 4,5,4',5'-dibenzo-3,3'-diethyl-9-methylthiacarbocyanine (DBTC) with diverse polyionic macromolecules has been investigated. Five different complex states have been observed, with corresponding spectral characteristics. The complex states and corresponding approximate spectral band maxima are: α state (570 m μ), β state (535 m μ), γ state (500–510 m μ), J state (620 to 650 m μ), β_a state (550 m μ , a hybrid or mixture), and the S state (470 m μ). For optimal reaction, a one-to-one ratio of dye to anion site on the polymer is generally required in the formation of the α , β , β_a , and J states. Little or no shift of spectral maxima for the complexes occurs with large ratios of sites to dye molecules. Titration data indicate that the J state arises through reaction of individual DBTC molecules with particular sites as a function of dye configuration and conformation to the site rather than being due to dye-dye interaction in a very large aggregate of dye molecules as previously supposed. The primary influence in formation of the α and β states may also be the conformation of the dye to the site and polymeric matrix, but dye-dye interaction may still occur. The γ complex is frequently transitory and may arise through simple adsorption of the dye from solution without altering the state of dye aggregation as it existed in solution. Effect of pH on the complexing reactions was minimal except with amphoteric macromolecules such as proteins. Apparently, cationic groups in the vicinity of the anionic complexing sites may become positively charged at low pH and repel the cationic dye. Variations of pH which should cause many magnitudes of change in the ratio of ionized and un-ionized carboxyl groups cause no changes in the stoichiometry of the complex reactions indicating that ionization is not a critical factor in formation of the complex.

Introduction

The metachromatic color changes of dyes, which result from interaction of the dye with ionic macromolecules, have long been of interest in histochemistry. The mechanisms for these metachromatic reactions have been under study for three decades, but much confusion still remains as to the nature of the reactions. Recent hypotheses, based on dye-dye interactions upon the polymeric matrix,²⁻⁴ seem to account satisfactorily for the relatively simple reactions of some dyes such as acridine orange. However, a dye such as 4,5,4',5'-dibenzo-3,3'-diethyl-9-methylthiacarbocyanine bromide (DBTC)⁵ reacts with polymeric anions to form at least five different and discrete complex states.^{6,7}

Such a complicated series of reactions has always been difficult to accommodate under the simple aggregation

(1) This work was supported by the National Aeronautics and Space Administration under Contract No. NASw-770.

(2) D. F. Bradley and M. K. Wolf, *Proc. Natl. Acad. Sci. U. S.*, **45**, 944 (1959).

(3) M. K. Wolf and D. F. Bradley, *Stain Technol.*, **35**, 44 (1960).

(4) A. L. Stone and D. F. Bradley, *J. Am. Chem. Soc.*, **83**, 3627 (1961).

(5) Abbreviations used in this paper include: DBTC, 4,5,4',5'-dibenzo-3,3'-diethyl-9-methyl-thiacarbocyanine; P, polymer anion site; D, dye molecule; RNase, ribonuclease; DNA, deoxyribonucleic acid.

(6) R. E. Kay, E. R. Walwick, and C. K. Gifford, *J. Phys. Chem.*, **68**, 1896 (1964).

(7) R. E. Kay, E. R. Walwick, and C. K. Gifford, *ibid.*, **68**, 1907 (1964).

theories previously advanced,^{2,3,8-10} and the studies presented below now demonstrate, unequivocally, the inadequacy of some of these theories as applied to the reactions of DBTC.

In particular, the concept of the complex which creates an intense, narrow absorption band (J band) at a longer wave length than that of the monomeric dye has had to be revised on the basis of these studies. This J band was previously thought to arise from interaction of dye molecules in a large aggregate of the dye, either as a nematic crystal or on a polymer matrix or micellar structure.^{6,7,9-11} It now appears the J band formed by the reactions of the dye with polymers is more likely to be due to reaction of individual dye molecules at isolated sites. This is more coincident with the original concept of Jelley,^{12,13} for whom this band was named, since he also considered it to be a molecular spectrum even in the nematic crystals.

In addition, it appears desirable to assume that the spectra of some of the other complex states may be caused by specific interaction of the dye with the polymer rather than by dye-dye interactions between adjacent dye molecules on the polymer. The more vital role of the polymer in the formation of the complexes may be further supported by the discovery that some of the dye-polymer complexes are almost completely independent of pH, suggesting that their formation is dependent upon forces other than the simple attraction of the negative anion site for the cationic dye.

Materials and Methods

Thiacarbocyanine Dye. Two samples of the dye, DBTC, were gifts of F. W. Mueller, Ansco, and J. A. Leermakers, Eastman Kodak Co. All operations during the preparation of the stock solutions ($1.2 \times 10^{-4} M$) were carried out in the dark or in minimal light to avoid photodecomposition of the dye. Stock and diluted working solutions were stored in brown polyethylene bottles, wrapped in aluminum foil, since the dye is readily adsorbed upon glass.

Biopolymers. We are indebted to K. Wilson and C. Smit, of Sunkist Corp., for the special pectin and polygalacturonic acid samples used in these studies. Their uniform methoxylpectin fractions (7.0, 9.4, 10.8, and 11.2% methoxyl) were isolated by ion-exchange fractionation of natural citrus pectin. Samples with enriched methoxyl (above 11.3%) were obtained by chemical esterification of citrus pectins, either by methylation with diazomethane or by acid-catalyzed esterification in methanol.

Methyl alginate was prepared by acid-catalyzed esterification of alginic acid. The alginic acid and

sodium alginate were purified from a commercial sodium alginate (Matheson Coleman and Bell) by repeated solvent precipitation.

Other preparations were obtained from commercial sources as follows: poly-L-glutamic acid, sodium salt, and poly-L-aspartic acid from Sigma Chemical Co.; bovine pancreas ribonuclease (5 times crystallized, salt free), oxidized ribonuclease, and poly-L-lysine hydrobromide from Mann Research Laboratories; bovine albumin (crystalline), protamine sulfate (clupeine), glycoprotein, human hemoglobin (2 times crystallized), and horseheart myoglobin from Nutritional Biochemicals Corp.; deoxyribonucleic acid, highly polymerized, α -chymotrypsin (3 times crystallized), pepsinogen, α -chymotrypsinogen, pepsin (2 times crystallized) from Worthington Biochemicals Corp.; chondroitin sulfate (sodium salt), hyaluronic acid (potassium salt), and polygalacturonic acid, from California Corp. for Biochemical Research; sodium polymetaphosphate, average degree of polymerization 18.5, from Victor Chemical Works.

Buffers. The spectra of the dye and its complexes are affected by high ionic strength so buffers were used at 0.001 to 0.002 *M* final concentration, unless otherwise specified. At such concentrations, none of the normal organic buffering anions had significant effect, and so it was possible to choose the most convenient buffer for obtaining the desired pH.

Titration Procedure. The following procedure was utilized for all titrations reported here. An appropriate portion of the biopolymer solution, the buffer, and sufficient water to make a standard volume were mixed in a spectrophotometer cuvette. The dye was then added, the solution mixed, and the absorption spectrum determined by scanning from 700 to 400 $m\mu$ in a Beckman DK-2A recording spectrophotometer. For each titration point, a new mixture was prepared at a different polymer concentration. It was not possible to titrate by addition of successive increments of the macromolecule⁴ since some titrations would not be reproducible, possibly as a result of formation of anomalous complexes. In some instances, to permit full equilibration, the final scan was delayed 5 to 10 min. following the addition of the dye. The dye concentration in the mixture was normally 10^{-5} or $2 \times 10^{-5} M$, but in some of the experiments, where it

(8) G. Scheibe, *Kolloid-Z.*, **82**, 1 (1938).

(9) G. Schiebe, *Angew. Chem.*, **50**, 212 (1937).

(10) G. Scheibe and V. Zanker, *Acta Histochem., Suppl.*, **1**, 6 (1958).

(11) S. E. Sheppard, *Rev. Mod. Phys.*, **14**, 303 (1942).

(12) E. E. Jelley, *Nature*, **139**, 631 (1937).

(13) E. E. Jelley, *ibid.*, **138**, 1009 (1936).

was desirable to have extremely large excesses of polymer sites, lower concentrations of dye were used. At the normal concentrations, the absorption peak maximum of the aqueous dye was at 508 $m\mu$, but at lower concentrations the peak shifted as much as 15 $m\mu$ toward longer wave lengths.

The stoichiometry of the reaction was determined from a plot of the decrease in absorbancy at 508 $m\mu$ against the P/D ratio, the molar ratio of macromolecule anion sites to dye molecules. In most cases, the initial points formed a straight line with a definite break as sites began to exceed available dye molecules (see Figure 1), and only slight interpolation was required for accurate determination of the equivalence values. Similar results could be obtained, in some instances, by plotting the change in absorbance at the band maximum for the dye-macromolecule complex. In some cases, the plots were curvilinear, indicating a higher dissociation constant for the complex. In such cases, the equivalence values were estimated as the value at the intersection of the straight line tangential to the curve at $P/D = 0$, with the straight line tangential to the curve at high P/D ratios.

Experimental Section

Upon titration of the dye with a polyanion molecule, at constant dye concentration, the absorption spectrum of the reaction mixture progressively changes with increasing P/D ratio until an equivalence point (usually at $P/D = 1$) is reached. After this point, little or no further change occurs, except in a few instances where extremely high ratios induce shifts toward new bands. As an example, the titration curve for the dye reaction with polyadenylic acid is shown in Figure 1. Titration with different macromolecules results in a number of distinct, stable spectral bands, each apparently characteristic of a certain type of complex. The various spectral bands obtained with the complexes are illustrated in Figure 2. Sheppard¹¹ designated several spectral bands of free dye as α , β , and γ , in order of decreasing wave length. The α band is given by the monomeric form of the dye while the other bands occur with some degree of dye aggregation. These designations have been retained for the free-dye bands at 575 $m\mu$ (α), 535 $m\mu$ (β), and 500–510 $m\mu$ (γ) and for the corresponding bands of dye-polymer complexes. Reference to the band at 650 $m\mu$ as a J band also follows Sheppard's terminology for the complex state. The sharp, intense band in the region of 470 $m\mu$, arising under special circumstances, does not correspond to previously described bands nor to known states of the free dye and has been termed, for convenience, the S band (short wave length band).

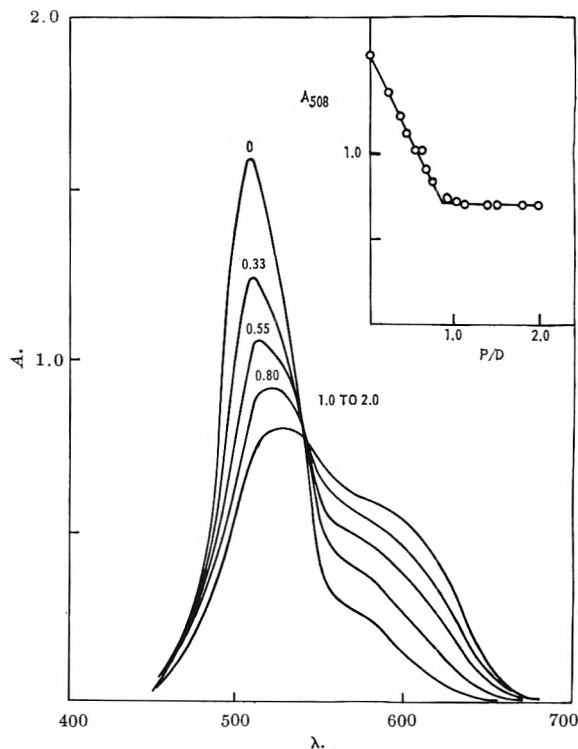


Figure 1. Titration of DBTC with polyadenylic acid. DBTC at $2 \times 10^{-5} M$. Titration procedure as in text. Buffered at pH 6.4 with sodium cacodylate, 0.001 M . Numbers on the curves indicate P/D ratio. A_{508} is absorbance at 508 $m\mu$.

A seemingly discrete state with an absorption band at 550 $m\mu$ is frequently found. Although the manner of transition from the aqueous dye to the complex producing the 550- $m\mu$ peak is characteristic of a change to a unique energy state, several pieces of experimental evidence suggest that this band may be either a hybrid or mixture of the α and β bands. It will be designated here as the β_a band. A similar hybrid in the 600- $m\mu$ region will be called the α_J band. Depending upon conditions (*e.g.*, pH and temperature) and the particular polymer associated with the dye, the bands may vary somewhat in position of maximum and in peak heights. However, they generally remain characteristic enough so that they can be considered to represent one of the complex states indicated above.

Formation of the Stoichiometric Complexes. The α State. The 570- $m\mu$ α band is formed when the dye reacts with polygalacturonic acid, alginic acid, native DNA, or follicle-stimulating hormone (Table I). The 570- $m\mu$ band is also found as a second band with a number of polymers which interact with the dye to form more than one band. The complex with polygalacturonic acid has a P/D ratio near unity; that with alginic acid requires a ratio of two sites per dye molecule; the P/D for the DNA stoichiometric complex

Table I: Summary of Complexing Reactions of DBTC with Various Macromolecules

Macromolecule	Type of complex ^a	γ_{max} , m μ	P/D ^b	Polymer equiv. weight ^c	Conditions
α group					
DNA, native	α	560-572	0.96		pH 7.0
Polygalacturonic acid	α	565	0.80		pH 7.0
Alginic acid	α	568	2.10		pH 8.2
Heparin, desulfated	α	565			pH 8.6
Follicle-stimulating hormone	α	570		9000	pH 7.2
β group					
Polyadenylic acid	β	528-530	0.98		pH 5-9
Polyaspartic acid	β	535	1.18		
DNA, denatured	β	535	1.04		
Polymetaphosphate	β	535-538	1.24		pH 1.5-10
Heparin	β	535	2.6		pH 7.6
γ group					
Albumin, bovine	γ	490-500			pH 8
Albumin, human	$\gamma \rightarrow J^d$	500 \rightarrow 500 + 650 ^d			
Hemoglobin	γ	495-505		1670	pH 8.6
Pepsin	$\gamma \rightarrow J$	500 \rightarrow 500 + 660 ^d		<3500	
Myoglobin	$\gamma \rightarrow J$	490 \rightarrow 490 + 650 ^d	(<4/10)	<3500	pH 7
Pepsinogen	$\gamma \rightarrow J$	508 \rightarrow 508 + 650 ^d			
Trypsin	$\gamma \rightarrow J$	508 \rightarrow 508 + 630 ^d			
Chymotrypsinogen	γ	508			pH 7.0
	$\gamma \rightarrow \alpha$	508-570	(5/13)	4500	pH 8.6
Polyglutamic acid	γ	502-510			pH <4
β_a group					
Polyglutamic acid	β_a	550	0.92		pH >4
Polyuridylic acid	β_a	545-560	1.06		pH 8
Chondroitin sulfate	β_a	555	0.98		
Alginic acid	β_a	552	1.04		
Alginic acid, 2/3 methyl ester	β_a	552	0.25		pH 8
Glycoprotein	β_a	548		1000	
Heparin, desulfated	β_a	552	1.0		pH 7-9
	αJ	605			pH 4.8
J group					
Pectin, 10.8 or 11.3% methoxyl (67% ester)	J	640	1.08, 0.98		pH 4-10
Pectin, 9.4% methoxyl (56% ester)	J	640	1.02		pH 4.8
Pectin, 7.0% methoxyl (41% ester)	J + α	615	1.2		pH 4-9
Pectin, 4.3% methoxyl (24% ester)	J + α	613			
Pectin, 13.3% methoxyl	J, α , γ	640, 570, 525	5.0		
Hyaluronic acid	J	635	2.28		pH 2-10
Ribonuclease, native	J	650	(7.3)	4500	pH >10
Ribonuclease, oxidized	J	650	(16/6)	3000	pH 5-10
Protamine sulfate	J, α , γ	655, 575, 525		560	pH >10
Glutamylglycine, thermal co- polymer	J	650		8000	pH 7.0
Gelatin	J	650		6700	pH 6.8
For other proteins in J group, see ref. 5					
S group					
Poly-L-lysine	S	470	40		pH >10
Polymetaphosphate + ZnCl ₂	S, β	475, 535			Large excess of sites

^a Designation of complex states follow the terminology in the text and as shown in Figure 2. ^b P/D is the experimental ratio of macromolecule anion sites to dye molecules required for the stoichiometric reaction to produce the indicated complex. Determined by the methods outlined in the text. The fractions in parentheses indicate the apparent ratios of titratable anion sites of proteins to dye in the complexes. ^c Polymer equivalent weight is the weight of the macromolecule required for reaction with one mole of dye. This is used in place of P/D for systems where the number of available sites may not be well defined. ^d Arrow indicates a time-dependent transition from the initial γ complex to the indicated final complex system.

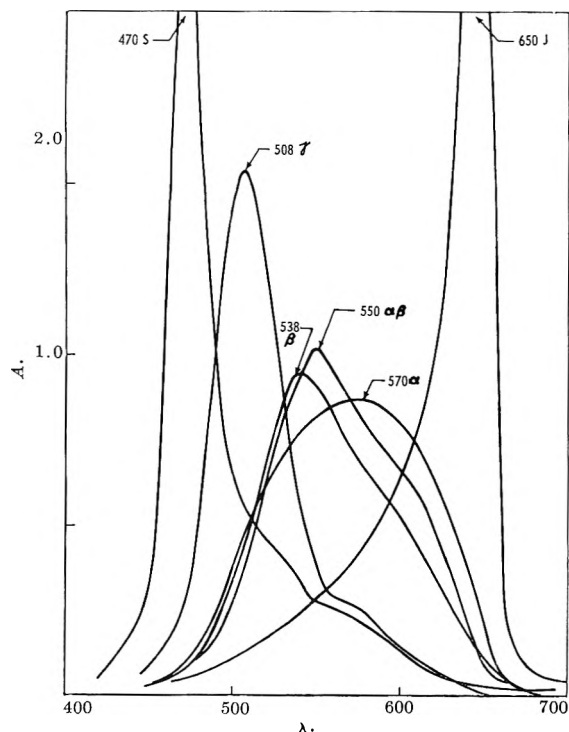


Figure 2. Examples of the DBTC-polyanion complex spectra. Spectra were obtained at stoichiometric reactions (except the 508- $m\mu$ peak) of dye and macromolecules. The 508- $m\mu$ curve (γ state) is that for chymotrypsinogen but is essentially identical with that for the aqueous dye at $2.0 \times 10^{-5} M$. The 470- $m\mu$ curve, S state, is for poly-L-lysine; the 538- $m\mu$ curve (β state) is for polyaspartic acid; the 550- $m\mu$ curve (β_a state) is for polyglutamic acid; the 570- $m\mu$ curve (α state) is for follicle-stimulating hormone; the 650- $m\mu$ (J state) is for pectin (10.8% methoxyl, fractionated sample).

is also unity as illustrated in Figure 3. Although the free-dye monomer and the α complex both have their peak maxima at the same wave length, the α -complex band is much weaker and more diffuse.

The β State. This band is formed upon reaction with such diverse polymers as polyadenylate, polyaspartate, polyphosphate, heparin, and denatured DNA. The P/D ratios required for complete reaction are close to unity for all of these except heparin, which shows a P/D ratio of 2.6 at full titration. Thus, all of the macromolecules which react with the dye to give a β band are characterized by relatively close spacing of the anionic groups on the polymer. The titration with polyadenylate, Figure 1, is characteristic of this group.

The γ State. The γ state in a complex is not always easy to demonstrate unequivocally. However, there are certain obvious cases which show that this state

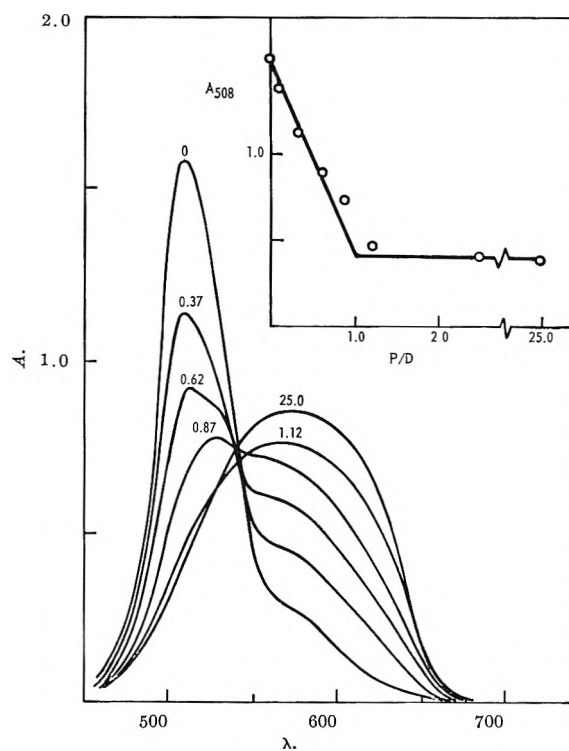


Figure 3. Titration of DBTC with native DNA. DBTC at $2 \times 10^{-5} M$. Titration procedure as in text. DNA solution 0.025% in DNA and $10^{-8} M$ in $MgCl_2$ was used in this titration. The reactions were buffered at pH 7.0 with 0.005 M cacodylate buffer. Numbers on the curves indicate P/D ratios.

may occur because of reaction of the dye with a polymer. Thus, as shown in Table I, addition of myoglobin, bovine albumin, human albumin, hemoglobin, or pepsin to the dye causes the peak to shift slightly to shorter wave lengths. In addition, numerous proteins, which do not cause a wave length shift, do create a drop in the absorbance of the band with a slight broadening of the peak. It can also be demonstrated, in several of these cases, that the dye is more stable to heat, light, and extremes of pH, than the free dye, which indicates that there is an interaction between the dye and the polymer. For example, at pH 2 the dye alone changes rapidly to a pale yellow color, but in the presence of polyglutamate the color remains stable, while the maximum shifts slightly to 502 $m\mu$. However, many of the γ -state complexes are apparently not entirely stable, and a slower reaction ensues, creating a shift to one of the more stable systems, as indicated in the data in Table I.

The β_a State. The β_a state is formed upon reaction of the dye with polyuridylic acid, chondroitin sulfate, polyglutamic acid, alginic acid (at P/D = 1), methyl alginate, and glycoprotein. The titration with polyuridylic acid (Figure 4) illustrates the formation of

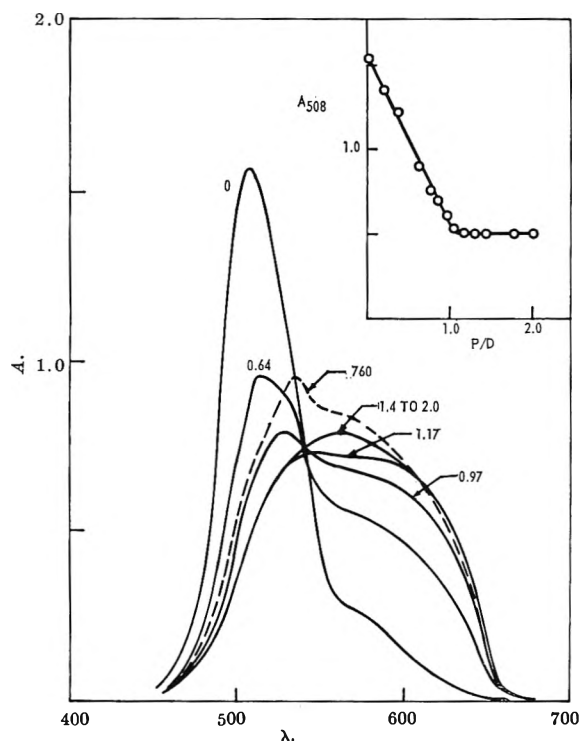


Figure 4. Titration of DBTC with polyuridylylate. DBTC at $2 \times 10^{-5} M$, buffered at pH 6.4 with cacodylate, 0.016 M . Numbers on curves indicate P/D ratios.

the β band. However, titrations to higher P/D ratios cause opposing changes in two of the β complexes. An increase to P/D = 2 with alginic acid causes a shift to the α band, while polyuridylylate ratios in excess of 200 cause shifts toward the β band. The characteristic β band may be reproduced by the reaction of some samples of partly denatured DNA. This band is obviously a mixture of the α band of native and β band of denatured DNA. Thus, the existing evidence seems to suggest that the 550- μ m band is a hybrid or mixture of the α and β states.

The J State. The unique spectrum of the J state is found, unequivocally, for such materials as pectin (degree of methylation more than 66 or 10.8% methoxyl content), hyaluronic acid, a number of proteins (oxidized ribonuclease will be the primary example), protamine (at higher pH), and a thermal polymer of glutamic acid and glycine. Pectin (Figure 5) and hyaluronic acid have been the only relatively uncomplicated molecules upon which to base stoichiometric studies. Pectins which are less than two-thirds methylated (10.8% methoxyl) also show an α component (Table I), but the reaction is complete at a P/D ratio of unity regardless of whether a pure J or an α plus J state is exhibited. However, in the hyaluronic acid reaction the dye apparently occupies only alternate sites (P/D = 2.3). The proteins have a reaction equivalent

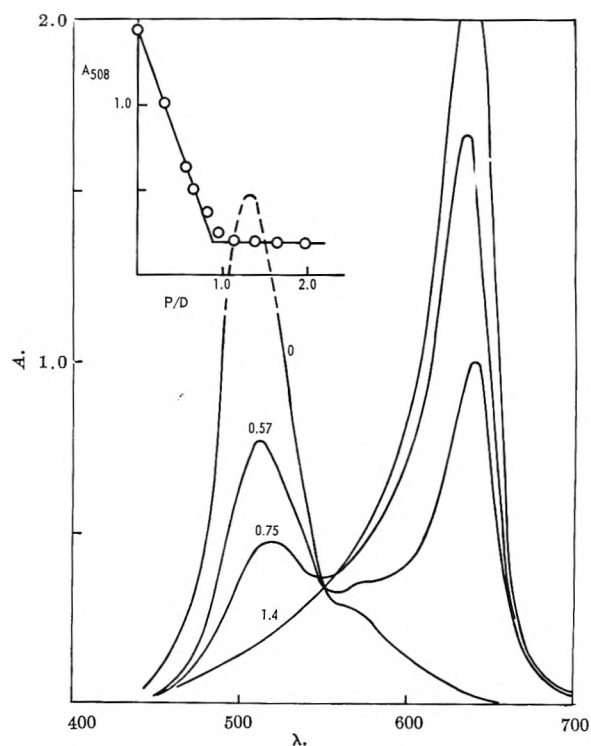


Figure 5. Titration of DBTC with pectin (10.8% methoxyl). DBTC at $2 \times 10^{-5} M$; solutions buffered at pH 4 with 0.001 M succinate. Numbers on curves indicate P/D ratios.

weight varying from about 2000 to 8000 per dye molecule (grams of protein per mole of dye), which varies rather widely with pH in some cases and with other environmental factors. It is difficult to determine, for proteins, the actual number of available anion sites since many of the carboxyl groups may be masked. Native ribonuclease reacts with the dye to give a J band only at a pH above its isoionic point. The native RNase contains eight carboxyl groups, and the titration requires only three to five dye molecules per molecule of RNase. The oxidized RNase, with eight cysteic acid residues added to the original carboxyls, requires between five and six dye molecules per molecule of RNase.

The S State. The S complex is an interesting but poorly defined state. It is found upon titration of the dye with polylysine hydrobromide, at a pH greater than 10, and as a secondary band in a number of other instances. It can also be produced with polymers which normally form other bands through the influence of specific cations at high P/D ratios, e.g., mixtures of $ZnCl_2$, at $10^{-3} M$, with polymetaphosphates. It also appears upon reaction with certain anions, such as borate, at high pH. The extent of the polylysine reaction is also dependent upon pH, with a greater reaction occurring as the pH increases beyond the initial

reaction point. This reaction is also inefficient with regard to the number of polymer sites required. Thus, about 40 polylysine residues are needed for each dye to obtain complete reaction at pH 11, and many more at pH 10.5. This suggests that the 470-m μ band may arise as a consequence of a complex among the cationic site on the polymer, hydroxyl ion (or other ion), and the dye.

Changes in Spectra Induced by High-Anion Site to Dye Ratios. As the P/D ratio is increased from zero to unity in the reaction of acridine orange with polymers, this dye demonstrates a hypsochromic shift to the β band. As the P/D ratio is still further increased, there is generally a tendency for the absorption spectrum to return to that of the monomeric dye, namely, the α band. It has been proposed^{2,3} that the β band, for acridine orange, is due to dye-dye interaction in a closely packed sequence of dye molecules on the polymeric matrix. As the ratio of sites to dye molecules becomes increasingly large, the dye molecules may then become randomly distributed at widely spaced, noninteracting sites, giving rise to the spectral characteristics of the monomeric dye. Since the number of excess sites required to promote this latter shift varies widely for different polymers, Bradley introduced the concept of the "stacking coefficient," which is the measure of the apparent tendency for dye molecules in the presence of excess sites to occupy sites adjacent to other dye molecules in preference to other available sites.

Previously,^{6,7} it has also been assumed that the α complex of DBTC with polymers is a monomer equivalent, while the β , β_a , and J complexes all involved some degree of dye-dye interaction. One would then expect that very high ratios of sites to DBTC would also cause some degree of shifting toward the α -complex spectrum in analogy to the acridine orange reactions. This hypothesis has been tested in a number of instances with DBTC (Table II).

Among the reactions tested, one, alginic acid, shifts from the β complex to the α complex at a low ratio (2:1). However, at still higher ratios (34:1) there is evidence for a shift back toward the shorter wave lengths, and the spectra show the presence of a γ component. The polyphosphate band also shifts in the expected direction, from a pure β band at 535 m μ to one with a significant α component having a maximum at 556 m μ . However, this only occurs at very high ratios, a ratio of 31,000 being required for the maximum shift. Further increases in P/D ratios produce no further changes.

Polyuridylic acid, at high ratios, shows an inverse shift, toward the β complex (see Figure 4, dashed curve).

Table II: Characteristics of the DBTC-Macromolecule Complexes at High P/D Ratios

Macromolecule ^a	P/D	λ_{\max} , m μ	pH
Polyadenylate (530)	10	530	7.0
	250	530	7.0
	708	533	7.0
Polyuridylyate (550)	28	550	7.0
	280	540	7.0
	765	535	7.0
Polyaspartate (535)	11	536	8.6
	20	538	7.0
	50	538	7.0
Polyglutamate (550)	10	550	8.6
	32	547	7.0
	480	547	7.0
Deoxyribonucleic acid (570)	11.5	570	7
	57	573	7
	115	574	7
	230	575	7
Pectin, 10.8% methoxyl (645)	11	655	5.0
	500	635, 595	5
	1,580	555, 635	5
Pectin, 7.0% methoxyl (590)	10	570	5.0
	330	595, 640	5
Polygalacturonic acid (565)	26	570	7.0
	53	560	7.0
Polymetaphosphate (535)	20	535	
	80	540	
	825	542	
	1,650	543	
	16,500	551	
	31,500	555	
80,000	555		
225,000	552		
Alginic acid	1.0	552	8.6
	2.1	575	8.6
	17	570	8.6
	34	564	8.6
	100	560	8.6

^a Figures in parentheses indicate λ_{\max} of the normal stoichiometric complex.

Pectin spectra also vary with P/D ratios. Pectins of relatively low methoxyl content show definite increases in a J-band component at high ratios (counter to the hypothesis), but the higher methoxyl samples (10.8% methoxyl), which demonstrate pure J bands at stoichiometric levels, acquire an α component at P/D ratios varying from 58 to 1580. None of the other complexing reactions tested showed significant variations in the ranges tested. Thus, of the four systems which show changes with increasing P/D ratios, only alginic acid and polymetaphosphate unequivocally shift in the direction which might be expected for a transition from a close-packed complex, with dye-dye interac-

tion, to more widely spaced, noninteracting complexes. In contrast, polyuridylylate and pectin (low methoxyl) produce changes in opposition to those expected.

These studies demonstrate that the DBTC complexes do not follow the simple behavior of those described for acridine orange, making it difficult to retain the simple dye-dye interaction hypothesis for these complexes.

Effects of Other Factors on the Complex. Anion Group. The anionic sites of the polyanions examined here include carboxyl, phosphate, sulfate, and cysteic acid groups. The carboxyl groups apparently may participate directly in forming any of the spectral species since representatives may be found in the J band (pectins, hyaluronic acid), the α complex (pectin and alginic acids), the β_a complex (polyglutamate), and the β complex (polyaspartate). The carboxyl groups of the proteins are probably also responsible for the formation of the γ complexes. The S band is also associated with polymers containing carboxyl groups, but only as a secondary band.

No polymer containing only phosphate anionic sites has been found specifically to form either the J complex or the S complex, but each of the other complexes forms with phosphate sites. These include DNA for the α , polyadenylate for the β , and polyuridylylate for the β_a complexes.

No complexes have yet been tested which rely only upon the sulfate or related groups so it is not possible to establish specificity for them. However, since the two sulfated representatives, chondroitin sulfate and heparin, show the β_a and the α bands, it may be assumed that these states are not excluded by sulfate.

The S complex, as noted previously, arises under special circumstances and appears to be associated with high pH. However, a small secondary band occasionally arises in the same region under some conditions (either excess dye or excess sites) with other polymers.

Thus, the nature of the anion site seems to have little direct influence upon the type of complex formed except that the carboxyl is more readily associated than the other groups with the J complex. An exception to this has arisen in recent, uncompleted studies where it has been found that polysaccharide-borate complexes (starch and borate) give a J-band reaction with the dye.

Anion Site Spacing. Anionic sites upon a polymeric matrix are tremendously more effective than the corresponding simple anions in creating the specific complexes with DBTC.^{6,7} It is quite apparent, therefore, that this selective specificity must reside in the rela-

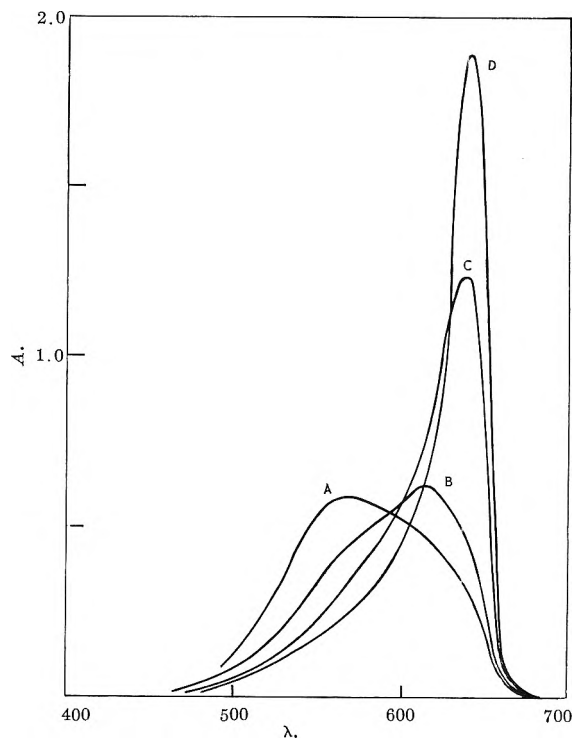


Figure 6. Change of DBTC-complex spectra with increasing pectin methylation. A: polygalacturonic acid (Sunkist sample, pH 7.0), P/D = 1.7. B: fractionated pectin, 4.3 and 7.0% methoxyl, pH 4.0 (identical curves), P/D = 2.5 and 1.4, respectively. C: fractionated pectin, 9.4% methoxyl, pH 4.0, P/D = 1.5. D: fractionated pectin, 10.8 and 11.3% methoxyl, pH 5.0, P/D = 1.3.

tion of the site complex to the polymeric matrix or in the interaction between the adjacent site complexes or in a combination of both of these factors. It is worthwhile to examine some of the potential spacing relationships in the complexing systems.

The experiments with the pectins are most pertinent to the question of effect of spacing. Pectic acid (polygalacturonic acid), which has a carboxyl group on each uronide unit, reacts with DBTC to form an α complex. Pectin, even with a methoxyl content as low as 4.3% (one out of four carboxyls methylated), shows a strong J band in addition to the α band upon reaction with DBTC. The J component shows only a slight increase for a pectin with 7.0% methoxyl (about one out of three groups esterified). However, as the methoxyl content increases to 9.4% (56% ester), the α component decreases rapidly as the J band increases until, at 10.8% methoxyl (two out of three carboxyls esterified), a pure J band is obtained in the DBTC reaction (Figure 6). Thus, as the average spacing between anionic groups in pectic acid and pectins is increased, there is a shift from the α -band to the J-band reaction. In the

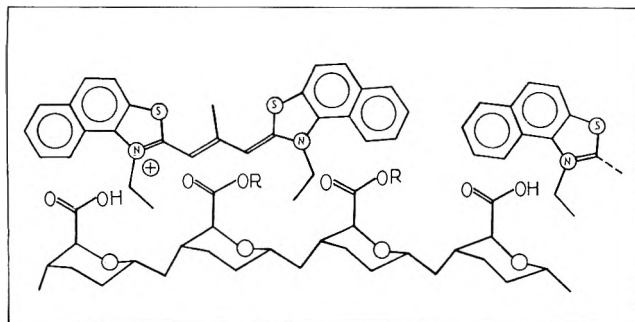


Figure 7. Relation of DBTC molecular length to pectin anion site spacing. This illustration only compares the length of the DBTC molecule with distance between anion sites on the pectin chain. No attempt has been made to indicate the actual spatial relations in this complex or the true conformation of either the dye or pectin molecules.

pectic acid, the anion groups are so closely spaced that there would be a high probability for interactions between adjacent dye molecules. Even if the conformations of the pectic acid made it impossible for adjacent dyes to interact (*e.g.*, carboxyls on alternating sides of the polymer chain), the dye is large enough so that overlapping could still occur between dyes on alternate sites. On the other hand, as illustrated in Figure 7, anion sites for the pectin having two-thirds of its carboxyls methylated are so widely spaced that interaction between dyes along the length of the polymer chain would be unlikely. Experiments to determine the effect of even greater spacing required chemical esterification of the pectin to obtain higher methoxyl contents. The chemically enriched samples, of 13 to 13.5% methoxyl, show extensive variations which depend upon the type of reaction used in esterification so these data cannot be applied to the question of spacing.

Hyaluronic acid (alternating glucuronic and acetylglucosamine units) does not react in a one-to-one anion site to dye ratio, only one dye reacting for every 2.3 carboxyl groups. A strong J band is also obtained for this polysaccharide, presumably as a result of the very wide spacing of the dyes on the polymer. These cases seem to contradict the concept that the J band is due to an interaction of dyes in a large aggregate, while the α band is formed when there is no dye-dye interaction in the complex.

Similar conclusions may be drawn from the ribonuclease data. A proposed structure and conformation of this protein¹⁴ would indicate that most of the anionic sites on the surface of the molecule are too widely spaced to permit interactions between dye molecules associated with them. Even allowing for errors in the conformation and secondary structure, a

relatively wide spacing is suggested by the primary structure, making it highly unlikely that the J band found with ribonuclease can be due to interaction between a large number of dye molecules in a large dye aggregate as previously proposed.

Effect of pH. Most amphoteric polymers, such as proteins and nucleic acids, either fail to react with the dye or show a much-reduced reaction at a pH at or below their isoionic point.⁷ Thus, native RNase reacts only at a pH greater than 9 and shows a full reaction only at a pH of 10 or greater, while oxidized RNase, with a much lower isoionic point, reacts strongly at pH 4.0. RNase, which has been treated with formaldehyde to eliminate the effect of lysine groups proximal to the anionic sites or treated with nitrous acid to reduce the basicity of the histidine groups, reacts at a lower pH (data to be published). A strong J band is found for nitrous acid treated (and dialyzed) oxidized RNase even at pH 3.0 (data to be published). Polyadenylate and polyuridylate also show some degree of sensitivity to low pH, but in each case it seems to reduce the intensity of the normal band with little shifting from the type of reaction observed. Polyglutamate shows a γ complex at low pH in place of its $\beta\alpha$ complex observed in neutral solutions. DNA acquires a β component in addition to its α band at low pH, but this is undoubtedly due to acid denaturation of the DNA.

On the other hand, the polysaccharide and polyphosphate complexes are relatively independent of pH. For example, the hyaluronic acid complex is unaffected with variation of pH from 2 to 10; the J band or α band of pectins and the β band with heparin show little change between pH 2.6 and 10; the β band of the polyphosphate complex is stable from pH 1.5 to 10, except for changes in the intensity of the peak. Alginate below pH 4 shows an α J hybrid rather than the normal α band, but this is probably due to precipitation of the free acid of the polysaccharide at low pH and consequent formation of micelles. Desulfated heparin also is affected by pH, in that an α J complex is observed at a pH below 5 while the $\beta\alpha$ complex is found above this pH. Again, this may be the result of a change in solubility of the polysaccharide.

Discussion

In earlier papers on the metachromatic reactions of DBTC with polymers,^{6,7} we assumed that the appearance of a specific spectral band in the complexing reaction indicated the presence of a specific state of dye aggregation. Thus, the α , β , γ , and J bands were

(14) H. P. Avey, C. H. Carlisle, and P. D. Shukla, *Brookhaven Symp. Biol.*, 15, 199 (1962).

Table III: Effect of pH on the DBTC Complexes

Complexing macromolecule	pH	λ_{\max} , ^a m μ	A_{\max} ^b	Buf-fering ^c agent	Complexing macromolecule	pH	λ_{\max} , ^a m μ	A_{\max} ^b	Buf-fering ^c agent
J-Band series					Alginate acid, 0.0006% [DBTC] = 2 \times 10 ⁻⁵ M				
Ribonuclease, native, 0.0022% [DBTC] = 10 ⁻⁵ M	8.0	508	0.63	T	2.0	642	0.59		
	8.6	512	0.53	T	2.5	625	0.83		
		645	0.04	T	3.1	610	0.97		
	9.1	512	0.52	0		570 s	0.89		
		645 s	0.13	0	3.4	605	0.98		
	9.4	525	0.32	0		570	0.92		
		645	0.54		4.2	570	1.09		
					8.6	570	1.13		
	10.1	530 s	0.13	0	10.5	570	1.02		
		650	1.51						
Ribonuclease, oxi- dized, 0.0022% [DBTC] = 10 ⁻⁵ M	11.5	630	0.73	0	Polygalacturonic acid, 0.0022% [DBTC] = 10 ⁻⁵ M				
	3.4	523	0.35	S	3.0	575	0.45	GG	
		565	0.22		4.0	568	0.52	S	
	3.8	526	0.28	S	7.0	652	0.52	C	
		580	0.33		8.6	560	0.49		
		653	0.59		β -Band group				
	4.2	530 s	0.19	S	Polymetaphosphate, 0.0067% [DBTC] = 2 \times 10 ⁻⁵ M	1.5	534	0.66	0
		650	1.25		3.5	536	0.94	0	
	5.0	650	1.46	S	4.9	538	0.96	0	
	6.1	650	1.78	C	6.7	534	1.16	0	
7.0	650	1.57	C	8.2	534	1.12	0		
8.1	645	1.31	T	9.8	535	1.01	0		
8.9	642	1.15	0	Polyadenylate					
10.6	603	0.63	0		530 p.p.t.	0.49	0		
11.1	593	0.61	0	2.3	575	0.42	0		
Hyaluronic acid, 0.002% [DBTC] = 2 \times 10 ⁻⁵ M	2.0	650	>2		3.4	520	0.84		
	7.0	650	>2			570 s	0.51		
	8.8	650	>2			540	1.04		
					4.0	570	0.86	S	
Pectin (10.8% meth- oxyl), 0.00073% [DBTC] = 10 ⁻⁵ M	2.6	645	0.23	0	8.2	530	0.89	T	
	3.05	643	1.29	S	11.5	530	0.97	0	
	8.4	642	1.69	T	Heparin, native, 0.006% [DBTC] = 2 \times 10 ⁻⁵ M				
	8.6	Dye curve	0	0	2.6	530	0.55	0	
Protamine, 0.007% [DBTC] = 10 ⁻⁵ M	9.9	525	0.35	0	4.0	535	0.71	0	
		575	0.35		8.8	530	0.82	0	
		650	0.45		11.3	533	0.84	0	
α -Band series					$\beta\alpha$ -Band group				
DNA, native, 0.014% in 0.2 mM MgCl ₂ [DBTC] = 2.7 \times 10 ⁻⁵ M	2.0	538	1.17	0	Polyglutamate, 0.0067% [DBTC] = 2 \times 10 ⁻⁵ M	2.0	502	0.77	0
		570	0.97		3.0	510	0.96	0	
	3.0	536	1.44	0	5.0	540	0.89	S	
		567	1.23		7.9	540	1.00	T	
	4.0	568	1.45	0	8.8	550	0.99	T	
	5.0	568	1.52	0	11.3	550	1.15	0	
	6.5	568	1.61	0	Polyuridylylate, 0.0067% [DBTC] = 10 ⁻⁵ M				
	7.4	565	1.68	0	6.3	560	0.79	0	
	8.8	568	1.59	0	8.2	555	0.82	T	
	10.0	565	1.49	0	Heparin, desulfated, 0.0067% [DBTC] = 2 \times 10 ⁻⁵ M				
11.5	572	1.26	0	4.8	610	0.99			
				9.3	555	0.90			
				10.5	553	0.93			
				11.0	552	0.90			

^a λ_{\max} indicates major peaks or shoulders (s) of the complex spectra. ^b Absorbancy at the indicated peak maxima with dye at indicated concentration. ^c Buffer symbols: 0, no buffer, adjusted to indicated pH with acid or base before addition of the dye; T, tris(hydroxyethyl)aminomethane; S, succinate; C, cacodylate; GG, glycylglycine. All buffers 0.001 to 0.003 M.

associated with progressively higher states of aggregation and polymerization of the dye on the surface of the polymers. These assumptions were then compatible

with our knowledge of the behavior of the dye in free solutions and with the theories advanced by other authors for the metachromatic reactions of dyes.

These hypotheses have all assumed that the different complex states were basically due to differences in degree or type of dye-dye interaction in the complex. The polyanion is presumed to play a passive part by providing a matrix with anion sites at intervals which would govern the distance of the dye molecules from one another. Thus, Bradley and co-workers²⁻⁴ for acridine orange propose that the α band is due to a monomeric species in both the complex and free dye, while the β and γ bands of the free dye in solution are due to dye-dye interactions in aggregates (dimers or higher), and equivalent interactions between dyes on adjacent anion sites are responsible for these bands in complexes. With respect to the J band, Jelley¹² believed these bands to be due to molecular species, but his ideas have been superseded by those of Scheibe¹⁰ and Sheppard,¹¹ whose theories require interaction between large numbers of dye molecules. Scheibe⁸ proposed that the J bands resulted from overlap of the "electron clouds" of the conjugated systems in adjacent dye molecules which permitted formation of a new "electron cloud" common to the entire polymer—essentially a superconjugated molecule. Scheibe's concept was criticized by Sheppard with the comment that the proposed complex would be "more metallic than metals." In its place, he offered a proposal that the J band arises from the formation of cells of dye molecules having coupled dipoles, with water molecules entering into the complex to act as the coupling agent between the dyes. With a series of such coupled dipole cells, excitation energy could be propagated along the entire length of a polymer or thread consisting of stacked cells. Although the need for a high aggregate was not implicit in this concept, since the spectra would be similar for small as well as large groups of cells, he assumed that the aggregates were actually responsible for the phenomenon. He also assumed that the J-band complex formed in reactions with polymeric substances, such as gelatin, was due to a similar aggregate formed at the surface of micelles of the polymer.

Our present data conflict with some of these concepts, most particularly with the mechanism for the J-band formation. Considering the stoichiometry and spacing relations in the complexing reactions of DBTC with pectin, it does not seem that the J band can arise in complexes as a consequence of highly organized, large aggregates of dye molecules. Since optimal reactions are always obtained with a maximum of one dye molecule per anion site, any aggregate would have to stretch along the surface of the macromolecule with spacing controlled by the distance between anionic sites. If sites are sufficiently close, the interaction phenomena could account for the J-band reaction.

Actually, the evidence suggests that there is a much greater probability for formation of the J complex when sites are sufficiently separated so that there is little chance for interaction between adjacent dye molecules in the macromolecule complex. Thus, methylation of the anion groups of pectic acid, which would decrease the chance of formation of any long surface aggregates of dye, causes a shift from the α complex to the J complex. A pure J band is obtained coincident with a degree of esterification which would create an average spacing between anion sites (two ester groups for every free carboxyl) just slightly greater than the full length of the extended DBTC molecule. It is true that carboxyls on adjacent turns of a helix structure would be sufficiently closely spaced to permit dye-dye interaction, but such conformation has not been indicated for pectin. Reactions with ribonuclease reinforce the conclusion that the J band may occur as the result of the interaction of individual DBTC molecules with isolated anion sites.

Similarly, the mechanism for the formation of the other complexes of DBTC must be modified to some degree. Although it has been attractive to assume that the α , β , and γ bands are due to increasing degrees of aggregation on the macromolecular surface, under the influence of specific site spacings, the present data are not entirely consistent with this concept. Different spectra are obtained for complexes with macromolecules having the same anionic groups with similar spacing between sites, as in the case of the varying reactions for different polynucleotides. On the other hand, similar spectra may be found for the complexes arising from the reaction of DBTC with polymers having extremely variant spacings as evidenced by the β band appearing with polymetaphosphate, polyaspartate, and polyadenylate. Finally, the aggregation theory requires that a shift to a "monomeric" complex should occur at very high ratios of anion site to dye.^{2,3} Increasing the anion site to dye ratio during formation of DBTC complexes may cause no change at all or may create shifts in either direction, toward or away from the supposed monomeric complex. Such behavior is very difficult to reconcile with a simple-aggregation, dye-dye interaction hypothesis. Even with a very high "stacking coefficient"³ (the measure of the tendency for a dye molecule to occupy sites adjacent to other dye molecules in preference to isolated sites), the reverse shifts cannot be explained except through the assumption of specific interactions between the site and the individual or aggregated dye molecules.

It seems that the reactions of DBTC with macromolecules might be better accommodated under a

hypothesis which does not stress, exclusively, the dye-dye interactions in the complexes but which considers, also, the conformations of the dye and its interactions with the polymer site and adjacent groupings. In this case, specific bands would be obtained owing to interactions of the dye with its site and/or neighboring dye molecules. These interactions would enforce certain conformations of the dye molecule and reinforce (increase transition probabilities) specific vibrational and electronic combinations in the dye molecule. This mechanism would be compatible with the concepts of Sheppard, who stated, with respect to the formation of the β and γ bands of the free cyanine dye: "We consider that the doublet or dimer formation accounts for the spectral deviation. But this is not because β or γ bands of higher frequency are new bands peculiar to the 'polymers' but because the doublet formation enhances the transition probabilities of bands produced in the molecule by coupling of the electronic transitions with vibrations." We are in agreement that dye interactions in the polymeric complexes create the observed spectral shifts, but it should not be assumed that it is only coupling between dye molecules which induces these effects; they may be similarly induced by a change in conformation of the dye as a result of its interaction with a specific polymeric structure. Thus, a large increase in anion site to dye ratios might cause no change at all or a change in either direction, depending upon whether dye-dye interaction is a significant factor in the stoichiometric complex and whether the dye reaction caused some conformational changes in the polymer at low or high ratios.

The α , β , γ , and J complexes could be readily accommodated under this hypothesis. The γ complex appears, frequently, to be a transitory state, and it may be that this complex arises through direct adsorption of the dye aggregate, in the same form as it exists in the aqueous solution, onto the polymer. A subsequent rearrangement may then occur, in some cases, which results in a more stable relation of dye molecule to site.

Unfortunately, little can be said at the present time about the intensely interesting S state since it has not

been observed in a sufficient number of cases to permit fitting it into the complexing-mechanism hypothesis. Since it appears occasionally as a secondary band under some conditions of excess site to dye relations, it is conceivable that it is another conformation related to the molecular J-band state.

The present studies have also reinforced some earlier observations that pH may have very little effect upon the formation of certain complexes. With amphoteric macromolecules, such as proteins, complex formation apparently may be prevented by a positively charged cationic group in the vicinity of the anion site. Changes in pH appear to have their effects mainly in altering such charges and permitting or preventing the formation of the normal complex at the anion site. The polysaccharide complexes, involving carboxyl groups, are unaffected by alterations in pH which change the relative concentrations of their ionized and un-ionized groups by many orders of magnitude. To a lesser degree, this is also true of the polyphosphates. Thus, it appears that the degree of ionization of the participating anion group has little or no final effect upon the complex, either as a directive factor or with regard to the equilibrium between the complex and its component parts. It is possible, however, that an anion site may be required for initial reaction, but, as the anionic sites are removed by the complexing, the ionized-nonionized equilibrium is rapidly re-established among the remaining groups, leading to further reaction with the dye.

It may be concluded that it is unlikely that the complex metachromatic reactions of DBTC, or related systems, will be explicable in terms of simple mechanisms. Instead, it is probable that the complex states involve multiple interactions and conformational relations. Any interpretation must consider the interactions between the dye and binding site, between neighboring bound dye molecules, and between neighboring binding sites as affected by the presence of the dye. It is particularly evident that the macromolecular binding site must be considered as a complicated unit in its interactions with the dye, rather than a simple anionic site reacting with the cationic dye.

The Formation Kinetics of the Nickel Monomalonate Complex Studied by the Temperature-Jump Method

by Francesco Paolo Cavasino

Institute of Physical Chemistry, University of Palermo, Palermo, Italy (Received June 22, 1966)

The kinetics of formation of the nickel monomalonate complex has been examined by the temperature-jump method at 15, 25, and 31° and at ionic strength 0.1 *M*. The experimental data are interpretable on the assumption that the following two reactions contribute significantly to the complex formation: $\text{Ni}^{2+} + \text{Mal}^{2-} \rightleftharpoons \text{NiMal}$ and $\text{Ni}^{2+} + \text{HMal}^- \rightleftharpoons \text{NiMal} + \text{H}^+$, where Mal^{2-} represents the malonate ion. The results suggest that the rate-determining step is the release of the "first" water molecule from the inner coordination sphere of the nickel ion. The kinetic data for the above reactions are virtually similar to those for the analogous reactions of nickel oxalate formation. All the equilibrium constants at 25° for each intermediate reaction leading to the nickel malonate and oxalate formation have also been evaluated and the steps, on which the different stability of these complexes depends, fixed.

Introduction

In recent years the study concerning the formation kinetics of metal complexes has been greatly developed thanks to the modern techniques which have allowed the investigation of fast reactions in solution with half-times down to about 10^{-9} sec.^{1,2} In particular, the relaxation methods²⁻¹⁰ have largely contributed to the development of these studies and to a better knowledge of the mechanism of such reactions. The conclusion drawn from these investigations is that the rate-determining step of complex formation is the release of a water molecule from the inner coordination sphere of the metal ion and that the rate for a given metal ion is independent of the nature of the entering ligand. (A dependence of the rate of water substitution on the ligands has been found, on the contrary, for metal ions of high charge density, *i.e.*, Fe^{3+} .) In the case of bidentate or multidentate ligands, two or more water molecules are to be replaced from the inner coordination sphere of the metal ion.

In the few kinetic studies existing at present in this field, the Ni^{2+} ion has usually been used as a coordinating ion. It has been suggested¹¹⁻¹⁴ that the rate of formation of a complex ion (1:1) with bidentate (*e.g.*, glycine) or multidentate (*e.g.*, triethylenetetramine) ligands is probably determined by dissociation of the

"first" coordinated water molecule. In order to obtain further information about the kinetics of formation of such complexes, the reaction of formation of nickel monomalonate has been studied at 15, 25, and 31° by the temperature-jump relaxation method.

- (1) L. De Maeyer and K. Kustin, *Ann. Rev. Phys. Chem.*, **14**, 5 (1963).
- (2) M. Eigen and L. De Mayer in "Technique of Organic Chemistry," Vol. VIII, 2nd Ed., S. L. Friess, E. S. Lewis, and A. Weissberger, Ed., Interscience Publishers, Inc., New York, N. Y., 1963, part 2, p. 895.
- (3) M. Eigen, *Discussions Faraday Soc.*, **17**, 194 (1954); **24**, 24 (1957).
- (4) M. Eigen, *Z. Elektrochem.*, **64**, 115 (1960).
- (5) L. De Maeyer, *ibid.*, **64**, 65 (1960).
- (6) M. Eigen in "Advances in the Chemistry of the Coordination Compounds," The Macmillan Co., New York, N. Y., 1961, p. 371.
- (7) M. Eigen, *Suomen Kemistilehti*, **34A**, 25 (1961).
- (8) M. Eigen and K. Tamm, *Z. Elektrochem.*, **66**, 107 (1962).
- (9) M. Eigen, *Pure Appl. Chem.*, **6**, 97 (1963).
- (10) M. Eigen and K. Kustin, *I.C.S.U. Rev.*, **5**, 97 (1963).
- (11) M. Eigen and R. G. Wilkins, to be published.
- (12) G. G. Hammes and J. I. Steinfeld, *J. Am. Chem. Soc.*, **84**, 4639 (1962).
- (13) J. I. Steinfeld and G. G. Hammes, *J. Phys. Chem.*, **67**, 528 (1963).
- (14) (a) G. H. Nancollas and N. Sutin, *Inorg. Chem.*, **3**, 360 (1964); (b) D. W. Margerum, D. B. Rorabacher, and J. F. G. Clarke, Jr., *ibid.*, **2**, 667 (1963).

Experimental Section¹⁵

A stock solution ($3.45 \times 10^{-1} M$) containing Ni^{2+} ion was prepared from $Ni(ClO_4)_2 \cdot 6H_2O$ (Fluka reagent grade) and doubly distilled water, and its concentration was estimated by a complexometric titration.¹⁶ Stock solutions of malonic acid ($5.65 \times 10^{-2} M$) and sodium perchlorate ($1 M$) were made by dissolving the appropriate weight of the substances (Fluka reagent grade) in doubly distilled water.

The temperature-jump apparatus was that described previously.¹⁷ The establishment of the chemical equilibria in solution, after the perturbation produced by the rapid increase in the temperature, was followed by the accompanying shift of hydrogen ion concentration. The shift was observed spectrophotometrically by adding a suitable indicator to the solutions (brom cresol green for $pH \geq 4.3$ and brom chlor phenol blue for $pH < 4.3$). The concentration of the indicator ($\leq 2.6 \times 10^{-5} M$) was such that the optical density of the solutions was in the range 0.3 to 0.7 at the appropriate wave length (λ 610 $m\mu$ for brom cresol green and λ 590 $m\mu$ for brom chlor phenol blue). The solutions containing nickel perchlorate and malonic acid indicated no appreciable absorption in the visible and near-ultraviolet range. The various solutions examined were obtained by mixing the necessary volume of stock solution of $Ni(ClO_4)_2$, malonic acid, and indicator and then adjusting the ionic strength to 0.1 M by the addition of $NaClO_4$ (1 M) solution and the pH by the addition of $HClO_4$ (1 M) or $NaOH$ (1 M).

All of the solutions exhibited a relaxation effect (Figure 1) which was characterized by a single relaxation time τ , according to the expression²

$$d\Delta C_i/dt = -\Delta C_i/\tau \text{ or } \log \Delta C_i = -t/2.3\tau + \text{constant} \quad (1)$$

where ΔC_i is the deviation of concentration of a given ionic species from its equilibrium value: $\Delta C_i = C_i - \bar{C}_i$ (C_i = actual concentration depending on the time; \bar{C}_i = equilibrium concentration). To ensure that the observed relaxation effects were due only to the reaction of complex formation, blank experiments were carried out with solutions containing $Ni(ClO_4)_2$ -indicator and malonic acid-indicator in the same condition of concentration, ionic strength, and pH; in no case was a relaxation effect observed. Measurements were made at 15, 25, and 31°, the temperature jump of 8° being included.

Results

Potentiometric studies¹⁸ on nickel malonate stability in solutions containing nickel ion in the presence of lower concentrations of malonate ion have shown the

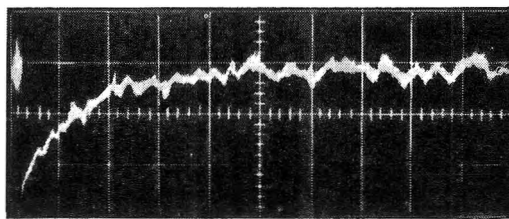
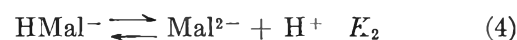
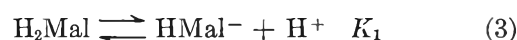
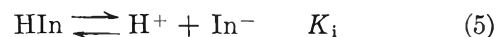


Figure 1. Experimental relaxation curve at 25°: $\Sigma[Ni] = 8.00 \times 10^{-3} M$; $\Sigma[Mal] = 2.00 \times 10^{-3} M$; $[H^+] = 0.41 \times 10^{-4} M$; $\mu = 0.1 M$; indicator is brom cresol green. The sweep rate is 2 msec./cm. The relaxation time evaluated from this curve is 2.27×10^{-3} sec.

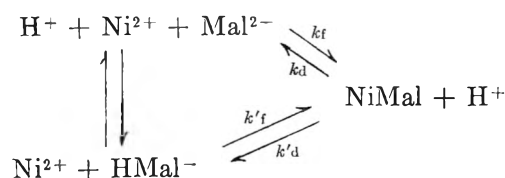
existence of the following equilibria (malonate ion is indicated by Mal^{2-})



For our solutions, the dissociation equilibrium concerning the indicator added has also to be taken into account



From the following considerations, the kinetic data obtained in this paper suggest that $NiMal$ formation occurs through two paths, according to the scheme



The equilibrium and rate constants are related by

$$K_C = k_t/k_d; K_C K_2 = k'_t/k'_d \quad (6)$$

Since the protolytic reactions occur rapidly compared to metal complex reactions, the rate law for the above scheme is given by

$$d(NiMal)/dt = k^*_t(Ni^{2+})(Mal^{2-}) - k^*_d(NiMal) \quad (7)$$

where

$$k^*_t = k_t + k'_t(H^+)/K_2 \text{ and } k^*_d = k_d + k'_d(H^+) \quad (8)$$

(15) The experimental part of this work was performed at the Max-Planck-Institut für physikalische Chemie, Göttingen, West Germany.

(16) A. I. Vogel, "A Text-book of Quantitative Inorganic Analysis," 3rd Ed., Longmans, Green and Co., London, 1961, p. 435.

(17) F. P. Cavasino and M. Eigen, *Ric. Sci. Riv.*, 4, 509 (1964).

(18) V. S. K. Nair and G. H. Nancollas, *J. Chem. Soc.*, 4367 (1961).

Table I: Relaxation Times and Equilibrium Concentrations ($\mu = 0.1 M$)

$\Sigma[\text{Ni}]$ $\times 10^4, M$	$\Sigma[\text{Mal}]$ $\times 10^4, M$	$[\text{Ni}^{2+}]$ $\times 10^4, M$	$[\text{NiMal}]$ $\times 10^4, M$	$[\text{Mal}^{2-}]$ $\times 10^4, M$	$[\text{HMal}^-]$ $\times 10^4, M$	$[\text{H}_2\text{Mal}]$ $\times 10^4, M$	$[\text{H}^+]$ $\times 10^4, M$	$\Sigma[\text{In}]$ $\times 10^4, M$	$[\text{In}^-]$ $\times 10^4, M$	$\tau \times 10^4$ sec.
$t = 15^\circ$										
60.0	10.0	54.1	5.9	0.74	3.39	0.04	0.27	0.20	0.08	67.4 ± 5.5
60.0	10.0	55.9	4.1	0.50	5.27	0.14	0.62	0.20	0.05	68.2 ± 4.2
60.0	30.0	52.1	7.9	1.02	20.13	1.01	1.15	0.11	0.05	67.3 ± 7.0
80.0	40.0	70.8	9.2	0.89	27.72	2.20	1.82	0.14	0.05	59.1 ± 3.0
80.0	40.0	73.1	6.9	0.65	29.09	3.34	2.63	0.18	0.05	62.4 ± 5.5
97.0	50.0	89.1	7.9	0.61	36.06	5.46	3.47	0.26	0.06	58.5 ± 3.5
80.0	40.0	75.2	4.8	0.43	29.59	5.14	3.98	0.26	0.05	62.7 ± 3.0
$t = 25^\circ$										
50.0	3.0	48.1	1.9	0.25	0.83	0.01	0.19	0.10	0.05	33.9 ± 2.2
40.0	3.0	38.4	1.6	0.25	1.18	0.01	0.26	0.20	0.09	43.8 ± 2.5
80.0	3.0	78.0	2.0	0.16	0.87	0.01	0.31	0.20	0.08	31.7 ± 1.7
60.0	10.0	54.9	5.1	0.59	4.23	0.07	0.41	0.20	0.06	28.4 ± 1.5
80.0	20.0	68.6	11.4	1.04	7.47	0.13	0.41	0.20	0.06	22.6 ± 1.0
60.0	30.0	47.7	12.3	1.61	15.72	0.36	0.55	0.23	0.06	26.9 ± 1.7
60.0	30.0	50.7	9.3	1.14	18.87	0.74	0.94	0.11	0.06	26.9 ± 1.4
80.0	40.0	68.0	12.0	1.10	25.56	1.41	1.32	0.12	0.06	23.8 ± 1.6
60.0	30.0	52.9	7.1	0.83	20.89	1.24	1.42	0.12	0.05	30.2 ± 2.4
106.0	10.0	102.3	3.7	0.23	5.71	0.34	1.42	0.12	0.05	30.6 ± 2.0
80.0	50.0	66.8	13.2	1.24	33.41	2.13	1.53	0.13	0.05	24.2 ± 1.5
80.0	50.0	68.7	11.3	1.03	34.84	2.79	1.92	0.15	0.05	24.6 ± 1.6
80.0	40.0	72.5	7.5	0.65	28.80	3.02	2.52	0.18	0.05	26.7 ± 2.2
80.0	50.0	72.5	7.5	0.64	36.91	5.00	3.25	0.18	0.04	29.0 ± 2.3
106.0	50.0	97.9	8.1	0.52	35.58	5.80	3.91	0.26	0.05	25.1 ± 1.3
80.0	50.0	73.9	6.1	0.51	37.08	6.32	4.09	0.24	0.05	25.9 ± 1.8
$t = 31^\circ$										
60.0	10.0	54.1	5.9	0.67	3.39	0.04	0.28	0.20	0.08	15.3 ± 1.2
60.0	10.0	55.9	4.1	0.45	5.30	0.14	0.65	0.20	0.05	22.4 ± 2.4
60.0	30.0	52.4	7.6	0.88	20.47	1.08	1.27	0.11	0.05	15.5 ± 2.2
80.0	40.0	70.3	9.7	0.84	27.45	2.04	1.79	0.14	0.05	14.6 ± 1.0
80.0	40.0	72.4	7.6	0.64	28.84	2.96	2.47	0.18	0.05	15.9 ± 1.5
80.0	40.0	73.5	6.5	0.54	29.37	3.62	2.97	0.18	0.04	17.0 ± 2.0
97.0	50.0	89.1	7.9	0.54	36.13	5.49	3.66	0.26	0.05	14.6 ± 1.0
97.0	50.0	89.9	7.1	0.48	36.23	6.18	4.11	0.26	0.05	14.8 ± 1.5

After the appropriate expansion of eq. 7, the following expression, valid in the neighborhood of equilibrium, is obtained

$$d\Delta[\text{NiMal}]/dt = -k^*_i\{[\text{Ni}^{2+}]/(1 + \alpha + \beta) + [\text{Mal}^{2-}] + 1/K_C\}\Delta[\text{NiMal}] \quad (9)$$

where

$$\alpha = [\text{H}^+]K_1\{1 + [\text{In}^-]/(K_i + [\text{H}^+]) + 2[\text{HMal}^-]/K_1\} : (K_2K_1\{1 + [\text{In}^-]/(K_i + [\text{H}^+]) + 2[\text{HMal}^-]/K_1\} + [\text{Mal}^{2-}]\{K_1 + 2[\text{H}^+]\})$$

$$\beta = [\text{H}^+]^2\{1 + [\text{In}^-]/(K_i + [\text{H}^+]) - [\text{Mal}^{2-}]/K_2\} : (K_2K_1\{1 + [\text{In}^-]/(K_i + [\text{H}^+]) - [\text{Mal}^{2-}]/K_2\} + 2[\text{Mal}^{2-}]\{K_1 + 2[\text{H}^+]\})$$

(The brackets indicate the equilibrium concentrations of the different species.)

Comparing eq. 9 with eq. 1 ($\Delta C_i = \Delta[\text{NiMal}]$), the reciprocal relaxation time is found to be

$$1/\tau = k^*_i\{[\text{Ni}^{2+}]/(1 + \alpha + \beta) + [\text{Mal}^{2-}] + 1/K_C\}$$

The term in braces in this expression may be evaluated from the equilibrium concentrations of the various species and from the equilibrium constants K_2 , K_1 , K_i , and K_C . By setting this term equal to A , we obtain from eq. 8

$$1/\tau A = k_t + k'_t(\text{H}^+)/K_2 \quad (10)$$

The equilibrium concentrations (Table I) which are necessary to determine the quantity A have been obtained from the concentrations of the species added ($\text{Ni}(\text{ClO}_4)_2$, malonic acid) and from the equilibrium

constants^{18,19} calculated by us at ionic strength 0.1 *M* (Table II). The concentration of hydrogen ion has been calculated from the pH measurements. Activity coefficients of the ions have been evaluated by means of Davies' equation.²⁰ For the equilibrium constants of the indicators, we have used the values of 2×10^{-5} and 10^{-4} for brom cresol green and brom chlor phenol blue, respectively, at the three temperatures investigated; this approximation is justified because a 10% variation of these constants does not influence the α and β values.

Table II: Equilibrium Constants ($\mu = 0.1 M$)

<i>t</i> , °C.	$K_C \times 10^{-2}$, <i>M</i> ⁻¹	$K_2 \times 10^3$, <i>M</i>	$K_1 \times 10^3$, <i>M</i>	$K_C K_2$ $\times 10^2$	$K_i \times 10^5$, <i>M</i>
15	1.46	5.85	2.29	8.54	2 ^a
25	1.60	5.67	2.40	9.07	10 ^b
31	1.63	5.49	2.41	8.95	

^a Brom cresol green. ^b Brom chlor phenol blue.

The relaxation times have been calculated by plotting $\log \Delta C_i$ vs. time, according to eq. 1. The values of ΔC_i and time are obtained from the experimental relaxation curves. Each value of the relaxation time is the average of four runs (Table I).

If the suggested mechanism is correct, a plot of the term $1/\tau A$ as a function of the equilibrium concentration of the hydrogen ions $[H^+] \equiv (H^+)$ (see eq. 10) should be linear. A linear behavior is in fact obtained at the three temperatures, as shown in Figure 2. From the slope and the intercept of these straight lines it is possible to determine k'_f/K_2 and k_f , respectively. The value of the complex formation rate constants, k_f and k'_f , estimated by the least-square method, and the values of the dissociation rate constants, k_d and k'_d , evaluated by eq. 6, are reported in Table III. The precision of the rate constants is about $\pm 13\%$.

Arrhenius energies of activation for the two reactions, E_f and E'_f (Table IV), have been estimated from the plots of $\log k_f$ and $\log k'_f$ against $1/T$. The linearity

Table III: Formation and Dissociation Rate Constants for Nickel Malonate Complex ($\mu = 0.1 M$)

$k_f \times 10^{-4}$, <i>M</i> ⁻¹ sec. ⁻¹	k_d , sec. ⁻¹	$k'_f \times 10^{-3}$, <i>M</i> ⁻¹ sec. ⁻¹	$k'_d \times 10^{-5}$, <i>M</i> ⁻¹ sec. ⁻¹	<i>t</i> , °C.
2.9	20	1.3	1.5	15
7.0	44	3.1	3.4	25
12.3	75	5.3	5.9	31

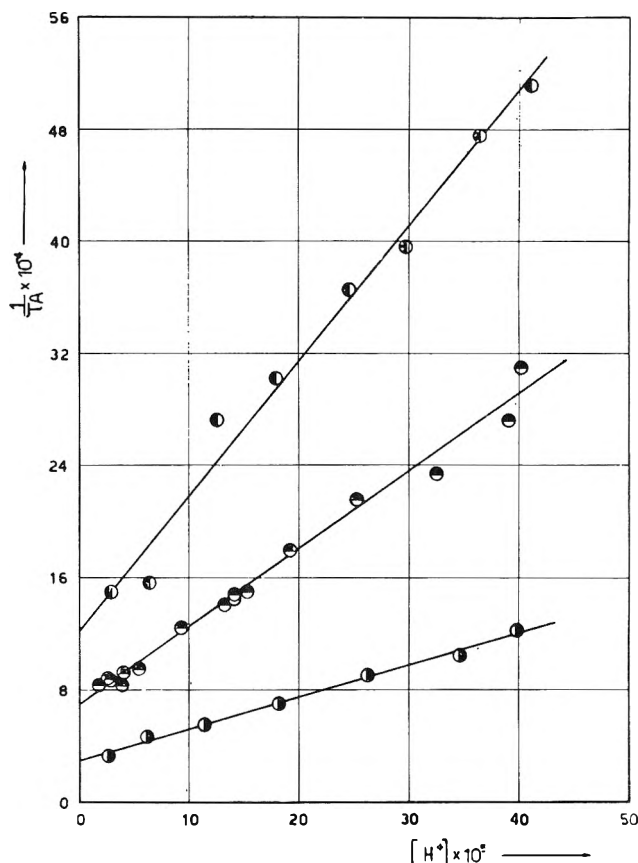


Figure 2. $1/\tau A$ vs. $1/[H^+]$ plot at 15° (○), 25° (◐), and 31° (●).

of these plots (Figure 3) suggests that the above scheme is valid for the temperature range investigated. Besides the energies of activation, we have also calculated (Table IV) the entropies of activation, ΔS_f^* and $\Delta S'_f^*$, from the expression²¹

$$\log PZ = \log (eRT/Nh) + \Delta S^*/2.3R$$

where PZ is the frequency factor obtained from the Arrhenius plots. The uncertainties in E_f and ΔS_f^* are about ± 3 kcal. mole⁻¹ and ± 7 cal. deg.⁻¹ mole⁻¹, respectively, and have been obtained by considering the error of 13% in the rate constants at the higher and lower temperatures. Other derived parameters, such as the heat and free energy of activation, are also reported in Table IV.

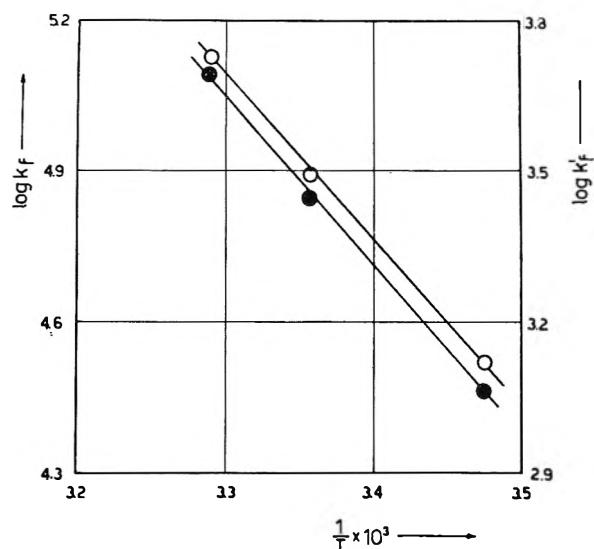
(19) R. A. Robinson and R. H. Stokes, "Electrolyte Solutions," 2nd Ed., Butterworths Scientific Publications, London, 1959, p. 520.

(20) C. W. Davies, *J. Chem. Soc.*, 2093 (1938).

(21) S. Glasstone, K. J. Laidler, and H. Eyring, "The Theory of Rate Processes," McGraw-Hill Book Co., Inc., London, 1941, pp. 199, 417.

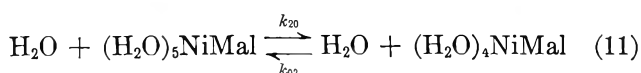
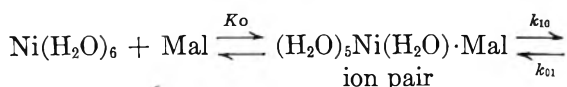
Table IV: Kinetic Data for the Nickel Malonate Formation at 25° ($\mu = 0.1 M$)

	$\text{Ni}^{2+} + \text{Mal}^{2-} \xrightleftharpoons[k_d]{k_f} \text{NiMal}$	$\text{Ni}^{2+} + \text{HMal}^- \xrightleftharpoons[k'_d]{k'_f} \text{NiMal} + \text{H}^+$
$k_f, M^{-1} \text{sec}^{-1}$	7.0×10^4	3.1×10^3
k_d	44 sec^{-1}	$3.4 \times 10^5 M^{-1} \text{sec}^{-1}$
$E_f, \text{kcal. mole}^{-1}$	16	15
$\Delta H^*_f, \text{kcal. mole}^{-1}$	15	14
$\Delta S^*_f, \text{cal. deg.}^{-1} \text{mole}^{-1}$	14	7
$\Delta G^*_f, \text{kcal. mole}^{-1}$	11	12
K_0, mole^{-1}	13	2
k_{10}, sec^{-1}	5.4×10^3	1.6×10^3
$\Delta G_0, \text{kcal. mole}^{-1}$	-1.5	-0.4
$\Delta S_0, \text{cal. deg.}^{-1} \text{mole}^{-1}$	15	8
$\Delta H_0, \text{kcal. mole}^{-1}$	3	2
$\Delta H^*_{10}, \text{kcal. mole}^{-1}$	12	12
$\Delta S^*_{10}, \text{cal. deg.}^{-1} \text{mole}^{-1}$	-1	-1

Figure 3. The temperature dependence of k_f (●) and k'_f (○).

Discussion

According to the suggestions of several authors concerning the various steps leading to the complex formation of a metal ion with uni- or bidentate ligands,^{6-14a} the reaction of nickel malonate formation from Ni^{2+} and malonate ion may be considered to occur as follows (the charges are omitted; malonate anion will be indicated by Mal)



where $(\text{H}_2\text{O})_5\text{NiMal}$ represents a half-bonded inter-

mediate, K_0 is the ion pair association constant, $K_{10} = k_{10}/k_{c1}$, and $K_{20} = k_{20}/k_{c2}$. The first step of this scheme leads to the formation of an ion pair, the second and the third correspond, respectively, to the substitution of the first and the second water molecules in the inner coordination sphere of the nickel ion. As the process of ion pair formation occurs rapidly compared to the rate of substitution of a coordinated water molecule,^{4,8,12} the reagents can always be considered in equilibrium with the ion pair.

The value of K_0 (Table IV) within a factor of about 2 or 3 has been calculated at 25° and at ionic strength 0.1 M by the equation

$$K_0 = (4\pi N a^3 / 3000) e^{-U(a)/kT} \quad (12)$$

where $U(a)$ is the Coulomb energy and a is the distance of closest approach of ion pair partners, which we have assumed equal to 5 Å.^{12-14a}

If the intermediate $(\text{H}_2\text{O})_5\text{NiMal}$ of scheme 11 is assumed to be in a steady state, it follows that

$$k_f = k_{10}k_{20}K_0 / (k_{c1} + k_{20})$$

and

$$k_d = k_{c2}k_{c1} / (k_{c1} + k_{20})$$

If $k_{20} \gg k_{c1}$, it is obtained

$$k_f = k_{10}K_0 \text{ and } k_d = k_{c1}/K_{20} \quad (13)$$

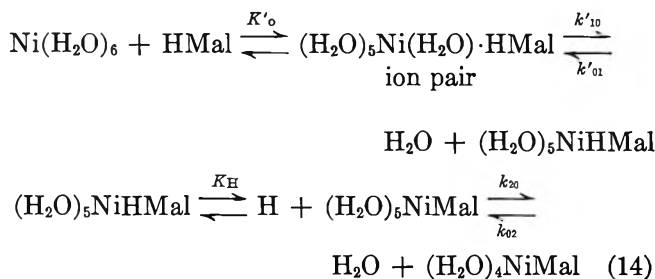
The value of k_{10} calculated in this work at 25° (Table IV) is of the same order of magnitude as the first-order rate constants for the reaction of Ni^{2+} with various unidentate ligands (Table V). Hence, one may assume that, in the case of the bidentate malonate ion, the over-all rate of complex formation is determined by the rate of elimination of the "first" water molecule from the inner coordination sphere

Table V: First-Order Rate Constants for the Nickel Monocomplex Formation at 25° ($\mu = 0.10\text{--}0.15\text{ M}$)

Ligand	$k_{10} \times 10^{-3}, \text{sec.}^{-1}$	Ref.
Water	27	22
Imidazole	16	12
Thiocyanate	~6	14a, 23
Sulfate ^a	15	8
Glycine	9	12
Diglycine	12	12
Triglycine	5	13
Oxalate	6	14a
Bioxalate	3	14a
Malonate	5	This work
Bimalonate	2	This work

^a At 20°.

of the nickel ion. This assumption can be confirmed by considering the kinetics of the reaction of Ni^{2+} with bimalonate ion. The nickel malonate formation from these reagents may be written schematically as follows (charges are neglected for brevity)



where K'_0 is the ion pair association constant, $K'_{10} = k'_{10}/k'_{01}$, K_{H} is the dissociation constant of the acid intermediate $(\text{H}_2\text{O})_5\text{NiHMal}$, and $K_{20} = k_{20}/k_{02}$. This scheme, compared to that previously considered (eq. 11), shows an additional step relative to the dissociation of $(\text{H}_2\text{O})_5\text{NiHMal}$. The value of the ion pair association constant, K'_0 , reported in Table IV, has been calculated by eq. 12 giving the value of 5 Å. to the distance of closest approach of the two ions. Since reactions 11 and 14 have the last step in common, by assuming that the rate constants k'_{10} and k'_{01} are comparable to k_{10} and k_{01} , it is clear that the rate-determining step of both reactions will be either the common elimination of the second water molecule or the elimination of the respective first water molecule.

Assuming the chemical species $(\text{H}_2\text{O})_5\text{NiMal}$ and $(\text{H}_2\text{O})_5\text{NiHMal}$ to be in a steady state and the dissociation rate constant of the acid intermediate to be greater than k'_{01} , we obtain

$$\begin{aligned} k'_t &= k'_{10}k_{20}K'_0/[k'_{01}(\text{H}^+)/K_{\text{H}} + k_{20}]; \\ k'_d &= k'_{01}k_{02}/K_{\text{H}}[k'_{01}(\text{H}^+)/K_{\text{H}} + k_{20}] \quad (15) \end{aligned}$$

If $k_{20} \gg k'_{01}(\text{H}^+)/K_{\text{H}}$, we have

$$k'_t = k'_{10}K'_0; \quad k'_d = k'_{01}/K_{20}K_{\text{H}} \quad (16)$$

In this case the over-all rate of reaction is determined by the elimination of the first coordinated water molecule. If $k_{20} \ll k'_{01}(\text{H}^+)/K_{\text{H}}$, we have

$$k'_t = k_{20}K'_0K'_{10}K_{\text{H}}/(\text{H}^+); \quad k'_d = k_{02}/(\text{H}^+) \quad (17)$$

In the latter case the rate-determining step should be the release of the second water molecule. When comparing the first equality of eq. 17 with the first of eq. 8, one can easily see that the second case cannot be valid as k'_t would not be dependent any more on (H^+) , which disagrees with the experimental data. It is then deduced that the rate-determining step of the reaction of Ni^{2+} ion with bimalonate ion is the elimination of the "first" water molecule. Consequently, the release of the "first" water molecule must also be the step which determines the over-all rate of the reaction between Ni^{2+} and malonate ion. The value of k'_{10} (Table IV) at 25° is also of the same order of magnitude as the corresponding first-order rate constants for various reactions of nickel ion (Table V). The differences may be due to the approximation in calculating K_0 by eq. 12 and also making $a = 5\text{ \AA}$. for all of the ligands. For comparison, the value of the rate constant for the exchange of a water molecule between the bulk of the solution and the inner coordination sphere of Ni^{2+} is also reported in Table V.

Further confirmation of the suggested mechanism can be obtained by comparing the parameters of activation ΔH^*_{10} and ΔS^*_{10} for the process of release of the first water molecule with the corresponding quantities for water exchange in the nickel ion. The variation of entropy (ΔS_0) for the formation of the ion pair between Ni^{2+} and malonate and bimalonate ions, respectively, may be approximately evaluated, according to the calculation by Nancollas and Sutin for the reaction of nickel oxalate formation,^{14a} from the expression

$$\Delta S_0 = -19.4(z_1z_2/a)$$

where a is the distance of closest approach of the ion pair partners (5 Å.). The variation of enthalpy (ΔH_0) for the same reactions can be determined by the Gibbs-Helmholtz equation

$$\Delta H_0 = -RT \ln K_0 + T\Delta S_0$$

The parameters of activation ΔH^*_{10} and ΔS^*_{10} are then calculated by the expressions

- (22) J. J. Swift and R. E. Connick, *J. Chem. Phys.*, **37**, 307 (1962).
 (23) A. G. Davies and W. M. Smith, *Proc. Chem. Soc.*, 380 (1961).

Table VI: Rate and Stepwise Equilibrium Constants for the Formation of Nickel Malonate and Oxalate Complexes at 25° ($\mu = 0.1 M$)

Reagents	$k_f, M^{-1} \text{ sec.}^{-1}$	k_d		$k_{10}, \text{sec.}^{-1}$	$k_{01}, \text{sec.}^{-1}$	K_0, mole^{-1}	K_{10}	K_H, mole	K_{20}	K_C, mole^{-1}	$K_C K_2$
		Sec.^{-1}	$M^{-1} \text{ sec.}^{-1}$								
$\text{Ni}^{2+} + \text{Mal}^{2-}$	7.0×10^4	44		5.4×10^3	~ 130	13	41	...	3	1.60×10^3	...
$\text{Ni}^{2+} + \text{HMal}^-$	3.1×10^3		3.4×10^5	1.6×10^3	~ 130	2	13	1.3×10^{-4}	3	...	9.07×10^{-3}
$\text{Ni}^{2+} + \text{Ox}^{2-}$	7.5×10^{4a}	3.6^a		6×10^{3a}	~ 130	13^a	48	...	33	2.08×10^{4a}	...
$\text{Ni}^{2+} + \text{HOx}^-$	5×10^{3a}		1.5×10^{3a}	3×10^{3a}	~ 130	2^a	21	2.4×10^{-3}	33	...	3.33^a

^a See ref. 14a.

$$\Delta S^*_{10} = \Delta S^*_f - \Delta S^*_0; \Delta H^*_{10} = \Delta H^*_f - \Delta H^*_0$$

As shown in Table IV, the values of ΔH^*_{10} and ΔS^*_{10} determined in this work are close to the corresponding values for the water exchange between the bulk solvent and the aquated nickel ion²² ($\Delta H^* = 11.6 \text{ kcal. mole}^{-1}$; $\Delta S^* = 0.6 \text{ cal. deg.}^{-1} \text{ mole}^{-1}$).

All the kinetic data for the nickel malonate complex formation are practically equal to those determined for the reaction of formation of nickel monooxalate.^{14a} Since the formation rate constants for nickel malonate and oxalate are similar (Table VI), the different stability of these complexes appears, of course, in the dissociation rate constant, which is greater for nickel malonate than for oxalate.

We have estimated (Table VI) all the stepwise equilibrium constants at 25° for nickel malonate complex formation from our experimental data and for nickel oxalate complex formation from the kinetic data of Nancollas and Sutin.^{14a} Since the mechanism is similar in the two cases, the following considerations are valid for the formation of both complexes. From the second equality of eq. 13 and 16, we have

$$k_d/k'_d = k_{01}K_H/k'_{01} \quad (18)$$

With the approximation $k_{01}/k'_{01} \approx 1$, i.e., by assuming that the breakage rate of the Ni-O bond is practically the same when the malonate or bimalonate ion is bonded to nickel, we have $k_d/k'_d = K_H$. The other equilibrium constants K_{20} , K'_{10} , and K_{10} can be expressed in the following terms, the product $K'_0K'_{10}$ being known

$$K_{20} = K_C K_2 / (K'_0 K'_{10}) K_H; \quad K'_{10} = (K'_0 K'_{10}) / K'_0;$$

$$K_{10} = K_C / K_0 K_{20}$$

As to the reaction between Ni^{2+} and the bimalonate ion, the only value of $K'_0K'_{10}$ given in the literature is 25.7 at 20° and $\mu = 0.1 M$.²⁴ We have also used the same value to calculate the above equilibrium constants at 25°. As to reaction of Ni^{2+} with bioxalate ion, no estimate of the value of the product $K'_0K'_{10}$

is reported in the literature. Nevertheless, an approximate value can be calculated by considering that $K'_0K'_{10}$ for the reaction of cobalt(II) with bimalonate ion at 20° and for $\mu = 0.1 M$ is 1.66 times greater than that for the analogous reaction with the bisuccinate ion.²⁴ Thus, if we assume that the same increase may be in $K'_0K'_{10}$ when passing from bimalonate ion to bioxalate ion and that this is also valid in the nickel case, the value of $K'_0K'_{10}$ should equal about $1.66 \times 25.7 \approx 43$.

By comparing the dissociation rate constants k_d for nickel malonate and oxalate, it is possible to determine on which step the respective stabilities of these complexes depend. From the eq. 13 we have

$$k_{d(\text{mal})}/k_{d(\text{ox})} = 12 = k_{01(\text{mal})}K_{20(\text{ox})}/k_{01(\text{ox})}K_{20(\text{mal})} \quad (19)$$

Since $k_{01(\text{mal})}$ is about equal to $k_{01(\text{ox})}$ (see Table VI), we conclude that the higher dissociation rate for the nickel malonate is due to the smaller value of the equilibrium constant K_{20} relative to the last step of reaction 11.

As to the dissociation rate constants k'_d , from eq. 16 we obtain

$$k'_{d(\text{mal})}/k'_{d(\text{ox})} = 227 =$$

$$k'_{01(\text{mal})}K_{11(\text{ox})}K_{20(\text{ox})}/k'_{01(\text{ox})}K_{11(\text{mal})}K_{20(\text{mal})}$$

Since $k'_{01(\text{mal})} \approx k'_{01(\text{ox})}$ (Table VI), the greater dissociation rate constant k'_d for the nickel malonate depends not only on the smaller value of the equilibrium constant K_{20} but also on the higher basicity of the intermediate $(\text{H}_2\text{O})_6\text{Ni}^+-\text{OCOCH}_2\text{COO}^-$.

Acknowledgment. The author wishes to thank Dr. Manfred Eigen for the kind hospitality in his laboratory and for helpful discussion and the Max-Planck-Institut für physikalische Chemie, Göttingen, West Germany, for financial support.

(24) E. Campi, *Ann. Chim.*, 53, 96 (1963).

Physical Adsorption on Low-Energy Solids. III. Adsorption of Ethane, *n*-Butane, and *n*-Octane on Poly(tetrafluoroethylene)

by Donald P. Graham

Contribution No. 385 from the Research and Development Division, Organic Chemicals Department, E. I. du Pont de Nemours & Co., Inc., Wilmington, Delaware (Received July 6, 1965)

Measurement of isotherms for adsorption of ethane, *n*-butane, and *n*-octane required separation of adsorption from absorption or solution in the solid. This separation was fortunately made possible by the great difference in the rates of the two processes. Ethane and *n*-butane were adsorbed with spreading pressures for a complete monolayer of 5.9 and 4.9 ergs/cm.², respectively, but *n*-octane, which does not spread on poly(tetrafluoroethylene), developed only 1.7 ergs/cm.² with deposition of a quantity equivalent to one monolayer. The greater part of this small spreading pressure was developed in the initial 10% of the deposition, indicating multilayer adsorption in patches with no real monolayer ever formed.

Introduction

Earlier papers^{1,2} have reported the adsorption of a number of nonpolar gases and vapors on the low-energy solids poly(tetrafluoroethylene) and polypropylene. All of the adsorptive materials, as liquids, spread with zero contact angle on the adsorbents and the calculated spreading pressures were in the range of 9 to 14 ergs/cm.².

The adsorbed films were characterized by high mobility and low density. In other words, a quantity of adsorbate equivalent to that required for a complete monolayer (if strongly bonded) appeared to be loosely bound in a film appreciably thicker than one molecular diameter.

This paper reports a continuation of the investigation using poly(tetrafluoroethylene) as the adsorbent and the hydrocarbons ethane, *n*-butane, and *n*-octane as adsorbates. This system was selected because the surface tensions of the adsorptive materials as liquids embrace the critical surface tension of poly(tetrafluoroethylene), which has been reported as ~ 18 dynes/cm.³ Thus, ethane and *n*-butane spread freely on poly(tetrafluoroethylene), but *n*-octane forms a finite contact angle.

Experimental Section

The poly(tetrafluoroethylene) used as the adsorbent was from the same sample used in the earlier investiga-

tion,¹ a powdered product marketed as Teflon 6. The surface area, determined by application of the B.E.T. equation to the nitrogen isotherm, was 11.67 m.²/g.

The ethane used was Phillips Research grade: 99.98% ethane, 0.02% propylene, and traces of ethylene and propane.

The *n*-butane was Phillips Pure grade: 99.35% *n*-butane, 0.33% isobutane, 0.10% neopentane, and 0.22% isopentane.

The *n*-octane was also Phillips Pure grade: 99.24% *n*-octane, 0.06% isooctanes, and 0.70% isononanes.

The equipment and methods of operation were the same employed in the earlier investigation¹ except for two points.

(1) In the adsorption of *n*-butane and *n*-octane, the thermocap relay controlling the temperature of the cryostat was activated by short-range mercury thermometers with 0.1° divisions. The ethylene gas thermometer was used for the ethane adsorption.

(2) The hydrocarbon adsorbates all showed considerable tendency to be absorbed (or dissolved) by the poly(tetrafluoroethylene) adsorbent. This is consistent with a previous observation that *n*-hexane is sorbed "between the polymer chains" of poly(tetra-

(1) D. P. Graham, *J. Phys. Chem.*, **66**, 1815 (1962).

(2) D. P. Graham, *ibid.*, **68**, 2788 (1964).

(3) H. W. Fox and W. A. Zisman, *J. Colloid Sci.*, **5**, 514 (1950).

fluoroethylene).⁴ Adsorption was separated from the process of absorption or solid solution, on the basis of the fact that the adsorption process was much faster than the diffusion-controlled absorption.

Each point on an isotherm was obtained as the zero time value of a plot of total amount sorbed vs. time. A 2-hr. period was used for ethane and *n*-butane, but only 1 hr. was used for *n*-octane because the plot began to flatten out after 1 hr. Since this method does not provide a true equilibrium measurement, some error is inescapable, but, owing to the much greater speed of adsorption vs. absorption, this error is probably very small. Of course, this situation precludes measurements at very low pressures, but these were of no interest because of the heterogeneity of the adsorbent. The inherent consistency of any appreciable error resulting from this refinement of the data is believed to ensure isotherms suitable for valid interpretation. The approximate magnitudes of the corrections to the "volume adsorbed" involved in removing the effects of solid solution are listed at the bottom of the list of physical constants of the adsorption systems in Table I. The dimensions of these corrections leave much to be desired as the rate of solution is probably determined by the amount of hydrocarbon actually at the interface, which is not a linear function of the relative pressure. In actual practice, this correction was determined experimentally for each point on each isotherm. An example is provided in Figure 1.

Table I: Physical Constants of Adsorption Systems

	Ethane	<i>n</i> -Butane	<i>n</i> -Octane
Latent heat of vaporization at T_{av} , cal./mole	3536	5380	9570
T_1 , °K.	179.6	263.2	293.2
T_2 , °K.	184.6	273.1	298.2
T_{av} , °K.	182.1	268.2	295.7
Vapor pressures of adsorptive materials at the adsorption temp., mm.			
$P_0(1)$ (at T_1)	578	514	10.5
$P_0(2)$ (at T_2)	764	772	14.08
Capacity of monolayer (V_m), ml. at STP/g. of adsorbent	1.80	1.07	0.591
Cross-sectional area/molecule, Å. ² (at T_{av})	23.5	39.5	71.5
Adsorbant surface area, m. ² /g.	11.67	11.67	11.67
Approximate initial rates of absorption by solid, (ml. at STP) (hr.) ⁻¹ (g. of adsorbent) ⁻¹ (P/P_0) ⁻¹	0.005	0.008	0.003

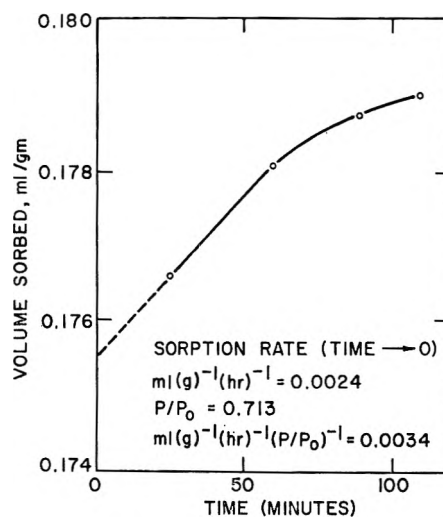


Figure 1. Total sorption of *n*-octane at 20° vs. time (an example of extrapolation to zero time).

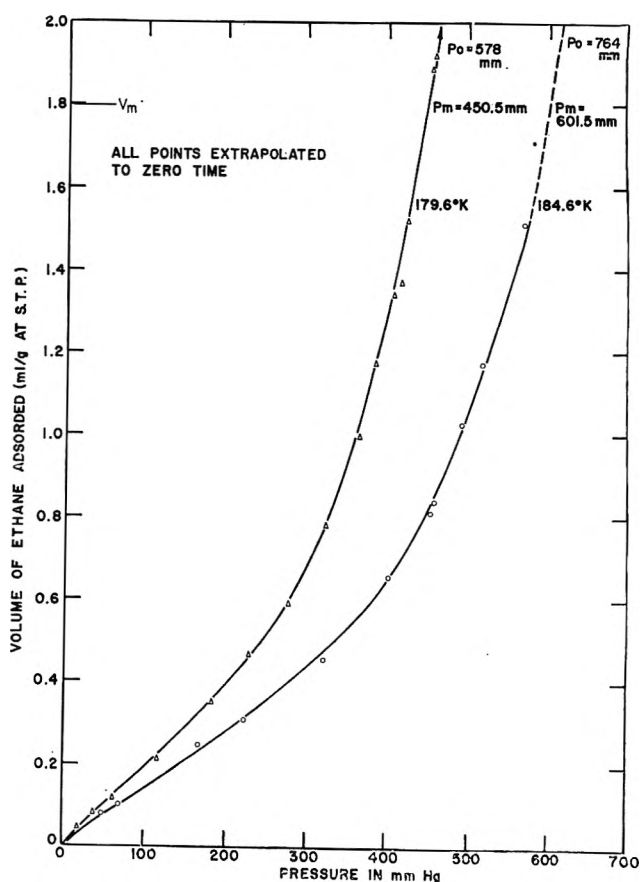


Figure 2. Adsorption of ethane on poly(tetrafluoroethylene) at 179.6 and 184.6°K.

(4) A. V. Kiselev and M. V. Serdobov, *Kolloidn. Zh.*, 25, 543 (1963).

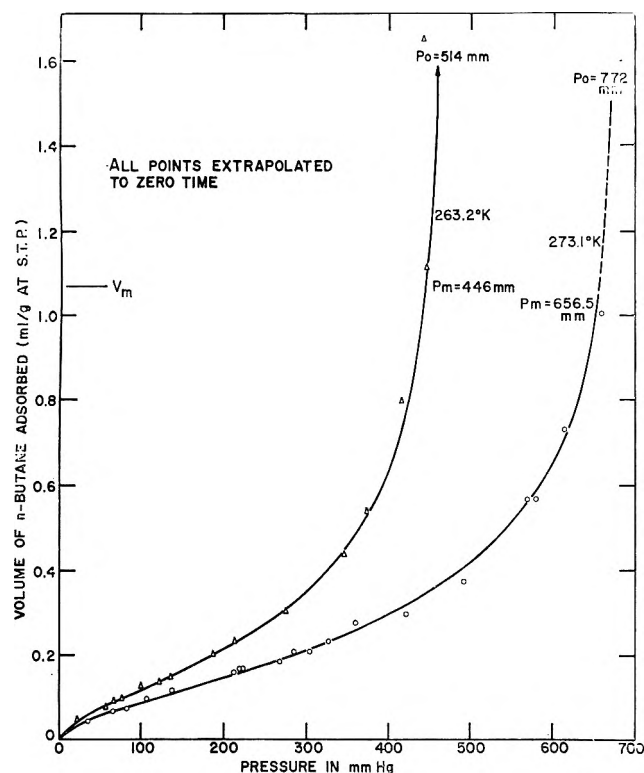


Figure 3. Adsorption of *n*-butane on poly(tetrafluoroethylene) at 263.2 and 273.1°K.

Results and Discussion

Adsorption Data. Adsorption isotherms were obtained at two temperatures for each system. Ethane and *n*-butane were studied at temperatures near their normal boiling points, but *n*-octane was studied at 20 and 25° to avoid the changes in crystallinity of the poly(tetrafluoroethylene) which would be expected at higher temperatures. The adsorption isotherms are shown in Figures 2 to 4.

Considerable hysteresis and poor reproducibility were experienced in the lower parts of the isotherms, due, in part, to adsorbent heterogeneity and porosity but made worse by the tendency for solid solution discussed earlier. However, the objectives of this paper depend upon those data representing approach to a completed monolayer rather than the measurements made at low coverage.

As was the case in the isotherms reported for other systems involving adsorbents of low surface energy,^{1,2} the isotherms show no "Point B" after deposition of a quantity of adsorbate equivalent to a true monolayer. However, this is not due to the low density of the adsorbed films, as was the case with N₂, Ar, and CF₄,^{1,2} but rather to the greater magnitude of the heats of self-condensation of the adsorptive hydrocarbons themselves.

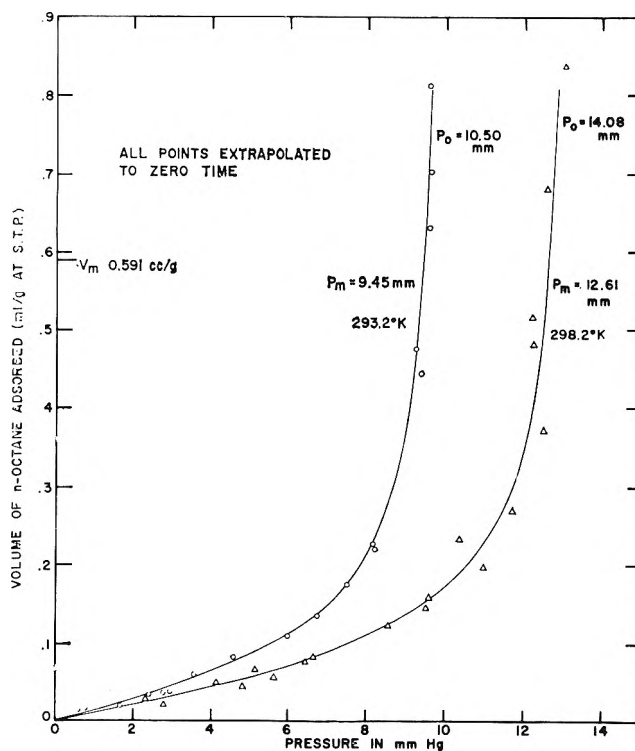


Figure 4. Adsorption of *n*-octane on poly(tetrafluoroethylene) at 293.2 and 298.2°K.

Owing to these properties of the isotherm, the quantities of adsorbed hydrocarbon representing one monolayer were determined for each system from an arbitrarily selected value for the molecular cross section of an adsorbed molecule and, from a value for the surface area of the adsorbent, determined separately (see Table I).

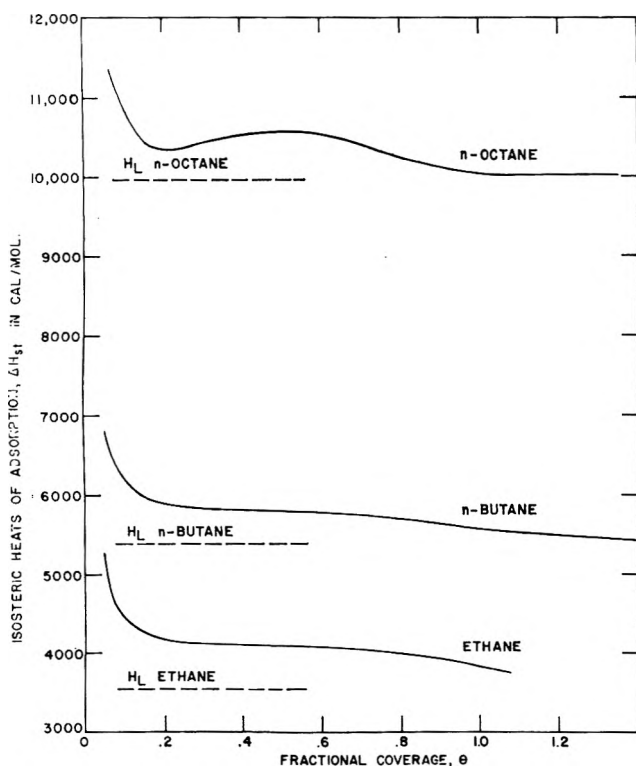
Isosteric Heats of Adsorption. Isosteric heats of adsorption of each of the three adsorptive hydrocarbons on poly(tetrafluoroethylene) were calculated by application of the Clausius-Clapeyron equation to the adsorption data. The results are plotted in Figure 5.

Owing to hysteresis, poor reproducibility, and magnification of any errors in the separation of adsorption from absorption, the uncertainty of the isosteric heats from low-coverage data (and even up to $\theta \sim 0.3$) was expected to be great. It is pertinent therefore to note that the high degree of heterogeneity indicated by the curves for these low-coverage heats is consistent with that observed in the course of earlier studies using the same adsorbent. This shows that the shape of the heat curves for this low-coverage region is at least qualitatively correct.

As stated before, the objectives of this research depend primarily on the upper part of the isotherms at coverages above $\theta \sim 0.5$, and these data are much

Table II: Comparison of Observed Entropy Changes with Those of Idealized Models Representing Site Adsorption and Mobile Adsorption

θ	$-\Delta H$, cal./mole	$-\Delta G$, cal./mole	$-\Delta S$	Std. diff. molar entropy of adsorption			
				Site adsorption		Mobile adsorption	
				Expt. $-\Delta S^{\circ}_i$	Theory gS°_{tr}	Expt. $-\Delta S^{\circ}_m$	Theory $gS^{\circ}_{tr} - aS^{\circ}_{tr}$
Ethane							
0.5	4,060	180	21.4	21.4	33.7	15.9	10.9
0.7	4,030	131	21.4	20.7		15.2	
0.85	3,990	106	21.3	17.9		14.8	
<i>n</i> -Butane							
0.5	5,750	169	20.8	20.8	37.8	15.6	11.9
0.7	5,720	112	20.9	19.2		14.9	
0.85	5,660	92	20.8	17.4		14.5	
<i>n</i> -Octane							
0.5	10,600	114	35.5	35.5	40.1	31.3	12.7
0.7	10,400	83	34.9	33.2		30.0	
0.85	10,200	72	34.3	30.9		29.0	

Figure 5. Isosteric heats of adsorption of ethane, *n*-butane, and *n*-octane on poly(tetrafluoroethylene).

better. If it is assumed that, at such high coverage, errors arising in the separation of adsorption from desorption cancel out, the degree of remaining uncertainty (as indicated by calculations from repeated "best curves" through the experimental points) is of the order of 5% for *n*-butane, less for ethane, and somewhat

more for *n*-octane. These uncertainties are, of course, carried on into the derived entropies but do not alter or weaken the conclusions.

In each case the heat drops from an initial high value (representing the strong sites on the adsorbent) to a level only a few hundred calories above the heat of condensation of the adsorptive material. After deposition of an amount of adsorbate equivalent to one monolayer, it drops to a value closely approaching the latent heat of condensation. This latter effect becomes more pronounced as the length of the hydrocarbon chain is increased, and, in the same sequence, there is an increasing tendency for the pressure at which multilayer deposition becomes important to approach the vapor pressure (P_0). The significance of these observations will be made clearer by consideration of the adsorbate mobility which follows.

Adsorbate Mobility. An indication of the extent of mobility *vs.* localization of adsorbed molecules is obtained from the entropy change in adsorption. As in the previous papers,^{1,2} adsorbate mobility is measured in terms of standard differential entropies of adsorption calculated from adsorption data and compared with those from theoretical, entropically ideal processes representing adsorption on fixed sites and as a mobile, two-dimensional gas. The method of calculation employed is that of de Boer and Kruyer.⁵ The results are reported in Table II.

In each case, the observed loss of entropy is less than that which would occur if the adsorbate were

(5) J. H. de Boer and S. Kruyer, *Proc. Koninkl. Ned. Akad. Wetenschap*, B55, 451 (1952).

localized although that condition is approached in the adsorption of octane. Expressed in terms of Table II, $-\Delta S_i$ (a combination of the experimentally observed entropy change with a configurational term) is smaller than ${}_gS^\circ_{tr}$ (the translational entropy of the adsorptive gas).

The test for mobile adsorption is a comparison of $-\Delta S_m$ (a combination of the experimental entropy change with a measure of the area over which an adsorbed molecule is free to move at a specified coverage) with ${}_gS^\circ_{tr} - {}_aS^\circ_{tr}$ (the difference between the translational entropy of the adsorptive gas and that of the adsorbate as an ideal, mobile, two-dimensional gas, or the entropy change resulting from loss of one degree of translational freedom).

Ethane and *n*-butane were adsorbed with entropy changes intermediate between those values representing two-dimensional mobility and localization. This restricted mobility is analogous to that reported in the previous paper² for ethane and carbon tetrafluoride on polypropylene.

n-Octane was more localized, particularly at low coverage, suggesting adsorption on strong sites followed by multilayer adsorption over these same strong sites to yield liquidlike multilayer patches.

Film Pressures. Film pressures or changes in the surface free energy with adsorption were calculated

from the adsorption data for a quantity of adsorbate equivalent to one complete monolayer by graphic integration of the Gibbs equation as described by Harkins.⁶ The values obtained for ethane and for *n*-butane (which, as liquids, spread on poly(tetrafluoroethylene) with zero contact angle) were 5.9 and 4.9 ergs/cm.², respectively. However, *n*-octane, which as a liquid forms a finite contact angle on poly(tetrafluoroethylene), was adsorbed with a film pressure of only 1.7 ergs/cm.², and most of this was developed in deposition of less than 10% of the quantity of adsorbate equivalent to one complete monolayer. This strongly supports other indications of adsorption in patches and the conclusion that, in the case of octane, no true monolayer was formed. The value of 1.7 ergs/cm.² is considerably lower than the value of 9 ergs/cm.² estimated by Melrose⁷ for decane on poly(tetrafluoroethylene) from contact angle and two-liquid adhesion-tension data but is in agreement with the results of measurements of the spreading pressure of *n*-octane on low-energy liquid surfaces.⁸

(6) W. D. Harkins, "The Physical Chemistry of Surface Films," Reinhold Publishing Corp., New York, N. Y., 1952, p. 211.

(7) J. C. Melrose, *Advances in Chemistry Series*, No. 43, American Chemical Society, Washington, D. C., 1964, p. 171.

(8) R. E. Johnson and R. H. Dettre, private communication awaiting publication.

Internal Pressure of Simple Liquids

by Umberto Bianchi, Giuseppe Agabio, and Antonio Turturro

Istituto di Chimica Industriale, Sezione V del Centro Nazionale di Chimica delle Macromolecole, Università di Genova, Genova, Italy (Received August 31, 1965)

Internal pressures $[(\partial U/\partial V)_T]$ have been measured for carbon tetrachloride, benzene, and cyclohexane over a range of temperature, both at constant pressure and at constant volume. $(\partial U/\partial V)_T$ is shown to decrease slightly by increasing the temperature at constant volume, thus showing the liquid intermolecular energy not to be, strictly speaking, a function of volume alone.

Introduction

Our previous work¹⁻⁴ on the internal pressure-temperature behavior of various polymers has often demanded a more extensive knowledge of some properties of simple liquids. In particular, we are interested in the comparison between energy-volume-temperature relationships for both simple and polymeric liquids (like an amorphous polymer well above its glass transition temperature T_g).

The internal pressure P_i , defined by

$$P_i = \left(\frac{\partial U}{\partial V}\right)_T = T\left(\frac{\partial P}{\partial T}\right)_V - P$$

can be determined by direct measurement of the thermal pressure coefficient $\gamma_V = (\partial P/\partial T)_V$, and its fundamental correlation with intermolecular energy makes this quantity particularly suited for our purposes.^{5,6}

This paper deals with a first group of measurements on the P_i change with temperature both at constant pressure and at constant volume, for three liquids: carbon tetrachloride, benzene, and cyclohexane.

A number of papers has recently been published on the equation of state (that is, an equation relating P , V , and T) for simple liquids and on their thermodynamic properties.^{7,8}

The general assumption is to consider the intermolecular energy U to depend only on the volume, while the temperature influences the intermolecular energy only through the alteration of the average distance of interaction between molecules.

This assumption is equivalent to writing

$$U = -\frac{a}{V^n} \quad (1)$$

where a is a constant (independent of T) and n is equal to or near unity.⁹

From (1) it follows

$$\left(\frac{\partial U}{\partial V}\right)_T = P_i = \frac{na}{V^{n+1}} \quad (2)$$

$$\left(\frac{\partial \ln P_i}{\partial T}\right)_P = -(n+1)\left(\frac{\partial \ln V}{\partial T}\right)_P = -(n+1)\alpha \quad (3)$$

$$\left(\frac{\partial \ln P_i}{\partial T}\right)_V = 0 \quad (3')$$

where α in eq. 3 is the cubical thermal expansion coefficient of the liquid.

Equations 3 and 3' show how the measurement of P_i over a temperature interval at constant pressure (eq. 3) and at constant volume (eq. 3') can provide a simple, direct way to test the assumption connected with eq. 1.

- (1) U. Bianchi, *Ric. Sci., IIA*, **32**, 651 (1962).
- (2) U. Bianchi and C. Rossi, *Chim. Ind. (Milan)*, **45**, 33 (1963).
- (3) U. Bianchi and E. Bianchi, *ibid.*, **45**, 657 (1963).
- (4) C. Rossi, U. Bianchi, and E. Bianchi, *J. Polymer Sci.*, **C4**, 699 (1963).
- (5) J. H. Hildebrand and R. L. Scott, "The Solubility of Nonelectrolytes," Reinhold Publishing Corp., New York, N. Y., 1950.
- (6) G. Allen, G. Gee, and G. J. Wilson, *Polymer*, **1**, 456 (1960).
- (7) E. B. Smith, *J. Chem. Phys.*, **36**, 1404 (1962).
- (8) P. J. Flory, R. A. Orwoll, and A. Vrij, *J. Am. Chem. Soc.*, **86**, 3507 (1964).
- (9) E. B. Smith and J. H. Hildebrand, *J. Chem. Phys.*, **31**, 145 (1959).

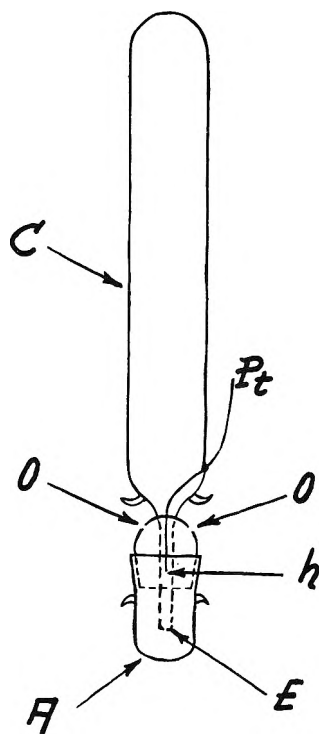


Figure 1. Pyrex glass cell used for P_i measurements on liquid samples.

Experimental Section

Materials. The solvents used were of high purity (RS according to the Carlo Erba reagents classification) and were distilled immediately before P_i measurements.

P_i Measurements. The experimental technique has been already described in detail²; we show in Figure 1 the cell used in these experiments.

C is a Pyrex glass cell, of about a 30-cc. capacity, which is first filled with the liquid to be studied and connected through the capillary end E to a vacuum line.

By repeated freezing with liquid nitrogen and melting under vacuum, the gas dissolved is eliminated. After disconnecting from the vacuum line, E is rapidly immersed in the Hg contained in A; by a suitable change in temperature, the liquid Hg meniscus is formed in h, *i.e.*, near the end of the platinum wire Pt.

The Hg in A is in electric contact, through the holes O, with some Hg contained at the bottom of the pressure vessel in which the cell is sealed.²

In this way, a lamp connected with a transformer through the platinum wire Pt and the Hg in A will reveal the position of the liquid Hg meniscus in the capillary tube E.²

Results

To measure the change of P_i by varying the temperature at constant pressure, we started with the measure-

ment of P_i at the lowest temperature, under an average pressure of 5 atm. Our practical experience has shown that the application of a small pressure increases the reproducibility of the results.

After performing three or four runs at the lowest temperature, the temperature is raised while the pressure is released; this results in some solvent coming out of the cell. At this point, a pressure of ~ 5 atm. is applied, and, by suitably changing the temperature, a new temperature is obtained, at which the liquid Hg meniscus in the cell is just in contact with the Pt wire. This makes possible the determination of P_i at this new temperature; by repetition of this procedure, we have studied the P_i behavior over some temperature intervals, as it is shown in Table I. Measurements of the function $P_i = P_i(T)$ at constant volume is simpler, as in going from the lowest to a higher temperature (at which P_i has to be measured) it is necessary simply to increase the pressure proportionally so that the liquid Hg meniscus is always kept in the same, initial, position. Results are shown in Table II. All P_i values in Tables I and II are averages over at least two independent measurements, the reproducibility being within 1% of the total value.

As has been pointed out previously,¹⁰ the experimental value of $\gamma = (\partial P/\partial T)_V$ has to be corrected for

Table I: P_i Values at Constant Pressure (at an Average Pressure of 5 atm.)

CCl ₄		C ₆ H ₆		C ₆ H ₁₂	
t , °C.	P_i , cal./cc.	t , °C.	P_i , cal./cc.	t , °C.	P_i , cal./cc.
21.5	82.7	26.3	90.7	22.3	78.6
22.4	82.5	32.2	89.2	28.9	76.9
26.7	81.3	36.7	88.4	35.2	75.9
36.8	79.2	43.8	86.6	37.2	76.1
45.1	77.4	48.4	85.9	45.0	73.8
53.8	76.2	54.1	83.9	52.8	72.6
60.0	75.0	54.4	83.6	60.3	70.6
		60.3	82.7		

Table II: P_i Values at Constant Volume

CCl ₄		C ₆ H ₆		C ₆ H ₁₂	
t , °C.	P_i , cal./cc.	t , °C.	P_i , cal./cc.	t , °C.	P_i , cal./cc.
21.5	82.7	26.3	90.7	29.4	77.3
22.4	82.5	32.0	90.7	36.9	77.3
28.7	82.5	37.7	90.4	44.8	76.3
34.9	81.7	43.9	89.5	52.2	76.6
41.7	81.6	50.0	89.0	59.9	76.3
48.0	81.6	55.5	89.4	66.5	76.2
55.3	81.3				

thermal expansion and compressibility of the Pyrex cell, using the equation

$$\gamma_V = \gamma \left(1 - \frac{\beta_g}{\beta_l} \right) + \frac{\alpha_g}{\beta_l} \quad (4)$$

where α_g = Pyrex thermal expansion coefficient (9.9×10^{-6} deg.⁻¹), β_g = Pyrex isothermal compressibility (3.0×10^{-6} atm.⁻¹), and β_l = liquid isothermal compressibility.

It is to be noted that our experimental data in Table II (V = constant) are not strictly values at constant volume because to keep the liquid Hg meniscus just in contact with the Pt wire does not mean a true constancy of the liquid volume.

This nonconstancy is obviously due to the change in temperature and pressure which affect the Pyrex cell volume.

This effect can be estimated by calculating the change in glass cell volume (*i.e.*, the volume of the liquid) by changing P and T . The glass cell volume is a function of T and P as

$$V_g = V_g^0(1 + \alpha_g \Delta T - \beta_g \Delta P) \quad (5)$$

In our case we have an average of 1° for ΔT and a corresponding change of 10 atm. for ΔP ; from eq. 5 we get

$$\frac{V_g - V_g^0}{V_g^0} = \alpha_g \Delta T - \beta_g \Delta P = -2 \times 10^{-5}$$

This means that the P_i values of Table II at different temperatures are not exactly at constant volume but refer to a liquid which is slightly contracting by increasing the temperature. The contraction is, however, very small.

Discussion of the Results

It is interesting, first of all, to compare our P_i values at 20° and about 1 atm. with equivalent values taken from literature.^{6,11-13} (See Table III.) As these data have not been obtained by the same method, the agreement is satisfactory and shows the accuracy with which P_i can be measured.

From Tables I and II we can calculate the slopes $(\partial \ln P_i / \partial T)_P$ and $(\partial \ln P_i / \partial T)_V$ which are collected in Table IV. It can be seen that $(\partial \ln P_i / \partial T)_P$ values are in fairly good agreement with -2α values, thus confirming the value $n = 1$ in eq. 2 and 3. This also confirms Gee's conclusion⁶ about the possibility of using eq. 3 (with $n = 1$) to calculate the change of P_i over small temperature intervals.

The most important point, however, is to note that $(\partial \ln P_i / \partial T)_V$ values are significantly different from zero (see eq. 3), their uncertainty being $\pm 10\%$.

Table III: Comparison among P_i Values at 20° , Taken from Different Sources^a

Liquid	P_i , cal./cc.				
	Ref. 6	Ref. 11	Ref. 12	Ref. 13	This work
CCl ₄	82.4	83.0	82.2	82.3	82.7
C ₆ H ₆	90.5	92.8	...	89.4	92.0
C ₆ H ₁₂	77.8	74.7	79.2

^a P_i values from ref. 6 are determined through sound velocity measurements; ref. 11 gave values of isothermal compressibility which, together with expansion coefficient data, have been used to calculate P_i values.

Table IV: Temperature Coefficients of $\ln P_i$ at Constant Pressure and at Constant Volume

Liquid	$10^4 \left(\frac{\partial \ln P_i}{\partial T} \right)_P$, °K. ⁻¹	$10^4 \left(\frac{\partial \ln P_i}{\partial T} \right)_V$, °K. ⁻¹	$10^4(-2\alpha)$, °K. ⁻¹
CCl ₄	-2.6	-0.46	-2.5
C ₆ H ₆	-2.7	-0.52	-2.6
C ₆ H ₁₂	-2.7	-0.40	-2.4

Moreover, we expect these values to be more negative than those quoted because they refer to an experiment in which, as previously noted, the volume of the liquid is slightly decreasing by increasing the temperature; the observed P_i values are thus a little higher than those referring to a liquid truly kept at constant volume, and consequently the absolute values of the slope $(\partial \ln P_i / \partial T)_V$ are decreased.

We can conclude that the intermolecular interaction energy of a liquid is not strictly a function of the volume alone and that, even keeping the volume constant, the temperature itself is capable of introducing an alteration, perhaps through a change in the average arrangement of each molecule and its neighbors.

Previous experimental results on CCl₄ and some fluorocarbons have been taken as evidence that $\gamma_V = (\partial P / \partial T)_V$ was constant over some 20° temperature interval (at constant volume).⁹ The evidence was based on the linearity of the pressure-temperature plot in these temperature intervals. The change of γ_V with temperature (at constant volume) is however too minute, and the temperature interval of 20° too small

(10) W. Westwater, H. W. Frantz, and J. H. Hildebrand, *Phys. Rev.*, **31**, 35 (1928).

(11) G. A. Holder and E. Whalley, *Trans. Faraday Soc.*, **58**, 2095 (1962).

(12) H. Benninga and R. L. Scott, *J. Chem. Phys.*, **23**, 1911 (1955).

(13) J. S. Rowlinson, "Liquids and Liquid Mixtures," Butterworths Scientific Publications, London, 1959.

to be able to discover the slight curvature in a plot of F against T .

Work is in hand to extend these measurements to other simple liquids, including polar compounds,

and to high molecular weight polymers, on which some preliminary results have been already published.¹

Acknowledgment. It is a pleasure to acknowledge the continuous interest of Prof. C. Rossi in this work.

NOTES

Barium-Iron-Oxygen Compounds with Varying Oxygen Content and Iron Valence

by Anna Clyde Fraker

Department of Engineering Research,
North Carolina State University at Raleigh,
Raleigh, North Carolina (Received May 24, 1965)

The hypothesis of Erchak and Ward¹ that barium-iron-oxide can accommodate different amounts of oxygen and that the structure maintains stability by varying iron valencies is supported by this paper, and a correlation between oxidation state and interatomic spacing is shown. Mössbauer measurements² of the perovskite BaFeO_3 compound reported by Derbyshire, Fraker, and Stadelmaier³ show that 76% of the iron is in the +4 valence state and 24% is in the +3 state. Thus the empirical formula for this compound is probably $\text{Ba}(\text{Fe}_3^{+4} \cdot \text{Fe}^{+3})\text{O}_{2.9}$ instead of the stoichiometric BaFeO_3 . Two +3 iron ions are formed for every oxygen ion which is lost.

The X-ray pattern of $\text{BaFeO}_{2.9}$ is shown in Figure 1A along with charts of two other materials which were equilibrated as described in Table I. The Mössbauer absorption spectrum of preparation A, Table I, as well as a mixture of preparation B and C is shown in Figure 2. In Figure 2A, the principal absorption peak corresponds to Fe^{+4} , the minor peak to Fe^{+3} . It is characteristic of these structures that their principal diffraction lines coincide and have comparable intensities. The X-ray patterns of materials B and C show a remarkable shift of the diffraction lines due to changes in the experimental conditions. This shift is associated with variations in ionic distances in the basic structure and must be attributed to the ionic radius of the iron. It is the size of the iron ion inside the octahedron which determines the lattice parameter

shift in the close-packed arrangement of barium and oxygen ions. The Fe-O distance which is listed in Table I was determined by dividing the interplanar spacing for the strongest diffraction peak by $\sqrt{2}$. This peak corresponds to {110} planes for the cubic structure of Figure 1A. It may be concluded from Table I that materials B and C are oxygen deficient, and Mössbauer measurements (Figure 2) of a mixture

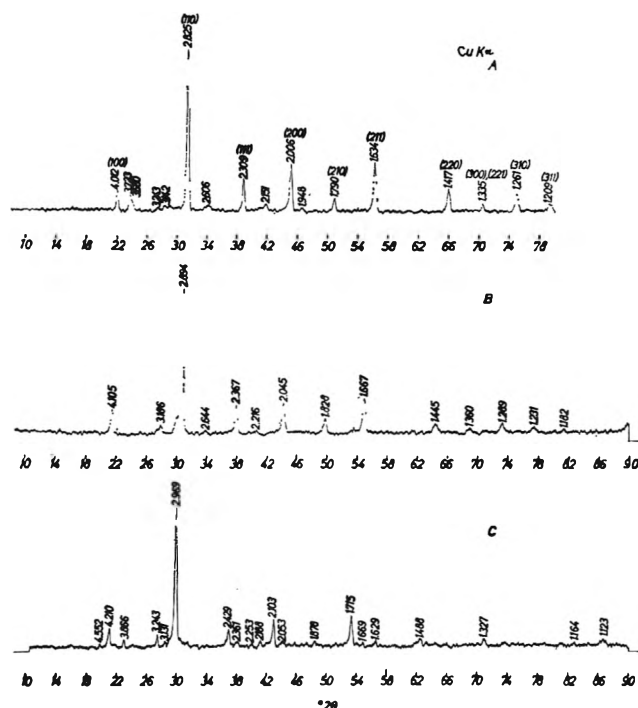


Figure 1.

(1) M. Erchak, Jr., and R. Ward, *J. Am. Chem. Soc.*, 68, 2093 (1946).

(2) Dr. Uri Shimony of the Massachusetts Institute of Technology, Cambridge, Mass., did the Mössbauer work.

(3) S. W. Derbyshire, A. C. Fraker, and H. H. Stadelmaier, *Acta Cryst.*, 14, 1293 (1961).

Table I^a

	A	B	C
Calcination temp. and atmosphere	1000° in closed tube or 700° in air	850–900° in air and quenched	950–1000° in air and quenched
Phases present	Barium-iron(IV) oxide and BaCO ₃	Barium-iron(III) oxide and BaO	Barium-iron(II) oxide and BaO
Valence and radius of iron ion	Fe ⁺⁴ 0.58 Å.	Fe ⁺³ 0.64 Å.	Fe ⁺² 0.76 Å.
Sum of radii, Fe–O	1.98 Å.	2.04 Å.	2.16 Å.
Distance Fe–O, obsd.	2.01 Å.	2.05 Å.	2.10 Å.
Mössbauer measurement of iron valence	76% Fe ⁺⁴ 24% Fe ⁺³	A mixture of materials B and C shows equal amounts of +3 and +2 iron	

^a The ionic radii in this table are those of Pauling and the oxygen radius is 1.40 Å. with the exception of the Fe⁺⁴ radius which is that assumed by C. Brisi, *Ann. chim.*, **45**, 431 (1955).

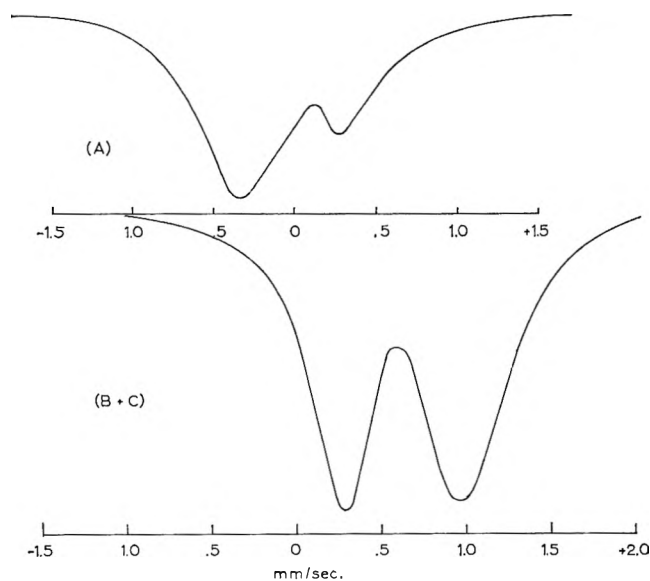


Figure 2.

of B and C show that no +4 iron is present in either of them. The discrepancy in the observed and calculated Fe–O distances in material A would also suggest that all iron is not in the +4 state.

Prior to calcination, the materials were prepared by a modified method of Clabaugh, Swiggard, and Gilchrist⁴ in which a mixed oxalate was precipitated. The initial ratio of barium to iron was 1.5:1. The excess barium is needed to make the reaction go to completion and some of this extra barium is washed out and any remaining excess later comes out as barium oxide or barium carbonate after calcination. Calculated X-ray intensities³ show that the excess barium does not remain as part of the barium-iron-oxygen compound.

An increase in temperature causes an oxygen loss

in these compounds, and this loss is compensated by the changing valence of the iron ion. As the oxygen loss occurs, the iron is reduced; however, upon reintroduction of oxygen to the structure, the iron again changes to a higher oxidation state. Since this is a reversible process, the material will tend toward an equilibrium compound for a given temperature and given oxygen partial pressure. This reversibility has been observed by taking material of Figure 1C and placing it into the furnace at 1000° in air and allowing it to cool slowly. The resultant structure is that of Figure 1A.

(4) W. S. Clabaugh, E. M. Swiggard, and R. Gilchrist, *J. Res. Natl. Bur. Std.*, **56**, 289 (1956).

The Hg(³P₁)-Sensitized Decomposition of *n*-Hexane Vapor

by Robert R. Kuntz

Department of Chemistry, University of Missouri, Columbia, Missouri (Received June 4, 1965)

The Hg(³P₁)-sensitized decomposition of alkanes leads to alkyl radicals and hydrogen atoms. Comparison of the liquid and vapor phase decompositions of *n*-pentane^{1,2} and isopentane^{2,3} indicates that similar processes are in operation in these media. The dispropor-

(1) R. A. Back, *Trans. Faraday Soc.*, **54**, 512 (1958).

(2) R. R. Kuntz and G. J. Mains, *J. Am. Chem. Soc.*, **85**, 2219 (1963).

(3) R. R. Kuntz, *J. Phys. Chem.*, **69**, 2291 (1965).

tiation/combination ratio for hexyl radicals produced in the liquid phase radiolysis⁴ compared to that observed in the liquid phase mercury-sensitized photolysis,² however, shows a large discrepancy. This brief study of the vapor phase mercury-photosensitized photolysis of *n*-hexane was made in order to learn more about the reactions of hexyl radicals and H atoms.

Experimental details are described elsewhere³ and will not be repeated here. Pure grade *n*-hexane from the Phillips Petroleum Co. was freed from olefin impurities by a gas chromatographic peak isolation technique on a 0.64 cm. \times 2.75 m. β,β -oxydipropionitrile column. Ethylene of stated 99.5% minimum purity was obtained from the Matheson Co. and used without further purification. Hexene-1 was obtained from K & K Laboratories and used without further purification since gas chromatographic analysis indicated no major impurities. Added ethylene and hexene-1 were kept at less than 2% of the reaction mixture to minimize quenching of excited mercury by these scavengers. All experiments were performed at 10-cm. of *n*-hexane pressure and 25°. Care was taken to remove hydrogen before it became sufficiently concentrated to quench an appreciable amount of excited mercury. In experiments with added ethylene, the light intensity was higher than in other experiments.

Results and Discussion

In Figure 1, the rate of hydrogen production is plotted against illumination time. Samples were taken at various intervals with the lowest conversion being about 0.05%. Gas chromatographic analyses of the liquid products indicate the olefins are predominantly hexene-2 and -3. Three dimer products were characterized by comparison with authentic samples produced in the liquid phase mercury-sensitized decomposition of *n*-hexane² and found to be 5,6-dimethyldecane, 4-ethyl-5-methylnonane, and 4,5-diethyloctane in the ratio 1:2:1.

The mechanism of mercury-photosensitized decompositions has been discussed in some detail.⁵ A simplified reaction scheme neglecting reactions of secondary products may be illustrated by reactions 1-5. Reactions 6 and 7 become important at very low conver-

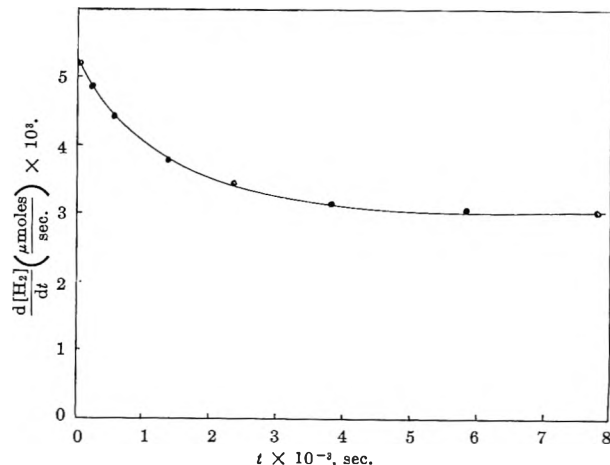
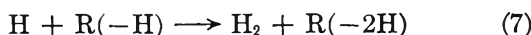
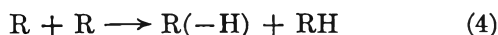
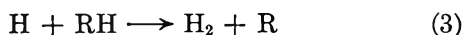
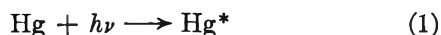


Figure 1. Hydrogen production as a function of photolysis time.

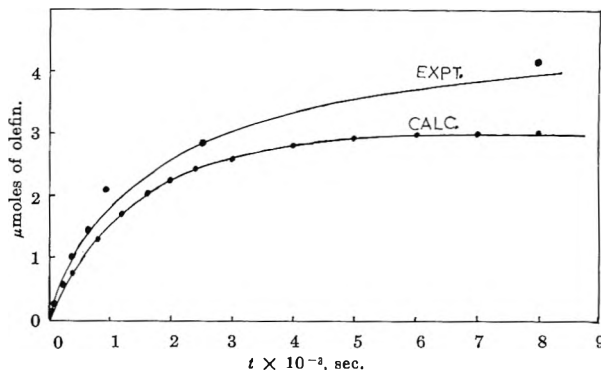


Figure 2. Olefin production as a function of photolysis time.

sions, owing to the greater reactivity of H atoms with olefins than with saturated hydrocarbons. Scavenger studies⁶ and dimer identifications² indicate the important radicals are 2- and 3-hexyl, each contributing about equally and comprising 99% of the total radical yield.

Under conditions of constant light intensity and low conversions, the initial rate of hydrogen production is a constant, K . From this simplified reaction mechanism, the rate of hydrogen production is given by eq. 1, where $[S]$ is the olefin concentration. The initial

$$\frac{d[\text{H}_2]}{dt} = \frac{k_3[\text{RH}] + k_7[\text{S}]}{k_3[\text{RH}] + (k_6 + k_7)[\text{S}]} K \quad (1)$$

conditions $[S] = 0$ and $t = 0$ give as the initial slope of the curve in Figure 1

(4) T. J. Hardwick, *J. Phys. Chem.*, **64**, 1623 (1960).

(5) Y. Rousseau, O. P. Strausz, and H. E. Gunning, *J. Chem. Phys.*, **39**, 962 (1963).

(6) R. A. Holroyd and G. W. Klein, *J. Phys. Chem.*, **67**, 2273 (1963).

$$\left(\frac{d^2[\text{H}_2]}{dt^2}\right)_{t=0} = \frac{Kk_6}{k_3[\text{RH}]} \frac{d[\text{S}]}{dt} \quad (\text{II})$$

Hydrogen production decreases from an extrapolated value of 5.30×10^{-9} mole/sec. to a plateau value of 3.00×10^{-9} mole/sec. This decrease may be attributed to the scavenging of H atoms by reaction 6. Since olefin is formed by reaction 4 and destroyed by reactions 6 and 7, it follows that the rate of olefin production is at least as great as the rate of hydrogen loss and undoubtedly greater because of reaction 7. Using $(5.30 - 3.00) \times 10^{-9}$ mole/sec. = 2.30×10^{-9} mole/sec. for $(d[\text{S}]/dt)_{\text{initial}}$, we obtain a value of 202 for k_6/k_3 . The importance of reaction 7 may be shown in the following manner. If we consider this reaction to be unimportant, then it may be shown that

$$\frac{d[\text{S}]}{dt} = \frac{d[\text{H}_2]}{dt} = \left(\frac{d[\text{H}_2]}{dt}\right)_{\text{plateau}} \quad (\text{III})$$

so a graphical integration of Figure 1 gives [S] as a function of photolysis time. This integration is shown in Figure 2 by the solid line and accompanied by the gas chromatographic determination of hexenes at various times. Thus $(d[\text{S}]/dt)_{\text{initial}}$ is somewhat greater than 2.30×10^{-9} mole/sec. From Figure 2, it would appear to be about 15% higher or 2.64×10^{-9} mole/sec. This would correspond to a k_6/k_3 value of 177 from the slope measurement. Rearrangement of eq. I (neglecting reaction 7) gives

$$\frac{K}{d[\text{H}_2]/dt} = 1 + \frac{k_6[\text{S}]}{k_3[\text{RH}]} \quad (\text{IV})$$

and k_6/k_3 may be calculated from each experimental point. The average value calculated in this manner using the calculated olefin content is 213, while the experimental points yield a value of 181.

The value of k_4/k_5 may be estimated in a similar manner. Since the material balance requires

$$\frac{d[\text{S}]}{dt} = \frac{d[\text{R}_2]}{dt} = 5.30 \times 10^{-9} \text{ mole/sec.} \quad (\text{V})$$

initially, and $d[\text{S}]/dt \geq 2.30 \times 10^{-9}$ mole/sec., then $d[\text{R}_2]/dt \leq 3.00 \times 10^{-9}$ mole/sec. and $k_4/k_5 \geq 2.30/3.00 = 0.77$. Using values calculated from the low-conversion experimental points in Figure 2, a value of 0.97 ± 0.08 can be obtained in the liquid phase mercury-photosensitized decomposition of *n*-hexane but is not similar to the value of 1.8–2.3 obtained by Hardwick⁴ in the liquid phase radiolysis.

In a few experiments, olefins were added. Rearrangement of eq. I gives eq. VI, where $d[\text{H}_2]/dt = K - (d[\text{H}_2]/dt)_{\text{scavenger}}$. Equation VI is plotted for

$$\frac{1}{d[\text{H}_2]/dt} = \frac{1}{K} \frac{k_3[\text{RH}]}{k_6[\text{S}]} + \frac{1}{K}(1 + k_7/k_6) \quad (\text{VI})$$

hexene-1 in Figure 3. A few determinations were made with ethylene as a scavenger at higher light intensities, and these also appear in Figure 3. The rate constant ratios for hexene-1 indicate $k_6/k_3 = 750$ and $k_7/k_6 = 0.12$. These values do not agree with the respective values 173 and 0.50 obtained in the liquid phase radiolysis,⁴ but they are in reasonable agreement with the values 419 and 0.02 in the mercury-sensitized *n*-pentane-pentene-1 system¹ and 818 and 0.07 in the mercury-sensitized *n*-butane-butene-1 system.⁷ The ratio of H atom addition to the predominant 2- and 3-hexene to abstraction from *n*-hexane (180) is much lower than the equivalent ratio (750) for addition of H atoms to hexene-1. This is consistent with the earlier work done with *n*-pentane (222:419)¹ and *n*-butane (354–445:818).⁷

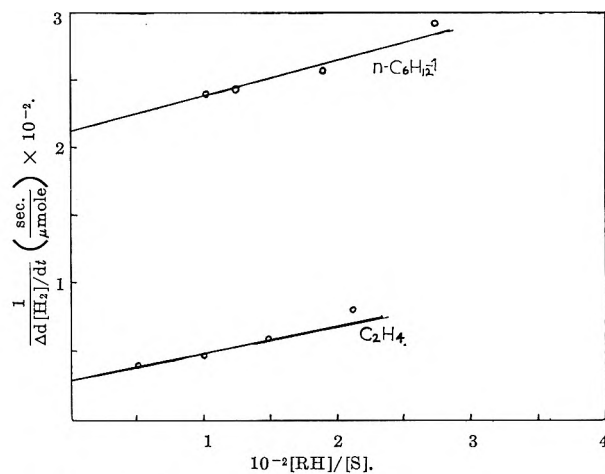


Figure 3. Plot of eq. VI.

If one fits a least-mean-square line to the ethylene experiments, a value of k_6/k_3 of 156 is obtained. This value compares to 422 obtained in the *n*-butane-ethylene system⁷ and 25,000 obtained in the ethane-ethylene system.⁸

Acknowledgment. The author gratefully acknowledges partial support for this study by the American Chemical Society Petroleum Research Fund. The author also wishes to thank Mr. Jonas Dedinas for some gas chromatographic analyses.

(7) K. R. Jennings and R. J. Cvetanović, *J. Chem. Phys.*, **35**, 1233 (1961).

(8) R. A. Back, *Can. J. Chem.*, **37**, 1834 (1959).

Enthalpies of Formation of Gaseous Tantalum Oxide and Tantalum Dioxide¹

by Oscar H. Krikorian and John H. Carpenter

Lawrence Radiation Laboratory, University of California, Livermore, California (Received June 12, 1965)

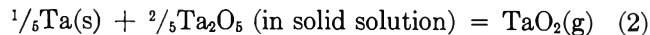
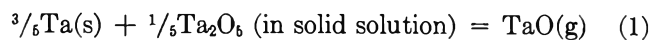
During recent mass spectrometric studies of the vapor pressures of molybdenum and technetium, the ions TaO^+ and TaO_2^+ were detected as impurities. The ions were formed by electron bombardment with 12.5-e.v. electrons and are believed to have originated directly from TaO and TaO_2 species vaporizing from tantalum rods contained in a rhenium filament heater. Gas-surface reactions seem unlikely as the source of the molecules, since residual gas pressures in the system were less than 1×10^{-7} torr, and ions of other oxide molecules such as those of molybdenum, technetium, or rhenium were not detectable.

Calculated pressures of TaO and TaO_2 are presented in Table I. Details of the experimental and calculational methods for obtaining pressures will be described later.² Briefly, a mixed molecular beam containing the tantalum oxides and molybdenum was produced from a tubular rhenium heater with a slit along one side. Tantalum rod and molybdenum sheet with effective areas of 1.5 and 1.8 mm.², respectively, were present in several compartments of the heater. Pressures were calculated from ion intensities by using the known pressures of molybdenum to calibrate the sensitivity of the mass spectrometer and by taking the sensitivity to vary as the inverse square root of mass. The Otvos and Stevenson method³ was used for the calculation of ionization cross sections and gave values of 52.5, 78.7, and 82.0 for the relative cross sections of Mo, TaO , and TaO_2 , respectively. The cross section of tantalum (75.4) was based on a configuration of $5d^3 6s^2$ for the outer electrons. Calculations of thermodynamic data in this paper have been based on thermodynamic tables prepared by AVCO.⁴

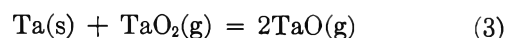
Table I: Pressures of TaO and TaO_2 above a Ta_2O_5 Solid Solution in Tantalum

T , °K.	$P_{\text{TaO}} \times 10^3$, atm.	$P_{\text{TaO}_2} \times 10^3$, atm.
2177	1.485	...
1924	0.015	...
2031	0.129	...
2258	6.06	...
2268	5.94	2.02

$\text{TaO}(\text{g})$ and $\text{TaO}_2(\text{g})$ are assumed to be formed by the reactions



where the Ta_2O_5 activity has been lowered by solution in tantalum. If the Ta_2O_5 activity remains fixed during the measurements, reactions 1 and 2 can be combined to give



A third-law treatment of reaction 3 using the pressures from Table I results in a ΔH°_{298} of reaction of 174.5 kcal./mole.

Reactions 1 and 2 cannot be treated by third-law methods since the Ta_2O_5 activity is not known. A second-law treatment may be used on reaction 1, however, by assuming that Ta_2O_5 forms an ideal solution in tantalum and that the enthalpy of solution of Ta_2O_5 in tantalum is zero. The data show little scatter and give a ΔH°_{298} of 63.0 kcal./mole for $\text{TaO}(\text{g})$. Combining this with the value of 174.5 kcal. for reaction 3 gives -48.5 kcal./mole for the ΔH°_{298} of $\text{TaO}_2(\text{g})$.

Measurements by Inghram, *et al.*,⁵ on mixtures of Ta_2O_5 and tantalum indicate a significantly different enthalpy change for reaction 3. Using the Otvos and Stevenson method³ for estimating cross sections, and the same thermodynamic functions as above,⁴ we calculate a ΔH°_{298} of 152.1 kcal./mole for reaction 3 when either Ta_2O_5 or a mixture of Ta_2O_5 and tantalum is heated in a tantalum Knudsen cell. Inghram, *et al.*, observed that as their samples became depleted with time, the TaO and TaO_2 pressures decreased. A decrease of about a factor of 7 in TaO pressure corresponded to a decrease of about a factor of 5 in TaO_2 pressure at 2200°K. The decrease in TaO_2 pressure would have been expected to be by a factor of about 50 if equilibrium of the TaO and TaO_2 with the same oxygen activity were maintained. The calculated ΔH°_{298}

(1) Work was performed under the auspices of the United States Atomic Energy Commission.

(2) O. H. Krikorian, J. H. Carpenter, and R. S. Newbury, "The Vapor Pressure of Technetium," paper presented at the 149th National Meeting of the American Chemical Society, Detroit, Mich., April 1965.

(3) J. W. Otvos and D. P. Stevenson, *J. Am. Chem. Soc.*, **78**, 546 (1956).

(4) S. L. Bender, *et al.*, AVCO Corporation Report AVCO-RAD-TR-61-12, May 1962; R. J. Barriault, *et al.*, AVCO Corporation Report AVCO-RAD-SR-62-186, Sept. 1962; H. L. Shick, *et al.*, AVCO Corporation Reports AVCO-RAD-SR-62-251, Dec. 1962, AVCO-RAD-SR-63-52, March 1963, AVCO-RAD-SR-63-105, June 1963, and AVCO-RAD-SR-63-183, Aug. 1963.

(5) M. G. Inghram, W. A. Chupka, and J. Berkowitz, *J. Chem. Phys.*, **27**, 569 (1957).

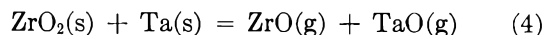
of reaction 3 for the depleted sample is 161.3 kcal./mole. Depletion of the samples led to an increase by a factor of 10 in the $\text{TaO}^+/\text{TaO}_2^+$ intensity ratio from the beginning to the very end of an experiment. This indicates a final ΔH_{298}° for reaction 3 that is intermediate between 161.3 and our value of 174.5 kcal./mole.

An explanation of the enthalpy discrepancies may be inferred from a discussion by Ackermann and Thorn.⁶ For tantalum crucibles containing Ta_2O_5 or other oxides at temperatures of 2000 to 2600°K., they have presented considerable evidence for the rapid diffusion of oxygen through the crucible walls followed by volatilization of $\text{TaO}(\text{g})$ from the outer surfaces. In addition, Goldstein, *et al.*,⁷ in a mass spectrometric study of vaporization of La_2O_3 from a tantalum cell found that oxygen from the La_2O_3 first dissolved in the tantalum and then vaporized from crucible surfaces at later times as $\text{TaO}(\text{g})$. It seems reasonable to assume that a similar solution of oxygen in tantalum occurred in the cell used by Inghram, *et al.*, and that an appreciable amount of the detected TaO^+ originated from the lid or from nearby shields. The TaO_2^+ , however, is believed to have originated primarily from the orifice.

The observed intensity changes in TaO^+ and TaO_2^+ may be accounted for by assuming the following: (a) for the initial Ta_2O_5 samples, the activity of O on the lid surface is about 0.3 of that in the cell, and the vaporization area of the cell lid for detection purposes is 10 times that of the orifice, and (b) the activity of O for the depleted sample is reduced by a factor of 2 in the cell, and by a factor of 100 on the lid compared to the initial conditions. For condition a, most of the TaO and about one-half of the TaO_2 originate from the lid, and with condition b, both TaO and TaO_2 originate predominantly from the orifice. Applying condition a, the ΔH_{298}° of reaction 3 is found to be 160.1 kcal./mole by third law, while condition b gives 161.3 kcal./mole for the depleted sample. If the effective vaporization area for TaO is increased by material vaporizing from shields or other sources, the ΔH_{298}° for reaction 3 will increase even more. Third-law treatments with conditions a and b give a ΔH_{298}° of 59.0 kcal./mole for $\text{TaO}(\text{g})$ and -42.6 kcal./mole for $\text{TaO}_2(\text{g})$.

Enthalpies of formation of $\text{TaO}(\text{g})$ and $\text{TaO}_2(\text{g})$, and of reaction 3, are summarized in Table II for the various determinations. Selected values give the greatest weight for the ΔH_{298}° of $\text{TaO}(\text{g})$ to this work, and for the ΔH_{298}° of $\text{TaO}_2(\text{g})$ to the revised results of Inghram, *et al.* Errors represent estimated standard deviations.

Inghram, *et al.*,⁵ also determined ΔH_{298}° of $\text{TaO}(\text{g})$ by mass spectrometry from the assumed reaction



The data show that the $\text{TaO}(\text{g})$ pressure is about 0.4 of that of $\text{ZrO}(\text{g})$ at 2288°K., after applying Otvos and Stevenson cross-section corrections. The $\text{TaO}(\text{g})$ pressure would be expected to equal that of $\text{ZrO}(\text{g})$ for reaction 4, or, if solution of oxygen in the tantalum occurred with subsequent vaporization of $\text{TaO}(\text{g})$ from the lid, observed $\text{TaO}(\text{g})$ pressures would be expected

Table II: Enthalpies of Formation of $\text{TaO}(\text{g})$ and $\text{TaO}_2(\text{g})$ and the Enthalpy of the Reaction $\text{Ta}(\text{s}) + \text{TaO}_2(\text{g}) = 2\text{TaO}(\text{g})$

Source	ΔH_{298}° (TaO), kcal./mole	ΔH_{298}° (TaO_2), kcal./mole	ΔH_{298}° , reaction, kcal./mole
Inghram, <i>et al.</i> ^a	53.3	-44.8	152.1
Inghram, <i>et al.</i> ^b (revised)	59.0	-42.6	160.7
This work	63.0	-48.5	174.5
Selected values	62 ± 4	-44 ± 4	168 ± 7

^a Results have been corrected by Otvos and Stevenson cross sections. Results for depleted samples were omitted. ^b The revised results of Inghram, *et al.*, are averaged from all of their runs after application of conditions a or b as described in the text.

to be higher than for $\text{ZrO}(\text{g})$. The situation is actually complex, and it would be difficult to obtain accurate thermodynamic data from this study. The phases are not characterized and may not be at equilibrium. The principal reaction in the cell is probably between a tantalum-rich phase with zirconium and oxygen in solid solution and an oxygen-deficient ZrO_2 phase containing dissolved tantalum to produce $\text{ZrO}(\text{g})$ along with lesser amounts of $\text{TaO}(\text{g})$ and $\text{TaO}_2(\text{g})$. Chupka, *et al.*,⁸ have found that addition of zirconium to ZrO_2 contained in a tantalum cell does not appreciably enhance the $\text{ZrO}(\text{g})$ pressure. This suggests that the activity of zirconium is high in the tantalum-rich phase postulated above.

From the conclusions presented here, dissociation energies may be calculated as 7.9 ± 0.2 e.v. for TaO and 15.1 ± 0.2 e.v. for TaO_2 . The average Ta-O bond strength in TaO_2 is about equal to that in TaO , thus correlating reasonably well with additivity rules. It is apparent that additional work is needed to establish

(6) R. J. Ackermann and R. J. Thorn in "Progress in Ceramic Science," Vol. 1, J. E. Burke, Ed., Pergamon Press, New York, N. Y., 1961, p. 76.

(7) H. W. Goldstein, P. N. Walsh, and D. White, *J. Phys. Chem.*, **64**, 1087 (1960).

(8) W. A. Chupka, J. Berkowitz, and M. G. Inghram, *J. Chem. Phys.*, **26**, 1207 (1957).

more definite values for the enthalpies of formation of gaseous tantalum oxides.

Acknowledgment. The authors wish to thank Drs. George Barton and Ray Newbury for use of the mass spectrometer facilities, and for assistance in making the measurements.

γ -Ray-Induced Isomerization of *cis*- and *trans*-1,2-Diphenylcyclopropane¹

by W. G. Brown

Chemistry Division, Argonne National Laboratory,
Argonne, Illinois (Received June 23, 1965)

In the expectation that characteristic differences in product patterns under different modes of excitation would be useful as mechanistic criteria, it was of interest to examine and compare the thermal, photochemical, and radiolytic isomerization of *cis*- and *trans*-1,2-diphenylcyclopropane. It happens that this system has been under investigation concurrently in other laboratories with respect to thermal² and photochemical³⁻⁵ transformations. The isomerizing action of γ -rays, here reported, is novel in relation to known examples⁶⁻⁹ of *cis-trans* interconversions under γ -ray excitation in that it involves inversion on a saturated carbon atom.

A diradical mechanism has been suggested in connection with each of the known modes of effecting isomerization though obviously, as others have noted, the differences in product distributions will demand some mechanistic differentiation. In the thermal equilibration,² which occurs in the liquid phase at temperatures as low as 190°, the equilibrium strongly favors the *trans* isomer and the geometrical isomerization is not accompanied by structural rearrangement to olefinic products.¹⁰ The activation energy, 33.5 kcal., is not inconsistent with a bond scission between the two phenyl substituted carbon atoms for which the energy requirement is estimated to be 24 kcal.¹¹ On the other hand, the diradical is considered⁴ a likely intermediate in the photochemical isomerization under 2537-Å. irradiation because of the explanation it offers for the by-products, *cis*- and *trans*-1,3-diphenylpropene and 1-phenylindane.¹² Finally, a version of this diradical, formulated with spins of the two odd electrons in parallel orientation, was proposed³ in connection with the sensitized photochemical isomerization. It is noted in a more recent communication⁵ that the

sensitized reaction generates no olefinic products when light adsorption is rigorously restricted to the sensitizer.

γ -Irradiation studies have been done in solution and on the pure isomers at temperatures above the melting point (37°) of the *cis* isomer. When irradiated as the crystalline solid at doses up to 3×10^{21} e.v./g., the *cis* isomer was unaffected.¹³ The pure liquids exhibited geometrical isomerization and, to a lesser extent than in photolysis, rearrangement to *cis*- and *trans*-1,3-diphenylpropene. No 1-phenylindane was detected. Polymer yield measurements, based on the weight of residue from high vacuum sublimation, were unsatisfactory, possibly because of a range of molecular weights; *G* values fell erratically in the range 0.5 to 4. The olefin yields, not determined precisely, were in the *G* range below 0.1. Yields for the *cis* \rightarrow *trans* and *trans* \rightarrow *cis* reactions, measured at conversions in the range 2 to 6%, were 5.7 ± 0.5 and 2.3 ± 0.2 , re-

(1) Based on work performed under the auspices of the U. S. Atomic Energy Commission.

(2) L. B. Rodewald and C. H. DePuy, *Tetrahedron Letters*, **40**, 2951 (1964).

(3) G. S. Hammond, P. Wyatt, C. D. DeBoer, and N. J. Turro, *J. Am. Chem. Soc.*, **86**, 2532 (1964).

(4) G. W. Griffin, J. Covell, R. C. Petterson, R. M. Dodson, and G. Klose, *ibid.*, **87**, 1410 (1965).

(5) G. S. Hammond and R. S. Cole, *ibid.*, **87**, 3256 (1965).

(6) A. Charlesby, *Radiation Res.*, **2**, 96 (1935).

(7) M. A. Golub, *J. Polymer Sci.*, **25**, 373 (1957).

(8) R. B. Cundall and P. A. Griffiths, *J. Am. Chem. Soc.*, **85**, 1211 (1963).

(9) J. Nosworthy, *Trans. Faraday Soc.*, **61**, 1138 (1965).

(10) Geometrical isomerization, presumably in the gas phase, can be observed in gas chromatography with inlet temperatures above 220°. At inlet temperatures up to 350° no olefinic products appear.

(11) From the heat of formation of bibenzyl(s) [G. S. Parks, T. J. West, B. F. Naylor, P. S. Fugii, and L. A. McLaine, *J. Am. Chem. Soc.*, **68**, 2524 (1946)], the heat of vaporization of bibenzyl [N. F. H. Bright, *J. Chem. Soc.*, 624 (1951)], and a newly determined value for the heat of formation of benzyl radical [S. J. Ashcroft, A. S. Carson, and J. B. Pedley, *Trans. Faraday Soc.*, **59**, 2713 (1963)], the heat of dissociation for the central bond in bibenzyl is given as $-10.5 - 17.3 + 2(39.7) = 51.6$ kcal. The assumption is then made that the dissociation energy for the 1,2 bond of 1,2-diphenylcyclopropane will be less by the amount of the strain energy of the cyclopropane ring which is taken to be 27.5 kcal. [H. A. Skinner and G. Pilcher, *Quart. Rev. (London)*, **17**, 285 (1963)].

(12) Experiments in this laboratory performed prior to the publication by Griffin, *et al.*,⁴ on photolysis in pentane solution with 2537-Å. radiation showed 1-phenylindane to be formed from the beginning from the *cis* isomer but it does not appear in short exposures of the *trans* isomer. Its formation from the latter evidently occurs by way of prior conversion to the *cis* isomer rather than through a common intermediate. It was also noted that, because of the reversibility of all isomerization reactions other than that leading to 1-phenylindane, this product accumulates and is eventually the major monomeric product. The olefinic products, formed in comparable *cis-trans* ratio from either starting material, would admit of a common intermediate.

(13) In photolysis the solid *cis* isomer, irradiated as a thin film in 2537-Å. light, produced essentially the same spectrum of C₁₅ products as in liquid phase or solution photolyses.

spectively. The irradiation of pure liquid *trans*-1,3-diphenylpropene revealed isomerization to the *cis* isomer (G 9.0 at 4% conversion and 5.4 at 12% conversion) but there was no detectable formation of cyclopropane derivatives. In benzene solution at 0.01 M the yields of products from *cis*- and *trans*-1,2-diphenylcyclopropane, at doses of $9-18 \times 10^{19}$ e.v./g., were as follows: *cis*-1,2-diphenylcyclopropane, —, 0.70; *trans* isomer, 0.92, —; *cis*-1,3-diphenylpropene, 0.05, 0.07; *trans* isomer, 0.03, 0.04. These yields are given as G values based on total energy absorbed. On more prolonged exposure, 2×10^{21} e.v./g., solutions of either isomer tended toward a *trans*:*cis* ratio of 1.15.

On the basis of product formation, it is evident that radiolysis represents a situation intermediate between direct and sensitized photolysis. The radiolysis in dilute benzene solution is necessarily a benzene sensitized process, since it is a consequence of energy absorbed primarily by the solvent, and the radiolysis of the neat liquids is perhaps best considered as self-sensitized. In benzene sensitized *cis*-*trans* isomerizations of olefins by γ -rays there is mounting evidence^{8,9} to show that triplet benzene is the effective species. It seems highly probable that this will prove true also of the inversions on a cyclopropane ring and thus that there will be a close mechanistic correlation with the sensitized photochemical reaction. The further conclusion is indicated that in radiolysis, and still more in direct photolysis, some fraction of the reaction, corresponding to the yields of rearrangement products, takes place by way of a more highly energized intermediate or by a different mechanism than is involved in sensitized photolysis.

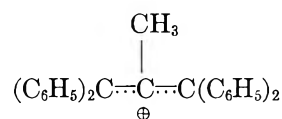
Electron Spin Resonance of 1,1-Diphenylethylene Adsorbed on Silica-Alumina Catalysts

by Francis R. Dollish and W. Keith Hall

Mellon Institute, Pittsburgh, Pennsylvania
(Received June 28, 1965)

Work on the optical spectra from 1,1-diphenylethylene (DPE) adsorbed on silica-alumina catalysts has been reviewed recently by Leftin and Hobson¹ and by Terenin.² Both attributed the band at $607 \text{ m}\mu$ (the blue species) to a cation radical. This assignment was first suggested by Leftin and Hall,³ who cited evidence supporting it but reported that they could not find the expected e.p.r. signal. However, shortly thereafter,

a weak e.p.r. resonance with unresolved hyperfine structure was reported for DPE adsorbed on silica-alumina^{4,5} and on the synthetic zeolites.⁶ Leftin, *et al.*,⁴ supposed that the paramagnetism stemmed from the blue species, but Rooney and Pink⁵ attributed it to a band at $330 \text{ m}\mu$ because they observed that addition of water to the sample eliminated the signal but did not affect the blue color. In agreement with this, Hall⁷ noted that paramagnetism, if present, was below his limit of detectability when the catalyst-hydrocarbon system was a deep blue-black. Hirschler⁸ summarized evidence supporting the view that the blue species is a carbonium ion formed from a dimeric or trimeric reaction product of DPE, a hypothesis which is consistent with the kinetic observations of Leftin and Hall.³ Rooney and Hathaway⁹ identified the blue carbonium ion as



The first objective of the present experiments was to confirm that the blue species is not paramagnetic. The second was to ascertain whether the weak paramagnetism found by others⁴⁻⁶ was due to a radical formed from DPE or from an impurity. In air, DPE is quite unstable. As received, it may contain up to 10% benzophenone and 1-2% biphenyl. To avoid complications due to impurities, freshly purified material must be used and contact with air avoided.

In contrast with the data of Rooney and Pink,⁵ Leftin, *et al.*,⁴ reported that the e.p.r. signal from chemisorbed DPE *increased* on addition of water vapor. They also noted that the signal intensity was enhanced by contact with hydrogen or argon but was decreased with oxygen. Effects of rare gases almost certainly must be of a physical nature. A similar apparent decrease in signal intensity on contact of perylene cation radicals with O_2 ⁵ has also been shown

(1) H. P. Leftin and M. C. Hobson, *Advan. Catalysis*, **14**, 115 (1963).

(2) A. N. Terenin, *ibid.*, **15**, 227 (1964).

(3) H. P. Leftin and W. K. Hall, *J. Phys. Chem.*, **64**, 382 (1960); **66**, 1457 (1962).

(4) H. P. Leftin, M. C. Hobson, and J. S. Leigh, *ibid.*, **66**, 1214 (1962).

(5) J. J. Rooney and R. C. Pink, *Trans. Faraday Soc.*, **58**, 1632 (1962).

(6) D. N. Stamires and J. Turkevich, *J. Am. Chem. Soc.*, **86**, 749 (1964).

(7) W. K. Hall, *J. Catalysis*, **1**, 53 (1962).

(8) A. E. Hirschler, *ibid.*, **2**, 428 (1963).

(9) J. J. Rooney and B. J. Hathaway, *ibid.*, **3**, 447 (1964).

Table I: Spectral Data from 1,1-Diphenylethylene Adsorbed on Silica-Alumina Catalyst AAA

A. Effect of purity and coverage				
	Nominal coverage, DPE molecules/g. $\times 10^{-19}$	Color	Spin-concentration, spins/g. $\times 10^{-16}$	Catalyst ^a lot
1. 86.8% (as received)	2.7	Greenish yellow	1.0	1
2. 99.9% (first g.l.p.c. purification)	2.0	Lemon yellow	1.9	1
3. 99.99% (second g.l.p.c. purification)	2.2	Lemon yellow	2.2	1
4. 86.8%	3.1	Yellow-green	0.9	2
5. 86.8%	27.9	Dark blue-green	0.6	2

B. Effect of pretreatment ^b				
	Nominal coverage, DPE molecules/g. $\times 10^{-19}$	Color	Width, ^c gauss	Nominal concentration, spins/g. $\times 10^{-16}$
1. Standard	3.5	Lemon yellow	8.40	0.8
2. Standard, sealed off with 5 mm. of O ₂	2.8	Light green	10.13	6.3
3. Reduced	3.1	Lemon yellow	10.59	0.03
4. Reduced, sealed off with 8 mm. of H ₂	2.9	Lemon yellow	8.59	0.03

^a Lot No. 1 consistently generated more radical ions than Lot No. 2 when tested with DPE, perylene, and pyrene. ^b The purity of DPE was 99.99%, and the catalyst used was Lot No. 2. ^c Width between points of maximum slope, measured vs. 0.1 M hydroquinone in alkaline ethanol in a dual cavity.

to be physical^{10,11}; the radical-ion concentration is actually increased by O₂. The final objective of the present work was to determine the saturation properties of the paramagnetic signal from DPE in the presence of various gases in order to clarify the effects of environment on the e.p.r. spectra of chemisorbed radicals.

Experimental Section

The equipment and high-vacuum procedures for the preparation of catalyst samples for electron spin resonance studies were given earlier.⁷ American Cyanamid Co. Aerocat (AAA) cracking catalyst (22.1% Al₂O₃, surface area, 450 m.²/g.) was used. Unless otherwise specified, the 1,1-diphenylethylene reagent (from the Aldrich Chemical Co.) was twice purified by preparative gas-liquid partition chromatography. The purity of the first product was 99.9%, and after the second chromatographic separation it was 99.99%.

The *standard pretreatment* of the catalyst consisted of treating the catalyst (1.5-g. charge) in flowing oxygen for 24 hr. at 540° and then evacuating it for 24 hr. at this temperature. When the O₂ treatment was followed by evacuation for 6 hr. before treatment with flowing H₂ for 24 hr. and a final evacuation for 24 hr., all at 540°, the catalyst was said to be *reduced*. The DPE (~13 mg.) was weighed in a capillary tube and placed in a reagent reservoir where it was degassed by the freeze-pump-thaw technique and sealed under

vacuum. Transfer of DPE to the catalyst was effected by rupturing a break-seal between the catalyst and reagent compartments and heating the assembly at 62° for 1 hr. Most samples reached a constant radical-ion concentration after 72 hr., and additional heating at 62° after this period did not lead to any change.

The electron spin measurements were carried out with a Varian X-band spectrometer (Model V-4500) with the microwave bridge in the low-power configuration and a 12-in. magnet; the magnetic field was modulated at 100 kc./sec. The Varian multipurpose cavity was used for the studies of the effects of added gases. For line-width determinations, the Varian dual cavity was used with an alkaline-ethanol solution of 0.1 M hydroquinone ($a_H = 2.368$ gauss) as a reference. Spin-concentration measurements were made by comparison of the first moment of the overmodulated derivative signals with those of 0.001 M 1,1-diphenyl-2-picrylhydrazyl in benzene ($\epsilon_{629m\mu} 14,590 M^{-1} \text{ cm.}^{-1}$ in CHCl₃¹²) using the same experimental conditions. The power entering the cavity arm was measured with a Hewlett-Packard 431B power meter using a 20-db. coupler.

(10) R. P. Porter and W. K. Hall, *J. Catalysis*, in press.

(11) B. D. Flockhart and R. C. Pink, *Talanta*, **9**, 931 (1962).

(12) J. W. Eastman, G. M. Androes, and M. Calvin, *J. Chem. Phys.*, **36**, 1197 (1962).

Results and Discussion

The results in Table I-A demonstrate that purity and coverage of DPE have a marked effect upon the color of the catalyst sample, indicating an increase in the 607-m μ band with increasing coverage and impurity level. The radical-ion concentration varied inversely. This behavior is consistent with the identification by Rooney and Hathaway⁹ of the blue species with an allylic carbonium ion, provided that an oxidizing agent is included among the impurities. Leftin and Hall³ demonstrated that the formation of the blue species was strongly catalyzed by oxidizing agents.

The effect of catalyst pretreatment upon the generation of radical ions is given in Table I-B. Treatment of the catalyst with hydrogen reduced the radical-ion concentration one order of magnitude. In the presence of oxygen, the spin-concentration was increased one order of magnitude over that obtained with the standard pretreatment. These data agree with earlier results^{7,10,13} for polynuclear aromatic hydrocarbons adsorbed on the same catalyst. If it is assumed that the extinction coefficient of the radical ion is close to that reported^{1,3} for the methyl-diphenylcarbonium ion in H₂SO₄ (ϵ 3×10^4 M⁻¹ cm.⁻¹), then the maximum radical-ion concentration observed in the O₂-treated sample would be sufficient to give an absorbance of only about 0.05. This suggests that the peak due to the radical ion is obscured by the background in the absorption spectra of DPE on this catalyst. The extinction coefficient of the 607-m μ band³ was shown to be at least 2.2×10^4 ; the absorbance of the 607-m μ band under similar conditions is about 3. Evidently, a cation radical is formed from pure DPE, but it does not correspond to the blue species.

In order to clarify some of the contradictory results^{4,5,7,10,11,13-15} concerning the effects of oxygen and other gases on the e.p.r. signal from adsorbed radical ions, a careful study was made of the saturation properties and line shape of the e.p.r. signal from DPE on silica-alumina catalyst AAA in various environments. Results at two power levels are contained in Table II. Reliable spin-concentrations can be calculated only from the integrated absorption area of curves taken under conditions of complete unsaturation. The effects of added hydrogen (C-1,2 and D-1,2) and argon (B-3,4,5) reported by Leftin⁴ can be accounted for mainly as changes in saturation level and not spin-concentration. The addition of small amounts of water vapor also results in a decrease in the saturation level (B-9 and D-3); however, large amounts of water do decrease the radical-ion concentration (B-10). These latter observations agree with those of Rooney and Pink.⁵ A small apparent lowering in spin-concen-

tration may also occur at high power with evacuated samples due to temperature elevation by absorption of microwave energy. The addition of H₂, Ar, and H₂O did not lead to any change in signal width or shape under unsaturated conditions; the width did increase at higher powers as the level of saturation increased. The addition of oxygen in all cases led to a reversible broadening of the signal width, *e.g.*, $\Delta H = 10.1, 13.0, 15.2,$ and 10.1 gauss for B-5 to B-8, respectively.

The effect of oxygen on e.p.r. spectra of DPE on silica-alumina is threefold. Exposure to oxygen unsaturates the signal (*e.g.*, A-2 and B-6); it can also lead to a change in signal shape from gaussian to lorentzian (B-7,8 and C-3) and it effects a real time-dependent increase in the spin-concentration (A-2 and C-3). The results of Imai, Ono, and Keii,¹⁵ who reported that the peak height from the anthracene radical ion first increased sharply and then decreased more slowly with oxygen pressure, can be understood in these terms. The initial increase is due mainly to unsaturation of the sample but partly to a real increase in radical concentration; the decrease in peak height is caused by a change in signal shape.

In the absence of oxygen, the line shape of DPE adsorbed on silica-alumina catalyst AAA is gaussian, consisting of an envelope of many unresolved proton hyperfine components broadened by incomplete averaging of the anisotropic terms of the hyperfine interaction and also by any perturbations of the applied magnetic field by random local fields of the solid. Upon the addition of 10 mm. of O₂, the signal became lorentzian in the wings while still retaining the gaussian shape in the center. At 20 mm. of O₂ and above, the signal width increased with increasing oxygen pressure, and the line shape was completely lorentzian. This broadening effect of oxygen has been observed in several carbonaceous materials,¹⁶⁻¹⁸ but variations in the line shape from gaussian to lorentzian were not reported. Ingram¹⁹ states that the interaction of the electron with the paramagnetic oxygen molecule can be viewed as a form of collision broadening or as an increased spin-lattice interaction since both reduce the characteristic relaxation time.

(13) J. K. Fogo, *J. Phys. Chem.*, **65**, 1919 (1961).

(14) D. M. Brouwer, *Chem. Ind. (London)*, **77** (1961); *J. Catalysis* **1**, 372 (1962).

(15) H. Imai, Y. Ono, and T. Keii, *J. Phys. Chem.*, **69**, 1082 (1965).

(16) D. E. G. Austin and D. J. E. Ingram, *Chem. Ind. (London)*, 981 (1956).

(17) L. S. Singer, *Proc. Conf. Carbon, 5th, University Park, Pa., 1961*, **2**, 37 (1963).

(18) A. J. Saraceno and N. D. Coggeshall, *J. Chem. Phys.*, **34**, 260 (1961).

(19) D. J. E. Ingram, "Free Radicals as Studied by Electron Spin Resonance," Butterworth and Co. Ltd., London, 1958, pp. 210-212.

Table II: Effect of Added Gases on Spectra from 1,1-Diphenylethylene Adsorbed on Silica-Alumina Catalyst AAA

Sample treatment	Power input into cavity, mw.			
	0.036	Signal height, arbitrary units	4.35	Signal height, arbitrary units
	Unsatd. spin-concentration, spins/g. $\times 10^{-16}$		% saturation	
A. 1. Standard	1.3	19	77	57
2. 10 mm. of O ₂ added for 1 hr.	2.1	33 ^b	41	258 ^b
3. O ₂ pumped out and 10 mm. of H ₂ added	2.4	34	64	160
B. 1. Standard, sealed off with 5 mm. of O ₂	8.2	25	13	284
2. O ₂ pumped out	7.5	22	63	110
3. 10 mm. of argon added	7.3	23	57	130
4. 100 mm. of argon added	7.5	22	28	203
5. Argon pumped out	6.6	21	64	100
6. 20 mm. of O ₂ added	6.4	8 ^a	12	88 ^a
7. 40 mm. of O ₂ added	5.2	4 ^a	13	46 ^a
8. O ₂ pumped out	7.2	21	31	168
9. 1.5×10^{13} H ₂ O/cm. ² added	6.8	23	27	217
10. 3.6×10^{14} H ₂ O/cm. ² added	1.0	4
C. 1. Reduced	0.3	5	63	22
2. 8 mm. of H ₂ added	0.5	8	61	41
3. H ₂ pumped out and 10 mm. of O ₂ added				
a. After 1 hr.	0.8	12 ^b	11	142 ^b
b. After 216 hr.	2.2	28 ^a	2	360 ^a
4. O ₂ pumped out	2.9	40 ^b	16	222 ^b
D. 1. Reduced, sealed off with 8 mm. of H ₂	0.3	7	25	69
2. H ₂ pumped off	0.6	10	66	45
3. Exposed to 10 mm. of H ₂ O	0.4	8	60	45

^a Signal shape is lorentzian. ^b Signal shape is a mixture of lorentzian in the wings and gaussian in the center. All signal shapes without superscript are gaussian.

The use of relative signal height to investigate the effects of oxygen is misleading, as can be seen by comparing B-5 to B-7. The measured decrease in spin-concentration in 40 mm. of O₂ was 23%, while the peak height decreased by a factor of 5. The signal, while enclosing approximately the same area, was altered in shape from gaussian to lorentzian. The situation was a little improved at high power due to a partial compensation between unsaturation and broadening in O₂.

The exact nature of the species responsible for the paramagnetic signal is not known; it may be the radical ion of the olefin or of a (rearranged) dimer. Morigagi, *et al.*,²⁰ published resolved e.p.r. spectra of 10^{-3} to 10^{-4} M DPE in tetrahydrofuran (yellow solution) in the presence of sodium metal, which they attributed to the DPE monomer anion with the approximate proton hyperfine splitting constants of $a_{para} = a_{ortho} = 6$ gauss, $a_{meta} = 1$ gauss, and $a_{\beta} = 3$ gauss. After heating the solution for 2 days at 100°, they obtained a green solution with a nine-line spectrum ($a_{para} = 5.4$ gauss, $a_{ortho} = 2.7$ gauss, $a_{meta} = \sim 0$), which was

ascribed to a polymer radical. Evans and Evans²¹ obtained an e.p.r. spectrum similar to that of Morigagi, *et al.*, for a solution of DPE in cyclohexane in contact with sodium-potassium alloy. Since the spin-concentration measured corresponded to 80% of the total DPE, they concluded that the anion radical was $\overset{\ominus}{\text{C}}\text{H}_2\text{-CPh}$ and they attributed a band at 630 μ to this species. It is well known that anthracene, which is quite similar to DPE from the spectroscopic viewpoint, forms both cation and anion radicals. It is not unlikely, therefore, that the monomeric cation radical is at least partly responsible for the paramagnetism.

Acknowledgment. This work was sponsored by the Gulf Research & Development Co. as part of the research program of the Multiple Fellowship on Petroleum.

(20) K. Morigagi, K. Kuwata, and K. Hirota, *Bull. Chem. Soc. Japan*, **33**, 952 (1960).

(21) A. G. Evans and J. C. Evans, *Trans. Faraday Soc.*, **61**, 1202 (1965).

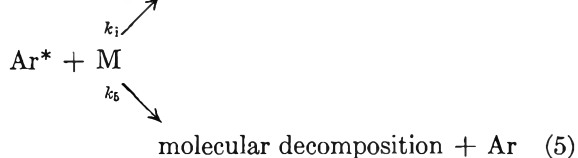
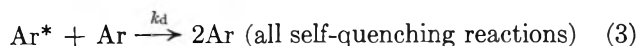
Energy Transfer between Molecules and Electronically Excited Atoms.¹ II

by M. M. Shahin and S. R. Lipsky

Department of Internal Medicine, Yale University School of Medicine, New Haven, Connecticut (Received July 8, 1965)

Recent investigations² on the nature of the excited species of argon formed through the action of β -radiation and the mechanisms of energy transfer from these species to various organic and inorganic molecules have provided a clearer understanding of experiments in rare gas sensitized radiolysis of organic compounds. We wish to report some relative values of rate constants for total quenching of these excited species and the efficiencies by which the organic molecules undergo ionization in the process of collision when the transferred energy exceeds their ionization potential.

Excited species of argon were formed by the action of tritium β -rays on argon gas flowing continuously through a microionization chamber³ at atmospheric pressure. The addition of various quantities of organic vapors (1:10³) caused changes in the degree of ionization which were measured by the change in the current collected in the ionization chamber. Following the treatment of Jesse⁴ and others,² we can write



Various values of k are the rate constants of the respective reactions; k_d describes all the steps through which the excited argon species will be destroyed in pure argon^{2a} and Ar^* refers to the electronically excited state of argon² with an energy of about 11.8 e.v. No higher excited states^{2b} of argon Ar^{**} (14–15 e.v.) are expected to participate in the ionization act as their high rate constant for reaction with argon atoms ($\text{Ar}^{**} + \text{Ar}, \text{Ar}_2^+ + e, k \approx 10^{-9}$ cc./sec.)⁵ is expected to make any competition for the organic molecules most unlikely since the relative concentration of argon to

that of the additive M is at least 10³. Application of the steady-state kinetics to the excited species of argon in such a system would yield the following Stern and Volmer type equation for the change in the rate of ion formation under saturation current measurements⁴

$$\frac{1}{\Delta R} = \frac{k_i + k_6}{K_2 k_i} + \frac{k_d}{K_2 k_i} \times \frac{1}{C}$$

where ΔR is the increase in the rate of formation of ions through reaction 4 when the organic compound M is added to a system of pure argon; K_2 is equal to k_2

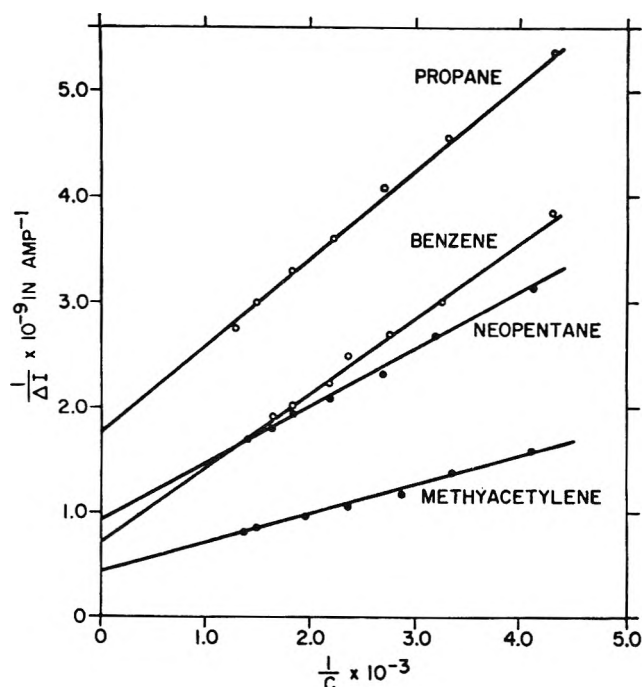


Figure 1. Variation of the inverse of the current increment vs. the inverse of the relative concentration of the organic vapor to that of argon. Saturation current measurements were made at 300 v./cm.

(A) and C is the ratio of the concentration of the organic molecule to that of argon present in the chamber. A plot of $1/\Delta R$ as measured by the current increment in the ionization chamber vs. $1/C$ will yield a straight

(1) This work was supported by grants from the National Aeronautics and Space Administration (NsG 192-61) and the National Institute of Health (HE-03558).

(2) (a) M. M. Shahin and S. R. Lipsky, *J. Chem. Phys.*, **41**, 2021 (1964); (b) G. S. Hurst, T. E. Bortner, and R. E. Glick, *ibid.*, **42**, 713 (1965).

(3) M. M. Shahin and S. R. Lipsky, *Anal. Chem.*, **35**, 467 (1963).

(4) W. P. Jesse and J. Sadauskis, *Phys. Rev.*, **100**, 1755 (1955).

(5) P. M. Becker and F. W. Lampe, *J. Chem. Phys.*, **42**, 3857 (1965).

line from which the relative values of the various parameters can be evaluated. Details of the experiments have been reported elsewhere.^{2a} Care has been taken to ensure that no excitation of argon gas occurs through acceleration of the electron in the field and corrections have been applied to the measured current increment in order to remove the effect of the change in electron drift velocity as the organic molecule is introduced into the system. Gas mixtures were all prepared and analyzed by mass spectrometry and further diluted to the required concentrations. The results for a number of gases are shown in Figure 1 and their relative rate constants as measured through the slopes and intercepts of the lines are tabulated in Table I. The over-all accuracy of the tabulated values is not considered to be better than 30%, owing to the accumulated errors including that involved in the extrapolation of the best drawn line through the data for intercept measurements. The relative values are regarded, however, to be more accurate.

Table I: Relative Rate Constants for Energy Transfer from Excited Argon Atoms to Various Organic Molecules

	$(k_i + k_s)/k_d$ $\times 10^{-3}$	k_i/k_d , rel.	$k_i/$ $(k_i + k_s)$, rel.
Acetylene	1.25	1.00	1.00
Methylacetylene	1.56	1.09	0.87
Ethylene	2.00	0.45	0.28
Propane	2.06	0.36	0.22
<i>n</i> -Butane	2.27	0.61	0.33
Neopentane	1.69	0.55	0.41
Acetone	2.10	0.48	0.29
Benzene	1.0	0.42	0.53

From the results in Table I, it is evident that the quenching of the excited species, although roughly similar for most of the gases, is not reflected in the ionization of the molecules. These results appear different from those of Hurst, *et al.*,^{2b} who have evaluated these rate constant ratios through computer calculations of their data which covered up to 100% of the organic gas, but by no means at the extremely low concentrations at which present measurements were made. The only other data available in the literature are those due to Jesse⁴ for acetylene and ethylene which if treated in this manner give the rate constant ratios $(k_i + k_s)/k_d$ of 1.5×10^3 and 2.6×10^3 , respectively. These values are similar to our 1.25×10^3 and 2.0×10^3 and contrast with 8.5×10^3 and 18.3×10^3 as deduced from the results of Hurst, *et al.*^{2b}

Enthalpy of Solid Solution for a Metastable Silver-Copper Alloy^{1a}

by Ronald K. Linde^{1b}

*W. M. Keck Laboratory of Engineering Materials,
California Institute of Technology, Pasadena, California
(Received July 8, 1965)*

Prior experimental work on the enthalpy of solid solution of Ag-Cu alloys has been confined to the narrow limits of compositions which exist as equilibrium solid solutions at elevated temperatures.² A liquid-quenching technique described in another paper³ has made possible the acquisition of data at a composition considerably beyond the limits of solid solubility which exist in the equilibrium phase diagram.⁴

By this technique suitable foils of single-phase metastable 75.0 atomic % Ag-Cu solid solutions were prepared (from Ag of purity $\geq 99.99\%$ and Cu of purity $>99.999\%$) and checked for single-phase composition (using X-ray diffraction). Half of the foils were retained in the metastable condition, while half were heated at 205° in an argon atmosphere for about 200 hr. and were checked by X-ray diffraction to ensure transformation to the stable state (≤ 0.2 atomic % solute in solution⁴). Foils were then cleaned (to remove oxides, etc.) by swabbing with a 28.46 wt. % HNO₃ solution, rinsed with distilled water, then swabbed with acetone, and allowed to dry in air.

The calorimeter consisted of a small, well-insulated double-walled dewar flask provided with a tight-fitting cover containing a small inlet door for introducing the specimen. For each experiment, a solution of 28.46 wt. % HNO₃ was added to the calorimeter, which was maintained at $23.0 \pm 0.5^\circ$ but which was held constant to within 0.01° during any given experiment. The foils were weighed into sample lots of 0.300 g. each and introduced into the acid solution after the temperature of the system had stabilized. The low rate of heat loss from the system made it possible to wait for all stirring to occur by natural convection currents. The rise in temperature when

(1) (a) This work was sponsored by the U. S. Atomic Energy Commission; (b) Poulter Laboratories, Stanford Research Institute, Menlo Park, Calif.

(2) (a) N. Swindells and C. Sykes, *Proc. Roy. Soc. (London)*, **A168**, 237 (1938); (b) R. A. Oriani and W. K. Murphy, *J. Phys. Chem.*, **62**, 199 (1958).

(3) R. K. Linde, *Trans. AIME*, in press.

(4) M. Hansen, "Constitution of Binary Alloys," 2nd Ed., McGraw-Hill Book Co., Inc., New York, N. Y., 1958, pp. 18-20.

the foils were dissolved in the acid was detected by two glass bead thermistors and recorded by means of a Wheatstone bridge circuit. (See Figure 1 for typical temperature records.)

The use of 25.16 ml. of acid solution in the case of transformed foils resulted in a temperature rise of $0.71 \pm 0.02^\circ$. In the case of metastable foils, 31.01 ml. was required to maintain the same temperature rise. It was thus possible to calculate the enthalpy difference from a knowledge of the heat capacity of the acid solution and without a precise knowledge of heat losses or of the energy equivalent of the entire calorimeter although this procedure precluded a meaningful measurement of the total energy release for a given type of foil.

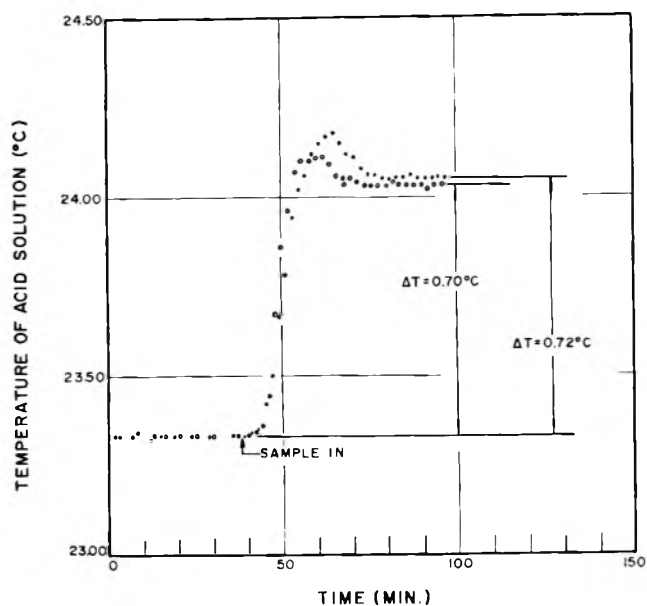


Figure 1. Two typical temperature records for dissolution of foils in acid solution.

As an indication of accuracy and a check that no significant error would be introduced by any uncompensated effects associated with changes in contact area encountered for the acid solution, several pairs of experiments were performed using specimen weights and amounts of acid solution substantially different from the values quoted above. Thus, for example, in one pair of experiments the quantities were adjusted so that the weight of each type of foil was doubled, while the contact area between the acid solution and the dewar walls was increased by 60%; the computed value of the enthalpy difference was unchanged, how-

ever. Experiments were repeated several times to ensure reproducibility.

When the metastable foils were dissolved, additional energy corresponding to the enthalpy of solid solution was released. Within the error limits stated below, the contribution from atoms in grain boundaries and other high-energy configurations could be considered the same for both types of foils (deduced primarily on the basis of microscopy and X-ray diffraction studies). All experimental conditions were kept identical. Thus, the enthalpy of solid solution should be closely equal to the enthalpy difference between the metastable and stable foils and can be calculated from the corresponding difference in amount of acid solution required to maintain the same temperature rise for both cases.

Results show an enthalpy of solid solution equal to 1150 ± 200 cal./g.-atom. By way of comparison, Scheil's analysis⁵ predicts a value of about 1110 cal./g.-atom, while Hardy's "sub-regular" model⁶ results in a value of 964 cal./g.-atom if any temperature dependence is neglected.

Heumann⁷ has computed the "distortional energy" (contribution to the enthalpy of solid solution due to difference in sizes of Ag and Cu atoms) for the composition in question to be about 1230 cal./g.-atom and has concluded that this represents, by far, the major factor in the enthalpy of solid solution. On the other hand, Oriani and Murphy^{2b} studied an 89 atomic % Ag-Cu alloy and concluded that the energetics for introducing solute species are independent of rigidity of the phase, despite the size difference between Ag and Cu atoms. A careful comparison between the most reliable experimental studies reported to date^{2,8} and the present investigation indicates that, in agreement with Scheil's prediction,⁵ the contribution of the phase rigidity may be of relatively minor importance for low solute concentrations but may be of considerable importance for high enough concentrations of Cu in Ag. On the other hand, even for high solute concentrations, the phase rigidity may not represent the only major factor in the enthalpy of solid solution.

The rapid-quench technique in its present state is not suitable for an extension of this work to include other new compositions.

(5) E. Scheil, *Z. Elektrochem.*, **49**, 242 (1943).

(6) H. K. Hardy, *Acta Met.*, **1**, 202 (1953).

(7) T. Heumann, *Z. Metallk.*, **42**, 182 (1951).

(8) O. Kubaschewski and J. A. Catterall, "Thermodynamic Data of Alloys," Pergamon Press Inc., New York, N. Y., p. 60.

The Photolysis of Trifluoronitrosomethane

by Rudolph C. White and Lloyd J. Parcell

Texaco Experiment Incorporated, Richmond, Virginia
(Received July 9, 1955)

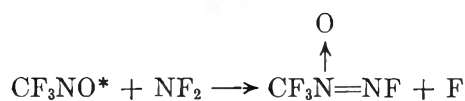
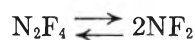
The unusual properties attributed to CF_3NO ,¹ and the publications by Mason,² elucidating the structure of the dimer of trifluoronitrosomethane as the N-nitritoamine and the photochemistry of both of these compounds, prompt us to report our work in this field.

We have irradiated CF_3NO in the gas phase (30 torr) with red light above 6000 Å. The irradiations were conducted in 10-cm. infrared cells constructed of aluminum with sodium chloride windows, Teflon with silver chloride windows, and Pyrex glass with sodium chloride windows. The progress of the reaction was followed by infrared analysis, and the products were subjected to mass spectral analysis. The irradiations were conducted for periods of up to 18 hr. In all cases, when light of wave length shorter than 6000 Å. was rigorously excluded, the primary products detected were $(\text{CF}_3)_2\text{NONO}$ and small amounts of NO_2 . The course of the reaction was not altered by the container material. This is in contrast to Mason's² report indicating a substantial surface effect in silica cells. When mixtures of CF_3NO and moist air in a Pyrex cell were irradiated overnight with red light, much less $(\text{CF}_3)_2\text{NONO}$ was obtained, and a multitude of products resulted, among which were CO_2 , COF_2 , CF_3NO_2 , SiF_4 , and others. When the trifluoronitrosomethane-air mixtures were allowed to stand overnight in the dark, no reaction was obtained. The photochemical reaction is, therefore, drastically altered by the presence of air and moisture.

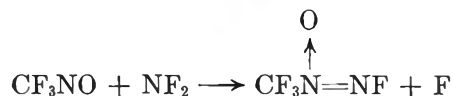
Our primary interest in CF_3NO is in utilizing the $n \rightarrow \pi^*$ transition as a mode of synthesis. The low energies involved in the transition should allow for the synthesis of compounds which have low bond energies. We have therefore irradiated mixtures of CF_3NO and N_2F_4 with red light. The ultraviolet irradiation of CF_3NO and N_2F_4 is reported to produce $\text{CF}_3\text{N}(\text{O})=\text{NF}$ and CF_3NF_2 as the primary products.³ When mixtures of CF_3NO and N_2F_4 (total pressures from 60 to 90 torr and mole ratios $\text{CF}_3\text{NO}:\text{N}_2\text{F}_4$ from 0.5 to 2.0) were irradiated overnight with red light, considerable amounts of $(\text{CF}_3)_2\text{NONO}$ were formed. No CF_3NF_2 was detected; however, mass spectral analysis indicated the presence of $\text{CF}_3\text{N}(\text{O})=\text{NF}^+$, or possibly some compound of higher molecular weight which would produce this ion. The course of the reaction

is obviously markedly different from the ultraviolet irradiation. This would appear to be additional evidence for an activated molecule mechanism for the photodimerization of CF_3NO . Tetrafluorohydrazine is known to be a source of free radicals,⁴ and considerable amounts of CF_3NF_2 would be expected if dissociation of CF_3NO into CF_3 and NO radicals were occurring. No reaction was obtained when $\text{CF}_3\text{NO}-\text{N}_2\text{F}_4$ mixtures were allowed to stand overnight in a stainless steel cylinder.

The formation of $\text{CF}_3\text{N}(\text{O})=\text{NF}$ is reasonable since CF_3NO^* can react with NF_2 radicals which are in equilibrium with N_2F_4 or can sensitize the N_2F_4 decomposition, $D(\text{N}_2\text{F}_4) = 21.5$ kcal., to give NF_2 radicals



or



The first scheme is more likely because of the absence of a dark reaction.

The stable free radical, $(\text{CF}_3)_2\text{NO}$, has recently been isolated⁵; however, this radical has not been detected in the photochemical reaction of CF_3NO with red light. When CF_3NO was irradiated with red light for long periods, low intensity m/e peaks have been obtained which may be attributed to $(\text{CF}_3)_2\text{NOCF}_3$. Mason² discusses a free-radical scheme which involves these two compounds; however, as she points out, there is a very strong thermochemical objection to such a process. Moreover, the irradiation of CF_3NO with ultraviolet by Dinwoodie and Haszeldine⁶ has yielded considerable amounts of $(\text{CF}_3)_2\text{NOCF}_3$. Since it appears that side reactions do not occur until the concentration of dimer has increased to an appreciable point, a feasible scheme to account for the deactivation of excited CF_3NO mole-

(1) J. E. Boggs, D. Coffey, Jr., and J. C. Davis, Jr., *J. Phys. Chem.*, **68**, 2383 (1964).

(2) J. Mason, *J. Chem. Soc.*, 4531, 4537 (1963).

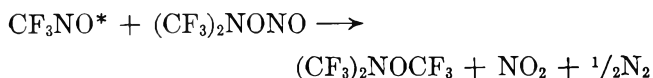
(3) J. W. Frazer, B. F. Holder, and E. F. Worden, *J. Inorg. Nucl. Chem.*, **24**, 45 (1962).

(4) C. B. Colburn, *Advan. Fluorine Chem.*, **3**, 92 (1963).

(5) W. D. Blackley and R. R. Reinhard, *J. Am. Chem. Soc.*, **87**, 802 (1965).

(6) A. H. Dinwoodie and R. N. Haszeldine, *J. Chem. Soc.*, 1675 (1965).

cules and to account for the side reactions observed upon long irradiation is the reaction of an activated CF_3NO molecule with the dimer



We have noticed an extremely slow, dark reaction on a sample of $(\text{CF}_3)_2\text{NONO}$ kept in a stainless steel cylinder for approximately 1 year. The primary product appears to be $(\text{CF}_3)_2\text{NNO}_2$. This may be an intramolecular rearrangement or a possible dissociation of $(\text{CF}_3)_2\text{NONO}$ into $(\text{CF}_3)_2\text{NO}$ and NO radicals and rearrangement upon recombination to form $(\text{CF}_3)_2\text{NNO}_2$.

The mass spectrum of $(\text{CF}_3)_2\text{NONO}$ has been determined with a Bendix time-of-flight mass spectrometer. A parent ion is not obtained even with a low ionizing voltage. The major peaks are due to CF_3^+ and NO^+ . Reasonably intense m/e peaks are obtained at 168 [$(\text{CF}_3)_2\text{NO}^+$] and 149 [$\text{CF}_3\text{N}(\text{=CF}_2)\text{O}^+$]. The 168 m/e peak further confirms the structure of the dimer as the N-nitritoamine. The failure to obtain a parent ion for this compound illustrates the relative ease of cleaving the nitrogen-oxygen bond under electron impact. The complete mass spectra and thermal decomposition studies on a series of perfluoro-nitrogen-oxygen compounds will be reported in detail at a later date.

Acknowledgment. The authors wish to thank Drs. P. L. Goodfriend and U. V. Henderson for helpful discussions on this subject. This work was partially supported by Air Force Rocket Propulsion Laboratory, Air Force Systems Command, United States Air Force, Edwards Air Force Base, Calif.

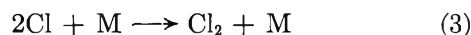
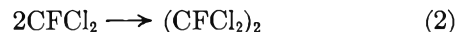
Photolysis of Fluorotrichloromethane¹

by Dana Marsh and Julian Heicklen

Aerospace Corporation, El Segundo, California
(Received July 23, 1965)

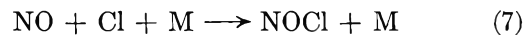
As a continuation of our program on fluorocarbon oxidations, we have examined the photochemistry of CFCl_3 in the presence of O_2 or NO . Earlier work² on the oxidation of CF_3 radicals had shown that the only carbon-containing product was CF_2O . We were curious to see if CFCl_2 radicals would oxidize in an analogous manner.

Upon exposure to the 2138-Å radiation of a zinc lamp, pure CFCl_3 showed no evidence of reaction as determined by *in situ* infrared analysis. This can be explained by the sequence of reactions



When a small amount of molecular chlorine has been formed by reaction 3, then reaction 5 becomes important and inhibits product formation. The products never reach sufficient concentrations to be detected.

Mixtures of CFCl_3 and NO were photolyzed, and infrared product bands were observed at 5.56, 6.19, and 8.8 μ . The band at 5.56 μ is the intense band of NOCl .³⁻⁵ Its growth was nonlinear and diminished with increasing exposure. It continued to grow, though very much more slowly, after exposure was terminated. It was clear that this band could not be associated with the same molecule as the other two bands. It is difficult to understand why NOCl formation should be inhibited with exposure time. More likely, the nonlinearity of the 5.56- μ band reflects a deviation from Beer's law similar to that for NO_2 .^{2b} The optical density of bands at 6.19 and 8.8 μ grew linearly with exposure time, and their ratio was invariant for all runs. Presumably, these two bands can be associated with CFCl_2NO . The relative quantum yields of formation of CFCl_2NO are reported in Table I. Ratios of CFCl_3 and NO used were such that the absorption of the radiation by NO was unimportant. Within the experimental error, $\Phi(\text{CFCl}_2\text{NO})$ is unchanged by variations in either the CFCl_3 or the NO pressures, thus suggesting that the absolute quantum yield is indeed unity. The mechanism that explains the result is



(1) This work was supported by the U. S. Air Force under Contract No. AF 04(695)-469.

(2) (a) H. S. Johnston, private communication (1965); (b) J. Heicklen, Aerospace Corp. Report TDR-469(5250-40)-12, May 1965.

(3) L. P. Kuhn and C. Butkiewicz, *J. Phys. Chem.*, **65**, 1085 (1961).

(4) W. G. Burns and H. J. Bernstein, *J. Chem. Phys.*, **18**, 1670 (1950).

(5) P. J. H. Woltz, E. A. Jones, and A. H. Nielsen, *ibid.*, **20**, 379 (1952).

Table I: Photolysis of CFCl_3 and NO Mixtures (λ 2138 Å., $T = 24^\circ$, $I_0 = 1.0 \times 10^{15}$ quanta/cm.² min.)

(CFCl_3), mm.	(NO), mm.	$\Phi(\text{CFCl}_2\text{NO})^a$
18.5	2.0	0.89
210	2.2	0.96
226	20	0.98
210	20	1.06
260	60	1.09

^a Average value assumed to be 1.00.

The slight growth of NOCl after exposure might result from the photolysis of Cl_2 from the overhead fluorescent room lights



followed by (7). The molecular chlorine would not be detected as it has no infrared absorption bands.

Mixtures of CFCl_3 and O_2 were photolyzed, and three infrared bands were found at 5.35, 5.46, and 9.08 μ . These bands correspond to those reported for CFCIO.⁶ Undoubtedly, Cl_2 also was produced. The optical density of the 5.35- μ band was monitored, and it grew linearly with exposure time. From the results, shown in Table II, it can be seen that $\Phi(\text{CFCIO})$ is

Table II: Photolysis of CFCl_3 and O_2 Mixtures (λ 2138 Å., $T = 24^\circ$, $I_0 = 1.0 \times 10^{15}$ quanta/cm.² min.)

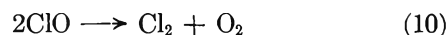
(CFCl_3), mm.	(O_2), mm.	$\Phi(\text{CFCIO})$
20.5	20.5	0.94
20	200	0.98
190	19.5	1.02
190	290	1.01
250	200	1.04
185 ^b	230	0.89

^a I_0 calculated assuming average value of $\Phi(\text{CFCIO}) = 1.00$.

^b 2.5 mm. of HI present for this run.

invariant to the pressures of the reactants. The incident intensity I_0 was estimated by assuming the average value of $\Phi(\text{CFCIO})$ to be unity. In one run, a small amount of HI was added (the HI absorbed only a few per cent of the radiation). The yield of CFCIO was unaffected, but an additional unidentified product band at 9.46 μ was found. When mixtures of CFCl_3 and HI without oxygen were photolyzed, the peak at 9.46 μ was still observed, and it was the only product peak.

The oxidation is indeed analogous to that for CF_3 radicals.^{2b} There are two mechanisms that can explain the oxidation. One mechanism is



The addition of HI would not alter the CFCIO yield. The other mechanism involves the addition reaction



which could be followed by



However, HI should scavenge the CFCl_2O_2 radical to give $\text{CFCl}_2\text{O}_2\text{H}$. Then the results could be explained only if $\text{CFCl}_2\text{O}_2\text{H}$ were a very reactive intermediate which immediately decomposed to CFCIO and HOCl.

Experimental Section

Trichloromonofluoromethane (Genetro 11) was obtained from the Allied Chemical Co. and showed about 2% impurities on analysis by gas chromatography. It was used directly after degassing twice at -196° . At the conclusion of photolysis, the impurity was still present at the same concentration, thus indicating that it did not enter the reaction. Nitric oxide, oxygen (extra dry grade 99.6% pure), and anhydrous HI were obtained from the Matheson Co. All were degassed twice at -196° . The NO was further purified by warming to -186° and collecting the volatile fraction, thus removing traces of N_2O , NO_2 , and water.

The infrared analyses were performed *in situ* in a Perkin-Elmer Model 13 Universal spectrometer. A T-shaped cell was used having 11.5-cm. infrared and 10.7-cm. ultraviolet path lengths. The ultraviolet light entered the stem of the T through a silica window. The top of the T had sodium fluoride windows at each end and was situated in the infrared beam. A low-pressure resonance zinc lamp obtained from the North American Phillips Co. was used. The 2138-Å. line was responsible for photolysis. The absorption coefficients, to base 10, were determined for CFCl_3 , NO, and HI at 2138 Å. in a Cary Model 15 spectrophotometer and are 1.00×10^{-3} , 0.24×10^{-3} , and 12.8×10^{-3} cm.⁻¹ mm.⁻¹, respectively.

The infrared absorption coefficient was estimated by passing samples of CFCIO of known absorbance

(6) A. H. Nielsen, T. G. Burke, P. J. H. Woltz, and E. A. Jones, *J. Chem. Phys.*, 20, 597 (1952).

through an F & M chromatograph with a silica gel column and by measuring the CO₂ peak. Fluoro-carbonyl compounds decompose quantitatively to CO₂ on this column; thus, the CO₂ corresponds to the CFCIO introduced. The absorption coefficient, to base 10, at 5.35 μ is 0.019 cm.⁻¹ mm.⁻¹. Assuming the CFCIO and the CFCl₂NO yields to be unity in the CFCl₃-O₂ and the CFCl₃-NO photolyses, respectively, yields values 0.0087 and 0.012 cm.⁻¹ mm.⁻¹ for the absorption coefficients, to base 10, for the 6.19- and 8.8- μ bands of CFCl₂NO, respectively.

Acknowledgment. The authors wish to thank Mrs. Barbara Peer for assistance with the manuscript.

Self-Diffusion Coefficients of Water

by Jui H. Wang

Kline Chemistry Laboratory, Yale University, New Haven, Connecticut (Received August 2, 1965)

The self-diffusion coefficients of water are of interest in many physicochemical and biological studies. A series of measurements of the self-diffusion of liquid water with H¹⁸O as tracer by means of the controlled-stirring, open-capillary method was carried out in 1954 in connection with our study of the solutions of proteins¹ and electrolytes.² In view of the frequent use by other workers of the two published self-diffusion coefficients of water, it seems desirable to report the other values determined in our earlier series of measurements.

The experimental details were already described in an earlier publication.³ The O¹⁸ atom per cent in the diffusion samples varied from 0.5 to 1.5%. The temperature was controlled to within $\pm 0.01^\circ$. The results are summarized in Table I.

The constancy of $D\eta/T$ shows that the effective volume of the diffusing species remains constant be-

tween 5 and 25°. Therefore, in spite of the tetrahedrally hydrogen-bonded structure of water,^{4,5} it is entirely adequate to describe its self-diffusion in terms of the movement of individual H₂O molecules.⁶ A linear plot of $\ln D$ vs. $1/T$ gives an apparent activation energy of 4.8 kcal./mole. Since each hydrogen bond is shared between two water molecules, this apparent activation energy is large enough to rupture completely two hydrogen bonds per activated molecule.

For a polar liquid with loose-packed structure such as the ice-like structure of water, self-diffusion and dielectric relaxation may involve essentially the same activation mechanism. If this is the case, then the dielectric relaxation time τ and self-diffusion coefficient D should be related by the simple equation, $D = \lambda^2/\tau$, where λ is the average distance between two successive equilibrium positions of a diffusing molecule. Since the density of water at 25° is only 0.3% smaller than that at 5°, λ^2 should remain practically constant in this temperature range. The dielectric relaxation data of Collie, Hasted, and Ritson⁷ enable us to compute λ^2 as listed in Table II. Using the average of the above values of $D\tau = \lambda^2$, we obtain a mean jumping distance of 3.7 Å. for self-diffusion in liquid water. This value compares interestingly with the observed O-O distances in ice I which are 2.76 Å. for the nearest neighbors and 4.51 Å. for the next nearest neighbors.

Table II

Temp., °C.	$\tau \times 10^{11}$, sec.	$D\tau \times 10^{16}$, cm. ²
5	9.43	13.4
10	7.96	13.3
15	6.87	13.5
25	5.23	13.4

Experimentally, the constancy of $D\eta/T$ and $D\tau$ with respect to T enables one to estimate with reasonable accuracy both D and τ at other temperatures from the viscosity data of water by either interpolation or even short extrapolation of these values.

Table I

Temp., °C.	Number of meas- urements	Self-diffusion coefficient of water, $D \times 10^6$, cm. ² /sec.	Viscosity, $\eta \times 10^3$, poise	$D\eta/T$ $\times 10^{10}$
5.00	8	1.426 \pm 0.018	15.188	7.77
10.00	6	1.675 \pm 0.025	13.077	7.73
15.00	8	1.97 \pm 0.020	14.404	7.79
25.00	6	2.57 \pm 0.022	8.937	7.70

- (1) J. H. Wang, *J. Am. Chem. Soc.*, **76**, 4755, 6423 (1954).
- (2) J. H. Wang, *J. Phys. Chem.*, **58**, 686 (1954).
- (3) J. H. Wang, C. B. Anfinsen, and F. M. Polestra, *J. Am. Chem. Soc.*, **76**, 4763 (1954).
- (4) J. D. Bernal and R. H. Fowler, *J. Chem. Phys.*, **1**, 515 (1933).
- (5) L. Pauling, *J. Am. Chem. Soc.*, **57**, 2680 (1935).
- (6) J. H. Wang, *ibid.*, **73**, 510 (1951).
- (7) C. H. Collie, J. B. Hasted, and D. M. Ritson, *Proc. Phys. Soc. (London)*, **60**, 145 (1948).

The Nuclear Magnetic Resonance Spectra of Three Unsymmetrical *o*-Dihalobenzenes

by William B. Smith and G. Mattney Cole

Department of Chemistry, Texas Christian University,
Fort Worth, Texas (Received August 9, 1966)

Recently, Martin and Dailey have reported the chemical shifts and coupling constants for a large series of disubstituted benzenes.¹ While the interplay of the several factors which determine the proton chemical shifts in such substances could not be completely delineated, they did note empirically a simple substituent additivity rule which allowed the calculation of the proton chemical shift in the *para*-disubstituted compounds with excellent accuracy.² While not quite so accurate, the application of these same substituent constants was found to apply to the *meta*-disubstituted compounds and to the two protons opposite to the substituents in the *ortho*-disubstituted examples. In the latter compounds, no correlation was found with the shifts of the protons adjacent to the substituents.²

We have now determined the n.m.r. parameters for three unsymmetrically substituted *ortho* dihalobenzenes. In part, our interest in these compounds stemmed from the observations of Martin and Dailey. The complexities of determining the parameters for an unsymmetrical four-spin system also presented an intriguing challenge.

The n.m.r. spectra of 1-chloro-2-bromo-, 1-chloro-2-iodo-, and 1-bromo-2-iodobenzene were determined in dilute solutions of carbon tetrachloride and are shown in Figures 1 and 2. Though the parameters for the symmetrical *ortho* dihalobenzenes have been reported before,^{1,3} these compounds were run again under the conditions used in this study, and the spectra were analyzed following the considerations of Grant, Hirst, and Gutowsky.³ The results of this study are given in Table I.

The spectra of an unsymmetrical four-spin system is determined by ten individual parameters (six coupling constants and four chemical shifts). The basis functions and matrices used in describing such a system have been given by Reilly and Swalen.⁴ In general, it is not possible to write down explicit formulas for the line frequencies and intensities for this case though under certain special conditions the matrices may be simplified to tractable expressions.^{4,5}

As will be noted in Table I, there is comparatively little variation among the six coupling constants for the three symmetrical dihalobenzenes, and it was

assumed as a first approximation that this would hold true for the unsymmetrical cases as well. Trial calculations using the Freqint IV A 1620 computer program and averaged values for the coupling constants and various trial values of the chemical shifts suggested that the spectral line frequencies of the 1-chloro-2-iodo- and 1-bromo-2-iodobenzene spectra could be well approximated as ABMX cases in which all off-diagonal matrix elements other than those involving J_{AB} are neglected. The energy levels for the ABMX case have been given by Reilly and Swalen,⁴ and explicit equations for the line frequencies are readily derived therefrom. Transitions were assigned according to the frequency sum rule given by Reilly and Swalen.⁴ Once the experimental line frequencies were assigned, the spectral parameters for these two cases were readily derived from the frequency and energy level equations. These values were checked and the intensities were calculated with the computer program. The parameters are given in Table I and the calculated spectra are shown in Figure 1. The average deviation was ± 0.1 c.p.s. for all 32 lines in both cases. As will be noted in Figure 1, the intensity fit is not exact in this approximation. When all off-diagonal elements were included in the calculation (ABCD case), the intensity pattern matched the experimental spectrum but the line positions shifted slightly. This indicated that a slight adjustment of the parameters was required. Since we did not have access to an iterative type program, no further improvement was attempted.

Examination of the 1-chloro-2-bromobenzene spectrum (Figure 2) clearly indicated that the system could only be treated as a true ABCD case. From our knowledge of the order of the lines in the two simpler cases, it was possible to construct an energy level diagram for this case again using the Reilly-Swalen sum rules. Several trial calculations indicated how variations in each parameter affected the energy levels. With this information, an exact ABCD solution was possible. The energy level table is shown in Figure 3. The line assignments correspond to those in Figure 2. The average deviation was ± 0.1 c.p.s. The parameters are given in Table I.

In keeping with the observations of others,^{1-3,6}

- (1) J. S. Martin and B. P. Dailey, *J. Chem. Phys.*, **37**, 2594 (1962).
- (2) J. S. Martin and B. P. Dailey, *ibid.*, **39**, 1722 (1963).
- (3) D. M. Grant, R. C. Hirst, and H. S. Gutowsky, *ibid.*, **38**, 470 (1963).
- (4) C. A. Reilly and J. D. Swalen, *ibid.*, **34**, 980 (1961).
- (5) See, for instance: (a) R. J. Abraham and H. J. Bernstein, *Can. J. Chem.*, **39**, 216 (1960); (b) N. V. Riggs, *Australian J. Chem.*, **16**, 521 (1963); (c) V. J. Kowalewski and D. G. Kowalewski, *J. Chem. Phys.*, **36**, 266 (1961); **37**, 2603 (1962).
- (6) H. Spiesscke and W. G. Schneider, *ibid.*, **35**, 731 (1961).

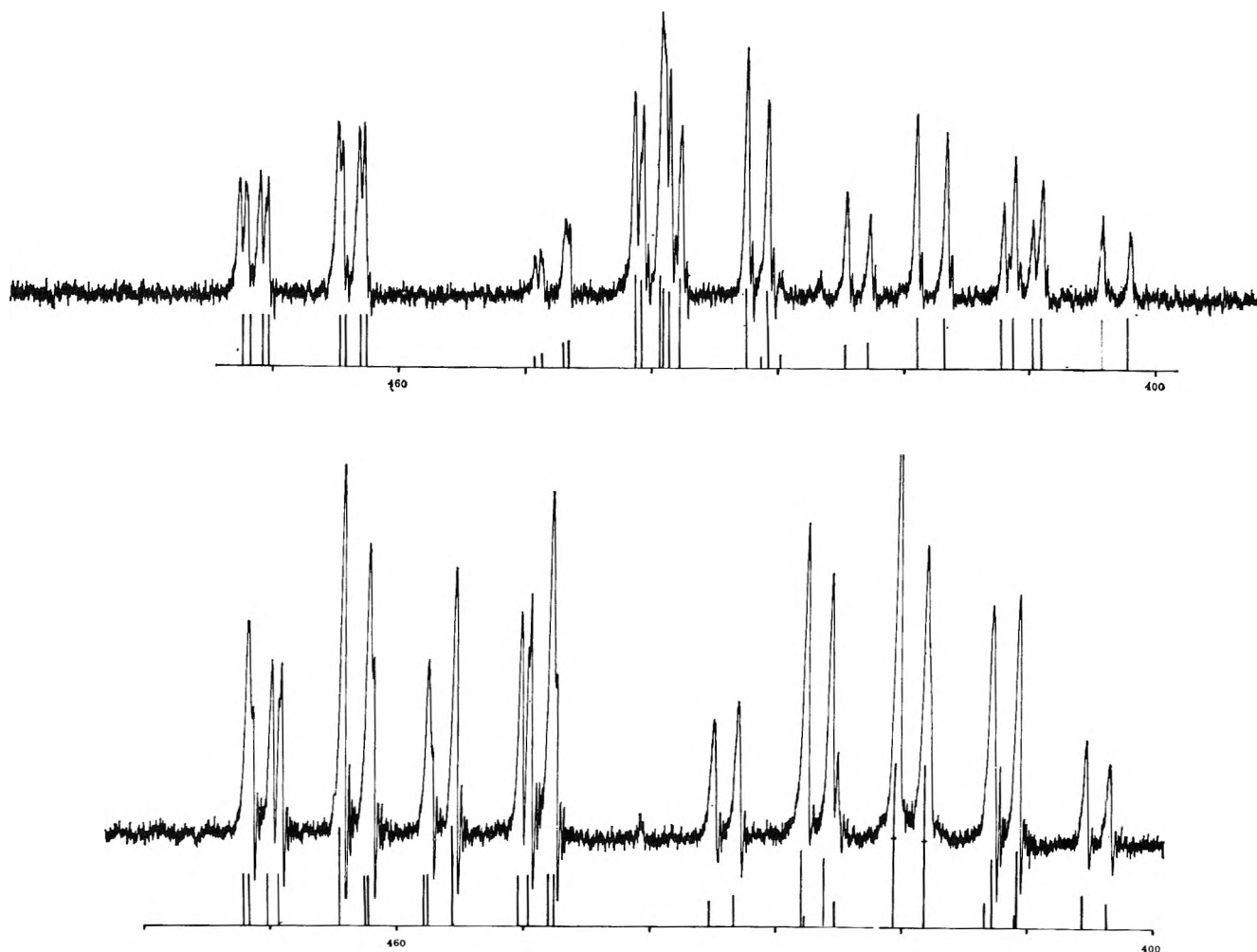


Figure 1. The n.m.r. spectra of 1-chloro-2-iodobenzene (upper) and 1-bromo-2-iodobenzene (lower). The calculated spectra are ABMX approximations.

Table I: N.m.r. Parameters for Dihalobenzenes^a

Dihalobenzenes	J_{34}	J_{45}	J_{56}	J_{25}	J_{46}	J_{36}	γ^3	γ^4	γ^5	γ
1,2-Dichloro	8.06	7.45	8.06	1.52	1.52	0.35	2.63 (2.80)	2.88 (2.95)	2.88 (2.95)	2.63 (2.80)
1,2-Dibromo	8.46	7.45	8.46	1.33	1.33	0.45	2.45 (2.70)	2.91 (2.93)	2.91 (2.93)	2.45 (2.70)
1,2-Diiodo	7.96	7.91	7.96	1.95	1.95	0.05	2.19 (2.63)	3.04 (3.07)	3.04 (3.07)	2.19 (2.63)
1-Chloro-2-bromo	8.26	7.45	8.26	1.33	1.62	0.50	2.47 (2.64)	2.99 (3.02)	2.86 (2.87)	2.62 (2.86)
1-Chloro-2-iodo	7.70	7.56	7.90	1.75	2.05	0.35	2.21 (2.43)	3.16 (3.16)	2.79 (2.87)	2.63 (2.99)
1-Bromo-2-iodo	7.96	7.20	8.20	1.60	1.64	0.40	2.22 (2.50)	3.12 (3.07)	2.90 (2.93)	2.45 (2.84)

^a Chemical shifts are in τ units. Values in parentheses are predicted from the values of Martin and Dailey.

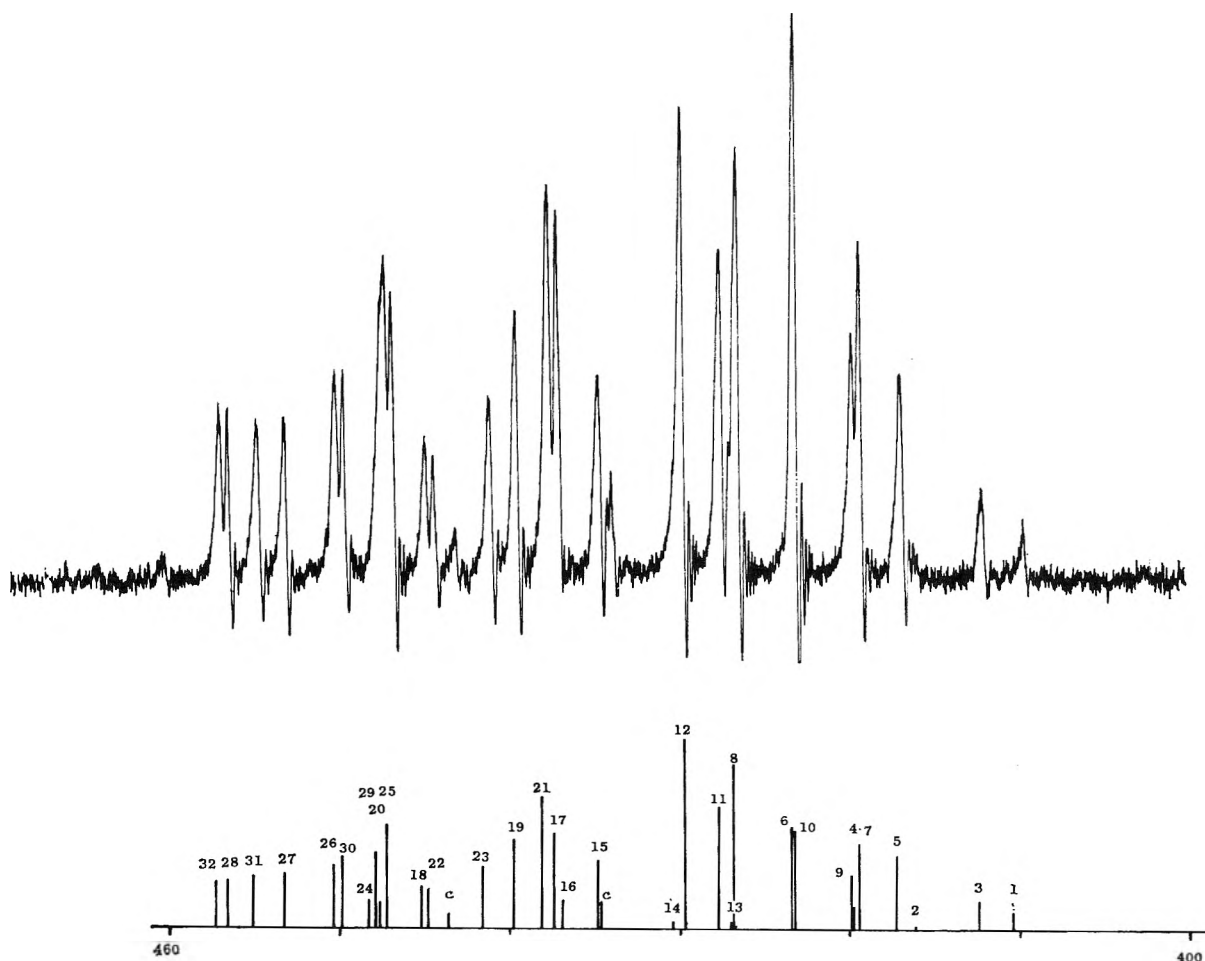


Figure 2. The n.m.r. spectrum of 1-chloro-2-bromobenzene. The calculated spectrum is an ABCD case.

the less shielded protons were assigned as being adjacent to the halogen substituents. As will be noted in Table I, there is only a slight and apparently random variation in the coupling constants for all six compounds. The values for the chemical shifts predicted from the Martin and Dailey relation are indicated in parentheses. In keeping with their observation, the agreement between the predicted and observed values is quite good for the remote pair of protons (4 and 5), and the predicted value is high by about 0.2–0.5 p.p.m. for the adjacent hydrogens (3 and 6).

Perhaps the most significant observation to be noted in Table I is the fact that the chemical shifts of the protons adjacent to a given halogen seem to be determined solely by the nature of that halogen and appear to be independent of the nature of the other substituent. Numerous discussions of the various factors contributing to the chemical shifts of aromatic protons have now appeared. The operation of "ring currents," inductive and substituent electric field effects, and the magnetic anisotropy of the substituent

have been considered.^{2,6,7} While it is generally agreed that substituent effects are at a minimum at a *meta* position, still the *meta*-substituent constants of Martin and Dailey² vary by a factor of 4 in going from chlorine to iodine, and the *meta* proton in iodobenzene is 0.23 τ upfield from that in chlorobenzene.⁶

The low-field shift of a proton located *ortho* to a halogen has been noted before, and both Spiesscke and Schneider⁶ and Martin and Dailey² have suggested the magnetic anisotropy of the halogen as the most likely explanation. The latter, however, noted that certain aspects of the magnetic anisotropy explanation were unsatisfactory; *i.e.*, the anisotropy was calculated also to affect more remote protons. Recently, Schaefer, Reynolds, and Yonemoto⁸ have also rejected the magnetic anisotropy argument and have suggested a short

(7) J. S. Martin, Thesis, Columbia University, 1962, and references therein.

(8) T. Schaefer, W. F. Reynolds, and T. Yonemoto, *Can. J. Chem.*, 41, 2969 (1963).

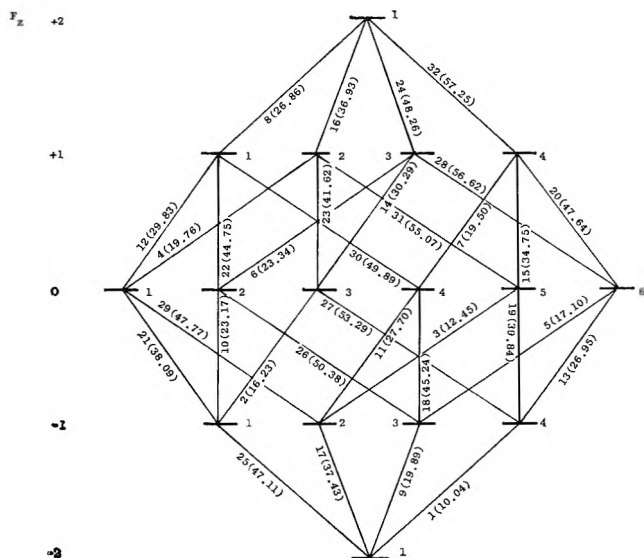


Figure 3. The energy level diagram for 1-chloro-2-bromobenzene showing the line assignments and frequencies (levels not to scale; add 400 c.p.s. to each frequency).

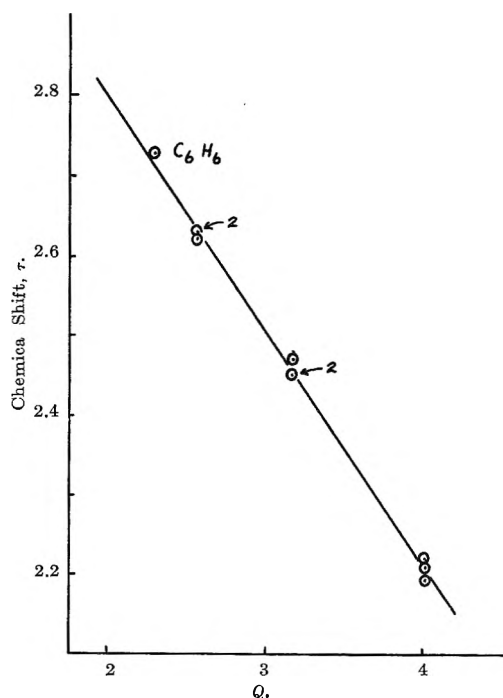


Figure 4. Plot of the chemical shift data of the *o*-hydrogens vs. the *Q* values of Hruska, Hutton, and Schaefer.

range van der Waals type interaction between the halogen and the adjacent proton. No quantitative calculations were attempted, and this explanation has been subsequently discarded in favor of a more reasonable explanation. Hruska, Hutton, and Schaefer⁹ have presented evidence that the low-field shift

results from an alteration in the paramagnetic term of the Ramsey shielding equation. A linear relation between the *ortho*-proton shifts for the aromatic halides was found with an empirical parameter, *Q*. This parameter was defined as P/Ir^3 , where *P* is the bond polarizability, *I* is the first ionization potential, and *r* is the bond length.

A plot of the chemical shifts for the various *ortho* protons in Table I against *Q* is shown in Figure 4. Benzene is also shown in the plot. As can be seen, the fit to the plot is excellent, and it is presumed that this mode of deshielding of the *ortho* protons dominates in these compounds. Reasonably, the additivity rule of Martin and Dailey would not be expected to hold in this situation.

Experimental Section

The compounds used in this study were all commercially available. Spectra were determined with a Varian A-60 at the ambient temperature of the probe (*ca.* 40°). Solutions of each compound were made up 5–10% by volume in carbon tetrachloride and outgassed. One drop of tetramethylsilane was added as an internal standard. The instrument was calibrated against chloroform. Each spectrum was recorded several times (4–10), and the averaged line positions were used in the calculations.

Acknowledgment. We wish to express our gratitude to the Robert A. Welch Foundation for its generous support of this work.

(9) F. Hruska, H. M. Hutton, and T. Schaefer, *Can. J. Chem.*, **43**, 2392 (1965).

Dissociation Constants for Some Nitrophenols and Salicylic Acid in Deuterium Oxide

by Paul K. Glasoe

Wittenberg University, Springfield, Ohio
(Received August 11, 1965)

In a report on the dissociation constants of some acids in deuterium oxide, Bell¹ noted the poor agreement between his result for 2,4-dinitrophenol and that reported earlier by McDougall and Long.² He also

(1) R. P. Bell and A. T. Kuhn, *Trans. Faraday Soc.*, **59**, 1789 (1963).

(2) A. C. McDougall and F. A. Long, *J. Phys. Chem.*, **66**, 429 (1962).

Table I: pK Values for Some Nitrophenols and for Salicylic Acid in Water and in Deuterium Oxide

Compound	Long and McDougall		Bell and Kubn		Martin and Butler		This work	
	pK_H	ΔpK	pK_H	ΔpK	pK_H	ΔpK	pK_H	ΔpK
<i>o</i> -Nitrophenol	7.19	0.75	7.25	0.57	7.22	0.60
<i>p</i> -Nitrophenol	7.26	0.48	7.24	0.56	7.14 ^a	0.58
2,4-Dinitrophenol	4.12	0.70	4.07	0.52	4.02	0.52	4.12	0.56
Salicylic acid	2.94	0.75	3.00	0.61 ^b	3.01	0.56

^a R. Robinson and A. Peiperl give the value 7.156: *J. Phys. Chem.*, **67**, 1723 (1963). ^b V. K. La Mer and S. Korman, *Science*, **83**, 624 (1936).

pointed out similar large discrepancies in the values reported by McDougall and Long and those of Martin and Butler³ for *o*-nitrophenol and *p*-nitrophenol. A summary of these values is given in Table I. Noting that the results of McDougall and Long were obtained using the glass electrode to measure pH or pD whereas his results and those of Martin and Butler were made using spectrophotometry, Bell suggests the possibility that the glass electrode is not wholly reliable in deuterium oxide solutions.

Since we have published several results for dissociation constants of acids in deuterium oxide using the glass electrode, we undertook the measurement of pK_H and pK_D for the nitrophenols in question using the procedure described in an earlier note.⁴ The solutions were in general very dilute, usually less than 0.01 *M*, owing to the low solubility of the nitrophenols in water. The ionic strength was kept around 0.05 by addition of KCl. It was found that the glass electrode was much more stable in such a solution than it was in the nitrophenol alone. In all cases, the pK values are corrected for the ionic strength using the Debye limiting law.

The values we have obtained are shown in Table I. In each case, our value checks reasonably well with Bell or with Martin and Butler. In view of these results, we conclude that in these cases the glass electrode gives proper results in deuterium oxide solutions.

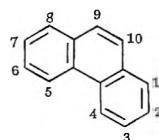
Long and McDougall² report a value for $pK_D - pK_H$ (or ΔpK) for salicylic acid of 0.75. This is much higher than that given by La Mer and Korman,⁵ 0.61. We have measured the pK_D and the pK_H for salicylic acid and obtain 0.56. We conclude that the deuterium isotope effect in salicylic acid is only slightly greater than that of "normal" carboxylic acids.^{1,6}

The Proton Magnetic Resonance Spectrum of Phenanthrene

by Robert C. Fahey and Gary C. Graham

Department of Chemistry, University of California at San Diego, La Jolla, California (Received August 18, 1966)

The proton n.m.r. spectrum of phenanthrene (Figure 1) contains two complex multiplet patterns. Because inter-ring coupling constants are usually negligibly small in aromatic hydrocarbons, the 9,10-protons should give rise to a single line. The intense line at



the center of the high-field multiplet is reasonably assigned to these protons.¹ The remaining lines in the spectrum comprise an ABCD pattern, the low-field multiplet of which has been assigned to the 4,5-protons based on studies of phenanthrene-9-*d*₁ and 4-methylphenanthrene.² An approximate analysis of the spectrum has been reported previously.³ We report here a complete analysis of the spectrum and compare our results with the earlier findings.

Spectra were measured at several concentrations (8.9 to 17.4%, w./v.) in CDCl₃ on a Varian HR-60 spectrometer. Peak positions were determined relative to tetramethylsilane as internal standard using the side-band technique. The spectra were analyzed using

(3) D. C. Martin and J. A. V. Butler, *J. Chem. Soc.*, 1366 (1939).
 (4) P. K. Glasoe and L. Ebersson, *J. Phys. Chem.*, **68**, 1560 (1964).
 (5) See footnote b of Table I.
 (6) C. K. Rule and V. K. La Mer, *J. Am. Chem. Soc.*, **60**, 1974 (1938).

(1) N. Jonathan, S. Gordon, and B. P. Dailey, *J. Chem. Phys.*, **36**, 2443 (1962).
 (2) H. J. Bernstein, W. G. Schneider, and J. A. Pople, *Proc. Roy. Soc. (London)*, **A236**, 515 (1956).
 (3) T. J. Batterham, L. Tsai, and H. Ziffer, *Australian J. Chem.*, **17**, 163 (1964).

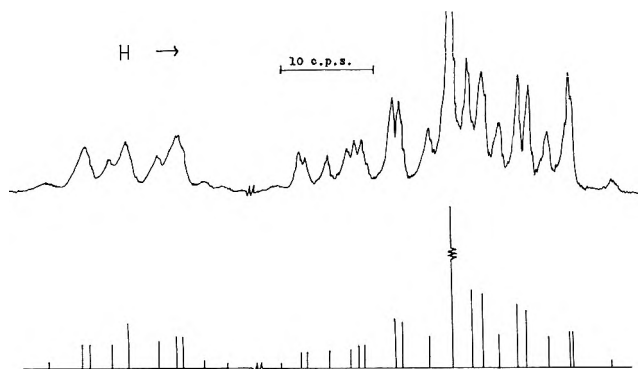


Figure 1. Observed and calculated proton n.m.r. spectra of phenanthrene at 60 Mc.

the procedure and iterative computer program described by Swalen and Reilly.⁴

A variety of different line assignments was tested corresponding to different chemical shift assignments and relative signs for the coupling constants. Only one assignment gave satisfactory agreement for both the line positions and the line intensities. The observed and calculated spectra for a 13% solution are given in Figure 1. The analysis was checked by comparing the observed 100-Mc. phenanthrene spectrum with that calculated from the parameters determined at 60 Mc., and good agreement was found. The coupling constants showed no significant variation with concentration over the range studied. The chemical shifts did vary, and values were extrapolated to infinite dilution. The results, together with values from the previous study, are shown in Table I.

Table I: Chemical Shifts and Coupling Constants for Phenanthrene

<i>i</i>	$\delta_{\text{TMS}} - \delta_{\text{H}_i}$, p.p.m.		<i>ij</i>	J_{ij} , c.p.s.	
	10% in CDCl_3^a	Inf. dil. in CDCl_3^b (± 0.005)		Ref. 3	This work (± 0.05)
1	8.125	7.855	12	8.4	8.11
2	7.825	7.570	13	1.6	1.31
3	7.883	7.612	14	0.5 ^c	0.66
4	8.933	8.648	23	7.3	7.20
9		7.702	24	1.6	1.24
			34	8.4	8.40

^a See ref. 3. ^b This work. ^c Assumed.

The coupling constants found here are generally similar to those reported earlier,³ but some differences do occur. It should be pointed out that the previous analysis was based on an interpolation procedure, and J_{14} was assumed to be 0.5 c.p.s. There is also

an appreciable discrepancy in the chemical shift values, our values for a 10% solution being consistently to lower field by 0.28 to 0.32 p.p.m. Independent spectra were obtained on two different Varian A-60 spectrometers. The chemical shifts of the 9,10-protons agreed satisfactorily (± 0.02 p.p.m.) with our other results, lending credence to their accuracy.

It may be noted that the low-field resonance lines are broader than the others. This might be the result either of long-range coupling or of a short relaxation time for the 4,5-protons. No significant narrowing of these lines was observed during spin-decoupling experiments in which the 9,10-proton resonance was irradiated.

Acknowledgment. We wish to express our appreciation to Varian Associates for supplying 60- and 100-Mc. n.m.r. spectra of phenanthrene, to Dr. E. Wadsworth of San Diego State College for making an A-60 spectrometer available for our use, and to the National Science Foundation for partial support of this work as well as for a grant-in-aid assisting the purchase of the n.m.r. spectrometer used in these studies.

(4) J. D. Swalen and C. A. Reilly, *J. Chem. Phys.*, **37**, 21 (1962).

Logarithmic Distribution Functions for Colloidal Particles

by E. P. Honig

Philips Research Laboratories, N. V. Philips' Gloeilampenfabrieken, Eindhoven, The Netherlands (Received August 31, 1965)

Recently, Espenscheid, Kerker, and Matijević¹ stated that a set of different logarithmic distribution functions $p_n(r)$ was obtained by varying a parameter n of the "general" logarithmic distribution function (eq. 21 of their paper), characterized by the three parameters n , r_n , and σ_n

$$p_n(r) = \frac{r^n \exp[-(\ln r - \ln r_n)^2 / 2\sigma_n^2]}{\sqrt{2\pi\sigma_n r_n^{n+1}} \exp[(n+1)^2 \sigma_n^2 / 2]} \quad (1)$$

However, it will be shown now that all distribution functions (1) can be reduced to the logarithmic normal distribution function, containing only two parameters: r_m and σ_n .

(1) W. F. Espenscheid, M. Kerker, and E. Matijević, *J. Phys. Chem.*, **68**, 3093 (1964).

Equation 1 can be rewritten as

$$p_n(r) = \frac{1}{\sqrt{2\pi\sigma_n r}} \left(\frac{r}{r_n}\right)^{n+1} \times \exp - \left[\frac{(\ln r/r_n)^2}{2\sigma_n^2} + (n+1)^2\sigma_n^2/2 \right]$$

or

$$p_n(r) = \frac{1}{\sqrt{2\pi\sigma_n r}} \exp - \left[\frac{(\ln r/r_n)^2}{2\sigma_n^2} - (n+1) \ln r/r_n + (n+1)^2\sigma_n^2/2 \right]$$

or

$$p_n(r) = \frac{1}{\sqrt{2\pi\sigma_n r}} \times \exp - \frac{[\ln r - \{\ln r_n + (n+1)\sigma_n^2\}]^2}{2\sigma_n^2} \quad (2)$$

The term $\ln r_n + (n+1)\sigma_n^2$ contains parameters

only; hence a new parameter r_m may be substituted, defined by

$$\ln r_m \equiv \ln r_n + (n+1)\sigma_n^2 \quad (3)$$

So

$$p_n(r) = \frac{1}{\sqrt{2\pi\sigma_n r}} \exp - \frac{(\ln r - \ln r_m)^2}{2\sigma_n^2} \quad (4)$$

The distribution function (1) is thus reduced to the logarithmic normal distribution function (4), where a single parameter r_m replaces the two parameters r_n and n . From an experimentally determined distribution curve *only* the parameters r_m and σ_n can be evaluated. In order to determine r_n and n separately, one must think of an experiment where r_n and n are connected by a relationship other than eq. 3; however, this does not seem possible because r_n and n have no physical significance. Hence, there is no reason to introduce a set of logarithmic distribution functions (by variation of the parameter n), and it is sufficient to deal with the logarithmic normal distribution function.

COMMUNICATIONS TO THE EDITOR

An Apparently Primary CH_5^+ Ion in the Mass Spectrum of 2-Methoxyethanol

Sir: We have observed the ion CH_5^+ in the mass spectrum of 2-methoxyethanol and have found that it is apparently a primary ion. This ion has been observed previously in the mass spectrometer,¹⁻¹⁰ but to our knowledge, this is the first time it has been recognized either as a primary ion or in a system which does not include methane.

We have identified this ion as part of a doublet appearing at m/e 17. In a spectrum of 2-methoxyethanol (Fisher certified reagent) dried over anhydrous CaSO_4 run on a Consolidated Electro Dynamics mass spectrometer Model 21-103C, we have observed this doublet, while in other samples dried with an excess of the CaSO_4 the lower mass peak (OH^+) is diminished to a shoulder on the higher mass peak. Accurate determination of the mass of the latter peak was done by measuring the accelerating voltage for this peak and comparing it to the voltages for the known peaks at m/e 15, 16, 18, and 19. The results are given in Table I. The peak at m/e 17 is about 80% of the height of the CH_4^+ peak at m/e 16. Therefore, it could not be due to $^{13}\text{CH}_4^+$.

Spectra were also run on a high-resolution Hitachi mass spectrometer, Model RMU-6D. In one of these, some NH_3 was added. To the second was added a

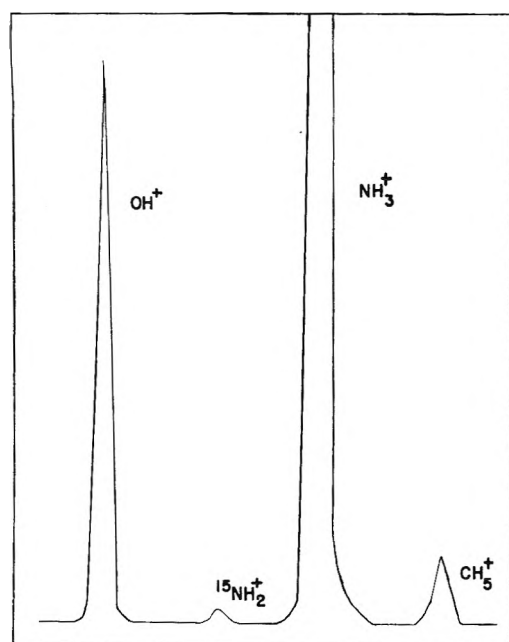


Figure 1. High-resolution spectrum of the multiplet at m/e 17 in 2-methoxyethanol with added ammonia.

small amount of CH_3D . It was expected that NH_3^+ should appear about 65% of the distance from the OH^+ to the CH_5^+ . The mass difference between CH_3D^+ and CH_5^+ is one part in 11,000, which is approximately the stated resolution for this instrument. The results are shown in Figures 1 and 2.

Table I: Determination of Exact Mass of m/e 17 Peak in the Mass Spectrum of Dry 2-Methoxyethanol

Trial	Mass found
1	17.0435
2	17.0377
3	17.0434
4	17.0441
5	17.0337
Av.	17.0405 \pm 0.0038 (av. dev.)

Expected masses^a: $\text{OH}^+ = 17.0022$; $\text{NH}_3^+ = 17.0260$; $\text{CH}_5^+ = 17.0386$

^a Calculated on the basis of automatic weights in J. H. Beynon and A. E. Williams, "Mass and Abundance Tables for Use in Mass Spectrometry," Elsevier Publishing Co., New York, N. Y., 1963, p. vii, and considering the mass of the electron.

Pressure dependence studies were made using the Consolidated instrument and measuring the pressure with a micromanometer. A typical set of data plotted as peak height *vs.* inlet pressure is shown in Figure 3. It can be seen that the relationship is linear.

(1) See the reviews by (a) C. E. Melton in "Mass Spectrometry of Organic Ions," F. W. McLafferty, Ed., Academic Press, New York, N. Y., 1963, Chapter 2; (b) J. Durup, "Les Reactions Entre Ions Positifs et Molecules en Phase Gazeuse," Gauthier-Villars, Paris, 1960, p. 20.

(2) A. Cassuto, *Advan. Mass Spectrometry, Proc. Conf., 2nd, Oxford, 1961*, 2, 296 (1963).

(3) G. R. Cook, J. A. R. Samson, and G. L. Weissler, U. S. Department of Commerce, Office of Technical Services, P. B. Report 145,185 (1959).

(4) F. H. Field, J. L. Franklin, and M. S. B. Munson, *J. Am. Chem. Soc.*, 85, 3575 (1963).

(5) C. E. Melton and W. H. Hamill, *J. Chem. Phys.*, 41, 1469 (1964).

(6) M. S. B. Munson, F. H. Field, and J. L. Franklin, *J. Am. Chem. Soc.*, 85, 3584 (1963).

(7) K. R. Ryan and J. H. Futrell, *J. Chem. Phys.*, 42, 824 (1965).

(8) N. N. Tunitskii and S. E. Kupriyanov, *Tr. Pervogo Vses. Soveshch. po Radiatsion. Khim., Akad. Nauk SSSR, Otd. Khim. Nauk, Moscow*, 7 (1958).

(9) H. von Koch, U. S. Department of Commerce Accession No. AD 603 091 (1964), Avail. CFSTI.

(10) S. Wexler, *J. Am. Chem. Soc.*, 85, 272 (1963).

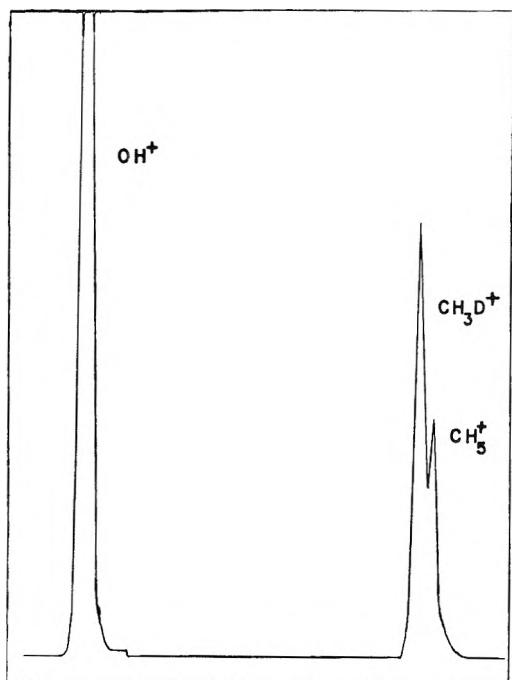


Figure 2. High-resolution spectrum of the multiplet at m/e 17 in 2-methoxyethanol with a small amount of added methane- d_1 .

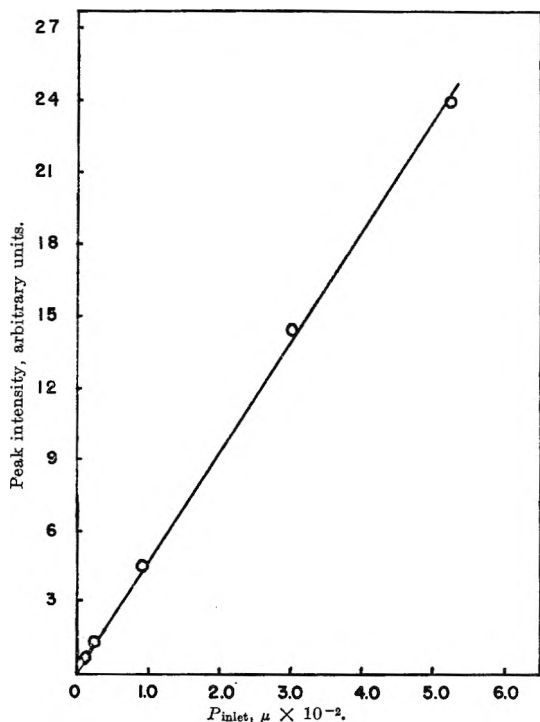


Figure 3. Peak intensity vs. the inlet pressure.

Isotopic studies to determine the mechanism of formation of this ion are in progress.

(11) Department of Chemistry, Northern Illinois University, DeKalb, Ill. 60115.

Acknowledgment. We wish to thank Mr. A. Struck of the Perkin-Elmer Corporation for obtaining some of the spectra mentioned in this communication.

MICHIGAN STATE UNIVERSITY
EAST LANSING, MICHIGAN

KERMIT R. WAY
MORLEY E. RUSSELL¹¹

RECEIVED AUGUST 30, 1965

Pulse Radiolysis of Fused Alkali Halides¹

Sir: The coloration of alkali halide crystals by ionizing radiation, by treatment with alkali metals, and by electrolysis, is well known. Coloration of alkali halides in the liquid state by solution of alkali metals or by electrolysis has often been reported²; however, coloration by ionizing radiation does not appear to have been studied. This communication reports some preliminary observations on coloration of alkali halide melts using the pulse radiolysis technique.

Two samples were used, one of pure KCl and the other an equimolar mixture of KCl and KBr. Samples were prepared from single-crystal material supplied by the Harshaw Chemical Co. and were held in ampoules made from 13-mm. tubes of Suprasil high-purity fused silica. Ampoules were evacuated before sealing. During measurements, the sample temperatures were maintained a few degrees above their melting points in an oven with an aperture for the light path.

The optical system consisted of a lamp passing white light through the center of the sample, through a monochromator, and to an S1 multiplier phototube whose output was suitably displayed on a dual-beam oscilloscope. Measurements could be made over the range 5000–11,000 Å.

Samples were irradiated by 4- μ sec. pulses of 30-Mev. electrons. The dose delivered was determined by a calorimetric method and was, typically, 10^5 rads/pulse.

With this arrangement, a moderate-to-strong absorption was observed to form during a pulse and to decay after a few microseconds. A typical oscilloscope trace is shown in Figure 1, curve A. A moderately intense radioluminescence was observed to interfere with measurements of absorption. This luminescence could be measured independently by closing a shutter between the lamp and the sample; a typical oscilloscope trace is shown in curve B of Figure 1. The absorption

(1) Research partially supported by the Air Force Cambridge Research Laboratories, Office of Aerospace Research, under Contract AF-19(628)-2926.

(2) See, for example, M. A. Bredig in "Molten Salt Chemistry," M. Blander, Ed., John Wiley and Sons, Inc., New York, N. Y., 1964, p. 367.

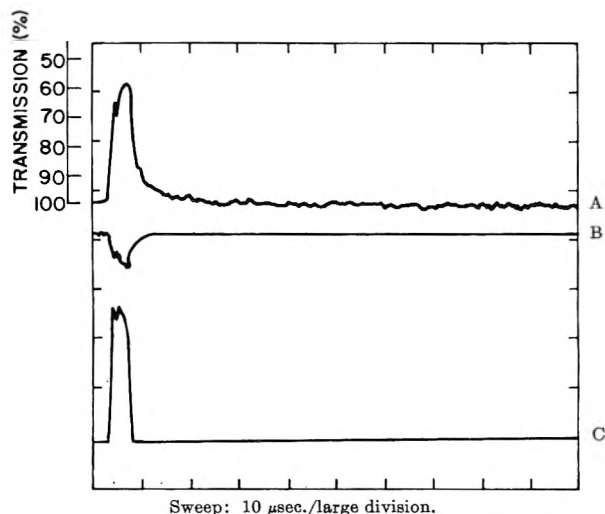


Figure 1. Tracing of oscilloscope photograph of light transmitted through and emitted from liquid KCl-KBr at 10,600 Å.: A, absorption signal; B, fluorescence signal, same gain as A; C, electron-beam current monitor signal.

signal could then be corrected by subtracting algebraically from it the corresponding fluorescence signal. The absorption was found to show a rise toward the infrared with a possible maximum near 10,000–11,000 Å., and the behavior was similar for both samples. The decay of the optical density shows a long-lived component with a time constant of $\sim 7 \mu\text{sec}$. Measurements on an empty tube showed that the silica container was not involved in these effects. No permanent absorption was observed: using chopped light and an a.c. amplifier and recorder, no absorption greater than 1% could be seen 1 sec. after delivering a dose of 10^6 rads. When allowed to cool in the absence of irradiation, the resulting crystals were not colored.

The absorption is thought to be similar to that produced by dissolving alkali metals in fused alkali halides. Mollwo³ found an absorption with a broad maximum at $\sim 10,000$ Å. for liquid KCl and KBr treated with alkali metal vapor. The absorption is tentatively attributed to a solvated electron or F center. The establishment of this identification will require further experiments both on metal solutions and by pulse radiolysis techniques.

(3) E. Mollwo, *Nachr. Akad. Wiss. Gottingen, Math-Physik Kl. II*, 1, 203 (1935).

GENERAL ATOMIC DIVISION
GENERAL DYNAMICS CORPORATION
SAN DIEGO, CALIFORNIA 92112

SANDRA J. BLACK
D. M. J. COMPTON

RECEIVED SEPTEMBER 22, 1965

Double Molecules in Gases

Sir: Possibly because the chemist is introduced to real gas behavior through the van der Waals equation, the presence of bound double molecules (as well as larger aggregates) in gases does not receive much attention in the literature. However, current statistical mechanical theories clearly point to such bound aggregates as a major source of the deviation from ideal gas behavior.¹

The question that remains unanswered is under what conditions these associated species are more important to kinetic and spectroscopic events than simple colliding pairs of molecules. The importance of double molecules in termolecular reaction kinetics will be discussed in a later publication. Our present concern lies with the possibility of direct observation of these bound pairs by their characteristic electronic absorption spectra.

There are at least three spectroscopic events that require two molecules in close proximity: (1) charge-transfer, (2) simultaneous, and (3) induced transitions. They are easily recognized because the absorbance due to such transitions is proportional to the square of the molecular concentration. Though a number of bands with this property can be found in the literature, seldom has the temperature of the gas been varied to determine whether the absorbing species is a bound pair or a colliding pair. If it is a colliding pair, the integrated band intensity should remain the same or increase slightly as the temperature is raised. On the other hand, a bound pair should dissociate as the temperature is raised decreasing the absorption in the band. We have found an ultraviolet band of bromine which displays this latter type of behavior.

The uppermost curve in Figure 1 shows the absorption spectrum of bromine vapor (130 torr, 14°, 10-cm. path) between 1850 and 2500 Å. Figure 2 shows the linear relationship between the absorbance in the band and the square of the concentration, indicating that the transition involves two molecules. The lower curves in Figure 1 illustrate the effect of raising the temperature of a fixed amount of bromine vapor. It is clear that the peak at 2080 Å. is rapidly removed as the temperature is increased from 14 to 200°. Further increases in temperature beyond 200° have little effect on the absorption in this region.

It seems reasonable to assume that the portion of the band which is removed by heating the cell is due to bound double molecules and that there is an

(1) D. E. Stogryn and J. O. Hirschfelder, *J. Chem. Phys.*, 31, 1531 (1959).

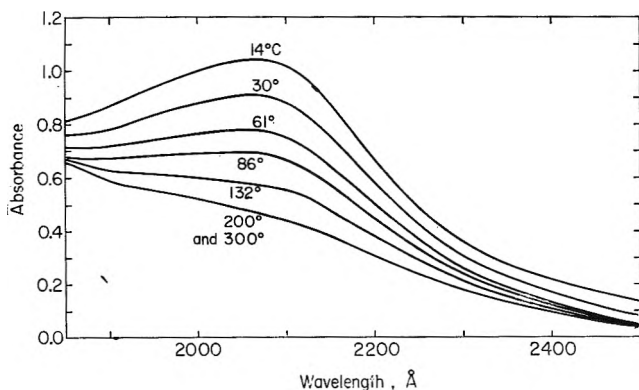


Figure 1. Ultraviolet absorption of bromine vapor. Path length, 10 cm.; $[\text{Br}_2] = 10^{-2} M$.

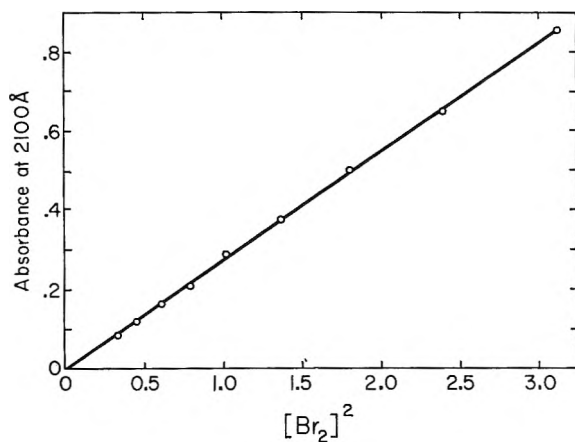


Figure 2. Relationship between $[\text{Br}_2]^2$ and the absorbance at 2100 Å.

underlying absorption due to colliding pairs and/or the tail of a stronger band at 1600 Å. reported by Cordes and Spomer.² With this assumption the absorbance due only to double molecules can be obtained by subtraction. A plot of $\log(A/T)$ against $(1/T)$ can then be used to calculate the enthalpy change (ΔH_2) in the formation of double molecules. Such a plot is shown in Figure 3. From the slope at 25° $\Delta H_2 = -2.6$ kcal. Hence, the bond energy $E = -\Delta U = 2.0$ kcal.

Because of a paucity of *PVT* data for the halogens, it is not possible to compare our value of the double-

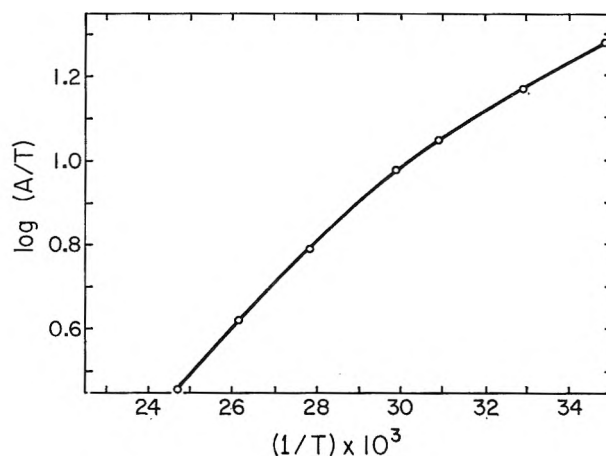


Figure 3.

molecule dissociation energy with that calculated from association theory.³ However, the value is consistent with that obtained from *PVT* data for hydrocarbons with boiling points similar to bromine.⁴

Two recent communications provide the only additional direct evidence for bound (nonpolar) double molecules in gases. Watanabe and Welsh⁵ have reported new absorption bands in hydrogen gas at 30°K. which they attribute to bound levels of $(\text{H}_2)_2$, and Robbins and Leckenby⁶ have reported mass spectrometric evidence for appreciable concentrations of species such as Ar_2 , Xe_2 , $(\text{N}_2)_2$, and $(\text{O}_2)_2$ in gases at 200 torr. There is little doubt that such species can be observed directly by techniques similar to those described in this paper since simultaneous, induced, or charge-transfer transition can be found for most molecules.

(2) H. Cordes and H. Spomer, *Z. Physik*, **63**, 334 (1930).

(3) E. A. Ogryzlo and G. Allard, *J. Chem. Educ.*, in press.

(4) J. O. Hirschfelder, F. T. McClure, and I. F. Weeks, *J. Chem. Phys.*, **10**, 201 (1942).

(5) A. Watanabe and H. L. Welsh, *Phys. Rev. Letters*, **13**, 810 (1964).

(6) E. J. Robbins and R. E. Leckenby, *Nature*, **206**, 1253 (1965).

CHEMISTRY DEPARTMENT
UNIVERSITY OF BRITISH COLUMBIA
VANCOUVER, CANADA

E. A. OGRYZLO
B. C. SANCTUARY

RECEIVED OCTOBER 11, 1965

ADDITIONS AND CORRECTIONS

1964, Volume 68

Kinko Shinzawa and Ikuzo Tanaka: The Photochemical Isomerization of α ,N-Diphenylnitron.

Page 1205. In line 10 of the Abstract, 0.28 should read 0.56, and 0.18 should read 0.36.

Pages 1210 and 1211. In Figures 5 and 8 the values of the vertical axes should be doubled.—KINKO KOYANO.

M. M. Breuer: The Binding of Phenols by Hair. II. Volume Changes Accompanying the Dilution of Aqueous Solutions of Phenols.

Page 2078. The sentence commencing on line 35 of the first column should read: The respective heats and entropies of association calculated from the values of K_1 and K_2 and the heats of dilution (Figure 6) in an analogous way as described before are +550 cal./mole, +1600 cal./mole, -1.60 e.u./mole, and +2.23 e.u./mole.—M. M. BREUER.

Y. Marcus and M. Givon: Anion Exchange of Metal Complexes. XIV. The Effect of Acidity on the Sorption of Lanthanides from Lithium Nitrate Solutions.

Page 2233. The view that dimerization of nitric acid has been found in a solution of a trialkylamine in toluene has been erroneously attributed to Högfeldt and Fredlund (ref. 19), being based on a pre-publication copy of their paper [*Acta Chem. Scand.*, **18**, 543 (1964)], kindly supplied by Dr. Högfeldt. Their paper only supports the formation of the dimeric complex $(R_3N \cdot HNO_3)_2$. The formation of the species $R_3NH^+ \cdot (NO_3^- \cdot HNO_3)^-$ has, however, recently been proposed by Tuck and co-workers [J. Bullock, S. Choi, D. Goodrick, D. Tuck, and E. Woodhouse, *J. Phys. Chem.*, **68**, 2687 (1964)] to explain their data on similar systems. The conclusions of the present paper are not based on species which may be present in amine systems, however.—Y. MARCUS.

Harold W. Kohn: Oxidation of Hydrocarbons Adsorbed on Oxide Catalysts Induced by Cobalt-60 γ -Rays.

Page 3134. The sentence beginning on the third line below eq. 4 should read: If 3 is zero order or fast... (instead of slow).—HAROLD W. KOHN.

1965, Volume 69

David L. Lydy, V. Alan Mode, and Jack G. Kay: Dissociation Constant and Degree of Dissociation for Tetraethylammonium Chloride in Ethylene Dichloride at 0, -15, and -30°.

Page 88. In Table II, Professor C. W. Davies has brought to our attention that the calculated minima in the degree of dissociation curves are much dependent upon the particular activity coefficient equation used. The relationship $\log f_{\pm} = -A\sqrt{\alpha C}$ gives the best agreement between calculated and observed values for the dissociation minima.

The third column of Table II, calculated on the basis of this limiting Debye-Hückel equation, should be corrected to read 1.92, 2.21, and 2.43 for the temperatures 0, -15, and -30°, respectively. The factor 5.3 is eliminated.—JACK G. KAY.

C. T. Stubblefield, J. L. Rutledge, and R. Phillips: The

Heats of Formation of Anhydrous Europium(II) Chloride and of the Aqueous Europium(II) Ion.

Page 991. In the Abstract, the value of the heat of formation of $EuCl_2(s)$ is reported incorrectly as -195.8 kcal./mole; it should be the same as that found in the text on p. 995, *viz.*, -192.8 kcal./mole.—C. T. STUBBLEFIELD.

Richard P. Wendt: The Estimation of Diffusion Coefficients for Ternary Systems of Strong and Weak Electrolytes.

Page 1229. Line 18, column 1, should read: B^{2z} , and C^{2z} , respectively. Valences of the ions. . . .

Page 1233. In eq. 59, the last term in the bracket should read

$$\frac{\nu_{16}\nu_{16}}{\nu_{16}C_1 + \nu_{26}C_2}$$

RICHARD P. WENDT

D. W. Placzek, D. F. Ring, and B. S. Rabinovitch: Deuterium Isotope Effects on Rates of Methylene Radical Insertion into C-H Bonds.

Page 1783. In column 2, lines 13-16, a kinetic equation of Majer, Capey, and Robb [J. R. Majer, W. D. Capey, and J. C. Robb, *Nature*, **203**, 294 (1964)] was termed inexact and a "more exact" formulation was cited (D. W. Placzek, Ph.D. Thesis, University of Washington, 1965). We thank Professor Robb for calling our attention to an arithmetic error in our derivation, correction of which renders it into his form which is exact. No results, computations, or conclusions are affected.—B. S. RABINOVITCH.

M. L. Hyder: The Radiolysis of Aqueous Nitrate Solutions.

Page 1858. A systematic error has been found in the calibration techniques used in this work which decreases all G values reported in the article. Correct G values may be obtained by multiplying the published values by 0.83. As a result, the measured value of $G_{e_{aq}^-}$ is decreased to 3.2 and the derived value of G_{-H_2O} becomes 3.9. These values are close to those reported by others who have studied alkaline solutions, including, in particular, Cheek and Linnenbom [C. H. Cheek and V. J. Linnenbom, *J. Phys. Chem.*, **67**, 1856 (1963)].

The qualitative conclusions discussed in this article are not affected by this correction.—M. L. HYDER.

Douglas C. Poland and Harold A. Scheraga: Hydrophobic Bonding and Micelle Stability.

Page 2442. We erroneously stated that "there is a glaring discrepancy between theory and experiment when the dependence of ΔH (for formation of the micelles) on chain length is considered." Actually, the experimental ΔH becomes more negative as chain length increases. This is exactly what the theory predicts [(a) G. Nemethy and H. A. Scheraga, *J. Chem. Phys.*, **36**, 3401 (1962), Figure 7. Figure 7 applies to the solution process; in applying it to the reverse process, the sign of ΔH must be changed. (b) G. Nemethy and H. A. Scheraga, *J. Phys. Chem.*, **66**, 1773 (1962), eq. 21 and the discussion following Table XI.] for *straight-chain* hydrocarbons; in the *branched* side chains of amino acids, the enthalpy of formation of a hydrophobic bond does become more positive as one goes from alanine-alanine to valine-valine to isoleucine-isoleucine (either in pair-

wise or in multiple interactions). Thus, all the experimental facts concerning the micelles discussed in the paper are in agreement with the theory (see ref. a and b above). This correction was pointed out to us by J. F. Goodman.—H. A. SCHERAGA.

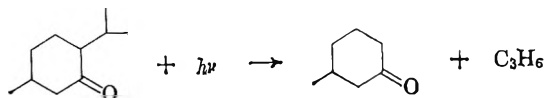
Leonard S. Silbert, B. F. Daubert, and Leo S. Mason: The Heats of Combustion, Formation, and Isomerization of Isomeric Monoglycerides.

Page 2887. In footnote 1, the year should be corrected to read 1953.—LEONARD S. SILBERT.

R. Srinivasan and Sheldon E. Cremer: Photochemical Rearrangement Reactions of 2-*n*-Propylcyclopentanone.

Page 3147. Srinivasan and Cremer are mistaken in making the statement that "Photochemical Rearrangement Reactions of

2-*n*-Propylcyclopentanone" appears to be the first instance in which the Norrish type II reaction has been observed to involve an alicyclic ketone. Bamford and Norrish [*J. Chem. Soc.*, 1521 (1938)] found that 1-menthone was photolyzed almost exclusively by this mechanism to propylene and 3-methylcyclohexanone.



PETER BORRELL
UNIVERSITY OF KEELE
STAFFORDSHIRE, ENGLAND

AUTHOR INDEX to Volume 69, 1965

- ABE, M., AND FUJITA, H. Binary Mixtures of θ -Solutions 3263
 ABU-HAMDIYYAH, M. The Effect of Urea on the Structure of Water and Hydrophobic Bonding 2720
 ABU-HAMDIYYAH, M., AND MYSELS, K. J. Alkyltripylamium Salts as Association Colloids in Concentrated Acid Media 1466
 ABU-ISA, I., AND DOLE, M. Specific Heat of Synthetic High Polymers. XII. Atactic and Isotactic Polystyrene 2668
 ACKER, T. See Odian, G., 2477
 ADAMS, C. R. See Schlaffer, W. G., 1530
 ADLER, G., AND PETROPOULOS, J. H. Electron Spin Resonance Spectroscopy of Irradiated Acrylamide 3712
 AFFSPRUNG, H. E. See Lin, T. F., 2980
 AGABIO, G. See Bianchi, U., 4392
 AKIMOV, I. See Terenin, A., 730
 ALBRIGHT, J. G., AND MILLS, R. A Study of Diffusion in the Ternary System, Labeled Urea-Urea-Water, at 25° by Measurements of Intradiffusion Coefficients of Urea 3120
 ALLEN, A. O. See Castorina, T. C., 3547
 ALLEN, E. R. See Cadle, R. D., 1611
 ALLEN, G. F. See Kulkarni, M. V., 2491
 ALLEN, M. C. See Blyholder, G., 3998
 ALLEN, R. J. See Chaberek, S., 641, 647, 2834, 2842
 ALLENDORF, H. D. See Rosner, D. E., 4290
 ALLRED, A. L. See Larsen, D. W., 2400
 ALUMBAUGH, R. L., PRITCHARD, G. O., AND RICKBORN, B. Nonstereospecific Mechanisms in the Photolysis of Cyclic Ketones 3225
 AMANO, A., AND UCHIYAMA, M. Kinetics of the Thermal Rearrangement between 3-Methyl-1,5-hexadiene and 1,5-Heptadiene 1278
 AMEY, R. L. On the Polarizability of Rare Gas Atoms 702
 AMIS, E. S. See Hefley, J. D., 2082
 ANBAR, M., AND HART, E. J. The Reaction of Haloaliphatic Compounds with Hydrated Electrons 271
 ANBAR, M., AND HART, E. J. The Reactivity of Metal Ions and Some Oxy Anions toward Hydrated Electrons 973
 ANBAR, M., AND HART, E. J. The Effect of Solvent and of Solutes on the Absorption Spectrum of Solvated Electrons 1244
 ANBAR, M., AND MEYERSTEIN, D. Isotope Effects in the Radiolysis and Photolysis of H₂O-D₂O Mixtures 698
 ANDERSEN, T. N. See Perkins, R. S., 3329
 ANDERSON, C. W. See Stern, J. H., 207
 ANDERSON, J. E., AND SLICHTER, W. P. Nuclear Spin Relaxation in Solid *n*-Alkanes 3099
 ANDO, T. See Tomita, Y., 404
 ANDRÉ, J. See Fripiat, J. J., 2185
 ANDRUS, R. W. See Tong, L. K. J., 2357
 ANGELL, C. A. Diffusion-Conductance Relations and Free Volume in Molten Salts 399
 ANGELL, C. A. Electrical Conductance of Concentrated Aqueous Solutions and Molten Salts: Correlation through Free Volume Transport Model 2137
 ANGELL, C. L., AND SCHAFFER, P. C. Infrared Spectroscopic Investigations of Zeolites and Adsorbed Molecules. I. Structural OH Groups 3463
 AQUILANTI, V. Rare Gas Sensitized Radiolysis of Methane 3434
 ARAI, S., AND DORFMAN, L. M. Pulse Radiolysis Studies. VIII. Kinetics of Formation of Triplet States of Aromatic Molecules in Acetone Solutions 2239
 ARAKAWA, T. See Peterson, D. B., 2880
 ARNETT, R. L. See Stacy, C. J., 3109
 ARNOLD, W. An Electron-Hole Picture of Photosynthesis 788
 ARON, C. See Rosoff, M., 21
 ARRINGTON, C. C., AND KISER, R. W. Chemical Species Containing P³² and S³⁵ Subsequent to the Neutron Irradiation of Thiourea 3202
 ASSOUR, J. M. On the Polymorphic Modifications of Phthalocyanines 2295
 ASTON, J. G., AND MISRA, D. N. Rates of the Simultaneous Oxidation and Reduction of Diphenylpicrylhydrazyl on Titanium Dioxide and Carbon Black. The Role of F-Centers in Catalytic Activity 3219
 ASTON, J. G. See Frankosky, M., 3126; Kikuchi, K., 3654
 ATKINSON, G., AND KOR, S. K. The Kinetics of Ion Association in Manganese Sulfate Solutions. I. Results in Water, Dioxane-Water Mixtures, and Methanol-Water Mixtures at 25° 128
 AVERY, J. S., AND MASON, R. Exciton States in Polymers 784
 BACK, R. A. See Dawes, D. H., 2385
 BADAWI, F. A. K. See Mukherjee, L. M., 2537
 BADDIEL, C. B., TAIT, M. J., AND JANZ, G. J. Nonaqueous Silver Nitrate Solutions. Spectral Studies in Acetonitrile 3634
 BAIR, H. E. See Karasz, F. E., 2657
 BAKER, F. B. See Newton, T. W., 176
 BALIGA, B. T., RANTAMAA, A. K., AND WHALLEY, E. Effect of Pressure on the Hydrolysis of the Ethyleniminium Ion 1751
 BARRIEREAU, R. E. Analytical Expressions for the Zero Pressure Thermodynamic Properties of Nitrogen Gas Including Corrections for the Latest Values of the Atomic Constants and the New Carbon-12 Atomic Weight Scale 495
 BARKER, C. K., CORDES, A. W., AND MARGRAVE, J. L. The Heats of Formation of Solid Tetrasulfur Tetranitride and Tetraselenium Tetranitride 334
 BARKER, C. K. See Kybett, B. D., 3603
 BARRADAS, R. G., HAMILTON, P. G., AND CONWAY, B. E. Esin and Markov Effect for Adsorbed Organic Ions and Molecules 3411
 BARRETT, J., FOX, M. F., AND MANSELL, A. L. The Photochemistry of Aqueous Sulfate Ion 2996
 BARTELL, L. S., GUILLORY, J. P., AND PARKS, A. T. Electron Diffraction Study of the Structure and Conformational Behavior of Cyclopropyl Methyl Ketone and Cyclopropanecarboxylic Acid Chloride 3043
 BARTER, C., AND WAGNER, C. D. Generation of Catalytic Activity in Silica Gel by Ionizing Radiation 491
 BARTON, L., WASON, S. K., AND PORTER, R. F. Thermochemistry of Interconversion of H₂B₂O₃(g) and H₂B₃O₃(g) 3160
 BARZYNSKI, H. F., HENTZ, R. R., AND BURTON, M. Radiolysis of Benzene and Benzene-Cyclohexane Mixtures in the Presence of Nickel Tetracarbonyl 2034
 BATES, R. G. See Gary, R., 2750
 BAUER, S. H., AND JEFFERS, P. The Dynamics of Cryosorption Pumping 3317
 BAUM, R. L. See Fordyce, J. S., 4335
 BAUTISTA, R. G., AND MARGRAVE, J. L. Langmuir Studies of the Sublimation of Strontium Fluoride and Barium Fluoride Single Crystals 1770
 BEAN, R. C., SHEPHERD, W. C., KAY, R. E., AND WALWICK, E. R. Spectral Changes in a Cationic Dye Due to Interaction with Macromolecules. III. Stoichiometry and Mechanism of the Complexing Reaction 4368
 BEAR, I. J., AND TURNBULL, A. G. The Heats of Formation of Beryllium Compounds. I. Beryllium Hydroxides 2828
 BEATTY, D. A. See Maciel, G. E., 3920
 BECKER, D. A., OKABE, H., AND McNESBY, J. R. Vacuum Ultraviolet Photochemistry. VIII. Propylene 538
 BECKER, R. See Harrah, L. A., 2487
 BECKER, R. S., AND ROY, J. K. The Spectroscopy and

- Photosensitization of Various Photochromic Spiropyrans. 1435
- BECKER, R. S. See Scott, D. R., 3207
- BECSEY, J. G. See Gustafsson, S. E., 1016
- BELL, W. E. See Norman, J. H., 1373
- BELTON, G. R., AND JORDAN, A. S. The Volatilization of Molybdenum in the Presence of Water Vapor. 2065
- BENDORAITIS, J. G., AND SALOMON, R. E. Optical Energy Gaps in the Monoclinic Oxides of Hafnium and Zirconium and Their Solid Solutions. 3666
- BENERITO, R. R. See Berni, R. J., 1882
- BEN-NAIM, A. On the Origin of the Stabilization of the Structure of Water by Nonelectrolytes. 1922
- BEN-NAIM, A. Thermodynamics of Aqueous Solutions of Noble Gases. I. 3240
- BEN-NAIM, A. Thermodynamics of Aqueous Solutions of Noble Gases. II. Effect of Nonelectrolytes. 3245
- BEN-NAIM, A., AND EGEL-THAL, M. Thermodynamics of Aqueous Solutions of Noble Gases. III. Effect of Electrolytes. 3250
- BENNETT, J. E. See McLure, I. A., 2759; Watson, A. E. P., 2753
- BENSON, G. C. See McLure, I. A., 2759; Watson, A. E. P., 2753
- BENSON, S. W., AND HAUGEN, G. The Elimination of HF from "Hot" Fluorinated Ethanes. An Estimation of the Activation Energies and Rate Parameters. 3898
- BERG, W. T. See Finke, H. L., 3030
- BERGER, J. E. Adsorption of Nonylphenoxyacetic Acid by Metals. 2598
- BERGMANN, E. D. See Radell, J., 928
- BERNARD, H. W. See Kikuchi, K., 3654
- BERNI, R. J., BENERITO, R. R., AND ZIFLE, H. M. Kinetics of the Zinc Fluoroborate and Hydrogen Ion Catalyzed Hydrolyses of the Diglycidyl Ether of 1,4-Butanediol and of Diglycidyl Ether. 1882
- BERNSTEIN, H. J. Bond and Interaction Contributions for Calculating the Heat of Formation, Diamagnetic Susceptibility, Molar Refraction and Volume, and Thermodynamic Properties of Some Substituted Methanes. 1550
- BERTOZZI, G. Surface Tension of Liquid Alkali Halide Binary Systems. 2606
- BESENBURCH, G., KANA'AN, A. S., AND MARGRAVE, J. L. Knudsen and Langmuir Measurements of the Sublimation Pressure of Cadmium(II) Fluoride. 3174
- BEVAN, R. B., JR. See Busey, R. H., 3471
- BEWIG, K. W., AND ZISMAN, W. A. The Wetting of Gold and Platinum by Water. 4238
- BHATNAGAR, O. N. See Gopal, R., 2382
- BHATTACHARYA, D. N., LEE, C. L., SMID, J., AND SZWARC, M. Studies of Ions and Ion Pairs in Tetrahydrofuran Solution. Alkali Metal Salts of Tetraphenylboride. 608
- BHATTACHARYA, D. N., LEE, C. L., SMID, J., AND SZWARC, M. Reactivities and Conductivities of Ions and Ion Pairs in Polymerization Processes. 612
- BHATTACHARYA, D. N., SMID, J., AND SZWARC, M. Alternative Paths in Anionic Propagation of Ion Pairs. Effect of Solvent and Counterion. 624
- BHAUMIK, M. L., AND EL-SAYED, M. A. Studies on the Triplet-Triplet Energy Transfer to Rare Earth Chelates. 275
- BIANCHI, U. Pressure Effects on Glass Transition in Polymers. 1497
- BIANCHI, U., AGABIO, G., AND TURTURRO, A. Internal Pressure of Simple Liquids. 4392
- BIERLEIN, J. A. See Gustafsson, S. E., 1016
- BILLICK, I. H., AND BOWEN, R. J. Application of a High Intensity, Multislit Rayleigh Interferometer to Sedimentation Studies. 4024
- BINDER, D. See Parkinson, W. W., 828
- BIRKETT, J. D., AND LYONS, P. A. Diffusion in Deuterio-Normal Hydrocarbon Mixtures. 2782
- BLACK, P. E. See Bywater, S., 2967
- BLACK, S. J., AND COMPTON, D. M. J. Pulse Radiolysis of Fused Alkali Halides. 4421
- BLACKBURN, P. E., AND BÜCHLER, A. The Thermodynamics of Vaporization in the Beryllium Oxide-Boron Oxide System. 4250
- BLAUER, J. A., GREENBAUM, M. A., AND FARBER, M. The Thermodynamic and Physical Properties of Beryllium Compounds. VII. Enthalpy and Entropy of Sublimation of Beryllium Fluoride. 1069
- BLAUER, J. A. See Ko, H. C., 2311
- BLOCH, F. W. See MacKenzie, D. R., 2526
- BLOCKER, N. K. See Sieck, L. W., 888
- BLUKIS, U., AND MYERS, R. J. Disulfur Monoxide. III. Its Infrared Spectrum and Thermodynamic Functions. 1154
- BLYHOLDER, G., AND ALLEN, M. C. Infrared Spectra and Bonding of Nitric Oxide Adsorbed on Nickel and Iron. 3998
- BOCKRIS, J. O'M., AND RICHARDS, S. R. Prediction of the Heats of Activation for Viscous Flow in Simple Non-metallic Liquids. 671
- BOCKRIS, J. O'M., RICHARDS, S. R., AND NANIS, L. Self-Diffusion and Structure in Molten Group II Chlorides. 1627
- BOCKRIS, J. O'M. See Gileadi, E., 3335
- BODENSEH, H. K., AND RAMSEY, J. B. Tetrapropylammonium Bromide: Ion Size Parameters in Solution and in the Solid State. 543
- BOEHM, C. See Nikitine, S., 745
- BOEYENS, J. C. A., AND HERBSTEIN, F. H. Molecular Compounds and Complexes. II. Exploratory Crystallographic Study of Some Donor-Acceptor Molecular Compounds. 2153
- BOEYENS, J. C. A., AND HERBSTEIN, F. H. Molecular Compounds and Complexes. III. The Crystal Structures of the Equimolar π -Molecular Compounds of Anthracene and Perylene with Pyromellitic Dianhydride. 2160
- BOGGS, J. E. See Davis, M. I., 3727
- BONE, L. I., AND FIRESTONE, R. F. Effects of Temperature in the Radiolysis of Methane and Propane. 3652
- BONNER, O. D., BREAZEALE, W. H., AND RUSHING, C. The Investigation of the Behavior of Some Divalent Salts of p-Toluenesulfonic Acid and Related Polymeric Acids in Aqueous Solutions. 4345
- BONNER, O. D., AND TORRES, A. L. The Determination of the Ionization Constants of Some Sulfonic Acids by Raman Measurements. 4109
- BONNER, O. D. See Durig, J. R., 3886
- BOPP, C. D. See Parkinson, W. W., 828
- BORCHERT, A. E. See Ramey, K. C., 3418
- BORGARDT, F. G. See Marshall, H. P., 25
- BORYTA, D. A. See Markowitz, M. M., 1114
- BOSMANS, H. See Fripiat, J. J., 2458
- BOTTER, F. Isotopic Equilibrium Separation Factors in the Hydrogen Solubility Process in Platinum-Palladium Alloys. 2485
- BOURDON, J. Spectral Sensitization of Chemical Effects in Solids. 705
- BOWEN, D. See Knight, J. A., 678
- BOWEN, R. J. See Billick, I. H., 4024
- BOYD, G. E., AND LARSON, Q. V. Production, Identity, and Annealing of the Radiolytic Products Formed in Crystalline Cesium Bromate by Cobalt-60 γ -Rays. 1413
- BOYD, G. E., AND LINDENBAUM, S. A Thermodynamic Calculation of the Ionic Strength Dependence of Ion-Exchange Reaction Selectivity Coefficients. 2378
- BOYD, G. E. See Lindenbaum, S., 2374; Schwarz, A., 4268
- BOYD, R. H., AND WANG, C. The Activity Coefficients of Solutes in Acid Solutions. II. The Relative Activity Coefficients of the Chloride and Silver Ions in Aqueous Sulfuric Acid. 3906
- BRACKETT, E. B. See Brackett, T. E., 3611
- BRACKETT, T. E., AND BRACKETT, E. B. The Lattice Energies of the Alkaline Earth Halides. 3611
- BRADSTREET, E. D. See Enns, T., 389
- BRANDT, W. W., AND BUDRYS, R. S. Sorption Rates Indicative of Structural Changes in Solid Polypeptides. 600
- BRANDT, W. W., AND BUDRYS, R. S. Comparison of Water Sorption and Deuterium-Hydrogen Exchange Sites in Poly-L-valine. 1432
- BRANDT, W. W. See Hartig, H., 335
- BREAZEALE, W. H. See Bonner, O. D., 4345; Durig, J. R., 3886

- BREDIG, M. A. Electrical Conductance and Density of Alkali Metal Nitrate Melts. 1753
- BREITER, M. W. Electrochemical Characterization of the Surface Composition of Heterogeneous Platinum-Gold Alloys. 901
- BREITER, M. W. Reactivity and Surface Composition. Anodic Methanol Oxidation on Platinum-Gold Alloys. 3377
- BRINEN, J. S., KOREN, J. G., OLMSTEAD, H. D., AND HIRT, R. C. Charge-Transfer Absorption and Luminescence Spectra of Alkyl Halide Salts of Pyridine. 3791
- BRISTOWE, W. W., KATAYAMA, M., AND TRUMBORE, C. N. γ -Radiolysis of Liquid Cyclopentanone. 807
- BRITT, A. D., AND KAISER, E. T. The Reaction of Triphenylphosphine with Alkali Metals in Tetrahydrofuran. 2775
- BRITTON, D. See van Thiel, M., 834
- BRODALE, G. E., AND GIAUQUE, W. F. The Heat of Hydration of Cobalt Sulfate Hexahydrate to Heptahydrate. Their Solubilities and Heats of Solution. 1268
- BRODMAN, B. W. See Radell, J., 928
- BROKAW, R. S. A Suggested Mechanism for the Hydrogen-Fluorine Reaction. 2488
- BROKAW, R. S. A Suggested Mechanism for the Hydrogen-Fluorine Reaction. II. The Oxygen-Inhibited Reaction. 2808
- BROOKS, W. V. F., CYVIN, S. J., AND KVANDER, P. C. Vibrational Mean-Square Amplitude Matrices. XVII. Mean-Square Perpendicular Amplitudes and Shrinkage Effects in Benzene Molecules. 1489
- BROWN, T. H., AND TAYLOR, R. L. The Use of Nonlinear Estimation Techniques in Simple Molecular Orbital Calculations. 2316
- BROWN, T. L., AND STARK, K. The Effect of Aromatic Solvents on Proton Magnetic Resonance Spectra. 2679
- BROWN, W. G. γ -Ray-Induced Isomerization of *cis*- and *trans*-1,2-Diphenylcyclopropane. 4401
- BRUCKENSTEIN, S. See Mukherjee, L. M., 2537
- BRUMBERGER, H., AND PANCIROV, R. Further Critical Opalescence Measurements on the Nitrobenzene-*n*-Heptane System. 4312
- BRUMMER, S. B. The Use of Large Anodic Galvanostatic Transients to Evaluate the Maximum Adsorption on Platinum from Formic Acid Solutions. 562
- BRUMMER, S. B. Comparison of Adsorbed Formic Acid and Carbon Monoxide on Platinum Electrodes. 1363
- BRUMMER, S. B., AND FORD, J. I. Galvanostatic Studies of Carbon Monoxide Adsorption on Platinum Electrodes. 1355
- BRUMMER, S. B., FORD, J. I., AND TURNER, M. J. The Adsorption and Oxidation of Hydrocarbons on Noble Metal Electrodes. I. Propane Adsorption on Smooth Platinum Electrodes. 3424
- BRYANT, J. T. See Pritchard, G. O., 664, 1085, 2804
- BYRCE, W. A. See Chrysochoos, J., 2453
- BUCHANAN, T. M. See Freeman, D. H., 1477
- BUCHER, J. J., AND DIAMOND, R. M. The Extraction of Perchloric Acid by Trilaurylamine. I. Aromatic Diluents. 1565
- BÜCHLER, A. See Blackburn, P. E., 4250
- BUDRYS, R. S. See Brandt, W. W., 600, 1432
- BUHL, A. See Schoonmaker, R. C., 3455
- BURGER, L. L. See Keder, W. E., 3075
- BURR, J. G. See Goodspeed, F. C., 1149; Yang, J. Y., 1157
- BURTON, M. See Barzynski, H. F., 2034; Hentz, R. R., 2027; Peterson, D. B., 2880
- BUSEY, R. H. The Entropy of $K_3Fe(CN)_6$ and $Fe(CN)_6^{3-}$ (aq). Free Energy of Formation of $Fe(CN)_6^{3-}$ (aq) and $Fe(CN)_6^{4-}$ (aq). 3179
- BUSEY, R. H., BEVAN, R. B., JR., AND GILBERT, R. A. The Heat Capacity of Potassium Hexabromorhenate-(IV) from 7 to 300°K. Manifestation of Thermal History Behavior. Antiferromagnetic Anomaly near 15°K. Entropy and Free Energy Functions. 3471
- BUTLER, B. D., AND TURNER, J. C. R. Soret Coefficients and Heats of Transport of Some Aqueous Electrolytes at 9°. 3598
- BUTLER, J. N. Interfacial Tension of Indium Amalgams in 0.1 M Perchloric Acid at 25°. 3817
- BYWATER, S., AND BLACK, P. E. Thermal Depolymerization of Polymethyl Methacrylate and Poly- α -methylstyrene in Solution in Various Solvents. 2967
- CADLE, R. D., AND ALLEN, E. R. Kinetics of the Reaction of O(³P) with Methane in Oxygen, Nitrogen, and Argon-Oxygen Mixtures. 1611
- CAHILL, J. A., AND GROSSE, A. V. Viscosity and Self-Diffusion of Liquid Thallium from Its Melting Point to About 1300°K. 518
- CALDER, G. V., AND GIAUQUE, W. F. The Entropy of Iodine Monochloride. Heat Capacity from 17 to 322°K. Vapor Pressure. Heats of Fusion and Vaporization. 2443
- CALDWELL, D. J. See Urry, D. W., 1603
- CALVERT, J. G. See Kerr, J. A., 1022
- CALVET, R. See Chaussidon, J., 2265
- CAPLAN, S. R. The Degree of Coupling and Efficiency of Fuel Cells and Membrane Desalination Processes. 3801
- CARLSON, H. G., AND WESTRUM, E. F., JR. 2,5-Dimethylthiophene. Heat Capacities and Thermodynamic Properties from 5 to 300°K. and Fusion of Stable and Metastable Phases. 1524
- CARMICHAEL, J. B., AND HEFFEL, J. Verification of the Flory Theory of Random Reorganization of Molecular Weight Distribution—Kinetics of Methylsiloxane Polymerization. 2213
- CARMICHAEL, J. B., AND HEFFEL, J. Equilibrium Molecular Weight Distribution of Cyclic and Linear Methylsiloxanes. 2218
- CARPENTER, J. H. See Krikorian, O. H., 4399
- CARPER, W. R., HEDGES, R. M., AND SIMPSON, H. N. Charge-Transfer Complexes and Donor Molecule Properties. I. Chloranil-Aniline Complexes. 1707
- CARR, R. W., JR., AND WALTERS, W. D. The Thermal Isomerization of Cyclobutene. 1073
- CARSON, J. L., KNIGHT, R. J., WATSON, I. D., AND WILLIAMSON, A. G. Solubilities of Fluorocarbons in Cyclohexane and 1,4-Dioxane. 3200
- CARTER, J. L., LUCCHESI, P. J., CORNEIL, P., YATES, D. J. C., AND SINFELT, J. H. Exchange of Deuterium with the Hydroxyl Groups of Alumina. 3070
- CARUSO, R., LOPREST, F. J., AND LUM, A. Heat of Formation of Hydrazinium Diperchlorate. 1716
- CASTELLANO, S., GÜNTHER, H., AND EBERSOLE, S. Nuclear Magnetic Resonance Spectra of 2,2-Bipyridyl. 4166
- CASTELLANO, S., AND LORENC, J. Nuclear Magnetic Resonance Spectra of Phenyl- and Diphenylacetylene. 3552
- CASTORINA, T. C., AND ALLEN, A. O. Radiolysis of Liquid Nitrogen Tetroxide. 3547
- CATER, E. D., LEE, T. E., JOHNSON, E. W., RAUH, E. G., AND EICK, H. A. Vaporization, Thermodynamics, and Dissociation Energy of Lanthanum Monosulfide. 2684
- CAVASINO, F. P. The Formation Kinetics of the Nickel Monomalonate Complex Studied by the Temperature-Jump Method. 4380
- CAVELL, E. A. S., JERRARD, H. G., SIMMONDS, B. A. W., AND SPEED, J. A. Dielectric Constants of Acetonitrile-Methanol Mixtures. 3657
- CHABEREK, S., AND ALLEN, R. J. Dye-Sensitized Photopolymerization Processes. II. A Comparison of the Photoactivities of Thionine and Methylene Blue. 647
- CHABEREK, S., ALLEN, R. J., AND GOLDBERG, G. Dye-Sensitized Photopolymerization Processes. III. The Photoreducing Activity of Some Dicarboxyl Compounds. 2834
- CHABEREK, S., ALLEN, R. J., AND SHEPP, A. Dye-Sensitized Photopolymerization Processes. IV. Kinetics and Mechanism of Thionine- β -Diketone-Acrylamide Systems. 2842
- CHABEREK, S., SHEPP, A., AND ALLEN, R. J. Dye-Sensitized Photopolymerization Processes. I. The Thionine-Nitrotripropionamide-Acrylamide System. 641
- CHAIRGE, P. See Scott, H., 1740
- CHANDRA, A. K., AND SANNIGRAHI, A. B. Hydrogen-Bonding Properties of Alcohols. 2494
- CHANG, E. T., AND WESTRUM, E. F., JR. The System Tetramethylmethane-Tetrachloromethane. Thermodynamics of Mixing in the Plastically Crystalline Region. 2176

- CHANG, J. Y. See Hentz, R. R., 2027
- CHANG, T. N. See Greenberg, S. A., 182, 553
- CHANG, Y. A., AND HULTGREN, R. The Dilatation Contribution to the Heat Capacity of Copper and α -Brass at Elevated Temperatures 4162
- CHAPIN, D. S., KAFALAS, J. A., AND HONIG, J. M. Electrical Properties of Ferromagnetic CrO_x ($1.89 < x < 2.02$) 1402
- CHAPMAN, I. D. See Hair, M. L., 3949
- CHAPPELL, W. H., JR. See Soulen, J. R., 3669
- CHAUSSIDON, J., AND CALVET, R. Evolution of Amine Cations Adsorbed on Montmorillonite with Dehydration of the Mineral 2265
- CHEN, F.-M. See Gutowsky, H. S., 3216
- CHÉNEBAULT, P., AND SCHÜRENKÄMPER, A. The Measurement of Small Surface Areas by the B.E.T. Adsorption Method 2300
- CHESICK, J. P. See Halberstadt, M. L., 429
- CHIANG, R. Intrinsic Viscosity-Molecular Weight Relationship for Fractions of Linear Polyethylene 1645
- CHIANG, T. C., AND HAMMAKER, R. M. An Infrared Study of the Dimerization of Trimethylacetic Acid in Carbon Tetrachloride Solution 2715
- CHIEN, J. C. W. On the Possible Initiation of Photo-oxidation by Charge-Transfer Excitation 4317
- CHRISTIAN, S. D., AND FOGEL, N. Discussion of an Apparent Violation of the Gibbs-Duhem Equation 2135
- CHRISTIAN, S. D. See Lin, T. F., 2980
- CHRISTNER, L. G. See Uytterhoeven, J. B., 2117
- CHRYSOCHOOS, J., AND BRYCE, W. A. Surface Effects in the Uninhibited and the Inhibited Pyrolyses of Isomeric Hexanes. IV. 2,3-Dimethylbutane (Diisopropyl) 2453
- CHU, B. Critical Opalescence of Binary Liquid Mixtures. The Debye Molecular Interaction Range 2329
- CIFERRI, A. See Puett, D., 141
- CLAES, P., AND RZAD, S. Electron Irradiation of Hydrocarbons. II. Model System for Radical Reactions and Diffusion in Radiolysis 1780
- CLARK, L. B., PESCHEL, G. G., AND TINOCO, I., JR. Vapor Spectra and Heats of Vaporization of Some Purine and Pyrimidine Bases 3615
- CLARK, L. W. Further Studies on the Decarboxylation of Picolinic Acid in Polar Solvents 2277
- CLARK, L. W. Further Studies on the Decarboxylation of β -Resorcylic Acid in Polar Solvents 3565
- CLARK, R. K., AND SCHMIDT, H. H. Gas-liquid Partition Chromatography in Benzene-Polyphenyl Systems and Polymer Statistical Thermodynamics 3682
- CLEVELAND, S. T., OKAJIMA, T., AND PEHLKE, R. D. Galvanic Cell Measurement of the Thermodynamic Interaction between Zinc and Lead in Dilute Solution in Liquid Tin 4085
- CLEVER, H. L., WESTRUM, E. F., JR., AND CORDES, A. W. Heat Capacities and Thermodynamic Properties of Globular Molecules. XIV. Tetraphosphorus Trisulfide, Tetraphosphorus Triselenide, and Tetraphosphorus Decasulfide between 5 and 350°K. 1214
- CLEVER, H. L., WONG, W.-K., AND WESTRUM, E. F., JR. Heat Capacities and Thermodynamic Properties of Globular Molecules. XIII. Transition and Fusion of Pentaerythrityl Chloride and Bromide, Transition of Pentaerythrityl Iodide 1209
- CLEVER, H. L., WULFF, C. A., AND WESTRUM, E. F., JR. Glutaronitrile. Calorimetrically Determined Thermal Properties from 5 to 350°K. and Statistical Gaseous Entropy 1983
- COETZEE, J. F., AND LOK, R. M.-S. A Differential Vapor Pressure Study of the Self-Association of Acids and Bases in 1,2-Dichloroethane and Certain Other Solvents 2690
- COETZEE, J. G., AND PADMANABHAN, G. R. Dissociation and Homoconjugation of Certain Phenols in Acetonitrile 3193
- COFFEY, D., JR. See Davis, M. I., 3727
- COHEN, N. See Heicklen, J., 1774
- COLE, G. M. See Smith, W. B., 4413
- COLE, S. A. See Weeks, B. M., 4131
- COLEMAN, A. E. See Sporck, C. R., 1066
- COLEMAN, C. F. Properties of Organic-Water Mixtures. II. Solubilities and Activity Coefficients of Sodium Chloride and Potassium Chloride in N,N-Dialkylamides Containing Water 1377
- COMPTON, D. M. J. See Black, S. J., 4421
- CONLEY, H. L., JR., AND MARTIN, R. B. Cupric Ion Catalyzed Hydrolyses of Glycine Ethyl Ester, Glycinamide, and Picolinamide 2914
- CONLEY, H. L., JR., AND MARTIN, R. B. Transition Metal Ion Promoted Hydrolysis of Amino Acid Esters 2923
- CONN, P. J., AND SWINEHART, D. F. A Thermodynamic Study of the Ionization of 3-Amino-4-methylbenzenesulfonic Acid 2653
- CONNOR, T. M., AND McLAUGHLAN, K. A. High Resolution Nuclear Resonance Studies of the Chain Conformation of Polyethylene Oxide 1888
- CONOCCHIOLI, T. J., TOCHER, M. I., AND DIAMOND, R. M. The Extraction of Acids by Basic Organic Solvents. V. Trioctyl Phosphine Oxide-HClO₄ and Trioctyl Phosphine Oxide-HReO₄ 1106
- CONWAY, B. E. See Barradas, R. G., 3411; Gilroy, D., 1259
- COOPER, D. E. See Yang, K., 1768
- COPELAND, B. K. W. See Levy, J. B., 408, 3700
- COPELAND, J. L., AND ZYBKO, W. C. The Solubility of Argon to 451 Atmospheres in Fused Sodium Nitrate at 369° 3631
- CORDES, A. W. See Barker, C. K., 334; Clever, H. L., 1214
- CORET, A. See Nikitine, S., 745
- CORNEIL, P. See Carter, J. L., 3070
- COURANT, R. A. See Horne, R. A., 2224, 3988
- COX, D. J. See Hill, J., 3032
- CRATIN, P. D., AND ROBERTSON, B. K. Nuclear Magnetic Resonance, Dielectric, Near-Infrared, and Cryoscopic Studies of Solubilized and Emulsified Water. The System Cyclohexane-Carbon Tetrachloride-Duomeen T Dioleate 1087
- CREMER, S. E. See Srinivasan, R., 3145
- CRISS, C. M. See Held, R. P., 2611
- CUBICCIOTTI, D. Thermodynamics of Vaporization of Liquid Thallous Iodide 1410
- CUBICCIOTTI, D., AND EDING, H. The Vapor Pressure and Enthalpy of Arsenic Triiodide and Its Absolute Entropy at 298°K. 2743
- CUBICCIOTTI, D., AND EDING, H. The Thermodynamic Functions above Room Temperature for Antimony and Bismuth Iodides and Their Absolute Entropies 3621
- CUBICCIOTTI, D., AND WITHERS, G. L. The Enthalpy of Formation and the Dissociation Energy of Thallium Monofluoride 4030
- CUBICCIOTTI, D. See Johnson, J. W., 1989, 3916; Keneshea, F. J., 3910; Rosztochy, F. E., 124, 1687
- CUKOR, P., AND LOTT, P. F. The Kinetics of the Reaction of Selenium(IV) with 2,3-Diaminonaphthalene 3232
- CULLINAN, H. T., JR., AND TOOR, H. L. Diffusion in the Three-Component Liquid System Acetone-Benzene-Carbon Tetrachloride 3941
- CUNDALL, R. B., AND GRIFFITHS, P. A. The Effect of Galvinoxyl on the Radiolysis of Benzene-Butene-2 Mixtures 1866
- CURRY, J., AND SHAW, R. W., JR. The Vapor Pressure of Copper Phthalocyanine 344
- CUSSLER, E. L., JR. Multicomponent Diffusion Involving High Polymers. II. Characterization of Polydispersity from Diffusion Data 1144
- CUSSLER, E. L., JR., AND LIGHTFOOT, E. N. Multicomponent Diffusion Involving High Polymers. I. Diffusion of Monodisperse Polystyrene in Mixed Solvents 1135
- CUSSLER, E. L., JR., AND LIGHTFOOT, E. N. Multicomponent Diffusion Involving High Polymers. III. Ternary Diffusion in the System Polystyrene 1-Polystyrene 2-Toluene 2875
- CYVIN, S. J. See Brooks, W. V. F., 1489
- CZANDERNA, A. W. The Reduction of $\text{CuO}_{0.67}$ in Hydrogen 3607
- DAASCH, L. A. High Resolution Mass Spectrum of Piperidine 3196
- DACEY, J. R. See Miller, G. H., 1434

- DAEN, J. See Jeffers, P. M., 2368; Miller, R. J., 3006
- DAHLGREN, G., AND SIMMERMAN, N. L. The Effect of Ethyl Substitution on the Kinetics of the Hydrolysis of Maleamic and Phthalamic Acid. 3626
- DAHLQVIST, K.-I., AND FORSÉN, S. Rotational Isomerism and Stereospecific Long-Range Spin Coupling in 2-Furaldehyde. 1760
- DAHLQVIST, K.-I., AND FORSÉN, S. The Barrier to Internal Rotation in 2-Furaldehyde. 4062
- DANIEL, J. L. See Williams, K. C., 250
- DANTI, A. See Koster, D. F., 486
- DANYLUK, S. S. See Gore, E., 89
- DAOUST, H. See Leonard, J., 1174
- DAUBERT, B. F. See Silbert, L. S., 2887
- DAURMAN, L., SALSER, G. E., AND TAJIMA, Y. A. Evidence for Nitrogen Trioxide in the Combustion of a Double-Base Propellant. 3668
- DAVIDSON, D. W. See Potts, A. D., 996
- DAVIES, R. H., AND TAYLOR, E. G. The Conductance of Some Alkali Metal Salts in Hydrogen Cyanide. 704
- DAVIS, D. F. See Fisher, F. H., 2595
- DAVIS, H. T., AND LUKE, K. D. Transport Properties of a Dense Fluid of Molecules Interacting with a Square-Well Potential. 869
- DAVIS, M. I., BOGGS, J. E., COFFEY, D., JR., AND HANSON, H. P. An Electron Diffraction Study of Trifluoronitrosomethane. 3727
- DAVIS, M. I., AND HANSON, H. P. A Gas Phase Electron Diffraction Investigation of Iron Pentacarbonyl. 3405
- DAVIS, M. I., AND HANSON, H. P. A Gas Phase Electron Diffraction Study of *cis*-Dichloroethylene. 4091
- DAVIS, W., JR., LAWSON, P. S., DEBRUIN, H. J., AND MROCHEK, J. Activities of the Three Components in the System Water-Nitric Acid-Uranyl Nitrate Hexahydrate at 25°. 1904
- DAWES, D. H., AND BACK, R. A. Isotopic Exchange in Nitrogen Gas Induced by γ -Radiation. 2385
- DAWSON, L. R., ZUBER, W. H., JR., AND ECKSTROM, H. C. Solvents Having High Dielectric Constants. XV. Thermodynamic Properties of Solutions of Hydrochloric Acid in *N*-Methylacetamide by Electromotive Force Measurements. 1335
- DEBRUIN, H. J. See Davis, W., Jr., 1904
- DE MAINE, P. A. D. See Thompson, C. C., Jr., 2766
- DEPHILLIPS, H. A., JR. See Klotz, I. M., 2801
- DERBYSHIRE, W. See Jonás, J., 1
- DESIENO, R. P. See Nash, C. P., 2139
- DETTE, R. H., AND JOHNSON, R. E., JR. Contact Angle Hysteresis. IV. Contact Angle Measurements on Heterogeneous Surfaces. 1507
- DIAMOND, R. M. See Bucher, J. J., 1565; Conocchioli, T. J., 1106; Jensen, C. H., 3440
- DIBBLE, E. See Whittaker, M. P., 2319
- DICKSON, D. S., MYERS, J. R., AND SAXER, R. K. The Vapor Pressure and Heat of Sublimation of Chromium. 4044
- DIJKGRAAF, C. Charge-Transfer Complexes of Titanium Tetrachloride, Titanium Tetrabromide, and Vanadium Oxytrichloride with Aromatic Hydrocarbons. 660
- DILLARD, J. G., AND KISER, R. W. Ionization and Dissociation of Ruthenium and Osmium Tetroxide. 3893
- DOBSON, G., AND HUGHES, G. The Radiation-Induced Oxidation of Organic Compounds. 1814
- DOBSON, G. R. The Mechanism of Photochromism in Metal Carbonyl Solutions. 677
- DOGLIOTTI, L. See Wettermark, G., 1584
- DOLE, M. See Abu-Isa, I., 2668
- DOLLISH, F. R., AND HALL, W. K. On the Interaction of Triphenylamine with Iodine and with Silica-Alumina Catalysts. 2127
- DOLLISH, F. R., AND HALL, W. K. Electron Spin Resonance of 1,1-Diphenylethylene Adsorbed on Silica-Alumina Catalysts. 4402
- D'ORAZIO, L. A., AND WOOD, R. H. Thermodynamics of the Higher Oxides. I. The Heats of Formation and Lattice Energies of the Superoxides of Potassium, Rubidium, and Cesium. 2550
- D'ORAZIO, L. A. See Wood, R. H., 2558, 2562
- DORER, F. H., AND RABINOVITCH, B. S. Unimolecular Decomposition of Product Olefins in Methylene Chemical Activation Systems. 1952
- DORER, F. H., AND RABINOVITCH, B. S. Unimolecular Reactions of Chemically Activated Species Produced in Systems of Methylene with Propene, Butene-1,3,3-Trifluoropropene, and 4,4,4-Trifluorobutene-1. 1964
- DORER, F. H., AND RABINOVITCH, B. S. An Experimental Generalization of Quantum Statistical Weight Effects in Nonequilibrium Unimolecular Reactions. 1973
- DORFMAN, L. M. See Arai, S., 2239
- DOUGLAS, E. Solubilities of Argon and Nitrogen in Sea Water. 2608
- DOUGLASS, D. C. See McCall, D. W., 2001
- DRESNER, L. The Exclusion of Ions from Charged Microporous Solids. 2230
- DUDA, J. L., AND VRENTAS, J. S. Mathematical Analysis of Multicomponent Free-Diffusion Experiments. 3305
- DULLIEN, F. A. L. See Robinson, R. L., Jr., 258
- DUNLOP, P. J. Relations between the Mutual and Tracer Diffusion Coefficients Associated with Isothermal Systems of Two Nonelectrolytes in an Un-ionized Solvent for the Limiting Case When the Physical and Chemical Properties of the Solutes Become Indistinguishable. 1693
- DUNLOP, P. J. Diffusion and Frictional Coefficients for Two Concentrated Compositions of the System Water-Mannitol-Sodium Chloride at 25°; Tests of the Onsager Reciprocal Relation. 4276
- DUNN, L. A., STOKES, R. H., AND HEPLER, L. G. The Volume Change on Neutralization of Strong Acids and Bases. 2808
- DUNN, R. L., AND HATFIELD, J. D. A Least-Squares Method for Calculating Diffusion Coefficients for Ternary Systems. 4361
- DUNN, R. L. See Elmore, K. L., 3520
- DURHAM, J. L. See Wade, W. H., 590
- DURIG, J. R., BONNER, O. D., AND BREAZEALE, W. H. Raman Studies of Iodic Acid and Sodium Iodate. 3886
- DURIGON, D. D. See Sandler, Y. L., 4201
- DWIGGINS, C. W., JR. A Small Angle X-Ray Scattering Study of the Colloidal Nature of Petroleum. 3500
- EARGLE, D. H., JR. See Kaiser, E. T., 2108
- EBERSOLE, S. See Castellano, S., 4166
- ECKSTROM, H. C. See Dawson, L. R., 1335
- EDING, H. See Cubicciotti, D., 2743, 3621
- EDMISTER, W. C. See Robinson, R. L., Jr., 258
- EDWARDS, R. K. See Martin, A. E., 1788; Yannopoulos, L. N., 2510
- EGEL-THAL, M. See Ben-Naim, A., 3250
- EICK, H. A. See Cater, E. D., 2684; Sturgeon, G. D., 3705
- ELIEZER, I. See Penciner, J., 2955
- ELLERSTEIN, S. M. On Obtaining the Kinetic Parameters of the Glass Transition. 2471
- ELLIOTT, G. R. B., AND LEMONS, J. F. Reply to Discussion of an Apparent Violation of the Gibbs-Duhem Equation. 2135
- ELLIOTT, G. R. B., LEMONS, J. F., AND SWOFFORD, H. S., JR. Solvent Vapor Pressures in Dilute Solutions of Gallium in Cadmium. 933
- ELLIS, R. B., AND FREEMAN, A. C. Surface Tension in the Reciprocal System K^+ , Cd^{+2} - Cl^- , Br^- 1443
- ELLISON, T. M. See Spencer, H. G., 2415
- ELMORE, K. L., HATFIELD, J. D., DUNN, R. L., AND JONES, A. D. Dissociation of Phosphoric Acid Solutions at 25°. 3520
- EL-SAYED, M. A. See Bhaumik, M. L., 275
- ELVING, P. J. See Turner, W. R., 1067
- EMERSON, M. F., AND HOLTZER, A. On the Ionic Strength Dependence of Micelle Number. 3718
- ENNS, T., SCHOLANDER, P. F., AND BRADSTREET, E. D. Effect of Hydrostatic Pressure on Gases Dissolved in Water. 389
- EPSTEIN, W. W. See Miles, M. H., 467
- ERB, R. A. Wettability of Metals under Continuous Condensing Conditions. 1306
- ERIKSON, T. A. The Surface Area of Liquids in Circular Tubes. 1809
- ESVAL, O. E., AND JOHNSON, J. S., JR. Equilibrium

- Ultracentrifugation of Hydrolyzed Lead(II) Perchlorate Solutions. 959
- EVANS, D. F., ZAWOYSKI, C., AND KAY, R. L. The Conductance of the Symmetrical Tetraalkylammonium Halides and Picrates in Acetonitrile at 25° 3878
- EVANS, D. F. See Kay, R. L., 4208, 4216
- EVANS, J. C., AND LO, G. Y.-S. Infrared Band Width of the Nitrate Ion ν_2 Mode. Ionic Lifetimes and a Solvent Isotope Effect. 3650
- EVANS, P. G., MILLER, G. R., AND KREEVOY, M. M. Comparison of Nuclear Magnetic Resonance, Thermal Maximum, and Scavenging Techniques for Rate Measurement. 4325
- EVANS, Y. C., AND LO, G. Y.-S. Interionic Vibrational Absorption Bands of Ion Aggregates in Benzene Solution. 3223
- EYRING, E. M. See Miles, M. H., 467; Whittaker, M. P., 2319
- EYRING, H. See James, M. R., 2351; Perkins, R. S., 3329; Ree, T. S., 3322; Urry, D. W., 1603
- EYRING, L. See Hyde, B. G., 1667
- FAHEY, R. C., AND GRAHAM, G. C. The Proton Magnetic Resonance Spectrum of Phenanthrene. 4417
- FAJER, J. Absorption Spectra of Piaselenol Radicals. . . . 1773
- FALCONER, W. E. See Salovey, R., 2345
- FALKENSTEIN, G. L. See Michaels, A. S., 1456
- FALLGATTER, M. B., AND HANRAHAN, R. J. Radiation Chemistry of Perfluorocyclohexane and Perfluorocyclobutane. Mass Spectroscopic Identification of Products. 2059
- FARBER, M. See Blauer, J. A., 1069; Frisch, M. A., 3001; Greenbaum, M. A., 4035; Ko, H. C., 2311; Singer, S., 799
- FARMER, J. B., GARDNER, C. L., AND McDOWELL, C. A. Electron Spin Resonance Line Shape of Triplet Triphenylene in Rigid Solution. 953
- FARMER, V. C., AND MORTLAND, M. M. An Infrared Study of Complexes of Ethylamine with Ethylammonium and Copper Ions in Montmorillonite. 683
- FARRELL, P. F., AND NEWTON, J. Ionization Potentials of Aromatic Amines. 3506
- FATOU, J. G., AND MANDELKERN, L. The Effect of Molecular Weight on the Melting Temperature and Fusion of Polyethylene. 417
- FATOU, J. G. See Mandelkern, L., 956
- FAUCHER, J. A. See Koleske, J. V., 4040
- FEDER, H. M. See Rudzitis, E., 2305
- FELD, M. See Jagur-Grodzinski, J., 628
- FENIMORE, C. P., AND JONES, G. W. Sulfur in the Burnt Gas of Hydrogen-Oxygen Flames. 3593
- FERNÁNDEZ-PRINI, R., AND PRUE, J. E. The Behavior of the Silver-Silver Iodide Electrode in the Presence of Tetraalkylammonium Ions. 2793
- FERRY, J. D. See Frederick, J. E., 346; Maekawa, E., 2811
- FILIPESCU, N. See Sager, W. F., 1092
- FINCH, A., AND GARDNER, P. J. Lattice Energies of Ionic Crystals. II. Some Group I-A and II-A Salts. 384
- FINKE, H. L., HOSSENLOPP, I. A., AND BERG, W. T. 1-Pentanethiol: Heat of Vaporization and Heat Capacity of the Vapor. 3030
- FINKE, H. L., MESSERLY, J. F., AND TODD, S. S. Thermodynamic Properties of *n*-Propyl-, *n*-Butyl-, and *n*-Decyl-Substituted Cyclohexane from 10 to 370°K. 2094
- FINKE, H. L. See Messerly, J. F., 353, 4304
- FIRESTONE, R. F. See Bone, L. I., 3652; Werner, H. R., 840
- FISCHER, E. See Greenspan, H., 2466
- FISHER, F. H. Multistate Dissociation and the Effect of Pressure on the Equilibrium on Magnesium Sulfate. . . 695
- FISHER, F. H., AND DAVIS, D. F. The Effect of Pressure on the Dissociation of Manganese Sulfate Ion Pairs in Water. 2595
- FISHMAN, E., AND SAUMAGNE, P. Near-Infrared Spectrum of Liquid Water from 30 to 374°. 3671
- FITZGIBBON, G. C., HOLLEY, C. E., JR., AND WADSÖ, I. The Heat of Formation of Lanthanum Oxide. 2464
- FLANAGAN, T. B. See Maeland, A., 3575; Simons, J. W., 3581, 3773
- FLAUTT, T. J. See Lawson, K. D., 3204, 4256
- FLEISCHER, P. C., JR. See Ryan, C. F., 3384
- FLEMING, D. M. See Wheelwright, E. J., 1220
- FLETCHER, A. N. See Heller, C. A., 3313
- FLURRY, R. L., JR. Molecular Orbital Theory of Electron Donor-Acceptor Complexes. I. A Simple Semi-empirical Treatment. 1927
- FOGEL, N. See Christian, S. D., 2135
- FORD, D. G. See Smith, W. R., 3587
- FORD, J. I. See Brummer, S. B., 1355, 3424
- FORDYCE, J. S., AND BAUM, R. L. Infrared Reflection Spectra of Molten Fluoride Solutions. Hydrolysis of Tantalum(V) in Potassium Fluoride-Lithium Fluoride. . 4335
- FOREST, E., AND SMYTH, C. P. Microwave Absorption and Molecular Structure in Liquids. LXIV. The Dielectric Behavior of Mixtures of Polar Nonassociative Liquids. 1302
- FORGACS, C., AND STEIN, G. Some Observations of Spectroscopic and Photoconductivity Effects in Permselective Membranes. 4221
- FORSÉN, S. See Dahlqvist, K.-I., 1760, 4062
- FOSTER, J. F. See Rao, V. S. R., 636, 656
- FOX, M. F. See Barrett, J., 2996
- FRAKER, A. C. Barium-Iron-Oxygen Compound with Varying Oxygen Content and Iron Valence. 4395
- FRANKLIN, J. L. See Natalis, P., 2935, 2943
- FRANKOSKY, M., AND ASTON, J. G. The Heat Capacity and Entropy of Hexamethylbenzene from 13 to 340°K. An Estimate of the Internal Rotation Barrier. 3126
- FREDERICK, J. E., AND FERRY, J. D. Dynamic Mechanical Properties of Dilute Solutions of Poly- α -methylstyrene. 346
- FREEMAN, A. C. See Ellis, R. B., 1443
- FREEMAN, D. H., PATEL, V. C., AND BUCHANAN, T. M. Electrolyte Uptake Equilibria with Low Cross-Linked Ion-Exchange Resins. 1477
- FREEMAN, D. H., AND SCATCHARD, G. Volumetric Studies of Ion-Exchange Resin Particles Using Microscopy. . . . 70
- FREEMAN, G. R. See Singh, A., 666
- FREI, Y. F., AND MILLER, I. R. Influence of Adsorbed Positively Charged Polyelectrolytes on Polarographic Currents of Cationic Depolarizers. II. 3018
- FREIFELDER, M., MATTOON, R. W., AND KRIESE, R. The Nuclear Magnetic Resonance Spectra of Some *N*-Monosubstituted Methylamines. 3645
- FREILING, E. C. See Scheidt, R. C., 1784
- FRIEDMAN, H. L. Calculation of the Hall Effect in Ionic Solutions. 2617
- FRIEDMAN, M. E., AND SCHERAGA, H. A. Volume Changes in Hydrocarbon-Water Systems. Partial Molal Volumes of Alcohol-Water Solutions. 3795
- FRIPIAT, J. J., JELLI, A., PONCELET, G., AND ANDRÉ, J. Thermodynamic Properties of Adsorbed Water Molecules and Electrical Conduction in Montmorillonites and Silicas. 2185
- FRIPIAT, J. J., LÉONARD, A., AND UYTTERHOEVEN, J. B. Structure and Properties of Amorphous Silicoaluminas. II. Lewis and Brønsted Acid Sites. 3274
- FRIPIAT, J. J., VAN CAUWELAERT, F., AND BOSMANS, H. Structure of Aluminum Cations in Aqueous Solutions. . 2458
- FRISCH, M. A., GREENBAUM, M. A., AND FARBER, M. The Heat of Formation of Aluminum(I) Chloride(g) and the Entropy of Aluminum(III) Chloride(g). 3001
- FRISCH, M. A., AND MARGRAVE, J. L. The Heat of Formation of Nitric Oxide(g). 3863
- FRIITZ, J. J. See Kikuchi, K., 3654
- FRYBURG, G. C. Enhanced Oxidation of Platinum in Activated Oxygen. III. Kinetics and Mechanism. . . 3660
- FUJIMORI, E. Two Phosphorescences and Electron Transfer in Dye-Disulphydryl Compound Complex. . . 940
- FUJITA, H. See Abe, M., 3263; Kobatake, Y., 3981
- FUNG, B.-M. The Electronegativity of Noble Gases. . . . 596
- FUOSS, R. M., ONSAGER, L., AND SKINNER, J. F. The Conductance of Symmetrical Electrolytes. V. The Conductance Equation. 2581
- FUOSS, R. M. See Skinner, J. F., 1437; Treiner, C., 2576

- FUTRELL, J. H., AND SIECK, L. W. Rare Gas Sensitized Radiolysis of Acetylene 892
 FUTRELL, J. H. See Sieck, L. W., 888
- GAGER, W. B. See Kircher, J. F., 189
 GANT, P. L. See Yang, K., 1768
 GARDNER, C. L. See Farmer, J. B., 953
 GARDNER, P. J. See Finch, A., 384
 GARG, S. K., AND KADABA, P. K. Dielectric Relaxation of Mixtures of D-polar Liquids 674
 GARG, S. K., AND SMYTH, C. P. Microwave Absorption and Molecular Structure in Liquids. LXII. The Three Dielectric Dispersion Regions of the Normal Primary Alcohols 1294
 GARLAND, C. W., LORD, R. C., AND TROIANO, P. F. An Infrared Study of High-Area Metal Films Evaporated in Carbon Monoxide 1188
 GARLAND, C. W., LORD, R. C., AND TROIANO, P. F. Infrared Spectrum of Carbon Monoxide Chemisorbed on Evaporated Nickel Films 1195
 GARLAND, C. W., TONG, S., AND STOCKMAYER, W. H. Diffusion in the System Cadmium Iodide-Water 1718
 GARLAND, C. W., TONG, S., AND STOCKMAYER, W. H. Diffusion of Chloroacetic Acid in Water 2469
 GARNETT, J. L., AND SOLLICH-BAUMGARTNER, W. A. Catalytic Deuterium-Exchange Reactions with Organics. XIX. π -Complex Adsorption in the Exchange of the Alkylbenzenes 1850
 GARNETT, J. L., AND SOLLICH-BAUMGARTNER, W. A. Catalytic Deuterium-Exchange Reactions with Organics. XX. A π -Complex Mechanism for the Isomerization and Isotope Exchange of *cis*- and *trans*-Stilbenes on Platinum Catalysts 3526
 GARRISON, W. M. See Weeks, B. M., 4131; Willix, R. L. S., 1579
 GARVER, E. E. See Hyde, B. G., 1667
 GARVIE, R. C. The Occurrence of Metastable Tetragonal Zirconia as a Crystallite Size Effect 1238
 GARY, R., BATES, R. G., AND ROBINSON, R. A. Dissociation Constant of Acetic Acid in Deuterium Oxide from 5 to 50°. Reference Points for a pD Scale 2750
 GATZ, C. R. See Young, R. A., 1763
 GAYNOR, A. J. See Macur, G., 3782
 GIAUQUE, W. F. See Brodale, G. E., 1268; Calder, G. V., 2443; Rao, R. V. G., 1272
 GIBSON, K. D. Moving Boundary Sedimentation in the Preparative Ultracentrifuge in the Absence of a Plateau Region 1820
 GIDDINGS, J. C. See James, M. R., 2351
 GILBERT, R. A. See Busey, R. H., 3471
 GILEADI, E., RUBIN, B. T., AND BOCKRIS, J. O'M. Electrodeposition of Ethylene on Platinum as a Function of Potential, Concentration, and Temperature 3335
 GILKERSON, W. R. See Nanney, T. R., 1338
 GILL, S. J., AND GLOGOVSKY, R. L. Influence of Pressure on the Reversible Unfolding of Ribonuclease and Poly- γ -benzyl-L-glutamate 1515
 GILROY, D., AND CONWAY, B. E. Kinetic Theory of Inhibition and Passivation in Electrochemical Reactions 1259
 GINTER, D. S., GINTER, M. L., AND INNES, K. K. Electronic Spectra of the Ga₂, In₂, and Tl₂ Molecules 2480
 GINTER, M. L. See Ginter, D. S., 2480; Kroll, M., 3671
 GLASOE, P. K. Dissociation Constants for Some Nitrophenols and Salicylic Acid in Deuterium Oxide 4416
 GLEISER, M. Free Energy of Formation of Chromium Carbide, Cr₃C₂ 1771
 GLEMZA, R., AND KOKES, R. J. Chemisorption of Oxygen on Zinc Oxide 3254
 GLEMZA, R. See Kokes, R. J., 17
 GLOGOVSKY, R. L. See Gill, S. J., 1515
 GOKCEN, N. A. Apparent Violations of Gibbs-Duhem Relations and the Limiting Laws of Dilute Solutions 3222
 GOKCEN, N. A. Diffusional Processes in Knudsen Cells 3538
 GOLAY, M. J. E. Note on Molecular Diffusion and Heat Conductivity in Liquids 1086
 GOLDBERG, G. See Chaberek, S., 2834
 GOLDBERG, P. See Guilbault, G. G., 3696
 GOLDSTEIN, H. W. See Trulson, O. C., 2531
 GOLL, R. J. See McDonald, C. C., 293
 GOLUB, M. A. The Radiation-Induced *cis-trans* Isomerization of Polybutadiene. IV 2639
 GÓMEZ-IBÁÑEZ, J. D., AND SHIEH, J. J. C. The Excess Free Energy of Mixtures of Cyclohexane and *n*-Hexadecane 1660
 GOODISMAN, J. Scaling in Isoelectronic Molecules 2520
 GOODSPEED, F. C., SCOTT, B. L., AND BURR, J. G. Photooxidation of Tertiary Nitrogen Compounds by Methylene Blue 1149
 GOPAL, R., AND BHATNAGAR, O. N. Studies on Solutions of High Dielectric Constant. VII. Cationic Transport Numbers of Potassium Bromide in *N*-Methylacetamide at Different Temperatures 2382
 GORDON, A. S., AND NORRIS, W. P. A Study of the Pyrolysis of Methyl Ethyl and Diethyl Carbonates in the Gas Phase 3013
 GORDON, B. E. See Smith, M. L., 3833
 GORDON, S. See Szutka, A., 289
 GORE, E., AND DANYLUK, S. S. A Nuclear Magnetic Resonance Investigation of Ether-Boron Halide Molecular Addition Compounds in Dichloromethane 89
 GOY, C. A., AND PRITCHARD, H. O. Kinetics and Thermodynamics of the Reaction between Iodine and Methane and the Heat of Formation of Methyl Iodide 3040
 GOY, C. A., SHAW, D. H., AND PRITCHARD, H. O. The Reactions of CN Radicals in the Gas Phase 1504
 GRAHAM, D. P. Physical Adsorption on Low-Energy Solids. III. Adsorption of Ethane, *n*-Butane, and *n*-Octane on Poly(tetrafluoroethylene) 4387
 GRAHAM, G. C. See Fahey, R. C., 4417
 GRAY, B. F., AND YANG, C. H. On the Unification of the Thermal and Chain Theories of Explosion Limits 2747
 GRAYBEAL, J. D. See Swiger, E. D., 949
 GRAYDON, W. F. See Worsely, M., 883
 GREEN, M. E. A Proposed Model for Electron Injection into Some Organic Semiconductors in the Dark 3510
 GREEN, P. J. See Swiger, E. D., 949
 GREENBAUM, M. A., WEIHER, J., AND FARBER, M. The Thermodynamic and Physical Properties of Beryllium Compounds. VIII. Heat of Fusion and High-Temperature Heat Capacity of Beryllium Oxide 4035
 GREENBAUM, M. A. See Blauer, J. A., 1069; Frisch, M. A., 3001; Ko, H. C., 2311
 GREENBERG, E., NATKE, C. A., AND HUBBARD, W. N. Fluorine Bomb Calorimetry. X. The Enthalpies of Formation of Niobium and Tantalum Pentafluorides 2089
 GREENBERG, E. See Porte, H. A., 2308
 GREENBERG, S. A., AND CHANG, T. N. Investigation of the Colloidal Hydrated Calcium Silicates. II. Solubility Relationships in the Calcium Oxide-Silica-Water System at 25° 182
 GREENBERG, S. A., AND CHANG, T. N. The Hydration of Tricalcium Silicate 553
 GREENSPAN, H., AND FISCHER, E. Viscosity of Glass-Forming Solvent Mixtures at Low Temperatures 2466
 GREGOR, H. P. See Liu, K.-J., 1248, 1252
 GREGORY, N. W. See Richards, R. R., 239
 GRIFFITH, O. H. Magnetic Resonance of the Triplet State of Oriented Pyrene Molecules 1429
 GRIFFITHS, P. A. See Cundall, R. B., 1866
 GRØNVOLD, F. See Westrum, E. F., Jr., 3192
 GROSSE, A. V. See Cahill, J. A., 518
 GROVE, E. L. See Macur, G., 3782
 GUILBAULT, G. G., KRAMER, D. N., AND GOLDBERG, P. A Kinetic Study of the Lipoamide Dehydrogenase-NADH-Dye Reaction 3696
 GUILLORY, J. P. See Bartell, L. S., 3043
 GUNN, S. R. Heats of Reaction of Boron Trifluoride with HF·3.75H₂O and of Diborane with Trimethylamine. Correlation of Thermochemical Data for Some Boron Compounds 1010
 GUNN, S. R. Comparison Standards for Solution Calorimetry 2902
 GUNNING, H. E. See Sherwood, A. G., 1732, 2323
 GÜNTHER, H. See Castellano, S., 4166
 GUPTA, A. R. Some Thermodynamic Aspects of Ion-Exchange Equilibria in Mixed Solvents 341
 GUSARSKY, E., AND TREININ, A. The Relation between

- Electrochemical and Spectroscopic Properties of the Halide and Pseudohalide Ions in Solution..... 3176
- GUSTAFSON, R. L., AND LIRIO, J. A. Interaction of Cross-Linked Polymethacrylic Acid with Polyvalent Metal Ions..... 2849
- GUSTAFSSON, S. E., BECSEY, J. G., AND BIERLEIN, J. A. Thermal Diffusion Measurements by Wave-Front-Shearing Interferometry..... 1016
- GUTOWSKY, H. S., AND CHEN, F.-M. Spin-Echo Nuclear Magnetic Resonance Studies of Chemical Exchange. V. Perfluorocyclohexane..... 3216
- GUTOWSKY, H. S. See Jonás, J., 1
- HABGOOD, H. W. Surface OH Groups on Zeolite X..... 1764
- HACKERMAN, N., AND WADE, W. H. A Microcalorimetric Study of Liquid-Liquid Displacement Phenomena..... 314
- HACKERMAN, N. See Venable, R. L., 317
- HAFEMANN, D. R. Charge Separation in Liquid Junctions..... 4226
- HAIR, M. L., AND CHAPMAN, I. D. The Adsorption of Hexachloroacetone on Alumina-Containing Surfaces... 3949
- HALBERSTADT, M. L., AND CHESICK, J. P. The Kinetics of the Thermal Isomerization of Ethylcyclopropane... 429
- HALE, D. See Rosenberg, H. M., 2490
- HALEEM, M. A., AND YANKWICH, P. E. Kinetics of the Decomposition of Oxalic Acid in Glycerine..... 1729
- HALEEM, M. A., AND YANKWICH, P. E. Kinetics of the Decomposition of Hydrogen Oxalate Ion in Glycerine Solution..... 2392
- HALL, A. C. A Study of Langmuir-Blodgett Layers on Metal Surfaces by the Method of Reflected Polarized Light..... 1654
- HALL, G. A., JR., AND HANRAHAN, E. S. Kinetics of the Decarboxylation of Phenylmalonic Acid..... 2402
- HALL, W. K. See Dollish, F. R., 2127, 4402; Larson, J. G., 3080; Uytterhoeven, J. B., 2117
- HALLA, F. Note on the Thermodynamics of the Formation of Dolomite..... 1065
- HALLER, I. See Srinivasan, R., 1775
- HALSEY, G. D., JR. See McClure, D. W., 3542
- HAMILTON, P. G. See Barradas, R. G., 3411
- HAMMAKER, R. M. See Chiang, T. C., 2715
- HAMORI, E., PRUSINOWSKI, L. R., SPARKS, P. G., AND HUGHES, R. E. Intrinsic Viscosity Studies of Stereoregular Poly(methyl methacrylate) in 2,2,3,3-Tetrafluoropropanol..... 1101
- HANNA, R. Lattice Energy of Some Cubic Oxides..... 2971
- HANNA, R. The Structure of Sodium Silicate Glasses and Their Far-Infrared Absorption Spectra..... 3846
- HANRAHAN, E. S. See Hall, G. A., Jr., 2402
- HANRAHAN, R. J. See Fallgatter, M. B., 2059; Hughes, B. M., 2707
- HANSON, H. P. See Davis, M. I., 3405, 3727, 4091
- HARDING, J. W. See Matsen, J. M., 522
- HARDWICK, R. See Haugen, G., 2988
- HARPST, J. A., HOLT, E., AND LYONS, P. A. Diffusion in Dilute Hydrochloric Acid-Water Solutions..... 2333
- HARPST, J. A. See Rodwin, L., 2783
- HARRAH, L. A., AND BECKER, R. The Electron Spin Resonance Associated with Photochromism in 2,2'-Dimethylbithrone..... 2487
- HARRINGTON, R. E., AND ZIMM, B. H. Degradation of Polymers by Controlled Hydrodynamic Shear..... 161
- HARRIS, E. L. Activity Coefficients of Cadmium Chloride in Mixed Aqueous Solution with Benzyltrimethylammonium Chloride..... 681
- HARRIS, G. M. See Wing, R. M., 4328
- HART, E. J. See Anbar, M., 271, 973, 1244; Szutka, A., 289
- HARTECK, P. See Rolfe, T. R., 849; Thompson, B. A., 3964
- HARTIG, H., AND BRANDT, W. W. Association of Secondary Amines with Tetrahydrofuran..... 335
- HARTMAN, K. O., AND HISATSUNE, I. C. The Kinetics of Calcium Formate Pyrolysis in Potassium Bromide Matrix..... 583
- HASEGAWA, I. See Ramey, K. C., 3418
- HASEGAWA, J. See Higuchi, T., 796
- HATFIELD, J. D. See Dunn, R. L., 4361; Elmore, K. L., 3520
- HAUGEN, G., AND HARDWICK, R. Ionic Association in Solutions of Thionine. II. Fluorescence and Solvent Effects..... 2988
- HAUGEN, G. See Benson, S. W., 3898
- HAWES, J. L., AND KAY, R. L. Ionic Association of Potassium and Cesium Chlorides in Ethanol-Water Mixtures from Conductance Measurements at 25°..... 2420
- HAWES, J. L. See Kay, R. L., 2787
- HAYON, E. Radiolysis of Heavy Water in the pD Range 0-14..... 2628
- HAYON, E., AND MOREAU, M. Electron Capture by Solutes in the Radiolysis of Methanol and Ethanol..... 4053
- HAYON, E., AND MOREAU, M. Reaction Mechanism Leading to the Formation of Molecular Hydrogen in the Radiation Chemistry of Water..... 4058
- HEDGES, R. M. See Carper, W. R., 1707
- HEFFEL, J. See Carmichael, J. B., 2213, 2218
- HEFLEY, J. D., AND AMIS, E. S. Electromotive Force Studies of Cadmium Chloride in Water, Water-Ethanol, and Ethanol Solutions..... 2082
- HEICKLEN, J., COHEN, N., AND SAUNDERS, D. The Multiplicity of CF₂..... 1774
- HEICKLEN, J., AND KNIGHT, V. Difluoroacetylene..... 2484
- HEICKLEN, J., AND KNIGHT, V. The Mercury-Photosensitized Decomposition of Perfluoropropene..... 3600
- HEICKLEN, J., AND KNIGHT, V. The Mercury-Photosensitized Oxidation of Perfluoropropene..... 3641
- HEICKLEN, J., WACHI, F., AND KNIGHT, V. The Infrared Spectra of Perfluorocyclopropane and *cis*- and *trans*-Perfluorobutene-2..... 693
- HEICKLEN, J. See Saunders, D., 3205; Marsh, D., 4410
- HEISKALA, V. H. Kinetics of Hydrogen Reduction of Uranium Trioxide..... 2012
- HEITNER-WIRGUIN, C., AND URBACH, V. Kinetics of Ion Exchange in the Phosphonic Resin Bio-Rex 63..... 3400
- HELD, R. P., AND CRISS, C. M. Thermodynamic Properties of Nonaqueous Solutions. I. Heats of Solution of Selected Alkali Metal Halides in Anhydrous N-Methylformamide..... 2611
- HELFFERICH, F. Ion-Exchange Kinetics. V. Ion Exchange Accompanied by Reactions..... 1178
- HELFFERICH, F. See Peterson, D. L., 1283
- HELLER, C. A., AND FLETCHER, A. N. Oxidation and Chemiluminescence of Tetrakis(dimethylamino)ethylene. I. Reversible Reactions of Oxygen with Tetrakis(dimethylamino)ethylene and *n*-Decane..... 3313
- HELLER, W. Remarks on Refractive Index Mixture Rules..... 1123
- HENTZ, R. R., CHANG, J. Y., AND BURTON, M. Abstraction Reactions of Hydrogen and Deuterium Atoms: Mercury-Photosensitized Decomposition of Mixtures of Cyclohexane and Cyclohexane-*d*₁₂..... 2027
- HENTZ, R. R. See Barzynski, H. F., 2034; Rojo, E. A., 3024
- HEPLER, L. G. Entropy and Volume Changes on Ionization of Aqueous Acids..... 965
- HEPLER, L. G. See Dunn, L. A., 2808; Hopkins, H. P., Jr., 2244
- HERBSTSTEIN, F. H. See Boeyens, J. C. A., 2153, 2160
- HERIC, E. L. On the Compressibility of Molten Alkali Halides..... 2785
- HERRON, J. T. Mass Spectrometric Study of the Reaction of Nitrogen Atoms with Ethylene..... 2736
- HERSH, C. K. See Macur, G., 3782
- HIGUCHI, T., AND HASEGAWA, J. Rate of Exchange of Chlorine between Dimethylchloramine and Succinimide..... 796
- HIKINO, T. See Uhara, I., 880
- HILDE, R. D. See Salmon, O. N., 804
- HILDEBRAND, J. H. See Shinoda, K., 605
- HILL, J., AND COX, D. J. Studies of the Sedimentation Velocity of Ovalbumin in Concentrated Salt Solutions. 3032
- HINTON, J. F., AND JOHNSTON, F. J. Halogen Displacement Reactions of Chloro- and Bromoacetic Acids in Water and Dioxane-Water Solutions..... 854
- HIRSHFELD, A. See Radell, J., 928
- HIRT, R. C. See Brinen, J. S., 3791

- HISATSUNE, I. C. See Hartman, K. O., 583
- HISHIKI, Y. See Namba, S., 774
- HOCH, M. See Narasimhamurty, H. V. L., 1420
- HOEGL, H. On Photoelectric Effects in Polymers and Their Sensitization by Dopants. 755
- HOFMEISTER, H. K., AND VAN WAZER, J. R. Exchange of Substituents on Nitrogen in Molten Ammonium Salts and Amines. 791
- HOLLEY, C. E., JR. See Fitzgibbon, G. C., 2464
- HOLMES, H. F., AND SECOY, C. H. Heats of Immersion in the Thorium Oxide-Water System. 151
- HOLMES, H. F., SHOUP, C. S., JR., AND SECOY, C. H. Electrokinetic Phenomena at the Thorium Oxide-Aqueous Solution Interface. 3148
- HOLROYD, R. A., AND KLEIN, G. W. Radical Yields in the Radiolysis of Unsaturated Hydrocarbons. 194
- HOLROYD, R. A., AND KLEIN, G. W. Radical Intermediates in the Mercury (³P) Photosensitized Decomposition of Cyclopropane. 2129
- HOLT, E. L., AND LYONS, P. A. Diffusion in Dilute Aqueous Acetic Acid Solutions. 2341
- HOLT, E. See Harpst, J. A., 2333
- HOLTZER, A. See Emerson, M. F., 3718
- HONIG, E. P. Logarithmic Distribution Functions for Colloidal Particles. 4418
- HONIG, J. M. See Chapin, D. S., 1402
- HOPKINS, H. P., JR., WU, C.-H., AND HEPLER, L. G. Thermochemistry of Aqueous Aminosulfonic Acids. Sulfamic and Sulfanilic Acids and Taurine. 2244
- HOPKINS, H. P., JR., AND WULFF, C. A. The Solution Thermochemistry of Polyvalent Electrolytes. I. Calcium Hydroxide. 6
- HOPKINS, H. P., JR., AND WULFF, C. A. The Solution Thermochemistry of Polyvalent Electrolytes. II. Silver Sulfate. 9
- HOPKINS, H. P., JR., AND WULFF, C. A. The Solution Thermochemistry of Polyvalent Electrolytes. III. Barium Hydroxide Octahydrate. 1980
- HOPKINS, H. P., JR. See Rupert, J. P., 3059
- HORMATS, E. I., AND UNTERLEITNER, F. C. Measurement of the Diffusion of Oxygen in Polymers by Phosphorescent Quenching. 3677
- HORMATS, E. I. See Unterleitner, F. C., 2516
- HORNE, R. A., AND COURANT, R. A. Protonic Conduction in the Water I Region. 2224
- HORNE, R. A., COURANT, R. A., JOHNSON, D. S., AND MARGOSIAN, F. F. The Activation Energy of Viscous Flow of Pure Water and Sea Water in the Temperature Region of Maximum Density. 3988
- HOSSENLOPP, I. A. See Finke, H. L., 3030
- HOU, K. C., AND PALMER, H. B. The Kinetics of Thermal Decomposition of Diacetylene in a Flow System. 858
- HOU, K. C., AND PALMER, H. B. The Kinetics of Thermal Decomposition of Benzene in a Flow System. 863
- HOUSEMAN, B. L. See Jasper, J. J., 310
- HOWARD, C. See Mandelkern, L., 956
- HOWERY, D. G., AND THOMAS, H. C. Ion Exchange on the Mineral Clinoptilolite. 531
- HUBBARD, W. N. See Greenberg, E., 2089; O'Hare, P. A. G., 4358; Porte, H. A., 2308; Rudzitis, E., 2305
- HUGHES, B. M., AND HANRAHAN, R. J. The Radiation Chemistry of Cyclopentane. 2707
- HUGHES, G. See Dobson, G., 1814
- HUGHES, R. E. See Hamori, E., 1101
- HUHEEY, J. E. The Electronegativity of Groups. 3284
- HULTGREN, R. See Chang, Y. A., 4162
- HUPF, H. B. See Lietzke, M. H., 2395
- HYDE, B. G., GARVER, E. E., KUNTZ, U. E., AND EYRING, L. Kinetic Studies on Reactions of Praseodymium Oxides in an Oxygen Atmosphere: $\text{PrO}_{1.33} + \text{O}_2 \rightarrow \text{PrO}_2$ 1667
- HYDE, S. M. See Verdin, D., 1992
- HYDER, M. L. The Radiolysis of Aqueous Nitrate Solutions. 1858
- IKEDA, T., AND KIMURA, H. Relative Determination of Soret Coefficients of Electrolytes. 41
- IKEDA, T., AND MATSUMOTO, M. Relative Determination of Soret Coefficients of Electrolytes. I. 3755
- IKEDA, R., NAKAMURA, D., AND KUBO, M. Pure Quadrupole Resonance of Halogens in Potassium Hexahalorhenates(IV) and Hexachlorotungstate(IV). 2101
- IMAI, H., ONO, Y., AND KEII, T. The Effect of Oxygen on the Electron Spin Resonance Spectra of Anthracene and Perylene Adsorbed on Silica-Alumina. 1082
- INGWALL, R. T. See Schrier, E. E., 298
- INNES, K. K. See Ginter, D. S., 2480
- INOUE, E., KOKADO, H., AND YAMAGUCHI, T. Hyper-sensitization of Photoconduction in Microcrystalline Zinc Oxide. 767
- ISE, N., AND OKUBO, T. Mean Activity Coefficient of Polyelectrolytes. I. Measurements of Sodium Polyacrylates. 4102
- ISE, N. See Okubo, T., 3690
- ISKANDER, G. R., See Razouk, R. I., 1805
- ITZEL, J. F., JR. See Poole, C. P., Jr., 3663
- IYER, A. S. See Narasimhamurty, H. V. L., 1420
- JACKSON, J. A., AND TAUBE, H. Chemical Shifts in the Nuclear Magnetic Resonance Absorption for Oxygen-17 in Oxy Ions. 1844
- JAGUR-GRODZINSKI, J., FELD, M., YANG, S. L., AND SZWARC, M. Electron Affinities of Aromatic Hydrocarbons in Tetrahydrofuran Solution. 628
- JAMES, D. G. L., AND SUART, R. D. The Reactivity of the Cyclic Polyenes toward Free Radicals. V. Cyclohexadiene-1,3 and the Isopropyl Radical. 2362
- JAMES, M. R., GIDDINGS, J. C., AND EYRING, H. Surface-Active and Interfacial Transfer in Gas-Liquid Chromatography. A New Tool for Measuring Interfacial Resistance. 2351
- JANZ, G. J. See Baddiel, C. B., 3634; Monahan, A. R., 1070
- JARVIS, N. L. Surface Viscosity of Monomolecular Films of Long-Chain Aliphatic Amides, Amines, Alcohols, and Carboxylic Acids. 1789
- JASPER, J. J., AND HOUSEMAN, B. L. The Thermodynamic Properties of Soluble Monolayers Produced by the Normal Alcohols (C₈ to C₁₂) at the Water-Octane Interface. 310
- JASPER, J. J., AND VAN DELL, R. D. The Shapes and Close-Pack Areas of Oriented Long-Chain Dipoles at the Water-Octane Interface. 481
- JAYNE, J. P. See Lunsford, J. H., 2182
- JEANCLAUDE, C. See Nikitine, S., 745
- JEFFERS, P. M., AND DEAN, J. Studies on Spreading, Collapse, and Temperature and Compression Rate Effects on Monolayers of α,ω -Dicarboxylic Acids. 2368
- JEFFERS, P. M. See Bauer, S. H., 3317
- JELLI, A. See Fripiat, J. J., 2185
- JENKINS, R. C. L. Sedimentation and Electrophoresis of Interacting Substances. IV. Theory of the Analysis of Interacting Systems by Differential Boundary Experiments. 3785
- JENNINGS, B. R., AND JERRARD, H. G. Light Scattering by Poly- γ -benzyl-L-glutamate Solutions Subjected to Electric Fields. 2817
- JENSEN, C. H., AND DIAMOND, R. M. Anion Exchange in Concentrated Solutions. 3440
- JERRARD, H. G. See Cavell, E. A. S., 3657; Jennings, B. R., 2817
- JOHANNES, W., AND WHITAKER, S. Thinning of Soap Films—The Effect of Surface Viscosity. 1471
- JOHARI, G. P., AND TEWARI, P. H. Dissociation Studies in High Dielectric Solvents. I. Conductance of Some 2-2 Salts in Formamide at 25°. 696
- JOHARI, G. P., AND TEWARI, P. H. Dissociation Studies in High Dielectric Solvents. IV. Conductance of Some 3-3 Complex Salts in Formamide at 25°. 2862
- JOHARI, G. P., AND TEWARI, P. H. Dissociation Studies in High Dielectric Solvents. V. Magnesium Sulfate as an Unassociated Salt in N-Methylformamide. 3167
- JOHARI, G. P. See Tewari, P. H., 2857
- JOHNSEN, R. H. Acetylene Production in the Radiolysis of Methane. 3218
- JOHNSEN, R. H. See Sieck, L. W., 1699
- JOHNSON, D. S. See Horne, R. A., 3988
- JOHNSON, E. R. See Prince, L. A., 359, 377

- JOHNSON, E. W. See Cater, E. D., 2684
 JOHNSON, G. K. See Kybett, B. D., 3603
 JOHNSON, J. S., JR. See Esvai, O. E., 959
 JOHNSON, J. W., CUBICCIOTTI, D., AND SILVA, W. F. The Critical Temperature and Coexistence Curve for Bismuth Bromide. 1989
 JOHNSON, J. W., SILVA, W. J., AND CUBICCIOTTI, D. The Vapor Pressure and Enthalpy of Vaporization of Molten Bismuth Chloride to the Critical Point. 3916
 JOHNSON, R. E., JR. See Dettre, R. H., 1507
 JOHNSON, S. L., AND RUMON, K. A. Infrared Spectra of Solid 1:1 Pyridine-Benzoic Acid Complexes; the Nature of the Hydrogen Bond as a Function of the Acid-Base Levels in the Complex. 74
 JOHNSON, V. See Tobolsky, A. V., 476
 JOHNSTON, F. J. The Radiolysis of Monodisperse Colloidal Sulfur. 2805
 JOHNSTON, F. J. See Hinton, J. F., 854
 JOLLEY, H. R. See Quist, A. S., 2726
 JONÁS, J., DERBYSHIRE, W., AND GUTOWSKY, H. S. Proton Resonance Spectra of Thiopyrones. 1
 JONES, A. D. See Elmore, K. L., 3520
 JONES, G. W. See Fenimore, C. P., 3593
 JONES, J. G. See Kilpatrick, M. L., 2248
 JONGENBURGER, H. S., AND WOOD, R. H. The Heats and Entropies of Dilution of the Perchlorates of Magnesium and Strontium. 4231
 JORDAN, A. S. See Belton, G. R., 2065
 JOYNER, T. B. The Thermal Decomposition of Solid Azidopentaamminecobalt(III) Azide. 1723
 KADABA, P. K. See Garg, S. K., 674
 KAFALAS, J. A. See Chapin, D. S., 1402
 KAISER, E. T., AND EARGLE, D. H., JR. Studies on the Anion Radicals of the Thianthrene Oxides. 2108
 KAISER, E. T. See Britt, A. D., 2775
 KAKIUCHI, K. Determination of an Equilibrium Constant for the Dimerization of the *Bacillus subtilis* α -Amylase Molecule. 1829
 KAMEI, H. The Proton Magnetic Resonance Study of the Protonation of Pyrazine. 2791
 KAMEI, A. M. See Low, M. J. D., 450
 KANA'AN, A. S. See Besenbruch, G., 3174
 KANDA, F. A., STEVENS, R. M., AND KELLER, D. V. The Barium-Sodium Equilibrium System. 3867
 KAPLAN, R. I. See Williams, K. C., 250
 KARABATSOS, G. J. See McFadden, W. H., 1742
 KARASZ, F. E., BAIR, H. E., AND O'REILLY, J. M. Thermal Properties of Atactic and Isotactic Polystyrene. 2657
 KATAYAMA, M. See Bristowe, W. W., 807
 KATZIN, L. I. See Singh, A., 3708
 KAY, J. G. See Lydy, D. L., 87
 KAY, R. E. See Bean, R. C., 4368
 KAY, R. L., AND EVANS, D. F. The Conductance of the Tetraalkylammonium Halides in Deuterium Oxide Solutions at 25°. 4216
 KAY, R. L., AND HAWES, J. L. The Association of Cesium Chloride in Anhydrous Methanol at 25°. 2787
 KAY, R. L., VIDULICH, G. A., AND VITUCCIO, T. The Temperature Coefficient of Conductance of Aqueous Sodium Sulfate around 32.4°. 4033
 KAY, R. L., ZAWOYSKI, C., AND EVANS, D. F. The Conductance of the Symmetrical Tetraalkylammonium Halides and Picrates in Methanol at 25 and 10°. 4208
 KAY, R. L. See Evans, D. F., 3878; Hawes, J. L., 2420
 KEARNS, D. R. The Temperature Dependence of the *cis-trans* Photoisomerization of Azo Compounds: Theoretical Considerations. 1062
 KEATING, K. B., AND ROZNER, A. G. Decomposition of Hydrogen Peroxide on Glass. 3658
 KEDER, W. E., AND BURGER, L. L. Proton Magnetic Resonance and Infrared Studies of Hydrogen Bonding in Tri-*n*-octylammonium Salt Solutions. 3075
 KEHL, W. L. See Swift, H. E., 3268
 KEII, T. See Imai, H., 1082
 KELLER, D. V. See Kanda, F. A., 3867
 KELLEY, R. D., KLEIN, R., AND SCHEER, M. D. Hydrogen Atom Addition of Olefins: Relative Rates at the Two Carbon Positions and Derived Heats of Formation of Several Alkyl Radicals. 905
 KELLNER, J. D. See Sundheim, B. R., 1204
 KENESHEA, F. J., AND CUBICCIOTTI, D. The Thermodynamics of Vaporization of Thallous Fluoride and Its Gaseous Dimerization. 3910
 KERR, J. A., AND CALVERT, J. G. The Formation and Decomposition Reactions of the Acetyl Radical and the Heat of Formation of the Acetyl Radical. 1022
 KEVAN, L. Radiolysis of Frozen Solutions. II. Sodium Nitrite Ices. 1080
 KEVAN, L. On Electron Trapping in Polycrystalline and in Glassy Alkaline Ices. 1081
 KIKUCHI, K., BERNARD, H. W., FRITZ, J. J., AND ASTON, J. G. The Directly Determined Magnetic Susceptibilities of Copper Acetylacetonate and Diphenylpicrylhydrazyl Adsorbed on Silica Gel from 1.40 to 4.2°K. 3654
 KILPATRICK, M., AND LOTT, S. K. Reaction of Flowing Steam with Refractory Metals. I. Molybdenum (1100-1700°). 1638
 KILPATRICK, M. See Kilpatrick, M. L., 2248
 KILPATRICK, M. L., KILPATRICK, M., AND JONES, J. G. The Nitration of Nitrobenzene with Nitronium Fluoroborate in Hydrogen Fluoride. 2248
 KIM, N. G. See Singer, S., 799
 KIMURA, H. See Ikeda, T., 41
 KIRCHER, J. F., SLEIMERS, F. A., MARKLE, R. A., GAGER, W. B., AND LEININGER, R. I. On the Degradation and Electron Spin Resonance Spectra of Irradiated Methacrylate Polymers. 189
 KISER, R. W. See Airington, C. C., 3202; Dillard, J. G., 3893; Winters, R. E., 1618, 3198
 KISHIMOTO, S. See Uhara, I., 880
 KISSINGER, L. W. See Ungnade, H. E., 1758
 KITAHARA, A. Solubility Behavior of Polyoxyethylene Nonylphenol Ethers in Cyclohexane and the Effect of Water by a Light-Scattering Method. 2788
 KLEIN, G. W. See Holroyd, R. A., 194, 2129
 KLEIN, R. See Kelley, R. D., 905
 KLEPPA, O. J., AND MESCHEL, S. V. Heats of Formation of Solid Solutions in the Systems (Na-Ag)Cl and (Na-Ag)Br. 3531
 KLOTZ, I. M., AND DEPHILLIPS, H. A., JR. Ion-Pair Formation in Aqueous Solutions of Butylammonium Isobutyrate. 2801
 KNIGHT, J. A., STOKES, R. A., AND BOWEN, D. Radiolysis of Cyanogen-Cyclohexane Mixtures. 678
 KNIGHT, R. J. See Carson, J. L., 3200
 KNIGHT, V. See Hecklen, J., 693, 2484, 3600, 3641
 KO, H. C., GREENBAUM, M. A., BLAUER, J. A., AND FARBER, M. The Enthalpy of Formation and Entropy of Aluminum(I) Fluoride(g). 2311
 KOBATAKE, Y., TAKEGUCHI, N., TOYOSHIMA, Y., AND FUJITA, H. Studies of Membrane Phenomena. I. Membrane Potential. 3981
 KOKADO, H. See Inoue, E., 767
 KOKES, R. J., AND GLEMZA, R. Thermodynamics of Adsorption of Carbon Dioxide on Zinc Oxide. 17
 KOKES, R. J. See Glemza, R., 3254
 KOLESKE, J. V., AND FAUCHER, J. A. Transitions in Gelatin and Vitrified Gelatin-Water Systems. 4040
 KOLLMANBERGER, A. See Smith, W. B., 4157
 KOLTHOFF, I. M., AND THOMAS, F. G. Electrode Potentials in Acetonitrile. Estimation of the Liquid Junction Potential between Acetonitrile Solutions and the Aqueous Saturated Calomel Electrode. 3049
 KONDO, K. See Nagasawa, M., 4005
 KOR, S. K. See Atkinson, G., 128
 KOREN, J. G. See Brinen, J. S., 3791
 KOSTER, D. F., AND DANTI, A. Proton Magnetic Resonance Studies of Ten Diolefins. 486
 KOTAKA, T. See Osaki, K., 3642, 4183
 KOYANO, K., AND TANAKA, I. The Photochemical and Thermal Isomerization of *trans*- and *cis*- α -Cyano- α -phenyl-N-phenylnitrones. 2545
 KRAMER, D. N. See Guilbault, G. G., 3696
 KRAMER, F. A., JR., AND WEST, R. The Proton Nuclear Magnetic Resonance Spectrum of 2,2'-Bipyridine. 673
 KRAUS, K. A. See Marcinkowsky, A. E., 303, 3968

- KRAUSE, F. P., AND LANGE, W. Aqueous Solubilities of *n*-Dodecanol, *n*-Hexadecanol, and *n*-Octadecanol by a New Method. 3171
- KREEVOY, M. M., SAPPENFIELD, D. S., AND SCHWABACHER, W. Rates of Mercapto Proton Exchange for 2-Mercaptoethanol in Aqueous Solution. 2287
- KREEVOY, M. M., AND SCHER, H. B. The Diffusion Coefficient of Atomic Mercury in Isocctane. 3814
- KREEVOY, M. M. See Evans, P. G., 4325
- KRESHECK, G. C., AND SCHERAGA, H. A. The Temperature Dependence of the Enthalpy of Formation of the Amide Hydrogen Bond; the Urea Model. 1704
- KRESHECK, G. C., SCHNEIDER, H., AND SCHERAGA, H. A. The Effect of D₂O on the Thermal Stability of Proteins. Thermodynamic Parameters for the Transfer of Model Compounds from H₂O to D₂O. 3132
- KRESHECK, G. C. See Schneider, H., 1310
- KRIESE, R. See Freifelder, M., 3645
- KRIKORIAN, O. H., AND CARPENTER, J. H. Enthalpies of Formation of Gaseous Tantalum Oxide and Tantalum Dioxide. 4399
- KRÖGER, F. A. The *P-T-z* Phase Diagram of the System Zinc-Tellurium. 3367
- KROLL, M., AND GINTER, M. L. Gas Phase Charge-Transfer Complexes. 3671
- KRONICK, P. L. Orientation in Pyridine-Iodine Complexes. 3178
- KRONICK, P. L. See Scott, H., 1740
- KUBO, M. See Ikeda, R., 2101
- KUBOKAWA, Y. Desorption of Olefins from Silica-Alumina Catalysts. 2676
- KUECKER, J. F. See Nightingale, E. R., Jr., 2197
- KULKARNI, M. V., ALLEN, G. F., AND LYONS, P. A. Diffusion in Carbon Tetrachloride-Cyclohexane Solutions. 2491
- KULKARNI, M. V., AND LYONS, P. A. Diffusion of Potassium Chloride in Methanol-Water Solutions. 2336
- KUMAR, P. See Mansingh, A., 4197
- KUNTZ, R. R. The Mercury-Photosensitized Decomposition of Isopentane. 2291
- KUNTZ, R. R. The Hg(³P₁)-Sensitized Decomposition of *n*-Hexane Vapor. 4396
- KUNTZ, U. E. See Hyde, B. G., 1667
- KURATA, M. See Osaki, K., 3642, 4183
- KURIAKOSE, A. K., AND MARGRAVE, J. L. Kinetics of the Reactions of Elemental Fluorine. IV. Fluorination of Graphite. 2772
- KURIAKOSE, A. K. See Poland, D. E., 158
- KUST, R. N. The Oxygen Electrode in Fused Alkali Nitrates. 3662
- KVANDE, P. C. See Brooks, W. V. F., 1489
- KYBETT, B. D., JOHNSON, G. K., BARKER, C. K., AND MARGRAVE, J. L. The Heats of Formation and Polymerization of Carbon Suboxide. 3603
- LABES, M. M. See Reucroft, P. J., 779; Scott, H., 1740
- LADD, M. F. C., AND LEE, W. H. The Thermodynamics of Crystalline Hydrates. 1840
- LADY, J. H. See Whetsel, K. B., 1596
- LA MAR, G. N. Proton Magnetic Resonance Line Widths, Ligand Exchange, and Electronic Relaxation Times for Some Arylphosphine Complexes of Cobalt(II) and Nickel(II). 3212
- LAMM, M. E., AND NEVILLE, D. M., JR. The Dimer Spectrum of Acridine Orange Hydrochloride. 3872
- LANDO, J. L. See Steigman, J., 2895
- LANGE, W. See Krause, F. P., 3171
- LANGFORD, C. H. See Stengle, T. R., 3299
- LANIER, R. D. Properties of Organic-Water Mixtures. III. Activity Coefficients of Sodium Chloride by Cation-Sensitive Glass Electrodes. 2697
- LANIER, R. D. Activity Coefficients of Sodium Chloride in Aqueous Three-Component Solutions by Cation-Sensitive Glass Electrodes. 3992
- LA PLANCHE, L. A., THOMPSON, H. E., AND ROGERS, M. T. Chain Association Equilibria. A Nuclear Magnetic Resonance Study of the Hydrogel Bonding of *N*-Monosubstituted Amides. 1482
- LA PLANCHE, L. A. See Rogers, M. T., 3648
- LARSEN, D. W., AND ALLRED, A. L. Halogen Complexes. III. The Association of 2,4,6-Trimethylpyridine and Trifluoroiodomethane. 2400
- LARSON, J. G., AND HALL, W. K. Studies of the Hydrogen Held by Solids. VII. The Exchange of the Hydroxyl Groups of Alumina and Silica-Alumina Catalysts with Deuterated Methane. 3080
- LARSON, Q. V. See Boyd, G. E., 1413
- LAUDELOUT, H., AND THOMAS, H. C. The Effect of Water Activity on Ion-Exchange Selectivity. 339
- LAURIE, V. W. See Swanson, T. B., 244
- LAWSON, K. D., AND FLAUTT, T. J. Measurement of the Spin-Lattice Relaxation Times of Dimethyloctylamine Oxide through the Critical Micelle Concentration. 3204
- LAWSON, K. D., AND FLAUTT, T. J. Nuclear Magnetic Resonance Absorption in Anhydrous Sodium Soaps. 4256
- LAWSON, P. S. See Davis, W., Jr., 1904
- LEE, C. L. See Bhattacharyya, D. N., 608, 612
- LEE, I. J., MUIR, W. M., AND LYMAN, D. J. Relationship between Parachor and Zisman's Critical Surface Tension of Polymers. 3220
- LEE, T. E. See Cater, E. D., 2684
- LEE, W. H. See Ladd, M. F. C., 1840
- LEEDER, J. D., AND WATT, I. C. The Role of Amino Groups in Water Absorption by Keratin. 3280
- LEIBOWITZ, M. Remarks on Förster's Theory of Transfer of Excitation Energy. 1061
- LEININGER, R. I. See Kircher, J. F., 189
- LEMLEY, J. See Schoonmaker, R. C., 3455
- LEMMON, R. M. See Smith, M. A., 3370
- LEMONS, J. F. See Elliott, G. R. B., 933, 2135
- LENDVAY, E. Photoluminescence of Adsorbed Dyes. 738
- LÉONARD, A. See Fripiat, J. J., 3274
- LEONARD, J., AND DAoust, H. Variation of Chain Dimensions of Polystyrene with Concentration. 1174
- LEVI, A. A. See Srinivasan, R., 1775
- LEVY, J. B., AND COPELAND, B. K. W. The Kinetics of the Hydrogen-Fluorine Reaction. II. The Oxygen-Inhibited Reaction. 408
- LEVY, J. B., AND COPELAND, B. K. W. The Kinetics of the Tetrafluorohydrazine-Fluorine Reaction. 3700
- LI, N. C. See Takahashi, F., 1622, 2950
- LICHTIN, N. N., AND WILSON, J. W. The Radiolysis of Methanol and Methanolic Solutions. IV. The Effect of Water on Peroxide Yields. 3673
- LIEBERMAN, M. L., AND WAHLBECK, P. G. The Thermodynamics of the Scandium-Hydrogen System. 3514
- LIEBERMAN, M. L., AND WAHLBECK, P. G. The Scandium-Yttrium-Hydrogen System. 3973
- LIETO, L. R. See Rosenthal, D., 1588
- LIETZKE, M. H., HUFF, H. B., AND STOUGHTON, R. W. Electromotive Force Studies in Aqueous Solutions at Elevated Temperatures. VI. The Thermodynamic Properties of HCl-NaCl Mixtures. 2395
- LIFSHTITZ, C., AND LONG, F. A. Appearance Potentials and Mass Spectra of Fluorinated Ethylenes. II. Heats of Formation of Fluorinated Species and Their Positive Ions. 3731
- LIFSHTITZ, C., AND LONG, F. A. Appearance Potentials and Mass Spectra of Fluorinated Ethylenes. III. Calculations Based on the Statistical Theory of Mass Spectra. 3737
- LIFSHTITZ, C., AND LONG, F. A. Appearance Potentials and Mass Spectra of C₂F₆, C₂F₆Cl, and *c*-C₃F₆. 3741
- LIFSHTITZ, C., AND LONG, F. A. Some Observations Concerning the Positive Ion Decomposition of C₂F₆ and C₃F₈ in the Mass Spectrometer. 3746
- LIGHTFOOT, E. N. See Cussler, E. L. Jr., 1135, 2875
- LIN, T. F., CHRISTIAN, S. D., AND AFFSPRUNG, H. E. Hydration of Acetone in 1,2-Dichloroethane. 2980
- LINDE, R. K. Enthalpy of Solid Solution for a Metastable Silver-Copper Alloy. 4407
- LINDENBAUM, S., AND BOYD, G. E. Thermodynamic Quantities in the Exchange of Lithium with Cesium Ion on Cross-Linked Polymethacrylate Ion Exchangers. 2374
- LINDENBAUM, S. See Boyd, G. E., 2378
- LIPPINCOTT, E. R. See Nagarajan, G., 2017
- LIPSKY, S. R. See Shanin, M. M., 4406
- LIRIO, J. A. See Gustafson, R. L., 2849

- LITMAN, B. J., AND SCHELLMAN, J. A. The $n-\pi^*$ Cotton Effect of the Peptide Linkage. 978
- LIU, K.-J., AND GREGOR, H. P. Influence of Electrolytes on the Solution Properties of Neutralized Poly-N-vinylimidazole. 1248
- LIU, K.-J., AND GREGOR, H. P. Metal-Polyelectrolyte Complexes. X. Poly-N-vinylimidazole Complexes with Zinc(II) and with Copper(II) and Nitrilotriacetic Acid. 1252
- LIVINGSTON, R. C. See Perkins, R. S., 3329
- LO, G. Y.-S. See Evans, J. C., 3223, 3650
- LOCKE, D. C. Gas-Solid Partition Chromatography with Real Carrier Gases. 3768
- LOEWENSTEIN, A., AND MARGALIT, Y. Nuclear Magnetic Resonance Studies of Nitriles and Isocyanides: Acetonitrile and Methyl Isocyanide. 4152
- LOFTUS, J., AND SATTERFIELD, C. N. Mechanism of Homogeneous Gas-Phase Partial Oxidation of *o*-Xylene. 909
- LOR, R. M.-S. See Coetzee, J. F., 2690
- LONG, F. A. See Lifshitz, C., 3731, 3737, 3741, 3746
- LOPREST, F. J. See Caruso, R., 1716
- LORD, R. C. See Garland, C. W., 1188, 1195
- LORENC, J. See Castellano, S., 3552
- LOTT, P. F. See Cukor, P., 3232
- LOTT, S. K. See Kilpatrick, M., 1638
- LOUGHRAN, E. D. See Ungnade, H. E., 1758
- LOW, M. J. D., AND KAMEL, A. M. The Thermal Decomposition of Cadmium Hydroxide. 450
- LUCASSEN, J. See van den Tempel, M., 1798
- LUCASSEN-REYNDERS, E. H. See van den Tempel, M., 1798
- LUCCHESI, P. J. See Carter, J. L., 3070
- LUKS, K. D. See Davis, H. T., 869
- LUM, A. See Caruso, R., 1716
- LUMRY, R., AND YUE, R. H.-S. Dielectric Dispersion of Protein Solutions Containing Small Zwitterions. 1162
- LUNSFORD, J. H., AND JAYNE, J. P. Formation of CO_2^- Radical Ions When CO_2 is Adsorbed on Irradiated Magnesium Oxide. 2182
- LUTINSKI, F. E. See Swift, H. E., 3268
- LYDY, D. L., MODE, V. A., AND KAY, J. G. Dissociation Constant and Degree of Dissociation for Tetraethylammonium Chloride in Ethylene Dichloride at 0, -15 , and -30° 87
- LYKLEMA, J., SCHOLTEN, P. C., AND MYSELS, K. J. Flow in Thin Liquid Films. 116
- LYMAN, D. J. See Lee, I. J., 3220
- LYNN, K. R. Kinetics of Base-Catalyzed Hydrolysis of Urea. 687
- LYONS, P. A. See Birkett, J. D., 2782; Harpst, J. A., 2333; Holt, E. L., 2341; Kulkarni, M. V., 2336, 2491; Rodwin, L., 2783
- MAATMAN, R. W. The Behavior of Alkali Metal Cations in the Pores of Silica Gel. 3196
- MAATMAN, R. W. See Williams, K. C., 250
- MABROUK, A. F. See Rohwedder, W. K., 1711
- MACIEL, G. E. Carbon-13 Chemical Shifts of Vinyl Carbons. 1947
- MACIEL, G. E., AND BEATTY, D. A. Carbon-13 Magnetic Resonance Study of Alkyl Cyanides, Isocyanides, Isocyanates, and Isothiocyanates. 3920
- MACIEL, G. E., AND SAVITSKY, G. B. Carbon-13 Magnetic Resonance Study of Some Saturated Heterocyclic Compounds. 3925
- MACIEL, G. E., AND TRAFICANTE, D. D. C^{13} Magnetic Resonance Study of the Protonation of Acetic and Benzoic Acids and Their Ethyl Esters in Concentrated Sulfuric Acid. 1030
- MACIEL, G. E. See Traficante, D. D., 1348
- MACKENZIE, D. R., BLOCH, F. W., AND WISWALL, R. H., JR. Radiation Chemistry of Some Cyclic Fluorocarbons. 2526
- MACKNIGHT, W. J. See Tobolsky, A. V., 476
- MACUR, G., GROVE, E. L., GAYNOR, A. J., AND HERSH, C. K. Viscosity of NaK 78 at Low Temperatures. 3782
- MAEKAWA, E., MANCKE, R. G., AND FERRY, J. D. Dynamic Mechanical Properties of Cross-Linked Rubbers. II. Effects of Cross-Link Spacing and Initial Molecular Weight in Polybutadiene. 2811
- MAELAND, A., AND FLANAGAN, T. B. X-Ray and Thermodynamic Studies of the Absorption of Hydrogen by Gold-Palladium Alloys. 3575
- MAGEE, E. M. See Matsen, J. M., 522
- MAINS, G. J. See Niki, H., 45
- MAJUMDAR, A. J., AND ROY, R. Polymorphism in Potassium Sulfate and Thallium Sulfate. 1684
- MALONE, T. J., AND MCGEE, H. A., JR. Mass Spectrometric Investigations of the Synthesis, Stability, and Energetics of the Low-Temperature Oxygen Fluorides. I. Dioxxygen Difluoride. 4338
- MANCKE, R. G. See Maekawa, E., 2811
- MANDELKERN, L., FATOU, J. G., AND HOWARD, C. The Nucleation of Long-Chain Molecules in Monomolecular Layers. 956
- MANDELKERN, L. See Fatou, J. G., 417
- MANSELL, A. L. See Barrett, J., 2996
- MANSINGH, A., AND KUMAR, P. A Method for Determining Dielectric Relaxation Times. 4197
- MARCINKOWSKY, A. E., NELSON, F., AND KRAUS, K. A. Diffusion Studies. I. Diffusion Coefficients in Liquids by a Radiometric Porous-Frit Method. 303
- MARCINKOWSKY, A. E., PHILLIPS, H. O., AND KRAUS, K. A. Properties of Organic-Water Mixtures. V. Self-Diffusion Coefficients of Na^+ in Alcohol-Water Mixtures at 25° 3968
- MARCUS, I. See Yang, J. Y., 3113
- MARCUS, Y. See Penciner, J., 2955
- MARGALIT, Y. See Loewenstein, A., 4152
- MARGOSIAN, F. F. See Horne, R. A., 3988
- MARGRAVE, J. L. See Barker, C. K., 334; Bautista, R. G., 1770; Besenbruch, G., 3174; Frisch, M. A., 3863; Kuriakose, A. K., 2772; Kybett, B. D., 3603; Poland, D. E., 158
- MARKLE, R. A. See Kircher, J. F., 189
- MARKOVITZ, H. The Reduction Principle in Linear Viscoelasticity. 671
- MARKOWITZ, M. M., AND BORYTA, D. A. The Differential Thermal Analysis of Perchlorates. VII. Catalytic Decompositions of the Alkali Metal Perchlorates by Manganese Dioxide. 1114
- MARSH, D., AND HEICKLEN, J. Photolysis of Fluorotrichloromethane. 4410
- MARSHALL, H. P., BORGARDT, F. G., AND NOBLE, P., JR. Thermal Decomposition of Hexanitroethane. 25
- MARSHALL, W. L. See Quist, A. S., 2726, 2984, 3165
- MARTIN, A. E., AND EDWARDS, R. K. The Uranium-Uranium Dioxide Phase Diagram at High Temperatures. 1788
- MARTIN, R. B. See Conley, H. L., Jr., 2914; 2923; Mathur, R., 668
- MASON, L. S. See Silbert, L. S., 2887
- MASON, R. See Avery, J. S., 784
- MASTERTON, W. L., AND SCHWARTZ, R. N. The Activity Coefficient of Trinitrotriethylaminecobalt(III) in Aqueous Salt Solutions. 1546
- MATHESON, M. S., AND RABANI, J. Pulse Radiolysis of Aqueous Hydrogen Solutions. I. Rate Constants for Reaction of e_{aq}^- with Itself and Other Transients. II. The Interconvertibility of e_{aq}^- and H^1 1324
- MATHESON, M. S. See Rabani, J., 53
- MATHESON, R. A. A Spectrophotometric Study of the Association of Cu^{2+} and SO_4^{2-} Ions in Aqueous Solutions of Constant Ionic Strength. 1537
- MATHEWS, W. K. See Vrbaški, T., 457
- MATHUR, R., AND MARTIN, R. B. Effects of Charge and Nickel Ion on Proton Chemical Shifts of Glycyl Peptides. 668
- MATSEN, J. M., HARDING, J. W., AND MAGEE, E. M. Chemical Reactions in Chromatographic Columns. 522
- MATSUI, T. See Takeshita, T., 4077
- MATSUMOTO, M. See Ikeda, T., 3755
- MATTHEWS, R. W., AND SANGSTER, D. F. Measurement by Benzoate Radiolytic Decarboxylation of Relative Rate Constants for Hydroxyl Radical Reactions. 1938
- MATTOON, R. W. See Freifelder, M., 3645

- MATUYAMA, E. Graphitic Acid of Pyrolytic Carbon and Its Heat Treatment. 2462
- McCALL, D. W., AND DOUGLASS, D. C. The Effect of Ions on the Self-Diffusion of Water. I. Concentration Dependence. 2001
- McCLELLAN, A. L., AND NICKSIC, S. W. Simultaneous Independent Hydrogen-Bonding Equilibria and Self-Association in Some Halomethanes and Haloethanes. 446
- McCLURE, D. W., AND HALSEY, G. D., JR. The Solubility of Hydrogen in Liquid Sodium. 3542
- McCULLOUGH, R. L., AND McMAHON, P. E. New Rotational States for Paraffins. 1747
- McCUSKER, P. A. See Wodetzki, C. M., 1045, 1056
- McDONALD, C. C., AND GOLL, R. J. Studies of Gaseous Atom-Molecule Reactions by Electron Paramagnetic Resonance Spectroscopy. 293
- McDONALD, R. A., AND OETTING, F. L. The Thermodynamic Properties and Allotropy of Beryllium Chloride between 13 and 715°K. 3839
- McDOWELL, C. A. See Farmer, J. B., 953
- McFADDEN, W. H., STEVENS, K. L., MEYERSON, S., KARABATSOS, G. J., AND ORZECH, C. E., JR. Specific Rearrangements in the Mass Spectra of Neopentyl Esters. 1742
- McGEE, H. A., JR. See Malone, T. J., 4338
- McKEWAN, W. M. See Turkdogan, E. T., 327
- McKOWN, G. L. See Swiger, E. D., 949
- McLAUCHLAN, K. A. See Connor, T. M., 1888
- McLEOD, D., JR. See Weltner, W., Jr., 3488
- McLURE, I. A., BENNETT, J. E., WATSON, A. E. P., AND BENSON, G. C. Excess Properties of Some Aromatic-Alicyclic Systems. II. Analyses of H^E and V^E Data in Terms of Three Different Theories of Molecular Solutions. 2759
- McLURE, I. A. See Watson, A. E. P., 2753
- McMAHON, P. E. See McCullough, R. L., 1747
- McNESBY, J. R. See Becker, D. A., 538
- MEIER, H. Sensitization of Electrical Effects in Solids. 719
- MEISELS, G. G., AND SWORSKI, T. J. Radiolysis of Ethylene. I. Yield of Hydrogen Atoms and Formation of Saturated Hydrocarbons. 815
- MEISELS, G. G., AND SWORSKI, T. J. Radiolysis of Ethylene. III. Identification of Ionic Intermediates and Formation of Excited Species by Application of Electrostatic Fields. 2867
- MELE, A. See Site, A. D., 4033
- MERKL, A. W. See Singer, S., 799
- MERRIGAN, J. A., AND RACK, E. P. Effects of Experimental Parameters on the (n, γ) -Activated Reactions of Bromine with Liquid Cyclohexane. 2795
- MERRIGAN, J. A., AND RACK, E. P. Evidence for Bromine-82m Isomeric Transition Activated Reactions in Saturated Hydrocarbons and Alkyl Halides. 2806
- MESCHEL, S. V. See Kleppa, O. J., 3531
- MESSERLY, J. F., TODD, S. S., AND FINKE, H. L. Low-Temperature Thermodynamic Properties of *n*-Propyl-, *n*-Butyl-, and *n*-Decyl-Substituted Cyclopentanes. 353
- MESSERLY, J. F., TODD, S. S., AND FINKE, H. L. Low-Temperature Thermodynamic Properties of *n*-Propyl- and *n*-Butylbenzene. 4304
- MESSERLY, J. F., See Finke, H. L., 2094
- MEYERS, E. A. See Serewicz, A. J., 1915
- MEYERSON, S. See McFadden, W. H., 1742
- MEYERSTEIN, D. See Anbar, M., 698
- MICHAELS, A. S., FALKENSTEIN, G. L., AND SCHNEIDER, N. S. Dielectric Properties of Polyanion-Polycation Complexes. 1456
- MICHAELS, A. S., MIR, L., AND SCHNEIDER, N. S. A Conductometric Study of Polycation-Polyanion Reactions in Dilute Aqueous Solution. 1447
- MIJNLIEFF, P. F., AND ZELDENRUST, H. Depolarization of Scattered Light by Optically Active Systems. 689
- MIKHAIL, R. SH. See Razouk, R. I., 1805
- MILES, D. See Urry, D. W., 1603
- MILES, M. H., EYRING, E. M., EPSTEIN, W. W., AND OSTLUND, R. E. Fast Reactions Involving Hydrogen Bonding in 2,2-Disubstituted Malonic Acids. 467
- MILLER, A. A. Radiation Yields of Carbon Monoxide and Dioxide for Some Aromatic Carbonyl Compounds. 1077
- MILLER, A. A. Volume-Energy Relations in Liquids at 0°K. 3190
- MILLER, A. R., AND SEARCY, A. W. Thermodynamic Stabilities as a Function of Composition for Indium Sulfide Phases from Mass Spectrometer Intensity vs. Time Data. 3826
- MILLER, D. G. A Simple Reduced Equation for the Estimation of Vapor Pressures. 3209
- MILLER, D. G. Definitive Test of the Onsager Reciprocal Relations in Isothermal Ternary Diffusion of Water-Sodium Chloride-Potassium Chloride. 3374
- MILLER, G. H., AND DACEY, J. R. The Importance of Xenon Fluorides in the Xenon-Photosensitized Reactions of the Perfluoroalkanes. 1434
- MILLER, G. R. See Evans, P. G., 4325
- MILLER, I. R. Effect of Adsorbed Polyelectrolytes on the Polarographic Currents. I. 2740
- MILLER, I. R. See Frei, Y. F., 3018
- MILLER, J. P. See Seward, R. P., 3156
- MILLER, R. J., AND DAEN, J. Shock Tube Studies on the Condensation of Various Vapors. 3006
- MILLS, R. The Intradiffusion and Derived Frictional Coefficients for Benzene and Cyclohexane in Their Mixtures at 25°. 3116
- MILLS, R. See Albright, J. G., 3120
- MIR, L. See Michaels, A. S., 1447
- MISRA, D. N. See Aston, J. G., 3219
- MIURA, M. See Yasunaga, T., 3214
- MODE, V. A. See Lydy, D. L., 87
- MODICA, A. P. Kinetics of the Nitrous Oxide Decomposition by Mass Spectrometry. A Study to Evaluate Gas-Sampling Methods behind Reflected Shock Waves. 2111
- MOELWYN-HUGHES, E. A. Interatomic Energy Constants of Mercury. 1740
- MONAHAN, A. R., AND JANZ, G. J. Reactivities of Perfluoroalkylnitriles toward Butadiene. 1070
- MOON, A. Y., POLAND, D. C., AND SCHERAGA, H. A. Thermodynamic Data from Fluorescence Spectra. I. The System Phenol-Acetate. 2960
- MOREAU, M. See Hayon, E., 4053, 4058
- MORITA, S. See Tasaka, M., 4191
- MORTLAND, M. M. See Farmer, V. C., 683
- MOSER, H. C. See Watkins, K. W., 1040; Yun, H. B., 1059
- MROCHEK, J. See Davis, W., Jr., 1904
- MUIR, W. M. See Lee, I. J., 3220
- MUKERJEE, P. Dimerization of Anions of Long-Chain Fatty Acids in Aqueous Solutions and the Hydrophobic Properties of the Acids. 2821
- MUKERJEE, P. Salt Effects on Nonionic Association Colloids. 4038
- MUKHERJEE, L. M., BRUCKENSTEIN, S., AND BADAWI, F. A. K. Equilibria in Ethylenediamine. III. Determinations of Absolute pK Values of Acids and Silver Salts. Establishment of a pH and pAg Scale. 2537
- MULAC, W. A. See Rabani, J., 53
- MULFORD, R. N. R., AND WIEWANDT, T. A. The Neptunium-Hydrogen System. 1641
- MULFORD, R. N. R. See Olson, W. M., 1223
- MULLER, N., AND ROSE, P. I. Nuclear Magnetic Resonance Dilution Shifts for Carboxylic Acids in Rigorously Dried Solvents. I. Acetic Acid in Acetic Anhydride, Acetone, and 1,4-Dioxane. 2564
- MUNSON, M. S. B. Ionic Reactions in Gaseous Acetylene. 572
- MUNSON, R. A. Kinetics of the Ortho-Pyro Interconversion in 100% Phosphoric Acid. 1761
- MURASE, T. See Nagasawa, M., 4005
- MYERS, J. R. See Dickson, D. S., 4044
- MYERS, R. J. See Blukis, U., 1154
- MYERS, R. T. Pure Acetic Acid and Acetic Anhydride and the Electrical Conductance and Dielectric Constant of This System. 700
- MYSELS, K. J. See Abu-Hamdiyyah, M., 1466; Lyklema, J., 116
- NAGARAJAN, G., LIPPINCOTT, E. R. AND STUTMAN, J. M. Mean Amplitudes of Vibration, Bastiansen-Morino Shrinkage Effect, Thermodynamic Functions, and Molecular Polarizability of Sulfur Trioxide. 2017

- NAGASAWA, M., MURASE, T., AND KONDO, K. Potentiometric Titration of Stereoregular Polyelectrolytes. . . . 4005
- NAGASAWA, M. See Tasaka, M., 4191
- NAKAMURA, D. See Ikeda, R., 2101
- NAMBA, S. Color Sensitization of Zinc Oxide with Cyanine Dyes. . . . 774
- NAMIKAWA, K. See Savitsky, G. B., 1425, 3105
- NANDI, P. K., AND NANDI, U. S. Reaction between Benzoyl Peroxide and Rhodamine 6GX Color Base. . . . 4071
- NANDI, U. S. See Nandi, P. K., 4071
- NANIS, L. See Bockris, J. O'M., 1627
- NANNEY, T. R., AND GILKERSON, W. R. The Dispersion of the Conductance of a Salt in Low Dielectric Solvents. 1338
- NARASIMHAMURTY, H. V. L., IYER, A. S., AND HOCH, M. Relation between Specific Heat and Total Emittance in Tantalum, Niobium, Tungsten, and Molybdenum. . . 1420
- NARVAEZ, R., AND TAYLOR, H. A. Sites for Hydrogen Adsorption on Zinc Oxide. . . . 2500
- NASH, C. P., AND DESIENO, R. P. Infrared Spectra of Molecules Adsorbed on Metal Powders Obtained from Electrically Exploded Wires. . . . 2139
- NATALIS, P., AND FRANKLIN, J. L. Ionization and Dissociation of Diphenyl and Condensed Ring Aromatics by Electron Impact. I. Biphenyl, Diphenylacetylene, and Phenanthrene. . . . 2935
- NATALIS, P., AND FRANKLIN, J. L. Ionization and Dissociation of Diphenyl and Condensed Ring Aromatics by Electron Impact. II. Diphenylcarbonyls and Ethers. . . . 2943
- NATH, N., AND SINGH, M. P. Mechanism of the Oxidation of Reducing Sugars (Hexoses) by Hexacyanoferrate(III) in Alkaline Medium and Lobry de Bruyn Transformation. . . . 2038
- NATKE, C. A. See Greenberg, E., 2089
- NAVON, G., AND STEIN, G. Rate Constants of Some Reactions of H Atoms in Aqueous Solution. . . . 1384
- NAVON, G., AND STEIN, G. Electron Transfer between Atomic Hydrogen and Cobalt(III) Complexes in Aqueous Solution. . . . 1390
- NEBEKER, E. B., AND PINGS, C. J. The Continuous Absorption Spectrum of Iodine Monochloride. . . . 2483
- NEIGHBOUR, F. See Verdin, D., 1992
- NELSON, F. See Marcinkowsky, A. E., 303
- NELSON, R. C. Minority Carrier Trapping and Dye Sensitization. . . . 714
- NELSON, R. C. See Smith, M. L., 3833
- NELSON, R. D., JR., AND SMYTH, C. P. Microwave Absorption and Molecular Structure in Liquids. LXI. The Dielectric Relaxation Mechanism for Molecules Similar in Structure to Diphenyl Ether. . . . 1006
- NEUMAN, R. C., JR., AND YOUNG, L. B. On the Relative Magnitudes of *cis* and *trans* Coupling across Carbon-Nitrogen Partial Double Bonds. . . . 1777
- NEUMAN, R. C., JR., AND YOUNG, L. B. Hindered Rotation and Carbon-13-Hydrogen Coupling Constants in Amides, Thioamides, and Amidines. . . . 2570
- NEVILLE, D. M., JR. See Lamm, M. E., 3872
- NEWTON, J. See Farrell, P. G., 3506
- NEWTON, T. W., AND BAKER, F. B. The Kinetics of the Reaction between Vanadium(II) and Uranium(VI). . . 176
- NICHOL, L. W., AND OGSTON, A. G. An Examination of the Johnston-Ogston Equation and the Moving Boundary Equation. . . . 1754
- NICHOL, L. W., AND OGSTON, A. G. Sedimentation Equilibrium in Reacting Systems of the Type $mA + nB \rightarrow C$ 4365
- NIGHTINGALE, E. R., JR., AND KUECKER, J. F. Viscosity of Aqueous Solutions. IV. Chloroamineplatinum(IV) Salts. Influence of Ionic Charge on the Viscosity *B*-Coefficient. . . . 2197
- NIKI, H., ROUSSEAU, Y., AND MAINS, G. J. The Hydrogen-Deuterium Exchange Reaction. I. 6^3P_1 Mercury Photosensitized. . . . 45
- NIKITINE, S., CORET, A., ZIELINGER, J. P., JEANCLAUDE, C., BOEHM, C., AND ZOUAGHI, M. The Relationship between Exciton Absorption and the Photoelectric Effect. . . . 745
- NISHIZAKI, Y. See Okubo, T., 3690
- NOBLE, P., JR. See Marshall, H. P., 25
- NORMAN, J. H., STALEY, H. G., AND BELL, W. E. Mass Spectrometric Knudsen Cell Measurements of the Vapor Pressure of Palladium and the Partial Pressure of Palladium Oxide. . . . 1373
- NORRIS, W. P. See Gordon, A. S., 3013; Smith, S. R., 1615
- NOWICKI, R. B. See Zajac, W. W., Jr., 2649
- NOYES, R. M. Revised Thermodynamic Properties of Aqueous Strontium Ion. . . . 3181
- NOYES, R. M. Diffusion Coefficients of Iodine Atoms in Carbon Tetrachloride. A Correction. . . . 3182
- NOYES, W. A., JR. See Zahra, A., 943
- O'BRIEN, J. F. See Ramey, K. C., 3418
- ODIAN, G., ACKER, T., AND PLETZKE, T. γ -Radiolysis of Ammonium Perchlorate. . . . 2477
- OETTING, F. L. See McDonald, R. A., 3839
- OGRYZLO, E. A., AND SANCTUARY, B. C. Double Molecules in Gases. . . . 4422
- OGSTON, A. G. See Nichol, L. W., 1754, 4365
- O'HARE, P. A. G., AND HUBBARD, W. N. Fluorine Bomb Calorimetry. XIII. The Enthalpy of Formation of Arsenic Pentafluoride. . . . 4358
- OHNISHI, R. See Takeshita, T., 4077
- OIWA, I. T. See Rosenthal, D., 1588
- OKABE, H. See Becker, D. A., 538
- OKAJIMA, T. See Cleveland, S. T., 4085
- OKUBO, T., NISHIZAKI, Y., AND ISE, N. Single-Ion Activity Coefficient of Gegenions in Sodium Polyacrylate. . . . 3690
- OKUBO, T. See Ise, N., 4102
- OLMSTEAD, H. D. See Brinen, J. S., 3791
- OLSON, W. M., AND MULFORD, R. N. R. The Decomposition Pressure and Melting Point of Thorium Mononitride. . . . 1223
- ONO, Y. See Imai, H., 1082
- ONSAGER, L. See Fuoss, R. M., 2581
- O'REILLY, J. M. See Karasz, F. E., 2657
- ORTTUNG, W. H., AND WARNER, J. Refractive Index Dispersion in Equine Hemoglobin Solutions. . . . 3188
- ORZECH, C. E., JR. See McFadden, W. H., 1742
- OSAKI, K., TAMURA, M., KOTAKA, T., AND KURATA, M. Normal Stresses and Dynamic Moduli in Polymer Solutions. . . . 3642
- OSAKI, K., TAMURA, M., KURATA, M., AND KOTAKA, T. Complex Modulus of Concentrated Polymer Solutions in Steady Shear. . . . 4183
- OSTERHOUDT, H. W., AND WILLIAMS, J. W. Sedimentation Equilibria in Polydisperse Pseudo-Ideal Solutions and at Low Centrifugal Field. . . . 1050
- OSTLUND, R. E., See Miles, M. H., 467
- PADMANABHAN, G. R. See Coetzee, J. F., 3193
- PALCO, A. A. See Rutenberg, A. C., 527
- PALMER, H. B. See Hou, K. C., 858, 863
- PANCIROV, R. See Brumberger, H., 4312
- PANSING, W. F. The Catalytic Cracking of Hexadecane—Effects of Impurities, Olefins, and Steam. . . . 392
- PANSON, G. S. See Rubin, J., 3089
- PAOLETTI, P., STERN, J. H., AND VACCA, A. Thermochemical Studies. XV. Thermodynamics of Protonation of Triethylenediamine, Triethylamine, Trimethylamine, and Ammonia in Aqueous Solution at 25°. . . . 3759
- PARCELL, L. J. See White, R. C., 4409
- PARFITT, G. D., SMITH, A. L., AND WALTON, A. G. The Role of Silver Nitrate Ion Pairs in the Alkyl Halide-Silver Nitrate Reaction. . . . 661
- PARKINSON, W. W., BOPP, C. D., BINDER, D., AND WHITE, J. E. A Comparison of Fast Neutron and γ -Irradiation of Polystyrene. I. Cross-Linking Rates. . . . 828
- PARKS, A. T. See Bartell, L. S., 3043
- PARRAVANO, G. See Sommerfeld, J. T., 102
- PASFIELD, W. H. The Partial Volumes of 1-Butanol in Dilute Aqueous Solutions at 30°. . . . 2406
- PASSAGLIA, E. See Stromberg, R. R., 3955
- PASSCHIER, A. A. See Stern, J. H., 207
- PATAPOFF, M. See Von Weysenhoff, H., 1756
- PATEL, V. C. See Freeman, D. H., 1477
- PATTERSON, A., JR. See Spinnler, J. F., 500, 508, 513, 658

- PAYNE, R. Structure of the Electrical Double Layer at a Mercury Electrode in the Presence of Adsorbed Nitrate Ions. 4113
- PEARCE, S. See West, W., 1894
- PEARSON, R. M. See Savitsky, G. B., 1425
- PEHLKE, R. D. See Cleveland, S. T., 4085
- PENCINER, J., ELIEZER, I., AND MARCUS, Y. Anion Exchange of Metal Complexes. XVI. Chloride Complexes of Zinc, Cadmium, and Mercury in Anhydrous Ethanol. 2955
- PERI, J. B. Infrared and Gravimetric Study of the Surface Hydration of γ -Alumina. 211
- PERI, J. B. A Model for the Surface of γ -Alumina. 220
- PERI, J. B. Infrared Study of Adsorption of Ammonia on Dry γ -Alumina. 231
- PERKINS, R. See Ree, T. S., 3322
- PERKINS, R. S., LIVINGSTON, R. C., ANDERSEN, T. N., AND EYRING, H. Voltage Transients of Freshly Produced Noble Metal Electrode Surfaces. 3329
- PERLMUTTER-HAYMAN, B. The Kinetics of the Hydrolysis of the Bichromate Ion. II. The Reaction in Acetate Buffer and the Acid Catalysis. 1736
- PESCHEL, G. G. See Clark, L. B., 3615
- PETERS, E. See von Hahn, E. A., 547
- PETERSON, D. B., ARAKAWA, T., WALMSLEY, D. A. G., AND BURTON, M. Energy-Transfer Processes in Dilute Solutions of Organometallics in Benzene. Radiation Chemistry and Luminescence Quenching. 2880
- PETERSON, D. B. See Wodetzki, C. M., 1045, 1056
- PETERSON, D. L., AND HELFFERICH, F. Toward a Generalized Theory of Gas Chromatography at High Solute Concentrations. 1283
- PETROPOULOS, J. H. See Adler, G., 3712
- PHILLIPS, H. O. See Marcinkowsky, A. E., 3968
- PHILLIPS, R. See Stubblefield, C. T., 991
- PIEROTTI, R. A. Aqueous Solutions of Nonpolar Gases. 281
- PINCHAS, S. The Integrated Absorption Intensity of the C=O Stretching Band of Carbon-13-Labeled Benzoic Acid. 2256
- PINCHAS, S., SADEH, D., AND SAMUEL, D. The Infrared Absorption of Oxygen-18-Labeled Phenol. 2259
- PINGS, C. J. See Nebeker, E. B., 2483
- PLACZEK, D. W., AND RABINOVITCH, B. S. The Thermal Isomerization of Trifluoromethyl- and Trifluoroethylcyclopropane. 2141
- PLACZEK, D. W., RING, D. F., AND RABINOVITCH, B. S. Deuterium Isotope Effects on Rates of Methylene Radical Insertion into C-H Bonds. 1782
- PLAZEK, D. J. Temperature Dependence of the Viscoelastic Behavior of Polystyrene. 3480
- PLETZKE, T. See Odian, G., 2477
- PLUMB, R. C., AND THAKKAR, N. Volta Potential Studies of the Aging of Gold Surfaces. 439
- POLAND, D. C., AND SCHERAGA, H. A. Hydrophobic Bonding and Micelle Stability. 2431
- POLAND, D. C. See Moon, A. Y., 2960
- POLAND, D. E., KURIAKOSE, A. K., AND MARGRAVE, J. L. The Oxidation of Titanium Monoxide at High Temperatures. 158
- POLITZER, P. The Electrostatic Forces within the Carbon Monoxide Molecule. 2132
- PONCELET, G. See Fripiat, J. J., 2185
- POOLE, C. P., JR., SWIFT, H. E., AND ITZEL, J. F., JR. Aluminum-27 Nuclear Magnetic Resonance of Trialkylaluminum Compounds. II. Variable-Temperature Studies. 3663
- POOLE, J. A. The Fluorescence of Benzene and Benzene- d_6 1343
- PORTE, H. A., GREENBERG, E., AND HUBBARD, W. N. Fluorine Bomb Calorimetry. XII. The Enthalpy of Formation of Ruthenium Pentafluoride. 2308
- PORTER, R. F., AND WASON, S. K. Reaction of Boroxine with $\text{BF}_3(\text{g})$. Infrared Spectrum and Stability of $\text{HBF}_2(\text{g})$ 2208
- PORTER, R. F. See Barton, L., 3160; Wason, S. K., 2461
- POTTS, A. D., AND DAVIDSON, D. W. Ethanol Hydrate. 996
- PRINCE, L. A., AND JOHNSON, E. R. The Radiation-Induced Decomposition of the Alkali and Alkaline Earth Perchlorates. I. Product Yields and Stoichiometry. 359
- PRINCE, L. A., AND JOHNSON, E. R. The Radiation-Induced Decomposition of the Alkali and Alkaline Earth Perchlorates. II. Mechanism of the Decomposition. 377
- PRITCHARD, G. O., AND BRYANT, J. T. An Anomaly in the Interaction of CF_2H Radicals. 1085
- PRITCHARD, G. O., BRYANT, J. T., AND THOMMARSON, R. L. The Reaction of Methyl Radicals with Methyl and Methylene Fluoride. 664
- PRITCHARD, G. O., BRYANT, J. T., AND THOMMARSON, R. L. The Reaction of Methylene with CF_2H_2 2804
- PRITCHARD, G. O., AND THOMMARSON, R. L. Photochemistry of the Fluoroketones. Heptafluoropropyl Ethyl Ketone. 1001
- PRITCHARD, G. O. See Alumbaugh, R. L., 3235
- PRITCHARD, H. O. See Goy, C. A., 1504, 3040
- PRUE, J. E. See Fernández-Prini, R., 2793
- PRUSINOWSKI, L. R. See Hamori, E., 1011
- PUETT, D., SMITH, K. J., JR., AND CIFERRI, A. Elasticity of Semicrystalline Polymers. 141
- PURCELL, W. P., AND SINGER, J. A. Electric Moment of Isonicotinamide in Benzene and Dioxane Solutions. 691
- PURCELL, W. P., AND SINGER, J. A. Benzene and Dioxane Electric Moments of N-Alkyl-Substituted Nicotinamides from Measurements in Mixed Benzene-Dioxane Solutions. 4097
- QUIST, A. S., AND MARSHALL, W. L. Assignment of Limiting Equivalent Conductances for Single Ions to 400° 2984
- QUIST, A. S., AND MARSHALL, W. L. Estimation of the Dielectric Constant of Water to 800° 3165
- QUIST, A. S., MARSHALL, W. L., AND JOLLEY, H. R. Electrical Conductances of Aqueous Solutions at High Temperature and Pressure. II. The Conductances and Ionization Constants of Sulfuric Acid-Water Solutions from 0 to 800° and at Pressures up to 4000 Bars. 2726
- RABANI, J., MULAC, W. A., AND MATHESON, M. S. The Pulse Radiolysis of Aqueous Tetranitro Methane. I. Rate Constants and the Extinction Coefficient of e_{aq}^- . II. Oxygenated Solutions. 53
- RABANI, J. See Matheson, M. S., 1324
- RABINOVITCH, B. S. See Dorer, F. H., 1952, 1934, 1973; Placzek, D. W., 1782, 2141; Whitten, G. Z., 4348
- RACK, E. P. See Merrigan, J. A., 2795, 2806
- RADELL, J., BRODMAN, B. W., HIRSHFELD, A., AND BERGMANN, E. D. Acidity and Autocatalysis of Esterification of Acetylenic and Fluoro Acids. 928
- RAI, D. K. See Singh, R. B., 3461
- RAMEY, K. C., O'BRIEN, J. F., HASEGAWA, I., AND BORCHERT, A. E. Nuclear Magnetic Resonance Study of Aluminum Alkyls. 3418
- RAMSEY, J. B. See Bodenseh, H. K., 543
- RANTAMAA, A. K. See Baliga, B. T., 1751
- RAO, R. V. G., AND GIAUQUE, W. F. The Heat Capacities and Entropies of Cobalt Sulfate Heptahydrate and Hexahydrate from 15 to 330°K 1272
- RAO, V. S. R., AND FOSTER, J. F. The Conformation of the Pyranose Rings in Mono-, Di-, and Polysaccharides at High pH by Proton Magnetic Resonance Studies. 636
- RAO, V. S. R., AND FOSTER, J. F. An Addition Complex between Carbohydrates and Dimethyl Sulfoxide as Revealed by Proton Magnetic Resonance. 656
- RAUH, E. G. See Cater, E. D., 2684
- RAZOUK, R. I., MIKHAIL, R. SH., AND ISKANDER, G. R. Adsorption of Cyclohexane on Aluminas Prepared by Thermal Decomposition of Aluminum Hydroxide *in Vacuo* and in Presence of Air. 1805
- REE, T. See Ree, T. S., 3322
- REE, T. S., REE, T., EYRING, H., AND PERKINS, R. The Reduced Thermodynamic Functions for the Significant Structure Theory of Simple Liquids. 3322
- REEVES, R. L. See Tong, L. K. J., 2357
- REEVES, R. R., JR. See Rolfes, T. R., 849; Thompson, B. A., 3964
- REID, W. E., JR. Some Electrochemical Aspects of

- Germanium Dissolution. Simultaneous Chemical and Electrochemical Oxidation. 2269
- REID, W. E., JR. Some Electrochemical Aspects of Germanium Dissolution. Valence States and Electrode Potential. 3168
- REUCROFT, P. J., RUDYJ, O. N., SALOMON, R. E., AND LABES, M. M. Effect of Gases on the Conductivity of Organic Solids. III. Sensitization of Bulk Photoconductivity in *p*-Chloranil Crystals. 779
- RICE, C. L., AND WHITEHEAD, R. Electrokinetic Flow in a Narrow Cylindrical Capillary. 4017
- RICE, F. O., AND WUNDERLICH, F. J. Concerning the Reaction $\text{NO}_2 + \text{NO}^* \rightarrow \text{N}_2\text{O} + \text{O}_2$ 2137
- RICHARDS, R. R., AND GREGORY, N. W. The Crystal Structure of Sodium Tetrachloroferrate(III). 239
- RICHARDS, S. R. See Bockris, J. O'M., 671, 1627
- RICHARDSON, J. W. See Smith, P. R., 3346
- RICKBORN, B. See Alumbaugh, R. L., 3225
- RIESZ, P. The Radiolysis of Acetone in Air-Free Aqueous Solutions. 1366
- RING, D. F. See Placzek, D. W., 1782
- ROBERTS, F. P. See Wheelwright, E. J., 1220
- ROBERTSON, B. K. See Cratin, P. D., 1087; Serewicz, A. J., 1915
- ROBERTSON, R. E. Polymer Order and Polymer Density. 1575
- ROBINSON, D. W. On the Nature of Valence-Shell Molecular Orbitals. 3357
- ROBINSON, R. A. See Gary, R., 2750
- ROBINSON, R. L., JR., EDMISTER, W. C., AND DULLIEN, F. A. L. Calculation of Diffusion Coefficients from Diaphragm Cell Diffusion Data. 258
- RODGERS, A. S. Kinetics of Fluorination. II. The Addition of Fluorine to *cis*- and *trans*-Perfluorobutene-2. 254
- RODWIN, L., HARPST, J. A., AND LYONS, P. A. Diffusion in the System Cyclohexane-Benzene. 2783
- ROE, R.-J. Parachor and Surface Tension of Amorphous Polymers. 2809
- ROGERS, M. T., AND LAPLANCHE, L. A. Proton Magnetic Resonance Spectra of *cis*- and *trans*- ^{15}N -*n*-Butylformamide. 3648
- ROGERS, M. T. See LaPlanche, L. A., 1482
- ROGERS, T. E., SWINEHART, J. H., AND TAUBE, H. The Exchange of Methanol between Solvated Cations and Solvent. II. 134
- ROHWEDDER, W. K., MABROUK, A. F., AND SELKE, E. Mass Spectrometric Studies of Unsaturated Methyl Esters. 1711
- ROJO, E. A., AND HENTZ, R. R. A Study of the Radiolysis and Luminescence Behavior of Dioxane-Benzene Mixtures. 3024
- ROLFES, T. R., REEVES, R. R., JR., AND HARTECK, P. The Chemiluminescent Reaction of Oxygen Atoms with Sulfur Monoxide at Low Pressures. 849
- ROQUITTE, B. C. The Thermal Unimolecular Decomposition of Norbornylene. 1351
- ROQUITTE, B. C. The Photochemistry of $\Delta^{2,5}$ -Bicyclo-[2.2.1]heptadiene. 2475
- ROSE, P. I. See Muller, N., 2564
- ROSENBERG, H. M., AND HALE, D. Solvent Shifts in Charge-Transfer Complex Spectra. 2490
- ROSENTHAL, D., OIWA, I. T., SAXTON, A. D., AND LIETO, L. R. Acid-Base Equilibria in Concentrated Salt Solutions. IV. Some Bases of Various Charge Types in Dilute Acid Solutions. 1588
- ROSNER, D. E., AND ALLENDORF, H. D. Kinetics of the Attack of Molybdenum by Dissociated Chlorine. 4290
- ROSOFF, M., AND ARON, C. Reaction Kinetics of Monomolecular Films of Chlorophyll *a* on Aqueous Substrates. 21
- ROSZTOCZY, F. E., AND CUBICCIOTTI, D. The Bismuth Iodide-Iodine Phase Diagram. 124
- ROSZTOCZY, F. E., AND CUBICCIOTTI, D. The Potassium-Iodine, Rubidium-Iodine, and Cesium-Iodine Phase Diagrams. 1687
- ROTLEVI, E., AND TREININ, A. The 300-m μ Band of NO_3^- 2645
- ROUSSEAU, Y. See Niki, H., 45
- ROWLAND, F. S. See Tang, Y. N., 4297
- ROY, J. K. See Becker, R. S., 1435
- ROY, R. See Majumdar, A. J., 1684
- ROZNER, A. G. See Keating, K. B., 3658
- RUBIN, B. T. See Gileadi, E., 3335
- RUBIN, J., AND PANSON, G. S. Hydrogen Bonding. II. Phenol Interactions with Substituted Pyridines. 3089
- RUDYJ, O. N. See Reucroft, P. J., 779
- RUDZITIS, E., FEDER, H. M., AND HUBBARD, W. N. Fluorine Bomb Calorimetry. XI. The Enthalpy of Formation of Yttrium Trifluoride. 2305
- RUFF, I. On the Role of Water in Electron-Transfer Reactions. I. 3183
- RUMON, K. A. See Johnson, S. L., 74
- RUPERT, J. P., HOPKINS, H. P., JR., AND WULFF, C. A. The Solution Thermochemistry of Polyvalent Electrolytes. IV. Sodium Carbonate, Sodium Bicarbonate, and Trona. 3059
- RUSHING, C. See Bonner, O. D., 4345
- RUSSELL, G. A. See Strom, E. T., 2131
- RUSSELL, M. E. See Way, K. R., 4420
- RUTENBERG, A. C., AND PALKO, A. A. Nuclear Magnetic Resonance Studies of Boron Trifluoride Addition Compounds. III. Rates and Mechanism for the Exchange of Boron Trifluoride Ethyl Ether-Boron Trifluoride and Tetrahydrofuran-Boron Trifluoride and between Ethyl Ether-Boron Trifluoride and Ethyl Sulfide-Boron Trifluoride. 527
- RUTLEDGE, J. L. See Stubblefield, C. T., 991
- RYAN, C. F., AND FLEISCHER, P. C., JR. The Gel Melting Point as a Measure of the Tacticity of Poly(methyl methacrylate). 3384
- RZAD, S. See Claes, P., 1780
- SADEH, D. See Pinchas, S., 2259
- SAGER, W. F., FILIPESCU, N., AND SERAFIN, F. A. Substituent Effects on Intramolecular Energy Transfer. I. Absorption and Phosphorescence Spectra of Rare Earth β -Diketone Chelates. 1092
- SAITO, S. See Wen, W.-Y., 3569
- SALMON, O. N., AND HILDE, R. D. Evidence of Structure and Dissociation Equilibrium in Liquid Iron Oxide from Iron Oxide Activity Data. 804
- SALMON, R. E. See Bendoraitis, J. G., 3666; Reucroft, P. J., 779
- SALOVEY, R., AND FALCONER, W. E. Radiation-Induced Reactions in *n*-Hexadecane. 2345
- SALSER, G. E. See Dauerman, L., 3668
- SAMS, J. R. See Wolfe, R., 1129
- SAMUEL, D. See Pinchas, S., 2259
- SANCTUARY, B. C. See Ogryzlo, E. A., 4422
- SANDLER, Y. L., AND DURIGON, D. D. The Desorption and Isotopic Exchange of Oxygen at a Silver Surface. 4201
- SANDSMARK, R. A. See Schlag, E. W., 1431
- SANGSTER, D. F. See Matthews, R. W., 1938
- SANNIGRAHI, A. B. See Chandra, A. K., 2494
- SAPPENFIELD, D. S. See Kreevoy, M. M., 2287
- SARAF, D. N. See Witherspoon, P. A., 3752
- SATTERFIELD, C. N. See Loftus, J., 909
- SAUERWEIN, W. See Sundheim, B. R., 4042
- SAUMAGNE, P. See Fishman, E., 3671
- SAUNDERS, D., AND HEICKLEN, J. Mercury-Photosensitized Isomerization of Perfluorobutene-2. 3205
- SAUNDERS, D. See Heicklen, J., 1774
- SAVITSKY, G. B., NAMIKAWA, K., AND ZWEIFEL, G. A. Relationship between the C^{13} Carbonyl Chemical Shifts and $n \rightarrow \pi^*$ Transition Energies in Cyclic and Bicyclic Ketones. 3105
- SAVITSKY, G. B., PEARSON, R. M., AND NAMIKAWA, K. Carbon-13 Chemical Shift Viewed as a Constitutive Property. II. Substituted Hydrocarbons. 1425
- SAVITSKY, G. B. See Maciel, G. E., 3925
- SAXER, R. K. See Kickson, D. S., 4044
- SAXTON, A. D. See Rosenthal, D., 1588
- SCATCHARD, G. See Freeman, D. H., 70
- SCHAFFER, P. C. See Angell, C. L., 3463
- SCHAEER, M. D. See Kelley, R. D., 905
- SCHIEDT, R. C., AND FREILING, E. C. Ion-Exchange Processes between Immiscible Molten Phases. 1784
- SHELLMAN, J. A. See Litman, B. J., 978

- SCHER, H. B. See Kreevoy, M. M., 3814
- SCHERAGA, H. A. See Friedman, M. E., 3795; Kresheck, G. C., 1704, 3132; Moon, A. Y., 2960; Poland, D. C., 2431; Schneider, H., 1310; Schrier, E. E., 298; Thomas, M. R., 3722
- SCHLÄFER, H. L. The Role of the Doublet State in the Photochemistry of Chromium(III) Complexes. 2201
- SCHLAFFER, W. G., ADAMS, C. R., AND WILSON, J. N. Aging of Silica and Alumina Gels. 1530
- SCHLAG, E. W., SANDSMARK, R. A., AND VALENCE, W. G. Computation of Statistical Complexions. III. An Exact High Speed Method. 1431
- SCHLEGEL, J. Acid-Base Reactions in Fused Salts. The Dichromate-Chlorate Reaction. 3638
- SCHMIDT, H. H. See Clark, R. K., 3682
- SCHMIDT, P. W. A Small Angle X-Ray Scattering Study of Colloidal Thorium Oxide. 3849
- SCHMILLEN, A. Luminescence of Doped Aromatic Crystals. 751
- SCHNEIDER, H., KRESHECK, G. C., AND SCHERAGA, H. A. Thermodynamic Parameters of Hydrophobic Bond Formation in a Model System. 1310
- SCHNEIDER, H. See Kresheck, G. C., 3132
- SCHNEIDER, N. S. See Michaels, A. S., 1447, 1456
- SCHOLANDER, P. F. See Enns, T., 389
- SCHOLTEN, P. C. See Lyklema, J., 116
- SCHONHORN, H. Surface Free Energy of Polymers. 1084
- SCHOONMAKER, R. C., BUHL, A., AND LEMLEY, J. Vaporization Catalysis. The Decomposition of Gallium Nitride. 3455
- SCHOR, R. See Smith, S. R., 1615
- SCHRIER, E. E., INGWALL, R. T., AND SCHERAGA, H. A. The Effect of Aqueous Alcohol Solutions on the Thermal Transition of Ribonuclease. 298
- SCHRIER, E. E. See Thomas, M. R., 3722
- SCHÜRENKÄMPER, A. See Chênebault, P., 2300
- SCHWABACHER, W. See Kreevoy, M. M., 2287
- SCHWAN, H. P. See Takashima, S., 4176
- SCHWARTZ, R. N. See Masterton, W. L., 1546
- SCHWARZ, A. AND BOYD, G. E. Thermodynamics of the Exchange of Tetramethylammonium with Sodium Ions in Cross-Linked Polystyrene Sulfonates at 25°. 4268
- SCHWARZ, W. M., AND SHAIN, I. Investigation of First-Order Chemical Reactions Following Charge Transfer by a Step-Functional Controlled Potential Method. The Benzidine Rearrangement
- SCOTT, B. L. See Goodspeed, F. C., 1149
- SCOTT, D. R., AND BECKER, R. S. The Ground State Electronic Configurations of Ferricenium and Dibenzenechromium Cations. 3207
- SCOTT, H., KRONICK, P. L., CHARGE, P., AND LABES, M. M. Conductive Salt of the Radical Cation of 1,6-Diaminopyrene and the Radical Anion of 7,7,8,8-Tetracyanoquinodimethane. 1740
- SCOTT, R. L. Phase Equilibria in Solutions of Liquid Sulfur. I. Theory. 261
- SEARCY, A. W. See Miller, A. R., 3826
- SECOY, C. H. See Holmes, H. F., 151, 3148
- SEELY, G. R. Photoreduction of Methyl Red Sensitized by Ethyl Chlorophyllide *a*. 821
- SEELY, G. R. Kinetics of the Ethyl Chlorophyllide Sensitized Photoreduction of Phenosafranin by Hydroazobenzene. 2633
- SEELY, G. R. On the Chlorophyllide-Sensitized Reduction of Azobenzene and Other Compounds. 2779
- SEERY, D. J. See van Thiel, M., 834
- SEIFERT, R. L. See Warner, T. B., 1034
- SELKE, E. See Rohwedder, W. K., 1711
- SERAFIN, F. A. See Sager, W. F., 1092
- SEREWICZ, A. J., ROBERTSON, B. K., AND MEYERS, E. A. The Crystal Structure of Pyridine Hydrogen Nitrate. 1915
- SEWARD, R. P., AND MILLER, J. P. Galvanic Cells with Molten Bisulfate Solvents. 3156
- SHAHIN, M. M. Energy Transfer between Molecules and Electronically Excited Atoms. II. 4406
- SHAIN, I. See Schwarz, W. M., 30
- SHANE, N. See Steigman, J., 968
- SHARPLESS, R. L. See Young, R. A., 1763
- SHAW, D. W. See Goy, C. A., 1504
- SHAW, R. W., JR. See Curry, J., 344
- SHEEHAN, W. F. Rydberg Potential Energy Function for Diatomic Molecules as Extended to Polyatomic Species and Activated Complex. 923
- SHEPHERD, W. C. See Bean, R. C., 4368
- SHEPP, A. See Chaberek, S., 641, 2842
- SHERWOOD, A. G., AND GUNNING, H. E. The Mercury-Photosensitized Decomposition of Acetylene in the Presence of Nitric Oxide. 1732
- SHERWOOD, A. G., AND GUNNING, H. E. The Photolysis of Mercury Divinyl. 2323
- SHIEH, J. J. C. See Gómez-Ibáñez, J. D., 1660
- SHIELDS, L. Electron Trapping in Rigid Ethanol-Methyl-2-tetrahydrofuran Mixtures. 3186
- SHIGA, T. An Electron Paramagnetic Resonance Study of Alcohol Oxidation by Fenton's Reagent. 3805
- SHIN, H. On the Calculation of the Vibrational De-excitation Probabilities. 1424
- SHIN, H. On the Effect of the Double-Impact Collision on Dissociation Rate Constants. 2411
- SHINODA, K., AND HILDEBRAND, J. H. Irregular Solutions of Iodine. 605
- SHOULDERS, B. A. See Smith, W. B., 579, 2022
- SHOUP, C. S., JR. See Holmes, H. F., 3148
- SIECK, L. W., BLOCKER, N. K., AND FUTRELL, J. H. The Radiolysis of Propane at Extremely Low Conversions. 888
- SIECK, L. W., AND JOHNSEN, R. H. The Vapor Phase Radiolysis of Ethanol. 1699
- SIECK, L. W. See Futrell, J. H., 892
- SILBERT, L. S., DAUBERT, B. F., AND MASON, L. S. The Heats of Combustion, Formation, and Isomerization of Isomeric Monoglycerides. 2887
- SILVA, W. J. See Johnson, J. W., 1989, 3916
- SIMMERMAN, N. L. See Dahlgren, G., 3626
- SIMMONDS, B. A. W. See Cavell, E. A. S., 3657
- SIMONS, J. W., AND FLANAGAN, T. B. Diffusion of Hydrogen in the α -Phase of the Palladium-Hydrogen System. 3581
- SIMONS, J. W., AND FLANAGAN, T. B. Absorption Isotherms of Hydrogen in the α -Phase of the Hydrogen-Palladium System. 3773
- SIMPSON, H. N. See Carper, W. R., 1707
- SINFELT, J. H., TAYLOR, W. F., AND YATES, D. J. C. Catalysis over Supported Metals. III. Comparison of Metals of Known Surface Area for Ethane Hydrogenolysis. 95
- SINFELT, J. H., YATES, D. J. C., AND TAYLOR, W. F. Kinetics of the Reaction of Cyclopropane with Hydrogen over a Series of Silica-Supported Metals. 1877
- SINFELT, J. H. See Carter, J. L., 3070; Taylor, W. F., 3857
- SINGER, J. A. See Purcell, W. P., 691, 4097
- SINGER, S., KIM, N. G., MERKL, A. W., AND FARBER, M. Chemical Synthesis with Ion Beams. 799
- SINGH, A., AND FREEMAN, G. R. γ -Radiation-Induced Isomerization of Cyclohexanone to 5-Hexenal in the Liquid Phase. 666
- SINGH, A., AND KATZIN, L. I. Optical Rotatory Dispersion of *d*-Camphor. 3708
- SINGH, M. P. See Nath, N., 2038
- SINGH, R. B., AND RAI, D. K. Potential Curves and Bond Strength of PO. 3461
- SITE, A. D., AND MELE, A. γ -Radiolysis of Ethylene Sensitized by "Inert" Gases. 4033
- SKINNER, J. F., AND FUOSS, R. M. Effect of Pressure on Conductance. I. Tetraisoamylammonium Picrate in Diethyl Ether and in Benzene. 1437
- SKINNER, J. F. See Fucss, R. M., 2581
- SLATES, R. V., AND SZWARC, M. Dissociative Equilibria in the Systems Aromatic Hydrocarbon + Na⁺ \rightleftharpoons Radical Anion + Na⁺. 4124
- SLICHTER, W. P. See Anderson, J. E., 3099
- SLIEMERS, F. A. See Kircher, J. F., 189
- SMID, J. See Bhattacharyya, D. N., 608, 612, 624
- SMITH, A. L. See Parfitt, G. D., 661
- SMITH, K. J., JR. See Puett, D., 141
- SMITH, M. A., AND LEMMON, R. M. A Study of the Radical Termination Mechanisms in the Radiolysis of Crystalline Choline Chloride. 3370

- SMITH, M. B. See Wu, Y. C., 1868, 1873
- SMITH, M. L., GORDON, B. E., AND NELSON, R. C. A Radiotracer Study of Competitive Adsorption at the Gold-Oil Interface. 3833
- SMITH, P. R., AND RICHARDSON, J. W. Electron Density Shifts during Chemical Bond Formation. 3346
- SMITH, R. W. See Wood, R. H., 2974
- SMITH, S. R., SCHOR, R., AND NORRIS, W. P. The Mass Spectra of the Three Monodeuterated Propenes. 1615
- SMITH, W. B., AND COLE, G. M. The Nuclear Magnetic Resonance Spectra of Three Unsymmetrical *o*-Dihalo-benzenes. 4413
- SMITH, W. B., AND KOLLMANSBERGER, A. Some Aspects of Gel Permeation Chromatography. 4157
- SMITH, W. B., AND SHOULDERS, B. A. The Nuclear Magnetic Resonance Spectra of Some 1,4-Dihetero-cyclohexanes. 579
- SMITH, W. B., AND SHOULDERS, B. A. The Nuclear Magnetic Resonance Spectra of Some 9,10-Bridged 9,10-Dihydroanthracenes. 2022
- SMITH, W. R., AND FORD, D. G. Adsorption Studies on Heterogeneous Titania and Homogeneous Carbon Surfaces. 3587
- SMYTH, C. P. See Forest, E., 1302; Garg, S. K., 1294; Nelson, R. D., Jr., 1006
- SNELL, F. M. Reciprocal Relations among Transport Coefficients. 2479
- SOLLICH-BAUMGARTNER, W. A. See Garnett, J. L., 1850, 3526
- SOMMERFELD, J. T., AND PARRAVANO, G. Oxygen Chemisorption on Ruthenium Dioxide. 102
- SOULEN, J. R., AND CHAPPELL, W. H., JR. Polymorphism in Palladium(II) Chloride. 3669
- SOUSA, J. See Wettermark, G., 1584
- SPARKS, P. G. See Hamori, E., 1101
- SPEED, J. A. See Cavell, E. A. S., 3657
- SPENCER, H. G., AND ELLISON, T. M. Effects of pH and Divalent Cations on the Transport of Univalent Cations across a Weak-Acid Membrane. 2415
- SPINNLER, J. F., AND PATTERSON, A., JR. The Wien Effect in Uranyl Ion Solutions. I. Uranyl Nitrate and Perchlorate from 5 to 65°. Negative Wien Effects. 500
- SPINNLER, J. F., AND PATTERSON, A., JR. The Wien Effect in Uranyl Ion Solutions. II. Uranyl Fluoride from 5 to 65°. 508
- SPINNLER, J. F., AND PATTERSON, A., JR. The Wien Effect in Uranyl Ion Solutions. III. Uranyl Sulfate from 5 to 65°. 513
- SPINNLER, J. F., AND PATTERSON, A., JR. The Wien Effect in Mixed Electrolyte Solutions. I. Reference Electrolytes. 658
- SPOECK, C. R., AND COLEMAN, A. E. Relation of Ring Size to Ultraviolet Extinction Coefficient in Cyclo-siloxanes Containing Phenyl Substituents on Silicon. 1066
- SRINIVASAN, R., AND CREMER, S. E. Photochemical Rearrangement Reactions of 2-*n*-Propylcyclopentanone. 3145
- SRINIVASAN, R., LEVI, A. A., AND HALLER, I. The Thermal Decomposition of Bicyclo[1.1.0]butane. 1775
- STACY, C. J., AND ARNETT, R. L. Intrinsic Viscosity of Linear Polyethylene in a θ -Solvent. 3109
- STALEY, H. G. See Norman, J. H., 1373
- STARK, K. See Brown, T. L., 2679
- STAUFFER, C. E. The Measurement of Surface Tension by the Pendant Drop Technique. 1933
- STEEL, B. J. Transport Numbers in Aqueous Potassium Chloride Solutions at 0°. 3208
- STEELE, W. A. Properties of Partially Localized Adsorbed Monolayers. 3446
- STEIGMAN, J., AND LANDO, J. L. Salting in by an Aqueous Polyelectrolyte Solution. 2895
- STEIGMAN, J., AND SHANE, N. Micelle Formation in Concentrated Sulfuric Acid as Solvent. 968
- STEIN, G. See Forgacs, C., 4221; Navon, G., 1384, 1390
- STEIN, H. N., AND STEVELS, J. M. Remarks on the Hydration of Tricalcium Silicate. 2489
- STENGLE, T. R., AND LANGFORD, C. H. The Outer Coordination Sphere. I. Nuclear Magnetic Resonance Relaxation Time Effects Produced by Paramagnetic Ions with Nonlabile Inner Coordination Spheres. 3299
- STEPHENS, R. D. See Strom, E. T., 2131
- STERN, J. H., ANDERSON, C. W., AND PASSCHIER, A. A. Thermodynamic Properties of Aqueous Solutions of Mixed Electrolytes. The Hydrochloric Acid-Potassium Chloride System from 40 to 0°. 207
- STERN, J. H. See Paoletti, P., 3759
- STEVELS, J. M. See Stein, H. N., 2489
- STEVENS, K. L. See McFadden, W. H., 1742
- STEVENS, R. M. See Kanda, F. A., 3867
- STEVENSON, D. P. On the Monomer Concentration in Liquid Water. 2145
- STOCKMAYER, W. H. See Garland, C. W., 1718, 2469
- STOKES, R. A. See Knight, J. A., 678
- STOKES, R. H. Tracer Diffusion in Binary Solutions Subject to a Dimerization Equilibrium. 4012
- STOKES, R. H. See Dunn, L. A., 2808
- STOUGHTON, R. W. See Lietzke, M. H., 2395
- STOUT, N. D. See Westrum, E. F., Jr., 1520
- STRENG, A. G., AND STRENG, L. V. Molar Extinction Coefficients of O₂F₂ in the Visible Range and a Comparison with Other Oxygen Fluorides. 1079
- STRENG, L. V. See Streng, A. G., 1079
- STROM, E. T., RUSSELL, G. A., AND STEPHENS, R. D. Electron Spin Resonance of Aliphatic Semiquinones. 2131
- STROMBERG, R. R., TUTAS, D. J., AND PASSAGLIA, E. Conformation of Polystyrene Adsorbed at the θ -Temperature. 3955
- STRONG, J. D. See Yang, J. Y., 1157
- STUBBLEFIELD, C. T., RUTLEDGE, J. L., AND PHILLIPS, R. The Heats of Formation of Anhydrous Europium(II) Chloride and of the Aqueous Europium(II) Ion. 991
- STURGEON, G. D., AND EICK, H. A. Samarium Borides. The Tetraboride-Hexaboride Conversion. 3705
- STUTMAN, J. M. See Nagarajan, G., 2017
- SUART, R. D. See James, D. G. L., 2362
- SULLIVAN, J. O., AND WARNECK, P. Rate Constant for the Reaction of Oxygen Atoms with Acetylene. 1749
- SUNDHEIM, B. R., AND KELLNER, J. D. Thermoelectric Properties of the Molten Silver Nitrate-Sodium Nitrate System. 1204
- SUNDHEIM, B. R., AND SAUERWEIN, W. A Rotating-Disk Thermocell. I. Theory. 4042
- SUNDHEIM, B. R. See Trieff, N. M., 2044
- SUSI, H. Hydrogen Bonding of Amide Groups in Dioxane Solution. 2799
- SWANSON, T. B., AND LAURIE, V. W. Electron Magnetic Resonance and Electronic Spectra of Tetrachloroferrate(III) Ion in Nonaqueous Solution. 244
- SWIFT, H. E., LUTINSKI, F. E., AND KEHL, W. L. Investigation of the Metallic Phases in Reduced, Impregnated Nickel and Nickel-Copper Silica-Alumina Catalysts. 3268
- SWIFT, H. E. See Poole, C. P., Jr., 3663
- SWIGER, E. D., GREEN, P. J., MCKOWN, G. L., AND GRAYBEAL, J. D. Nuclear Quadrupole Resonance of Bi²⁰⁹ in BiBr₃. 949
- SWINEHART, D. F. See Conn, P. J., 2653
- SWINEHART, J. H. See Rogers, T. E., 134
- SWOFFORD, H. S., JR. See Elliott, G. R. B., 933
- SWORSKI, T. J. See Meisels, G. G., 815, 2867
- SZUTKA, A., THOMAS, J. K., GORDON, S., AND HART, E. J. Rate Constants of Hydrated Electron Reactions with Some Aromatic Acids, Alkyl Halides, Heterocyclic Compounds, and Werner Complexes. 289
- SZWARC, M. See Bhattacharyya, D. N., 608, 612, 624; Jagur-Grodzinski, J., 628; Slates, R. V., 4124
- TAIT, M. J. See Baddiel, C. B., 3634
- TAJIMA, Y. A. See Dauerman, L., 3668
- TAKAHASHI, F., AND LI, N. C. Hydrogen-Bonding Studies of Some Hindered Phenols with *N*-Methylacetamide and *N,N'*-Dimethylacetamide. 1622
- TAKAHASHI, F., AND LI, N. C. Proton Magnetic Resonance Studies of Hydrogen Bonding in Amine-Acetamide-Chloroform Systems. 2950
- TAKAHASHI, Y., AND WESTRUM, E. F., JR. Uranium

- Monoselenide. Heat Capacity and Thermodynamic Properties from 5 to 350°K. 3618
- TAKAHASHI, Y. See Westrum, E. F., Jr., 1520, 3192
- TAKASHIMA, S. A Study of Proton Fluctuation in Protein. Experimental Study of the Kirkwood-Shumaker Theory 2281
- TAKASHIMA, S., AND SCHWAN, H. P. Dielectric Dispersion of Crystalline Powders of Amino Acids, Peptides, and Proteins 4176
- TAKEGUCHI, N. See Kobatake, Y., 3981
- TAKESHITA, T., OHNISHI, R., MATSUI, T., AND TANABE, K. Acid Property and Structure of a Solid Metal Sulfate Catalyst. Change in Structure of Nickel Sulfates with Heating 4077
- TAMURA, M. See Osaki, K., 3642, 4183
- TANABE, K. See Takeshita, T., 4077
- TANAKA, I. See Koyano, K., 2545
- TANG, Y.-N., AND ROWLAND, F. S. Recoil Tritium Reaction: Ring Opening and Alkyl Replacement in Substituted Cyclopropanes 4297
- TANOURA, M. See Yasunaga, T., 3214
- TASAKA, M., MORITA, S., AND NAGASAWA, M. Membrane Potential in Nonisothermal Systems 4191
- TAUBE, H. See Jackson, J. A., 1844; Rogers, T. E., 134
- TAYLOR, E. G. See Davies, R. H., 704
- TAYLOR, H. A. See Narvaez, R., 2500
- TAYLOR, R. L. See Brown, T. H., 2316
- TAYLOR, W. F., SINFELT, J. H., AND YATES, D. J. C. Catalysis over Supported Metals. IV. Ethane Hydrogenolysis over Dilute Nickel Catalysts 3857
- TAYLOR, W. F. See Sinfelt, J. H., 95, 1877
- TERANISHI, S. See Wade, W. H., 590
- TERENIN, A., AND AKIMOV, I. Some Experiments on the Photosensitization Mechanism of Semiconductors by Dyes 730
- TEWARI, P. H., AND JOHARI, G. P. Dissociation Studies in High Dielectric Constant Solvents. III. Conductance of Magnesium Sulfate in Dioxane-Formamide Mixture at 25° 2857
- TEWARI, P. H. See Johari, G. P., 696, 2862, 3167
- THAKKAR, N. See Plumb, R. C., 439
- THEARD, L. M. Effects of Additives on the Radiolysis of Cyclohexane Vapor at 100° 3292
- THOMAS, F. G. See Kolthoff, I. M., 3049
- THOMAS, H. C. See Howery, D. G., 531; Laudelout, H., 339
- THOMAS, J. K. See Szutka, A., 289
- THOMAS, M. R., SCHERAGA, H. A., AND SCHRIER, E. E. A Near-Infrared Study of Hydrogen Bonding in Water and Deuterium Oxide 3722
- THOMMARSON, R. L. See Pritchard, G. O., 664, 1001, 2804
- THOMPSON, B. A., REEVES, R. R., JR., AND HARTECK, P. The Bromine Ultraviolet Lamp. Studies of the Oxygen-Ozone and Carbon Dioxide Equilibria 3964
- THOMPSON, C. C., JR., AND DE MAINE, P. A. D. Solvent Effects on Charge-Transfer Complexes. II. Complexes of 1,3,5-Trinitrobenzene with Benzene, Mesitylene, Durene, Pentamethylbenzene, or Hexamethylbenzene 2766
- THOMPSON, H. B. See LaPlanche, L. A., 1482
- THOMPSON, T. E. See Tsang, Y., 4242
- THOMSON, W. J. See Williams, K. C., 250
- TIEN, H. T. Interaction of Alkali Metal Cations with Silica Gel 350
- TIEN, H. T. Formation Constants of Silver(I) Cyanide Complexes in Equimolar Sodium-Potassium Nitrate Melts 3763
- TIMMONS, C. O., AND ZISMAN, W. A. Investigation of Fatty Acid Monolayers on Metals by Contact Potential Measurements 984
- TINOCO, I., JR. See Clark, L. B., 3615
- TOBOLSKY, A. V., JOHNSON, V., AND MacKNIGHT, W. J. Cleavage Reactions in Cross-Linked Urethane Elastomers 476
- TOCHER, M. I. See Conocchioni, T. J., 1106
- TODD, S. S. See Finke, H. L., 2094; Messerly, J. F., 353, 4304
- TOMBALAKIAN, A. S. See Worsely, M., 883
- TOMITA, Y., ANDO, T., AND UENO, K. Infrared Spectra of Nitrilotriacetate Chelates in Aqueous Solution 404
- TONG, L. K. J., REEVES, R. L., AND ANDRUS, R. W. The Effect of Solubilization by Surfactants on the Kinetics of Alkaline Decomposition of Indoaniline Dyes 2357
- TONG, S. See Garland, C. W., 1718, 2469
- TOOR, H. L. See Cullinan, H. T., Jr., 3941
- TOPOL, L. E. Thermodynamic Considerations in Molten Metal Salt Solutions 11
- TORRES, A. L. See Bonner, O. D., 4109
- TOYOSHIMA, Y. See Kobatake, Y., 3981
- TRAFICANTE, D. D., AND MACIEL, G. E. Carbon-13 Magnetic Resonance Spectra of 1-Substituted 1-Hexynes 1348
- TRAFICANTE, D. D. See Maciel, G. E., 1030
- TREINER, C., AND FUOSS, R. M. Electrolyte-Solvent Interaction. XVI. Quaternary Salts in Cyanoethylsucrose-Acetonitrile Mixtures 2576
- TREININ, A. See Gusarsky, E., 3176; Rotlevi, E., 2645
- TRIEFF, N. M., AND SUNDHEIM, B. R. The Effect of Solvent on the Acid-Base Kinetics of the Excited State of β -Naphthol 2044
- TROIANO, P. F. See Garland, C. W., 1188, 1195
- TRULSON, O. C., AND GOLDSTEIN, H. W. Mass Spectrometric Study of Zirconium Diboride 2531
- TRUMBORE, C. N. See Bristowe, W. W., 807
- TSANG, Y., AND THOMPSON, T. E. The Use of Combined Schlieren and Absorption Optics in an Electrophoretic Study of the Reversibly Interacting System Dextran Sulfate-Carboxyhemoglobin 4242
- TSCHIKOW-ROUX, E. The C-C Bond Dissociation Energy in C_2F_6 1075
- TURKDOGAN, E. T., MCKEWAN, W. M., AND ZWELL, L. Rate of Oxidation of Iron to Wustite in Water-Hydrogen Gas Mixtures 327
- TURNBULL, A. G. See Bear, I. J., 2828
- TURNER, J. C. R. See Butler, B. D., 3598
- TURNER, M. J. See Brummer, S. B., 3424
- TURNER, W. R., AND ELVING, P. J. Electrooxidation of the Tetraphenylborate Ion in Aqueous Solution at the Platinum Disk Electrode 1067
- TURTURO, A. See Bianchi, U., 4392
- TUTAS, D. J. See Stromberg, R. R., 3955
- UCHIYAMA, M. See Amano, A., 1278
- UENO, K. See Tomita, Y., 404
- UHARA, I., KISHIMOTO, S., YOSHIDA, Y., AND HIKINO, T. Dislocations as Active Centers of Catalysis and Chemical Action in Silver 880
- UNGER, I. Triplet State of Fluorobenzene 4284
- UNGNAD, H. E., LOUGHRAN, E. D., AND KISSINGER, L. W. 1,2-Dinitrotetrafluoroethane, Absorption Spectra and Bonding with Solvents 1758
- UNTERLEITNER, F. C., AND HORMATS, E. I. Rates of Decay of Phosphorescence from Triphenylene in Acrylic Polymers 2516
- UNTERLEITNER, F. C. See Hormats, E. I., 3677
- URBACH, V. See Heitner-Wirguin, C., 3400
- URRY, D. W., MILES, D., CALDWELL, D. J., AND EYRING, H. Optical Rotatory Dispersion of L-Cysteine-Cobalt Systems 1603
- UTIYAMA, H. Physicochemical Studies on Isotactic Polystyrene 4138
- UYTTERHOEVEN, J. B., CHRISTNER, L. G., AND HALL, W. K. Studies of the Hydrogen Held by Solids. VIII. The Decationated Zeolites 2117
- UYTTERHOEVEN, J. B. See Fripiat, J. J., 3274
- VACCA, A. See Paoletti, P., 3759
- VALANCE, W. G. See Schlag, E. W., 1431
- VALLEAU, J. P. Concerning the "Osmotic Term" in the Conductance Theory of Fuoss and Onsager 1745
- VAN CAUWELAERT, F. See Fripiat, J. J., 2458
- VAN DELL, R. D. See Jasper, J. J., 481
- VAN DEN TEMPEL, M., LUCASSEN, J., AND LUCASSEN-REYNDERS, E. H. Application of Surface Thermodynamics to Gibbs Elasticity 1798
- VAN THIEL, M., SEERY, D. J., AND BRITTON, D. Shock Waves in Chemical Kinetics. The Dissociation of Molecular Chlorine 834

- VAN WAZER, J. R. See Hofmeister, H. K., 791
- VENABLE, R. L., AND WADE, W. H. Pore Area and Adsorption Hysteresis for Packed Spheres. 1395
- VENABLE, R. L., WADE, W. H., AND HACKERMAN, N. Heats of Immersion. VIII. Differential Heats of Adsorption as a Function of Particle Size for the Alumina-Water System. 317
- VERDIN, D., HYDE, S. M., AND NEIGHBOUR, F. The Radiation-Induced Oxidation of *p*-Xylene Sensitized by Organic Bromine Compounds. 1992
- VIDULICH, G. A. See Kay, R. L., 4033
- VISCO, R. E. Kinetics and Equilibria of the System Indium(III)-Indium(I)-Indium(0) in Acidic Solution. 202
- VITUCCIO, T. See Kay, R. L., 4033
- VLADIMIROFF, T. Observations Concerning Directly and Nondirectly Bonded ¹³C-H Couplings with Respect to Symmetry Considerations. 3197
- VON HAHN, E. A., AND PETERS, E. The Role of Copper(I) in the Kinetics of Hydrogen Reduction of Aqueous Cupric Sulfate Solutions. 547
- VON WEYSENHOFF, H., AND PATAPOFF, M. Validity and Limitations of the Gas Titration of Atomic Nitrogen with Nitric Oxide. 1756
- VRBAŠKI, T. Kinetics of Processes Occurring on the Catalyst Surface during the Oxidation of *o*-Methylbenzyl Alcohol over Vanadia. 3092
- VRBAŠKI, T., AND MATHEWS, W. K. The Catalytic Vapor Phase Oxidation of *o*-Methylbenzyl Alcohol. 457
- VRENTAS, J. S. See Duda, J. L., 3305
- WACHI, F. See Hecklen, J., 693
- WADE, W. H. The Coordination Number of Small Spheres. 322
- WADE, W. H., TERANISHI, S., AND DURHAM, J. L. The Dehydration of Ethanol on Aluminas of Various Specific Surface Areas. 590
- WADE, W. H. See Hackerman, N., 314; Venable, R. L., 317, 1395
- WADSO, I. See Fitzgibbon, G. C., 2464
- WAGNER, C. D. See Barter, C., 491
- WAHLBECK, P. G. See Lieberman, M. L., 3514, 3973; Yannopoulos, L. N., 2510
- WALL, L. A. See Yu, H., 2072
- WALMSLEY, D. A. G. See Peterson, D. B., 2880
- WALTERS, W. D. See Carr, R. W., Jr., 1073
- WALTON, A. G. See Parfitt, G. D., 661
- WALWICK, E. R. See Bean, R. C., 4368
- WANG, C. See Boyd, R. H., 3906
- WANG, J. H. Self-Diffusion Coefficients of Water. 4412
- WARNECK, P. See Sullivan, J. O., 1749
- WARNER, J. See Orttung, W. H., 3188
- WARNER, T. B., AND SEIFERT, R. L. Electronic Commutator Determination of E° of Formation and Related Thermodynamic Quantities for Molten Lead Chloride. 1034
- WASON, S. K., AND PORTER, R. F. Infrared Spectrum of HBBr₂(g). 2461
- WASON, S. K. See Barton, L., 3160; Porter, R. F., 2208
- WATKINS, K. W., AND MOSER, H. C. Reaction of Tritium Atoms with Films of Solid Ethylene. Disproportionation and Combination of Ethyl Radicals at 63°K. 1040
- WATSON, A. E. P., MCLURE, I. A., BENNETT, J. E., AND BENSON, G. C. Excess Properties of Some Aromatic-Alicyclic Systems. I. Measurements of Enthalpies and Volumes of Mixing. 2753
- WATSON, A. E. P. See McLure, I. A., 2759
- WATSON, I. D. See Carson, J. L., 3200
- WATT, I. C. See Leeder, J. D., 3280
- WAY, K. R., AND RUSSELL, M. E. An Apparently Primary CH₃⁺ Ion in the Mass Spectrum of 2-Methoxyethanol. 4420
- WEEKS, B. M., COLE, S. A., AND GARRISON, W. M. Reactions of Alanine with the Reducing Species Formed in Water Radiolysis. 4131
- WEIHER, J. See Greenbaum, M. A., 4035
- WEINSTEIN, J. See Wettermark, G., 1584
- WELLS, P. R. Common Scaling of the Hammett and Taft Equations. 1787
- WELTNER, W., JR., AND McLEOD, D., JR. Spectroscopy of Titanium, Zirconium, and Hafnium Oxides in Neon and Argon Matrices at 4 and 20°K. 3488
- WEN, W.-Y., AND SAITO, S. Activity Coefficients and Molal Volumes of Two Tetraethanolammonium Halides in Aqueous Solutions at 25° 3569
- WENDT, R. P. The Estimation of Diffusion Coefficients for Ternary Systems of Strong and Weak Electrolytes. 1227
- WENTORF, R. H., JR. The Behavior of Some Carbonaceous Materials at Very High Pressures and High Temperatures. 3063
- WERNER, H. R., AND FIRESTONE, R. F. Kinetics of the γ -Ray-Induced Decomposition of Chloroform. 840
- WEST, R. See Kramer, F. A., Jr., 673
- WEST, W., AND PEARCE, S. The Dimeric State of Cyanine Dyes. 1894
- WESTRUM, E. F., JR., TAKAHASHI, Y., AND GRØNVOLD, F. λ -Type Thermal Anomaly in Tetrauranium Enneaoxide at 348°K. 3192
- WESTRUM, E. F., JR., TAKAHASHI, Y., AND STOUT, N. D. The Heat Capacity and Thermodynamic Properties of Hypostoichiometric Thorium Dicarbide from 5 to 350°K. 1520
- WESTRUM, E. F., JR. See Carlson, H. G., 1524; Chang, E. T., 2176; Clever, H. L., 1209, 1214, 1983; Takahashi, Y., 3618
- WETTERMARK, G., WEINSTEIN, J., SOUSA, J., AND DOGLIOTTI, L. Kinetics of *cis-trans*-Isomerization of *para*-Substituted *N*-Benzylideneanilines. 1584
- WHALLEY, E. See Baliga, B. T., 1751
- WHEELWRIGHT, E. J., FLEMING, D. M., AND ROBERTS, F. P. Calorimetric Determination of the Mean β -Energy and Half-Life of Promethium-147. 1220
- WHEITSEL, K. B., AND LADY, J. H. Infrared Studies of Amine Complexes. III. Association of Aniline and *N*-Methylaniline with Benzene, *N,N*-Dimethylaniline, Pyridine, and *N,N*-Dimethylcyclohexylamine. 1596
- WHITAKER, S. See Johannes, W., 1471
- WHITE, J. E. See Parkinson, W. W., 828
- WHITE, R. C. AND PARCELL, L. J. The Photolysis of Trifluoronitrosomethane. 4409
- WHITEHEAD, R. See Rice, C. L., 4017
- WHITTAKER, M. P., EYRING, E. M., AND DIBBLE, E. Kinetics of Uranyl Ion Hydrolysis and Polymerization. 2319
- WHITTEN, G. Z., AND RABINOVITCH, B. S. The Chemically Activated Decomposition of *n*-Butane and of Isobutane. 4348
- WIEWANDT, T. A. See Mulford, R. N. R., 1641
- WILLIAMS, J. W. See Osterhoudt, H. W., 1050
- WILLIAMS, K. C., DANIEL, J. L., THOMSON, W. J., KAPLAN, R. I., AND MAATMAN, R. W. Reactions of Aqueous Salts with High Area Aluminas. 250
- WILLIAMSON, A. G. See Carson, J. L., 3200
- WILLIX, R. L. S., AND GARRISON, W. M. The Effect of Cupric Ion on the Radiation Chemistry of Aqueous Glycine. 1579
- WILSON, J. W. See Lichtin, N. N., 3673; Schlafer, W. G., 1530
- WING, R. M., AND HARRIS, G. M. Mechanism of the Solid-State Thermal Decomposition of Potassium Trisoxalatochromium(III) Trihydrate. 4328
- WINKEL, D. Theoretical Refinement of the Pendant Drop Method for Measuring Surface Tensions. 348
- WINTERS, R. E., AND KISER, R. W. Ions Produced by Electron Impact with the Dimetallic Carbonyls of Cobalt and Manganese. 1618
- WINTERS, R. E., AND KISER, R. W. Ionization Potentials and Mass Spectra of Cyclopentadienylmolybdenum Dicarboxyl Nitrosyl and 1,3-Cyclohexadieneiron Tricarbonyl. 3198
- WISWALL, R. H., JR. See MacKenzie, D. R., 2526
- WITHERS, G. L. See Cubicciotti, D., 4030
- WITHERSPOON, P. A., AND SARAF, D. N. Diffusion of Methane, Ethane, Propane, and *n*-Butane in Water from 25 to 43° 3752
- WODETZKI, C. M., McCUSKER, P. A., AND PETERSON, D. B. Effect of Density on the Radiolysis of Ethane. 1045
- WODETZKI, C. M., McCUSKER, P. A., AND PETERSON, D. B. Effect of Additives in Radiolysis of Ethane at High Densities. 1056
- WOLFE, R., AND SAMS, J. R. The Virial Theory of Adsorption and the Surface Areas of Solids. 1129
- WONG, W.-K. See Clever, H. L., 1209

- WOOD, R. H., AND D'ORAZIO, L. A. Thermodynamics of the Higher Oxides. II. Lattice Energies of the Alkali and Alkaline Earth Peroxides and the Double Electron Affinity of the Oxygen Molecule. 2558
- WOOD, R. H., AND D'ORAZIO, L. A. Thermodynamics of the Higher Oxides. III. The Lattice Energy of Potassium Ozonide and the Electron Affinity of Ozone. 2562
- WOOD, R. H., AND SMITH, R. W. Heats of Mixing of Aqueous Electrolytes. I. Concentration Dependence of 1-1 Electrolytes. 2974
- WOOD, R. H. See D'Orazio, L. A., 2550; Jongenburger, H. S., 4231
- WORSELY, M., TOMBALAKIAN, A. S., AND GRAYDON, W. F. Cation Interchange across Ion-Exchange Membranes. 883
- WU, C.-H. See Hopkins, H. P., Jr., 2244
- WU, Y. C., SMITH, M. B., AND YOUNG, T. F. Heats of Mixing of Electrolytes Having Common Ions. 1868
- WU, Y. C., SMITH, M. B., AND YOUNG, T. F. Heats of Mixing of Electrolytes of the 1-1 Charge Type. 1873
- WULFF, C. A. See Clever, H. L., 1983; Hopkins, H. P., Jr., 6, 9, 1980; Rupert, J. P., 3059
- WUNDERLICH, B. Specific Heat of Polyethylene Single Crystals. 2078
- WUNDERLICH, F. J. See Rice, F. O., 2137
- YAMAGUCHI, T. See Inoue, E., 767
- YANG, C. H. See Gray, B. F., 2747
- YANG, J. Y., AND MARCUS, I. Radiolysis of Cyclohexane- d_{12} -Cyclopentane Mixtures. 3113
- YANG, J. Y., STRONG, J. D., AND BURR, J. G. Linear Energy Transfer Effects in the Radiolysis of Liquid Aromatic Hydrocarbons. 1157
- YANG, K., GANT, P. L., AND COOPER, D. E. Determination of Potential Parameters for Gas-Solid Interactions from Quantum Effects in Physical Adsorption. 1768
- YANG, S. L. See Jagur-Grodzinski, J., 628
- YANKWICH, P. E., AND ZAVITSANOS, P. D. Pyrolysis of Magnesium Oxalate: Kinetics and Stoichiometry. 442
- YANKWICH, P. E., AND ZAVITSANOS, P. D. Carbon Isotope Effects in the Pyrolytic Decomposition of Magnesium Oxalate. 918
- YANKWICH, P. E. See Haleem, M. A., 1729, 2392
- YANNOPOULOS, L. N., EDWARDS, R. K., AND WAHLBECK, P. G. The Thermodynamics of the Yttrium-Hydrogen System. 2510
- YAO, Y.-F. Y. Adsorption of Gases on Alkali Fluorides. 2472
- YAO, Y.-F. Y. Adsorption of Polar Molecules on Metal Oxide Single Crystals. 3930
- YASUNAGA, T., TANOURA, M., AND MIURA, M. The Abnormal Relation between the Velocity of Sound and the Temperature in Sodium Sulfate Solution. 3214
- YATES, D. J. C. The Stability of Metallic Cations in Zeolites. 1676
- YATES, D. J. C. See Carter, J. L., 3070; Sinfelt, J. H., 95, 1877; Taylor, W. F., 3857
- YOSHIDA, Y. See Uhara, I., 880
- YOUNG, L. B. See Neuman, R. C., Jr., 1777, 2570
- YOUNG, R. A., GATZ, C. R., AND SHARPLESS, R. L. Ion-Catalyzed Recombination of Atomic Nitrogen and the Pink Glow. 1763
- YOUNG, T. F. See Wu, Y. C., 1868, 1873
- YU, H., AND WALL, L. A. Radiolytic Stress Relaxation of an Ethylene-Propylene Copolymer. 2072
- YUE, R. H.-S. See Lumry, R., 1162
- YUN, H. B., AND MOSER, H. C. Disproportionation and Combination of Tritium-Labeled Isopropyl Radicals. 1059
- ZAHRA, A., AND NOYES, W. A., JR. The Photochemistry of Methyl Isopropyl Ketone. 943
- ZAJAC, W. W., JR., AND NOWICKI, R. B. The Acidity Function, H_0 , of Hydrogen Bromide in Acetic Acid-Water Mixtures. 2649
- ZANGEN, M. Solvent Extractions from Molten Salts. IV. Kinetics of the Formation of Mercury(II) Bromide Species. 1835
- ZAVITSANOS, P. D. See Yankwich, P. E., 442, 918
- ZAWOYSKI, C. See Evans, D. F., 3878; Kay, R. L., 4208
- ZELDENRUST, H. See Mijnlief, P. F., 689
- ZIELINGER, J. P. See Nikitine, S., 745
- ZIELINSKI, M. Carbon-13 Isotope Effects in the Oxidation of Acetic Acid. 1428
- ZIFFLE, H. M. See Berni, R. J., 1882
- ZIMM, B. H. See Harrington, R. E., 161
- ZISMAN, W. A. See Bewig, K. W., 4238; Timmons, C. O., 984
- ZOUAGHI, M. See Nikitine, S., 745
- ZUBER, W. H., JR. See Dawson, L. R., 1335
- ZWEIFEL, G. See Savitsky, G. B., 3105
- ZWELL, L. See Turkdogan, E. T., 327
- ZYBKO, W. C. See Copeland, J. L., 3631

SUBJECT INDEX to Volume 69, 1965

- Absorption, exciton, relationship between photoelectric effect and, 745; role of amino groups in absorption of water by keratin, 3280; of hydrogen by gold-palladium alloys, 3575; charge-transfer, and luminescence spectra of alkyl halide salts of pyridine, 3791; n.m.r., in anhydrous sodium soaps, 4256
- Acetaldehyde hydrate, rates of dehydration of, 4325
- Acetate, phenol-, system, use of fluorescence measurements to determine association constants for weak complexes, 2960
- Acetic acid, -acetic anhydride mixtures, electrical conductance and dielectric constant of, 700; C^{13} magnetic resonance study of protonation of, 1030; oxidation of, C^{13} isotope effects, 1428; diffusion in dilute aqueous solution of, 2341; chemical shift of hydroxyl proton of, as function of concentration in acetic anhydride, acetone, and 1,4-dioxane, 2564; dissociation constant in deuterium oxide, reference points for pD scale, 2750
- Acetic anhydride, -acetic acid mixtures, electrical conductance and dielectric constants, 700
- Acetone, radiolysis of, in air-free aqueous solutions, 1366; existence of monomer and monomer monohydrate in 1,2-dichloroethane, 2980; -benzene-carbon tetrachloride system, diffusion in, 3941
- Acetonitrile, quaternary salts in cyanoethylsucrose-acetonitrile mixtures, 2576; liquid junction potential between acetonitrile solution and aqueous saturated calomel electrode, 3049; spectral studies of nonaqueous solutions of silver nitrate in, 3634; -methanol mixtures, dielectric constants of, 3657; n.m.r. study, 4152
- Acetyl radical, formation and decomposition reactions of, 1022
- Acetylene, gaseous, ionic reactions in, 572; rare gas sensitized radiolysis of, 892; Hg-photosensitized decomposition of, in presence of NO, 1732; production in radiolysis of methane, 3218
- Acetylenic acids, acidity and autocatalysis of esterification of, 928
- Acid sites, Lewis and Brønsted, structure and properties of amorphous silicoaluminas, 3274
- Acidity function, of hydrogen bromide in acetic acid-water mixtures, 2649
- Acids, extraction by basic organic solvents, 1106
- Acridine orange hydrochloride, dimer spectrum of, 3872
- Acrylamide, thionine-nitrotropionamide-acrylamide system, dye-sensitized photopolymerization processes, 641; kinetics and mechanism of thionine- β -diketone-acrylamide systems, photopolymerization processes, 2842; irradiated, e.s.r. spectra of, 3712
- Activation energy, of viscous flow of pure and sea water in temperature region of maximum density, 3988
- Activity, of FeO in liquid iron oxide, 804; of three components in system water-nitric acid-uranyl nitrate hexahydrate, 1904
- Activity coefficients, of cadmium chloride in mixed aqueous solution with benzyltrimethylammonium chloride, 681; of NaCl and KCl in N,N-dialkylamides containing water, 1377; of trinitrotriamminecobalt(III) in aqueous salt solution, 1546; of NaCl by cation-sensitive glass electrodes, 2697; and molal volumes of two tetraethanolammonium halides, 3569; single-ion, of gegenions in sodium polyacrylate, 3690; relative, of chloride and silver ions in aqueous sulfuric acid, 3906; of NaCl in aqueous three-component solutions by cation-sensitive glass electrodes, 3992; mean, of sodium polyacrylate, 4102; for divalent salts of *p*-toluenesulfonic, dibenzylsulfonic, and 1,2,3-triphenylpropanetrilsulfonic acid, 4345
- Adsorption, equilibrium, of carbon dioxide on zinc oxide, 17; of ammonia on dry γ -alumina, 231; on smooth Pt from HCOOH solutions using large anodic galvanostatic transients, 562; virial theory of, and surface area of solids, 1129; CO, on Pt electrodes, galvanostatic studies of, 1355; of cyclohexane on aluminas prepared by thermal decomposition of aluminum hydroxide *in vacuo* and in air, 1805; of gases on alkali fluorides, 2472; hydrogen, on zinc oxide, 2500; of nonylphenoxyacetic acid by metals, 2598; electrochemical, of organic ions and molecules, Esin and Markov effect, 3411; of propane on smooth Pt electrodes, 3424; of CO, N₂, O₂, and Ar on heterogeneous titania and homogeneous carbon surfaces, 3587; competitive, radiotracer study at gold-oil interface, 3833; of polar molecules on metal oxide single crystals, 3930; of hexachloroacetone on alumina-containing surfaces, 3949; of ethane, *n*-butane, and *n*-octane on poly(tetrafluoroethylene), 4387
- Aging, of silica and alumina gels, 1530
- Alanine, reactions with reducing species formed in water radiolysis, 4131
- Alcohol, aqueous, effect on thermal transition of ribonuclease, 298; -water solutions, partial molal volumes of, 3795; e.p.r. study of oxidation by Fenton's reagent, 3805
- Alcohols, normal primary, three dielectric dispersion regions of, 1294; long-chain aliphatic, surface viscosity of monomolecular films of, 1789; H-bonding properties of, 2494
- Alkali fluorides, adsorption of gases on, 2472
- Alkali halides, liquid binary systems, surface tension of, 2606; molten, compressibility of, 2785; pulse radiolysis of, 4421
- Alkali metal cations, interaction with silica gel, 350; behavior in pores of silica gel, 3196
- Alkali metal halides, heats of solution in anhydrous N-methylformamide, 2611
- Alkali metal perchlorates, catalytic decomposition by manganese dioxide, 1114
- Alkali metals, reaction of triphenylphosphine with, in tetrahydrofuran, 2775
- Alkali metal salts, conductance of, in hydrogen cyanide, 704
- Alkaline earth halides, lattice energies for, 3611
- Alkaline earth perchlorates, product yields and stoichiometry in radiation-induced decomposition of, 359; mechanism of radiation-induced decomposition, 377
- Alkali nitrates, fused, oxygen electrodes in, 3662
- Alkali perchlorates, product yields and stoichiometry in radiation-induced decomposition of, 359; mechanism of radiation-induced decomposition, 377
- n*-Alkanes, solid, nuclear spin relaxation in, 3099
- Alkylbenzenes, π -complex adsorption in exchange of, 1830
- Alkyl cyanides, C^{13} magnetic resonance study, 3920
- Alkylcyclopropanes, vibrationally excited, structural isomerization of, quantum statistical weight effects, 1973
- Alkyl halides, rate constants of hydrated electron reactions with, 289; -silver nitrate reaction, silver nitrate ion pairs in, 661
- Alkyl isocyanates, C^{13} magnetic resonance study, 3920
- Alkyl isocyanides, C^{13} magnetic resonance study, 3920
- Alkyl isothiocyanates, C^{13} magnetic resonance study of, 3920
- Alkyltropylium salts, as association colloids in concentrated acid media, 1466
- Allotropy, of beryllium chloride, 3839
- Alloys, platinum-gold, electrochemical characterization of surface composition of, 901
- γ -Alumina, infrared and gravimetric study of surface hydration of, 211; model for surface of, 220; dry, infrared study of adsorption of ammonia on, 231
- Alumina gel, aging of, 1530
- Aluminas, reactions of aqueous salts with high area aluminas, 250; -water system, differential heats of adsorption as function of particle size for, 317; having various specific surface areas, dehydration of ethanol on, 590; prepared by thermal decomposition of aluminum hydroxide *in vacuo* and in air, adsorption of cyclohexane on both, 1805; exchange of deuterium with hydroxyl groups of, 3070; exchange of hydroxyl groups of, with deuterated methane, 3080; metallic phases in reduced, impregnated Ni and Ni-Cu silica-alumina catalysts, 3268
- Aluminum alkyls, n.m.r. study of, 3418
- Aluminum cations, structure of, in aqueous solutions, 2458
- Aluminum(I) chloride(g), heat of formation of, 3001
- Aluminum(III) chloride(g), entropy of, 3001
- Aluminum(I) fluoride(g), enthalpy of formation and entropy of, 2311
- Amides, N-monosubstituted, n.m.r. study of hydrogen bonding of, 1482; long-chain aliphatic, surface viscosity of monomolecular films of, 1789; hindered rotation and C^{13} -H coupling constants in, 2570; hydrogen bonding of amide groups in dioxane solution, 2799

- Amidines, hindered rotation and C^{13} -H coupling constants in, 2570
- Amine complexes, association of aniline and N-methylaniline with benzene, N,N-dimethylaniline, pyridine, and N,N-dimethylcyclohexylamine, 1596
- Amines, secondary, association with tetrahydrofuran, 335; exchange of substituents on nitrogen in molten ammonium salts and, 791; long-chain aliphatic, surface viscosity of monomolecular films of, 1789; aromatic, ionization potentials, 3506
- Amino acid esters, transition metal ion promoted hydrolyses of, 2923
- Amino acids, dielectric dispersion of crystalline powders of, 4176
- Amino groups, role in water absorption by keratin, 3280
- 3-Amino-4-methylbenzenesulfonic acid, thermodynamic study of ionization of, 2653
- Ammonia, infrared study of adsorption of, on dry γ -alumina, 231; thermodynamics of protonation of, 3759
- Ammonium ion, limiting equivalent conductance to 300°, 2984
- Ammonium perchlorate, γ -radiolysis of, 2477
- Ammonium salts, molten, exchange of substituents on nitrogen in, 791
- Aniline, association with benzene, N,N-dimethylaniline, pyridine, and N,N-dimethylcyclohexylamine, 1596; chloranil-, complexes, charge-transfer complexes and donor molecule properties, 1707; p.m.r. studies of hydrogen bonding in amine-acetamide-chloroform systems, 2950
- Anion exchange, of chloride complexes of zinc, cadmium, and mercury in anhydrous ethanol, 2955; in concentrated solutions, 3440
- Anodic organic reactions, kinetic theory of inhibition and passivation in, 1259
- Anthracene, effect of oxygen on e.s.r. spectra of, 1082; crystal structures of equimolar π -molecular compounds of, and perylene with pyromellitic dianhydride, 2160; triplet states of, 2239
- Antimony iodide, thermodynamic functions and absolute entropy, 3621
- Argon, solubility in sea water, 2608; solubility in water and dilute aqueous nonelectrolyte solutions, 3245; solubility in water and aqueous solutions of electrolytes, 3250; adsorption on heterogeneous titania and homogeneous carbon surfaces, 3587; solubility to 451 atm. in fused sodium nitrate, 3631
- Aromatic acids, rate constants of hydrated electron reactions with, 289
- Arsenic pentafluoride, enthalpy of formation of, 4358
- Arsenic triiodide, vapor pressure, enthalpy, and absolute entropy, 2743
- Arylphosphine complexes, of Co(II) and Ni(II), p.m.r. line widths, ligand exchange and electronic relaxation times for, 3212
- Association, ion, kinetic study in manganese sulfate solutions using ultrasonic absorption, 128; of secondary amines with tetrahydrofuran, 335; self-, in halomethanes and haloethanes, 446; of Cu^{2+} and SO_4^{2-} in aqueous solutions of constant ionic strength, 1537; of aniline and N-methylaniline with benzene, N,N-dimethylaniline, pyridine, and N,N-dimethylcyclohexylamine, 1596; of 2,4,6-trimethylpyridine and trifluoroiodomethane, 2400; ionic, of KCl and CsCl in ethanol-water mixtures, 2420; self-, of acids and bases in 1,2-dichloroethane and other solvents, differential vapor pressure study, 2690; of cesium chloride in anhydrous methanol, 2787; ionic, of thionine, fluorescence and solvent effects, 2988
- Association constants, for tetrapropylammonium bromide in acetone and ethylidene chloride, 543; use of fluorescence measurements to determine, for weak complexes, 2960
- Azidopentaamminecobalt(III) azide, solid, thermal decomposition of, 1723
- Azobenzene, chlorophyllide-sensitized reduction of, 2779
- Azo compounds, temperature dependence of *cis-trans* photoisomerization of, 1062
- Bacillus subtilis* α -amylase, equilibrium constant for dimerization of, 1829
- Barium, -sodium equilibrium system, 3867; -iron-oxygen compounds with varying oxygen content and iron valence, 4395
- Barium hydroxide octahydrate, solution thermochemistry of, 1980
- Benzanthracene, triplet state of, 2239
- Benzene, thermal decomposition in flow system, 863; fluorescence of, 1343; molecules, mean-square perpendicular amplitudes and shrinkage effects in, 1489; -butene-2 mixtures, effect of galvinoxyl on, 1866; radiolysis of benzene-cyclohexane mixtures and, in presence of nickel tetracarbonyl, 2034; solvent effects on charge-transfer complexes of 1,3,5-trinitrobenzene with, 2766; diffusion in cyclohexane-benzene system, 2783; dioxane-, mixtures, radiolysis and luminescence behavior of, 3024; intradiffusion and derived frictional coefficients for, and cyclohexane in their mixtures, 3116; -polyphenyl systems, gas-liquid partition chromatography, 3682; diffusion in system acetone-benzene-carbon tetrachloride, 3941; electric moments of N-alkyl substituted nicotinamides from measurements in benzene-dioxane solutions, 4097
- Benzene- d_6 , fluorescence of benzene and, 1343
- Benzidine rearrangement, development of method for electrode processes in which first-order chemical reaction follows charge transfer, 30
- Benzoate, radiolytic decarboxylation of, determination of relative rate constants for hydroxyl radical reactions, 1938
- Benzoic acid, pyridine-, complex, infrared study of hydrogen bond in, 74; C^{13} magnetic resonance study of protonation of, 1030; C^{13} -labeled, integrated absorption intensity of C=O stretching band of, 2256
- Benzoyle peroxide, reaction with Rhodamine 6GX color base, 4071
- N-Benzylideneanilines, *para*-substituted, kinetics of *cis-trans* isomerization of, 1584
- Benzyltrimethylammonium chloride, activity coefficients of cadmium chloride in mixed aqueous solution with, 681
- Beryllium chloride, thermodynamic properties and allotropy of, 3839
- Beryllium fluoride, enthalpy and entropy of sublimation, 1069
- Beryllium hydroxides, thermodynamic properties of, 2828
- Beryllium oxide, heat of fusion and high temperature heat capacity of, 4035; -boron oxide system, thermodynamics of vaporization in, 4250
- Bichromate ion, kinetics of hydrolysis of, in acetate buffer and acid catalysis, 1736
- $\Delta^{2,5}$ -Bicyclo[2.2.1]heptadiene, photochemistry of, 2475
- Bio-Rex 63, kinetics of ion exchange in phosphonic resin, 3400
- Biphenyl, mass spectra and appearance potentials of principal ions of, 2935
- 2,2'-Bipyridine, proton n.m.r. spectrum of, 673
- 2,2'-Bipyridyl, n.m.r. spectra of, 4166
- Bismuth, bismuth iodide-iodine phase diagram, 124
- Bismuth-209, nuclear quadrupole resonance in solid $BiBr_3$, 949
- Bismuth bromide, nuclear quadrupole coupling of Bi^{209} nucleus in solid $BiBr_3$, 949; critical temperature and coexistence curve for, 1989
- Bismuth chloride, molten, vapor pressure and enthalpy of vaporization of, 3916
- Bismuth iodide, thermodynamic functions and absolute entropy, 3621
- Bisulfate ion, limiting equivalent conductance to 400°, 2984
- Bisulfates, fused, as solvents in galvanic cells, 3156
- Bond dissociation energy, C-C, in C_2F_6 , 1075
- Bond formation, chemical, electron density shifts during, 3346
- Bond strength, of PO, 3461
- Boron, infrared spectrum of $HbBr_2(g)$, 2461; thermochemistry of interconversion of $H_2B_2O_5(g)$ and boroxine gas, 3160
- Boron halide, ether-, molecular addition compounds in dichloromethane, n.m.r. study, 89
- Boron oxide, thermodynamics of vaporization in beryllium oxide-, system, 4250
- Boron trifluoride, exchange between ethyl ether- BF_3 and tetrahydrofuran- BF_3 and between ethyl ether- BF_3 and ethyl sulfide- BF_3 , 527; heat of reaction with $HF \cdot 3.75H_2O$, 1010; reaction of boroxine with, infrared spectrum and stability of $HBF_2(g)$, 2208
- Boroxine, reaction with $BF_3(g)$, infrared spectrum and stability of $HBF_2(g)$, 2208
- α -Brass, dilation contribution to heat capacity of copper and, at elevated temperatures, 4162
- Bromate ions, radiolysis by Co^{60} γ -rays, identification of species formed, 1413
- Bromine, surface tension in reciprocal system K^+ , Cd^{+2} - Cl^- , Br^- , 1443; effect of experimental parameters on (n, γ)-activated reactions of, with liquid cyclohexane, 2795; evidence for Br^{82m} isomeric transition activated reactions in saturated hydrocar-

- bonds and alkyl halides, 2806; heats of formation of solid solutions in systems (Na-Ag)Cl and (Na-Ag)Br, 3531
- Bromine ultraviolet lamp, studies of oxygen-ozone and CO₂ equilibria, 3964
- Bromoacetic acid, halogen displacement reactions of, 854
- Butadiene, reactivity of perfluoroalkylnitriles toward, 1070
- n*-Butane, diffusion in water, 3752; adsorption on poly(tetrafluoroethylene), 4387; chemically activated decomposition of, 4402
- 1,4-Butanediol, diglycidyl ether of, kinetics of zinc fluoroborate and hydrogen ion catalyzed hydrolyses of, 1882
- 1-Butanol, partial volumes of, in dilute aqueous solutions, 2406
- Butene-2, benzene-, mixtures, effect of galvinoxyl on radiolysis of, 1866
- t*-Butylamine, p.m.r. studies of hydrogen bonding in amine-acetamide-chloroform systems, 2950
- Butylammonium isobutyrate, ion-pair formation in aqueous solutions of, 2801
- n*-Butylbenzene, low-temperature thermodynamic properties of, 4304
- ¹⁵N-*n*-Butylformamide, *cis*- and *trans*-, p.m.r. spectra of, 3648
- Cadmium, solvent vapor pressures in dilute solutions of Ga in Cd, 933; surface tension in reciprocal system K⁺, Cd⁺²-Cl⁻, Br⁻, 1443; Ga-, system, discussion of apparent violation of Gibbs-Duhem equation, 2135; anion exchange of chloride complexes of, 2955; Ga-Cd system, apparent violation of Gibbs-Duhem relation, 3222
- Cadmium chloride, activity coefficients of, in mixed aqueous solution with benzyltrimethylammonium chloride, 681; e.m.f. studies in water, water-ethanol, and ethanol, 2082
- Cadmium fluoride, Knudsen and Langmuir measurements of sublimation pressure of, 3174
- Cadmium hydroxide, thermal decomposition of, 450
- Cadmium iodide, -water system, diffusion in, 1718
- Calcium formate, pyrolysis in KBr matrix, kinetic study, 583
- Calcium hydroxide, solution thermochemistry of, 6
- Calcium oxide, solubility relationships in CaO-silica-water system, 182
- Calomel electrode, aqueous saturated, liquid junction potential between acetonitrile solution and, 3049
- Calorimetry, mean β -energy and half-life of promethium-147, 1220; solution, comparison standards for, 2902
- d*-Camphor, optical rotatory dispersion, 3708
- Carbohydrates, addition complex between dimethyl sulfoxide and, 656
- Carbon, graphitic acid of pyrolytic carbon and its heat treatment, 2462; adsorption on heterogeneous titania and homogeneous carbon surfaces, 3587
- Carbon-13, isotope fractionation in pyrolytic decomposition of magnesium oxalate, 918; chemical shifts of vinyl carbons, 1947
- Carbonaceous materials, behavior at high temperatures and pressures, 3063
- Carbon dioxide, thermodynamics of adsorption on zinc oxide, 17; radiation yields of, for aromatic carbonyl compounds, 1077; formation of CO₂⁻ radical ions when CO₂ is adsorbed on irradiated MgO, 2182; bromine ultraviolet lamp, studies of oxygen-ozone and CO₂ equilibria, 3964; photosensitization with Hg 6 ³P₁ atoms, 4047
- Carbon-13-hydrogen couplings, directly and nondirectly bonded, observations with respect to symmetry, 3197
- Carbon monoxide, radiation yields of, for aromatic carbonyl compounds, 1077; chemisorbed on evaporated nickel films, infrared spectrum, 1195; galvanostatic studies of CO adsorption on Pt electrodes, 1355; comparison of adsorbed formic acid and, on Pt electrodes, 1363; electrostatic forces within CO molecule, 2132; adsorption on heterogeneous titania and homogeneous carbon surfaces, 3587; effect of oxygen adsorbed in skin of Pt electrode on determination of CO adsorption, 4048; adsorbed, estimation of, on smooth Pt by anodic stripping, correction for electrode oxidation, 4049
- Carbon suboxide, heats of formation and polymerization, 3603
- Carbon tetrachloride, cyclohexane-, Duomeen T Diolate system, demonstration of two distinct water species in, 1087; -perfluorocyclic oxide, critical opalescence of mixture, 2329; diffusion in CCl₄-cyclohexane solutions, 2491; diffusion in acetone-benzene-carbon tetrachloride system, 3941
- Carbonyls, dimanganese and dicobalt, ions produced by electron impact with, 1618
- Carboxyhemoglobin, electrophoresis of reversibly interacting system dextran sulfate-, 4242
- Carboxylic acids, long-chain aliphatic, surface viscosity of monomolecular films of, 1789
- Catalysis, comparison of metals of known surface area for ethane hydrogenolysis, 95; effects of impurities, olefins, and steam on catalytic cracking of hexadecane, 392; autocatalytic effect of Cu(I) in hydrogen reduction of aqueous cupric sulfate, 547; influence of alumina particle size for dehydration of ethanol, 590; dislocations as active centers of, and chemical action in silver, 880; auto-, of esterification of acetylenic and fluoro acids, 928; aging of silica and alumina gels, 1530; kinetics of cyclopropane-hydrogen reaction over silica-supported metals, 1877; kinetics of processes occurring on catalyst surface during oxidation of *o*-methylbenzyl alcohol over vanadia, 3092; metallic phases in reduced, impregnated Ni and Ni-Cu silica-alumina catalysts, 3265; ethane hydrogenolysis over dilute Ni catalysts, 3857; acid property and structure of solid metal sulfate catalyst, 4077
- Cations, metallic, stability in zeolites, 1676
- Cesium, -iodine phase diagrams, 1687; thermodynamic quantities in exchange of Li⁺ with Cs⁺ on cross-linked polymethacrylate ion exchangers, 2374
- Cesium chloride, ionic association of, in ethanol-water mixtures, 2420; association in anhydrous methanol, 2787
- Cesium superoxide, heat of formation and lattice energy of, 2550
- Cetyl alcohol, use in glass-liquid chromatographic work, measurement of interfacial resistance, 2351
- Charge-transfer complexes, gas phase, 3671
- Chemical shifts, proton, effects of charge and nickel ion on, of glycol peptides, 668; C¹³, viewed as constitutive property for substituted hydrocarbons, 1425; in n.m.r. absorption for O¹⁷ in oxy ions, 1844; C¹³ of vinyl carbons, 1947; of hydroxyl protons of acetic acid as function of concentration in acetic anhydride, acetone, and 1,4-dioxane, 2564; effect of aromatic solvents on p.m.r. spectra, 2679; C¹³ carbonyl, relation between $n \rightarrow \pi^*$ transition energies and, in cyclic and bicyclic ketones, 3105; C¹³, for alkyl cyanides, isocyanides, isocyanates, and isothiocyanates, 3920; for compounds of the type $\underline{X(CH_2)_n}$, 3925
- Chemical synthesis, with ion beams, 799
- Chemiluminescence, resulting from reaction of oxygen atoms with sulfur monoxide, 849; of tetrakis(dimethylamino)-ethylene, 3313
- Chemisorption, oxygen, on ruthenium dioxide, 102; infrared spectrum of CO chemisorbed on evaporated Ni films, 1195; of oxygen on zinc oxide, 3254
- Chloranil, -aniline complexes, charge-transfer complexes and donor molecule properties, 1707
- p*-Chloranil, sensitization of bulk photoconductivity in, 779
- Chlorate ion, dichromate ion-, reaction in fused salts, 3638
- Chloride complexes, of zinc, cadmium, and mercury in anhydrous ethanol, anion exchange, 2955
- Chloride ion, limiting equivalent conductance to 400°, 2984; activity coefficient in aqueous sulfuric acid, 3906
- Chlorides, molten group II, self-diffusion and structure in, 1627
- Chlorine, rate of exchange of, between dimethylchloramine and succinimide, 796; molecular, dissociation using shock waves, 834; surface tension in reciprocal system K⁺, Cd⁺²-Cl⁻, Br⁻, 1443; heats of formation of solid solutions in system (Na-Ag)Cl and (Na-Ag)Br, 3531; dissociated, kinetics of attack of molybdenum by, 4290
- Chloroacetic acid, halogen displacement reactions of, 854; diffusion in water, 2469
- Chloroamineplatinum(IV) salts, influence of ionic charge on viscosity β -coefficient of, 2197
- Chloroform, kinetics of γ -ray-induced decomposition of, 840
- Chlorophyll *a*, reaction kinetics of monomolecular films of, 21
- Chlorophyllide, -sensitized reduction of azobenzene and other compounds, 2779
- Choline chloride, crystalline, radical termination mechanisms in radiolysis of, 3370
- Chromatography, chemical reactions in chromatographic columns, 522; gas, theoretical study at high solute concentrations, 1283; gas-liquid, use of glass bead column for measuring interfacial resistance, 2351; gas-liquid partition, in benzene-polyphenyl systems and polymer statistical thermodynamics,

- 3682; gas-solid partition, with real carrier gases, 3768; gel permeation, 4157
- Chromium, electrical properties of ferromagnetic CrO_x ($1.89 < x < 2.02$), 1402; role of doublet state in photochemistry of Cr(III) complexes, 2201; vapor pressure and heat of sublimation of, 4044
- Clinoptilolite, ion exchange on, 531
- Cobalt, exchange of methanol between solvated Co^{+2} and solvent, 134; electron transfer between atomic hydrogen and Co(III) complexes in aqueous solution, 1390; optical rotatory dispersion of L-cysteine-cobalt systems, 1603; p.m.r. line widths, ligand exchange, and electronic relaxation times for arylphosphine complexes of Co(II) , 3212
- Cobalt sulfate hydrates, heat of hydration of cobalt sulfate hexahydrate to heptahydrate, 1268; heat capacities and entropies of cobalt sulfate heptahydrate and hexahydrate, 1272
- Collisions, double-impact, effect on dissociation rate constants, 2411
- Colloids, association, alkyltropylium salts, 1466; in petroleum, small angle X-ray scattering study of, 3500; nonionic association, salt effects on, 4038; logarithmic distribution functions for, 4418
- Complexes, addition, between carbohydrates and dimethyl sulfoxide by p.m.r., 656; charge-transfer, of titanium tetrachloride, titanium tetrabromide, and vanadium oxotrichloride with aromatic hydrocarbons, 660
- Complex modulus, of concentrated polymer solutions in steady shear, 4183
- Complex salts, 3-3, conductance in formamide, 2862
- Compressibility, of molten alkali halides, 2785
- Condensation, of vapors, shock tube studies, 3006
- Conductance, diffusion-, relations and free volume in molten salts, 399; of alkali metal salts of tetraphenylboride, 608; of some 2-2 salts in formamide, 696; of acetic acid-acetic anhydride system, 700; of alkali metal salts in hydrogen cyanide, 704; of tetra-*n*-butylammonium picrate in low dielectric solvent, 1338; of tetraisoamylammonium picrate in diethyl ether and benzene, 1437; polycation-polyanion reaction in dilute aqueous solution, 1447; electrical, of concentrated aqueous solutions and molten salts, correlation through free volume transport model, 2137; limiting equivalent, of quaternary salts in cyanoethylsucrose-acetonitrile mixtures, 2576; theoretical equation for symmetrical electrolytes, 2581; Hall, general expressions and numerical results for ideal and limiting-law terms of, 2617; of sulfuric acid-water solutions, high temperature-pressure study, 2726; of magnesium sulfate in dioxane-formamide mixture, 2857; of 3-3 complex salts in formamide, 2862; limiting equivalent, for single ions to 400° , 2984; of symmetrical tetraalkylammonium halides and picrates, 3878; temperature coefficient of, of aqueous sodium sulfate, 4033; of symmetrical tetraalkylammonium halides and picrates in methanol, 4208; of tetraalkylammonium halides in deuterium oxide solutions, 4216
- Conduction, salt of radical cation of 1,6-diaminepyrene and radical anion of 7,7,8,8-tetracyanoquinodimethane, 1740; electrical, relation between mobility of water molecules and, in montmorillonites and silicas, 2185; protonic, in water I region, 2224
- Conductivities, of ions and ion pairs in polymerization processes, 612; heat, and molecular diffusion in liquids, 1086
- Conformation, of pyranose rings in mono-, di-, and polysaccharides at high pH, 636; of polystyrene adsorbed at θ -temperature, 3955
- Coordination number, of small spheres, 322
- Copper, complexes of ethylamine with copper ions in montmorillonite, 683; poly-*N*-vinylimidazole complex with Cu(II) , 1252; metallic phases in reduced, impregnated Ni and Ni-Cu silica-alumina catalysts, 3268; reduction of $\text{CuO}_{0.67}$ in hydrogen, 3607; dilation contribution to heat capacity of, and α -brass at elevated temperatures, 4162; enthalpy of solid solution for metastable Ag-Cu alloy, 4407
- Copper acetylacetonate, adsorbed on silica gel, magnetic susceptibilities of, 3654
- Copper phthalocyanine, vapor pressure of, 344
- Coupling constants, C^{13} -H, in amides, thioamides and amidines, 2570
- Cracking, catalytic, of hexadecane, effects of impurities, olefins, and steam, 392
- Critical opalescence, measurements on nitrobenzene-*n*-heptane system, 4312
- Critical temperature, and coexistence curve for bismuth bromide, 1989
- Cryosorption pumping, dynamics of, 3317
- Crystallinity, elasticity of semicrystalline polymers, 141
- Crystals, ionic, lattice energies, 384; doped aromatic, luminescence of, 751; polyethylene single, specific heat of, 2078; exploratory study of 18 equimolar π -molecular compounds formed between pairs of electron donors and acceptors, 2153
- Crystal structure, of sodium tetrachloroferrate(III), 239; of pyridine hydrogen nitrate, 1915; of equimolar π -molecular compounds of anthracene and perylene with pyromellitic dianhydride, 2160
- Cubic oxides, lattice energy of, 2971
- Cupric ion, spectrophotometric study of association of Cu^{2+} and SO_4^{2-} ions, 1537; effect on radiation chemistry of aqueous glycine, 1579
- Cupric sulfate, role of Cu(I) in kinetics of hydrogen reduction of, 547
- Cyanide radicals, reaction of CN radicals in gas phase, 1504
- Cyanine dyes, color sensitization of zinc oxide with, 774; dimeric state of, 1894
- Cyanoethylsucrose, -acetonitrile mixtures, quaternary ammonium salts in, 2576
- Cyanogen, -cyclohexane mixtures, radiolysis of, 678
- α -Cyano- α -phenyl-*N*-phenylnitrones, *cis*- and *trans*-, photochemical and thermal isomerization of, 2545
- Cyclobutene, thermal isomerization of, 1073
- Cyclohexadiene-1,3, reaction with isopropyl radical, 2362
- 1,3-Cyclohexadienyltricarboxyl, ionization potentials and mass spectra of, 3198
- Cyclohexane, dehydrogenation of, in chromatographic column, 522; cyanogen-, mixtures, radiolysis of, 678; -carbon tetrachloride-Duomeen T Dioleate system, demonstration of two distinct water species in, 1087; and *n*-hexadecane, excess free energy of mixtures of, 1660; adsorption on aluminas prepared by thermal decomposition of aluminum hydroxide *in vacuo* and in air, 1805; radiation-induced oxidation of, 1814; -cyclohexane- d_{12} mixtures, Hg-photosensitized decomposition of, 2027; radiolysis of benzene-, mixtures in presence of nickel tetracarbonyl, 2034; *n*-propyl-, *n*-butyl-, and *n*-decyl-substituted, thermodynamic properties, 2094; diffusion in CCl_4 -cyclohexane solutions, 2491; -benzene, diffusion in system, 2783; liquid, effects of experimental parameters on (n, γ)-activated reactions of bromine with, 2795; -cyclopentane mixtures, comparison of radiolysis yields of dimer and olefin with corresponding nondeuterated mixtures, 3113; intradiffusion and derived frictional coefficients for benzene and, in their mixtures, 3116; effect of additives on radiolysis of vapor of, 3292
- Cyclohexanone, γ -radiation-induced isomerization of, to 5-hexenal in liquid phase, 666
- Cyclopentadienylmolybdenum dicarbonyl nitrosyl, ionization potentials and mass spectra of, 3198
- Cyclopentane, radiation chemistry of, 2707; -cyclohexane- d_{12} mixtures, comparison of radiolysis yields of dimer and olefin with corresponding nondeuterated mixtures, 3113
- Cyclopentanes, *n*-propyl-, *n*-butyl-, and *n*-decyl-substituted, low-temperature thermodynamic properties of, 353
- Cyclopentanone, liquid, γ -radiolysis of, 807
- Cyclopropane, reaction with hydrogen over silica-supported metals, kinetics, 1877; Hg (^3P) photosensitized decomposition of, radical intermediates, 2129
- Cyclopropanecarboxylic acid chloride, electron diffraction study of structure and conformational behavior of, 3043
- Cyclopropanes, substituted, recoil tritium reaction, ring opening and alkyl replacement in, 4297
- Cyclopropyl methyl ketone, electron diffraction study of structure and conformational behavior of, 3043
- Cyclosiloxanes, relation of ring size to ultraviolet extinction coefficient in, containing phenyl substituents on silicon, 1066
- L-Cysteine, -cobalt systems, optical rotatory dispersion of, 1603
- n*-Decane, reversible reactions of oxygen with tetrakis(dimethylamino)ethylene and, 3313
- Decarboxylation, radiolytic, of benzoate, relative rate constants for hydroxyl radical reactions, 1938; of picolinic acid in polar solvents, 2277; of phenylmalonic acid, kinetic study, 2402; of β -resorcylic acid in polar solvents, 3565

- Decomposition, thermal, of hexanitroethane, 25; radiation-induced, of alkali and alkaline earth perchlorates, product yield and stoichiometry, 359; radiation-induced, of alkali and alkaline earth perchlorates, mechanism, 377; thermal, of cadmium hydroxide, 450; thermal, of calcium formate in KBr matrix, 583; γ -ray induced, of chloroform, 840; thermal, of diacetylene in flow system, 858; thermal, of benzene in flow system, 863; pyrolytic, of magnesium oxalate, 918; catalytic, of alkali metal perchlorates by manganese dioxide, 1114; thermal unimolecular, of norbornylene, 1351; thermal, of solid azidopentaamminecobalt(III) azide, 1723; of oxalic acid in glycerine kinetic study, 1729; Hg-photosensitized, of acetylene in presence of NO, 1732; unimolecular, of product olefins in methylene chemical activation systems, 1952; Hg-photosensitized, of cyclohexane-cyclohexane- d_{12} mixtures, 2027; nitrous oxide, mass spectra study of kinetics, 2111; Hg (3P) photosensitized, of cyclopropane, radical intermediates, 2129; Hg-photosensitized, of isopentane, 2291; of hydrogen oxalate ion in glycerine solution, kinetic study, 2392; of gallium nitride, 3455; Hg-photosensitized, of perfluoropropene, 3600; of hydrogen peroxide on glass, 3658; solid-state thermal, of potassium trisoxalatochromium(III) trihydrate, 4328; chemically activated, of *n*-butane and isobutane, 4348; Hg (3P_1)-sensitized, of *n*-hexane vapor, 4396
- Decomposition pressure, of thorium mononitride, 1223
- Degradation, mechanical, of polymers by controlled hydrodynamic shear, 161; of irradiated methacrylate polymers, 189
- Dehydration, of ethanol on aluminas of various specific surface areas, 590; of aliphatic and aromatic saturated montmorillonites, 2265; of acetaldehyde hydrate, 4325
- Depolarization, of scattered light by optically active systems, 689
- Depolymerization, thermal, of polymethyl methacrylate and poly- α -methylstyrene in solution in various solvents, 2967
- Desalination processes, membrane, degree of coupling and efficiency of fuel cells, 3801
- Desorption, of olefins from silica-alumina catalysts, 2676; and isotopic exchange of oxygen at silver surface, 4201
- Deuterium, hydrogen-, exchange reaction, 6^3P_1 Mercury photosensitized, 45; -water mixtures, isotope effects in radiolysis and photolysis of, 698; comparison of water sorption and D-H exchange sites in poly-L-valine, 1432; exchange with hydroxyl groups of alumina, 3070
- Deuterium oxide, effect on thermal stability of proteins, 3132; near-infrared study of H bonding in water and, 3722; conductance of tetraalkylammonium halides in, 4216
- Dextran sulfate, -carboxyhemoglobin, electrophoresis of reversibly interacting system, 4242
- Diacetylene, kinetics of thermal decomposition of, in flow system, 858
- Diamagnetic susceptibility, bond and interaction contributions for calculating, 1550
- 2,3-Diaminonaphthalene, kinetics for reaction of Se(IV) with, 3232
- 1,6-Diaminopyrene, conductive salt of radical cation of, 1740
- Diaphragm cell, use of data in calculation of diffusion coefficients, 258
- Dibenzenechromous cation, ground state electronic configuration of, 3207
- Diborane, heat of reaction with trimethylamine, 1010
- Dicarbonyls, photoreducing activity of, 2834
- α,ω -Dicarboxylic acids, studies on spreading, collapse, and temperature and compression rate effects on monolayers of, 2368
- cis*-Dichloroethylene, gas phase electron diffraction study of, 4091
- Dichromate ion, -chlorate ion reaction in fused salts, 3638
- Dicobalt octacarbonyl, mass spectra study of, 1618
- Dielectric constants, for acetic acid-acetic anhydride mixtures, 700; complex, of benzene solutions of several organic compounds, 1006; for normal primary alcohols, 1294; for mixtures of polar nonassociative liquids, 1302; of water to 800°, 3165; of acetonitrile-methanol mixtures, 3657; of crystalline powders of glycine, tyrosine, glycylglycine, and ovalbumin, 4176
- Dielectric properties, of polyanion-polycation complexes, 1456
- Dielectric relaxation, mechanism for molecules similar to diphenyl ether, 1006
- Diethyl carbonates, pyrolysis in gas phase, 3013
- Diethylglycine, photooxidation by methylene blue, 1149
- Diffusion, -conductance relations and free volume in molten salts, 399; thermal, measurements by wave-front-shearing interferometry, 1016; molecular, and heat conductivity in liquids, 1086; of monodisperse polystyrene in mixed solvents, 1135; self-, and structure in molten group II chlorides, 1627; iso-thermal ternary, derivation of equation relating mutual and tracer diffusion coefficients to certain limiting cross-term diffusion coefficients and thermodynamic properties of system, 1693; in system cadmium iodide-water, 1718; self-, for water, dependence on ionic concentration, 2001; of KCl in methanol-water solutions, 2336; in dilute aqueous acetic acid solutions, 2341; of chloroacetic acid in water, 2409; in carbon tetrachloride-cyclohexane solutions, 2491; in deuterio-normal hydrocarbon mixtures, 2782; in cyclohexane-benzene system, 2783; multicomponent, in polystyrene 1-polystyrene 2-toluene system, 2875; study in ternary system, labeled urea-urea-water, 3120; free-, mathematical analysis of multicomponent experiments, 3305; isothermal ternary, of water-sodium chloride-potassium chloride, test of Onsager reciprocal relations in, 3374; volume and surface, in Knudsen cells, effect on vapor pressure measurements, 3538; of hydrogen in α -phase of palladium-hydrogen system, 3581; of oxygen in polymers, use of phosphorescent quenching, 3677; of methane, ethane, propane, and *n*-butane in water, 3752; in system acetone-benzene-carbon tetrachloride, 3941; tracer, in binary solutions subject to dimerization equilibrium, 4012
- Diffusion coefficient, of atomic mercury in isoctane, 3814
- Diffusion coefficients, calculation from diaphragm cell diffusion data, 258; determination in liquids by a radiometric porous-frit method, 303; estimation of, for ternary systems of strong and weak electrolytes, 1227; of iodine atoms in carbon tetrachloride, correction, 3182; exact procedure for calculating of $(N - 1)^2$ independent, from free-diffusion experiments, 3305; for two concentrated compositions of system water-mannitol-sodium chloride, 4276; least-squares method for calculating, for ternary systems, 4361
- 1,3-Difluoroacetone, anomaly in interaction of CF_2H radicals, 1085
- Difluoroacetylene, preparation and purification of, 2484
- Diglycidyl ether, kinetics of zinc fluoroborate and hydrogen ion catalyzed hydrolyses of, 1882
- o*-Dihalobenzenes, unsymmetrical, n.m.r. spectrum of three, 4413
- 1,4-Diheterocyclohexanes, n.m.r. spectra of, 579
- 9,10-Dihydroanthracenes, 9,10-bridged, n.m.r. spectra of, 2022
- β -Diketone, thionine- β -diketone-acrylamide systems, kinetics and mechanism for photopolymerization processes, 2842
- Dimanganese decacarbonyl, mass spectra study of, 1618
- Dimercaptopropanol, complex with cationic dye, 940
- Dimerization, of *bacillus subtilis* α -amylase molecule, equilibrium constant, 1829; of cyanine dyes, 1894; of trimethylacetic acid in CCl_4 , infrared study, 2715; of anions of long-chain fatty acids in aqueous solutions, 2821; gaseous, of thallos fluoride, 3910; of solute, tracer diffusion coefficient, ≤ 0.12
- N,N'*-Dimethylacetamide, hydrogen-bonding studies of hindered phenols with, 1622; p.m.r. studies of hydrogen bonding in amine-acetamide-chloroform systems, 2950
- 2,2'-Dimethylbianthrone, e.s.r. associated with photochromism, 2487
- 2,3-Dimethylbutane, surface effects in uninhibited and inhibited pyrolysis of, 2453
- Dimethylchloramine, rate of exchange of chlorine between, and succinimide, 796
- Dimethyloctylamine oxide, spin-lattice relaxation times of, through c.m.c., 3204
- Dimethyl sulfoxide, addition complex between carbohydrates and, 656
- 2,5-Dimethylthiophene, heat capacities and thermodynamic properties, 1524
- Diolefins, p.m.r. studies of, 486
- Dioxane, -benzene mixtures, radiolysis of luminescence behavior of, 3024; electric moments of *N*-alkyl-substituted nicotinamides from measurements in mixed benzene-dioxane solutions, 4097
- Dioxygen difluoride, mass spectra study of synthesis, stability and energetics of, 4338
- Diphenylacetylene, mass spectra and appearance potentials of principal ions of, 2935; n.m.r. spectra of, 3552
- Diphenylcarbonyls, electron impact studies of principal ions in mass spectra of, 2943
- 1,2-Diphenylcyclopropane, *cis*- and *trans*-, γ -ray-induced isomerization of, 4401

- 1,1-Diphenylethylene, e.s.r. of, 4402
- Diphenylpicrylhydrazyl, rates of simultaneous oxidation and reduction of, on titanium dioxide and carbon black, 3219; adsorbed on silica gel, magnetic susceptibilities of, 3654
- Dipole moments, of isonicotinamide in benzene and dioxane solutions, 691
- Dipoles, long-chain, shapes and close-pack areas of, at water-octane interface, 481; dielectric relaxation of mixtures of dipolar liquids, 674
- Dislocations, as active centers of catalysis and chemical action in silver, 880
- Dispersion, dielectric, of protein solutions containing small zwitterions, 1162; of conductance of tetra-*n*-butylammonium picrate in low dielectric solvents, 1338; dielectric, of crystalline powders of amino acids, peptides, and proteins, 4176
- Displacement phenomena, liquid-liquid, microcalorimetric study of, 314
- Dissociation, multistate, and effect of pressure on equilibrium on magnesium sulfate, 695; of molecular chlorine, 834; of manganese sulfate ion pairs in water, effect of pressure, 2595; of diphenylcarbonyls and ethers by electron impact, 2943; magnesium sulfate as unassociated salt in *N*-methylformamide, 3167; and homoconjugation of certain phenols in acetonitrile, 3193; of phosphoric acid solutions, 3520; of ruthenium and osmium tetroxide, 3893
- Dissociation constant, for tetraethylammonium chloride in ethylene dichloride, 87; for reaction $\text{HCl} \rightleftharpoons \text{H}^+ + \text{Cl}^-$ in ethylenediamine, 2537; of acetic acid in deuterium oxide, 2750; for nitrophenols and salicylic acid in deuterium oxide, 4416
- Dissociation energy, of lanthanum monosulfide, 2684; of thallium monofluoride, 4030
- Distribution functions, logarithmic, for colloidal particles, 4418
- Disulfur monoxide, infrared spectrum and thermodynamic functions, 1154
- n*-Dodecanol, aqueous solubility of, 3171
- Dolomite, thermodynamics of formation of, 1065
- Donor-acceptor molecular compounds, exploratory crystallographic study of, 2153; crystal structures of anthracene and perylene with pyromellitic dianhydride, 2160
- Duomeen T Dioleate, cyclohexane-carbon tetrachloride-, system, demonstration of two distinct water species in, 1087
- Durene, solvent effects on charge-transfer complexes of 1,3,5-trinitrobenzene with, 2766
- Dyes, minority carrier trapping and dye sensitization, 714; adsorbed, photoluminescence of, 738; phosphorescence and electron transfer in dye-disulfhydryl compound complex, 940; cyanine, dimeric state of, 1894; kinetics of lipoamide dehydrogenase-NADH-dye reaction, 3696; stoichiometry of reaction of 4,5,4',5'-dibenzo-3,3'-diethyl-9-methylthiacarbocyanine with diverse polyionic macromolecules, 4368
- Elasticity, Gibbs, application of surface thermodynamics to, 1798
- Electric moments, benzene and dioxane, of *N*-alkyl-substituted nicotinamides from measurements in mixed benzene-dioxane solutions, 4097
- Electrode potential, of germanium, 3168
- Electrode processes, study of first-order chemical reactions following charge transfer using a controlled potential method, 30
- Electrokinetic flow, in narrow cylindrical capillary, 4017
- Electrokinetic phenomena, at thorium oxide-aqueous solution interface, 3148
- Electrolytes, reference, Wien effect, 658; strong and weak, estimation of diffusion coefficients for ternary systems of, 1227; having common ions, heats of mixing of, 1868; of 1-1 charge type, heats of mixing of, 1873; aqueous, concentration dependence as indicated in heats of mixing studies, 2974; aqueous, Soret coefficients and heats of transfer for, 3598
- Electron affinities, of aromatic hydrocarbons in tetrahydrofuran solution, 628; of oxone, 2562
- Electron density, shifts during chemical bond formation, 3346
- Electron diffraction, study of structure and conformational behavior of cyclopropyl methyl ketone and cyclopropanecarboxylic acid chloride, 3043; gas phase, investigation of iron pentacarbonyl, 3405; study of trifluoronitrosomethane, 3727; gas phase, study of *cis*-dichloroethylene, 4091
- Electron donor-acceptor complexes, semiempirical linear combination of molecular orbitals description of, 1927
- Electronegativity, of noble gases, 596; calculated values for 99 groups, 3284
- Electronic commutator method, for determination of E° of formation and related thermodynamic values for molten lead chloride, 1034
- Electron-transfer reactions, role of water in, 3183
- Electron trapping, in rigid ethanol-methyl-2-tetrahydrofuran mixtures, 3186
- Electrons, hydrated, determination of extinction coefficient, 53; hydrated, reaction of haloaliphatic compounds with, 271; hydrated, reactions with aromatic acids, alkyl halides, heterocyclic compounds, and Werner complexes, kinetic study, 289; hydrated, reactivity of metal ions and oxy anions toward, 973; trapped, in polycrystalline and glassy alkaline ices, 1081; solvated, effect of solvent and of solutes on absorption spectrum of, 1244; hydrated, rate constants for reaction of e_{aq}^- with itself and other transients, interconvertibility of e_{aq}^- and H, 1324
- Electrooxidation, of tetraphenylborate ion in aqueous solution at Pt disk electrode, 1067
- Electrophoresis, of interacting substances differential boundary experiments, 3785; of interacting system dextran sulfate-carboxyhemoglobin, 4242
- Electrosorption, of ethylene on Pt as function of potential, concentration, and temperature, 3335
- Emittance, total, relation to specific heat in Ta, Nb, W, and Mo, 1420
- Energy constants, interatomic, of mercury, 1740
- Energy transfer, intermolecular triplet-triplet, between aromatic carbonyls and aromatic hydrocarbons, and rare earth chelates, 275; between molecules and electronically excited atoms, 4406
- Enthalpy, of arsenic triiodide and its absolute entropy, 2743; measurements for eight binary aromatic-alicyclic systems, 2753; excess, analyses of data in terms of different theories of molecular solutions, 2759; of condensed phases of antimony and bismuth iodides, 3621; of solid solution for metastable silver-copper alloy, 4407
- Enthalpy of formation, of amide hydrogen bond, temperature dependence, 1704; for niobium and tantalum pentafluorides, 2089; of yttrium trifluoride, 2305; of ruthenium pentafluoride, 2308; and entropy of aluminum(I) fluoride(g), 2311; and dissociation energy of thallium monofluoride, 4030; of arsenic pentafluoride, 4358; of gaseous tantalum oxide and tantalum dioxide, 4399
- Enthalpy of fusion, for glutaronitrile, 1983
- Enthalpy of mixing, for tetramethylmethane-tetrachloromethane system, 2176
- Enthalpy of solution, for barium hydroxide octahydrate, 1980; standard, of sodium carbonate, sodium bicarbonate, and trona, 3059
- Enthalpy of sublimation, of beryllium fluoride, 1069
- Enthalpy of transfer, from water to deuterium oxide for model compounds, 3132
- Enthalpy of vaporization, of molten bismuth chloride, 3916
- Entropy, and volume changes on ionization of aqueous acids, 965; of cobalt sulfate heptahydrate to hexahydrate, 1272; statistical gaseous, for glutaronitrile, 1983; of aluminum(I) fluoride (g), 2311; of iodine monochloride, 2443; absolute, of arsenic triiodide, also vapor pressure and enthalpy, 2743; of aluminum (III) chloride(g), 3001; of hexamethylbenzene, 3126; of potassium ferricyanide and ferricyanide ion, 3179; absolute, for bismuth and antimony iodides, 3621
- Entropy of dilution, of perchlorates of magnesium and strontium, 4231
- Entropy of sublimation, of beryllium fluoride, 1069
- Entropy of transfer, from water to deuterium oxide for model compounds, 3132
- Equilibria, ion-exchange, thermodynamic aspects of, in mixed solvents, 341; chain association, equations and application, 1482; acid-base, in concentrated salt solutions, bases of various charge types in dilute acid solutions, 1588
- Equilibrium constant, for dimerization of *Bacillus subtilis* α -amylase molecule, 1829; charge-transfer, for series of aniline-chloranil complexes, 1707
- Esin and Markov effect, for adsorbed organic ions and molecules, 3411
- Esterification, of acetylenedicarboxylic acid and perfluoro acids with unfluorinated alcohols, 928
- Ethane, hydrogenolysis of, comparison of metals of known surface area for, 95; effect of density on radiolysis of, 1045; effect of additives in radiolysis of, 1056; diffusion in water, 3752;

- hydrogenolysis over dilute Ni catalysts, 3857; hot fluorinated, elimination of HF from, 3898; adsorption on poly(tetrafluoroethylene), 4387
- Ethanol, dehydration on aluminas, 590; vapor phase radiolysis of, 1699; -methyl-2-tetrahydrofuran mixtures, electron trapping in, 3186; electron capture by solutes in radiolysis of, 4053
- Ethanol hydrate, existence below -73.5° as indicated by low-frequency dielectric studies and thermal analysis, 996
- Ether, -boron halide molecular addition compounds, n.m.r. study in dichloromethane, 89
- Ethers, electron impact studies of principal ions in mass spectra of, 2943
- Ethylamine ion, complexes with ethylammonium and copper ions in montmorillonite, 683
- Ethylammonium, complexes of ethylamine with, in montmorillonite, 683
- Ethyl chlorophyllide, sensitized photoreduction of phenosafranin by hydrazobenzene, 2633
- Ethyl chlorophyllide *a*, photoreduction of methyl red sensitized by, 821
- Ethylcyclopropane, kinetics of thermal isomerization of, 429;
- Ethylene, radiolysis of, yield of hydrogen atoms and formation of saturated hydrocarbons, 815; solid, reaction of tritium atoms with films of, 1040; -propylene copolymer, radiolytic stress relaxation, 2072; mass spectra study of reaction of nitrogen atoms with, 2736; application of electrostatic fields in radiolysis of, 2867; electrosorption of, on Pt as function of potential, concentration, and temperature, 3335; γ -radiolysis of, sensitized to inert gases, 4033
- Ethylenediamine, dissociation constant for reaction $\text{HCl} \rightleftharpoons \text{H}^+ + \text{Cl}^-$ in, establishment of pH and pAg scale in, 2537
- Ethylenes, fluorinated, appearance potentials from fragment ions to determine heats of formation of hydrofluorocarbon radicals and ions, 3731; fluorinated, calculations based on statistical theory of mass spectra, 3737
- Ethyl radicals, disproportionation and combination of, 1040
- Europium, heat of formation of anhydrous europium(II) chloride and of aqueous europium(II) ion, 991
- Exchange reactions, hydrogen-deuterium, 6^3P ; mercury photo-sensitized, 45; of boron trifluoride between ethyl ether-boron trifluoride and tetrahydrofuran-boron trifluoride and between ethyl ether-boron trifluoride and ethyl sulfide-boron trifluoride, 527; for chlorine between dimethylchloramine and succinimide, 796; π -complex adsorption in exchange of alkylbenzenes, 1850; rates of mercapto proton exchange for 2-mercaptoethanol in aqueous solution, 2287; isotopic exchange in nitrogen gas induced by γ -radiation, 2385; deuterium exchange with surface hydroxyl groups of alumina, 3070; hydroxyl groups of alumina and silica-alumina catalysts with deuterated methane, 3080; π -complex mechanism for isomerization and isotope exchange of *cis*- and *trans*-stilbenes on Pt catalysts, 3526; isotopic exchange of oxygen at silver surface, 4201
- Excitation energy, remarks on Förster's theory of transfer of, 1061
- Exciton states, in polymers, 784
- Explosions, unification of thermal and chain theories of explosion limits, 2747
- Extinction coefficients, of hydrated electron, from radiolysis study of aqueous tetranitromethane, 53; ultraviolet, relation of ring size to, in cyclosiloxanes containing phenyl substituents on silicon, 1066; molar, of O_2F_2 in visible range, 1079
- Extraction, of acids by basic organic solvents, 1106; of perchloric acid by trilaurylamine, role of aromatic diluent, 1565
- Fatty acids, studies of monolayers on metals by contact potential measurements, 984; dimerization of anions of, hydrophobic properties of, 2821
- Faujasite crystals, number of hydroxyl groups at exterior surfaces of, 4050
- Fenton's reagent, e.p.r. study of alcohol oxidation by, 3805
- Ferricenium cation, ground state electronic configuration of, 3207
- Ferricyanide ion, entropy and free energy of formation of, 3179
- Ferrocyanide ion, free energy of formation of, 3179
- Films, monomolecular, of chlorophyll *a* on aqueous substrates, kinetic study, 21; flow in thin liquid, 116; high-area metal, evaporated in carbon monoxide, infrared study, 1188; soap, effect of surface viscosity on thinning of, 1471; study of Langmuir-Blodgett layers on metal surfaces by reflected polarized light, 1654; monomolecular, surface viscosity for long-chain aliphatic amides, amines, alcohols, and carboxylic acids, 1789; studies on spreading, collapse, and temperature and compression rate effects on monolayers of α,ω -dicarboxylic acids, 2368
- Fluid theory, transport properties of dense fluid of molecules interacting with square-well potential, 869
- Fluorescence, remarks on Förster's theory of transfer of excitation energy, 1061; of benzene and benzene-*d*₆, 1343; use of measurements to determine association constants for weak complexes, phenol-acetate system, 2960; use in study of ionic association in solutions of thionine, 2988
- Fluorides, hydrolysis of Ta(V) in KF-LiF, 4335
- Fluorine, addition to *cis*- and *trans*-perfluorobutene-2, 254; hydrogen-, reaction, oxygen inhibited, 408; suggested mechanism for H_2 -F reaction, 2488; kinetics of fluorination of graphite, 2772; reaction of methylene with CF_2H_2 , 2804; hydrogen-fluorine reaction, suggested mechanism, 2808; kinetics of tetrafluorohydrazine-fluorine reaction, 3700
- Fluoro acids, acidity and autocatalysis of esterification of, 928
- Fluorobenzene, triplet state of, 4284
- Fluorocarbon gases, C-C bond dissociation energy in C_2F_6 , 1075
- Fluorocarbons, cyclic, radiation chemistry of, 2526; solubilities in cyclohexane and 1,4-dioxane, 3200; appearance potentials and mass spectra of C_2F_6 , $\text{C}_3\text{F}_8\text{Cl}$, and *c*- C_3F_8 , 3741; observations on positive ion decomposition of C_2F_6 and C_3F_8 in mass spectrometer, 3746
- Fluorotrichloromethane, photolysis of, 4410
- Formation constants, of silver(I) cyanide complexes in equimolar sodium-potassium nitrate melts, 3763
- Formic acid, adsorption on smooth Pt from, using large anodic galvanostatic transients, 562; adsorbed, comparison with carbon monoxide on Pt electrodes, 1363
- Free energy, surface, of polymers, 1084; excess, of mixtures of cyclohexane and *n*-hexadecane, 1660
- Free energy of dissolution, standard, for isolated metal atoms with molten chlorides of that metal, 11
- Free energy of formation, of ferricyanide ion and ferrocyanide ion, 3179
- Free volume, diffusion-conductance relations and, in molten salts, 399
- Frictional coefficients, derived, for benzene and cyclohexane in their mixtures, 3116; for two concentrated compositions of system water-mannitol-sodium chloride, 4276
- Frozen solutions, radiolysis of sodium nitrate ices, 1080; electron trapping in polycrystalline and glassy alkaline ices, 1081
- Fuel cells, degree of coupling and efficiency of, membrane desalination processes, 3801
- 2-Furaldehyde, barrier to internal rotation in, 4062
- Fusion, of pentaerythrityl chloride, bromide, and iodide, 1209; of stable and metastable phases of 2,5-dimethylthiophene, 1524
- Gallium, solvent vapor pressures of dilute solutions of Ga in Cd, 933; -Cd system, discussion of apparent violation of Gibbs-Duhem equation, 2135; electronic spectra of Ga, In, and Tl₂ molecules, 2480; -Cd system, apparent violation of Gibbs-Duhem relations, 3222
- Gallium nitride, decomposition of, 3455
- Galvanic cells, with molten bisulfate solvents, 3156; measurement of thermodynamic interaction between zinc and lead in dilute solution in liquid tin, 4085
- Galvinoxyl, effect on radiolysis of benzene-butene-2 mixtures, 1866
- Gases, nonpolar, aqueous solutions of, 281; effect of hydrostatic pressure on gases dissolved in water, 389; adsorption on alkali fluorides, 2472; double molecules in, 4422
- Gegenions, single-ion activity coefficients of, in sodium polyacrylate, 3690
- Gelatin, transitions in, and vitrified gelatin-water systems, 4040
- Gel melting point, as measure of tacticity of poly(methyl methacrylate), 3384
- Germanium, simultaneous chemical and electrochemical oxidation of, 2269; electrochemical aspects of dissolution, 3168
- Gibbs-Duhem equation, discussion of apparent violation of, 2135; reply to discussion of apparent violation of, 2135
- Gibbs-Duhem relations, apparent violation, Ga-Cd system, 3222
- Glass, pressure effects on glass transition in polymers, 1497; transition, kinetic parameters of, 2471; decomposition of hydrogen peroxide on, 3658
- Glass electrodes, cation-sensitive, activity coefficients of sodium chloride by, 2797

- Glutaronitrile, thermal properties and statistical gaseous entropy of, 1983
- Glycinamide, cupric ion catalyzed hydrolysis of, 2914
- Glycine, radiation chemistry of, effect of cupric ion, 1579
- Glycine ethyl ester, cupric ion catalyzed hydrolyses of, 2914
- Glycyl peptides, effect of charge and nickel ion on proton chemical shifts of, 668
- Gold, Volta potential studies of aging of gold surfaces, 439; platinum-, alloys, heterogeneous, electrochemical characterization of surface composition of, 901; anodic methanol oxidation in Pt-Au alloys, 3377; -oil interface, radiotracer study of competitive adsorption at, 3833; wetting of, by water, 4238
- Graphite, kinetics for fluorination of, 2772
- Graphitic acid, of pyrolytic carbon and its heat treatment, 2462
- Hafnium oxides, spectroscopy of, in neon and argon matrices, 3488; monoclinic, optical energy gaps in, 3666
- Halide ion, relation between electrochemical and spectroscopic properties of pseudohalide ions and, 3176
- Haloaliphatic compounds, reaction with hydrated electrons, 271
- Haloethanes, hydrogen-bonding equilibria and self-association in, 446
- Halogens, pure quadrupole resonance in potassium hexahalo-rhenates(IV) and hexachlorotungstate(IV), 2101
- Halomethanes, hydrogen-bonding equilibria and self-association in, 446
- Heat capacity, of pentaerythritol iodide, chloride, and bromide, 1209; of cobalt sulfate heptahydrate and hexahydrate, 1272; of hypostoichiometric thorium dicarbide, 1520; of 2,5-dimethylthiophene, 1524; of solid and liquid glutaronitrile, 1983; of iodine monochloride, 2443; of 1-pentanethiol vapor, 3030; and entropy of hexamethylbenzene, 3126; of potassium hexabromorhenate(IV), 3471; of uranium monoselenide, 3618; high-temperature, of beryllium oxide, 4035; dilation contribution to, of copper and α -brass at elevated temperatures, 4162
- Heat of activation, prediction of, for viscous flow in simple non-metallic liquids, 671
- Heat of adsorption, differential, as function of particle size for alumina-water system, 317
- Heat of combustion, of isomeric monoglycerides, 2887
- Heat of dilution, of perchlorates of magnesium and strontium, 4231
- Heat of formation, of solid tetrasulfur tetranitride and tetraselenium tetranitride, 334; of alkyl radicals, 905; of anhydrous europium(II) chloride and aqueous europium(II) ion, 991; of acetyl radical, 1022; bond and interaction contributions for calculating, 1550; of hydrazinium diperchlorate, 1716; of lanthanum oxide, 2464; of superoxides of potassium, rubidium, and cesium, 2550; of beryllium hydroxides, 2828; of isomeric monoglycerides, 2887; of aluminum(I) chloride(g), 3001; for methyl iodide, 3040; of solid solutions in system (Na-Ag)Cl and (Na-Ag)Br, 3531; and polymerization of carbon suboxide, 3603; of hydrofluorocarbon radicals and ions, 3731; of nitric oxide(g), 3863
- Heat of fusion, of iodine monochloride, 2443; of beryllium oxide, 4035
- Heat of hydration, of cobalt sulfate hexahydrate to heptahydrate, 1268
- Heat of immersion, in thorium oxide-water system, 151
- Heat of mixing, of electrolytes having common ions, 1868; of electrolytes of 1-1 charge type, 1873; of aqueous alkali metal halide and nitrate solutions of same ionic strength, 2974
- Heat of reaction, of boron trifluoride with HF-3.75H₂O and of diborane with trimethylamine, 1010
- Heat of solution, of cobalt sulfate hexahydrate and heptahydrate, 1268; of alkali metal halides in anhydrous N-methylformamide, 2611
- Heat of sublimation, of chromium, 4044
- Heat of transport, for aqueous electrolytes, 3598
- Heat of vaporization, of 1-pentanethiol vapor, 3030; of purine and pyrimidine bases, 3615
- Hemoglobin, equine solutions, refractive index dispersion in, 3188
- 1,5-Heptadiene, thermal rearrangement between 3-methyl-1,5-hexadiene and, 1278
- Heptafluoropropyl ethyl ketone, photolysis of, 1001
- n*-Heptane, -perfluorocyclic oxide, critical opalescence of mixture, 2329; critical opalescence measurements on nitrobenzene-system, 4312
- Heterocyclic compounds, rate constants of hydrated electron reactions with, 289; saturated, C¹³ magnetic resonance study of, 3925
- Hexachloroacetone, adsorption on alumina-containing surfaces, 3949
- Hexacyanoferrate(III), use in oxidation of reducing sugars in alkaline medium, 2038
- Hexadecane, effects of impurities, olefins, and steam on catalytic cracking of, 392; and cyclohexane, excess free energy of mixtures of, 1660; radiation-induced reactions in, 2345
- n*-Hexadecanol, aqueous solubility of, 3171
- Hexamethylbenzene, solvent effects on charge-transfer complexes of 1,3,5-trinitrobenzene with, 2766; heat capacity and entropy of, estimate of internal rotation barrier, 3126
- n*-Hexane, Hg(²⁰¹Pi)-sensitized decomposition of vapor of, 4396
- Hexanitroethane, thermal decomposition of, 25
- 5-Hexenal, liquid phase γ -radiation-induced isomerization of cyclohexanone to, 666
- 1-Hexynes, 1-substituted, C¹³ magnetic resonance spectra of, 1348
- Homoconjugation, of certain phenols in acetonitrile, 3193
- Hydrates, crystalline, thermodynamics of, 1840
- Hydration, surface, of γ -alumina, infrared and gravimetric study of, 211; of tricalcium silicate, 553, 2489; of acetone in 1,2-dichloroethane, 2980
- Hydrazinium diperchlorate, heat of formation of, 1716
- Hydrazobenzene, kinetics of ethyl chlorophyllide sensitized photoreduction of phenosafranine by, 2633
- Hydrocarbons, unsaturated, radical yields in radiolysis of, 194; displacement of, from high energy metal oxide surfaces by water, heat effects, 314; aromatic, electron affinities of, in tetrahydrofuran solution, 628; aromatic, charge-transfer complexes of titanium tetrachloride, titanium tetrabromide, and vanadium oxytrichloride with, 660; saturated, formation in ethylene radiolysis, 815; liquid aromatic, LET effects in radiolysis of, 1157; substituted, C¹³ chemical shift viewed as constitutive property, 1425; diffusion in deuterio-normal mixtures, 2782; aromatic, dissociative equilibrium in systems aromatic hydrocarbons⁺, Na⁺ \rightleftharpoons radical anion⁻ + Na⁺, 4124
- Hydrochloric acid, -potassium chloride system, thermodynamic properties of, 207; thermodynamic properties of solution of, in N-methylacetamide by e.m.f. measurements, 1335; -water solutions, diffusion in, 2333; thermodynamic properties of HCl-NaCl mixtures, 2395; dissociation constant for reaction HCl \rightarrow H⁺ + Cl⁻ in ethylenediamine, 2537
- Hydrofluorocarbon, radicals and ions, heats of formation of, 3731
- Hydrogen, -deuterium exchange reaction, 6³P₁ mercury photosensitized, 45; -fluorine reaction, oxygen inhibited, 408; pulse radiolysis of aqueous hydrogen systems, 1324; comparison of water sorption and D-H exchange sites in poly-L-valine, 1432; neptunium-, system, 1641; reaction of cyclopropane with, over silica-supported metals, 1877; solubility process in Pt-Pd alloys, isotopic equilibrium separation factors in, 2485; -fluorine reaction, suggested mechanism, 2488; adsorption on zinc oxide, 2500; -yttrium system, thermodynamics of, 2510; -fluorine reaction, suggested mechanism for, 2808; thermodynamics of scandium-hydrogen system, 3514; solubility in liquid Na, 3542; absorption of, by gold-palladium alloys, 3575; diffusion in α -phase of palladium-hydrogen system, 3581; -oxygen flames, sulfur in burnt gas of, 3593; absorption isotherms of, in α -phase of hydrogen-palladium system, 3773; scandium-yttrium-, system, 3973; molecular, reaction mechanism leading to formation of, in radiation chemistry of water, 4058
- Hydrogen atoms, yield in ethylene radiolysis, 815; addition to olefins, relative rates at the two carbon positions, 905; rate constants of some reactions of, in aqueous solution, 1384; electron transfer from, and Co(III) complexes in aqueous solution, 1390; abstraction reactions of D atoms and, Hg-photosensitized decomposition of cyclohexane-cyclohexane-*d*₁₂ mixtures, 2027
- Hydrogen bonds, in solid 1:1 pyridine-benzoic acid complexes, 74; in fast reactions of 2,2-disubstituted malonic acids, 467; n.m.r. study of H bonding in N-monosubstituted amides, 1482; between hindered phenols and N-methylacetamide and N,N'-dimethylacetamide, 1622; amide, temperature dependence of enthalpy of formation of, 1704; H-bonding properties of simple alcohols, both as proton donors and acceptors, 2494; formed by amide groups in dioxane solution, 2799; p.m.r. studies of amine-acetamide-chloroform systems, 2950; p.m.r. and infra-

- red study of, in tri-*n*-octylammonium salt solutions, 3075; H-bonding equilibrium constants of substituted pyridines to phenol, 3089; near-infrared study in water and deuterium oxide, 3722
- Hydrogen bromide, acidity function of, in acetic acid-water mixtures, 2649
- Hydrogen fluoride, elimination of HF from hot fluorinated ethanes, activation energies and rate parameters, 3898
- Hydrogen ion, limiting equivalent conductance to 400°, 2984
- Hydrogenolysis, of ethane, comparison of catalytic activities of Ni, Co, and Pt, 95; of ethane over dilute Ni catalysts, 3857
- Hydrogen oxalate ion, kinetics of decomposition in glycerine solution, 2392
- Hydrogen peroxide, decomposition on glass, 3658; effect of water on yields of, in radiolysis of methanol, 3673
- Hydrolysis, base-catalyzed, of urea, 687; of bichromate ion in acetate buffer and acid catalysis, 1736; of diglycidyl ether of 1,4-butanediol and of diglycidyl ether, zinc fluoroborate and hydrogen ion catalyzed, 1882; of uranyl ion, kinetics of, 2319; cupric ion catalyzed, of glycine ethyl ester, glycynamide, and picolinamide, 2914; of amino acid esters, promoted by transition metal ions, 2923; of maleamic and phthalamic acid, effect of ethyl substitution on kinetics of, 3626; of tantalum(V) in KF-LiF, 4335
- Hydrophobic bonds, thermodynamic parameters of, in model system, 1310; effect of urea on water structure and, 2720
- Hydroxide ion, limiting equivalent conductance to 300°, 2984
- Hydroxyl groups, of alumina, exchange of deuterium with, 3070; of alumina and silica-alumina catalysts, exchange with deuterated methane, 3080; structural, infrared study of zeolites and adsorbed molecules, 3463; number at exterior surfaces of faujasite crystals, 4050
- Hydroxyl radical, relative rate constants for reactions of, benzoate radiolytic decarboxylation, 1938
- Hysteresis, adsorption, and pore area for packed spheres, 1395
- Indium, kinetics and equilibria of system In(III)-In(I)-In(0) in acidic media, 202; electronic spectra of Ga₂, In₂, and Tl₂ molecules, 2480; amalgams, interfacial tension in perchloric acid solutions, 3817
- Indium sulfide, thermodynamic stabilities as function of composition for phases of, 3826
- Indoaniline dyes, kinetics of alkaline decomposition of, 2357
- Interaction scheme, application to molecular properties of substituted methanes, 1550
- Interfacial tension, of indium amalgams in perchloric acid solutions, 3817
- Interferometer, high intensity, multislit Rayleigh, application to sedimentation studies, 4024
- Interferometry, wave-front-shearing, thermal diffusion measurements by, 1016
- Internal rotation barrier, estimate for hexamethylbenzene, 3126; in 2-furaldehyde, 4062
- Intradiffusion coefficient, and derived frictional coefficients for benzene and cyclohexane in their mixtures, 3116; of urea, from diffusion study of system, labeled urea-urea-water, 3120
- Iodic acid, Raman studies of, 3886
- Iodine, phase diagram for bismuth iodide-iodine, 124; irregular solutions of, 605; phase diagrams of KI-I₂, Rb-I₂, and CsI-I₂ systems, 1687; interaction of triphenylamine with, spectra study, 2127; reaction with methane, heat of formation of methyl iodide, 3040; orientation in pyridine-iodine complexes, 3178
- Iodine atoms, diffusion coefficients of, correction, 3182
- Iodine monochloride, thermodynamic properties of, 2443; continuous absorption spectrum of, 2483
- Ion aggregates, interionic vibrational absorption bands of, in benzene, 3223
- Ion beams, chemical synthesis with, 799
- Ion exchange, resins, volumetric studies of resin particles using microscopy, 70; selectivity, effect of water activity on, 339; on mineral clinoptilolite, 531; membranes, cation interchange across, 883; accompanied by reaction, 1178; resins, low-cross linked electrolyte uptake equilibria with, 1477; kinetics of, in phosphonic resin Bio-Rex 63, 3400
- Ionic strength, thermodynamic calculation of dependence of ion-exchange reaction selectivity coefficients on, 2378
- Ionization, of aqueous acids, entropy and volume changes, 965; of 3-amino-4-methylbenzenesulfonic acid, thermodynamic study, 2653; and dissociation of diphenyl and condensed ring aromatics by electron impact, 2935; of diphenylcarbonyls and ethers by electron impact, 2943; and dissociation of ruthenium and osmium tetroxide, 3893
- Ionization constants, for 3-amino-4-methylbenzenesulfonic acid, 2653; of sulfuric acid-water solutions at high temperatures and pressures, 2726; of sulfonic acids by Raman spectra, 4109
- Ionization potentials, of cyclopentadienylmolybdenum dicarbonyl nitrosyl and 1,3-cyclohexadieneiron tricarbonyl, 3198; of aromatic amines, 3506
- Ion pairs, AgNO₃, in alkyl halide-silver nitrate reaction, 661; manganese sulfate, effect of pressure on dissociation of, 2595; formation in aqueous solutions of butylammonium isobutyrate, 2801
- Iron, rate of oxidation of, to wüstite in water-hydrogen gas mixtures, 327; Ba-Fe-O compounds with varying oxygen content and iron valence, 4395
- Iron oxide, liquid, structure and dissociation equilibrium in, 804
- Iron pentacarbonyl, gas phase electron diffraction investigation of, 3405
- Irradiation, fast neutron and γ -, of polystyrene, 828
- Isobutane, chemically activated decomposition of, 4348
- Isoelectronic molecules, scaling in, 2520
- Isomerization, thermal, of ethylcyclopropane, 429; γ -radiation-induced, of cyclohexanone to 5-hexenal in liquid phase, 666; thermal, of cyclobutene, 1073; *cis-trans*, of *para*-substituted N-benzylideneanilines, 1584; structural, of series of vibrationally excited alkylcyclopropanes, quantum statistical weight effects, 1973; thermal, of trifluoromethylcyclopropane and trifluoroethylcyclopropane, 2141; photochemical and thermal, of *trans*- and *cis*- α -cyano- α -phenyl-N-phenylnitrones, 2545; radiation-induced *cis-trans*, of polybutadiene, 2629; of isomeric monoglycerides, 2887; Hg-photosensitized, of perfluorobutene-2, 3205; π -complex mechanism for, and isotope exchange of *cis*- and *trans*-stilbenes on Pt catalysts, 3526; γ -ray-induced, of *cis*- and *trans*-1,2-diphenylcyclopropane, 4401
- Isonicotinamide, electric moment of, in benzene and dioxane solutions, 691
- Isopentane, Hg-photosensitized decomposition of, 2291
- Isopropyl radicals, tritium-labeled, disproportionation and combination of, 1059; reactivity with cyclohexadiene-1,3, 2362
- Isotherms, absorption, of hydrogen in α -phase of hydrogen-palladium system, 3773
- Isotope effects, in radiolysis and photolysis of H₂O-D₂O mixtures, 698; C¹³, in pyrolytic decomposition of magnesium oxalate, 918; C¹³, in oxidation of acetic acid, 1428; in Hg-photosensitized decomposition of cyclohexane-cyclohexane-*d*₁₂ mixtures, 2027
- Keratin, role of amino groups in water absorption by, 3280
- Ketones, cyclic and bicyclic, relationship between C¹³ carbonyl chemical shifts and $n \rightarrow \pi^*$ transition energies in, 3105; cyclic, nonstereospecific mechanisms in photolysis of, 3225
- Knudsen cells, diffusional processes in, effect on vapor pressure measurements, 3538
- Lanthanum monosulfide, vaporization, thermodynamics, and dissociation energy of, 2684
- Lanthanum oxide, heat of formation of, 2464
- Lattice energies, for group I-A and II-A salts, 384; of superoxides of potassium, rubidium, and cesium, 2550; of alkali and alkaline earth peroxides and double electron affinity of oxygen molecule, 2558; of potassium ozonide, 2562; of cubic oxides, 2971; for alkaline earth halides, 3611
- Lead, galvanic cell measurement of thermodynamic interaction between zinc and, in dilute solution in liquid, tin, 4085
- Lead chloride, molten, electronic commutator determination of E° of formation and related thermodynamic values for, 1034
- Lead(II) perchlorate, hydrolyzed, equilibrium ultracentrifugation of, 959
- Light scattering, measurements on optically active systems, 689; by poly- γ -benzyl-L-glutamate solutions subjected to electric fields, 2817
- Lipoamide dehydrogenase, -NADH-dye reaction, kinetic study, 3696
- Liquid junction potentials, between acetonitrile and aqueous saturated calomel electrode, 3049; calculation by computer simulation method, 4226
- Liquids, surface area of, in circular tubes, 1809; volume-energy

- relations at 0°K. in, 3190; reduced thermodynamic functions for significant structure theory of, 3322; internal pressure of simple, 4392
- Lithium, thermodynamic quantities in exchange of Li^+ with Cs^+ on cross-linked polymethacrylate ion exchangers, 2374
- Lithium ion, limiting equivalent conductance to 300°, 2984
- Luminescence, of doped aromatic crystals, 751
- Luminescence behavior, radiolysis and, of dioxane-benzene mixtures, 3024
- Magnesium, heats and entropies of dilution of perchlorates of, 4231
- Magnesium oxalate, pyrolysis, kinetics and stoichiometry, 442; carbon isotope effects in pyrolytic decomposition of, 918
- Magnesium sulfate, multistate dissociation and effect of pressure on equilibrium on, 695; conductance studies in dioxane-formamide, 2857; as unassociated salt in N-methylformamide, 3167
- Magnetic susceptibilities, of copper acetylacetonate and diphenylpicrylhydrazyl adsorbed on silica gel, 3654
- Maleamic acid, effect of ethyl substitution on kinetics of hydrolysis of, 3626
- Malonic acids, 2,2-disubstituted, fast reactions involving hydrogen bonding, 467
- Manganese dioxide, catalyst for decomposition of alkali metal perchlorates, 1114
- Manganese sulfate, kinetics of ion association in solutions of, using ultrasonic absorption, 128; ion pairs, effect of pressure on dissociation of, 2595
- Mannitol, frictional and diffusion coefficients for system water-mannitol-sodium chloride, 4276
- Melting point, of thorium mononitride, 1223
- Membrane phenomena, effect of pH and divalent cations on transport of univalent cations across weak-acid membrane, 2415; equation for electric potential, 3981; membrane potential in nonisothermal systems, 4191; spectroscopic and photoconductivity effects in permselective membranes, 4221
- Mercaptoethanol, complex with cationic dye, 940
- 2-Mercaptoethanol, rates of mercapto proton exchange for, in aqueous solution, 2287
- Mercury, interatomic energy constants of, 1740; anion exchange of chloride complexes of, 2955; atomic, diffusion coefficient in isoctane, 3814; electrode, structure of electrical double layer at, in presence of adsorbed nitrate ions, 4113
- Mercury(II) bromide, kinetics for formation of, 1835
- Mercury divinyl, photolysis of, 2323
- Mesitylene, solvent effects on charge-transfer complexes of 1,3,5-trinitrobenzene with, 2766
- Metal carbonyl solutions, mechanism of photochromism in, 677
- Metal complexes, interaction of cross-linked polymethacrylic acid with polyvalent metal ions, 2849
- Metal dissolution reaction, kinetic theory of inhibition and passivation in, 1259
- Metals, wettability of, under continuous condensing conditions, 1306
- Metal wires, infrared spectra of molecules adsorbed on metal powders obtained from electrically exploded wires, 2139
- Methacrylate polymers, irradiated, degradation and e.s.r. spectra of, 189
- Methane, kinetics of reaction of $\text{O}(^3\text{P})$ with, in oxygen, nitrogen and argon-oxygen mixtures, 1611; reaction with iodine, heat of formation of methyl iodide, 3040; deuterated, exchange of hydroxyl groups of alumina and silica-alumina catalysts with, 3080; acetylene production in radiolysis of, 3218; rare gas sensitized radiolysis of, 3434; effect of temperature in radiolysis of, 3652; diffusion of, in water, 3752
- Methanes, substituted, bond and interaction contributions for calculating heat of formation, diamagnetic susceptibility, molar refraction and volume and thermodynamic properties of, 1550
- Methanol, exchange between solvated cations and solvent, 134; anodic oxidation of, in platinum-gold alloys, 3377; -acetonitrile mixtures, dielectric constants of, 3657; radiolysis of, effect of water on peroxide yields, 3673; electron capture by solutes in radiolysis of, 4053
- 2-Methoxyethanol, apparently primary CH_5^+ ion in mass spectrum of, 4420
- N-Methylacetamide, thermodynamic properties of solution of HCl in, 1335; hydrogen-bonding studies of hindered phenols with, 1622; p.m.r. studies of hydrogen bonding in amine-acetamide-chloroform systems, 2950
- Methylamines, N-monosubstituted, n.m.r. spectra of, 3645
- N-Methylaniline, association with benzene, N,N-dimethylaniline, pyridine, and N,N-dimethylcyclohexylamine, 1596
- o-Methylbenzyl alcohol, catalytic vapor phase oxidation, 457; oxidation of, over vanadia, kinetics of processes occurring on catalyst surface during reaction, 3092
- Methylene, reaction with propene, butene-1, 3,3,3-trifluoropropene, and 4,4,4-trifluorobutene-1, rates for chemically activated species that arise, 1964; reaction with CF_2H_2 , 2804
- Methylene blue, comparison of photoactivities of thionine and, 647; photooxidation of tertiary nitrogen compounds by, 1149
- Methylene fluoride, reaction of methyl radicals with, 664
- Methylene esters, unsaturated, mass spectrometric studies of, 1711
- Methyl ethyl carbonates, pyrolysis in gas phase, 3013
- Methyl fluoride, reaction of methyl radicals with, 664
- 3-Methyl-1,5-hexadiene, thermal rearrangement between, and 1,5-heptadiene, 1278
- Methyl isocyanide, n.m.r. study of, 4152
- Methyl isopropyl ketone, photochemistry of, 943
- Methyl radicals, reaction with methyl and methylene fluoride, 664
- Methyl red, photoreduction of, when sensitized by ethyl chlorophyllide a, 821
- Methylsiloxanes, polymerization, kinetics of, 2213; cyclic and linear, equilibrium molecular weight distribution of, 2218
- Methyl-2-tetrahydrofuran, ethanol-, mixtures, electron trapping in, 3186
- Micelles, formation in concentrated sulfuric acid as solvent, 968; hydrophobic bonding and micelle stability, 2431; ionic strength dependence of micelle number, 3718
- Microporous solids, charged, exclusion of ions from, 2230
- Molar volume, of two tetraethanolammonium halides, 3569
- Molar refraction, bond and interaction contributions for calculating, 1550
- Molar volume, bond and interaction contributions for calculating, 1550
- Molecular orbitals, use of nonlinear estimation techniques in calculations, 2316; valence-shell, 3357
- Molecular solutions, analyses of excess enthalpy and volume data in terms of different theories of, 2759
- Molecular vibrations, mean-square perpendicular amplitudes and shrinkage effects in benzene molecules, 1489
- Molecular weight, effect on melting temperature and fusion of polyethylene, 417; intrinsic viscosity-molecular weight relationship for fractions of linear polyethylene, 1645
- Molecular weight distribution, verification of Flory theory of random reorganization of, in kinetics of methylsiloxane polymerization, 2213; equilibrium of cyclic and linear methylsiloxanes, 2218
- Molybdenum, relation between specific heat and total emittance in Ta, Nb, W, and, 1420; reaction of flowing steam with, 1638; volatilization of, in presence of water vapor, 2065; kinetics of attack of, by dissociated chlorine, 4290
- Monoglycerides, isomeric, heats of combustion, formation, and isomerization of, 2887
- Monolayers, soluble, of normal alcohols, thermodynamic properties of, at water-octane interface, 310; interfacial, of octane-soluble dipoles, structural arrangement, 481; fatty acid, on metals, study by contact potential measurements, 984; properties of partially localized adsorbed, 3446
- Montmorillonite, infrared study of complexes of ethylamine with ethylammonium and copper ions in, 683; aliphatic and aromatic saturated, dehydration of, 2265
- Naphthalene, triplet states of, 2239
- β -Naphthol, effect of solvent on acid-base kinetics of excited state of, 2044
- Neopentyl esters, specific rearrangements in mass spectra of, 1742
- Neptunium, -hydrogen system, 1641
- Nickel, exchange of methanol between solvated nickel and solvent, 134; p.m.r. line widths, ligand exchange, and electronic relaxation times for arylphosphine complexes of Ni(II), 3212; investigation of metallic phases in reduced, impregnated Ni and Ni-Cu silica-alumina catalysts, 3268; ethane hydrogenolysis over dilute Ni catalysts, 3857
- Nickel monomalonate complex, formation kinetics of, by temperature jump method, 4380
- Nickel sulfates, change in structure with heating, 4077

- Nickel tetracarbonyl, effect in radiolysis of benzene and benzene-cyclohexane mixtures, 2034
- Nicotinamide adenine dinucleotide, reduced form, kinetics of lipoamide dehydrogenase-NADH-dye reaction, 3696
- Nicotinamides, N-alkyl substituted, benzene and dioxane electric moments of, from measurements in mixed benzene-dioxane solutions, 4097
- Niobium, relation between specific heat and total emittance in Ta, W, Mo, and, 1420
- Niobium pentafluoride, enthalpy of formation, 2089
- Nitrate ion, 300-m μ band of, 2645; infrared band width of, ν_2 mode, ionic lifetimes and solvent isotope effect, 3650; adsorbed on Hg electrode, structure of electrical double layer, 4113
- Nitrate solutions, radiolysis of, 1858
- Nitric acid, water-, uranyl nitrate hexahydrate system, activities of components in, 1904
- Nitric oxide, heat of formation of NO(g), 3863; infrared spectra and bonding of, adsorbed on Ni and Fe, 4998
- Nitrioltriacetic acid, complex with poly-N-vinylimidazole, 1252
- Nitrioltriacetate chelates, infrared spectra of, in aqueous solution, 404
- Nitrioltripropionamide, -acrylamide system, dye photopolymerization processes, 641
- p*-Nitroaniline, reaction with poly(*p*-styrenesulfonic acid), salting in process, 2895
- Nitrobenzene, synthesis of, by interaction of NO₂⁺ ion beam with gaseous benzene, 799; nitration of, with nitronium fluoroborate in HF, 2248; -*n*-heptane system, critical opalescence measurements on, 4312
- Nitrogen, exchange of substituents on, in molten ammonium salts and amines, 791; tertiary compounds, photooxidation by methylene blue, 1149; solubility in sea water, 2608; adsorption on heterogeneous titania and homogeneous carbon surfaces, 3587
- Nitrogen atoms, mass spectra study for reaction with ethylene, 2736
- Nitrogen dioxide, concerning the reaction NO₂ + NO* → N₂O + O₂, 2137
- Nitrogen gas, analytical expression for zero pressure thermodynamic properties of, 495; isotopic exchange induced by γ -radiation, 2385
- Nitrogen tetroxide, radiolysis of liquid, 3547
- Nitrogen trioxide, evidence in combustion of double-base propellant, 3668
- Nitronium fluoroborate, nitration of nitrobenzene with, in HF, 2248
- Nitrophenols, dissociation constants in deuterium oxide, 4416
- Nitrous oxide, kinetics of decomposition of, mass spectra study, 2111
- Noble gases, electronegativity of, 596; thermodynamics of aqueous solutions of, 3240; thermodynamics of aqueous solutions of, effect of nonelectrolytes, 3245; thermodynamics of aqueous solutions of, effect of electrolytes, 3250
- Noble metals, voltage transients of freshly produced electrode surfaces of, 3329
- Nonlinear estimation technique, use in simple molecular orbital calculations, 2316
- Nonylphenoxyacetic acid, adsorption of, by metals, 2598
- Norbornylene, thermal unimolecular decomposition of, 1351
- Nucleation, of long-chain molecules in monomolecular layers, 956
- n*-Octadecanol, aqueous solubility of, 3171
- n*-Octane, adsorption on poly(tetrafluoroethylene), 4387
- Oil, radiotracer study of competitive adsorption at gold-oil interface, 3833
- Olefins, relative rates of H-atom addition to two positions of unsymmetric alkyl-substituted ethylenes, 905; product, unimolecular decomposition of, in methylene chemical activation systems, 1952; desorption from silica-alumina catalysts, 2676
- Onsager reciprocal relation, test in isothermal ternary diffusion of water-sodium chloride-potassium chloride, 3374; test of, on system water-mannitol-sodium chloride, 4276
- Opalescence, critical, of binary liquid mixtures, 2329
- Optical properties, of built-up layers of barium stearate on evaporated gold films, 1654
- Optical rotatory dispersion, of L-cysteine-cobalt systems, 1603; of *d*-camphor, 3708
- Organometallics, energy-transfer processes in dilute solutions of, 2880
- Osmium tetroxide, ionization and dissociation of, 3893
- Osmotic pressure, of polystyrene solutions, 1174
- Outer coordination sphere, n.m.r. relaxation time effects produced by paramagnetic ions with nonlabile inner coordination spheres, 3299
- Ovalbumin, sedimentation velocity in concentrated salt solutions, 3032
- Oxalic acid, kinetics of decomposition of, in glycerine, 1729
- Oxidation, of titanium monoxide at high temperatures, 158; of iron to wüstite in water-hydrogen gas mixtures, 327; catalytic vapor phase, of *o*-methoxybenzyl alcohol, 457; homogeneous gas-phase partial, of *o*-xylene, 909; C¹³ isotope effects in oxidation of acetic acid, 1428; radiation-induced, of organic compounds, 1814; radiaticn-induced, of *p*-xylene sensitized by organic bromines, 1992; of reducing sugars by hexacyanoferrate(III) in alkaline medium, 2038; simultaneous chemical and electrochemical, of germanium, 2269; of *o*-methylbenzyl alcohol over vanadia, kinetics of processes occurring on catalyst surface, 3092; and reduction of diphenylpicrylhydrazyl on titanium dioxide and carbon black, 3219; and chemiluminescence of tetrakis(dimethylamino)ethylene, 3313; anodic, of methanol in platinum-gold alloys, 3377; Hg-photosensitized, of perfluoropropene, 3641; of Pt in activated oxygen, kinetics and mechanism, 3660; of alcohol by Fenton's reagent, 3805; electrode, correction for, in estimation of adsorbed CO on smooth Pt by anodic stripping, 4049
- Oxygen, chemisorption on ruthenium dioxide, 102; chemiluminescent reaction of oxygen atoms with sulfur monoxide, 849; effect on e.s.r. spectra of anthracene and perylene adsorbed on silica-alumina, 1082; atomic, kinetics of reaction of O(³P) with methane in oxygen, nitrogen, and argon-oxygen mixtures, 1611; molecule, double electron affinity of, lattice energies of alkali and alkaline earth peroxides, 2558; chemisorption on zinc oxide, 3254; adsorption studies on heterogeneous titania and homogeneous carbon surfaces, 3587; sulfur in burnt gas of hydrogen-oxygen flames, 3593; enhanced oxidation of Pt in, kinetics and mechanism, 3660; diffusion in polymers, use of phosphorescent quenching, 3677; -ozone and CO₂ equilibria, bromine ultraviolet lamp, 3964; in skin of Pt electrode, effect on determination of CO adsorption, 4048; desorption and isotopic exchange of, at silver surface, 4201; Ba-Fe-O compounds with varying oxygen content and iron valence, 4395
- Oxygen-17, chemical shifts in n.m.r. absorption for, in oxy ions, 1844
- Oxygen electrode, in fused alkali nitrates, 3662
- Oxy ions, chemical shifts in n.m.r. absorption for O¹⁷ in, 1844
- Ozone, electron affinity of, 2562; bromine ultraviolet lamp, studies of oxygen-ozone and CO₂ equilibria, 3964
- Palladium, vapor pressure of, mass spectrometric Knudsen cell measurements, 1373; isotopic equilibrium separation factors in hydrogen solubility process in Pt-Pd alloys, 2485; absorption isotherms of hydrogen in α -phase of H₂-Pd system, 3773
- Palladium(II) chloride, polymorphism in, 3669
- Palladium oxide, partial pressure of, mass spectrometric Knudsen cell measurements, 1373
- Parachol, relationship between Zisman's critical surface tension of polymers and, 3220
- Pendant drop method, for surface tension, refinement, 348
- Pentaerythrityl halides, heat capacities and thermodynamic properties of, 1209
- Pentamethylbenzene, solvent effects on charge-transfer complexes of 1,3,5-trinitrobenzene with, 2766
- 1-Pentanethiol, heat of vaporization and heat capacity of vapor, 3030
- Peptide linkage, $n-\pi^*$ Cotton effect, 978
- Peptides, dielectric dispersion of crystalline powders of, 4176
- Perchlorates, of magnesium and strontium, heats and entropies of dilution of, 4231
- Perchloric acid, extraction by trioctyl phosphine oxide, 1106; extraction into tri-laurylamine, role of aromatic diluent, 1565
- Perfluoroalkanes, importance of xenon fluorides in Xe-photosensitized reactions of, 1434
- Perfluoroalkyl nitriles, reactivities toward butadiene, 1070
- Perfluorobutene-2, *cis*- and *trans*-, addition of fluorine to, 254;

- cis*- and *trans*-, infrared spectra of, 693; Hg-photosensitized isomerization of, 3205
- Perfluorocyclic oxide, critical opalescence of two mixtures of, with *n*-heptane and with carbon tetrachloride, 2329
- Perfluorocyclobutane, radiation chemistry of, spectroscopic identification of products, 2059
- Perfluorocyclohexane, radiation chemistry of, spectroscopic identification of products, 2059; spin-echo n.m.r. spectra studies of chemical exchange in perfluorocyclohexane, 3216
- Perfluorocyclopropane, infrared spectra of, 693
- Perfluoropropene, Hg-photosensitized decomposition of, 3600; Hg-photosensitized oxidation of, 3641
- Peroxides, alkali and alkaline earth, lattice energies of, and double electron affinity of oxygen molecule, 2558
- Perrenic acid, extraction by trioctyl phosphine oxide, 1106
- Perylene, effect of oxygen on e.s.r. spectra of, 1082; crystal structures of equimolar π -molecular compounds of anthracene and, with pyromellitic dianhydride, 2160
- Petroleum, small angle X-ray scattering study of colloidal nature of, 3500
- Phase diagrams, for bismuth iodide-iodine, 124; of KI-I₂, RbI-I₂, and CsI-I₂ systems, 1687; *P-T-x*, for system zinc-tellurium, 3367
- Phase equilibria, in solutions of liquid sulfur, 261
- Phenanthrene, mass spectra and appearance potentials of principal ions of, 2935; p.m.r. spectrum of, 4417
- Phenol, O¹⁸ labeled, infrared absorption of, 2259; -acetate system, use of fluorescence measurements to determine association constant, 2960; H-bonding equilibrium constants of substituted pyridines to, 3089
- Phenols, hindered, hydrogen-bonding studies of, with *N*-methylacetamide and *N,N'*-dimethylacetamide, 1622; dissociation and homoconjugation in acetonitrile, 3193
- Phenosafranine, kinetics of ethyl chlorophyllide sensitized photo-reduction of, by hydrazobenzene, 2633
- Phenylacetylene, n.m.r. spectra of, 3552
- Phenylmalonic acid, kinetics of decarboxylation of, 2402
- Phosphorescence, and electron transfer in dye-disulfhydryl compound complex, 940; decay rate from triphenylene molecules in acrylic polymers, 2516
- Phosphoric acid, dissociation of solutions of, 3520
- Phosphorus, potential curves and bond strength of PO, 3461
- Photochemistry, vacuum ultraviolet, for propylene, 538; of chromium(III) complexes, role of doublet state in, 2201; of $\Delta^{3,5}$ -bicyclo[2.2.1] heptadiene, 2475; of aqueous sulfate ion, 2996
- Photochromism, in metal carbonyl solutions, 677; of 2,2'-dimethylbianthrone, e.s.r. spectra, 2487
- Photoconduction, hypersensitization of, in microcrystalline zinc oxide, 767
- Photoconductivity, bulk, sensitization of, in *p*-chloranil crystals, 779; effects in permselective membranes, 4221
- Photoelectric effect, relationship between exciton absorption and, 745; in polymers and their sensitization by dopants, 755
- Photoisomerization, *cis-trans*, of azo compounds, temperature dependence, 1062
- Photoluminescence, of adsorbed dyes, 738
- Photolysis, isotope effects in, of H₂O-D₂O mixtures, 698; of heptafluoropropyl ethyl ketone, 1001; of ketene in propene, butene-1, 3,3,3-trifluoropropene, and 4,4,4-trifluorobutene-1 1964; of nitrogen dioxide, 2137; of mercury divinyl, 2323; rearrangement reactions of 2-*n*-propylcyclopentanone, 3145; of cyclic ketones, nonstereospecific mechanisms, 3225; of trifluoronitrosomethane, 4409; of fluorotrichloromethane, 4410
- Photooxidation, of tertiary nitrogen compounds by methylene blue, 1149; possible initiation of, by charge-transfer excitation, 4317
- Photopolymerization, dye-sensitized, thionine-nitrotripropionamide-acrylamide system, 641; dye-sensitized, comparison of photoactivities of thionine and methylene blue, 647; dye-sensitized, use of dicarbonyls as photoinitiators with thionine and methylene blue, 2834; dye-sensitized, kinetics and mechanism of thionine- β -diketone-acrylamide systems, 2842
- Photoreduction, of methyl red sensitized by ethyl chlorophyllide *a*, 821; ethylchlorophyllide sensitized, of phenosafranine by hydrazobenzene, 2633
- Photosensitization, mechanism of semiconductors by dyes, 730; of CO₂ with Hg 6 ¹P₁ atoms, 4047
- Photosynthesis, electron-hole picture of, 788
- Phthalamic acid, effect of ethyl substitution on kinetics of hydrolysis of, 3626
- Phthalocyanines, polymorphic modifications of, 2295
- Picolinamide, cupric ion catalyzed hydrolysis of, 2914
- Picolinic acid, decarboxylation in polar solvents, 2277
- Piperidine, high resolution mass spectrum of, 3196
- Platinum, -gold alloys, heterogeneous, electrochemical characterization of surface composition of, 901; -Pd alloys, hydrogen solubility process in, 2485; electroadsorption of ethylene on, as function of potential, concentration, and temperature, 3335; -gold alloys, anodic methanol oxidation in, 3377; electrodes, propane adsorption on, 3424; enhanced oxidation of, in activated oxygen, kinetics and mechanism, 3660; electrode, effect of oxygen absorbed in skin of, on determination of CO adsorption, 4048; wetting of, by water, 4238
- Polarizability, of rare gas atoms, 702; molecular, for sulfur trioxide, 2017
- Polar molecules, adsorption on metal oxide single crystals, 3930
- Polarographic currents, effect of adsorbed polyelectrolytes on, 2740
- Polarography, influence of adsorbed positively charged polyelectrolytes on polarographic currents of cationic depolarizers, 3018
- Poly- γ -benzyl-L-glutamate, influence of pressure on reversible unfolding of, 1515; light scattering studies on samples in dichloroethane, 2817
- Polybutadiene, radiation-induced *cis-trans* isomerization of, 2639; effects of cross-link spacing and initial molecular weight in, 2811
- cis*-1,4-Polybutadiene, viscosity behavior of, and polystyrene in mixed θ -solvents, 3263
- Polydispersity, from diffusion data on polymers, 1144
- Polyelectrolytes, conductometric study of polycation-polyanion reactions, 1447; dielectric properties of polyanion-polycation complexes, 1456; adsorbed, effect on polarographic currents, 2740; salting in by aqueous polyelectrolyte solution, 2895; adsorbed positively charged, influence on polarographic currents of cationic depolarizers, 3018; stereoregular, potentiometric titration of, 4005; mean activity coefficients of sodium polyacrylates, 4102
- Polyenes, cyclic, reactivity toward free radicals, 2362
- Polyethylene, effect of molecular weight on melting temperature and fusion of, 417; linear, intrinsic viscosity-molecular weight relationship for fractions of, 1645; single crystals, specific heat, 2078; linear, intrinsic viscosity in θ -solvent, 3109
- Polyethylene oxide, high resolution nuclear resonance studies of chain conformation of, 1888
- Polymerization, reactivities and conductivities of ions and ion pairs in, 612; anionic, of styrene in dioxane, effect of solvent and counterion, 624; degree of, for lead(II) perchlorate solutes using equilibrium ultracentrifugation, 959; of uranyl ion, kinetics of, 2319; of carbon suboxide, 3603
- Polymers, semicrystalline, elasticity of, 141; degradation of, by controlled hydrodynamic shear, 161; photoelectric effect in, and their sensitization by dopants, 755; exciton states in, 784; surface free energy of, 1084; characterization of polydispersity from diffusion data, 1144; pressure effects on glass transition in, 1497; amorphous, attempt at assigning order from polymer density, 1575; radiolytic stress relaxation of ethylene-propylene copolymer, 2072; amorphous, parachor and surface tension of, 2809; ternary diffusion in system polystyrene 1-polystyrene 2-toluene, 2875; relationship between parachor and Zisman's critical surface tension of, 3220; normal stresses and dynamic moduli in polymer solutions, 3642; diffusion of oxygen in, use of phosphorescent quenching, 3677; complex modulus of concentrated solutions of, in steady shear, 4183
- Polymethacrylate ion exchangers, cross-linked, thermodynamic quantities in exchange of Li⁺ and Cs⁺ on, 2734
- Polymethacrylic acid, cross-linked, interaction with polyvalent metal ions, 2849
- Poly(methyl methacrylate), stereoregular, intrinsic viscosity studies in 2,2,3,3-tetrafluoropropanol, 1101; depolymerization in solution in various solvents, 2967; ge. melting point as measure of tacticity of, 3384
- Poly- α -methylstyrene, dilute solutions of, dynamic mechanical properties of, 346; thermal depolymerization in solution in various solvents, 2967
- Polymorphism, in potassium sulfate and thallium sulfate, 1684; in palladium(II) chloride, 3669

- Polyoxyethylene nonylphenol ethers, solubility behavior in cyclohexane and effect of water, 2788
- Polypeptides, solid, sorption rates indicative of structural changes in, 600
- Polyphenyls, gas-liquid partition chromatography in benzene-polyphenyl systems and polymer statistical thermodynamics, 3682
- Polystyrene, comparison of fast neutron and γ -irradiation of, 828; monodisperse, diffusion in mixed solvents, 1135; variation of chain dimension with concentration for, 1174; atactic and isotactic, thermal properties of, 2657; atactic and isotactic, specific heat, 2668; -polystyrene-toluene system, ternary diffusion in, 2875; phase equilibrium and viscosity behavior of *cis*-1,4-polybutadiene and, in mixed Θ -solvents, 3263; temperature dependence of viscoelastic behavior of, 3480; conformation of molecules adsorbed at Θ -temperature, 3955; isotactic, physicochemical studies on, 4138; cross-linked sulfonates, thermodynamics of exchange of tetramethylammonium with sodium ions in, 4268
- Polystyrenesulfonic acid, ion-exchange membranes of, having variable porosity, 883
- Poly(*p*-styrenesulfonic acid), reaction between *p*-nitroaniline and, 2895
- Poly(tetrafluoroethylene), adsorption of ethane, *n*-butane and *n*-octane on, 4387
- Polyurethanes, cleavage reactions in cross-linked urethane elastomers, 476
- Poly-L-valine, comparison of water sorption and D-H exchange sites in, 1432
- Poly-N-vinylimidazole, neutralized, influence of electrolytes on solution properties of, 1248; complexes with zinc(II), copper (II) and nitrilotriacetic acid, 1252
- Porous-frit method, combined with radiometric techniques for determination of diffusion coefficients, 303
- Potassium, surface tension in reciprocal system K^+ , Cd^{+2} - Cl^- , Br^- , 1443; phase diagrams of $KI-I_2$ system, 1687; viscosity of NaK 78 at low temperature, 3782
- Potassium bromide, cationic transport numbers in *N*-methylacetamide, 2382
- Potassium chloride, -hydrochloric acid system, thermodynamic properties of, 307; solubility and activity coefficients of, in *N,N*-dialkylamides containing water, 1377; diffusion in methanol-water solutions, 2336; ionic association of, in ethanol-water mixtures, 2420; transport numbers in solution of, 3208; test of Onsager reciprocal relation in isothermal diffusion of water- $NaCl$ - KCl , 3374
- Potassium ferricyanide, entropy of, 3179
- Potassium hexabromorhenate(IV), heat capacity, thermal history behavior, antiferromagnetic anomaly, entropy, and free energy functions, 3471
- Potassium ion, limiting equivalent conductance to 400°, 2984
- Potassium ozonide, lattice energy of, 2562
- Potassium sulfate, polymorphism in, 1684
- Potassium superoxide, heat of formation and lattice energy of, 2550
- Potassium trisoxalatochromium(III) trihydrate, solid-state thermal decomposition of, 4328
- Potential, Volta, study of aging of gold surfaces, 439; thermo-electric, in Soret steady state, for $AgNO_3$ - $NaNO_3$ system, 1204; e.m.f. studies of cadmium chloride in water, water-ethanol, and ethanol, 2082; appearance, and mass spectra of fluorinated ethylenes, 3731; appearance, and mass spectra of fluorinated ethylenes, calculations based on statistical theory of mass spectra, 3737; appearance, and mass spectra of C_3F_6 , and C_3F_5Cl , and *c*- C_3F_6 , 3741; appearance, for positive ions formed by C-C and C-F bond ruptures in $C_2F_6^+$ and $C_3F_8^+$, 3746
- Potential energy curves, for P-O interactions, 3461
- Potentiometric titrations, of stereoregular polyelectrolytes, 4005
- Praseodymium oxides, reactions in an oxygen atmosphere, 1667
- Pressure, hydrostatic, effect on gases dissolved in water, 389
- Probabilities, vibrational de-excitation, calculation of, 1424
- Promethium-147, mean β -energy and half-life of, 1220
- Propane, radiolysis at low conversions, 888; adsorption on smooth Pt electrodes, 3424; effect of temperature in radiolysis of, 3652; diffusion in water, 3752
- Propellant, double-base, evidence for nitrogen trioxide in combustion of, 3668
- Propenes, monodeuterated, mass spectra of, 1615
- n*-Propylbenzene, thermodynamic properties of, 4304
- 2-*n*-Propylcyclopentanone, photochemical rearrangement reactions of, 3145
- Propylene, vacuum ultraviolet photochemistry of, 538; ethylene-, copolymers, radiolytic stress relaxation of, 2072
- Proteins, proton fluctuation in, experimental study of Kirkwood-Shumaker theory, 2281; effect of deuterium oxide on thermal stability of, 3132; dielectric dispersion of crystalline powders of, 4176
- Protein solutions, dielectric dispersion of, 1162
- Protonation, of acetic and benzoic acids and ethyl esters in concd. sulfuric acid, C^{13} magnetic resonance study, 103; of pyrazine, p.m.r. study, 2791
- Proton fluctuation theory, Kirkwood-Shumaker, attempt at experimental verification by study of pH dependence of dielectric increment of proteins, 2281
- Purine bases, vapor spectra and heats of vaporization of, 3615
- Pyranose rings, conformation of, in mono-, di-, and polysaccharides at high pH, 636
- Pyrazine, p.m.r. study of protonation of, 2791
- Pyrene, magnetic resonance of triplet state of orientated pyrene molecules, 1429
- Pyridine, -benzoic acid complexes, infrared study, nature of hydrogen bond in, 74; -iodine complexes, orientation in, 3178; alkyl halide salts of, charge-transfer absorption and luminescence spectra of, 3791
- Pyridine hydrogen nitrate, crystal structure of, 1915
- Pyridines, substituted, phenol interactions with, 3089
- Pyrimidine bases, vapor spectra and heats of vaporization of, 3615
- Pyrolysis, of magnesium oxalate, kinetics and stoichiometry, 442; uninhibited and inhibited, of isomeric hexanes, surface effects in, 2453; of methyl ethyl and diethyl carbonates in gas phase, 3013
- Pyromellitic dianhydride, crystal structures of equimolar π -molecular compounds of anthracene and perylene with, 2160
- Quaternary ammonium salts, in cyanoethylsucrose-acetonitrile mixtures, 2576
- Radiation chemistry, of aqueous glycine, effect of cupric ion, 1579; of perfluorocyclohexane and perfluorocyclobutane, 2059; of some cyclic fluorocarbons, 2526; of cyclopentane, 2707; of perphenyl compounds of Sn, Pb, As, Sb, and Bi, 2880; of water, reaction mechanism leading to formation of molecular hydrogen, 4058
- Radical-ion salts, of 1,6-diaminopyrene and 7,7,8,8-tetracyanoquinodimethane, 1740
- Radicals, yielded in radiolysis of unsaturated olefins, 194
- Radiolysis, pulse, of aqueous tetranitromethane, 53; of unsaturated hydrocarbons, radical yields, 194; of cyanogen-cyclohexane mixtures, 678; isotope effects in, of H_2O - D_2O mixtures, 698; γ -, of liquid cyclopentanone, 807; of ethylene, hydrogen atom yield and formation of saturated hydrocarbons, 815; of propane at low conversions, 888; rare gas sensitized, of acetylene, 892; of ethane, effect of density on, 1045; of ethane at high densities, effect of additives, 1056; of sodium nitrite ices, 1080; of liquid aromatic hydrocarbons, LET effects, 1157; pulse, of aqueous hydrogen solutions, 1324; of acetone in air-free aqueous solutions, 1366; of bromate ions by cobalt-60 γ -rays, identification of species formed, 1413; vapor phase, of ethanol, 1699; of aqueous nitrate solutions, 1858; of benzene-butene-2 mixtures, effect of galvinoxyl on, 1866; of benzene and benzene-cyclohexane mixtures in presence of nickel tetracarbonyl, 2034; pulse, for identification of aromatic triplet states in electron-irradiated solutions, 2239; γ -, of ammonium perchlorate, 2477; of heavy water in pD range 0-14, 2628; of monodisperse colloidal sulfur, 2805; of ethylene, application of electrostatic fields, 2867; and luminescence behavior of dioxane-benzene mixtures, 3024; of cyclohexane- d_{12} -cyclopropane mixtures, comparison of dimer and olefin yields with corresponding nondeuterated mixtures, 3113; acetylene production in, of methane, 3218; of cyclohexane vapor, effect of additives on, 3292; of crystalline choline chloride, radical termination mechanisms, 3370; rare gas sensitized, of methane, 3424; of liquid nitrogen tetroxide, 3547; of methane and propane, effect of temperature, 3652; of methanol and methanolic solutions, effect of water on peroxide yields, 3673; γ -, of ethylene sensitized by inert gases, 4033; of methanol and ethanol, electron capture by solutes in, 4053; of water, reac-

- tions of alanine with reducing species formed in, 4131; pulse, of fused alkali halides, 4421
- Rare earth chelates, intermolecular triplet-triplet energy transfer between aromatic carbonyls and hydrocarbons and, 275
- Rare earths, β -diketone chelates of, absorption and phosphorescence spectra of, 1092
- Rare gas atoms, polarizability of, 702
- Reaction velocity, of monomolecular films of chlorophyll *a* on aqueous substrates, 21; and mechanism for thermal decomposition of hexanitroethane, 25; for ion association in manganese sulfate solutions, 128; for vanadium(II)-uranium(VI) reaction, 176; of homogeneous oxidation of In(I) ion by H^+ in perchloric acid, 202; fluorine addition to *cis*- and *trans*-perfluorobutene-2, 254; rate constants of hydrated electron reactions with some aromatic acid, alkyl halides, heterocyclic compounds, and Werner complexes, 289; for oxidation of iron to wüstite in water-hydrogen gas mixtures, 327; for oxygen-inhibited hydrogen-fluorine reaction, 408; for thermal isomerization of ethylcyclopropane, 429; for magnesium oxalate pyrolysis, 442; for BF_3 exchange reactions, 527; for calcium formate pyrolysis in KBr matrix, 583; of base-catalyzed hydrolysis of urea, 687; dissociation of molecular chlorine using shock waves, 834; for γ -ray-induced decomposition of chloroform, 840; for halogen displacement reactions of chloro- and bromoacetic acids, 854; for thermal decomposition of diacetylene, 858; for thermal decomposition of benzene in flow system, 863; ion exchange accompanied by reaction, 1178; kinetic theory of inhibition and passivation in electrochemical reactions, 1259; for thermal rearrangement between 3-methyl-1,5-hexadiene and 1,5-heptadiene, 1278; for e_{aq}^- with itself and other transients, 1324; for reactions of H atoms in aqueous solution, 1384; computation of statistical complexions, exact high speed method, 1431; for reactions of CN radicals in gas phase, 1504; of *cis-trans* isomerization of *para*-substituted *N*-benzylideneanilines, 1584; for reaction of $O(^3P)$ with methane in oxygen, nitrogen, and argon-oxygen mixtures, 1611; for praseodymium oxide reactions in an oxygen atmosphere, 1667; for decomposition of oxalic acid in glycerine, 1729; for hydrolysis of bichromate ion in acetate buffer, 1736; for formation of mercury(II) bromide species, 1835; for cyclopropane-hydrogen reaction over silica-supported metals, 1877; of zinc fluoroborate and hydrogen ion catalyzed hydrolyses of diglycidyl ether of 1,4-butanediol and of diglycidyl ether, 1882; measurement by benzoate radiolytic decarboxylation for hydroxyl radical reactions, 1938; for chemically activated species produced in systems of methylene with olefins, 1964; for structural isomerization of series of vibrationally excited alkylcyclopropanes, 1973; for hydrogen reduction of uranium trioxide, 2012; effect of solvent on acid-base kinetics of excited state of β -naphthol, 2044; for methylsiloxane polymerization, 2213; formation of triplet states of aromatic molecules, 2239; for mercapto proton exchange for 2-mercaptoethanol in aqueous solution, 2287; for uranyl ion hydrolysis and polymerization, 2319; alkaline decomposition of indoaniline dyes, effect of solubilization by surfactants, 2357; kinetic study of addition and metathesis between isopropyl radical and cyclohexadiene-1,3, 2362; for decomposition of hydrogen oxalate ion in glycerine solution, 2392; decomposition of phenylmalonic acid, 2402; effect of double-impact collision on dissociation rate constants, 2411; decay rate of phosphorescence from triphenylene in acrylic polymers, 2516; for ethyl chlorophyllide sensitized photo-reduction of phenosafranin by hydrazobenzene, 2633; for fluorination of graphite, 2772; and mechanism of thionine-, β -diketone-acrylamide systems, 2842; for transition metal ion promoted hydrolyses of amino acid esters, 2923; for iodine-methane reaction, 3040; for exchange of deuterium with surface hydroxyl groups of alumina, 3070; for processes occurring on catalyst surface during oxidation of *o*-methylbenzyl alcohol over vanadia, 3092; for selenium(IV)-2,3-diaminonaphthalene reaction, 3232; of ion exchange in phosphonic resin Bio-Rex 63, 3400; effect of ethyl substitution on hydrolysis of maleamic and phtalamic acid, 3626; for oxidation of Pt in activated oxygen, 3660; for lipoamide dehydrogenase-NADH-dye reaction, 3696; for tetrafluorohydrazine-fluorine reaction, 3700; for attack of molybdenum by dissociated chlorine, 4290; comparison of methods to determine rates of dehydration of acetaldehyde hydrate, 4325; for nickel monomalonate complex studies by temperature jump method, 4380
- Rearrangements, thermal, between 3-methyl-1,5-hexadiene and 1,5-heptadiene, 1278; specific, in mass spectra of neopentyl esters, 1742
- Reduced equation, for estimation of vapor pressure, 3209
- Reduction, chlorophyllide-sensitized, of azobenzene and other compounds, 2779; simultaneous oxidation and, of diphenylpicrylhydrazyl on titanium dioxide and carbon black, 3219; of $CuO_{0.67}$ in hydrogen, 3607
- Refractive index, remarks on rules for mixtures, 1123
- Refractive index dispersion, in equine hemoglobin solutions, 3188
- Relaxation, dielectric, of mixtures of dipolar liquids, 674
- Relaxation times, spin-lattice, of dimethyloctylamine oxide through c.m.c., 3204; electronic, for arylphosphine complexes of Co(II) and Ni(II), 3212; n.m.r., produced by paramagnetic ions with nonlabile inner coordination spheres, 3299; dielectric, method for determining, 4197
- Resistance, interfacial, use of glass bead column in measurement of, 2351
- Resistivity, electrical properties of ferromagnetic CrO_x ($1.89 < x < 2.02$), 1402
- Resonance, pure quadrupole, of halogens in potassium hexahalo-rhenates(IV) and hexachlorotungstate(IV), 2101
- β -Resorcylic acid, decarboxylation in polar solvents, 3565
- Rhodamine 6GX, reaction with benzoyl peroxide, 4071
- Ribonuclease, effect of aqueous alcohol solutions on thermal transition of, 298; influence of pressure on reversible unfolding of, 1515
- Rubidium, phase diagrams of RbI-I₂ system, 1687
- Rubidium superoxide, heat of formation and lattice energies of, 2550
- Ruthenium dioxide, oxygen chemisorption on, 102
- Ruthenium pentafluoride, enthalpy of formation of, 2308
- Ruthenium tetroxide, ionization and dissociation of, 3893
- Rydberg potential energy function, diatomic, extended to polyatomic species, 923
- Saccharides, mono-, di-, and poly-, conformation of pyranose rings in, at high pH, 636
- Salicylic acid, dissociation constant in deuterium oxide, 4416
- Salting in process, by aqueous polyelectrolyte solution, 2895
- Salts, molten, diffusion-conductance relations and free volume in, 399
- Samarium borides, tetraboride-hexaboride conversion, 3705
- Scaling, in isoelectronic molecules, 2520
- Scandium, -hydrogen system, thermodynamics of, 3514; -yttrium-hydrogen system, 3973
- Sea water, solubility of argon and nitrogen in, 2608; activation energy of viscous flow in temperature region of maximum density, 4988
- Sedimentation, equilibria, in polydisperse pseudo-ideal solutions and at low centrifugal fields, 1050; moving boundary, in preparative ultracentrifuge in absence of plateau region, 1820; velocity, of ovalbumin in concentrated salt solutions, 3032; and electrophoresis of interacting substances, differential boundary experiments, 3785; application of high intensity, multislit Rayleigh interferometer to studies of, 4024; equilibrium in reacting systems of type $mA + nB \rightleftharpoons C$, 4365
- Selectivity coefficients, ion-exchange reaction, thermodynamic calculation of ionic strength dependence of, 2378
- Selenium, kinetics for selenium(IV)-2,3-diaminonaphthalene reaction, 3232
- Self-diffusion, of liquid thallium from melting point to 1300°K., 518
- Self-diffusion coefficients, for water, as function of ionic concentration, 2001; of sodium ion in alcohol-water mixtures, 3968; of water, 4412
- Semiconductors, photosensitization mechanism of, by dyes, 730; organic, proposed model for electron injection into, in dark, 3510
- Semiquinones, aliphatic, e.s.r. of, 2131
- Sensitization, spectral, of chemical effects in solids, 705; dye, and minority carrier trapping, 714; of electrical effects in solids, 719; hyper-, of photoconduction in microcrystalline zinc oxide, 767; color, of zinc oxide with cyanine dyes, 774; of bulk photoconductivity in *p*-chloranil crystals, 779
- Shock tube studies, on condensation of vapors, 3006
- Shock waves, in dissociation of molecular chlorine, 834
- Shrinkage effects, in benzene molecules, 1489; Bastiansen-Morino, for sulfur trioxide, 2017

- Significant structure theory, of simple liquids, reduced thermodynamic functions for, 3322
- Silica, solubility relations in calcium oxide-silica-water system, 182; metallic phases in reduced, impregnated Ni and Ni-Cu silica-alumina catalysts, 3268
- Silica-alumina catalysts, exchange of hydroxyl groups of, with deuterated methane, 3080
- Silica gel, interaction of alkali metal cations with, 350; generation of catalytic activity by ionizing radiation, 491; aging of, 1530; behavior of alkali metal cations in pores of, 3196
- Silicoaluminas, amorphous, structure and properties of, Lewis and Brønsted acid sites, 3274
- Silver, dislocations as active centers of catalysis and chemical action in, 880; Ag-AgI electrode, behavior in presence of tetraalkylammonium ions, 2793; heats of formation of solid solutions in systems (Na-Ag)Cl and (Na-Ag)Br, 3531; -copper alloy, enthalpy of solid solution for metastable, 4407
- Silver bromide, spectral sensitization of chemical effects in, 705
- Silver(I) cyanide complexes, formation constants in equimolar sodium-potassium nitrate melts, 3763
- Silver ion, activity coefficient of, in aqueous sulfuric acid, 3906
- Silver nitrate, solution thermochemistry of, 9; ion pairs, in alkyl halide-silver nitrate reaction, 661; -sodium nitrate system, molten, thermoelectric properties, 1204; Raman, infrared, and n.m.r. spectra of, in acetonitrile, 3634
- Soaps, anhydrous sodium, n.m.r. absorption in, 4256
- Sodium, heats of formation of solid solutions in systems (Na-Ag)Cl and (Na-Ag)Br, 3531; viscosity of NkK 78 at low temperatures, 3782; Ba-Na equilibrium system, 3867; dissociative equilibrium in systems aromatic hydrocarbon⁻, Na⁺ ⇌ radical anion⁻ + Na⁺, 4124
- Sodium bicarbonate, solution thermochemistry of, 3059
- Sodium carbonate, solution thermochemistry of, 3059
- Sodium chloride, solubility and activity coefficients in N,N-dialkylamides containing water, 1377; thermodynamic properties of HCl-NaCl mixtures, 2395; activity coefficients by cation-sensitive glass electrodes, 2697; test of Onsager reciprocal relations in isothermal ternary diffusion of H₂O-NaCl-KCl system, 3375; activity coefficients in aqueous three-component solutions by cation-sensitive glass electrodes, 3992; diffusion and frictional coefficients for system water-mannitol-sodium chloride, 4276
- Sodium iodate, Raman studies of, 3886
- Sodium ion, limiting equivalent conductance to 400°, 2984; self-diffusion coefficients in alcohol water mixtures, 3968; thermodynamics of exchange of tetramethylammonium with, in cross-linked polystyrene sulfonates, 4268
- Sodium nitrate, silver nitrate, system, molten, thermoelectric properties, 1204
- Sodium nitrite ices, radiolysis of, 1080
- Sodium polyacrylates, single-ion activity coefficient of gegenions in, 3690; mean activity coefficients of, 4102
- Sodium silicate glasses, structure and far-infrared absorption spectra of, 3846
- Sodium sulfate, abnormal relation between velocity of sound and temperature in, 3214; temperature coefficient of conductance of, 4033
- Sodium tetrachloroferrate(III), crystal structure of, 239
- Solubility, of reaction mixtures of calcium oxide, silica, and water, and hydrated tricalcium silicate in water, 182; of non-polar gases in water, theory, 281; of cobalt sulfate hexahydrate and heptahydrate, 1268; and activity coefficients of NaCl and KCl in N,N-dialkylamides containing water, 1377; of argon and nitrogen in sea water, 2608; behavior of polyoxyethylene nonylphenol ethers in cyclohexane and effect of water, 2788; aqueous, of *n*-dodecanol, *n*-hexadecanol, and *n*-octadecanol, 3171; of fluorocarbons in cyclohexane and 1,4-dioxane, 3200; of argon in water and dilute aqueous nonelectrolyte solutions, 3245; of argon in water and aqueous solutions of electrolytes, 3250; of hydrogen in liquid Na, 3542; equilibrium, of hydrogen as function of gold content in gold-palladium alloys, 3575; of argon to 451 atm. in fused sodium nitrate, 3631
- Solubilization, by surfactants, effect on kinetics of alkaline decomposition of indoaniline dyes, 2357
- Solvent extraction, for study of kinetics of reactions in molten salt phase, 1835
- θ-Solvents, binary mixtures of, 3263
- Soret coefficients, relative determination for electrolytes, 41; and heats of transport of aqueous electrolytes, 3598; of electrolytes, relative determination, 3755
- Sorption, rates for solid polypeptides, 600; water, comparison with deuterium-hydrogen exchange sites in poly-L-valine, 1432
- Sound, abnormal relation between velocity of, and temperature in sodium sulfate solution, 3214
- Specific heat, relation between, and total emittance in Ta, Nb, W, and Mo, 1420; of polyethylene single crystals, 2078; of atactic and isotactic polystyrene, 2668
- Spectra, p.r.s., of thiopyrones, 1; infrared, of solid 1:1 pyridine-benzoic acid complexes, 74; n.m.r., study of ether-boron halide molecular addition compounds in dichloromethane, 89; e.s.r., of irradiated methacrylate polymers, 189; infrared, study of adsorption of ammonia on dry γ-alumina, 231; e.m.r. and electronic, of tetrachloroferrate(III) ion in nonaqueous solution, 244; e.p.r., studies of gaseous atom-molecule reactions, 293; infrared, of nitrotriacetate chelates in aqueous solution, 404; p.m.r. of ten diolefins, 486; n.m.r., of 1,4-diheterocyclohexanes, 579; infrared, study of complexes of ethylamine with ethylammonium and copper ions in montmorillonite, 683; infrared, of perfluorocyclopropane and *cis*- and *trans*-perfluorobutene-2, 693; photoconductivity, of HgI₂, PbI₂, GaSe, and Cu₂O crystals, 745; nuclear quadrupole resonance, of Bi²⁰⁹ in BiBr₃, 949; e.s.r., of photoexcited triplet state of triphenylene in rigid solution, 953; C¹³ magnetic resonance study of protonation of acetic and benzoic acids, 1030; e.s.r., effect of oxygen on, of anthracene and perylene adsorbed on silica-alumina, 1082; absorption and phosphorescence, of rare earth β-diketone chelates, 1092; infrared, of disulfur monoxide, 1154; infrared, of high-area metal films evaporated in CO, 1188; infrared, of carbon monoxide chemisorbed on evaporated nickel films, 1195; absorption, of solvated electrons, effect of solvent and of solutes on, 1244; C¹³m.r., of 1-substituted 1-hexynes, 1348; mass, Knudsen cell measurements of vapor pressure of Pd and partial pressure of PdO, 1373; magnetic resonance of triplet state of oriented pyrene molecules, 1429; of photochromic spiropyrans, 1435; n.m.r., of hydrogen bonding of N-monosubstituted amides, 1482; study of association of Cu²⁺ and SO₄²⁻ ions in aqueous solution at constant ionic strength, 1537; infrared, study of association of aniline and N-methylaniline with benzene, N,N-dimethylaniline, pyridine, and N,N-dimethylcyclohexylamine, 1596; mass, of three monodeuterated propenes, 1615; mass, of dimanganese decacarbonyl and dicobalt octacarbonyl, 1618; mass, study of unsaturated methyl esters, 1711; mass, specific rearrangements in, of neopentyl esters, 1742; n.m.r. absorption, chemical shifts in, for O-17 in oxy ions, 1844; high resolution nuclear resonance, of chain conformation of polyethylene oxide, 1888; n.m.r., of 9,10-bridged 9,10-dihydroanthracenes, 2022; identification of products in radiolysis of perfluorocyclohexane and perfluorocyclobutane, 2059; e.s.r. of anion radicals of thianthrene oxides, 2108; infrared absorption bands for decaionated zeolites, 2117; in study of interaction of triphenylamine with iodine and with silica-alumina catalysts, 2127; e.s.r., of aliphatic semiquinones, 2131; infrared, of molecules adsorbed on metal powders obtained from electrically exploded wires, 2139; infrared, and stability of HBF₂(g), 2208; infrared absorption, of O¹⁸ labeled phenol, 2259; infrared, of HBBr₂(g), 2461; electronic, of Ga₂, In₂, and Tl₂ molecules, 2480; continuous absorption, of iodine monochloride, 2483; e.s.r., associated with photochromism in 2,2'-dimethylbianthrone, 2487; charge-transfer complex, solvent shifts in, 2490; mass, of zirconium diboride, 2531; n.m.r. dilution shifts for acetic acid in acetic anhydride, acetone, and 1,4-dioxane, 2564; 300-mμ band of NO₃⁻, 2645; p.m.r., effect of aromatic solvents on, 2679; infrared, study of dimerization of trimethylacetic acid in CCl₄, 2715; mass, for reaction of nitrogen atoms with ethylene, 2736; p.m.r., study of protonation of pyrazine, 2791; mass, ionization and dissociation of diphenyl and condensed ring aromatics by electron impact, 2935; p.m.r., of hydrogen bonding in amine-acetamide-chloroform systems, 2950; p.m.r. and infrared, of hydrogen bonding in tri-*n*-octylammonium salt solutions, 3075; n.m.r. spin relaxation, in solid *n*-alkanes, role of specific molecular motions in effecting spin relaxation, 3099; relation between electrochemical and spectroscopic properties of halide and pseudohalide ions in solution, 3176; high resolution, of piperidine, 3196; mass, of cyclopentadienylmolybdenum dicarbonyl nitrosyl and 1,3-cyclohexadienyltricarbonyl, 3198; p.m.r.

- line widths, ligand exchange, and electronic relaxation times for arylphosphine complexes of Co(II) and Ni(II), 3212; spin-echo n.m.r., studies of perfluorocyclohexane, 3216; interionic vibrational absorption bands of ion aggregates in benzene, 3223; n.m.r., of aluminum alkyls, 3418; infrared investigation of zeolites and adsorbed molecules, structural OH groups, 3463; of titanium, zirconium, and hafnium oxides in neon and argon matrices, 3488; n.m.r., of phenyl- and diphenylacetylene, 3552; of purine and pyrimidine bases, 3615; Raman, infrared, and n.m.r., of silver nitrate solutions in acetonitrile, 3634; n.m.r., of N-monosubstituted methylamines, 3645; p.m.r., of *cis*- and *trans*-¹⁹N-*n*-butylformamide, 3648; Al²⁷ n.m.r., of trialkyl-aluminum compounds, 3663; near infrared, of liquid water, 3671; e.s.r., of irradiated acrylamide, 3712; near-infrared, of hydrogen bonding in water and deuterium oxide, 3722; mass, use of appearance potential of fragment ions from fluorinated ethylenes to calculate heats of formation of hydrofluorocarbon radicals and ions, 3731; mass, of fluorinated ethylenes, calculations based on statistical theory of mass spectra, 3737; mass, of C₃F₆, C₂F₅Cl, and *c*-C₃F₆, 3741; luminescence, of alkyl halide salts of pyridine, 3791; mass, use of mass spectrometer intensity *vs.* time data to determine thermodynamic stabilities as function of composition for indium sulfide, 3826; far-infrared absorption, of sodium silicate glasses, 3846; absorption, of cationic dye acridine orange hydrochloride, 3872; Raman, of iodic acid and sodium iodate, 3886; C¹³ magnetic resonance, of alkyl cyanides, isocyanides, isocyanates, and isothiocyanates, 3920; infrared, of hexachloroacetone, 3949; infrared, and bonding of nitric oxide adsorbed on Ni and Fe, 3998; Raman, determination of ionization constants of sulfonic acids, 4109; n.m.r., of nitriles and isocyanides, 4152; n.m.r., of 2,2'-bipyridyl, 4166; absorption, changes due to different gegenions in permselective membranes, 4221; n.m.r., method to determine rate of dehydration of acetaldehyde hydrate, 4325; infrared reflection, of molten fluoride solutions, 4335; mass, study of dioxygen difluoride, 4338; changes in cationic dye due to interaction with macromolecules, 4368; e.s.r., of 1,1-diphenylethylene adsorbed on silica-alumina catalysts, 4402; n.m.r., of three unsymmetrical *o*-dihalobenzenes, 4413; p.m.r., of phenanthrene, 4417; apparently primary CH₅⁺ ion in mass spectrum of 2-methoxyethanol, 4420
- Spheres, packed, pore area and adsorption hysteresis for, 1395
- Spiropyrans, photochromic, spectroscopy and photosensitization of, 1435
- Steam, flowing, reaction with molybdenum metal, 1638
- Stilbenes, *cis*- and *trans*-, π -complex mechanism for isomerization and isotope exchange on Pt catalyst, 3526
- Stress relaxation, use in study of cleavage of cross-linked polyurethane elastomers, 476; radiolytic, of ethylene propylene copolymer, 2072
- Strontium, heats and entropies of dilution of perchlorates of, 4231
- Strontium ion, aqueous, revised thermodynamic properties of, 3181
- Sublimation pressure, of cadmium(II) fluoride by Knudsen and Langmuir techniques, 3174
- Succinimide, rate of exchange of chlorine between dimethylchloramine and, 796
- Sugars, reducing, oxidation by hexacyanoferrate(III) in alkaline medium, 2038
- Sulfamic acid, thermochemistry of, 2244
- Sulfanilic acid, thermochemistry of, 2244
- Sulfate ion, association of Cu²⁺ and SO₄²⁻ ions in aqueous solutions of constant ionic strength, 1537; limiting equivalent conductance to 400°, 2984; photochemistry of, 2996
- Sulfonic acids, ionization constants of, by Raman measurements, 4109
- Sulfur, liquid, phase equilibria in solutions of, 261; monodisperse colloidal, radiolysis of, 2805; in burnt gas of hydrogen-oxygen flames, 3593
- Sulfuric acid, concentrated, micelle formation in, 968; -water solutions, conductances and ionization constants at high temperatures and pressures, 2726
- Sulfur monoxide, study of mechanism of light emission from reaction of oxygen atoms with, 849
- Sulfur trioxide, mean amplitudes of vibration, shrinkage effects, thermodynamic functions, and molecular polarizability of, 2107
- Surface area, of solids, and virial theory of adsorption, 1129; of liquids in circular tubes, 1809; small, measurement by B.E.T. adsorption method, 2300
- Surface charge, direct measure of, in presence of electrode reaction, 4051
- Surface tension, theoretical refinement of pendant drop method, 348; in reciprocal system K⁺, Cd²⁺-Cl⁻, Br⁻, 1443; measurement by pendant drop techniques, 1933; of liquid alkali halide binary systems, 2606; of amorphous polymers, 2809; Zisman's critical, relationship between parachor and, 3220
- Tacticity, of poly(methyl methacrylate), gel melting point as measure of, 3384
- Tantalum, relation between specific heat and total emittance in Nb, W, Mo, and, 1420; hydrolysis of Ta(V) in KF-LiF, 4335
- Tantalum dioxide, enthalpy of formation of gaseous, 4399
- Tantalum oxide, enthalpy of formation of gaseous, 4399
- Tantalum pentafluoride, enthalpy of formation, 2089
- Taurine, thermochemistry of, 2244
- Tellurium, *P-T-x* phase diagram for Zn-Te system, 3367
- Temperature coefficient, of conductance of sodium sulfate, 4033
- Tetraalkylammonium halides, symmetrical, conductance of, 3878; symmetrical, conductance in methanol, 4208; conductance in deuterium oxide solutions, 4216
- Tetraalkylammonium ions, behavior of Ag-AgI electrode in presence of, 2793
- Tetraalkylammonium picrates, symmetrical, conductance of, 3878; symmetrical, conductance in methanol, 4208
- Tetrachloroferrate(III) ion, e.m.r. and electronic spectra of, 244
- Tetrachloromethane, thermodynamics of mixing in plastically crystalline region for tetramethylmethane-tetrachloromethane system, 2176
- 7,7,8,8-Tetracyanoquinodimethane, conductive salt of radical anion of, 1740
- Tetraethanolammonium halides, activity coefficients and molal volumes, 3569
- Tetraethylammonium chloride, dissociation in ethylene dichloride, 87
- Tetrafluorohydrazone, -fluorine reaction, kinetics of, 3700
- Tetrahydrofuran, association of secondary amines with, 335
- Tetraisoamylammonium picrate, conductance in diethyl ether and benzene, 1437
- Tetrakis(dimethylamino)ethylene, reversible reactions of oxygen with, and *n*-decane, 3313
- Tetramethylammonium, thermodynamics of exchange of, with sodium ions in cross-linked polystyrene sulfonates, 4268
- Tetramethylmethane, -tetrachloromethane, thermodynamics of mixing in plastically crystalline region, 2176
- Tetranitromethane, aqueous, pulse radiolysis of, 53
- Tetraoxygen difluoride, molar extinction coefficient of O₄F₂ in visible range, 1079
- Tetraphenylborate ion, electrooxidation in aqueous solution at Pt disk electrode, 1067
- Tetraphenylboride, conductance of alkali metal salts of, 608
- Tetraphosphorus decasulfide, thermal properties of, 1214
- Tetraphosphorus triselenide, thermal properties of, 1214
- Tetraphosphorus trisulfide, thermal properties of, 1214
- Tetrapropylammonium bromide, ion size parameters in solution and solid state, 543
- Tetraselenium tetranitride, heat of formation of, 334
- Tetrasulfur tetranitride, heat of formation of, 334
- Tetrauranium enneaoxide, λ -type thermal anomaly in, 3192
- Thallium, viscosity and self-diffusion from melting point to 1300°K., 518; electronic spectra of Ga₂, In₂, and Tl₂ molecules, 2480
- Thallium monofluoride, enthalpy of formation and dissociation energy of, 4030
- Thallium sulfate, polymorphism in, 1684
- Thallos fluoride, thermodynamics of vaporization of, gaseous dimerization, 3910
- Thallos iodide, thermodynamics of vaporization of, 1410
- Thermocell, rotating-disk, 4042
- Thermochemistry, solution, for calcium hydroxide, 6; solution, of silver sulfate, 9; solution, of barium hydroxide octahydrate, 1980; of aqueous sulfamic and sulfanilic acids and taurine, 2244; solution, of sodium carbonate, sodium bicarbonate, and trona, 3059; of interconversion of H₂B₂O₃(g) and H₃B₃O₃(g), 3160
- Thermodynamic functions, for sulfur trioxide, 2017
- Thermodynamic properties, for adsorption of carbon dioxide on zinc oxide, 17; of equimolar solutions of HCl and KCl, 207; of soluble monolayers produced by normal alcohols (C₈ to C₁₂)

- at water-octane interface, 310; low-temperature, of *n*-propyl-, *n*-butyl-, and *n*-decyl-substituted cyclopentanes, 353; zero pressure, of nitrogen gas, analytic expression, 495; of dolomite, 1065; of disulfur monoxide, 1154; of pentaerythrityl chloride, bromide, and iodide, 1209; of tetraphosphorus trisulfide, tetraphosphorus triselenide, and tetraphosphorus decasulfide, 1214; of HCl in *N*-methylacetamide by e.m.f., 1335; of hypostoichiometric thorium dicarbide, 1520; of 2,5-dimethylthiophene, 1524; bond and interaction contributions for calculating, 1550; of *n*-propyl-, *n*-butyl-, and *n*-decyl-substituted cyclohexane, 2094; of adsorbed water molecules and electrical conduction in montmorillonites and silicas, 2185; in exchange of lithium with cesium ion on cross-linked polymethacrylate ion exchangers, 2374; of HCl-NaCl mixtures, 2395; of yttrium-hydrogen system, 2510; of atactic and isotactic polystyrene, 2657; of lanthanum monosulfide, 2684; of beryllium compounds, 2828; for methane-iodine reaction, 3040; of aqueous strontium ion, 3181; of aqueous solutions of noble gases, 3240; of aqueous solutions of noble gases, effect of nonelectrolytes, 3245; of aqueous solutions of noble gases, effect of electrolytes, 3250; of scandium-hydrogen system, 3514; of uranium monoselenide, 3618; for benzene in polyphenyls, use of gas-liquid partition chromatography, 3682; of protonation of triethylenediamine, triethylamine, trimethylamine, and ammonia, 3759; and allotropy of beryllium chloride, 3839; low-temperature, of *n*-propyl and *n*-butylbenzene, 4304
- Thermodynamics, surface, application to Gibbs elasticity, 1798; of crystalline hydrates, 1840
- Thermoelectric properties, of molten AgNO₃-NaNO₃ system, 1204
- Thianthrene oxides, arion radicals of, 2108
- Thioamides, hindered rotation and C¹³-H coupling constants in, 2570
- Thionine, -nitrotripropionamide-acrylamide system, dye-sensitized photopolymerization processes, 641; comparison of photoactivities of methylene blue and, 647; - β -diketone-acrylamide systems, kinetics and mechanism of, 2842; ionic association in solution, fluorescence and solvent effects, 2988
- Thiopyrones, proton resonance spectra of, 1
- Thourea, chemical species containing P³² and S³⁵ subsequent to neutron irradiation of, 3202
- Thorium dicarbide, hypostoichiometric, heat capacity and thermodynamic properties of, 1520
- Thorium mononitride, decomposition pressure and melting point of, 1223
- Thorium oxide, -water system, heats of immersion, 151; -aqueous solution interface, electrokinetic phenomena at, 3148; colloidal, small angle X-ray scattering study of, 3849
- Tin, galvanic cell measurement of thermodynamic interaction between zinc and lead in dilute solution in liquid tin, 4085
- Titania, adsorption of CO, N₂, O₂, and Ar, 3587
- Titanium monoxide, oxidation at high temperatures, 158
- Titanium oxide, spectroscopy of, in neon and argon matrices, 3488
- Titanium tetrabromide, charge-transfer complexes with aromatic hydrocarbons, 660
- Titanium tetrachloride, charge-transfer complexes with aromatic hydrocarbons, 660
- p*-Toluenesulfonic acid, behavior of divalent salts of, in aqueous solution, 4345
- Transition, thermal, of ribonuclease, effect of aqueous alcohol solutions on, 298; of pentaerythrityl chloride, bromide, and iodide, 1209; thermal, of ribonuclease and poly- γ -benzyl-L-glutamate, 1515
- Transition energies, $n \rightarrow \pi^*$, in cyclic and bicyclic ketones, relationship between C¹³ carbonyl chemical shifts and, 3105
- Transition metals, hydrolyses of amino acid esters promoted by transition metal ions, 2923
- Transport, of univalent cations across weak-acid membrane, effect of pH and divalent cations on, 2415
- Transport coefficients, reciprocal relations among, 2479
- Transport numbers, cationic, of KBr in *N*-methylacetamide, 2382; in aqueous potassium chloride solutions, 3208
- Transport properties, of dense fluid of molecules interacting with square-well potential, 869
- Trialkylaluminum compounds, Al²⁷ n.m.r. spectra of, 3663
- Tricalcium silicate, hydration of, 553, 2489
- Triethylamine, thermodynamics of protonation of, 3759
- Triethylenediamine, thermodynamics of protonation of, 3759
- Trifluoroethylcyclopropane, thermal isomerization of, 2141
- Trifluoroiodomethane, association with 2,4,6-trimethylpyridine, 2400
- Trifluoromethylcyclopropane, thermal isomerization of, 2141
- Trifluoronitrosomethane, electron diffraction study of, 3727; photolysis of, 4409
- Trilaurylamine, extraction of perchloric acid by, role of aromatic diluent, 1565
- Trimethylacetic acid, infrared study of dimerization of, in CCl₄, 2715
- Trimethylamine, heat of reaction of diborane with, 1010; thermodynamics of protonation of, 3759
- 2,4,6-Trimethylpyridine, association with trifluoroiodomethane, 2400
- 1,3,5-Trinitrobenzene, complexes with benzene, mesitylene, durene, pentamethylbenzene, or hexamethylbenzene, 2766
- Trinitrotri-*amminecobalt*(III), activity coefficient of, in aqueous salt solution, 1546
- Tri-*n*-octylammonium salt solutions, p.m.r. and infrared studies of hydrogen bonding in, 3075
- Tri-*n*-octyl phosphine oxide, extraction of HClO₄ and HReO₄ by, 1106
- Triphenylamine, interaction with iodine and silica-alumina catalysts, 2127
- Triphenylene, triplet state in rigid solution, electron spin resonance spectrum of, 953; rate of decay of phosphorescence from, in acrylic polymers, 2516
- Triphenylphosphine, reaction with alkali metals in tetrahydrofuran, 2775
- Tritium, recoil, ring opening and alkyl replacement in substituted cyclopropanes, 4297
- Tritium atoms, reactions with films of solid ethylene, 1040
- Trona, solution thermochemistry of, 3059
- Tungsten, relation between specific heat and total emittance in Ta, Nb, Mo, and, 1420
- Ultracentrifugation, equilibrium, of hydrolyzed lead(II) perchlorate solutions, 959
- Ultracentrifuge, preparative, moving boundary sedimentation in, 1820
- Uranium, kinetics of V(II)-U(VI) reaction, 176
- Uranium monoselenide, heat capacity and thermodynamic properties, 3618
- Uranium trioxide, kinetics of hydrogen reduction of, 2012
- Uranyl fluoride, Wien effect, 508
- Uranyl ion, kinetics for hydrolysis and polymerization of, 2319
- Uranyl nitrate, Wien effect, 500
- Uranyl nitrate hexahydrate, water-nitric acid- system, activities of components, 1904
- Uranyl perchlorate, Wien effect, 500
- Uranyl sulfate, Wien effect, 513
- Urea, kinetics of base-catalyzed hydrolysis of, 687; effect on water structure and hydrophobic bonding, 2720; diffusion study in system, labeled urea-urea-water by measurement of intradiffusion coefficients of, 3120
- Vanadia, oxidation of *o*-methylbenzyl alcohol over, kinetics of processes occurring on catalyst surface, 3092
- Vanadium, kinetics of V(II)-U(VI) reaction, 176
- Vanadium oxytrichloride, charge-transfer complexes with aromatic hydrocarbons, 660
- Vaporization, thermodynamics of, for liquid thallos iodide, 1410; of lanthanum monosulfide, 2684; of gallium nitride, 3455; thermodynamics of, for thallos fluoride, gaseous dimerization, 3910; thermodynamics of, in beryllium oxide-boron oxide system, 4250
- Vapor pressure, of copper phthalocyanine, 344; solvent, in dilute solutions of gallium in cadmium, 933; of Pd and partial pressure of PdO, 1373; of water and nitric acid over water-nitric acid-uranyl nitrate hexahydrate system, 1904; of iodine monochloride, 2443; differential study, of self-association of acids and bases in 1,2-dichloroethane and other solvents, 2690; and enthalpy of arsenic triiodide and its absolute entropy, 2743; simple reduced equation for estimation of, 3209; and enthalpy of vaporization of molten bismuth chloride, 3916; and heat of sublimation of chromium, 4044
- Vinyl compounds, C¹³ chemical shifts for, 1947
- Viscoelasticity, linear, reduction principle in, 671
- Viscoelastic properties, of dilute solutions of poly- α -methylstyrene, 346; effects of cross-link spacing and initial molecular

- weight in polybutadiene, 2811; temperature dependence of viscoelastic behavior of polystyrene, 3480
- Viscosity, and self-diffusion of liquid thallium from melting point to 1300°K., 518; intrinsic, studies of stereoregular poly(methyl methacrylate) in 2,2,3,3-tetrafluoropropanol, 1101; surface, effect on thinning of soap films, 1471; intrinsic, -molecular weight relationship for fractions of linear polyethylene, 1645; surface, of monomolecular films of long-chain aliphatic amides, amines, alcohols, and carboxylic acids, 1789; of aqueous solutions of chloroamineplatinum(IV) salts, 2197; of glass-forming solvent mixtures, 2466; macroscopic, for quaternary salts in cyanoethylsucrose-acetonitrile mixtures, 2576; intrinsic, of linear polyethylene in Θ -solvent, 3109; of *cis*-1,4-polybutadiene and polystyrene in mixed Θ -solvents, 3263; of NaK 78 at low temperatures, 3782; of pure water and sea water in region of maximum density, 3988
- Volatilization, of molybdenum in presence of water vapor, 2065
- Volume, partial, of 1-butanol in dilute aqueous solution, 2406; excess, analyses of data in terms of different theories of molecular solutions, 2759; partial molal, of alcohol-water solutions, 3795
- Volume change, on neutralization of strong acids and bases, 2808
- Volume of mixing, measurements for eight aromatic-alicyclic systems, 2753
- Voltage transients, of freshly produced noble metal electrode surfaces, 3329
- Water, thorium oxide- system, heats of immersion, 151; solubility relations in calcium oxide-silica-water system, 182; alumina- system, differential heats of adsorption as function of particle size for, 317; -deuterium mixtures, isotope effects in radiolysis and photolysis of, 698; solubilized and emulsified, n.m.r., dielectric, near-infrared, and cryoscopic studies of, 1087; desorption isotherms for, from packed spheres and commercial gel, 1395; sorption, comparison with deuterium-hydrogen exchange sites in poly-L-valine, 1432; diffusion in cadmium iodide-water system, 1718; nitric acid-uranyl nitrate hexahydrate system, activities of components in, 1904; stabilization of structure by nonelectrolytes, 1922; effect of ions on self-diffusion of, 2001; liquid, monomer concentration in, 2145; adsorbed, relation between electrical properties and thermodynamic properties of, 2185; protonic conduction in water I region, 2224; diffusion in dilute HCl-water solutions, 2333; heavy, radiolysis in pD range 0-14, 2628; effect of urea on structure of, and on hydrophobic bonding, 2720; sulfuric acid-water solutions, conductances and ionization constants at high temperatures and pressures, 2726; estimation of dielectric constant to 800°, 3165; role in electron-transfer reactions, 3183; two-structure model, use in discussion of thermodynamics of aqueous solutions of noble gases, 3240; absorption by keratin, role of amino groups in, 3280; -sodium chloride-potassium chloride, isothermal ternary diffusion of, test of Onsager reciprocal relations in, 3374; liquid, near-infrared spectrum of, 3671; effect on peroxide yields in radiolysis of methanol and methanolic solutions, 3673; near-infrared study of H bonding in deuterium oxide and, 3722; partial molal volumes of alcohol-water solutions, 3795; activation energy of viscous flow of, in maximum density temperature region, 3988; reaction mechanism leading to formation of molecular hydrogen in radiation chemistry of, 4058; radiolysis, reactions of alanine with reducing species formed in, 4131; wetting of gold and platinum by, 4238; diffusion and frictional coefficients for system water-mannitol-sodium chloride, 4276; self-diffusion coefficients, 4412
- Water activity, effect on ion-exchange selectivity, 339
- Werner complexes, rate constants of hydrated electron reactions with, 289
- Wettability, of metals under continuous condensing conditions, 1306; of heterogeneous surface as function of coverage by regions of different intrinsic wettabilities, 1507
- Wien effect, in uranyl ion solutions, 500; for uranyl fluoride, 508; in uranyl sulfate, 513; for reference electrolyte solutions, 658
- Wüstite, rate of oxidation of iron to, in water-hydrogen gas mixtures, 327
- Xenon fluorides, in Xe-photosensitized reactions of perfluoroalkanes, 1434
- o*-Xylene, homogeneous gas-phase partial oxidation of, 909
- p*-Xylene, sensitized by organic bromine compounds, radiation-induced oxidation of, 1992
- Yttrium, -hydrogen system, thermodynamics of, 2510; scandium-yttrium-hydrogen system, 3973
- Yttrium trifluoride, enthalpy of formation of, 2305
- Zeolites, stability of metallic cations in, 1676; decationated, study of hydrogen held by solids, 2117; infrared investigation of, structural OH groups, 3463
- Zinc, poly-N-vinylimidazole complex with Zn(II), 1252; anion exchange of chloride complexes of, 2955; -tellurium, system, *P-T-x* system of, 3367; galvanic cell measurement of thermodynamic interaction between, and lead in dilute solution in liquid tin, 4085
- Zinc oxide, spectral sensitization of chemical effects in, 705; microcrystalline, hypersensitization of photoconduction in, 767; color sensitization of, with cyanine dyes, 774; sites for hydrogen adsorption on, 2500
- Zirconia, metastable tetragonal, occurrence as a crystallite size effect, 1238
- Zirconium diboride, mass spectrometric study of, 2531
- Zirconium oxides, spectroscopy of, in neon and argon matrices, 3488; monoclinic, optical energy gaps in, 3666
- Zwitterions, small, dielectric dispersion of protein solutions containing, 1162